K. K. Pant
Sanjay Kumar Gupta
Ejaz Ahmad   *Editors*

Catalysis for Clean Energy and Environmental Sustainability

Biomass Conversion and Green Chemistry – Volume 1

Springer

Catalysis for Clean Energy and Environmental Sustainability

K. K. Pant • Sanjay Kumar Gupta • Ejaz Ahmad
Editors

Catalysis for Clean Energy and Environmental Sustainability

Biomass Conversion and Green Chemistry - Volume 1

Springer

Editors
K. K. Pant
Department of Chemical Engineering
Indian Institute of Technology Delhi
New Delhi, Delhi, India

Sanjay Kumar Gupta
Department of Civil Engineering
Indian Institute of Technology Delhi
New Delhi, Delhi, India

Ejaz Ahmad
Department of Chemical Engineering
Indian Institute of Technology
(ISM) Dhanbad
Dhanbad, Jharkhand, India

Dedicated to:
To Our Parents, Families
& Prof. K.K. Pant's Late Father Shri
Pitamber Pant Ji

Preface

Biomass conversion to value-added chemicals and fuels via green catalytic routes continues to be the most sought-after research topic worldwide. In this regard, an array of homogeneous catalysts such as mineral acids, ionic liquids, deep eutectic solvents, heterogeneous catalysts such as zeolites, metal oxides, metal-organic framework, noble metal catalysts, and a combination thereof have been employed and found useful. However, the successful commercialization of these catalytic materials is still a challenging task due to recyclability and scalability issues. Moreover, recent research is focused on developing green and eco-friendly catalytic materials for the production of clean energy and environmental sustainability. However, most of the data is scattered and presented in experimental articles, whereas a theoretical insight into the catalytic reaction mechanism and catalyst support interaction is missing. Therefore, it is of utmost importance to develop mechanistic insight into the product-selective catalytic processes for biomass and biomass-derived feedstock conversion. Accordingly, volume I of the book focuses on recent advances in catalytic materials and processes for biomass conversion and green chemistry.

Overall, volume I of the book consists of 27 chapters covering all the aspects of biomass conversion technologies and green chemistry that include high- and low-temperature processes for biomass conversion, bio-catalytic and chemo-catalytic routes for value-added chemicals production from biomass-derived platform chemicals, production of biopolymers, biochar production, and emerging technologies such as photocatalysis and biohydrometallurgy. Although an application-oriented approach towards understanding biomass conversion catalysis has been employed, the mechanistic and fundamental aspects of catalytic materials in hydrogenation, oxidation, dehydration, carbonylation, and esterification/etherification and other pertinent reactions have been discussed extensively. We understand that this book will serve as ready reference material on recent advances in biomass conversion and biofuels production technologies using green catalytic processes for young researchers and prominent scientists and academicians worldwide from chemical engineering, chemistry, biochemistry, biotechnology, mechanical engineering, and interdisciplinary areas of research.

The overall flow and content is the outcome of several rounds of discussion, reviews, and revisions. Therefore, the editors are highly indebted to all the reviewers for their precious time, thoughtful comments, and valuable suggestions without which it would not have been possible to reach this stage. The editors would also like to thank all the authors for their patience during several rounds of revisions and timely responses. The editors would also like to sincerely thank Springer Nature for timely publication of the book and highly indebted to the Springer Nature team members, especially Mr. Dinesh Vinayagam (Production Editor), Mr. Aaron Schiller, Mr. Joseph Quatela, and Ms. Amelie von Zumbusch, for their constant support throughout the process starting from proposal stage to final book publication. The editors would like to thank and acknowledge the support of their lab members Dr. Shireen Quereshi and Mr. Prashant Ram Jadhao for their backend work, follow up with contributors, maintaining the record of all the documents, and assistance in chapters review from the time of proposal to the publication of both the books. The editors are also highly indebted and obliged to their family members for their patience, care, and unconditional support to complete both the volumes of the book.

New Delhi, Delhi, India   K. K. Pant
New Delhi, Delhi, India   Sanjay Kumar Gupta
Dhanbad, Jharkhand, India   Ejaz Ahmad

Contents

ix

Thermochemical Conversion of Biomass and Upgrading of Bio-Products to Produce Fuels and Chemicals

Hessam Jahangiri, João Santos, Andreas Hornung, and Miloud Ouadi

Abstract The considerable growth in energy demands and limited fossil fuel sources, together with environmental concerns, have forced the study of renewable, green and sustainable energy sources. Biomass and its residues can be transformed into valued chemicals and fuels with several thermal conversion processes, which are combustion, gasification and pyrolysis. Combustion is a chemical process that involves the rapid reaction of substances with oxygen, producing heat. Gasification produces synthesis gas at high temperatures (800–1200 °C) to generate heat and power. Pyrolysis has been applied for many years for charcoal formation, while intermediate and fast pyrolysis processes have become of significant interest in recent years. The reason for this interest is that these processes provide different bio-products (bio-oil, synthesis gas and biochar), which can be applied directly in various applications or as a sustainable energy carrier. The present chapter covers an overview of the fundamentals of slow, intermediate and fast pyrolysis, followed by the properties and applicability of the pyrolysis products. This study also identifies the features and advantages of the thermo-catalytic reforming (TCR) process in comparison with other technologies. This report presents a comprehensive literature review of bio-oil production and upgrading methods. In addition, the most common catalysts and supports for different upgrading methods are introduced. Finally, the current pathways for 2-methylfuran (2-MF) formation and the selection of xylose-rich biomass are discussed.

H. Jahangiri (✉)
School of Chemical Engineering, University of Birmingham, Edgbaston, Birmingham, UK

School of Water, Energy and Environment, Cranfield University, Cranfield, UK
e-mail: h.jahangiri@bham.ac.uk

J. Santos · M. Ouadi
School of Chemical Engineering, University of Birmingham, Edgbaston, Birmingham, UK

A. Hornung
School of Chemical Engineering, University of Birmingham, Edgbaston, Birmingham, UK

Fraunhofer UMSICHT, Fraunhofer Institute for Environmental, Safety and Energy Technology, Sulzbach-Rosenberg, Germany

Friedrich-Alexander University Erlangen-Nuremberg, Erlangen, Germany

Abbreviations

Al	Aluminium
APR	Aqueous phase reforming
BFB	Bubbling fluidized bed
C	Atomic carbon
C_2H_2	Acetylene
C_2H_4	Ethylene
C_2H_6	Ethane
C_3H_6	Propylene
C_3H_8	Propane
CaO	Calcium oxide
CeO_2	Cerium dioxide
CFB	Circulating fluidized bed
CH_3OH	Methanol
CH_4	Methane
CHP	Combined heat and power
CO	Carbon monoxide
Co	Cobalt
CO_2	Carbon dioxide
Cu	Copper
Ga	Gallium
H	Atomic hydrogen
H_2	Hydrogen
H_2O	Water or water vapour
HC	Hydrocarbon
HDO	Hydrodeoxygenation
HHV	Higher heating value
K_2O	Potassium oxide
KOH	Potassium hydroxide
M	Monomer
MCM	Mobil Composition of Matter
MF	Methylfuran
MgO	Magnesium oxide
MnO	Manganese(II) oxide
Mo	Molybdenum
Mtoe	Millions of tonnes of oil equivalent
MW	Molecular weight
MW_{th}	Megawatts thermal
N_2	Nitrogen

N$_2$O	Nitrous oxide
Na$_2$CO$_3$	Sodium carbonate
NaOH	Sodium hydroxide
Ni	Nickel
NO	Nitric oxide
NO$_2$	Nitrogen dioxide
NO$_x$	Nitrogen oxides
O	Atomic oxygen
O$_2$	Oxygen
O$_3$	Ozone
OECD	Organisation for Economic Co-operation and Development
OH	Hydroxyl radicals
OHS	Oat hulls
PAH	Polycyclic aromatic hydrocarbons
PCB	Polychlorinated biphenyls
Pd	Palladium
PFD	Process flow diagram
PPM	Parts per million
Pt	Platinum
S	Seconds
SAPO	Silicoaluminophosphate
SB	Sugarcane bagasse
SBA	Santa Barbara Amorphous
SG	Second generation
SiO$_2$	Silica
SO$_2$	Sulphur dioxide
TCR	Thermo-catalytic reforming
TiO$_2$	Titanium dioxide
UK	United Kingdom
UO$_2$	Uranium dioxide
USA	United States of America
Zn	Zinc
ZrO$_2$	Zirconia
ZSM	Zeolite Socony Mobil

1 Introduction

One of the main segments of renewable resources is bioresources. The fossil fuel-based energy transition to sustainable alternatives to meet the growing need for fuels, chemicals and energy is a significant challenge facing industrial growth. The energy consumption of the world since the 1990s and also predicted demands for future decades are shown in Fig. 1. This figure represents that the world's energy
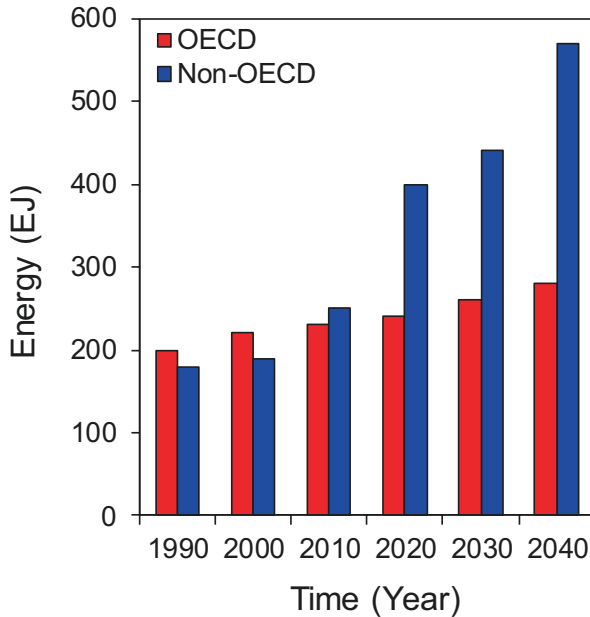
Fig. 1 Energy consumption of the world between 1990 and 2040 [3]

consumption has increased considerably from the 1990s towards the 2020s and also that it will increase significantly further in future. Much of the world's energy consumption occurs between non-OECD nations (outside the Organisation for Economic Co-operation and Development) due to expanding population and strong economic growth. Nowadays, sustainable biomass feedstock development for the production of biochemicals and biofuels is significantly considered around the world with extensive work being conducted to convert scientific and academic improvements into profitable reality [1–3].

The word biofuel refers to any solid, gas or liquid fuels that are produced from plant materials, wastes and residues which can replace petroleum fuels. The most suitable alternative for petroleum-based fuels are biofuels, which can be used for transport and do not face the limitations of fossil fuels [4]. The increase in energy consumption over the past decades, the significant growth in energy demands in the future and limited sources of fossil fuels have all enforced scientists and researchers to study more about sustainable sources of energy.

Another motivation and incentive for scientists to explore renewable and green sources of energy were environmental concerns and global climate change issues. The most well-known reason for the phenomenon of global warming is the effect of greenhouse gases. "Greenhouse gas" refers to the atmospheric gases which emit and absorb radiation at particular wavelengths in the thermal infrared radiation spectrum transmitted by the surface of the earth, clouds and the atmosphere itself.

Table 1 Top 10 producers of world oil [9]

Producers	Energy (Mtoe)	Total oil (%)
Venezuela	144	3.3
Kuwait	160	3.7
United Arab Emirates	160	3.7
Iran	168	3.9
Iraq	175	4.0
China	215	5.0
Canada	221	5.1
Russia	533	12.3
United States	567	13.1
Saudi Arabia	572	13.2
Others	1416	32.7
World	4331	100

Carbon dioxide (CO_2), nitrous oxide (N_2O), water vapour (H_2O), methane (CH_4) and ozone (O_3) are the main greenhouse gases in the atmosphere [5]. These greenhouse gases trap the heat of emitted atmospheric radiation within the surface-troposphere process. This fact is named "the effects of greenhouse" [5, 6]. The evidence of ice core data and in situ measurements proved that the concentration of greenhouse gases such as CH_4, CO_2 and N_2O has considerably increased during the last centuries and caused an increment of global temperature [7].

To decrease the emission of greenhouse gases and hence decrease global temperatures, it is required to change the energy sources that are used by industries into renewable and green sources. It has been reported by the International Energy Agency that 60% of all greenhouse gas emissions and 69% of all CO_2 emissions are correlated with energy [8]. Fossil fuel combustion for producing energy increases the concentration of carbon dioxide, which is the primary source of pollution. Today, the main location for production of crude oil is in the Middle East, with about 32% of the world's proven oil reserves [9]. Furthermore, Norway and the UK are the first and second largest liquid producers in Europe, respectively [9]. Table 1 shows the top 10 producers of world crude oil. Therefore, development of renewable transport fuels (bio-oils) is an important topic to be discussed in order to reduce pollution and enhance energy security for consumers of crude oil.

2 Renewable Resources

In 2018, it was reported by the Department of Energy and Climate Change in the UK that one of the most profound sources of emissions of greenhouse gases is from the transport sector. It was estimated that 33% of CO_2 emission was from the transport sector [10]. However, biofuels are non-toxic and biodegradable and can prevent

the emissions of carbon compared to fossil fuels. Moreover, their sustainability and renewability should also be highlighted. Biodegradable biofuels prevent underground water and soil pollution and therefore provide a lower level of environmental risk compared to non-renewable fuels [11].

Biofuels can be applied in different types of vehicles from trucks to airplanes with the requirements in engine modifications or the infrastructure of fuel distribution. The application of biofuels can lead to a considerable reduction in CO_2 emissions of 50–80% in comparison with fossil fuels [12]. Biofuels have three forms: solid, gas and liquid. The liquid biofuel can be a replacement for the present fossil diesel or petrol.

3   Biofuel Classes

Biofuels are characterized into two main classes. The first is "primary biofuels", and the second is "secondary biofuels". The traditional form of producing biofuels for generating heat and electricity is from "primary biofuels", which is utilized through direct combustion of natural materials. This kind of biofuel is not an appropriate energy source for large-scale industrial processes due to its environmental risks, low efficiency and toxicity [13].

"Secondary biofuels" are the other class of biofuels, which are obtained through biomass processing and produced in the form of gas (biogas or synthesis gas), liquid (bio-liquid) and solid charcoal (biochar) which are used as transport fuels or for other industrial applications. The second class of biofuel itself is also categorized into three groups according to their processing technology and their feedstock, known as the first, second and third generations of biofuels [14]. In the next section, first, second and third generations of biofuels will be explained.

3.1   First Generation

First-generation biofuels are mostly obtained from sugars, oil-rich food crops or starch which includes oils (biodiesel) and alcohols (bioethanol) [13, 15, 16]. The required technology for the production of first-generation biofuels is known and has been subjected to considerable process development. Furthermore, the production of these types of biofuels is simple on a commercial scale. One of the most crucial challenges in this generation of biofuels is the research on the cost optimization for processes where their products are intended to compete with their non-renewable competitors [15].

Another critical problem associated with this type of biofuel is the rivalry between fuel and food production from edible crops [17, 18]. This is the most important criticism for the use of first-generation biofuels and has caused considerable increases in the prices of food in many countries that produce biofuels [19, 20].

Aside from the competition between food and fuel, another main concern regarding first generation of biofuels is deforestation. For example, massive tracts of peatland and rainforest have been cleared all for the plantation of palm oil [21]. Therefore, first generation of biofuels is the least favoured source of energy, due to disagreements regarding the final greenhouse gas emissions, energy balance and doubtful social sustainability [14, 16, 22].

3.2 Second Generation

Second-generation biofuels (biofuel SG or biofuel 2.0) are obtained from non-food biomass such as lignocellulosic feedstock materials like straw, cereal, residues and forests. Therefore cellulose is the primary component of the biomass feedstock for second-generation biofuels which are also known as cellulosic fuels [23, 24]. Since the second generation of biomass feedstock does not require the use of agricultural land, the issue of fuel versus food is undebatable [25, 26]. The major advantages of second-generation biofuels over first generation biofuels are as follows [27, 28]:

- An abundant and wide range of feedstocks can be processed.
- They are more efficient and need less farmland.
- They have a better environmental performance.
- They have lower costs.

3.3 Third Generation

Third-generation biofuels are formed from microalgae and microbes as alternative energy resources [14, 29]. However, cellulose fermentation is defined as a third-generation biofuel process which is used to produce bioethanol [30]. Microalgae are unicellular or multi-cellular photosynthetic microorganisms. Microalgae can convert sunlight and CO_2 into lipids, carbohydrates and a large amount of proteins. Also, it removes phosphorus and nitrogen from wastewater and fertilizer, resulting in pollution reduction [31, 32]. There are several processes for the conversion of algae into biofuels such as liquefaction, pyrolysis, gasification, anaerobic digestion, extraction, fermentation and transesterification [16, 33–35].

Second-generation biofuels have some drawbacks, such as their pre-treatment requirement and the need for facilities on a large scale with complex processes and relatively low production yields. These reasons have prevented the full commercialization of second-generation biofuels [36, 37]. However, third-generation biofuels to some extent do not need as sophisticated methods of production, large-scale facilities and high amounts of energy. Therefore, third generation can be considered a viable source of renewable energy depending on its final end use [25].

4   Biomass Conversion Methods

There are a couple of methods of converting biomass into useful chemicals and energy carriers. Figure 2 shows the primary conversion methods that are currently used for the production of transport fuels and chemicals.

4.1   *Combustion*

Combustion is an exothermic reaction between an oxidant and fuel which produces flue gas, ash and heat. Combustion happens at high temperatures (850–1000 °C). The combustion of biomass is a complicated process containing homogenous and heterogeneous reactions. Drying, devolatilization, gasification and char combustion are the main steps when heating biomass. Several pre-treatment steps are needed to meet combustion requirements such as sizing and drying the biomass. Excess air ratio and temperature are the essential parameters in the combustion process [38, 39]. The most efficient reactor for high moisture and ash content materials is the fluidized bed combustor since it could reach complete thermal oxidation [40, 41]. The main disadvantage of combustion is the production of a massive amount of flue gases and bottom ashes [42].
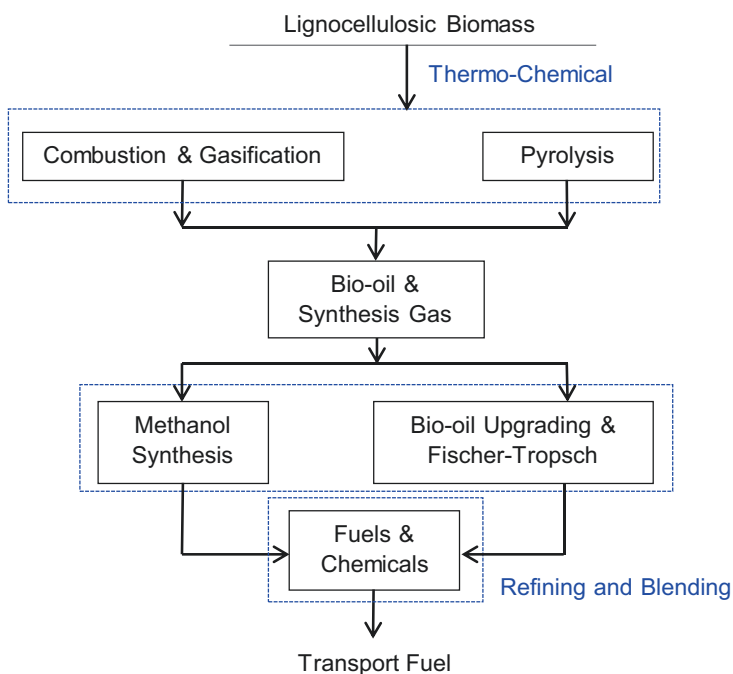
Fig. 2 Thermochemical procedures for conversion of lignocellulosic biomass into fuels and chemicals

4.2   Gasification

Biomass partial combustion at a high temperature (800–1200 °C) with a low oxygen level produces combustible gases that mainly consist of CO, CO_2, N_2, H_2O, H_2 and CH_4 [43, 44]. This gas mixture is called "synthesis gas" or "syngas" which has several applications in furnace oil, direct heat, internal combustion engines and methanol production in an economically beneficial way [43]. Furthermore, Fischer-Tropsch synthesis process can convert syngas into liquid hydrocarbons [45–47]. The three main gasification reactors are fixed bed gasifier (updraft and downdraft) [48, 49], fluidized bed gasifier and entrained flow gasifier [50, 51]. The reactor configurations are shown in Fig. 3.

Fixed bed gasifiers are generally suitable for small-scale power generations (<20 MW_{th} for updraft gasifiers and <5 MW_{th} for downdraft gasifiers). Downdraft fixed bed gasifiers produce comparatively clean gas with a low level of tars, while updraft gasifiers produce very dirty gas with a high level of tars [51, 52].

In a fluidized bed gasifier, the feedstock can be processed with either a bed of sand or a mixture of inorganic materials (alkali metals and dolomite) with char. The fluidized bed gasifier has a high tolerance to different sizes of particles compared with fixed bed gasifiers [53]. In regard to entrained flow gasifier, the reaction happens at high temperature (>1000 °C) in the presence of suspended particles. Entrained flow gasifier produces gas with high quality and low level of tars, and also it is usually aimed for large-scale power plant (>100 MW_{th}) [52].

The chemistry of gasification is complicated. The reaction steps can be defined as follows [52]:

- Drying: The moisture content of the material is decreased in this stage, and it varies between 5% and 35% at 100 °C temperature.
- Devolatilization (pyrolysis): Thermal decomposition happens in the absence of oxygen in this step. This step produces pyrolysis vapours (non-condensable and condensable) and biochar. The condensable vapour fraction creates liquid tars.
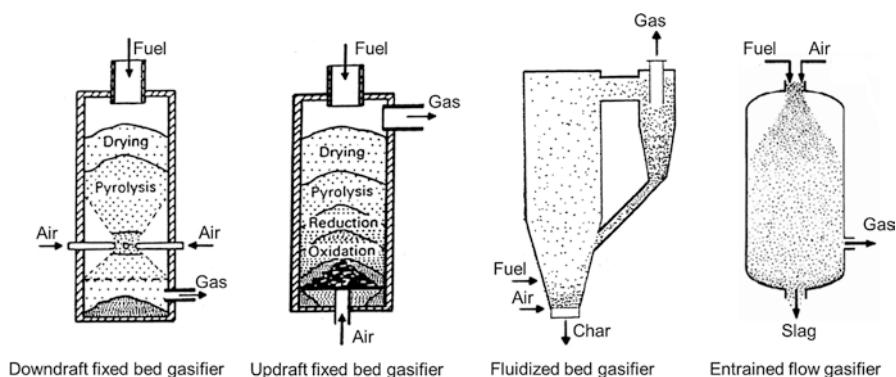
Fig. 3 Downdraft and updraft fixed bed, fluidized bed and entrained flow gasifiers. (Reproduced with permission from [49, 50], Copyright © 2000 and 2016, Elsevier)

- Oxidation: In this step, the reaction takes place between organic vapours, solid carbonized material and oxidizing agent, producing CO_2. The H_2 is oxidized to form water. Furthermore, partial carbon oxidation might happen if O_2 is in sub-stoichiometric quantities and produces CO.
- Reduction: In this stage, the reduction process happens to remove oxygen from the produced gases to form combustible gases at a high temperature (800–1200 °C). The main reactions are water gas reaction, Boudouard reaction, water gas shift reaction and methanation reaction.

4.3 Pyrolysis

Biomass pyrolysis is biomass decomposition through heating in the absence of oxygen. Pyrolysis is an endothermic process. It occurs in a temperature range from 200 °C to 800 °C in comparison with gasification, which is from 800 °C to 1200 °C [54]. Pyrolysis is the first phase of both combustion and gasification. Pyrolysis is divided into different categories which are fast, intermediate, slow and torrefaction [55, 56]. Residence time is an essential factor in biomass pyrolysis.

Torrefaction and slow pyrolysis have hours and days solid residence times. Intermediate pyrolysis has minutes solid residence time, while biomass fast pyrolysis has a very short solid/vapour residence time, which is around 2 s [57]. The characteristics of the main three groups are presented in Table 2. Figure 4 shows the different products of biomass pyrolysis with different methods (mass balance). This figure shows that longer residence time reactions (slow pyrolysis and torrefaction) favour charcoal production, while shorter residence time reactions (intermediate and fast) favour liquid and gas production. Fast pyrolysis reaction yields the maximum amount of liquid (75%) and the least char content (12%) in comparison with other biomass pyrolysis reactions [57, 58].

Common pyrolysis reactors are bubbling fluidized bed (BFB), circulating fluidized bed (CFB), cyclone (vortex), rotating cone, ablative, screw and auger or kiln, which are shown in Fig. 5. The fluidized bed pyrolysers deliver high heat transfer rates by applying solid-gas heat transfer mediums. However, the maximum particle size for fluidized beds should be less than 6 mm [52]. In a cyclone pyrolyser, the material particles are entrained in a hot inert vapour (gas or steam) flow and then move into the reactor to be melted on the heated reactor wall. One of the issues with cyclone pyrolyser is scale-up [59].

The rotating cone reactor pyrolyses the material on a high-speed rotating cone with the presence of hot sand (capable of having fast heating rates). The ablative pyrolyser presses the biomass against a hot surface, making fast biomass disintegration. The ablative system can process small-size materials, and the heat supply is problematic [52, 57]. The auger (kiln) or screw reactor transfers the biomass particles using a conveyer or screw system. The screw system can pyrolyse different sizes of materials. Furthermore, it is reported that the vacuum reactor can be used as a pyrolyser but has slower heating rates in comparison with other reactors, and the process is costly and complicated [52, 57].

Table 2 Characteristics of slow, intermediate and fast pyrolysis [52, 57]

Process	Conditions
Slow	Solid residence time (h/days), ~290–400 °C
Intermediate	Solid residence time (min), ~400 °C
Fast	Solid residence time (s), ~500 °C

Fig. 4 Different products from biomass pyrolysis. (Reproduced with permission from [57], Copyright © 2012, Elsevier)
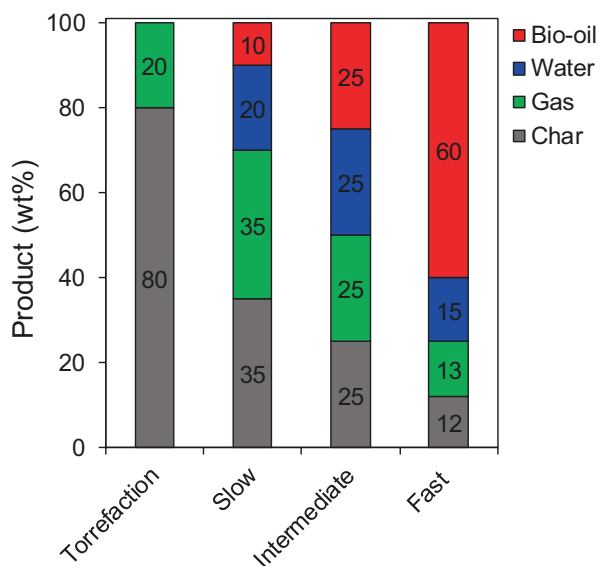
5 Fundamentals of Slow, Intermediate and Fast Pyrolysis

Typically, slow pyrolysis is a batch system despite the existence of a few works using the continuous process [60, 61]. It involves slow heating rates, low temperatures (normally below 300 °C) and long residence time, and the biochar is the primary bio-product [62]. The majority of the slow pyrolysis works are oriented for biochar formation and utilization; however, the liquids and gases can also be used as a fuel at the production site [63]. In addition, the high amount of acetic acid and other acid compounds in the oil make this pyrolysis liquid suitable for pesticide applications [64]. This process can tolerate water present in the biomass, which has a straight effect on biochar properties, promoting the formation of activated carbon [65]. For biochar production, moisture content between 15% and 20% is the usual range [62]. The feedstock particle size can differ from wood logs to pellets. Wood is the most common biomass for slow pyrolysis, and this process can work with rice straw, palm, bamboo, sugarcane bagasse and nutshells [66, 67].

Carbonization is the oldest method for biomass processing and consequent char production, where the solid residue is the desirable product [65]. Slow pyrolysis products without condensation of the vapours can be utilized to deliver heat to the
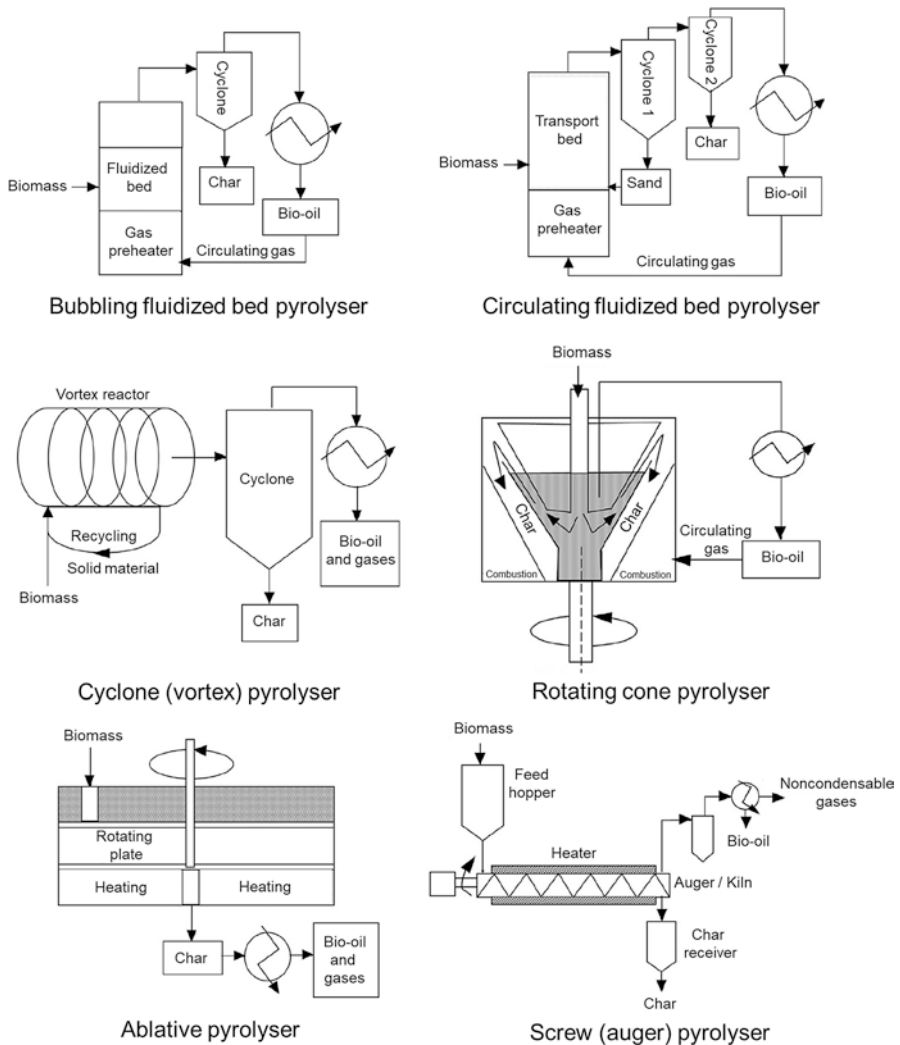
Fig. 5 Different kinds of pyrolysers. (Reproduced with permission from [59], Copyright © 2019, Elsevier)

system [68]. Torrefaction is another approach to apply slow pyrolysis, operating with mild temperatures (225–300 °C) to improve the biomass fuel properties and the respective calorific value [69]. During torrefaction, surplus, volatiles and moisture are extracted from the biomass, while the main compounds (cellulose, hemicellulose and lignin) are partially degraded, originating the organic volatiles [70]. The final material is solid called "torrefied" biomass, and it is easier to be stored and transported due to the reduction of volume and weight, improving the energy density per unit volume [71]. Torrefied feedstock needs less power to be ground, and its

hydrophobic features make this solid residue more resistant in terms of water absorption [69, 70]. Torrefaction is also considered as a biomass pre-treatment for pelletization, combustion, pyrolysis and gasification, originating a syngas with lower tar content and making these thermochemical processes more efficient and more comfortable to operate [71].

Intermediate pyrolysis works with the modest heating rates (100–500 °C/min), gentle temperatures (about 400 °C), the vapour residence time in seconds, the solid residence time in minutes and effective cooling system for the organic gases to reduce thermal post-degradation. Moderately, intermediate pyrolysis produces equal yields of gas, solids and liquids. Intermediate pyrolysis can produce energy vectors with enhanced physicochemical properties which depend on process parameters and feedstock [72, 73]. In comparison with other pyrolysis technologies, this procedure is capable of pyrolysing fine particles (from chopping, shredding and grinding) and also bulky feedstocks (briquettes, pellets and chips) [73]. Furthermore, intermediate pyrolysis can convert a diverse range of feedstocks (such as sewage sludge, algae, grass, food and market waste, agricultural waste, industrial and forest residues, de-inking sludge, digestate and others) into valuable products [54, 74].

Fast pyrolysis is a continuous process, and it requires a short vapour residence time and high heating rate (up to 1000 °C/s), which produces a high amount of liquids (on a dry basis, 75 wt%) [73, 75]. However, woody biomass fast pyrolysis liquid is a mixture of bio-oil and aqueous phase, which cannot be separated easily. Fast pyrolysis bio-oil has a low calorific value (17 MJ/kg) and high water (25 wt%), oxygen (38 wt%) and viscosity (40–100 mm^2/s) [57]. During fast pyrolysis, the organic material degrades very fast, forming char and pyrolysis gases, which are condensed, generating the bio-oil and non-condensable gaseous compounds considered as remaining products [76]. The aim of fast pyrolysis is to avoid extra breaking of the pyrolysis products into non-condensable elements to maximize the liquid yields (the desirable product) controlling the following process conditions [57, 77, 78]:

- Very high heating rate is up to 1000 °C to raise the heat transfer on the feedstock particles.
- The reaction temperature is about 500 °C and vapour temperature between 400 and 450 °C. These conditions maximize the yield of bio-oil at the expense of permanent gases and char.
- Short solid and vapour residence times are usually less than 2 s to reduce secondary reactions.
- Fine biomass particle size is normally less than 3 mm to guarantee quick reactions, higher thermal conductivity and heat transfer in fluidized bed reactors.
- Feed moisture content is below 10 wt% to decrease the water in the bio-oil.
- High condensation efficiency is needed for organic gases to reduce thermal post-degradation and increase bio-oil formation and collection.
- Quick extraction of the biochar is required to reduce vapour cracking.

Theoretically, fast pyrolysis is able to convert any kind of biomass. However, this process has only shown consistent and reasonable results using woody feedstocks

[76]. The feedstock composition and the process parameters influence the type of pyrolysis chemical mechanisms in the reactor, but the reactions taking place are a combination of depolymerization, rearrangement, breaking and dehydration [78]. Bio-oil production through fast pyrolysis has some benefits such as high thermal efficiency, atmospheric pressure conditions and the simplicity of the operation [79]. This pyrolytic liquid can be applied as an energy vector or for production of chemical compounds [80]. The secondary products of fast pyrolysis (solid residue and gas fraction) are also considered to be valuable materials for heat and power generation [80].

5.1 Comparison Between Slow, Intermediate and Fast Pyrolysis

Products from the intermediate process present different properties compared to the slow and fast pyrolyses. Intermediate and slow pyrolyses are the most appropriate methods to produce biochar, while intermediate pyrolysis provides shorter solid residence times [73]. Additionally, slow pyrolysis is a restricted method mainly applied for the formation of char, and it is hardly seen to produce bio-oil [75].

The main difference between intermediate and fast pyrolysis technologies is the solid residence times which produce a dissimilar heat transfer to the materials. Intermediate pyrolysis enhances the components' thermal cracking and conducts a superior control of the chemical reactions, thus improving the physicochemical properties of biofuel [81]. Intermediate pyrolysis bio-oil showed a low level of tars, ashes and viscosity, and it led to a more natural separation between the aqueous phase and organic phase, which is in contrast with fast pyrolysis bio-oil [75, 82].

Another limitation of fast pyrolysis is the processing of different feedstocks, which need to have low water contents and fine particle sizes when processed by a fluidized bed reactor [83]. This process requires extra filters and post-cyclones to extract the dust and char present in the pyrolysis gases. Furthermore, fast pyrolysis is only well succeeded in converting woody feedstocks, and normally the bio-oil produced is rich in ashes, water, tars and acids [54, 84].

The benefits of mixing biochar with fresh biomass were proven via intermediate pyrolysis. The extended residence time of the solid residue has a catalytic effect in the bio-oil quality, increasing the calorific value, producing lighter organic compounds (mostly aromatics such as toluene, benzene and ethylbenzene and olefins) and reducing the moisture content and viscosity [74, 83]. Intermediate pyrolysis biochar, bio-oil and gas have suitable physical and chemical properties which can be applied as energy vectors.

The biochar can be applied as a solid fuel in combustion and gasification plants to produce power and heat [75]. It can also be an optimum soil fertilizer/conditioner (depending on feedstock), which can sequester carbon from the soil [85]. The bio-oil showed a low level of water, oxygen, viscosity and tar, hence a suitable fuel to

combust in engines, boilers and other power and heat plants [86]. The upgraded intermediate pyrolysis bio-oil can be blended with diesel and gasoline and used as a transportation fuel in engines [87]. The gas phase showed a low ash content and a suitable calorific value, which can be utilized in combined heat and power (CHP) processes [85].

5.2   Pyrolysis Products

The three main products from the pyrolytic process of biomass are biochar, bio-oil and permanent gas fraction. Their properties and yields are influenced mainly by biomass composition and pyrolysis conditions.

5.2.1   Biochar

Biochar is an aromatic polycyclic carbon and solid residue formed after the pyrolysis conversion of carbonaceous biomass characterized by a high proportion of carbon, low volatility and small amounts of hydrogen and oxygen [81]. However, thermo-catalytic reforming (TCR) biochar is free of polycyclic aromatic hydrocarbons (PAHs) and polychlorinated biphenyls (PCBs), and it contains a low level of dioxins, hence a reliable and valid carbon source in terms of safety, health and environmental concerns [88]. TCR technology is discussed in details in the next section (Sect. 6).

Usually, char is extracted from the gas fraction in the cyclone step, and it contains most of the inorganic material existing in the original feed. The physical and chemical features of the biochar are affected by the pyrolysis parameters and feedstock composition. Process conditions can vary, and thus the higher heating value (HHV) can be between 20 and 36 MJ/kg and the carbon amount between 53 and 96 wt% [89]. Additionally, during pyrolysis, the biochar production may range from 10 to 40 wt% depending on the conditions of the process. In terms of physical properties, the temperature can increase the surface area between 100 and 500 m^2/g due to the formation of a microporous structure [90]. Below 400 °C, there is an incomplete elimination of biomass volatiles, and consequently, the alteration of the char surface area is insignificant. From 400 to 900 °C, the surface area of the biochar starts to increase gradually [89].

Biochar has the capacity to retain water in different soils (up to 25% in comparison with no added biochar) and to provide carbon, nitrogen and inorganics for agricultural fields, improving the quality of the crops [91]. Moreover, it is extremely stable when introduced in the soil environment, and it can perform carbon sequestration due to its rounded structures [92]. For those reasons, biochar is considered to be an optimum fertilizer and soil amendment being utilized for hundreds of years as an eco-friendly solution to improve and remediate the quality of the soils [93].

Energy production is also one of the ways to valorize the biochar from pyrolysis. It can be a solid fuel for combustion, fulfilling the heating necessities for pyrolysis. Biochar can also be gasified to produce syngas/hydrogen [94, 95]. Some works explored the biochar microscopic surface area for the elimination of contaminants in gas and water by the adsorption of metal ions from water and the removal of SO_2 or NO_x present in the gas [96, 97]. Additionally, biochar can be used as a catalyst in relation to its inorganic compositions and surface properties [98].

5.2.2   Bio-oil

Bio-oil is a dark brown organic liquid produced from the pyrolytic conversion of biomass, and it is the most interesting energy vector in the pyrolysis process [89]. This oil is formed through a quick condensation of the organic vapours, and it results in the thermal breaking and depolymerization of lignin, hemicellulose and cellulose [99]. Bio-oil is composed of water, nitrogen and hundreds of chemical species such as esters, alkenes, aldehydes, ethers, ketones, acids, furans, alcohols, sugars, phenols and other oxygenated compounds, making this pyrolysis product reactive and thermodynamically unstable [100, 101]. For that reason, it is essential to upgrade the bio-oil for fuel engine applications.

Viscosity is a relevant requirement for the pyrolysis oil, impacting the pumping performance of the engine. According to some studies, the viscosity of the oil should be no more than 20 mm^2/s at 40 °C [102]. The bio-oil properties are affected by some processing conditions such as solid residence time, heating rate, temperature, kind of biomass and particle size of the feed. Some secondary pyrolysis reactions produce water, which is present in the bio-oil composition, creating two fractions (a mixture of the organic phase and aqueous phase). The aqueous phase is a combination of water-soluble compounds (mostly phenol, acetic acid and hydroxyl acetone) and due to its limited chemical properties (such as heating value) cannot be applied as a fuel vector [103].

It is reported that catalytic reforming implementation in intermediate pyrolysis process can separate the organic phase from the aqueous phase and also improve the heating value of biofuel in pyrolysis [104]. A catalytic treatment via reforming, which promotes water gas shift reactions, helps to valorize the aqueous phase, producing green hydrogen [105]. The organic fraction can be exploited as a fuel (directly or upgraded to improve the oil quality) or for the production of chemical compounds. Generation of heat and power through gas turbines/engines, furnaces, combustors and boilers is one of the applications for the organic phase of the bio-oil without catalytic conversion which has shown success [106, 107].

For transportation purposes, the pyrolysis oil can be treated via either the upgrading processes (such as hydrodeoxygenation (HDO), emulsification, hydrocracking and catalytic esterification) or mixing with gasoline and diesel to be used in engines [94]. Valuable chemicals can also be extracted in the organic phase to be applied in flavouring additives, pharmaceutical compounds, preservatives, fertilizing materials and resin components [80, 108].

5.2.3   Biogas

Biogas and/or syngas produced in pyrolysis is the consequence of the degradation and cracking of big particles from the original biomass. It is mostly composed of CO, CO_2, H_2, CH_4 and other light hydrocarbons such as C_2H_6, C_3H_8 and C_3H_6 [109]. If the condensation process is not efficient, the pyrolytic gas can contain some volatiles such as xylenes, benzene, acetaldehyde, pentane and toluene [76].

The composition of the pyrolysis gas is influenced by the reactor parameters, the chemical structure and the particle size of the materials. Cellulose and hemicellulose decomposition enhances the production of CO and CO_2 because of thermal cracking of carboxyl and carbonyl groups [110]. The reforming of aromatics and methoxy groups present in the lignin produces a gas rich in CH_4 and H_2 [111]. Light hydrocarbons result in the degradation of methylene and ethylene bonds [112]. The water content in the biomass is another factor affecting the syngas yield [113]. The particle size of the material also influences the composition and yield of the gaseous product. Bigger particle size inhibits the cracking reactions of hydrocarbons and volatiles, producing less CO and H_2 and subsequently more CO_2 and light hydrocarbons [114]. Additionally, larger particles have a negative impact on the heating rate of biomass, decreasing the gas yield for higher biochar production [89].

In terms of temperature, when there is an increment, the thermal cracking, devolatilization and degradation of biomass are stimulated. Concurrently, secondary reactions such as dehydrogenation, decarboxylation, deoxygenation and decarbonylation favour the production of volatiles [115]. As a consequence, the pyrolysis vapour is richer in H_2 and CO, but it contains less CO_2 and hydrocarbon gases. The combustible gases of the pyrolytic gas (CO, H_2, CH_4 and other hydrocarbon gases) can be combusted as a fuel in industrial facilities, generating heat and power [94]. If the syngas contains a high level of H_2, it can be used for fuel cell applications. However, high H_2 yields are not normally obtained via fast or slow pyrolysis, unlike the intermediate and TCR technologies [116, 117].

5.3   Biomass Thermal Decomposition

Pyrolysis thermal mechanisms for the conversion of biomass can be designated in a simultaneous combination of fragmentation, isomerization, condensation, dehydration, rearrangement, aromatization, cracking, depolymerization and char formation [78, 118]. The components of biomass (lignin, hemicellulose, cellulose, water, inorganics and extractives) and the reactor factors have a significant influence in the pyrolysis reactions. Figure 6 shows the chemical composition of biomass.

The pyrolysis reactions can be classified as primary and secondary. Depolymerization, fragmentation and charring (char formation) are part of the primary reactions (Fig. 7) [55]. Depolymerization is the prevailing mechanism of pyrolysis, and it implies the breaking of the monomer's bonds, producing volatiles and gases [98, 102]. Fragmentation is responsible for the formation of

incondensable vapours and short-chain compounds due to the linkage disintegration between the monomers and polymer [119]. Charring reactions cause the condensation of benzene rings during the pyrolytic process, stimulating the production of char [120].

The components obtained during primary reactions are not chemically stable, and for that reason, they suffer recombination and cracking reactions (secondary reactions). During recombination reactions, heavier elements are produced or placed on biochar surface, while lighter elements are formed by the cracking of primary compounds [121]. Additionally, the biochar formed can also promote secondary reactions. Morf et al. [119] showed that the secondary reactions are the dominant reactions, affecting the properties and the quality of the pyrolysis products.

Under 500 °C, the main reactions occurring in pyrolysis are mostly decarbonylation, depolymerization, dehydration and decarboxylation [122]. The biomass structure is not significantly changed until 200 °C [102]. The production of C_2 hydrocarbons and CH_4 is attributed to the rupture of the alkyl components in the C-H bonds [89]. Between 250 and 500 °C, the decomposition of hemicellulose (220–350 °C) and cellulose (315–400 °C) occurs, where the depolymerization activity is quite intense, achieving the best bio-oil yield from 400 to 500 °C [111]. The main reactions are dehydrogenation, fragmentation and aromatization when the temperature is above 500 °C [77]. Above 550 °C, more gas is formed due to the fragmentation process, and close to 600 °C, there are more aromatic rings in the biochar, demonstrating the existence of aromatization reactions [111]. The most stable compound is lignin, but it is the hardest biomass element to be degraded. Its chemical decomposition occurs from 160 to 900 °C; however, the most relevant weight loss is between 350 and 600 °C [123].

Lignin contributes to a larger formation of biochar, while a higher percentage of cellulose and hemicellulose in the biomass produces more bio-oil [124]. Biomass rich in lignin has a negative impact on bio-oil quality, causing high viscosity, low stability, high average molecular weight and worse combustion performance [125].
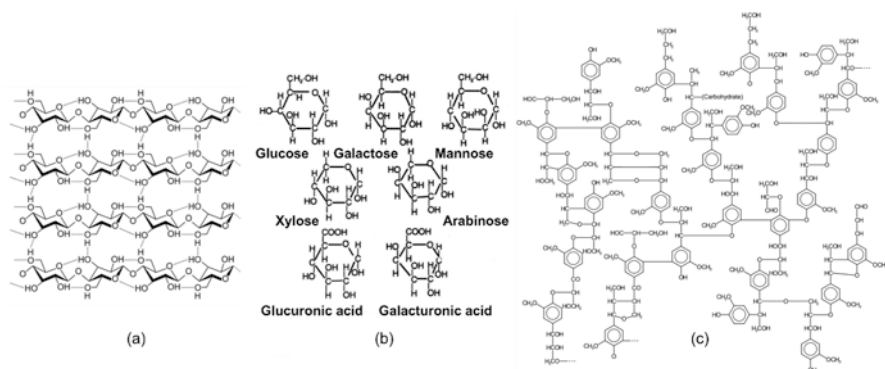
Fig. 6 Biomass compounds: (**a**) cellulose, (**b**) hemicellulose and (**c**) lignin. (Reproduced with permission from [81], Copyright © 2017, Elsevier)
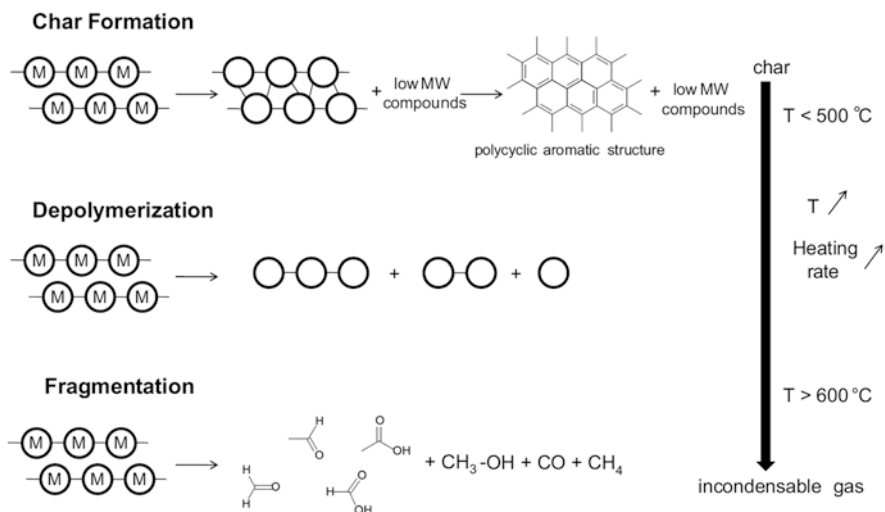
Fig. 7 Pyrolysis primary reactions (MW, molecular weight; M, monomer). (Reproduced with permission from [55], Copyright © 2014, Elsevier)

On the other hand, a higher proportion of cellulose and hemicellulose benefits pyrolysis oil properties, making it more suitable as a fuel due to the presence of arabinose, galactose, mannose, xylose and glucose in their composition. The biomass extractives are the non-structural elements (sugars, fatty acids, proteins, phenolics, resin oils and sterols) that can be removed with solvents such as hexane, ethanol, benzene, toluene and water [126]. Wood extractives lead to a loss of bio-oil formation and levoglucosan production, and its extraction can cause a reduction of 64% and 34% in oxygen and hydrogen present in the biochar, respectively [127].

Inorganic compounds are converted to ash after thermal reaction, and they promote biomass degradation, charring, water reactions, non-condensable vapour production and a decrease of bio-oil yields [128]. Ash composition and content can influence the chemical properties and the distribution of the pyrolytic products [125]. Alkali metals can affect the thermal degradation reactions of pyrolysis, creating macro-polymer substances through the disintegration of monomers (ring breaking) [128].

6 Pyroformer and Thermo-Catalytic Reforming (TCR)

6.1 *Pyroformer*

Pyroformer is an intermediate pyrolysis system which is patented by Hornung and Apfelbacher (Fig. 8). This system was one of the first intermediate pyrolysis reactors after the Haloclean rotary kiln system (cycled-spheres reactor) [73]. Pyroformer

is essentially an auger screw reactor inclosing a carbon steel compartment (horizontal position), including two co-axial rotating screws [73]. This reactor operates at a pressure of up to 1 MPa, its heating system is external through heating bands, and the design is appropriate to process high ash content biomass and to maximize the contact time between organic vapours and pyrolysis biochar [74].

Throughout the process, the internal screw transports a mix of fresh feedstock and recycled char fraction along the reactor, which is heated at standard pyrolysis temperatures [129]. The external screw carries the biochar back to the inlet zone, increasing the heat transfer of the feedstock [75]. The biochar layer in the reactor controls the heating rate and protects the feed from extremely high temperatures, thus avoiding fast pyrolysis reactions [73]. Biomass is transformed into char, vapours and volatile gases. The remaining biochar (that is not recycled in the reactor) exits to the solid drop-out pipe of the Pyroformer, and the pyrolysis gas phase moves through the gas outlet pipe [74].

The novelty of this system is the effect of biochar recycling which creates an additional catalytic impact in the system. This catalytic impact improved the bio-oil quality in comparison with fast pyrolysis bio-oil due to oil formation with lower molecular weight, less water content and less heavy tar formation, and also applying biochar increased gas fuel yields (H_2 and CO), thus generating a considerably higher heating value biofuels [130].

6.2 Thermo-Catalytic Reforming (TCR)

TCR innovation is about combining the intermediate pyrolysis (which was developed from the Pyroformer process) with post-catalytic reforming (treatment). TCR was designed and developed by Fraunhofer UMSICHT to produce valuable chemical and biofuels from waste materials [72]. TCR process flow diagram (PFD) is
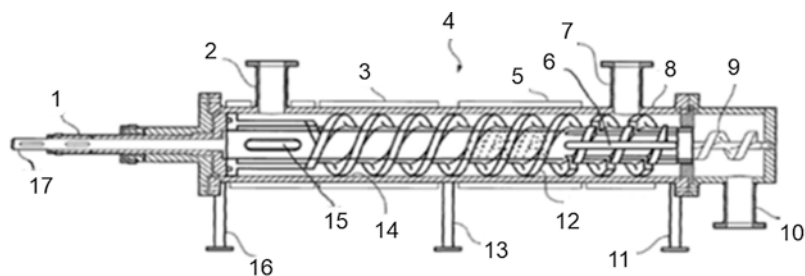
1. External screw shaft; 2. feed inlet pipe; 3, 4, 5 and 8. electrical heating bands; 6. external screw slot; 7. gas outlet pipe; 9. internal screw; 10. solid drop out pipe; 11, 13 and 16. supports; 12 and 14. external screw; 15. external screw slot; 17. internal screw shaft.

Fig. 8 Pyroformer reactor system. (Reproduced with permission from [74], Copyright © 2013, Elsevier)

represented in Fig. 9. TCR procedure has two crucial stages which are (1) intermediate pyrolysis at mild temperatures in which biomass thermal heating happens in the absence of oxygen and (2) reforming step at raised temperatures in which vapour catalytic cracking occurs to improve the formation of organic vapours and syngas with superior physicochemical properties [129].

In the TCR technology, the intermediate pyrolysis step happens at 400–500 °C in an auger reactor with solid residence times between 5 and 10 min [133]. Biochar is being formed during the intermediate pyrolysis of biomass in the auger reactor, and then it is collected in the reforming section (fixed bed reactor). The reforming treatment is executed between produced vapours and biochar, thus generating a catalytic effect in all products and enhancing their physicochemical properties [134].

The post-reformer temperature is between 500 and 700 °C [135]. The higher temperature of post-reformer produces a higher yield of syngas. The upgraded vapours are then condensed and generate three different products which are syngas fraction (27–44 wt%), a bio-oil fraction (6–11 wt%) and an aqueous phase (21–26 wt%). The significant compounds of syngas are H_2 and methane [134]. During the reforming step, different kinds of chemical reactions take place, which are as follows [72]:

1. $C + H_2O \leftrightarrow H_2 + CO$ (Water gas reaction).
2. $CO + H_2O \leftrightarrow CO_2 + H_2$ (Water gas shift reaction).
3. $CH_4 + H_2O \leftrightarrow CO + 3H_2$ (Steam reforming reaction).
4. $C + 2H_2 \leftrightarrow CH_4$ (Hydrogasification reaction).
5. $CO_2 + C \leftrightarrow 2CO$ (Boudouard reaction).
6. $C + \frac{1}{2}O_2 \leftrightarrow CO$ (Partial oxidation reaction).

1. Feed Hopper
2. Auger Reactor
3. Post Reformer
4. Cyclone
5. Shell and Tube Heat Exchanger
6. Scrubber
7. Bio-oil Collection Vessel
8. Ice Bath
9. Biodiesel Wash Bottle
10. Isopropanol Wash Bottle
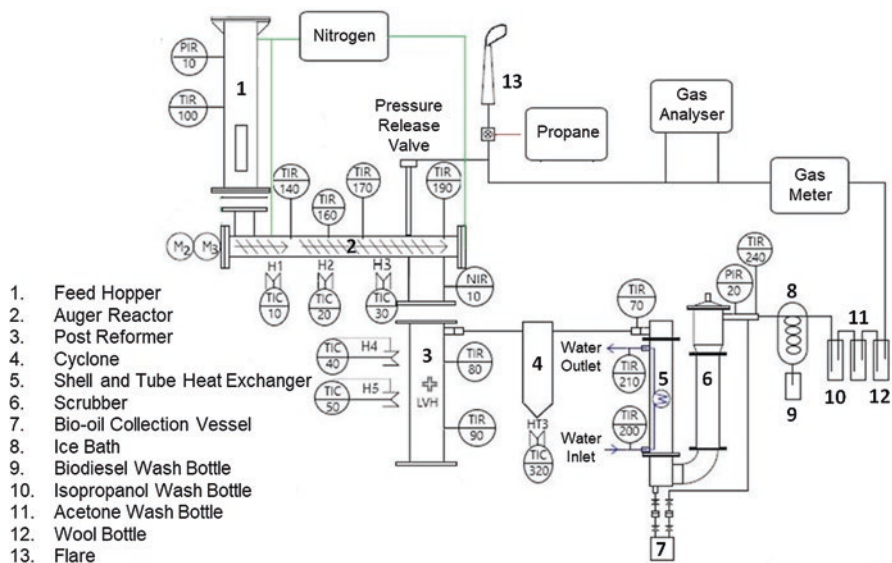11. Acetone Wash Bottle
12. Wool Bottle
13. Flare

Fig. 9 TCR process flow diagram (PFD). (Reproduced with permission from [131], Copyright © 2020, Elsevier)

During the experiment, the solid fraction (char) remains in the post-reformer and is only extracted intermittently throughout the process. To guarantee an efficient separation between the organic liquid component and the gas fraction, TCR has a cooling system working with temperatures from −3 to +10 °C to cool down the vapours from the post-reformer. Before being routed to an exhaust system, the gas phase goes directly to a gas analyser and calorimeter to quantify its composition and the HHV [136]. To avoid the contamination of the gas analyser from aerosols and other impurities, the plant is installed with active carbon bag filter and with gas wash bottles containing biodiesel, isopropanol, acetone and wool [72].

In addition to agricultural, organic and industrial wastes with a high water and ash contents (low ash melting points as well), the TCR process is also able to convert plastic residues [137]. Technically, TCR can convert feedstocks with moisture content up to 20%, which is beneficial in terms of energy consumption as it can be used for avoiding the drying step [138].

TCR products can be used in diverse applications from different areas. The gas fraction can generate heat and power through CHP, bio-oil can be blended with diesel and gasoline to be applied in engines, and char can be involved in combustion or gasification processes and as fertilizer or soil conditioner [138]. TCR is a safe technology operating without the utilization of externally sourced solvents, catalysts or any chemical product, and it works at atmospheric pressure [139]. Its flexibility in terms of plant control provides a large variety of value-added products such as an improved quality bio-oil that is simple to transport and store, stable and energy-dense biochar with similar features to anthracitic coal and syngas rich in H_2 [72, 140]. Another advantage of this process is the efficient design, which can convert most of the introduced energy from the original biomass [139].

6.2.1 Comparison Between TCR and Other Technologies

Table 3 shows the characteristics of the bio-oil produced from a woody biomass fast pyrolysis and TCR. The bio-oil of fast pyrolysis has many disadvantages, which are as follows [82, 141, 142]:

- A high oxygen content with a complicated mixture of compounds.
- A high acid number.
- It is strongly corrosive.
- It has low higher heating value.
- It has poor chemical stability, and its phase can be changed with time.

Therefore, fast pyrolysis bio-oil should be upgraded in different ways such as catalytic cracking and hydrotreatment to produce valued chemicals and transport fuels. The role of catalysis and different methods for bio-oil upgrading will be illustrated in detail in the next section (Sect. 7).

TCR technology can produce TCR oil with superior physicochemical fuel properties in comparison with the bio-oil of fast pyrolysis. TCR oil is low in acidity

Table 3 Bio-oil properties from woody biomass pyrolysis

Properties	Fast pyrolysis [57, 82, 144]	TCR [145, 146]
Mass balance		
Bio-oil (wt%)	60	7.0
Water content (wt%)	15	14
Gas (wt%)	13	58
Char (wt%)	12	21
Bio-oil		
Moisture content (wt%)	15–30	6–8.4
Acid number (mg KOH/g)	88–126	9.3–30.1
Viscosity (mm^2/s)	40–100	12.1–36.5
HHV (MJ/kg)	16–19	32.8–35.5
Bio-oil elemental analysis		
C (wt%)	54–58	72.2–78.6
H (wt%)	5.5–7.0	7.0–7.4
N (wt%)	0–0.2	2.2–2.6
O (wt%)	35–40	11.4–17.9
Ash (wt%)	0–0.2	0–0.05

(9.3–30.1 mg KOH/g) and low in oxygen content (11.4–17.9 wt%) and has a higher heating value (32.8–35.5 MJ/kg), which is in contrast with bio-oil properties of fast pyrolysis (Table 3). TCR crude bio-oil phase separates easily from the water phase and has a very high calorific value which is totally miscible with conventional fossil fuels and crude oil [75, 82].

There is no need for extensive pre-treatment steps or expensive precious metals or zeolite catalysts to be added into the reactor [131, 132]. TCR process is well compatible with all range of waste organic feedstocks, which are high in moisture and ash contents, such as paper sludge, sewage sludge, municipal solid waste, anaerobic digestate and others [135, 143]. Additionally, TCR produces a notable amount of green H_2 which can be separated and purified for hydrotreatment of the bio-oil and crude oil in a petroleum refinery [140].

Another reason which makes TCR process economically attractive for bio-oil production is that TCR system has been designed to process the biomass in one single step and there are no additional feeds required (feedstock goes in, and phase-separated products come out) even at small scales. This process is cheaper than reactors with multiple feeds and processing steps to upgrade the bio-oil.

In the reforming section, the char catalyses the cracking of heavy oxygenated compounds present in the vapour phase and promotes reforming to synthesis gas and condensable organic vapours, leading to a lower molecular weight, non-corrosive, less viscous (easier to pump) and significantly deoxygenated oil fraction, thus avoiding the problems associated with fast pyrolysis oil [82, 141, 142].

TCR biochar is an excellent fuel source for gasification as it produces a tar-free synthesis gas that could be used as a further source for hydrogen production. The key advantage of utilizing this approach is that it reduces demand for externally sourced H_2 for refining, which further increases the process economics and

Fig. 10 Diagram of Van Krevelen for bio-oil from the TCR of woody biomass [145, 146], fast pyrolysis of woody biomass [57, 82] and hydrotreated bio-oil from woody biomass fast pyrolysis over nickel-based catalysts [148]
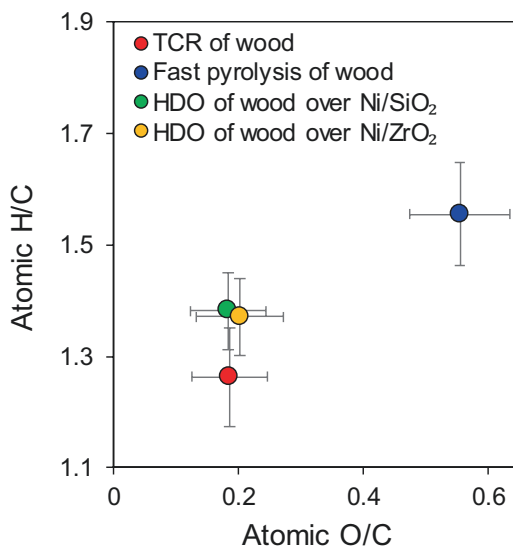
sustainability credentials. In addition, the hydrogen yields can be maximized by injection of steam (which can be TCR aqueous phase) into the TCR system, which promotes a water gas shift reaction [129, 140]. This is in contrast to fast pyrolysis that needs an outside source of H_2 to improve the bio-oil properties [147].

The Van Krevelen diagram represents the O/C and H/C ratios for varied technologies (Fig. 10). The O/C and H/C of bio-oil from the TCR of woody biomass were 0.19 and 1.27, respectively [145, 146]. However, the bio-oil from fast pyrolysis of woody biomass has considerably higher values of O/C (0.56) and H/C (1.56) than TCR results [57, 82]. Additionally, the O/C and H/C of hydrotreated bio-oils from fast pyrolysis of woody biomass over Ni-based catalysts are slightly different from the TCR values [148]. Therefore, TCR displayed significant enhancement of bio-oil properties and stability characteristics.

7   Upgrading of Bio-oil

Fast pyrolysis bio-oils have a lot of drawbacks such as thermal instability, high oxygen content and high viscosity and corrosiveness. Therefore, fast pyrolysis bio-oil upgrading should be performed to decrease the oxygen content and acidity before its application [57, 80]. There are different methods to upgrade bio-oil, which are emulsification, filtration, polar solvent, catalytic and TCR cracking, hydrotreatment, aqueous phase processing, esterification, transesterification and ketonization.

7.1   Emulsification

The most straightforward pathway to upgrade bio-oil is to mix it with diesel directly to be used as a transport fuel. Generally, fast pyrolysis bio-oils are immiscible with hydrocarbons, but the aid of a surfactant can emulsify them. It is reported that emulsified bio-oil with different ratios of diesel (25, 50 and 75 wt%) provides a more stable bio-oil than the original [106, 149]. The use of emulsions for a long term will affect a stainless steel engine and its sub-assemblies because of the corrosiveness of the emulsified bio-oil. Furthermore, other disadvantages of this method are the surfactant costs and the high energy requirement [57].

7.2   Filtration

Hot vapour filtration is reported as an appropriate method to decrease the alkali content to less than 10 ppm and ash content of bio-oil lower than 0.01 wt%. This filtration provides higher bio-oil quality with lower biochar. Biochar is an active catalyst, and it cracks the vapours and decreases the yield up to 20%. There is not much information about the performance of hot vapour filters, although it should be similar to that of hot gas filters for a gasification reaction [150]. Furthermore, filtration of a liquid which has a very small particle size (below 5μm) is not easy because of its physical and chemical nature [150].

7.3   Polar Solvent

Polar solvents are useful for homogenizing and reducing the bio-oil viscosity for many years. Methanol has displayed a huge effect on bio-oil stability. Furthermore, Diebold and Czernik [151] tested different additives, ethanol, acetone and methanol. All these additives reduced the ageing rate of bio-oil. Moreover, it is reported that the viscosity of bio-oil was decreased significantly by adding 10 wt% of methanol to bio-oil, which was the best additive [151].

7.4   Catalytic Cracking

A catalytic pyrolysis reaction can produce fuel-ranged hydrocarbons in a single step from the biomass [152]. Zeolites or silica can be added to the biomass fast pyrolysis reaction to convert vapours of pyrolysis into aromatic hydrocarbons in a single step [153–155]. Zeolite catalysts are the most popular for upgrading bio-oil through catalytic pyrolysis, and these include HZSM-5, zeolite beta, SAPO-34, zeolite Y,

ZSM-5 and mordenite [89]. The zeolite pore size affects the formation of aromatics and coke, and larger pores are related to higher yields of coke [156]. Another relevant factor is the acidity of the zeolite, where lower acidity levels produce more coke and fewer aromatics [157].

HZSM-5 and ZSM-5 zeolite catalysts are the most tested in catalytic pyrolysis. ZSM-5 has less selectivity, acidity and thermochemical stability than HZSM-5. Therefore, HZSM-5 is a more attractive catalyst for aromatics production, and it promotes catalytic reactions in the biomass such as aromatization, decarbonylation, cracking, isomerization, decarboxylation, cyclization, oligomerization, deoxygenation and alkylation [89, 158]. HZSM-5 was tested in a pyrolysis fixed bed reactor for converting microalgae, and the produced bio-oil presented a lower oxygen content (19.6 wt%) and a higher calorific value (32.6 MJ/kg) compared to no catalytic treatment at the same conditions [159]. Zhang et al. [160] and Stephanidis et al. [161] used the same zeolite to pyrolyse corncobs and beech wood respectively, and the bio-oil in both studies showed a higher calorific value (30–35 MJ/kg) and aromatics content and a decrement of oxygenated compounds.

Some works have experimented ZSM-5 catalyst in a pyrolysis fixed bed reactor using glucose, rice husks, maple wood and furans as feedstock [156, 162]. The general results were a substantial reduction in the yield and oxygen content of the bio-oil. The chemical structure of ZSM-5 was also altered by adding some metals such as Zn, Ni, Mo, Ga, Co, Pd and Pt. This modification influenced the alkylation and cyclization reactions, increasing the zeolite acidity and the aromatics yields, especially using Ga metal [163, 164]. Zeolite catalysts favour the production of coke which is deposited on the surface of catalyst filling the respective pores. Consequently, the catalyst is deactivated, reducing its durability, and the formed coke also absorbs the bio-oil organics, resulting in lower quality and quantity, thus increasing the cost of the process [89].

Mesoporous catalysts, including Al-SBA-15, MCM-41 and Al-MCM-41, are also an option for catalytic pyrolysis of materials. The last works developed in a circulating fluid bed reactor demonstrated the effect of mesoporous catalysts in the pyrolysis oil composition, increasing the phenolics content and reducing the concentration of acids (carboxylic acid) and carbonyls [165]. Moreover, an increment of the silica/alumina ratio in this kind of catalyst led to an increase of the organics and aromatics in the bio-oil but a lower liquid production [166]. The use of mesoporous catalysts shows a clear indication of upgrading treatment; however, the deoxygenation process is incomplete [165].

Some works investigated the application of mineral catalysts such as MgO, dolomite, SiO_2, CaO, limestone and K_2O through pyrolysis of cellulose, pine sawdust, lignin and poplar wood using a fixed bed reactor at 500 °C [167, 168]. CaO and MgO (basic oxides) inhibited the production of tar and phenolics in the bio-oil, while coke and gaseous products presented higher levels [168]. Alternatively, the use of acid oxides indicated more tar formation. In another research, Na_2CO_3 catalyst produced a very unstable bio-oil, but the application of Pt enhanced the quality and the stability of the same pyrolysis oil [157].

7.5 TCR Cracking

Ex situ and in situ catalytic pyrolysis (Fig. 11) are used to upgrade and develop the properties of the bio-oil. In comparison with the in situ process, ex situ technology is more efficient in eliminating oxygen from the pyrolysis bio-oil due to the lower homogeneity of the applied catalyst [157]. Additionally, the ex situ process has a higher selectivity and flexibility to produce more specific compounds, because the catalyst is placed in an external reactor, and thus the final products can be easily produced [169]. However, the main inconveniences of this route are the quick catalyst deactivation and the high cost of the technology, particularly for industrial units [170].

During the in situ process (Fig. 11), the catalyst is introduced into the reactor to favour thermal cracking reactions and to convert heavy components present in the bio-oil to lighter ones [171]. However, a higher cracking rate requires more catalyst, and a consequence is the extra production of coke [167]. In situ pyrolysis can improve the formation of aromatics and low molecular weight compounds in the bio-oil [169]. However, this integrated catalytic system is limited and less flexible owing to the use of a single reactor operating at the same parameters for the pyrolytic and catalytic reactions [172]. The main challenge of in situ catalytic pyrolysis is to find a robust, active and stable catalyst that is easy to regenerate and can resist the reactor's mechanical environment and enhance the quality of the bio-oil by reducing its oxygen and coke content [173].

TCR technology is able to minimize some negative aspects of the current in situ and ex situ catalytic routes such as coke formation, limitation/flexibility of the process, selection of a proper catalyst and the economic viability for larger plants. The biomass conversion occurs in the intermediate pyrolysis reactor, and then vapours undergo the catalytic treatment in a different reactor (called the reforming unit). The catalyst is the biochar generated in the previous step (auger intermediate pyrolysis
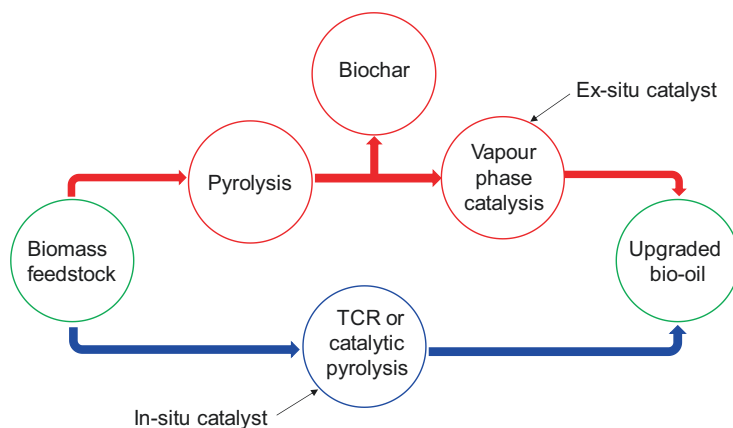

Fig. 11 In situ and ex situ catalytic pyrolysis. (Reproduced with permission from [174], Copyright © 2017, Elsevier)

reactor) which is constantly produced throughout the process, thus avoiding the concern of selecting an adequate catalyst that is easy to regenerate.

Biochar formed via TCR can be considered as an inexpensive sacrificial catalyst. It has excellent chemical and morphologic characteristics such as structure, surface area and high active sites, making this carbonized solid catalytically active in converting organic vapours to high-quality pyrolysis liquids [139, 145]. It has been proven that upgrading treatment of the volatiles before their condensation is presently the most efficient way to minimize the amount of water and oxygen in the pyrolysis liquid, which leads to a higher calorific value bio-oil composed of low molecular weight elements [81].

7.6 Hydrotreatment

Hydrotreatment reaction removes O_2 as water and CO_2 by a catalytic reaction with H_2. Active catalysts for a hydrotreatment reaction are Co–Mo and Ni–Mo supported on Al_2O_3 and zeolites. Pindoria et al. tested hydrotreatment upgrading in a two-step reactor. In the first step, hydrocracking was performed without catalysts, and in the second step, zeolite catalytic hydrotreatment was operated with the same pressure (4 MPa) but lower temperatures (300–400 °C) in comparison with the first step [175]. The experiment showed that the zeolite catalyst becomes deactivated during the reaction not because of the carbon content but because of volatile component embodiments which block the zeolite active sites. The hydrotreatment process formed a lot of water and some impure bio-oils [175]. Furthermore, this process needs superior techniques and complicated equipment and has a high cost [82].

7.7 Aqueous Phase Processing

Aqueous phase reforming (APR) of materials such as glucose, glycerol and sorbitol can produce light alkanes and hydrogen in a single reaction vessel. Alkane production is performed with a bifunctional reaction pathway which forms hydrogen and CO_2 at low temperatures (150–265 °C) on an active metal catalyst such as Pd or Pt and then dehydration of sorbitol over a solid acid catalyst (alumina and silica). These steps are followed on the metal catalyst by hydrogenation of the dehydrated reaction intermediates. The produced hydrogen converts sorbitol into an alkane, CO_2 and H_2O. A large bio-oil fraction is water-soluble, and the aqueous phase contains mainly oxygenated hydrocarbons [176–178].

7.8   Esterification and Transesterification

Highly acidic biomass oils need an initial acid esterification stage to change acid into esters in the presence of acid catalysts and alcohol. The main factors in an esterification reaction are temperature, alcohol types such as methanol or ethanol, reaction time, the alcohol/oil molar ratio and homogenous or heterogeneous acid catalysts [179]. Most active heterogeneous catalysts for esterification reaction are sulphated zirconia [180], tungstated zirconia [181], acidic resins [182], zeolites [183] and 12-tungstophosphoric acid on SBA-15 (heteropoly acids) [184]. Catalytic success was limited to ester lower than C_{10} in either alcohols or carboxylic acids [185].

However, long-chain fatty acids are an alternative fuel with the superiorities of being non-toxic, renewable and having low emissions and a biodegradable profile. Vegetable oil transesterification with CH_3OH in the presence of an appropriate catalyst is the most common process for the production of biodiesel. It involves the alcoholysis of triglycerides in the presence of a catalyst to form fatty acid methyl esters (FAME). However, FAME needs further upgrading to be used as a fuel [190]. Homogenous basic catalysts such as KOH and NaOH are the most common catalysts for the transesterification process [186, 187]. Furthermore, a calcium-based catalyst supported on MgO seems to be a reliable catalyst for the reaction of transesterification due to its low cost and high activity [188, 189].

7.9   Ketonization

Ketonization (ketonic decarboxylation) reaction transforms two molecules of a carboxylic acid into water, carbon dioxide and ketone [191, 192]. More stable products are formed by the ketonization reaction with higher energy content. The catalytic ketonization reaction is a promising process to upgrade the free fatty acids because it removes oxygen and carboxylic acid in the reaction. Then long-chain ketones can be transported to the refinery station for isomerization and hydrocracking to produce diesel-ranged fuels [190]. This reaction is a reliable reaction for upgrading the carboxylic acid, which is derived from biomass fast pyrolysis to produce transportable fuels [193, 194].

Furthermore, over 70% of fast pyrolysis bio-oil contains mostly carboxylic acid, carboxylic esters, alcohol and ethers [195]. The large volume of carboxylic acids in the bio-oil causes corrosion during storage and transport [150]. Thus, an essential step for upgrading bio-oil is acid removal. Therefore, the ketonization reaction is a suitable method not only for removing the oxygen and carboxylic acid content of bio-oil but also for producing C-C bonds between low molecule weights of acids. Then, ketone products can simply couple with other products of bio-oil with hydrogenation or aldol condensation to make longer chain molecules which form the fuel-ranged hydrocarbons [192, 196, 197].

Amphoteric metal oxide catalysts such as ZrO_2 [198, 199], MnO [200, 201], CeO_2 [202, 203] and UO_2 [204, 205] are the most active catalysts for the ketonization reaction. The basic and acidic characteristics of catalysts play a significant part in the ketonization reaction. Different characterizations showed that CeO_2, TiO_2, ZrO_2 and MnO have both acidic and basic properties which confirmed the amphoteric characteristics of these metal oxides [206–209]. In the metal oxide catalysts generally, metal cations are Lewis acid sites, but oxygen anions are Lewis base sites.

Pham et al. reported that oxygen anions must perform as Brønsted basic sites instead of Lewis basic sites for surface carboxylate formation in the ketonization reaction. It is stated that the adjacent Lewis acid (stabilizes and activates another carboxylic acid) and presence of Brønsted basic (carboxylates formation) on most oxide catalysts are the keys for the ketonization reaction [210].

There are substantially fewer studies about ketonization of carboxylic acid over zeolite catalysts in comparison with metal oxide catalysts. The following catalysts were tested in the ketonization reaction which are HZSM-35, HZSM-34, HZSM-11, HZSM-5, zeolite beta, erionite and mordenite. It was found that HZSM-5, HZSM-11 and zeolite beta are the most active zeolite catalysts in comparison with other zeolites for acetic acid conversion into acetone [211, 212].

8 Current State of the Art for Furfural and 2-Methylfuran Production

Furfural is an essential oxygenated compound having C=O and C=C bonds with the high stability of the C=C bond due to its location inside a one five-member ring and six electrons [213]. Furfural can be produced from renewable biomass and agricultural wastes rich in xylose (such as sugarcane bagasse, oat hulls and corncobs), and it can be applied for the formation of essential non-petroleum-derived chemicals (such as 2-methylfuran (2-MF) and furfuryl alcohol), competing with crude oil [214].

This compound can also be used in many industrial processes such as pharmaceutical, plastics, oil refining and agrochemical industries where it is transformed into perfume intermediates, chemical solvents, medicine compounds and pesticides [215]. Furfural is obtained through the following steps: production of pentose such as xylose, submitting the hemicellulose material to hydrolysis and the final conversion into furfural by acid-catalysed dehydration of pentose (Fig. 12) [216].

Presently, furfural production is an energy-intensive process due to long side reactions which causes a decrease of furfural yield because of extensive residence times and the necessity for substantial waste disposal. The need for high-pressure steam to heat the reaction is also a drawback in this process [216]. Concentrated sulphuric acid, which is particularly corrosive and extremely toxic, is used as a catalyst. This brings serious issues compared to homogeneous catalytic reactions such as problematic separation and reprocessing of the product contamination and

mineral acid [217]. For these reasons, enhancements to the chemical technology behind the furfural production are necessary to improve the sustainability of furan-based chemical productions.

Irradiation of microwave is suggested as an alternative technique to improve the dehydration process for furfural production. This process offers fast and efficient heating which promotes better reaction rates and avoids the production of certain by-products and so results in higher furfural yields [218, 219]. Heterogeneous catalytic conversion using solid catalysts has taken a relevant role in converting pentose into furfural due to its high selectivity and high reaction. Moreover, it can be recycled easily, offering more environmentally attractive properties for practical operations [220].

Humins, solid carbonaceous species, are the undesired co-product obtained during the production of furfural from xylose. Humin is responsible for the low furfural yields (between 45% and 50%) using an industrial batch process [221]. In the last few years, some works have shown different ways to achieve better furfural yields by inhibiting the humin production. One technique is to apply organic solvents (methyl isobutyl ketone and ethyl acetate) to absorb furfural from the aqueous fraction [222]. Supercritical CO_2 has also been used to extract furfural [223]. However, due to furfural's affinity to polymerize in storage, it is not a suitable option as a fuel candidate [224].

The option of transforming furfural to 2-MF is mentioned in several current works because of its high calorific value and high octane number, making 2-MF a promising biofuel [95, 225]. To produce 2-MF first, it is necessary to convert furfural to furfuryl alcohol (2-furanmethanol) through hydrogenation and then apply HDO in the intermediate furfuryl alcohol to get the desired product 2-MF as shown in Fig. 13 [226, 227].

Developing a new way to produce 2-MF from biomass-derived chemicals is extremely desirable, not only from the perspective of the green sustainable chemistry but also to mitigate the fossil energy crisis by using a large number of biomass resources available efficiently [226]. All these reasons can boost furfural production through the TCR process, followed by an HDO treatment, to achieve the desired formation of 2-MF. Compared to hydrocarbons, 2-MF has a better combustion efficiency (caused by its oxygen atom) and higher octane number [220]. Therefore, 2-MF can be mixed with gasoline to be applied as fuel for vehicles [228].
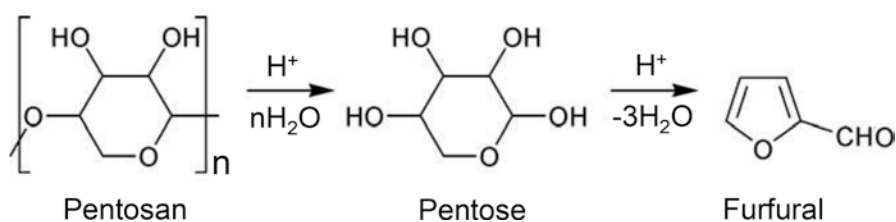

Fig. 12 The reaction mechanism of pentosan acidic degradation to furfural. (Reproduced with permission from [213], Copyright © 2005, Elsevier)

HDO works in the presence of a catalyst under H_2 pressure, and it is classified to be the most efficient way to upgrade pyrolysis bio-oil [229]. This process converts aldehydes, oxygenated and unsaturated elements, into hydrocarbons because HDO selectivity cleaves the C-O/C=O bonds (carbonyl group) of the oxygenated compounds and at the same time preserving the C-C/C=C bonds [224, 230]. This step is quite relevant to improve the oil properties for fuel applications removing aromatics from the bio-oil and subsequently to increase the affinity between temperature and viscosity [58, 100].

HDO can be divided into two different classes, high and atmospheric pressure. The first one applies high H_2 pressure to hydrogenate aromatic rings, reducing the oxygen content present in acids, phenols, esters and aldehydes [231]. There are several reactions that take place during this method according to the bio-oil chemical composition, including dehydration, hydrogenation, hydrocracking, decarboxylation and hydrogenolysis [232]. Atmospheric H_2 pressure has similar conditions compared to high pressure; however, it differs in the type of catalyst, operating conditions (mainly pressure) and in the role of H_2 on the upgrading reaction [233]. The scientific community has used HDO atmospheric pressure in industrial scales for lignin compounds to minimize the operation cost [232].

One of the main difficulties of HDO is to have low consumption of H_2 with an efficient deoxygenation process [231]. In terms of H_2 consumption, HDO can be defined in two categories: in situ H_2 source and ex situ H_2 source. In situ H_2 source uses the same autoclave for H_2 production and to treat the pyrolysis oil, avoiding issues with H_2 storage and transportation [233]. On the other hand, ex situ H_2 source requires industrial H_2 from water electrolysis or fossil fuels as an H_2 donor, making this process less desired [234]. This method also needs high H_2 pressures (up to 30 MPa) to solubilize H_2 in the liquid fraction to reduce the oxygen amount of the pyrolysis oil [235].

It has also been reported the use of external H_2 during the hydrogenation of furfural to 2-MF adding various noble metal and bimetallic catalysts [226]. This situation can lead to a number of obstacles connected to hydrogen utilization, such as the cost to compress, storage and transport (especially in isolated locations), the reactor design, issues related to solubility and dilution of hydrogen, which increase the cost and complexity of the process [215, 236]. A different way to provide hydrogen to convert furfural to 2-MF may be the catalytic transfer hydrogenation, where the H_2 molecule is replaced for the hydrogen donor. In this process, alcohols are a good
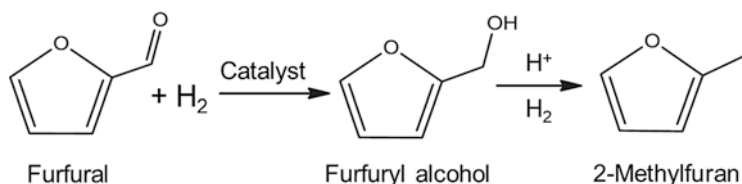

Fig. 13 Hydrogenation and HDO of furfural to 2-methylfuran. (Reproduced with permission from [220], Copyright © 2014, Elsevier)

option as hydrogen donors because they are not corrosive, and they may be obtained from ethanol or butanol using biomass as a substrate [237, 238].

The biggest challenge of having a competent and reasonable HDO is the selection of the catalyst which should be efficient, economical and environmentally friendly. The catalyst stability may be an issue to convert furfural into 2-MF due to the high temperatures, which increases the energy cost and the coke production as well [220]. The deactivation catalysts during the 2-MF production through furfural hydrogenation is the main issue of the process because of the production of undesired co-products (furan, tetrahydrofuran and C-4 compounds) [239]. Additionally, this method of conversion is quite exothermic (142 kJ/mol), causing difficulties in terms of temperature control [240].

Chromium-based catalysts were described as efficient for 2-MF production, while their toxicity makes them less attractive [224]. Molybdenum carbide has a high selectivity to convert furfural into 2-MF, but it presents very acidic features, stimulating the polymerization of furfural and creating an unstable environment for the HDO process [241]. Although precious metals such as ruthenium and palladium showed a good furfural conversion yield, they are extremely expensive, easily deactivated, hard to regenerate and not economically viable [215]. Mesoporous silica catalysts contain large surface areas, and they can convert 82% of furfural; nevertheless, the process is extremely slow (more than 25 h), and it leads to the formation and deposit of carbon in the catalyst substrate, which leads to catalyst deactivation and consequent reduction of HDO reactions between the surface and the product [220].

Copper-based catalysts are mentioned as the most promising option to convert furfural into 2-MF [226, 242]. Recently, the combination between Cu and Zn or Cu and Mn as a catalyst showed strong stability and efficiency in 2-MF production by HDO. The good interaction among these two groups of metals brings the production of mixed oxide phases and, consequently, a breakage of the C-O bond [228, 239]. Moreover, the combination between manganese/zinc Cu-based catalysts and Al_2O_3 and SiO_2 supports increases the selectivity and activity of the HDO process [239]. Both catalytic supports are cheap, practical to be used in industry, and they promote the interaction and dispersion of copper, improving the catalytic performance [226].

8.1 Xylose-Rich Biomass

One of the most accessible and inexpensive green resources for the biofuel production and bioenergy area is lignocellulosic agricultural wastes [243]. Present approaches to exploit biomass such as pure cellulose extraction or combustion to produce electricity are damaging the environment and not profitable for the industry [244]. Therefore, thermochemical processes become more prevalent for converting biomass into valued products and thus establishing a different pathway for the application of lignocellulosic residues regarding profitability and sustainability [81].

Lignocellulosic materials are commonly composed of lignin (10–25%), hemicellulose (20–40%) and cellulose (40–60%). Hemicellulose biomass is getting more appreciation because of its high xylan content. This xylan content is mainly formed by xylose which is an interesting chemical in the biofuel industry [244]. According to the previous section, furfural can be obtained using lignocellulosic feedstocks containing a high level of xylose. Furfural has an annual production of 250,000 tonnes, and the present method to extract this chemical compound from xylose sources is the acid-catalysed dehydration [245]. Oat hulls (OHS) and sugarcane bagasse (SB) have been recognized as one of the most promising xylose-rich biomass for furfural production [220].

Presently, oat is one of the main produced cereals around the world, and its hull, which is a residue from the process of oat milling, has a high potential as a renewable biomass source because of its availability. OHS is a suitable feedstock to produce gaseous and liquid fuels through advanced thermochemical processes (gasification and pyrolysis) [246].

OHS is generally formed from lignin (17–20%), hemicellulose (32–35%) and cellulose (35–45%) [247]. OHS has a low ash content (4.5–5.5%), and also it does not require to be milled when treated because of its particle size and homogenous morphological structure [247]. Due to the high amount of hemicellulose, oat hulls are a good source of furfural and xylose (pentose sugars) [248]. However, some kinetic parameters of oat hulls need to be understood to develop this process [246].

Nowadays, OHS is mostly used to produce energy from combustion because of its HHV (16 MJ/kg) [249]. This residue shows a practical nutritive value and is applied in the human and animal food industry [246]. Furthermore, it is reported that OHS can be used for ethanol production through chemical hydrolysis [247]. Therefore, OHS can be considered as a renewable resource for biofuel production due to its potential and availability [249].

Sugarcane is the most prominent farming harvest in the world. Bagasse can be obtained from sugarcane milling to extract its juice for production of sugar or ethanol, which is the main residue of sugarcane [250]. The raw SB is made in many countries, and its production is more significant and efficient in sub-tropical and tropical climates [251]. Brazil and India are the leading SB producers in the world, and this industry represents a relevant role for the energy needs in developing countries [252]. Normally, 1000 kg of fresh sugarcane can generate 280 kg of dry bagasse, 110 kg of sugar and 45 kg of molasses [250]. For ethanol production, cane straw and bagasse residues represent around 35% of the total sugarcane weight [253].

SB has a lamella structure, and it is formed from lignin (20–25%), hemicellulose (20–30%), cellulose (40–50%) and low ash content (1.5–3%) [250]. Presently, more than 500 sugarcane species are cultivated in Brazil, and 20 new species have been created every single year [253]. However, the chemical compositions of the different SB species do not diverge significantly from the main compounds [253]. The cellulose elements of SB have crystalline and amorphous structures that require to be submitted to thermochemical and physical treatments to reach to the polysaccharides components [252]. In order to increase the SB particle surface area, milling is a suitable physical approach. Thermochemical treatments are ammonia, alkaline

hydroxide, steam explosion and acid reagents, which convert the crystalline structure of SB into polysaccharide elements [254–256]. The results of these thermochemical processes on the chemical structure of the SB can be analysed via enzyme digestion, electron miscopy and X-ray diffraction [252].

Presently, SB can be utilized in many applications such as cancer treatment, animal feed, and production of furfural, sugar, pulp and ethanol [252, 253]. Furthermore, SB is a suitable feedstock to be applied as a renewable resource due to its low cost and high availability [252, 257]. SB is mostly used for power and heat generation through combustion route, which is not energy efficient [250, 253]. However, SB can be applied for the production of biofuel through advanced thermochemical processes due to its high caloric value and availability, thus making this material a valuable feedstock for pyrolysis technology [250].

9   Conclusion

Renewable and sustainable energy sources have received attention because of the increase in demand for fossil fuels and concerns regarding climate change. Biofuels are characterized into "primary biofuels" and "secondary biofuels". The traditional form of biofuel for heat and electricity generation is categorized in "primary biofuels". The second class of biofuels is characterized into first, second and third generations. First-generation biofuels are mainly produced from sugar, food crops and starch. Second-generation biofuels are formed from non-food biomass, and third-generation biofuels are made from microbes and microalgae. Pyrolysis is an advanced thermal conversion method for converting biomass into useful chemicals and energy carriers. Pyrolysis methods can be divided into three primary types which are fast, intermediate and slow pyrolysis. Slow pyrolysis is suitable for biochar formation and utilization. The main difference between slow, intermediate and fast pyrolysis methods is the solid residence times that cause a different heat transfer to the material.

TCR is a novel technology that combines the intermediate pyrolysis with post-catalytic treatment (catalytic reforming) in a single-step upgrading. In the reforming stage, vapour catalytic cracking happens to encourage the formation of syngas and organic vapours with lower molecular weight compounds. TCR bio-oil has superior physicochemical fuel characteristics in comparison with other technologies. TCR bio-oil of woody biomass is low in oxygen content (11.4–17.9 wt%), low in viscosity (12.1–36.5 mm²/s) and low in acidity (9.3–30.1 mg KOH/g) and has a very high heating value (32.8–35.5 MJ/kg) compared to bio-oil of fast pyrolysis. TCR bio-oil can be separated simply from the water phase and is totally miscible with conventional fossil fuels. There is no need for using expensive catalysts such as zeolite or/ and precious metal oxide catalysts in this process. TCR technology is well compatible with different ranges of feedstocks that are high in ash and moisture contents. Furthermore, TCR produces a significant amount of green H_2 for hydrotreatment of bio-oil and can be maximized by injection of steam into the system that promotes a

water gas shift reaction. However, fast pyrolysis needs an outside source of H_2 to improve the bio-oil properties.

In this chapter, different methods such as zeolite cracking, hydrotreatment, esterification, transesterification, ketonization and others were discussed in detail to upgrade bio-oil. 2-Methylfuran (2-MF) can be one of the promising fuels to be used in engines. Furfural can be converted into 2-MF through hydrogenation and HDO reactions. Copper-based catalysts have been reported as one of the most promising options to convert furfural into 2-MF in terms of stability and efficiency. However, this process is not profitable or efficient due to the high cost of solvents, catalysts and outside sources of hydrogen. These facts can encourage 2-MF production using TCR process, which may be a more economically viable process and thus has started to attract more attention as an alternative process route. Overall, this report showed different potentials for converting wastes into sustainable fuels and useful energy vectors.

References

1. Gilland B (1995) World-population, economic-growth, and energy demand, 1990–2100—a review of projections. Popul Dev Rev 21(3):507–539
2. OECD (2016) OECD economic outlook. OECD, Paris
3. Sieminski A (2014) International energy outlook. Energy information administration (EIA), Washington, DC, p 18
4. Saladini F, Patrizi N, Pulselli FM, Marchettini N, Bastianoni S (2016) Guidelines for emergy evaluation of first, second and third generation biofuels. Renew Sustain Energy Rev 66:221–227
5. Easterbrook DJ (2016) Chap. 9—Greenhouse gases. In: Evidence-based climate science, 2nd edn. Elsevier, Amsterdam, pp 163–173
6. Rees RM, Flack S, Maxwell K, Mistry A (2014) Air: Greenhouse gases from Agriculture A2. In: Van Alfen NK (ed) Encyclopedia of agriculture and food systems. Academic Press, Oxford, pp 293–304
7. Yang Z, Wei T, Moore JC, Chou J, Dong W, Dai R et al (2016) A new consumption-based accounting model for greenhouse gases from 1948 to 2012. J Clean Prod 133:368–377
8. Bennaceur K, Gielen D, Kerr T, Tam C (2008) CO2 capture and storage: a key carbon abatement option. OECD, Paris
9. Birol F (2016) Key world energy statistics. International Energy Agency (IEA), Washington, DC
10. Department for Business EIS (2018) 2018 UK Greenhouse gas emissions, provisional figures. National Statistics, London
11. Demirbas A (2008) Biodiesel. Springer, Berlin
12. McCollum D, Yang C (2009) Achieving deep reductions in US transport greenhouse gas emissions: scenario analysis and policy implications. Energy Policy 37(12):5580–5596
13. Chakraborty S, Aggarwal V, Mukherjee D, Andras K (2012) Biomass to biofuel: a review on production technology. Asia-Pac J Chem Eng 7:S254–SS62
14. Nigam PS, Singh A (2011) Production of liquid biofuels from renewable resources. Prog Energ Combust 37(1):52–68
15. Alonso DM, Bond JQ, Dumesic JA (2010) Catalytic conversion of biomass to biofuels. Green Chem 12(9):1493–1513

16. Singh A, Nigam PS, Murphy JD (2011) Renewable fuels from algae: an answer to debatable land based fuels. Bioresour Technol 102(1):10–16
17. Searchinger T, Heimlich R, Houghton RA, Dong FX, Elobeid A, Fabiosa J et al (2008) Use of US croplands for biofuels increases greenhouse gases through emissions from land-use change. Science 319(5867):1238–1240
18. Fargione J, Hill J, Tilman D, Polasky S, Hawthorne P (2008) Land clearing and the biofuel carbon debt. Science 319(5867):1235–1238
19. Patil V, Tran KQ, Giselrod HR (2008) Towards sustainable production of biofuels from microalgae. Int J Mol Sci 9(7):1188–1195
20. Righelato R, Spracklen DV (2007) Environment—carbon mitigation by biofuels or by saving and restoring forests? Science 317(5840):902
21. Danielsen F, Beukema H, Burgess ND, Parish F, Bruhl CA, Donald PF et al (2009) Biofuel plantations on forested lands: double jeopardy for biodiversity and climate. Conserv Biol 23(2):348–358
22. Demirbas A (2011) Competitive liquid biofuels from biomass. Appl Energy 88(1):17–28
23. Jansen RA (2012) Second generation biofuels and biomass: essential guide for investors, scientists and decision makers. Wiley, Hoboken, NJ
24. Sims REH, Mabee W, Saddler JN, Taylor M (2010) An overview of second generation biofuel technologies. Bioresour Technol 101(6):1570–1580
25. Liew WH, Hassim MH, Ng DKS (2014) Review of evolution, technology and sustainability assessments of biofuel production. J Clean Prod 71:11–29
26. Speight JG (2011) The biofuels handbook. Royal Society of Chemistry, Cambridge
27. Carriquiry MA, Du X, Timilsina GR (2011) Second generation biofuels: economics and policies. Energy Policy 39(7):4222–4234
28. Antizar-Ladislao B, Turrion-Gomez JL (2008) Second-generation biofuels and local bioenergy systems. Biofuels Bioprod Biorefin 2(5):455–469
29. Huang C, Zong MH, Wu H, Liu QP (2009) Microbial oil production from rice straw hydrolysate by Trichosporon fermentans. Bioresour Technol 100(19):4535–4538
30. Carere CR, Sparling R, Cicek N, Levin DB (2008) Third generation biofuels via direct cellulose fermentation. Int J Mol Sci 9(7):1342–1360
31. Zhu LD, Hiltunen E, Antila E, Zhong JJ, Yuan ZH, Wang ZM (2014) Microalgal biofuels: flexible bioenergies for sustainable development. Renew Sustain Energy Rev 30:1035–1046
32. Zhu LD, Ketola T (2012) Microalgae production as a biofuel feedstock: risks and challenges. Int J Sust Dev World 19(3):268–274
33. Demirbaş A (2008) Production of biodiesel from algae oils. Energy Sources Pt A Recov Utilization Environ Eff 31(2):163–168
34. Kita K, Okada S, Sekino H, Imou K, Yokoyama S, Amano T (2010) Thermal pre-treatment of wet microalgae harvest for efficient hydrocarbon recovery. Appl Energy 87(7):2420–2423
35. Tsukahara K, Sawayama S (2005) Liquid fuel production using microalgae. J Jpn Petrol Inst 48(5):251–259
36. Picazo-Espinosa R, González-López J, Manzanera M (2011) Bioresources for third-generation biofuels. In: Biofuel's engineering process technology, vol 6, pp 115–133
37. Singh A, Olsen SI, Nigam PS (2011) A viable technology to generate third-generation biofuel. J Chem Technol Biotechnol 86(11):1349–1353
38. Khan AA, de Jong W, Jansens PJ, Spliethoff H (2009) Biomass combustion in fluidized bed boilers: potential problems and remedies. Fuel Process Technol 90(1):21–50
39. Jenkins BM, Baxter LL, Miles TR Jr, Miles TR (1998) Combustion properties of biomass. Fuel Process Technol 54(1–3):17–46
40. Oral J, Sikula J, Puchyr R, Hajny Z, Stehlik P, Bebar L (2005) Processing of waste from pulp and paper plant. Clean Prod 13(5):509–515
41. Gopal P, Sivaram N, Barik D (2019) Paper industry wastes and energy generation from wastes. In: Energy from toxic organic waste for heat and power generation. Elsevier, Amsterdam, pp 83–97

42. Quina MJ, Bordado JC, Quinta-Ferreira RM (2011) Air pollution control in municipal solid waste incinerators. In: The impact of air pollution on health, economy, environment and agricultural sources. InTech, Rijeka

43. Cherubini F (2010) The biorefinery concept: using biomass instead of oil for producing energy and chemicals. Energ Conver Manage 51(7):1412–1421

44. Kamm B, Gruber PR, Kamm M (2000) Biorefineries—industrial processes and products. Ullmann's encyclopedia of industrial chemistry. Wiley-VCH Verlag GmbH & Co. KGaA, Weinheim

45. Iqbal S, Davies TE, Morgan DJ, Karim K, Hayward JS, Bartley JK et al (2016) Fischer Tropsch synthesis using cobalt based carbon catalysts. Catal Today 275:35–39

46. Jahangiri H, Bennett J, Mahjoubi P, Wilson K, Gu S (2014) A review of advanced catalyst development for Fischer-Tropsch synthesis of hydrocarbons from biomass derived syn-gas. Cat Sci Technol 4(8):2210–2229

47. Mahmoudi H, Jahangiri H, Doustdar O, Akbari N, Wood J, Tsolakis A, et al (2020) Maximizing paraffin to olefin ratio employing simulated nitrogen-rich syngas via Fischer-Tropsch process over Co3O4/SiO2 catalysts. Fuel Processing Technology 208:106477

48. Ahmad AA, Zawawi NA, Kasim FH, Inayat A, Khasri A (2016) Assessing the gasification performance of biomass: a review on biomass gasification process conditions, optimization and economic evaluation. Renew Sustain Energy Rev 53:1333–1347

49. Warnecke R (2000) Gasification of biomass: comparison of fixed bed and fluidized bed gasifier. Biomass Bioenergy 18(6):489–497

50. Heidenreich S, Müller M, Foscolo PU (2016) Chap. 2—fundamental concepts in biomass gasification. In: Heidenreich S, Müller M, Foscolo PU (eds) Advanced biomass gasification. Academic Press, New York, pp 4–10

51. Reed TB, Das A (1988) Handbook of biomass downdraft gasifier engine systems. Biomass Energy Foundation, Golden, CO

52. Ouadi M, Fivga A, Jahangiri H, Saghir M, Hornung A (2019) A review of the valorization of paper industry wastes by thermochemical conversion. Ind Eng Chem Res 58(35):15914–15929

53. Pfeifer C, Rauch R, Hofbauer H (2004) In-bed catalytic tar reduction in a dual fluidized bed biomass steam gasifier. Ind Eng Chem Res 43(7):1634–1640

54. Mahmood ASN, Brammer JG, Hornung A, Steele A, Poulston S (2013) The intermediate pyrolysis and catalytic steam reforming of brewers spent grain. J Anal Appl Pyrolysis 103:328–342

55. Collard F-X, Blin J (2014) A review on pyrolysis of biomass constituents: mechanisms and composition of the products obtained from the conversion of cellulose, hemicelluloses and lignin. Renew Sustain Energy Rev 38:594–608

56. Klaas M, Greenhalf C, Ouadi M, Jahangiri H, Hornung A, Briens C, et al (2020) The effect of torrefaction pre-treatment on the pyrolysis of corn cobs. Results Eng 7:100165

57. Bridgwater AV (2012) Review of fast pyrolysis of biomass and product upgrading. Biomass Bioenergy 38:68–94

58. Xiu S, Shahbazi A (2012) Bio-oil production and upgrading research: a review. Renew Sustain Energy Rev 16(7):4406–4414

59. Dhyani V, Bhaskar T (2019) Chap. 9—pyrolysis of biomass. In: Pandey A, Larroche C, Dussap C-G, Gnansounou E, Khanal SK, Ricke S (eds) Biofuels: alternative feedstocks and conversion processes for the production of liquid and gaseous biofuels, 2nd edn. Academic Press, New York, pp 217–244

60. Cong H, Mašek O, Zhao L, Yao Z, Meng H, Hu E et al (2018) Slow pyrolysis performance and energy balance of corn stover in continuous pyrolysis-based poly-generation systems. Energy Fuel 32(3):3743–3750

61. Crombie K, Mašek O (2014) Investigating the potential for a self-sustaining slow pyrolysis system under varying operating conditions. Bioresour Technol 162:148–156

62. Park J, Lee Y, Ryu C, Park YK (2014) Slow pyrolysis of rice straw: analysis of products properties, carbon and energy yields. Bioresour Technol 155:63–70

63. Stamatov V, Honnery D, Soria J (2006) Combustion properties of slow pyrolysis bio-oil produced from indigenous Australian species. Renew Energy 31(13):2108–2121
64. Hagner M, Tiilikkala K, Lindqvist I, Niemelä K, Wikberg H, Källi A et al (2018) Performance of liquids from slow pyrolysis and hydrothermal carbonization in plant protection. In: Waste biomass valorization, pp 1–12
65. Carrier M, Hugo T, Gorgens J, Knoetze H (2011) Comparison of slow and vacuum pyrolysis of sugar cane bagasse. J Anal Appl Pyrolysis 90(1):18–26
66. Aziz AA, Deraman M (2013) Pore structure of carbon granules prepared from slow pyrolysis of oil palm empty fruit bunch fibres. J Oil Palm Res 25(2):216–227
67. Moreira R, Orsini RD, Vaz JM, Penteado JC, Spinace EV (2017) Production of biochar, bio-oil and synthesis gas from cashew nut shell by slow pyrolysis. Waste Biomass Valor 8(1):217–224
68. Antal MJ, Gronli M (2003) The art, science, and technology of charcoal production. Ind Eng Chem Res 42(8):1619–1640
69. Prins MJ, Ptasinski KJ, Janssen FJJG (2006) Torrefaction of wood: Part 1. Weight loss kinetics. J Anal Appl Pyrolysis 77(1):28–34
70. van der Stelt MJC, Gerhauser H, Kiel JHA, Ptasinski KJ (2011) Biomass upgrading by torrefaction for the production of biofuels: a review. Biomass Bioenergy 35(9):3748–3762
71. Batidzirai B, Mignot APR, Schakel WB, Junginger HM, Faaij APC (2013) Biomass torrefaction technology: techno-economic status and future prospects. Energy 62:196–214
72. Neumann J, Meyer J, Ouadi M, Apfelbacher A, Binder S, Hornung A (2016) The conversion of anaerobic digestion waste into biofuels via a novel thermo-catalytic reforming process. Waste Manag 47:141–148
73. Hornung A (2013) Intermediate pyrolysis of biomass. Woodhead Publ Ser En 40:172–186
74. Ouadi M, Brammer JG, Yang Y, Hornung A, Kay M (2013) The intermediate pyrolysis of de-inking sludge to produce a sustainable liquid fuel. J Anal Appl Pyrolysis 102:24–32
75. Yang Y, Brammer JG, Mahmood ASN, Hornung A (2014) Intermediate pyrolysis of biomass energy pellets for producing sustainable liquid, gaseous and solid fuels. Bioresour Technol 169:794–799
76. Pattiya A (2018) 1—Fast pyrolysis. In: Rosendahl L (ed) Direct thermochemical liquefaction for energy applications. Woodhead Publishing, Cambridge, pp 3–28
77. Blanco A, Chejne F (2016) Modeling and simulation of biomass fast pyrolysis in a fluidized bed reactor. J Anal Appl Pyrolysis 118:105–114
78. Dickerson T, Soria J (2013) Catalytic fast pyrolysis: a review. Energies 6(1):514–538
79. Oasmaa A, Kuoppala E, Solantausta Y (2003) Fast pyrolysis of forestry residue. 2. Physicochemical composition of product liquid. Energy Fuel 17(2):433–443
80. Czernik S, Bridgwater AV (2004) Overview of applications of biomass fast pyrolysis oil. Energy Fuel 18(2):590–598
81. Dhyani V, Bhaskar T (2018) A comprehensive review on the pyrolysis of lignocellulosic biomass. Renew Energy 129:695–716
82. Zhang Q, Chang J, Wang TJ, Xu Y (2007) Review of biomass pyrolysis oil properties and upgrading research. Energ Conver Manage 48(1):87–92
83. Hornung A, Apfelbacher A, Sagi S (2011) Intermediate pyrolysis: a sustainable biomass-to-energy concept—biothermal valorisation of biomass (BtVB) process. J Sci Ind Res 70(8):664–667
84. Abu El-Rub Z, Bramer EA, Brem G (2004) Review of catalysts for tar elimination in biomass gasification processes. Ind Eng Chem Res 43(22):6911–6919
85. Kebelmann K, Hornung A, Karsten U, Griffiths G (2013) Thermo-chemical behaviour and chemical product formation from polar seaweeds during intermediate pyrolysis. J Anal Appl Pyrolysis 104:131–138
86. Ouadi M, Kay M, Brammer J, Hornung A (2012) Waste to power. Tappi J 11(2):55–64
87. Hossain AK, Ouadi M, Siddiqui SU, Yang Y, Brammer J, Hornung A et al (2013) Experimental investigation of performance, emission and combustion characteristics of an indirect injec-

tion multi-cylinder CI engine fuelled by blends of de-inking sludge pyrolysis oil with bio-diesel. Fuel 105:135–142

88. Ghidotti M (2017) Analytical methods for the characterisation of volatile and water-soluble organic compounds in biochar. In: Relationships with thermal stability and seed germination. Alma

89. Hu X, Gholizadeh M (2019) Biomass pyrolysis: a review of the process development and challenges from initial researches up to the commercialisation stage. J Energy Chem 39:109–143

90. Chen W, Yang H, Chen Y, Chen X, Fang Y, Chen H (2016) Biomass pyrolysis for nitrogen-containing liquid chemicals and nitrogen-doped carbon materials. J Anal Appl Pyrolysis 120:186–193

91. Mollinedo J, Schumacher TE, Chintala R (2015) Influence of feedstocks and pyrolysis on biochar's capacity to modify soil water retention characteristics. J Anal Appl Pyrolysis 114:100–108

92. Laird DA (2008) The charcoal vision: a win-win-win scenario for simultaneously producing bioenergy, permanently sequestering carbon, while improving soil and water quality. Agron J 100(1):178–181

93. Hood-Nowotny R, Watzinger A, Wawra A, Soja G (2018) The impact of biochar incorporation on inorganic nitrogen fertilizer plant uptake; an opportunity for carbon sequestration in temperate agriculture. Geosciences 8(11):420

94. Goyal HB, Seal D, Saxena RC (2008) Bio-fuels from thermochemical conversion of renewable resources: a review. Renew Sustain Energy Rev 12(2):504–517

95. Huber GW, Iborra S, Corma A (2006) Synthesis of transportation fuels from biomass: chemistry, catalysts, and engineering. Chem Rev 106(9):4044–4098

96. Ahmad M, Rajapaksha AU, Lim JE, Zhang M, Bolan N, Mohan D et al (2014) Biochar as a sorbent for contaminant management in soil and water: a review. Chemosphere 99:19–33

97. Mohan D, Sarswat A, Ok YS, Pittman CU (2014) Organic and inorganic contaminants removal from water with biochar, a renewable, low cost and sustainable adsorbent—a critical review. Bioresour Technol 160:191–202

98. Mullen CA, Boateng AA, Goldberg NM, Lima IM, Laird DA, Hicks KB (2010) Bio-oil and bio-char production from corn cobs and stover by fast pyrolysis. Biomass Bioenergy 34(1):67–74

99. Lede J, Diebold JP, Peacocke GVC, Piskorz J (1997) The nature and properties of intermediate and unvaporized biomass pyrolysis materials. In: Bridgwater AV, Boocock DGB (eds) Developments in thermochemical biomass conversion, vol 1/2. Springer, Dordrecht, pp 27–42

100. Isahak WNRW, Hisham MWM, Yarmo MA, T-y YH (2012) A review on bio-oil production from biomass by using pyrolysis method. Renew Sustain Energy Rev 16(8):5910–5923

101. Milne T, Agblevor F, Davis M, Deutch S, Johnson D (1997) A review of the chemical composition of fast-pyrolysis oils from biomass. In: Bridgwater AV, Boocock DGB (eds) Developments in thermochemical biomass conversion, vol 1/2. Springer, Dordrecht, pp 409–424

102. Garcìa-Pérez M, Chaala A, Pakdel H, Kretschmer D, Rodrigue D, Roy C (2006) Multiphase structure of bio-oils. Energy Fuel 20(1):364–375

103. Zhang S, Yan Y, Li T, Ren Z (2005) Upgrading of liquid fuel from the pyrolysis of biomass. Bioresour Technol 96(5):545–550

104. Hornung U, Schneider D, Hornung A, Tumiatti V, Seifert H (2009) Sequential pyrolysis and catalytic low temperature reforming of wheat straw. J Anal Appl Pyrolysis 85(1):145–150

105. Li H, Xu Q, Xue H, Yan Y (2009) Catalytic reforming of the aqueous phase derived from fast-pyrolysis of biomass. Renew Energy 34(12):2872–2877

106. Chiaramonti D, Bonini M, Fratini E, Tondi G, Gartner K, Bridgwater AV et al (2003) Development of emulsions from biomass pyrolysis liquid and diesel and their use in engines—part 2: tests in diesel engines. Biomass Bioenergy 25(1):101–111

107. Gust S (1997) Combustion experiences of flash pyrolysis fuel in intermediate size boilers. In: Bridgwater AV, Boocock DGB (eds) Developments in thermochemical biomass conversion, vol 1/2. Springer Netherlands, Dordrecht, pp 481–488

108. Balat M (2011) An overview of the properties and applications of biomass pyrolysis oils. Energy Sources Pt A Recov Utilization Environ Eff 33(7):674–689

109. Park YK, Yoo ML, Heo HS, Lee HW, Park SH, Jung SC et al (2012) Wild reed of Suncheon Bay: potential bio-energy source. Renew Energy 42:168–172

110. Uddin MN, Daud WMAW, Abbas HF (2014) Effects of pyrolysis parameters on hydrogen formations from biomass: a review. RSC Adv 4(21):10467–10490

111. Yang HP, Yan R, Chen HP, Lee DH, Zheng CG (2007) Characteristics of hemicellulose, cellulose and lignin pyrolysis. Fuel 86(12–13):1781–1788

112. Guoxin H, Hao H, Yanhong L (2009) Hydrogen-rich gas production from pyrolysis of biomass in an autogenerated steam atmosphere. Energy Fuel 23(3):1748–1753

113. Dasappa S, Paul PJ, Mukunda HS, Rajan NKS, Sridhar G, Sridhar HV (2004) Biomass gasification technology—a route to meet energy needs. Curr Sci India 87(7):908–916

114. Hasan MDM, Wang XS, Mourant D, Gunawan R, Yu C, Hu X et al (2017) Grinding pyrolysis of Mallee wood: effects of pyrolysis conditions on the yields of bio-oil and biochar. Fuel Process Technol 167:215–220

115. He M, Xiao B, Liu S, Hu Z, Guo X, Luo S et al (2010) Syngas production from pyrolysis of municipal solid waste (MSW) with dolomite as downstream catalysts. J Anal Appl Pyrolysis 87(2):181–187

116. Santos J, Ouadi M, Jahangiri H, Hornung A (2020) Valorisation of lignocellulosic biomass investigating different pyrolysis temperatures. J Energy Inst 93(5):1960–1969

117. Bashir MA, Jahangiri H, Hornung A, Ouadi M (2021) Deoxygenation of Bio-oil from Calcium-Rich Paper-Mill Waste. Chem Eng Technol 44(1):194–202

118. Vamvuka D (2011) Bio-oil, solid and gaseous biofuels from biomass pyrolysis processes—an overview. Int J Energ Res 35(10):835–862

119. Morf P, Hasler P, Nussbaumer T (2002) Mechanisms and kinetics of homogeneous secondary reactions of tar from continuous pyrolysis of wood chips. Fuel 81(7):843–853

120. Van de Velden M, Baeyens J, Brems A, Janssens B, Dewil R (2010) Fundamentals, kinetics and endothermicity of the biomass pyrolysis reaction. Renew Energy 35(1):232–242

121. Zhang L, Hu X, Hu K, Hu C, Zhang Z, Liu Q et al (2018) Progress in the reforming of bio-oil derived carboxylic acids for hydrogen generation. J Power Sources 403:137–156

122. Shen J, Wang X-S, Garcia-Perez M, Mourant D, Rhodes MJ, Li C-Z (2009) Effects of particle size on the fast pyrolysis of oil mallee woody biomass. Fuel 88(10):1810–1817

123. Williams PT, Besler S (1996) The influence of temperature and heating rate on the slow pyrolysis of biomass. Renew Energy 7(3):233–250

124. Akhtar J, Saidina Amin N (2012) A review on operating parameters for optimum liquid oil yield in biomass pyrolysis. Renew Sustain Energy Rev 16(7):5101–5109

125. Fahmi R, Bridgwater AV, Donnison I, Yates N, Jones JM (2008) The effect of lignin and inorganic species in biomass on pyrolysis oil yields, quality and stability. Fuel 87(7):1230–1240

126. Roy C, Pakdel H, Brouillard D (1990) The role of extractives during vacuum pyrolysis of wood. J Appl Polym Sci 41(1–2):337–348

127. Kallioinen A, Vaari A, Rättö M, Konn J, Siika-aho M, Viikari L (2003) Effects of bacterial treatments on wood extractives. J Biotechnol 103(1):67–76

128. Scott DS, Paterson L, Piskorz J, Radlein D (2001) Pretreatment of poplar wood for fast pyrolysis: rate of cation removal. J Anal Appl Pyrolysis 57(2):169–176

129. Santos J, Ouadi M, Jahangiri H, Hornung A (2019) Integrated intermediate catalytic pyrolysis of wheat husk. Food Bioprod Process 114:23–30

130. Yang Y, Brammer JG, Ouadi M, Samanya J, Hornung A, Xu HM et al (2013) Characterisation of waste derived intermediate pyrolysis oils for use as diesel engine fuels. Fuel 103:247–257

131. Fivga A, Jahangiri H, Bashir MA, Majewski AJ, Hornung A, Ouadi M (2020) Demonstration of catalytic properties of de-inking sludge char as a carbon based sacrificial catalyst. J Anal Appl Pyrolysis 146:104773

132. Santos J, Jahangiri H, Bashir MA, Hornung A, Ouadi M (2020) The Upgrading of Bio-Oil from the Intermediate Pyrolysis of Waste Biomass Using Steel Slag as a Catalyst. ACS Sustain Chem Eng 8(50):18420–32

133. Hornung A (2014) Transformation of biomass theory to practice preface. In: Transformation of biomass: theory to practice, pp Xvii–Xviii

134. Neumann J, Binder S, Apfelbacher A, Gasson JR, Ramírez García P, Hornung A (2015) Production and characterization of a new quality pyrolysis oil, char and syngas from digestate—introducing the thermo-catalytic reforming process. J Anal Appl Pyrolysis 113:137–142

135. Ouadi M, Bashir MA, Speranza LG, Jahangiri H, Hornung A (2019) Food and market waste—a pathway to sustainable fuels and waste valorization. Energy Fuel 33(10):9843–9850

136. Neumann J, Jager N, Apfelbacher A, Daschner R, Binder S, Hornung A (2016) Upgraded bio-fuel from residue biomass by thermo-catalytic reforming and hydrodeoxygenation. Biomass Bioenergy 89:91–97

137. Ouadi M, Greenhalf C, Jaeger N, Speranza LG, Hornung A (2018) Thermo-catalytic reforming of co-form (R) rejects (waste cleansing wipes). J Anal Appl Pyrolysis 132:33–39

138. Kirby ME, Hornung A, Ouadi M, Theodorou MK (2017) The role of thermo-catalytic reforming for energy recovery from food and drink supply chain wastes. Energy Procedia 123:15–21

139. Ahmad E, Jager N, Apfelbacher A, Daschner R, Hornung A, Pant KK (2018) Integrated thermo-catalytic reforming of residual sugarcane bagasse in a laboratory scale reactor. Fuel Process Technol 171:277–286

140. Ouadi M, Jaeger N, Greenhalf C, Santos J, Conti R, Hornung A (2017) Thermo-catalytic reforming of municipal solid waste. Waste Manag 68:198–206

141. Zhang L, Liu R, Yin R, Mei Y (2013) Upgrading of bio-oil from biomass fast pyrolysis in China: a review. Renew Sustain Energy Rev 24:66–72

142. Lin YC, Huber GW (2009) The critical role of heterogeneous catalysis in lignocellulosic biomass conversion. Energ Environ Sci 2(1):68–80

143. Conti R, Jäger N, Neumann J, Apfelbacher A, Daschner R, Hornung A (2017) Thermocatalytic reforming of biomass waste streams. Energ Technol 5(1):104–110

144. Mullen CA, Boateng AA, Mihalcik DJ, Goldberg NM (2011) Catalytic fast pyrolysis of White oak wood in a bubbling fluidized bed. Energy Fuel 25(11):5444–5451

145. Jager N, Conti R, Neumann J, Apfelbacher A, Daschner R, Binder S et al (2016) Thermo-catalytic reforming of woody biomass. Energy Fuel 30(10):7923–7929

146. Santos J, Ouadi M, Jahangiri H, Hornung A (2020) Thermochemical conversion of agricultural wastes applying different reforming temperatures. Fuel Process Technol 203:106402

147. Guo C, Rao KTV, Yuan Z, He S, Rohani S, Xu C (2018) Hydrodeoxygenation of fast pyrolysis oil with novel activated carbon-supported NiP and CoP catalysts. Chem Eng Sci 178:248–259

148. Carriel Schmitt C, Gagliardi Reolon MB, Zimmermann M, Raffelt K, Grunwaldt J-D, Dahmen N (2018) Synthesis and regeneration of nickel-based catalysts for hydrodeoxygenation of beech wood fast pyrolysis bio-oil. Catalysts 8(10):449

149. Chiaramonti D, Bonini A, Fratini E, Tondi G, Gartner K, Bridgwater AV et al (2003) Development of emulsions from biomass pyrolysis liquid and diesel and their use in engines—part 1: emulsion production. Biomass Bioenergy 25(1):85–99

150. Bridgwater AV (2012) Upgrading biomass fast pyrolysis liquids. Environ Prog Sustain 31(2):261–268

151. Diebold JP, Czernik S (1997) Additives to lower and stabilize the viscosity of pyrolysis oils during storage. Energy Fuel 11(5):1081–1091

152. Carlson TR, Vispute TR, Huber GW (2008) Green gasoline by catalytic fast pyrolysis of solid biomass derived compounds. ChemSusChem 1(5):397–400

153. Pattiya A, Titiloye JO, Bridgwater AV (2008) Fast pyrolysis of cassava rhizome in the presence of catalysts. J Anal Appl Pyrolysis 81(1):72–79

154. Pattiya A, Titiloye JO, Bridgwater AV (2010) Evaluation of catalytic pyrolysis of cassava rhizome by principal component analysis. Fuel 89(1):244–253
155. Carlson TR, Tompsett GA, Conner WC, Huber GW (2009) Aromatic production from catalytic fast pyrolysis of biomass-derived feedstocks. Top Catal 52(3):241–252
156. Jae J, Tompsett GA, Foster AJ, Hammond KD, Auerbach SM, Lobo RF et al (2011) Investigation into the shape selectivity of zeolite catalysts for biomass conversion. J Catal 279(2):257–268
157. Nguyen TS, Zabeti M, Lefferts L, Brem G, Seshan K (2013) Catalytic upgrading of biomass pyrolysis vapours using faujasite zeolite catalysts. Biomass Bioenergy 48:100–110
158. Duman G, Pala M, Ucar S, Yanik J (2013) Two-step pyrolysis of safflower oil cake. J Anal Appl Pyrolysis 103:352–361
159. Pan P, Hu C, Yang W, Li Y, Dong L, Zhu L et al (2010) The direct pyrolysis and catalytic pyrolysis of Nannochloropsis sp. residue for renewable bio-oils. Bioresour Technol 101(12):4593–4599
160. Zhang H, Xiao R, Huang H, Xiao G (2009) Comparison of non-catalytic and catalytic fast pyrolysis of corncob in a fluidized bed reactor. Bioresour Technol 100(3):1428–1434
161. Stephanidis S, Nitsos C, Kalogiannis K, Iliopoulou EF, Lappas AA, Triantafyllidis KS (2011) Catalytic upgrading of lignocellulosic biomass pyrolysis vapours: effect of hydrothermal pretreatment of biomass. Catal Today 167(1):37–45
162. Williams PT, Nugranad N (2000) Comparison of products from the pyrolysis and catalytic pyrolysis of rice husks. Energy 25(6):493–513
163. Engtrakul C, Mukarakate C, Starace AK, Magrini KA, Rogers AK, Yung MM (2016) Effect of ZSM-5 acidity on aromatic product selectivity during upgrading of pine pyrolysis vapors. Catal Today 269:175–181
164. Li J, Li X, Zhou G, Wang W, Wang C, Komarneni S et al (2014) Catalytic fast pyrolysis of biomass with mesoporous ZSM-5 zeolites prepared by desilication with NaOH solutions. Appl Catal Gen 470:115–122
165. Iliopoulou EF, Antonakou EV, Karakoulia SA, Vasalos IA, Lappas AA, Triantafyllidis KS (2007) Catalytic conversion of biomass pyrolysis products by mesoporous materials: effect of steam stability and acidity of Al-MCM-41 catalysts. Chem Eng J 134(1):51–57
166. Adam J, Antonakou E, Lappas A, Stöcker M, Nilsen MH, Bouzga A et al (2006) In situ catalytic upgrading of biomass derived fast pyrolysis vapours in a fixed bed reactor using mesoporous materials. Micropor Mesopor Mat 96(1):93–101
167. French R, Czernik S (2010) Catalytic pyrolysis of biomass for biofuels production. Fuel Process Technol 91(1):25–32
168. Zhang C, Hu X, Guo H, Wei T, Dong D, Hu G et al (2018) Pyrolysis of poplar, cellulose and lignin: effects of acidity and alkalinity of the metal oxide catalysts. J Anal Appl Pyrolysis 134:590–605
169. Yildiz G, Pronk M, Djokic M, van Geem KM, Ronsse F, van Duren R et al (2013) Validation of a new set-up for continuous catalytic fast pyrolysis of biomass coupled with vapour phase upgrading. J Anal Appl Pyrolysis 103:343–351
170. Gholizadeh M, Gunawan R, Hu X, de Miguel Mercader F, Westerhof R, Chaitwat W et al (2016) Effects of temperature on the hydrotreatment behaviour of pyrolysis bio-oil and coke formation in a continuous hydrotreatment reactor. Fuel Process Technol 148:175–183
171. Foster AJ, Jae J, Cheng Y-T, Huber GW, Lobo RF (2012) Optimizing the aromatic yield and distribution from catalytic fast pyrolysis of biomass over ZSM-5. Appl Catal Gen 423–424:154–161
172. Lappas AA, Kalogiannis KG, Iliopoulou EF, Triantafyllidis KS, Stefanidis SD (2016) Catalytic pyrolysis of biomass for transportation fuels. advances in bioenergy: the sustainability challenge, pp 45–56
173. Wang K, Johnston PA, Brown RC (2014) Comparison of in-situ and ex-situ catalytic pyrolysis in a micro-reactor system. Bioresour Technol 173:124–131

174. Wang SR, Dai GX, Yang HP, Luo ZY (2017) Lignocellulosic biomass pyrolysis mechanism: a state-of-the-art review. Prog Energ Combust 62:33–86

175. Pindoria RV, Megaritis A, Herod AA, Kandiyoti R (1998) A two-stage fixed-bed reactor for direct hydrotreatment of volatiles from the hydropyrolysis of biomass: effect of catalyst temperature, pressure and catalyst ageing time on product characteristics. Fuel 77(15):1715–1726

176. Cortright RD, Davda RR, Dumesic JA (2002) Hydrogen from catalytic reforming of biomass-derived hydrocarbons in liquid water. Nature 418(6901):964–967

177. Huber GW, Cortright RD, Dumesic JA (2004) Renewable alkanes by aqueous-phase reforming of biomass-derived oxygenates. Angew Chem Int Ed 43(12):1549–1551

178. Huber GW, Dumesic JA (2006) An overview of aqueous-phase catalytic processes for production of hydrogen and alkanes in a biorefinery. Catal Today 111(1–2):119–132

179. ADd O, AFd S, Pimentel MF, Pacheco JGA, Pereira CF, Larrechi MS (2017) Comprehensive near infrared study of Jatropha oil esterification with ethanol for biodiesel production. Spectrochim Acta A Mol Biomol Spectrosc 170:56–64

180. Juan JC, Zhang JC, Yarmo MA (2008) Efficient esterification of fatty acids with alcohols catalyzed by Zr(SO(4))(2) center dot 4H(2)O under solvent-free condition. Catal Lett 126(3–4):319–324

181. Park YM, Chung SH, Eom HJ, Lee JS, Lee KY (2010) Tungsten oxide zirconia as solid superacid catalyst for esterification of waste acid oil (dark oil). Bioresour Technol 101(17):6589–6593

182. Ozbay N, Oktar N, Tapan NA (2008) Esterification of free fatty acids in waste cooking oils (WCO): role of ion-exchange resins. Fuel 87(10–11):1789–1798

183. Costa AA, Braga PRS, de Macedo JL, Dias JA, Dias SCL (2012) Structural effects of WO3 incorporation on USY zeolite and application to free fatty acids esterification. Micropor Mesopor Mat 147(1):142–148

184. Brahmkhatri V, Patel A (2011) 12-Tungstophosphoric acid anchored to SBA-15: an efficient, environmentally benign reusable catalysts for biodiesel production by esterification of free fatty acids. Appl Catal A Gen 403(1–2):161–172

185. Mantri K, Nakamura R, Miyata Y, Komura K, Sugi Y (2007) Multi-valent metal salt hydrates as catalysts for the esterification of fatty acids and alcohols. Mater Sci Forum 539–543:2317–2322

186. Xie W, Zhao L (2014) Heterogeneous CaO–MoO3–SBA-15 catalysts for biodiesel production from soybean oil. Energ Conver Manage 79:34–42

187. Lee AF, Bennett JA, Manayil JC, Wilson K (2014) Heterogeneous catalysis for sustainable biodiesel production via esterification and transesterification. Chem Soc Rev 43(22):7887–7916

188. Benjapornkulaphong S, Ngamcharussrivichai C, Bunyakiat K (2009) Al2O3-supported alkali and alkali earth metal oxides for transesterification of palm kernel oil and coconut oil. Chem Eng J 145(3):468–474

189. Xie W, Liu Y, Chun H (2012) Biodiesel preparation from soybean oil by using a heterogeneous CaxMg2 − xO2 catalyst. Catal Lett 142(3):352–359

190. James OO, Maity S, Mesubi MA, Usman LA, Ajanaku KO, Siyanbola TO et al (2012) A review on conversion of triglycerides to on-specification diesel fuels without additional inputs. Int J Energ Res 36(6):691–702

191. Parida K, Mishra HK (1999) Catalytic ketonisation of acetic acid over modified zirconia: 1. Effect of alkali-metal cations as promoter. J Mol Catal A Chem 139(1):73–80

192. Bayahia H, Kozhevnikova EF, Kozhevnikov IV (2015) Ketonisation of carboxylic acids over Zn-Cr oxide in the gas phase. Appl Catal Environ 165:253–259

193. Iliopoulou EF (2010) Review of C-C coupling reactions in biomass exploitation processes. Curr Org Synth 7(6):587–598

194. Gaertner CA, Serrano-Ruiz JC, Braden DJ, Dumesic JA (2010) Ketonization reactions of carboxylic acids and esters over Ceria-Zirconia as biomass-upgrading processes. Ind Eng Chem Res 49(13):6027–6033

195. Aguado R, Olazar M, Jose MJS, Aguirre G, Bilbao J (2000) Pyrolysis of sawdust in a conical spouted bed reactor. Yields and product composition. Ind Eng Chem Res 39(6):1925–1933
196. Nie L, Resasco DE (2012) Improving carbon retention in biomass conversion by alkylation of phenolics with small oxygenates. Appl Catal A Gen 447:14–21
197. Zapata PA, Faria J, Ruiz MP, Resasco DE (2012) Condensation/hydrogenation of biomass-derived oxygenates in water/oil emulsions stabilized by nanohybrid catalysts. Top Catal 55(1–2):38–52
198. Gliński M, Kijeński J (2000) Decarboxylative coupling of heptanoic acid. Manganese, cerium and zirconium oxides as catalysts. Appl Catal Gen 190(1–2):87–91
199. Okumura K, Iwasawa Y (1996) Zirconium oxides dispersed on silica derived from Cp2ZrCl2, [(i-PrCp)2ZrH(μ-H)]2, and Zr(OEt)4 characterized by x-ray absorption fine structure and catalytic ketonization of acetic acid. J Catal 164(2):440–448
200. Gliński M, Kijeński J (2000) Catalytic ketonization of carboxylic acids synthesis of saturated and unsaturated ketones. React Kinet Catal L 69(1):123–128
201. Parida KM, Samal A, Das NN (1998) Catalytic ketonization of monocarboxylic acids over Indian Ocean manganese nodules. Appl Catal Gen 166(1):201–205
202. Randery SD, Warren JS, Dooley KM (2002) Cerium oxide-based catalysts for production of ketones by acid condensation. Appl Catal A Gen 226(1–2):265–280
203. Dooley KM, Bhat AK, Plaisance CP, Roy AD (2007) Ketones from acid condensation using supported CeO2 catalysts: effect of additives. Appl Catal A Gen 320:122–133
204. Nagashima O, Sato S, Takahashi R, Sodesawa T (2005) Ketonization of carboxylic acids over CeO2-based composite oxides. J Mol Catal A Chem 227(1–2):231–239
205. Pestman R, Koster RM, vanDuijne A, Pieterse JAZ, Ponec V (1997) Reactions of carboxylic acids on oxides 0.2. Bimolecular reaction of aliphatic acids to ketones. J Catal 168(2):265–272
206. Zaki MI, Hasan MA, Pasupulety L (2001) Surface reactions of acetone on Al2O3, TiO2, ZrO2, and CeO2: IR spectroscopic assessment of impacts of the surface acid-base properties. Langmuir 17(3):768–774
207. Zaki MI, Hasan MA, Al-Sagheer FA, Pasupulety L (2001) In situ FTIR spectra of pyridine adsorbed on SiO2-Al2O3, TiO2, ZrO2 and CeO2: general considerations for the identification of acid sites on surfaces of finely divided metal oxides. Colloid Surf A 190(3):261–274
208. Martin D, Duprez D (1997) Evaluation of the acid-base surface properties of several oxides and supported metal catalysts by means of model reactions. J Mol Catal A Chem 118(1):113–128
209. Jahangiri H, Osatiashtiani A, Bennett JA, Isaacs MA, Gu S, Lee AF et al (2018) Zirconia catalysed acetic acid ketonisation for pre-treatment of biomass fast pyrolysis vapours. Cat Sci Technol 8(4):1134–1141
210. Pham TN, Sooknoi T, Crossley SP, Resasco DE (2013) Ketonization of carboxylic acids: mechanisms, catalysts, and implications for biomass conversion. ACS Catal 3(11):2456–2473
211. Vervecken M, Servotte Y, Wydoodt M, Jacobs L, Martens JA, Jacobs PA (1986) Zeolite-induced selectivity in the conversion of the lower aliphatic carboxylic acids. In: Setton R (ed) chemical reactions in organic and inorganic constrained systems. Springer, Dordrecht, pp 95–114
212. Jahangiri H, Osatiashtiani A, Ouadi M, Hornung A, Lee AF, Wilson K (2019) Ga/HZSM-5 catalysed acetic acid ketonisation for upgrading of biomass pyrolysis vapours. Catalysts 9(10):841
213. Danon B, Marcotullio G, de Jong W (2014) Mechanistic and kinetic aspects of pentose dehydration towards furfural in aqueous media employing homogeneous catalysis. Green Chem 16(1):39–54
214. Zeitsch KJ (2000) Furfural production needs chemical innovation. Chem Innov 30(4):29–32
215. Panagiotopoulou P, Vlachos DG (2014) Liquid phase catalytic transfer hydrogenation of furfural over a Ru/C catalyst. Appl Catal A Gen 480:17–24
216. Dias AS, Pillinger M, Valente AA (2005) Dehydration of xylose into furfural over micro-mesoporous sulfonic acid catalysts. J Catal 229(2):414–423

217. Weingarten R, Cho J, Conner WC, Huber GW (2010) Kinetics of furfural production by dehydration of xylose in a biphasic reactor with microwave heating. Green Chem 12(8):1423–1429
218. de la Hoz A, Diaz-Ortiz A, Moreno A (2005) Microwaves in organic synthesis. Thermal and non-thermal microwave effects. Chem Soc Rev 34(2):164–178
219. Qi XH, Watanabe M, Aida TM, Smith RL (2008) Catalytic dehydration of fructose into 5-hydroxymethylfurfural by ion-exchange resin in mixed-aqueous system by microwave heating. Green Chem 10(7):799–805
220. Yan K, Wu GS, Lafleur T, Jarvis C (2014) Production, properties and catalytic hydrogenation of furfural to fuel additives and value-added chemicals. Renew Sustain Energy Rev 38:663–676
221. Montane D, Salvado J, Torras C, Farriol X (2002) High-temperature dilute-acid hydrolysis of olive stones for furfural production. Biomass Bioenergy 22(4):295–304
222. Vlachos DG, Caratzoulas S (2010) The roles of catalysis and reaction engineering in overcoming the energy and the environment crisis. Chem Eng Sci 65(1):18–29
223. Sako T, Sugeta T, Nakazawa N, Otake K, Sato M, Ishihara K et al (1995) High-pressure vapor-liquid and vapor-liquid-liquid equilibria for systems containing supercritical carbon-dioxide, water and furfural. Fluid Phase Equilibr 108(1–2):293–303
224. Xiong K, Wan WM, Chen JGG (2016) Reaction pathways of furfural, furfuryl alcohol and 2-methylfuran on Cu(111) and NiCu bimetallic surfaces. Surf Sci 652:91–97
225. Lange JP, van der Heide E, van Buijtenen J, Price R (2012) Furfural—a promising platform for lignocellulosic biofuels. ChemSusChem 5(1):150–166
226. Dong F, Zhu YL, Zheng HY, Zhu YF, Li XQ, Li YW (2015) Cr-free Cu-catalysts for the selective hydrogenation of biomass-derived furfural to 2-methylfuran: the synergistic effect of metal and acid sites. J Mol Catal A Chem 398:140–148
227. Ordomsky VV, Schouten JC, van der Schaaf J, Nijhuis TA (2013) Biphasic single-reactor process for dehydration of xylose and hydrogenation of produced furfural. Appl Catal A Gen 451:6–13
228. Srivastava S, Jadeja GC, Parikh J (2016) A versatile bi-metallic copper-cobalt catalyst for liquid phase hydrogenation of furfural to 2-methylfuran. RSC Adv 6(2):1649–1658
229. De S, Saha B, Luque R (2015) Hydrodeoxygenation processes: advances on catalytic transformations of biomass-derived platform chemicals into hydrocarbon fuels. Bioresour Technol 178:108–118
230. Ren H, Yu WT, Salciccioli M, Chen Y, Huang YL, Xiong K et al (2013) Selective hydrodeoxygenation of biomass-derived oxygenates to unsaturated hydrocarbons using molybdenum carbide catalysts. ChemSusChem 6(5):798–801
231. Cheng SY, Wei L, Julson J, Rabnawaz M (2017) Upgrading pyrolysis bio-oil through hydrodeoxygenation (HDO) using non-sulfided Fe-Co/SiO2 catalyst. Energ Conver Manage 150:331–342
232. Pourzolfaghar H, Abnisa F, Daud WMAW, Aroua MK (2018) Atmospheric hydrodeoxygenation of bio-oil oxygenated model compounds: a review. J Anal Appl Pyrolysis 133:117–127
233. Yang T, Shi L, Li R, Li B, Kai X (2019) Hydrodeoxygenation of crude bio-oil in situ in the bio-oil aqueous phase with addition of zero-valent aluminum. Fuel Process Technol 184:65–72
234. Muradov N (2017) Low to near-zero CO2 production of hydrogen from fossil fuels: status and perspectives. Int J Hydrogen Energy 42(20):14058–14088
235. Duan P, Savage PE (2011) Catalytic hydrotreatment of crude algal bio-oil in supercritical water. Appl Catal Environ 104(1):136–143
236. Gandarias I, Requies J, Arias PL, Armbruster U, Martin A (2012) Liquid-phase glycerol hydrogenolysis by formic acid over Ni-Cu/Al2O3 catalysts. J Catal 290:79–89
237. Chia M, Dumesic JA (2011) Liquid-phase catalytic transfer hydrogenation and cyclization of levulinic acid and its esters to gamma-valerolactone over metal oxide catalysts. Chem Commun 47(44):12233–12235

238. Jae J, Zheng WQ, Lobo RF, Vlachos DG (2013) Production of Dimethylfuran from Hydroxymethylfurfural through catalytic transfer hydrogenation with Ruthenium supported on carbon. ChemSusChem 6(7):1158–1162

239. Zheng H-Y, Zhu Y-L, Huang L, Zeng Z-Y, Wan H-J, Li Y-W (2008) Study on Cu–Mn–Si catalysts for synthesis of cyclohexanone and 2-methylfuran through the coupling process. Cat Com 9(3):342–348

240. Yang J, Zheng H-Y, Zhu Y-L, Zhao G-W, Zhang C-H, Teng B-T et al (2004) Effects of calcination temperature on performance of Cu–Zn–Al catalyst for synthesizing γ-butyrolactone and 2-methylfuran through the coupling of dehydrogenation and hydrogenation. Cat Com 5(9):505–510

241. Nakagawa Y, Tamura M, Tomishige K (2013) Catalytic reduction of biomass-derived furanic compounds with hydrogen. ACS Catal 3(12):2655–2668

242. Sitthisa S, Resasco DE (2011) Hydrodeoxygenation of Furfural over supported metal catalysts: a comparative study of Cu, Pd and Ni. Catal Lett 141(6):784–791

243. Chareonlimkun A, Champreda V, Shotipruk A, Laosiripojana N (2010) Catalytic conversion of sugarcane bagasse, rice husk and corncob in the presence of TiO2, ZrO2 and mixed-oxide TiO2–ZrO2 under hot compressed water (HCW) condition. Bioresour Technol 101(11):4179–4186

244. Boussarsar H, Roge B, Mathlouthi M (2009) Optimization of sugarcane bagasse conversion by hydrothermal treatment for the recovery of xylose. Bioresour Technol 100(24):6537–6542

245. Lichtenthaler FW, Peters S (2004) Carbohydrates as green raw materials for the chemical industry. C R Chim 7(2):65–90

246. Qazanfarzadeh Z, Kadivar M (2016) Properties of whey protein isolate nanocomposite films reinforced with nanocellulose isolated from oat husk. Int J Biol Macromol 91:1134–1140

247. Skiba EA, Budaeva VV, Baibakova OV, Zolotukhin VN, Sakovich GV (2017) Dilute nitric-acid pretreatment of oat hulls for ethanol production. Biochem Eng J 126:118–125

248. Lawford HG, Rousseau JD, Tolan JS (2001) Comparative ethanol productivities of different Zymomonas recombinants fermenting oat hull hydrolysate. Appl Biochem Biotechnol 91(3):133–146

249. Valdebenito F, Pereira M, Ciudad G, Azocar L, Briones R, Chinga-Carrasco G (2017) On the nanofibrillation of corn husks and oat hulls fibres. Ind Crop Prod 95:528–534

250. Varma AK, Mondal P (2017) Pyrolysis of sugarcane bagasse in semi batch reactor: effects of process parameters on product yields and characterization of products. Ind Crop Prod 95:704–717

251. Chauhan MK, Varun, Chaudhary S, Kumar S, Samar (2011) Life cycle assessment of sugar industry: a review. Renew Sustain Energy Rev 15(7):3445–3453

252. Jain A, Wei YZ, Tietje A (2016) Biochemical conversion of sugarcane bagasse into bioproducts. Biomass Bioenergy 93:227–242

253. Rocha GJD, Nascimento VM, Goncalves AR, Silva VFN, Martin C (2015) Influence of mixed sugarcane bagasse samples evaluated by elemental and physical-chemical composition. Ind Crop Prod 64:52–58

254. Chandel AK, Antunes FAF, Freitas WLC, da Silva SS (2013) Sequential acid-base pretreatment of sugarcane bagasse: a facile method for the sugars recovery after enzymatic hydrolysis. J Bioprocess Eng Biorefin 2(1):11–19

255. Maryana R, Oktaviani K, Tanifuji K, Ohi H (2014) Comparison between acid sulfite and soda-AQ delignification methods for effective bio-ethanol production from sugarcane bagasse and oil palm empty fruit bunch. In: 2014 Pan Pac Conf TAPPI; May 28; Taiwan, pp E46–E52

256. Ramos LP, da Silva L, Ballem AC, Pitarelo AP, Chiarello LM, Silveira MHL (2015) Enzymatic hydrolysis of steam-exploded sugarcane bagasse using high total solids and low enzyme loadings. Bioresour Technol 175:195–202

257. Al Arni S (2018) Comparison of slow and fast pyrolysis for converting biomass into fuel. Renew Energy 124:197–201

Biochemical Conversion of Residual Biomass: An Approach to Fuel Gas and Green Fertilizers

Carmen Mateescu and Andreea-Daniela Dima

Abstract Energy demand growth along with intensified global efforts to promote circular economy for solving environmental problems while obtaining high value-added products has increased the interest for valorization of the residual biomass that is abundantly generated in agriculture and various industries. This chapter is an overall contribution aiming to emphasize and clarify some theoretical and practical aspects on the biochemical conversion of biomass into fuel gases (biomethane and biohydrogen) and other valuable by-products. The residual biomass is very diverse, but the quality of the substrate and the biochemical technology, as well as the processing parameters, determine the type and composition of the conversion products. Hence, particular attention is given to substrate evaluation and pretreatment techniques for increasing the conversion yields and the process economic viability. The metabolic pathways of microbial processes and the technological parameters are analysed and discussed for both biomethane and biohydrogen. Some current and innovative methods of biogas upgrading with a focus on the market applications of the biochemical conversion to fuel gases are comprehensively approached. Also, the chapter presents an overview on the technological possibilities and economic benefits of using by-products as green fertilizers for agriculture, briefly mentioning some other ways for waste recovery to value-added products. In addition to analysing current achievements in this field of research, the chapter aims to identify gaps and bring to light some issues that need to be studied in greater depth so as to make the biochemical conversion processes of biomass feasible and widely applicable in industry.

Keywords Biomass · Waste · Biomethane · Biohydrogen · Fertilizers

C. Mateescu (✉)
National Institute for Research and Development in Electrical Engineering ICPE-CA, Bucharest, Romania
e-mail: carmen.mateescu@icpe-ca.ro

A.-D. Dima
University Politehnica of Bucharest, Bucharest, Romania

1 Introduction

Limited conventional fuel reserves, but also the increasing greenhouse gas emissions leading to extreme climatic phenomena, have urged the concerns of scientists and energy project developers around the world in implementing solutions for transition from fossil-based resources to zero-carbon renewable fuels [1]. A report released by the World Energy Council in 2019 stated that technological innovations, climate change and more tense geopolitics have become fundamental drivers to reshape the world of energy; thus, the use of sustainable bioenergy is expected to increase by one-third in 2040 from today's levels [2].

Worldwide, there is a steady increase in the interest of the public and private environment in developing projects aimed at capitalizing residual biomass for the production of green energy and value-added by-products [3]. Residual biomass, also named 'waste biomass', is addressed to biomass that is not produced for its direct use, for example, as energy source, but is a waste product generated in other agricultural or technological processes. Residual biomass may include landscape biomass (agricultural and forestry), animal manure, biodegradable fraction of municipal waste [4] and algal biomass remaining after oil extraction [5–7].

Using waste biomass as raw material for new technological processes has become a requirement much promoted by energy and environmental policies over the past decade within the concept of circular bioeconomy, offering important advantages for sustainability, such as no additional land required to produce biomass; waste reduction for new production chains, thus contributing to a closed-loop resource use; avoidance of GHG emissions from residual biomass if left to rot on the ground; etc. [3, 4].

There are several approaches used for biomass conversion to produce bioenergy, which may be classified into the following two major categories: thermochemical conversion (combustion for heat or electricity, pyrolysis to bio-oil and charcoal, catalytic liquefaction to marketable liquids and gasification to syngas) and biochemical conversion to produce biogas, biohydrogen, bioethanol and biodiesel [8, 9]. Regarding biochemical conversion, it includes three types of different processes, which are anaerobic digestion, alcoholic fermentation and photobiological reactions, all of them involving microorganisms or enzymes to transform biopolymers in gaseous or liquid biofuels [10]. Besides enzymes which are biological catalysts aimed to lower the activation energy for biochemical reactions, some researches have also proved that mineral catalysts such as zeolites added to the fermentation mass in anaerobic digestion processes can facilitate microbial fermentation and increase the biomass to biomethane conversion yields. More specifically, zeolites can help the anaerobic digestion processes by adsorbing ammonia and other toxicants in the system, thus shortening the duration of the lag phase of microbial growth and accelerating methane production [11, 12].

With attention focused exclusively on the biochemical conversion processes, this chapter aims to examine and discuss currently applied technologies and recent research trends for the residual biomass recovery to fuel gas (biomethane and

biohydrogen) and valuable by-products through biochemical processes catalysed by specific enzymes and microorganisms.

Hence, the main scope of the contribution is to provide insight into the theoretical and practical aspects on the effective biochemical conversion of various organic substrates via two different biochemical pathways: anaerobic digestion (AD) and dark fermentation (DF). Both biochemical routes are catalysed by enzymes and coenzymes which are responsible for the decomposition of organic compounds with complex structures to compounds with smaller molecules that generate fermentation gases. Anaerobic digestion and dark fermentation processes are very similar in terms of degradation steps, but each has its own specificity which makes biomass conversion switching towards biogas or biohydrogen. In this chapter, biomass biochemical conversion processes are presented and analysed, with emphasis on the operational and process parameters that have to be considered for effective and economically viable biotechnological conversion. Given that microbial processes generate both useful products to be used in various applications and some unwanted chemicals, including hydrogen sulphide, ammonia, siloxanes, volatile organic compounds, etc., which are corrosive or harmful, an important topic discussed in the chapter concerns the processes of gas stream cleaning and upgrading.

Green chemistry is an economic direction that has got increasing attention in recent years. By-products resulting from biochemical conversion processes of residual biomass are actually raw materials for many industries. Also, another important aim of this chapter is to bring attention to the main directions for the use of secondary products as organic fertilizing materials, as well as for the synthesis of intermediates for the chemical industry, composite and adsorbent materials, algal biomass growth for biofuel industry, etc. Finally, some gaps and issues that need to be prospected in depth are emphasized to make these processes economically and commercially viable. Further exploration on the biomass to biogas and biohydrogen processing techniques is needed to expand these technologies on a large scale and replace the available non-renewable energy resources that are exhausted at a much faster rate than they are generated.

2   Potential Substrates for Biochemical Conversion to Fuel Gas

Resources that are generally used as substrates in biochemical processes for energy production include energy crops, agro-industrial residues and by-products, lignocellulosic products, algae and other aquatic plants or organic-loaded wastewaters, such as municipal sewage sludge, residual waters from zootechnical industry and animal excreta, etc. [13]. On the other hand, the trend in energy production is increasingly focusing on waste recovery, which means a broader approach in energy production is emerging, which does no longer consider singular issues, but a combination of factors sourcing political, environmental, economic and social policies.

Some of the conventional substrates for energy production, particularly energy crops, have been the subject of controversies like the 'food-versus-fuel debate', discussing about the pressure that fuel crops pose on agricultural land use, which may have caused increased prices on edibles, feed and fibres [14]. Consequently, in 2018, the EU Parliament stepped in to settle the conflict by releasing a new directive which promoted the use of renewable sources for energy production. By different provisions, this directive reinforced the sustainability criteria of bioenergy which includes the indirect land use change caused by biofuel production from agricultural crops [15]. Research in this field is meant to develop technologies that provide the best opportunities for answering strategic requirements at local, regional and global levels, focusing on waste recovery strategies.

Moreover, according to a report released by the World Bank in 2018, the annual production of residues is assumed to rise by 70%, reaching 3.40 billion tonnes in 2050 [16], which is mainly influenced by expected rapid population growth around the world, from 7.7 billion at the end of 2019 to over 9.1 billion in 2050 [17, 18]. In other words, world population growth causes higher demand for edibles and other basic commodities, which will lead in turn to the amplification of agro-industrial activities [19] and to an alarming increase in the volume of agricultural residues and food industry waste and wastewaters. On the other side, the amount of municipal waste is expected to go up with increasing population density. Broadly speaking, the share of organic residuals in the amount of municipal waste is about 64%, but this could withstand important differences at regional level, depending on several features, such as geographical position and climate, standard of living, education, and local waste management policies [16]. Waste must be therefore managed in a sustainable way, with priority on recycling and advanced processing to obtain reusable products, as provided within a circular economy [20].

Waste biomass or organic residuals could be used as valuable renewable raw materials in the manufacturing of several products (biofuels, polymers and chemicals, building products, resins, enzymes, etc.). Unfortunately, only a low volume of organic waste is currently directed to become a feedstock in electricity generation processes or towards obtaining value-added products [19, 21], although conventional technologies have greatly improved and novel processes have also been developed [22]. Anaerobic digestion (AD) is one of the most promising waste management technologies, as it can provide both garbage sanitation and energy generation in the form of biogas. At present, biogas production units bring high economic benefits at industrial scale [23], promoting pollution reduction and local development. Not yet established extensively, dark fermentation (DF) is another waste-to-energy emerging process, used for biohydrogen production from substrates such as crop and farm residuals, industrial organic waste and wastewaters, sewage sludge, etc. [24].

Crop residues, which are primarily lignocellulosic materials, are among the most widespread biomass wastes. This type of vegetal waste is considered as plentiful, easily available resource, and many research activities have been directed towards increasing the possible use of lignocellulosic biomass in biomethane and biohydrogen production. Despite its abundance, lignocellulosic biomass, including some

agricultural waste, forestry residuals and energy crops, have a lower biodegradability compared to other sorts of biomass, explained by the high content of recalcitrant biopolymer structures in their composition. Progress is being made to enhance biodegradability of cellulose, hemicellulose and lignin structures in lingo-cellulosic biomass, but some efforts should still be done for their efficient conversion to fuel gas [25]. For instance, after crop harvesting, large quantities of residuals that are not adequate for animal feed can be biochemically converted to produce second-generation liquid biofuels, biomethane and biohydrogen, thus significantly contributing to social and environmental sustainability [22]. At present, about 5% of residues coming from the main agricultural crops are used for biogas production, but this share is assumed to increase to 25% by 2030 and to 50% by 2050 [26]. The range of suitable substrates for biogas production expands continuously as additional materials are tested for their biochemical methane potential and substrate pretreatment strategies are being developed. For example, Córdoba et al. fermented spent sawdust from mushroom cultivation and obtained a biogas potential of about 200 mL/gVS biogas, at a rough biomethane concentration of 70%, showing that although the value is not high compared to other feedstock materials, *Gymnopilus pampeanus* has the ability to improve the biodegradation of sawdust [27].

Huge quantities of residual biomass are also generated by the livestock industry. Studies have shown that the manure of about 25 billion animal units from farming worldwide, mainly referring to those from piggeries, dairy farms and poultry farms, could be collected and used to obtain substantial quantities of biomethane in anaerobic digestion processes. This could be translated by up to 370 billion m^3 fuel gas or 3800 TWh energy produced globally [26].

Food waste is another potential substrate for fuel gas production. It is permanently generated in the domestic and industrial sectors, being commonly unavoidable, responsible for financial loss and requiring immediate disposal. The World Biogas Association estimates that one-third of the food quantity being produced annually becomes unsuitable for human consumption or for animal feeding and it is directly dumped to landfill [28]. Due to its high humidity (70–90%) and the wide organic fraction content, food waste is considered a suitable substrate for biomethane or biohydrogen production in fermentation processes which successfully serve for energy and nutrient recovery. Thereby, one tonne of wet food waste used as substrate in anaerobic digestion could generate 150–180 m^3 biogas, while the total amount of residuals coming from the food industry would provide up to 100 billion m^3 pure biomethane or 1100 TWh energy in the form of heat and electricity [26]. Moreover, several strategies for increasing biomethane production from biodegradable municipal wastes have been developed in numerous experimental studies, either by optimization of process factors or by using additives, such as Fe_3O_4 nanoparticles or urea-capped Fe_3O_4 nanoparticles [29, 30]. Research results are encouraging since optimal fermentation conditions could provide efficient bioconversion of waste, meaning that higher biomethane production, better nutrient recovery and shorter fermentation durations would be obtained.

Moreover, the annual volume of sewage sludge is expected to increase in line with the demographic growth and level of urbanization [31]. A proper stabilization

of sewage sludge may be done through biochemical conversion in anaerobic digesters, by which the organic component diminishes its biological activity, pathogens and weed seeds, as well as its unpleasant odour. About 300 TWh energy could be obtained if wastewater treatment plants would collect the sewage sludge of each household and couple the purification stages to fermentative processes. Additionally, algae seem to gain increasing interest for valorization in biofuel production; taking into account their high productivities and implementing economically viable technologies using algal biomass are a burning issue [32]. Macroalgae and microalgae are considered renewable and inexpensive feedstock for third-generation biofuels [7, 33].

Biogas-obtaining substrates have various advantages with minimum preliminary processing requirements if recovered by anaerobic digestion (high moisture, high buffering capacity, rich microbial flora) [34]. The biochemical methane potential (BMP) of some common substrates for anaerobic digestion is presented in Table 1.

Biohydrogen may be theoretically produced by dark fermentation from any organic substrate that is rich in proteins, fats and carbohydrates. Nevertheless, for biohydrogen fermentative processes, carbohydrate-rich organic matter has proved to give the largest production. Energy crops rich in sugars (e.g. sugar beet and cane) and grains that are rich in starch (e.g. wheat and corn) are some of the most suitable feedstocks for biohydrogen production. However, exploiting crops for hydrogen production falls in the same food-versus-fuel controversy as in the case of biogas production. In this view, using residues from harvesting and processing of carbohydrate-rich crops not intended for food industry is a better solution, more economically viable and environmentally sustainable. Carbohydrates from waste materials are thus key substrates for dark fermentation [34]. Simple sugars provide short fermentation time, while for more complex sugars, pretreatment strategies for hydrolysis of carbohydrate polymers (cellulose and hemicellulose, strongly bonded to lignin) into monosaccharides are required. Substrates rich in complex sugars have shown encouraging results for biohydrogen production, making agriculture

Table 1 BMP of several organic materials

Substrate	BMP (mL CH_4/g vs. substrate)	Reference
Cow manure	530	Lee et al. [35]
Biological sludge and sewage sludge	212–221	Nielfa et al. [36]
Sunflower oil cake	227	Raposo et al. [37]
Rice straw	300–380	Lei et al. [38] and Zhang and Zhang [39]
Potato waste	148–237	Achinas et al. [40] and Dima et al. [41]
Waste glycerol+glucose	100–300[a]	Sawasdee et al. [42]
Algal biomass	188–335	Mussgnug et al. [43]

[a]Results expressed in mL CH_4/g COD substrate

Table 2 Biochemical hydrogen potential (BHP) of several organic materials

Substrate	BHP (mL H_2/g vs. substrate)	Reference
Glucose	200	Riazi and Chiaramonti [45]
Sucrose	58.9–157.1[a]	Dellosso Penteado et al. [46] and Pecorini et al. [47]
Food waste	25.0–101.6	Alibardi and Cossu [48] and De Gioannis [49]
Organic waste mixtures	78–135	Alibardi and Cossu [50]
Corn stalk waste with acidification	149.7	Zhang et al. [51]
Wheat straw	68.1	Fan et al. [52]
Apple and potato processing wastewaters	0.7–2.8[b]	Van Ginkel et al. [53]

[a]Results originally expressed in moles H_2/moles substrate and recalculated in mL H_2/g substrate
[b]Results expressed in L H_2/L wastewater

and forestry residuals a zero cost potential feedstock for hydrogen production, although careful calculation of energy input required along with the pretreatment method should be made [44]. Crude glycerol, which is a co-product in the production process of biodiesel, could also be used to obtain hydrogen with a potential growth of biodiesel production economics.

Other complex waste and wastewaters, including solid residuals from food industry and agro-based industries; domestic organic wastes; wastewaters from the juice, dairy and meat industries; oil-based industry residuals, etc., have also been studied in fermentative hydrogen production processes. These types of feedstock have lower conversion efficiencies compared to carbohydrate-based waste since they contain proteins and fats [34]. Table 2 shows some results on biohydrogen production in batch tests using different types of feedstock.

In both biohydrogen and biogas production processes, the quality of the substrate has a great impact upon the process performance. Various other factors such as feedstock pretreatment strategies, bacterial consortia, technological parameters, etc. may influence the results regarding fuel gas outcome; therefore, plant operators should correlate the substrate selection with the specific characteristics of the technology to be used.

3 Overview on Pretreatment Strategies to Improve Conversion Yields

Biochemical conversion of complex biomass to fuel gas typically encounters difficulties in breaking down the rigid chains of biopolymers which are hard to access or even inaccessible to microorganisms if not made available by pretreatments [54]. In anaerobic digestion processes with biogas production, it has been found that

hydrolysis of biopolymers is a rate-determining step. Some studies have shown that methanogenesis can also be considered a process stage that may control the decomposition rate at certain ratios between the microorganisms responsible for hydrolysis and methanogenesis, respectively [55].

Lignocellulosic biomass that represents a huge amount of renewable bioresources available worldwide contains much lignin which is the biopolymer responsible for impairing cellulose and hemicellulose hydrolysis [56, 57]. Lignin is embedding cellulose and hemicellulose in the cell to sustain its structure, but in microbial decomposition processes lignin blocks the microbial attack in the hydrolysis stage [58]. A very eloquent schematic representation of the biopolymers chains that make up the structure of lignocellulosic biomass is made by Hernández-Beltrán et al. and adapted in Fig. 1.

Algal biomass is currently considered a very promising feedstock for food technology and pharmaceuticals, but increasingly special attention is granted for the algal-based renewable fuel production [60]. Microalgal cell walls are composed of macromolecules with low biodegradability or low bioavailability that are hardly accessible to fermentative microorganisms. Macroalgae cell walls are composed of proteins and carbohydrates with complex structures that have high chemical and mechanical resistance, which impede the access of bacteria for the biochemical decay of the biopolymers [61].

Pretreatment techniques are mandatory biorefining steps for lignocellulosic and algal biomass solubilization [62]. Pretreatment helps to reduce the crystallinity of cellulose, increases its porosity and improves the liquefaction, thus facilitating the biopolymer release [63]. It was demonstrated that biomass pretreatment may enhance the hydrolysis rate up to tenfold [64]. Also, pretreatment has great benefit
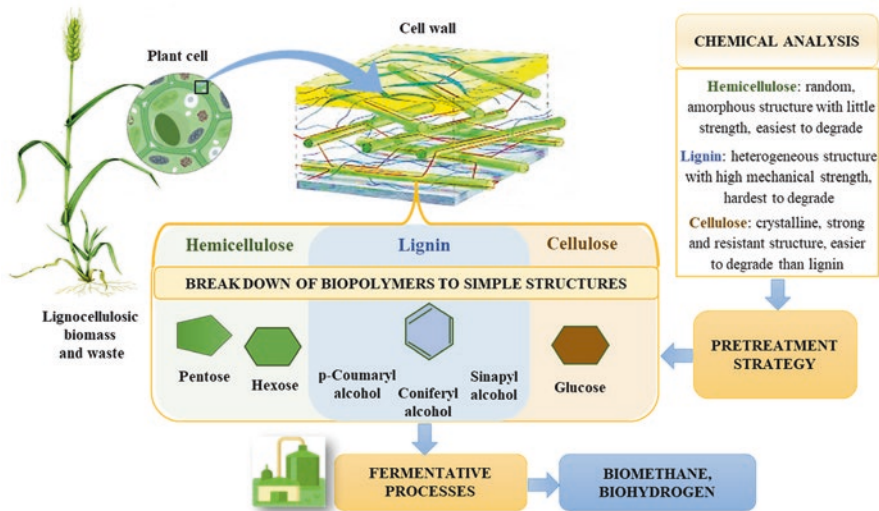
Fig. 1 Biopolymers in lignocellulosic materials and process steps (adapted from [59])

for increasing the efficiency of the bioconversion process; research and development may diminish the overall process cost [65]. In deciding for a pretreatment step, it is important that it can justify its impact on the residual biomass processing cost, capital costs, biomass feedstock costs and operating costs [56]. The pretreatment method should be selective, efficient but also economical so as not to exceed 40% of the overall cost of processing [66]. Prior to the biomass pretreatment step, the mechanical processing and preconditioning like shredding, grinding, chipping, blending, etc. should be avoided if possible, since this would add significant costs to the whole biorefining process [67].

In the last decade, extensive research has been undertaken throughout the world for developing various reliable and cost-effective pretreatment techniques for degradation of lignin from residual biomass and for improving process efficiency in algal biomass recovery to produce renewable liquid and gaseous fuels. In scientific papers, numerous classifications of the pretreatment techniques have been presented, including mechanical, thermal, chemical and biological techniques and combinations thereof such as physico-chemical, bio-physico-chemical, mecano-chemical and thermo-chemical, addressed and adapted to different types of substrates [58]. However, all these pretreatment methods may be broadly grouped into three classes—physical, chemical and biological methods—with the mention that the physical pretreatment techniques are the most diverse, including mechanical, thermal, electrical pretreatment, irradiation, etc. [68]. Figure 2 shows a centralization of the biomass pretreatment methods for anaerobic fermentation processes with the production of fuel gas and fermented residual material.

In the industrial practice, some combinations of the mentioned techniques have become more efficient and advantageous options in terms of bioconversion efficiency and costs throughout the bioprocessing chain. Even a combination of three pretreatments (e.g. mechanical, thermal and chemical pretreatment) can be efficient while contributes to the cost optimization and to the improvement of the energy balance of the technological pretreatment stage [69].

Physical pretreatment aims at reducing the biomass particle size by applying an external physical force and may include various techniques such as mechanical beating, sonication, milling, cavitation, extruding, microwave irradiation, deflaking, dispersing, refining, etc. [70]. The physical pretreatment methods are fairly eco-friendly, and in general they do not produce toxic compounds, but the major disadvantage is that they are high-energy consumption options [71].

Chemical pretreatments (acidic, alkaline, oxidative, ionic liquids, organosolv process, deep eutectic solvents, etc.) result in the disruption of the inter- and intra-molecular forces and chemical bonds that hold together the biomass components [58, 71]. Although chemical pretreatment methods have proven effective in accelerating the hydrolysis step, they are less applied since they may increase the risk of inhibition of microbial activity due to the effect of some compounds with toxic effect. In addition, chemical pretreatment often generates environmentally harmful chemicals, such as aldehydes, phenolic acids, furfural, etc. [64, 72]. Moreover, chemical treatment can result in losses of organic matter causing decrease in the

BIOMASS PRETREATMENT METHODS		
PHYSICAL PRETREATMENT	**CHEMICAL PRETREATMENT**	**BIOLOGICAL PRETREATMENT**

• Mechanical
  ○ Milling
  ○ Grinding
  ○ Chipping
  ○ Extrusion
• Thermal
  ○ Hydrothermal
  ○ Steam explosion
  ○ Liquid hot water (LHW)
• Irradiation
  ○ Microwave irradiation
  ○ Ultrasonication
  ○ γ-irradiation
• High voltage pulse discharge
	• Acid treatment
	• Alkaline treatment
	• Mixed treatment (acid for hemicellulose, followed by alkali for lignin removal)
	• Organosolv
	• Ionic liquids
	• Deep eutectic solvents
	• Alkaline hydrogen peroxide
	• Ammonia fiber explosion (AFEX)
	• Supercritical CO2 explosion
		• Microbial pretreatment using bacterial strains isolated from soil, fish gut, rumen fluid etc.
		• Enzymatic pretreatment involving enzymes produced by fungi and bacteria (such as glucanases, cellobiase, xylanases, pectinase, laccases, manganese peroxidases, protease etc.)

Fig. 2 Pretreatment methods to enhance biomass conversion to fuel gas

biogas potential of the biomass substrate. For all these reasons, chemical pretreatment is a less popular option [73].

While the conventional physical and chemical pretreatment methods require expensive materials and devices and imply a high energy consumption, the biological pretreatments are less energy consuming and less polluting and have low disposal costs. They involve microorganisms with cellulolytic and hemicellulolytic abilities which contain degrading enzymes and produce the biomass biopolymer decomposition [64]. Biological enzymatic pretreatment methods operate with mild conditions, and even if these methods lead to a lower methane yield in anaerobic digesters compared to the thermal methods, they have lower energy requirements [74]. In recent years, biological pretreatment methods have become increasingly used and common due to many advantages compared to non-biological methods, mainly related to an enhanced total biogas and methane yield. However, the potential of these techniques is far from being sufficiently explored and exploited [75]. The effectiveness of the biological pretreatment methods is negatively affected by the microbial growth rate which is fairly slow [76].

It is unanimously accepted that each pretreatment option has its specific advantages and disadvantages, but a cost-effective pretreatment method that should be also environmentally friendly to completely decompose the recalcitrant compounds from biomass for fuel gases and other value-added products is not yet decided.

Furthermore, the mechanisms of the processes in each technique are not yet well discovered so that an optimization of the operational and technological conditions is possible [71]. Hence, further research for the development of advanced residual biomass pretreatment technologies with adequate reaction mechanism control, also fitted to the particularities of various biomass and for minimal costs, are still needed [65].

4   Biochemical Routes and Metabolic Pathways

Residual biomass generated abundantly from numerous economic sectors is a very valuable resource through the organics content that can be recovered by bioconversion into fuel gases and a mineralized product much attractive for crop eco-fertilization. Anaerobic fermentative bioprocesses such as anaerobic digestion with biomethane generation and dark fermentation with biohydrogen production have attracted increased interest in the research environment in the current context of the need to replace conventional fuels with green fuels produced mainly from municipal, agro-industrial wastes and crop residuals [77].

The biological methanation involves methanogens that use carbon dioxide, hydrogen and other simple precursors (acetate, methylamine, formate, etc.) resulted as metabolism products from biochemical decomposition of complex biopolymers, followed by the conversion of simple molecules into methane and other gases [78]. A schematic representation of degradation steps involved in fermentative biomass breakdown for biogas and biohydrogen production by anaerobic digestion and dark fermentation respectively is shown in Fig. 3.

Besides biomethane that has been largely exploited, biohydrogen produced from carbohydrate-rich substrates through biological processes using microorganisms is believed to be another key energy carrier for the future [79].

Anaerobic conversion of the organics-loaded substrate to produce fuel gases takes place on very diverse and complex biochemical pathways, specific to microbial metabolism, involving a wide spectrum of fermentative microbial species (bacteria and fungi) through the enzymes they produce. The various microbial species require specific environment conditions in terms of acidity, temperature and nutrient concentrations that would ensure optimum growth [80].

Under metabolic interaction the fermentative microorganisms work together to decompose the organic matter to the final metabolic products.

The full mechanism of methanogenesis is particularly complex, as some aspects of biochemical pathways have not been elucidated so far. The biochemical processes go successively through the following four biochemical transformation steps: hydrolysis of complex biopolymers; acidogenesis to organic acids, aldehydes and alcohols; acetogenesis involving the formation of acetate, CO_2 and H_2; and methanogenesis which is the final stage of conversion having methane as product of interest, along with other gases [90, 81].
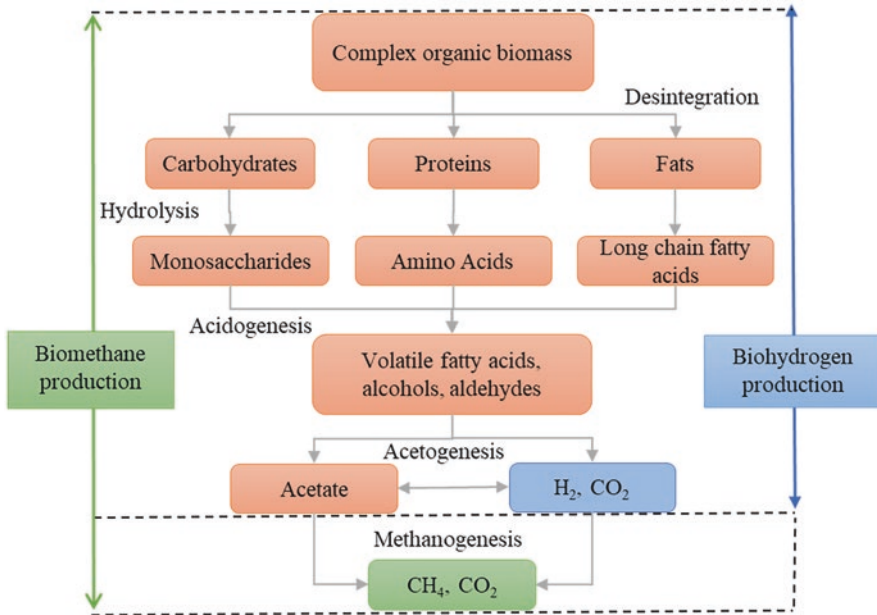
Fig. 3 Biodegradation steps for biomass breakdown to biogas and biohydrogen

Hydrolysis is a slow step that limits the speed of the overall process, when enzymes (exo-enzymes) secreted by groups of aerobic or optionally anaerobic microorganisms attack the complex molecules of the organic matter (cellulose, starch, pectin, hemicelluloses, proteins and fats) and convert them into soluble compounds with simpler molecules (cellobiose, sucrose, maltose, xylobiose, fatty acids, amino acids and peptides, nitrogenous bases, etc.) [82]. The hydrolytic microorganisms are more resistant than other species; they can easily adapt to different acidities of the environment and cope much better with sharp variations in environmental conditions, but they are also not very sensitive to various harmful compounds from the fermentation medium [83].

Acidogenesis, in which hydrolysis products are transformed into simple organic acids (formic, acetic, propionic, butyric, valerianic, lactic, malic, etc.), alcohols (methyl, ethyl, propyl, butanediol, etc.) and numerous gases (carbon dioxide, hydrogen, ammonia, hydrogen sulphide). Acidogenesis runs much faster than the other anaerobic digestion stages, but the accumulation of fatty acids in the fermentation slurry is considered one of the major causes responsible for the failure of the digester before the methane production start [54, 84].

Acetogenesis, where fatty acids are converted into acetate, hydrogen, bicarbonates, formic acid and methanol. During acetogenesis, hydrogen is also produced, but it is rapidly consumed by hydrogenotrophic methanogens [54, 85]. Acetate may be produced also in acidogenesis stage from glycerol and from long-chain fatty acid oxidation [84].

Methanogenesis, the final stage of the anaerobic digestion process, where ca. 2/3 of the biomethane is produced by acetoclastic methanogenesis starting from acetic acid but the remaining 1/3 of the biomethane is produced from hydrogen and CO_2 by hydrogenotrophic methanogenesis. Biochemical pathway studies showed that methanogenesis from methanol, methylamines and formate also occurs [86]. Some other gases besides methane and carbon dioxide, which resulted during the second stage of the fermentation process (hydrogen sulphide and ammonia), may be found in the biogas mixture. It was proved that methanogenic species represent microbial groups most sensitive to the environment conditions (acidity, temperature, inhibitors) in anaerobic digestion. Also, they have a significantly slower regeneration time of 5–16 days compared to acidogenic bacteria which have a regeneration time of less than 36 h [87]. The main chemical reactions describing the biochemical steps and the enzymes involved in the metabolic reactions are briefly presented in Table 3.

In anaerobic fermentative processes for biomethane, various microbial consortiums must co-exist in the fermentation mass in a proper biochemical balance, although they disturb each other in terms of optimal growth conditions. Methanogens may become inactive or even die if the environment conditions in the fermentation reactor are not appropriate or constant. When any process unbalance occurs, the acidogenic bacteria start growing fast and make the volatile fatty acids increase sharply, automatically leading to slowing down or even stopping biogas production [91].

Due to the complex and interactive dynamics of the different microbial groups in anaerobic digestion, with a disproportionate quantity of various microbial groups that have a direct influence on the overall process reaction rate, the anaerobic digestion for producing biomethane is a very much unstable biochemical process, with the risk of process failure in case of any slight variations of the environmental parameters [81].

Hydrogen may be regarded as one of the most interesting fuels of the future since hydrogen combustion is an eco-friendly energy generation process as it releases only water vapours. Currently, hydrogen is produced largely by chemical processes from natural gases, hydrocarbons or coal and also by water electrolysis, but only a small part is generated from biomass, as seen in Fig. 4. The main beneficiaries of hydrogen synthesis are chemical industries, mostly for producing fertilizers and petroleum derivatives [34].

However, using non-renewable sources to obtain hydrogen is not a very attractive option in terms of environmental impact; sustainability of hydrogen production and storage still remains an important challenge. As a cleaner solution, biochemical hydrogen synthesis has been adopted to minimize CO_2 emissions. Biological processes for producing hydrogen are less energy consuming and have a great potential to be implemented as a more advantageous alternative to regular methods. Moreover, they could use low value feedstock, such as waste biomass and other industrial or municipal organic residuals [24].

Biological pathways to produce biohydrogen can use both autotrophic and heterotrophic microorganisms. The process is catalysed by anaerobic bacteria and/or algae, and it runs in aqueous environment at normal temperature and pressure

Table 3 Biochemical reactions in anaerobic fermentative processes

Process stage	Responsible enzymes	Chemical reactions and metabolic products	Reference
Hydrolysis	Esterases, glycosidases, cellulases, β-glucosidase, β-xylanase, β-xylosidase, β-mannosidase, α-galactosidase, peptidases, lipase, etc.	$(C_6H_{10}O_5)n + nH_2O \rightarrow n(C_6H_{12}O_6)$	Abbasi et al. [88], Bharathiraja et al. [81], Deepanraj et al. [89], Sikora et al. [90] and Van et al. [83]
Acidogenesis	Glucosidases, dehydrogenase, dehydratases, decarboxylase, glycine reductase, acetate kinase	$n(C_6H_{12}O_6) \rightarrow 3nCH_3COOH$ $C_6H_{12}O_6 + 2H_2O \rightarrow 2CH_3COOH + 4H_2 + CO_2$ $C_6H_{12}O_6 + 2H_2 \rightarrow 2CH_3CH_2COOH + 2H_2O$ $C_6H_{12}O_6 \rightarrow CH_3CH_2CH_2COOH + 2H_2 + 2CO_2$ $C_6H_{12}O_6 \rightarrow 2CH_3CH_2OH + 2CO_2$ $C_6H_{12}O_6 \rightarrow 2CH_3CHOHCOOH$	Abbasi et al. [88], Deepanraj et al. [89], Sikora et al. [90] and Van et al. [83]
Acetogenesis	Decarboxylase, dehydrogenase/acetyl-CoA synthase, acetate kinase, oxidoreductase, alcohol dehydrogenase, etc.	$CH_3CH_2OH + H_2O \rightarrow CH_3COOH + 2H_2$ $2CH_3CH_2OH + 2CO_2 \rightarrow CH_4 + 2CH_3COOH$ $CH_3CH_2COOH + 2H_2O \rightarrow CH_3COOH + 3H_2 + CO_2$ $CH_3CH_2CH_2COOH + 2H_2O \rightarrow 2CH_3COOH + 2H_2$ $CH_3CHOHCOOH + H_2O \rightarrow CH_3COOH + CO_2 + 2H_2$ $2CO_2 + 4H_2 \rightarrow CH_3COOH + 2H_2O$	Abbasi et al. [88], Deepanraj et al. [89], Sikora et al. [90] and Van et al. [83]
Methanogenesis	Dehydrogenase, methyl-reductase, methyl-transferase, acetate kinase, etc.	$CH_3COOH \rightarrow CH_4 + CO_2$ $CO_2 + 4H_2 \rightarrow CH_4 + 2H_2O$	Abbasi et al. [88], Deepanraj et al. [89], Sikora et al. [90], Van et al. [83]
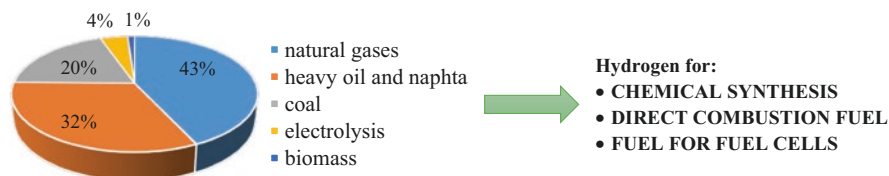
Fig. 4 Sources of hydrogen and main applications

conditions. At sites where large amounts of residual biomass are available, small-scale installations for hydrogen production are efficient solutions for waste treatment, while eliminating transportation costs associated to their disposal [24, 92]. Conversion processes could be though classified in various ways, depending on particularities, but the two major options for producing biohydrogen are the light-independent (in darkness) and the light-dependent processes. The main processes by which biohydrogen can be biochemically generated are shown in Fig. 4. All these biological pathways are alternative options for producing renewable fuel gas, and their development could lead to important benefits in the renewable energy production landscape.

Among biochemical conversion processes to biohydrogen, dark fermentation is extensively used for various organic waste and algal biomass recovery. Given its higher production rates and with the advantage to possibly treat large amounts of organic wastes, dark fermentation is the most promising and the most studied technology for hydrogen gas production [93].

In dark fermentation that takes place in anoxic conditions, biohydrogen is generated as a metabolic product from the activity of heterotrophic anaerobic bacteria whose growth implies oxidative degradation of the organic substrates. Figure 1 shows schematically the pathways of biomass conversion into biohydrogen by dark fermentation. There is a strong similarity between the stages of anaerobic digestion and dark fermentation as both are anaerobic fermentation processes. Dark fermentation is related to anaerobic digestion, with the mention that the common process stages are limited to hydrolysis, acidogenesis and acetogenesis. After these stages, the biochemical processes of producing biomethane, respectively biohydrogen, are conducted to different pathways; differences that induce the shift of biochemical reactions towards the production of either biomethane or biohydrogen lay in the operating conditions. In dark fermentation, the growth of methanogens must be inhibited, and several strategies as operating at low hydraulic retention time or at pH lower than 6.5 could be employed, as well as the inoculum pretreatment or use of selected bacteria strains, etc. [94].

Degradation products from substrate decay ensure the metabolic energy required for bacterial growth, as well as the necessary building blocks. During this process, electrons are generated and tend to be protonated for fulfilling the electrical stability of the environment; therefore, molecular hydrogen is formed.

Depending on the temperature regime, different fermentative microorganisms (e.g. *Enterobacter* sp., *Clostridium* sp.) participate in the biohydrogen production.

Other microbial species also produce hydrogen but on low amounts that are considered unsuitable for high-scale dark fermentation units (*Vibrionaceae* sp., *Veillonellaceae* sp., etc.). As seen in Fig. 5, glucose was taken as example for carbohydrate compounds. By strictly anaerobic bacterial fermentation, 4 moles of biohydrogen are generated by 1 mole of glucose in processes where the acetic acid is the end-product. In case of butyrate as end-product, 2 additional moles of biohydrogen are generated by other bacteria species. Fermentation of carbohydrates leads mainly to acetic and butyric acids in addition to biohydrogen [95].

Besides this theoretical potential, in practice, the fermentation pathways, substrate type and end-products are significantly influencing the hydrogen production; therefore, the process parameters involved in the metabolic balance must be strictly monitored and adjusted. High yields of biohydrogen can be obtained if residual biomass is rich in sugars; this type of biomass is the most recommended organic substrate for dark fermentation; therefore, the process viability can be improved if

Biohydrogen (H_2) production pathways

Biophotolysis of water
a) Direct biophotolysis (by green algae)
$$2H_2O + \text{light energy} \rightarrow 2H_2 + O_2$$
b) Indirect biophotolysis (by cyanobacteria)
$$12H_2O + 6CO_2 + \text{light energy} \rightarrow C_6H_{12}O_6 + 6O_2 + 6H_2O \text{ and}$$
$$C_6H_{12}O_6 + 12H_2O + \text{light energy} \rightarrow 12H_2 + 6CO_2 + 6H_2O$$

Photodecomposition of organic compounds (by photosynthetic bacteria)
$$CH_3COOH + 2H_2O + \text{light energy} \rightarrow 4H_2 + 2CO_2$$

Dark fermentation of organic compounds
$$C_6H_{12}O_6 + 2H_2O \rightarrow 2CH_3COOH + 2CO_2 + 4H_2$$
$$C_6H_{12}O_6 + 2H_2O \rightarrow CH_3CH_2CH_2COOH + 2CO_2 + 2H_2$$

Hybrid systems
a) Use of fermentative and photosynthetic bacteria
Stage 1. Dark fermentation (facultative anaerobes)
$$C_6H_{12}O6 + 2H_2O \rightarrow 2CH_3COOH + 2CO_2 + 4H_2$$
Stage 2. Photo-fermentation (photosynthetic bacteria)
$$2CH_3COOH + 4H_2O \rightarrow 8H_2 + 4CO_2$$
b) Bioelectrochemical bioreactor assisted conversion
$$C_6H_{12}O_6 + 2H_2O \rightarrow 4H_2 + 2CO_2 + 2CH_3COOH$$
Anode: $CH_3COOH + 2H_2O \rightarrow 2CO_2 + 8e^- + 8H^+$
Cathode: $8H^+ + 8e^- \rightarrow 4H_2$

Fig. 5 Hydrogen production biochemical pathways (adapted after [24, 92])

available, inexpensive, high-carbohydrate content and easily biodegradable fermentation materials are used [96].

Apart from dark fermentation, some other biochemical processes for biomass-to-biohydrogen conversion are used at smaller extent, as shown in Fig. 5. Biophotolysis of water is a technique in which green algae and cyanobacteria decompose water into hydrogen and oxygen. Within the direct biophotolysis, H_2-producing green algae generate hydrogen gas mostly with the aid of hydrogenase enzyme (e.g. *Chlamydomonas reinhardtii*, *Platymonas subcordiformis*, *Chlorella fusca*, etc.), under anaerobic conditions. But there are also some other types of algae (e.g. *Dunaliella salina*) that do not use hydrogenase enzyme for biophotolysis [97]. By biophotolysis, cyanobacteria, which are photoautotrophic microorganisms and contain photosynthetic pigments, use hydrogenase enzyme as well as nitrogenase enzyme to produce biohydrogen. Some examples of such cyanophytes include *Calothrix* sp., *Oscillatoria* sp., *Anabaena* sp., etc., from which *Anabaena variabilis* has recently got increased attention due to its high hydrogen production potential.

Under nitrogen-deficient conditions, biohydrogen is produced by photosynthetic bacteria from reduced organic acids, catalysed by nitrogenase enzyme, and using light energy. The potential of photoheterotrophic bacteria to use light energy in decomposing organic compounds for hydrogen production has also been investigated [34].

In hybrid systems using fermentative and photosynthetic bacteria, the anaerobic fermentation of the substrate produces low molecular weight intermediates that are then submitted to photosynthetic bacterial attack in a photo-bioreactor. In the case of glucose, after the first stage of the process (dark fermentation), the metabolite product of the bacteria is acetic acid which is further reacted to carbon dioxide and hydrogen. In total, 12 moles of biohydrogen are theoretically expected, as seen in Fig. 5—Hybrid systems (a).

Bioelectrochemical bioreactor-assisted conversion is another type of hybrid system in which microbial fuel cells generate electrons and protons during organic matter decomposition by bacteria. The electrolyte carries the protons towards the cathode, while electrons travel towards the cathode via a circuit, generating electrical current, and oxygen reacts to electrons and protons forming reduced compounds. In a bioelectrochemical microbial reactor, in order to decompose acetate, a theoretical voltage of 0.11 V was applied to eliminate oxygen and evolve hydrogen. Even though the real necessary voltage was found higher (0.25 V) to counter system resistance, this voltage is significantly lower than what is required for water electrolysis with hydrogen production in alkaline media (1.8–2 V) [92, 98].

5   Conversion Technological Parameters

The proper running of the fuel gas production processes in both anaerobic digestion and dark fermentation processes relies on the system capability to prove suitable environmental conditions for specific microbial communities' growth. This is a very

important aspect as major disturbances in the microbial equilibria generally lead to ceased gas production and consequently to important financial loses for industrial plants. There are various factors affecting the performance of biomethane and biohydrogen obtaining processes, but most commonly, they are classified as related either to the fermentation substrate characteristics or to process/operational conditions. Figure 6 shows the factors with major influence on anaerobic digestion and dark fermentation processes.

Metabolic pathways of anaerobic digestion and dark fermentation are very similar processes in terms of degradation steps, but each has its own specificity which makes biomass conversion switching towards biogas or biohydrogen. Hence, a comparative discussion of optimal factors in anaerobic digestion and dark fermentation is made below.

Among the requisite characteristics of the organic substrate for obtaining high biomethane yields in the anaerobic digestion processes, the proper carbon-to-nitrogen (C/N) ratio of the feedstock must be carefully controlled. A ratio from 20 to 30 is generally considered optimal, as the consumption of organic carbon by bacteria is much faster than that of nitrogen. On the other hand, good results have also been obtained for other C/N ratios, associated to the biodegradability of the carbon source, which make substrate biodegradability another important characteristic of the feedstock [25]. As for dark fermentation to produce biohydrogen, organic matter with C/N ratio higher than 30 has been associated with increased production [25]. Also, in both processes, proper gas yields were observed when good-quality inoculum with high specific bacteria load was used [47, 91]. Moreover, the inoculum-to-substrate ratio adjustment is essential for process kinetics optimization taking into consideration the nature of both substrate and inoculum [99].

The buffering capacity of the environment, as sum of buffer capacities of the feedstock materials and inoculum, should be also carefully adjusted for the deed that degradation reactions during the fermentation result in different acidity species and subsequently to a drop in pH values or very basic fermentation mass. Drastic changes in the pH lead to unwanted degradation products and poor gas production yields. For example, lignocellulosic materials are characterized by high carbon-to-nitrogen ratios and low buffering capacities, unlike animal manure or sewage sludge which have in reverse low C/N ratios and high buffer capacities. For a good conversion to fuel gas, mixtures of several feedstock materials to balance the physico-chemical properties of substrate are recommended [100].

SUBSTRATE CHARACTERISTICS

- C/N ratio
- Inoculum type
- Buffering capacity
- Nutrients
- Inhibitors

PROCESS PARAMETERS

- Temperature
- pH
- Organic loading
- Fermentation time
- Mixing
- Pressure and aeration

Fig. 6 Factors affecting biomass conversion into fuel gas in fermentative processes

Employed to adjust the properties of the substrate and fulfil the requirements of an efficient bioconversion in anaerobic digestion processes, co-digestion of organic materials has also proven a good strategy. Co-digestion can enhance the digester's performance by its influence on the cumulative biogas/biomethane production, lag phase time length and production rate.

Some inhibitions may occur in the fermentative processes due to unappropriate nutrients necessary for metabolic growth of useful microflora. For instance, Fe, Ni and Co are essential nutrients for high conversion of acetate into methane by aceto-clastic bacteria. Fe and Ni microelements were similarly reported to enhance biohy-drogen production. Light and heavy metal ions, phenolic compounds, ammonia and other metabolites or toxic compounds brought within the substrate may negatively affect the biogas and biohydrogen productions alike, depending on their concentration [24, 87].

Thermal regime is particularly a relevant factor highly altering the fuel gas production in anaerobic digestion and dark fermentation processes. Generally, higher temperatures have been associated with increased fuel generation, but in such case the biochemical processes may become more prone to imbalances at even small variations of environmental conditions within the digester. Increasing temperature is reflected in higher costs for heating and requires more careful process monitoring and control. Fermentation can take place at various temperature ranges, conventionally classified in several categories. Most fermentative processes are developed at ambient (15–27 °C) temperatures, at mesophilic (30–45 °C) temperatures or moderate thermophilic (50–60 °C) temperatures. Cryophilic (<10 °C), extreme thermophilic (65–80 °C) and hyperthermophilic (>80 °C) conditions are scarcely used [44, 87, 95]. It has been noticed that to a certain level, temperature augmentation improves the reactions kinetics, but the optimal digestion temperature for each project should be set for every specific configuration as it may vary with the composition of raw materials, reactor type, bacterial specificity from inoculum, etc. [44]. Thus, even though the fermentation at higher temperatures is typically more efficient than at lower temperatures, a temperature range that simultaneously preserves the advantages of fast microbial multiplication and high process efficiency should be pursued.

The optimal pH for methanogenesis under anaerobic digestion should range between 6 and 7.5, while the dark fermentation requires optimal pH values from 5.5 to 6.0; for this low pH, repression of methanogenic microorganisms is promoted while indirectly increasing H_2 production [34].

Organic loading in the digester is a good indicator of nutrient level availability for consumption by microorganisms, and it is also directly linked to the reactor performance. The operator responsible for the biomethane/biohydrogen production facility should have minimal information on the biodegradability of the substrates so as not to overload the system nor to operate the reactor at under-capacity. For continuous systems, the organic loading rate, which may be defined as the mass of volatile solids entering the digestion tank in unit time, should take into account the limits of the reactor. For example, a sudden increase in the organic loading rate may cause a fast release of volatile organic acids, which accumulate, leading to

acidification in the fermentation medium and causing process imbalance. For undisturbed fermentation and optimum production of fuel gas, it is necessary that constant organic loadings should be provided [87].

The fermentation time (in batch operation) and the hydraulic retention time (in continuous operation) are process parameters with decisive influence on the production yield. Thus, under batch operation mode, the biogas production in anaerobic digesters is ceasing when the substrate has been exhausted. The complete fermentation process could last from several days to weeks or months depending on the fermentation temperature [101].

For biohydrogen, the duration of dark fermentation in batch regime is usually short, of about 2–3 days on average, but some experimental results indicate good hydrogen yields at hydraulic retention time shorter than 14 h [102–105]. In selecting the hydraulic retention time lengths for continuous processes, several factors should be considered. The optimal period for mesophilic anaerobic digesters is between 10 and 20 days of fermentation, but this could depend on the reactor design or particularly on the substrate biodegradability [106]. For example, a short hydraulic retention time, usually less than 3 days, may induce reduction of the methanogens which are slowly growing and promote acidogenic bacteria growth, thus favouring the hydrogen production. On the other hand, a too high feeding rate would lead to poor hydrolysis of the substrate [94, 107].

The influence of homogenization on the fermentation outcome has been studied at a larger extent for anaerobic digestion than for dark fermentation. Mechanical stirring inside the reactor can improve the availability of microorganisms in the substrate by increasing their contact with the substrate. Homogenization could be also ensured by feedstock hydrodynamics as well as by the gas flowing inside the reactor, in connexion to the hydraulic retention time [108]. In case of mass mixing, the hydraulic retention time is reduced, and reactions in the fermenter are fostered.

On the other side, the need for mixing should be well assessed since excessive mixing increases the energy consumption, but mass agitation may negatively influence the balance of microorganisms, with effect on the fuel gas production. Besides ensuring the substrate homogenization within the reactor, mass mixing is also useful for balancing the temperature and for preventing scum, sediment or any inactive areas to be developed. Slight mixing can ensure the homogeneous concentration of nutrients and metabolic products of microorganisms [87].

Pressure influence on biomethane/biohydrogen production has not been largely investigated, neither explained from a biochemical perspective. The pressure effect is supposed to be associated to various syntrophic phenomena between microbial species like acetogens and methanogens and usually held responsible for hydrogen exchange between species [109]. Some experiments demonstrated that by increasing the hydrostatic pressure inside the reactor, the methanogenesis was negatively affected [91].

Regarding dark fermentation processes in continuous biohydrogen synthesis, the biochemical pathways were found sensitive to hydrogen concentration increments which switched the metabolic pathways towards the formation of other chemical products such as ethanol, butanol, propanone, lactate, etc. System response to the

hydrogen concentration decreases with increasing temperature [81]. The study of pressure influence on fermentative processes requires in-depth analysis and could be a prospective research topic.

6   Biogas Upgrading Methods

Methane is the component of biogas that decides its energy value; methane concentration in biogas varies between 50% and 70%. The second major component found in high concentration in biogas is carbon dioxide which accounts the non-combustible share of biogas. Except for methane, the other biogas components contained in minor amounts (water, nitrogen, oxygen, hydrogen sulphide, ammonia, siloxanes, volatile organic compounds, etc.) are practically unwanted components, that may cause damage in various ways and have to be removed through cleaning and upgrading processes, with the main scope to protect the metallic parts and raise the calorific power of biogas [110].

Among the compounds to be removed from biogas so as to allow the use of biomethane in combustion and transport processes is hydrogen sulphide, which is produced from sulphate reduction and is found in biogas in concentrations up to 4000 ppmv. Hydrogen sulphide is corrosive to engines, pipes, gas storage tanks, compressors, etc. but is also an inhibitor for catalytic reforming. Moreover, it is well known that sulphur dioxide is generated by burning H_2S, which is a pollutant for the environment. Hence, the many potential problems that sulphur hydrogen can cause require its removal from biogas through an upgrade process before its use as a fuel [111]. Biogas produced from wastewaters can contain siloxanes formed from the organic silicon compounds which arrive in sewage sludge due to the various uses of silicon-containing compounds in households and industries [112]. Even if they are found in low concentrations of up to 10.6 ppmv [112], the presence of siloxanes in biogas is associated with serious problems since silicone oxides may generate sticky residues by combustion. This unwanted residue can be deposited in the engines and valves causing severe malfunction [110]. Biogas upgrading is aiming at obtaining purified biogas, namely, biomethane, which is very close to natural gas standards after removing carbon dioxide and other impurities such as water, hydrogen sulphide, siloxanes, etc. [113].

At present, the technologies for biogas upgrading are very diverse and very efficient; the choice of the most optimal process takes into account the application for which the biomethane will be used. There are big differences between the quality requirements of biogas for stationary CHP engines, where the concentrations of water vapour and hydrogen sulphide in biogas must not exceed 1000 ppmv, while in biogas for transport and biogas injected into the gas grid, carbon dioxide and other impurities must be removed so as to upgrade the biogas to >95% methane, according to specific national standards [1].

Several conventional and commercially available technologies for biogas physical upgrading are currently used for various applications, water scrubbing, organic

solvent scrubbing, pressure swing adsorption and membrane-based upgrading, while other emerging technologies (for instance, cryogenic methods) for biogas upgrading are still under developing stage [111]. Also, some chemical methods for converting CO_2 into valuable products are successfully applied: amine chemical scrubbing, methanation reaction and methanol and syngas synthesis are used as biogas upgrading via CO_2 removal and CO_2 utilization technologies [111, 114, 115].

Besides the conventional technologies, the biological biogas upgrading method has been researched and developed as an alternative to the currently available technologies. According to Bassani, this newly developed method involves hydrogenotrophic methanogens to react CO_2 from biogas and H_2 from external source, thus producing additional CH_4 through biochemical pathways. Table 4 summarizes the main features of each of the conventional biogas upgrading methods widely applied commercially. The emerging technologies which proved good results in removing contaminants like CO_2, H_2S and siloxanes but still need more in-depth research before being implemented on the market are briefly presented in Table 5.

The techniques presented in Tableq 4 and Table 5 are suitable for removing various unwanted components from biogas, but a single method cannot ensure the complex purification to biomethane; in general, it is recommended that two or more processes be combined to achieve the effective removal of biogas' unwanted components. The choice between one conventional/emerging biogas upgrading technology and another is specific to each case and depends on the biogas' quality requirements for the given application, but all the mentioned upgrading technologies have different advantages and disadvantages [1].

Carbon dioxide removal from biogas can be achieved by water or organic solvent scrubbing and also by separation by various means (with membranes, pressure, cryogenic, adsorption, etc.). Water scrubbing is most commonly used for removing CO_2 but also for H_2S, although some organic absorbents (i.e. polyethylene glycol-based solvents) can retain CO_2 more efficiently [117]. Nevertheless, in order to avoid solvent deterioration due to H_2S contaminant in the biogas stream, a complete H_2S removal using activated carbon should be applied prior to organic scrubbing. In case the recovery of H_2S from the solvent is not achieved, the capacity of the solvent for CO_2 absorption will be greatly diminished [128].

Hydrogen sulphide removal from gas streams can be done through many technologies, but selecting the best one has to take into account several factors such as the composition of the gas and its final use, H_2S concentration and the absolute quantity of H_2S to be removed, variability and volume of the gas to be treated, etc. [129]. Among the traditional methods for removing H_2S from biogas, the followings dominate the market: adsorption on activated carbon, molecular sieves, iron and zinc oxides, alkaline solids, water or solvent scrubbing and membrane purification.

In the past year, increased attention has been paid to the biotechnological methods (air/oxygen dosing to biogas reactor, biofilters) that have proved the same or even higher efficiency in H_2S removal than the physical-chemical methods [121, 129]. The biological methods are innovative alternatives still under development. Yet, many large-scale biogas facilities are equipped with H_2S removal units which operate on the principle of biological H_2S oxidation by aerobic bacteria [110].

Table 4 Commercially available biogas upgrading technologies

Method type	Upgrading technology	Principle	CH_4 purity [%]	Reference
Physical methods	Water physical scrubbing	Biogas stream flows through a counter flow water in a column. CO_2's higher solubility in water makes the water absorb CO_2, thus enriching the CH_4 content of biogas. The method required biogas drying and water regeneration to remove CO_2 by desorption	96–98	Adnan et al. [114], Bauer et al. [116] and Munoz et al. [117]
	Organic solvent scrubbing	The same as in the case of water scrubbing, except for the use of organic solvents (e.g. polyethylene glycol) instead of water. Cooling and heating of the solvent are needed during the procedure	96–98	Adnan et al. [114] and Bassani [115]
	Pressure swing adsorption	A water solution of amines (a mixture of monoethanolamine or di-methyl ethanol amine DEA and piperazine) binds with CO_2 molecules in the biogas; then, the amine solution is regenerated by a stripper that releases CO_2 into the atmosphere	>99	Adnan et al. [114], An et al. [118], Augelleti et al. [119] and Bassani [115]
	Membrane separation	Dry or wet separation of biogas components using selective membranes (organic polymer polyimide; inorganic zeolites, silica; activated carbon membranes, metallic-based materials; mixed polymer-ceramic, polymer-carbon, etc.) as a permeable material for CH_4, N_2, H_2S, CO_2, H_2O	92–96	Bassani [115], Bassani [111], Bauer et al. [116], Harasimowicz et al. [120] and Khan et al. [121]
Chemical methods	Amine or alkali/salt chemical scrubbing	Biogas-liquid mass transfer principle in a countercurrent flow, using absorbents such as mono-, di-, triethanolamine, methyl diethanolamine with a stripper piperazine or alkali aqueous solutions	99.9	Andriani et al. [122] and Munoz et al. [117]
	Methanation (Sabatier reaction)	Reaction of CO_2 with H_2 for producing CH_4 and H20 (Sabatier reaction), on selective catalysts (nickel or heterogeneous catalysts: copper-, iron-, zinc- or ceria-based oxides), at temperatures of ~500 °C and pressure of 5–10 MPa		Adnan et al. [114], Klankermayer et al. [123], Sun et al. [124] and Wang et al. [9]

Table 5 Emerging technologies for biogas upgrading

Method type	Upgrading technology	Principle	CH$_4$ purity [%]	Reference
Physical method	Cryogenic separation	Progressive decrease in biogas temperature followed by biogas compressing and then separating liquefied CH$_4$ from the rest of gases (CO$_2$ and other components such as H$_2$O, H$_2$S, halogens, etc.) that are gradually removed	98.5	Angelidaki et al. [110], Munoz et al. [117], Grande and Blom [11]
Biological method	Hydrogen-assisted methanogenesis	Bioconversion of CO$_2$ to CH$_4$ with the use of external H2 (preferably produced from water electrolysis) through two different metabolic pathways: (a) Directly, involving hydrogenotrophic methanogenic archaea (most frequently *Methanobacterium* and *Methanothermobacter* species), based on the eq. (1): $4H_2 + CO_2 \rightarrow CH_4 + H_2O$ $\Delta G^o = -130.7$ KJ/mol (1) (b) Indirectly, involving homoacetogenic bacteria that convert CO$_2$ to acetate, followed by acetoclastic methanogens to produce CH$_4$ from acetic acid, as in eqs. (2) and (3): $4H_2 + 2CO_2 \rightarrow CH_3COOH + 2H_2O$ $\Delta G^o = -104.5$ KJ/mol (2) $CH3COOH \rightarrow CH_4 + CO_2$ $\Delta G^o = -31.0$ KJ/mol (3)	98–100	Angelidaki et al. [110], Kougias et al. [125], Kougias et al. [113], Agneessens et al. [126], Mulat et al. [127] and Bassani et al. [115]

Siloxanes are completely synthetic organic compounds included in cosmetics, deodorants, shampoos, soaps, food additives, drugs and anti-foam products [112]. They are generally found in significant concentrations of up to 400 mg/m3 in biogas derived from municipal waste [130, 131]. Siloxanes must be removed from the biogas stream, as by burning they are oxidized to microcrystalline silicon oxide that can deposit in the combustion chamber causing severe damages to engines [112]. The most common and effective techniques for removing siloxanes from biogas are physical processes such as absorption/adsorption or condensation [1, 132].

7 By-product Management Options and Advanced Processing

Biogas is the main product with economic value resulting from the recovery of residual biomass by anaerobic fermentation, but a valuable by-product is also the liquid material left in the digester. It is rich in trace elements and basic nutrients for

plant growth (N, P, K) and can be used in agriculture due to its excellent qualities for soil fertilization. Digestate proves improved fertilizer efficiency compared to raw animal manure, because it has a more homogeneous texture and has a better ability to release nutrients, a better carbon/nitrogen ratio and much lower odours [133]. Other more in-depth studies that have compared the fertilizing performance of digestate and some types of manure have shown that digestate is better suited for clay soils and high levels of organic matter, while pig and cattle manure are more suitable for sandy soils with lower content of organic compounds [134]. It can be estimated that for every 1 tonne of organic waste treated by anaerobic digestion, around 400 kg of liquid digestate and 300–400 kg of fibre digestate can be generated [77]. Digestate management is a complex task that involves adequate solutions for storage, processing, transportation and utilization and should be economical and in compliance with environmental protection measures [135].

Despite the many advantages that this by-product can bring to agriculture or other sectors through bioprocessing, there are also many challenges that, if not well managed, can make the investment in the biogas plant unprofitable. Since digestate contains >90% water, it requires large space for storage, and such auxiliary facilities significantly augment the cost of the anaerobic digestion plant. Digestate processing to volume reduction and nutrient concentration involves drying, evaporation and retention of other pollutants (ammonia) or contaminants (heavy metals, organic pollutants, pathogens, etc.), but some of these techniques require high energy or reagent consumption, some generate residual products, etc. [135]. If used directly as a soil fertilizer, the digestate is discharged from the digester and transported outside the facility by gas pipelines or with the help of special tanks [133], but the cost of transportation is an important issue to be assessed in planning a viable biogas plant.

Before making the decision on the best management option for recovering the digestate effectively and economically, it is mandatory to know its physico-chemical characteristics as the quality of the digestate is taken into account in the decision of supply to end users [135]. The application of digestate to arable lands is limited on the one hand by the maximum level of nitrogen allowed to be supplied to the land, which, in most of the EU member states, is 170 kg nitrogen/hectare/year, as stipulated by Directive 91/676/EEC [136]. On the other hand, many countries have adopted national and local regulations regarding the quality parameters of the digestate resulting from the anaerobic digestion of the sewage sludge which is known to contain heavy metals. Regulations encourage decentralized anaerobic digestion and allow land application of the digestate only for on-farm product [137].

Use of digestate in agricultural farms for soil fertilization cannot cover the need to manage the entire amount of digestate generated in huge quantities from tens of thousands of large-scale biogas plants operating worldwide. The biggest biogas plants of a size greater than 20 MW being constructed at the moment generate over 400,000 t/year digestate [138].

Although valuable, such increasingly generated anaerobic digestion by-product raises concerns about transportation costs, emissions of pollutant gases over long-term storage but also in terms of the large amount of nitrogen content that limits the digestate use exclusively for agricultural crops [139, 140].

More recent research has been directed towards testing and implementing alternative ways of digestate recovery to minimize the impact on the environment and add value to the technological solution of the residual biomass energy recovery. Also, digestate management aims to open new business opportunities for the manufacture and sale of products based on digestate and thus reduce the operating costs of biogas plants [137].

The recovery of valuable components from the digestate can be achieved by processing it through various mechanical, physical, chemical, biological or combined techniques [141]. Digestate management strategies are expected to be focused on biorefinery processes to produce marketable materials. Thus, as alternatives for digestate recovery, some scientists have developed optimized procedures to transform solid digestate into high-quality compost [142, 143]. Use of solid digestate for vermiculture is another option for its efficient capitalization [144]. Other studies tested and implemented methods for making solid fuels after drying and pelletizing solid fraction of the digestate [145], or it can be just dried and incinerated for energy recovery [137]. Incineration is a proper management way for reducing the volume and the polluting organic matter content in digestate; some elements (P, K, Ca) which are collected in the bottom ash could be recovered to be used for soil fertilization [146]. Biochar that can be obtained from pyrolysis of digestate is not only a valuable adsorbent material; some researchers proved that biochar can enhance the anaerobic digestion performance, since it can act as an adsorbent for the process inhibitory compounds and stand for microbial growth or electric conductor allowing electron transfer. Also, they proved that biochar is an effective adsorbent to be used for upgrading biogas [147]. Other studies regarding digestate processing aimed at producing bio-oil to be used as fuel for engines [148, 149]. Digestate can be used for industrial purposes to produce composite materials and as building material [138].

The liquid phase resulted after filtration of the digestate is rich in ammonium nitrogen, carrying ca. 70–80% of the total NH_4^+-N [146]. Therefore, the liquid digestate may have various beneficiaries to exploit its nutrient-rich composition. It is mainly used for agriculture or can be recirculated to the digester instead of process water for diluting the biomass feedstock and supplying fermentative microbiota. Another option for liquid digestate management is to utilize nutrients, such as nitrogen and phosphorus, and organic matter for cultivating mixotrophic microalgae, thus enhancing the biomass productivity in bioreactors and supply feedstock for the biorefinery industries [137, 150]. Digestate use as a carbon source in microbial fuel cell reactors has gained popularity in the last decade [151, 152]. Figure 7 displays the main management options of the advanced recovery of the by-products resulting from the biomass residues' anaerobic bioconversion within the concept of circular bioeconomy.

Catalytical conversion of anaerobically digested biomass takes place in catalytic reactors that produce pyrolysis gaseous mixtures which could be used as feedstocks in the production of chemicals/source of hydrogen/running of gas turbines for generation of power. Advanced techniques of catalytical biomass conversion through supercritical water gasification has been investigated by Güngören Madenoğlu for
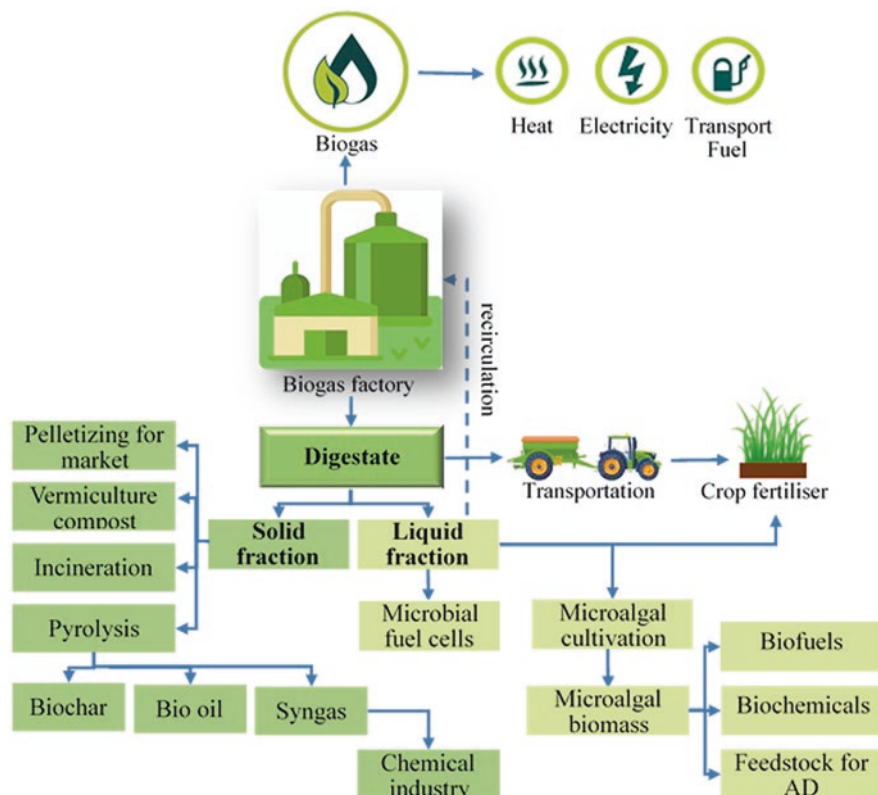
Fig. 7 Digestate management options for the materials' advanced recovery

different reaction temperatures and alkali catalysts (KOH, NaOH, LiOH and K_2CO_3) to produce methane, hydrogen and aqueous products (aliphatic hydrocarbons, phenol, substituted phenols, N-heterocyclic, substituted N-heterocyclics and substituted benzene) that can be used for various chemical synthesis [153].

Related studies revealed that some metallic catalysts (e.g. Ru/C) may result in high methane production, while alkali catalysts (NaOH, K_2CO_3, etc.) may accelerate hydrogen production [154, 155].

Compared to thermochemical conversion, the biochemical conversion is much slower and does not require much external energy, but the reaction pathways involve biocatalysts to convert the organic components into intermediates and final products. Biomass conversion into biochar, bio-oils and gaseous intermediates by thermochemical methods requires heat and/or various catalysts [156].

In dark fermentation, hydrogen yields are influenced by the metabolic pathways that are followed; a large part of the organic fraction fed in the bioreactor remains in the liquid phase at the end of the conversion process, in the form of alcohols, fatty acid unfermented material and other by-products. Under optimal fermentation conditions, the organic matter found in the effluent is about 60–70% from the organic
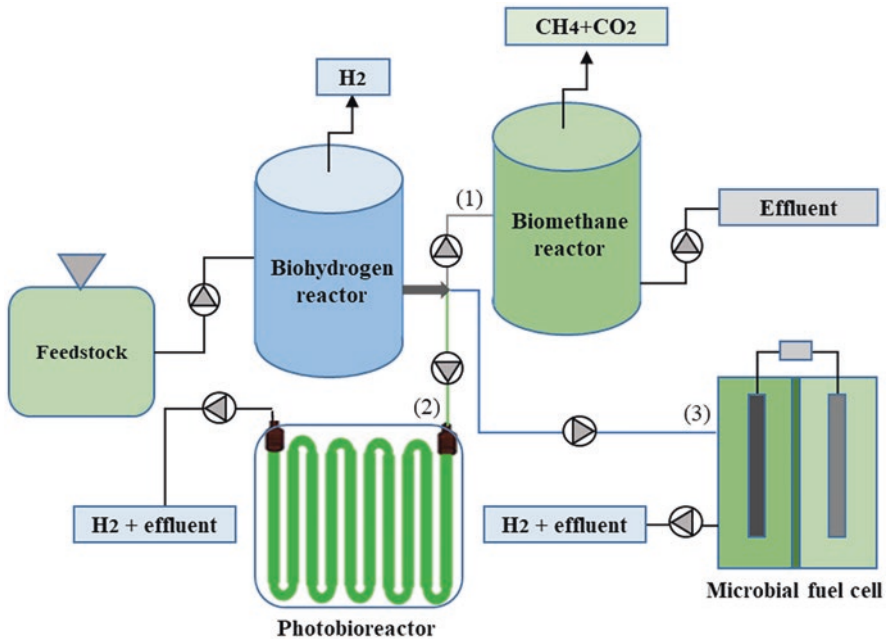
Fig. 8 Two-stage integrated systems for biohydrogen and biomethane recovery by anaerobic digestion (1); additional hydrogen recovery by photo-fermentation (2); additional hydrogen recovery in a microbial fuel cell (3) (adapted after [96])

matter fed into the bioreactor [93]. For increasing the energetic yields, one approach is to couple dark fermentation with other processes from which a second useable form of energy can be obtained. The remaining organic matter from dark fermentation could be thus reused either to produce biomethane or to recover additional biohydrogen by photo-fermentation or in a modified microbial fuel cell [93, 96]. Advanced fuel gas recovery could be carried out in a two-stage process as seen in Fig. 8.

Integrated technologies offer several advantages such as higher net energy recovery and better waste stabilization. The two (multi-)step processes are promising technologies, but their practical applicability is fairly narrow, and further research is still required in order to enhance their viability.

8   Future Prospects and Innovative Research Directions

Numerous social, economic and environmental reasons have increasingly driven interest in bioenergy production worldwide, but in the last decade vast research work has been reported on anaerobic digestion and dark fermentation processes as well. Important advances have been made in several research directions, but there
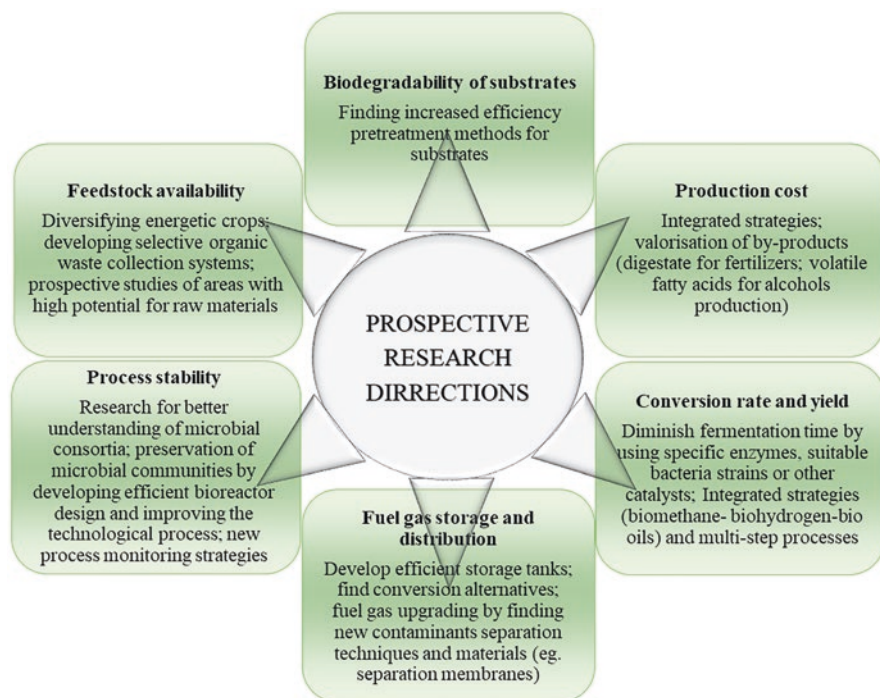
Fig. 9 Research directions for advances in biochemical conversion to fuel gas and by-products

are still many aspects that should be closely investigated for further improvements of fuel gas production [14, 157]. In Fig. 9, important research directions which require further prospects and some innovative developing optimization strategies for biomethane/biohydrogen production processes are summarized.

The biogas production technologies have reached a technological maturity level which makes them feasible for large-scale application; the future goals of research in the field should be more focused on controlling biochemical process stability, increasing feedstock availability and lowering production costs, as well as on biogas upgrading to make it suitable as transport fuel [158].

Compared to anaerobic digestion which has been more widely investigated, dark fermentation is still a rather immature practice, not sufficiently developed to be commercially available. The main challenge in dark fermentation is that the conversion efficiency of the process as a whole is still low in comparison to theoretical data. Since about 67–85% of the substrate leaves the reactor before being decomposed, many efforts still need to be made to increase the conversion efficiency of the substrate and thus the production of biohydrogen [34]. Scaling-up the biohydrogen production systems and developing continuous pilot-scale or industrial-scale bioreactors are currently still a challenge. Improvement of dark fermentation energetic yields requires a deeper knowledge of microorganisms' biology and interactions, selection of appropriate substrates and pretreatment strategies. Also, further

investigations regarding possible joinder of dark fermentation with other waste-to-energy management options, such as anaerobic digestion, are required in order to get a better substrate conversion [96].

In both cases, the metabolic engineering of microbial strains emerges as an innovative new research direction. For instance, developing thermophilic bacteria strains able to ferment lignocellulosic or other heavily biodegradable biomass, also able to withstand environmental conditions' sharp variations during fermentation stages, and have a better behaviour against competing species could be a good approach to increase fuel gas production in fermentative processes. Moreover, gene encoding could be used to develop microorganisms which selectively follow biochemical pathways in order to obtain higher production yields and a cleaner gas requiring less purification or upgrading [157].

The development of some new degradation biocatalysts such as different types of enzymes with broader spectrum of applications and more effective in the hydrolysis of biopolymers should be explored in further research. Thus, enzyme-producing microorganisms could be successfully used to increase the biochemical process performance, being able to act as microbial catalysts of biochemical reactions. The type and characteristics, but also the amount of biocatalysts, may highly influence the fermentation process stability and the conversion rates, which make the cost of their production to be considered evenly [40]. On the other hand, prior or along with developing advanced biocatalysts, a higher comprehension of biochemical processes that affect anaerobic digestion and dark fermentation should be followed. A deeper understanding of microorganisms' interactions among each other and with their environment, for example, by molecular analysis, enables the development of a knowledge-based process control which uses reproducible forecasts on how the fermentation systems reacts to varying external influences for process optimization [159].

Pushing forward the existing technology for obtaining fuel gas is also an important challenge, being correlated to the need of improving bioreactor designs, reducing the hydraulic retention time without affecting the gas production rate, enhancing gas storage volume, etc. [160]. Moreover, advances in the fermentation process monitoring and control are still to be made. The existing limitations in bioprocesses monitoring are considered one of the major challenges opposing progress in the fuel gas production field.

Developing new monitoring techniques and equipment or improving the existent ones (such as biosensors, optical sensors, immunosensors, etc.) could lead to adequate operation of bioreactors and higher production yields along with higher financial gain and process sustainability [161]. Additionally, developing integrated or multi-stage processes is a promising possibility for obtaining enhanced conversion yields of organic matter to fuel gas. An example of such a system is the coupling of dark fermentation with biomethane production in anaerobic digesters, providing a better use of the discharged substrate [93, 96].

The need to obtain pure gases represents another challenge of the bioconversion processes, as either high financial investments in maintaining optimum operational conditions or enhanced upgrading techniques for gas purification and elimination of

trace gases are required. Regarding the latter, various techniques for gas upgrading have been employed, whether physico-chemical, biological or combined techniques, but there are still some inconveniences that need to be surpassed. For instance, membranes employed in gas separation are costly and fragile, while catalysts in chemical hydrogenation process are easily degenerated and need periodical replacement [110].

Other exploitable directions could be the reduction of handling cost associated to the fermentation effluent and mitigation of its potentially hazardous influence on the environment. In this purpose, several approaches could bring proper results: advanced separation of useful chemicals, low-energy-consuming concentration techniques for further use as fertilizer, improved recovery techniques for water savings, etc. [162].

Further expectations in the fuel gas production using anaerobic digestion and dark fermentation processes rest also on engineering and scientific advances in the sector of feedstock supply. Although fermentation can be conducted on a wide variety of possible substrates out of which organic wastes are preferred, ensuring continuous feedstock to the processes may be sometimes a challenge for constant fuel gas production. Catch crops, which are plants not intended for food but grown intercropped with food crops, contributing to the enrichment of the soil, have been previously investigated for bioethanol productions; their degradation to biohydrogen and biogas should also be considered. The selection of new substrates and their subsequent processing to make them suitable for fuel gas production should take into account some criteria such as availability, biodegradability, cost (of production/processing/transportation), chemical composition and contaminants, etc. [157, 163]. Developing effective pretreatment techniques of lignocellulosic biomass which is recalcitrant to degradation is also a key point in widening substrates choices for biomass-to-fuel gas conversion processes [40].

To summarize, there are still multiple directions for possible improvements of anaerobic digestion and dark fermentation to be approached towards increasing global process efficiency, so as to bring important contribution to developing sustainable bio-based fuel gas industry while supporting the circular economy.

9   Conclusions

Residual biomass is an inexhaustible energy resource derived from human, animal and plant waste. It contains organic matter that stores the energy produced in plants by photosynthesis, energy that is transferred through the food chain to animals and human beings and finally to their waste. Energy recovery from residual biomass may partially replace fossil fuels but also help in maintaining environmental balance by reducing greenhouse gas emissions and soil and water pollution.

Biomass biochemical conversion technologies can provide environment-friendly option for producing gaseous and liquid fuels with the help of specific enzymes as biological catalysts to break down biopolymers from biodegradable waste into

various intermediates and final products. Although the biochemical conversion is much slower than thermochemical conversion, it is the most suitable and economical option for treating wet waste since not much external energy is required. There are two different approaches for the biochemical conversion processes to fuel gases (anaerobic digestion, dark fermentation), but the process parameters are those which decide the biochemical conversion pathway and implicitly the metabolism products; nevertheless, for a better recovery of the organic matter, the two processes can be integrated in the same project.

During the last decade, important advances have been made in the research of enzymatically catalysed bioconversion processes for the production of biomethane and biohydrogen so that currently these technologies are already commercial. However, there are still many aspects to be further investigated in more detail such as biomass pretreatment, biochemical process stability and microbial metabolism knowledge, optimal process parameters, shortening of fermentation time, gas purification, by-product reuse options, etc., so as to increase the organic fraction recovery to valuable products and make the investment more feasible.

References

1. Kapoor R, Ghosh P, Kumar M, Kumar Vijay V (2019) Evaluation of biogas upgrading technologies and future perspectives: a review. Environ Sci Pollut Res 26:11631–11661
2. World Energy Council (2019) World energy scenarios, exploring innovation pathways to 2040. https://www.worldenergy.org/assets/downloads/Scenarios_Report_FINAL_for_website.pdf. Accessed 8 Jan 2020
3. Casoni AI, Gutierrez VS, Volpe MA, Hoch PM (2018) Synthesis of value added product processes from residual biomass. Comput Aided Chem En 44:397–402
4. Pfau S (2015) Residual biomass: a silver bullet to ensure a sustainable bioeconomy? In: The European Conference on Sustainability, Energy & the Environment, Conference Proceedings. The International Academic Forum, Nagoya, pp 295–312
5. Krishnan S, Din MF, Mat Taib S, Ling YE, Aminuddin E, Chelliapan S, Mishra P, Rana S, Nasrullah M, Sakinah M, Wahid ZA, Singh L (2018) Utilization of micro–algal biomass residues (MABRS) for bio–hythane production—a perspective. J Appl Biotechnol Bioeng 5(3):162–165
6. Pal P, Chew KW, Yen HW, Lim JW, Lam MK, Show PL (2019) Cultivation of oily microalgae for the production of third-generation biofuels. Sustainability 11:5424–5440
7. Saad MG, Dosoky NS, Zoromba MS, Shafik HM (2019) Algal biofuels: current status and key challenges. Energies 12(10):1920. https://doi.org/10.3390/en12101920
8. Aiguo GW, Danielle A, Hua S (2017) Catalytic biomass valorization. In: Tumuluru JS (ed) Biomass volume estimation and valorization for energy, vol 42. IntechOpen, London, pp 493–660. https://www.intechopen.com/books/biomass-volume-estimation-and-valorization-for-energy/catalytic-biomass-valorization
9. Wang W, Wang S, Ma X, Gong J (2011) Recent advances in catalytic hydrogenation of carbon dioxide. Chem Soc Rev 40:3703–3727
10. Lee SY, Sankaran R, Chew KW, Tan CH, Krishnamoorthy R, Chu DT (2019) Waste to bioenergy: a review on the recent conversion technologies. BMC Energy 1:4. https://doi.org/10.1186/s42500-019-0004-7

11. Grande CA, Blom R (2014) Cryogenic adsorption of methane and carbon dioxide on zeolites 4A and 13X. Energy Fuels 28(10):6688–6693. https://doi.org/10.1021/ef501814x

12. Li R, Liu D, Zhang Y, Zhoua J, Tsang YF, Liu Z, Duan N, Zhang Y (2019) Improved methane production and energy recovery of post-hydrothermal liquefaction waste water via integration of zeolite adsorption and anaerobic digestion. Sci Total Environ 651(1):61–69

13. Sayara T, Sánchez A (2019) A review on anaerobic digestion of lignocellulosic wastes: pretreatments and operational conditions. Appl Sci 9:4655. https://doi.org/10.3390/app9214655

14. Prasad S, Ingle AP (2019) Impacts of sustainable biofuels production from biomass. In: Rai M, Ingle AP (eds) Sustainable bioenergy: advances and impacts. Elsevier, Amsterdam, pp 327–346. https://doi.org/10.1016/b978-0-12-817654-2.00012-5

15. European Commission (2018). https://ec.europa.eu/energy/en/topics/renewable-energy/biofuels/sustainability-criteria. Accessed 13 Jan 2020

16. Kaza S, Yao LC, Bhada-Tata P, Van Woerden F (2018) What a Waste 2.0: a global snapshot of solid waste management to 2050. Urban Development, 2018. World Bank, Washington, DC. © World Bank. https://openknowledge.worldbank.org/handle/10986/30317 License: CC BY 3.0 IGO

17. European Commission Report (2019) Global food supply and demand. Consumer trends and trade challenges, Brussels https://ec.europa.eu/info/sites/info/files/food-farming-fisheries/farming/documents/market-brief-food-challenges-sep2019_en.pdf. Accessed 10 Jan 2020

18. Perea-Moreno MA, Samerón-Manzano E, Perea-Moreno AJ (2019) Biomass as renewable energy: worldwide research trends. Sustainability 11(3):863. https://doi.org/10.3390/su11030863

19. Tripathi N, Hills CD, Singh RS, Atkinson CJ (2019) Biomass waste utilisation in low-carbon products: harnessing a major potential resource. NPJ Clim Atm Sci 2:35. https://doi.org/10.1038/s41612-019-0093-5

20. Pires A, Martinho G (2019) Waste hierarchy index for circular economy in waste management. Waste Manag 95:298–305

21. Woiciechowski AL, Pedroni Medeiros AB, Rodrigues C, de Souza Vandenberghe LP, de Andrade Tanobe VO, Dall'Agnol A, Gazzoni DL, Soccol CR (2016) Feedstocks for biofuels. In: Soccol CR et al (eds) Green Fuels Technology, Green Energy and Technology. Springer International, Cham. https://doi.org/10.1007/978-3-319-30205-8_2

22. Karakashev D, Zhang Y (2018) Bioenergy and biochemicals production from biomass and residual resources. Energies 11(8):2125. https://doi.org/10.3390/en11082125

23. Achinas S, Euverink GJ (2019) Rambling facets of manure-based biogas production in Europe: Abriefing. Renew Sustain Energy Rev 75:954–971. https://doi.org/10.1016/j.rser.2019.109566

24. Ghimire A, Frunzo L, Pirozzi F, Trably E, Escudie R, Lens PNL, Esposito G (2015) A review on dark fermentative biohydrogen production from organic biomass: process parameters and use of by-products. Appl Energy 144:73–95

25. Lin L, Xu F, Ge X, Li Y (2019) Biological treatment of organic materials for energy and nutrients production—anaerobic digestion and composting. Adv Bioenerg 4:121–181

26. World Biogas Association (WBA) (2019) Global potential of biogas. Lead Author Jain S. Report. https://www.worldbiogasassociation.org/global-potential-of-biogas/. Accessed 14 Jan 2020

27. Córdoba V, Colavolpe MB, Fernández M, Santalla E, Albertó E (2016) Potential methane production of spent sawdust used in the cultivation of Gymnopilus pampeanus. J Environ Chem Eng 4:4418–4425

28. World Biogas Association (WBA) (2018) Global food waste management: an implementation guide for cities. Report, https://www.worldbiogasassociation.org/food-waste-management-report/. Accessed 14 Jan 2020

29. Ali A, Mahar RB, Abdelsalam EM, Sherazi STH (2018) Kinetic modeling for bioaugmented anaerobic digestion of the organic fraction of municipal solid waste by using Fe3O4 nanoparticles. In: Waste and biomass valorization. https://doi.org/10.1007/s12649-018-0375-x

30. Ali A, Mahar RB, Sherazi STH (2019) Methane augmentation of anaerobic digestion of food waste in the presence of Fe3O4 and carbamide capped Fe3O4 nanoparticles. In: Waste and biomass valorization. https://doi.org/10.1007/s12649-019-00732-8

31. Hanum F, Yuan LC, Kamahara H, Aziz HA, Atsuta Y, Yamada T, Daimon H (2019) Treatment of sewage sludge using anaerobic digestion in Malaysia: current state and challenges. Front Energy Res 7:19. https://doi.org/10.3389/fenrg.2019.00019

32. Viesturs D, Melece L (2014) Advantages and disadvantages of biofuels: observations in Latvia. In: Engineering for rural development. Proceedings, Jelgava, May 2014, vol 13, pp 210–215

33. Tirpan Cioroiu DR, Parvulescu OC, Dobre T, Raducanu C, Koncsag C, Mocanu A, Duteanu N (2018) Slow pyrolysis of cystoseira barbata brown macroalgae. Rev Chim (Bucharest) 69(3):553–556

34. Bharathiraja B, Sudharsanaa T, Bharghavi A, Jayamuthunagai J, Praveenkumar R (2016) Biohydrogen and biogas—an overview on feedstocks and enhancement process. Fuel 185:810–828

35. Lee JP, Lee JS, Park SC (1999) Two-phase methanization of food wastes in pilot scale. Appl Biochem Biotech 77–79:585–593

36. Nielfa A, Cano R, Fdz-Polanco M (2014) Theoretical methane production generated by the co-digestion of organic fraction municipal solid waste and biological sludge. Biotech Rep 5:14–21

37. Raposo F, Borja R, Rincon B, Jimenez AM (2008) Assessment of process control parameters in the biochemical methane potential of sunflower oil cake. Biomass Bioenergy 32:1235–1244

38. Lei Z, Chen J, Zhang Z, Sugiura N (2010) Methane production from rice straw with acclimated anaerobic sludge. Effect of phosphate supplementation. Bioresour Technol 101:4343–4348

39. Zhang R, Zhang Z (1999) Biogasification of rice straw with an anaerobic-phased solids digester system. Bioresour Technol 68:235–245

40. Achinas S, Li Y, Achinas V, Euverink GJW (2019) Biogas potential from the anaerobic digestion of potato peels: process performance and kinetics evaluation. Energies 12:2311. https://doi.org/10.3390/en12122311

41. Dima AD, Mateescu C, Parvulescu OC, Lungulescu EM, Nicula NO (2019) Theoretical and experimental results on the recovery of potato processing residuals by anaerobic digestion. Rev Chim (Bucharest) 70(7):2524–2529

42. Sawasdee V, Haosagul S, Pisutpaisal N (2019) Co-digestion of waste glycerol and glucose to enhance biogas production. Int J Hydrogen Energy 44:29575–29582

43. Mussgnug JH, Klassen V, Schluter A, Kruse O (2010) Microalgae as substrates for fermentative biogas production in a combined biorefinery concept. J Biotechnol 150:51–56

44. Ntaikou I, Antonopoulou G, Lyberatos G (2010) Biohydrogen production from biomass and wastes via dark fermentation: a review. Waste Biomass Valor 1:21–39

45. Riazi MR, Chiaramonti D (2017) Biofuels production and processing technology—technology & engineering. CRC, Boca Raton, FL

46. Dellosso Penteado E, Zampol Lazaro C, Kimiko Sakamoto I, Zaiat M (2013) Influence of seed sludge and pretreatment method on hydrogen production in packed-bed anaerobic reactors. Int J Hydrogen Energy 38:6137–6145

47. Pecorini I, Baldi F, Iannelli R (2019) Biochemical hydrogen potential tests using different inocula. Sustainability 11(3):622. https://doi.org/10.3390/su11030622

48. Alibardi L, Cossu R (2015) Composition variability of the organic fraction of municipal solid waste and effects on hydrogen and methane production potentials. Waste Manag 36:147–155

49. De Gioannis G, Muntoni A, Polettini A, Pomi R, Spiga D (2017) Energy recovery from one- and two-stage anaerobic digestion of food waste. Waste Manag 68:595–602

50. Alibardi L, Cossu R (2016) Effects of carbohydrate, protein and lipid content of organic waste on hydrogen production and fermentation products. Waste Manag 47:69–77

51. Zhang ML, Fan YT, Xing Y, Pan CM, Zhang GS, Lay JJ (2007) Enhanced biohydrogen production from cornstalk wastes with acidification pretreatment by mixed anaerobic cultures. Biomass Bioenergy 31(4):250–254

52. Fan YT, Zhang YH, Zhang SF, Hou HW, Ren BZ (2006) Efficient conversion of wheat straw wastes into biohydrogen gas by cow dung compost. Bioresour Technol 97(3):500–505

53. Van Ginkel SW, Oh SE, Logan BE (2005) Biohydrogen gas production from food processing and domestic waste waters. Int J Hydrogen Energy 30:1535–1542. Biofuels Production and Processing Technology editat de M.R. Riazi, David Chiaramonti, 2017—Technology & Engineering

54. Meegoda JN, Li B, Patel K, Wang LB (2018) A review of the processes, parameters, and optimization of anaerobic digestion. Int J Environ Res Public Health 15(10):2224. https://doi.org/10.3390/ijerph15102224

55. Ma J, Frear C, Wang Z, Yu L, Zhao Q, Li X, Chen S (2013) A simple methodology for rate-limiting step determination for anaerobic digestion of complex substrates and effect of microbial community ratio. Bioresour Technol 134:391–395

56. Kumar AK, Sharma S (2017) Recent updates on different methods of pretreatment of lignocellulosic feedstocks: a review. Bioresour Bioprocess 4:7. https://doi.org/10.1186/s40643-017-0137-9

57. Yang L, Xu F, Ge X, Li Y (2015) Challenges and strategies for solid-state anaerobic digestion of lignocellulosic biomass. Renew Sustain Energy Rev 44:824–834

58. Karuppiah T, Azariah VE (2019) Biomass pretreatment for enhancement of biogas production. In: Banu JR (ed) Anaerobic digestion. IntechOpen, London. https://doi.org/10.5772/intechopen.82088

59. Hernández-Beltrán JU, Hernández-De Lira IO, Cruz-Santos MM, Saucedo-Luevanos A, Hernández-Terán F, Balagurusamy N (2019) Insight into pretreatment methods of lignocellulosic biomass to increase biogas yield: current state, challenges, and opportunities. Appl Sci 9:3721. https://doi.org/10.3390/app9183721

60. Mateescu C, Dima AD (2019) Enzymatic pretreatment of algal biomass for enhanced conversion to biogas. J Eng Sci Innov 4(4):361–370

61. Kim HT, Yun EJ, Wang D, Chung JH, Choi IG, Kim KH (2013) A high temperature and low acid pretreatment and agarose treatment of agarose for the production of sugar and ethanol from red seaweed biomass. Bioresour Technol 136:582–587

62. Hom-Diaz A, Passos F, Ferrer I, Vicent T, Blanquez P (2016) Enzymatic pretreatment of microalgae using fungal broth from Trametes versicolor and commercial laccase for improved biogas production. Algal Res 19:184–188

63. Tamilarasan K, Kavitha S, Rajesh Banu J, Arulazhagan P, Tae Yeom I (2017) Energy-efficient methane production from macroalgal biomass through chemo disperser liquefaction. Bioresour Technol 228:156–163

64. Aftab MN, Iqbal I, Riaz F, Karadag A, Tabatabaei M (2019) In: El-Fatah Abomohra A (ed) Biomass for bioenergy—recent trends and future challenges. IntechOpen, London. https://doi.org/10.5772/intechopen.84995

65. Mosier N, Wyman C, Dale B, Elander R, Lee YY, Holtzapple M, Ladisch M (2005) Features of promising technologies for pretreatment of lignocellulosic biomass. Bioresour Technol 96(6):673–686

66. Bhutto AW, Qureshi K, Harijan K, Abro R, Abbas T, Bazmi AA, Karim S, Yu G (2017) Insight into progress in pre-treatment of lignocellulosic biomass. Energy 122:724–745

67. Shah FA, Mahmood Q, Rashid N, Pervez A, Raja IA, Shah MM (2015) Co-digestion, pretreatment and digester design for enhanced methanogenesis. Renew Sustain Energy Rev 42:627–642

68. Patinvoh RJ, Osadolor OA, Chandolias K, Horváth IS, Taherzadeh MJ (2016) Innovative pretreatment strategies for biogas production. Bioresour Technol 224:13–24

69. Moset V, Xavier CDAN, Feng L, Wahid R, Møller HB (2018) Combined low thermal alkali addition and mechanical pre-treatment to improve biogas yield from wheat straw. J Clean Prod 172:1391–1398

70. Dahadha S, Amin Z, Lakeh AAB, Elbeshbishy E (2017) Evaluation of different pretreatment processes of lignocellulosic biomass for enhanced biomethane production. Energy Fuel Energy Fuels 31(10):10335–10347

71. Baruah J, Nath BK, Sharma R, Kumar S, Deka RC, Baruah DC, Kalita E (2018) Recent trends in the pretreatment of lignocellulosic biomass for value-added products. Front Energy Res 6:141. https://doi.org/10.3389/fenrg.2018.00141

72. Córdova O, Santis J, Ruiz-Fillipi G, Zuñiga ME, Fermoso FG, Chamy R (2018) Microalgae digestive pretreatment for increasing biogas production. Renew Sustain Energy Rev 82:2806–2813

73. Torres LM, Espinosa L (2008) Effect of alkaline pretreatment on anaerobic digestion of solid wastes. Waste Manag 28:2229–2234. https://doi.org/10.1016/j.wasman.2007.10.006

74. Passos F, Hom-Diaz A, Blanquez P, Vicent T, Ferrer I (2016) Improving biogas production from microalgae by enzymatic pretreatment. Bioresour Technol 199:347–351

75. Wagner AO, Lackner N, Mutschlechner M, Prem EV, Markt R, Illmer P (2018) Biological pretreatment strategies for second-generation lignocellulosic resources to enhance biogas production. Energies 11:1797

76. Parthiba Karthikeyan O, Trably E, Mehariya S, Bernet N, Wong JWC, Carrere H (2018) Pretreatment of food waste for methane and hydrogen recovery: a review. Bioresour Technol 249:1025–1039

77. Premier GC, Kim JR, Massanet-Nicolau J, Kyazze G, Esteves S, Penumathsa B, Rodríguez R, Maddy J, Dinsdale J, Guwy AJ (2013) Integration of biohydrogen, biomethane and bio-electrochemical systems. Renew Energy 49:188–192

78. Martinez-Perez N, Cherryman SJ, Premier GC, Dinsdale RM, Hawkes DL, Hawkes FR, Kyazze G, Guwy AJ (2007) The potential for hydrogen-enriched biogas production from crops: scenarios in the UK. Biomass Bioenergy 31:95–104

79. Show KY, Lee DJ, Zhang ZP (2011) Production of biohydrogen: current perspectives and future prospects. In: Pandey A, Larroche C, Ricke SC, Dussap CG, Gnansoinou E (eds) Biofuels alternative feedstocks and conversion processes. Academic Press, Amsterdam, pp 467–479

80. Cysneiros D, Banks CJ, Heaven S, Karatzas KAG (2012) The effect of pH control and 'hydraulic flush' on hydrolysis and volatile fatty acids (VFA) production and profile in anaerobic leach bed reactors digesting a high solids content substrate. Bioresour Technol 123:263–271

81. Bharathiraja B, Sudharsanaa T, Jayamuthunagaib J, Praveenkumarc R, Chozhavendhand S, Iyyappan J (2018) Biogas production—a review on composition, fuel properties, feed stock and principles of anaerobic digestion. Renew Sustain Energy Rev 90:570–582

82. Dobre T, Pârvulescu OC, Răducanu C, Tricǎ B, Jinescu G (2018) Stochastic modelling of poly-saccharide hydrolysis. J Eng Sci Innov 3(1):25–38

83. Van DP, Fujiwara T, Tho BL, Toan PS, Minh GH (2020) A review of anaerobic digestion systems for biodegradable waste: configurations, operating parameters, and current trends. Environ Eng Res 25(1):1–17

84. Cirne DG, Paloumet X, Björnsson L, Alves MM, Mattiasson B (2007) Anaerobic digestion of lipid-rich waste—effects of lipid concentration. Renew Energy 32:965–975

85. Stams AJM, Plugge CM (2009) Electron transfer in syntrophic communities of anaerobic bacteria and archaea. Nat Rev Microbiol 7:568–577

86. Lovley DR, Klug MJ (1983) Methanogenesis from methanol and methylamines and aceto-genesis from hydrogen and carbon dioxide in the sediments of a eutrophic lake. Appl Environ Microbiol 45:1310–1315

87. Deublein D, Steinhauser A (2008) Biogas from waste and renewable resources: an introduction. Wiley, Hoboken, NJ. ISBN 978-3-527-31841-4

88. Abbasi T, Tauseef SM, Abbasi SA (2012) Anaerobic digestion for global warming control and energy generation—an overview. Renew Sustain Energy Rev 16:3228–3242

89. Deepanraj B, Sivasubramanian V, Jayaraj S (2014) Biogas generation through anaerobic digestion process—an overview. Res J Chem Environ 18(5):80–93

90. Sikora A, Detman A, Mielecki D, Chojnacka A, Błaszczyk M (2019) Searching for metabolic pathways of anaerobic digestion: a useful list of the key enzymes. In: Banu R (ed) Anaerobic digestion. IntechOpen, London, pp 485–544. ISBN: 978-1-83881-850-0

91. Mateescu C (2016) Influence of the hydrostatic pressure on biogas production in anaerobic digesters. Rom Biotechnol Lett 21(5):11941–11948

92. Das D, Veziroglu N (2008) Advances in biological hydrogen production processes. Int J Hydrogen Energy 33(21):6046–6057

93. Antonopoulou G, Ntaikou I, Stamatelatou K, Lyberatos G (2011) Biofuels chemical and biolo-chemical conversion processes and technologies: Biological and fermentative production of hydrogen. In: Luque R, Campelo J, Clark J (eds) Handbook of biofuels production. Woodhead Publishing, Cambridge, pp 305–346. https://doi.org/10.1533/9780857090492.2.305

94. Sołowski G (2018) Biohydrogen production—sources and methods: a review. Int J Bioprocess Biotech. https://doi.org/10.20911/IJBBT-101.100001

95. Hawkes FR, Dinsdale R, Hawkes DL, Hussy I (2002) Sustainable fermentative hydrogen production: challenges for process optimisation processes. Int J Hydrogen Energ 27:1339–1347

96. Tapia-Venegas E, Ramirez-Morales JE, Silva-Illanes F, Toledo-Alarcon J, Paillet F, Escudie R, Lay CH, Chu CY, Leu HJ, Marone A, Lin CY, Kim DH, Trably E, Ruiz-Filippi G (2015) Biohydrogen production by dark fermentation: scaling-up and technologies integration for a sustainable system. Rev Environ Sci Biotechnol 14(4):761–785

97. Sharma S, Singh RN, Tripathi S (2013) Biohydrogen from algae: fuel of the future. Int. Res J Environ Sci 2(4):44–47

98. Liu H, Got S, Logan BE (2005) Electrochemically assisted microbial production of hydrogen from acetate. Environ Sci Technol 39:4317–4320

99. Cappai G, De Gioannis G, Muntoni A, Spiga D, Boni MR, Polettini A, Pomi R, Rossi A (2018) Biohydrogen production from food waste: influence of the inoculum-to-substrate ratio. Sustainability 10:4506. https://doi.org/10.3390/su10124506

100. Ghimire A, Luongo V, Frunzo L, Pirozzi F, Lens PNL, Esposito G (2017) Continuous biohydrogen production by thermophilic dark fermentation of cheese whey: use of buffalo manure as buffering agent. Int J Hydrogen Energy 42(8):4861–4869

101. Bravim da Silva O, Silva Carvalho L, Carneiro de Almeida G, Davies de Oliveira J, Souza Carmo T, Skorupa Parachin N (2017) Biogas—turning waste into clean energy. IntechOpen, London. https://doi.org/10.5772/64262

102. Cardoso V, Romao BB, Silva FTM, Santos JG, Batista FRX, Ferreira JS (2014) Hydrogen production by dark fermentation. Chem Eng Trans 38:481–486

103. Florio C, Micoli L, Ausiello A, Pasquale V, Turco M, Pirozzi D, Toscano G, Dumontet S (2018) Mesophilic dark fermentation of food waste for biohydrogen production in a mixed batch reactor. Chem Eng Trans 67:67–72

104. Venkata Mohan S, Bhaskar YV, Krishna TM, Chandrasekhara Rao N, Lalit Babu V, Sarma PN (2007) Biohydrogen production from chemical wastewater as substrate by selectively enriched anaerobic mixed consortia: influence of fermentation pH and substrate composition. Int J Hydrogen Energy 32:2286–2295

105. Vijaya Bhaskar Y, Venkata Mohan S, Sarma PN (2008) Effect of substrate loading rate of chemical wastewater on fermentative biohydrogen production in biofilm configured sequencing batch reactor. Bioresour Technol 99:6941–6948

106. Zupančič GD, Grilc V (2012) Anaerobic treatment and biogas production from organic waste. In: Kumar S (ed) Management of organic waste. InTech, Rijeka, pp 1–28. http://www.intechopen.com/books/management-of-organic-waste/anaerobic-treatment-and-biogas-production-from-organic-wastes

107. Han SK, Shin HS (2004) Performance of an innovative two-stage process converting food waste to hydrogen and methane. J Air Waste Manag Assoc 54:242–249

108. Trad Z, Fontaine JP, Larroche C, Vial C (2016) Multiscale mixing analysis and modeling of biohydrogen production by dark fermentation. Renew Energy 98:264–282

109. Anukam A, Mohammadi A, Naqvi M, Granström K (2019) A review of the chemistry of anaerobic digestion: methods of accelerating and optimizing process efficiency. Processes 7:504. https://doi.org/10.3390/pr7080504

110. Angelidaki I, Treu L, Tsapekos P, Luo G, Campanaro S, Wenzel H, Kougias PG (2018) Biogas upgrading and utilization: current status and perspectives. Biotechnol Adv 36(2):452–466

111. Bassani I (2017) Hydrogen assisted biological biogas upgrading. PhD Thesis, Kgs. Technical University of Denmark, DTU Environment, Lyngby

112. Bailon Allegue L, Hinge J (2012) Report biogas and bio-syngas upgrading. Danish Technological Institute, Taastrup

113. Kougias PG, Treu L, Benavente DP, Boe K, Campanaro S, Angelidaki I (2017b) Ex-situ biogas upgrading and enhancement in different reactor systems. Bioresour Technol 225:429–437

114. Adnan AI, Ong MY, Nomanbhay S, Chew KW, Show PL (2019) Technologies for biogas upgrading to biomethane: a review. J Bioeng 6:92. https://doi.org/10.3390/bioengineering6040092

115. Bassani I, Kougias PG, Treu L, Angelidaki I (2015) Biogas upgrading via hydrogenotrophic methanogenesis in two-stage continuous stirred tank reactors at mesophilic and thermophilic conditions. Environ Sci Technol 49:12585–12593

116. Bauer F, Hulteberg C, Persson T, Tamm D, Granskning B (2013) Biogas upgrading—review of commercial technologies. SGS Rapport 270. Swedish Gas Technology Centre, Malmö

117. Munoz R, Meier L, Diaz I, Jeison D (2015) A review on the state-of-the-art of physical/chemical and biological technologies for biogas upgrading. Rev Environ Sci Biotechnol 14:727–759

118. An H, Feng B, Su S (2011) CO_2 capture by electrothermal swing adsorption with activated carbon fibre materials. Int J Greenh Gas Con 5:16–25

119. Augelletti R, Conti M, Annesini MC (2017) Pressure swing adsorption for biogas upgrading. A new process configuration for the separation of biomethane and carbon dioxide. J Clean Prod 140:1390–1398

120. Harasimowicz M, Orluk P, Zakrzewska-Trznadel G, Chmielewski AG (2007) Application of polyimide membranes for biogas purification and enrichment. J Hazard Mater 144:698–702

121. Khan IU, Dzarfan Othman HM, Hashim H, Matsuura T, Ismail AF, Arzhandi RDM, Azelee WI (2017) Biogas as a renewable energy fuel—a review of biogas upgrading, utilization and storage. Energ Conver Manage 150:277–294

122. Andriani D, Wresta A, Atmaja T, Saepudin A (2014) A review on optimization production and upgrading biogas through CO_2 removal using various techniques. Appl Biochem Biotechnol 172:1909–1928

123. Klankermayer J, Wesselbaum S, Beydoun K, Leitner W (2016) Selective catalytic synthesis using the combination of carbon dioxide and hydrogen: catalytic chess at the interface of energy and chemistry. Angew Chem Int Ed 55:7296–7343

124. Sun X, Kang X, Zhu Q, Ma J, Yang G, Liu Z, Han B (2016) Very highly efficient reduction of CO_2 to CH_4 using metal-free N-doped carbon electrodes. Chem Sci 7:2883–2887

125. Kougias PG, Campanaro S, Treu L, Zhu X, Angelidaki I (2017a) A novel archaeal species belonging to methanoculleus genus identified via de-novo assembly and metagenomic binning process in biogas reactors. Anaerobe 46:23–32

126. Agneessens LM, Ottosen LDM, Voigt NV, Nielsen JL, de Jonge N, Fischer CH, Kofoed MVW (2017) In-situ biogas upgrading with pulse H_2 additions: the relevance of methanogen adaption and inorganic carbon level. Bioresour Technol 233:256–263

127. Mulat DG, Mosbæk F, Ward AJ, Polag D, Greule M, Keppler F, Nielsen JL, Feilberg A (2017) Exogenous addition of H_2 for an in situ biogas upgrading through biological reduction of carbon dioxide into methane. Waste Manag 68:146–156

128. Sun Q, Li H, Yan J, Liu L, Yu Z, Yu X (2015) Selection of appropriate biogas upgrading technology—a review of biogas cleaning, upgrading and utilization. Renew Sustain Energy Rev 51:521–532
129. Bailon Allegue L, Hinge J (2014) Biogas upgrading. Evaluation of methods for H2S removal. Danish Technological Institute, Taastrup
130. Kajolina T, Aakko-Saksa P, Roine J, Kall L (2015) Efficiency testing of three biogas siloxane removal systems in the presence of D5, D6, limonene and toluene. Fuel Process Technol 139:242–247
131. Ryckebosch E, Drouillon M, Vervaeren H (2011) Techniques for transformation of biogas to biomethane. Biomass Bioenergy 35:1633–1645
132. Kapoor R, Subbarao PM, Vijay VK, Shah G, Sahota S, Singh D, Verma M (2017) Factors affecting methane loss from a water scrubbing based biogas upgrading system. Appl Energy 208:1379–1388
133. Al Seadi T, Rutz D, Heinz P, Köttner M, Finsterwalder T, Volk S, Janssen R (2008) Biogas handbook. University of Southern Denmark, Esbjerg. ISBN 978-87-992962-0-0
134. Risberg K, Cederlund H, Pell M, Arthurson V, Schnürer A (2017) Comparative characterization of digestate versus pig slurry and cow manure e chemical composition and effects on soil microbial activity. Waste Manag 61:529–538
135. Vilanova Plana P, Noche B (2016) A review of the current digestate distribution models: storage and transport. WIT Trans Ecol Environ 202:345–357
136. Möller K, Müller T (2012) Effects of anaerobic digestion on digestate nutrient availability and crop growth: a review. Eng Life Sci 12(3):242–257
137. Logan M, Visvanathan C (2019) Management strategies for anaerobic digestate of organic fraction of municipal solid waste: current status and future prospects. Waste Manag Res 37(1):27–39
138. Fuchs W, Drosg B (2013) Assessment of the state of the art of technologies for the processing of digestate residue from anaerobic digesters. Water Sci Technol 67(9):1984–1993
139. Monlau F, Sambusiti C, Ficara E, Aboulias A, Barakata A, Carrère H (2015a) New opportunities for agricultural digestate valorization: current situation and perspectives. Energ Environ Sci 8:2600–2621
140. Monlau F, Sambusiti C, Antoniou N, Barakat A, Zabaniotou A (2015b) A new concept for enhancing energy recovery from agricultural residues by coupling anaerobic digestion and pyrolysis process. Appl Energy 148:32–38
141. Monfet E, Aubry G, Avalos Ramirez A (2018) Nutrient removal and recovery from digestate: a review of the technology. Biofuels 9(2):247–262
142. Bustamante MA, Restrepo AP, Alburquerque JA, Pérez-Murcia MD, Paredes C, Moral R, Bernal MP (2013) Recycling of anaerobic digestates by composting: effect of the bulking agent used. J Clean Prod 47:61–69
143. Torres-Climent A, Martin-Mata J, Marhuenda-Egea F, Moral R, Barber X, Perez-Murcia MD, Paredes C (2015) Composting of the solid phase of digestate from biogas production: optimization of the moisture, C/N ratio, and pH conditions. Commun Soil Sci Plan 46:197–207
144. Hanc A, Vasak F (2015) Processing separated digestate by vermicomposting technology using earthworms of the genus Eisenia. Int J Environ Sci Technol 12:1183–1190
145. Nagy D, Balogh P, Gabnai Z, Popp J, Oláh J, Bai A (2018) Economic analysis of pellet production in co-digestion biogas plants. Energies 11:1135. https://doi.org/10.3390/en11051135
146. Peng W, Pivato A (2017) Sustainable management of digestate from the organic fraction of municipal solid waste and food waste under the concepts of back to earth alternatives and circular economy. Waste Biomass Valor 10(2):465–481
147. Fabbri D, Torri C (2016) Linking pyrolysis and anaerobic digestion (Py-AD) for the conversion of lignocellulosic biomass. Curr Opin Chem Biol 38:167–173
148. Hossain AK, Serrano C, Brammer JB, Omran A, Ahmed F, Smith DI, Davies PA (2016) Combustion of fuel blends containing digestate pyrolysis oil in a multi-cylinder compression ignition engine. Fuel 171:18–28

149. Opatokun SA, Strezov V, Kan T (2015) Product based evaluation of pyrolysis of food waste and its digestate. Energy 92:349–354
150. Zhu L (2015) Microalgal culture strategies for biofuel production: a review. Biofuels Bioprod Biorefin 9:801–814
151. Di Domenico EG, Petroni G, Mancini D, Geri A, Di Palma L, Ascenzioni F (2015) Development of electroactive and anaerobic ammonium-oxidizing (Anammox) biofilms from digestate in microbial fuel cells. Biomed Res Int 2015:351014. https://doi.org/10.1155/2015/351014
152. Wu S, Lv T, Lua Q, Ajmala Z, Dong R (2017) Treatment of anaerobic digestate supernatant in microbial fuel cellcoupled constructed wetlands: evaluation of nitrogen removal, electricity generation, and bacterial community response. Sci Total Environ 580:339–346
153. Güngören Madenoğlu T (2018) Evaluation of anaerobically digested biomass in catalytic supercritical water gasification for biofuel production. Anadolu Uni J Sci Techn A App Sci Eng 19(2):407–421
154. Ning D, Ramin A, Ajay KD, Janusz AK (2014) Catalytic gasification of cellulose and pinewood to H2 in supercritical water. Fuel 118:416–425
155. Pooya A, Sami K, Friederike S, Faraz A, Ramin F (2012) Hydrogen production from cellulose, lignin, bark and model carbohydrates in supercritical water using nickel and ruthenium catalysts. Appl Catal B Environ 117–118:330–338
156. Basu P (2010) Biomass gasification and pyrolysis practical design. Elsevier, Oxford
157. Sen B (2015) Recent advances in hydrogen production by dark fermentation technology. In: Sivakumar S, Sharma UC, Prasad R (eds) Energy science and technology: hydrogen and other technologies, vol 11. Studium Press LLC, Houston, TX, pp 159–181
158. Fallde M, Eklund M (2014) Towards a sustainable socio-technical system of biogas for transport: the case of the city of Linkoping in Sweden. J Clean Prod 98:17–28. https://doi.org/10.1016/j.jclepro.2014.05.089
159. Theuerl S, Klang J, Prochnow A (2019) Process disturbances in agricultural biogas production—causes, mechanisms and effects on the biogas microbiome: a review. Energies 12:365. https://doi.org/10.3390/en12030365
160. Prasad S, Rathore D, Singh A (2017) Recent advances in biogas production. Chem Eng Process Tech 3(2):1038
161. Scheper TH, Lammers F (1994) Fermentation monitoring and process control. Curr Opin Biotechnol 5(2):187–191
162. Nardin F, Mancini M, Unterhofer T, Mazzetto F (2014) New solutions for digestate solid/liquid separation to apply on small alpine farm biogas plants. In: Proceedings International Conference of Agricultural Engineering, Zurich, July 2014
163. Chatellard L, Marone A, Carrère H, Trably E (2016) Trends and challenges in biohydrogen production from agricultural waste. In: Singh A, Rathore D (eds) Biohydrogen production: sustainability of current technology and future perspective. Springer, Berlin, pp 69–95. https://doi.org/10.1007/978-81-322-3577-4_4

Bio-Catalytic Itaconic Acid and Bio-Based Vinyl Monomer Production Processes

Kalpana Avasthi, Ashish Bohre, Basudeb Saha, and Blaž Likozar

Abstract The production of polymers in the present society has relied heavily on fossil resources. It is not impossible to imagine the world without plastic-based materials. The production of plastic globally has surpassed 8300 million metric tons that utilized around 7% of fossil fuels. The limited availability of fossil-based sources has driven the research and development to find out alternative sources for the synthesis of polymers. In this regard lignocellulosic biomass is an interesting feedstock for the synthesis of polymers. However, the overall production cost of the as-synthesized sustainable polymers is the major obstacle that needs to be addressed. This chapter described the sustainable bio-catalytic pathways for the production of four important sustainable vinyl monomers: itaconic acid, acrylic acid, methacrylic acid, and styrene. Annual production of these monomers exceeds 26 million tons, *albeit* from non-renewable feedstocks. They provide the backbone to produce polyesters, polyacrylates, polystyrene adhesives, protective coatings, paints, resins, rubbers, and other copolymers.

Keywords Monomers · Biomass · Catalysis · Sustainability · Metabolic engineering

K. Avasthi · A. Bohre (✉) · B. Likozar (✉)
Department of Catalysis and Chemical Reaction Engineering, National Institute of Chemistry, Ljubljana, Slovenia
e-mail: ashish.bohre@ki.si; blaz.likozar@ki.si

B. Saha (✉)
Catalysis Center for Energy Innovation, University of Delaware, Newark, DE, USA

RiKarbon, Inc., Newark, DE, USA
e-mail: bsaha@udel.edu; bsaha@rikarbon.com

1 Introduction

With increasing global energy demand and ecological concerns related to the consumption of fossil-based feedstocks, there is a need to develop alternative fuels from sustainable, non-food resources. The effective utilization of abundantly available, inexpensive residues of agricultural and forest biomass to produce liquid fuels and biogenic materials can play a crucial role in addressing this concern [1]. The production of polymers heavily depends upon non-renewable feedstocks. However, due to the finite nature of fossil-based feedstocks, it is necessary to find alternative sustainable feedstocks like lignocellulosic biomass. Presently, 8300 million metric tons per year (Mt) of polymers are produced from fossil resources that utilized ~7% fossil fuels worldwide [2].

The finite nature of fossil-based sources and their environmental impact have driven the need to produce polymers from sustainable feedstocks [3]. The sustainable polymers have the capability to replace the conventional fossil-derived polymers. However the high production cost and inferior performance are the two main obstacles that render its commercialization limited [4].

Biomass-derived vinyl monomers such as itaconic acid (IA), acrylic acid (AA), methacrylic acid (MAA), styrene (ST), etc. are important substrates for sealing materials, household plastics, adhesive resins, and textile fiber applications. The vast majority of vinyl monomers in industries are derived from fossil fuels through several commercial processes. Apart from the utilization of unsustainable feedstocks, low product yield, multiple steps, and formation of toxic side products are the other major drawbacks associated with industrial processes.

To address these drawbacks, the production of vinyl monomers has been directed towards sustainable bio-catalytic processes utilizing bio-based feedstocks. As a result, several research articles and patents have appeared recently that have shown the benefits of sustainable vinyl monomer production [5, 6].

Vinyl monomers are industrially important commodity chemicals, which are widely used to produce polyesters, polyacrylates, polystyrene adhesives, protective coatings, paints, resins, rubbers, and other copolymers [7]. The chemical structure of vinyl monomers contains an active double bond that can be further functionalized to yield versatile synthetic intermediates and polymers. In this chapter, recent bio-catalytic transformation strategies applied to the production of vinyl monomers from biomass-derived feedstocks are discussed. Focus is given to four important vinyl monomers: IA, AA, MAA, and ST. Each of these is produced at over 26 million tons per annum from petroleum feedstock with current market prices of about $2500 per metric (Fig. 1) [8].

2 Itaconic Acid

Itaconic acid (IA) is a versatile chemical derived from the fermentation of carbohydrate feedstocks [9, 10]. It is composed of unsaturated dicarboxylic acid functionalities that make it an attractive building block to produce several novel copolymers.
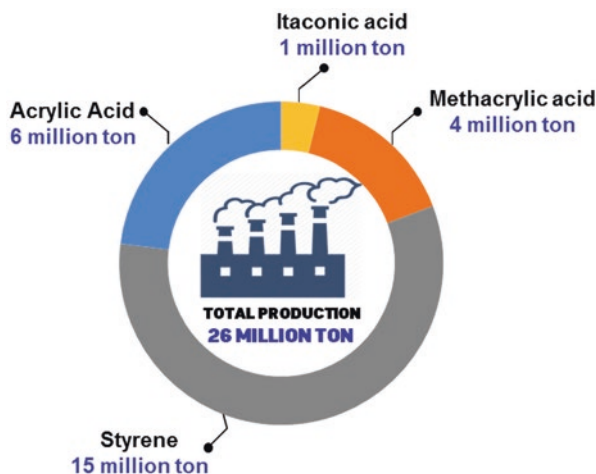
Fig. 1 Global annual production of the four most important vinyl monomers

It has also been utilized for the synthesis of polyester-based renewable polymers, synthetic resins, rubbers, and coatings [11]. Owing to its promising applications, the US Department of Energy has identified IA as the most useful and promising chemical produced from bio-based material, which appealed to the scientific community towards the development of a scalable technology for IA production and usage [12].

The synthetic route of IA was initially reported in 1837 by the high-temperature decarboxylation of citric acid [13]. Since the 1960s, industries have been producing IA by fermentation of glucose using filamentous fungus *Aspergillus terreus* (*A. terreus*) with product intensity of 80 g L^{-1} and production volume of about one million tons per year [14]. In 2009, a research group from the University of New Hampshire developed the homopolymer of IA, which was licensed to Itaconix® [15].

The current industrial process faced several challenges like dependence on selected microorganism strains and the sensitivity of *A. terreus* to substrate impurities [16]. To overcome these challenges, many studies have been conducted in the recent past [17]. In particular, they cover genetic modification of the microorganism, morphological engineering of utilization *A. terreus* of low-cost substrates, and use of alternative microorganisms. Such technical developments are briefly reviewed in the following section.

2.1 Global Production and Applications of Bio-Based IA

The global production of IA is around one million tons per year, mostly used for the production of polymer and copolymer [18]. Commercial-scale production of IA was started in 1945 by Pfizer Company. Since then, Rhodia (1995, France), Iwata Chemical (1970, Japan), and Cargill (1996, USA) have also initiated

commercial-scale IA production [19]. Most IA production (about 76%) facilities are located in China [20]. After China, Alpha Chemika (India) and Itaconix Co. (USA) are the major IA producers [21].

As a result of the EU restriction on the use of sodium tri(poly)phosphate to prevent eutrophication in the industrial production of detergents, polyitaconic acid (a derivative of IA) was used instead. In 2015, Germany was the leading producer of IA in the EU with market size of $2.8 million [22].

2.2   Bio-Catalytic Pathway for the Production of IA

IA is exclusively produced by submerged batch culture process using a high-producing strain of *A. terreus* [23, 24]. In this process high sugar (glucose or sucrose) concentration and continuous supply of high amounts of oxygen are needed, which make the process expensive. Another drawback is that the growth of *A. terreus* fungus is sensitive to phosphate impurities [25, 26]. The following sections described the use of different fungi, yeasts, and bacteria for IA biosynthesis.

2.2.1   IA Production by Fungi

Ustilago maydis   Ustilago maydis (*U. maydis*) is a biotrophic organism that can be utilized for the synthesis of IA [27]. Advantages such as unicellular growth pattern, lower sensitivity to impurities, homogenous oxygenation, and easy genetic manipulation make this fungus a possible alternative to *A. terreus*. The production process of IA by both of these fungi is different. Using *Ustilago* and related species, IA is produced at pH above 5, whereas comparatively low pH is required in the case of *A. terreus.* In addition, IA production by most *Ustilago* species is triggered under nitrogen-limited environment, whereas phosphate limitation applies to *A. terreus*. *U. maydis* follows an uncommon metabolic pathway different from the reported pathway of *A. terreus* (Fig. 2) [28]. Despite the very different lifestyles of these fungi, the function of transporters involved in the synthesis of IA is likely similar in both cases [29]. The activities of such transporters are significantly affected by either amino acid sequence or primary structure of the protein and underlying biosynthetic pathways. Wierckx et al. showed that the mitochondrial tricarboxylate transporter from *A. terreus* (At_MttA) allows greater itaconate yield in *U. maydis* than overexpressing the natural mitochondrial tricarboxylate transporter (mtt1) [30].

Most *U. maydis*-catalyzed fermentation reaction was performed on a lab scale in shake flasks. Guevarra and Tabuchi synthesized various carboxylic acids with the aid of this fungus with IA yield of 53 g L^{-1} [31]. Klement et al. reported the production of IA from glucose using *U. maydis* wild-type strain MB215 under nitrogen-restricted conditions, and the optimum IA concentration achieved was 20 g L^{-1} [32]. Nitrogen limitation is crucial for the effective production of IA. The main problem
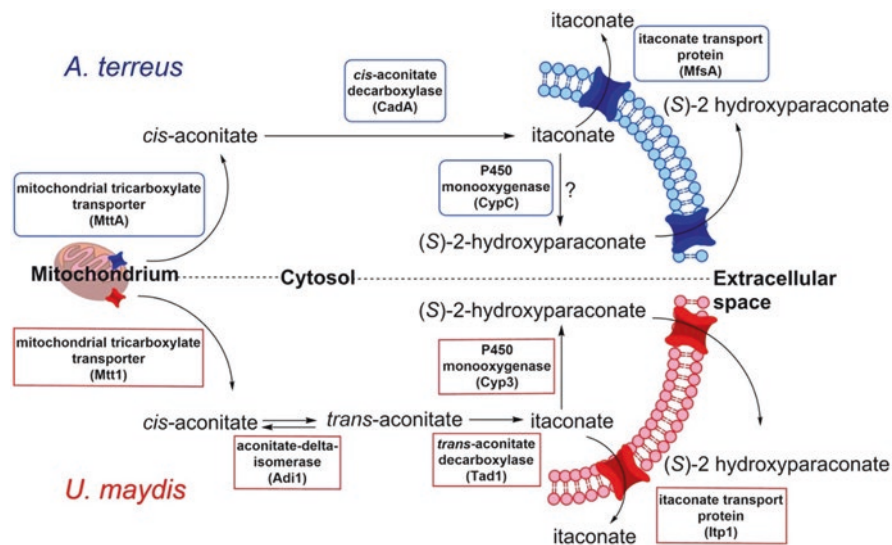
Fig. 2 Itaconate and (*S*)-2-hydroxyparaconate biosynthesis pathways of *U. maydis* and *A. terreus*, a comparison. (Reproduced with permission from [30]. Copyright (2019) Elsevier)

associated with small-scale production is that the control of pH is very difficult and sampling from the shake flasks causes oxygen limitations that affect IA production [16]. In order to avoid the limitation and produce IA under more industrially relevant conditions, Maassen et al. proposed a new method in which cultivation was performed in a stirred batch where pH can be constantly controlled [33]. The authors reported an optimum 0.74 g L^{-1} h^{-1} rate of IA production from glucose (200 g L^{-1}) and ammonium (75 mM). It was found that the yield of IA can be further improved by reducing the concentration of glucose.

In 2016, Geiser et al. proposed that *U. maydis* also produces 2-hydroxyparaconate as a second metabolite along with IA by controlled pulsed fed-batch fermentation process [34]. It is possible to increase IA production up to 67% after deleting the enzyme responsible for the degradation of IA into 2-hydroxyparaconate. Such genetic engineering can be beneficial for improved titer of IA. Wierckx et al. recently proposed an integrated process by gene knockouts, overexpression of genes, and replacement of promoter to improve IA yield [35]. This combined approach yielded 220 g L^{-1} IA titer, the highest ever achieved from *U. maydis* and *A. terreus*. A high level of malate was also produced under these conditions. The IA yield can be further increased by removal/inactivation of the enzyme that promotes the formation of malate intermediate.

Ustilago cynodontis Ustilago cynodontis (*U. cynodontis*) is another smut fungus belonging to the *Ustilaginaceae* family and commonly known as a natural producer of IA [36]. It features relatively high pH resistance properties compared to other smut fungi and is beneficial for the production of IA in batch fermentations.

Utilization of such pH-resistant fungi can reduce the cost of alkalization required to back titrate the produced acids and minimize the waste formation. Guevarra and Tabuchi first described the production of IA and 2-hydroxyparaconic in unbuffered media from glucose by *U. cynodontis* [37]. In this study, the growth of cells was investigated at different temperatures. Low temperature (25 °C) was found to be the best for cell growth and resulted in the highest organic acid titers. In 2014, Geiser et al. screened 68 strains of the *Ustilaginaceae* family for the synthesis of carboxylic acids, polyols, and glycolipids from glucose [36]. Among the tested fungi, *U. cynodontis* was identified as an efficient producer of IA with 3.3 g L^{-1} titer under relatively low pH. In a most recent pioneer work, Hosseinpour et al. applied morphological and metabolic engineering to generate an efficient pH-tolerant host to produce IA under biotechnologically relevant environments [38]. The yeast-like morphology of *U. cynodontis* was preserved by disturbing the signal transduction route and by deletions of *ras2*, *fuz7*, and *ubc3* genes under stress-inducing conditions. This metabolically engineered strain produced 21 g L^{-1} IA in a fed-batch fermentation process with pulse feeding at pH 3.8.

Aspergillus niger *Aspergillus niger* (*A. niger*) was identified as an emerging alternative for the synthesis of IA. *A. niger* is presently employed to synthesize citric acid on an industrial scale [39]. The biotechnological route to produce citric acid is similar to IA. It is beneficial because the current fermentation setup of citric acid can be employed to produce IA on a commercial scale from this fungus. *A. niger* cannot produce IA naturally because it lacks the essential enzyme cis-aconitate decarboxylase (*cadA*) [40, 41]. Sole expression of the enzyme is not adequate because such genetically modified strain produces very low concentration of IA (0.05 g L^{-1}). Li et al. demonstrated that 2.5 g L^{-1} IA could be achieved by overexpression of a mitochondrial carrier or a plasma membrane carrier [42]. In 2013, Maassen et al. showed that co-overexpression of *cadA* (encoding a cis-aconitate decarboxylase) and *acoA* (encoding a aconitase decarboxylase) genes in the cytosol and mitochondria doubles the productivity of IA from glucose [43]. Interestingly, expression of *acoA*, *mttA* (encoding a putative mitochondrial transporter), and *mfsA* genes (encoding a plasma membrane transporter) in the *A. niger* strain led to 24 times higher IA yield (4 g g^{-1}) compared to *CadA* [39].

In 2016, Hossain et al. genetically modified wild *A. niger* by incorporating a cytosolic citrate synthase (*citB*) gene. The resulting strains produced about 26.2 g L^{-1} of IA with a production rate of 0.35 g L^{-1} h^{-1} in batch cultivations without yielding any by-products [44]. They proposed that by-product formation was suppressed by the overexpression of citrate synthase that also improved the biosynthesis pathway toward IA. For improved yield of IA, the same research group recently expanded the cytosolic acetyl-CoA pool by introducing *acl1* and *acl2* genes that encode together for ATP-citrate lyase (ACL). Using fused *A. niger* cells, very high IA titer volume, up to 42.7 g L^{-1}, from glucose was reported [45]. They found that metabolic engineering of ACL increases glycolytic flux that leads to an enhanced IA

yield in *A. niger*. The fermentation conditions of IA can be enhanced by using nitrogen supplementation that reduces IA-induced weak-acid stress.

Along with the editing of specific genes, a variety of promoters have also been utilized to improve gene expression and increase the production of IA [10]. In 2011, Steiger et al. developed six novel promoters for *A. niger*. They obtained a 0.6 g L^{-1} titer of IA with the PmbfA promoter, while other promoters were not active for such transformation [46]. Li et al. introduced *gpdA* promoter to control *cadA* gene expression. The recombinant strain *A. niger* produced a relatively low titer (0.6 g L^{-1}) of IA [40]. To achieve a higher IA titer, Blumhoff et al. applied P*pki* and P*icdA* promoters to *A. niger*. Both promoters increased the expression of genes entailed in the fermentation process and increased the titer of IA to 1.4 g L^{-1} [43]. In 2017, Yin et al. designed a low-pH-induced promoter Pgas that dynamically controls gene expression in *A. niger* and produced IA at a titer of 5 g L^{-1} [47]. This promoter worked well even at very low pH (2.0), and the strength of the promoter was not dependent on acid ion concentration or type of acid used.

2.2.2 IA Production by Bacteria

Escherichia coli *Escherichia coli* (*E. coli*) is one of the most versatile organisms used as a host for the industrial synthesis of various chemicals [48]. *E. coli* strains have relatively shorter cultivation times for IA production compared to fungi. It is a stable bacterial strain that thrives under different growth conditions. Moreover, its flexibility towards genetic manipulation is excellent. Because of these advantages over fungi, several molecular cloning and genetic modification techniques have been introduced for the synthesis of IA. The biosynthesis of IA from *E. coli* was first achieved in 2011 by Li et al. [40]. They produced 0.08 g L^{-1} IA in Luria-Bertani (LB) medium with expression of *cad* gene under its inducible T7 promoter in culture of *E. coli*. The low activity of *E. coli* is associated with the fact that the key enzyme that is encoded by the *cad* gene and catalyzes this transformation was primarily present in inclusion bodies. To increase the titers of IA, Vuoristo et al. engineered *E. coli* by employing citrate synthase and aconitase from *Corynebacterium glutamicum* and by eliminating the genes encoding phosphate acetyltransferase and lactate dehydrogenase [49]. However such modifications only managed to increase IA production up to 0.69 g L^{-1}. Following a similar approach, Okamoto et al. observed that the inactivation of isocitrate dehydrogenase gene (*icd*) is beneficial for IA production and can enhance the yield of IA. *E. coli* produced 4.34 g L^{-1} I A from glucose by expression of T7-inducible *cad* gene along with *icd* inactivation after 105 h cultivation in LB medium [50]. The intracellular metabolism of *E. coli* strain was further engineered by applying a synthetic protein scaffold that improved metabolite synthesis with low expression levels of pathway enzymes [51]. The engineered strain produced 6.57 g L^{-1} IA in basic media (pH 8.5) from glucose.

Metabolic modelling is a promising approach to confirm that the engineered strains are capable to produce a desired product [52]. Harder et al. successfully

applied minimal cut set concept-based modelling approach to design a high IA producer strain [53]. In this approach, a plasmid (*pCadCS*) carrying a specific gene was introduced into *E. coli*. The derived *E. coli* strain produced 32 g L^{-1} IA from glucose in fed-batch culture. Despite the benefits, production of IA from *E. coli* by adopting the model-based approach was not advanced significantly.

To improve IA production, Yang et al. described a novel strategy by self-assembling aconitase (*aco*) and cis-aconitate decarboxylase (*cad*) enzymes in *E. coli* [54]. The IA production improved up to 8.7 g L^{-1} by adopting this strategy. To make a more divisible and efficient multi-enzyme device, this research group introduced citrate synthase (gltA) and developed sequential multi-enzymatic complex reactors (MECRs) in *E. coli* (Fig. 3) [55]. The obtained MECRs had a nanoscale particle-like structure with diameters from 50 to 120 nm. The productivity of the developed MECRs was greater to unassembled and linearly self-assembled strains.

In 2017, Kim et al. developed a whole-cell bioconversion with *E. coli* to produce IA [24]. They reported that the activity of aconitase and cis-aconitate decarboxylase could be enhanced by regulating the expression of multiple *cadA* genes. As a result, excellent IA titer of 41.6 g L^{-1} was achieved from citrate under buffer-free conditions. Performing such bioconversion in the absence of buffer decreases the manufacture cost and side products released during purification. The stability and reusability of *E. coli* were further increased by the immobilization on barium alginate [56]. The immobilized cells were stable and can be reused four times, enabling the possibility of IA production in a continuous system.

Corynebacterium glutamicum *Corynebacterium glutamicum* (*C. glutamicum*) is another gram-positive bacteria that has been used for the synthesis of IA from glu-
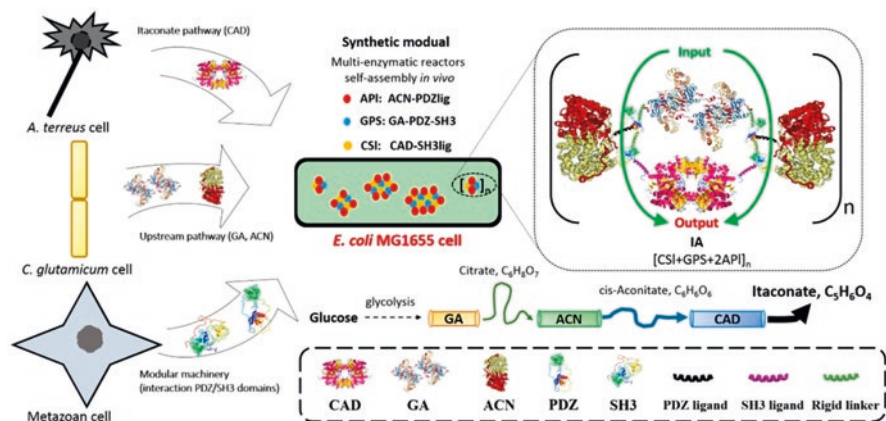
Fig. 3 Systematic strategies showing self-assembling of multi-enzymatic complex reactors of the heterogeneous dimeric GA, monomeric ACN, and dimeric CAD using protein-peptide interaction domains and ligands (mouse SH3 and PDZ domains/ligands). The scheme shown on the right represents the putative self-assembly mechanism to produce IA from citric acid using a sequential catalytic flux (green arrows). (Reproduced with permission from [55]. Copyright (2018) American Chemical Society)

cose [57]. It is tolerant to IA and can overcome the feedback inhibition problem. Otten et al. have explored the capability of *C. glutamicum* for glucose-based synthesis of IA [58]. They produced genetically engineered *C. glutamicum* immobilization of *A. terreus* CadA with *E. coli* maltose-binding protein. These modifications boosted the activity of *C. glutamicum*, resulting in IA titers of 7.80 g L^{-1} under nitrogen-limited growth conditions.

2.2.3 IA Production by Yeasts

When compared to fungi and bacteria, yeasts have some additional advantages including lower energy requirements, lower susceptibility to infectious agents, and ability to perform post-translational modifications. Despite such impressive features, little advancements have been made in utilization of yeast to produce IA. Few examples of IA production using yeast are described below.

Yarrowia lipolytica Yarrowia lipolytica (*Y. lipolytica*) is an oleaginous yeast for efficient production of IA [59]. In 2015, Alper et al. first demonstrated the inherent activity of *Y. lipolytica* to produce IA [60]. Different parameters such as media, enzyme localization, and metabolic pathways were screened and optimized to obtain 4.6 g L^{-1} titers of IA from glucose in a bioreactor. They found that *Y. lipolytica* is capable of growing under low pH and high-shear stress conditions. Motivated by this work, Zhao et al. enhanced the activity of *Y. lipolytica* by overexpressing a series of genes [61]. The overexpression of mitochondrial cis-aconitate transporter (MTT) gene substantially altered the organic acid profile of *Y. lipolytica*. The engineered strain produced 22.03 g L^{-1} IA from glucose which is the highest achieved from yeast under industrially relevant conditions.

Saccharomyces cerevisiae Saccharomyces cerevisiae (*S. cerevisiae*) is a non-pathogenic yeast known for its rapid growth, high tolerance to shear stress, and high pH resistance properties [62]. Blazeck et al. proposed a systematic approach for the synthesis of IA by *S. cerevisiae* [63]. In this approach, a hybrid promoter was first used to optimize pathway expression within *S. cerevisiae*. Next, three effective genetic targets were identified by in silico computational genome-scanning analysis. This collective approach resulted in IA productivity of 0.16 g L^{-1} from glucose. Young et al. applied iterative algorithm to develop substantial strain libraries that improves IA yield [64]. The most promising pathways to IA were identified through automated strain construction in which three libraries were designed to screen different parameters. This algorithmic design strategy produced 0.85 g L^{-1} IA, the highest yet reported by yeasts. Two other known IA producer yeasts are *Pseudozyma antarctica* and the genus *Candida*. *P. antarctica* was the most active and produced 30 g L^{-1} IA from glucose in flask fermentation under nitrogen-limited growth conditions [65, 66].

2.3 Production of IA from Different Sustainable Feedstocks

Glucose is the preferred feedstock for industrial production of IA that contributes to more than 25% of the total IA manufacturing cost. However, the high cost of glucose ($0.35–$0.60 kg^{-1}) has driven R&D initiatives towards utilization of alternative inexpensive raw materials to make IA production economically competitive to petrochemical-based products [66]. Starch-rich sources (corn, potato, and cassava) have emerged as compelling alternatives because of their high purity, low cost, and abundance [67]. Corn starch undergoes gelatinization when subjected to heating. Thus, hydrolysis of corn starch is performed by using mineral acid or enzymes that prevent gelatinization of corn starch. When hydrolysis of corn starch was performed over enzymes, hydrochloric or sulfuric acid before fermentation, *A. terreus* cells essentially needed a supplementary nitrogen source to begin the fermentation [68].

Although corn starch contains low concentrations of nitrogen, it is insufficient for cell growth. In contrast, when hydrolysis is performed with nitric acid, fermentation proceeded well without additional ingredients. This indicates that nitric acid works as an acid as well as nitrogen source for *A. terreus*. Acid-hydrolyzed sample of corn starch was subjected to fermentation at pH 2 before autoclaving at 121 °C for 20 min. Higher than 60 g L^{-1} IA was yielded in flask fermentation from 140 g L^{-1} of corn starch by *A. terreus* TN-484 [69]. Petruccioli et al. found that the productivity of IA was significantly affected by the degree of hydrolysis [67]. They achieved 18.40 g L^{-1} IA titers from corn starch saccharified at 85 dextrose equivalents by *A. terreus* NRRL 1960. The yield of IA was further increased to 63% by ultraviolet, chemical, and mixed mutagenic treatment of wild-type *A. terreus SKR10* strains [70].

The synthesis of IA from corn starch is a time-consuming and multiple-step process. To reduce the overall production time, Li et al. proposed an integrated process in which saccharification and fermentation steps were combined by overexpressing the glucoamylase gene in *A. terreus* strain. The IA titer reached 77.60 g L^{-1} by genetically engineered *A. terreus* from liquefied corn starch [26]. Researchers have also screened other starch-rich wastes for the production of IA. Potato starch wastes yielded high amounts of IA, which could be due to the higher glucose content [71]. *A. terreus* from mangrove soil has been recently isolated and utilized for the production of IA in a large volume (3 L) bioreactor [72]. The deionization of potato waste removed the inhibitory ions like phosphate and improved the yield of IA. Under optimized fermentation conditions, 29.69 g L^{-1} IA was produced by *A. terreus* strain C1.

In search of new alternative microorganisms, *E. coli* and *A. niger* species have been successfully tested for the production of IA from starch-rich feedstocks. Okamoto et al. proposed a direct IA production process by employing α-amylase expressing *E. coli* [73]. In this process, two α-amylases from *Bacillus amyloliquefaciens* NBRC 15535^T (BBA) and *Streptococcus bovis* NRIC 1535 (SBA) were selected for hydrolysis of starch. With 1% starch released from SBA hydrolysate, *E. coli* produced 0.15 g L^{-1} IA after 69 h cultivation by pH-stat method, while BBA displayed no noticeable activity. Gnanasekaran et al. investigated the feasibility of

A. niger species for the production of IA from inexpensive starch-based edible feedstocks [74]. They achieved IA titers of 15.65 g L^{-1} from 120 g L^{-1} corn starch through submerged batch fermentation in 168 h.

Utilization of starch-rich sources for production of IA is a good alternative; however, it competes with our food sources. Therefore, non-food renewable raw material is highly desirable. In this regard, lignocellulosic biomass has grown substantial attention, as it is abundant, inedible, carbon-neutral renewable source and extensively used for the production of biofuels and bio-products [75]. Xylose, a pentose sugar, has also been employed as a feedstock for the synthesis of IA with immobilized *A. terreus* TKK 200–5-21,960 [76]. It yielded very low amounts of IA even after a long fermentation period (165 h) in a continuous bioreactor. To improve the productivity of IA, Saha et al. screened 100 *A. terreus* strains, among which 20 *A. terreus* strains effectively produced IA from xylose and arabinose [77]. The highest amount of IA obtained was 36.4 g L^{-1} from 80 g L^{-1} mannose in a shake flask by strain NRRL 1961. Krull et al. described IA production from lignocellulosic biomass. They performed fermentation of agricultural residue "wheat chaff" by *A. terreus* [78]. It was found that alkaline pretreatment and subsequent enzymatic saccharification are essential for effective IA production. The wild-type strain *A. terreus* DSM 23081 produced 27.70 g L^{-1} IA.

Jatropha curcas (*J. curcas*) seed cake is another promising agro-waste that can be fermented for the production of IA. In 2007, Rao et al. proposed IA production route from *J. curcas* seed cake by using *A. terreus*. The fermentation was performed at various temperatures, times, pH, and agitation speeds. The highest IA yield (24.4 gL^{-1}) was achieved after 120 h of fermentation [79]. To improve the yield of IA, El-Imam et al. treated *J. curcas* seed cake in 50% sulfuric acid. The resulting slurry was fermented by *A. terreus* at 1.5 pH, which gave 48.7 g L^{-1} IA after 24 h [80]. In 2017, Omojasola et al. performed the fermentation of *J. curcas* seed cake by *A. terreus* and *A. niger fungi* [81]. The optimized fermentation conditions showed higher IA yield from *A. niger* (290 g L^{-1}) compared to *A. terreus* (218 g L^{-1}) at pH 3.5 on the eighth day.

Apart from corn starch, lignocellulosic residues, and *J. curcas* seed cake, glycerol has been identified as a potential substrate to produce IA. *E. coli* scvCadA_No8 produced a 7.2 g L^{-1} yield of IA from glycerol in 2 L fed-batch fermentation reactor under nitrogen-limited conditions [82]. Chang et al. metabolically engineered *E. coli* by overexpression of *Corynebacterium glutamicum* pyruvate carboxylase for production of IA [83]. Using this strain, they achieved 43 g L^{-1} IA titers from glycerol. In addition to *E. coli*, *U. vetiveriae* TZ1 has also been used as a promising organism for the production of IA, which achieved maximum IA titers of 34.70 g L^{-1} at a rate of 0.09 g L^{-1} h^{-1} from 196 g L^{-1} glycerol [84]. Gnanasekaran et al. recently utilized superfluous algal biomass hydrolysate and purified glycerol for the production of IA by *A. niveus* [85]. In this process glycerol was first pre-treated with lipid extracted *Gracilaria edulis* algal biomass residual and then fermented by *A. niveus*. After 168 h of incubation, 31.55 g L^{-1} of IA was produced from glycerol in a shake flask.

Sugarcane bagasse has been proven as a promising biomass to produce IA [86]. Haigh et al. recently compared economic viability of different bio-based feedstocks and concluded that utilization of sugarcane bagasse can help to reduce the cost of IA production and make IA biorefinery commercially viable [87]. Life cycle assessment for production of IA from sugarcane bagasse was also conducted recently by Görgens and co-workers [88]. Paranthaman et al. developed an integrated process for IA production by using less expensive sugarcane bagasse in place of refined glucose [89]. In this process, four fungi, namely, *Aspergillus oryzae*, *Aspergillus niger*, *Aspergillus flavus*, and *Penicillium* sp., were chosen and improved their activities in solid-state fermentation. Under the best fermentation conditions and pH, *A. niger* yielded the highest IA level (8.24 mg kg^{-1}) in a shake flask. In 2018, Dinakarkumar et al. screened and fermented different agro-wastes using *Aspergillus niveus*. They achieved the best results with sugarcane bagasse [90].

3 Acrylic Acid

AA is an essential monomer for the manufacture of various industrial and consumer products [91]. AA market size was about $11,006 million in 2013 and is anticipated to reach $18,824 million by 2020 [92]. According to global opportunity analysis and industry forecast, global consumption of AA is expected to reach 8169 kilotons by 2020 [93]. However, renewable feedstock-derived AA is not cost-competitive to petroleum-derived AA because of maturity of petrochemical industries and processing [94]. Environmental sustainability and demand-supply imbalance of petroleum warrant production of bio-based AA and acrylates from glycerol, sugar, LA, acrolein, and intermediate feedstocks [95].

3.1 Bio-catalytic Routes to Acrylic Acid

Currently, *Clostridium propionicum*, obtained from coupled oxidation/reduction of alanine, is used to produce AA [96, 97], under its acrylate form from *Clostridium propionicum* bacteria. In 1981, O'Brien et al. tested resting cells of *Clostridium propionicum* for biotransformation of propionate to AA [98]. However, the less stability of anaerobic cells under an aerobic environment resulted in relatively low yield of AA (up to 18%). In 1990, the same group used sweet whey as an initial substrate for acrylate production in a two-step process [99]. In the first step, sweet whey was converted to propionic acid and acetic acid in 70 h by a co-culture of *Lactobacillus bulgaricus* and *Propionibacterium shermanii*. In the second step, propionate was converted into acrylate by resting cells of *Clostridium propionicum*. In this process, maximum acrylate of 0.133 mmol g^{-1} AA was produced in 6 h. When *Clostridium propionicum* was grown on bio-based LA, and provided with methylene blue as an electron acceptor, it produced 144 mg L^{-1} AA [97]. It was found that

during the biotransformation to AA from *Clostridium propionicum*, the produced AA reduced the growth of *Clostridium propionicum* and affected the yield.

In 2012, Luo group has systematically examined the toxic effects of AA on the development of *Clostridium propionicum*; the group also tested many mutants to grow at 43.06 mM concentration of AA [100]. To overcome the limitations of *Clostridium propionicum*, Tong et al. reported a recombinant *Escherichia coli* strain to prepare AA using glycerol as a renewable feedstock [101]. This recombinant strain produced a small amount—37.7 mg L^{-1} AA—under shaking flask conditions. Ahmed et al. isolated *Rhodococcus ruber* AKSH-84 microorganisms from petroleum-contaminated sludge samples capable of performing biotransformation of acrylonitrile to AA [102]. Under the optimized conditions, *Rhodococcus ruber* AKSH-84 produced 92 mol.% AA. In 2015, Gnanadesikan and co-worker patented a method for manufacturing AA, acrylonitrile, and 1,4-butanediol from 1,3-propanediol through microbial fermentation [103]. Cho et al. reported a novel approach in which AA was produced (0.12 g L^{-1}) from glucose via 3-HP, 3-HP-CoA, and acryloyl-CoA pathways over *Escherichia coli* [92].

4   Methacrylic Acid

MAA and methyl methacrylate (MMA) are essential monomers for the production of poly(methyl methacrylate) (PMMA), which is used to manufacture various end-user products such as electronics, paints, and coatings to improve polyvinyl chloride stiffness and artificial bone replacement parts. In 2018, the total available PMMA market is estimated at ~ $7 billion and an anticipated market size of $11.65 billion in 2022, representing a 17% growth [104]. This data estimates that a bio-based PMMA will hold 24% of the total PMMA market. Presently, PMMA is produced using multi-step chemical processes from fossil feedstocks that lead to high production costs and selling price of PMMA [105]. Bio-based PMAA, currently representing an estimated $951 million market size, is promising for the environment and in terms of costs.

The majority of MAA is used to produce plastics, optical glasses, lenses, moldings, fibers, resins, and others. The copolymer of MAA is also an essential component found in surface coatings, paints, adhesives, and emulsion polymers [106]. The properties of MAA-derived polymers include good mechanical strength, scratch resistant, and outstanding optical properties. PMMA is lighter than glass and exhibits excellent toughness, rigidity, and transparency. The growing demand of lightweight parts in vehicles caused increased demand for PMMA in the automotive sector. The pipe materials and vacuum insulation panels used in constructions are made from PMMA. The growing construction activates in the Asia-Pacific posed an increased demand for PMMA. The excellent transparent properties of PMMA have boosted its consumption in the lighted signs for advertising and directions.

4.1   Bio-catalytic Routes to Methacrylic Acid

The biotechnological production of MAA has received significantly less attention compared to the chemical routes. The first report of the biotechnological production of MAA was published in 1990 [107]. In this report, nitrilase-rich *Rhodococcus rhodochrous* J1 cells were used for the biotransformation of methacrylonitrile to MAA. Under the optimized reaction conditions, 3.02 Mol. MAA was produced in 24 h with a 100% molar conversion yield from methacrylonitrile. A patent filed by Burgard et al. disclosed the biosynthesis of MAA from renewable sugar feedstock by metabolically engineered cells or organisms [108]. The optimum yield of MAA was attained from succinyl-CoA, alpha-ketoglutarate, and acetyl-CoA precursors, respectively, via 3-hydroxyisobutyrate pathway.

In 2012, Pyo et al. proposed an interesting route for the production of MAA from 2-methyl-1,3-propanediol (2 M1,3PD), an industrial by-product, by the combination of bio- and chemo-catalysis [109]. The oxidative biotransformation of 2 M1,3PD to 3-hydroxy-2-methylpropionic acid (3H2MPA) was investigated by using resting cells of *Gluconobacter oxydans* in a bioreactor. After 3 h and at 25–30 °C using 5–10 g substrate and 2.6 g cell (dry weight) per liter, a selectivity of 95% 3H2MPA was obtained with 95–100% conversion of 2 M1,3PD. *Gluconobacter oxydans* cells were active for the biotransformation of up to 20 g per L of substrate in a continuous reactor. The chemical transformation of 3H2MPA to MAA was achieved by a titanium dioxide catalyst. Over 95% conversion and 95% overall yield of MAA were obtained at 210 °C. These results seem impressive, but the catalyst stability was not disclosed.

5   Styrene

ST is an industrially important commodity substance, widely used to produce polystyrene plastics, polyesters, protective coatings, resins, rubbers, and other copolymers The worldwide demand for ST has been witnessing high growth mainly in packaging and construction industries. It was anticipated that most of ST is consumed in automotive and construction as an end-user application. The global market of ST is expected to reach around 33 million in 2023, increasing around 2% per year in the period 2017–2023 [110]. About 80% of the world's ST capacity is based on ethylbenzene technology. In 2017, over 98% of ethylbenzene was consumed for the production of ST. About 35% of the total ST is used to produce polystyrene (PS). The other main end uses of ST include ABS resins, unsaturated polyester resins, SB latex, and SB rubber. ST is also the key ingredient for expandable polystyrene, which is expected to grow in the future [111]. Expandable polystyrene has the largest market share in China and Central Europe. Northeast Asia remains the dominant player. The fastest growing regions are the Middle East and Africa, with anticipated yearly growth rates of 8% and more than 20%, respectively.

Polystyrene is produced in different forms for different applications. For example, solid polystyrene is used to manufacture medical devices such as test tubes, petri dishes, CD cases, smoke detectors, containers for food, etc. [112] Polystyrene film is used to manufacture packaging and glazing materials and light diffusers, take-out containers, cassette cases, etc. Polystyrene foam is used for the production of cups for hot beverages, insulator for refrigerators, protective packaging, food packaging, etc.

5.1 Bio-catalytic Routes to Styrene

Due to the high potential of styrene (ST), bio-catalytic transformation to produce ST has received considerable attention in recent years [113, 114]. Glucose is predominantly used as an initial precursor for the biological production of ST [115]. In 2011, Mckenna et al. screened numerous enzymes for the biological production of ST from glucose [116]. In the biosynthesis pathway to ST, L-phenylalanine was first produced as an intermediate precursor from glucose, which further undergoes enzymatic transformation to ST, as shown in Scheme 1. In the first step, phenylalanine is deaminated to *trans*-cinnamic acid by phenylalanine ammonia lyase (PAL) encoded by PAL2 from *Arabidopsis thaliana*. In the second step, *trans*-cinnamic acid is decarboxylated to ST via the expression of a suitable phenylacrylate decarboxylase (PADC). This process produced 264 mg L^{-1} of ST in shake flask culture; a critical limitation in this study was the toxicity of ST. When the production of ST reached 300 mg L^{-1}, both growth and the formation of other by-products were ceased.

Later on, the scope of this process was further extended to produce chiral aromatic building blocks (*S*)-styrene oxide and (*R*)-1,2-phenylethanediol from glucose by using ST monooxygenase (SMO) or ST dioxygenase (SDO) enzymes [117]. When SMO and SDO were introduced into the stains, 1.32 g L^{-1} of (S)-styrene oxide and 1.23 g L^{-1} of (R)-1,2-phenylethanediol were produced, respectively. In 2014, Nielsen et al. developed a biosynthesis pathway to produce ST by engineered
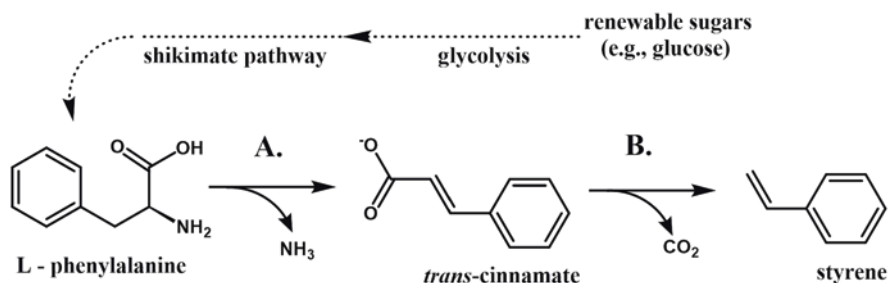
Scheme 1 Enzymatic pathway to convert L-phenylalanine into styrene via the intermediate trans-cinnamate

Saccharomyces cerevisiae (*S. cerevisiae*) [118]. The engineered strain produced 29 mg L^{-1} of ST at a glucose yield of 1.44 mg g^{-1}.

In another approach, Xian et al. have examined four PAL isoenzymes, *Arabidopsis thaliana* (AtPAL2), *Fagopyrum tataricum* (FtPAL), *Petroselinum crispum* (PcPAL), and *Artemisia annua* (AaPAL), to produce ST in *E. coli* [119]. AtPAL2 has shown optimum enzyme activity among the investigated isoenzymes. When isopropyl myristate was used as a solvent shake flask fermentation medium, the ST concentration reached 350 mg L^{-1} after 48 h. Techno-economic assessment of bio-based ST production from glucose by engineered *Escherichia coli* was performed by Claypool et al. [120]. According to the assumption of this analysis, a 45 Gg per annum bio-based ST plant is projected to yield 99.9% pure ST monomer at a MESP of 1.90 \$ kg^{-1}. The analysis concluded that the selling price of bio-based ST is competitive to petroleum-derived ST.

The most direct route to bio-based ST via bio-catalytic decarboxylation of *trans*-cinnamic acid was first reported in 1995 by Middelhoven et al. [121]. In this report, the culture of the yeast *Cryptococcus elinovii* was grown on cinnamic acid to produce ST. However smaller amount of ST (13 mg) was yielded due to the toxicity of ST. The decarboxylation of cinnamic acid and derivatives was also performed over plant cell cultures [122]. Among different plant cell cultures, the cells of *Camellia sinensis* produced 30% ST at room temperature. In 2013, a new study showed that forest waste is a very useful sustainable platform for manufacturing bio-based ST [123]. In this study the fungal strain was cultivated on various lignocellulosic biomass such as fresh leaves, wood, bark of Scots pine, Norway spruce, and Silver Birch. Authors achieved maximum production rates of 52.5 lg h^{-1}, 41 lg h^{-1}, and 27 lg h^{-1} ST from the mature bark of oak and potato dextrose broth, respectively.

Lian et al. utilized red oak-derived pyrolytic sugars for the production of ST [124]. A maximum of 240 mg L^{-1} ST was obtained from levoglucosan. In another study, ST was produced from glucose, cellobiose, and xylo-oligosaccharides using a co-culture system of phenylalanine ammonia lyase and phenylacrylic acid decarboxylase expressing in *Streptomyces lividans* strain. The co-cultures of *S. lividans*/p-encP and *S. lividans*/FDC1 produced a maximum of 30 mg L^{-1} ST after 7 days of cultivation from glucose [125].

6   Concluding Remarks

Rapid consumption of petroleum products coupled with environmental concerns necessitated the replacement of non-renewable carbons with renewable alternatives such as biomass for transportation fuels and chemicals. The described vinyl monomers are important compounds, which have application in food, pharmaceuticals, polymers, and fine chemicals. The chapter has covered the recent advancements in the production of IA, AA, MAA, and ST monomers. Several filamentous and non-filamentous fungi, bacteria, and yeasts have been used as bio-catalysts with great potential. Despite significant scientific advancements and technological know-how,

none of the reported approaches are commercially practiced to date. Future research should focus on strain development by genetic engineering to improve the final titer of vinyl monomers. The development of solid-state fermentation is another promising direction to reduce production cost. In order to reduce the production cost and mitigate competition with food values, it is also essential to use cheaper, alternative feedstocks such as lignocellulosic biomass and glycerol.

References

1. Matar S, Hatch LF (2001) Chemistry of petrochemical processes. Elsevier, Amsterdam
2. Hillmyer MA (2017) The promise of plastics from plants. Science 358(6365):868–870
3. Deneyer A, Peeters E, Renders T, Van den Bosch S, Van Oeckel N, Ennaert T, Szarvas T, Korányi TI, Dusselier M, Sels BF (2018) Direct upstream integration of biogasoline production into current light straight run naphtha petrorefinery processes. Nat Energy 3(11):969
4. Mika LT, Csefalvay E, Nemeth A (2017) Catalytic conversion of carbohydrates to initial platform chemicals: chemistry and sustainability. Chem Rev 118(2):505–613
5. Sikarwar VS, Zhao M, Clough P, Yao J, Zhong X, Memon MZ, Shah N, Anthony EJ, Fennell PS (2016) An overview of advances in biomass gasification. Energ Environ Sci 9(10):2939–2977
6. Bohre A, Dutta S, Saha B, Abu-Omar MM (2015) Upgrading furfurals to drop-in biofuels: an overview. ACS Sustain Chem Eng 3(7):1263–1277
7. Yu AZ, Serum EM, Renner AC, Sahouani JM, Sibi MP, Webster DC (2018) Renewable reactive diluents as practical styrene replacements in biobased vinyl Ester thermosets. ACS Sustain Chem Eng 6(10):12586–12592
8. Satoh K (2015) Controlled/living polymerization of renewable vinyl monomers into bio-based polymers. Polym J 47:527
9. Kumar S, Krishnan S, Samal SK, Mohanty S, Nayak SK (2017) Itaconic acid used as a versatile building block for the synthesis of renewable resource-based resins and polyesters for future prospective: a review. Polym Int 66(10):1349–1363
10. Bafana R, Pandey RA (2018) New approaches for itaconic acid production: bottlenecks and possible remedies. Crit Rev Biotechnol 38(1):68–82
11. Cunha da Cruz J, Machado de Castro A, Camporese Sérvulo EF (2018) World market and biotechnological production of itaconic acid. 3 Biotech 8(3):138
12. Hajian H, Yusoff WMW (2015) Itaconic acid production by microorganisms: a review. Curr Res J Biol Sci 7(2):37–42
13. Paolo CG (1962) Process for preparing itaconic acid, and 2, 3-butadienoic acid. US 3025320A
14. Robert T, Friebel S (2016) Itaconic acid—a versatile building block for renewable polyesters with enhanced functionality. Green Chem 18(10):2922–2934
15. Durant Y, Cao M, Chirat M (2011) Polycarboxylic acid polymers. Google Patents
16. Kuenz A, Gallenmüller Y, Willke T, Vorlop K-D (2012) Microbial production of itaconic acid: developing a stable platform for high product concentrations. Appl Microbiol Biotechnol 96(5):1209–1216
17. Nuss P, Gardner KH (2013) Attributional life cycle assessment (ALCA) of polyitaconic acid production from northeast US softwood biomass. Int J Life Cycle Assess 18(3):603–612
18. El-Imam AA, Du C (2014) Fermentative itaconic acid production. J Biodivers Biopros Dev 1(1):1–8

19. Okabe M, Lies D, Kanamasa S, Park EY (2009) Biotechnological production of itaconic acid and its biosynthesis in Aspergillus terreus. Appl Microbiol Biotechnol 84(4):597–606
20. Saha BC (2017) Emerging biotechnologies for production of itaconic acid and its applications as a platform chemical. J Ind Microbiol Biotechnol 44(2):303–315
21. Kuenz A, Krull S (2018) Biotechnological production of itaconic acid—things you have to know. Appl Microbiol Biotechnol 102(9):3901–3914
22. De Carvalho JC, Magalhaes A, Soccol CR (2018) Biobased itaconic acid market and research trends—is it really a promising chemical. Chim Oggi Chem Today 36:56–58
23. Kubicek CP, Punt P, Visser J (2011) In: Hofrichter M (ed) Industrial applications. Springer, Berlin, Heidelberg, pp 215–234
24. O'Neill LAJ, Artyomov MN (2019) Itaconate: the poster child of metabolic reprogramming in macrophage function. Nat Rev Immunol 19(5):273–281
25. Saha BC, Kennedy GJ (2019) Phosphate limitation alleviates the inhibitory effect of manganese on itaconic acid production by Aspergillus terreus. Biocatal Agric Biotechnol 18:101016
26. Huang X, Chen M, Lu X, Li Y, Li X, Li J-J (2014) Direct production of itaconic acid from liquefied corn starch by genetically engineered Aspergillus terreus. Microb Cell Fact 13:108–108
27. Olicón-Hernández DR, Araiza-Villanueva MG, Pardo JP, Aranda E, Guerra-Sánchez G (2019) New insights of Ustilago maydis as yeast model for genetic and biotechnological research: a review. Curr Microbiol 76(8):917–926
28. Geiser E, Przybilla SK, Friedrich A, Buckel W, Wierckx N, Blank LM, Bölker M (2016a) Ustilago maydis produces itaconic acid via the unusual intermediate trans-aconitate. J Microbial Biotechnol 9(1):116–126
29. Wierckx N, Agrimi G, Lübeck PS, Steiger MG, Mira NP, Punt PJ (2020) Metabolic specialization in itaconic acid production: a tale of two fungi. Curr Opin Biotechnol 62:153–159
30. Hosseinpour Tehrani H, Geiser E, Engel M, Hartmann SK, Hossain AH, Punt PJ, Blank LM, Wierckx N (2019a) The interplay between transport and metabolism in fungal itaconic acid production. Fungal Genet Biol 125:45–52
31. Guevarra ED, Tabuchi T (1990a) Accumulation of Itaconic, 2-Hydroxyparaconic, Itatartaric, and malic acids by strains of the genus Ustilago. Agric Biol Chem 54(9):2353–2358
32. Klement T, Milker S, Jäger G, Grande PM, Domínguez de María P, Büchs J (2012) Biomass pretreatment affects Ustilago maydis in producing itaconic acid. Microb Cell Fact 11(1):43
33. Maassen N, Panakova M, Wierckx N, Geiser E, Zimmermann M, Bölker M, Klinner U, Blank LM (2014) Influence of carbon and nitrogen concentration on itaconic acid production by the smut fungus Ustilago maydis. Eng Life Sci 14(2):129–134
34. Geiser E, Przybilla SK, Engel M, Kleineberg W, Büttner L, Sarikaya E, Hartog Td, Klankermayer J, Leitner W, Bölker M, Blank LM, Wierckx N (2016b) Genetic and biochemical insights into the itaconate pathway of Ustilago maydis enable enhanced production. Metab Eng 38:427–435
35. Hosseinpour Tehrani H, Becker J, Bator I, Saur K, Meyer S, Rodrigues Lóia AC, Blank LM, Wierckx N (2019b) Integrated strain- and process design enable production of 220 g L−1 itaconic acid with Ustilago maydis. Biotechnol Biofuels 12(1):263
36. Geiser E, Wiebach V, Wierckx N, Blank LM (2014) Prospecting the biodiversity of the fungal family Ustilaginaceae for the production of value-added chemicals. Fungal Biol Biotechnol 1(1):2
37. Guevarra ED, Tabuchi T (1990b) Production of 2-Hydroxyparaconic and Itatartaric acids by Ustilago cynodontis and simple recovery process of the acids. Agric Biol Chem 54(9):2359–2365
38. Hosseinpour Tehrani H, Tharmasothirajan A, Track E, Blank LM, Wierckx N (2019c) Engineering the morphology and metabolism of pH tolerant Ustilago cynodontis for efficient itaconic acid production. Metab Eng 54:293–300

39. van der Straat L, Vernooij M, Lammers M, van den Berg W, Schonewille T, Cordewener J, van der Meer I, Koops A, de Graaff LH (2014) Expression of the Aspergillus terreus itaconic acid biosynthesis cluster in Aspergillus Niger. Microb Cell Fact 13(1):11

40. Li A, van Luijk N, ter Beek M, Caspers M, Punt P, van der Werf M (2011) A clone-based transcriptomics approach for the identification of genes relevant for itaconic acid production in Aspergillus. Fungal Genet Biol 48(6):602–611

41. Kanamasa S, Dwiarti L, Okabe M, Park EY (2008) Cloning and functional characterization of the cis-aconitic acid decarboxylase (CAD) gene from Aspergillus terreus. Appl Microbiol Biotechnol 80(2):223–229

42. Li A, Pfelzer N, Zuijderwijk R, Brickwedde A, van Zeijl C, Punt P (2013) Reduced by-product formation and modified oxygen availability improve itaconic acid production in Aspergillus Niger. Appl Microbiol Biotechnol 97(9):3901–3911

43. Blumhoff ML, Steiger MG, Mattanovich D, Sauer M (2013a) Targeting enzymes to the right compartment: metabolic engineering for itaconic acid production by Aspergillus Niger. Metab Eng 19:26–32

44. Hossain AH, Li A, Brickwedde A, Wilms L, Caspers M, Overkamp K, Punt PJ (2016) Rewiring a secondary metabolite pathway towards itaconic acid production in Aspergillus Niger. Microb Cell Fact 15(1):130

45. Hossain AH, van Gerven R, Overkamp KM, Lübeck PS, Taşpınar H, Türker M, Punt PJ (2019) Metabolic engineering with ATP-citrate lyase and nitrogen source supplementation improves itaconic acid production in Aspergillus Niger. Biotechnol Biofuels 12(1):233

46. Blumhoff M, Steiger MG, Marx H, Mattanovich D, Sauer M (2013b) Six novel constitutive promoters for metabolic engineering of Aspergillus Niger. Appl Microbiol Biotechnol 97(1):259–267

47. Yin X, Shin H-D, Li J, Du G, Liu L, Chen J (2017) Pgas, a low-pH-induced promoter, as a tool for dynamic control of gene expression for metabolic engineering of Aspergillus Niger. Appl Environ Microbiol 83(6):e03222–e03216

48. Pontrelli S, Chiu T-Y, Lan EI, Chen FYH, Chang P, Liao JC (2018) Escherichia coli as a host for metabolic engineering. Metab Eng 50:16–46

49. Vuoristo KS, Mars AE, Sangra JV, Springer J, Eggink G, Sanders JPM, Weusthuis RA (2015) Metabolic engineering of itaconate production in Escherichia coli. Appl Microbiol Biotechnol 99(1):221–228

50. Okamoto S, Chin T, Hiratsuka K, Aso Y, Tanaka Y, Takahashi T, Ohara H (2014) Production of itaconic acid using metabolically engineered *Escherichia coli*. J Gen Appl Microbiol 60(5):191–197

51. Tran K-NT, Somasundaram S, Eom GT, Hong SH (2019) Efficient Itaconic acid production via protein–protein scaffold introduction between GltA, AcnA, and CadA in recombinant Escherichia coli. Biotechnol Prog 35(3):e2799

52. Fatma Z, Hartman H, Poolman MG, Fell DA, Srivastava S, Shakeel T, Yazdani SS (2018) Model-assisted metabolic engineering of Escherichia coli for long chain alkane and alcohol production. Metab Eng 46:1–12

53. Harder B-J, Bettenbrock K, Klamt S (2016) Model-based metabolic engineering enables high yield itaconic acid production by Escherichia coli. Metab Eng 38:29–37

54. Yang Z, Gao X, Xie H, Wang F, Ren Y, Wei D (2017) Enhanced itaconic acid production by self-assembly of two biosynthetic enzymes in Escherichia coli. Biotechnol Bioeng 114(2):457–462

55. Yang Z, Wang H, Wang Y, Ren Y, Wei D (2018) Manufacturing multienzymatic complex reactors in vivo by self-assembly to improve the biosynthesis of Itaconic acid in Escherichia coli. ACS Synth Biol 7(5):1244–1250

56. Moon Y-M, Gurav R, Kim J, Hong Y-G, Bhatia SK, Jung H-R, Hong J-W, Choi TR, Yang SY, Park HY, Joo H-S, Yang Y-H (2018) Whole-cell immobilization of engineered Escherichia coli JY001 with barium-alginate for Itaconic acid production. Biotechnol Bioprocess Eng 23(4):442–447

57. Becker J, Rohles CM, Wittmann C (2018) Metabolically engineered Corynebacterium glutamicum for bio-based production of chemicals, fuels, materials, and healthcare products. Metab Eng 50:122–141

58. Otten A, Brocker M, Bott M (2015) Metabolic engineering of Corynebacterium glutamicum for the production of itaconate. Metab Eng 30:156–165

59. Markham KA, Alper HS (2018) Synthetic biology expands the industrial potential of Yarrowia lipolytica. Trends Biotechnol 36(10):1085–1095

60. Blazeck J, Hill A, Jamoussi M, Pan A, Miller J, Alper HS (2015) Metabolic engineering of Yarrowia lipolytica for itaconic acid production. Metab Eng 32:66–73

61. Zhao C, Cui Z, Zhao X, Zhang J, Zhang L, Tian Y, Qi Q, Liu J (2019) Enhanced itaconic acid production in Yarrowia lipolytica via heterologous expression of a mitochondrial transporter MTT. Appl Microbiol Biotechnol 103(5):2181–2192

62. Kwak S, Jin Y-S (2017) Production of fuels and chemicals from xylose by engineered Saccharomyces cerevisiae: a review and perspective. Microb Cell Fact 16(1):82

63. Blazeck J, Miller J, Pan A, Gengler J, Holden C, Jamoussi M, Alper HS (2014) Metabolic engineering of Saccharomyces cerevisiae for itaconic acid production. Appl Microbiol Biotechnol 98(19):8155–8164

64. Young EM, Zhao Z, Gielesen BEM, Wu L, Benjamin Gordon D, Roubos JA, Voigt CA (2018) Iterative algorithm-guided design of massive strain libraries, applied to itaconic acid production in yeast. Metab Eng 48:33–43

65. Levinson WE, Kurtzman CP, Kuo TM (2006) Production of itaconic acid by Pseudozyma Antarctica NRRL Y-7808 under nitrogen-limited growth conditions. Enzyme Microb Technol 39(4):824–827

66. Tabuchi T, Sugisawa T, Ishidori T, Nakahara T, Sugiyama J (1981) Itaconic acid fermentation by a yeast belonging to the genus Candida. Agric Biol Chem 45(2):475–479

67. Petruccioli M, Pulci V, Federici F (1999) Itaconic acid production by Aspergillus terreus on raw starchy materials. Lett Appl Microbiol 28(4):309–312

68. Mondala AH (2015) Direct fungal fermentation of lignocellulosic biomass into itaconic, fumaric, and malic acids: current and future prospects. J Ind Microbiol Biotechnol 42(4):487–506

69. Yahiro K, Shibata S, Jia S-R, Park Y, Okabe M (1997) Efficient itaconic acid production from raw corn starch. J Ferment Bioeng 84(4):375–377

70. Reddy CSK, Singh RP (2002) Enhanced production of itaconic acid from corn starch and market refuse fruits by genetically manipulated Aspergillus terreus SKR10. Bioresour Technol 85(1):69–71

71. Bafana R, Sivanesan S, Pandey RA (2017) Itaconic acid production by filamentous Fungi in starch-rich industrial residues. Indian J Microbiol 57(3):322–328

72. Bafana R, Sivanesan S, Pandey R (2019) Optimization and scale up of itaconic acid production from potato starch waste in stirred tank bioreactor. Biotechnol Prog 35

73. Okamoto S, Chin T, Nagata K, Takahashi T, Ohara H, Aso Y (2015) Production of itaconic acid in Escherichia coli expressing recombinant α-amylase using starch as substrate. J Biosci Bioeng 119(5):548–553

74. Gnanasekaran R, Dhandapani B, Gopinath KP, Iyyappan J (2018a) Synthesis of itaconic acid from agricultural waste using novel Aspergillus niveus. Prep Biochem Biotechnol 48(7):605–609

75. Petridis L, Smith JC (2018) Molecular-level driving forces in lignocellulosic biomass deconstruction for bioenergy. Nat Rev Chem 2(11):382–389

76. Kautola H (1990) Itaconic acid production from xylose in repeated-batch and continuous bioreactors. Appl Microbiol Biotechnol 33(1):7–11

77. Saha BC, Kennedy GJ (2017) Mannose and galactose as substrates for production of itaconic acid by Aspergillus terreus. Lett Appl Microbiol 65(6):527–533

78. Krull S, Eidt L, Hevekerl A, Kuenz A, Prüße U (2017) Itaconic acid production from wheat chaff by Aspergillus terreus. Process Biochem 63:169–176

79. Rao DM, Hussain SJ, Rangadu VP, Subramanyam K, Krishna GS, Swamy A (2007) Fermentatative production of itaconic acid by Aspergillus terreus using Jatropha seed cake. Afr J Biotechnol 6(18)
80. El-Imam AMA, Kazeem MO, Odebisi MB, Abidoye AO (2013) Production of itaconic acid from Jatropha curcas seed cake by Aspergillus terreus. Not Sci Biol 5(1):57–61
81. Alfy H (2017) Control of soybean stem Fly Melanagromyza sojae (Diptera: Agromyzidae) by sticky color traps in soybean field. Egypt Acad J Bio Sci F Toxicol Pest Control 9(2):7–13
82. Jeon H-G, Cheong D-E, Han Y, Song JJ, Choi JH (2016) Itaconic acid production from glycerol using Escherichia coli harboring a random synonymous codon-substituted 5′-coding region variant of the cadA gene. Biotechnol Bioeng 113(7):1504–1510
83. Chang P, Chen GS, Chu H-Y, Lu KW, Shen CR (2017) Engineering efficient production of itaconic acid from diverse substrates in Escherichia coli. J Biotechnol 249:73–81
84. Zambanini T, Hosseinpour Tehrani H, Geiser E, Merker D, Schleese S, Krabbe J, Buescher JM, Meurer G, Wierckx N, Blank LM (2017) Efficient itaconic acid production from glycerol with Ustilago vetiveriae TZ1. Biotechnol Biofuels 10(1):131
85. Gnanasekaran R, Dhandapani B, Iyyappan J (2019) Improved itaconic acid production by Aspergillus niveus using blended algal biomass hydrolysate and glycerol as substrates. Bioresour Technol 283:297–302
86. Sindhu R, Gnansounou E, Binod P, Pandey A (2016) Bioconversion of sugarcane crop residue for value added products—an overview. Renew Energy 98:203–215
87. Nieder-Heitmann M, Haigh KF, Görgens JF (2018) Process design and economic analysis of a biorefinery co-producing itaconic acid and electricity from sugarcane bagasse and trash lignocelluloses. Bioresour Technol 262:159–168
88. Nieder-Heitmann M, Haigh KF, Görgens JF (2019) Life cycle assessment and multi-criteria analysis of sugarcane biorefinery scenarios: finding a sustainable solution for the south African sugar industry. J Clean Prod 239:118039
89. Paranthaman R, Kumaravel S, Singaravadivel K (2014) Bioprocessing of sugarcane factory waste to production of Itaconic acid. Afr J Microbiol Res 8(16):1672–1675
90. Gnanasekaran R, Saranya P, Yuvashree S, Yuvaraj D, Saravanan A, Smila KH, Anli Dino A (2018b) Itaconic acid production by Novel Aspergillus Niveus in solid state fermentation using agrowastes. Int J Eng Technol 7(3.34):6
91. Makshina EV, Canadell J, van Krieken J, Peeters E, Dusselier M, Sels BF (2019) Bio-acrylates production: recent catalytic advances and perspectives of the use of lactic acid and their derivates. ChemCatChem 11(1):180–201
92. Chu HS, Ahn J-H, Yun J, Choi IS, Nam T-W, Cho KM (2015) Direct fermentation route for the production of acrylic acid. Metab Eng 32:23–29
93. Droesbeke MA, Du Prez FE (2019) Sustainable synthesis of renewable terpenoid-based (meth) acrylates using the CHEM21 green metrics toolkit. ACS Sustain Chem Eng 7:11633
94. Baskar G, Aiswarya R, Kalavathy G, Pandey A, Gnansounou E, Raman JK, Kumar RP (2020) Refining biomass residues for sustainable energy and bioproducts. Elsevier, Amsterdam, pp 135–147
95. Kadar J, Heene-Würl N, Hahn S, Nagengast J, Kehrer M, Taccardi N, Collias D, Dziezok P, Wasserscheid P, Albert J (2019) Acrylic acid synthesis from lactide in a continuous liquid-phase process. ACS Sustain Chem Eng 7(7):7140–7147
96. Ohara T, Sato T, Shimizu N, Prescher G, Schwind H, Weiberg O, Marten K, Greim H (2000) Acrylic acid and derivatives. Ullmann's encyclopedia of industrial chemistry. Wiley-VCH, Weinheim
97. Danner H, Ürmös M, Gartner M, Braun R (1998) Biotechnological production of acrylic acid from biomass. Appl Biochem Biotechnol 70(1):887–894
98. Kirk T, Hollaender A (1981) In: Hollaender A (ed) Trends in the biology of fermentations for fuels and chemicals. Plenum Press, New York, p 131
99. O'Brien DJ, Panzer CC, Eisele WP (1990) Biological production of acrylic acid from cheese whey by resting cells of Clostridium propionicum. Biotechnol Prog 6(4):237–242

100. Jyoti G, Bhoi S, Sahu DK (2019) Production and isolation of n-butyl acrylate using pervaporation-aided esterification reaction: kinetics and optimization. Chem Eng Technol 42(3):617–627

101. Tong W, Xu Y, Xian M, Niu W, Guo J, Liu H, Zhao G (2016) Biosynthetic pathway for acrylic acid from glycerol in recombinant Escherichia coli. Appl Microbiol Biotechnol 100(11):4901–4907

102. Kamal A, Kumar MS, Kumar CG, Shaik TB (2011) Bioconversion of acrylonitrile to acrylic acid by Rhodococcus ruber strain AKSH-84. J Microbiol Biotechnol 21(1):37–42

103. Gnanadesikan V, Singh R, Dasari R, Alger M (2018) Process for manufacturing acrylic acid, acrylonitrile and 1, 4-butanediol from 1, 3-propanediol. Google Patents

104. Ali U, Karim KJBA, Buang NA (2015) A review of the properties and applications of poly (methyl methacrylate)(PMMA). Poly Rev 5(4):678–705

105. Ouzas A, Niinivaara E, Cranston ED, Dubé MA (2018) In situ Semibatch emulsion polymerization of 2-ethyl hexyl acrylate/n-butyl acrylate/methyl methacrylate/cellulose nanocrystal nanocomposites for adhesive applications. Macromol React Eng 12(3):1700068

106. Bohre A, Ali MA, Ocepek M, Grilc M, Zabret J, Likozar B (2019) Copolymerization of biomass-derived carboxylic acids for biobased acrylic emulsions. Ind Eng Chem Res 58(43):19825–19831

107. Nagasawa T, Nakamura T, Yamada H (1990) Production of acrylic acid and methacrylic acid using Rhodococcus rhodochrous J1 nitrilase. Appl Microbiol Biotechnol 34(3):322–324

108. Burk MJ, Burgard AP, Osterhout RE, Sun J, Pharkya P (2015) Microorganisms for producing methacrylic acid and methacrylate esters and methods related thereto. European Patent EP2694663A4

109. Pyo S-H, Dishisha T, Dayankac S, Gerelsaikhan J, Lundmark S, Rehnberg N, Hatti-Kaul R (2012) A new route for the synthesis of methacrylic acid from 2-methyl-1, 3-propanediol by integrating biotransformation and catalytic dehydration. Green Chem 14(7):1942–1948

110. Jaymand M (2014) Recent progress in the chemical modification of syndiotactic polystyrene. Polym Chem 5(8):2663–2690

111. Chaukura N, Gwenzi W, Bunhu T, Ruziwa DT, Pumure I (2016) Potential uses and value-added products derived from waste polystyrene in developing countries: a review. Resour Conserv Recy 07:157–165

112. Ramli Sulong NH, Mustapa SAS, Abdul Rashid MK (2019) Application of expanded polystyrene (EPS) in buildings and constructions: a review. J Appl Polym 136(20):47529

113. Oelschlägel M, Zimmerling J, Tischler D (2018) A review: the styrene metabolizing cascade of side-chain oxygenation as biotechnological basis to gain various valuable compounds. Front Microbiol 9:490

114. Jang YS, Kim B, Shin JH, Choi YJ, Choi S, Song CW, Lee J, Park HG, Lee SY (2012) Bio-based production of C2–C6 platform chemicals. Biotechnol Bioeng 109(10):2437–2459

115. Hope C (1987) Cinnamic acid as the basis of a medium for the detection of wild yeasts. J Int Brewing 93(3):213–215

116. McKenna R, Nielsen DR (2011) Styrene biosynthesis from glucose by engineered E. coli. Metab Eng 13(5):544–554

117. McKenna R, Pugh S, Thompson B, Nielsen DR (2013) Microbial production of the aromatic building-blocks (S)-styrene oxide and (R)-1, 2-phenylethanediol from renewable resources. Biotechnol J 8(12):1465–1475

118. McKenna R, Thompson B, Pugh S, Nielsen DR (2014) Rational and combinatorial approaches to engineering styrene production by Saccharomyces cerevisiae. Microb Cell Fact 13(1):123

119. Liu C, Men X, Chen H, Li M, Ding Z, Chen G, Wang F, Liu H, Wang Q, Zhu Y (2018) A systematic optimization of styrene biosynthesis in Escherichia coli BL21 (DE3). Biotechnol Biofuels 11(1):14

120. Claypool JT, Raman DR, Jarboe LR, Nielsen DR (2014) Technoeconomic evaluation of bio-based styrene production by engineered Escherichia coli. J Ind Microbiol Biotechnol 41(8):1211–1216

121. Middelhoven WJ, Gelpke MDS (1995) Partial conversion of cinnamic acid into styrene by growing cultures and cell-free extracts of the yeastCryptococcus elinovii. Antonie Van Leeuwenhoek 67(2):217–219
122. Takemoto M, Achiwa K (2001) Synthesis of styrenes through the biocatalytic decarboxylation of trans-cinnamic acids by plant cell cultures. Chem Pharm Bull 49(5):639–641
123. Azeem M, Borg-Karlson AK, Rajarao GK (2013) Sustainable bio-production of styrene from forest waste. Bioresour Technol 144:684–688
124. Lian J, McKenna R, Rover MR, Nielsen DR, Wen Z, Jarboe LR (2016) Production of bio-renewable styrene: utilization of biomass-derived sugars and insights into toxicity. J Ind Microbiol Biotechnol 43(5):595–604
125. Fujiwara R, Noda S, Tanaka T, Kondo A (2016) Styrene production from a biomass-derived carbon source using a coculture system of phenylalanine ammonia lyase and phenylacrylic acid decarboxylase-expressing Streptomyces lividans transformants. J Biosci Bioeng 122(6):730–735

Biological and Environmental Degradations of Polyamides, Polylactic Acid, and Chitin for Future Prospects

Mohammad Asif Ali, Sukhdev Singh, Maninder Singh, and Gargi Joshi

Abstract Lately, the development of biobased polymers has been gaining attraction worldwide. Bio-based materials such as polyamide (PA), polylactic acid (PLA), and chitin have been in great demand. They hold great value in a variety of fields including in the automobile industry, packaging materials, as well as biomedical applications. For example, the biodegradable drug-eluting stents with flexibility, high mechanical property, and targeted drug releasing property can replace the conventional ones to prevent restenosis. This chapter presents the recent trends and developments of polyester, polyamide, and chitin and the future scientific challenges in the degradation of these polymers. Moreover, it presents the promising development of polyester, polyamide, and chitin degradation as well as the ways of improving their functionalities and wide range of applications towards the efficient waste management.

Keywords Biodegradable polymer · Polyamide · Polyester · Biopolymer · Chitin

1 Introduction

Accumulation of plastic waste in soil and sea has been a significant and challenging environmental concern because of their long-lasting capability to stay in the sea/soil without deterioration and generated at a rate approaching 400 Mt year^{-1} [1]. Since the beginning of the plastic age after World War II [2], scientists have developed various types of polymers depending on the necessities for mass consumption such as polyester and polyamide [2, 3]. Plastics find applications in almost all areas of our life, and their versatile properties such as lightness,

---

M. Asif Ali, S. Singh, M. Singh and G. Joshi contributed equally to this work.

M. A. Ali (✉) · M. Singh · G. Joshi
Graduate School of Advanced Science and Technology, Energy and Environment Area, Japan Advanced Institute of Science and Technology, Nomi, Ishikawa, Japan

S. Singh
iSm2-Stereo, Faculty des Sciences, Aix-Marseille University, Marseille, France

durability, corrosion-resistant, ease of processing, and high productivity make them highly desirable to society [1–4]. There is also a steep increase in the demand of plastic, in the areas of medicine, pharma sector, agriculture sector, packaging, and end-user industries in the past few decades [4, 5]. Since most of the plastics are synthesized from the petroleum based monomers, it is now high time to replace these petroleum-based/non-degradable polymers with degradable polymers for all commercial applications [1, 4]. However, there are several undesirable outcomes of plastic waste such as microplastics and their impact on the environment. Notably, the most concerning aspect of plastic use is its impact on our environment and ecosystem. The non-degradable nature of accumulated plastic leads to a significant problem of waste management all over the world [3, 5]. For this reason, biodegradable polymers are highly requisite for our environment and the betterment of our society. For the last two decades, scientists are trying to develop polymers that are not detrimental to the ground and living things and can be degraded quickly [1, 2]. The solution lies in the development of bio-based or degradable plastics that can be prepared from biomass or synthetic materials [1, 6]. Nylon™ is a basic term that represents an important class of polyamides [6]. Amide linkages in the polyamide exhibit high thermomechanical properties, higher softening temperature because of hydrogen bonding, which provides chain symmetry polyamide founds its application in the bristles, ropes, fishing net, biomedical application, an automobile engine [7]. Polyamide are partially degradable and can be broken down into small parts after the action of microorganisms such as bacteria or genetically altered bacteria, fungi, insects, and alga [2, 7]. There is also well-known synthetic or bio-based polyester which has a low softening temperature and their desirable lower strength because of chemical structure, and derived from a microorganism such as polylactic acid (PLA). Polyhydroxyalkanoates (PHAs) [8–11] are considered as biodegradable polymers and have shown great potential as replacement of petroleum-based products [7]. Polysaccharides are biologically relevant, quite often heterogeneous polymers comprising of monosaccharide moieties interacting via glycosidic linkages [12–16]. Chitin, being abundantly available, is one of the preferred choices for composite preparation as it imparts biodegradability and biocompatibility. In the present study, we will discuss the synthesis and properties of polyesters, polyamide, and chitin that are prepared from renewable sources or bio-based materials.

2   Polyester

Polyester is a synthetic fiber and is one of the most commonly used polymers that contain an ester functional group [8, 10, 11]. For the last two decades, scientists are trying to develop polymers that are not detrimental to the environment and living things and can be degraded easily [7, 9–11] (Fig. 1).
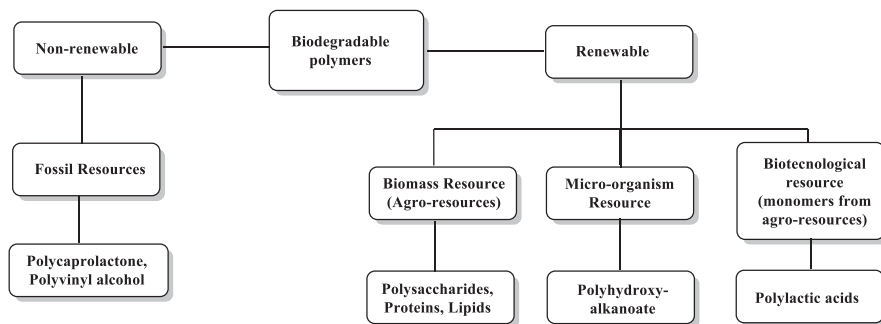
Fig. 1 Classification of biodegradable polymers based on their resources

2.1 Biodegradable Polyesters

Biodegradable polymers are the polymers that can be broken down by bacterial or microbial decomposition after their intended use. The polymers with high molecular weight are degraded to lower-molecular-weight compounds (such as CO_2, NO_2, water, biomass, and salts) [8], and the action of microorganisms and enzymes does the job of decomposition. Polyesters are the form of polymers that are synthesized from a dicarboxylic acid and a diol. They are the most representative examples of environmentally benign polymeric materials. The desired properties of polyesters depend on their mode of production and the resulting orientation of the polymer chains. Predominantly, the aliphatic polyesters are biodegradable because they have hydrolyzable ester bonds and relatively short aliphatic chains [8, 12, 14, 15].

Biodegradable polyesters are classified into three types:

1. *Polylactic acids (PLA)*: Polyesters obtained from bio-monomers and prepared by biotechnological method.
2. *Polyhydroxyalkanoates (PHA)*: Polyesters prepared by a microorganism.
3. *Polycaprolactones (PCL)*: Polyesters prepared from mineral oils (fossil materials)

In the present chapter, we will discuss the synthesis and properties of polyesters, mainly PLA and PHA, that are prepared from renewable sources or bio-based materials.

3 Polylactic Acids

Polylactic acid (PLA), also known as polylactide, is the polymer made from monomeric units of lactic acid. It was discovered by Wallace Carothers in 1932 when he obtained PLA form lactic acid. The two terms, polylactic acids and polylactide, are used interchangeably, but there is a scientific difference between these two. PLA is mainly obtained from two processes, direct polycondensation or polymerization

(DP) and ring-opening polymerization (ROM). The PLA obtained from DP is known as polylactic acid, whereas it is known as polylactide if obtained from ROM (Fig. 2). Since PLA is mostly obtained from corn starch, PLA is also regarded as "corn plastic."

3.1 Production of PLA from Renewable Sources

PLA is a hydrophobic polymer which is composed of two enantiomeric forms of lactic acid: L-(+)-Lactic acid and D-(−)-Lactic acid. Both enantiomers are useful in industrial application; however, L-(+)-Lactic acid is involved in cellular metabolism, and hence, it is more useful in biomedical applications. Starting from pure lactic acid (D or L isomer), we can get the pure form of poly-D (or L) isomer. Pure L-(+)-Lactic acid will produce poly-L-Lactic acid (abbreviated as PLLA), D-(−)-Lactic acid will lead to poly-D-Lactic acid (PDLA), and if the mixture of D, L-lactic acid is employed, it will produce poly-D, L-lactic acid (PDLLA) [12, 14, 15]. Monomers for the synthesis of PLA are obtained from petroleum sources (mainly lactonitrile that lead to D, L-lactic acid) and renewable sources (such as corn starch that give L-lactic acid). From lactic acid monomers, the polymerization was performed using direct polymerization (DP), ring-opening polymerization, and azeotropic dehydration process (Fig. 3) [7, 8].

3.2 Direct Polymerization (DP)

Lactic acid contains both OH and COOH groups that are allowed to condensate. As a result of polycondensation, metal catalysts are generally used to remove water at high temperatures and pressures.

This process produces PLA of low to medium M_W of polymer.

Direct polymerization of lactic acid involves three steps:

1. Removal of water produced.
2. Polycondensation of oligomers.
3. Melt condensation of oligomers to produce high-molecular-weight (M_W) polylactic acid.
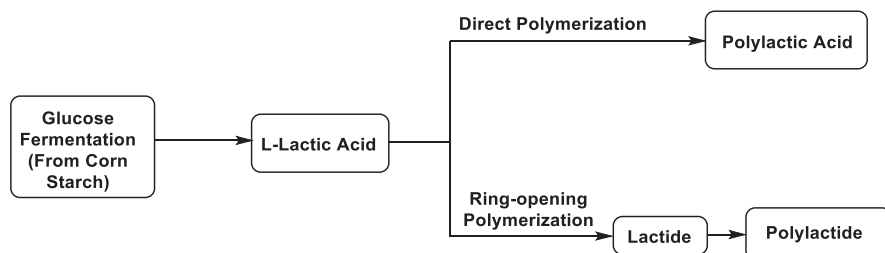
Fig. 2 The general route for the production of PLA from renewable resources
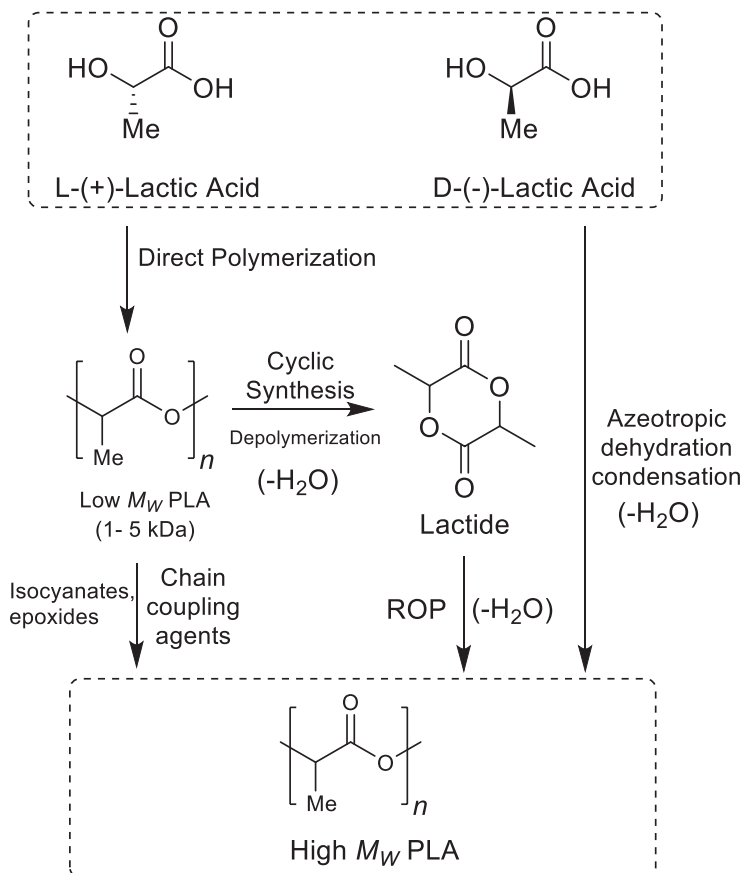
Fig. 3 Principle routes to prepare PLA

In direct polymerization, lactide is formed and decomposed simultaneously, and hence, it is not used for large-scale production. Though this method produces low-quality PLA which is useless, using a melt condensation step, this methodology can be used to obtain PLA of high M_w.

3.3 Ring-Opening Polymerization (ROP)

To obtain PLA of high M_w, ring-opening polymerization (ROP) is generally applied.

ROP usually involves three steps:

1. Polycondensation of LA monomers to produce low M_w PLA (direct polymerization)

2. Formation of lactide by depolymerization of low M_W PLA.
3. Polymerization of lactide ring-opening in the presence of a catalyst to produce high M_W PLA.

Though ROP produces PLA of high M_W and without side products, the process is complicated and time-consuming because additional purification is required, and this increases the cost of production. In the ROP method, the high purity of lactide is essential, which is used as a monomer. The impurities in lactide lead to undesirable effects on the properties of the PLA obtained.

3.4 Azeotropic Dehydration Polycondensation (ADP)

In the DP technique, the biggest issue is the removal of by-product (mainly water) from the viscous mixture at the end of the process. Azeotropic dehydration is the technique that is mainly applied to overcome the difficulty of by-product removal. In this method, water is efficiently removed by using appropriate azeotropic solvents in a single step, and high M_W PLA is produced. The conditions applied for azeotropic removal of water are usually controlled by manipulation of equilibrium between polymer and monomer in the organic solvent and at a temperature less than the melting point of PLA. This avoids the formation of impurities by depolymerization and racemization. Therefore, the selection of solvent and condition applied is critical to have the desired properties in the PLA produced. Also, in this approach, a Soxhlet extractor with molecular sieve (3 Å) inside was mounted simultaneously with azeotropic solvents to remove traces of water from the refluxed solvent, and a polymer of $M_W \sim 30,000$ g mol^{-1} was obtained [10, 11, 13, 16].

3.5 Solid-State Polymerization (SSP)

This is another technique of polymerization of lactic acid, which mainly goes through two steps:

1. Melt state to produce oligomer at high temperature (usually between 150 and 200 °C).
2. Solid state to further increase M_W at a temperature between melting temperature (T_m) and glass temperature (T_g) of PLA.

Further, in the second step, the prepolymer (in the form of semi-crystallized powder, chip, the pellet of fibers) of relatively low M_W is usually pulverized and dried thoroughly before heating, and this leads to heat distribution homogeneously among the dry particles that produce PLA of high M_W. This method produces PLA with better quality and properties because of the excellent control of side reactions and avoiding decomposition at low temperatures. However, this approach is time-consuming [17].

3.6　Enzymatic Polymerization (EP)

Enzymatic polymerization is a greener approach for the synthesis of PLA and generally applied to the ROP of lactide. For enzymatic polymerization of lactides, several lipases are used, e.g., *Candida antarctica* lipase B (CAL-B), *Pseudomonas cepacia* (lipase PS), *porcine pancreatic lipase* (PPL), etc. The enzymatic polymerization can be carried out in bulk, and organic solvents like toluene or ionic liquids can be used. CAL-B-catalyzed reactions in different solvents led to high-molecular-weight PLA (around M_W 40,000) [18].

3.7　Mechanical and Thermal Properties of PLA

The three polylactic acids, PLA, PLLA, and PDLLA, have different stereochemistry, and this leads to their different mechanical properties. Some physical properties of different PLAs are summarized in the Table 1 [19].

The thermal properties of PLA depend on its structural parameters, such as its M_W and its stereoisomeric composition. The relation between glass transition temperature (T_g) and molecular weight (M_w) was described by following the Flory-Fox equation

$$T_g = T^\infty - \frac{K}{M_w}$$

where T_g is the glass transition temperature, T^∞ the glass transition temperature at infinite molecular weight, M_w the molecular weight, and K the constant related to the free volume of the end groups for the polymer chains. This equation describes the dependency of T_g on the average M_W of the polymer. With the increase in average M_W, the first T_g increases rapidly and then becomes constant after reaching a particular value. These also explain that with the increase in the L-isomer content of the polymer, the T_g increases at the infinite molecular weight.

Table 1 Properties of various PLAs

Polymer	σ (MPa)	E (GPa)	ε (%)	T_g (°C)	T_m (°C)	ρ (g/cm³)
PLA	21–60	0.35–0.5	2.5–6.0	45–60	150–162	1.21–1.25
PLLA	15–70	2.7–4.14	3.0–10.0	55–65	170–200	1.24–1.30
PDLLA	27–50	1.0–3.45	2.0–10.0	50–60	260–280	1.25–1.27

Tensile strength (σ), elastic modulus (E), ultimate strain (ε), glass transition (T_g) temperature, melting temperature (T_m), density (ρ) of the polymer

4 Polyhydroxyalkanoates

Because of limited petroleum resources, the scientific community is trying to produce biodegradable and environment benign polymers. Polyhydroxyalkanoates (PHAs) are the most important candidates in terms of their properties and biodegradability. Since 1980, various companies have produced PHAs at large scale (summary in Table 2). PHAs are mostly used for packaging and biomedical applications such as drug delivery and tissue engineering [13, 16]. Some prominent examples of various PHAs and their biosynthetic routes are discussed as follows:

4.1 Polyhydroxybutyrates (PHB)

Polyhydroxybutyrates (PHBs) are biopolymers that are synthesized by many types of bacteria. PHB (Fig. 4) is a reserve linear polymer having R-(−)-3-hydroxybutyric acid as a repeating monomer unit (act as a chiral center), which is attributed to its optical activity. It was first discovered by French bacteriologist M. Lemoigne of the Institut Pasteur in 1923 as a reserve material in a bacterial cell, and later, it was confirmed by Stanier and co-workers that the reserve serves as intracellular food and energy source to prevent starvation when essential elements are not available.

4.2 Synthesis of PHB

The synthesis of PHB can be achieved in bacterium *A. eutrophus* (also *R. eutropha*) starting from acetyl-CoA using a sequential reaction of three different enzymes: 3-ketothiolase (phbA gene), acetoacetyl-CoA reductase (phbB gene), and PHB synthase (phbC gene). The biosynthetic pathway of PHB production is illustrated in Fig. 5. In the first step, 3-ketothiolase promotes the formation of acetoacetyl-CoA moiety by Claisen condensation of two molecules of acetyl-CoA. Then in the second step, NADPH-dependent acetoacetyl-CoA reductase catalyzes the stereoselective reduction of acetoacetyl-CoA formed in the first step to R-(−)-3-hydroxybutyryl-CoA. In the final stage, the enzyme PHB synthase polymerizes R-(−)-3-hydroxybutyryl-CoA to form PHB.

4.3 Properties of PHB

PHB is a promising biodegradable plastic and can be an excellent alternative to petrochemical plastics. This is due to its biocompatibility, biodegradability, and versatile properties that make it an eco-friendly substitute for synthetic polymers.

Table 2 Different types of polyesters and their producers [12–15, 17–19]
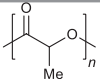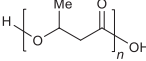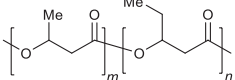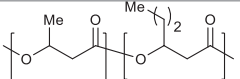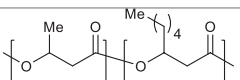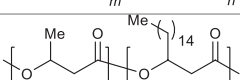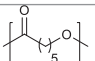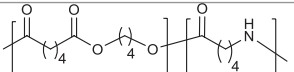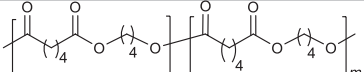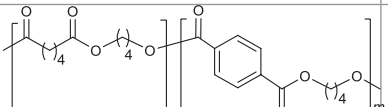
Polyester	General name		Chemical structure and full name	Commercial name (manufacturers)
Agro-based resources	PLA		Polylactic acid	• PLA (Galactic, Belgium) • CPLA (Dainippon Ink Chem., Japan) • NatureWorks (Cargill Dow LLC, USA) • Lacea (Mitsui Chemicals, Japan)
	PHA	PHB		• Biopol (Monsanto-Metabolix, USA) • BioCycle (Copersucar, Brazil)
		PHBV		
		PHBHHx		• Nodax (Procter & Gamble, USA)
		PHBO		
		PHBOd		
Fossil-based (petroleum resources)	PCL			• CAPA (Solvay, Belgium) • Tone (Union Carbide, USA) • Celgreen (Daicel, Japan)
	PEA			• BAK (Bayer, Germany)
Aliphatic co-polyesters	PBSA			• Bionolle (Showa Highpolymer, Japan) • Skygreen (SK Chemicals, Korea) • EnPol (Ire Chemical Ltd., Korea) • Lunare SE (Nippon Shokubai, Japan)
Aromatic co-polyesters	PBAT			• Ecoflex (BASF, Germany) • PHEE (Dow Chemicals, USA) • Biomax (DuPont, USA) • Eastar Bio (Eastman Chemical, USA)

Fig. 4 Structure of
optically active PHB
or P(3HB)
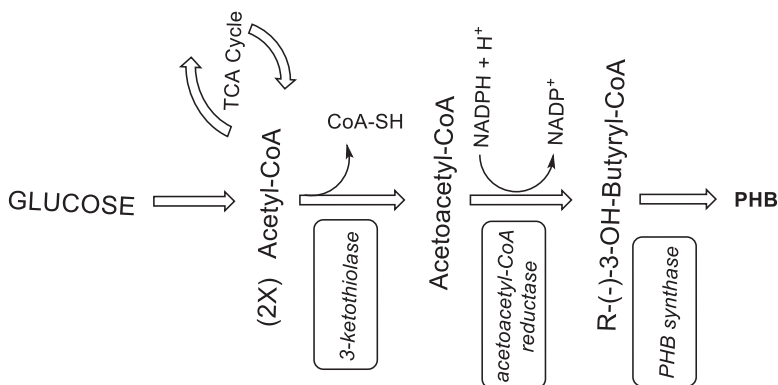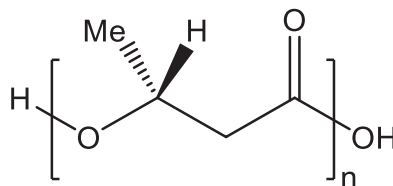
Fig. 5 Biosynthesis of PHB

PHB is a partially crystalline polymer that has material properties similar to
polypropylene (PP). Some of the essential physical properties of PHB are
summarized in Table 3, along with PP. According to Table 3, the strength parameters
(tensile strength, Young's modulus) of PHB and PP are similar, and most physical
properties (crystallinity, melting temperature, and glass transition temperature (T_g))
are mostly the same with others fiber. However, there is a difference in toughness
(elongation at break). While the less ductile PHB breaks at 5%, the propylene
exceeds 400%. This property of PHB is improved by making copolymer with higher
PHAs, which reduces crystallinity [20]. Due to high crystallinity of PHB, it
undergoes thermal decomposition at its melting point. This makes its processing
very difficult and limits its commercial use. To improve properties of PHB, the
solution is to make its copolymer with higher PHAs such as PHBV. PHBV is less
brittle and less stiff than homopolymer PHB. The physical properties of PHB can be
modulated by changing the ratio of HB and HV during its synthesis [13, 16, 20].

4.4 Polyhydroxyvalerate (PHBV)

Polyhydroxy-butyrate-*co*-valerate (abbreviated as PHBV or PHBHV), also known
as ENMAT Y1000 (Helian Polymer), is a linear aliphatic polyester which is obtained
by the insertion of 3-hydroxyvalerate units to the PHB biopolymer [13, 16, 21–23].
PHBV is obtained by bacterial synthesis (*R. eutropha*) from non-genetically

Table 3 Properties of PHB in comparison with polypropylene (PP)

Property	PHB	PP
Density ρ (g/cm^3)	1.25	0.91
Tensile strength σ (MPa)	40	38
Elastic modulus E (GPa)	3.5zz	1.5
Elongation at break ε (%)	6	400
Glass transition Temperature T_g (°C)	15	5
Melting temperature T_m (°C)	175	176
Degree of crystallinity X (%)	80	70

modified feedstock (glucose), and its non-toxic, 100% biodegradable nature makes it biocompatible with many types of cells.

4.5 Synthesis of PHBV

Similar to PHB, PHBV [21–23] is also synthesized by three enzymes 3-ketothiolase, acetoacetyl-CoA reductase, and PHA synthase. Several PHAs with monomers ranging from C$_3$ to C$_5$ have been synthesized in bacterium *A. eutrophus*. The addition of propionic acid to a medium with glucose produces a copolymer comprising 3-hydroxybutyrate, and 3-hydroxyvalerate gives PHBV whose biosynthetic pathway is shown in Fig. 6.

4.6 Poly(3-hydroxybutyrate-co-3-hydroxyhexanoate) (PHBHHx)

PHBHH$_x$ is a co-polyester that consists of 3-hydroxybutyrate (3HB) and 3-hydroxyhexanoate (3HH$_x$) repeating units [22, 24]. As compared to other PHA family members, PHBHH$_x$ (Fig. 7) has better biodegradability and adjustable mechanical properties (crystallinity, melting point, flexibility, ductility, etc.), which are mainly dependent on the 3HH$_x$ content of the polymer. Some of the properties are summarized in Table 4 [21–24].
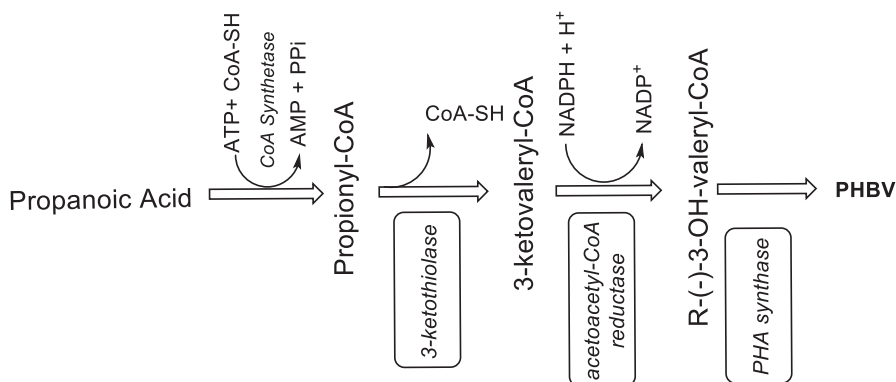
Fig. 6 Biosynthesis of PHBV
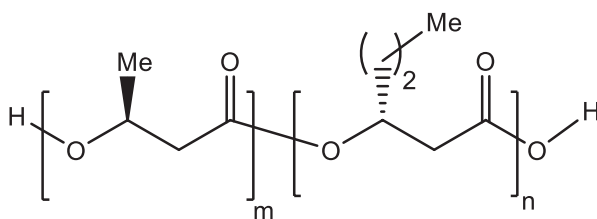
Fig. 7 Structure of PHBHHxPHBHH$_x$ is produced on similar fermentation methods as other PHAs like PHB and PHBV. The substrates are bio-based generated aliphatic fatty acid and soybean oil. Apart from this, it can also be prepared in agricultural crops, which is a cheaper process as compared to bacterial fermentation. A variety of plants can be used, such as corn, sugarcane, and switch grass. The process PHBHH$_x$ goes through various modifications in biosynthetic pathways of fatty acids and amino acids (in plastids and peroxisome) in different compartments of a cell (Fig. 8).

5 Polyamides

Polyamides are the class of the polymers with repeating and interlinked structural amide linkages (-NH-CO-). Nylon™ having integral amide groups is one of the families of polyamide materials [25–27]. Nylon™ is generally referred to as synthetic polyamide materials synthesized using the aliphatic monomers [28–31]. Generally, the polymers obtained via condensation reaction of diacids and diamines are referred to as AABB-type, and from lactams, it is referred to as AB-type as shown in Fig. 9. There are many synthetic techniques employed for the synthesis of polyamides, and two fundamental processes are used to obtain the desired polyamide material: one method is polycondensation of diacids and diamines, and the other is ring-opening polymerization of the lactam ring such as caprolactam (Fig. 10) [32, 33].

There are various types of nylons, and the associated number tells us the type of Nylon™, for example, Nylon 66 or polyamide 66 (PA 66). Number suffixing

Table 4 Properties of PHBVs

Polymer	T_g (°C)	T_m (°C)	σ (MPa)	ε (%)
PHB	4	175	40	6
P(HB-co-10%HHx)	-1	127	21	400
P(HB-co-17%HHx)	−2	120	20	850
Polypropylene	5	176	38	400
Low-density polyethylene	−30	176	10	620

Glass transition temperature (T_g), melting temperature (T_m), tensile strength (σ), elongation at break (ε)

describes the number of carbon atoms present in the polyamide structure of the amine and acid, respectively. Various polyamide materials and monomers used are described in Table 5, and the structures of the monomers used (Fig. 11) for the syntheses of polyamides are shown in Table 5.

Some of the outstanding characteristics of Nylon™ are given below:
- Excellent durability in the equilibrium moisture content.
– Excellent mechanical properties meaning it has superior strength and elastic modulus.
– Excellent chemical stability and excellent physical stability.
– Outstanding flame retardant properties, and the flame retardant grades are rated UL 94VO.
– Wonderful heat resistance properties.

5.1 Degradation of Polyamides

It is seen from the genetic and biochemical studies that microorganisms can degrade various polyamides. Following is the description of the degradation of polyamides and different oligomers of Nylon™ [34, 35]. In vivo studies have been reported for PA 6, particularly for intrauterine devices (IUD) [36, 37]. In 2 years or longer, breaks were found in the string of the tail. From the prepared samples, PA 66 was found to be unaffected in the presence of esterase [38] but degrades to a small extent in the presence of papain, trypsin, and chymotrypsin. Recently, biochemical studies on the biodegradation of nylon-6,6 by a lignin-degrading fungus were reported [39, 40]. There are many strains selected for submerged cultures of synthetic medium for degradation using white-rot fungi. Like all natural polymers such as proteins or peptides, they are prone to biodegradation. Polyamides have the same chemical moieties like peptides or proteins, but their strong intermolecular hydrogen bonding, high crystallinity, and less polarity make them non-biodegradable. However, degradation of low-molecular-weight polyamides or homopolymers into oligomers can be achieved using microorganisms or enzymatic degradation. Bacteria-degraded oligomers and monomers are also reported [36, 37, 39, 40]. According to the IUPAC terminology, biodegradable polymers undergo chain scission, thus resulting in
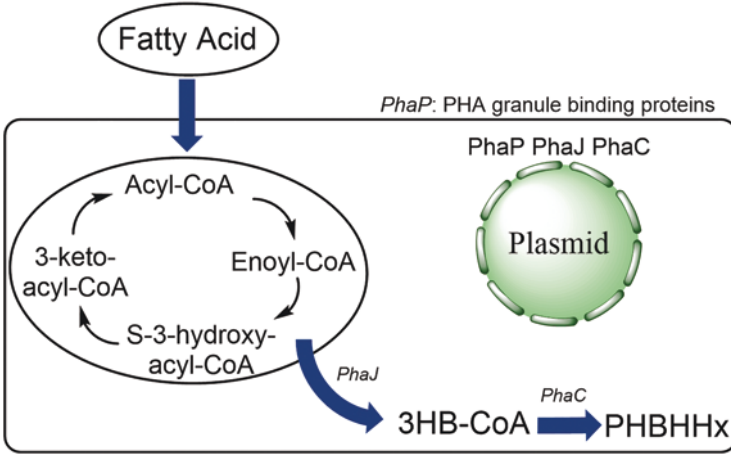
Fig. 8 PHBHHx production through metabolic engineering

AABB-type

AB-type
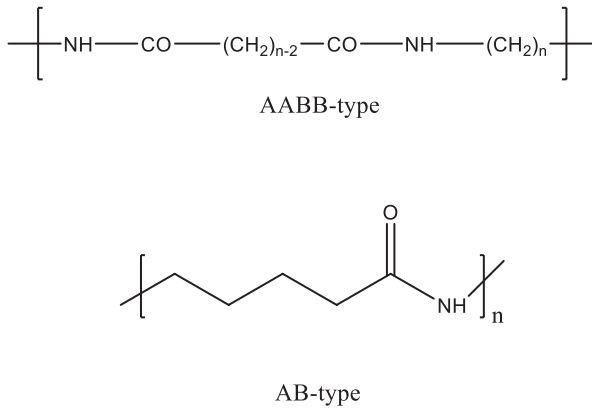
Fig. 9 Types of polymerization depending on the synthetic procedure

lower molecular mass of the polyamide. Though bio-based materials are composed mainly or in part of many biological products provided by the biomass, it does not support the fact that the material is biodegradable. Some of the aliphatic polyamides are susceptible to biodegradation by microorganisms (fungi or bacteria) [31, 34, 39]. The term biodegradation was assumed to be due to the endogenous enzymatic hydrolysis of an amide bond of polyamide. Thermophilic bacteria with optimum growth at 55 °C isolated from soil by enrichment culture technique at 60 °C were found to degrade PA 66 and PA 12. PA 6 and PA 66 are also degraded by some marine bacteria such as *Brevundimonas vesicularis*, *Bacillus cereus*, *Bacillus sphaericus*, and *Vibrio furnissii* at 35 °C. Many reports have shown the degradation of PA 66 using white-rot fungi. These strains produce peroxidase, which has found

Caprolactam　　　　　　　　　　　　　　　　　　Nylon 6
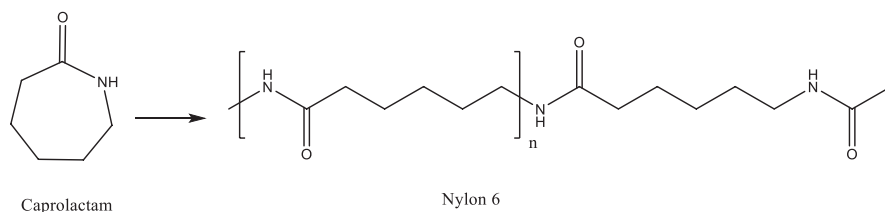
Fig. 10 Basic ring-opening polymerization of caprolactam to synthesize Nylon 6

Table 5 Monomers used in the synthesis of the desired Nylon type

Type of polyamide	Monomers
Nylon 66	1,6-Hexamethylene diamine and adipic acid
Nylon 46	1,4-Diamino butane and adipic acid
Nylon 610	1,6-Hexamethylene diamine and sebacic acid
Nylon 612	1,6-Hexamethylene diamine and 1,12-dodecanedioic acid
Nylon 666	A copolymer of nylon 6/nylon 66
Nylon 6	Caprolactam
Nylon 12	Laurolactam
Nylon1012	1,10-Diamino decane and 1,12-dodecanedioic acid
Polyphthalamide	Any diamine and terephthalic acid/ isophthalic acid

use in the bioremediation of many types of environmental pollutants, which gives some possibility of recycling PA 66. The lignolytic fungi *Phanerochaete chrysosporium* can degrade PA 6, which is a direct analog of degradable polyester or poly(ε-caprolactone). Possible mechanism of PA degradation is oxidation of the methylene group near to the amide linkage (due to N-atom) with the peroxidase enzyme and the obtained radical then undergoes stepwise oxidation with releasing degradation products. The lack of aromatic units makes in PA unsusceptible to degradation, but copolymerization promotes better biodegradability [28, 31, 34].

5.2 Effect of Moisture Absorption on the Thermomechanical Properties of Polyamides

Polyamides at the molecular level having amide linkages are hydrophilic and, thus, can absorb water quite easily, which causes the change in the physical properties of the polyamide material. In ordinary atmospheric conditions (relative humidity 60% and temperature 23 °C), water absorption is 3.5% for PA 6, 2.5% for PA 66, and
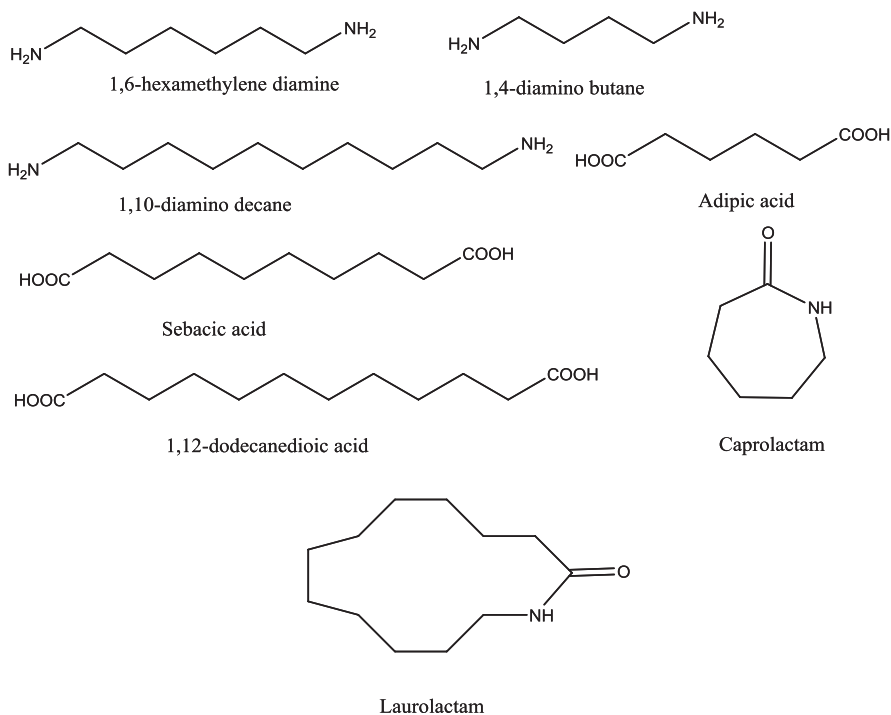
Fig. 11 Monomers used in the synthesis of various types of polyamides

1.5% for PA 610. Thus, moisture absorption has a severe effect on the amidic linkages such as it can cause plasticizing, thus lowering the glass transition temperature and reducing both elastic modulus and strength at break. The effect of moisture on the main properties of polyamides are summarized in Table 6 [27, 28, 31, 34].

6 Chitin

Polysaccharides are biologically relevant, quite often heterogeneous polymers comprising of monosaccharide moieties interacting via glycosidic linkages. Their source of origin ranges from cyanobacteria to plants to animals. Similarly, they portray a variety of functions, the primary one being energy storage apart from structural support, inter−/intracellular communication, host-guest recognition, etc. [41]. Commercially, the polysaccharides are crucial owing to their biocompatibility in the food industry as thickening agents, in cosmetics, fillers in composite materials, and also in drug delivery systems [42, 43]. Considering the routes of application of polysaccharides, their degradation is inevitable after particular time [44–46]. Chitin, being abundantly available, is one of the preferred choices for composite preparation

Table 6 Effects of moisture on the main properties of PAs

Properties	Effect
Elastic modulus	Decrease
Breaking strength	Decrease
Elongation at break	Increase
Impact resistance	Increase
Creep resistance	Decrease
Dielectric strength	Decrease
Dielectric constant	Increase
Electrical resistivity	Increase

as it imparts biodegradability and biocompatibility. Similar to cellulose nanofibers, chitin nanofibrils have also been designed, and this provides an added advantage for material fabrication. Depending on the route of preparation, followed by surface modification, chitin nanofibers/nanowhiskers show different dimensions and surface charges.

Additionally, degraded chitin offers low-molecular-weight substitutes (Fig. 12), which have proved beneficial as they overcome the limitation set by chitin's insolubility.

Antimicrobial Agents Shows high activity against pathogens, and this fact is being explored for antimicrobial food packaging.

Anti-diabetes Showed decreased progress of diabetes mellitus as well as increased calcium and iron absorption.

Agriculture Contributor to carbon and nitrogen cycles in the environment.

Food Industry It is frequently used as a thickening agent, dietary fiber, and preservative.

Biomedical Applications It is used in drug delivery systems apart from contact lenses, dental implants, as encapsulating material, etc.

Discussed below are some of the most frequently employed techniques used for the degradation of polysaccharides.

Enzymatic Degradation A broad class of depolymerase that targets the glycosidic bond is known to benefit from this purpose, including glycosyltransferases, lyases, and hydrolases. Microbial enzymes are abundantly found in nature and identified for the generation of oligosaccharides having further practical use as dietary supplements and recently also for medicinal purposes. Figure 13 shows chitobiose and N-acetylglucosamine as the breakdown products of chitin by the action on the β-1,4 linkage [46–48].
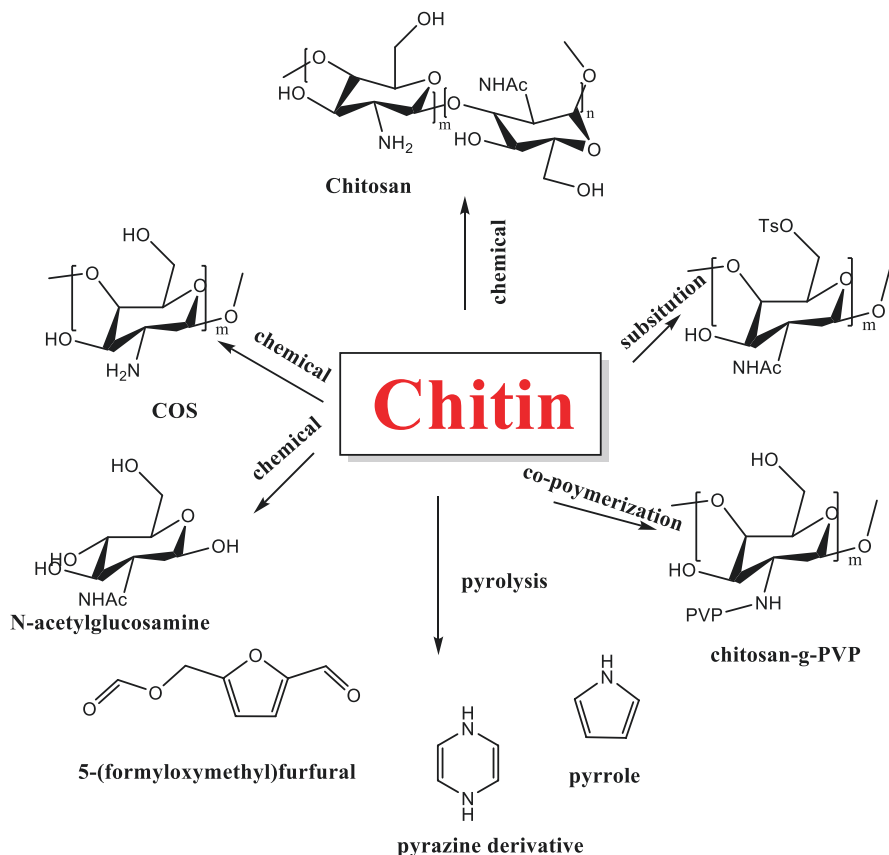
Fig. 12 Overview of conversion of chitin biomass into various products [47]

Chitin biodegradation within the soil by associated bacteria helps in nutrient cycling, as it provides the essential nitrogen and carbon. Also, this management promotes plant's defense against invaders, subsequently increasing the crop yield. Although the enzymatic approach promises high selectivity and specificity, the associated cost and complicated multistep reaction conditions in the laboratory downplay these advantages.

Alkaline/Acidic Degradation Early works avoided the use of alkali as solutions for carbohydrates because it led to their degradation combined with oxidation, resulting in a complex mixture of products. However, it was later realized that alkaline degradation in the absence of oxygen could be extremely helpful in structural analysis and avoiding the methylation route. The alkali can have multiple interaction points, end groups, and hydroxyl groups or by O-substitution, depending on the polysaccharide chain. Similarly, the use of strong acids for the degradation of polysaccharides was severely limited due to the associated problems of instrumental
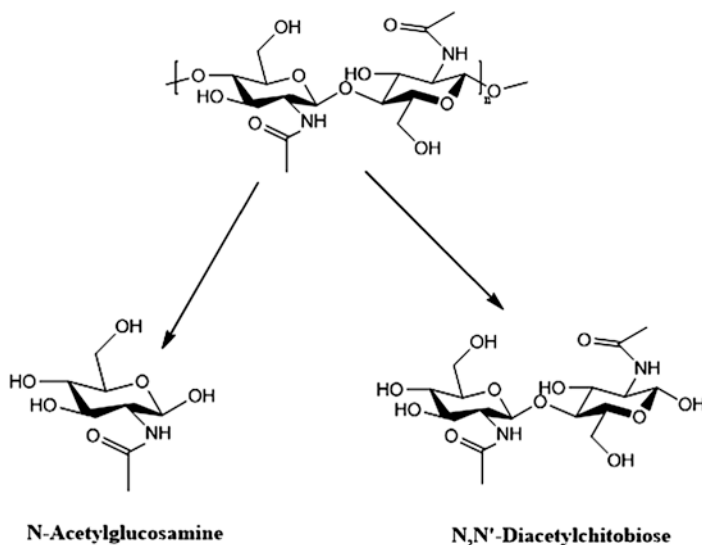
Fig. 13 Structure of animal polysaccharide, chitin, and its components after degradation [46–48]

design, uncontrolled hydrolysis of monosaccharides, and regeneration of acid and also from the perspective of ecological safety.

Sonication It was evident that the use of chemicals and optimized requirements of enzymatic reactions are too tricky for the study of carbohydrates. In contrast, ultrasonic treatment is an efficient alternative with ease of use and adaptability. It involves the use of sound waves with frequencies above the human hearing limit, i.e., 20 kHz. The process entails acoustic cavitation in the solution as a result of the generation of rapidly expanding and contracting water bubbles. This mainly causes increased temperature and pressure environment for ultimate degradation. The molecular weight, viscosity, and the solvent used are some of the factors governing the output of sonolysis apart from the ultrasonic intensity and frequency. The breakdown is initiated from the weakest point in the macromolecular structure, and longer chains are broken into smaller fragments within a short duration of time without altering the native structure. The best part is that it is a green technology, economically feasible with no clean-up requirements.

7 Conclusion

In conclusion, a polymer needs to get adapted to the ecosystem or the biological life cycle because all carbon-based material is part of the ecosystem. Thus, polymers should follow the rules of nature of degradability without harming the ecosystem. A significant imbalance in the conversion rate (consumption and renewal) of

biomass into fossil fuels, especially petroleum-based materials can cause disturbance in carbon dioxide levels in the ecosystem (producing more carbon dioxide than conversion into fossil fuels) and is not managed usefully, which can be harmful to the environment. This imbalance can be restored using renewable resources such as biomass for the synthesis of polymer. By doing this, carbon dioxide renewed equals consumption, which makes it sustainable. Many materials are reported every year, which have a shallow impact on the environment. It is justified that the production of eco-friendly and sustainable polyamides from the biomass has become famous for the economic and biological point of view. With the consumption rate in the world market, the production of polyamide is also growing. The bio-based materials not only are reusable but are suitable for the ecosystem, which minimize plastic waste and are highly energy-efficient and biodegradable. Also, non-biodegradable polyamides can be made biodegradable if suitable microorganisms are found for the degradation of the polyamide. However, finding suitable microorganisms does not ensure that such a polymer will become susceptible to organic recycling or will degrade in the environment.

References

1. Chamas A, Moon H, Zheng J, Qiu Y, Tabassum T, Jang JH, Omar MA, Scott SL, Suh S (2020) Degradation rates of plastics in the environment. ACS Sustain Chem Eng 8(9):3494–3511. https://doi.org/10.1021/acssuschemeng.9b06635
2. Agarwal S (2020) Biodegradable polymers: present opportunities and challenges in providing a microplastic-free environment. Macromol Chem Phys 221:2000017. https://doi.org/10.1002/macp.202000017
3. Mülhaupt R (2013) Green polymer chemistry and bio-based plastics: dreams and reality. Macromol Chem Phys 214:159–174. https://doi.org/10.1002/macp.201200439
4. Rydz J, Sikorska W, Kyulavska M, Christova D (2015) Polyester-based (bio) degradable polymers as environmentally friendly materials for sustainable development. Int J Mol Sci 16(1):564–596. https://doi.org/10.3390/ijms16010564
5. McKeown P, Kamran M, Davidson MG, Jones MD, Román-Ramírez LA, Wood J (2020) Organocatalysis for versatile polymer degradation. Green Chem 22:3721–3726. https://doi.org/10.1039/D0GC01252A
6. Ali MA, Kaneko T (2019) Syntheses of aromatic/heterocyclic derived bioplastics with high thermal/mechanical performance. Ind Eng Chem Res 58:15958–15974. https://doi.org/10.1021/acs.iecr.9b00830
7. Iwata T (2015) Biodegradable and bio-based polymers: future prospects of eco-friendly plastics. Angew Chem Int Ed 54:3210–3215. https://doi.org/10.1002/anie.201410770
8. Leja K, Lewandowicz G (2010) Polymer biodegradation and biodegradable polymers—a review. Polish J Environ Stud 19(2):255–266
9. Rudnik E (2013) Compostable polymer materials: definitions, structures, and methods of preparation. In: Handbook of biopolymers and biodegradable plastics, pp 189–211. https://doi.org/10.1016/B978-008045371-2.50004-4
10. Rydz J, Sikorska W, Kyulavska M, Christova D (2015) Int J Mol Sci 16:564–596. https://doi.org/10.3390/ijms16010564
11. Tsui A, Wright ZC, Frank CW (2013) Annu Rev Chem Biomol Eng 4:143–170. https://doi.org/10.1146/annurev-chembioeng-061312-103323

12. Luyt AS, Malik SS (2019) Can biodegradable plastics solve plastic solid waste accumulation, plastics to energy: fuel, chemicals, and sustainability implications, plastics to energy. Elsevier, Amsterdam, pp 403–423. https://doi.org/10.1016/B978-0-12-813140-4.00016-9

13. Agwuncha SC, Sadiku ER, Ibrahim ID, Aderibigbe BA, Owonubi SJ, Agboola O, Reddy AB, Bandla M, Varaprasad K, Bayode BL, Ray SS (2017) Poly(lactic acid) biopolymer composites and nanocomposites for biomedicals and biopackaging applications. In: Handbook of composites from renewable materials, vol 8. Wiley-Scrivener, Hoboken, NJ, pp 135–170. https://doi.org/10.1002/9781119441632.ch153

14. Bari E, Morrell JJ, Sistani A (2019) Durability of natural/synthetic/biomass fiber-based polymeric composites: laboratory and field tests, durability and life prediction in biocomposites. In: Fibre-reinforced composites and hybrid composites, vol 1. Elsevier Woodhead Publishing, Cambridge, pp 15–26. https://doi.org/10.1016/B978-0-08-102290-0.00002-7

15. Amass W, Amass A, Tighe B (1998) A review of biodegradable polymers: uses, current developments in the synthesis and characterization of biodegradable polyesters, blends of biodegradable polymers and recent advances in biodegradation studies. Polym Int 47:89–144. https://doi.org/10.1002/(SICI)1097-0126(1998100)47:2<89::AID-PI86>3.0.CO;2-F

16. Hu Y, Daoud WA, Cheuk KKL, Lin CSK (2016) Newly developed techniques on polycondensation, ring-opening polymerization and polymer modification: focus on poly(lactic acid). Materials 9:133. https://doi.org/10.3390/ma9030133

17. Vouyiouka S, Theodoulou P, Symeonidou A, Papaspyrides CD, Pfaendner R (2013) Solid state polymerization of poly(lactic acid): some fundamental parameters. Polym Degrad Stab 98(12):2473–2481. https://doi.org/10.1016/j.polymdegradstab.2013.06.012

18. Takwa M, Wittrup ML, Hult K, Martinelle M (2011) Rational redesign of Candida antarctica lipase B for the ring-opening polymerization of D,D-lactide. Chem Commun 47:7392–7394. https://doi.org/10.1039/c1cc10865d

19. Casalini T, Rossi F, Castrovinci A, Perale G (2019) A perspective on polylactic acid-based polymers use for nanoparticles synthesis and applications. Front Bioeng Biotechnol 7:259. https://doi.org/10.3389/fbioe.2019.00259

20. Roopan SM, Surendra TV et al (2015) Preparation and properties of biopolymers: a critical review. In: Thakur VK, Thakur MK (eds) Handbook of polymers for pharmaceutical technologies: structure and chemistry, vol 3. Wiley-Scrivener, Hoboken, NJ, pp 541–553

21. Poupart R, Haider A, Babinot J, Kang I-K, Malval J-P, Lalevée J, Andalloussi SA, Langlois V, Versace DL (2015) Photoactivable surface of natural poly(3-hydroxybutyrate-co-3-hydroxyvalerate) for antiadhesion applications. ACS Biomater Sci Eng 1(7):525–538. https://doi.org/10.1021/acsbiomaterials.5b00002

22. Slater S, Houmiel KL, Tran M, Mitsky TA, Taylor NB, Padgette SR, Gruys KJ (1998) Multiple β-Ketothiolases mediate poly(β-Hydroxyalkanoate) copolymer synthesis in Ralstonia eutropha. J Bacteriol 180(8):1979–1987. https://doi.org/10.1128/JB.180.8.1979-1987.1998

23. Fuentes MAV, Thakur S, Wu F, Misra M, Gregori S, Mohanty AK (2020) Study on the 3D printability of poly (3-hydroxybutyrate-co-3-hydroxy valerate)/poly(lactic acid) blends with chain extender using fused filament fabrication. Sci Rep 10:11804. https://doi.org/10.1038/s41598-020-68331-5

24. Meereboer KW, Misra M, Mohanty AK (2020) Review of recent advances in the biodegradability of polyhydroxyalkanoate (PHA) bioplastics and their composites. Green Chem 22:5519–5558. https://doi.org/10.1039/D0GC01647K

25. McKeen LW (2017) 8—Polyamides (Nylons). In: McKeen L (ed) Plastics design library, 4th edn. William Andrew Publishing, Burlington, MA, pp 187–227. https://doi.org/10.1016/B978-0-12-813292-0.00008-3

26. Kobayashi S, Mullen K (2015) Encyclopedia of polymeric nanomaterials. In: Ali MA (ed) Polyamide syntheses. Springer, Berlin, pp 1750–1762

27. Gong X, Chen X, Zhou Y (2018) Advanced weaving technologies for high-performance fabrics. In: McLoughlin J, Sabir T (eds) Woodhead publishing series in textiles. Woodhead Publishing, Cambridge, pp 75–112. https://doi.org/10.1016/B978-0-08-100904-8.00004-3

28. Su WF (2013) In: Su WF (ed) Step polymerization BT—principles of polymer design and synthesis. Springer, Berlin, pp 111–136. https://doi.org/10.1007/978-3-642-38730-2_6

29. Jiang Y, Loos K (2016) Enzymatic synthesis of biobased polyesters and polyamides. Polymers 8(7):243. https://doi.org/10.3390/polym8070243

30. Huang SJ, Edelman PG (1995) An overview of biodegradable polymers and biodegradation of polymers. In: Scott G, Gilead D (eds) Degradable polymers. Springer, Dordrecht. https://doi.org/10.1007/978-94-011-0571-2_2

31. Misra M, Panday JK (eds) (2015) Biocomposites: design and mechanical performance. Woodhead Publishing, Cambridge. https://doi.org/10.1016/C2014-0-02693-7

32. Hu X, Zhu N, Fang Z, Guo K (2017) Continuous flow ring-opening polymerizations. React Chem Eng 2:20–26. https://doi.org/10.1039/C6RE00206D

33. Becker G, Wurm FR (2018) Functional biodegradable polymers via ring-opening polymerization of monomers without protective groups. Chem Soc Rev 47:7739–7782

34. Yamano N, Kawasaki N, Ida S, Nakayama Y, Nakayama A (2017) Biodegradation of polyamide 4 in vivo. Polym Degrad Stab 137:281–288

35. Negoro S (2005) Biodegradation of nylon and other synthetic polyamides. Biopolymers Online. https://doi.org/10.1002/3527600035.bpol9018

36. Ghosh M, Roy SK, Kar AB (1975) Effect of a copper intrauterine contraceptive device and nylon suture on the estradiol 17β-6, 7-H3 and progesterone 1, 2-H3 in the rat uterus. Contraception 11:45–51. https://doi.org/10.1016/0010-7824(75)90049-9

37. Kyulavska M, Toncheva-Moncheva N, Rydz J (2019) Biobased polyamide ecomaterials and their susceptibility to biodegradation. In: Martínez L, Kharissova O, Kharisov B (eds) Handbook of ecomaterials. Springer, Cham. https://doi.org/10.1007/978-3-319-68255-6_126

38. Smith R, Oliver C, Williams DF (1987) The enzymatic degradation of polymers in vitro. J Biomed Mater Res 21:991–1003. https://doi.org/10.1002/jbm.820210805

39. Ali MA, Kaneko T (2017) Microbe-derived Itaconic acid: novel route to biopolyamides. Microbial applications. Springer-Verlag, Berlin, pp 279–289. https://doi.org/10.1007/978-3-319-52669-0_15

40. Lee J, Seo WG, Kim J et al (2017) Amide-based oligomers for low-viscosity composites of polyamide 66. Macromol Res 25:1000–1006. https://doi.org/10.1007/s13233-017-5129-2

41. Kadokawa JI (2018) Enzymatic preparation of functional polysaccharide hydrogels by phosphorylase catalysis. Pure Appl Chem 90(6):1045. https://doi.org/10.1515/pac-2017-0802

42. Shamshina JL, Berton P, Rogers RD (2019) Advances in functional chitin materials: a review. ACS Sustain Chem Eng 7(7):6444–6457. https://doi.org/10.1021/acssuschemeng.8b06372

43. Nielsen UN, Ayres E, Wall DH, Bardgett RD (2011) Soil biodiversity and carbon cycling: a review and synthesis of studies examining diversity-function relationships. Eur J Soil Sci 62:105–116. https://doi.org/10.1111/j.1365-2389.2010.01314.x

44. Kaoutari A, Armougom F, Gordon JI, Raoult D, Henrissat B (2013) The abundance and variety of carbohydrate-active enzymes in the human gut microbiota. Nat Rev Microbiol 11:497–504. https://doi.org/10.1038/nrmicro3050

45. Jardine A, Sayed S (2016) Challenges in the valorisation of chitinous biomass within the biorefinery concept. Curr Opin Green Sustain Chem 2:34–39. https://doi.org/10.1016/j.cogsc.2016.09.007

46. Berton P, Shamshina JL, Ostadjoo S, King CA, Rogers RD (2018) Enzymatic hydrolysis of ionic liquid-extracted chitin. Carbohydr Polym 199:228–235. https://doi.org/10.1016/j.carbpol.2018.07.014

47. Alvarez-Vasco C, Zhang X (2013) Alkaline hydrogen peroxide pretreatment of softwood: hemicellulose degradation pathways. Bioresour Technol 150:321–327. https://doi.org/10.1016/j.biortech.2013.10.020

48. BelHaaj S, Magnin A, Petrier C, Boufi S (2013) Starch nanoparticles formation via high power ultrasonication. Carbohydr Polym 92:1625–1632. https://doi.org/10.1016/j.carbpol.2012.11.022

Plant Microbial Fuel Cell as a Biomass Conversion Technology for Sustainable Development

D. A. Jadhav, D. Ghosal, A. D. Chendake, S. Pandit, and T. K. Sajana

Abstract Plant photosynthesis is one of nature's best gifts to humankind for converting solar energy into chemical energy in the form of carbohydrates and energy. Plant microbial fuel cells (PMFCs) or photosynthetic MFCs integrate the principles of photosynthesis and fuel cell to convert such synthesized carbohydrates and organic matter into electricity by microbial oxidation in the rhizosphere of plants. Also, plants utilize nutrients from effluent streams for self-growth and metabolism, reducing the nutrient load and heavy metal concentration, and are capable to degrade contaminants. Performance of PMFC is governed by various parameters such as selection of plant species, rhizodeposits, design of MFC, electrode properties, inoculum characteristics, wastewater properties, etc. This chapter discussed the basics of PMFC to applications for real field. According to applications, PMFC designs can be varied as constructed MFC, microbial carbon capture cells, microbial solar cells, floating islands, hydroponics-MFC, and paddy field MFC. Thus, simultaneous organic matter degradation, biomass recovery, oxygen release for cathodic reduction, CO_2 sequestrations, nutrient removal, and heavy metal removal along with electricity generation can be achieved in PMFC.

D. A. Jadhav (✉)
Department of Agricultural Engineering, Maharashtra Institute of Technology,
Aurangabad, Maharashtra, India
e-mail: deepak.jadhav1795@gmail.com

D. Ghosal
Department of Chemical Engineering, CV Raman Global University,
Bhubaneswar, Odisha, India

A. D. Chendake
Shiv Shankar College of Agricultural Engineering,
Mirajgaon, Ahmednagar, Maharashtra, India

S. Pandit
Department of Life Sciences, School of Basic Sciences and Research, Sharda University,
Greater Noida, Uttar Pradesh, India

T. K. Sajana
Department of Agricultural and Food Engineering, Indian Institute of Technology Kharagpur,
Kharagpur, West Bengal, India

1   Introduction

Water and energy crisis and wastewater treatment are major environmental concerns of the present era. Utilization of conventional fossil fuels for energy generation resulted in carbon emission and caused severe environmental damage issues. Over limited availability of fossil fuels, researchers are looking forward to recover the energy from renewable energy sources. Biomass can be an effective non-conventional renewable energy source with minimal harm to the environment. Biomass as feed-stock can be effectively utilized for bioethanol and biodiesel generation and as bio-fuel source and contribute for circular economy. At present, biomass energy contributes about 12–15% of renewable energy in India [1].

Biomass fuels provided about 5% of the total primary energy use in the United States in 2017. Of that 5%, about 46% was from biofuels (mainly ethanol), 44% was from wood and wood-derived biomass, and 10% was from the biomass in municipal waste [2]. In the present era, researchers are looking forward for harvesting the energy from such renewable biomass source. Bioenergy can be harvested from the organic biomass in the form of bioethanol, biodiesel, bioheat, and biopower as well as biogas. Individual process of bioenergy synthesis has advantages and limitations based on various biomass utilized. Bioelectrochemical system is the recent waste-to-energy technique utilized to generate power, employing bacteria for oxidation of organic matter present in wastewater. This chapter provides space of consideration for the utilization of plants for bioelectricity generation through advanced plant microbial fuel cell during wastewater treatment.

2   Microbial Fuel Cell

Anodic oxidation of organic matter from wastewater and cathodic reaction using electron acceptors can be bioelectrochemically grouped together in microbial fuel cell (MFC) technology with the aim of harvesting electricity during wastewater treatment. MFC consists of anodic chamber for oxidation and cathodic chamber for reduction, separated by cation exchange membrane (CEM). Electrons generated after anodic oxidation are utilized for electric current production, and protons migrated through CEM are utilized for cathodic reduction to form water. Being an electrochemical system, MFC provides flexible platform for controlling electro-chemical reactions, and being a biological system, it provides platform for microbes to select the substrate. Hence, performance of MFC mainly depends on wastewater characteristics, operating conditions, design aspects, inoculum properties, and material properties.

Wastewater contains high content of carbohydrates, organic matter, and nutrients, which can be suitable substrate for microbial oxidation in anodic chamber. Some biomass needs pretreatment method so that it can be easily biodegraded in MFC.

3   Plant Microbial Fuel Cell

During the photosynthesis process, plants such as trees, shrubs, and algae utilize solar energy and turn it into chemical energy. During photosynthesis, light energy transfers electrons from water to produce carbohydrates. Thus carbon dioxide is reduced along with oxidation of water to release oxygen. Thus, oxygen- and energy-rich organic carbohydrate molecules produced during photosynthesis serve as counterbalance reaction for CO_2 respiration by all organisms and oxygen release during photosynthesis.

In plant MFC (PMFC), several small growing plants such as algae, rice plant, water hyacinth, and other shrubs are used for photosynthesis process. In MFC, oxygen serves as a terminal electron acceptor released by plants for cathodic reduction. Also, utilization of carbon dioxide by the plants resulted into carbohydrate synthesis which serves as organic matter for microbial oxidation in anodic processes (Fig. 1). Some plant species have properties of adsorption of heavy metals and other toxic elements from wastewater and hence are used for heavy metal removal in MFC. Thus, simultaneous organic matter removal, heavy metal removal, and toxicity reduction along with simultaneous electricity generation can be achieved in plant MFC. Also carbon sequestration from industrial plant and need of external aeration can be reduced with such advanced application of MFC technology.

Similar to conventional MFC, the performance of plant MFC is governed by various parameters such as selection of plant species, rhizodeposits, design of MFC, electrode properties, inoculum characteristics, wastewater properties, etc. Several design variations and electrode orientations have been adopted while taking into account the root zone depth of plant as well as creating anoxic-oxic zone separation.

4   Factors Governing Performance of Plant MFC

Plant MFC generally combines the principle of plant photosynthesis and bioelectrochemical system, which is dependent on microbial, electrochemical, material, environmental, and engineering parameters. Hence, performance of plant MFC is governed by several constraints such as plant species, operating conditions, wastewater characteristics, inoculum properties, and design aspects. However, operating conditions need to be optimized for getting better performance from plant MFC in terms of power generation and wastewater treatment. Table 1 summarizes the performance of plant MFCs with variations in governing parameters.
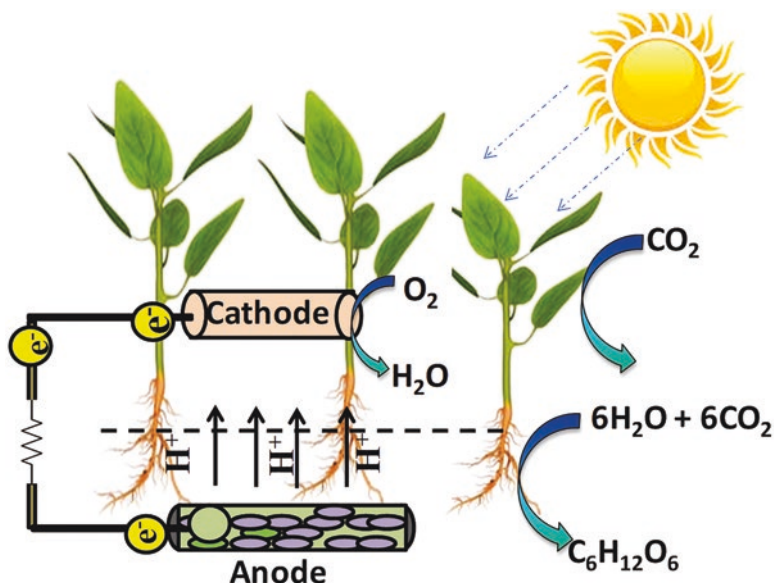
Fig. 1 Schematic diagram of plant microbial fuel cell

Table 1 Factors affecting the performance of plant MFC

Parameters	MFC design	Wastewater treatment (%)	Power density (mW/m²)	References
Plant species	*Ipomoea aquatic* plant	COD—92%; TN—90%	12.42	Liu et al. [3]
Electrode material	Stainless steel (SS) vs. graphite (G)	–	0.35 (SS); 0.12 (G)	Pamintuan and Sanchez [4]
Electrode placement	5 cm deep soil and 3 cm overlaying water	–	0.72	Deng et al. [5]
Electrode design	Flat plate design	COD—85%	440	Helder et al. [6]
Operating conditions	Soil water content (water logged soil)	–	10.13	Nguyen and Nitisoravut [7]
	Temperature 34 °C and 41 °C	–	1.9; 0.6	

4.1 Plant Species

Selection of plant species in plant-MFC greatly affects the performance of MFC due to rate of biomass formation, oxygen release rate, as well as root zone depth of plant. Several plant species such as *Ipomoea aquatica* and *Phragmites australis*, lemon grass, algae, and rice plants are widely used for plant and constructed wet-land MFC. Marshy grasses, lemon grasses, and locally available grasses are widely

preferred during treatment of saline effluent and industrial wastewater in MFC. Moreover, macrophytes or hydrophytes play an important role in phytoremediation in case of constructed wetland MFC due to plant metabolism to absorb heavy metals and other nutrients [8]. Even in paddy field, methane emission can be controlled by competition with electrogenic microbes, and hence methane emission is reduced in paddy field MFC. On the other hand, locally available mixed culture algae can support the high rate of biomass production and oxygen release for cathodic reduction and mostly used for carbon sequestration in microbial carbon capture cells. Thus, depending upon the characteristics of plants and local availability, plant species have been selected for MFC applications.

4.2   Operating Conditions

The operating conditions such as pH, salinity, and substrate flow and characteristics and inoculum conditions control the rate of microbial metabolism during substrate oxidation in MFC. In paddy fields, rice plants are sensitive for low salinity-deficient conditions below the salinity level of 0.6 S/m [9]. In such conditions, electrolyte salinity can be improved by addition of phosphate buffer solution in wastewater or selection of seawater plant species for plant MFC. Similarly, increase of salt concentration in electrolyte also has negative impact on the growth of plant species in MFC. Additionally, pH is one of the major indicators determining the proton gradient and flow between anodic and cathodic chamber. Most of plant metabolism are best suited at neutral pH conditions and enhance the release of rhizodeposition from plant roots [8]. In plant MFC, rate of rhizodeposition discharge depends on temperature conditions as well as humidity level which directly affect the current production in plant MFC.

4.3   Design Aspects

Electrode material selection mostly depends on the microbial attachment and biofilm formation, cost, and high conductive surface area. In case of sediment or plant MFC, placing of electrodes in soil and maintaining the water interface control the proton transfer diffusion. Deng et al. [5] studied the effect of electrode positions on various soil and water depths. Results showed that MFC with 5-cm-deep soil and 3-cm overlaying water exhibited the highest power density of 0.72 mW/m^2 with decrease in ohmic resistance. Also electron spacing is dependent on root zone depth of plant as there is possibility of covering of anode with branches of roots and unavailable for microbial biofilm growth. Lower electrode spacing supports the submergence of anode in a support matrix near the rhizosphere to obtain organic substrates in the influent as well as reduce the proton diffusion losses. Like typical MFC, electrode material, architectural design, and catalyst selection affect the energy recovery in plant MFC [10, 11].

5   Variations in Plant MFC

Plant MFC is a promising technology utilizing the correlation between plant and microbes at rhizosphere of root zone. Root system of aquatic plant exudates acts as substrate for bacteria in rhizosphere for oxidation. Based on plant-microbe harmony at the soil interface and plant species used in such coupled biosystem, different variations in plant MFC design such as constructed wetland MFC (CW-MFC), microbial carbon capture cells (MCCs), microbial solar cells (MSCs), floating islands, hydroponics-MFC, and paddy field MFC were used for practical applications as discussed below (Fig. 2). Table 2 compared the performance of different plant MFCs based on applications for wastewater treatment and power generation.

5.1   *Constructed Wetland MFC (CW-MFC)*

The integration of conventional constructed wetland (CW) system and microbial fuel cell (MFC) exerts symbiotic relationship between plant bacteria present in the rhizosphere of aquatic plants through the formation of root exudates as endogenous substrates for oxidation (Fig. 3) and a microbial activity [16, 20]. Different wetland plants such as *Phragmites australis* were used in CW-MFC under upflow conditions to maximize the redox potential gradient across the substrate. Similar CW-MFC was capable to remove nitrate by 86.5%, soluble chemical oxygen demand (sCOD) by 92%, phosphate removal efficiency of 56.3%, and total suspended solid removal efficiency of 78.4% along with energy recovery of 33.52 mW/m^3 during treatment of graywater [21].

During comparison of air cathode CW-MFC and typical CW-MFC, the removal efficiency of COD and NO_3-N as well as power density (4.21 mW/m^2) in CW-ACMFC was slightly higher than that of CW-MFC, which might be resulted from the growth and metabolism of microorganisms and plant stimulated by a higher voltage [22]. In some CW-MFC, additional filtration media (sand filter layer) were provided to serve as a medium for protons to move in and to facilitate the simple filtration of sewage during upflow of substrate [23]. Such CW-MFC can serve as a polishing treatment for sewage treatment plant along with its advantages: easy operation, inexpensive, wide availability, and recyclability.

5.2   *Microbial Carbon Capture Cells (MCCs)*

To address the issue of carbon storage and utilization, the modified MFC system such as microbial carbon capture cell (MCC) has a potential to provide a sustainable and effective solution by utilizing the concept of carbon capture and conversion to algal biomass using algal biocathode, treating wastewater simultaneously and facilitating energy recovery in the form of electricity.
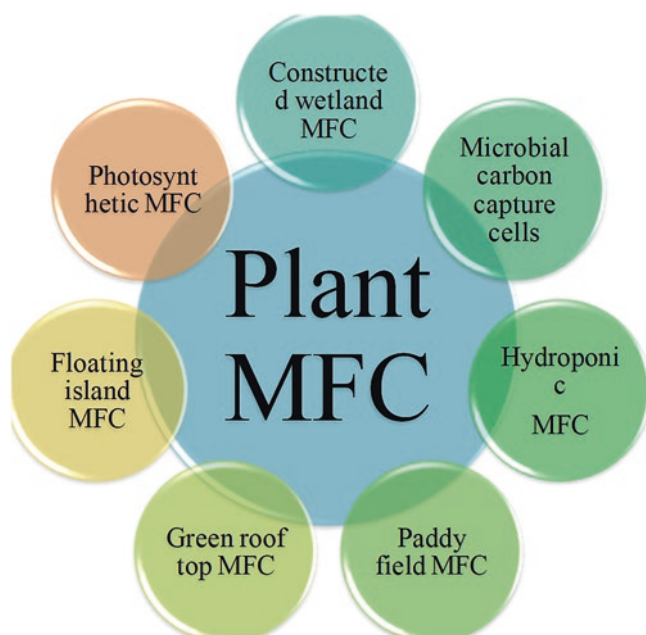
Fig. 2 Variation in design of plant MFC based on applications

Table 2 Variation in design of plant MFC for different applications

MFC design	Plants and design aspects	Wastewater treatment (%)	Power generation	References
Constructed wetland MFC	Vertical flow MFC	COD—86%	0.302 W/m³	Fang et al. [12]
Microbial carbon capture cell	Air lift-type MFC; microalgae	COD—87%; NH₃-N—70%; P—69%	0.97 W/m³	Hu et al. [13]
Photosynthetic MFC	*Synechocystis* sp. PCC 6803; single-chamber MFC	–	1.3 mW/m²	Zou et al. [14]
Floating island MFC	Floating type, brewery wastewater	COD—86.47%	8 mW/m²	An et al. [15]
Hydroponic MFC	Upflow mode; ceramic separator; *Canna indica*	COD—86.2%	0.25 W/m³	Khuman et al. [16]
Paddy field MFC	Depth of anode electrode	–	14.44 mW/m²	Lu et al. [17]
Rooftop MFC	*Chlorophytum comosum*; electrode	–	744 µW/m²	Tou et al. [18]
Sediment MFC	*Acorus tatarinowii*, anode position	–	7 mW/m²	Liu et al. [19]

Fig. 3 Pictorial view of laboratory scale constructed wetland MFC during initial stage of construction

MCCs consist of integration of MFC system and algal species in cathodic chamber for CO_2 sequestration (Fig. 1). The use of algal species in cathodic chamber generates oxygen available for cathodic reduction during photosynthesis and, thus, reduces the cost of external aeration.

In MCC, carbon dioxide produced during oxidation of organic matter in the anodic chamber can be further used to produce the useful biomass with photosynthetic activities of algae, attaining simultaneous electricity generation, CO_2 sequestration, wastewater treatment, and biomass production. Thus, anodic off-gas into algae-grown cathode is demonstrated to be an effective way for CO_2 emission reduction during wastewater treatment with simultaneous electricity generation without the need for external aeration [24]. The various factors such as algal growth kinetics, density, light intensity, and CO_2 supply and other operating conditions govern the performance of MCC [25, 26].

5.3 Microbial Solar Cells (MSCs)

Microbial solar cells (MSCs) are modified version of MFC in which integration of photosynthetic organism such as plants and algae is used for the conversion of solar energy into electrical energy via chemical routes. He et al. [27] designed self-sustained phototrophic MFC with self-assembly of a synergistic

phototrophic-heterotrophic cathode biofilm from a sediment microbial fuel cell (SMFC). Molecular taxonomic analysis showed that the presence of cyanobacteria and microalgae predominated in the water phase as photosynthetic organisms along with dominance of electrogenic population in sediment for electricity generation. Application of MSC with reversible biocathode was proposed by Strik et al. [28] to address the issue of pH imbalance across the membrane due to acid formation at anode and alkali formation at cathode. Micro-sized MSC (57-μL) through photosynthetic reactions of cyanobacteria *Synechocystis* sp. PCC 6803 in the anodic chamber was capable to generate the power density of 7.09 nW/cm^2 [29]. The photosynthetic organism, i.e., cyanobacteria, serves as a sustainable and effective catalyst for cathodic reactions in MSC, similar to the photosynthesis process in plants. Such advanced MSC in combination with photoelectric cell is useful to produce electricity, methane, hydrogen, and other biofuels during wastewater treatment [30].

5.4 Paddy Field MFC

Apart from rice as food source, environmental concern has been raised with emission of methane from paddy field. From this point of view, several research studies have been conducted on application of MFC in paddy field for in situ electricity generation, methane emission, and wastewater treatment. PMFC with rice plants (*Oryza sativa* L.) and biochar anode produced power density of 11.1 mW/m^2 along with reduction in methane emission by 39% and were found to be effective as compared to soil-based MFC [31]. In reality, paddy MFC is more suitable in sediment conditions due to availability of high organic matter in soil. In such MFC, anode is set in paddy field before rice transplantation. Rhizosphere microbe oxidizes photosynthesized organic matter excreted from rice roots and generates electron for energy recovery [32]. Current production in paddy MFC reduced methane generation by half when operated in closed circuit conditions as compared to MFC with open circuit conditions [33]. The microbial taxonomic analyses revealed the presence of *Desulfobulbus*, *Geobacter* sp., *Methanobacterium*, and *Clostridiaceae* microbes in paddy field suitable for MFC applications.

5.5 Floating Islands

Floating island is generally an artificially constructed MFC in hydroponic system for plant growth and wastewater treatment and serves as a polishing treatment for the removal of organic matter and nutrient content from wastewater. Such system is capable to remove the contaminants from effluent stream intermittently with effective heavy metal removal. Recently, Yadav et al. [34] developed integrated drip hydroponic MFC system for treatment of domestic wastewater. Such system achieved ammonia, COD, and phosphate removal efficiency of 35%, 83%, and

72%, respectively. The integration of *Cymbopogon citratus* (lemon grass) plants in the integrated system through adsorption and filtration processes resulted in higher wastewater treatment efficiency and power generation (31.88 mW/m^2).

5.6 Other Variations

Photosynthetic MFC, based on plant photosynthesis, generates electrical energy from organic matter synthesized by sunlight, by heterotrophs, or by photosynthetic organisms [35]. Most of planted sediment MFCs used for real-field applications contains aquatic plants to mimic the constructed wetland system for degradation of contaminants [19]. Liu et al. [19] reported that position of anode across the depth of sediment is important factor and planted sediment MFC did not improve the power generation when roots of the plants are placed on electrode surface (Table 1). In the concept of implementing MFC at rooftop of a building, green roof MFC under outdoor conditions produced lower power output of 88 mW/m^2 as compared to that in control laboratory conditions (440 mW/m^2) [36]. In a study of seven *Sedum* species in green roof MFC, positive relationship between water content of plant growth media and power output was reported by Tapia et al. [37], and it was concluded that current and water gradually decrease over time at a similar rate after providing irrigation.

6 Summary and Outlook

To harvest the solar energy, photovoltaic cells and plant MFC can provide the solution for trapping the renewable energy from the sun. However, PMFC offers sustainable and efficient approach for electricity generation and contaminant degradation over photovoltaic cells. Such PMFC can be implemented at agricultural field without disturbing the tillage operation and reduced greenhouse gas emission from paddy field along with in situ electric supply for operating different electronic sensors [38]. As PMFC mimics the natural system, hence real-field application of such MFC can be possible with only cost of electrode assembly and electronic circuit system required and thus reduces the cost of membrane, reactor assembly, collectors, and mediators as required in typical MFC. Apart from the low cost, it also offers ease in design and fabrication, no technical assistance required, and minimal carbon dioxide and methane emission with cost-effective solution for wastewater treatment [39]. A major challenge in PMFC is the low power production which can be overcome by integrating the system with conventional wastewater treatment system [40].

7   Conclusion

At current scenario, water and energy crises are two important concerns the whole world is facing nowadays. Bioelectrochemical system such as plant microbial fuel cell provides a novel way to trap solar energy by integrating advantages of MFC for effluent treatment and energy recovery. Research on PMFC is still in the early stage of growth, and the limitation of low-power output can be overcome by using effective catalyst and mediators and controlling mass diffusion losses. PMFC is a multi-disciplinary system dealing with biology, electrochemistry, material science, environmental chemistry, and engineering economics. During integration of plant photosynthesis with MFC, the soil system and the plant can provide a heterogeneous microenvironment for microbes and substrates. Due to the self-food-synthesizing ability of plants and photosynthetic organisms, plant-microbe interaction plays an encouraging role in long-term operation due to the continuous availability of nutrients and the adaptation of electrogenic population in system [8]. Variations in design promote the application of PMFC to be coupled with constructed wetland, algal treatment, hydroponic system, and marine sediment. Thus, PMFC provides a novel and alternative solution for energy generation from plant biomass source to achieve the sustainable development and energy positive system.

References

1. Mohnish B, Suchithra TV (2018) Electricity generation from living plants using microbial fuel cells. Int J Eng Technol 7(4):534–537
2. Webpage 1. https://www.eia.gov/energyexplained/biomass/. Accessed 18 May 2020
3. Liu S, Song H, Li X, Yang F (2013) Power generation enhancement by utilizing plant photosynthate in microbial fuel cell coupled constructed wetland system. Int J Photoenergy 2013:1
4. Pamintuan KRS, Sanchez KM (2019) Power generation in a plant-microbial fuel cell assembly with graphite and stainless steel electrodes growing Vigna Radiata. In: IOP conference series: materials science and engineering, vol 703. IOP Publishing, Bristol, p 012037
5. Deng H, Wu YC, Zhang F, Huang ZC, Chen Z, Xu HJ, Zhao F (2014) Factors affecting the performance of single-chamber soil microbial fuel cells for power generation. Pedosphere 24(3):330–338
6. Helder M, Strik DPBTB, Hamelers HVM, Buisman CJN (2012) The flat-plate plantmicrobial fuel cell: the effect of a new design on internal resistances. Biotechnol Biofuels 5:70
7. Nguyen V, Nitisoravut R (2019) Bioelectricity generation in plant microbial fuel cell using forage grass under variations of circadian rhythm, ambient temperature, and soil water contents. In: 2019 IEEE Asia Power and Energy Engineering Conference (APEEC). IEEE, Piscataway, NJ, pp 240–244
8. Regmi R, Nitisoravut R, Ketchaimongkol J (2018) A decade of plant-assisted microbial fuel cells: looking back and moving forward. Biofuels 9:1–8. https://doi.org/10.1080/1759726 9.2018.1432272
9. Zeng L, Lesch SM, Grieve CM (2003) Rice growth and yield respond to changes in water depth and salinity stress. Agric Water Manag 59(1):67–75

10. Jadhav DA, Deshpande PA, Ghangrekar MM (2017a) Enhancing the performance of single-chambered microbial fuel cell using manganese/palladium and zirconium/palladium composite cathode catalysts. Bioresour Technol 238:568–574

11. Mathuriya AS, Jadhav DA, Ghangrekar MM (2018) Architectural adaptations of microbial fuel cells. Appl Microbiol Biotechnol 102(22):9419–9432

12. Fang Z, Song H, Cang N, Li X (2013) Performance of microbial fuel cell coupled constructed wetland system for decolorization of azo dye and bioelectricity generation. Bioresour Technol 144:165–171

13. Hu X, Liu B, Zhou J, Jin R, Qiao S, Liu G (2015) CO_2 fixation, lipid production, and power generation by a novel air-lift-type microbial carbon capture cell system. Environ Sci Technol 49(17):10710–10717

14. Zou Y, Pisciotta J, Billmyre RB, Baskakov IV (2009) Photosynthetic microbial fuel cells with positive light response. Biotechnol Bioeng 104(5):939–946

15. An J, Kim D, Chun Y, Lee SJ, Ng HY, Chang IS (2009) Floating-type microbial fuel cell (FT-MFC) for treating organic-contaminated water. Environ Sci Technol 43(5):1642–1647

16. Khuman CN, Bhowmick GD, Ghangrekar MM, Mitra A (2020) Effect of using a ceramic separator on the performance of hydroponic constructed wetland-microbial fuel cell. J Hazard Toxic Radioactive Waste 24(3):04020005

17. Lu Y, Liu L, Wu S, Zhong W, Xu Y, Deng H (2019) Electricity generation from paddy soil for powering an electronic timer and an analysis of active exoelectrogenic bacteria. AMB Express 9(1):1–7

18. Tou I, Azri YM, Sadi M, Lounici H, Kebbouche-Gana S (2019) Chlorophytum microbial fuel cell characterization. Int J Green Energy 16(12):947–959

19. Liu B, Ji M, Zhai H (2018) Anodic potentials, electricity generation and bacterial community as affected by plant roots in sediment microbial fuel cell: effects of anode locations. Chemosphere 209:739–747

20. Guadarrama-Pérez O, Gutiérrez-Macías T, García-Sánchez L, Guadarrama-Pérez VH, Estrada-Arriaga EB (2019) Recent advances in constructed wetland-microbial fuel cells for simultaneous bioelectricity production and wastewater treatment: a review. Int J Energy Res 43(10):5106–5127

21. Araneda I, Tapia NF, Lizama Allende K, Vargas IT (2018) Constructed wetland-microbial fuel cells for sustainable greywater treatment. Water 10(7):940

22. Yan D, Song X, Weng B, Yu Z, Bi W, Wang J (2018) Bioelectricity generation from air-cathode microbial fuel cell connected to constructed wetland. Water Sci Technol 78(9):1990–1996

23. Wang G, Guo Y, Cai J, Wen H, Mao Z, Zhang H, Wang X, Ma L, Zhu M (2019) Electricity production and the analysis of the anode microbial community in a constructed wetland-microbial fuel cell. RSC Adv 9(37):21460–21472

24. Wang X, Feng Y, Liu J, Lee H, Li C, Li N, Ren N (2010) Sequestration of CO_2 discharged from anode by algal cathode in microbial carbon capture cells (MCCs). Biosens Bioelectron 25(12):2639–2643

25. Jadhav DA, Jain SC, Ghangrekar MM (2017b) Simultaneous wastewater treatment, biomass production and electricity generation in clayware microbial carbon capture cells. Appl Biochem Biotechnol 183(3):1076–1092

26. Jadhav DA, Neethu B, Ghangrekar MM (2019) Microbial carbon capture cell: advanced bioelectrochemical system for wastewater treatment, electricity generation and algal biomass production, application of microalgae in wastewater treatment: domestic and industrial wastewater treatment: biorefinery approaches of wastewater treatment, 2. Springer International Publishing AG, Cham. ISBN: 978-3-030-13908-7

27. He Z, Kan J, Mansfeld F, Angenent LT, Nealson KH (2009). Self-sustained phototrophic microbial fuel cells based on the synergistic cooperation between photosynthetic microorganisms and heterotrophic bacteria. Environ Sci Technol 43(5):1648–1654

28. Strik DP, Hamelers HV, Buisman CJ (2010) Solar energy powered microbial fuel cell with a reversible bioelectrode. Environ Sci Technol 44(1):532–537

29. Yoon S, Lee H, Fraiwan A, Dai C, Choi S (2014) A microsized microbial solar cell: a demonstration of photosynthetic bacterial electrogenic capabilities. IEEE Nanotechnol Mag 8(1):24–29

30. Fischer F (2018) Photoelectrode, photovoltaic and photosynthetic microbial fuel cells. Renew Sustain Energy Rev 90:16–27

31. Khudzari JM, Gariépy Y, Kurian J, Tartakovsky B, Raghavan GV (2019) Effects of biochar anodes in rice plant microbial fuel cells on the production of bioelectricity, biomass, and methane. Biochem Eng J 141:190–199

32. Kouzuma A, Kaku N, Watanabe K (2014) Microbial electricity generation in rice paddy fields: recent advances and perspectives in rhizosphere microbial fuel cells. Appl Microbiol Biotechnol 98(23):9521–9526

33. Arends JB, Speeckaert J, Blondeel E, De Vrieze J, Boeckx P, Verstraete W, Rabaey K, Boon N (2014) Greenhouse gas emissions from rice microcosms amended with a plant microbial fuel cell. Appl Microbiol Biotechnol 98:3205–3217

34. Yadav RK, Chiranjeevi P, Patil SA (2020) Integrated drip hydroponics-microbial fuel cell system for wastewater treatment and resource recovery. Bioresour Technol Rep 9:100392

35. Rosenbaum M, He Z, Angenent LT (2010) Light energy to bioelectricity: photosynthetic microbial fuel cells. Curr Opin Biotechnol 21(3):259–264

36. Helder M, Strik DP, Timmers RA, Raes SM, Hamelers HV, Buisman CJ (2013) Resilience of roof-top plant-microbial fuel cells during Dutch winter. Biomass Bioenergy 51:1–7

37. Tapia NF, Rojas C, Bonilla CA, Vargas IT (2017) Evaluation of *Sedum* as driver for plant microbial fuel cells in a semi-arid green roof ecosystem. Ecol Eng 108:203–210

38. Kabutey FT, Zhao Q, Wei L, Ding J, Antwi P, Quashie FK, Wang W (2019) An overview of plant microbial fuel cells (PMFCs): configurations and applications. Renew Sustain Energy Rev 110:402–414

39. Qi X, Ren Y, Liang P, Wang X (2018) New insights in photosynthetic microbial fuel cell using anoxygenic phototrophic bacteria. Bioresour Technol 258:310–317. https://doi.org/10.1016/j.biortech.2018.03.058

40. Jadhav DA, Das I, Ghangrekar MM, Pant D (2020) Moving towards practical applications of microbial fuel cells for sanitation and resource recovery. J Water Proc Eng 38:101566

Catalytic and Non-Catalytic Hydrothermal Liquefaction of Microalgae

Eleazer P. Resurreccion and **Sandeep Kumar**

Abstract Hydrothermal liquefaction (HTL) is an attractive thermochemical pathway that converts microalgal cells into biocrude which can be upgraded and refined into drop-in transportation fuel. HTL is propitious from an environmental sustainability standpoint because the reaction requires medium temperatures (200–400 °C) and high pressures (5–25 MPa) (subcritical and supercritical conditions) for a relatively short period of time (10–60 min) without the need for dewatering and drying of the microalgal culture (wet microalgae with cultivation culture). Instead, water provides dual use to the reaction: as a solvent and as a catalyst. At HTL conditions, water is a reactive nonpolar species with high miscibility in organics. It solubilizes even the recalcitrant microalgal components such as lignin to produce biocrude, aqueous, gaseous, and solid products. This chapter discusses the process and chemistry of microalgae HTL, the role of water in the reaction, the difference between catalytic and non-catalytic HTL as it applies to microalgae, and perspectives and direction on the state of research for microalgae HTL.

Keywords Microalgae · Hydrothermal liquefaction · Biocrude · Subcritical water · Algaenans · Decarboxylation

1 Introduction

The production of sustainable liquid fuels from renewable sources has become increasingly challenging in recent years due to the substantial energy demand brought about by rising population. This demand is largely supplied by limited fossil fuel reserves with remarkable effect on global climate change [1]. The world's

E. P. Resurreccion (✉)
Department of Civil Engineering Technology, Montana State University-Northern,
Havre, MT, USA
e-mail: e.p.resurreccion@gmail.edu

S. Kumar
Department of Civil and Environmental Engineering, Old Dominion University,
Norfolk, VA, USA
e-mail: skumar@odu.edu

energy is 80% derived from fossil fuels, and with current consumption, fossil fuel reserves are projected to be depleted within the next few decades [2, 3]. Action plans have been taken to transition into alternative renewable and sustainable energy sources. Among these sources, biomass such as dedicated energy crops, agricultural wastes, forest products, aquatic plants, and municipal wastes present a viable feedstock because these materials can sequester CO_2 through photosynthesis and they can be transformed into liquid or gaseous fuels. Biomass-derived fuels are not food-based, and they do not interfere with the food supply chain unlike corn ethanol or soybean biodiesel. Some areas of the world lack fossil reserves, but they have abundant supply of biomass which can be capitalized to achieve energy security [4]. Nonfood biomass is also referred as lignocellulosic feedstock. The fuel ("biofuel") derived from biomass has a net energy ratio (i.e., lower heating value embodied in the biomass versus fossil energy requirement in producing the fuel) and has lower greenhouse gas emissions relative to petroleum [5].

Algae are especially appealing because they have high biomass yields and high photosynthetic efficiency [6–8]. They grow approximately ten times faster than terrestrial plants, have low footprint, and require marginal land and water for cultivation. These characteristics make algae-based biofuel suitable to address environmental, land-use, and food issues associated with food crop biomass [9, 10]. Microalgae are unicellular algae cultivated in fresh, brackish, or marine water requiring less arable land [11] and are measured in micrometers. In contrast, macroalgae are multicellular organisms capable of growing tens of meters in fresh, brackish, or marine water. This chapter focuses on microalgae as biomass feedstock.

Conversion methods for microalgae into biofuels are classified into two categories: (1) *biochemical (*e.g.*, alcohol fermentation, anaerobic digestion, hydrogen production)* and (2) *thermochemical (combustion, carbonization, liquefaction, gasification, hydrothermal, pyrolysis)* [2, 12]. Figure 1 shows all conversion technologies employed in microalgae. Out of those methods, *hydrothermal liquefaction* (HTL) is the most promising because it utilizes microalgae cells (presence or absence of lipids) without dewatering or drying (as wet biomass), therefore significantly lowering fossil energy costs [14–18]. Unlike HTL, gasification (dry) and pyrolysis demand the reduction of microalgae's water content [19]. In the case of direct combustion, water level must be lower than 10 wt% to be effective [6, 7, 20]. HTL entails the reaction of biomass in water at high temperature (250–350 °C) and pressure (5–15 MPa) in the presence of solvent (water or alcohol) yielding biocrude, a dark viscous liquid immiscible in water [8]. The process can occur with or without a catalyst. Biocrude is very viscous, rich in oxygen and nitrogen, and easily deteriorates when stored for prolonged periods of time. The high operating pressure maintains water at liquid or supercritical state. The biocrude has higher heating value and lower oxygen content than pyrolysis bio-oil, the product of other microalgae conversion methods. Despite these desirable characteristics, biocrude requires further upgrading to be adapted as drop-in transportation fuels (i.e., direct fuel substitute to petrol) due to its low hydrogen-to-carbon (H/C) ratio, high heteroatom content, and substantial high-boiler fractions (i.e., components with relatively high boiling points). The most common method of upgrade is through hydrotreating in which the
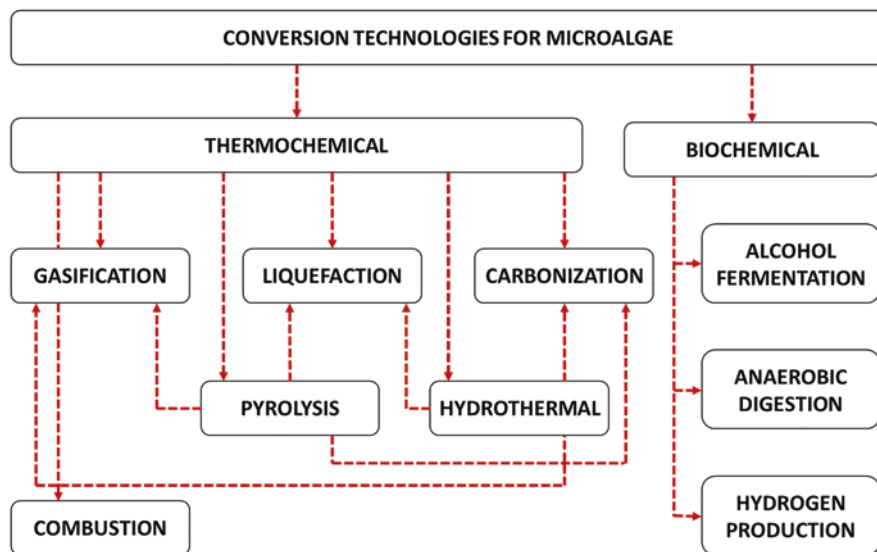
Fig. 1 Conversion technologies for microalgae. Major conversion pathways are *thermochemical* and *biological*. The thermochemical pathway consists of *combustion*, *carbonization*, *liquefaction*, *gasification*, *hydrothermal*, and *pyrolysis*. Hydrothermal can be combined with carbonization, liquefaction, and gasification to form *hydrothermal carbonization* (*HTC*), *hydrothermal liquefaction* (*HTL*), and *hydrothermal gasification* (*HTG*) (modified and adapted with permission from [13])

biocrude is allowed to react with H_2 at high temperature and pressure in the presence of a catalyst [21, 22]. HTL biocrude also has lower moisture content than pyrolysis bio-oil, at a value of around 25–50 wt% [17, 23, 24]. Yet, biocrude from microalgae has relatively low energy content because around only 40% of carbon and 35% of hydrogen in the feedstock are converted to biocrude, while the rest remain the aqueous phase (i.e., low organics) [25]. Solvents are used to liquefy microalgae in order to improve biocrude yield and quality (high quality: low density, low viscosity). These organic solvents include toluene, ethanol, methanol, 1-methyl naphthalene, and 1,4-dioxane [26–29]. The use of organic solvents permits the HTL reaction to proceed at milder temperature compared to HTL reaction without solvent.

2 Process Description in Microalgae HTL

Hydrothermal liquefaction (HTL) is a biomass-to-liquid conversion route typically carried out in water at medium temperatures (200–400 °C) and high pressures (5–25 MPa) for 10–60 min yielding biocrude, aqueous, gaseous, and solid phases with or without catalyst [4, 30]. Although biocrude is not outright produced as a drop-in transportation fuel, its energy content is comparable to petroleum [31]

and thus suitable to be upgraded and co-refined in any existing fossil fuel refinery. A critical substance in any HTL reactions is water. Water acts not only as a solvent but also as a catalyst at elevated temperatures and pressures because at such conditions water is highly reactive and nonpolar with high miscibility with organics [12]. Water at supercritical conditions is ideal for hydrolytic reactions due to changes in its dielectric properties which enable it to solubilize recalcitrant components of biomass such as lignin [32, 33]. HTL is suitable to processing microalgae and aquatic biomass in that the process employs wet microalgae (with the cultivation culture), thereby efficiently converting the feedstock to biofuel fractions. Without water removal and drying operation, HTL consumes about 50% less energy than conventional biodiesel production (i.e., lipid extraction followed by transesterification of lipids) which demands essentially dry microalgae feedstock (~ 90 wt%) [7]. Drying step alone accounts to 20–30% of the total process cost [20]. Because HTL utilizes the entire microalgae (lipids + microalgae residue), lipid content in microalgae is not a limiting factor [11, 34]. A generalized process flow in catalytic microalgae HTL is shown in Fig. 2.

The interest in HTL conversion technology has significantly increased over the last decade demonstrated by studies focusing on temperature variations [36], reaction times (5–120 min) [36–38], strain types (*Botryococcus braunii*, *Spirulina platensis*, *Chlorella vulgaris*, *Nannochloropsis* sp., or *Desmodesmus* sp., *among others*) [36–40] or catalyst types (homogeneous, heterogeneous) with yield around 50–60 wt% biocrude [31, 39, 41]. Most of these investigations employed high-lipid microalgae [37], although some studies suggested that low-lipid but high-growth rate microalgae are applicable [36]. As indicated above, the conventional biofuel production approach of subjecting microalgae to thermal drying, solvent extraction, and transesterification to generate biodiesel is extremely costly, exacerbated by the use of organic solvents with adverse effects to humans and the environment. Moreover, the approach exploits high-lipid (20–50 wt%) microalgae with low productivity that produces substantial amount of microalgae residue [11]. Unless disposition to the residue is applied (e.g., anaerobic digestion, combustion, fertilizer), the approach is untenable from an environmental and economic standpoint. In order to be economically feasible, revenues from all product and co-product streams must be optimized. Among all microalgae conversion technologies, it appears that HTL has the potential to maximize profit since it processes the entire microalgae (lipids
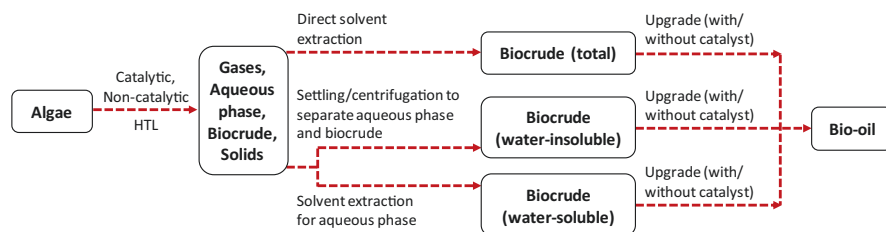
Fig. 2 Generalized process flow in the catalytic HTL of microalgae (modified and adapted with permission from [35])
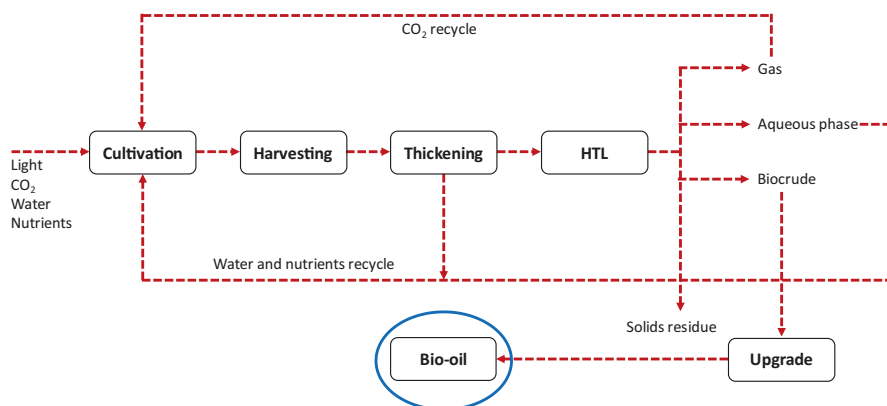
Fig. 3 Microalgae biorefinery scheme using HTL with upgrade (modified and adapted with permission from [36])

+ microalgae residue) to generate a singular product stream (bio-oil). HTL is a promising microalgae biofuel production method because it (1) operates at relatively medium temperatures (200–400 °C), (2) requires lower energy compared to other thermochemical conversion techniques, and (3) delivers product with high value. Unlike the transesterification route, the dewatering process in HTL consumes only 12% of the total energy demand [42]. A holistic microalgae biorefinery scheme utilizing HTL is presented in Fig. 3. It consists of five major steps: cultivation, harvesting, thickening, HTL, and upgrade.

Microalgae cultivation is accomplished through an open pond reactor (OPS) or a closed photobioreactor (PBR) [7, 43, 44]. Axenic cultures are grown in a PBR to prevent contamination. In most microalgal culture, sterility is not a requirement, and therefore OPS is preferred operating at a much lower cost. The microalgae grown in an OPS are harvested and concentrated (thickening) to a desired loading rate via recycling water and nutrients back to the OPS. In the case of PBR, recycling of the extracted water from thickening is typically not done to avoid system contamination [7]. Thickening has three steps: autoflocculation, sedimentation, and centrifugation/filtration [2, 7]. Microalgae can enter the HTL step as either a whole biomass or a microalgae residue if valuable co-products such as lipids or proteins are extracted post-thickening. Co-product extraction is achieved by mechanical disruption, pulse electric field (PEF), ultrasound, or a combination of either of the three. Whether whole biomass or microalgae residue, HTL converts the feedstock into gaseous phase, aqueous phase, biocrude, and solid residue. The gas, predominantly CO_2, is recycled back to the OPS or PBR as organic carbon source to growing culture. A combination of protein (high-value co-product) extraction and HTL boosts the microalgae refinery's sustainability due to (1) maximizing utilization potential by recycling a significant portion of the nitrogen-rich aqueous phase and (2) lowering nitrogen content of the biocrude [36]. However, adding an extra protein

extraction step reduces the overall bio-oil yield, and trade-off must be evaluated. The biocrude undergoes upgrade to produce bio-oil. Catalytic upgrade of biocrude oil is discussed in Sect. 8.

3   Mass, Energy, and Nutrient Balance in Microalgae HTL

Regardless of microalgae species, the mass balance of the HTL process share similar trends; that is, the main fractions are (1) biocrude (bio-oil if upgraded), (2) organics in the aqueous phase, (3) solid residues, and (4) gaseous phase, typically lower in concentrations. High-value chemical co-products may be delivered. Biocrude, solid residues, and the gaseous phase are measured gravimetrically, while the aqueous phase is determined by calculating the mass difference from the input feedstock. Inadvertent overestimation of the organics in the water is commonly achieved by incorporating the losses in the system.

Energy balance in HTL is presented in terms of two energy ratios: (1) energy recovery (ER) and (2) energy consumption (EC). ER ratio is loosely defined as the ratio of the energy embodies in main product, in this case biocrude, to the total input energy required in HTL (E_{in}/E_{out}) [36, 45, 46]. However, there are discrepancies among researchers in calculating ER [47, 48]. Across various energy platforms, EC calculations give rise to substantially different values making reporting ambiguous. Some researchers strictly include biocrude bioenergy as E_{in}, while some include co-product energy in the form of bioelectricity and, to a lesser extent, the gaseous phase energy. The ambiguity is easily resolved by employing energy return on investment (EROI), which explicitly includes all energy products in the numerator and all energy consumption in the denominator without premature crediting of co-products [39, 48]. In terms of EC ratio, researchers are uniform in defining it as the ratio of the HTL energy demand versus the energy embodied in the biocrude [39, 45, 49]. Comparatively, the heating value of a typical microalgae is around 20 MJ/kg [50], while biocrude has a value of 43 MJ/kg [38, 51]. It was reported by Brown et al. that the heating value of the gaseous phase is 4 MJ/kg [38] from the HTL of *Nannochloropsis* sp. for 60 min at 350 °C. In perspective, the average lower heating value for methane is 50 MJ/kg, for propane 46.4 MJ/kg, and for butane 45 MJ/kg [52], implying that the gaseous phase contains low fraction of these gases. Below is a typical mass and atomic balance (dry basis, mass fraction) of *Spirulina platensis* undergoing HTL for 60 min at 350 °C [45] (Fig. 4).

A significant portion of nutrients is recovered in the aqueous medium coming out of HTL which is subsequently recovered as nutrient-rich culture medium during microalgae cultivation. Specifically, around 40–75% of N in aqueous phase is recovered [36, 45]. HTL utilizes various catalysts which affect the percent nitrogen recovered. In combination, both lipid yield and nutrients recycle are optimized to render HTL economically viable method in converting microalgae to biofuel. Integrated microalgal cultivation, HTL, and nutrient recycling are tenable approaches from an energy and mass balance approach [31, 53, 54].
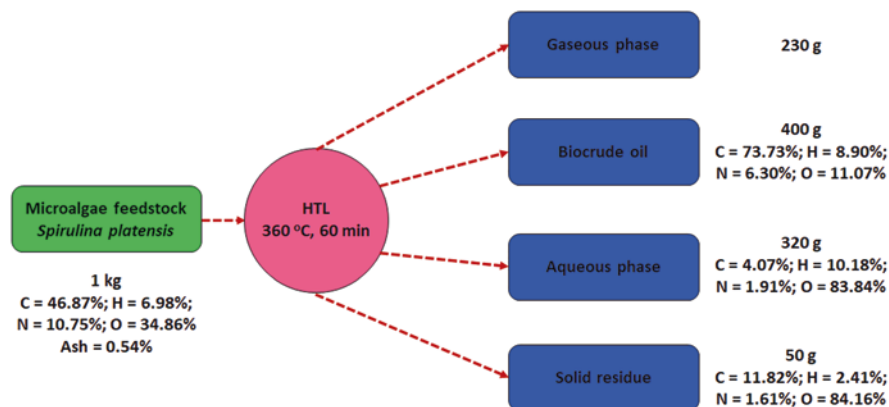
Fig. 4 Mass and atomic balance (dry basis) in the HTL of *Spirulina platensis*, bio-oil (biocrude oil), and solid residue (modified and adapted with permission from [40])

4 Role of Media in Microalgae HTL

Water plays a critical role in HTL. At normal temperature, water is a polar liquid and does not react with organic compounds. Elevated temperature (superheated water) leads to the breaking of strong hydrogen bonds which makes water less polar and behave more like an organic solvent and, consequently, highly reactive and miscible with organic components. Under these conditions, the dielectric constant (relative permittivity), ε_r, of water decreases substantially. For example, dielectric constant reduces from 78.85 to 19.66 with a temperature increase from 25 °C to 300 °C. Secondly, an increase in temperature increases the self-ionization (dissociation) of water. Water dissociates into hydronium ion ($H3O^+$) and hydroxide ions (OH^-) as a reversible reaction. The ionic product of water (K_W), written as molar concentrations of the ionic products of water, increases considerably (1×10^{-14} to 1×10^{-12}) with an increase in temperature from normal to subcritical range:

$$K_W = \left[H3O^+\right]\left[OH^-\right] \tag{1}$$

With the increase in the dissociation constant, water acts as a catalyst and accelerates the rate of both acid- and base-catalyzed reactions. These two factors make water, at an elevated temperature, a good solvent for nonpolar hydrophobic hydrocarbons and lead to fast and efficient reactions. The phase diagram of water depicting the dominant reaction in each region is shown in (Fig. 5).
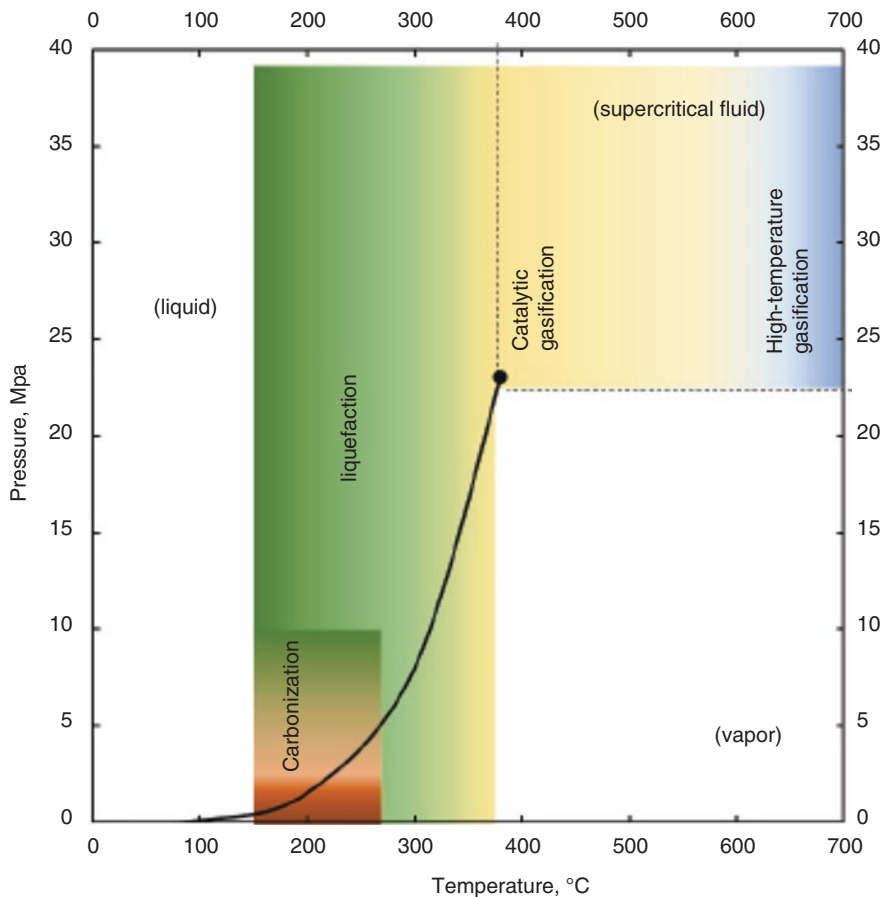
Fig. 5 Hydrothermal processing regimes superimposed with the phase diagram of water. To the left of the triple point are liquefaction and carbonization. To the upper right of the triple point are catalytic gasification and high-temperature gasification, both within the supercritical region (printed with permission from [17])

5 Chemistry of HTL

Subcritical water acts as a hot pressurized liquid solvent in HTL. Subcritical water is maintained at a pressure where the operating temperature becomes higher than its boiling point of 100 °C up to its critical point of 374 °C (i.e., similar to superheated water in a pressure cooker). At subcritical condition, the solubility of hydrophobic organic compounds in water is improved due to water's low permittivity (78 F m^{-1} (25 °C, 0.1 MPa) to 14.07 F m^{-1} (350 °C, 20 MPa)) [18]. Thus, hydrolysis is promoted yielding higher concentrations of H$^+$ and OH$^-$ ions (greater water ion product) than those in water at STP. Conversely, supercritical water is ideal for gasification where radical reactions are pronounced. HTL is affected by temperature, reaction

time, catalyst amount, and microalgae's ash content, although the extent to which each of these factors affects HTL mechanism has not been fully understood. Microalgae subjected to hot compressed liquid water near its critical point (374 °C, 22.1 MPa) is subjected to two competing reactions: *hydrolysis* (depolymerization or decomposition) into smaller units that are highly reactive and *repolymerization* of the units to form bio-oil, gas, aqueous phase, and solid residue [25, 38, 55]. Varying the process condition such as increasing reaction time or temperature may lead to increase in solid fraction yield and a decrease in the biocrude oil yield [56–58]. Increasing the reaction time decreases the viscosity of the biocrude oil which in turn lowers its concentration in the liquid phase [49].

A 2011 study compared the individual HTL characteristics of the three components of microalgae (lipids, proteins, and carbohydrates) with the HTL characteristics of various microalgae strains [39]. The study proposed that the biocrude oil conversion yield for the HTL of any microalgal strain is 55–80 w/w% in lipids, 11–18 w/w% in proteins, and 6–15 w/w% in carbohydrates, all of which are much lower compared to experiments performed by authors who utilized microalgae with very low lipid content [59, 60]. Another study [61] showed that at reaction temperatures below 250 °C, HTL of lipids and algaenans significantly contributes to the composition of the resulting biocrude. Conversely, at reaction temperatures between 300 and 375 °C, HTL of proteins and carbohydrates produces the majority of the components in the biocrude, with an elevated level of nitrogen due to the decomposition of amines in proteins.

A generalized equation was empirically developed by Biller and Ross [39] to estimate the percent biocrude oil yield (w/w) from the HTL of *Nannochloropsis oculata* and *Chlorella vulgaris* with known data on lipid, protein, and carbohydrate contents and yields via Eq. (2). However, the equation cannot be applied to other microalgal strain because microalgal components in other strains do not behave independently during HTL and cannot be linearly added to produce a single biocrude oil yield value. Instead, their interactions are characterized via cross-linking mechanisms [61]:

$$Bio\,Y = (Lip\,C)(Lip\,Y) + (Pro\,C)(Pro\,Y) + (Car\,C)(Car\,Y) \qquad (2)$$

where

Bio Y = Biocrude oil yield (w/w %)
Lip C = Lipid content (w/w %)
Lip Y = Lipid yield (w/w %)
Pro C = Protein content (w/w %)
Pro Y = Protein yield (w/w %)
Car C = Carbohydrate content (w/w %)
Car Y = Carbohydrate yield (w/w %)

5.1 Microalgae Components

Lipids. Lipids are nonpolar compounds that are hydrophobic, usually occurring in the form of triglycerides (TAGs), an aliphatic compound consisting of a glycerol backbone attached to three fatty acids [62]. Upon hydrolysis, TAGs easily decompose to produce 1 mole of glycerol (by-product) and 3 moles of free fatty acids (FFAs) (main product) in hot compressed water without catalyst [18]. The glycerol produced is then converted via HTL into methanol, acetaldehyde, propionaldehyde, acrolein, allyl alcohol, ethanol, formaldehyde, and gas products (CO, CO_2, and H_2) [62, 63]. The FFAs can be converted into long-chain hydrocarbons although they are thermally stable [14]. At ambient temperature, lipids are typically insoluble in solvents, but as temperature increases, they become more polar and soluble. The solubility of lipids in water is enhanced if the water's dielectric constant is within subcritical conditions (e.g., 350 °C, 20 MPa) [17]. The glycerol produced during HTL is a mixture of fatty acids, methanol, and salts that is soluble in water [64]. The higher the lipid content of a microalgae species, the higher the biocrude oil yield from HTL.

Proteins. Proteins consist of several monomer units of amino acids joined by peptide bonds. The majority of the nitrogen in microalgae is found in proteins. The HTL process inadvertently incorporates most of the nitrogen in proteins to the biocrude oil, therefore affecting the biocrude oil's properties. Proteins are easily hydrolyzable to produce low yields of amino acids [65] because the peptide bonds in proteins are more stable than the glycosidic bonds in glucose/starch. Amino acid yields during HTL are also low (~10%) since they can further undergo (1) *decarboxylation* to produce carbonic acid and amines and (2) *deamination* to produce ammonia and organic acids [14, 17]. The degradation products of an amino acid include CO_2, CO, CH_4, hydrogen, short-chain hydrocarbons (alkanes, alkenes), alcohols ($\leq$ C5), aldehydes, amides, and carboxylic acids [12]. These products can repolymerize to form long-chain hydrocarbons and aromatic compounds such as phenols or nitrogen heterocyclics such as indole or pyrrole [14, 49, 66, 67]. The amino acid (activation energy: 148–166 kJ/mol) decomposition is a first-order kinetic reaction described by the Arrhenius equation [68]. Amino acids degrade very quickly, usually decomposing more than 70% within 20–30 s at around 350 °C [69].

Carbohydrates. Carbohydrates are a collective term for monosaccharides, oligosaccharides, and polysaccharides. It can exist as cellulose, hemicellulose, and lignin. In the case of microalgae subjected to hydrothermal conditions, its carbohydrate content are not converted directly into biocrude oil. Rather, HTL degrades the carbohydrates into polar compounds such as organic acids (i.e., acetic, formic, lactic), aldehydes, benzenes, and alcohols [17, 18, 39]. The aldehyde and benzene fractions are then converted to long-chain hydrocarbons forming the biocrude oil [14].

Algaenans. Algaenans are recalcitrant biopolymers existing in the cell walls of green microalgae. They consist of hydrocarbons with variable lengths and alkyl-aromatics [61]. No study has been done to analyze their degradation behavior and

chemical pathways during HTL because they are resistant to hydrothermal conditions and chemical treatments [14].

5.2 Microalgae HTL Products

As presented in Fig. 4, HTL utilizes microalgae feedstock and produces a mixture of gaseous product, biocrude oil, an aqueous phase, and a solid residue. Biocrude oil has low oxygen content (10–20%) compared to the aqueous phase and solid residue [8]. It consists of a mixture of straight-chain and aromatic hydrocarbons with varying O/C and H/C ratios, depending upon the nature of the microalgae feedstock. A typical microalgae-based biocrude oil has a heating value of 35–40 MJ/kg as a result low O/C and H/C ratios, relative to raw microalgae with a heating value of 15–25 MJ/kg. Biocrude oil can be upgraded to high-quality fuels or can be directly co-fired with coal. Aviation gasoline, biojet fuel, and renewable diesel are the main products of biocrude oil upgrade. Unlike petroleum-based diesel or biodiesel obtained from transesterification of microalgae lipids, renewable diesel can be used directly in diesel-powered vehicles because it is compatible with diesel engines and their distribution infrastructure. Upgrading of HTL biocrude oil is also easily accomplished within existing petroleum refineries. The emission controls within these refineries are also capable of removing sulfur from HTL fuel products to meet stringent local, state, and federal fuel requirements (e.g., ULSD). The aqueous stream coming out of the HTL process contains large amounts of oxygen and nutrients. The chemicals in the nutrients such as nitrates, phosphates, and sulfates can be recycled back to the microalgae pond as source of nutrient during cultivation [6, 7, 38, 70]. CO_2 can be extracted from the gaseous mixture and recycled back to the microalgae pond as carbon source [7]. Similar to the aqueous phase, the solid residue (biochar) is high in oxygen and nitrogen which can be utilized as land amendment.

Biocrude Oil. Biocrude oil is a viscous liquid mixture of hydrocarbons with varying lengths. This is derived from carbohydrates, fatty acids, amino acids, and organic acids that are primary end products of the photosynthetic carbon fixation pathway (i.e., Calvin-Benson cycle). Biocrude oil from microalgae HTL has three major components: lipids (fatty acids, sterols), proteins (peptides), and insoluble fraction (algaenans, asphaltenes) [61]. It is dark and chemically similar to petroleum crude oil [46]. Its energy content is lower than petroleum fuel oil (~70–95%) [38]. The biocrude oil yield reported as mass fraction of the dry input microalgae, from the HTL at 350 °C of *Nannochloropsis* sp., is 43 ± 2 [38], while that from *Spirulina platensis* is 39.9 [40]. These values are higher than those predicted by Eq. (2): 27.7 ± 8.3 for *Nannochloropsis* sp. and 18.0 ± 6.4 for *Spirulina platensis* [14]. Other studies investigated the effects of homogenous catalyst on biocrude oil yield from microalgae under hydrothermal conditions [57, 71, 72]. Results ranged from 14.2 to 67 wt%. The typical elemental compositions (wt%) of biocrude oil from direct catalytic HTL of microalgae are reported as follows: 73.7–76.1% C,

8.6–11.1% H, 8.3–11.1% O, and 3.9–6.3% N with a higher heating value of 34.5 to 40.1 MJ/kg [14, 36]. The N content leads to the formation of NO_x emission during combustion. Although sulfur content is below detection limit, it ranges between 0.5 and 1% [38, 45]. Microalgal biocrude consists of cyclic N and O compounds (e.g., pyrrolidinedione, piperidinedione), cyclic oxygenates (e.g., phenol), and cyclic nitrogenates (e.g., pyrimidine, pyrazine) derived from protein derivatives (peptides and/or cyclic peptides) and carbohydrates [38, 39, 73].

Aqueous Phase. The aqueous phase is an organic-rich HTL fraction consisting mainly of phosphate, ammonium, acetate, K^+, Na^+, and Mg^{2+} [31, 72]. This phase can be recycled and fed into the growth culture medium because of its high nitrogen content [53, 74]. Because this aqueous phase is rich in organics, recycling it supplies the necessary carbon source needed by certain heterotrophic microalgae strains. Alternatively, this phase can also be gasified at supercritical conditions (i.e., >647.1 K, >22.1 MPa), in combination with the solid residue to generate a hydrogen-rich and methane-rich fuel gas (syngas). In a 2018 study, a modeling platform was developed for the combined gasification of three species of microalgae (*Nannochloropsis oculate*, *Fucus serratus*, and *Scenedesmus almeriensis*) combined with tar [75]. The model handled variations in O_2 which improved performance and efficiency, utilized steam that produced hydrogen, and employed CO_2 absorber that recycled carbon and generated high-quality syngas. Microalgae's protein and carbohydrate fraction contributed to the production of H_2, while the fatty acid component led to the production of CH_4 [76].

Solid Residue. The solid outcome in microalgae HTL is an oxygen-rich residue with high ash content but exceedingly small percent of hydrogen, nitrogen, and sulfur. It is also known as char which can be used as fertilizer/soil amendment due to its nutrient load or as catalyst. Figure 4 revealed that solid residue yield is about 5 wt% of the total *Spirulina platensis* feedstock with the following elemental composition: 11.82% C, 2.41% H, 1.61% N, 84.16% O, and 0.61% S [40]. Investigations from other studies reported yields below 10% [25, 49, 72]. Char serves as feedstock for other thermochemical process such as gasification and carbonization (both pyrolytic and hydrothermal) and combustion.

Gaseous Phase. The gaseous phase consists of CO_2, CH_4, H_2, CO, and C_2 and represents approximately 20% of microalgae feedstock [36, 45, 38]. Gaseous products increased by 20% accompanied by a decrease in biocrude oil yield if reaction temperature is increased from 350 °C to 380 °C [38]. CO_2 and H_2 (662 mmol/mol and 297 mmol/mol, respectively) are the main components of the gaseous phase, and CH_4, N_2, C_2H_4, and C_2H_6 are the minor components [38]. Changing the residence time from 60 to 120 min increased the gaseous phase by 48% [40]. CO occurs at very low concentration because [75] it is a highly reactive and unstable radical that easily forms CO_2 via the water-gas shift reaction ([4, 77] oxygen removal is achieved via decarboxylation (i.e., removes carboxyl group and releases CO_2) and not decarbonylation (releases CO) [36]. CO_2 can be recycled into the growth medium as an inorganic carbon source for the microalgae, while H_2 can be used in the upgrade of the generated biocrude oil.

5.3 Reaction Pathways

The production of biocrude oil from the hydrothermal liquefaction of microalgae biomass has been recently touted as an attractive route to utilizing microalgae's embodied energy into a more effective energy carrier with low coke formation [78, 79]. HTL's chemistry and process conditions (200–380 °C) [80, 81] allow the recycle elements such as O and N into the aqueous and gaseous product streams while extracting C and H from the hydrocarbons embedded in the microalgae biomass [82]. The process is initialized by hydrolyzing lipids, proteins, and carbohydrates into smaller, unstable, and reactive molecules [35]. The decomposition and depolymerization typically occur for a noticeably short period of time, while the repolymerization to produce biocrude oil takes much longer [59]. Water plays an essential role in cleaving the macromolecule bonds and permits the adequate separation of the biocrude oil from other phases after HTL reaction.

HTL of microalgae involves three subsequent phases. The first phase is the hydrolysis of the major components (lipids, proteins, carbohydrates) into their building blocks (monomers). Hydrolysis results into lipids turning into 1 mole of glycerol and 3 moles of fatty acids, proteins into different amino acids or peptides, and carbohydrates into monosaccharides or polysaccharides (reducing and nonreducing sugars). The second phase is the parallel reaction of the monomers which includes dehydration and cracking. Finally, the third phase is the cross-reaction of the intermediate products such as Maillard reaction between amino acids and reducing sugars, decarboxylation of fatty acids, and decarboxylation of amino acids [83, 84]. Lipids generate straight-chain and cyclic hydrocarbons (hydroxyl and carboxyl groups), while proteins and carbohydrates produce heteroatoms [84]. These heteroatoms are N- and O-containing compounds [61, 85–88].

A typical reaction network for microalgae HTL is as follows: Glycerol from lipids is converted into *acrolein* and *1,3-dioxan-5-ol*. The fatty acids, on the other hand, are converted into *alkanes* and *alkenes* via decarboxylation and into *fatty acid amides* if reacted with NH_3 [87, 89]. The amino acids from proteins can undergo three routes: (1) decarboxylation to form ketones and amines, which in turn can be converted into *alkanes*; (2) deamination to form ammonia and organic acids, which in turn can be converted into *alkanes*; and (3) nucleophilic reaction to form *cyclic amines* [61, 62]. The sugars from carbohydrates are converted *into 5-hydroxymethylfural*, *lactic acid*, *acetic acid*, *formic acid*, and *pyruvaldehyde.* These intermediates can then react with an amide to form amides [10]. A reducing sugar can also undergo dimerization or Maillard reaction with NH_3 to form a slew of N- and O-containing compounds such as *pyrazine*, *cyclic oxygenates*, *indole*, *quinoline*, *pyrazine derivatives*, and *phenol derivatives* [90, 91].

In general, the formation of biocrude oil via HTL from microalgae primarily involves deoxygenation and denitrogenation [82], with deoxygenation occurring via decarboxylation and dehydration [92]. Biocrude oil has abundant hydrocarbons, phenols, free fatty acids, and N- and O-containing heteroatoms [38, 39]. Upgrading the biocrude oil improves its C/H ratio, HHV, viscosity, and alkane fraction.

Hydrogenation. Hydrogenation is a chemical reaction between molecular hydrogen (H_2) and an unsaturated hydrocarbon (e.g., alkene) in the presence of Ni, Pd, or Pt catalyst to saturate (remove double bond) the hydrocarbon. The 3 moles of fatty acids derived from the hydrolysis of lipids consist of unsaturated C-O double bonds. These double bonds and other C-C double bonds and double bonds in aromatic compounds can react with hydrogen to transform these compounds into saturated hydrocarbons or saturated aromatics via catalytic hydrogenation. Metal catalysts such as Ni, Ru, Pt, and Pd can be used. Hydrogenation enhances the quality of the biocrude oil by removing the heteroatoms. One example is the hydrogenation of phenol in the presence of Ni catalyst to cyclohexenol (1-, 2-, or 3-cyclohexenol) and the subsequent hydrogenation to cyclohexanol [93]. Another example is the conversion of five-member rings with one heteroatom from unsaturated to saturated: (1) oxygen with H_2 and Raney nickel, oxole (furan) → oxacyclopentane (tetrahydrofuran); (2) sulfur with H_2 and Pd/C, thiol (thiophene) → thiacyclopentane (tetrahydrothiophene); and (3) nitrogen with H_2 and Pt, azole (pyrrole) → azacyclopentane (pyrrolidine) [29, 93, 94].

Hydrogenation is initialized when H_2 is cleaved and absorbed on the surface of the catalyst. Alkene (e.g., C-H) is then absorbed to the catalyst surface via the weak π bonds. A hydrogen atom is transferred to the alkene, forming a C-H bond. A second hydrogen atom is transferred to the alkene, forming a second C-H bond. The two hydrogens are finally added to the same face of the double bond (syn addition) to produce saturated alkane.

Deoxygenation. The produced biocrude oil has high viscosity and low energy content due to its high oxygen content of about 6–15 wt% [72, 95]. Improvement of biocrude oil quality entails upgrading or the removal of oxygen to produce CO_2, H_2O, and CO via catalytic deoxygenation. Deoxygenation types are (1) generation of CO_2 and R-H from the decomposition of carboxylic acid (decarboxylation), (2) generation of H_2O and R-H from the reaction of ketone with H_2 (hydrodeoxygenation), and (3) generation of H_2O and ester from the reaction of carboxylic acid and alcohol (dehydration). The conversion of phenol to cyclohexane is a *hydrodeoxygenation* process with the following steps: *hydrogenation* of phenol using Pd catalyst, *dehydration* of cyclohexanol using acid catalyst, and *hydrogenation* of cyclohexene using Pd catalyst [82]. The hydrodeoxygenation of phenol is accomplished using other metal catalysts such as Ni/ZrO2, Ru/C, Ni/Al$_2$O$_3$, Pd/C, and Pt/C [93]. Ni-supported catalyst is found to be more effective than metal-supported catalyst in the hydrodeoxygenation of phenol because Ni catalyst requires metal oxides which facilitate dissociation of the O-H bond [93]. The choice of a suitable catalyst ensures the success of hydrodeoxygenation of complex aromatic compounds. For instance, the hydrogenation of methoxyphenol is actively mediated by the sulfide form of cobalt-molybdenum, nickel-molybdenum, and nickel-tungsten [96].

Decarboxylation. Decarboxylation is a type of catalytic deoxygenation that removes CO_2 from the carboxyl group and produces straight-chain hydrocarbons (alkanes, alkenes). It improves biocrude quality by increasing the hydrocarbon content of HTL-produced biocrude oil in the presence or absence of a catalyst. A study

by Biller et al. validated that the decarboxylation of fatty acids to form alkanes is achieved in the presence of Na_2CO_3 [39]. The upgraded biocrude oil is found to contain higher straight-chain alkanes, higher HHV, lower fraction of high boilers, and lower oxygen relative to crude bio-oil. The catalysts Pd/C, Pt/C, Pt/Al$_2$O$_3$, Raney-Ni, and HZSM-5 are also beneficial in upgrading biocrude from direct catalytic HTL because they enhance alkane fractions and lower fatty acid content resulting in a better quality biocrude [41, 83, 97–99]. Alkali catalysts (NaOH, KOH) are appropriate in the monomolecular decarboxylation of stearic acid, while metal oxide catalysts (CeO_2, Y_2O_3, ZrO_2) are suitable for the bimolecular decarboxylation of stearic acid [100].

Denitrogenation. After HTL, the N from the microalgae biomass is partitioned in the biocrude oil as N-containing compounds, in the aqueous phase as HCN and NH_3, and in the solid phase [72, 82]. N-containing compounds can be heterocyclic (ring compounds with at least two different elements in its ring) such as pyrazine, cyclic oxygenates, indole, quinoline, and pyrrole or non-heterocyclic such as aliphatic amines (straight-chain amines), aniline (amino group with phenyl group attachment), and nitrile ($C \equiv N^-$). Heterocyclic compounds and the phenyl group for aniline need to be saturated (i.e., removal of double bonds) before the C-N bond is destroyed. Typical denitrogenation reaction requires the addition of H_2 via catalytic hydrodenitrogenation. As an example, the mechanism of pyridine hydrodenitrogenation was proposed by Duan and Savage under hydrothermal conditions using Pt/γ-Al$_2$O$_3$ as the most effective catalyst [101]. The study presented four sequential steps to (1) removal of double bonds in the cyclic ring (saturation) by addition of H to form piperidine, (2) cleavage of C-N bond by addition of H to form pentylamine, (3) hydrolysis by addition of H_2O to form n-pentanol and NH_3, and (4) dehydration by removal of H_2O and hydrogenation by addition of H_2 to form n-pentane.

Desulfurization. The amino acid composition of microalgae determines the S-containing heteroatoms in the biocrude oil, at about <1 wt% [8, 14, 102]. In reference, ULSD has a maximum diesel content of 15 ppm (0.0015 wt%) since 2006 [103]. Sulfur is significantly reduced during microalgae HTL and biocrude oil upgrading to prevent the formation of So$_x$ during fuel use. It has been determined that Ni/SiO$_2$-Al$_2$O$_3$ catalyst promotes more efficient removal of S in the biocrude oil below the detection limit than Ru/C or CoMo/Al$_2$O$_3$ catalysts [95]. Although there are limited studies in literature regarding the desulfurization of microalgae HTL and biocrude oil upgrading, the mechanism of S removal has been investigated in petroleum biocrude. The catalytic dehydrogenation of petroleum biocrude significantly removes S-containing compounds such as mercaptans and disulfides and to a lesser degree thiols (thiophenes) with benzene ring(s) (benzothiophenes or dibenzothiophenes) [104, 105]. The body of research on the desulfurization of microalgae HTL and biocrude oil upgrading focuses on the effects heterogeneous catalysts such as Pt/C and Pd/C on catalytic activity and regeneration. Nevertheless, further research is warranted in developing catalysts which effectively removes S while maintaining high-quality and high-yield biocrude oil.

Table 1 Summary of non-catalytic hydrothermal liquefaction (HTL) of microalgae

Biomass type	Temp (°C)	Press (MPa)	Time (min)	Key findings	Ref
Nannochloropsis sp. *Scenedesmus*, *Spirulina*	200–500 300	– 10–12	60 30	Maximum biocrude oil yield was 43 wt% achieved at 350 °C and 60 min. The HHV of oil was 39 MJ/kg Optimum biocrude oil yield was 24–45 wt% with 35–57 MJ/kg HHV of oil	Brown et al. [38] Vardon et al. [8]
Dunaliella tertiolecta Chlorella pyrenoidosa Microcystis viridis	300–380 280 300–340	5–30 – –	10–100 120 30–60	Maximum biocrude oil yield was 36.9 wt% achieved at 360 °C, 30 min, and 10 wt% algae feed. The HHV of oil was 26.62 MJ/kg Maximum biocrude oil yield was 39 wt% Optimum biocrude oil yield was 33–40 wt%	Zou et al. [59] Yu et al. [99] Yang et al. [25]

6 Non-catalytic Microalgae HTL

Wet microalgal biomass can undergo HTL with or without catalyst. Catalyst improves biocrude oil yield, but without it, yield is highly dependent on temperature and algae strain species [106]. An investigation on the marine microalgae *Nannochloropsis* sp. revealed that the optimum biocrude oil (HHV oil = 39 MJ/kg) yield of 43 wt% was achieved at 350 °C and 60 min [38]. In a study by [8], *Scenedesmus* and *Spirulina* species subjected on HTL at 300 °C, 10–12 MPa, and 30 min generated 24–45 wt% biocrude oil having 35–57 MJ/kg HHV [8]. The maximum biocrude oil yield for the HTL of *Dunaliella tertiolecta* (HHV oil = 26.62 MJ/kg) performed at 360 °C, 30 min, and 10 wt% solid feedstock concentration was 36.9 wt% [59]. HTL of *Chlorella pyrenoidosa* at 280 °C and 120 min reaction time yield 39 wt% biocrude oil [99], and HTL of *Microcystis viridis* at 300–340 °C and 30–60 min reaction time yield 33–40 wt% biocrude oil [25]. Still, caution must be exercised in subjecting these microalgal species to extremely high temperatures because such conditions minimize yield through recondensation reaction which leads to coke formation [107]. Ideally, non-catalytic HTL of microalgae must be carried out below the critical point of water (374 °C, 22 MPa) since within this regime the high ionic constant and low dielectric constant of water brought about by its weak hydrogen bond effectively hydrolyze microalgae's organic components [32, 108]. With the hydrolysis of lipids, proteins, and carbohydrates in hot compressed water, biocrude oil yield is increased [106, 109]. Table 1 summarizes the various reaction conditions in the non-catalytic HTL of microalgae.

7 Catalytic Microalgae HTL and Valorization

Catalysts are used in the HTL of microalgae to enhance biocrude oil yield, to increase rates of reactions, and to minimize the production of the solid phase (char). Catalysts can either be homogenous (water-soluble) or heterogeneous

(non-water-soluble). The role of catalysts is to facilitate the degradation of the biomass into biocrude oil at hydrothermal conditions or to upgrade biocrude oil into fuel grade with appropriate hydrocarbon composition. Homogeneous catalysts such as salts of Na and K have been extensively investigated in the HTL of microalgae [41, 56, 57]. Na and K salts promote the formation of CO_2 and H_2 by hastening the water gas shift reaction. These salts also increase the HHV of biocrude oil [18]. These catalysts maintain water in the biomass, thereby promoting decarboxylation (deoxygenation via the removal of CO_2). However, evidence suggests that homogeneous catalysts increase the oxygen content of biocrude oil [72]. In contrast, heterogeneous catalysts are used in the valorization or upgrade of biocrude oil. They inadvertently reduce biocrude oil yield due to increased gas phase formation, and there are also challenges associated with intra-particle diffusion limitations, fouling, and sintering [12]. Despite this, a research confirmed that a slight increase in biocrude oil yield and a pronounced gain in HHV were realized when a heterogeneous catalyst was employed [31].

Catalytic microalgae HTL uses water as solvent. Water below the critical point (i.e., subcritical water or hot compressed water) makes the hydrophobic organic components of the microalgae more soluble and the presence of ions conducive for intermediate reactions necessary in the production of biocrude [56]. Water above the critical point (i.e., supercritical water (SCW)), on the contrary, promotes the production of radical species and gaseous hydrocarbons (CH_4, C2–C4 gases).

Regardless of the type of catalyst or solvent, HTL involves the degradation of the macrocomponents of microalgae, the rate of which depends on the species/strain [110]. Specifically, lipids degrade into fatty acids and glycerol, while carbohydrates depolymerize into aldehydes and ketones [32, 111]. The fatty acids produced from lipids are further decarboxylated to form corresponding straight-chain hydrocarbons (alkanes, alkenes), depending on the R-structure. Proteins are hydrolyzed at hydrothermal conditions to produce amino acid monomers which are further converted into N-containing compounds such as amines, ammonia, etc. The algaenan component of microalgae can be converted into alkanes, a potential "drop-in" fuel in replacement for gasoline, diesel, and jet fuel [17, 61]. The mechanisms of these reactions are yet to be fully understood, although catalysts' role has been regarded by studies to promote or deter the intermediate reactions of depolymerization [61, 112]. Thus, the actual composition of biocrude oil is dependent not only on microalgal species/strain but also on catalyst's activity.

7.1 Homogeneous Catalysis

Homogeneous catalysts are catalysts that are soluble at room temperature in the solvent medium used in the reaction system. They were first developed for use in the HTL of algae biomass and are almost exclusively used for that purpose. They exist in the form of organic acids (e.g., CH_3COOH, $HCOOH$), their organic salts (e.g., CH_3COONa, $HCOONa$), alkali salts (e.g., Na_2CO_3, KOH), and cations of transition elements (e.g., Co^{3+}, Zn^{2+}). Homogeneous catalysts aid in breaking the C-C bond in

the biomass to facilitate hydrolysis and dehydration to produce hydrocarbons, N-containing compounds, oxygenates, gases, and solids. They improve biocrude oil yield and reduce char production. However, homogeneous catalysts do not easily facilitate the generation of "drop-in" fuels or the use of homogenous catalysts during the upgrading of biocrude oil from the liquefaction of microalgae and tend to produce hydrocarbons unfit for fuel use (i.e., gasoline, jet fuel, diesel) [58, 61, 98].

Na_2CO_3, $Ca_3(PO_4)_2$, and NiO were studied by Jena et al. in the HTL of *Spirulina platensis* and upgrading of its associated biocrude oil [44]. HTL conditions were 300–350 °C and 25 wt% algae concentration. Na_2CO_3 produced the highest yield of biocrude oil at 59 wt%, compared to the other two catalysts which lowered yield. Na_2CO_3 is the most widely used homogeneous catalyst, as confirmed in this study and many other studies [25, 61, 72, 73, 113, 114]. Na_2CO_3 as a catalyst has numerous advantages. First, it increases the biocrude oil's C5 to C18 hydrocarbons by 45 wt% as well as stimulates benzene, toluene, ethylbenzene, and xylene production [115]. Second, its effectiveness is due to its high reactivity in the formation of CH_3COONa, an organic salt instrumental in decarbonylation, dehydration, and hydroxylation reactions [78]. Third, it increases HHV and H and C contents of the biocrude oil while it simultaneously lowers the oil's O, N, and S contents [19, 116–118]. However, it also has negative effects. First, it is sensitive to loading amount which directly raises solution pH and cost associated with recovery and reuse [119]. Second, the use of Na_2CO_3 saponifies the lipids and forms sodium aliphatate, a solid residue [19, 117, 120]. Third, it reacts with the organic acids produced via decarboxylation [19]. Thus, Na_2CO_3 lowers organic acid concentration and increases CO_2 fraction in the gas phase.

Alkali catalysts in general are sensitive to temperature. For example, using Na_2CO_3 at 240 °C results in effective depolymerization of proteins to N- and O-containing heteroatoms than using Na_2CO_3 at 280 °C [120]. In a similar manner, Na_2CO_3 produces higher biocrude oil yields at 300 °C than at 350 °C [77]. Alkali catalysts such as KOH facilitates the production of additional 5–10 wt% biocrude oil compared to the non-catalytic reaction, as exhibited in an HTL experiment using *Cyanidioschyzon merolae* at 180–300 °C for 30 min with 10 wt% loading [121]. One of the drawbacks in using alkali catalysts is they have limited effect to intermediate reactions necessary to generate fuels with high content of hydrocarbons. These reactions include isomerization, decarboxylation of organic acids, and aromatization [78]. They are also nonrecyclable, and their disposal at the end of the liquefaction process contribute to environmental pollution.

Organic acids such as CH_3COOH and HCOOH are homogeneous catalysts responsible in the increase of gas fraction and decrease in biocrude oil viscosity. CH_3COOH and HCOOH raise the gas fraction of the HTL process by 16–22 wt% and 30 wt%, respectively [72]. Interestingly, the S content of biocrude oil is doubled by using organic acid catalysts compared to alkali catalysts [72]. Comparatively, catalytic activity of homogeneous catalysts as a function of biocrude oil yield is Na_2CO_3 > CH_3COOH > KOH > HCOOH [72]. Collectively, homogeneous catalysts still do not gain industrial acceptance as catalyst of choice in mediating HTL microalgae reactions despite their apparent benefits. The reasons stemmed from their

chemical properties. First, carbonate-, hydroxide-, and carboxylic acid-based catalysts have low effectiveness in catalyzing fatty acid decarboxylation, isomerization, and aromatization [78]. These reactions improve biocrude oil yield. Second, they inhibit denitrogenation, deoxygenation, and desulfurization [78]. These reactions improve biocrude oil quality. Third, they are consumed in the reaction and are difficult to recycle [60]. Fourth, they advance corrosion of tanks and equipment by increasing the pH of the HTL reaction [122]. Insomuch as all these disadvantages are concerned, scientists direct their research efforts to heterogeneous catalysts.

7.2 Heterogeneous Catalysis

To overcome the negative consequences of homogenous catalyst-mediated HTL of microalgae biomass, heterogeneous catalysts are widely adopted. They are primarily employed in the valorization or upgrading of biocrude oil. They are solid and insoluble in the reaction medium [81, 123, 124], have high recyclability after several uses [24, 68], have low corrosion rate [10, 113, 115], and have high catalytic activity. Heterogeneous catalysts elicit intermediate reactions [13, 109] through subsequent adsorption-desorption of reactants into their surface. Extensively researched heterogeneous catalysts include metals (e.g., Ru, Pd, Pt, Ni) supported on Al_2O_3, activated carbon, or zeolite, metal oxides, and molecular sieves [35]. Heterogeneous catalysts come in many forms such as oxides (SiO_2 and Al_2O_3), zeolites, and metals supported by C (e.g., Pd/C and Pt/C). Of primary interest to researchers are their catalytic activity and their effects on the biocrude oil products including gaseous phase, aqueous phase, and solid residue.

   In a review by Xu and colleagues [35], these following findings are highlighted about heterogeneous catalysts. The catalytic deoxygenation performance of metal catalysts such as Ru/C, Pt/Al_2O_3, Pt/C, NiO, Ni/SiO_2-Al_2O_3, Ni-Mo/Al_2O_3, $CoMo/\gamma$-Al_2O_3, $Co/Mo/Al_2O_3$, and cesium on zeolite socony mobil-5 (Ce/HZSM-5) were excellent at 2–51 wt% (i.e., percent of microalgae components that are deoxygenized). $Co/Mo/Al_2O_3$ was found to have the highest deoxygenating efficiency. In terms of hydrogenation, Pd/C, Pt/Al_2O_3, Pt/C, NiO, Ni-Mo/Al_2O_3, and Ce/HZSM-5 demonstrated 1–52 wt%. The ability of Pt/Al_2O_3, Ni/Al_2O_3, $Co/Mo/Al_2O_3$, and Ce/HZSM-5 in increasing carbon content of the biocrude oil was demonstrated to be 9–15 wt%. Moreover, these heterogeneous catalysts were shown to increase C and H and to lower O (i.e., raise HHV): Ru/C, Pt/Al_2O_3, Pt/C, NiO, Ni-Mo/Al_2O_3, $Co/Mo/Al_2O_3$, Ce/HZSM-5, and $Ca_3(PO_4)_2$. With respect to desulfurization, Ru/C, Pd/C, Pt/C, Ni/SiO_2-Al_2O_3, $CoMo/\gamma$-Al_2O_3, and Ce/HZSM-5 showed 6–100 wt% efficiency, with Ni/SiO_2-Al_2O_3 demonstrating the highest activity with or without H_2. Meanwhile, NiO and $Ca_3(PO_4)_2$ exhibited unfavorable desulfurization activity. The removal of N (denitrogenation), on the other hand, was positively mediated by Ru/C, Pt/Al_2O_3, Pt/C, Ni/SiO_2-Al_2O_3, Ni/Al_2O_3, Ni-Mo/Al_2O_3, Ce/HZSM-5, and $Ca3(PO_4)_2$ at approximately 10 wt% efficiency. In comparison to metal catalysts, zeolite has lower catalytic efficiency with respect to biocrude oil yield and quality,

albeit cheap to produce. Notably, molecular sieve catalysts such as HZSM-5 have high catalytic cracking effects (i.e., produce more alkanes, alkenes, and ketones in biocrude oil with minimal organic acids) but quite inexpensive [26, 50, 105]. Interestingly, ideal microalgae HTL and biocrude oil upgrading conditions utilizing these heterogeneous catalysts are close to 350 °C and 60 min. Some of these recent studies are outlined herein. They discuss catalytic effects from a purely biocrude oil yield and quality standpoint.

In a study involving the upgrade of *Chlorella vulgaris* and *Nannochloropsis occulta* sp., Pt/Al_2O_3, Ni/Al_2O_3, and Co/Al_2O_3 were used as catalysts by impregnating the alumina support with the metal at 20 wt%, 6 wt%, and 20 wt%, respectively [31]. Experimental conditions included 350 °C, 1 h, and 1:9 catalyst/water ratio. Results for the *Chlorella vulgaris* showed that the use of Pt/Al_2O_3 and Co/Al_2O_3 increased biocrude oil yield by 3%, while the use of Ni/Al_2O_3 decreased biocrude oil yield by 6% from the yield without catalysts (36 wt%). In the case of *Nannochloropsis occulta* sp., all three catalysts lowered biocrude oil yield. Pt/Al_2O_3 and Co/Al_2O_3 were effective in cleaving C-C and C-O bonds, and they also reinforced the occurrence of deoxygenation of oxygenates, which were mostly generated from carbohydrates in the biomass. In another *Nannochloropsis occulta* sp. investigation, Duan and colleagues demonstrated that Pd/C and $CoMo/Al_2O_3$ raised biocrude oil yield by 22 wt% and 20 wt%, respectively, from 35 wt% without catalyst [97]. Another metal-supported catalyst study utilized Pd/C in the liquefaction of *Nannochloropsis* sp. in a system that isolated the catalyst from the biocrude oil and solid residue [98]. Similar to the Duan study, biocrude oil was increased to 40 wt% and 38 wt% at 10-bar and 30-bar H_2 pressure, respectively, from the 35 wt% yield in the uncatalyzed control.

Nickel supported by rare-earth and ammonia exchange (Ni/REHY) catalyst was researched by Yang et al. in the HTL and upgrading of *Dunaliella* sp. at 200 °C, 2 MPa, 1 h, and 2 g Ni/REHY at 90 mL solvent [98]. A biocrude oil yield of 35 wt% was achieved for the reaction without catalyst, 52 wt% yield for REHY-mediated reaction, and 72 wt% yield for Ni/REHY-mediated reaction. Raney nickel (Raney-Ni) and zeolite socony mobil-5 (H-ZSM-5) catalyst systems were utilized by Zhang et al. in the HTL of *Chlorella* sp. using ethanol as solvent [125]. Reaction conditions were as follows: 200–300 °C temperature range, 2.8–2.9 MPa pressure range, and 30 min reaction time. Although there was no significant increase in biocrude oil yield for both catalytic experimental setups across the range of temperatures and pressures, product analysis revealed the formation of gasoline-range hydrocarbons. Such chemicals indicate bond cleavage, depolymerization, and hydrogenation processes took place. A rise in biocrude oil yield from 32 wt% (uncatalyzed) to 38 wt% (H-ZSM-5) and 52 wt% (Ce/H-ZSM-5) was realized in Xu et al.'s study that employed *C. pyrenoidosa* sp. liquefaction [126]. The study concluded that the incorporation of Ce in the zeolite enhanced yield in terms of both biocrude oil and hydrocarbons.

The quality of high-yield biocrude oil was investigated with regard to its N content through the valorization of *Cyanobacteria* microalgae using magnesium aluminum-layered double oxide/zeolite socony mobil-5 (MgAl-LDO/HZSM-5)

catalyst [118]. Greater than 41% of the biocrude oil generated had extraordinarily little N. The extreme lowering of biocrude oil N was attained at 550 °C, 10 K/min heating rate, and 0.75 catalyst/substrate ratio.

There is little question that heterogeneous catalysts offer a superior task in forming high-yield and high-quality biocrude oil. However, biocrude oil is not the sole basis in their large-scale industry adoption. Other parameters that are directly or indirectly affected by the type of heterogeneous catalyst need further evaluation. These catalyst properties include (1) stabilization, (2) effects on gaseous products, and (3) other factors.

Stabilization. Heterogeneous catalysts can precipitate, sinter, dissolve, or diffuse as a result of microalgal impurities and reaction condition [14]. High N and O concentrations, extreme temperatures and pressures, and prolonged reaction times contribute to the catalyst's deactivation [127]. The studies detailed prior are bench-scale investigations that pertain mostly to catalytic effects on biocrude yield and quality but not on the heterogeneous catalyst's recoverability from its solid products [123]. More studies concerning fundamental knowledge on *recyclability* and methods of preventing *deactivation* are warranted.

Effects on Gaseous Products. Gas yield (approximately 5 wt% of product yield) and composition are considerably affected by heterogeneous catalyst. The composition of H_2, CH_4, CO, CO_2, and C_2 varies depending upon the catalyst employed [128, 129]. Metal catalysts such as Ru/C, Pd/C, Pt/Al_2O_3, Pt/C, Raney-Ni, Ni-Mo/Al_2O_3, and HZSM-5 generally increase CO_2 concentration in the gas phase and hydrocarbons in the biocrude oil via decarboxylation reaction [1, 105, 120]. Ru/C and Ni/SiO_2-Al_2O_3 are also responsible for increasing H_2, CH_4, and C_2H_6 fractions in the gas phase, also via decarboxylation reaction [122]. The presence of significant amount of CH_4 and C_2H_6 in the gas phase is also linked to the use of Pt/C catalyst which is known to promote cracking during microalgal liquefaction [130].

Other Factors. The nature of material support base by heterogeneous catalyst dictates which reaction is favored in an HTL setup. Catalysts with similar support base influence similar chemical reactions, but when they are altered, biocrude oil yield and quality are modified. For example, the catalysts Pt/Al_2O_3, Ni/Al_2O_3, and $Co/Mo/Al_2O_3$ all share similar aluminum oxide base which at 350 °C generated individual specific biocrude oil yield from *Nannochloropsis* HTL [31]. Nonetheless, when Al_2O_3 was changed to Pt/C, Ni/SiO_2-Al_2O_3, or CoMo/γ-Al_2O_3, the yield for all three catalyst-mediated experiments were increased [41, 131]. Certain metals are linked to certain reactions. For instance, Pt-based catalyst enhances hydrogenation, while Co-Mo promotes deoxygenation [41]. Changes in reaction temperature using a particular metal catalyst affect biocrude oil yield [31]. A study verified that the biocrude oil yield for all experiments using Pd/C, Pd/Al_2O_3, Pt/C, Pt/Al_2O_3, and Raney-Ni catalysts at 240 °C increased when temperature is raised to 280 °C [99]. Lastly, the reaction atmosphere (i.e., presence or absence of H_2) in conjunction with metal catalyst or zeolite dictated the yield and quality of biocrude oil. For example, zeolite with H_2 increased the biocrude oil yield, while zeolite without H_2 decreased it [41] (Table 2).

Table 2 Summary of catalyst, microalgae species, experimental conditions, and biocrude oil yield for catalytic hydrothermal liquefaction (HTL) of microalgae

Catalyst	Microalgae	Temp (°C), time (min)	Yield (wt%)	Ref
Ru/C	*Nannochloropsis* sp.	350, 60	+43	Duan and Savage [41]
Pd/Al_2O_3	*Chlorella pyrenoidosa*	280, 30	+8	Yu et al. [99]
Pd/C	*Chlorella pyrenoidosa*	280, 30	+4	Yu et al. [99]
Pd/C	*Nannochloropsis* sp.	350, 60	+63	Duan and Savage [41]
Pt/Al_2O_3	*Nannochloropsis oc.*	350, 60	−12	Biller et al. [31]
Pt/C	*Nannochloropsis* sp.	350, 60	+34	Duan and Savage [41]
Pt/Al_2O_3	*Chlorella pyrenoidosa*	280, 30	+7	Yu et al. [99]
Pt/C	*Chlorella pyrenoidosa*	280, 30	+6	Yu et al. [99]
NiO	*Spirulina platensis*	350, 60	−23	Jena and Das [73]
Ni/Al_2O_3	*Nannochloropsis oc.*	350, 60	−47	Biller et al. [31]
$Ni/SiO_2-Al_2O_3$	*Nannochloropsis* sp.	350, 60	+44	Duan and Savage [41]
Raney-Ni	*Chlorella pyrenoidosa*	280, 30	+12	Yu et al. [99]
$Ni-Mo/Al_2O_3$	*Nannochloropsis Salina*	340, 30	+41	Li et al. [86]
$Co-Mo/Al_2O_3$	*Nannochloropsis oc.*	350, 60	−26	Biller et al. [31]
$Co-Mo/\gamma--Al_2O_3$	*Nannochloropsis* sp.	350, 60	+54	Duan and Savage [41]
Zeolite	*Nannochloropsis* sp.	350, 60	+29	Duan and Savage [41]
HZSM-5	*Chlorella pyrenoidosa*	300, 20	+3	Xu et al. [126]
Ce/HZSM-5	*Chlorella pyrenoidosa*	300, 20	+47	Xu et al. [126]
$Ca_3(PO_4)_2$	*Spirulina platensis*	350, 60	−12	Jena and Das [73]

8 Biocrude Oil Valorization

The production of high-quality fuel containing specific types of hydrocarbons relies on the valorization or upgrading of the biocrude oil obtained from the HTL of algae biomass. As mentioned in the previous section, the upgrade of biocrude oil uses heterogeneous catalysts. Most of the time, HTL of the algae biomass is carried out uncatalyzed followed by catalyzed upgrading of the biocrude oil. Upgrading ensures the conversion of oxygenates into hydrocarbons [45]. Zeolite is the most widely used heterogeneous catalyst for upgrading biocrude oil because of its unique structure and acidity [117, 132, 133]. The body of research on zeolite has been considerably applied to pyrolysis [134–136]. The valorization process removes O in the intermediate products through a combination of processes such as cracking, decarboxylation, and decarbonylation. Typical temperatures range between 300 and 500 °C [107, 131, 137]. The suitable choice of zeolite is critical for the following reasons. First, it affects the composition of the gaseous phase (e.g., alkanes, CO_2,

and CO) and the aqueous phase (e.g., organics). Second, it determines the amount of alkanes necessary to satisfy the requirements for gasoline, jet fuel, and diesel. Such amount is a function of the nature of the metal species in the zeolite. Third, it determines the degree of the dehydration process which determines the amount of water vapor in the gaseous phase. The goal of biocrude oil valorization is to satisfy the ASTM D 6751 biodiesel standard [138] in terms of the following properties: S content, total acid number, viscosity, density, HHV, and distillation temperature at which 90 wt% of O-containing compounds are converted to fuel-range hydrocarbons (alkanes and aromatics). The O from oxygenates, mainly produced from carbohydrates, lowers the HHV and energy density of the fuel and therefore must be diminished (deoxygenation). The N and S from these compounds must also be reduced since (1) they cause the release of NO_x and SO_x that pollutes air and (2) they degrade combustion engines through corrosion (denitrogenation and desulfurization) [97, 139, 140]. One of the most efficient and effective upgrading methods is hydrothermal valorization, a process implemented at high temperatures with water as exclusive H donor (or in combination with added H_2) and heterogeneous catalyst to eliminate O, N, and S heteroatoms [141, 142].

Recent studies on biocrude valorization primarily centered on zeolites and metal catalysts, as these catalysts have been shown to consistently produce high-quality (yield, hydrocarbons) fuels. Zeolites and metal-modified zeolites, in particular, are effective in generating alkanes and aromatics [143, 144]. Zeolites enhance octane properties of fuels through mediating hydrogenation and isomerization reactions critical to increasing isomer concentration in the fuel [145, 146]. Zeolites were shown (1) to effectively mediate dehydration, isomerization, and alkylation of HTL-derived biocrude oil from algae, (2) to not get deactivated by coking, and (3) to possess high tolerance to steam [78]. One of these studies compared the catalytic activities of HZSM-5 and Pt/Al$_2$O$_3$ catalysts in upgrading *Scenedesmus almeriensis-* and *Nannochloropsis gaditana*-derived biocrude oil [14]. Temperature was set at 400 °C, reaction period at 4 h, and catalyst concentration at 0.3 g/0.55 mL DI water. Results indicated that the yields for both catalysts employed to both algae were remarkably similar under the experimental condition applied. Specifically, the fuel products contained significant concentrations of pentadecane and hexadecane, while the gaseous products composed of C1–C4 alkanes, CO_2, and CO. The authors hypothesized that pentadecane, hexadecane, and C1–C4 alkanes were produced from the hydrogenation of alkenes, while CO_2 and CO were produced from decarboxylation of fatty acids.

The zeolite HZSM-5 was compared to metal catalysts Pt/C and Mo$_2$C by Duan and Savage [143]. Results showed that at 430 °C, S-, O-, and N-containing compounds were greatly reduced using the three catalysts, with Mo$_2$C mediating the highest saturated hydrocarbons at 76 wt%. However, when the temperature was raised to 530 °C, Pt/C and HZSM-5 mediated 90 wt% aromatics, while Mo$_2$C mediated only 88 wt% aromatics. Duan and colleagues again tested zeolite in terms of the effect of the catalyst's structure on its activity and selectivity [147]. The results revealed that activity is independent of structure, while selectivity is structure-dependent. Duan and colleagues followed this study with an evaluation of different

kinds of zeolites and SAPO-x catalysts with various structures and acidities [147]. They utilized these catalysts to upgrade biocrude oil from HTL of algae. They found out that at 400 °C, 6 MPa H_2, 10 wt% catalyst, and supercritical H_2O, yield was highly dependent on the structure. The HSAPO-11 catalyst had the lowest upgrading efficiency at 42.4 wt% and the lowest hydrocarbon yield at 80 wt%, while the HMCM-41 catalyst had the highest upgrading efficiency at 54.5 wt% and the highest hydrocarbon yield at 95.6 wt%. In another study, the zeolite HZSM-5 was used in upgrading biocrude oil with H_2 at high pressure [148]. Temperatures (400–500 °C) and catalyst loadings (5–50 wt%) were varied. All S-, O-, and N-containing compounds were significantly reduced, and the highest alkane yield was achieved at 400 °C. The authors hypothesized that the dominant upgrading reactions were hydrotreating (hydrodesulfurization, hydrodeoxygenation, hydrodenitrogenation), hydrogenation, hydrocracking, and aromatization [97].

In terms of metal catalysts, Raney-Ni catalyst was found to be more effective than Ru/C or a combination of Raney-Ni and Ru/C because it mediated a fuel product with 87 wt% alkanes, in contrast to the other two catalysts which mediated fuel products with <60 wt% alkanes [141]. Zhang et al. has shown in their experiment that the yields mediated by these three catalysts were as follows: Ru/C > Pt/C > Mo_2C at 350 °C and 6 MPa H_2 pressure [144]. It has been shown that the deoxygenation activities of Pt/γ-Al_2O_3, Ru/C, Ru/C + alumina, MCM-41 (100% Si), and Ru/C + Mo_2C in algae valorization were high [35]. Ru/C + alumina, MCM-41 (100% Si), Pt/γ-Al_2O_3, Pt/C, and Pd/C were excellent for hydrogenation, and Ru/C + Pt/C was ideal for desulfurization [35].

A method of improving a heterogeneous catalyst's activity is to combine two or more of them, known as the two-component or multicomponent catalyst system, respectively. This is done to improve the catalyst's ability to remove heteroatoms from biocrude oil (i.e., better-quality fuel with high concentration of fuel-range hydrocarbons) or increase fuel yield [95, 147]. An example is the combination of Ru/C with Raney-Ni (Ru/C + Raney-Ni). Introducing H_2 to the biocrude oil at 400 °C in the presence of the two-component catalyst system boosted the fuel's yield and C and H contents. In fact, fuel yield reached 77.2 wt%, HHV was determined to be 45.2 MJ/kg, and energy yield (i.e., ratio of the energy contained in fuel versus the energy contained in biocrude oil) reached 86 wt% [141]. In a similar manner, a multicomponent system of catalysts containing Ru/C + Pt/C, Ru/C + Mo_2C, and Ru/C + Pt/γ-Al_2O_3 achieved enhanced deoxygenation, denitrogenation, and desulfurization activities [95].

Lastly, solvent plays an important role in microalgae valorization. Water is the commonly used solvent, and it influences the catalytic activities of heterogeneous catalysts. Some of the documented effects of water on catalyst and fuel are as follows: (1) Using subcritical water, increasing Pt/C-sulfide catalyst from 0 to 20 wt%, lowers S and O contents, raises C and H contents, and increases the energy density and HHV of the fuel [142]; (2) using water, the catalytic activity of HZSM-5 is improved [107] which stimulates decarboxylation to generate more CO_2 [143].

Some of the challenges associated with heterogeneous catalysts in microalgae valorization include (1) deactivation due to solid residue (coke) formation [115,

149], (2) "poisoning" due to S-containing compounds [30], and (3) reduction in surface area and pore volume. In the third case, Ni/C, ZSM5, 5% Ru/C, and 5% Pt/C used in upgrading biocrude oil at 350 °C for 10 h with H_2 caused such reduction (93% surface area, 78% pore volume) because of the development of heavy products unable to adsorb on catalyst surface [115]. The primary issue, therefore, that must be addressed through research of catalytic upgrading of fuel is catalytic stability. Stability dictates fuel quality which determines it compliance to ASTM D 6751.

9   Perspectives and Direction on the State of Research (SOR) for Microalgae HTL

Hydrothermal technologies utilize subcritical or supercritical water to process any form of biomass. It is divided into four regions, depending upon reaction temperature and pressure: carbonization, liquefaction, catalytic gasification, and high-temperature gasification. This chapter focused on hydrothermal liquefaction (HTL). The state of the art of HTL technology began with terrestrial biomass [17, 18]. Since the 1940s, the technology has been developed, but it was not until the oil crisis of 1973 that it has expanded to other alternative biomass feedstock which aimed at reducing foreign petroleum oil dependence. Early challenges associated with HTL technology were (1) the ability to inject the reactor with high concentration of biomass, (2) the optimum feed rate at which no mechanical problem exists, and (3) the suitable reactor condition and catalyst type that allow the production of fuel with consistent and reliable fuel-range hydrocarbons. Several companies have attempted to develop and commercialize HTL technology. One of them is the "CatLiq Process" from SCF Technologies, a Danish company. The process converts a continuous input of organic waste to biocrude oil at subcritical conditions (350 °C and 25 MPa) using homogeneous (K_2CO_3) and heterogeneous (zirconia) catalysts [150].

Although HTL is a mature technology, no pilot- and demo-scale implementation has succeeded over the past 50 years. A combination of technological and economic issues prevented the achievement of a demonstration scale. An advantage for HTL is its ability to process dilute, high-liquid feedstock, making it suitable for algae input at 5–10 wt% concentration [7]. Yet, no large-scale HTL implementation using microalgae as feedstock has been realized thus far. There is no single limiting factor, but a multitude of challenges prevent the commercialization of microalgae HTL. These are as follows:

1. Impurities and heterogeneities (e.g., particle size) in the feedstock solution which can potentially precipitate, plug the reactor, and poison the catalyst's active sites.
2. Difficulty in maintaining the minimum microalgae concentration of about 5–10 wt%.
3. Low heat transfer efficiency and recovery efficiency.
4. Low biocrude oil yield.

5. Corrosive biocrude oil (tanks, pipes, and reactors must be made of stainless steel to prevent corrosion caused by subcritical or supercritical water).
6. Lack of use for by-products such as aqueous phase and solid residue.
7. Negative overall energy balance due to liquid pumping and heat losses.
8. Unclear understanding of the kinetics of catalytic reaction.
9. Unstable and nonrecyclable heterogeneous catalyst in a continuous mode of operation.

Direction on the SOR for microalgae HTL is subdivided into four aspects: microalgae, residence time, heating rate, and separation. These aspects are expected to address the challenges identified above to establish a commercial biorefinery based on microalgae HTL in the foreseeable future.

Microalgae. Microalgae feedstock is fed into the HTL reactor as a dilute solution. Thus, significant operational cost is incurred in the form of pumping energy use. The optimum microalgae-to-water ratio remains unclear since recent investigations on microalgae feedstocks showed contradicting results. As an example, a high microalgal load (>10 wt% microalgae solution) requires high water heating energy, but the water content is not sufficient to dissolve and stabilize the algal cells [26, 59]. Recent research has proposed microalgae forms such as pulverized dried samples [58, 59], intact microalgae cells in the form of paste [25, 38, 39, 41, 151], or freeze-dried pulverized cells mixed with deionized water [31, 39, 60, 72]. However, these forms can inadvertently alter fuel yield, fuel composition, or extractability of some macroelements. The paste microalgae form appears to precisely track the fate and transport of nutrients during the HTL and upgrading process, and it seems to illustrate a more realistic scenario within the context of commercial-scale HTL plant. Further research on these forms is warranted.

Residence Time. Residence time is defined as the period during which the maximum temperature is maintained for HTL, not accounting for the heating and cooling periods. Currently, residence time for microalgae HTL is still too long. To achieve high biocrude oil yield, reaction must take place at high temperature and low residence time. Most studies in literature applied 60 min. Up until recently, Kumar and colleagues invented a method called flash hydrolysis, a type of HTL with reaction time in the seconds range [119]. The technology significantly lowers operational and energy costs. Still, the development of heterogeneous catalyst that is stable, recyclable, and suitable to fast-heating condition presents an opportunity for future research.

Heating Rate. The effects of heating rate on biocrude oil yield are still unclear. Only a few studies provide information on this parameter [31, 36, 38, 39, 41]. Some research suggests that increasing heating (e.g., 100 °C/min) rate has a positive correlation on biocrude oil formation [31, 39, 41, 38]. Design and optimization research of heat transfer system for large-scale reactors which solve microalgae's low heat transfer coefficient and variabilities of reaction enthalpies must be performed.

Separation. Almost all studies in literature utilized organic solvents in separating the HTL products from each other. These solvents include dichloromethane, chloroform, acetone, THF, or hexane. There is no information available on the potential

effects of these solvents on biocrude oil yield and quality. Further, there is no data pertaining to the influence of the solvent to the microalgae loaded. An organic solvent is typically added to the biocrude oil and later evaporated. The process can also evaporate lighter volatile organics in the biocrude oil which reduces the yield. If a commercial microalgae HTL and upgrading is to be pursued, solvent-based separation is inappropriate due to intermittent operational pause. A more feasible scenario is to immediately separate the water-insoluble fraction of the biocrude oil from the water-soluble fraction and then apply solvent-free methods such as gravitation and centrifugation. These two methods require deep exploration.

References

1. International Energy Agency (IEA) (2017) World energy outlook 2017. A report by the Organization for Economic Cooperation and Development (OECD) of the International Energy Agency (IEA), Paris
2. Brennan L, Owende P (2010) Biofuels from microalgae—a review of technologies for production, processing, and extractions of biofuels and co-products. Renew Sustain Energy Rev 14(2):557–577. https://doi.org/10.1016/j.rser.2009.10.009
3. Guo M, Song W, Buhain J (2015a) Bioenergy and biofuels: history, status, and perspective. Renew Sustain Energy Rev 42:712–725. https://doi.org/10.1016/j.rser.2014.10.013
4. Akhtar J, Amin NAS (2011) A review on process conditions for optimum bio-oil yield in hydrothermal liquefaction of biomass. Renew Sustain Energy Rev 15(3):1615–1624. https://doi.org/10.1016/j.rser.2010.11.054
5. Kumar D, Murthy GS (2012) Life cycle assessment of energy and GHG emissions during ethanol production from grass straws using various pretreatment processes. Int J Life Cycle Assess 17(4):388–401. https://doi.org/10.1007/s11367-011-0376-5
6. Bessette A, Stuart BJ, Resurreccion EP, Kumar S (2020) Algae-powered sustainable community design life cycle assessment and techno-economic analysis. ACS Sustain Chem Eng 8(4):1916–1922. https://doi.org/10.1021/acssuschemeng.9b06256
7. Resurreccion EP, Colosi LM, White MA, Clarens AF (2012) Comparison of algae cultivation methods for bioenergy production using a combined life cycle assessment and life cycle costing approach. Bioresour Technol 126:298–306. https://doi.org/10.1016/j.biortech.2012.09.038
8. Vardon DR, Sharma BK, Blazina GV, Rajagopalan K, Strathmann TJ (2012) Thermochemical conversion of raw and defatted algal biomass via hydrothermal liquefaction and slow pyrolysis. Bioresour Technol 109:178–187. https://doi.org/10.1016/j.biortech.2012.01.008
9. Lin L, Cunshan Z, Vittayapadung S, Xiangqian S, Mingdong D (2011) Opportunities and challenges for biodiesel fuel. Appl Energy 88(4):1020–1031. https://doi.org/10.1016/j.apenergy.2010.09.029
10. Searchinger T, Heimlich R, Houghton RA, Dong F, Elobeid A, Fabiosa J, Tokgoz S, Hayes D, Yu T-H (2008) Use of U.S. croplands for biofuels increases greenhouse gases through emissions from land-use change. Science 319(5867):1238–1240. https://doi.org/10.1126/science.1151861
11. Chisti Y (2007) Biodiesel from algae. Biotechnol Adv 25(3):294–306. https://doi.org/10.1016/j.biotechadv.2007.02.001
12. Juneja A, Kumar S, Tumuluru JS (2018) Hydrothermal liquefaction: a promising technology for high moisture biomass conversion. In: Tumuluru JS (ed) Biomass preprocessing and pretreatments for production of biofuels. CRC, Boca Raton, FL, p 9781498765473

13. Tekin K, Karagöz S (2013) Non-catalytic and catalytic hydrothermal liquefaction of biomass. Res Chem Intermed 39:485–498. https://doi.org/10.1007/s11164-012-0572-3

14. Barreiro DL, Prins W, Ronsse F, Brilman W (2013) Hydrothermal liquefaction (HTL) of microalgae for biofuel production: state of the art review and future prospects. Biomass Bioenergy 53:113–127. https://doi.org/10.1016/j.biombioe.2012.12.029

15. Castello D, Pedersen TH, Rosendahl LA (2018) Continuous hydrothermal liquefaction of biomass: a critical review. Energies 11(11):3165. https://doi.org/10.3390/en11113165

16. Kamio E, Takahashi S, Noda H, Fukuhara C, Okamura T (2008) Effect of heating rate on liquefaction of cellulose by hot compressed water. Chem Eng J 137(2):328–338. https://doi.org/10.1016/j.cej.2007.05.007

17. Peterson AA, Vogel F, Lachance RP, Fröling M, Antal MJ Jr, Tester JW (2008) Thermochemical biofuel production in hydrothermal media: a review of sub- and super-critical water technologies. Energ Environ Sci 1:32–65. https://doi.org/10.1039/b810100k

18. Toor SS, Rosendahl L, Rudolf A (2011) Hydrothermal liquefaction of biomass: a review of subcritical water technologies. Energy 36(5):2328–2342. https://doi.org/10.1016/j.energy.2011.03.013

19. Chakinala AG, Brilman DWF, van Swaaij WPM, Kersten SRA (2010) Catalytic and non-catalytic supercritical water gasification of microalgae and glycerol. Ind Eng Chem Res 49:1113–1122. https://doi.org/10.1021/ie9008293

20. Asiedu A, Stuart B, Resurreccion E, Kumar S (2017) Techno-economic analysis of protein concentrate produced by flash hydrolysis of microalgae. Environ Prog Sustain Energy 37(2):881–890. https://doi.org/10.1002/ep.12722

21. Elliott DC (2007) Historical developments in hydroprocessing bio-oils. Energy Fuel 21(3):1792–1815. https://doi.org/10.1021/ef070044u

22. Mortensen PM, Grunwaldt J-D, Jensen PA, Knudsen KG, Jensen AD (2011) A review of catalytic upgrading of bio-oil to engine fuels. Appl Catal A Gen 407(1–2):1–19. https://doi.org/10.1016/j.apcata.2011.08.046

23. Park H-J, Dong J-I, Jeon J-K, Park Y-K, Yoo K-S, Kim S-S, Kim J, Kim S (2008) Effects of the operating parameters on the production of bio-oil in the fast pyrolysis of Japanese larch. Chem Eng J 143(1–3):124–132. https://doi.org/10.1016/j.cej.2007.12.031

24. Savage PE, Levine RB, Huelsman CM (2010) Hydrothermal processing of biomass. In: Crocker M (ed) Thermochemical conversion of biomass to liquid fuels and chemicals. Royal Society of Chemistry, Cambridge, pp 190–219

25. Yang YF, Feng CP, Inamori Y, Maekawa T (2004) Analysis of energy conversion characteristics in liquefaction of algae. Resour Conserv Recycl 43(1):21–33. https://doi.org/10.1016/j.resconrec.2004.03.003

26. Huang H, Yuan X, Zeng G, Wang J, Li H, Zhou C, Pei X, You Q, Chen L (2011) Thermochemical liquefaction characteristics of microalgae in sub- and supercritical ethanol. Fuel Process Technol 92(1):147–153. https://doi.org/10.1016/j.fuproc.2010.09.018

27. Matsui T, Nishihara A, Ueda C, Ohtsuki M, Ikenaga N, Suzuki T (1997) Liquefaction of micro-algae with iron catalyst. Fuel 76(1):1043–1048. https://doi.org/10.1016/S0016-2361(97)00120-8

28. Xuan X, Wang J, Zeng G, Huang H, Pei X, Li H, Liu Z, Cong M (2011) Comparative studies of thermochemical liquefaction characteristics of microalgae using different solvents. Energy 36(11):6406–6412. https://doi.org/10.1016/j.energy.2011.09.031

29. Zhao C, Kou Y, Lemonidou AA, Li X, Lercher JA (2009) Highly selective catalytic conversion of phenolic bio-oil to alkanes. Angew Chem 121(22):4047–4050. https://doi.org/10.1002/anie.200900404

30. Elliott DC (2015) Biofuel from fast pyrolysis and catalytic hydrodeoxygenation. Curr Opin Chem Eng 9:59–65. https://doi.org/10.1016/j.coche.2015.08.008

31. Biller P, Riley R, Ross AB (2011) Catalytic hydrothermal processing of microalgae: decomposition and upgrading of lipids. Bioresour Technol 102(7):4841–4848. https://doi.org/10.1016/j.biortech.2010.12.113

32. Guo Y, Yeh T, Song W, Xu D, Wang S (2015b) A review of bio-oil production from hydrothermal liquefaction of algae. Renew Sustain Energy Rev 48:776–790. https://doi.org/10.1016/j.rser.2015.04.049

33. Kumar S, Gupta RB (2008) Hydrolysis of microcrystalline cellulose in subcritical and supercritical water in a continuous flow reactor. Ind Eng Chem Res 47(23):9321–9329. https://doi.org/10.1021/ie801102j

34. Yu G, Zhang Y, Schideman L, Funk TL, Wang W (2011a) Hydrothermal liquefaction of low lipid content microalgae into bio-crude oil. Trans ASABE 54(1):239–246. https://doi.org/10.13031/2013.36241

35. Xu D, Lin G, Guo S, Wang S, Guo Y, Jing Z (2018) Catalytic hydrothermal liquefaction of algae and upgrading of biocrude: a critical review. Renew Sustain Energy Rev 97:103–118. https://doi.org/10.1016/j.rser.2018.08.042

36. García Alba L, Torri C, Samori C, van der Spek J, Fabbri D, Kersten SRA, Brilman WF (2012) Hydrothermal treatment (HTT) of microalgae: evaluation of the process as conversion method in an algae biorefinery concept. *Energy Fuel* 26(1):642–657. https://doi.org/10.1021/ef201415s

37. Dote Y, Sawayama S, Inoue S, Minowa T, Yokoyama S-y (1994) Recovery of liquid fuel from hydrocarbon-rich microalgae by thermochemical liquefaction. Fuel 73(12):1855–1857. https://doi.org/10.1016/0016-2361(94)90211-9

38. Brown TM, Duan P, Savage PE (2010) Hydrothermal liquefaction and gasification of *Nannochloropsis sp*. Energy Fuel 24(6):3639–3646. https://doi.org/10.1021/ef100203u

39. Biller P, Ross AB (2011) Potential yields and properties of oil from the hydrothermal liquefaction of microalgae with different biochemical content. Bioresour Technol 102(1):215 225. https://doi.org/10.1016/j.biortech.2010.06.028

40. Jena U, Das KC, Kastner JR (2011) Effect of operating conditions of thermochemical liquefaction on biocrude production from *Spirulina platensis*. Bioresour Technol 102(10):6221–6229. https://doi.org/10.1016/j.biortech.2011.02.057

41. Duan P, Savage PE (2011a) Hydrothermal liquefaction of a microalgae with heterogeneous catalysts. Ind Eng Chem Res 50(1):52–61. https://doi.org/10.1021/ie100758s

42. Xu L, Brilman DWF, Withag JAM, Brem G, Kersten SRA (2011) Assessment of a dry and a wet route for the production of biofuels from microalgae: energy balance analysis. Bioresour Technol 102(8):5113–5122. https://doi.org/10.1016/j.biortech.2011.01.066

43. Mata TM, Martins AA, Caetano NS (2010) Microalgae for biodiesel production and other applications: a review. Renew Sustain Energy Rev 14(1):217–232. https://doi.org/10.1016/j.rser.2009.07.020

44. Patil V, Tran K-Q, Giselrød HR (2008) Towards sustainable production of biofuels from microalgae. Int J Mol Sci 9(7):1188–1195. https://doi.org/10.3390/ijms9071188

45. Jena U, Das KC (2011) Comparative evaluation of thermochemical liquefaction and pyrolysis for bio-oil production from microalgae. Energy Fuel 25(11):5472–5482. https://doi.org/10.1021/ef201373m

46. Ross AB, Biller P, Hall C (2010a) Catalytic hydrothermal processing of microalgae with integrated nutrient recycling. In: Proceedings of the 19th European biomass conference and exhibition, 06/06–10/2011, Berlin, Germany

47. Quinn JC, Smith TG, Downes CM, Quinn C (2014) Microalgae to biofuels lifecycle assessment—multiple pathway evaluation. Algal Res 4:116–122. https://doi.org/10.1016/j.algal.2013.11.002

48. Zhang Y, Colosi LM (2013) Practical ambiguities during calculation of energy ratios and their impacts on life cycle assessment calculations. Energy Policy 57:630–633. https://doi.org/10.1016/j.enpol.2013.02.039

49. Minowa T, Yokoyama S, Kishimoto M, Okakura T (1995) Oil production from algal cells of *Dunaliella tertiolecta* by direct thermochemical liquefaction. Fuel 74(12):1735–1738. https://doi.org/10.1016/0016-2361(95)80001-X

50. Jonker JGG, Faaij APC (2013) Techno-economic assessment of microalgae as feedstock for renewable bio-energy production. Appl Energy 102:461–475. https://doi.org/10.1016/j.apenergy.2012.07.053

51. Biller P, Sharma BK, Kunwar B, Ross AB (2015) Hydroprocessing of bio-crude from continuous hydrothermal liquefaction of microalgae. Fuel 159(1):197–205. https://doi.org/10.1016/j.fuel.2015.06.077

52. US Department of Commerce (US DOC) (1982) Heating valued of natural gas and its components. A technical report by the National Bureau of Standards, Center for Chemical Physics, Chemical Thermodynamics Division, Washington, DC, USA. https://nvlpubs.nist.gov/nistpubs/Legacy/IR/nbsir82-2401.pdf. Accessed 3 Oct 2020

53. Minowa T, Sawayama S (1999) A novel microalgal system for energy production with nitrogen cycling. Fuel 78(10):1213–1215. https://doi.org/10.1016/S0016-2361(99)00047-2

54. Tsukahara K, Kimura T, Minowa T, Sawayama S, Yagishita T, Inoue S, Hanaoka T, Usui Y, Ogi T (2001) Microalgal cultivation in a solution recovered from the low-temperature catalytic gasification of the microalga. J Biosci Bioeng 91(3):311–313. https://doi.org/10.1016/S1389-1723(01)80140-7

55. Demirbas, A (2000) Mechanisms of liquefaction and pyrolysis reactions of biomass. Energ Conver Manage 41(6):633–646. https://doi.org/10.1016/S0196-8904(99)00130-2

56. Anastasakis K, Ross AB (2011) Hydrothermal liquefaction of the brown macro-alga *Laminaria saccharina:* effect of reaction conditions on product distribution and composition. Bioresour Technol 102(7):4876–4883. https://doi.org/10.1016/j.biortech.2011.01.031

57. Zhou D, Zhang L, Zhang S, Fu H, Chen J (2010) Hydrothermal liquefaction of macroalgae *Enteromorpha prolifera* to bio-oil. Energy Fuel 24(7):4054–4061. https://doi.org/10.1021/ef100151h

58. Zou S, Wu Y, Yang M, Imdad K, Li C, Junmao T (2010a) Production and characterization of bio-oil from hydrothermal liquefaction of microalgae *Dunaliella tertiolecta* cake. Energy 35(12):5406–5411. https://doi.org/10.1016/j.energy.2010.07.013

59. Zou S, Wu Y, Yang M, Li C, Tong J (2010b) Bio-oil production from sub- and supercritical water liquefaction of microalgae *Dunaliella tertiolecta* and related properties. Energ Environ Sci 3(8):1073–1078. https://doi.org/10.1039/C002550J

60. Yu G, Zhang Y, Schideman L, Funk T, Wang Z (2011b) Distributions of carbon and nitrogen in the products from hydrothermal liquefaction of low-lipid microalgae. Energ Environ Sci 4(11):4587–4595. https://doi.org/10.1039/C1EE01541A

61. Torri C, Garcia Alba L, Samori C, Fabbri D, Brilman DWF (2012) Hydrothermal treatment (HTT) of microalgae: detailed molecular characterization of HTT oil in view of HTT mechanism elucidation. Energy Fuel 26(1):658–671. https://doi.org/10.1021/ef201417e

62. Bühler W, Dinjus E, Ederer HJ, Kruse A, Mas C (2002) Ionic reactions and pyrolysis of glycerol as competing reaction pathways in near- and supercritical water. J Supercrit Fluids 22(1):37–53. https://doi.org/10.1016/S0896-8446(01)00105-X

63. Aysu T, Demirbas A, Bhengu AS, Kücük MM (2015) Evaluation of *Eremurus spectabilis* for production of bio-oils with supercritical solvents. Process Saf Environ 94:339–349. https://doi.org/10.1016/j.psep.2014.08.005

64. Lehr V, Sarlea M, Ott L, Vogel H (2007) Catalytic dehydration of biomass-derived polyols in sub- and supercritical water. Catal Today 121(1–2):121–129. https://doi.org/10.1016/j.cattod.2006.11.014

65. Rogalinski T, Liu K, Albrecht T, Brunner G (2008) Hydrolysis kinetics of biopolymers in subcritical water. J Supercrit Fluids 46(3):335–341. https://doi.org/10.1016/j.supflu.2007.09.037

66. Anastasakis K, Ross AB (2015) Hydrothermal liquefaction of four brown macro-algae commonly found on the UK coasts: an energetic analysis of the process and comparison with biochemical conversion methods. Fuel 139:546–553. https://doi.org/10.1016/j.fuel.2014.09.006

67. Raikova S, Smith-Baedorf H, Bransgrove R, Barlow O, Santomauro F, Wagner JL, Allen MJ, Bryan CG, Sapsford D, Chuck CJ (2016) Assessing hydrothermal liquefaction for the

production of bio-oil and enhanced metal recovery from microalgae cultivated on acid mine drainage. Fuel Process Technol 142:219–227. https://doi.org/10.1016/j.fuproc.2015.10.017

68. Sato N, Quitain AT, Kang K, Daimon H, Fujie K (2004) Reaction kinetics of amino acid decomposition in high-temperature and high-pressure water. Ind Eng Chem Res 43(13):3217–3222. https://doi.org/10.1021/ie020733n

69. Klingler D, Berg J, Vogel H (2007) Hydrothermal reactions of alanine and glycine in sub- and supercritical water. J Supercrit Fluids 43(1):112–119. https://doi.org/10.1016/j.supflu.2007.04.008

70. Zhou Y, Schideman L, Yu G, Zhang Y (2013) A synergistic combination of algal wastewater treatment and hydrothermal biofuel production maximized by nutrient and carbon recycling. Energ Environ Sci 6(12):3765–3779. https://doi.org/10.1039/C3EE24241B

71. Bach Q-V, Sillero MV, Tran K-Q, Skjermo J (2014) Fast hydrothermal liquefaction of a Norwegian macro-alga: screening tests. Algal Res 6(Part B):271–276. https://doi.org/10.1016/j.algal.2014.05.009

72. Ross AB, Biller P, Kubacki ML, Li H, Lea-Langton A, Jones JM (2010b) Hydrothermal processing of microalgae using alkali and organic acids. Fuel 89(9):2234–2243. https://doi.org/10.1016/j.fuel.2010.01.025

73. Jena U, Das KC, Kastner JR (2012) Comparison of the effects of Na_2CO_3, $Ca_3(PO_4)_2$, and NiO catalysts on the thermochemical liquefaction of microalga *Spirulina platensis*. Appl Energy 98:368–375. https://doi.org/10.1016/j.apenergy.2012.03.056

74. Tsukahara K, Sawayama S (2005) Liquid fuel production using microalgae. J Jpn Petrol Inst 48(5):251–259. https://doi.org/10.1627/jpi.48.251

75. Adnan MA, Hossain MM (2018) Gasification performance of various microalgae biomass—a thermodynamic study by considering tar formation using Aspen plus. Energ Conver Manage 165(1):783–793. https://doi.org/10.1016/j.enconman.2018.03.078

76. Jiao K, Chang J, Zeng X, Ng I-S, Xiao Z, Sun Y, Tang X, Lin L (2017) 5 aminolevulinic acid promotes arachidonic acid biosynthesis in the red microalga *Porphyridium purpureum*. Biotechnol Biofuels 10(168). https://doi.org/10.1186/s13068-017-0855-4

77. Elliott DC, Searlock, J L (1983) Aqueous catalyst systems for the water-gas shift reaction. 1. Comparative catalyst studies. Ind Eng Chem Prod Res Dev 22(3):426–431. https://doi.org/10.1021/i300011a008

78. Galadima A, Muraza O (2018) Hydrothermal liquefaction of algae and bio-oil upgrading into liquid fuels: role of heterogenous catalysts. Renew Sustain Energy Rev 81(Part 1):1037–1048. https://doi.org/10.1016/j.rser.2017.07.034

79. Koley S, Khadase MS, Mathimani T, Raheman H, Mallick N (2018) Catalytic and non-catalytic hydrothermal processing of *Scenedesmus obliquus* biomass for bio-crude production – a sustainable energy perspective. Energ Conver Manage 163(1):111–121. https://doi.org/10.1016/j.enconman.2018.02.052

80. Pearce M, Shemfe M, Sansom C (2018) Techno-economic analysis of solar integrated hydrothermal liquefaction of microalgae. Appl Energy 166:19–26. https://doi.org/10.1016/j.apenergy.2016.01.005

81. Saber M, Nakhshiniev B, Yoshikawa K (2016a) A review of production and upgrading of algal bio-oil. Renew Sustain Energy Rev 58:918–930. https://doi.org/10.1016/j.rser.2015.12.342

82. Tian C, Li B, Liu Z, Zhang Y, Lu H (2014) Hydrothermal liquefaction for algal biorefinery: a critical review. Renew Sustain Energy Rev 38:933–950. https://doi.org/10.1016/j.rser.2014.07.030

83. Chen Y, Wu Y, Ding R, Zhang P, Liu J, Yang M, Zhang P (2015) Catalytic hydrothermal liquefaction of *D. tertiolecta* for the production of bio-oil over different acid/base catalysts. AICHE J 61(4):118–128. https://doi.org/10.1002/aic.14740

84. Yeh TM, Dickinson JG, Franck A, Linic S, Thompson LT Jr, Savage PE (2013) Hydrothermal catalytic production of fuels and chemicals from aquatic biomass. J Chem Technol Biotechnol 88(1):13–24. https://doi.org/10.1002/jctb.3933

85. Helou C, Marier D, Jacolot P, Abdennebi-Najar L, Niquet-Léridon C, Tessier FJ, Gadonna-Widehem P (2014) Microorganisms and Maillard reaction products: a review of the literature and recent findings. J Amino Acids 46:267–277. https://doi.org/10.1007/s00726-013-1496-y

86. Li H, Hu J, Zhang Z, Wang H, Ping F, Zheng C, Zhang H, He Q (2014) Insight into the effect of hydrogenation on efficiency of hydrothermal liquefaction and physico-chemical properties of biocrude oil. Bioresour Technol 163:143–151. https://doi.org/10.1016/j.biortech.2014.04.015

87. Peterson AA, Lachance RP, Tester JW (2010) Kinetic evidence of the Maillard reaction in hydrothermal biomass processing: glucose-glycine interactions in high-temperature, high pressure water. Ind Eng Chem Res 49(5):2107–2117. https://doi.org/10.1021/ie9014809

88. Wang Y, Ho CT (2010) Dicarbonyl intermediates: a control factor in the Maillard reaction. ACS Symp Ser 1042(3):27–34

89. Chen Y, Wu Y, Zhang P, Hua D, Yang M, Li C, Chen Z, Liu J (2012) Direct liquefaction of *Dunaliella tertiolecta* for bio-oil in sub/supercritical ethanol-water. Bioresour Technol 124:190–198. https://doi.org/10.1016/j.biortech.2012.08.013

90. Kruse A, Krupka A, Schwarzkopf V, Gamard C, Henningsen T (2005) Influence of proteins on the hydrothermal gasification and liquefaction of biomass. 1. Comparison of different feedstocks. Ind Eng Chem Res 44(9):3013–3020. https://doi.org/10.1021/ie049129y

91. Kruse A, Maniam P, Spieler F (2007) Influence of proteins on the hydrothermal gasification and liquefaction of biomass. 2. Model compounds. Ind Eng Chem Res 46(1):87–96. https://doi.org/10.1021/ie061047h

92. Balat M (2008) Mechanisms of thermochemical biomass conversion processes. Part 3: reactions of liquefaction. Energy Source Pt A 30(7):649–659. https://doi.org/10.1080/10407780600817592

93. Mortensen PM, Grunwaldt JD, Jensen PA, Jensen AD (2013) Screening of catalysts for hydrodeoxygenation of phenol as a model compound for bio-oil. ACS Catal 3(8):1774–1785. https://doi.org/10.1021/cs400266e

94. Chu Y, Wei Z, Yang S, Li C, Qin X, Min E (1999) NiMoN$_x$/γ-Al$_2$O$_3$ catalyst for HDN of pyridine. Appl Catal A Gen 176(1):17–26. https://doi.org/10.1016/S0926-860X(98)00225-7

95. Xu Y, Duan P, Wang B (2015) Catalytic upgrading of pretreated algal oil with a two component catalyst mixture in supercritical water. Algal Res 9:186–193. https://doi.org/10.1016/j.algal.2015.03.011

96. Elliott DC, Baker EG (1986) Catalytic hydrotreating of biomass liquefaction products to produce hydrocarbon fuels. An interim report by the Pacific Northwest Laboratory, operated by Battelle for the US Department of Energy, DE-AC06-76RLO 1830, Springfield, VA, USA. https://pdfs.semanticscholar.org/e0a5/ed3035f73585b268ad3c81c1fe3413562639.pdf. Accessed 6 Oct 2020

97. Duan P, Savage PE (2011b) Catalytic hydrotreatment of crude algal bio-oil in supercritical water. Appl Catal Environ 104(1–2):136–143. https://doi.org/10.1016/j.apcatb.2011.02020

98. Yang L, Li Y, Savage PE (2014a) Catalytic hydrothermal liquefaction of a microalga in a two-chamber reactor. Ind Eng Chem Res 53(30):11939–11944. https://doi.org/10.1021/ie5020684

99. Yu G, Zhang Y, Guo B, Funk T, Schideman L (2014) Nutrient flows and quality of biocrude oil produced via catalytic hydrothermal liquefaction of low-lipid microalgae. Bioenergy Res 7:1317–1328. https://doi.org/10.1007/s12155-014-9471-3

100. Watanabe M, Iida T, Inomata H (2006) Decomposition of a long chain saturated fatty acid with some additives in hot compressed water. Energ Conver Manage 47(18–19):3344–3350. https://doi.org/10.1016/j.enconman.2006.01.009

101. Duan P, Savage PE (2011c) Catalytic hydrothermal hydrodenitrogenation of pyridine. Appl Catal Environ 108–109:54–60. https://doi.org/10.1016/j.apcatb.2011.08.007

102. Nautiyal P, Subramanian KA, Dastidar MG (2014) Production and characterization of biodiesel from algae. Fuel Process Technol 120:79–88. https://doi.org/10.1016/j.fuproc.2013.12.003

103. United States Environmental Protection Agency (US EPA). Diesel Fuel Standards and Rulemakings. https://www.epa.gov/diesel-fuel-standards/diesel-fuelstandards-and-rulemakings (Accessed 09/01/2020).

104. Babich IV, Moulijn JA (2003) Science and technology of novel processes for deep desulfurization of oil refinery streams: a review. Fuel 82(6):607–631. https://doi.org/10.1016/S0016-2361(02)00324-1

105. Ishihara A, Dumeignil F, Lee J, Mitsuhashi K, Qian EW, Kabe T (2005) Hydrodesulfurization of sulfur-containing polyaromatic compounds in light gas oil using noble metal catalysts. Appl Catal A Gen 289(2):163–173. https://doi.org/10.1016/j.apcata.2005.04.056

106. Prapaiwatcharapan K, Sunphorka S, Kuchonthara P, Kangvansaichol K, Hinchiranan N (2015) Single- and two-step hydrothermal liquefaction of microalgae in a semi-continuous reactor: effect of the operating parameters. Bioresour Technol 191:426–432. https://doi.org/10.1016/j.biortech.2015.04.027

107. Barreiro D, Gómez BR, Ronsse F, Hornung U, Kruse A, Prins W (2016) Heterogeneous catalytic upgrading of biocrude oil produced by hydrothermal liquefaction of microalgae: state of the art and own experiments. Fuel Process Technol 148:117–127. https://doi.org/10.1016/j.fuproc.2016.02.034

108. Akiya N, Savage PE (2002) Roles of water for chemical reactions in high-temperature water. Chem Rev 102(8):2725–2750. https://doi.org/10.1021/cr000668w

109. Tekin K, Karagöz S, Bektaş S (2014) A review of hydrothermal biomass processing. Renew Sustain Energy Rev 40:673–687. https://doi.org/10.1016/j.rser.2014.07.216

110. Wang Z, Adhikari S, Valdez P, Shakya R, Laird C (2016) Upgrading of hydrothermal liquefaction biocrude from algae grown in municipal wastewater. Fuel Process Technol 142:147–156. https://doi.org/10.1016/j.fuproc.2015.10.015

111. Costanzo W, Hilten R, Jena U, Das KC, Kastner JR (2016) Effect of low temperature hydrothermal liquefaction on catalytic hydrodenitrogenation of algae biocrude and model macromolecules. Algal Res 13:53–68. https://doi.org/10.1016/j.algal.2015.11.009

112. Faeth JL, Valdez PJ, Savage PE (2013) Fast hydrothermal liquefaction of *Nannochloropsis sp.* to produce biocrude. Energy Fuel 27(3):1391–1398. https://doi.org/10.1021/ef301925d

113. Sawayama S, Minowa T, Yokoyama S-Y (1999) Possibility of renewable energy production and CO_2 mitigation by thermochemical liquefaction of microalgae. Biomass Bioenergy 17(1):33–39. https://doi.org/10.1016/S0961-9534(99)00019-7

114. Shuping Z, Yulong W, Mingde Y, Kaleem I, Chun L, Tong J (2010) Production and characterization of bio-oil from hydrothermal liquefaction of microalgae *Dunaliella tertiolecta* cake. Energy 35(12):5406–5411. https://doi.org/10.1016/j.energy.2010.07.013

115. Shakya R, Whelen J, Adhikari S, Mahadevan R, Neupane S (2015) Effect of temperature and Na_2CO_3 catalyst on hydrothermal liquefaction of algae. Algal Res 12:80–90. https://doi.org/10.1016/j.algal.2015.08.006

116. Busca G (2014) Heterogeneous catalysts and biomass conversion. In: Heterogeneous catalytic materials: solid state chemistry, surface chemistry and catalytic behavior, 1st edn. Elsevier, Amsterdam, pp 429–446

117. Emdadi L, Oh SC, Wu Y, Oliaee SN, Diao Y, Zhu G, Liu D (2016) The role of external acidity of meso−/microporous zeolites in determining selectivity for acid-catalyzed reactions of benzyl alcohol. J Catal 335:165–174. https://doi.org/10.1016/j.jcat.2015.12.021

118. Gao L, Sun J, Xu W, Xiao G (2017) Catalytic pyrolysis of natural algae over mg-Al layered double oxides/ZSM-5 (MgAl-LDO/ZSM-5) for producing bio-oil with low nitrogen content. Bioresour Technol 225:293–298. https://doi.org/10.1016/j.biortech.2016.11.077

119. Garcia-Moscoso JL, Obeid W, Kumar S, Hatcher PG (2013) Flash hydrolysis of microalgae *(Scenedesmus sp.)* for protein extraction and production of biofuel intermediates. J Supercrit Fluids 82:183–190. https://doi.org/10.1016/j.supflu.2013.07.012

120. Guan Q, Wei C, Ning P, tian S, Gu J (2013) Catalytic gasification of algae *Nannochloropsis sp.* in sub/supercritical water. Proc Environ Sci 18:844–848. https://doi.org/10.1016/j.proenv.2013.04.113

121. Muppaneni T, Reddy HK, Selvaratnam T, Dandamudi KPR, Dungan B, Nirmalakhandan N, Schaub T, Holguin FO, Voorhies W, Lammers P, Deng S (2017) Hydrothermal liquefaction of *Cyanidioschyzon merolae* and the influence of catalysts on products. Bioresour Technol 223:91–97. https://doi.org/10.1016/j.biortech.2016.10.022

122. Yang C, Jia L, Chen C, Liu G, Fang W (2011) Bio-oil from hydro-liquefaction of *Dunaliella sauna* over Ni/REHY catalyst. Bioresour Technol 102(6):4580–4584. https://doi.org/10.1016/j.biortech.2010.12.111

123. Saber M, Golzary A, Hosseinpour M, Takahashi F, Yoshikawa K (2016b) Catalytic hydrothermal liquefaction of microalgae using nanocatalyst. Appl Energy 183:566–576. https://doi.org/10.1016/j.apenergy.2016.09.017

124. Saha P, Jeon H, Mishra PK, Rhee H-W, Kwak JH (2016) N–H and S–H insertions over cu(I)-zeolites as heterogeneous catalysts. J Mol Catal A Chem 417:10–18. https://doi.org/10.1016/j.molcata.2016.02.031

125. Zhang J, Chen W-T, Zhang P, Luo Z, Zhang Y (2013) Hydrothermal liquefaction of *Chlorella pyrenoidosa* in sub- and supercritical ethanol with heterogeneous catalysts. Bioresour Technol 133:389–397. https://doi.org/10.1016/j.biortech.2013.01.076

126. Xu Y, Zheng X, Yu H, Hu X (2014) Hydrothermal liquefaction of *Chlorella pyrenoidosa* for bio-oil production over Ce/HZSM-5. Bioresour Technol 156:1–5. https://doi.org/10.1016/j.biortech.2014.01.010

127. Lababpour A (2018) Continuous hydrothermal liquefaction for biofuel and biocrude production from microalgal feedstock. ChemBioEng Rev 5(2):90–103. https://doi.org/10.1002/cben.201700017

128. Xu D, Savage PE (2014) Characterization of biocrudes recovered with and without solvent after hydrothermal liquefaction of algae. Algal Res 6(Part A):1–7. https://doi.org/10.1016/j.algal.2014.08.007

129. Xu D, Savage PE (2015) Effect of reaction time and algae loading on water-soluble and insoluble biocrude fractions from hydrothermal liquefaction of algae. Algal Res 12:60–67. https://doi.org/10.1016/j.algal.2015.08.005

130. Yang W, Li X, Liu S, Feng L (2014b) Direct hydrothermal liquefaction of undried macroalgae *Enteromorpha prolifera* using acid catalysts. Energ Conver Manage 87:938–945. https://doi.org/10.1016/j.enconman.2014.08.004

131. Yang C, Li R, Cui C, Liu S, Qiu Q, Ding Y, Wu Y, Zhang B (2016a) Catalytic hydroprocessing of microalgae derived biofuels: a review. Green Chem 18:3684–3699. https://doi.org/10.1039/C6GC01239F

132. Piemonte V, Capocelli M, Orticello G, Di Paola L (2016) Bio-oil production and upgrading: new challenges for membrane applications. In: Figoli A, Cassano A, Basile A (eds) Membrane technologies for biorefining. Woodhead Publishing, Cambridge, pp 263–287

133. Tempelman CHL, Zhu X, Gudun K, Mezari B, Shen B, Hensen EJM (2015) Texture, acidity and fluid catalytic cracking performance of hierarchical faujasite zeolite prepared by an amphiphilic organosilane. Fuel Process Technol 139:248–258. https://doi.org/10.1016/j.fuproc.2015.06.025

134. Kan T, Strezov V, Evans TJ (2016) Lignocellulosic biomass pyrolysis: a review of product properties and effects of pyrolysis parameters. Renew Sustain Energy Rev 57:1126–1140. https://doi.org/10.1016/j.rser.2015.12.185

135. Naqvi SR, Uemura Y, Yusup S, Sugiur Y, Nishiyama N, Naqvi M (2015) The role of zeolite structure and acidity in catalytic deoxygenation of biomass pyrolysis vapors. Energy Procedia 75:793–800. https://doi.org/10.1016/j.egypro.2015.07.126

136. Plana-Pallejà J, Abelló S, Berrueco C, Montané D (2016) Effect of zeolite acidity and mesoporosity on the activity of Fischer–Tropsch Fe/ZSM-5 bifunctional catalysts. Appl Catal A Gen 515:126–135. https://doi.org/10.1016/j.apcata.2016.02.004

137. Tran NH, Bartlett JR, Kannangara GSK, Milev AS, Volk H, Wilson MA (2010) Catalytic upgrading of biorefinery oil from micro-algae. Fuel 89(2):265–274. https://doi.org/10.1016/j.fuel.2009.08.015

138. Knothe G (2006) Analyzing biodiesel: standards and other methods. J Am Oil Chem Soc 83(10):823–833. https://doi.org/10.1007/s11746-006-5033-y

139. Roussis SG, Cranford R, Sytkovetskiy N (2012) Thermal treatment of crude algae oils prepared under hydrothermal extraction conditions. Energy Fuel 26(8):5294–5299. https://doi.org/10.1021/ef300798b

140. Yang L, Li Y, Savage PE (2016b) Near- and supercritical ethanol treatment of biocrude from hydrothermal liquefaction of microalgae. Bioresour Technol 211:779–782. https://doi.org/10.1016/j.biortech.2016.03.151

141. Bai X, Duan P, Xu Y, Zhang A, Savage PE (2014) Hydrothermal catalytic processing of pretreated algal oil: a catalyst screening study. Fuel 120:141–149. https://doi.org/10.1016/j.fuel.2013.12.012

142. Duan P, Bai X, Xu Y, Zhang A, Wang F, Zhang L, Miao J (2013a) Catalytic upgrading of crude algal oil using platinum/gamma alumina in supercritical water. Fuel 109:225–233. https://doi.org/10.1016/j.fuel.2012.12.074

143. Duan P, Savage PE (2011d) Catalytic treatment of crude algal bio-oil in supercritical water: optimization studies. Energ Environ Sci 4:1447–1456. https://doi.org/10.1039/C0EE00343C

144. Zhang C, Duan P, Xu Y, Wang B, Wang F, Zhang L (2014) Catalytic upgrading of duck-weed biocrude in subcritical water. Bioresour Technol 166:37–44. https://doi.org/10.1016/j.biortech.2014.05.022

145. Anderson J, DiCicco DM, Ginder JM, Kramer U, Leone TG, Raney-Pablo HE, Wallington TJ (2012) High octane number ethanol–gasoline blends: quantifying the potential benefits in the United States. Fuel 97:585–594. https://doi.org/10.1016/j.fuel.2012.03.017

146. Pasadakis N, Gaganis V, Foteinopoulos C (2006) Octane number prediction for gasoline blends. Fuel Process Technol 87(6):505–509. https://doi.org/10.1016/j.fuproc.2005.11.006

147. Duan P, Wang B, Xu Y (2015) Catalytic hydrothermal upgrading of crude bio-oils produced from different thermo-chemical conversion routes of microalgae. Bioresour Technol 186:58–66. https://doi.org/10.1016/j.biortech.2015.03.050

148. Li Z, Savage PE (2013) Feedstocks for fuels and chemicals from algae: treatment of crude bio-oil over HZSM-5. Algal Res 2(2):154–163. https://doi.org/10.1016/j.algal.2013.01.003

149. Duan P, Xu Y, Bai X (2013b) Upgrading of crude duckweed bio-oil in subcritical water. Energy Fuel 27(8):4729–4738. https://doi.org/10.1021/ef4009168

150. Nielsen RP, Olofsson G, Søgaard EG (2012) CatLiq—high pressure and temperature catalytic conversion of biomass: the CatLiq technology in relation to other thermochemical conversion technologies. Biomass Bioenergy 39:399–402. https://doi.org/10.1016/j.biombioe.2012.01.035

151. Vardon DR, Sharma BK, Scott J, Yu G, Wang W, Schideman L, Zhang Y, Strathmann TJ (2011) Chemical properties of biocrude oil from the hydrothermal liquefaction of *Spirulina* algae, swine manure, and digested anaerobic sludge. Bioresour Technol 102(17):8295–8303. https://doi.org/10.1016/j.biortech.2011.06.041

Catalytic and Non-Catalytic Methods for Biodiesel Production

Zakir Hussain, Mohd Belal Haider, Mata Mani Tripathi, and Rakesh Kumar

Abstract In this chapter, the technical difficulties of conventional base-catalyzed transesterification and conventional esterification process using concentrated sulfuric acid in a homogeneous form have been discussed in detail. The use of low-quality feedstocks like waste vegetable oils and non-edible oils for biodiesel production has been explored. To address the mass transfer limitations in the conventional transesterification process, the addition of a phase transfer catalyst such as tetramethylammonium bromide (TMAB) has been investigated. Thereafter, the esterification of Karanja oil with high free fatty acid content through a non-catalytic method has been discussed. Kinetic modeling of the non-catalytic esterification along with process simulation in Aspen Plus was performed. Finally, the potential application of corncob-derived solid acid catalyst (SAC) for the esterification of oleic acid to produce biodiesel has been discussed.

Keywords Biodiesel · Waste vegetable oils · Solid acid catalyst

1 Introduction

Renewable energy is the energy supply that may be without difficulty replenished like biomass from plants, solar energy from the sun, hydropower from flowing water, geothermal energy from the heat inside the earth, and wind energy from flowing air [1, 2]. Nonrenewable energy is the energy supply whose sources like fossil fuels (natural gas, coal, hydrocarbon gas liquids, and petroleum products) and nuclear fuels cannot be replenished easily. Fossil fuels are the primary source of energy around the world. Energy plays a pivotal role in our survival, and there are many efforts around the world toward conserving energy by using less of an energy service. Energy consumption is increasing day by day resulting in more demand for

Z. Hussain
Department of Chemical Technology, Loyola Academy, Secunderabad, Telangana, India

M. B. Haider · M. M. Tripathi · R. Kumar (✉)
Department of Chemical Engineering and Engineering Sciences, Rajiv Gandhi Institute of Petroleum Technology, Jais, Amethi, Uttar Pradesh, India
e-mail: rkumar@rgipt.ac.in

fossil fuels, and simultaneously depleting fossil fuel sources alarm us to look for their alternatives. Today, all the energy sources are in great demand due to the industrial advancement through which countries are prospering economically. According to the Energy Information Administration (United States), a total energy of 406 quadrillion British thermal units (BTU) was consumed around the world in the year 2000, and the energy demand is anticipated to increase to 769.8 quadrillions BTU by 2035 [3]. There is an approximately 47.25% increase in anticipated energy demand between the years 2000 and 2035. A large portion of energy demand is met using the combustion of the main source of energy like fossil fuel. However, the rapid exhaustion of fossil fuels and environmental concerns due to their usage evoked the search for many promising alternative green energy sources like biofuels [4]. Exploration and exploitation of various alternative energy sources have gained huge attention over the past few decades. The contribution of biofuels in meeting inevitably increasing energy demand is very important because of the aforementioned concerns with mainstream fossil fuels.

Among the portfolio of biofuels, biodiesel is considered to be the best alternate for diesel fuel as a result of its high net energy returns (~90%). Moreover, biodiesel has been recognized around the world as a green fuel and considered as the best option in contrast to diesel fuel. Citing the eco-friendly nature of the biodiesel, central and state governments of various countries are framing policies to enlarge its utilization [5]. Biodiesel is considered a renewable fuel, which produces lesser greenhouse gas emissions and has a par excellence lubricating property. Also, biodiesel is inherently free of sulfur unlike petroleum-based diesel [6]. Biodiesel is an alkyl ester of long-chain fatty acids derived from the reaction between oil/fat and alcohol. Industrially, biodiesel is produced by transesterification of oil and alcohol using a base catalyst like KOH or NaOH [7]. This process is limited by low mutual solubility between the oil and alcohol phases. These phases are nonhomogeneous or immiscible in each other, limiting the mass transfer through interphase. This raises the need for a phase transfer catalytic process involving the formation of an intermediate complex that can solubilize the organic (oil) and inorganic (alcohol) phases.

The commercialization of biodiesel on a large scale is limited by the high cost of production. The high cost of production using current technology is due to its requirement of high-quality feedstock and also its intolerance to impurities (free fatty acid (FFA) and water) present in the low-quality feedstock. The common feedstock for biodiesel production involves edible and non-edible oils. Pure fatty acids are costlier compared to edible oils which in turn are costlier than non-edible oils. Moreover, the widespread use of edible oils for fuel may elevate the crisis of food against the comfort of fuel. Therefore, non-edible and waste vegetable oils are the most preferred feedstock to lower biodiesel production costs. However, non-edible oils may have higher amount of FFA content than edible oils. The FFA present in oils reacts with the alkali to form soap which results in the difficult product purification and low biodiesel yield [8]. Subsequently, it is essential to restrict the FFA content present in feed oil preceding the base-catalyzed transesterification reaction. Therefore, need arises to adopt certain reaction criterion which governs the adaptability of the single-step (only transesterification) or two-step (esterification to

lower FFAs followed by transesterification) process based on the FFA content. In a two-step process, esterification plays a major role in limiting FFA content and makes the oil with high FFA content useful to produce biodiesel.

Esterification of non-edible oils containing high FFA content is carried out using concentrated sulfuric acid in a homogeneous form as a catalyst. However, homogeneous acid is usually nonrecyclable and inflicts severe environmental issues and corrosion problems [9]. Besides, it was observed that a substantial amount of water effluents is produced during the washing of homogeneously catalyzed biodiesel and also exhibited a significant product (biodiesel) loss. A high cost of raw material (oil) and all the above-highlighted disadvantages result in the addition of cost for biodiesel production in each stage which is responsible for high biodiesel price. Certainly, the cost of biodiesel production can be lowered by using non-edible and waste vegetable oils. However, the disadvantage of lower solubility between reactants and also environmental hazards involved in the conventional process can only be mitigated using an effective process modification and (or) efficient catalyst.

1.1 Feedstock for Biodiesel Production

The common feedstock for biodiesel production involves various pure fatty acids (palmitic, linoleic, stearic, linolenic, and oleic acids), edible oils (soybean, peanut, rice bran, cottonseed, palm, and sunflower), and non-edible oils (waste vegetables, Karanja, neem, Jatropha, polanga, rubber seed, mahua, palm fatty acid distillates, algal). Biodiesel is typically made by reacting triglyceride (ester of three fatty acids and glycerol molecule) present in vegetable oils with alcohol. High-quality biodiesel can also be produced by reacting pure fatty acids with alcohol [6, 10, 11]. However, generally complex heterogeneous blends of various fatty acids known as vegetable oils are the preferable sources to produce biodiesel because of their low cost than pure fatty acids. Usually, vegetable oils are categorized into two groups such as edible and non-edible oils based on their composition, source, and application. Edible oils like palm, peanut, rice bran, soybean, and sunflower are widely used to produce high-quality biodiesel. However, the widespread use of edible oils for fuel may elevate the crisis of food against the comfort of fuel [12]. The use of edible oils for biodiesel production increases the cost of biodiesel which also limits its commercialization. Waste vegetable oils and non-edible oils like Karanja, Jatropha, date seed, castor, rubber seed, mahua, some nontraditional seeds, and algae oils are preferred sources to produce biodiesel. In general, non-edible and waste vegetable oils contain a high amount of FFAs and water but later have an advantage of no gum content in the oil. Thus, non-edible and waste vegetable oils are low-quality oils which are mostly available at a lower cost, and using these oils in biodiesel production lowers the cost of biodiesel to a substantial extent [13]. Therefore, non-edible oils and waste vegetable oils are the highly preferred feedstock to produce biodiesel, and their composition has been given in Table 1.

Table 1 Fatty acid composition of waste vegetable oil and Karanja oil

S. no.	Fatty acids	% Mass	
		Waste vegetable oil	Karanja oil
1	Caprylic (C8:0)	0.02	–
2	Capric (C10:0)-	0.02	–
3	Lauric (C12:0)-	0.22	–
4	Myristic (C14:0)-	0.79	–
5	Palmitic (C16:0)-	44.10	4.20
6	Palmitoleic (C16:1)	0.21	–
7	Stearic (C18:0)-	4.12	2.90
8	Oleic (C18:1)-	39.00	66.80
9	Linoleic (C18:2)-	10.52	17.60
10	Linolenic (C18:3)-	0.13	–
11	Arachidic (C20:0)-	0.15	3.80
12	Behenic (C22:0)-	0.06	4.70
13	Lignoceric (C24:0)-	0.05	–
14	Others	0.61	–

1.2   Conventional Catalysts for Biodiesel Production

Industrial-scale biodiesel is produced by transesterification of oil and alcohol using a conventional base catalyst like KOH or NaOH which requires high-quality feedstocks [7]. Reaction like transesterification of vegetable oil with alcohol or esterification of FFA with alcohol is used to produce biodiesel. Principally, the only transesterification of triglycerides (a single-step process or a two-step process) is used to produce high-quality biodiesel [5]. A single-step base-catalyzed transesterification process can be used when high-quality vegetable oil whose FFA content is less than 3 wt% is available. In any case, a two-step process that can be carried out in either of two approaches is preferred for oils containing greater than 3 wt% FFA. In one approach, FFAs in the oil undergo esterification first to produce an esterified product, and in a due course, triglycerides present in the esterified oil are subjected to transesterification to give high-quality biodiesel. This approach is suitable only when FFA in the oil is not much higher than the FFA limit set for the single-step process. In another approach, FFAs are produced first by hydrolysis of triglycerides present in vegetable oil, and subsequently, biodiesel is produced by esterification of FFAs. This approach is particularly useful when utilizing oils containing a very high amount of FFA like jojoba oil, date seed oil, mahua, palm fatty acid distillates, Jatropha oil, and Karanja oil to produce biodiesel. Therefore, the conventional transesterification and esterification processes and their disadvantages in handling the sustainable and cheaper feedstocks are discussed in subsequent sections.

1.3 Base-Catalyzed Transesterification

Many types of catalysts like alkali, acid, and enzymes can be used for biodiesel production. Among these, the alkali-catalyzed transesterification is the most widely used since it gives a high yield at mild reaction conditions [14]. The mechanism of alkali-catalyzed transesterification reaction is shown in Fig. 1. The overall transesterification reaction is in which 1 mole of triglyceride (the major component of oil) reacts with 3 moles of alcohol (e.g., methanol) to form 3 moles of fatty acid alkyl ester or fatty acid methyl ester or biodiesel and 1 mole of glycerol (Fig. 1a). The transesterification mechanism involves the formation of alkoxide and protonated base by mixing alcohol with a base catalyst (Fig. 1b). The formed alkoxide initiates the nucleophilic attack on the triglyceride molecule, and on exchanging ions, they form one molecule of biodiesel and diglyceride, respectively (Fig. 1c) [15, 16]. Similarly, the same approach is followed in converting diglyceride to monoglycerides (Fig. 1d) and subsequently monoglyceride to biodiesel and glycerol molecules (Fig. 1e).

Conventional single-step base (KOH and NaOH)-catalyzed transesterification process is popularly used to produce biodiesel on a commercial scale. However, this process is limited by interphase mass transfer and low quality of feedstock.

1.3.1 Interphase Mass Transfer

The mass transfer between oil and methanol phases plays a critical role during the transesterification reaction [17]. Since oil (nonpolar) and alcohol (polar) are two dissimilar species, they suffer from limited solubility in each other [7]. Moreover, Boocock et al. [18–20] confirmed that the base-catalyzed reaction between vegetable oil and methanol is not homogeneous. Due to this non-homogeneity, base-catalyzed transesterification reaction was characterized to be associated with very slow reaction rates at the initial and final stages of the reaction [21, 22]. The slow reaction rates during the initial stage of the reaction are due to the immiscibility of the reactants. At the final stage of the reaction, glycerol being a polar compound formed during the reaction extracts the catalyst, which remains separated from reactants resulting in slow reaction rates. These slow reaction rates at the initial and final stages of the reaction result in the reaction to be slow or would stop the reaction without complete conversion of reactants [21]. Therefore, the mass transfer resistance between phases limits the conventional base-catalyzed transesterification process.

(A) Overall reaction
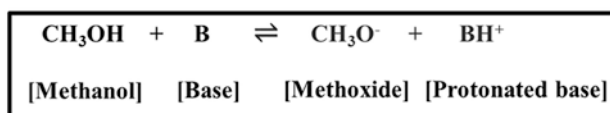
$$CH_3OH \;+\; B \;\rightleftharpoons\; CH_3O^- \;+\; BH^+$$

[Methanol]   [Base]   [Methoxide] [Protonated base]

(B) Formation of methoxide and protonated base catalyst

(C) Nucleophilic attack of methoxide on triglyceride to form biodiesel and diglyceride

Fig. 1 Alkali-catalyzed transesterification reaction (**a–e**). (**a**) Overall reaction. (**b**) Formation of methoxide and protonated base catalyst. (**c**) Nucleophilic attack of methoxide on triglyceride to form biodiesel and diglyceride. (**d**) Nucleophilic attack of the second molecule of methoxide on diglyceride. (**e**) Nucleophilic attack of the third molecule of methoxide on monoglyceride

$$\begin{array}{c}
CH_2\text{-O-}\overset{\overset{\displaystyle O}{\|}}{C}\text{-R}_1\\
|\\
CH\text{-O-}\overset{\overset{\displaystyle O}{\|}}{C}\text{-R}_2\\
|\\
CH_2\text{-OH}
\end{array}
\quad + \quad CH_3O^- \quad \rightleftharpoons \quad
\begin{array}{c}
CH_2\text{-O-}\overset{\overset{\displaystyle O}{\|}}{C}\text{-R}_1\\
|\\
CH\text{-O}^-\\
|\\
CH_2\text{-OH}
\end{array}
\quad + \quad CH_3\text{-}\overset{\overset{\displaystyle O}{\|}}{C}\text{-OR}_2$$

[Biodiesel]

$$\begin{array}{c}
CH_2\text{-O-}\overset{\overset{\displaystyle O}{\|}}{C}\text{-R}_1\\
|\\
CH\text{-O}^-\\
|\\
CH_2\text{-OH}
\end{array}
\quad + \quad BH^+ \quad \rightleftharpoons \quad
\begin{array}{c}
CH_2\text{-O-}\overset{\overset{\displaystyle O}{\|}}{C}\text{-R}_1\\
|\\
CH\text{-OH}\\
|\\
CH_2\text{-OH}
\end{array}
\quad + \quad B$$

[Monoglyceride]

(D) Nucleophilic attack of the second molecule of methoxide on diglyceride

$$\begin{array}{c}
CH_2\text{-O-}\overset{\overset{\displaystyle O}{\|}}{C}\text{-R}_1\\
|\\
CH\text{-OH}\\
|\\
CH_2\text{-OH}
\end{array}
\quad + \quad CH_3O^- \quad \rightleftharpoons \quad
\begin{array}{c}
CH_2\text{-O}^-\\
|\\
CH\text{-OH}\\
|\\
CH_2\text{-OH}
\end{array}
\quad + \quad CH_3\text{-}\overset{\overset{\displaystyle O}{\|}}{C}\text{-OR}_1$$

[Biodiesel]

$$\begin{array}{c}
CH_2\text{-O}^-\\
|\\
CH\text{-OH}\\
|\\
CH_2\text{-OH}
\end{array}
\quad + \quad BH^+ \quad \rightleftharpoons \quad
\begin{array}{c}
CH_2\text{-OH}\\
|\\
CH\text{-OH}\\
|\\
CH_2\text{-OH}
\end{array}
\quad + \quad B$$
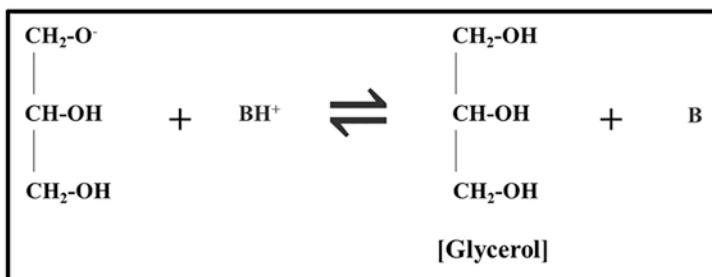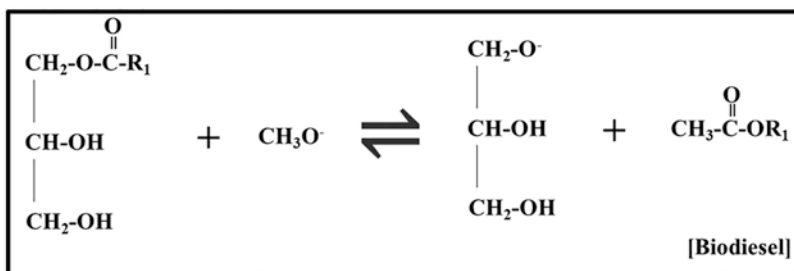
[Glycerol]

(E) Nucleophilic attack of the third molecule of methoxide on monoglyceride

Fig. 1 (continued)

1.3.2 Sensitivity to Feedstock

Biodiesel production using waste vegetable and non-edible oils can lower the biodiesel cost substantially. However, to produce biodiesel through a single-step base-catalyzed transesterification route, high-quality oil without FFA and water is required since the presence of water and FFA in the feedstock is counterproductive. The presence of water fragments the triglyceride to diglyceride (Fig. 2a), diglyceride to monoglyceride (Fig. 2b), and monoglyceride to glycerol (Fig. 2c) and a molecule of FFA in each step as shown in Fig. 2. Consequently, the FFA reacts with the base catalyst and forms soaps by saponification as shown in Fig. 3 which counters the transesterification and complicates product purification.

Since transesterification is the main reaction mechanism in biodiesel formation, hydrolysis of triglycerides and saponification of FFAs are considered as side reactions [5, 7, 8]. The hydrolysis reaction fragments the triglycerides and forms FFAs which are the main reactants for saponification resulting in the formation of soaps ultimately. The formed soap particles form an emulsion with the water present within the solution and result in the formation of gels which increases the viscosity of reactants [23]. The increased viscosity and a lower amount of triglycerides for transesterification result in the lower biodiesel yield [24]. Moreover, the formed soaps obstruct the reaction progress and cause lower yield of biodiesel. Furthermore, due to the presence of soaps, the loss of produced biodiesel to glycerol (by-product) phase may be increased during the washing of crude biodiesel [7, 8, 25]. The soap present in the ester phase tends to gather at the surface of the two liquids [26]. During washing, the soap particles trapped inside the ester layer form emulsion with the water which causes hindrance in the purification of ester and results in the loss of biodiesel yield [27]. This results in a higher water requirement for washing crude biodiesel during purification whose cost indeed adds to the total cost of biodiesel production. Therefore, the sensitivity to impurities in feedstock limits the use of a single-step base-catalyzed transesterification process. The limitations of using a single-step base-catalyzed transesterification process could be overcome by incorporating another solvent or catalyst in the reaction system.

The use of a solvent may offer an advantage to enhance the reaction by initiating the process which could dissolve each ionic and valence species, and because of this, the basic strength and nucleophilicity of the anions effectively increase. One way to hypothesize this phenomenon is by using the very fact that reducing the intensity of ion-pairing and eliminating the associated impact of a hydroxylic solvent (like methanol) mostly increase the basic strength and nucleophilicity of anions [7, 28]. Therefore, this increased nucleophilicity will enhance the reaction to a greater extent. The solvents which exhibit this type of phenomenon are phase transfer catalysts and dipolar aprotic solvents. The use of dipolar aprotic solvents like dimethylformamide (DMF) or dimethyl sulfoxide (DMSO) can improve the nucleophilicity and basic strength [29, 30]. However, these solvents aren't readily separable from the reaction product, and their separation might require the following various other processes to purify crude biodiesel:
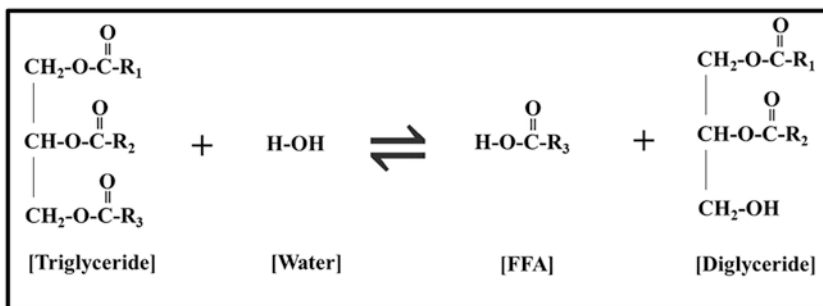
(A) Triglyceride fragment to free fatty acid and diglyceride
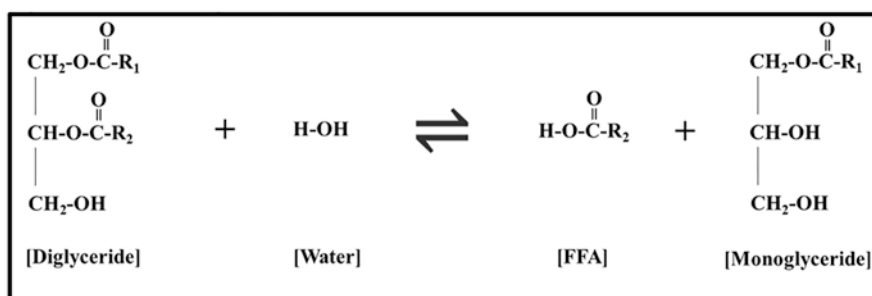
(B) Diglyceride fragment to free fatty acid and monoglyceride
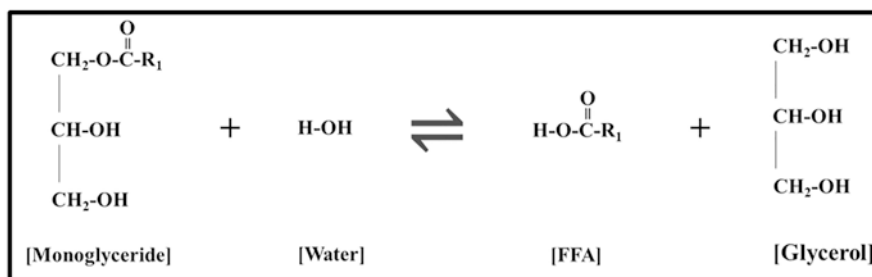
(C) Monoglyceride fragment to free fatty acid and glycerol

Fig. 2 Hydrolysis reaction of triglyceride (**a–c**). (**a**) Triglyceride fragment to free fatty acid and diglyceride. (**b**) Diglyceride fragment to free fatty acid and monoglyceride. (**c**) Monoglyceride fragment to free fatty acid and glycerol

AOH   +   H-OH   ⇌   A$^+$ +   OH

[Alkali catalyst]   [water]

$+$

$$\underset{H-O-C-R_1}{\overset{O}{\parallel}}$$

[FFA]

Where,
A = Alkali group (Na or K)

⇅

$$\underset{AO-C-R_1}{\overset{O}{\parallel}}   +   H-OH$$

[Alkali Soap]
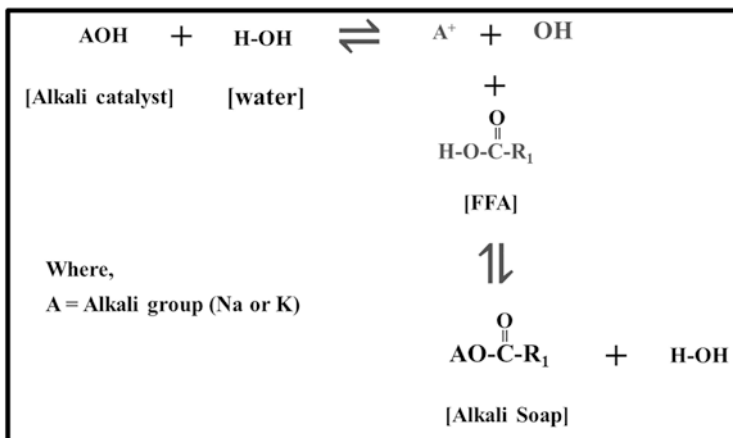
Fig. 3 Saponification reaction of free fatty acids

1. Washing with a larger excess volume of water
2. Distillation of the used solvent and subsequent centrifugation, filtration, and further washing of the by-product
3. Extraction using a unique water-immiscible solvent in multiple stages, washing with water, and subsequent evaporation of the solvent used for extraction

Such procedures are interminable, tedious, inefficient, and not eco-friendly by generating a large volume of effluent containing harmful solvents which are difficult to recycle.

1.4   Acid-Catalyzed Esterification

Since single-step base-catalyzed transesterification is sensitive to FFA in feedstock, the FFA content in the feed oil needs to be lowered before transesterification reaction [5]. The FFA content in the feed oil can be lowered using several pretreatment techniques such as neutralization and stripping off FFA as soap, distillation, and esterification. In the first two techniques (neutralization and stripping and distillation), there will be a loss of FFA as soaps and waste, whereas in the esterification process, FFA can be converted to biodiesel, and thus esterification is the most efficient process to reduce FFA content of oil [13].

Esterification is a reversible reaction carried out in the presence or absence of the acid catalyst (homogeneous/heterogeneous) in which the equimolar amount of fatty acid alkyl ester (biodiesel) and water can be produced by reacting equimolar quantities of FFA and alcohol [5] as shown in Fig. 4a. The esterification mechanism involves the protonation of the carboxylic group to give carbocation (Fig. 4b). Then the methanol initiates the nucleophilic attack on the carbocation as soon as it is

$$H\text{-}O\text{-}\overset{\overset{O}{\|}}{C}\text{-}R_1 \quad + \quad CH_3\text{-}OH \quad \underset{}{\overset{H^+}{\rightleftharpoons}} \quad R_1\text{-}\overset{\overset{O}{\|}}{C}\text{-}OCH_3 \quad + \quad H\text{-}OH$$

[FFA]   [Methanol]   [Biodiesel]   [Water]

(A) Overall reaction

$$H\text{-}O\text{-}\overset{\overset{O}{\|}}{C}\text{-}R_1 \quad \rightleftharpoons \quad \left[H\text{-}O\text{-}\overset{\overset{+OH}{\|}}{C}\text{-}R_1 \quad \rightleftharpoons \quad H\text{-}O\text{-}\overset{\overset{OH}{|}}{\underset{+}{C}}\text{-}R_1 \right]$$

[FFA]   [Carbocation]

(B) Protonation of the carboxylic group of FFA to form a carbocation

$$H\text{-}O\text{-}\overset{\overset{OH}{|}}{\underset{+}{C}}\text{-}R_1 \quad + \quad CH_3OH \quad \rightleftharpoons \quad \begin{matrix} OH \\ | \\ R_1\text{-}C\text{-}OH \\ | \\ +O\text{-}H \\ | \\ CH_3 \end{matrix}$$

[Tetrahedral Intermediate]

(C) Nucleophilic attack of methanol on carbocation

$$\begin{matrix} OH \\ | \\ R_1\text{-}C\text{-}OH \\ | \\ +O\text{-}H \\ | \\ CH_3 \end{matrix} \underset{}{\overset{-H^+}{\rightleftharpoons}} \begin{matrix} OH \\ | \\ R_1\text{-}C\text{-}OH \\ | \\ O \\ | \\ CH_3 \end{matrix} \underset{}{\overset{H^+}{\rightleftharpoons}} \begin{matrix} H \quad H \\ O^+ \\ | \\ R_1\text{-}C\text{-}OH \\ | \\ O \\ | \\ CH_3 \end{matrix} \rightleftharpoons \begin{matrix} H \\ O \\ \| \\ R_1\text{-}C\text{-}OCH_3 \end{matrix} + H_2O$$

$$\updownarrow -H^+$$

$$R_1\text{-}\overset{\overset{O}{\|}}{C}\text{-}OCH_3$$

[Biodiesel]

(D) Formation of biodiesel

Fig. 4 Esterification reaction mechanism (**a**–**d**). (**a**) Overall reaction. (**b**) Protonation of the carboxylic group of FFA to form a carbocation. (**c**) Nucleophilic attack of methanol on carbocation. (**d**) Formation of biodiesel

formed and results in a tetrahedral intermediate (Fig. 4c). Finally, the formed tetrahedral intermediate results in biodiesel and water with a series of protonation and deprotonation steps (Fig. 4d).

It is possible to produce biodiesel using non-edible oils having high FFA content using an acid-catalyzed esterification process which can catalyze both esterification and transesterification simultaneously [5, 31]. Conventionally, concentrated sulfuric acid in a homogeneous form is used as the esterification catalyst. However, homogeneous acid is usually non-recoverable and nonrecyclable; hence, utilization of this acid imposes severe environmental issues and corrosion problems, generates large volumes of unprocessed effluents, and causes loss of product during washing [5, 13]. To mitigate these disadvantages, a non-catalytic esterification route and heterogeneous catalytic processes can be explored.

1.5 Kinetics of Biodiesel Production

The kinetics of the conventional homogeneous base-catalyzed transesterification was determined by various researchers [32–35]. Consider the overall transesterification reaction (Eq. 1) in which vegetable oil is assumed to be entirely composed of triglycerides:

$$\text{Triglyceride}\,(A) + 3\text{Methanol}\,(B) \underset{k_r}{\overset{k_f}{\rightleftharpoons}} 3\text{Biodiesel}\,(C) + \text{Glycerol}\,(D) \qquad (1)$$
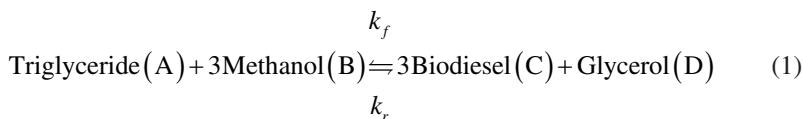
Rate expression can be written as

$$-r_A = k_f C_A^\alpha C_B^\beta - k_r C_c^\gamma C_D^\delta \qquad (2)$$

Mole balances can be written as

$$C_A = C_{Ao}\,(1 - X_A), \quad C_B = C_{Ao}\,(m - 3X_A) \quad C_C = 3C_{Ao}X_A \quad C_D = 3C_{Ao}X_A \qquad (3)$$

where m is the ratio of C_{Bo}/C_{Ao}.

Combining Eqs. (2) and (3) gives

$$\frac{dX_A}{dt} = k_f C_{Ao}^{(\alpha+\beta-1)}\,(1 - X_A)^\alpha\,(m - 3X_A)^\beta - 3^\gamma k_r C_{Ao}^{(\gamma+\delta-1)} X_A^{(\gamma+\delta)} \qquad (4)$$

The parameters α, β, γ, and δ are the order of the reaction for triglyceride, methanol, biodiesel, and glycerol, respectively, and are independent of the reaction conditions.

Similarly, the esterification reaction can be represented as

$$\text{FFA}(O) + \text{Methanol}(M) \underset{k_r}{\overset{k_f}{\rightleftharpoons}} \text{Biodiesel}(F) + \text{Water}(W) \tag{5}$$
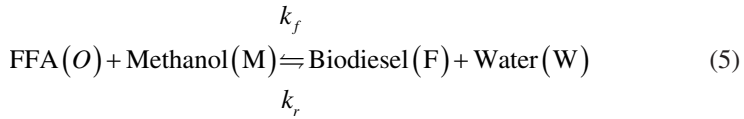
Many studies used a solid catalyst to produce biodiesel and modeled the experimental data using pseudo-homogeneous models [10, 36, 37]. For example, Cardoso et al. [10] used tin(II) chloride dihydrate (SnCl$_2$. 2H$_2$O) to produce biodiesel from oleic acid and ethanol and modeled the kinetics based on pseudo-homogeneous assumption. They assumed first-order kinetics and considered only the forward reaction with a rate expression given in Eq. (6):

$$-r_o = k_f C_O \tag{6}$$

Esterification of oleic acid with methanol was carried out by Tesser et al. [36] and used the ion-exchange polymeric resin (Relite CFS). The data were modeled considering equilibrium reaction and second-order-type pseudo-homogeneous rate expression (Eq. 7). Similarly, Zubir and Chin [37] carried out the ethanolysis of oleic acid and used a similar expression to model the kinetics:

$$-r_o = \left(k_f C_O C_M - k_r C_F C_W \right) C_{\text{Catalyst}} \tag{7}$$

The two popular kinetic models used to describe heterogeneously catalyzed esterification reaction are Langmuir-Hinshelwood-Hougen-Watson (LHHW) and Eley-Rideal (ER) [14, 38, 39]. Unlike homogeneous kinetic models, these models are characterized by an increased number of temperature-dependent parameters, usually one for each reacting species, representing the adsorption phenomenon on the catalyst surface.

1.6 *Phase Transfer Catalysis*

Phase transfer catalysis is a process that facilitates the interphase mass transfer of species present in two immiscible phases to accelerate the reaction [17]. The chemical compound which is involved in this process is referred to as phase transfer catalyst (PTC). Phase transfer catalysis is the widely adopted technique in many industrial processes owing to their faster, cleaner reactions and greatly simplified ramp-up which do not necessitate strict anhydrous conditions. In the system of two mutually insoluble phases (liquid-liquid or solid-liquid), the distinguishable mechanism of PTC is that it forms an intermediate complex [7]. This intermediate complex is mostly soluble in an organic compound and facilitates the transfer of inorganic ions into the organic phase easily. Such techniques are notably helpful in reactions that are base-catalyzed and associated with nucleophilic displacements.

Since oil and methanol are two mutually insoluble phases and transesterification is a base-catalyzed process that is associated with a nucleophilic attack mechanism, using PTC can enhance the process and dampens the technical disadvantages associated with the conventional biodiesel production process.

The efficacy of most of the conventional homogeneous reactions depends on the mutual solubility of the dissimilar species (organic and inorganic) participating in the reaction [17, 40]. In contrast, the reaction rates will be very low during direct organic synthesis reactions in a reaction system of sparingly soluble reactants carried out using conventional catalysts. This disadvantage raises the need for PTC which can offer a distinct route to mutually solubilize the dissimilar species. During phase transfer catalysis, PTC forms a complex with the reactant present in phase 1, and this complex diffuses into another reactant present in phase 2 and reacts. After the reaction, PTC diffuses back to phase 1 and promotes the process further. Since the vegetable oil and methanol are mutually insoluble and form distinct phases, the concentration of two reactants in any single phase will be very low for good reaction rates. Moreover, strict anhydrous conditions are required by the transesterification using base catalyst whose reaction rates are frequently considered to be controlled by diffusion and characterized by a slow reaction rate. Therefore, enhancing the mass transfer between the phases can overcome the difficulty of the reaction between them. There are several ways to overcome the mass transfer limitation and enhance the contact between two phases such as the use of large excess alcohol, mechanical mixing, using polar aprotic solvents or inert cosolvent, ultrasonic and hydrodynamic cavitation, and supercritical conditions. However, these techniques are associated with one or more drawbacks like the high cost of solvent or require a very excessive amount of solvents, the high cost of operations, generation of huge amounts of effluents, and higher capital costs [22, 41]. It was evident that eliminating the mass transfer limitations using cosolvent (which forms pseudo-homogeneous phase) or catalyst-free processes (conducted at high temperature and pressure), faster transesterification rates could be achieved [18–20]. So, phase transfer catalysis is also a promising technique that can be explored to enhance the reaction rates between reactants forming two immiscible phases. There are many types of PTCs such as onium salts (quaternary ammonium, sulfonium, phosphonium, or arsonium salts), crown ether groups, and cryptates [17]. Among those quaternary ammonium salts are most widely used because of the less interference of their ions in reactions [17, 42] and also they are much cheaper than other PTCs [43]. Tetramethylammonium (TMA) cations are a type of quaternary ammonium salts known to possess properties of PTC, and they are cations with four methyl groups attached to the central nitrogen atom. These cations are associated with some anionic groups such as bromide, iodide, hydroxide, and chloride. There are many studies which used PTCs (such as tetramethylammonium bromide, tetramethylammonium hydroxide, cetyltrimethylammonium bromide, tetrabutylammonium hydroxide, tetrabutylammonium acetate, tetrabutylammonium nitrate, benzyl trimethyl ammonium hydroxide, tetrabutylammonium hydrogen sulfate, 18-crown-6 ether, and choline hydroxide) as a process enhancer for conventional base-catalyzed transesterification process [7, 21, 22, 44, 45]. All this literature reports the improved reaction and enhanced

production and properties of the biodiesel. However, tetramethylammonium bromide (TMAB) was never used for this purpose as per our knowledge, and we propose TMAB as a new PTC to enhance the conventional transesterification process.

2 Biodiesel from Waste Vegetable Oil

The waste vegetable oil contains contaminants that are removed by fiber cloth placed on a Buchner funnel. Thereafter, the oil was heated at 120 °C for 45 min with continuous stirring to remove the moisture present in the oil. A typical experimental setup for the transesterification reaction is shown in Fig. 5. It consists of a three-necked round-bottom flask with a condenser fitted to one neck. Cooling water is circulated through the condenser to condense methanol vapors formed during the reaction. The second neck is fitted with a thermometer to measure the temperature of the reaction mixture. The third neck is used to introduce the reactants and to withdraw the samples at frequent time intervals. A plate heater with a magnetic stirrer was used to heat the reaction content in the flask at a uniform stirring rate.

Then the experiments were carried out at various methanol to oil molar ratios using KOH and NaOH as catalysts and tetramethylammonium bromide (TMAB) as phase transfer catalyst (PTC). The temperature of the reaction was maintained at 65 °C. After completion of the reaction (typically after 90 min), by-product glycerin was separated from the ester layer (biodiesel), and the biodiesel was purified by washing with hot water [12].
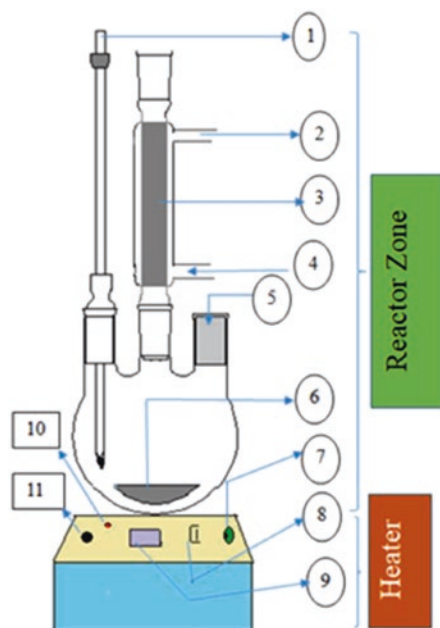
Nomenclature:

Reactor Zone

1) Thermometer
2) An Outlet for cooling water
3) Reflux condenser
4) Inlet for cooling water
5) Inlet for feed
6) Magnetic stirrer

Heater

7) Controller for agitation speed
8) On/off power switch
9) Speed indicator
10) On/off power indicator
11) Controller for temperature

Fig. 5 Schematic of the experimental setup [12]

2.1   Effect of TMAB

The transesterification of waste vegetable oil was conducted in the presence of TMAB using NaOH/KOH catalysts. It was observed that the addition of tetramethylammonium bromide lowers the methanol requirement. The methanol to oil molar ratio was reduced from 9:1 to 7.5:1 as given in Fig. 6. The lower methanol requirement is due to the increased solubility of the intermediate complex in the presence of tetramethylammonium bromide as compared to the conventional process.

Moreover, the washability characteristics and properties of the final biodiesel were enhanced. The reason behind improved washability is because of the assimilation of water content during the reaction by tetramethylammonium bromide which is a hygroscopic quaternary ammonium salt. In the conventional process (alkali-catalyzed transesterification reaction), the presence of water makes the reaction partially shift toward hydrolysis and saponification and makes the process vulnerable [7]. Therefore, adding TMAB to the process assimilates the water content, and due to this, soap formation is suppressed. Diminished soap formation can be directly related to the less water requirement for washing, and the crude biodiesel can be washed easily. This makes the overall process with TMAB as PTC relatively more economical than the existing conventional and commercial process.
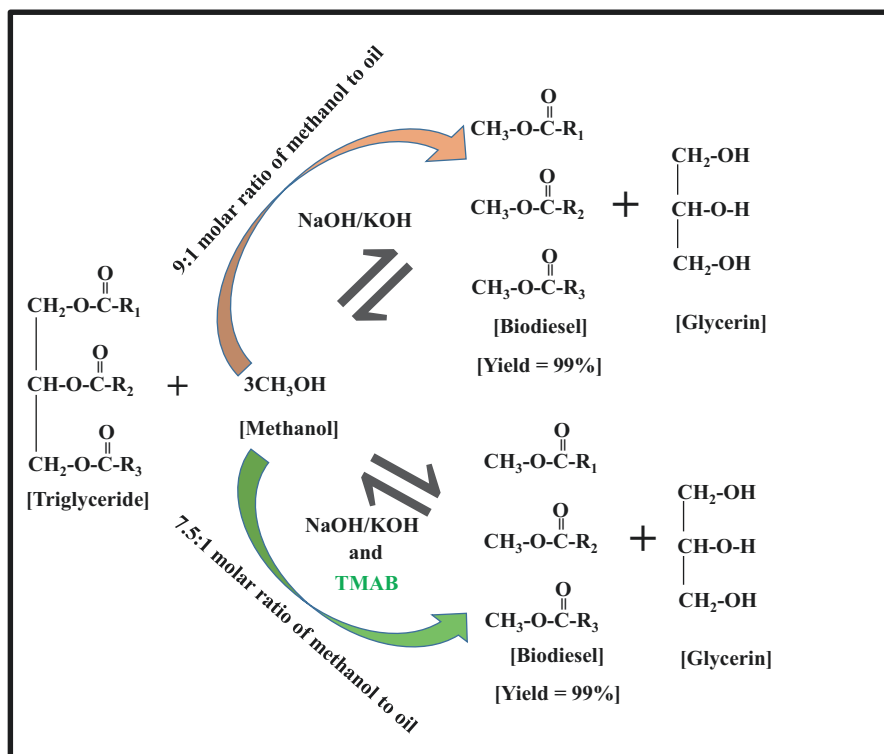
Fig. 6 Effect of tetramethylammonium bromide (TMAB) on biodiesel production

3   Non-catalytic Process for Biodiesel Production

The non-catalytic processes are the highly focused area in biodiesel production and also known as the thermal processes in which the reaction is carried out at a high-temperature and high-pressure conditions. Usually, they are highly controlled reactions monitored with utmost safety and can mitigate the drawbacks associated with a homogeneous catalyst [46]. The non-catalytic supercritical methanol process explored by many studies achieved a yield of biodiesel as high as 97% in a very short period. However, there are limitations in the supercritical methanol process which limits its commercialization. The limitations of the supercritical process like thermal degradation of esters, higher capital, and operating cost can be mitigated using the non-catalytic subcritical esterification process [47, 48]. Together curbing the limitation of the supercritical process, the ester yield and conversion in the non-catalytic subcritical esterification process are nearly equal to that of other processes. Many studies were already conducted through the non-catalytic route and observed good results. For example, at 270 °C and 200 bar using 1:0.9 rapeseed oil to methanol ratio (v/v), Minami and Sake [49] achieved a product yield of nearly 94%. A 60% conversion of C18 fatty acids non-catalytically was reported by Melo Junior et al. [50] in a short period (60 min) under microwave irradiation. Rani et al. [51] achieved a conversion of ~95% in 5 h using 1:4 Jatropha oil to methanol ratio (w/v), 190 °C, and 27.1 bar. Experiments conducted by Cho et al. [52] with palm fatty acid distillate and methanol achieved a final product acid value of fewer than 0.5 mg KOH/g in 3 h at 290 °C and 8.5 bar. The investigation by Pinnarat and Savage [11] revealed that the non-catalytic esterification under subcritical conditions can be carried out smoothly with the advantage of tolerating a moderate amount of water content in the feed oil. Moreover, they reported that the presence of a moderate amount of water enhances the effectiveness of the subcritical esterification process.

3.1   Experimental Procedure

The details of the experimental setup are available elsewhere [13]. It consists of a small batch reactor of 25 mL capacity made of stainless steel and fitted with a pressure gauge that is placed inside a jacketed vessel. Heating and mechanical agitation were carried out using a magnetic stirrer, and the chiller was used to ensure the constant temperature inside the reactor. There was a provision to introduce the inert gas for maintaining the constant pressure.

The soluble impurities of Karanja oil were removed by washing thoroughly with hot deionized water (~80 °C). Thereafter, the oil was dried and a trace amount of water was removed by treating dried oil with silica gel. The key to the biodiesel production through the non-catalytic route is the maintenance of volumetric filling fraction (f). "f" is given as the volume of reactants charged to the reactor divided by the total reactor volume [13]. The reactant amounts must be selected to meet the required phase equilibrium criteria set by the value of "f" which controls the phases

that coexist at reaction conditions. The value of "f" must be selected in such a way that the reactants remain in the homogeneous phase. A higher value of "f" should be maintained to have a liquid-phase reaction under subcritical conditions. Phase equilibrium calculations were performed using the "*Flash2*" subroutine of Aspen Plus software [11, 13]. The required input for the phase equilibrium calculation in "*Flash2*" subroutine was the composition of feed streams, temperature, and pressure or vapor fraction. The required pressure of the reactor to maintain the reactants in a single phase at a fixed temperature was obtained from the simulation result.

The reactor was charged with appropriate amounts of reactants. Inert gas (argon) was used to maintain the desired pressure inside the reactor. The effect of temperature, reaction time, agitation speed, and oil to methanol ratio on the conversion was studied. The samples were withdrawn at various intervals to analyze acid values (Eq. 8) and the corresponding conversion (Eq. 9) [9, 13]:

$$\text{Acid Value} = \frac{56.1 \times N \times V}{W} \tag{8}$$

where

N is the normality of standard potassium hydroxide solution
V is the volume of standard potassium hydroxide used, mL
W is the weight of the sample, gram

$$\text{Conversion}(\%) = \frac{(\text{Acid Value})_{t=0} - (\text{Acid Value})_{t=t}}{(\text{Acid Value})_{t=0}} \times 100 \tag{9}$$

3.2 Kinetic Modeling and Simulation

The simulation studies have been done for the non-catalytic biodiesel production process to check the commercial viability [13, 53–55]. The required kinetic parameters to simulate the process were calculated by modeling the experimental data. The experimental data was modeled assuming the reaction as reversible (Eq. 10). Further, the reaction was assumed to be pseudo-first order in the forward direction and bimolecular second order in a backward direction. Applying all the above assumptions, a final expression (Eq. 11) for the reaction conversion was obtained:

$$\text{FFA} + \text{M} \underset{k_f}{\overset{k_r}{\rightleftharpoons}} \text{ME} + \text{H}_2\text{O} \tag{10}$$

$$X = \frac{X_e \left[\exp\left(\frac{k_f' t (2 - X_e)}{X_e} \right) - 1 \right]}{\exp\left(\frac{k_f' t (2 - X_e)}{X_e} \right) - (X_e - 1)} \tag{11}$$

Table 2 Estimated kinetic parameters [13]

T °C	X_e	k_f' (min^{-1})	k_r (g/mgKOH min)	R^2
190	0.941	0.295	3.09E-4	0.991
200	0.950	0.372	3.31E-4	0.997
210	0.956	0.469	3.60E-4	0.995
220	0.962	0.641	4.18E-4	0.987

3.2.1 Kinetic Parameters

The experimental results show that a conversion value of FFA nearly 96.21% can be achieved in 7 h at 220 °C using 1:6 oil/methanol ratio (w/v). Then the experimental data were fitted in Eq. (11), and nonlinear regression was done to calculate the kinetic parameters at each temperature. The proposed model was fitted well with experimental data and obtained parameters are given in Table 2.

3.2.2 Process Simulation

A 1050 kg/h capacity esterification process was simulated by incorporating the obtained kinetic parameters into the Aspen Plus software after importing the required databanks and specifying all the species present in the esterification reaction [13]. The overall flow sheet was optimized using the optimization tool of Aspen Plus. The simulation results show that 99.85% oleic acid conversion can be achieved against the experimental conversion of 96.21% Karanja oil. The little deviation in the conversion predicted through simulation and experimental value may be attributed to the difference in reactant choice in simulation and experiment. In simulation, oleic acid was used as a single reactant to represent FFA. However, in experiments, Karanja oil was used whose FFA may contain a complex blend (homogeneous/heterogeneous) of various fatty acids.

4 Heterogeneous Catalytic Process for Biodiesel Production

Solid acid catalyst (SAC) is especially important when employing low-quality oils with FFA content for biodiesel production. There were many SACs used for biodiesel production such as protonated-Nafion, sulfated zirconia, Amberlyst, and niobic acid. However, these catalysts are associated with many disadvantages such as fast deactivation, high cost of synthesis, poor stability, small pore size, low acid density, low porosity, and usually hydrophilic which results in poor tolerance toward the water [56]. Moreover, they are not much suitable for esterification reaction because their activity decreases in the presence of water, and water is one of the products of the esterification reaction. For example, because of low protonic acid densities in the case of zeolites and niobic acid, they tend to lose their activity more

easily in the presence of water. On the other hand, higher amounts of protonic groups are present in Nafion, but their catalytic activity is very much lower than the conventional catalyst, concentrated sulfuric acid [6, 56]. Owing to these disadvantages, a new class of low-cost carbon-based catalysts were developed which offer an environmentally benign and economically feasible biodiesel production process.

The low-cost alternative SACs for the high-cost traditional SACs are carbon-based SACs derived from various natural and waste materials. The low-cost carbon-based SACs which show high potential for esterification can be derived using sugars (glucose and sucrose), polysaccharides (starch and cellulose), and biomass (coconut shell, bamboo, wood powder, lignin, and bagasse). Owing to various other prolific applications and higher cost of sugars and polysaccharides, more attention was given to the environmentally benign and cheaper carbon alternatives like biomass. Therefore, much research was still in progress to find various potential waste biomass materials and their transformation to value-added products. As a part of this novel approach, corncob was used to synthesize SAC for biodiesel production [5].

4.1 Corncob-Based Catalyst

A fresh corncob was made free from kernels, sun-dried, ground, and screened to a size between 72 and 100 mesh numbers. To increase the surface area of carbon, phosphoric acid was impregnated at various ratios for different intervals of time and kept for soaking at room temperature. Then the samples were carbonized and washed thoroughly using dilute HCL and hot deionized water to remove phosphates and polyphosphates formed on the surface. Finally, the carbonized samples were sulfonated using the concentrated sulfuric acid at various temperatures for different intervals of time in the presence of an inert atmosphere [5]. A detailed parametric study was done involving all the catalyst preparation variables such as impregnation time and ratio, carbonization time and temperature, and sulfonation time and temperature. The final synthesized catalyst was analyzed qualitatively using FTIR for the presence of various functional groups ($-SO_3H$, $-COOH$, and $-OH$). The structural properties of the catalyst were evaluated by X-ray diffraction (XRD). The surface area, average pore diameter, pore volume, and pore size distribution were estimated using adsorption-desorption isotherm data fitted to Brunauer-Emmett-Teller (BET) equation.

A three-necked round-bottom flask of 250 mL capacity was fitted with a Dean and Stark apparatus and used to test the catalyst activity for esterification of oleic acid and methanol. The reaction was carried out at 338 K and 1:9 oleic acid to methanol molar ratio using 10 wt% catalyst [5]. The optimal catalyst synthesis parameters were found to be as impregnation time = 5 h and ratio = 1, carbonization time = 8 h, and temperature = 723 K and sulfonation time = 15 h and

temperature = 393 K. The catalyst synthesized at optimum conditions gave maximum conversion (~95%) of oleic acid due to the highest total acid density (5.56 mmol/g), surface area (641 m^2/g), and mesoporous structure. Further, it was observed that the synthesized catalyst may be reused up to 20 cycles after washing with n-hexane.

5   Conclusions

Waste vegetable oils and non-edible oils are the best feedstock for biodiesel production to lower the cost and to avoid the ethical issues in using virgin vegetable oils. Moreover, to dampen the disadvantages of the conventional biodiesel production processes such as limited interphase mass transfer, sensitivity to free fatty acids in the feedstock, slow reaction rates, and rigorous anhydrous conditions, a phase transfer catalyst can be explored. Conventional single-step base (KOH and NaOH)-catalyzed transesterification process requires free fatty acid content in the oil to be less than 3 wt%. Waste vegetable oils contain water, and a slightly higher amount of free fatty acids is not a good feedstock for biodiesel production through the conventional route. The addition of phase transfer catalysts such as TMAB can enhance the mass transfer between the reactants and lower down the methanol requirement.

Non-edible oils containing a very high amount of free fatty acids (usually much greater than 3 wt%) are also not suitable for biodiesel production through the conventional route. The addition of TMAB enhances the mass transfer between the reactants which results in a higher yield of biodiesel. However, due to the presence of a very high amount of free fatty acids in non-edible oils, there is a large tendency of reaction between the FFA and the base catalyst rather than the reaction between triglycerides and methanol or free fatty acid and methanol. The addition of TMAB does not offer any advantage in such cases. Therefore, the content of free fatty acids in the oil needs to be reduced before transesterification. This raises the need for a two-step biodiesel production process in which the first step would be esterification. Among various techniques, esterification is the volume-efficient process to lower the free fatty acids and uses concentrated sulfuric acid in a homogeneous form. To mitigate the drawbacks of a conventional homogeneous esterification process, a non-catalytic esterification route can be explored.

Concentrated sulfuric acid is associated with several drawbacks, and the non-catalytic route requires elevated reaction conditions which are associated with the high cost of production. Due to these drawbacks, research efforts are focused on the low-cost solid acid catalysts, which offer an environmentally benign and economically feasible biodiesel production process. The combination of low-quality feedstock and mild reaction conditions can lower the biodiesel cost to a substantial extent. Moreover, the solid acid catalysts like novel corncob-based solid acid catalyst offer huge eco-friendly benefits together with the recyclability and reusability.

References

1. Apergis N, Payne JE (2012) Renewable and non-renewable energy consumption-growth nexus: evidence from a panel error correction model. Energy Econ 34:733–738
2. Suman P, Meghavathu D, Sridevi V, Hussain Z (2018) Desalination studies on two single sloped solar stills with heat absorbing material on aluminium basin. In: Emerging trends in engineering, science and technology for society, energy and environment. CRC, Taylor & Francis Group, Boca Raton, FL. ISBN:978-0-8153-5760-5
3. Sarin A (2012) Biodiesel: production and properties. Royal Society of Chemistry, Cambridge. ISBN: 978-1-84973-472-1
4. Demirbas A (2009) Progress and recent trends in biodiesel fuels. Energ Conver Manage 50:14–34
5. Hussain Z, Kumar R (2018) Synthesis and characterization of Novel Corncob-based solid acid catalyst for biodiesel production. Ind Eng Chem Res 57(34):11645–11657
6. Narkhede N, Patel A (2013) Biodiesel production by esterification of oleic acid and transesterification of soybean oil using a new solid acid catalyst comprising 12-tungstosilicic acid and zeolite hβ. Ind Eng Chem Res 52:13637–13,644
7. Hussain Z, Meghavathu D, Kumar R (2018) Effect of quaternary ammonium salt addition to conventional biodiesel production. Int J Eng Technol 7(4.5):220–223
8. Devi KG, Meghavathu D, Velluri S, Mehtha CC, Hussain Z (2015) Qualitative production of biodiesel using waste vegetable oil. i-Manager's J Fut Eng Technol 10:1–11
9. Hussain Z, Kumar R (2018) Esterification of free fatty acids in Karanja oil using Novel Corncob-derived solid acid catalyst. Mater Today Proc 5(9):18045–18051
10. Cardoso AL, Neves SCG, Da Silva MJ (2008) Esterification of oleic acid for biodiesel production catalyzed by $SnCl_2$: a kinetic investigation. Energies 1:79–92
11. Pinnarat T, Savage PE (2010) Noncatalytic esterification of oleic acid in ethanol. J Supercrit Fluids 53:53–59
12. Hussain Z, Kumar R, Meghavathu D (2018) Glimpses of dynamic biodiesel product pricing model. Int J Eng Technol 7(4.5):224–227
13. Hussain Z, Kumar R (2018) Esterification of free fatty acids: experiments, kinetic modeling, simulation and optimization. Int J Green Energy 15:629–640
14. Lien YS, Hsieh LS, Wu JCS (2010) Biodiesel synthesis by simultaneous esterification and transesterification using oleophilic acid catalyst. Ind Eng Chem Res 49:2118–2121
15. Guan Q, Li Y, Chen Y, Shi Y, Gu J, Li B, Miao R, Chen Q, Ning P (2017) Sulfonated multi-walled carbon nanotubes for biodiesel production through triglycerides transesterification. RSC Adv 7:7250–7258
16. Thangaraj B, Ramachandran KB, Raj SP (2013) Alkaline catalytic transesterification for palm oil biodiesel and characterisation of palm oil biodiesel. J Biofuels 4:79–87
17. Madhusudana Rao J, Rao TB (1994) Asymmetric synthesis using phase transfer catalysis. J Indian Inst Sci 74:373–400
18. Boocock DGB (2003) Single-phase process for production of fatty acid methyl esters from mixtures of triglycerides and fatty acids, United States Patent. Patent No. US6642399B2
19. Boocock DGB, Konar SK, Mao V, Lee C, Buligan S (1998) Fast formation of high-purity methyl esters from vegetable oils. J Am Oil Chem Soc 75:1167–1172
20. Boocock DGB, Konar SK, Mao V, Sidi H (1996) Fast one-phase oil-rich processes for the preparation of vegetable oil methyl esters. Biomass Bioenergy 11:43–50
21. Zhang Y, Stanciulescu M, Ikura M (2009) Rapid transesterification of soybean oil with phase transfer catalysts. Appl Catal Gen 366:176–183
22. Hailegiorgis SM, Mahadzir S, Subbarao D (2011) Reactive extraction of Jatropha curcas l assisted by phase transfer catalyst for the production of biodiesel. In: National Postgraduate Conference, pp 1–5
23. Meng X, Chen G, Wang Y (2008) Biodiesel production from waste cooking oil via alkali catalyst and its engine test. Fuel Process Technol 89:851–857

24. Agarwal M, Singh K, Upadhyaya S, Chaurasia SP (2012) Potential vegetable oils of Indian origin as biodiesel feedstock—an experimental study. Journal of Scientific and Industrial Research (India) 71:285–289
25. Hussain Z, Haider Mohammad B, Kumar R (2016) Usagespecific biodiesel production with and without catalytic booster. Mater Today Proc 3:4115–4120
26. Stavarache C, Vinatoru M, Nishimura R, Maeda Y (2005) Fatty acids methyl esters from vegetable oil by means of ultrasonic energy. Ultrason Sonochem 12:367–372
27. Phan AN, Phan TM (2008) Biodiesel production from waste cooking oils. Fuel 87:3490–3496
28. Guan Q, Shang H, Liu J, Gu J, Li B, Miao R, Chen Q, Ning P (2016) Biodiesel from transesterification at low temperature by $AlCl_3$ catalysis in ethanol and carbon dioxide as cosolvent: process, mechanism and application. Appl Energy 164:380–386
29. Talebian-Kiakalaieh A, Amin NAS, Mazaheri H (2013) A review on novel processes of biodiesel production from waste cooking oil. Appl Energy 104:683–710
30. Meher L, Vidyasagar D, Naik S (2006) Technical aspects of biodiesel production by transesterification—a review. Renew Sustain Energy Rev 10:248–268
31. Vijaya Lakshmi C, Viswanath K, Venkateshwar S, Satyavathi B (2011) Mixing characteristics of the oil-methanol system in the production of biodiesel using edible and non-edible oils. Fuel Process Technol 92:1411–1417
32. Tiwari P, Garg S (2016) Study of reversible kinetic models for alkali-catalyzed Jatropha curcas transesterification. Biomass Convers Biorefin 6:61–70
33. Freedman B, Butterfield RO, Pryde EH (1986) Reaction conditions employed in kinetic studies. J Am Oil Chem Soc 63:1375–1380
34. Darnoko D, Cheryan M (2000) Kinetics of palm oil transesterification in a batch reactor. J Am Oil Chem Soc 77:1263–1267
35. Noureddini H, Zhu D (1997) Kinetics of transesterification of soybean oil. J Am Oil Chem Soc 74:1457–1463
36. Tesser R, Di Serio M, Guida M, Nastasi M, Santacesaria E (2005) Kinetics of oleic acid esterification with methanol in the presence of triglycerides. Ind Eng Chem Res 44:7978–7982
37. Zubir MI, Chin SY (2010) Kinetics of modified Zirconia-catalyzed heterogeneous esterification reaction for biodiesel production. J Appl Sci 10:2584–2589
38. Lerkkasemsan N, Abdoulmoumine N, Achenie L, Agblevor F (2011) Mechanistic modeling of palmitic acid esterification via heterogeneous catalysis. Ind Eng Chem Res 50:1177–1186
39. Shahid A, Jamal Y, Khan SJ, Khan JA, Boulanger B (2018) Esterification reaction kinetics of acetic and oleic acids with ethanol in the presence of Amberlyst 15. Arab J Sci Eng 43:5701–5709
40. Gokel GW (1995) A review of "phase-transfer catalysis fundamentals, applications, and industrial perspectives. C. M. Starks, C. L. Liotta, M. Halper. Chapman and Hall, New York, 1994, 9.25″ × 6.25″; xiv + 668 pp. ISBN 0-412-04071-9". Supramol Chem 5:237
41. Lifka J, Ondruschka B (2004) Influence of mass transfer on the production of biodiesel. Chem Eng Technol 27:1156–1159
42. Zhao D, Ren H, Wang J, Yang Y, Zhao Y (2007) Kinetics and mechanism of quaternary ammonium salts as phase-transfer catalysts in the liquid-liquid phase for oxidation of thiopene. Energy Fuel 21:2543–2547
43. Starks CM, Halper M (1994) Phase transfer catalysis. Springer, Dordrecht. ISBN: 978–94–011-0687-0
44. Hailegiorgis SM, Mahadzir S, Subbarao D (2011) Enhanced in situ ethanolysis of Jatropha curcas L. in the presence of cetyltrimethylammonium bromide as a phase transfer catalyst. Renew Energy 36:2502–2507
45. Huang YQ (2013) Synthesis of biodiesel by phase transfer catalysis. Appl Mech Mater 291–294:355–358
46. Hussain Z, Kumar R (2018) Kinetics & simulation of non-catalytic esterification. Mater Today Proc 5(9):18287–18296

47. Shin HY, Lim SM, Bae SY, Oh SC (2011) Thermal decomposition and stability of fatty acid methyl esters in supercritical methanol. J Anal Appl Pyrolysis 92:332–338
48. Quesada-Medina J, Olivares-Carrillo P (2011) Evidence of thermal decomposition of fatty acid methyl esters during the synthesis of biodiesel with supercritical methanol. J Supercrit Fluids 56:56–63
49. Minami E, Saka S (2006) Kinetics of hydrolysis and methyl esterification for biodiesel production in two-step supercritical methanol process. Fuel 85:2479–2483
50. Melo-Júnior CAR, Albuquerque CER, Fortuny M, Dariva C, Egues S, Santos AF, Ramos ALD (2009) Use of microwave irradiation in the noncatalytic esterification of C18 fatty acids. Energy Fuel 23:580–585
51. Rani KNP, Neeharika TSVR, Kumar TP, Satyavathi B, Chintha S (2016) Kinetics of non-catalytic esterification of free fatty acids present in Jatropha oil. J Oleo Sci 65:441–445
52. Cho HJ, Kim SH, Hong SW, Yeo YK (2012) A single step non-catalytic esterification of palm fatty acid distillate (PFAD) for biodiesel production. Fuel 93:373–380
53. Haas MJ, McAloon AJ, Yee WC, Foglia TA (2006) A process model to estimate biodiesel production costs. Bioresour Technol 97:671–678
54. West AH, Posarac D, Ellis N (2008) Assessment of four biodiesel production processes using HYSYS. plant. Bioresour Technol 99:6587–6601
55. Lee S, Posarac D, Ellis N (2011) Process simulation and economic analysis of biodiesel production processes using fresh and waste vegetable oil and supercritical methanol. Chem Eng Res Design 89:2626–2642
56. Lou WY, Guo Q, Chen WJ, Zong MH, Wu H, Smith TJ (2012) A highly active bagasse-derived solid acid catalyst with properties suitable for production of biodiesel. ChemSusChem 5:1533–1541

Castor Oil-Based Derivatives as a Raw Material for the Chemical Industry

Sagar Dhanuskar, S. N. Naik, and K. K. Pant

Abstract The use of fossil derived petrochemical products are expected to decrease due to the depletion of fossil resources and increasing environmental issues such as the impact of greenhouse gases, global warming, and rising population. Interest in plant oil-based rather than petroleum-based fuels is increasing as it is a renewable resource and easily availfd ble. Plant vegetable oil, like castor oil, has shown attractive physical and chemical properties in comparison with fossil fuels. The Castor oil derivatives are a combination of saturated and unsaturated fatty acid esters linked to the backbone of glycerol. Castor oil contains nearly 90% of ricinoleic acid having hydroxyl group, a double bond, a carboxylic group, and a long chain of hydrocarbon and also having different methods to convert into an essential bio-based alternative for petroleum-based industrial chemicals applications. Therefore, this chapter underlines the importance of castor oil or derivatives with its expected global market growth in the manufacture of such diverse materials and its geographical availability. Overall, this chapter provides a summary of castor oil, its development, and its resources.

Keywords Castor oil · Castor oil industry · Chemistry of castor oil · Renewable chemicals · Ricinoleic acid

S. Dhanuskar
Centre for Rural Development and Technology, Indian Institute of Technology Delhi, New Delhi, Delhi, India

Department of Chemical Engineering, Indian Institute of Technology Delhi, New Delhi, Delhi, India

S. N. Naik
Centre for Rural Development and Technology, Indian Institute of Technology Delhi, New Delhi, Delhi, India

K. K. Pant (✉)
Department of Chemical Engineering, Indian Institute of Technology Delhi, New Delhi, Delhi, India
e-mail: kkpant@chemical.iitd.ac.in

1   Introduction

In today's world, increasing the effects of greenhouse gases, quick industrial development, global economic growth, environmental contamination, increased population, and natural resources loss are concern to problems which affects the environment. In addition to eliminating the existing harms caused by environmental degradation, people are looking for green technologies that creates fresh and good quality, safety, clean and sustainable energy resources for the better future. So this motivates researchers to quest for innovative approaches to incorporate the use of sustainable energy with the adequate technology for the production of products needed by different industries [1]. Plant oils are the oils derived from plant resources like castor oil, olive oil, soybean oil, and linseed oil [2] and getting more attention since they found an appropriate way of producing alternative options for the application in increasing energy demand and environmental awareness. Castor oil shows the properties in the development of most technologies that are cost-effective renewable resources and numerous uses as sustainable resources for the chemical based industries [3]. Castor oil derivatives serve as a raw material to produce solvents, lubricants, paints, polymers, and jet fuels in the chemical industry.

2   Castor Oil Background

Castor plants *(Ricinus communis)* are part of the large spurge family (Euphorbiaceae), which cultivate naturally under different climatic conditions [4]. Castor oil plant initially belonging to India and Africa and then imported from India to China around 1400 years ago [5]. Castor seed contains 50% of oil, which can be easily extracted, and transformed into different derivatives which can be used in the development of new generation technologies for various chemical industry such as drugs, personal care products, perfumes, lubricants and biofuels [1]. Castor oil with easy to grow properly, across the tropical, subtropics and temperate zones, and castor oil are biodegradability, low costs, renewable, and eco-friendly with all this qualities the demand castor oil is continuously increased as an alternative option [4]. Castor oil and its derivatives used as raw material more than 700 industries and due to the unique chemical structure, it continued to increase as plant oil resource.

Castor oil is getting more significance attraction because of its unique physicochemical characteristic, particularly in comparison with the most conventional edible and non-edible oils due to the presence of ricinoleic acid. The high amount of ricinoleic acid content (85–90%) in castor oil which is a multipurpose compound and this acid has three functional groups. This ricinoleic acid has a carboxylic acid, a double bond, and secondary alcohol or hydroxyl group that give a wide range of opportunities to convert or modify castor oil in several useful derivatives products based on the different applications anticipated (Fig. 1) [4]. The carboxylic group can contribute to a wide variety of esterified products, while hydrogenation,
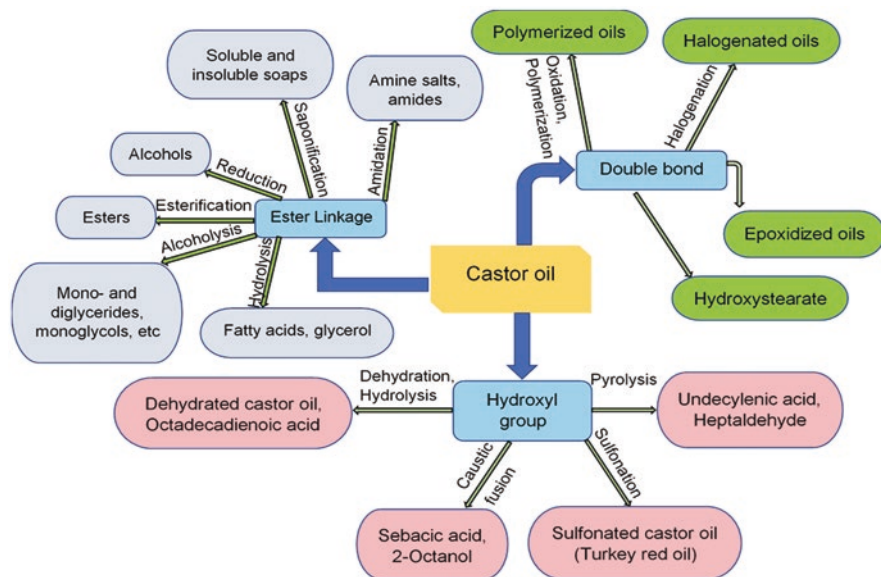
Fig. 1 Possible castor oil reactions for the production important industrial castor oil derivatives

epoxidation, or vulcanization can modify the single point of unsaturation. On the other hand, the carbon-12 hydroxy functional group, which may be acetylated or alkoxylated, can be eliminated through dehydration to improve the unsaturation of oil [6].

Castor oil and its derivatives have gain revolutionary importance in industries application as it has low-cost efficiency and renewable nature. This paper the distribution and production of the castor oil around the world, and brief discussion of castor oil different reactions that converts into derivatives which are used in the industrial applications. The potential reactions are with the castor oil are caustic fusion, dehydration, epoxidation, hydrogenation, hydrolysis, pyrolysis, polymerization, sulphonation, and transesterification.

3 Castor Distribution and Production

The Castor plants is unspecific, seeds increase at various rates varying broadly in size, shape, and color with approximately 45–55% by weight of oil, and geographic locations also places an important role in growing seeds on average or fully matured. The castor plant has a leaf throughout the year, in flowers from July to September, and from September to November the seeds ripen. Throughout the winter, the castor seeds are placed in a capsule of reddish-green spiny fruit and spread by water and wind [7, 8]. The seeds have very different and unique spots, primarily covering the

surface shades of light brown with shades of dark brown. The castor seeds are unsafe, so intake of the seeds can cause abdominal, vomiting and human-mortal diarrhea pain [9, 10]. Castor plants are perennial and fast-growing plant around 10–12 m high but grow steadily smaller around 1–3 m annually in the temperate region. The stem of the plant is hollow, and light green often tinged with red and leaves are huge, bright reddish-brown color of vein. During summer, blossoms are always reddish-green and kept in a bundle at the ends of the branches [3].

Castor is an oil plant is non-edible and has large number properties. Over the past decade, castor oil production has increased drastically due to ease of accessibility, inexpensive, non-food competition, high boiling point, and viscosity, tremendous ability as a renewable bio-based synthetic product which are environmental friendly [4, 11]. Castor oil is mostly produced in India, Africa, South America, Brazil, China. India leads the world in the production and export of castor oil and in India the major states producing castor seed in Gujarat, followed by Andhra Pradesh and Rajasthan. India is delivering castor oil total world production is about 85%, which estimated at about US$ 1.2 billion per annum and although the leading importer is the United States, the European Union, Japan, Brazil, and China [5, 12, 13].

4   Extraction and Refining

Extraction of castor oil from the castor seeds from a combination of processes, such as solvent extraction, and mechanical pressing [3, 14]. Before the extraction process, the castor beans will be subjected to many processess in the direction of preparing for extraction. In the *clearing* process, foreign materials and dirt are removed from the castor bean. In the process *drying*, the castor beans are dried at a temperature at 60 °C for few hours for the outermost covering breaks, and the beans are sheds. During the *winnowing* process, castor seeds shell is removed nibs to take off the covering and to get the large amount of yield; and throughout *grinding* process, the castor seeds are crushed to form a paste (*cake*) softening or cracking the cell walls to allow castor fat for extraction [3, 14] (Fig. 2). The mechanical pressing approach is preferred over the solvent extraction system because it requires low costs, lower investments, and its offers better environmental protection. The disadvantages of mechanical pressing are only extract on about 45–55% of oil and the remaining oil in the cake extracted by solvent extraction which increases the work and extraction expenses which make the operation environmentally unfriendly. Generally castor seeds, on average containing 45–55% by weight of oil depending on the size, geographic position, and extraction process [3, 4].

Castor oil extract from then beans contains some amount of free fat, unsaturated fats, hydrocarbons, toxic proteins, gums, foreign matter, soil matter, mono- and diacylglycerols, and other contaminants that are removed by the refining process. Removal of impurities such as free fatty acid, colloidal, and colouring matter by two processes in the refining process via chemical and physical refining process. Using procedures like settling, and filtration is used in the standard refining method for the

```
                    ┌─────────────────────────────┐
                    │ Cleaned dried castor oil seed │
                    └─────────────────────────────┘
                                  │
                                  ▼
┌───────────────┐      ┌─────────────────────────┐
│ Hulls or shells │◄────│ Dehulling or deshelling │
└───────────────┘      └─────────────────────────┘
                                  │
                                  ▼
                       ┌───────────────────┐
                       │  Crush into pulp   │
                       └───────────────────┘
                                  │
                                  ▼
┌───────────────┐      ┌───────────────────┐
│      Oil      │◄─────│   Screw pressing   │
└───────────────┘      └───────────────────┘
        │                         │
        ▼                         ▼
┌───────────────┐      ┌───────────────────┐
│ Water refining │      │ Pulpdried to flakes │
└───────────────┘      └───────────────────┘
                                  │
                                  ▼
                ┌───────────────────┐      ┌───────────────────┐
                │ Solvent extractor │◄─────│ Solvent (Hexane)  │
                └───────────────────┘      └───────────────────┘
```
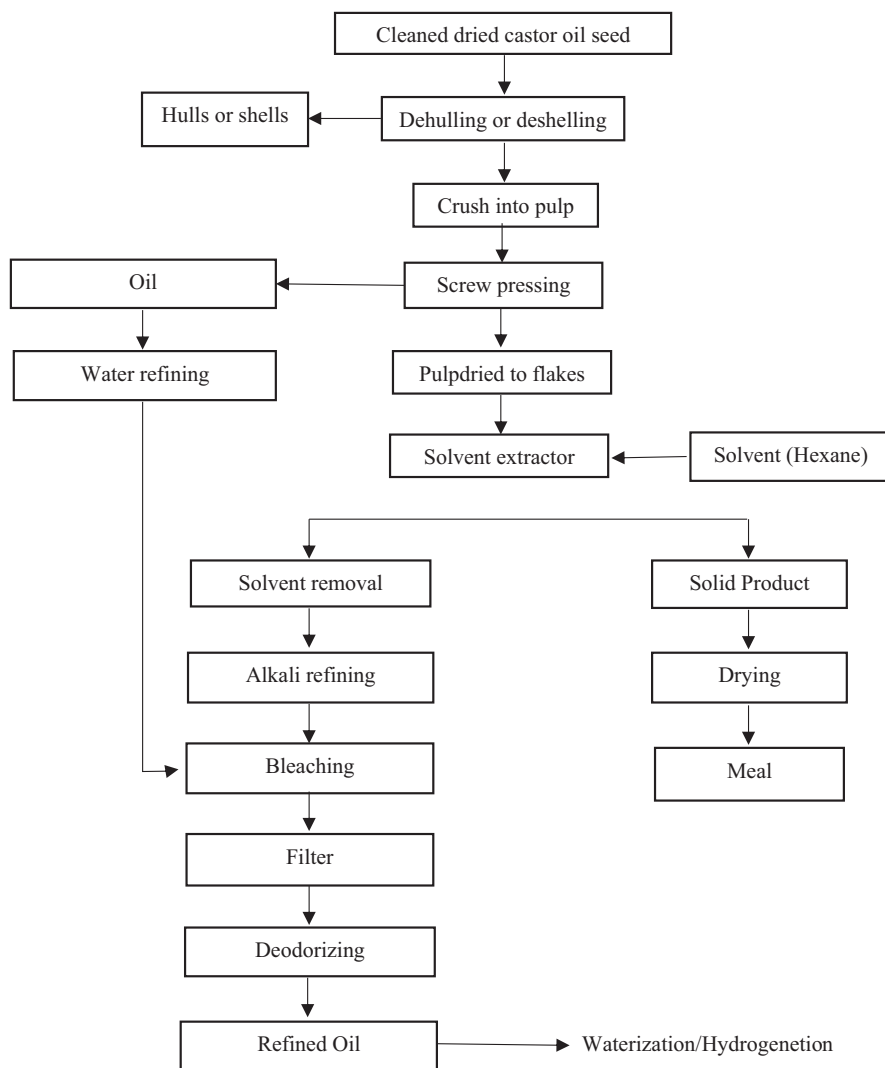
Fig. 2 The Modified procedure for the extraction and preparation of castor oil [3, 14, 15]

removing of solid and colloidal material. Degumming is used when extracting castor oil containing the dissolved and scattered protein compounds, and other compounds including gums, phospholipids, and solation metal material. In the process of neutralization, the castor oil is undergoing the alkali treatment using caustic soda solution to remove the excess free fatty acids. In the Deodorization nitrogen or steam stripping operations to remove the volatile components found in the extracted castor oil. Castor oil decolouring or bleaching is used to remove of colouring material [3, 6, 15].
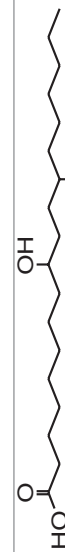
5 Composition and Physicochemical Parameters of Castor Oil

Castor oil has different physicochemical properties from all other non-edible oil, and its properties are discussed in given Table 1. Castor oil has a unique chemical composition as compared to other vegetable oils and the fatty acid composition of castor oil consist up to 90% ricinoleic acid, and rest other fatty acids present and following composition and structure are shown in the Table 2. The high content presence of ricinoleic acid in castor oil has provide a wide area of application in the chemical industry. In the ricinoleic acid presence of the carboxylic group, a double bond and hydroxyl group favor the castor oil for various chemical reactions, modification, and transformations as a renewable resource. For instance, the existence of a carboxylic group allows castor oil to be transformed through a few reactions are esterification, amidation. The existence of a double bond allows the transformation of castor oil many reactions, for example, hydrogenation carbonylation and epoxidation. Besides, the hydroxyl group may also take part in reactions such as dehydration, alkali splitting, halogenation, alkoxylation, sulfonation, and its products are sebacic acid, 2-octanol, 10-undecenoic acid, heptaldehyde, red turkey oils, urethane polymers, etc. Castor oil is entirely biodegradable, renewable and the chemical

Table 1 Physicochemical parameters of castor oil [5, 16–18]

Physical and chemical parameters	Average result
Moisture, %	0.30
Density g/mL	0.95–0.96
Refractive index @ 28 °C	1.79
Fire point (°C)	256
Flash point (°C)	225
Smoke point (°C)	215
Viscocity (cps)	0.425
Colour (TU)	14.0
pH	5.8
Turbidity	5.0
Free fatty acid	
Acid value	5.7
Saponification value (mgKOH/g oil)	180.77
Peroxide value (Meq/kg)	158.64
Iodine value (Wiji's)	85.9
Unsaponifiable matter, %	0.7
Specific gravity (at 30 °C)	0.96
Hydroxyl value	154.6
Thermal conductivity (W/m °C)	4.73
Specific heat (kJ/kg/K)	0.09
Melting point (°C)	−2 to −5
Water content (ppm)	367

Table 2 Free fatty acids composition of castor oil [19]

Fatty acid	Structure	Composition (%w/w)
Ricinoleic acid		89.5%
Linoleic acid		4.2%
Oleic acid		3%
Stearic acid		1%
Palmitic acid		1%
Dihydroxystearic acid		0.7%
Linolenic acid		0.3%
Eicosanoic acid		0.3%

transformations into various castor oil-based products. Castor oil-based products are produced entirely environmentally friendly, biodegradable, and sustainable.

6 Castor Oil Products Significant Applications in Industries

Researchers are now emphasizing on the edible oils as the industrial raw materials in the area of research. The using of edible oils as a raw material for chemical reactions is related to major environmental issues, the price of vegetable oil has increased significantly, which inevitably influence the economic feasibility of edible-oil-based goods. Consequently, the collection of edible vegetable oils cannot be deemed a potential feedstock to a different industrial reaction. The production of industrials chemical products made from non-edible oils is one possible way to get the better control on such limitations. In this case of castor oil consisting of ricinoleic acid around 90% and small quantities of oleic and palmitic acids, many non-edible oils having higher in unsaturated oleic acid and lower in saturated palmitic acid. Castor oil can therefore distinguish between other edible and non-edible oils, making it the raw materials of greatest interest for the industries.

6.1 Dehydration

Iodine content in the castor oil is low and is thus referred to as a non-drying oil. Although, it is non-drying when its dehydration gives semi-drying or drying oil. Ricinoleic acid dehydration is a catalyzed acid reaction that eliminates the hydroxyl group and forms a new double bond. Dehydration is typically done at a temperature around 250 °C using most commonly employed catalysts such as concentrated sulfuric acid, sodium bisulfate, phosphoric acid, phthalic anhydride, and acid-activated clay are most widely used under inert atmosphere or vacuum [3, 20–24].

This mechanism, the hydroxonium is developed by electrophilic attack by a proton against the unshared electron pairs of the carbon-12 hydroxyl group, and the carbonium ion is generate by a loss of water, and ejection of a proton from either carbon-11 or carbon-13 [25–27]. Since dehydrated castor oil commonly has a ratio of 4:1 to 3:1 between nonconjugated and conjugated dienoic acid,it is easier to remove hydrogen from the 13-carbon atom than in an 11-carbon atom.

As shown in Fig. 3, ricinoleic acid dehydration requires the elimination of the hydroxyl group and one of its α hydrogen presents on one of the carbon-connected hydroxyl group forming conjugated and nonconjugated linoleic acids. Typically conjugated acid is polymerized and other anti-polymerizing agents such as sodium sulfite or zinc chloride, or aluminum chloride [28]. Many potential side reactions with estolide are developed during the dehydration of ricinoleic due to heat acceleration. Dehydrated castor oil-based protective coating, varnishes, lubricants, soaps, paints, inks, alkyd resins system provide properties like quick-drying, durability, chemical tolerance, metals adhesion, high gross and water quality [1, 4, 29].
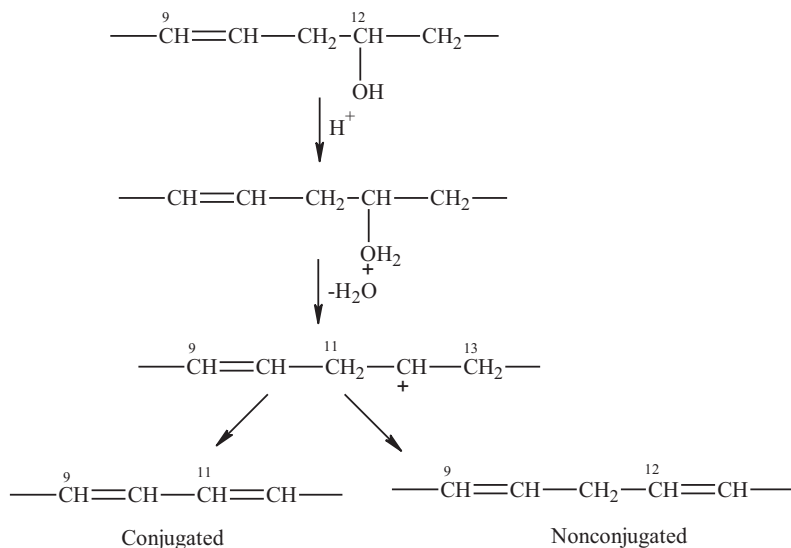
Fig. 3 Chemical mechanism of dehydration of ricinoleic acid to form an isomeric mixture of unsaturated fatty acids

6.2 Hydrogenation

Castor oil contains both a carboxyl group and an extremely reactive hydroxyl group, much like an unsaturation state that can be removed by hydrogenation. In the hydrogenation, a hydrogen molecule from a hydroxyl group is decreased to generate hydrogenated castor oil achieved using standard Raney nickel catalyst of 2% at 150 °C and 150 psi with hydrogen pressure with high hydroxyl value and low Iodine value [30–32]. Hydrogenation of castor oil has a high melting point compared with other oils, enhanced storage conditions, odor, and enhanced oxidative and thermal stability. Hydrogenated castor oil, 12-Hydroxystearic acid, and methyl-12-Hydroxystearic acid are produced by hydrogenation followed by hydrolysis and esterification of castor oil. Hydrogenation of castor oil (HCO) is obtained from a route of catalytic transfer hydrogenation (CTH) [19] (Fig. 4).

The advantage of catalytic transfer hydrogenation is due to the organic molecules used at atmospheric temperature and pressure as a hydrogen donor and thus resulting in low energy consumption. In addition, the catalytic transfer hydrogenation doesn't need a specific reactor, and the solvent can even be used as a hydrogen donor in the presence of a catalyst. The CTH process with catalyst Pd/C and various hydrogen donor solvent for soy [33], sunflower [34], and castor [4, 35] oils. There are other groups of hydrogen donor that were used for CTH reactions: hydrazine [36], dioxane [37], primary and secondary alcohols, indoline, hydroaromatic hydrocarbons [38], formic acid, methanol [39], formate, phophinates, and phosphinic acid. The catalyst was increasingly effective, minimizing the degree of secondary reactions (ether formation, hydrolysis, and others). Palladium is inadequate for
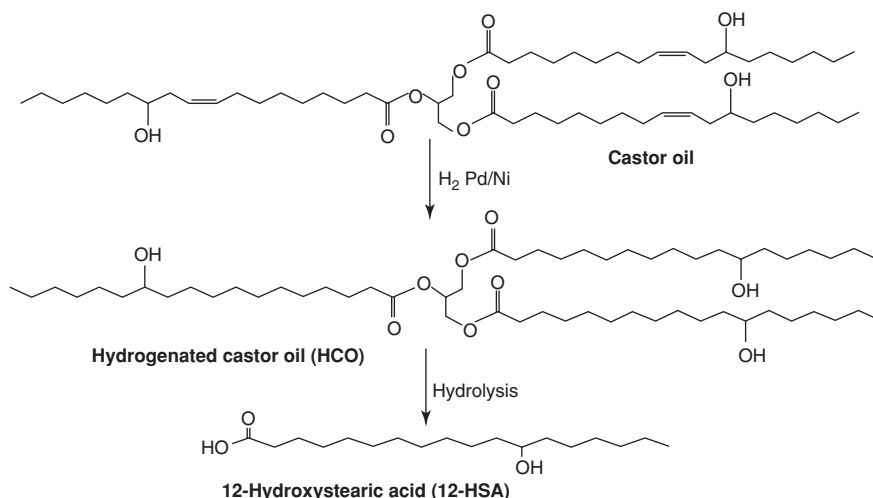
Fig. 4 Hydrogenation of castor oil by catalytic transfer [4, 19]

hydrogenation because the process is enhanced at low selectiveness due to nonselective and generated significant amounts of trans acids during the reaction [40]. Hydrogenated castor oil are soluble in hot organic solvents like ether and chloroform and insoluble in water and most organic solvents [41].

The hydrogenated castor oil is valuable because of the long shelf life for lubricant industries due to its excellent quality of insolubility, water-resistance, and maintenance of its lubricity. Also, HCO's polarity and surface wetting properties are valuable cosmetics, solid lubricant, paint additives, production of formed plastics and rubber products, wax production, polishing, carbon paper, candles, and crayons [1, 4, 6, 42]. After saponification and acid hydrolysis of hydrogenated castor oil 12-Hydroxystearic acid is produced and converted into methyl-12-Hydroxystearic acid. 12-Hydroxystearic acid is a significant material is used in the industry for polymer materials [42, 43]. All these products are useful for the preparation of metallic soaps such as lithium, calcium, etc. for use in multipurpose greases and lubricants [44, 45].

6.3 *Transesterification*

In the Transesterification reaction, the castor oil with low molecular weight alcohols is reacted to generated biodiesel (methyl ricinoleate) in the presence of homogeneous base or acid catalysts [46, 47]. The process required three necked batch reactor which equipped with a reflux condenser, a magnetic stirrer and digital thermometer. In transesterification of oils require minimum amount of catalyst (to avoid saponification and cost reduction) with reaction temperature (55–65 °C) and

the reaction time (2–8 h), a molar ratio of alcohol to oil 6:1 and methanol (to minimize the cost of recovery after reaction). Transesterification reactions are a reversible reaction that requires excess alcohol to shift the equilibrium towards biodiesel formation. Transesterification of castor oil reduces the molecular weight, acid value, saponification value, and viscosity of the castor oil by varying the molar ratio, reaction time, catalyst concentration increasing kinematic viscosity and specific gravity [1, 4, 48]. As the biodiesel is nontoxic, biodegradable and environmentally friendly fuel, the ignition of biodiesel discharges less emissions of carbon dioxide, sulfur dioxide, unburned hydrocarbons, and particulate matter [17]. The volatility increased during the transesterification reaction and during the reaction monitoring the cetane number and heating value for higher yield of biodiesel [49, 50].

The reaction process is addressed in the transesterification reaction below (Eq. 1) where the base interacts with the alcohol, forming an alkoxide and the protonated catalyst. The alkoxide nucleophilic attack on the triglyceride carbonyl group produces a tetrahedral intermediate (Eq. 2) from which the alkyl ester and the corresponding diglyceride anion form (Eq. 3). The latter deprotonates the catalyst and thus regenerates the active specie (Eq. 4) which can now react with a second alcohol molecule to start another catalytic cycle. The same mechanism converts diglycerides and monoglycerides to a mixture of alkyl esters and glycerol [51–54] (Fig. 5).

Increased biodiesel production from castor oil resulted in glycerol overproduction, which is also an important root for the different solvents, for example, propylene glycols, glycerol ethers, and esters [55]. Glycerol has also shown potential as a renewable solvent and reduction agents used in hydrogenation reactions to transfer metal-catalyst and the creation of nanoparticles, a high-boiling organic solvent to improve enzymatic hydrolysis, and aliphatic polyester synthesis [4, 56–58].
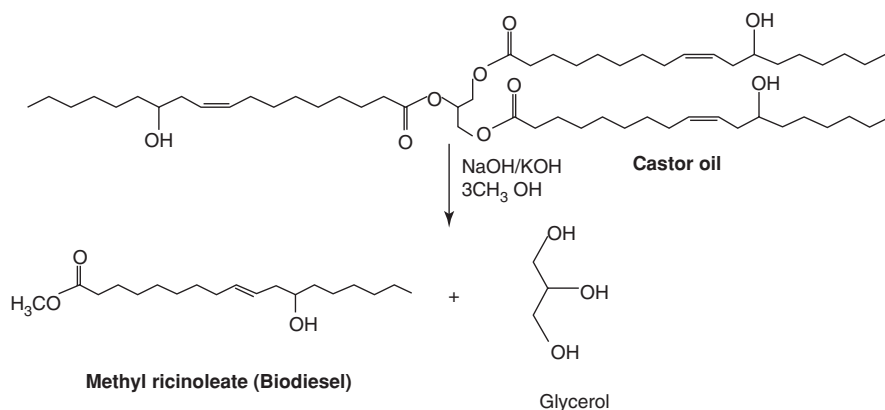
Fig. 5 Transesterification of castor oil [4, 50]

6.4   Oxidation

Triglycerides-based oils are mainly restricted to their oxidation stability by the degree of unsaturated double bonds. In several reactions like oxidation, unsaturated carbon-carbon bonds serve as active sites [59]. Most triglyceride-based oils contain unsaturated fatty acids and are vulnerable to oxidation. The higher the unsaturation level, the more double bonds the oil will become sensitive to oxidation. The oxidation mechanism of castor oil has been well investigated and a famous representation of the oil is shown in Fig. 6 [60, 61]. The development of free radicals initiates castor oil oxidation. The elimination of hydrogen atom in the methylene group from next to a double bond can easily lead to free radical formation. Free reacts rapidly with oxygen to form a peroxy radical. Radical peroxy can attack another lipid molecule to remove a hydrogen atom to form a hydroperoxide and another free radical, propagating the oxidation process [62]. Castor oil oxidation is taken at a temperature of about 80–130 °C in the presence of blowing air or oxygen with or without a catalyst, and mixing is required for the formation of clear and viscous oxidized or blown castor oil with varying viscosity. This process is a mixture of oxidation and polymerization; therefore, it is called oxidative polymerization. Oxidized castor oils are excellent non-migrating, non-volatile cellulosic resin plasticizers, poly (vinyl butyral), polyamides, shellac, and natural and synthetic rubber. Since blown castor oil high acid value, imparting oil and solvent resistance to produce the high viscosity materials with increased viscosity, and compatibility and decreased solubility. This oil is used as excellent pigment grinding media and as an ink foundation, lubricating oils, plasticize in adhesives, hot melts, and hydraulic oils [6, 9, 63, 64].
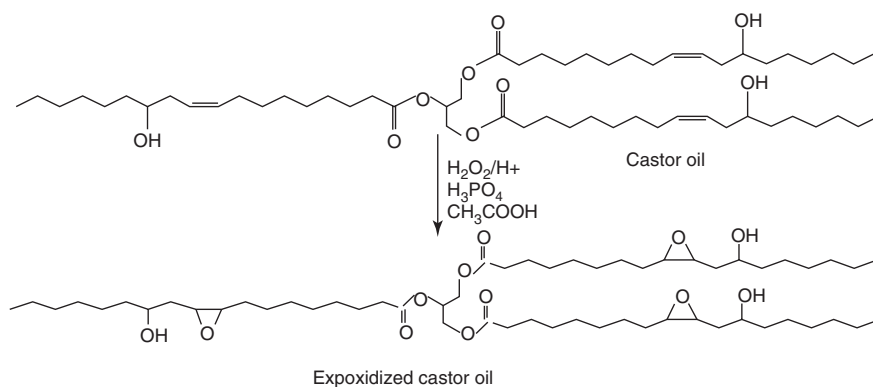
Fig. 6 Epoxidation of castor oil

6.5   Epoxidation

Epoxidation reactions in which peracid is used either pre-formed or produced during the reaction as acetic acid is used as a carrier of oxygen with hydrogen peroxide as a donor of oxygen. Castor oil fatty acids or their alkyl esters are reacted with peracids when catalysts to produce epoxides. Castor oil can be epoxidized with hydrogen peroxide at both 30% and 70%. The reactions to be subjected to 30% hydrogen peroxide with 60 °C are added during a 4 h period when the mixture of castor and methyltri-n-octylammonium(MTTP) is undergoing a reaction. The reaction mixture is mixed vigorously for another 4 h before cooling to room temperature and addition of toluene for extraction and separating of organic layer and dried by anhydrous sodium sulfate. Epoxidized castor oil (ECO) was recovered in 94% yield after the elimination of the solvent on a rotary evaporator. In addition, powdered calcium carbonate was added and agitated in the alternate process by which castor oil and MTTP combine the mixture thoroughly at 60 °C. Using a syringe pump, 70% Hydrogen peroxide was introduced dropwise by stirring over 2 h. The mixture has been kept at 60 °C for 9 h under intense agitation conditions before cooling to room temperature. In 70% hydrogen peroxide chloroform is used for the extraction and drying remaining product dried over sodium sulfate. 90% yield of ECO was obtained when the solvent was drained from a rotary evaporator [1, 43, 65]. Acid catalysts, enzymes, tungsten-based catalysts, transition metal complexes, ion exchange resin, Ti (IV)-grafted silica catalyst [66] and methyl-tri-n-octyl ammonium diperoxotungstophosphate [67] are various forms of catalysts for epoxidation reactions.

Mechanism of epoxidation reaction is explained in the three consecutive reactions:

a) $RCOOH + H_2O_2 \rightleftharpoons RCOOOH + H_2O$

b) $RCOOOH + R'CH=CHR'' \longrightarrow R'\overset{O}{\overset{/\,\backslash}{CH-CH}}R'' + RCOOH$

c) $R'\overset{O}{\overset{/\,\backslash}{CH-CH}}R'' + RCOOH \longrightarrow R'CHOH-CHR''(OCOR)$
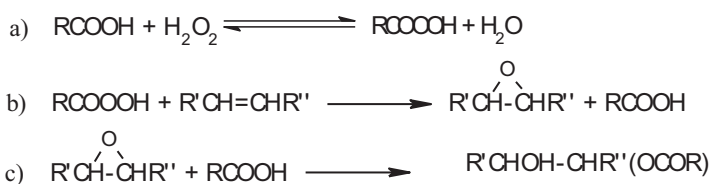
Reaction (b), the present step of epoxidation, does not requires a catalyst and is the fastest of the three reactions. Both acids are catalyzed in the reactions (a) and (c). Even if resins of sulfonic acid are equivalent to other strong acids in catalytic formation of peracid (reaction a), the by- product formation is not catalyzed (reaction c), when raw material is used with relatively high molecular weight. Many of the Most of the resin catalysts advantages are based on the distinction from other strong acids [68].

The epoxidation products are known as oxirane compounds or epoxides. In addition, the epoxides play an important role in the production of alcohols, glycols, polyols, and other polymers due to highly reactive. Epoxidation castor oil is used in

products like plasticizers and polymer stabilizers, high-temperature lubricants, dispersions of polyurethane, paints, coatings, and adhesives, nanocomposites, surfactants, hydraulic oils, and biodiesel [69–73]. The method is flexible; it can use several biological and inorganic catalysts to make the process is less energy-intensive [1, 43].

6.6 Ozonolysis

Various methods through which functional groups may introduced into vegetable oil structures such as epoxidation, hydroformylation, and ozonolysis by treating the double bond. In specific, ozonolysis is best way to get a terminal process to breaking carbon-carbon double bonds to give compounds with primary alcohols, aldehydes and carboxylic acids relying upon the reaction conditions [74]. The Ozone is used as an effective oxidizing agent for splitting and oxidization of alkenes, which are then reduced in castor oil to alcohol by a fast reduction agent such as sodium borohydride ($NaBH_4$) and lithium aluminum hydride. In ozonolysis, the oxidative cleavage method is the perfect reaction performed without a catalyst at a low temperature of 25–45 °C, and its decomposition occurs at 60–100 °C, which is less energy consumption for industries. This ozonolysis technique has recently applied to soyabean oil, castor oil, canola oil, and triolein, resulting in polymers such as polyurethane (PU), polyethers, and polyesters being condensed. After ozonolysis dangling chains which are saturated fatty acids are left unaffected and in polymer structures as side chains to enhance hydrophobicity and affect the mechanical and physical properties of the resulting polymers [74]. The ozonolysis process is highly oxygen reactive, which can lead to several side reactions, which can create several by-products unless the process performed in controlled conditions [1, 43, 75] (Fig. 7).

In fact, the process of ozonolysis reaction is ionic in nature. In the postulates of the mechanism (Fig. 8), the initial ozone reactions with unsaturated bond were electrophilic to form an initial unstable ozonide (I) that decomposes readily to give a zwitterion (II) and a carbonyl fragment (III). Then such fragments can be mixed to produce standard ozonide (IV). The zwitterion can, dimerize to a diperoxide (V) or polymerize to a higher molecular weight peroxide (VI). Loan et al. has reconciled this obvious inconsistency of the function by postulating a solvent cage that inhibits cleavage products from participation in "cross" or exchange reactions [76].

6.7 Sulfation

In the sulfation process, the SO_3 group is introduced into an organic compound to produce the structural function of the C-OSO_3. Sulfated castor oil is often named as Turkey Red Oil or sulfuric acid esters because of the reddish sulfur color derived
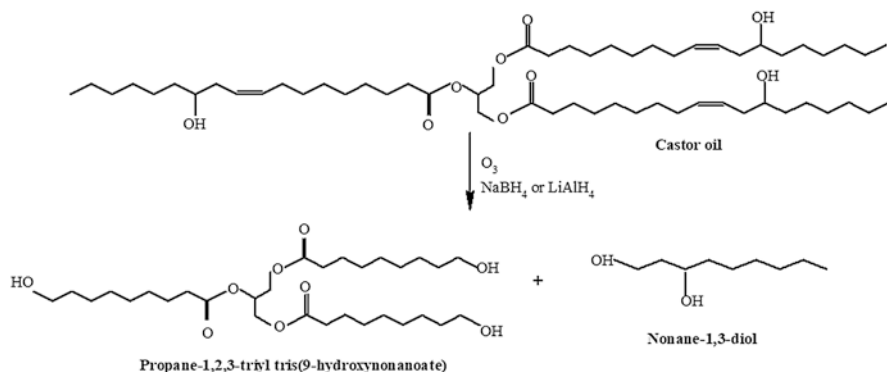
Fig. 7 Ozonolysis and reduction of castor oil into products
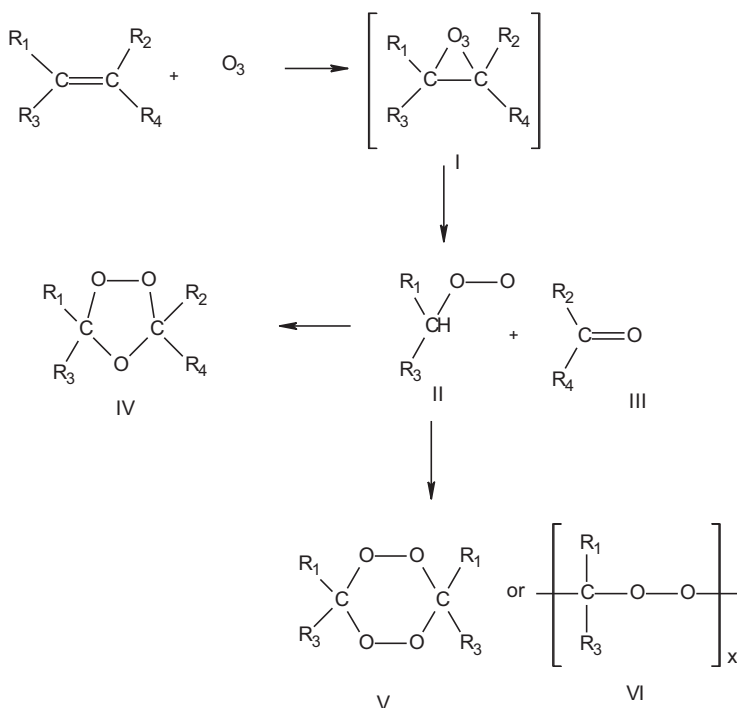
Fig. 8 Mechanism of Ozonolysis

from the castor oil hydroxyl group reacted with the sulfuric acid. Sulfation is a batch process, the reaction is conducted at temperature 25–30 °C is done by reacting 3–4 h of castor oil with sulfuric acid with continuous agitation and cooling [1, 4, 43, 77, 78]. Using catalysts in chemical reactions improves the rate of reaction and affects orientation in certain situations. Catalysts for sulfation of castor oil the with

sulfuric acid concentrate at low temperature have been tested for mercury, mercurous sulfate, vanadium pentoxide, copper sulfate, and pyridine. Their impact on generation of sulfuric esters was investigated by determining in deciding a mixed sulfuric trioxide produced during reaction process at intervals. Two reactions are leading to the forming of ester in sulfation of castor oil In the sulfation of castor oil, two reactions contribute to ester formation; (1) ricinoleic acid reaction in ae -OH group, and (2) the double bond of ricinoleic acid attachment. The double bond reaction continuous at a slightly slower rate. Other reactions like glycerides hydrolysis and sulfonic acid production, lactones, lactides, and estolides exist. The formation of esters is important in the wetting action as it brings the radical hydrophilic OSO_2OH amid the chain fatty acid ester, giving a balanced structure to the molecule. Taking sulfuric ester formation, there two opposite reactions possible: (1) ester formation and (2) ester hydrolysis produced by the water while excess acid is present. The hydrolysis of ester will be favoured by a negative catalyst and may also encourage other side reactions that would use large amounts of sulfuric acid, thereby decreasing the acid concentration or ester formation available.

The sulfation process requires temperature, and this is due to the very strong acid application, which does not require elevated reaction temperatures. Turkey- red oil is commonly used in textiles, cosmetics, wetting, emulsifying, and dispersing agents, production of detergents which is used in lubricants, softened materials, shampoos, and dyestuff formulation [1, 4, 43, 79–81] (Fig. 9).

6.8 Pyrolysis

In the case of hydrocarbons, at higher temperatures pyrolysis continues formation of free radical. It is likely that a free radical mechanism can also require a pyrolysis reaction of castor oil derivatives. The reaction was also shown to be more successful in producing of the targeted oleochemicals in the presence of free radical-yielding initiators [4, 82]. Castor oil or its fatty acid esters molecules break down in the process of pyrolysis to obtained undecylenic acid or its esters and heptaldehyde. At the same time, the key products are formed using either thermal pyrolysis or using thermal pyrolysis and catalytic pyrolysis. Ricinoleic acid found in the fatty acids of castor oil to produce undecylenic acid or its esters and heptaldehyde at a higher temperature (>400 °C) under atmospheric pressure. The reaction was performed with and without catalysts but some are different types of catalysts are used such as metals (Al, Tl, Ti, Ce, Th, W, Mo), glass and ploy (vinyl chloride) are employed. The mechanism of pyrolysis of castor oil indicated that when H atom of the OH group attaches itself mesomerically to C atom in the molecule to form a six membered ring separated between, C_3 and C_4 during heating and gives $Me(CH_2)_5CHO$ and $H_2C:CH_2(CH_2)_7CO_2H_4$ between the O and H linkage of the six-membered ring.

According to this, the methanolysis of castor oil yields methyl ricinoleate of castor oil favored because of excessive viscosity, polymerized materials, and toxic gases throughout reaction. Different groups have studied with or without a catalyst
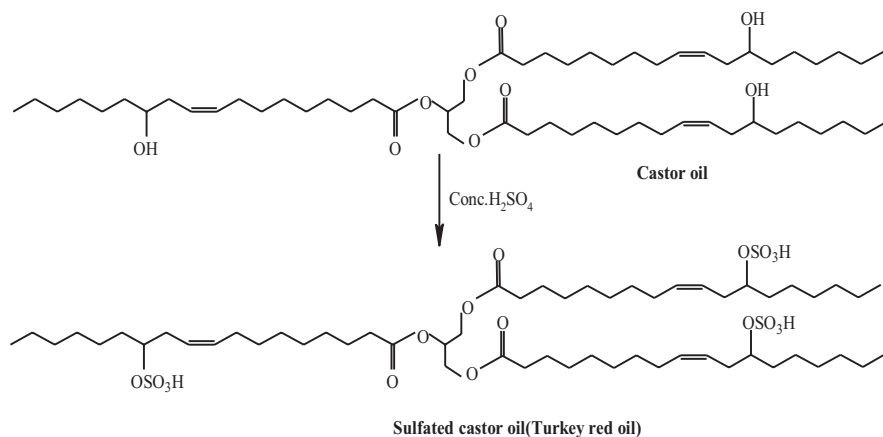
Fig. 9 Sulfonation of castor into Turkey red oil

at different temperature ranges from 400 to 550 °C to provide effective conversion and improve product efficiency [42, 83–91] (Fig. 10).

Undecylenic acid and heptaldehyde are valuable cosmetics raw materials (C11 and C7 aldehydes are used in soaps, shampoos, talcum powders, and perfume formulations), pharmaceuticals, and polymeric materials [42, 83, 84, 87]. Heptaldehyde is utilized as an organic solvent for polymers, insecticides, elastic products, resins, and plastics. Undecylenic acid as a source of bactericides and fungicides. 10-undecenoic acid was an important source for the manufacture of antibiotics and antitumor medicines. 10-undecenoic acid is also used in the application for Athlete's Foot remedy and nylon 11 [3, 4, 6, 43, 92–96].

6.9   Alkali Splitting

Alkali splitting reaction is the most important industrial procedure in which castor oil and its esters are converted into sebacic acid, and 2-octanol is used in the oleochemical industry. The ricinoleate molecule of castor oil produces sebacic acid and 2-octanol in a batch or continuous procedure with the presence of a large amount of alkali at high temperature with an effective catalyst [42, 97, 98]. Castor oil and its ester and alkali with equimolar ratio, 10-hydroxydecanoic acid, and 2-octanone are the main components when the reaction is done at temperature 180–200 °C and long reaction time [42, 85, 97]. Sebacic acid and 2-octanol are produced with 2:1 ratio of alkali: methyl ricinoleate at a higher temperature 250–270 °C and with reaction time for few hours and also find the application in the production of alcohols with high boiling range [3, 42, 43, 85, 99].

Mechanism indicates ricinoleic acid dehydration as the first stage of pyrolysis in presence of alkali resulting in the formation of β, γ-keto acid isomerizing to α,
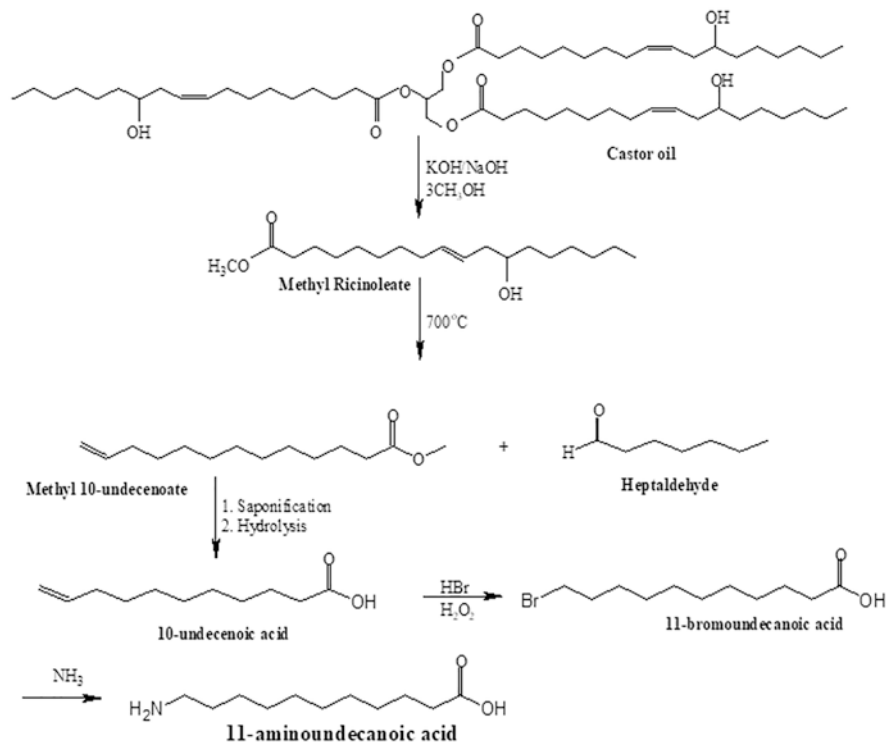
Fig. 10 Conversion of castor oil into 10-undecenoic acid and heptaldehyde

β-keto acid in the presence of alkali. In the presence of water, this keto acid sub-jected to a retroaldol fission to produce methyl hexyl ketone and decanoic acid aldehyde. From the first step of dehydrogenation the methyl hexyl ketone takes hydrogen to form 2-octanol. On the other hand, the decanoic acid may have two potential reactions. One of these reactions is a reversible hydrogenation reaction (hydrogen supplied from the first dehydrogenation stage) to form 10-hydroxy deca-noic acid, while the other reaction is the oxidation of decanoic acid aldehyde to produce sebacic acid in the presence of alkaline. In this reaction, many high boiling points (>300 °C) chemically inert thinners are white mineral oil, therminol, m-cresol, paratherm NF, glycol oil, and petroleum oil to enhance the yield and purity of the product and also minimize frothing and solidify reaction mixture [18, 100, 101]. Sebacic acid and its compounds are used in producing the dioctyl seba-cate (DOS), which is used in jet lubrication and lubricant in air-cooled combustion engines and used as plasticizers for production of vinyl resins, coatings, perfumes, cosmetics, and candles (Fig. 11).

In Additional as hexamethylenediamine is used in nylon 6–10 synthesis with sebacic acid [6, 18, 102, 103]. 2-Octanol finds uses in the coal industry as a floating agent and as a processing solvent for plasticizing, dehydrating, and anti-bubbling
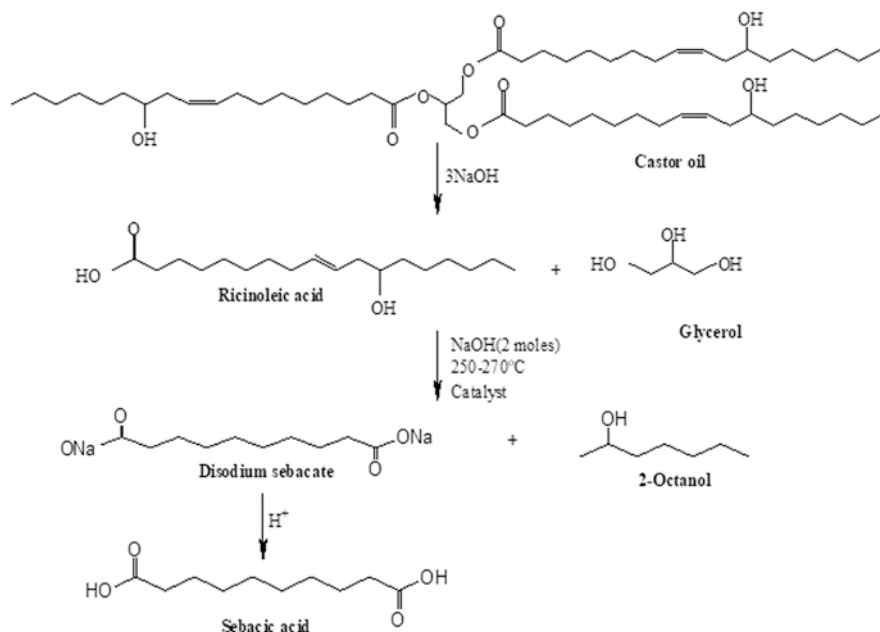
Fig. 11 Conversion of castor oil into sebacic acid and 2-octanol

agent [6, 18, 89, 104]. This process is green since the process uses water and is thus a more environmentally friendly option [1, 3, 4, 6, 43].

7 Polymer Goods Based on Castor Oil

Scientists must concentrate on discovering an alternative to use sustainable resources as raw materials to produce polymeric materials due to the scarcity of sustainable natural resources and rising environmental issues. Castor oil-based biopolymers have many advantages over the petroleum-based monomers polymer procedure are cheap, better properties, biodegradable, non-toxic, and have carbon footprints [4, 105, 106]. The hydroxyl group of ricinoleic acid present in castor oil is used in production castor oil-based biopolymers are polyurethanes, polyamides, polyethers, polyesters, and poly(2-hydroxyethylmethacrylate) [1, 3, 4, 43, 107–111].

Polyurethane (PU) is a class of polymer compounds containing urethane linkages (-NHCOO-) prepared from the polyaddition reaction between organic isocyanates and hydroxyl group molecules like castor oil. When castor oil reacts with the isocyanate (NCO) to maintain the NCO/OH ratio at 1.6. The reaction was at 45 °C with a constant stirring of 2 h. The dynamics of kinetics have become quite complex. Such that, for the first step, the process of polyurethane preparation method, at a particular heating rate, defined as a simple and uniform kinetic form, is assumed

to be of nth order (or, more specifically, would have an obvious reaction order of n): ath order in relation to OH and bth order in relation of NCO). Since all the systems used in the reactions had an NCO/OH ratio of 1 it resulted in [NCO] = [OH] at any point during polymerization process. The kinetic expression, associated to a specific velocity k_n, can therefore written as

$$-\frac{d[NCO]}{dt} = -\frac{d[OH]}{dt} = k_n [NCO]^a [OH]^b = k_n [NCO]^n, \tag{1}$$

$$\frac{d\alpha}{dt} = K_n (1-\alpha)^n, \tag{2}$$

where

$$\alpha = [NCO]_0 - \frac{[NCO]}{[NCO]_0} \tag{3}$$

is the degree of conversion, $K_n = k_n [NCO]_0^{n-1}$, $[NCO]_0$ being the initial concertration of NCO groups at time $t = 0$.

If the complete reaction between all NCO groups and all OH groups had an enthalpy of $\Delta H \_ 0$, then $\alpha = \frac{H(t)}{\Delta H_0}$, (where $H(t)$ is the accumulated energy liberated at a time t during the reaction), and Eq. (2) could be rewritten as

$$\frac{1}{\Delta H_0} \frac{dH}{dt} = K_n \left(1 - \frac{H(t)}{\Delta H_0}\right)^n \tag{4}$$

The specific velocity $k \_ n$ can be related to the temperature T through an Arrhenius dependence relationship.

$$k_n = A_0 e^{-E_A/RT} \tag{5}$$

where R is the universal gas constant, A_0 is an apparent frequency factor, E_A an apparent energy of activation. Substitution of (5) in (4) finally yields:

$$dH / dt = \frac{A_0}{(\Delta H_0))^{n-1}} e^{-\frac{E_A}{RT}} [\Delta H_0 - H(t)]^n, \tag{6}$$

Time and temperature are related by the heating rate:

$$T = T_0 + \beta \Rightarrow dT = \beta dr, \tag{7}$$

where T_0 is the initial temperature and β is the heating rate. Substitution of (7) in (4) would result in

$$dH/dt = \frac{\beta A_0}{(\Delta H_0))^{n-1}} e^{-\frac{E_A}{RT}} \left[\Delta H_0 - H(T) \right]^n, \tag{8}$$

Equation (8) is the final step to solved, so that the resulting curves $H(T) * T$ would be adjusted to the data with the parameters E_A, ΔH_0, and A_0 from this the values of $H(T)$ is obtained through numerical integration of dH/dt. There is other way to find out parameters value through Eq. (4) $\frac{dH}{dt}$, T, and $H(t)$ can be obtained from the data.

The use of organic isocyanates in this process is toxic and highly reactive for the production of PU, which produces the more dangerous component, phosgene, which has an impact on the environment [4, 112]. The processing of castor oil polyurethanes reveals excellent properties due to its hydrophobicity and environmental friendliness. Polyurethanes based on castor oil has been used in various application such as thermoplastic to thermosetting materials, rigid, semirigid and flexible foams, sealants, adhesives, biomedical implants, coatings, and cast elastomers [4]. Castor oil-based polyurethanes products such as a polyol, adipic acid, polyethylene terephthalate, and polyethylene glycol (PEG) are used in the application insulated coatings and rates of biodegradation are documented for biomedical implants and tissue engineering elsewhere [4, 43, 111]. The reaction of castor oil by using curing agent 1,6 hexamethylene diamine (HMDA) was used to synthesize epoxy-terminated polyurethane prepolymers [111].

Polyurethane organoclay nanocomposites are used in the application of coatings, adhesives, and automotive, and are formulated with a mixture of polypropylene glycol polyol and DCO (15%) [113]. Lil and Nal have applied to castor oil-based polyurethane, in the preparation of polymer electrolyte films used in the application for electrochemical devices, and this work also shows that polyurethane from castor oil-based can be used in polymer electrolytes as an option bio-based polymer membrane [114]. The ricinoleic acid present in castor oil gives antibacterial activity to undecylenic acid for polyesters synthesis. A part nylon-12,12 Dimethyl 1,12-dodecanedioate is produced from methoxycarbonylation of undecylenic acid or its esters [4, 115]. Overall, the most important green raw material is castor oil for chemical and polymer industries, and castor oil biopolymers have tremendous potential in the global polymer market and the environment [3, 4].

8 Conclusions

Castor oil is a primary green resource and one of the better fossil fuel alternatives. Castor oil derivatives have various uses in the chemical industry, agriculture, cosmetics, and pharmaceutical. Castor oil has a carboxylic acid, a double bond (between C9 and C10), and a functional group of secondary alcohol or hydroxyl (at C12). The presence of functional groups of castor oil has the potential to produces a wide range of industrial materials as an alternative for petroleum-based products. The castor oil has a unique chemical structure other than non-edible oils present, which

shows the more significant environmental concerns and its readily available, cheap, non-food competition. Castor oil hydroxyl group strengthens the chemical interactions in the preparation of metal oxides and nanoparticles from carboxylic acid and alcohol with different types of molecular materials like polymer, isocyanates, acids, and dodecanoyl chloride and synthesis of precursors for the preparation of metal oxide and nanoparticles from the carboxylic acid and alcohol. Castor oil production is increased due to its tremendous potential for chemical transformation as a renewable bio-resource and used as a raw material to manufacture a range of end products.

References

1. Chauke NP, Mukaya HE, Nkazi DB (2019) Chemical modifications of castor oil: a review. Sci Prog 102(3):199–217. https://doi.org/10.1177/0036850419859118
2. Bhatia S, Yean-Sang O, Twaiq FA, Mohamed AR (2003) Production of biofuel from palm oil. In: Proceedings of 5th International Petroleum Conference and Exhibition (PETROTECH-2003), New Delhi, pp 9–12
3. Mutlu H, Meier MAR (2010) Review article. Castor oil as a renewable resource for the chemical industry. Eur J Lipid Sci Technol 112(1):10–30. https://doi.org/10.1002/ejlt.200900138
4. Mubofu EB (2016) Castor oil as a potential renewable resource for the production of functional materials. Sustain Chem Process 4:1–12. https://doi.org/10.1186/s40508-016-0055-8
5. Patel VR, Dumancas GG, Viswanath LCK, Maples R, Subong BJJ (2016) Castor oil: properties , uses , and optimization of processing parameters in commercial production. Light Insights 9:1–12. https://doi.org/10.4137/LPI.S40233.TYPE
6. Ogunniyi DS (2006) Castor oil : a vital industrial raw material. Bioresour Technol 97:1086–1091. https://doi.org/10.1016/j.biortech.2005.03.028
7. Brickell C (2010) RHS encyclopedia of plants and flowers. Dorling Kindersley, London
8. Downey RK (1989) Brassica species. In: Oil crops of Teh world, pp 339–362
9. Kroschwitz JI, Nees F (1995) Kirk/Othmer Encyclopedia of chemical technology, Vols. 3-10. Angew Chem En Ed 34(22):2564
10. Lakshminarayana G, Paulose MM, Kumari BN (1984) Characteristics and composition of newer varieties of Indian castor seed and oil. J Am Oil Chem Soc 61(12):1871–1872
11. Pavaskar M, Kshirsagar A (2013) Global castor oil and Indian monopoly. Financial Vis 1:15–19
12. FAO (2008) Disponível em: <http://faostat.fao.org>. Acesso Em, 6
13. Scarpa A, Guerci A (1982) Various uses of the castor oil plant (Ricinus communis L.) a review. J Ethnopharmacol 5(2):117–137
14. Kemper TG (2005) Oil extraction. Baileys Industrial Oil Fat Products 5:63–68
15. Ali MF, El Ali BM, Speight JG (2005) Handbook of industrial chemistry. McGraw-Hill, New York
16. Nangbes JG, Nvau JB, Buba WM, Zukdimma AN (2013) Extraction and characterization of castor (Ricinus Communis) seed oil. Int J Eng Sci 4(5):2319–1813. https://doi.org/10.1016/j.indcrop.2012.07.022
17. Pena R, Romero R, Martinez SL, Ramos MJ, Martinez A, Natividad R (2009) Transesterification of castor oil: effect of catalyst and co-solvent. Ind Eng Chem Res 48(3):1186–1189
18. Vasishtha AK, Trivedi RK, Das G (1990) Sebacic acid and 2-octanol from castor oil. J Am Oil Chem Soc 67(5):333–337. https://doi.org/10.1007/BF02539685
19. Alwaseem H, Donahue CJ, Marincean S (2014) Catalytic transfer hydrogenation of castor oil. J Chem Educ 91(4):575–578. https://doi.org/10.1021/ed300476u

20. Bhowmick DN, Sarma SAN (1977) Dehydration of castor oil. Ind Eng Chem Prod Res Dev 16(1):107–111
21. Forbes WC, Neville HA (1940) Catalytic methods for increasing the unsaturation of long-chain fatty compounds dehydration of castor oil. Ind Eng Chem 32(4):555–558
22. Grummitt O, Marsh D (1953) Alternative methods for dehydrating castor oil. J Am Oil Chem Soc 30(1):21–25
23. Priest GW, Mikusch JD v (1940) Composition and analysis of dehydrated castor oil. Ind Eng Chem 32(10):1314–1319
24. Radlove SB, DeJong WM, Falkenburg LB (1948) A continuous process for the dehydration of castor oil. J Am Oil Chem Soc 25(8):268–271
25. Ramamurthi S, Manohar V, Mani VVS (1998) Characterization of fatty acid isomers in dehydrated castor oil by gas chromatography and gas chromatography-mass spectrometry techniques. J Am Oil Chem Soc 75(10):1297–1303
26. Tunc EA, Nezihe A, Elif D, Yılmaz O (2011) Microwave heating application to produce dehydrated castor oil, pp 398–403
27. Yan C, Ding J, Ma T, Shao R, Xu W, He J, Wang P (2017) Dehydration of castor oil over NaHSO4/MCM-41 catalyst modified by n-Dodecyltriethoxysilane. Z Anorg Allg Chem 643(12):772–779
28. Achaya KT (1971) Chemical derivatives of castor oil. J Am Oil Chem Soc 48(11):758–763. https://doi.org/10.1007/BF02638537
29. Shende PG, Jadhav AB, Dabhade SB (2002) Polyesteramide resins from dehydrated castor oil and various dibasic acids. Pigm Resin Technol 31(5):310–314
30. Sreenivasan B, Kamath NR, Kane JG (1957) Studies on castor oil. II. Hydrogenation of castor oil. J Am Oil Chem Soc 34(6):302–307
31. Trivedi RK, Vasishtha AK (1988) Low pressure hydrogenation of castor oil. J Am Oil Chem Soc 65(9):1467–1469
32. Wehrman MD, Lindberg S, Schultz KM (2016) Quantifying the dynamic transition of hydrogenated castor oil gels measured via multiple particle tracking microrheology. Soft Matter 12(30):6463–6472
33. Martinelli M, de Souza Schneider RC, Baldissarelli VZ, von Holleben ML, Caramao EB (2005) Castor oil hydrogenation by a catalytic hydrogen transfer system using limonene as hydrogen donor. J Am Oil Chem Soc 82(4):279–283
34. Devi BLAP, Karuna MSL, Rao KN, Saiprasad PS, Prasad RBN (2003) Microwave-assisted catalytic transfer hydrogenation of safflower oil. J Am Oil Chem Soc 80(10):1003–1005
35. Kulkarni MG, Sawant SB (2003) Some physical properties of castor oil esters and hydrogenated castor oil esters. Eur J Lipid Sci Technol 105(5):214–218
36. Ratnayake WMN, Pelletier G (1992) Positional and geometrical isomers of linoleic acid in partially hydrogenated oils. J Am Oil Chem Soc 69(2):95–105
37. Tagawa T, Nishiguchi T, Fukuzumi K (1978) Transfer hydrogenation and transfer hydrogenolysis: XII. Selective hydrogenation of fatty acid methyl esters by various hydrogen donors. J Am Oil Chem Soc 55(3):332–336
38. Zucolotto M (1994) Esterioquímica e mecanismo de hidrogenação catalítica heterogênea por transferência de hidrogênios de moléculas de hidroaromáticas. Dissertação de Mestrado, Instituto de Química, UFRGS, Porto Alegre
39. Xiang Y, Li X, Lu C, Ma L, Zhang Q (2010) Water-improved heterogeneous transfer hydrogenation using methanol as hydrogen donor over Pd-based catalyst. Appl Catal A Gen 375(2):289–294
40. De Souza Schneider RC, Lara LRS, Ceolin MM, Kaercher JA, Schneider M (2013) Environmental impact of castor oil catalytic transfer hydrogenation. Clean Technol Environ Policy 15(6):977–985. https://doi.org/10.1007/s10098-012-0567-1
41. Shripathi Rao H, Chari KS, Aggarwal JS (1962) Hydrogenation of castor oil: part i-influence of variables on hydrogenation efficiency. J Sci Ind Res 21D:89–92

42. Naughton FC (1974) Production, chemistry, and commercial applications of various chemicals from castor oil. J Am Oil Chem Soc 51(3):65–71

43. Prasad RBN, Rao BVSK (2017) Chemical derivatization of castor oil and their industrial utilization. In: Fatty acids. https://doi.org/10.1016/b978-0-12-809521-8.00008-8

44. Ishchuk YL, Dugina LN, Krasnokutskaya ME, Godun BA (1986) Influence of composition of technical 12-hydroxystearic acid on properties of anhydrous calcium greases. Chem Technol Fuels Oils 22(8):402–405

45. Ishchuk YL, Ishchuk LP, Maskaev AK, Kotok AA (1974) Influence of adding oleic and ricinoleic acids to 12-hydroxystearic acid on the structure and properties of lithium greases. Chem Technol Fuels Oils 10(11):833–835

46. Deshpande DP, Haral SS, Gandhi SS, Ganvir VN (2012) Transeterification of Castor oil. ISCA J Eng Sci 1(1):2–7

47. Nakarmi A, Joshi S (2014) Study on castor oil and its conversion into biodiesel by transesterification method. Nepal J Sci Technol 15(1):45–52

48. Encinar JM, Gonzalez JF, Pardal A, Martinez G (2010) Transesterification of rapeseed oil with methanol in the presence of various co-solvents. In: Proceedings Venice, pp 1–17

49. Bello EI, Mogaji TS, Agge M (2011) The effects of transesterification on selected fuel properties of three vegetable oils. J Mech Eng Res 3(7):218–225

50. Sreenivas PR, Venkata Sekhar K (2011) Development of biodiesel from castor oil. Int J Energy Sci 1(3):192–197. http://scholar.google.com/scholar?hl=en&btnG=Search&q=intitle:Development+of+Biodiesel+from+Castor+Oil#0%5Cnhttp://scholar.google.com/scholar?hl=en&btnG=Search&q=intitle:Development+of+biodiesel+from+castor+oil%230

51. Demirbas A (2009) Progress and recent trends in biodiesel fuels. Energ Conver Manage 50(1):14–34

52. Encinar JM, González JF, Pardal A (2012) Transesterification of castor oil under ultrasonic irradiation conditions. Preliminary results. Fuel Process Technol 103:9–15

53. Murugesan A, Umarani C, Subramanian R, Nedunchezhian N (2009) Bio-diesel as an alternative fuel for diesel engines—a review. Renew Sustain Energy Rev 13(3):653–662

54. Schuchardt U, Sercheli R, Vargas RM (1998) Transesterification of vegetable oils: a review. J Braz Chem Soc 9(3):199–210

55. Díaz-Álvarez A, Cadierno V (2013) Glycerol: a promising green solvent and reducing agent for metal-catalyzed transfer hydrogenation reactions and nanoparticles formation. Appl Sci 3(1):55–69

56. Brioude M d M, Guimarães DH, Fiúza R d P, Prado LAS d A, Boaventura JS, José NM (2007) Synthesis and characterization of aliphatic polyesters from glycerol, by-product of biodiesel production, and adipic acid. Mater Res 10(4):335–339

57. Meher LC, Sagar DV, Naik SN (2006) Technical aspects of biodiesel production by transesterification—a review. Renew Sustain Energy Rev 10(3):248–268

58. Zhao X, Cheng K, Liu D (2009) Organosolv pretreatment of lignocellulosic biomass for enzymatic hydrolysis. Appl Microbiol Biotechnol 82(5):815

59. Adhvaryu A, Erhan SZ, Liu ZS, Perez JM (2000) Oxidation kinetic studies of oils derived from unmodified and genetically modified vegetables using pressurized differential scanning calorimetry and nuclear magnetic resonance spectroscopy. Thermochim Acta 364(1–2):87–97

60. Hamilton RJ, Kalu C, Prisk E, Padley FB, Pierce H (1997) Chemistry of free radicals in lipids. Food Chem 60(2):193–199

61. Porter NA, Caldwell SE, Mills KA (1995) Mechanisms of free radical oxidation of unsaturated lipids. Lipids 30(4):277–290

62. Fox NJ, Stachowiak GW (2007) Vegetable oil-based lubricants—a review of oxidation. Tribol Int 40(7):1035–1046

63. Kirk RE, Othmer DF (1953) Encyclopedia of chemical technology, vol 2. The Interscience Encyclopedia, New York

64. Weiss EA (1971) Castor, sesame and safflower. Leonard Hill Books, London

65. Sinadinović-Fišer S, Janković M, Borota O (2012) Epoxidation of castor oil with peracetic acid formed in situ in the presence of an ion exchange resin. Chem Eng Process Process Intensification 62:106–113
66. Abdullah BM, Salimon J (2010) Epoxidation of vegetable oils and fatty acids: catalysts, methods and advantages. J Appl Sci 10(15):1545–1553
67. Chakrapani S, CRIVELLO* JV (1998) Synthesis and photoinitiated cationic polymerization of epoxidized castor oil and its derivatives. J Macromol Sci Pt A Pure Appl Chem 35(1):1–20
68. Chadwick AF, Barlow DO, D'addieco AA, Wallace JG (1958) Theory and practice of resin-catalyzed epoxidation. J Am Oil Chem Soc 35(7):355–358
69. de Luca MA, Martinelli M, Jacobi MM, Becker PL, Ferrão MF (2006) Ceramer coatings from castor oil or epoxidized castor oil and tetraethoxysilane. J Am Oil Chem Soc 83(2):147–151
70. DeHonor Márquez E, Nieto Alarcón JF, Vigueras Santiago E, Hernández López S (2018) Effective and fast epoxidation reaction of linseed oil using 50 wt% hydrogen peroxide. Am J Chem 8(5):99–106
71. Fürmeier S, Metzger JO (2003) Fat-derived aziridines and their N-substituted derivatives: biologically active compounds based on renewable raw materials. Eur J Org Chem 2003(4):649–659
72. Salimon J, Salih N, Yousif E (2011) Synthetic biolubricant basestocks from epoxidized ricinoleic acid: improved low temperature properties. Kemija u Industriji: Časopis Kemičara i Kemijskih Inženjera Hrvatske 60(3):127–134
73. Thamaraichelvi C, Priyatharsini C, Barathiselvam C (2016) Development of bio-based nanocomposite from epoxidized castor oil, layered silicate and their characterization. IOSR J Appl Chem 9(2):26–29
74. Sun J, Aly KI, Kuckling D (2017) Synthesis of hyperbranched polymers from vegetable oil based monomers via ozonolysis pathway. J Polym Sci A Polym Chem 55(12):2104–2114
75. Omari A, Mgani QA, Mubofu EB (2015) Fatty acid profile and physico-chemical parameters of castor oils in Tanzania. Green Sustain Chem 5:154–163
76. Loan LD, Murray RW, Story PR (1965) The mechanism of ozonolysis. Formation of cross ozonides. J Am Chem Soc 87(4):737–741
77. Rangarajan S, Palaniappan NP (1958) Catalysts in sulfation of castor oil. Ind Eng Chem 50(12):1787–1788
78. Zamiri R, Zakaria A, Abbastabar H, Darroudi M, Husin MS, Mahdi MA (2011) Laser-fabricated castor oil-capped silver nanoparticles. Int J Nanomedicine 6:565
79. Bishai AM, Hakim IK (1995) Electrical properties of an insulating varnish. Polym Int 36(4):315–324
80. Gherca D, Pui A, Cornei N, Cojocariu A, Nica V, Caltun O (2012) Synthesis, characterization and magnetic properties of MFe2O4 (M= co, mg, Mn, Ni) nanoparticles using ricin oil as capping agent. J Magnet Magnet Mater 324(22):3906–3911
81. Santhanam N, Balu M, Sreevatsan S (2015) Production and uses of key castor oil oleochemicals. White paper
82. Li H, Niu S, Lu C (2017) Pyrolysis characteristics of castor oil through thermogravimetric coupled with Fourier transform infrared spectroscopy. Process Eng 205:3705–3710. https://doi.org/10.1016/j.proeng.2017.10.292
83. Anderson D (2005) A primer on oils processing technology. Baileys Ind Oil Fat Prod 4:31–45
84. Domsch A (1994) Chemistry and application of undecylenic acid and derivatives thereof for cosmetics. Seifen Öle Fette Wachse 120(6):322–329
85. Flinn RA (1978) Castor oil cracking products. Encyclop Chem Process Design 6:401–420
86. Gupta AS, Aggarwal JS (1954) 10-Undecenoic acid and heptaldehyde from castor oil. J Sci Ind Res B 13:277–280
87. Hunting ALL (1981) Properties and uses of undecylenic acid and derivatives. Cosmet Toiletrics 96:29–34
88. Maher KD, Bressler DC (2007) Pyrolysis of triglyceride materials for the production of renewable fuels and chemicals. Bioresour Technol 98(12):2351–2368

89. Sudipta D, Prakash C, Sujan S, Gajanan S, Mall BK (2011) Synthesis of biodiesel by pyroly-sis of castor oil. Asian J Chem 23(6):2614–2618
90. Vernon AA, Ross HK (1936) Some characteristics of the residue from the cracking of castor oil. J Am Chem Soc 58(12):2430–2433
91. Vishwanadham B, Rao HS, Sadasivudu D, Khan AA (1995) Pyrolysis of castor oil methylest-ers to 10-undecenoic acid and heptaldehyde. Indian J Chem Technol 2(3):119–128
92. Lligadas G, Ronda JC, Galià M, Cádiz V (2010) Oleic and undecylenic acids as renewable feedstocks in the synthesis of polyols and polyurethanes. Polymers 2(4):440–453
93. Mustafa J, Khan SI, Ma G, Walker LA, Khan IA (2005) Synthesis and in vitro cytotoxic activity of N-, F-, and S-ether derivatives of podophyllotoxin fatty acid adducts. Lipids 40(4):375–382
94. Rahman VPM, Mukhtar S, Ansari WH, Lemiere G (2005) Synthesis, stereochemistry and biological activity of some novel long alkyl chain substituted thiazolidin-4-ones and thiazan-4-one from 10-undecenoic acid hydrazide. Eur J Med Chem 40(2):173–184
95. Van der Steen M, Stevens CV (2009) Undecylenic acid: a valuable and physiologically active renewable building block from castor oil. ChemSusChem 2(8):692–713. https://doi.org/10.1002/cssc.200900075
96. Van der Steen M, Stevens CV, Eeckhout Y, De Buyck L, Ghelfi F, Roncaglia F (2008) Undecylenic acid: a valuable renewable building block on route to Tyromycin a derivatives. Eur J Lipid Sci Technol 110(9):846–852
97. Dytham RA, Weedon BCL (1960) Organic reactions in strong alkalis-III: fission of keto-and hydroxy-acids. Tetrahedron 8(3–4):246–260
98. Hargreaves GH, Owen LN (1947) 143. Reactions of carbinols in the presence of alkali. Part II. The scission of ricinoleic acid. J Chem Soc (Resumed):753–756
99. Diamond MJ, Binder RG, Applewhite TH (1965) Alkaline cleavage of hydroxy unsaturated fatty acids. I. Ricinoleic acid and lesquerolic acid. J Am Oil Chem Soc 42(10):882–884
100. Logan RL, Udeshi SV (2002). Method for preparing sebacic acid and octanol-2. Google Patents
101. Ries CD, Totah TS (1999). Method for preparing cleaved products from castor oil or deriva-tives thereof. Google patents
102. Kim J, Hefferan TE, Yaszemski MJ, Lu L (2009) Potential of hydrogels based on poly (eth-ylene glycol) and sebacic acid as orthopedic tissue engineering scaffolds. Tissue Eng Part A 15(8):2299–2307
103. Tang J, Zhang Z, Song Z, Chen L, Hou X, Yao K (2006) Synthesis and characteriza-tion of elastic aliphatic polyesters from sebacic acid, glycol and glycerol. Eur Polym J 42(12):3360–3366
104. Goswami D, De S, Basu JK (2012) Effects of process variables and additives on mustard oil hydrolysis by porcine pancreas lipase. Braz J Chem Eng 29(3):449–460
105. Cangemi JM, dos Santos AM, C Neto S, Chierice GO (2008) Biodegradation of polyurethane derived from castor oil. Polímeros 18(3):201–206
106. Nayak PL (2000) Natural oil-based polymers: opportunities and challenges. J Macromol Sci Pt C Polym Rev 40(1):1–21
107. Mallu P, Somashekar R (2000) Synthesis and characterization of castor oil based polyurethane-polyacrylonitrile interpenetrating polymer networks. Bull Mater Sci 23(5):413
108. O'Lenick AJ Jr, Lavay C (2002) Polymeric castor polyesters. Google Patents
109. Prashantha K, Pai KVK, Sherigara BS, Prasannakumar S (2001) Interpenetrating polymer networks based on polyol modified castor oil polyurethane and poly (2-hydroxyethylmethacrylate): synthesis, chemical, mechanical and thermal properties. Bull Mater Sci 24(5):535–538
110. Sokolsky-Papkov M, Shikanov A, Ezra A, Vaisman B, Domb AJ (2008) Fatty acid-based biodegradable polymers: synthesis and applications. ACS Publications, Washington, DC
111. Yeganeh H, Hojati-Talemi P (2007) Preparation and properties of novel biodegradable polyurethane networks based on castor oil and poly (ethylene glycol). Polym Degrad Stab 92(3):480–489

112. Slocombe RJ, Hardy EE, Saunders JH, Jenkins RL (1950) Phosgene derivatives. The preparation of isocyanates, carbamyl chlorides and cyanuric acid1. J Am Chem Soc 72(5):1888–1891
113. Alaa MA, Yusoh K, Hasany SF (2015) Synthesis and characterization of polyurethane–organoclay nanocomposites based on renewable castor oil polyols. Polym Bull 72(1):1–17
114. Ibrahim S, Ahmad A, Mohamed NS (2015) Characterization of novel castor oil-based polyurethane polymer electrolytes. Polymers 7(4):747–759
115. Totaro G, Cruciani L, Vannini M, Mazzola G, Di Gioia D, Celli A, Sisti L (2014) Synthesis of castor oil-derived polyesters with antimicrobial activity. Eur Polym J 56:174–184

Sustainability of the Catalytic Process for Biomass Conversion: Recent Trends and Future Prospects

Rohidas Bhoi, Virendra Kumar Saharan, Suja George, and Sonal

Abstract Depleting conventional resources and increasing energy demand have placed immense pressure on the environment and forced mankind to look for alternate and sustainable energy resources. Biomass is a promising resource which is environment friendly as well as sustainable. Lignocellulosic biomass can be fractionated into cellulose, hemicelluloses, and lignin, out of which the structure of lignin makes catalytic processing more challenging. The selection of suitable solvent, catalysts, and reaction conditions for biomass conversion has a vital role in the yield and composition of targeted products. Biomass can be converted into oil, gas, and char using a suitable catalyst and conversion processes. Valuable chemicals and transportation fuel can be generated from oil obtained from sustainable biomass such as agricultural waste, forestry products, inedible plants, etc. The product obtained from most of the conversion processes is a complex mixture of chemicals demanding further separation and upgradation. Catalytic oil upgradation is necessary before being used as a transportation fuel. It is essential to identify the basic/platform components that can be produced from biomass and serve as feedstock for the synthesis of the majority of the chemicals. Catalyst can facilitate the selective transformation of molecules provided it is sustainable in terms of its activity and regeneration. An emerging approach integrates various routes of biomass conversion technologies such as catalytic pyrolysis, hydrolysis, and liquefaction over a suitable solid catalyst to transform biomass into useful chemicals and fuels. This chapter summarizes the technological challenges to selectively convert biomass to oil or basic chemicals and fuels by catalytic processes.

R. Bhoi

Department of Chemical Engineering, Malaviya National Institute of Technology, Jaipur, Rajasthan, India

Department of Chemical Engineering, Indian Institute of Technology Bombay, Mumbai, Maharashtra, India

V. K. Saharan · S. George · Sonal (✉)
Department of Chemical Engineering, Malaviya National Institute of Technology, Jaipur, Rajasthan, India
e-mail: sonal.chem@mnit.ac.in

1 Introduction

Biomass has the potential to produce value-added chemicals and has the potential to become an alternative to fossil fuels. It is a stored solar energy in the form of chemical bonds of carbon-hydrogen by photosynthesis or the metabolic activity of the organism. The reason for the search for an alternate form of energy is the depletion of fossil fuel reserves, as well as the emission of greenhouse gases and its impact on the environment due to the consumption of fossil fuels. The potential of biomass can be gauged from the fact that it is recognized as the fourth largest source of energy. The other sources being crude oil, coal, and natural gas [1].

Utilization of biomass as a fuel source is sustainable that will help to balance out the net emission of CO_2 by the interplay between photosynthesis and biorefinery. Biomass is mainly obtained from lignocellulose, lipid, and starchy crops. There are various methods for conversion of biomass, viz., catalytic processes like biochemical (fermentation and enzymatic hydrolysis) and thermochemical (combustion, pyrolysis, and gasification) processes, transesterification, and isomerization, etc. [2]. These processes make use of both homogeneous and heterogeneous catalysts with relative advantages and disadvantages. The choice of conversion process depends on factors such as type of feedstock, the volume of biomass, targeted chemicals, reactor type, etc.

1.1 Biomass Resources

A complex linkage exists between biomass for energy and materials, biomass for food production, biomass for energy use, water requirement, and their impact on biodiversity and climate change. Figure 1 illustrates the complexity by showing key relationships and assumptions. Biomass feedstock can be classified into three groups, viz., (1) agricultural waste, municipal solid waste, and forest residue, (2) surplus forestry, and (3) biomass produced via cropping system. Altogether, the three categories could produce 500 EJ/year of energy. As far as category one is concerned, the biomass supply is almost inevitable. However, conventional uses of biomass can affect its availability for energy applications. Approximately 100 EJ/year of energy is estimated from this source, i.e., biomass residue [3]. The second source, surplus forestry, indicates the possible growth of surplus forests that can account for 60–100 EJ/year of energy worldwide. The availability depends on sustainable forest management principles [3]. The third category includes the
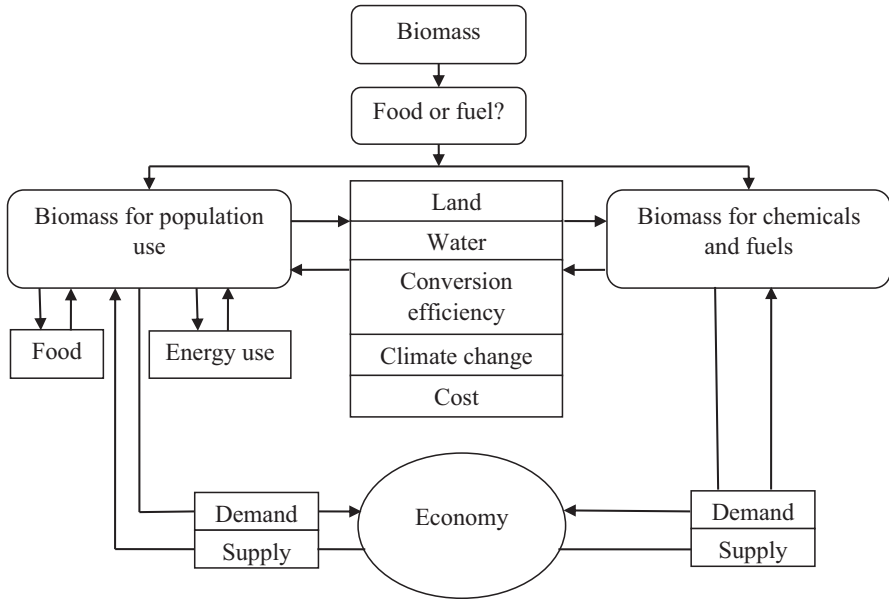
Fig. 1 Key relationships relevant to the assessment of biomass potentials
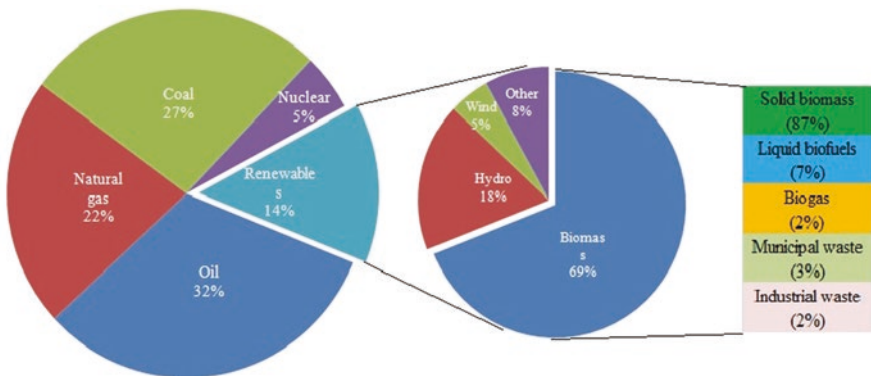
Fig. 2 Bioenergy share in world energy demand in the year 2017

possible surplus land available for energy crops. The better quality land, which is not utilized for main crops and requires less water and fertilizer, can be used for this purpose. The potential contribution from the third source is estimated to be 120 EJ/ year. The arid land (water scarce and degraded) can be used for energy crops and can account for 70 EJ/year [3]. The contribution will depend on the choice of energy and planting rate and will be influenced by the water availability, environmental constraints, logistic issues, etc. The share of bioenergy in total energy demand in the year 2017 is shown in Fig. 2 [4]. The bioenergy share is 3% of the agriculture and energy sector, and less than 1% of agriculture land is used for an energy crop.

Another source of biomass is microalgae and macroalgae (seaweed) as a feedstock for bioenergy but is limited due to its relatively low dry matter content. So it is difficult to evaluate the sustainability and economic competitiveness of algal biomass [3].

Even though the potentials of biomass can be evaluated, the question remains as to how effectively this potential can be utilized? Factors like economic and environmental impact have to be taken into account while evaluating the utilization of biomass potential. Typically, USD 3–4/GJ is considered as a threshold value to compare it with fossil fuel price. Higher fossil fuel price and government incentives in favor of bioenergy can certainly make it more sustainable [3].

The land for agriculture and for bioenergy crops will compete with each other, and preference will be given to agriculture in the countries with an agricultural-based economy, like India. Additionally, the land will be constrained by environmental and logistical factors. The modern and efficient methods of agriculture can free part of the land for bioenergy crops. It is apparent that the first generation of food crops will contribute in a major way compared to second-generation energy crops. The selection of conversion technology is chosen on the basis of feedstock availability and suitability. The various available technologies are elaborated in the following sections. A huge estimate of ten billion tons of dry biomass is produced annually, which is equivalent to 10% of the global energy demand. This biomass could generate energy equivalent to two billion tons of standard coal [5].

1.2   Components of Lignocellulosic Biomass

The biomass is available at a low cost, and there are no competing interests between lignocellulosic biomass and food source. The three basic components of lignocellulosic biomass are (1) hemicellulose consisting of five-carbon sugar polymers (20–35%), (2) cellulose consisting of six carbon glucose polymers (35–50%), and (3) lignin consisting of aromatic compound polymers (10–25%). Hemicellulose is easy to hydrolyze and can be converted at mild operating conditions due to the low degree of polymerization. Cellulose is a straight-chain polymer and can be depolymerized into glucose, which is further decomposed into useful chemicals and fuels. The processing of cellulose and hemicelluloses involves similar reactions but yields different products. Lignin is an amorphous polymer and has aromatic functionality. The structure of hemicellulose and lignin varies from biomass to biomass. The decomposition behavior of each of these components is different from each other and depends on temperature, heating rate, and contamination. Hemicellulose and lignin can affect the degradation of cellulose but will not hinder each other's process. As a rule of thumb, cellulose leads to bio-oil formation, and lignin leads to bio-char formation. Also, higher volatile matter leads to bio-oil and syngas formation, and high fixed carbon leads to bio-char formation.
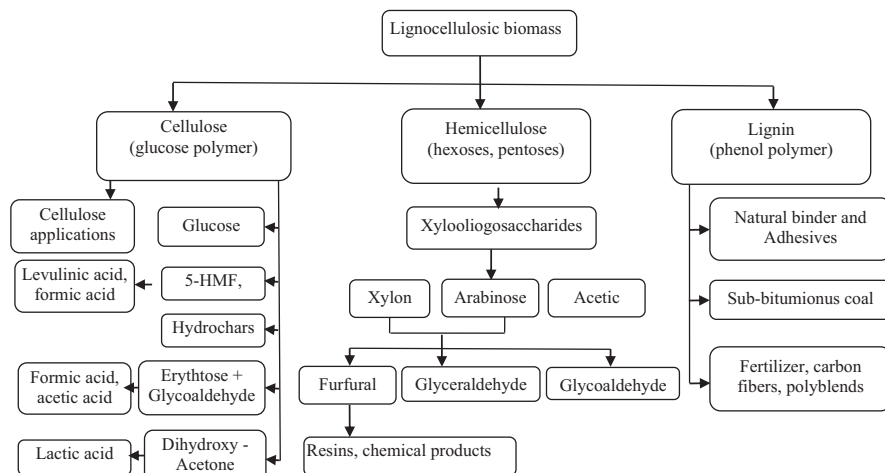
Fig. 3 Representation of products from lignocellulose based biorefinery

Biomass moisture content has a significant influence on the heat transfer process and product distribution. High moisture content helps to increase the bio-oil yield, which is a poor fuel that contains nearly 50% water and highly oxygenated products. The overview of lignocellulosic feedstock-based biorefinery is shown in Fig. 3. As can be seen, the biorefinery is analogous to petroleum refinery and can produce multiple products ranging from chemicals to fuels.

In biomass processing, the three components are separated and processed separately. Typically, pretreatment steps to remove hemicellulose and lignin from biomass. Cellulose is deconstructed into glucose monomer and is the feedstock for useful products, i.e., 5-hydroxymethylfurfural (5-HMF). Xylan is the major component (8–25%) representing hemicelluloses and used to produce furfural and its derivatives [6]. Lignin is a major source of aromatic functionality and consists of p-coumaryl alcohol monomer, coniferyl alcohol monomer, and sinapyl alcohol monomer. Lignin is a source for high carbon and contains nearly 40% possible energy of biomass.

1.3 Biomass Conversion Strategies

Biomass as a resource is complex and extremely varied in nature, and one or more conversion steps are needed to convert it into a usable energy form. Biomass can be used without being fractionated, such as combustion, but with low efficiency. For efficient use, each lignocellulosic fraction needs to be isolated for processing, as each one of them has a distinct structure. Typically, the following conversion

strategies incorporating various catalysts are adapted for the conversion of lignocel-lulosic biomass to useful products:

1. Chemical
2. Thermal
3. Microbiological

Chemical catalytic processing is gaining importance as the resultant product exhibits properties similar to petroleum-based products. These processes are conducted at mild operating conditions relative to non-catalytic methods and can be tuned to get the desired product distribution. The various useful chemical processes are catalytic pyrolysis, hydroprocessing, hydrolysis, dehydration, oxidation, isomerization, transesterification, etc. Homogeneous, as well as heterogeneous, catalysts can be used for the catalytic process. Homogeneous catalyst has a high turnover frequency (TOF); however, it poses problems like toxicity, corrosivity, reusability, and complex postprocess separation. Hence, heterogeneous catalysts are a better option compared to their homogeneous counterpart. As shown in Fig. 3, hemicelluloses are used to produce furfural, lignin is used to produce aromatic compounds, and cellulose is used to produce levulinic acid or glucose. All of this can be achieved by using conventional as well as modified catalysts such as zeolites and silica monometallic as well as bimetallic catalysts [6]. During biomass processing, the C-C coupling reactions such as oligomerization, aldol condensation, and ketonization use acid or metal oxide catalysts, whereas reforming, hydrogenolysis, hydrogenation, and oxidation use bimetallic catalysts. Bimetallic catalysts are preferred over monometallic catalysts due to their increased catalytic activity, modified selectivity, and improved catalyst stability. In the case of simple processing, the entire biomass is subjected to thermochemical processes such as gasification, pyrolysis, etc. The biological route utilizes living microorganisms (enzymes, bacteria) to degrade biomass feedstock and produce liquid and gaseous fuels.

   The abovementioned technologies can be used independently or in combination, such as thermochemical processing (catalytic pyrolysis/gasification). The choice of conversion route will depend on many factors such as type of feedstock, targeted products, the volume available, and readiness of the technology. In addition, handling, transport, and storage of the biomass are cumbersome and sometimes costlier, making the whole process uneconomical. So all factors needs to be considered while selecting a suitable process for biomass conversion.

2   Catalytic Processes for Biomass Conversion

The catalyst requirement for biomass conversion is different from the petroleum industry. Petroleum feedstocks are oxygen-deficient, whereas biomass is rich in oxygen. Hence, conversion strategy differs as the addition of functional groups, and removal of it is required for petroleum and biomass feedstocks, respectively. Biomass molecules are highly complex and vicious and pose mass transfer limitations

whenever heterogeneous catalysts are used. The energy density of biomass can be increased through the removal of oxygen and can be achieved through various conversion processes mentioned earlier. Thermal processes are nonselective, whereas chemical processes are selective such as dehydration, hydrogenolysis, decarboxylation, and decarbonylation. The catalyst then affects the conversion rates and the selectivity of the products but suffers from deactivation. Many catalysts for biomass conversion have been tested, but few found suitable on the basis of stability, selectivity, and reusability. Most of the catalysts are tested with model components, and the problem appears when real feedstocks with impurities are used. Bimetallic catalysts seem to be promising as the catalyst properties can be modified to handle real feedstocks [6].

The porosity of the catalysts plays a vital role in biomass conversion. Porous materials with mixed pores (micro, meso, and macro), compared with single-mode pores, are more suitable for biomass conversion [7]. As an important step in processing, biomass is converted to platform chemicals through various routes. There are five platforms reported in the literature. They are the sugar platform, thermochemical or syngas platform, biogas platform, carbon-rich chain platform, and plant product platform. The sugar platform focuses on the fermentation of sugar extracted from biomass; the thermochemical platform focuses on the gasification/pyrolysis of biomass feedstock; the biogas platform decomposes the biomass through anaerobic digestion with the help of microorganism, carbon-rich platform converts oil and fats via etherification/transesterification; and plant product platform is the biorefinery operations in a plant kingdom itself rather than in an industrial plant. Sometimes, the plant strains are genetically modified to produce more feedstock or chemicals than it does naturally. Presented below is the list of top 12 chemical products that form the building blocks of the biorefinery by evaluating their potential market, their derivatives, and the technical complexity of the synthesis pathways [8]; these are:

• 1,4- Succinic, 1,4-fumaric, and 1,4-malic acids	• 2,5-Furandicarboxylic acid
• 3-Hydroxy propionic acid	• Aspartic acid
• Glucaric acid	• Glutamic acid
• Itaconic acid	• Levulinic acid
• 3-Hydroxybutyrolactone	• Glycerol
• Sorbitol	• Xylitol/arabinitol

2.1 Catalytic Processes for Lignocellulosic Biomass Conversion

In this section, the various catalytic processes for the conversion of biomass into fuels and valuable chemicals are discussed. The chemical processes for biomass conversion are sensitive to reaction conditions and nature of solvents and catalysts and produce a complex mixture of products requiring further separation and

upgrading. An integrated processing approach with a multifunctional catalyst will be beneficial for biomass conversion.

2.1.1   Catalytic Hydrolysis-Acid/Alkaline Catalysts

The biomass must be pretreated to improve the product yield in downstream processing. The pretreatment changes the biomass structure that can be achieved either by physical, chemical, and thermal processing or sometimes by a combination of these treatment methods. The aim of pretreatment is to decrystallize cellulose, separate hemicellulose, and break the lignin seal. During hydrolysis, the cellulosic component of lignocellulosic biomass is converted to glucose and xylose as the main products. However, due to its crystalline form and hydrogen bonding, the hydrolysis of cellulose is significantly difficult and requires the use of strong liquid acid as a catalyst [9]. This process yields reducing sugars, which is furthermore converted to useful chemicals. Among the different liquid acids, mineral acids (H_2SO_4 and HCl), as well as organic acids (carboxylic acid, p-toluenesulfonic acid), can be used as a catalyst. Dilute acids are used to avoid corrosion of process equipment and also the degradation of glucose and xylose to products such as 5-HMF. Dilute H_2SO_4 has been used commercially for the production of furfural from cellulosic biomass. It is also used for the hydrolysis of hemicelluloses to sugar products such as xylose. The limited solubility of cellulose in water is a major issue; hence, solvents like ethanol are commonly used. The effect of reaction conditions such as temperature and acid concentration was investigated with four timber species (aspen, balsam fir, basswood, and red maple) and switchgrass. They were subjected to hydrolysis in the presence of dilute H_2SO_4 in an identical reaction condition (temperature, 160–190 °C; H_2SO_4 concentration, 0.25–1% (w/v), particle size (28—10/20 mesh)). The maximum product yield was 94% for xylose and 13.6% for glucose. Both temperature and acid concentration have a strong influence on the reactions [10]. Various solid catalysts used for hydrolysis are discussed in subsequent sections of this chapter.

In alkaline hydrolysis, lower temperatures and pressures are utilized compared to acid hydrolysis, but the treatment time runs in a few hours to a few days as against minutes or seconds for the acid catalyst. The treatment effectiveness largely depends on the lignin content of the biomass material. Sodium, calcium, potassium, and ammonium hydroxides are the commonly used alkaline agents, of which sodium hydroxide is widely used. The enzymatic hydrolysis of cellulose is one of the reactions influenced by alkali pretreatment [10].

2.1.2   Catalytic Solvolysis of Lignocellulosic Biomass

In solvolysis, an organic molecule modifies the chemical and physical properties of cellulose so that it can be in contact with the catalyst for a longer time. The organic molecule acts both as solvent and reactant, and therefore it has a significant effect on the product formation. For example, solvent methanol in the presence of dilute

H_2SO_4 reacts with lignocelluloses to give methyl glycoside. A mixture of methanol in water and ethanol in water was tested to be suitable for liquefaction of lignocelluloses [11]. Comparatively, the solvolysis of cellulose (in water or alcohol or mixture) is difficult than hemicelluloses and lignin due to its chemical structure. The typical solvents used for this solvolysis are acetone, ethylene glycol, toluene, etc. The solvolysis method is also used for lignin extraction along with other pretreatment methods such as acid/alkaline hydrolysis and reductive or oxidative catalytic fractionation. Non-catalytic solvolysis of lignocellulosic biomass is possible but requires longer reaction time and results in low product yield.

2.1.3 Hydrothermal Liquefaction of Lignocellulosic Biomass

The objective of the liquefaction process is to maximize the production of C_1–C_6 compounds over xylose and glucose. Compared with the catalytic hydrolysis process, the hydrothermal process targets the deep degradation of lignocellulosic biomass that involves isomerization and dehydration of glucose. The final distribution of the product depends on the type of catalyst used. An advantage of the hydrothermal treatment is that it does not get affected by the presence of water in biomass, whereas other processes require pre-drying of biomass. Numerous halide, sulfate, and alkaline catalysts are used for the hydrothermal liquefaction process such as $CrCl_3$, $FeCl_3$, $CuCl_3$, $NiSO_4$, $CoSO_4$, KOH, $Ca(OH)_2$, etc. The use of halide/sulfate catalysts promotes the formation of levulinic acid, furans, and formic acid, whereas alkaline catalysts give bio-oil and phenolic compounds as major products. The hydrothermal reaction is typically carried out at ~500 K in order to convert cellulose completely. In the case of bio-oil, higher reaction temperature (>500 K) and longer reaction times lead to the formation of secondary products, thereby decreasing the bio-oil yield. The separation of the products produced from catalytic hydrothermal liquefaction requires multiple extraction steps with different types of solvents due to the complex mixture of liquid, gases, and tar. At present, it is uneconomical to produce bio-oil by hydrothermal liquefaction when compared with petro-diesel and gasoline. Hydrothermal liquefaction is energy-intensive and time-consuming [9]. Therefore, innovative separation methods are required for the separation of products obtained from hydrothermal liquefaction. Comparatively, the fast pyrolysis method discussed in the following section is more promising.

2.1.4 Catalytic Pyrolysis

Pyrolysis is a high-temperature decomposition process carried out in the absence of oxygen and can be used to convert lignocellulosic biomass to bio-oil in the absence of oxygen. Pyrolysis of biomass results in three products, namely, oil, gas, and solid char. Pyrolysis operating parameters such as residence time and heating rate can be tuned to get the maximum of oil or gas or char. Furthermore, pyrolysis can be classified as slow pyrolysis (heating rate <20 °C/min, residence time >15 min), fast

pyrolysis (heating rate 10–200 °C/s, residence time 0.5–10 s), and flash pyrolysis (heating rate >1000 °C/s, residence time <0.5 s). Slow pyrolysis is traditionally used for maximizing solid yield, whereas fast, as well as flash, pyrolysis is preferred for bio-oil yield [1]. Pyrolysis reduces the H/C ratio of the products against hydrogenation that improves the H/C ratio. The reactions that take place during pyrolysis are depolymerization, dehydration, decarboxylation, esterification, condensation, cyclization, etc. The bio-oil obtained by biomass pyrolysis is a complex mixture of organic acids, ketones, esters, and aromatic compounds. Pyrolysis oil is acidic in nature and contains aqueous as well as organic phases. Hence, further treatment is necessary to get useful fuel-like products. The major factors that affect the progress of pyrolysis are biomass heating rate, operating temperature, residence time, and the catalyst [9]. The pyrolysis process can be improved by proper selection of heating rate, operating temperature, catalyst, and residence time.

Catalyst helps in enhancing the rate of cracking of higher molecules into the smaller ones. Each catalyst exhibits its own kinetics that results in varied product distribution under a different set of operating parameters. The catalytic pyrolysis process can be classified into three different groups, viz., catalyst pre-added in the feedstock, catalyst added into the primary reactor, and catalyst in the secondary reactor located downstream to the primary reactor. The heterogeneous catalysts used in the pyrolysis process are divided into four catalytic groups, viz., dolomite type, Ni-type, alkali metal, and noble metal catalysts [12]. A bimetallic catalyst is a promising option for biomass upgrading using pyrolysis. Fast pyrolysis is a proven technology to convert renewable feedstocks to an energy-rich liquid product (~17 MJ/kg). Fast pyrolysis utilizes heating of biomass at a high rate and rapid cooling of vapor (residence time <2 s), thereby minimizing the secondary cracking reactions and polymerization. Fast pyrolysis is two to three times more economical than liquefaction and gasification but exhibits a complex reaction mechanism.

Catalytic pyrolysis is preferred as it increases the reaction rate and exhibits selectivity toward the desired product. Acid and base, in homogeneous as well as heterogeneous forms, are used as catalysts. The pretreatment of the biomass also has positive effects on pyrolysis. The widely used catalysts for pretreatment of biomass are H_2SO_4, HCl, H_3PO_4, and Lewis acids. For example, pinewood sawdust was treated with phosphoric acid before being subjected to fast pyrolysis, which increased the formation of levoglucosan content. Levoglucosan was further converted to syngas [13]. In the case of supported heterogeneous catalyst, the activity change with the change of support was evident from the pyrolysis of cellulose to produce 5-methyl furfural at 773–1073 K. The catalyst SO_4^{2-} supported on TiO_2 yield furfural, while SO_4^{2-} supported on ZrO_2 yield furan [9]. The solvent also plays an important role in pyrolysis by dissolving lignocellulosic biomass or reaction intermediates and thereby increases the yield of products. It was observed that the yield of levoglucosenone and furfural is found to increase when pyrolysis of cellulose is carried out at 473 K for 6 min using H_2SO_4 as a catalyst and tetramethyl sulfone ($C_4H_8O_2S$) as a solvent [14]. The acid and alkaline catalysts used in pyrolysis exhibit a corrosive effect and have its effect on the stability of the bio-oil. Hence, the

use of phosphates, sulfates, and chlorides is suggested in place of these catalysts [15]. Use of zeolite-based catalysts such as ZSM-5 and MCM-41 has an advantage such that selective pyrolysis can be conducted to obtain bio-oil containing hydrocarbons, much like the gasoline. However, the catalyst activity may decrease as a result of coke formed on the catalyst surface [16]. The lignocellulose biomass, along with catalyst and reaction condition, should be selected carefully to get the desired product.

2.1.5   Catalytic Gasification

Gasification is the process of obtaining gaseous products such as H_2 and syngas by thermochemical conversion of biomass in an oxygen-deficient environment. The product syngas is further converted to hydrocarbon fuel through Fischer-Tropsch synthesis. The gasification followed by Fischer-Tropsch is referred to as indirect liquefaction of lignocellulosic biomass. Another route to make syngas is partial oxidation of lignocellulosic biomass at elevated temperatures (800–900 °C). Air is used as a source of oxygen; hence, separation of nitrogen becomes a problem in biomass gasification. The tar formed during gasification contains polyaromatic hydrocarbons, and its conversion to useful products requires multiple processes. To avoid tar formation, steam gasification is preferred where water at supercritical conditions is used to improve the solubility of biomass in water, thereby reducing the mass transfer limitations. Under supercritical conditions (673 K and 1 MPa), cellulose was converted to methane over Ru/TiO_2 catalyst, and a 44% yield of methane was obtained [17]. The catalyst can deactivate due to coke formation. Also, the tar formation can block and foul the downstream process equipment. The best way is to convert tar into syngas using a multifunctional catalyst and remove bio-char by catalytic combustion. One of the risks associated with biomass gasification is incomplete combustion leading to the emission of toxic gases and particulate matter.

2.1.6   Integrated Processing

In integrated processing, two or more processes are combined together to produce the desired product. For example, in hydroprocessing, hydrogenation follows the hydrolysis, solvolysis, liquefaction, and pyrolysis. In the integrated approach, the depolymerization is followed by an in-situ decomposition to yield commodity chemicals and fuels. On decomposition, the oxygenated molecule is obtained, which is further deoxygenated/hydrogenated to get new C-C bonds. The commonly used catalysts for hydrogenation are Pt, Ru, and Pd and for hydrolysis are liquid acids. When a multifunctional catalyst ($Pt/\gamma-Al_2O_3$) is used, the process of decomposition and hydrogenation occurs simultaneously. For example, a gasoline-like product is obtained (carbon yield, 57%; octane number, 96.5) when maple

wood is hydrolyzed using H_2SO_4 and then hydrogenated over metal Ru and Pt catalyst in an integrated process. The process was carried out at 433 K [18].

2.2 Advanced Heterogeneous Catalysts for Biomass Conversion

Heterogeneous catalysts are characterized by size, shape, and porosity. The nanosize metal catalyst shows improved properties such as selectivity, durability, reusability, and other such properties compared to their bulk counterparts [19]. This is beneficial for biomass conversion as it results in improved interaction between active sites and reacting molecules. The porosity of the solid catalyst is an important tunable property that can influence the product selectivity. The widely used porous catalysts for biomass processing are zeolites and silica. Multipore catalysts (micro, meso, and macro) are preferred over monopore catalyst to overcome certain drawbacks of monopore catalyst such as mass transfer limitation resulting in poor selectivity, catalyst deactivation, and low conversion.

2.2.1 Zeolites, Silica, and Metal Oxides

Porous materials are classified as micropore (diameter up to 2 nm), mesopore (diameter between 2 and 50 nm), and macropore (diameter above 50 nm). Zeolites are microporous materials with tunable Brønsted and Lewis acidity that makes them suitable candidates for biomass conversion. For example, sugarcane bagasse has been fast pyrolyzed to aromatics (yield 12.4%) and olefins (yield 10.9%) using zeolite catalysts. Also, HZSM zeolites are used for catalytic hydrolysis of furfuryl alcohol to levulinic acid with a 70% yield. Zeolites are also used for various conversion processes such as upgrading glycerol to valuable chemicals, aromatic hydrocarbons from furans, phenolic components from lignin, etc. [2]. Zeolites as support can accommodate various metals, and their oxides and can be used in application such as biomass pyrolysis (Fe/HZSM-5), glycerol upgradation (Sn/HZSM-5), and production of other biomass-derived components (Pt/(NH₄-USY).

Zeolite suffers from mass transfer limitations due to its microporous nature. This can be overcome by the use of silica that has a mesoporous structure. Silica can accommodate different functional groups and has a high BET surface area (400–1400 m²/g), tunable pore diameters, and optimized acid sites [20]. Therefore, the mesoporous silica catalysts are ideal candidates for the conversion of bulky biomass molecules. For example, glucose is converted to 5-hydroxymethylfurfural (5-HMF) over SiO_2-Al_2O_3 catalyst. Similarly, lignin can be converted to aromatic hydrocarbon using silica-based catalysts [21]. Aluminum-doped silica catalyst with varying silica-alumina ratio was used for the conversion of lignin to aromatics. For example, Al-SBA-15 (Si/Al = 50) was used for pyrolysis of corncob to selectively

get 2-methoxy phenylacetate [22]. Also, the MCM-41 catalyst was found to be useful for converting ethanol to ethylene at temperatures above 350 °C [23]. For the conversion of cellulose to hydrogen, a higher hydrogen yield was obtained with Ni/KIT6 and Ni/SBA15 [24]. The better performance of the silica-supported catalyst is attributed to higher BET surface area and reduced diffusional resistance due to large pore diameter. The bimetallic catalyst can also be supported on silica (CoCu/SBA-15) and used for hydrogenation reactions such as furfural to furan. In a similar reaction, about 99% conversion of furfural can be achieved with 80% selectivity to furfuryl alcohol. The high conversion is due to the synergistic effect of metal-metal and metal-support interactions [25].

Metal, metal oxides, and their combinations are the commonly used catalysts for oxidation and hydrogenation reactions. In general, the metals present on the left side of the transition metal series in the periodic table exhibit good activity for oxidation reactions in their bulk form. At the same time, many materials (like Au for oxidation) that do not exhibit any activity in their bulk form become active catalysts at the nanoscale (1–100 nm) due to improved surface and electronics properties [26]. Hence, careful selection of metal catalysts for the oxidation process requires information of their position in the periodic table as well as their properties at the nanoscale. Mixed metal oxides exhibit attractive catalytic activity due to their enriched acid-base, redox, and surface area properties. However, their oxidizing ability for biomass oxidation can reduce due to excess basicity. As biomass conversion is conducted at harsh hydrothermal conditions, the hydrothermal stability of the catalyst is of paramount importance. Importantly, metal oxides such as TiO_2, ZrO_2, CeO_2, and ZrO_2 exhibit higher hydrothermal stability [27]. Despite all these advantages, the control over the aggregation of metal nanoparticles during synthesis and reaction remains a great challenge. This can be tackled by depositing the nanoparticles on high surface area metal oxide support. Metal-support interaction enhances the properties of nanoparticles [28]. For example, $PtSn/\gamma-Al_2O_3$ was able to convert mono- and polysaccharides with higher yield compared to PtSn/C [29]. A well-dispersed Ni nanoparticle on SiO_2 was used in the levulinic acid hydrogenation to γ-valerolactone and performed well due to the presence of optimum porosity and highly dispersed nanoparticles [30].

2.2.2 Micro- and Mesoporous Catalysts for Catalytic Processing of Edible/Non-edible Biomass

The edible biomass comprises lipids and starch, whereas non-edible biomass includes lignocellulosic materials. Among the edible biomass feedstocks, sugarcane or corn is converted to bioethanol via the fermentation route, whereas edible oils (sunflower, soybean, safflower, and palm), as well as non-edible oils (jatropha, karanja), are converted to biodiesel via catalytic transesterification with alcohols (methanol or ethanol). Both homogeneous (methanolic NaOH and KOH) and heterogeneous catalysts (ZnO/HZMS-5, PbO/HZSM-5) are used for transesterification reactions [31–33]. Homogeneous transesterification reactions are

carried out at mild reaction conditions (temperature 60–70 °C, atmospheric pressure), whereas heterogeneous catalyst reactions are performed at higher temperatures (100–180 °C) and pressures (20–40 bar).

The non-edible biomass, i.e., all plant-based residues, are converted to syngas or bio-oil through thermochemical routes. The biodiesel synthesis from non-edible and waste cooking oils is gaining momentum as these oils are available at a cheaper rate and do not have competing usage. Vegetable oil and bio-oil can also be converted to biogasoline via catalytic cracking but require proper catalyst and reactor setup. The product of cracking comprises an organic liquid, gas, coke, and some amount of water. The organic liquid is a mixture of hydrocarbons having properties similar to gasoline, kerosene, and diesel fractions. The catalysts used for catalytic cracking of oil include alumina, silica (SBA-15), zeolites (HZSM-5), and silica-alumina [34]. For example, a fixed bed reactor was used for catalytic cracking of canola oil to biogasoline over a variety of zeolites under different reaction conditions. Among the various zeolites used, HZSM-5 was found to be the most effective catalyst with a 100% conversion of canola oil. The reaction was carried over a temperature range of 573–773 K. The reaction product contained a high yield of aromatic compounds [35].

Several carbon-based catalysts (multiwalled carbon nanotubes, CNT-P-SO$_3$H) have shown excellent performance for the transesterification of oils and fats. Apart from thermochemical routes, the non-edible biomass is converted to valuable products/platform chemicals via a catalytic process such as hydrolysis, solvolysis, etc. The platform chemicals obtained are further converted to valuable products through isomerization, dehydration, hydrodeoxygenation, hydrogenolysis, etc. The various microporous, mesoporous, and nanoparticle catalysts are presented in Table 1.

2.3 Functionalized Heterogeneous Catalyst

Heterogeneous catalysts are preferable over homogeneous ones due to the ease of separation, reusability, tolerance to moisture, and thermal stability. To make the biomass conversion process more energy efficient, multifunctional catalysts can play a major role with an adequate amount of acid, base, and redox-active sites. Various multifunctional catalysts are discussed in the following section accommodating such features and can be applied to biomass conversion. The multifunctional catalyst can reduce few energy-intensive steps in the overall process, thereby improving the process efficiency.

2.3.1 Carbon-Based Catalysts

Carbon material catalysts have a high surface area, tailorable porosity, and higher hydrophobicity. These properties make them suitable catalysts for biomass valorization. They can act as support as well as active phase catalyst. However, the

Table 1 Microporous, mesoporous, and nanoparticle catalysts used for biomass conversion

Reaction	Catalyst	Conv/ yield, %	Reaction conditions	Remark	Ref
Isomerization and dehydration of glucose to HMF	Mesoporous AlSiO in THF/ H_2O-NaCl biphasic system	91.7/63	Temp: 160 °C, Time: 90 min	High catalytic activity after four reaction cycles. High surface area and a large number of active sites	[20]
Dehydration of glucose to HMF	HZSM-5 zeolite	80/42	Biphasic aqueous NaCl+ MIBK system, 190 °C, 30 min	The activity of the zeolite catalyst is better than the silica catalyst, short reaction time	[36]
Hydrodeoxygenation of guaiacol to cyclohexane	Pt/HMFI-90	100/93	Liquid phase, 180 °C, 5 bar, 5 h	Higher activity of acidic support, reducibility in Pt has a significant effect	[37]
Hydrodeoxygenation of anisole to cyclohexane	Ni/Al-SBA-15	99.8/95	Liquid phase, 220 °C, 50 bar, 2 h	A synergetic effect between support and active phases	[38]
Hydrogenation of furfural to furan	Pd NPs/S-$_1$-OH	100/99.9	Gas-phase, 250 °C, atm pressure	Wettability-driven selective hydrogenation	[39]
Hydrogenation of furfural to tetrahydrofurfuryl alcohol	CuNi/MgAlO	99/95	Liquid phase, 150 °C, 40 bar, 3 h	High activity and selectivity compared to monometallic catalysts	[40]
Hydrogenation of HMF to DMF	Cu-Zn nanoalloy (<150 nm)	100/97	Temp: 220 °C, 20 bar, 18 h	A synergetic effect between Cu and Zn	[41]
Aerobic oxidation of HMF to 2,5-furan-carboxylic acid	Ni-doped MnO_x nanowires	100/94	Temp: 100 °C, 8 bar, 28 h	The special property makes oxygen to be easy come and easy go	[42]

yield of carbon catalysts such as CNTs and graphene is low, and the production cost is high that limits their applications. The preparation cost of carbon catalyst can be brought down by using low-cost substrate like biomass. The carbon catalysts made from various biomass sources are described below.

Biomass-Derived Carbon Catalysts

The widely used carbon catalysts are carbon black and activated carbon. They are primarily utilized as a support material for heterogeneous catalysts such as Ru/C and Pd/C in reductive catalytic fractionation process to separate cellulose, hemicellulose, and lignin [5]. The carbon catalyst from biomass (wood, bamboo,

bagasse) can be obtained by various carbonization techniques such as pyrolysis, gasification, hydrothermal carbonization, etc. Sometimes, the carbon-based functionalized catalysts are prepared from municipal waste, complex industrial sludge, etc. This approach of converting biomass and waste into catalysts can benefit in two ways; the first one is the reduced cost of material fabrication, and the second one is the reduction in environmental pollution by utilizing waste. The properties of carbon material (surface area, pore configuration) are highly influenced by activation techniques and other key parameters such as source material, type of activation agent, time, and temperature [43].

Carbon material acts as excellent support for active catalyst phases. One such example is ionic liquids (ILs) supported on the carbon-based sulfonated catalyst. A high yield (47–65%) of 5-hydroxymethylfurfural was obtained when inulin was reacted at 100 ℃ for 60 min using ILs supported on carbon material. The catalyst performed well compared to conventional solid acid catalysts with high reusability. The carbon-based catalysts are expected to perform at par with their conventional counterparts. To verify this, four amorphous carbon-based sulfonated catalysts were prepared from D-xylose, cellulose, lignin, cellulose, and wood and compared with cation resin, HZSM-5, sulfated zirconia, and Amberlyst-15. All four carbon-based catalysts showed comparable catalytic activity over the conventional solid acid catalysts [44]. In another study, a carbon catalyst prepared via hydrothermal carbonization of water hyacinth was used for oleic acid esterification and also for xylose dehydration to furfural. The solid acid bearing the highest acidity (WH-PTSA-220) showed maximum catalyst activity, whereas catalyst prepared with high temperature (WH-PTSA-240) had shown favorable reusability due to enhance graphitization and hydrophobicity of the carbon surface [45]. The one-pot catalytic synthesis, developed by the Sels group, converts crystalline cellulose into simple alkanes using a modified Ru/C catalyst [46]. A series of bimetallic nanocatalysts supported on carbon (PtMn/C, PtFe/C, PtNi/C, PtZn/C, etc.) are reported to be used for the efficient oxidative conversion of glycerol to glyceric acid. Ninety-one percent of glycerol was converted within 8 h at 60 °C, with a 50% yield of glyceric acid. Carbon support is chosen because of its inert behavior in acidic environment [47].

Graphene-Based Catalysts

The advancement in graphene-based catalysts has paved a new way for its application in biomass processing. Graphene, along with graphene oxide (GO) and reduced graphene oxide (rGO), is increasingly used for biomass conversion. Graphene oxide is synthesized by oxidation of graphite, and reduced graphene oxide is synthesized by reduction of graphene oxide. Graphene per se has limited catalyst activity, which can be enhanced by the doping of heteroatoms such as nitrogen, boron, or sulfur. Graphene-based supports can be synthesized from biomass, and biomass-derived chemicals, for example, glucose to graphene [48]. It also facilitates the anchoring of various acid-base functionalities and metal nanoparticles (NPs). Graphene-based

materials are preferred for the process involving adsorption and surface reactions owing to its high BET surface area of about 2600 m^2/g [49]. Fructose dehydration to 5-hydroxymethylfurfural (5-HMF) was carried out using GO in the presence of isopropanol mediated dimethyl sulfoxide (DMSO), and 87% yield of HMF was obtained. The high performance of the catalyst was attributed to the synergistic effect between hydrogen bonding and fructose [50].

In the process of producing fuel precursors, the hydroxyalkylation/alkylation condensation of 2-methyl furan with hydroxyl group-containing compounds is catalyzed by improved GO (IGO) to yield C_{12} to C_{21} fuel precursors in liquid form. The IGO was highly selective to C_{15} fuel precursor (yield 95% at 60 °C) and found to be a promising acid catalyst for C-C coupling reactions when compared with commonly used framework zeolites [51]. GO-based materials have the potential to become alternative conventional catalysts and need focused efforts for their development. Though there are numerous advantages of graphene-based catalysts, the synthesis of graphene and its derivatives remains a challenge [48]. Also, attention is to be paid for possible health issues for humans.

Carbon Nanotubes (CNTs) as Catalysts

Carbon nanotubes are used as catalyst support and show excellent performance for stabilizing metal nanoparticles (NPs), metal oxides, and acid/base functionalities. It also prevents particle aggregation on the support surface, thereby suppressing the formation of metal complex on the catalyst surface. For example, sorbitol was converted to ethylene glycol and 1,2-propanediol over Ru/CNTs catalyst. The reaction results can be further improved by the addition of WOx to Ru/CNTs due to synergy between WO_x and Ru. The catalyst was recycled several times and found to be stable against leaching and poisoning. The yield of ethylene glycol and 1,2-propanediol was reported as 25.6% and 34.6%, respectively, when the reaction is conducted using Ru0.25WO$_x$/CNTs at 205 °C and 5.0 MPa. This can be the alternate route for the production of ethylene glycol and 1,2-propanediol, which, at present, produced commercially from petroleum-derived ethylene and propylene [52]. In another study, 2,5-diformylfuran (DFF) was produced by aerobic oxidation for biomass-based 5-hydroxymethylfurfural (5-HMF) over vanadium dioxide immobilized on polyaniline-functionalized CNTs (VO$_2$-PANI/CNT). The maximum yield of DFF was 96% when 100% 5-HMF was converted with O_2 as the oxidant. The selective adsorption of HMF on the catalyst surface inhibited the undesired oxidation of DFF, resulting in higher yield [53].

CNT-based solid acid catalyst (CNT-P-SO$_3$H) showed excellent results for transesterification as well as esterification reactions to produce biodiesel. The catalyst suffered a loss of partial activity after six cycles, which cannot be regenerated [54]. A multiwalled carbon nanotube (Net$_3$-MWCNT) catalyst with a grafted amino group is also reported for the transesterification reaction. The 77% conversion of glyceryl tributyrate was observed after 8 h. The conversion was on the higher side compared to commonly used hydrotalcite catalyst (51%

conversion) under identical conditions [55]. Thus, CNTs provide a good option as catalysts and support for the biomass conversion process.

2.3.2 Metal-Organic Frameworks (MOFs) as Catalysts

Zeolites are known for their well-defined porous structures. Similarly, the metal-organic frameworks (MOFs) exhibit zeolite-like structure and a potential alternative to zeolites as well as metal oxide catalysts. MOFs perform better in selected reactions such as fructose dehydration in dimethyl sulfoxide (DMSO). MOFs are highly crystalline and possess required acid, base, and redox functionalities. It can also allow the immobilization of functional groups like $-SO_3H$ and $-NH_2$ as well as metal nanoparticles such as Ru, Pd, Cu, etc. MOFs exhibit mesoporous structures and are highly tunable materials in terms of pore size and anchoring of active phases. Approximately 20,000 MOFs are reported in the literature, but all may not be suitable for biomass conversion. The MOFs with a certain degree of thermal, chemical, and water stability only are suitable for biomass conversion. For example, zinc-carboxylate MOFs have shown poor water tolerance and are not suitable, whereas MIL-type compounds (MIL101-Cr, MIL-53Al-NH_2, UiO-66) exhibit higher water stability [56]. MOFs have also been used as active catalyst phase, catalyst support as well as a precursor material for the catalyst. MOFs and their composites are discussed in the following section.

MOF-Supported Metal Nanoparticles (NPs)

MOFs have shown greater properties to prevent agglomeration of NPs, hence improving their catalytic activities. Ning et al. [57] prepared Pt/MOF-5 by confining Pt nanoparticles into the pores of MOF-5 and used for conversion of furfural derived from biomass. Furan-2-acrolein was selectively produced from furfural (selectivity 90.7%) using Pt/MOF-5 as a catalyst. The catalyst showed good activity for the conversion of furfural (84.1%) in the presence of ethanol as a solvent. The catalyst was active after five reaction cycles due to the synergistic effect between NPs and MOF. The other MOF-supported catalysts used for furfural conversion are Pt/UIO-66-NH_2 and Pt/UIO-66. Hydrogenation of furfural to furfuryl alcohol was carried out with Ru NPs supported on several MOFs supports such as Zr6-NDC, UiO-66, MIL-140A, and UiO-67. High selectivity of furfuryl alcohol was obtained under mild reaction conditions. Ru/UiO-66 was found to be the most stable catalyst resulting in the highest activity and reusability for five reaction cycles without appreciable loss of activity.

γ-Valerolactone (GVL) is an important platform chemical and produced from ethyl levulinate derived from biomass via hydrogenation and transesterification reactions. Ethyl levulinate can also be obtained by esterification of levulinic acid with ethanol [58]. The MOF catalyst (UiO-66) with various functionalities (-SO_3H,

-NH$_3$, and –NO$_2$) is used for this reaction. The catalytic activity of UiO-66 reduced when functionalized with –NH$_2$ and –NO$_2$ for both hydrogenation and transesterification reactions owing to the poor dispersion of Ru. On the other hand, –SO$_3$H-functionalized MOF showed increased activity (22% higher yield of GVL) for transesterification reaction when compared with Ru/UiO-66 [59].

Acid-Functionalized MOFs

The reaction that is primarily explored using acid MOFs is the production of a 5-HMF form of glucose, which is a two-step reaction that involves isomerization (glucose to fructose) followed by dehydration (fructose to 5-HMF). The isomerization requires Lewis acidity, and dehydration requires Brønsted acidity. It is, therefore, beneficial if the catalyst possesses Lewis as well as Brønsted acidity for the single-step conversion of glucose. These bifunctional characteristics can be induced by partial modification of the metal-organic framework. UiO-66 is one such example where the organic linker of the zirconium organic framework is replaced with 2-monocular-benzene-1,4-dicarboxylate. The catalyst was recyclable and showed higher selectivity for 5-HMF and fructose up to 90%. Similarly, NU-1000 (acidic zirconia modified by phosphate) was used for glucose conversion via the isomerization-dehydration mechanism with higher selectivity [7]. To prevent the side reactions, the Lewis and Brønsted active sites were purposely poisoned as both Lewis and Brønsted acidities were required, but at reduced level. It was also observed through the isotope tracer studies that the isomerization-dehydration mechanism is the favored mechanism over the direct-dehydration mechanism. The direct-dehydration mechanism utilizes phosphate-modified titania and bare niobia as catalysts [60]. The presence of water as a solvent is essential to carry out glucose to 5-HMF conversion. This was verified by conducting a reaction with MIL-101Cr (MIL-SO$_3$H) catalysts in pure tetrahydrofuran (THF) as a solvent. No product was formed. The findings suggest that the presence of water for glucose conversion is indispensable. Therefore, the catalyst should have tolerance for water as a large amount of water is generated during a dehydration reaction.

Productions of levulinic acid and 5-HMF from glucose are competing reactions and highly sensitive to the catalyst used. For example, MIL-SO$_3$H favored the formation of 5-HMF over levulinic acid (molar ratio 1:0.3). On the other hand, Amberlyst-15 and H$_2$SO$_4$ favored levulinic acid over 5-HMF with molar ratio of 3:1 and 10:1, respectively. The catalyst did not show good reusability, and reactivation remains a challenge [61]. The kinetics of conversion of fructose to 5-HMF reveal that MIL-101Cr-SO$_3$H-promoted reaction follows pseudo-first-order kinetics with an activation energy of 55 kJ/mol. The reaction was conducted in the presence of dimethyl sulfoxide (DMSO) at 120 °C for 60 min. The high yield (90%) of 5-HMF was obtained with the full conversion of fructose [62]. The results highlight MOFs as promising alternative solid acid catalysts for biomass conversion.

Bifunctionalized MOFs

MOFs are tailorable and offer the opportunity to introduce acid, base, or both functionality and metal-active sites. This property of MOFs makes them an ideal material to be used as a bifunctional catalyst. For example, palladium supported on amine-functionalized MOF (Pd/MIL-101(Al)-NH_2) is used for hydrogenation of 5-HMF to 2,5-hydroxymethyl-tetrahydrofuran (DHMTHF). The metallic site and free amine moiety are observed to be the controlling factors in the conversion of 5-HMF to DHMTHF. The amine moiety in the MOF is crucial in uniform dispersion of Pd nanoparticles on amine-functionalized support. When 5-HMF is fully converted, a 96% yield of DHMTHF is obtained under optimal reaction conditions. The reaction was carried out at a low temperature of 30 °C in an aqueous medium. The MOF support could stabilize the Pd nanoparticles efficiently as only a marginal (0.03%) amount of Pd was leached after five cycles (60 h) of operation. However, the selectivity for DHMTHF was reduced from 96% to 80% [63].

An important platform chemical is γ-valerolactone (GVL), which is used for the synthesis of useful chemicals. GVL is synthesized by hydrogenation of levulinic acid and further converted to ethyl valerate (EV yield 83%) in the presence of ethanol via hydrodeoxygenation (HDO) over a bimetallic catalyst (Pd/MIL-101-SO_3H) [64]. GVL can also be produced from methyl levulinate (ML) by using Ru nanoparticles deposited on the Zr-based metal-organic framework (SO_3H-UiO-66). The catalyst showed duel functionality, and about 100% yield of GVL was obtained. Alternately, if GVL is produced by a two-step method, i.e., hydrogenation of methyl levulinate over Ru/C catalyst to produce intermediate (4-hydroxypentanoic acid methyl ester) followed by conversion of this intermediate in the absence of metal catalyst, the yield was very limited [65].

Sorbitol is an important chemical and widely used as a sweetener in the food industry as a moisture controller in medical and cosmetic applications and feedstock for hydrogen and alkane production. Sorbitol can be obtained by hydrogenation of cellulose and also by hydrolysis of cellobiose. Both the reactions can be catalyzed by the bifunctional catalyst supported on MOF, i.e., Ru-PTA/MIL-100(Cr). The important factor for cellulose and cellobiose conversion was the ratio of active acid sites (n_A) to the number of Ru surface atoms (n_{Ru}). The optimum ratio of two catalytic activities for maximum conversion was $8.84 < (n_A/n_{Ru}) < 12.90$. Ruthenium (Ru) promoted hydrogenation reaction, and PTA/MIL-100(Cr) was active for hydrolysis reactions. Though the leaching of metal was not significant (0.006%), the catalyst activity decreased significantly. The yield of sorbitol was 95.1% for fresh catalysts and decreased to 8.5% when the catalyst was reused for the reaction. The loss in activity was attributed to the catalyst poisoning by insoluble substrates [66]. It is, therefore, expected that the MOF catalysts could serve as novel catalysts for biomass upgrading by metal/acid dual functionality but need improvement in catalyst stability. The synchronized effect among the metal and acid functionality in the presence of an environmentally benign solvent will be the key to the catalytic process.

Bimetallic MOF-Derived Catalysts

The MOF catalysts suffer from low hydrothermal and chemical stability, which can be addressed by MOF-derived carbon-based metal and metal oxides. The carbon material has high stability for the chemical and hydrothermal environment. A bimetallic catalyst (CuNi@C), prepared by impregnation of nickel nitrate onto Cu-based MOFs, was utilized for conversion of furfural to cyclopentanone at 130 °C, 5 MPa for 5 h. As a result, a 96.9% yield of the product was obtained. Cyclopentanone has wide applications in insecticide, medicine, and perfume industries. It can also be used as a solvent in the electronics industry [67]. In another work, the $CuCo_{0.4}/C$-873 catalyst is tested for the conversion of furfural to furfuryl alcohol. The catalyst is derived from Co-doped Cu-BTC MOF by thermolysis in a nitrogen environment at a temperature ranging from 773 K to 1073 K.; the doping of the cobalt helped inefficient dispersion of Co and Cu nanoparticles. The thermolysis temperature has an effect on the chemical state of the catalyst. At the best catalytic performance, 98.7% furfural was converted with high selectivity of furfural alcohol (97.7%) [68].

The Ni nanoparticle catalyst generated in situ with the help of MOF precursor (MIL-77(Ni)) is used for hydrotreatment of lignocellulosic biomass to avoid the disadvantages of supported catalysts such as metal leaching, coke deposition, polymerization of unstable species, less water tolerance, etc. The catalyst was found to be ten times more active than a conventional catalyst, i.e., $Ni/SiO_2\text{-}Al_2O_3$. The higher activity is attributed to high purity and crystallinity due to in situ generation and the robust MOF network [69].

Overall, MOFs are a good alternative to microporous zeolites, mesoporous silica, and carbon-based catalysts. It offers numerous advantages such as reduced mass transfer resistance, improved surface properties, and efficient immobilization of functional groups. However, its uses as a catalyst get restricted due to high synthesis cost, leaching of active species, and low hydrothermal stability. Thus, directed efforts are required toward the structure-activity analysis of MOFs to be widely accepted as a catalyst for biomass conversion [5].

2.3.3 Solid-Phase Ionic Liquid (IL)-Based Catalyst

Ionic liquids (ILs) are generally in the liquid state at room temperature and have a melting point below 100 °C. They are organic salts and are increasingly used as an alternative solvent to conventional volatile solvents. They consist of organic cation and inorganic or organic anions. The advantages of ILs are their extremely low vapor pressure and high thermal stability, which are helpful in developing the greener technologies and sometimes referred to as green solvents [70]. Additionally, ILs possess tunable physical properties by virtue of the different combination of cations and anions. The properties of ILs, such as viscosity, density, melting point, solubility, and acidity, can be tuned. Theoretically, it is possible to synthesize 10^{18}

types of ILs, but only about 1000 types of ionic liquids have been synthesized to date. The drawbacks of ionic liquids are high preparation cost, active phase leaching, and poor recyclability that can be overcome by solid-phase ILs [5].

Depolymerization of cellulose is a critical step to obtain platform chemicals such as fructose, glucose, xylose, etc. Cellulose is insoluble in most of the common industrial solvents due to its high degree of crystallinity, thus hampering the catalytic activity in the depolymerization step and demanding for harsh reaction conditions. Due to this reason, depolymerization of cellulose to glucose under mild reaction conditions still remains a challenge [70]. ILs are excellent solvents for cellulose dissolution that can be helpful in the depolymerization of cellulose through hydrolysis, alcoholysis, etc. The key advantages of ILs are efficient functionalization, promising reusability, and lower amount requirement for the reaction. The cost of functionalized ILs is a crucial factor that needs due consideration. Depending on the solubility of biomass molecule in ILs, a careful selection of coupled catalyst-solvent system is necessary. An understanding of molecular interaction between the feedstock molecule, catalyst, and solvent is necessary for the development of new catalytic systems. The post-reaction separation technologies for catalyst, solvent, and biomass products are necessary. There is a limited success for the depolymerization of lignin using ILs. Therefore, more opportunities are available for research in this domain [71]. Even though the ILs have several advantages over conventional catalysts, handling of ILs is difficult owing to its viscous nature. Also, the leaching of ILs in reaction mixture limits their practical applications in biomass conversion. To address these issues, researchers have combined ILs with solid catalyst and developed a new class of functionalized catalyst, namely, "solid-state ILs." The ILs are deposited in the form of a film on the support material with a high specific surface area, thus creating a homogeneous environment for reactions [5]. This way, the use of solid-state ILs is more practical in biomass conversion.

Supported IL-Based Catalysts

The ionic liquid immobilized on solid support offers several advantages than using the ILs themselves. Both inorganic and organic materials can be used as supports. Inorganic supports offer better thermal stability and low on cost and easy to prepare, i.e., alumina and silica [72]. Various carbohydrates (cellulose, sucrose, glucose) were converted to furans with a functional ILs supported on silica nanoparticles with different acidity. The dual acid-functionalized supported ionic liquid (SIL) (IL-SO_3H-HSO_4/SiO_2) was effective for high conversion (99%) of sugars. The reusability of the ILs/SiO_2 was also investigated for dehydration of fructose with IL-SO_3H-HSO_4/SiO_2 at the optimized conditions. Consistent conversion (99%) of fructose was obtained for five reaction cycles that suggest no leaching of immobilized functional groups (SO_3H and $-HSO_4$) during the repeated process [73]. ILs immobilized on mixed metal oxides, and silica gels are investigated for biodiesel synthesis from waste cooking oil. The mixed oxide catalysts (Mg + Al), in its pristine form, exhibited low activity for the conversion of waste cooking oil by

transesterification due to the high acidity of the oil. Their activity improved after the immobilization of ILs due to increased basic strength and basicity of supports. The biodiesel yields catalyzed by IL/Mg-Al and IL/Mg-Al-La catalysts were 85.4% and 98.7%, respectively [74]. When waste cooking oil is transesterified with methanol at 60 °C for 20 h with ILs supported on silica gel, 87.58% yield of biodiesel was observed [75].

Polymeric IL-Based Catalysts

The ionic liquids are promising candidates for various applications and named after the mobility of ions in ionic liquids. The ILs are neither liquids nor solids and do not have advantages of liquids or solids. This limits their applicability due to leakage issues and high viscosity. Polymeric ionic liquids (PILs) can address this problem without losing the features of ILs. PILs are formed by the polymerization of ionic liquids [76]. They can combine the functionalities of polymer and ILs and act as bifunctional catalysts. They have high thermal stability, better corrosion resistance, and flexibility of available structures. The dehydration process of 5-HMF from glucose/fructose can be catalyzed by a series of PILs (mono- and bifunctional polymeric ionic liquids). The PILs performed well compared to solid-supported ionic liquids like ILs on silica and showed consistent activity for five reaction cycles without significant loss of activity [77]. Among the other reusable PILs are poly(3-butyl-1-vinylimidazolium chloride) combined with $CrCl_2$, P[BVIM]Cl-$CrCl_2$, which was found suitable for dehydration of glucose and fructose to yield 68.8% HMF at 120 °C for 3 h. However, the recyclability test indicates poor performance compared to its analogous catalyst, i.e., P[BVIM]Cl-Et_2AlCl [78]. PILs are also found suitable for oleic acid esterification to yield 92.6% biodiesel. The biodiesel yield slightly decreased to 89.3% after six runs, indicating the consistent performance of the catalyst. The catalyst, 1-vinyl-3-(3-sulfopropyl) imidazolium hydrogen sulfate [VSIM][HSO_4], was synthesized from Brønsted acidic ionic liquid through free radical polymerization from a novel approach, where Fe_3O_4 particles acted as hard template [79].

2.3.4   Magnetic Iron Oxide-Based Catalysts

Magnetic catalysts are different from other solid catalysts due to their easy separation from the reaction mixture by the permanent magnet. They are mainly represented by ferrous, cobalt, and nickel, especially ferrous. The commonly used magnetic catalyst/support includes alloys (FePt, CoPt), metals (Fe, Co, Ni), and iron oxides (FeO, Fe_2O_3, Fe_2O_4). Among them, Fe_2O_4 is widely used for catalytic purposes [80]. Magnetic acid catalysts are used for the conversion of cellulose to glucose, fructose to 5-hydroxymethylfurfural (5-HMF), and 5-HMF to 5-ethoxymethylfurfural (5-EMF) via hydrolysis, dehydration, and etherification processes, respectively. These catalysts also find their use in transesterification reactions to synthesize biodiesel. The catalysts

Table 2 Summary of functionalized heterogeneous catalyst used for biomass conversion

Reaction	Class	Catalyst	Conv/ yield, %	P, bar	T, K	Remark	Ref
Oxidation of glycerol to glyceric acid	Carbon-based	Pt_9Sn_1/C	91/50	1	333	The catalyst was active for four reaction cycles without loss of activity	[47]
Hydrogenolysis of glycerol to lactic acid	Carbon-based	Cu-Pd/RGO	56.2/49.5	14	413	Reasonably good activity for three cycles	[82]
Fructose to lactic acid	MOF	MIL-100(Fe)	>99/32	1	463	Catalyst was active for four reaction cycles	[83]
Methyl levulinate—GVL	MOF	$Ru-SO_3H-$ UiO-66	100/81	5	353	The catalyst was active for five reaction cycles	[65]
Dehydration of glucose to HMF	ILs	$CrCl_2-Im-$ SBA-15	50/35	1	423	Catalyst deactivation after two reaction cycles	[84]
Esterification of oleic acid to biodiesel	ILs	Microporous poly-IL	92.6/92.6	1	353	The catalyst was active for six reaction cycles	[79]

mentioned in Sect. 2.3.2 are effective for biomass conversion, but sometimes they are difficult to separate due to the viscous nature of the reaction mixture. This provides an opportunity for the use of a magnetic catalyst as it can be easily separated with external magnate material. Core-shell $Fe_3O_4@SiO_2$ magnetic nanoparticle is one such catalyst used for biodiesel production [81]. Magnetic sulfonated mesoporous silica (Fe_3O_4-SBA-SO_3H) was used as a catalyst for hydrolysis of cellobiose and found efficient for 98% conversion of cellobiose at 120 ºC, whereas the conversion is only 54% when H_2SO_4 is used as a catalyst under identical conditions. The catalyst can be easily recyclable from the hydrolysis solution with the help of an external magnet. The catalyst is also stable and showed consistent activity for three experimental runs. A summary of the functionalized heterogeneous catalyst used for biomass conversion is presented in Table 2.

2.4 Bimetallic Catalysts

Biomass conversion processes such as reforming, hydrogenolysis, hydrogenation, and oxidation are catalyzed by metals and yield product as well as byproducts. Byproducts can complicate the separation process and seriously affect the yield of the desired product. It is necessary to minimize the production of side products. It can be done by the addition of a second metal, as a support or promoter, to enhance selectivity to a particular product. The second metal can alter the catalytic activity,

selectivity, and stability of the first one. It can be achieved by one of the methods mentioned here:

- Altering the geometry
- Altering the electron properties of active sites
- Stabilizing the active metal
- Chemical bonding with a reaction intermediate and transition state
- Bifunctional effects by providing different functions in the reaction mechanism

The use of a bimetallic catalyst is advantageous, but the exact mechanism is not known. The information on the molecular and electronic level can help to establish the relationship between experimental results and catalyst modification. One may propose an analogy between catalysts used in petroleum refining and biomass conversion, but may not be appropriate as petroleum refining needs the addition of functional groups, whereas biomass conversion requires removal/replacement of functional groups. The transformation of cellulose, hemicelluloses, and lignin using bimetallic catalysts is discussed in the following section.

2.4.1 Cellulose Conversion Using the Bimetallic Catalyst

Cellulose is made up of biopolymers and depolymerized to its monomer, glucose ($C_6H_{12}O_6$), by hydrolysis. Glucose is further converted to platform chemicals such as levulinic acid and 5-hydroxymethylfurfural (5-HMF) by a dehydration reaction. Glucose can be upgraded to valuable chemicals by decreasing the functionality (aqueous-phase reforming) as well as increasing the functionality (oxidation). Aqueous-phase reforming produces H_2 and alkanes, whereas oxidation yields acids. Glucose mainly consists of aldehydes and alcohols. Oxidation of aldehydes produces carboxylic acid (gluconic acid) and that of alcohol produces glucuronic and keto acids. The most common monometallic catalysts used for glucose conversion are Pt and Pd. A second metal, Bi, is added to increase their activity as well as selectivity toward gluconic acid. The presence of Bi prevents the deactivation of Pd (by absorbing O_2 that would otherwise oxidize Pd) and limits the formation of byproducts. The promotion of Pd with other metals was not as effective as PdBi [85]. The possible oxidation products that can be produced from glucose are glucuronic acid, gluconic acid, 5-keto-glucose, glucaric acid, 5-keto-gluconic acid, and 2,5-diketogluconic acid. Other catalysts used for cellulose oxidation are PbPt, AuPt, AuRh, etc.

Glucose, the monomer of cellulose, can also be converted to various alcohols such as hexitols, sorbitols, and diols by hydrogenation. Ni and Ni-based catalysts are primarily used for glucose hydrogenation, but leaching of catalysts is a real issue. To improve the catalyst activity, promoters like Sn, Mo, Cr, and Fe are used that increase the rate of glucose formation by four to five times. When Fe/Cr is added to Ni, the selectivity of sorbitol was reached to as high as 98% [86]. Ru-based catalyst is reportedly stable for hydrogenation of glucose to produce sorbitols, but is expensive. Hexitols can be produced by hydrogenolysis (hydrogenation followed by dehydration) over the Pt-Ni catalyst. The yield of hexitols was 47.4% at 100% conversion of glucose over the Pt-Ni

catalyst. The results were even better with hexitol yield up to 53.2% and 54.2%, respectively, for Pd-Ni and Ru-Ni catalyst at 100% conversion of glucose.

2.4.2 Hemicellulose Conversion Using the Bimetallic Catalyst

Hemicellulose is a polymer with C_5 sugars, mainly xylose. Xylose is converted to xylitol by hydrogenation using a different metal catalyst. The catalyst Ru-Ni is commonly used to produce xylitol. For catalyst deactivation due to leaching, deposition is a common issue. Xylitol is a common sweetener used in the food industry. A platform chemical, furfural, can be obtained by dehydration of xylose and further hydrogenated to 2-methylfuran, furfural alcohol, and furan. The Cu-chromite is the most widely used commercial catalyst for hydrogenation [87]. The other bimetallic catalysts used for hemicellulose conversion are Cu/C, Cu/MgO, NiCu/SiO$_2$, CuCO/SiO$_2$, etc. Furfural yield of 98% was reported at 473 K over Cu/MgO and CuCo/SiO$_2$ catalyst [6].

2.4.3 Lignin Conversion Using the Bimetallic Catalyst

Lignin is a significant fraction of biomass, and its effective utilization will ensure the economic feasibility of the biomass conversion. Commercially, lignin is used in a very inefficient manner as 98% of it is burned to fulfill energy demand in pulp mills, whereas only 2% is utilized toward chemical production. So for the sustainable operation of biorefinery, lignin conversion to chemicals through technological advancement is necessary [88, 89]. Lignin possesses aromatic functionality, and products like benzene, phenol, and cyclohexanes can be made from it through cracking via hydrogenation and hydrodeoxygenation (HDO). Bimetallic catalysts such as sulfide, CoMo, and NiMo are used for lignin hydrogenation and HDO. The catalysts PtSn and PtRh are also reported to be used for lignin conversion. Among the catalysts, at a lower temperature (<673 K), all Rh-based catalysts are active than sulfide, CoMo, and NiMo catalysts. Owing to its complexity, model components such as phenol, cresol, anisole, etc. are used to study the conversion of lignin. Zhang et al. (2014) [90] conducted the catalytic hydrogenolysis of lignin using NiRu (Ni = 85% and Ru = 15%) to obtain aromatic chemicals and fuel-grade hydrocarbons. The results with bimetallic catalysts show better performance than monometallic Ni and Ru. The best result for pinene transformation was obtained using bimetallic Au-Cu/TiO$_2$ catalyst with higher selectivity for verbenone product due to the synchronized effect between bimetals and their support [91].

2.4.4 Catalytic Conversion of Glycerol Using the Bimetallic Catalyst

Bimetallic catalysts are used for the conversion of biomass-derived glycerol to valuable chemicals. Glycerol can be valorized through hydrogenolysis, hydrogenation, and oxidation reactions. Hydrogenolysis involves breaking of bonds with the help

of hydrogen. Glycerol is converted to polyols, alcohols via hydrogenolysis over the temperature range of 373–523 K and at 200 bar using monometallic catalysts. The selectivity and yield of hydrogenolysis can be greatly improved over bimetallic catalysts. Hydrogenolysis is sometimes referred to as hydrodeoxygenation (HDO) when used for the removal of oxygen. For example, the ethylene glycol was produced over Ni/Al_2O_3, but the selectivity was improved when palladium/iridium/rhodium was added to Ni/Al_2O_3 as the second metal. Glycerol can be oxidized in two ways: (1) oxidation of secondary alcohol to give dihydroxyacetone and hydroxypiruvic acid and (2) oxidation of primary alcohol to give glyceraldehydes and glyceric acid. The most commonly used bimetallic catalyst for glycerol oxidation was AuPd in basic medium and PtBi in acidic medium [6]. The summary of the bimetallic catalysts used for the conversion of biomass-derived chemicals is given in Table 3.

Table 3 Summary of bimetallic catalysts used for the conversion of biomass-derived chemicals

Feedstock	Reaction	Catalysts	Conv.	Selectivity	P, bar	T, K	Remark	Ref
Ethylene glycol	Aqueous-phase reforming	Pt/Al_2O_3	>90%	88% (H_2), 8% (alkane)	56	338	90% activity lost in 2 days. No restoration of activity	[92]
Sorbitol	Aqueous-phase reforming	RANEY® $Ni_{14}Sn$	>90%	46% (H_2), 31% (alkane)	51	538	Consistent activity for H_2 production for 340 h without regeneration	[92]
Glycerol	Hydrogenolysis	Ru-Co/ZrO_2	56.2%	70.3% (1,2 PDO), 18.0% (EG)	50	453	A synergetic effect between Ru and Co observed	[93]
Glycerol	Hydrogenolysis	CuAg/Al_2O_3	27%	96% (1,2 PDO)	15	473	The catalyst showed higher activity than commercial chromite catalyst	[94]
Guaiacol (lignin)	Deoxygenation	PtSn/Inconel	>80%	–	1	673	Higher rate of catalyst deactivation	[95]
o-Cresol (lignin)	Hydrodeoxygenation	CoMO/Al_2O_3	23%	65% (C_6H_6)	50	573	Activity of the catalyst is low	[96]

3 Current Challenges and Future Opportunities

In order to reduce the dependence on fossil fuels, large-scale production of fuels and chemicals from lignocellulosic biomass is necessary. But this is very challenging due to variations in supply, composition, and properties. Many technologies devised at laboratory/pilot plant scale are technically viable but economically not feasible. To make the process economically feasible, a multidisciplinary approach, including chemistry, material science, and process engineering, is required. The efficiency of various technologies and yield of the products depends on many factors such as type of biomass, pretreatment method, biomass composition, catalyst activity, etc. In the following section, the major concerns regarding technologies and the use of catalysts for biomass conversion are discussed.

3.1 The Selectivity of Desirable Products

It is essential to tune the porosity and structure of the catalyst to selectively produce the desired products. The pore dimension of the solid catalyst influences the diffusion properties of the reacting species. Zeolites ordered mesoporous silica and metal-organic frameworks (MOFs) are the materials that can be used as a catalyst for biomass conversion. These materials also act as support for metals and metal oxides with excellent stabilizing effects. One of the reasons for low conversion and selectivity of complex and viscous biomass molecules is the inaccessibility of active catalyst sites. The active sites are located inside the porous catalyst materials and become difficult to access due to diffusional limitations. Due to this reason, multimode porous materials are preferred over single-mode porous materials for enhanced selectivity. For example, large biomass molecules (lignin, triglycerides, polysaccharides) cannot access the catalytically active sites in zeolites due to small pore diameters. In that case, catalyst materials with mixed pores (micro, meso, and macro) such as hierarchical zeolites are useful. Zeolites offer numerous advantages, such as acidity, porosity, and shape selectivity. Of these, tunable Brønsted/Lewis acidity is a vital feature for biomass conversion and can influence conversion and selectivity. Both Brønsted and Lewis acidities are required for effective biomass conversion. For example, during the conversion of 2,5-dimethylfuran, zeolites with strong Lewis acid sites (Na-Y) favored the formation of toluene, whereas Brønsted acid zeolites (H-β and H-Y) favored *p*-xylene formation.

Another parameter that can affect the selectivity of the desired product is the biomass to catalyst ratio. In fast catalytic pyrolysis of *Pongamia pinnata* seeds using USY zeolites, more aromatic hydrocarbons were produced (4.7% to 52.5%) when the ratio of biomass to catalyst increased for five times [2]. Mesoporous SiO_2-based materials (SBA, KIT, MSU, COK) offer similar properties to zeolites but with larger pores. Larger pores can offer access to active catalyst sites, thereby enhancing the biomass conversion. During the condensation of furfuryl alcohol to butyl levulinate,

propylsulfonic acid-functionalized SBA-15 offered 96% yield of butyl levulinate with 100% selectivity [5]. Hence, it is important to select a catalyst with appropriate porosity, pore structure, and acidity to achieve maximum conversion and selectivity of the desired product.

3.2 Deactivation and Reusability of the Catalyst

Deactivation of the catalyst is evaluated by subjecting it to the loss of activity with increasing time on stream. Among the various reasons for deactivation, coking is a major one for the deactivation of catalysts in biomass conversion reactions. The other possible ways of catalyst deactivation are blockage of pore or active sites by insoluble byproducts/intermediates, metal leaching, sintering, decrease in specific surface area, loss of pore volume, etc. Sometimes, the basic metal oxides (MgO) can form hydroxides, which are more soluble in water and tend to leach. Also, the reaction byproducts can accumulate on the active catalytic site, thereby restricting the accessibility resulting in a low conversion. In the case of zeolites, degradation due to desilication or dealumination at harsh hydrothermal conditions is one of the ways of catalyst deactivation [2]. In order to avoid pore blockage in microporous zeolites, incorporation of larger size metal should be avoided. Many of the catalysts presented in this chapter showed good catalytic activity up to five reaction cycles, but their applicability at commercial scale and for real biomass feedstock needs to be tested. Fouling of MOF catalysts by humin formation is common in biomass conversion that can be prevented by using a proper solvent such as ethanol in case of selective conversion of glucose to 5-HMF [61]. Temperature can also influence deactivation as observed in catalytic cracking of fatty acid mixture; the order of deactivation over the composite catalyst was almost constant at moderate rate, whereas ZSM-5 deactivation order decreased with increasing temperature. The same order of deactivation was also observed for used palm oil cracking [97].

3.3 Kinetic/Mechanistic Aspects

Kinetic data obtained by careful evaluation of reaction parameters helps in process scale-up, technology transfer, and evaluation of economic feasibility. Due to the large number of complex reactions taking place in biomass conversion, it is not easy to explain kinetics at the molecular level. Few kinetic studies are discussed here. In the case of catalytic cracking of vegetable oil, a simplified lumped kinetics is presented by the grouping of components having similar chemical functions [34]. The complexity of the model varies according to the degree of lumping. Adding more lumps will make the process of kinetic parameters more intrinsic; thus, more kinetic parameters need to be estimated, and accordingly, more experimental information is required. For vegetable oil cracking, three, four, and six lumped

models were reported. The cracking of palm fatty acid mixture and used palm oil was reported to follow first-order kinetics [97], whereas the cracking of used vegetable oil over sulfated zirconia followed second-order kinetics. The reactions were carried out over a temperature range of 673–723 K and in the presence of composite catalysts (HZSM-5 and MCM-41/ZSM-5) in a fixed bed microreactor. The proposed model was adequate with a 10% deviation in the experimental and predicted values [98].

Kinetic of fructose to 5-HMF reaction reveals that MIL-101Cr-SO$_3$H-promoted reaction follows the pseudo-first-order kinetics with the observed activation energy of 55 kJ/mol [62]. In the case of glucose to 5-HMF reaction, the isomerization-dehydration mechanism is the prominent reaction pathway, compared to the phosphate-modified titania and bare niobia, which proposes direct-dehydration mechanism [61]. Though the use of bimetallic catalyst is advantageous, the exact mechanism is not known. The information on the molecular and electronic level can help to establish the relationship between experimental results and catalyst modification. Proposing a robust kinetic model still remains a challenge due to multiple and complex reactions that take place during biomass conversion.

4 Conclusions

The chapter has summarized various aspects of biomass conversion to useful chemicals having properties similar to those obtained from petrochemicals. It can be achieved by various processes such as hydration, solvolysis, pyrolysis, gasification, etc. Numerous catalysts with varying degrees of efficiency and reusability are presented in this chapter. The advantages and disadvantages of such catalysts are presented for a wide range of feedstocks and intermediate components. The commonly used catalyst, microporous zeolites, mesoporous silica, metal nanoparticles, and bimetallic materials have shown promising performance for model components of biomass. But their performance with real biomass feedstock remains a challenge. Due to this reason, not many commercial technologies are available. For example, the biomass pyrolysis to produce bio-oil is still an immature technology compared to fossil oil. It has to overcome many technical and economic challenges.

Overall, more opportunities are available for research in biomass conversion, but one needs to follow certain restraints for efficient utilization of biomass. These are as follows:

(a) Detailed understanding of the properties of components such as cellulose, hemicelluloses, and lignin. This will help to understand the mechanism of its catalytic conversion.
(b) Identification of the specific sources for cellulose, hemicelluloses, and lignin components and targeted product out of it.

(c) Preparation of the suitable catalysts based on their acidity/basicity, operating conditions, reusability, shape of catalyst particle, metal interaction, etc.

(d) As the product of lignocellulosic biomass is a complex one, novel reactor and separators should be developed. Process intensification to reduce waste and maximize product and energy efficiency will lead to an economically feasible design.

References

1. Jahirul MI, Rasul MG, Chowdhury AA, Ashwath N (2012) Biofuels production through biomass pyrolysis—a technological review. Energies 5:4952–5001. https://doi.org/10.3390/en5124952

2. Sudarsanam P, Peeters E, Makshina EV, Parvulescu VI, Sels BF (2019) Advances in porous and nanoscale catalysts for viable biomass conversion. Chem Soc Rev 48:2366–2421. https://doi.org/10.1039/c8cs00452h

3. Bauen A, Berndes G, Junginger M, Londo M, Vuille F (2009) Bioenergy—a sustainable and reliable energy source—a review of status and prospects. IEA Bioenergy:1–108

4. Global Bioenergy Statistics (2019) World Bioenergy Association 2019, p 58

5. Sudarsanam P, Zhong R, Van Den Bosch S, Coman SM, Parvulescu VI et al (2018) Functionalised heterogeneous catalysts for sustainable biomass valorisation. Chem Soc Rev 47:8349–8402. https://doi.org/10.1039/C8CS00410B

6. Alonso DM, Wettstein SG, Dumesic JA (2012) Bimetallic catalysts for upgrading of biomass to fuels and chemicals. Chem Soc Rev 41:8075–8098. https://doi.org/10.1039/c2cs35188a

7. Amin MH, Sudarsanam P, Field MR, Patel J, Bhargava SK (2017) Effect of a swelling agent on the performance of Ni/Porous Silica catalyst for CH4-CO2 reforming. Langmuir 33:10632–10644. https://doi.org/10.1021/acs.langmuir.7b02753

8. Fernando S, Adhikari S, Chandrapal C, Murali N (2006) Biorefineries: current status, challenges, and future direction. Energy Fuel 20:1727–1737. https://doi.org/10.1021/ef060097w

9. Zhou C, Xia X, Lin C, Tong D, Beltramini J (2011) Catalytic conversion of lignocellulosic biomass to fine chemicals and fuels. Chem Soc Rev 40:5588–5617. https://doi.org/10.1039/c1cs15124j

10. Kumar P, Barrett DM, Delwiche MJ, Stroeve P (2009) Methods for pretreatment of lignocellulosic biomass for efficient hydrolysis and biofuel production. Ind Eng Chem Res 48:3713–3729. https://doi.org/10.1021/ie801542g

11. Cheng S, DCruz I, Wang M, Leitch M, Xu C (2010) Highly efficient liquefaction of woody biomass in hot-compressed alcohol-water co-solvents. Energy Fuel 24:4659–4667. https://doi.org/10.1021/ef901218w

12. Han J, Kim H (2008) The reduction and control technology of tar during biomass gasification / pyrolysis: an overview. Renew Sustain Energy Rev 12:397–416. https://doi.org/10.1016/j.rser.2006.07.015

13. Dobele G, Rossinskaja G, Dizhbite T, Telysheva G, Meier D, Faix O (2005) Application of catalysts for obtaining 1, 6-anhydrosaccharides from cellulose and wood by fast pyrolysis. J Anal Appl Pyrolysis 74:401–405. https://doi.org/10.1016/j.jaap.2004.11.031

14. Kawamoto H, Saito S, Hatanaka W, Saka S (2007) Catalytic pyrolysis of cellulose in sulfolane with some acidic catalysts. J Wood Sci 53:127–133. https://doi.org/10.1007/s10086-006-0835-y

15. Chen MQ, Wang J, Zhang MX, Chen MG, Zhu XF, Min FF et al (2008) Catalytic effects of eight inorganic additives on pyrolysis of pine wood sawdust by microwave heating. J Anal Appl Pyrolysis 82:145–150. https://doi.org/10.1016/j.jaap.2008.03.001

16. Pattiya A, Titiloye JO, Bridgwater AV (2008) Fast pyrolysis of cassava rhizome in the presence of catalysts. J Anal Appl Pyrolysis 81:72–79. https://doi.org/10.1016/j.jaap.2007.09.002

17. Osada M, Sato T, Watanabe M, Adschiri T, Arai K (2004) Low-temperature catalytic gasification of lignin and cellulose with a ruthenium catalyst in supercritical water. Energy Fuel 18:327–333

18. Li N, Tompsett GA, Zhang T, Shi J, Wyman CE, Huber GW (2011) Renewable gasoline from aqueous phase hydrodeoxygenation of aqueous sugar solutions prepared by hydrolysis of maple wood. Green Chem 13:91–101. https://doi.org/10.1039/c0gc00501k

19. Wang D, Astruc D (2017) The recent development of efficient Earth-abundant transition-metal nanocatalysts. Chem Soc Rev 46:816–854. https://doi.org/10.1039/c6cs00629a

20. Li X, Xia Q, Nguyen VC, Peng K, Liu X, Essayem N et al (2016) High yield production of HMF from carbohydrates over silica-alumina composite catalysts. Cat Sci Technol 6:7586–7596. https://doi.org/10.1039/c6cy01628f

21. Custodis VBF, Karakoulia SA, Triantafyllidis KS, Van Bokhoven JA (2016) Catalytic fast pyrolysis of lignin over high-surface-area mesoporous aluminosilicates: effect of porosity and acidity. ChemSusChem 9:1134–1145. https://doi.org/10.1002/cssc.201600105

22. Jeenpadiphat S, Kasiban C, Tungasmita DN (2016) Corncob to value-added chemical transformation by metal/beta zeolite and metal/mesoporous SBA-15 catalytic pyrolysis. J Chem Technol Biotechnol 91:2519–2528. https://doi.org/10.1002/jctb.4852

23. Haishi T, Kasai K, Iwamoto M (2011) Fast and quantitative dehydration of lower alcohols to corresponding olefins on mesoporous silica catalyst. Chem Lett 40:614–616. https://doi.org/10.1246/cl.2011.614

24. Grams J, Potrzebowska N, Goscianska J, Michalkiewicz B, Ruppert AM (2016) Mesoporous silicas as supports for Ni catalyst used in cellulose conversion to hydrogen rich gas. Int J Hydrogen Energy 41:8656–8667. https://doi.org/10.1016/j.ijhydene.2015.12.146

25. Li S, Wang Y, Gao L, Wu Y, Yang X, Sheng P et al (2018) Short channeled Ni-Co/SBA-15 catalysts for highly selective hydrogenation of biomass derived furfural to tetrahydrofurfuryl alcohol. Microporous Mesoporous Mater 262:154–165. https://doi.org/10.1016/j.micromeso.2017.11.027

26. Hashmi ASK, Hutchings GJ (2006) Gold catalysis. Angew Chem Int Ed 45:7896–7936. https://doi.org/10.1002/anie.200602454

27. Chakinala AG, Chinthaginjala JK, Seshan K, Van Swaaij WPM, Kersten SRA, Brilman DWF (2012) Catalyst screening for the hydrothermal gasification of aqueous phase of bio-oil. Catal Today 195:83–92. https://doi.org/10.1016/j.cattod.2012.07.042

28. Tauster SJ, Fung SC, Garten RL (1978) Strong metal-support interactions. Group 8 Noble Metals supported on TiO2. J Am Chem Soc 100:170–175. https://doi.org/10.1021/ja00469a029

29. Tathod AP, Dhepe PL (2015) Efficient method for the conversion of agricultural waste into sugar alcohols over supported bimetallic catalysts. Bioresour Technol 178:36–44. https://doi.org/10.1016/j.biortech.2014.10.036

30. Varkolu M, Raju Burri D, Rao Kamaraju SR, Jonnalagadda SB, van Zyl WE (2017) Hydrogenation of levulinic acid using formic acid as a hydrogen source over Ni/SiO2 catalysts. Chem Eng Technol 40:719–726. https://doi.org/10.1002/ceat.201600429

31. Bhoi R, Sen N, Singh KK, Mahajani SM, Shenoy KT, Rao H et al (2014) Transesterification of sunflower oil in microreactors. Int J Chem React Eng 12. https://doi.org/10.1515/ijcre-2013-0105

32. Singh D, Bhoi R, Ganesh A, Mahajani S (2014) Synthesis of biodiesel from vegetable oil using supported metal oxide catalysts. Energy Fuel 28:2743–2753. https://doi.org/10.1021/ef500045x

33. Bhoi R, Mahajani S (2018) Investigation of spontaneous emulsification and its relevance in biodiesel synthesis. React Chem Eng 3:171–181. https://doi.org/10.1039/c7re00205j

34. Taufiqurrahmi N, Bhatia S (2011) Catalytic cracking of edible and non-edible oils for the production of biofuels. Energ Environ Sci 4:1087–1112. https://doi.org/10.1039/c0ee00460j

35. Uatikaneni SPR, Adjaye JD, Bakhshp NN (1995) Catalytic conversion of Canola oil to fuels and chemicals over various cracking catalysts. Can J Chem Eng 73:484–497

36. Moreno-Recio M, Santamaría-González J, Maireles-Torres P (2016) Brönsted and Lewis acid ZSM-5 zeolites for the catalytic dehydration of glucose into 5-hydroxymethylfurfural. Chem Eng J 303:22–30. https://doi.org/10.1016/j.cej.2016.05.120

37. Hellinger M, Carvalho HWP, Baier S, Wang D, Kleist W, Grunwaldt JD (2015) Catalytic hydrodeoxygenation of guaiacol over platinum supported on metal oxides and zeolites. Appl Catal A Gen 490:181–192. https://doi.org/10.1016/j.apcata.2014.10.043

38. Sankaranarayanan TM, Berenguer A, Ochoa-Hernández C, Moreno I, Jana P, Coronado JM et al (2015) Hydrodeoxygenation of anisole as bio-oil model compound over supported Ni and Co catalysts: effect of metal and support properties. Catal Today 243:163–172. https://doi.org/10.1016/j.cattod.2014.09.004

39. Wang C, Liu Z, Wang L, Dong X, Zhang J, Wang G et al (2018) Importance of Zeolite wettability for selective hydrogenation of Furfural over Pd@Zeolite catalysts. ACS Catal 8:474–481. https://doi.org/10.1021/acscatal.7b03443

40. Wu J, Gao G, Li J, Sun P, Long X, Li F (2017) Efficient and versatile CuNi alloy nanocatalysts for the highly selective hydrogenation of furfural. Appl Catal Environ 203:227–236. https://doi.org/10.1016/j.apcatb.2016.10.038

41. Bottari G, Kumalaputri AJ, Krawczyk KK, Feringa BL, Heeres HJ, Barta K (2015) Copper-Zinc alloy nanopowder: a robust precious-metal-free catalyst for the conversion of 5-Hydroxymethylfurfural. ChemSusChem 8:1323–1327. https://doi.org/10.1002/cssc.201403453

42. Yu K, Liu Y, Lei D, Jiang Y, Wang Y, Feng Y et al (2018) M3+O(-Mn4+)2 clusters in doped MnO: X catalysts as promoted active sites for the aerobic oxidation of 5-hydroxymethylfurfural. Cat Sci Technol 8:2299–2303. https://doi.org/10.1039/c7cy02455j

43. Ma Q, Yu Y, Sindoro M, Fane AG, Wang R, Zhang H (2017) Carbon-based functional materials derived from waste for water remediation and energy storage. Adv Mater 29:1605361. https://doi.org/10.1002/adma.201605361

44. Kang S, Ye J, Zhang Y, Chang J (2013) Preparation of biomass hydrochar derived sulfonated catalysts and their catalytic effects for 5-hydroxymethylfurfural production. RSC Adv 3:7360–7366. https://doi.org/10.1039/c3ra23314f

45. Laohapornchaiphan J, Smith CB, Smith SM (2017) One-step preparation of carbon-based solid acid catalyst from Water Hyacinth leaves for esterification of oleic acid and dehydration of xylose. Chem Asian J 12:3178–3186. https://doi.org/10.1002/asia.201701369

46. Op De Beeck B, Dusselier M, Geboers J, Holsbeek J, Morré E, Oswald S et al (2015) Direct catalytic conversion of cellulose to liquid straight-chain alkanes. Energ Environ Sci 8:230–240. https://doi.org/10.1039/c4ee01523a

47. Dou J, Zhang B, Liu H, Hong J, Yin S, Huang Y et al (2016) Carbon supported Pt9Sn1 nanoparticles as an efficient nanocatalyst for glycerol oxidation. Appl Catal Environ 180:78–85. https://doi.org/10.1016/j.apcatb.2015.06.007

48. Das VK, Shifrina ZB, Bronstein LM (2017) Graphene and graphene-like materials in biomass conversion: paving the way to the future. J Mater Chem A 5:25131–25143. https://doi.org/10.1039/c7ta09418c

49. Bai S, Shen X (2012) Graphene-inorganic nanocomposites. RSC Adv 2:64–98. https://doi.org/10.1039/c1ra00260k

50. Wang H, Kong Q, Wang Y, Deng T, Chen C, Hou X et al (2014) Graphene oxide catalyzed dehydration of fructose into 5-hydroxymethylfurfural with isopropanol as cosolvent. ChemCatChem 6:728–732. https://doi.org/10.1002/cctc.201301067

51. Dutta S, Bohre A, Zheng W, Jenness GR, Núñez M, Saha B et al (2017) Solventless C-C Coupling of low carbon Furanics to high carbon fuel precursors using an improved graphene oxide carbocatalyst. ACS Catal 7:3905–3915. https://doi.org/10.1021/acscatal.6b03113

52. Guo X, Guan J, Li B, Wang X, Mu X, Liu H (2015) Conversion of biomass-derived sorbitol to glycols over carbon-materials supported Ru-based catalysts. Sci Rep 5:1–9. https://doi.org/10.1038/srep16451

53. Guo Y, Chen J (2015) Bicomponent assembly of VO2 and polyaniline-functionalized carbon nanotubes for the selective oxidation of biomass-based 5-Hydroxymethylfurfural to 2,5-Diformylfuran. ChemPlusChem 80:1760–1768. https://doi.org/10.1002/cplu.201500292

54. Liu H, Chen J, Chen L, Xu Y, Guo X, Fang D (2016) Carbon nanotube-based solid sulfonic acids as catalysts for production of fatty acid methyl ester via transesterification and esterification. ACS Sustain Chem Eng 4:3140–3150. https://doi.org/10.1021/acssuschemeng.6b00156

55. Tessonnier JP, Villa A, Majoulet O, Su DS, Schlögl R (2009) Defect-mediated functionalization of carbon nanotubes as a route to design single-site basic heterogeneous catalysts for biomass conversion. Angew Chem Int Ed 48:6543–6546. https://doi.org/10.1002/anie.200901658

56. Herbst A, Janiak C (2017) MOF catalysts in biomass upgrading towards value-added fine chemicals. CrstEngComm 19:4092–4117. https://doi.org/10.1039/c6ce01782g

57. Ning L, Liao S, Cui H, Yu L, Tong X (2018) Selective conversion of renewable Furfural with Ethanol to produce Furan-2-acrolein mediated by Pt@MOF-5. ACS Sustain Chem Eng 6:135–142. https://doi.org/10.1021/acssuschemeng.7b01929

58. Ahmad E, Alam MI, Pant KK, Haider MA (2016) Catalytic and mechanistic insights into the production of ethyl levulinate from biorenewable feedstocks. Green Chem 18:4804–4823. https://doi.org/10.1039/c6gc01523a

59. Yang J, Huang W, Liu Y, Zhou T (2018) Enhancing the conversion of ethyl levulinate to γ-valerolactone over Ru/UiO-66 by introducing sulfonic groups into the framework. RSC Adv 8:16611–16618. https://doi.org/10.1039/c8ra01314d

60. Oozeerally R, Burnett DL, Chamberlain TW, Walton RI, Degirmenci V (2018) Exceptionally efficient and recyclable heterogeneous metal–organic framework catalyst for glucose isomerization in water. ChemCatChem 10:706–709. https://doi.org/10.1002/cctc.201701825

61. Herbst A, Janiak C (2016) Selective glucose conversion to 5-hydroxymethylfurfural (5-HMF) instead of levulinic acid with MIL-101Cr MOF-derivatives. New J Chem 40:7958–7967. https://doi.org/10.1039/c6nj01399f

62. Chen J, Li K, Chen L, Liu R, Huang X, Ye D (2014) Conversion of fructose into 5-hydroxymethylfurfural catalyzed by recyclable sulfonic acid-functionalized metal-organic frameworks. Green Chem 16:2490–2499. https://doi.org/10.1039/c3gc42414f

63. Chen J, Liu R, Guo Y, Chen L, Gao H (2015) Selective hydrogenation of biomass-based 5-hydroxymethylfurfural over catalyst of palladium immobilized on amine-functionalized metal-organic frameworks. ACS Catal 5:722–733. https://doi.org/10.1021/cs5012926

64. Zhang D, Ye F, Guan Y, Wang Y, Hensen EJM (2014) Hydrogenation of γ-valerolactone in ethanol over Pd nanoparticles supported on sulfonic acid functionalized MIL-101. RSC Adv 4:39558–39564. https://doi.org/10.1039/c4ra05250a

65. Lin Z, Cai X, Fu Y, Zhu W, Zhang F (2017) Cascade catalytic hydrogenation-cyclization of methyl levulinate to form γ-valerolactone over Ru nanoparticles supported on a sulfonic acid-functionalized UiO-66 catalyst. RSC Adv 7:44082–44088. https://doi.org/10.1039/c7ra06293a

66. Chen J, Wang S, Huang J, Chen L, Ma L, Huang X (2013) Conversion of cellulose and cellobiose into sorbitol catalyzed by ruthenium supported on a polyoxometalate/metal-organic framework hybrid. ChemSusChem 6:1545–1555. https://doi.org/10.1002/cssc.201200914

67. Wang Y, Sang S, Zhu W, Gao L, Xiao G (2016) CuNi@C catalysts with high activity derived from metal-organic frameworks precursor for conversion of furfural to cyclopentanone. Chem Eng J 299:104–111. https://doi.org/10.1016/j.cej.2016.04.068

68. Wang Y, Miao Y, Li S, Gao L, Xiao G (2017) Metal-organic frameworks derived bimetallic Cu-Co catalyst for efficient and selective hydrogenation of biomass-derived furfural to furfuryl alcohol. Mol Catal 436:128–137. https://doi.org/10.1016/j.mcat.2017.04.018

69. Čelič TB, Grilc M, Likozar B, Tušar NN (2015) In situ generation of Ni nanoparticles from metal-organic framework precursors and their use for biomass hydrodeoxygenation. ChemSusChem 8:1703–1710. https://doi.org/10.1002/cssc.201403300

70. Zhang Q, Zhang S, Deng Y (2011) Recent advances in ionic liquid catalysis. Green Chem 13:2619–2637. https://doi.org/10.1039/c1gc15334j

71. Zhang Z, Song J, Han B (2017) Catalytic transformation of lignocellulose into chemicals and fuel products in ionic liquids. Chem Rev 117:6834–6880. https://doi.org/10.1021/acs.chemrev.6b00457

72. Skoda-Földes R (2014) The use of supported acidic ionic liquids in organic synthesis. Molecules 19:8840–8884. https://doi.org/10.3390/molecules19078840

73. Xu H, Zhao H, Song H, Miao Z, Yang J, Zhao J et al (2015) Functionalized ionic liquids supported on silica as mild and effective heterogeneous catalysts for dehydration of biomass to furan derivatives. J Mol Catal A Chem 410:235–241. https://doi.org/10.1016/j.molcata.2015.09.020

74. Sun J, Yang J, Li S, Xu X (2016) Basic ionic liquid immobilized oxides as heterogeneous catalyst for biodiesel synthesis from waste cooking oil. Cat Com 83:35–38. https://doi.org/10.1016/j.catcom.2016.05.002

75. Cao Y, Zhou H, Li J (2016) Preparation of a supported acidic ionic liquid on silica-gel and its application to the synthesis of biodiesel from waste cooking oil. Renew Sustain Energy Rev 58:871–875. https://doi.org/10.1016/j.rser.2015.12.237

76. Eftekhari A, Saito T (2017) Synthesis and properties of polymerized ionic liquids. Eur Polym J 90:245–272. https://doi.org/10.1016/j.eurpolymj.2017.03.033

77. Li H, Zhang Q, Liu X, Chang F, Zhang Y, Xue W et al (2013) Immobilizing Cr3+ with SO3H-functionalized solid polymeric ionic liquids as efficient and reusable catalysts for selective transformation of carbohydrates into 5-hydroxymethylfurfural. Bioresour Technol 144:21–27. https://doi.org/10.1016/j.biortech.2013.06.063

78. Liu DDJ, Chen EYX (2013) Polymeric ionic liquid (PIL)-supported recyclable catalysts for biomass conversion into HMF. Biomass Bioenergy 48:181–190. https://doi.org/10.1016/j.biombioe.2012.11.020

79. Wu Z, Chen C, Guo Q, Li B, Que Y, Wang L et al (2016) Novel approach for preparation of poly (ionic liquid) catalyst with macroporous structure for biodiesel production. Fuel 184:128–135. https://doi.org/10.1016/j.fuel.2016.07.004

80. Liu B, Zhang Z (2016) Catalytic conversion of biomass into chemicals and fuels over magnetic catalysts. ACS Catal 6:326–338. https://doi.org/10.1021/acscatal.5b02094

81. Chiang YD, Dutta S, Chen CT, Huang YT, Lin KS, Wu JCS et al (2015) Functionalized Fe3O4@Silica Core-Shell Nanoparticles as Microalgae Harvester and Catalyst for Biodiesel Production. ChemSusChem 8:789–794. https://doi.org/10.1002/cssc.201402996

82. Jin X, Dang L, Lohrman J, Subramaniam B, Ren S, Chaudhari RV (2013) Lattice-matched bimetallic CuPd-graphene nanocatalysts for facile conversion of biomass-derived polyols to chemicals. ACS Nano 7:1309–1316. https://doi.org/10.1021/nn304820v

83. Huang S, Yang KL, Liu XF, Pan H, Zhang H, Yang S (2017) MIL-100(Fe)-catalyzed efficient conversion of hexoses to lactic acid. RSC Adv 7:5621–5627. https://doi.org/10.1039/c6ra26469g

84. Degirmenci V, Pidko EA, Magusin PCMM, Hensen EJM (2011) Towards a selective heterogeneous catalyst for glucose dehydration to 5-Hydroxymethylfurfural in water: CrCl2 catalysis in a thin immobilized ionic liquid layer. ChemCatChem 3:969–972. https://doi.org/10.1002/cctc.201000426

85. Karski S, Paryjczak T, Witoñska I (2003) Selective oxidation of glucose to gluconic acid over bimetallic Pd-Me catalysts (Me = Bi, Tl, Sn, Co). Kinet Catal 44:618–622. https://doi.org/10.1023/A:1026133820538

86. Hoffer BW, Crezee E, Mooijman PRM, Van Langeveld AD, Kapteijn F, Moulijn JA (2003) Carbon supported Ru catalysts as promising alternative for Raney-type Ni in the selective hydrogenation of D-glucose. Catal Today 79–80:35–41. https://doi.org/10.1016/S0920-5861(03)00040-3

87. Rao R, Dandekar A, Baker RTK, Vannice MA (1997) Properties of copper chromite catalysts in hydrogenation reactions. J Catal 171:406–419. https://doi.org/10.1006/jcat.1997.1832

88. Zakzeski J, Weckhuysen BM (2011) Lignin solubilization and aqueous phase reforming for the production of aromatic chemicals and hydrogen. ChemSusChem 4:369–378. https://doi.org/10.1002/cssc.201000299

89. Ahmad E, Pant KK (2018) Lignin conversion: A key to the concept of lignocellulosic biomass-based integrated biorefinery. Elsevier B.V., Amsterdam. https://doi.org/10.1016/B978-0-444-63992-9.00014-8

90. Zhang J, Teo J, Chen X, Asakura H, Tanaka T, Teramura K et al (2014) A series of NiM (M = Ru, Rh, and Pd) bimetallic catalysts for effective lignin hydrogenolysis in water. ACS Catal 4:1574–1583. https://doi.org/10.1021/cs401199f

91. Ajaikumar S, Ahlkvist J, Larsson W, Shchukarev A, Leino AR, Kordas K et al (2011) Oxidation of α-pinene over gold containing bimetallic nanoparticles supported on reducible TiO2 by deposition-precipitation method. Appl Catal A Gen 392:11–18. https://doi.org/10.1016/j.apcata.2010.10.015

92. Shabaker JW, Huber GW, Dumesic JA (2004) Aqueous-phase reforming of oxygenated hydrocarbons over Sn-modified Ni catalysts. J Catal 222:180–191. https://doi.org/10.1016/j.jcat.2003.10.022

93. Feng J, Zhang Y, Xiong W, Ding H, He B (2016) Hydrogenolysis of glycerol to 1,2-propanediol and ethylene glycol over ru-co/zro2 catalysts. Catalysts 6:1–13. https://doi.org/10.3390/catal6040051

94. Zhou J, Guo L, Guo X, Mao J, Zhang S (2010) Selective hydrogenolysis of glycerol to propanediols on supported Cu-containing bimetallic catalysts. Green Chem 12:1835–1843. https://doi.org/10.1039/c0gc00058b

95. González-Borja MÁ, Resasco DE (2011) Anisole and guaiacol hydrodeoxygenation over monolithic Pt-Sn catalysts. Energy Fuel 25:4155–4162. https://doi.org/10.1021/ef200728r

96. Jongerius AL, Jastrzebski R, Bruijnincx PCA, Weckhuysen BM (2012) CoMo sulfide-catalyzed hydrodeoxygenation of lignin model compounds: an extended reaction network for the conversion of monomeric and dimeric substrates. J Catal 285:315–323. https://doi.org/10.1016/j.jcat.2011.10.006

97. Ooi YS, Zakaria R, Mohamed AR, Bhatia S (2004) Catalytic cracking of used palm oil and palm oil fatty acids mixture for the production of liquid fuel: kinetic modeling. Energy Fuel 18:1555–1561. https://doi.org/10.1021/ef049948v

98. Charusiri W, Yongchareon W, Vitidsant T (2006) Conversion of used vegetable oils to liquid fuels and chemicals over HZSM-5, sulfated zirconia and hybrid catalysts. Korean J Chem Eng 23:349–355. https://doi.org/10.1007/BF02706733

Understanding Biomass Chemistry Using Multiscale Molecular Modeling Approach

Shelaka Gupta

Abstract Catalytic upgradation of lignocellulosic biomass to produce value-added fuels and chemicals is technologically challenged due to the complexity of the biomass-derived substrates as well as the reaction media. In order to develop a potential biorefinery, fundamental understanding of the interaction of biomass-derived platform molecules with the catalyst surface and solvent and their behavior during a conversion process needs to be developed. In this regard, computational chemistry methods such as ab initio density functional theory (DFT), classical molecular dynamics (MD), ab initio molecular dynamics (AIMD), Car-Parrinello molecular dynamics (CPMD), etc. have made a valuable contribution. This chapter briefly describes the role of these methods in understanding the reaction mechanism on the catalyst surface and the role of solvents in biomass conversion processes and pyrolysis chemistry.

Keywords Biomass chemistry · Density functional theory · Classical molecular dynamics · Ab initio molecular dynamics · Car-Parrinello molecular dynamics · Acid catalysis

1 Introduction

Lignocellulosic biomass, an inedible form of biomass, can be upgraded to a variety of value-added fuels and chemicals [1]. The overall strategy for the production of biorenewables is to reduce the oxygen content present in biomass. The US Department of Energy (DOE) in 2004 identified 12 biobased value added platform chemicals [2]. Heterogeneous catalysis has played an important role in the upgradation of these biomass-derived platform molecules [3]. Catalytic reactions such as hydrogenation [4], hydrodeoxygenation (HDO) [5], ring-opening (RO) and decarboxylation [6], decarbonylation [7], etc. have been employed to selectively remove the oxygen content present in biomass-derived platform molecules to

S. Gupta (✉)
Department of Chemical Engineering, Indian Institute of Technology Hyderabad, Kandi, Sangareddy, Telangana, India
e-mail: shelaka@che.iith.ac.in

produce fuels and chemicals. However, since most of these reactions are carried out in the solvent phase at high temperatures, stability of the catalyst remains a challenge [8]. Therefore, rational design and development of the catalyst is believed to be a key factor for determining the success of this sustainable process for which a complete molecular-level understanding is required.

Experimnetal techniques may provide some insights about the reaction mechanism however they are still insufficient to construct the detailed reaction mechanism and thus are open to multiple interpretations especially in the field of biomass upgradation owing to the complexity of catalysts, substrates, and reaction media. Advances in high-performance computing and computational methods have made computational design of the catalyst a reality, and the field has reached enough maturity to ensure that the reactions can be described accurately [9]. Computational chemistry methods can predict the properties of a chemical system and allow insights into the reaction that are inaccessible through experiments. These properties are either accessed through quantum chemical method based on the electronic structure calculations such as density functional theory (DFT) [10], or classical force fields to describe the dynamics of atoms with respect to time in the system without considering the behavior of the electrons such as classical molecular dynamic simulations (MD) [11]. In order to study the dynamics during chemical transformations such as bond breaking and formation or charge distribution, ab initio molecular dynamics (AIMD) [12], Car-Parrinello molecular dynamics (CPMD) [13], metadynamics (MTD) [14], etc. are used.

Some of the key findings based on molecular modeling-based investigation in the field of biomass valorization are summarized in this chapter. The chapter first discusses about the role of computational chemistry in understanding the reaction mechanism of different reactions that are generally employed in biomass upgradation which is crucial for the catalyst design. Further, since most of these reactions are carried out in the presence of solvents, the role of molecular dynamic simulations to understand the effect of solvents in affecting the reaction mechanism and changing the yields is discussed. The last section highlights the role of CPMD calculations combined with metadynamics in revealing the biomass pyrolysis chemistry.

2 Reaction Mechanism

2.1 Acid-Catalyzed Conversion of Carbohydrates

Lignocellulosic biomass comprises of three components: cellulose, hemicellulose, and lignin [15]. Upon acid-catalyzed hydrolysis, these components yield C6 and C5 sugar monomers such as glucose and xylose [15]. Glucose can be upgraded to a variety of biofuels and chemicals [16]. Among these chemicals, 5-hydroxymethylfurfural (5-HMF) has emerged as a potential platform molecule for the production of polymers [17], chemicals, and biofuels [18]. Glucose can

either be directly dehydrated to produce 5-HMF [19] or is first isomerized to produce fructose which upon dehydration produces 5-HMF. Out of these, the second route has received considerable attention [20]. Lewis acid catalyst (e.g., Sn-BEA [21], Ti-BEA [22], tungstite [23], etc.) has played a vital role in the isomerization of glucose to produce fructose. DFT simulations by Yang et al. [21] showed that the O1H hydroxyl group of glucose gets coordinated in the presence of hydroxylated defect lattice Sn sites in zeolite (Sn-BEA) (Fig. 1) which lead to proton transfer in two steps from the O1H to O5 followed by RO and formation of acyclic glucose (Fig. 1(i) (1a–1c)). The RO was followed by deprotonation of O2H (Fig. 1(i) (1c–1d)) and aldose-ketose isomerization through a hydride shift from C2 to C1 (Fig. 1(i) (1d–1e)). The intermediate thus formed underwent a conformational transition (Fig. 1(i) (1e–1f)), ring closure (Fig. 1(i) (1f–1 g)), and protonation to form fructose (Fig. 1(i) (1g–1h)). In another study, it was shown that the presence of Lewis acid sites (W^{6+}) provides a cooperated reaction environment on the surface which promotes the rate determining C2-C1 H-shift reaction in glucose conversion to fructose [23]. Further addition of dopants such as Nb^{5+} and Ti^{4+} was found to be effective in lowering the overall barrier for glucose isomerization. Apart from zeolites, base-metal catalyst such as MgO, NaOH, Mg-Al hydrotalcites, etc. [25, 26] and ionic liquids such as tetrabutyl ammonium proline, etc. [27] have been shown to provide good activity for this isomerization reaction.
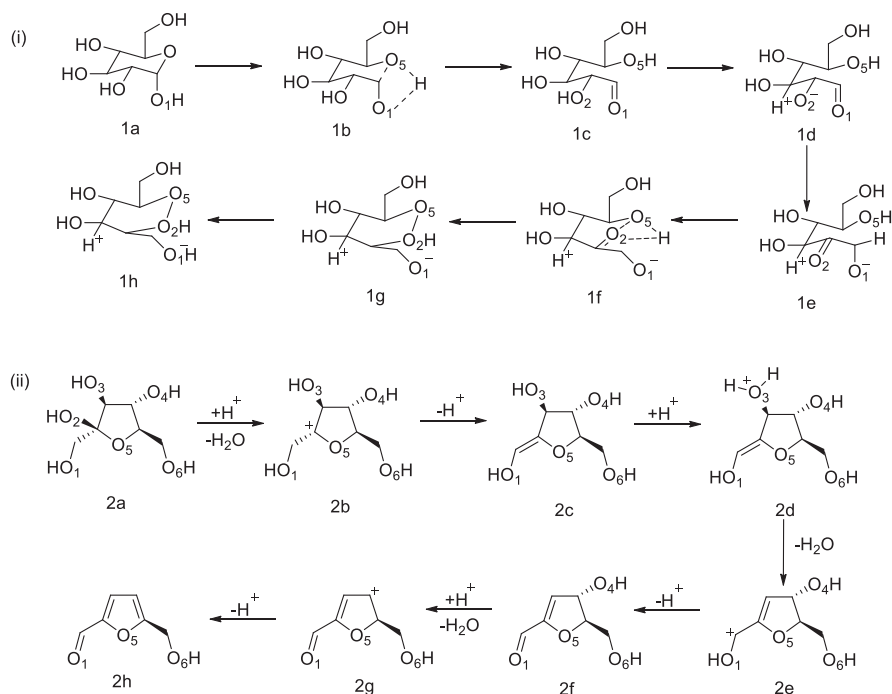
Fig. 1 Mechanistic insights into glucose isomerization to fructose on Sn-BEA catalyst [21] and furfural conversion to 5-HMF [24]

Under Brønsted acidic environment, fructose has been shown to undergo dehydration to produce 5-HMF. Yang et al. analyzed 100 reaction pathways by utilizing DFT simulations to identify the main reaction channel for obtaining 5-HMF from glucose [24]. The simulations showed that the dehydration of fructose is initiated by the protonation of O2H as shown in Fig. 1(ii) with subsequent removal of water resulting in the formation of carbocationic intermediate (Fig. 1(ii) (2a–2b)). Dehydration is followed by deprotonation which results in a C–C double bond (Fig. 1(ii) (2b–2c)). Subsequently, two more water molecules are removed (Fig. 1(ii) (2d–2h) which led to the formation of 5-HMF [24].

Similarly, the hemicellulosic part of biomass upon hydrolysis produces C5 sugars such as xylose which can be converted to furfural, another class of platform molecule that can be upgraded to C4 to C5 molecules which find applications as fuels (2-methylfuran, 2-methyltetrahydrofuran, etc.), fuel additives, and value-added chemicals (butanediol, gamma valerolactone, etc.) [28]. Heterogeneous catalyst such as H-zeolites [29], modified mesoporous silicas [30], sulfonated graphene oxides [31], ion exchange resins [32], etc. have been employed for the production of furfural from xylose. Similar to glucose conversion to 5-HMF, it has been observed that in the presence of a Lewis acid catalyst, xylose first gets isomerized to produce xylulose [33]. A six-membered transition state was formed during the formation of xylulose with a barrier of 150.8 kJ/mol in water [34] in which hydrogen from O2H migrated to O of the aldehyde group and another H from C2 migrates to C1. On undergoing hydrogenation-cyclization and dehydrations, xylulose can be converted to furfural [34].

2.2 Hydrogenation Reactions

Hydrogenation is the most common reaction carried out for biomass upgradation and is generally carried out at moderate pressure (10–30 bar) and temperature (370–420 K) conditions in the presence of metal catalyst (Pd, Ni, Pt, Ru, or Cu) to either saturate the C=C or C=O bonds present in the multifunctional biomass-derived platform molecules [35]. The type of bond hydrogenated depends upon the choice of the catalyst. Selective hydrogenation of C=O bond present outside the furan ring in furfural and 5-HMF produces furfuryl alcohol (FA) and 2,5-bishydroxymethylfuran (BHMF) in the presence of noble metal (Ru/MSN-Zr [36], Pt/MCM-41 [37], Ir/TiO$_2$ [38], etc.) or non-noble metal catalyst such as Cu-ZnO at mild reaction conditions (T = 25–120 °C, P_{H2} = 8–60 bar) in polar solvents [39]. Addition of oxophilic promoters such as Fe [40], Re [41], etc. in these metal catalysts provided better selectivity at low temperature (~50 °C) and pressure conditions (8 bar). DFT simulations have also been used to explain the observed selectivity trends for C=O or C=C bond hydrogenation. Using DFT simulations, it was showed that Cu has less affinity for C=C bond, and as a result, furfural prefers to bind through η1(O)-aldehyde due to which carbonyl in furan ring forms a direct bond with the surface of Cu via the lone pairs present on the oxygen and favors C=O

bond hydrogenation [42]. Further hydrogenation proceeds via either an alkoxide (path 1) or hydroxyalkyl (path 2) intermediate as shown in Fig. 2. However, the activation barrier for path 2 was found to be lower than path 1 which indicated that the first hydrogen atom will attack the oxygen atom of the carbonyl group rather than the C atom which was in line with the diffuse reflectance infrared Fourier transform spectroscopy (DRIFTS) studies in which this intermediate was observed [42]. In contrast with group eight metals, furan ring bound in η2 (C,O)-aldehyde configuration in which both oxygen and carbon of the carbonyl group bonded with the metal atoms and underwent hydrogenation to FA by forming hydroxyalkyl intermediate. On the other hand, C=C bond hydrogenation present in 5-HMF and furfural furan ring produces 5-hydroxymethyl-tetrahydrofurfural (HMTHFA) and tetrahydrofurfural which on undergoing self-condensation reaction can be used as a diesel component [43]. In the presence of relatively more active and high surface area catalyst such as Pd/C [38], Ni/SiO$_2$, etc., complete hydrogenation of furfural and 5-HMF can be achieved to produce tetrahydrofurfuryl alcohol (THFA) and 2,5-bishydroxymethyltetrahydrofuran (BHMTHF) that can be used as a green solvent [44]. Metals with strong affinity for C=C bonds and those which favor parallel adsorption of furan ring are employed for THFA and BHMTHFA production [45]. In order to prevent further dehydroxylation, hydrogenation reaction is carried out in biphasic solvent.

Some studies have also reported hydrogenation reaction of biomass-derived platform molecules to be structure sensitive when carried over transition metal catalyst.
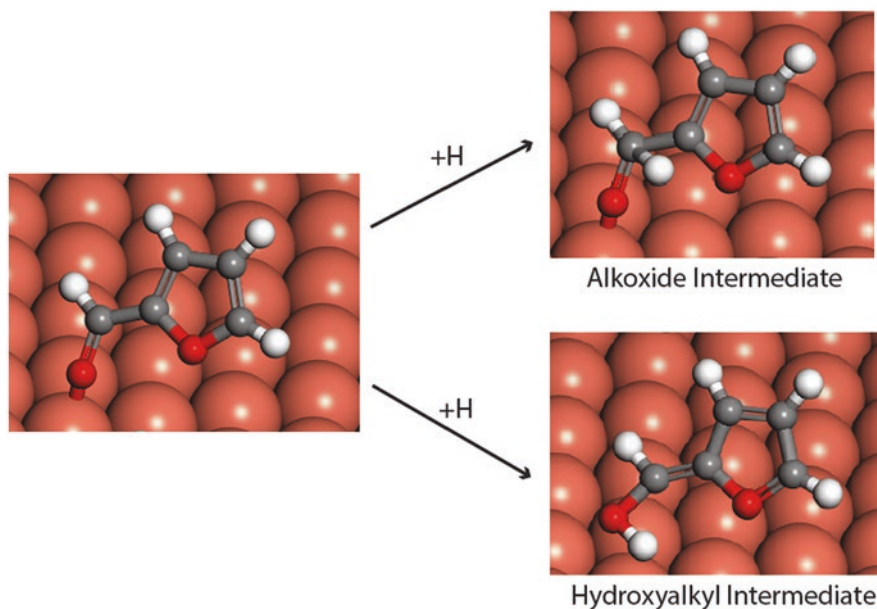
Fig. 2 Adsorption geometry of furfural and intermediates on Cu (111) surface via alkoxide or hydroxyalkyl pathway [42]

For example, vapor-phase furfural hydrogenation when carried out on Pt nanoparticles of different shapes (cubes, spheres, octahedral) and sizes (1.5–7.1 nm) exhibited structure sensitivity [46]. Product selectivity toward furfuryl alcohol increased from 1 to 66% on increasing the size of the Pt nanoparticles. Under similar reaction conditions, smaller nanoparticles showed higher selectivity for decarbonylation reaction, thus favoring furan formation. Additionally, octahedral particles favored furfuryl alcohol production, whereas cubes produced equal amount of furan and FA. Similar structure sensitivity was reported in lignin-derived phenol hydrogenation over Pd catalyst where Pd cubes (100) exhibited higher selectivity toward cyclohexanone (~90%) irrespective of the reaction time (~40 h) [47]. In contrast, Pd octahedra (111) and spherical particles having both (111) and (100) exhibited higher selectivity toward cyclohexanol on increased reaction time (>20 h). The selectivity trends were explained using DFT simulations which showed that the activation barriers for cyclohexanone hydrogenation on Pd (100) (Fig. 3, E_a = 97 kJ/mol (2a–2b) and 101 kJ/mol (2b–2c)) were higher as compared to Pd (111) (Fig. 3, E_a = 77 (1a–1b) and 57 kJ/mol (1b–1c)) [47].

2.3 Hydrodeoxygenation Reactions

Hydrodeoxygenation (HDO) reactions form an important class of reaction in biomass upgradation to produce hydrocarbons because of their ability to selectively remove the oxygen content present in biomass which in turn improves the effective H/C ratio. Noble (Pd, Pt, Ru, etc.) or non-noble (Fe, Ni, or Cu) metal catalysts show lower selectivity toward HDO products as they promote other side reactions such as decarboxylation or decarbonylation [48]. Apart from metal catalysts, sulfided transition state metal catalysts (Mo, Co, and Ni) have been studied for the HDO of bio-oil. Sulfided Ni-Mo and Co-Mo catalyst supported on Al_2O_3 exhibited higher yield for deoxygenated products for different HDO reactions [49]. However, these sulfided catalysts are prone to deactivation due to the presence of oxygenated molecules and aqueous environment [50]. On the other hand, bifunctional catalysts having both metal and acid sites and bimetallic catalysts which contain a combination of reducing (Ni, Pt, Pd, Rh, etc.) and oxophilic metals (Fe, Co, Mo, Re, W, Cr, etc.) have shown higher selectivity for HDO reactions [51]. Bimetallic catalysts such as Pt-WO$_x$/C, Rh-ReO$_x$/SiO$_2$, Ir-ReO$_x$/SiO$_2$, etc. have shown high selectivity to produce terminal diols from biomass-derived cyclic ethers [52]. Chia et al. by utilizing DFT simulations showed that under aqueous environment when Ir is present near the vicinity of Re, the hydroxyl group is adsorbed on the oxophilic Re atom and is responsible for donating a proton to the cyclic ethers for the formation of carbenium ion which leads to RO via the sterically hindered C–O bond [53] hydrogenolysis (Fig. 4a). The ring-opened intermediate upon undergoing hydride transfer formed oxocarbenium ion which on further addition of hydrogen led to terminal diol formation (Fig. 4a). Similarly, bimetallic catalysts such as PdFe/C [55], NiFe/SiO$_2$ [5], Pd/Fe$_2$O$_3$ [56], etc. have been seen to be highly efficient for the HDO reaction
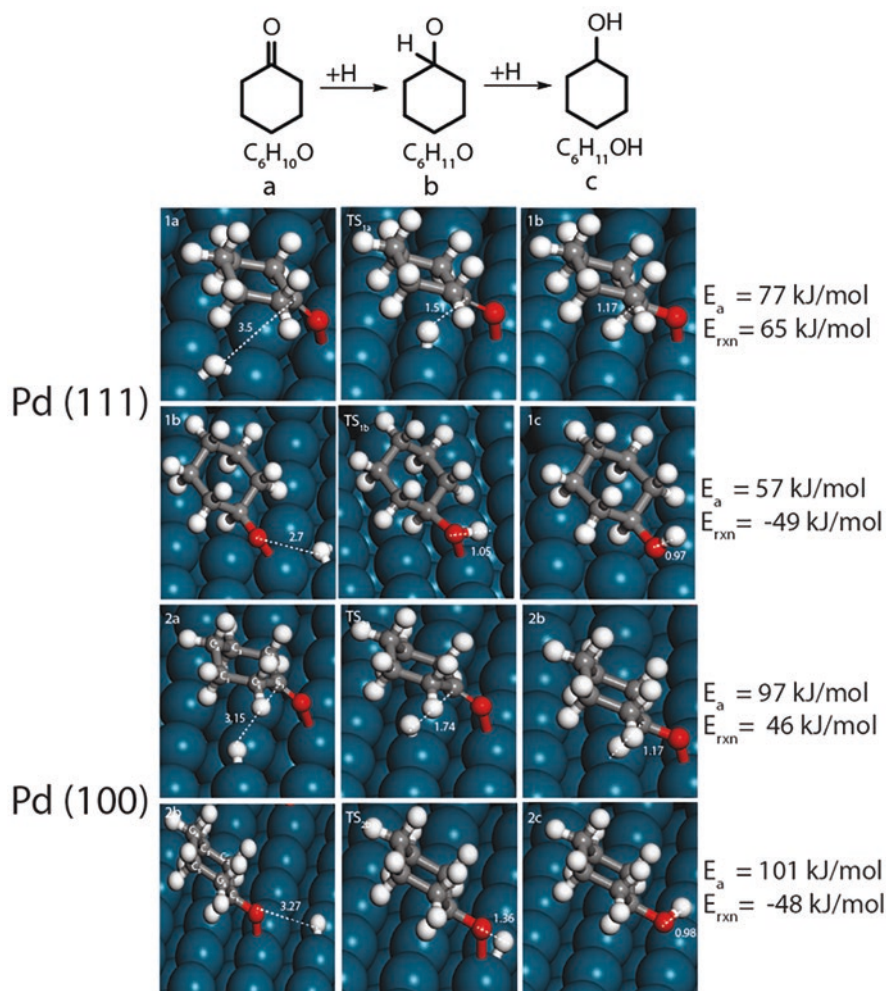
Fig. 3 Reactant, product, and transition structures for cyclohexanone hydrogenation to cyclohexanol on Pd (111) and Pd (100) surface [47]
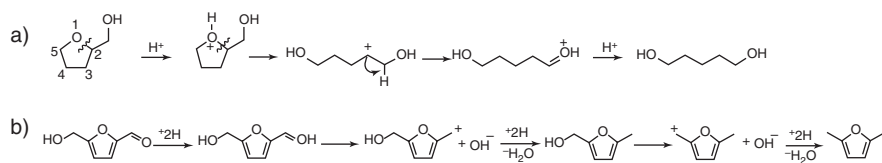
Fig. 4 DFT suggested routes for the (**a**) RO of cyclic ethers to produce terminal alcohols [53] and (**b**) HDO of 5-HMF to 2,5-DMF [54]

of lignin-derived molecules such as phenol, cresol, guaiacol, syringol, etc. to produce arenes. In contrast, monometallic catalysts such as Ru and Pd before catalyzing the HDO reaction tend to hydrogenate the aromatic ring. High selectivity for arenes on these bimetallic catalysts is ascribed either to the oxophilicity or to the perpendicular adsorption of phenolics which enhances the C–O bond cleavage and inhibits hydrogenation of aromatic ring. Similarly, PdZn bimetallic catalyst showed higher selectivity for the HDO reaction of 5-HMF to 2,5-dimethylfuran (2,5-DMF) [54]. Experimental studies by Saha et al. showed that Pd alone exhibited low conversion and selectivity for the reaction [57]. However, on addition of Zn, both conversion (~99%) and selectivity (~85%) increased. By utilizing DFT simulations, Gupta et al. showed that when oxophilic Zn is present on the steps of Pd catalyst, the activation barriers for the HDO steps decrease which in turn helps in improving the conversion and selectivity [54] (Fig. 4b). For the HDO of biomass-derived platform molecules, Jalid et al. by utilizing micro kinetic model (MKM) studied the reactivity trends for the C–O bond hydrogenolysis in ethanol on the steps of transition metal catalyst [58]. The study showed that reaction conditions affected the bimetallic catalyst design for carrying out HDO reaction. At 523 K, the metal catalyst followed the order Co > Ru > Ir > Rh > Ni > Fe > Pt > Pd > Cu > Re > Ag > Au, whereas at 373 K, Cu, Pt, Rh, Ir, Ru, Ni, and Co were found to be more selective. More specifically, three bimetallic catalysts (Co_3Ni, Co_3Fe, and Ni_3Fe) exhibited maximum turnover for the HDO product.

2.4 RO and Decarboxylation Reactions of Biomass-Derived Lactones and Cyclic Esters

Apart from hydrogenation and HDO reactions, RO and decarboxylation reactions have been found to be effective for the deoxygenation of biomass-derived platform molecules to produce value-added fuels and chemicals [59]. Several studies have reported the RO and decarboxylation of the biomass-derived platform molecule γ-valerolactone (GVL) to produce renewable fuels and chemicals [60]. In the presence of Brønsted acid catalyst such as SiO_2/Al_2O_3 at 648 K temperature and under 35 bar H_2 pressure, GVL underwent RO to produce pentenoic acid which upon undergoing decarboxylation formed isomers of butene (~92%) [59]. However, in the presence of Lewis acid catalyst (γ-Al_2O_3), selectivity toward α-butene, a commercially relevant polymer precursor, was found to be higher but in lieu of dropped overall yield (~43%) [61]. The overall yield of butene was retrieved back (~80%) on adding tungsten oxide to γ-Al_2O_3 which was attributed to the presence of Brønsted acidity. Thus, the presence of both Lewis and Brønsted acid catalysts was found to be essential for the production of linear alpha olefins from lactones. By utilizing DFT simulations, Gupta et al. showed that in the presence of Brønsted acid environment, oxocarbenium ions are formed via protonation of carbonyl oxygen of GVL [62] (Fig. 5a). These oxocarbenium ions then led to GVL RO to form
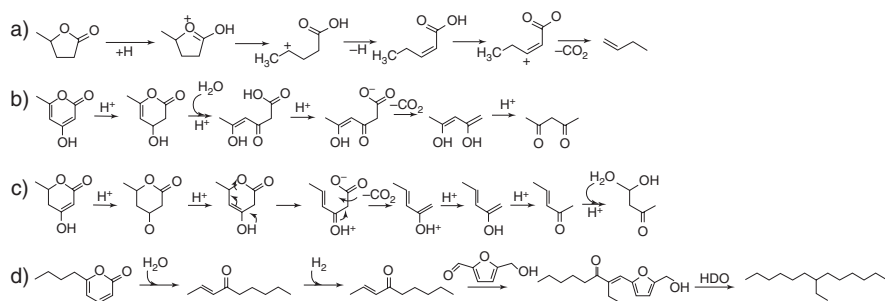
Fig. 5 RO and decarboxylation mechanism of (**a**) GVL [62], (**b**) TAL [63], (**c**) DHHMP [6], and (**d**) 6PP [64]

γ-carbenium ion on a Lewis acid catalyst with a reduced activation barrier of $E_a = 13$ kJ/mol [65]. Under Brønsted acid environment, the stability of oxocarbenium ions determined RO rates in lactones [62].

On the other hand, polyketide biosynthesis route provides platform molecules with variable no. of carbon atom in contrast to biomass-derived aqueous sugars having C5–C6 atoms [66]. Shanks and co-workers demonstrated triacetic acid lactone (TAL) as a potential platform produced via polyketide biosynthesized route to produce value-added fuels and chemicals [63]. TAL underwent RO and decarboxylation to produce CO_2 and 2,4-pentanedione with complete conversion without any acid catalyst in the presence of water at a much lower temperature (<100 °C) than that needed for GVL RO [63] (Fig. 5b). By utilizing DFT simulations, it was observed that the RO takes place via nucleophilic addition of water on the carbonyl group of the 2-pyrone molecule [6]. On partial hydrogenation and keto-enol tautomerization, TAL produced 3,6-dihydro-4-hydroxy-6-methylpyran-2-one (DHHMP). DHHMP was observed to undergo RO and decarboxylation to produce 3-pentanone via retro-Diels-Alder (rDA) reaction mechanism (Fig. 5c). High reactivity of DHHMP via rDA reaction was attributed to a double bond present at C_4–C_5 position. In another DFT study by our group, the substituent type present at the C4 position and the nature of the solvent were observed to affect the RO barrier [67]. 2-Pyrone containing electron-donating group at the C4 position exhibited lower activation barriers in comparison to the one with electron-withdrawing substituent. The reactivity of the 2-pyrones was correlated with the frontier molecular orbital (FMO) theory where a linear relationship was proposed between the FMO gap of the products formed and activation barrier [68]. In comparison to nonpolar solvents, higher stabilization of transition state in polar solvents reduced the RO activation barrier. In addition to it, Car-Parrinello molecular dynamics (CPMD) simulations showed that the dynamic behavior of the solvent due to the differential interaction of the solvent with the transition and the reactant state reduced the barrier for the rDA reactions [69]. Similar to TAL, Alam et al. identified 6-amyl-alpha pyrone (6PP) as another platform molecule to produce food graded flavoring agent and C15–C16 range fuel [64]. At 498 K, 6PP underwent RO and

decarboxylation to produce non-2-en-4-one which further upon hydrogenation yielded 4-nonanone, a known food flavoring agent. 4-Nonanone was upgraded to C15–C16 range diesel fuel by undergoing aldol condensation with 5-HMF in the presence of MgO–CaO base catalyst followed by HDO [64] (Fig. 5d).

3 Solvent Effects

The catalytic conversion of lignocellulose biomass is generally carried out in aqueous solutions, and the kinetics and selectivity of such reactions can be tuned by varying the temperature, pressure, and solvent composition [70, 71]. Some reactions have shown improvement in performance by altering the solvent composition. For example, the yield of acid-catalyzed conversion reaction showed an increase in the presence of mixed solvent environment [72, 73]. However, solvent selection for a new process requires either trial and error experiments or simulation methods that are computationally expensive. Ab initio DFT simulations can probe mechanistic details of reaction; however, the simulations are computationally expensive which makes the screening of multiple solvent compositions infeasible. In contrast, classical molecular dynamic (MD) simulations allow characterization of larger molecules surrounded by complex solvent environment with reduced computational burden [74]. With the use of classical molecular dynamic (MD) simulations in combination with experiments, the rate of acid-catalyzed reactions in biomass conversion in a mixture of solvents can be estimated [75]. Classical MD simulations were used to explain the selectivity trends for Brønsted acid-catalyzed dehydration of 1,2-propanediol which when carried out in pure water showed higher selectivity toward propanal (~41%) than acetone (~5). Similar selectivity trends were observed for aqueous mixtures of the aprotic solvents except for aqueous dimethyl sulfoxide solution wherein acetone (selectivity ~48%) was formed as the major product. Classical MD simulations were used to calculate the free energy difference ($\Delta\Delta G$) between the reactant and the product, and the value of $\Delta\Delta G$ was correlated to the rate of formation of the product which indicated that the stabilization of the product relative to the reactant in solvent-mediated environment enhanced the selectivity [76]. Classical MD simulations were also used to explain the increase in yield of 5-HMF from glucose in the presence of aqueous mixture of dimethyl sulfoxide (DMSO) and acetonitrile as the solvents [77]. Using MD simulation, it was observed that acetonitrile increased the coordination between water and glucose which lead to an increase in the isomerization of glucose to fructose [77]. The stability of hydronium ions formed during acid-catalyzed biomass conversion reactions in mixed solvent environment has been shown to affect the reaction kinetics [78]. Water-rich local solvent domains were formed near the hydronium ion which was attributed to the increased stability of hydronium ion. Molecular dynamic simulations were also used to unravel the interaction between lignin and cellulose in the two solvent system (THF-water) [79]. THF in water was found to dissolve and disaggregate the lower weight lignin molecules which allowed molecules to separate

out from cellulosic fraction as well as from each other. Also introduction of THF leads to formation of random coil conformations instead of compact modules observed in case of water [79].

However, classical MD simulations cannot be used to simulate the phenomena (bond formation and breaking, charge distribution) associated with the changes in electronic structures. As an alternative to study the dynamics during chemical transformations, ab initio molecular dynamics (AIMD) simulations can be used. AIMD simulations were used to understand the effect of polar aprotic solvents such as GVL in the presence of salt containing Cl$^-$ ions on the acid-catalyzed dehydration kinetics of fructose [80]. A ten times increase in reactivity with more than 80% yield was observed for fructose dehydration to 5-HMF during the experiments in the presence of GVL. This increase in reactivity was explained by using AIMD simulations which showed that the initial dehydration proceeded by the protonation and water elimination from C2 of the fructose molecule which resulted in the formation of an oxocarbenium ion which was followed by deprotonation to form enol (Fig. 6(i)). The apparent activation barrier for these two steps was calculated to be 93 kJ/mol in water. Further simulations showed that hydrophilic domains were formed with the addition of GVL near the fructose that was surrounded with GVL domains. The hydrophilic domain leads to easier transfer of the protons and stabilization of the transition states due to localized Cl$^-$ anions and protons [80]. The overall activation barrier reduced to 74 kJ/mol for a solution of 75 wt% GVL. In another study by Gupta et al., it was proposed that in Brønsted acid environment, the RO of GVL takes place via formation of oxocarbenium ion intermediate using DFT
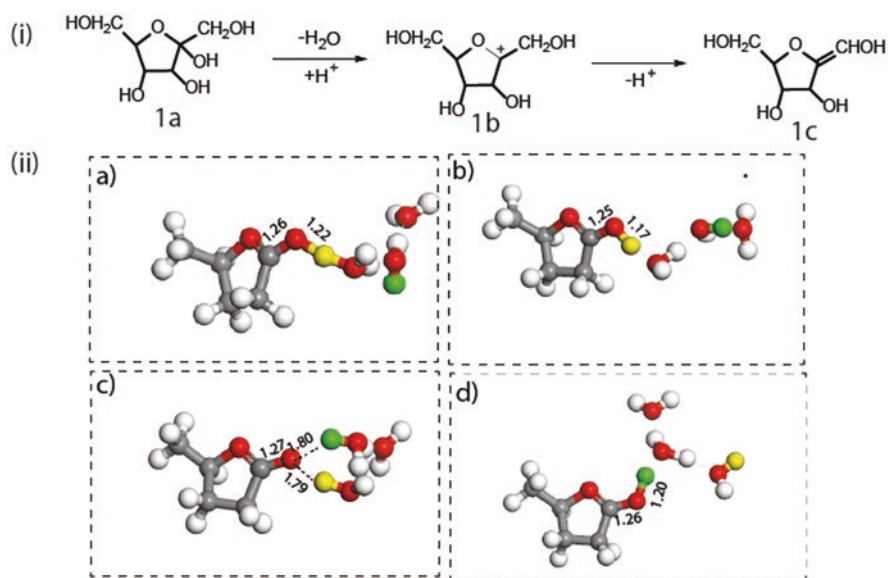
Fig. 6 AIMD predicted mechanism for (i) fructose dehydration in GVL-water mixture [80] and (ii) formation of GVL oxocarbenium ion in the presence of Brønsted acidic proton in water [62]

as explained previously [62]. Further AIMD simulations showed that the oxocarbenium ions were found to be stable for 2.5 ps in the reaction environment containing water [62] (Fig. 6(ii)). However, AIMD simulations are computationally very expensive. Another alternative approach to this is Car-Parrinello AIMD (CPMD) which combines quantum mechanics and classical MD. However, CPMD calculation takes a longer time. Metadynamics [81] is used as a method to accelerate the dynamics of CPMD calculations. To understand the solvent dynamics effects on the rDA reaction of partially saturated 2-pyrones containing electron-withdrawing and electron-donating substituents, CPMD simulation in conjunction with metadynamics was used. In the presence of solvent phase, the RO and decarboxylation barrier were lowered, and the effect was more pronounced for the 2-pyones containing electron-donating substituent [69]. The decrease in the barrier was attributed to the differential stabilization of the transition and reactant state due to the structuring and dynamics of solvent molecules [69].

4 Pyrolysis Chemistry

High degree of polymerization in cellulose and hemicellulose renders use of DFT simulations in studying the pyrolysis reaction and mechanism. Moreover, pyrolysis reactions are carried out in condensed phase, whereas most of the DFT simulations are done in gas phase. Recent studies of pyrolysis chemistry were performed by AIMD simulations in condensed environment and at finite temperature [82]. A simulation cell of periodically repeated two units of cellulose Iβ was used to mimic the solid cellulose by Agarwal et al. [82] Using CPMD metadynamics, they found that at 327 °C, ring contraction of glucopyranose to glucofuranose led to depolymerization with a lowest free energy barrier of 20 kJ/mol (Fig. 7(i)) and at 600 °C precursor to levoglucosan was formed with a free energy barrier of 36 kcal/mol [82] (Fig. 7(ii)). On the other hand, Mettler et al. used α-cyclodextrin as a model compound for cellulose [83] and suggested direct formation of furanic compounds from cellulose instead of cellulose decomposition to glucose [83]. They observed that the cleavage of glycosidic linkage between two glucose units leads to furan ring formation followed by formation of carbonyl group at C1 position (Fig. 7(iii)). This is followed by RO of the pyran ring. In order to satisfy the valency of pyran O, it undergoes ring closure again but at C2 which is followed by dehydration to form the furan ring [83]. Therefore, for small-scale cellulose pyrolysis system having ~100 atoms, CPMD-metadynamics appears to be a useful approach. This limits detailed description of pyrolysis of cellulose in complex environment.

The reactive force field (ReaxFF) [84, 85] is another promising approach that can model complex reactive system. Zheng et al. constructed a large cellulose model having 7572 atoms containing six long chains and each containing 60 glycopyranoses for conducting ReaxFF simulation [86]. The simulations were performed at 500–1400 K for 250 ps. The ReaxFF simulation results showed that the reaction
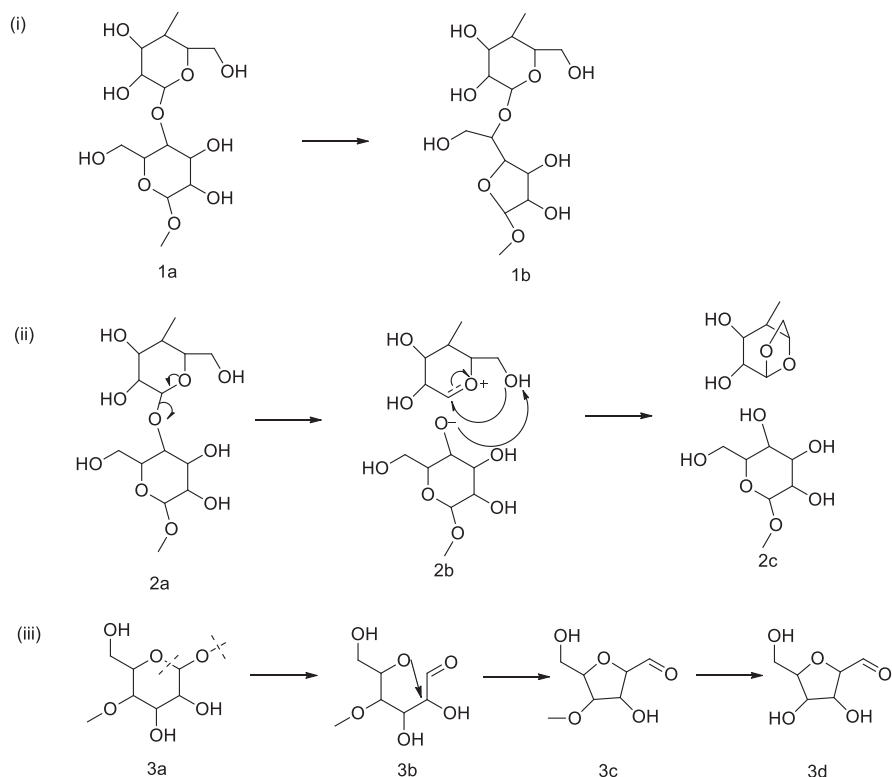
Fig. 7 Chemical pathway for the (i) ring contraction of glucopyranose to glucofuranose, (ii) depolymerization of glucopyranose into LGA, and (iii) conversion of α-cyclodextrin to furan obtained using CPMD simulations

proceeded by the release of gases initially, and at 800 K, bio-oil production was maximum. The major products observed in the cellulose pyrolysis simulation were glycolaldehyde, levoglucosan, 2-hydroxy-propionaldehyde, hydroxyl-acetone, H_2O, CO, and CO_2 which was in good agreement with the experiments. The maximum yield of levoglucosan was observed to be at lower temperatures, whereas higher temperature favored glycolaldehyde. Using ReaxFF MD simulations for a large lignin model having 15,920 atoms, Zheng et al. studied the reaction pathways for different linkages in lignin pyrolysis. Cα/Cβ ether bond cracking was found to be the dominant pathway for β-O-4, α-O-4, and α-O-4 and β-5 linkages. Whereas γ-O-α and β-β linkage bond cracking of Cα-O ether bond and the RO of aryl monomer were found to be equally important [87]. For the other β-1, β-2, β-5, 4-O-5, and 5-5 linkages, RO pathway dominated. At low temperature, Cα/Cβ ether bond cracking was observed, whereas aryl RO took place at higher temperatures.

5   Conclusion

Fundamental understanding of physicochemical interactions during biomass valorization is needed for the development of sustainable biomass processes. This chapter reviews some of the recent studies on the implementation of molecular simulation methods (DFT, MD, AIMD, CPMD-metadynamics, ReaxFF, etc.) to address the challenges related to developing biomass conversion technologies such as screening of solvents, understanding the mechanism and reaction kinetics in liquid-phase biomass reactions, and developing a reaction network for condensed phase biomass pyrolysis. However, there are only few studies which take into account solvation environment dynamics, temperature effects, condensed phase biomass processing environment, etc. With the availability of higher parallel computing packages, there exits an opportunity where this predictive computational modeling at different scales can be used to fully explore the biomass processing.

References

1. Bardhan SK, Gupta S, Gorman ME, Haider MA (2015) Biorenewable chemicals: feedstocks, technologies and the conflict with food production. Renew Sust Energ Rev 51:506–520
2. Werpy T, Petersen G (2004) Top value added chemicals from biomass volume I — results of screening for potential candidates from sugars and synthesis gas. Biomass. https://doi.org/10.2172/15008859
3. Alonso DM, Bond JQ, Dumesic JA (2010) Catalytic conversion of biomass to biofuels. Green Chem 12:1493
4. Nakagawa Y, Tamura M, Tomishige K (2013) Catalytic reduction of biomass-derived furanic compounds with hydrogen. ACS Catal 3:2655–2668
5. Nie L et al (2014) Selective conversion of m-cresol to toluene over bimetallic Ni-Fe catalysts. J Mol Catal A Chem 388–389:47–55
6. Chia M et al (2013) Mechanistic insights into ring-opening and decarboxylation of 2-pyrones in liquid water and tetrahydrofuran. J Am Chem Soc 135:5699–5708
7. Sitthisa S, An W, Resasco DE (2011) Selective conversion of furfural to methylfuran over silica-supported NiFe bimetallic catalysts. J Catal 284:90–101
8. Schwartz TJ, Neill BJO, Shanks BH, Dumesic JA (2014) Bridging the chemical and biological catalysis gap: challenges and outlooks for producing sustainable chemicals. ACS Catal 4:2060–2069
9. Grajciar L et al (2018) Towards operando computational modeling in heterogeneous catalysis. Chem Soc Rev 47:8307–8348
10. Sholl DS, Steckel JA (2009) Density functional theory a practical introduction. Wiley, New York
11. Rapaport DC (2011) The art of molecular dynamics simulation. Cambridge University Press, Cambridge. https://doi.org/10.1017/CBO9780511816581
12. Hassanali AA, Cuny J, Verdolino V, Parrinello M (2014) Aqueous solutions: state of the art in ab initio molecular dynamics. Philos Trans R Soc A 372:1–32
13. Car R, Parrinello M (1985) Unified approach for molecular dynamics and density-functional theory. Phys Rev Lett 55:2471–2474
14. Barducci A, Bonomi M, Parrinello M (2011) Metadynamics. WIREs Comput Mol Sci 1:826–843

15. Wyman CE et al (2005) Coordinated development of leading biomass pretreatment technologies. Bioresour Technol 96:1959–1966
16. Song J, Fan H, Ma J, Han B (2013) Conversion of glucose and cellulose into value-added products in water and ionic liquids. Green Chem 15:2619–2635
17. Mishra DK et al (2017) MnCo2O4 spinel supported ruthenium catalyst for air-oxidation of HMF to FDCA under aqueous phase and base-free conditions. Green Chem 19:1619–1623
18. James OO et al (2010) Towards the conversion of carbohydrate biomass feedstocks to biofuels via hydroxymethylfurfural. Energy Environ Sci 3:1833–1850
19. Tang J et al (2017) Insights into the kinetics and reaction network of aluminum chloride-catalyzed conversion of glucose in NaCl-H2O/THF biphasic system. ACS Catal 7:256–266
20. Xin H et al (2017) Dehydration of glucose to 5-hydroxymethylfurfural and 5-ethoxymethyl-furfural by combining Lewis and Brønsted acid. RSC Adv 7:41546–41551
21. Yang G, Pidko EA, Hensen EJM (2013) The mechanism of glucose isomerization to fructose over Sn-BEA zeolite : a periodic density functional theory study. ChemSusChem 6:1688–1696
22. Gounder R-B, Davis ME (2013) Titanium-beta zeolites catalyze the stereospecific isomerization of D-glucose to L-sorbose via intramolecular C5−C1 hydride shift. ACS Catal 3:1469–1476
23. Li G, Pidko EA, Hensen EJM (2016) A periodic DFT study of glucose to fructose isomerization on tungstite (WO3·H2O): influence of group IV − VI dopants and cooperativity with hydroxyl groups. ACS Catal 6:4162–4169
24. Yang G, Pidko EA, Hensen EJM (2012) Mechanism of Bronsted acid-catalyzed conversion of carbohydrates. J Catal 295:122–132
25. Delidovich I, Palkovits R (2014) Catalytic activity and stability of hydrophobic Mg-Al hydrotalcites in the continuous aqueous-phase isomerization of glucose into fructose. Cat Sci Technol 4:4322–4329
26. Delidovich I, Palkovits R (2015) Structure-performance correlations of Mg-Al hydrotalcite catalysts for the isomerization of glucose into fructose. J Catal 327:1–9
27. Zhang X et al (2019) Glucose aqueous isomerization catalyzed by basic ionic liquids. ACS Sustain Chem Eng 7:13247–13256
28. Li X, Jia P, Wang T (2016) Furfural: a promising platform compound for sustainable production of C4 and C5 chemicals. ACS Catal 6:7621–7640
29. Kim SB et al (2011) Dehydration of D-xylose into furfural over H-zeolites. Korean J Chem Eng 28:710–716
30. Bhaumik P, Dhepe PL (2014) Effects of careful designing of SAPO-44 catalysts on the efficient synthesis of furfural. Catal Today 251:66–72
31. Lam E et al (2011) Carbocatalytic dehydration of xylose to furfural in water. Carbon N Y 50:1033–1043
32. Larreategui A, Requies J, Güemez MB, Arias PL (2011) Furfural production from xylose using sulfonic ion-exchange resins (Amberlyst) and simultaneous stripping with nitrogen. Bioresour Technol 102:7478–7485
33. Choudhary V, Pinar AB, Sandler SI, Vlachos DG, Lobo RF (2011) Xylose isomerization to xylulose and its dehydration to furfural in aqueous media. ACS Catal 1:1724–1728
34. Wang M, Liu C, Li Q, Xu X (2015) Theoretical insight into the conversion of xylose to furfural in the gas phase and water. J Mol Model 21:296
35. Chheda JN, Huber GW, Dumesic JA (2007) Liquid-phase catalytic processing of biomass-derived oxygenated hydrocarbons to fuels and chemicals. Angew Chem Int Ed Engl 46:7164–7183
36. Chen J et al (2013) Immobilized Ru clusters in nanosized mesoporous zirconium silica for the aqueous hydrogenation of furan derivatives at room temperature. ChemCatChem 5:2822–2826
37. Chatterjee M, Ishizaka T, Kawanami H (2014) Selective hydrogenation of 5-hydroxymethyl-furfural to 2,5-bis-(hydroxymethyl)furan using Pt/MCM-41 in an aqueous medium: a simple approach. Green Chem 16:4734–4739

38. Cai H, Li C, Wang A, Zhang T (2014) Biomass into chemicals: one-pot production of furan-based diols from carbohydrates via tandem reactions. Catal Today 234:59–65
39. Wang Y, Zhao D, Rodr D, Len C (2019) Recent advances in catalytic hydrogenation of furfural. Catalysts 9:1–33
40. Yu L et al (2015) Robust and recyclable nonprecious bimetallic nanoparticles on carbon nanotubes for the hydrogenation and hydrogenolysis of 5-hydroxymethylfurfural. ChemCatChem 7:1701–1707
41. Tamura M, Tokonami K, Nakagawa Y, Tomishige K (2013) Rapid synthesis of unsaturated alcohols under mild conditions by highly selective hydrogenation. Chem Commun 49:7034–7036
42. Sitthisa S, Sooknoi T, Ma Y, Balbuena PB, Resasco DE (2011) Kinetics and mechanism of hydrogenation of furfural on Cu/ SiO2 catalysts. J Catal 277:1–13
43. Huber GW, Chheda JN, Barrett CJ, Dumesic JA (2005) Production of liquid alkanes by aqueous-phase processing of biomass-derived carbohydrates. Science 823:1446–1450
44. Tang X et al (2017) Chemoselective hydrogenation of biomass derived 5-hydroxymethylfurfural to diols: key intermediates for sustainable chemicals, materials and fuels. Renew Sust Energ Rev 77:287–296
45. Vorotnikov V, Mpourmpakis G, Vlachos DG (2012) DFT study of furfural conversion to furan, furfuryl alcohol, and 2-methylfuran on Pd(111). ACS Catal 2:2496–2504
46. Pushkarev VV, Musselwhite N, An K, Alayoglu S, Somorjai GA (2012) High structure sensitivity of vapor-phase furfural decarbonylation/hydrogenation reaction network as a function of size and shape of Pt nanoparticles. Nano Lett 12:5196–5201
47. Porwal G et al (2019) Mechanistic insights into the pathways of phenol hydrogenation on Pd nanostructures. ACS Sustain Chem Eng 7:17126–17136
48. Hausoul PJC, Negahdar L, Schute K, Palkovits R (2015) Unravelling the Ru-catalyzed hydrogenolysis of biomass- based polyols under neutral and acidic conditions. ChemSusChem 8:3323–3330
49. Hočevar B, Grilc M, Huš M, Likozar B (2019) Mechanism, ab initio calculations and microkinetics of straight-chain alcohol, ether, ester, aldehyde and carboxylic acid hydrodeoxygenation over Ni-Mo catalyst. Chem Eng J 359:1339–1351
50. Mikkola JP et al (2000) Deactivation kinetics of Mo-supported raney Ni catalyst in the hydrogenation of xylose to xylitol. Appl Catal A Gen 196:143–155
51. Robinson AM, Hensley JE, Will Medlin J (2016) Bifunctional catalysts for upgrading of biomass-derived oxygenates: a review. ACS Catal 6:5026–5043
52. Kim S et al (2019) Recent advances in hydrodeoxygenation of biomass-derived oxygenates over heterogeneous catalysts. Green Chem 21:3715–3743
53. Chia M et al (2011) Selective hydrogenolysis of polyols and cyclic ethers over bifunctional surface sites on rhodium À rhenium catalysts. J Am Chem Soc 133:12675–12689
54. Gupta S, Khan TS, Saha B, Haider MA (2019) Synergistic effect of Zn in a bimetallic PdZn catalyst: elucidating the role of undercoordinated sites in the hydrodeoxygenation reactions of biorenewable platforms. Ind Eng Chem Res 58:16153–16163
55. Sun J et al (2013) Carbon-supported bimetallic Pd-Fe catalysts for vapor-phase hydrodeoxygenation of guaiacol. J Catal 306:47–57
56. Hong Y et al (2014) Synergistic catalysis between Pd and Fe in gas phase hydrodeoxygenation of m-cresol. ACS Catal 4:3335–3345
57. Saha B, Bohn CM, Abu-Omar MM (2014) Zinc-assisted hydrodeoxygenation of biomass-derived 5-hydroxymethylfurfural to 2,5-Dimethylfuran. ChemSusChem 7:3095–3101
58. Jalid F, Khan TS, Mir FQ, Haider MA (2017) Understanding trends in hydrodeoxygenation reactivity of metal and bimetallic alloy catalysts from ethanol reaction on stepped surface. J Catal 353:265–273
59. Bond JQ, Martin Alonso D, West RM, Dumesic JA (2010) Y-valerolactone ring-opening and decarboxylation over SiO2/Al2O3 in the presence of water. Langmuir 26:16291–16298
60. Alonso DM, Bond JQ, Serrano-Ruiz JC, Dumesic JA (2010) Production of liquid hydrocarbon transportation fuels by oligomerization of biomass-derived C9 alkenes. Green Chem 12:992

61. Wang D, Hakim SH, Alonso DM, Dumesic JA (2013) A highly selective route to linear alpha olefins from biomass-derived lactones and unsaturated acids. Chem Commun 49:7040–7042
62. Gupta S, Arora R, Sinha N, Alam MI, Haider MA (2016) Mechanistic insights into the ring-opening of biomass derived lactones. RSC Adv 6:12932–12942
63. Chia M, Schwartz TJ, Shanks BH, Dumesic JA (2012) Triacetic acid lactone as a potential biorenewable platform chemical. Green Chem 14:1850–1853
64. Alam MI et al (2016) Development of 6-amyl-α-pyrone as a potential biomass-derived platform molecule. Green Chem 18:6399–6696
65. Khan TS, Gupta S, Bandodkar P, Alam MI, Haider MA (2018) On the role of oxocarbenium ions formed in Brønsted acidic condition on γ-Al2O3 surface in the ring-opening of γ-valerolactone. Appl Catal A Gen 560:66–72
66. Awakawa T et al (2013) 4-Hydroxy-3-methyl-6-(1-methyl-2-oxoalkyl)pyran-2-one synthesis by a type III polyketide synthase from Rhodospirillum centenum. Chembiochem 14:1006–1013
67. Gupta S, Alam MI, Khan TS, Sinha N, Haider MA (2016) On the mechanism of retro-Diels-Alder reaction of partially saturated 2-pyrones to produce biorenewable chemicals. RSC Adv 6:60433–60445
68. Khan TS, Gupta S, Alam I, Haider MA (2016) Reactivity descriptor for the retro Diels – Alder reaction of partially saturated 2-pyrones: DFT study on substituents and solvent e fects. RSC Adv 6:101697–101706
69. Shrivastav G, Khan TS, Agarwal M, Haider MA (2018) A Car-Parrinello molecular dynamics simulation study of the retro Diels-Alder reaction for partially saturated 2-pyrones in water. J Phys Chem C 122:11599–11607
70. He J et al (2017) Production of levoglucosenone and 5-hydroxymethylfurfural from cellulose in polar aprotic solvent–water mixtures. Green Chem 19:3642–3653
71. Fowler FW, Katritzky AR, Rutherford RJD (1971) The correlation of solvent effects on physical and chemical properties. J Chem Soc B: 460–469
72. Mukherjee S, Vannice MA (2006) Solvent effects in liquid-phase reactions: I. Activity and selectivity during citral hydrogenation on Pt/SiO2 and evaluation of mass transfer effects. J Catal 243:108–130
73. Foresman JB, Keith TA, Wiberg KB, Snoonian J, Frisch MJ (1996) Solvent effects. 5. Influence of cavity shape, truncation of electrostatics, and electron correlation on ab initio reaction field calculations. J Phys Chem 100:16098–16104
74. Neurock M (2003) Perspectives on the first principles elucidation and the design of active sites. J Catal 216:73–88
75. Walker TW et al (2018) Universal kinetic solvent effects in acid-catalyzed reactions of biomass-derived oxygenates. Energy Environ Sci 11:617–628
76. Chew AK et al (2020) Effect of mixed-solvent environments on the selectivity of acid-catalyzed dehydration reactions. ACS Catal 10:1679–1691
77. Overton JC, Zhu X, Mosier NS (2019) Molecular dynamics simulations and experimental verification to determine mechanism of cosolvents on increased 5-hydroxymethylfurfural yield from glucose. ACS Sustain Chem Eng 7:12997–13003
78. Varghese JJ, Mushrif SH (2019) Origins of complex solvent effects on chemical reactivity and computational tools to investigate them: a review. React Chem Eng 4:165–206
79. Patri AS et al (2019) A multifunctional cosolvent pair reveals molecular principles of biomass deconstruction. J Am Chem Soc 141:12545–12557
80. Mellmer MA et al (2019) Effects of chloride ions in acid-catalyzed biomass dehydration reactions in polar aprotic solvents. Nat Commun 10:1–10
81. Laio A, Gervasio FL (2008) Metadynamics: a method to simulate rare events and reconstruct the free energy in biophysics, chemistry and material science. Rep Prog Phys 71:126601
82. Agarwal V, Dauenhauer PJ, Huber GW, Auerbach SM (2012) Ab initio dynamics of cellulose pyrolysis: nascent decomposition pathways at 327 and 600 °C. J Am Chem Soc 134:14958–14972

83. Mettler MS et al (2012) Revealing pyrolysis chemistry for biofuels production: conversion of cellulose to furans and small oxygenates. Energy Environ Sci 5:5414–5424
84. van Duin ACT, Dasgupta S, Lorant F, Goddard WA (2001) ReaxFF: a reactive force field for hydrocarbons. J Phys Chem A 105:9396–9409
85. Russo MF, van Duin ACT (2011) Atomistic-scale simulations of chemical reactions: bridging from quantum chemistry to engineering. Nucl Instrum Methods Phys Res Sect B 269:1549–1554
86. Zheng M et al (2016) Initial reaction mechanisms of cellulose pyrolysis revealed by ReaxFF molecular dynamics. Fuel 177:130–141
87. Zhang T, Li X, Guo L (2017) Initial reactivity of linkages and monomer rings in lignin pyrolysis revealed by ReaxFF molecular dynamics. Langmuir 33:11646–11657

Levulinic Acid- and Furan-Based Multifunctional Materials: Opportunities and Challenges

Sreedhar Gundekari, Rajathsing Kalusulingam, Bhavesh Dakhara, Mariappan Mani, Joyee Mitra, and Kannan Srinivasan

Abstract Currently, the world's requirement for energy and chemicals is satisfied by tapping petroleum, coal, and natural gas resources. The continuously escalating energy demands for the betterment of life necessitate the search for alternate sources of energy. Sustainability, probably the "word of this century," will be a prime force in stimulating scientists and technologists to look for alternate options in making fuels, chemicals and polymers that are irreplaceable in our lives. Renewable biomass, having useful carbon atoms, could be explored with significant potential to produce chemicals and materials that include polymers. The approach also has an intrinsic advantage of balancing CO_2 emission, thereby aiding our environment. Researchers worldwide have made considerable advancements on biomass value addition for producing fuels, chemicals and materials. Broadly, biomass are categorized as lignocellulose and lipid-based wherein the former offers humungous scope of reaction chemistries that are deployable in a biorefinery akin to petro-refinery. Among them, levulinic acid (LA), 5-hydroxymethylfurfural (HMF) and 2,5-furandicarboxylic acid (FDCA) and their related products render multifunctional properties with diverse opportunities for applications. In the last decade, intense research has been carried out on these molecules. In this chapter, we shall discuss the background of these platform chemicals, multifarious catalytic

S. Gundekari
Inorganic Materials and Catalysis Division, CSIR-Central Salt and Marine Chemicals Research Institute, Gijubhai Badheka Marg, Bhavnagar, 364002, Gujarat, India

Department of Chemistry, Chaitanya Deemed to be University, Hanamkonda, Warangal, 506001, Telangana, India

R. Kalusulingam · M. Mani · J. Mitra · K. Srinivasan (✉)
Inorganic Materials and Catalysis Division, CSIR-Central Salt and Marine Chemicals Research Institute, Gijubhai Badheka Marg, Bhavnagar, 364002, Gujarat, India

Academy of Scientific and Innovative Research, CSIR-HRDC Campus, Sector-19, Kamla Nehru Nagar, Ghaziabad, 201002, U.P., India
e-mail: joyeemitra@csmcri.res.in; skannan@csmcri.res.in

B. Dakhara
Inorganic Materials and Catalysis Division, CSIR-Central Salt and Marine Chemicals Research Institute, Gijubhai Badheka Marg, Bhavnagar, 364002, Gujarat, India

291

approaches made and process tools deployed, in particular for γ-valerolactone, LA-based plasticizers, HMF and FDCA. Challenges on these approaches and possible strategies to overcome them will also be discussed.

Keywords Biomass valorization · Levulinic acid derivatives · γ-Valerolactone · Furan compounds · 5-Hydroxymethylfurfural · 2,5-Furandicarboxylic acid

1   Introduction

At present, the world's energy and chemical requirements are largely met through fossilized sources like petroleum, coal and natural gas. The improvement in the quality of life and, consequently, the increasing demand for energy necessitate the search for alternate and sustainable solutions to energy crisis. Sustainability, arguably the "word of this century," has been instrumental in stimulating scientists and technologists to explore alternative options in making fuels, chemicals and polymers that facilitate our daily lives. Carbon-rich biomass is the only renewable source that could be explored with significant potential for producing chemicals including polymers. This is de facto an attractive option considering the balance between the availability and consumption patterns. The approach also has an intrinsic advantage of reducing indispensability on fossil fuels to an extent besides reducing CO_2 emission, thereby benefitting our environment. Researchers all over the world have enthusiastically contributed to the value addition of biomass for producing chemicals. Many countries with strong roots in agriculture, availability of extensive forest/agro-resources and vast coastline for marine macro−/micro-algae are likely to generate non-edible/waste biomass which can potentially be harnessed to produce chemicals sustainably in the years to come.

Generally, lignocellulosic biomass consists of 38–50% cellulose, 23–32% hemicellulose and 15–25% lignin, which constitute about 80–90% of the total biomass. Cellulose is a non-branched water-insoluble polysaccharide consisting of several hundreds to tens of thousands of glucose units linked through 1,4-β-glycosidic ether bonds. Cellulose is the most abundant biopolymer synthesized by nature; its amount is estimated at approximately 2×10^9 tons/year [1]. Hemicellulose is a polymeric network connecting lignin and cellulose. Although lower in molecular weight than cellulose, hemicellulose consists of C6 sugars (glucose, mannose and galactose) and C5 sugars (arabinose, xylose and so on). Lignin is a complex three-dimensional cross-linked amorphous polymer consisting of three major methoxylated phenylpropanoid units (coumaryl alcohol, coniferyl alcohol and sinapyl alcohol) connected by strong C–O (~60–70%) and C–C (~25–35%) linkages [2, 3]. Thus, the primary components have great potential for the production of diverse chemicals [4].

The Department of Energy (USA) with NREL (National Renewable Energy Laboratory) and PNNL (Pacific Northwest National Laboratory) have conducted an extensive study to identify valuable sugar-based building blocks [5]. Of the 300

initially selected candidates, a list of 30 interesting chemicals was obtained through an iterative process. The list was further reduced to 12 building blocks considering potential markets, complexity of synthetic pathway, functionality of molecule and abundance. Of these 12 platform molecules, some are obtained through biochemical methods and some others via thermochemical pathway. 1,4-Diacids (succinic, fumaric and malic), 3-hydroxypropionic acid, aspartic acid, glutamic acid and itaconic acid were obtained from biochemical pathway. Xylitol, 2,5-furandicarboxylic acid, levulinic acid, glucaric acid, sorbitol and 3-hydroxybutyrolactone were reported through thermochemical pathway.

From the last decade, our research group is associated with biomass conversion, working on heterogeneous catalytic approaches for the conversion and value addition of the above-mentioned platform molecules including the preparation of xylitol, sorbitol, succinic acid, 5-hydroxymethylfurfural (HMF) and 2,5-furandicarboxylic acid (FDCA). We have also focused on the valorization of levulinic acid into various value-added products by finding efficient catalysts and synthetic protocols. In this chapter, we have covered a brief outline of levulinic acid synthesis, state of the art on catalytic interventions for preparation of levulinic acid-based products such as γ-valerolactone, arylated-γ-lactones and 4,4-diaryl-substituted pentanoic acid/esters. A summarized report on HMF preparation and its selective conversion into FDCA using ruthenium-based catalysts has also been discussed here. The end of the chapter discusses the challenges of the mentioned conversions.

2   Levulinic Acid

Levulinic acid (LA), a keto carboxylic acid from biomass, is an important building block for fuels and chemicals harnessed by catalytic transformations. LA ($C_5H_8O_3$) is a white crystalline solid (<30 °C), soluble in aqueous and in common organic solvents including polar solvents. LA is a potential intermediate for making alkyl/aryl-substituted cyclic lactones, aliphatic alcohols including diols, cyclic/acyclic amides, ketals, esters, acid halides, diketones, amino/halo-substituted keto carboxylic acids, alkane/alkenes, valeric acid/esters, cyclic ethers, etc.

2.1   Preparation of Levulinic Acid

LA is mainly prepared from cellulose-derived glucose by involving two steps. In the first step of the reaction, glucose isomerizes to fructose and is subsequently dehydrated to HMF. In the second step, HMF under hydrolysis in aqueous medium forms LA along with formic acid as a by-product (Scheme 1) [6]. The conversion in the presence of alcoholic medium forms alkyl levulinates and alkyl formates [7]. Many reports reveal the direct conversion of lignocellulose biomass (wheat straw, pulp
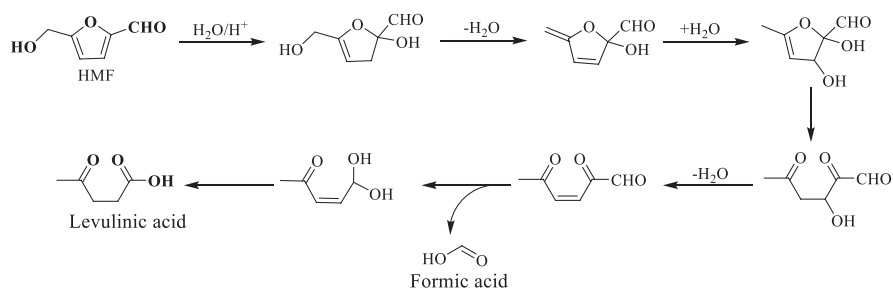
Scheme 1 Simplified reaction mechanism for the production of LA via HMF path

slurry, sorghum grain, corn starch, water hyacinth, bagasse and rice husk) to LA using homogeneous acid catalysts [6, 8–13]. Reports of LA preparation are also available from cellulose, glucose and HMF individually, and these conversions mainly used homogeneous catalysts including mineral acids, super acids, metal halides and acidic ionic liquids. In the course of the past few years, researchers have also developed many solid acid catalysts [14–25].

The hemicellulose-based xylose is also a precursor for the preparation of LA and its esters through furfural and furfuryl alcohol as intermediates (Scheme 2). Furfural undergoes selective hydrogenation using metal-supported catalysts with furfuryl alcohol as the product. Furfuryl alcohol in the presence of water results in LA and LA esters (alkyl levulinates) in alcoholic medium. Furfuryl alcohol conversion to LA involves acid catalysts including homogeneous acid catalysts (mineral acids), acidic ionic liquids and solid acid catalysts [26–30].

2.2   Applications of Levulinic Acid

Multiple functionalities of LA including carboxyl, carbonyl and so on facilitate its participation in various organic transformations including oxidation, hydrogenation, hydrocyclization, reductive amination, condensation, etc. (Scheme 3) [31]. We are extensively working on the preparation of γ-valerolactone, arylated-γ-lactones and 4,4-disubstituted pentanoic acid/esters. A detailed discussion pertaining to these chemical transformations has been covered in the following sections.

2.2.1   Hydrocyclization of Levulinic Acid to γ-Valerolactone

LA under H_2 environment primarily results in useful products such as γ-valerolactone (Gvl), 1,4-pentanediol (1,4-PDO), 2-methyltetrahydrofuran (2-MTHF) and pentanoic acid, depending on the catalytic system and reaction parameters [32–35]. All these LA derivatives are industrially relevant; for example, Gvl is an attractive platform chemical and has various applications in the production of biofuels, i.e. valeric
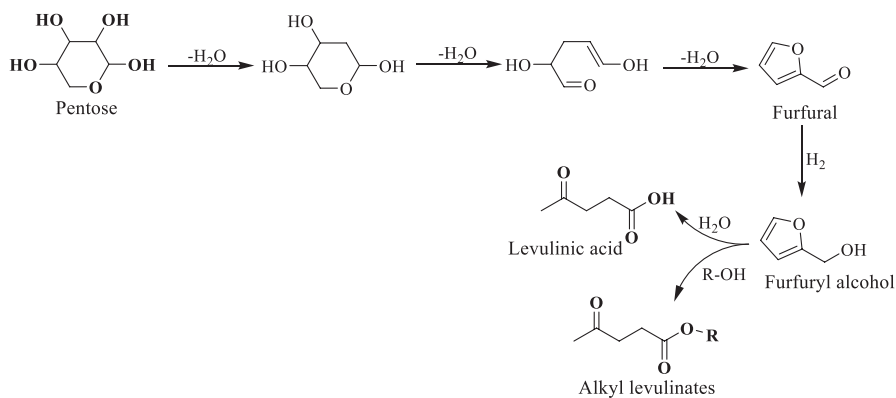
Scheme 2 Simplified reaction mechanism for the production of LA from furfural via furfuryl alcohol as intermediate
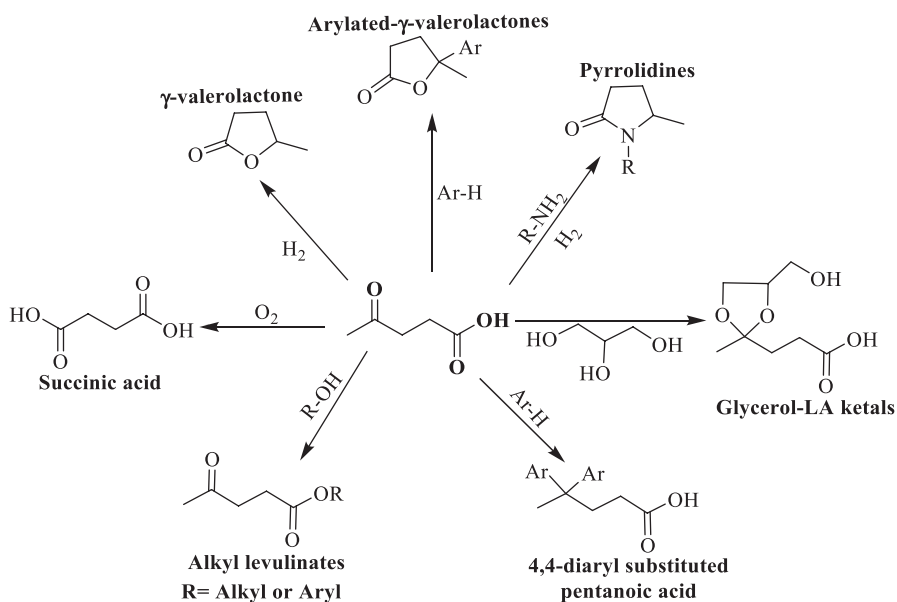
Scheme 3 Catalytic organic transformation of LA to industrially valuable products

esters [36], aromatic hydrocarbons [37], liquid alkanes [38, 39], polymer intermediates, i.e. α-methylene-γ-valerolactone, 1,4-pentanediol and adipic acid [40–42]. In addition, Gvl itself is a green solvent for organic transformations including the conversion of lignocellulose components (Fig. 1) [43–50].

Generally, the mechanistic pathway for the conversion of LA to Gvl involves two routes [51]. *Path-a* culminates in the hydrogenation of LA to γ-hydroxypentanoic acid prior to an intramolecular esterification to obtain Gvl, and *path-b* follows the esterification of the enol form of LA to α-angelica lactone (α-AL) and its
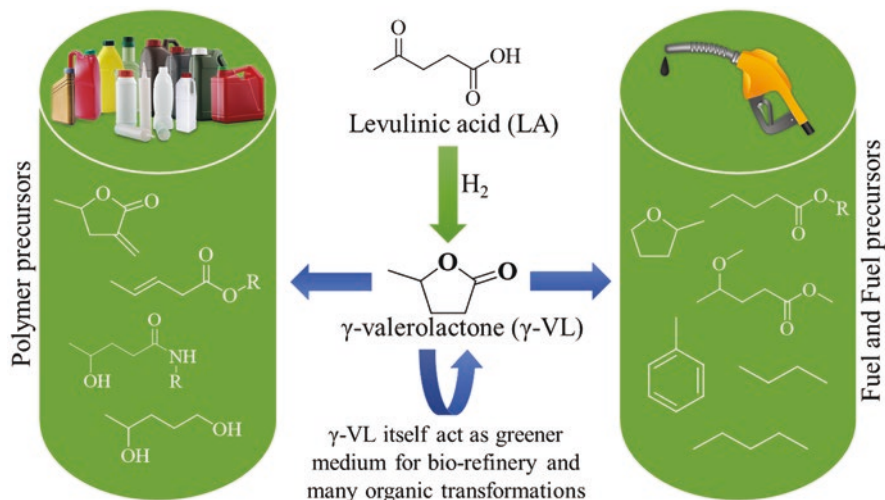
Fig. 1 Applications of Gvl in the preparation of polymers and fuel intermediates
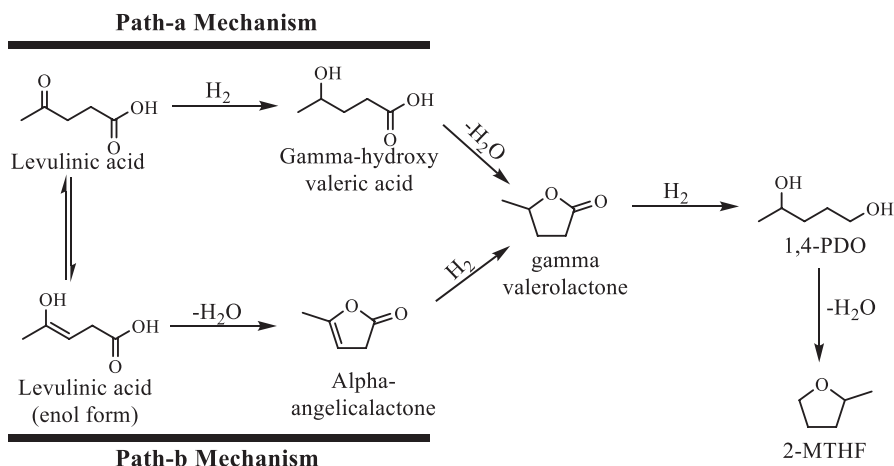
Scheme 4 Reaction mechanism for hydrocyclization of LA to Gvl

subsequent hydrogenation to Gvl (Scheme 4). Over-hydrogenation results in the ring opening of Gvl forming 1,4-pentanediol as its product, under acidic conditions. At higher temperatures, diol undergoes cyclization to 2-methyltetrahydrofuran (2-MTHF).

Various research groups explored the catalytic hydrocyclization of LA and levulinates to Gvl using heterogeneous and homogeneous catalytic routes under batch and continuous flow conditions with molecular hydrogen, alcohols and formic acid as hydrogen sources [35, 52–57]. The homogeneous catalysts such as complexes of Ru/Ir/Pd, etc. were found to be quite active for this conversion. However, inherent

problem of separation and catalyst disposal are bottlenecks in homogeneous catalytic systems. Often expensive chemicals and multistep reaction protocols are required for catalyst preparation, thus limiting their applicability in large scales.

Non-noble metal-supported heterogeneous catalysts including Fe, Ni, Cu, Cr, Co and Mo were reported towards this hydrocyclization. Raney Ni® and Cu-/Ni- metal supported and combination of these two are exclusively reported using three hydrogen sources (H_2 gas, isopropanol and formic acid) in either static or continuous vapour phase. The Zr-based catalysts were mainly reported for Meerwein-Ponndorf-Verley (MPV) of levulinic acid followed by cyclization to Gvl using alcohol as hydrogen source. Heterogeneous catalytic systems based on supported noble metals such as Ru, Pd, Pt and Au are active towards LA to Gvl conversion. Among these, Ru catalysts are most active under comparatively milder reaction conditions.

Layered double hydroxide (LDH) materials were found to be attractive in many catalytic applications because of its multifunctionality and tunable nature. Pristine LDH, calcined LDH (CLDH), LDH-derived *ex situ* and *in situ* catalysts and metal supported on LDH materials were extensively reported for levulinic acid conversion to Gvl. The following section reviewed the prior art of this conversion using LDH materials including the contribution from our group.

Hydrocyclization of LA to Gvl Using Layered Double Hydroxide-Based Materials

LDH-Derived Catalysts for Hydrocyclization of LA to Gvl

The LDH-derived catalysts for LA to Gvl conversion, were first reported by Yan et al. who introduced Cu-Cr, Cu-Al and Cu-Fe CLDH catalyst precursors (derived from LDH by calcination). All the mentioned CLDH catalyst precursors showed good catalytic activity for Gvl (yield 90.7% for Cu-Cr, 87.3% for Cu-Al and 87.3% for Cu-Fe) (Table 1, entries 1–4). The Cu^{2+} oxide of CLDH generates Cu(0) under reaction conditions (200 °C, 70 bar H_2 for 10 h in water) confirmed by PXRD, which is the active catalyst for hydrogenation. The authors observed a decrease in the catalytic activity (in the case of Cu-Cr) upon reuse because of carbon deposits on the surface of the catalyst during the reaction. To avoid this problem, they reactivated the catalyst by calcination (550 °C for 3 h) and was rewarded with similar catalytic activity up to monitored three reaction cycles [58–60].

Li research group demonstrated a series of Al-LDH-based catalyst precursors using different metals such as Fe, Cu, Ni and Co. From these M-Al LDH (M = metal) precursors, the active catalyst species was prepared by reduction under H_2 (50 mL/min) at 700 °C for 2.5 h, and obtained catalysts are denoted as $M(0)/Al_2O_3$. Among the catalysts screened by the Li group, Co/Al_2O_3 (derived from Co-Al LDH) showed excellent activity towards LA to Gvl conversion with 100% conversion and >99% selectivity at 180 °C, 50 bar H_2 for 3 h in 1,4-dioxane medium (Table 1, entries 5–9). The LDH precursor-derived Co/Al_2O_3 is more active than Co/γ-Al_2O_3 (prepared by Co impregnation on γ-Al_2O_3 followed by reduction) and Co/Al_2O_3-CR (derived from Co-Al LDH through calcination followed by pre-reduction), suggesting that

Table 1 Prior art of LA hydrocyclization to Gvl using LDH-derived catalysts and supported LDH catalysts

Entry	Catalyst precursor	Catalyst	Calcination	External reduction	Reaction conditions	Reactivation for reusable studies	LA or its esters conv. (%)	Gvl yield (%)	Sel. (%) Gvl	References
1	Cu-Cr CLDH	In situ-formed Cu(0) from Cu^{2+} oxide under conditions	Cu-Cr LDH to Cu-Cr CLDH at 950 °C for 10 h	–	200 °C, 70 bar H$_2$ for 10 h in aqueous medium	550 °C for 3 h	100	90.7%	–	[58]
2	Cu-Al CLDH	In situ-formed Cu(0)	LDH to CLDH	–	200 °C, 70 bar H$_2$ for 10 h in aqueous medium	–	98.3	87.3	–	[59, 60]
3	Cu-Cr CLDH	In situ-formed Cu(0)	(oxide form) at 950 °C for 10 h				>99	90.7	–	
4	Cu-Fe LDH	In situ-formed Cu(0)					>99	81.5–90.1	–	
5	Fe-Al LDH	2Fe/Al$_2$O$_3$	–	700 °C for 2.5 h under H$_2$	180 °C, 50 bar H$_2$ for 3 h in 1,4-dioxane medium	–	0.5	–	>99	[61]
6	Cu-Al LDH	2Cu/Al$_2$O$_3$	–			–	2	–	>99	
7	Ni-Al LDH	2Ni/Al$_2$O$_3$	–			–	39	–	>99	
8	Co-Al LDH	2Co/Al$_2$O$_3$	–			–	43	–	>99	
9	Co-Al LDH	4Co/Al$_2$O$_3$	–			External reduction under H$_2$ flow (50 mL/min) at 700 °C for 1 h	100		>99	
10	Ni-Cu-Al-Fe LDH	Ni(0)-Cu(0)/AlFe LDH	–	500 °C for 3 h under H$_2$	140 °C, 20 bar H$_2$ for 3 h in methanol	–	100	78.5	–	[62]
11	Ni-Cu-Mg-Al-Fe LDH	Ni(0)-Cu(0)/MgAlFe LDH	–			500 °C for 3 h under H$_2$	100	98.1	–	

Entry	Catalyst precursor	Catalyst	Calcination	External reduction	Reaction conditions	Reactivation for reusable studies	LA or its esters conv. (%)	Gvl yield (%)	Sel. (%) Gvl	References
12	Cu-Ni-Mg-Al CLDH	Cu(0)-Ni(0)/MgAl CLDH	600 °C for 6 h	140 °C for 2 h under H$_2$ (30 bar)	140 °C, 30 bar H$_2$ for 3 h in dioxane	140 °C for 2 h under H$_2$ (30 bar)	100	100	–	[63]
13	Ni-Zr-Al CLDH	Ni(0)/Zr-Al$_2$O$_3$/NF CLDH	500 °C for 4 h	600 °C for 2 h in H$_2$/Ar	250 °C and ambient pressure Continuous process	–	99.5	–	98.2	[64]
14	Ni-Al CLDH	Ni(0)/Al$_2$O$_3$/NF CLDH				–	89.7	–	85.3	
15	Mg-Al LDH	Mg-Al CLDH	500 °C for 6 h		270 °C under N$_2$ flow, and in situ hydrogen transfer from formic acid	Calcination at 450 °C for 1 h	100	–	98	[65]
16	–	Physical mixture of MgO-Al$_2$O$_3$	–	–,	Continuous process	–	74	–	86	
17	–	Mg-Al LDH	–	–		–	68	–	95	
18	NiO-Al$_2$O$_3$	NiO/Al$_2$O$_3$	400 °C for 4 h	650 °C for 3 h under H$_2$ flow	160 °C, 30 bar H$_2$ for 1 h	–	21.6	–	98–99	[66]
19	NiO-MgO	Ni(0)/MgO				–	43	–	98–99	
20	Ni-Mg-Al CLDH	Ni(0)/Mg-Al CLDH					100	–	>99	
21	Ni-Al LDH	Ni(0)/boehmite	–	–	200 °C, 30 bar H$_2$ for 6 h	–	100	100	–	[67]

(continued)

Table 1 (continued)

Entry	Catalyst precursor	Catalyst	Calcination	External reduction	Reaction conditions	Reactivation for reusable studies	LA or its esters conv. (%)	Gvl yield (%)	Sel. (%) Gvl	References
22	$Cu_2(OH)_2CO_3/$ AlOOH	Cu/AlOOH	200 °C for 5 h	–	180 °C for 5 h; IPA as H_2 source and as medium	Washing with IPA for three times	96	90.5	–	[68]
23	CuO/Al_2O_3	Cu/Al_2O_3	500 °C	Under H_2 atm. 500 °C for 5 h	180 °C for 5 h in IPA medium	–	88	78	–	
24	Ni-Al-Ti LDH	Ni(0)/ Al_2O_3-TiO_2	450 °C for 5 h	H_2 (30 mL/min) for 2 h at 450 °C	80 °C; 10 wt% aqueous feed, H_2 flow rate 20 mL/min (GHSV = 56.72 mL/g s). Catalyst weight 0.02 g	Flushing with N_2 at 110 °C/30 min and then reduction with H_2 at 450 °C/30 min	99.9	–	99.9	[69]
25	Ni-Ti LDH	Ni(0)/TiO_2		H_2 (30 mL/min) for 2 h at 450 °C		–	10.9	–	95.3	
26	Ni-Al LDH	Ni(0)/Al_2O_3		H_2 (30 mL/min) for 2 h at 450 °C		–	14.9	–	96.6	
27	Al_2O_3@ Ni-Cu-Al LDH	Al_2O_3@NiCu	500 °C for 5 h	H_2/Ar (10/90, v/v) flow at 600 °C for 3 h	220 °C for 6 h; IPA as H_2 source and as medium under N_2 atm.	–	91.6	–	89.3	[70]

Entry	Catalyst precursor	Catalyst	Calcination	External reduction	Reaction conditions	Reactivation for reusable studies	LA or its esters conv. (%)	Gvl yield (%)	Sel. (%) Gvl	References
28	Ru(O/OH)/ Mg-La CLDH	Ru(0)/Mg-La CLDH	650 °C (LDH to CLDH)	650 °C under H$_2$/ Ar flow	80 °C, 5 bar H$_2$ for 4 h	–	92	–	>99	[71]
29	Pt(O/OH)/ Mg-Al CLDH	Pt(0)/Mg-Al CLDH	550 °C for 6 h (LDH to CLDH)	480 °C under H$_2$	Room temperature, 30 bar H$_2$ for 24 h	–	100	>99	–	[72]
30	Ru(O/OH)/ Mg-Al LDH	Ru(0)/Mg-Al LDH	–	–	80 °C, 10 bar H$_2$ for 30 min	–	100	>99	–	[73]
31	HRO/Mg-Al LDH	Ru(0)/Mg-Al LDH	–	–	80 °C, 10 bar H$_2$ for 30 min	–	100	>99	–	
32	Cu source with Mg-Al LDH (colloidal deposition)	Cu supported on MgAl-LDH	300 °C for 5 h	–	260 °C, 10 bar H$_2$, and 30 mL/min flow rate of H$_2$	–	87.5	–	95	[74]

the synthesis protocol of Co/Al$_2$O$_3$ (derived from Co-Al LDH) greatly affected the catalytic performance. The used Co/Al$_2$O$_3$ catalyst was recovered from the reaction mixture by magnetic separation. The authors observed that, after reaction, the Co nanoparticle surface underwent oxidation to cobalt oxide in air during catalyst separation. Thus, prior to each run (while reusability), the used catalyst was washed with water and re-reduced under H$_2$ flow (50 mL/min) at 700 °C for 1 h. The activity of the Co/Al$_2$O$_3$ was maintained up to four reaction cycles following this pretreatment procedure [61].

Magnetic catalyst (Ni(0)-Cu(0)/MgAlFe LDH) was reported by Chen research group for Gvl synthesis in methanol medium with 98.1% yield and full conversion of LA (Table 1, entries 10 and 11). The magnetically active catalyst (Ni(0) and Cu(0)) is prepared from LDH precursor by prior or external reduction in H$_2$ atmosphere at 500 °C for 3 h. The prior reduction temperature of LDH affected the catalytic activity; increased yield of Gvl was observed by increasing the reduction temperature from 350 to 500 °C, and further increment (>500 °C) resulted in a decrease in the selectivity of Gvl because of particle sintering at high temperature. Decrease in catalytic activity of the material (Ni(0)-Cu(0)/MgAlFe LDH) was observed in the reusability studies with increase in the number of cycles. Thus, to maintain the catalyst activity, the used catalyst was reactivated by prior reduction (500 °C for 3 h) for each cycle, and the methodology showed good reusability [62].

Kantam research group reported LDH-derived active catalyst Cu(0)-Ni(0)/MgAl LDH for this conversion with 100% yield of Gvl at relatively mild reaction conditions (140 °C, 30 bar H$_2$ pressure for 3 h) in 1,4-dioxane solvent (Table 1, entry 12). Calcination (600 °C for 6 h) followed by prior reduction (140 °C, 30 bar H$_2$ for 2 h) procedure was used to generate the active catalyst (Ni(0) and Cu(0)) from its LDH precursor via intermediate metal oxides (CLDH). In this case also, gradual decrease in catalytic activity of LDH-derived material was observed upon reuse (66% yield at fourth cycle). Hence, to improve reusability, the catalyst was reactivated at 140 °C, 30 bar H$_2$ for 2 h, and it showed better catalytic activity (fourth cycle 92%) as compared with un-reactivated catalyst [63].

Li and co-researchers disclosed Zr containing Ni catalyst such as Ni(0)/Zr-Al CLDH for vapor-phase continuous production of Gvl from neat LA at 250 °C and ambient H$_2$ pressure (Table 1, entries 13 and 14). The active catalyst is prepared from Ni-Zr-Al LDH catalyst precursor by calcination (500 °C for 4 h in static air) followed by reduction (600 °C for 2 h in H$_2$/Ar atmosphere). The active LDH-derived catalyst (Ni(0)/Zr-Al LDH) exhibited the highest selectivity of Gvl (97.7%) as compared to Zr-free catalyst such as Ni/Al$_2$O$_3$ (85.3%), and the acidity of Zr enhanced the cyclization of reaction intermediate (γ-hydroxy pentanoic acid) to Gvl via **path-a** mechanism (Scheme 4) [64].

Chary et al. reported in situ hydrogen transfer (from formic acid) for Gvl preparation from LA in continuous mode. In this methodology, it was observed that Mg-Al CLDH (derived from Mg-Al LDH calcination at 500 °C for 6 h) was an efficient catalytic material by considering stability and activity as compared with physical mixture of MgO-Al$_2$O$_3$ and as-synthesized Mg-Al LDH (without calcination). Under the reaction conditions (270 °C and N$_2$ flow), Mg-Al CLDH showed

complete LA conversion with 98% Gvl selectivity (Table 1, entries 15–17). Reactivated (calcination at 450 °C for 1 h) MgO-Al$_2$O$_3$ CLDH showed good results during reusability studies as compared to the spent catalyst [65].

Fu and co-authors studied several Ni-supported catalysts for this conversion by varying the supports such as MgO, Al$_2$O$_3$ and Mg-Al CLDH. Among these supports, Ni(0) on Mg-Al CLDH (derived from Ni-Mg-Al LDH through calcination followed by reduction) showed the highest yield (99.7%) of Gvl in 1,4-dioxane medium at 160 °C, 30 bar H$_2$ for 1 h. High surface area and uniform dispersion of Ni on Mg-Al CLDH was the reason for better catalytic activity as compared to other examined catalysts (Table 1, entries 18–20). They also conducted reusability of CLDH-derived active catalyst (Ni/Mg-Al CLDH) and showed good recyclability even in the absence of reactivation [66].

The above-mentioned synthetic protocol for the generation of active catalyst from LDH precursor consumes a significant amount of energy. To avoid these drawbacks, we recently reported Ni-Al LDH catalyst precursor (without calcination or pre-reduction) for this conversion in water. Interestingly, Ni(0)/boehmite (Ni-Al LDH-derived) was obtained during the reaction and confirmed by PXRD and TEM. The PXRD of NiAl-LDH showed the presence of (003), (006), (012), (015), (018), (110) and (113) planes that are characteristic of hydrotalcite (Fig. 2), which completely converted to (020), (120), (140) and (051) planes of boehmite (JCPDS Card No. 01-074-290), and (111) with (200) for Ni (0) (JCPDS Card No.: 00-004-0850). Platelet-like morphology of NiAl-LDH underwent a change to hexagonal rods of boehmite with embedded spherical Ni(0) particles having <20 nm size as shown in Fig. 3. The generated active catalyst (Ni(0)/boehmite) showed superior catalytic activity towards the reaction with 100% yield of Gvl (Table 1, entry 21). The active catalyst was recyclable up to four cycles without any activation and only a minor decrease in LA conversion in each cycle, maintaining the Gvl selectivity [67].

Ma et al. disclosed in situ-reduced nano-Cu/AlOOH catalyst for alkyl levulinates to Gvl using Cu$_2$(OH)$_2$CO$_3$/AlOOH-LDH precursor using 2-propanol as hydrogen source [68]. Under optimized condition (180 °C for 5 h), the in situ-reduced catalyst showed 90.5% yield of Gvl (96% conversion of methyl levulinate) with Cu/Al molar ratio 3/1 (Table 1, entry 22). The pre-reduced catalyst Cu/Al$_2$O$_3$ has lower activity towards the reaction and resulted in 78% yield of Gvl because of the agglutination of active catalytic Cu(0) metal particles on Al$_2$O$_3$ (Table 1, entry 23). The in situ Cu/AlOOH catalyst has strong acidic sites (obtained from TPD analysis) and could reasonably enhance the reaction. Various alcohols as hydrogen sources including primary (methanol, ethanol, 1-propanol and 1-butanol), secondary (2-propanol and 2-butanol) and tertiary (t-butanol) alcohols were studied for the reaction using Cu$_2$(OH)$_2$CO$_3$/AlOOH-LDH precursor. It was observed that primary and tertiary alcohols are inefficient for hydrogen generation and cannot participate in the reaction, wherein secondary alcohols such as 2-propanol and 2-butanol showed remarkable activity to obtain Gvl. Using the in situ catalyst, authors identified significant loss in Gvl yield while increasing the number of catalytic cycles, and they
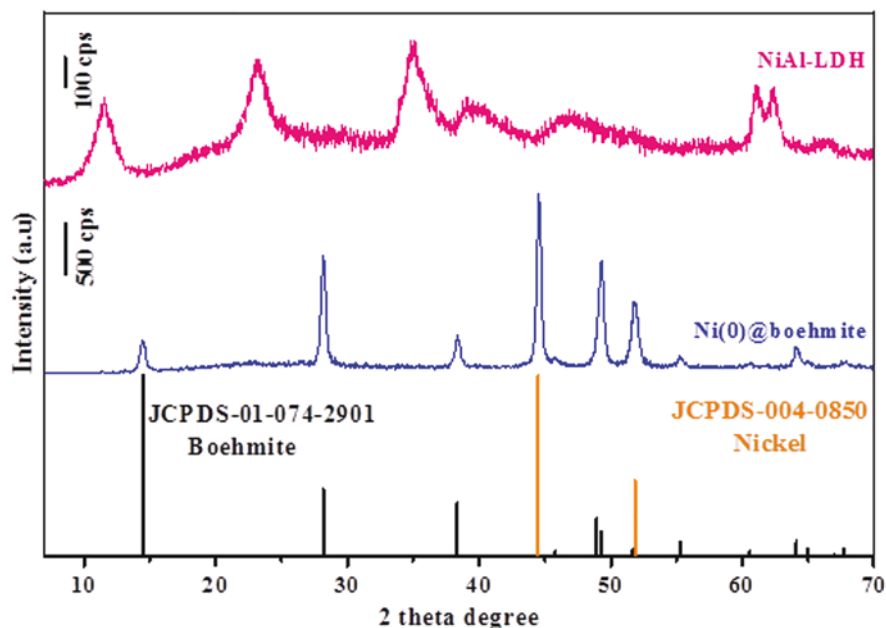
Fig. 2 Powder XRD pattern for NiAl-LDH (catalyst precursor) and Ni(0)@boehmite (catalyst obtained after the reaction). The XRD pattern for Ni(0)@boehmite matched well with nickel (JCPDS Card No: 004-0850; stick pattern included) and boehmite (JCPDS Card No: 01-074-290)
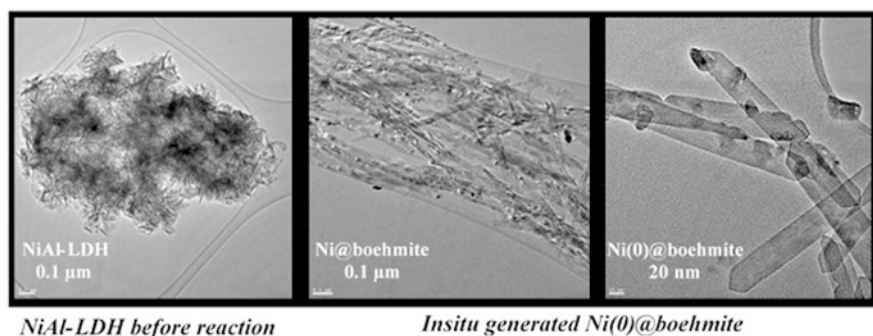
Fig. 3 TEM images showing the morphology and crystallinity of NiAl-LDH catalyst precursor and Ni(0)@boehmite catalyst at different magnifications (catalyst obtained after the reaction)

rationalized this from the increase (50 nm from 35 nm) in Cu(0) metal particles size by the TEM analysis of the spent catalyst.

Aytam research group reported ex situ-reduced $Ni(0)/Al_2O_3$-TiO_2 catalyst, derived from Ni-Al-Ti LDH precursor [69]. The mixed metal catalyst has high catalytic activity for vapor-phase hydrocyclization of LA to Gvl as compared with $Ni(0)/TiO_2$ and $Ni(0)/Al_2O_3$ (Table 1, entries 24–26). The high concentration of

Lewis acidic sites (confirmed by DRIFT) along with metallic Ni active sites on the surface (confirmed by CO pulse chemisorption) in $Ni(0)/Al_2O_3$-TiO_2 supports the higher activity of the material. The Lewis acidity of support (Al_2O_3-TiO_2), i.e. peaks at 1630–1600/cm and 1450/cm, influences the dehydration of LA for the formation of angelica lactone (path-b mechanism in Scheme 4) which underwent subsequent hydrogenation to Gvl using active metallic Ni(0). The catalyst was also tested for transfer hydrocyclization of LA with formic acid as hydrogen donor, resulting in higher angelica lactone yield compared to desired Gvl which may be due to insufficient hydrogen (obtained from decomposition formic acid) or deactivation/leaching of active Ni metal under such acidic conditions. The catalyst is active up to 17 h time-on-stream using molecular hydrogen, and a further increase in time and/or increase in reaction cycles, a decrease in the conversion of LA is observed due to carbon (coke formation) deposition on the catalyst.

Transfer hydrocyclization of ethyl levulinate to Gvl using hierarchical multilevel-supported bimetallic catalyst (derived from Al_2O_3@NiCuAl-LDH precursor) was reported [70]. The bimetallic NiCu catalyst with 0.5 Cu/Ni molar ratio resulted in high activity (89% yield of Gvl) in the presence of isopropanol as hydrogen source (Table 1, entry 27). Alumina-supported bimetallic catalyst (NiCu) has highest density of acidic and basic sites. Lewis acidic sites of catalytic material can interact with carbonyl group of ethyl levulinate through the electron pair on the oxygen atom and are active for C=O hydrogenation. The basic sites of the catalyst are also responsible for MPV reduction and facilitate ethyl levulinate activation. As-fabricated bimetallic NiCu catalyst has good stability and activity for recycling studies. The bimetallic catalyst shows no metal leaching and no particle agglomeration during the reaction.

LDH-Supported Metal Catalysts for Hydrocyclization of LA to Gvl

LDH materials as catalytic support were also reported for hydrocyclization of LA. Venugopal group reported Ru(0)/Mg-La CLDH prepared by impregnation procedure using $RuCl_3$ with Mg-La CLDH in aqueous medium. The Ru(0)-supported CLDH catalyst was the first basic supported catalyst for this reaction which showed good catalytic activity (92% LA conversion with >99% Gvl selectivity) in toluene medium at 80 °C, 5 bar H_2 for 4 h (Table 1, entry 28) [71]. Furthermore, Rajaram group also reported Pt-supported Mg-Al CLDH for LA to Gvl conversion in aqueous medium at room temperature, 30 bar H_2 for 24 h with >99% yield of Gvl (Table 1, entry 29) [72].

Our group reported in situ-generated Ru(0)/MgAl-LDH catalyst from Ru(O/OH)/LDH and hydrous ruthenium oxide (HRO)/MgAl LDH during the reaction. The in situ-regenerated catalysts showed remarkable catalytic activity with >99% yield of Gvl under mild reaction conditions (80 °C, 10 bar H_2 for 30 min) in water (Table 1, entries 30 and 31). The Ru(0)/Mg-Al LDH material is prepared by wet impregnation (Mg-Al LDH with $RuCl_3$ solution) followed by in situ reduction during the reaction [73]. The main advantage of this invention is to avoid prior

reduction for preparation of Ru(0) from ruthenium precursor. Prior reduction of catalysts mostly consumes more energy and sometimes may even be higher than the input energy used for the reaction.

Cu-supported MgAl-LDH catalyst (prepared from colloidal deposition method) was reported by Asiri research group for hydrocyclization of LA to Gvl under vapour phase using fixed-bed reactor [74]. At optimized conditions, i.e. 260 °C, 10 bar H_2, and 30 mL/min H_2 flow rate, the 3% Cu/MgAl-LDH catalyst (0.5 g) showed 87.5% conversion of LA (WHSV = 0.456/h) with 95% selectivity of Gvl (Table 1, entry 32). Three per cent Cu loading enhances the overall acidity of the material which initiates the intramolecular esterification of γ-hydroxy pentanoic acid to obtain Gvl. Increasing the temperature to >260 °C decreased the selectivity of Gvl because of the onset of competing reactions such as the dehydration of LA to angelica lactone and ring opening of obtained Gvl into valeric acid. The spent Cu/MgAl-LDH catalyst shows decrease in activity towards the reaction and is associated with Cu particle size increment (5.3 nm from 2 nm) due to agglomeration as well as decrease in the surface area and acidity.

2.2.2 Arylated-γ-Lactones from Levulinic Acid and Aromatics

Preparation of arylated-γ-lactones (Agvls) was demonstrated by Yonezawa research group using homogeneous catalysts such as methanesulfonic acid (MsOH), triflic acid (TfOH) and polyphosphoric acid (PPA) [75]. Among these, triflic acid catalyst showed the highest yield of corresponding lactones. *m*-Br anisole, *o*-Br anisole and unsubstituted anisole ended with 84, 46, and 81% yields of desired Agvls at room temperature for 8 h (Scheme 5). However, homogeneous catalysts used are difficult to remove from the product mixture and pollute the environment while disposing. Homogeneous acid catalyst needs to be neutralized after reaction with large amount of bases which demands additional energy and chemical input and increases the overall process cost.

A patent by Hattori *et al.*, in JP 2011201847-A, disclosed the preparation of Agvls from levulinic acid with aromatics using various solid acid catalysts [76]. The reactions were performed under microwave irradiation in the presence of solvents. The drawback of this invention is the formation of multiple products under microwave irradiation, rendering poor selectivity for the desired product. Another drawback of this invention is the use of microwave irradiation that poses difficulty and challenges for scale-up operations as these are to be prepared in bulk scale (in tonnage) where conventional heating in batch or continuous reactors would be more
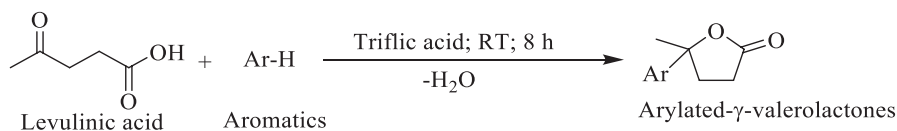
Scheme 5 Preparation of Agvls from levulinic acid with aromatics using triflic acid

feasible technologically. Also, various chlorinated high boiling solvents such as 1,2-dichlorobenzene were used that are not environmentally friendly and have recyclability issues.
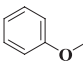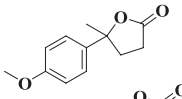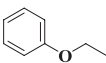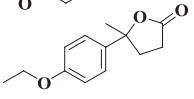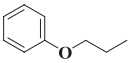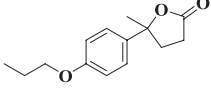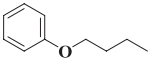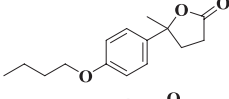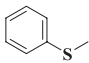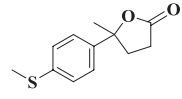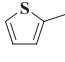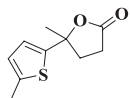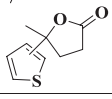
We reported this transformation under solvent-free conditions using conventional heating. Various zeolites were identified for preliminary screening owing to their properties, i.e. high crystallinity, thermal stability, tunable acidity, reusability and shape selectivity, which find use in industrially relevant transformations especially in petrochemicals. Among zeolites screened, Na/H-β, Na-Y, and Na-ZSM-5, Na-β and H-β were found active for the mentioned conversion. The high activity of β-zeolite is attributed to its unique pore topology and the presence of local structural defects through octahedral extra-framework aluminium (AlO_6) that render Lewis acidic properties in the material, resulting in the observed conversion and product selectivity. H-β zeolite fared better compared to Na-β. Under optimized condition, the highest yield of γ-lactone was obtained with anisole: LA 4:1 molar ratio in the absence of solvent at 150 °C using 50 wt% catalyst loading after 12 h (Table 2, entry 1).

Substrate scope was extended from ethoxy to butoxy benzenes. Increasing the alkyl chain length had a positive effect on LA conversion with a selectivity for *para*-substituted γ-lactones (Table 2, entries 2–4). Aromatic hydrocarbon cumene did not participate in the reaction. Inability of the relatively less electron-rich aromatic ring in cumene to take part in the nucleophilic attack on the carbonyl carbon of levulinic acid could be a reason for its inactive nature (Scheme 6). The ring electron density was increased by the lone pair of electron present on the heteroatom and in the substrates with electron-donating substituents. Thioanisole showed 83% selectivity of *para*-isomeric γ-lactone (Table 2, entry 5). This synthetic protocol was further explored with 2-methylthiophene and thiophene, which resulted in the selective formation of γ-lactone (90% and 80%) with 93% and 96% LA conversion (Table 2, entries 6 and 7).

Recyclability of H-β catalyst was also studied. Organic carbon that adhered to the used catalyst (UH-β) surface was removed by calcination in air at 550 °C for 3 h. The used calcined catalyst (UH-βC) and fresh H-β catalyst showed comparable yield and selectivity for the synthesis of γ-lactone. A scalability study at 10 g of LA with anisole showed an increase in γ-lactone yield with time. After 6, 12, 18 and 24 h, 38, 62, 80 and 90% yield of *para*-substituted γ-lactone was obtained with 95, 94, 92 and 90% selectivity, respectively.

Mechanistic investigation for the formation of Agvls (Scheme 6) suggests that the lone pairs of the keto carbonyl group of LA interact with Lewis acidic sites of aluminium in zeolitic framework, present due to local defects [77, 78]. A partial positive charge generated on the keto carbon is responsible for the nucleophilic attack resulting in the formation of γ-hydroxy pentatonic acid intermediate. This unstable species underwent intramolecular esterification to γ-lactone on removal of water [79]. The higher activity of H-β zeolite compared to Na-β is possibly due to the presence of Bronsted acidic protons on H-β zeolite.

Table 2 Synthesis of Agvls from LA with various aromatics using H-β zeolite catalyst[a]

Entry	Aromatic	Lactone	Conv. (%)[b]	Sel. (%)[c]
1			90	91
2			70	86
3			74	85
4			78	86
5			48	83
6[d]			93	90
7[e, f]			96	80

[a]LA to aromatic molar ratio is 1:4 (LA (4.3 mmol), aromatics (17.2 mmol)), H-β (50 wt% w.r.t. LA), 150 °C for 12 h. [b]conversion of LA, [c]isolated yield of Agvls, [d]110 °C, [e]85 °C, [f]GC-MS conversion and yield.

[a]LA to aromatic molar ratio is 1:4 (LA (4.3 mmol), aromatics (17.2 mmol)), H-β (50 wt% w.r.t. LA), 150 °C for 12 h
[b]Conversion of LA
[c]Isolated yield of Agvls
[d]110 °C
[e]85 °C
[f]GC-MS conversion and yield

2.2.3 Synthesis of 4,4-Diryl-Substituted Pentanoic Acid/Esters from Levulinic Acid and Aromatics

Preparation of Diphenolic Acid

Bisphenol A (BPA), a popular plasticizer prepared from the acid-catalysed condensation of phenol and acetone (2:1 ratio), is a commercial polymer precursor, used for thermoplastic polymers, polycarbonates and epoxy resins and is also used in the making of paper currencies by several countries [80, 81]. Diphenolic acid (DPA), a structural analogue and a potential alternate to BPA, is a lignocellulose-derived
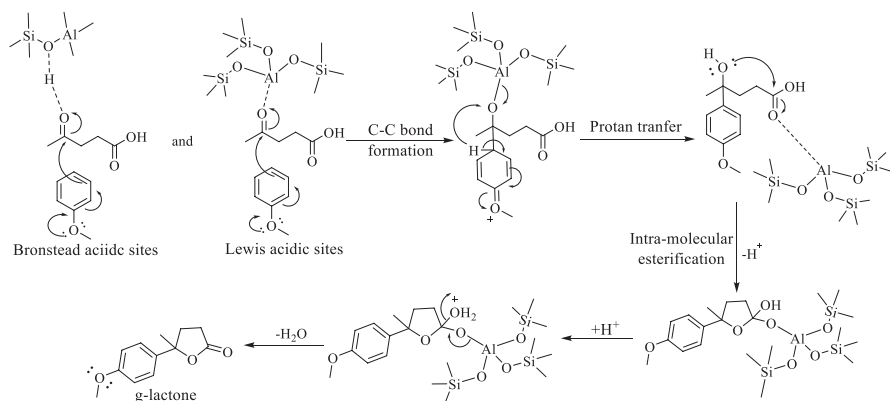
Scheme 6 Mechanistic pathway for Agvls formation from LA with anisole using β-zeolite

bisphenol having diaromatic-substituted moiety as 4,4-bis(4-hydroxyphenyl)valeric acid, prepared on condensation of LA with phenol under acid-catalysed reaction (Scheme 7) [82]. Many catalysts are reported for this conversion. Initially, the reaction was reported with Bronsted mineral acids (H_2SO_4 and HCl) [83]. However, these are toxic and corrosive, and hence homogeneous mineral acids were replaced by insoluble heterogeneous catalysts.

The insoluble cesium-substituted Keggin-type heteropolyacid such as $Cs_{1.5}H_{4.5}P_2W_{18}O_{62}$ showed 70.5% yield of DPA with 88% selectivity of p,p'-DPA isomer at 150 °C, molar ratio of phenol to LA 4:1 for 10 h [84]. The heteropolyacid catalyst revealed good reusability for three repetitive runs.

A water-tolerant solid acid catalyst, i.e. mesoporous $H_3PW_{12}O_{40}$/SBA-15 (obtained from sol-gel co-condensation), has been reported for DPA synthesis [85–87]. The $H_3PW_{12}O_{40}$/SBA-15 has high surface area, well-defined pore size and uniform distributed catalytic sites. The SBA with 15.7% loading of $H_3PW_{12}O_{40}$ showed better activity towards the reaction, 80% conversion of levulinic acid with 2.9:1 ratio of DPA (p,p') isomer to DPA (o,p') isomer. The high pore size of catalytic material facilitates the accessibility of the reactive sites in the framework for the reactants. The $H_3PW_{12}O_{40}$/SBA-15 catalyst is regenerated by calcination (420 °C) and was recycled for five reaction cycles with almost similar catalytic activity.

Sels research group reported a new class of acid catalyst, i.e. sulfonated hyperbranched poly(arylene oxindoles) (SHPAOs) in combination with thiol co-catalyst. Using SHPAO catalyst, various thiol compounds, e.g. benzylthiol, ethanethiol, 1-propanethiol, 1-butanethiol, 2-propanethiol and 2-methyl-2-propanethiol, were explored at 200 °C for 16 h under inert atmosphere and absence of solvent [88, 89]. The less sterically hindered co-catalyst/additive ethanethiol showed high yield of DPA (52.9%) with high selectivity of p,p' isomer (19.5 ratio of the p,p'-DPA to the o,p'-DPA isomer). The role of thiol promoter in catalytic mechanism cycle is mentioned in Scheme 8.
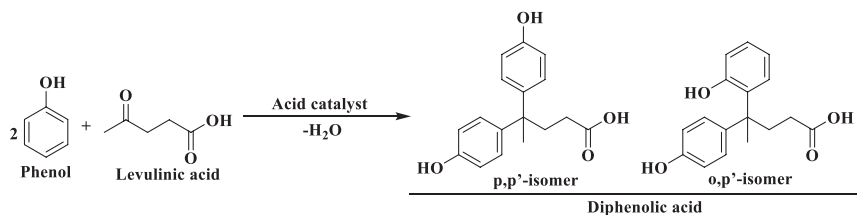
Scheme 7 Preparation of diphenolic acid from levulinic acid with phenol
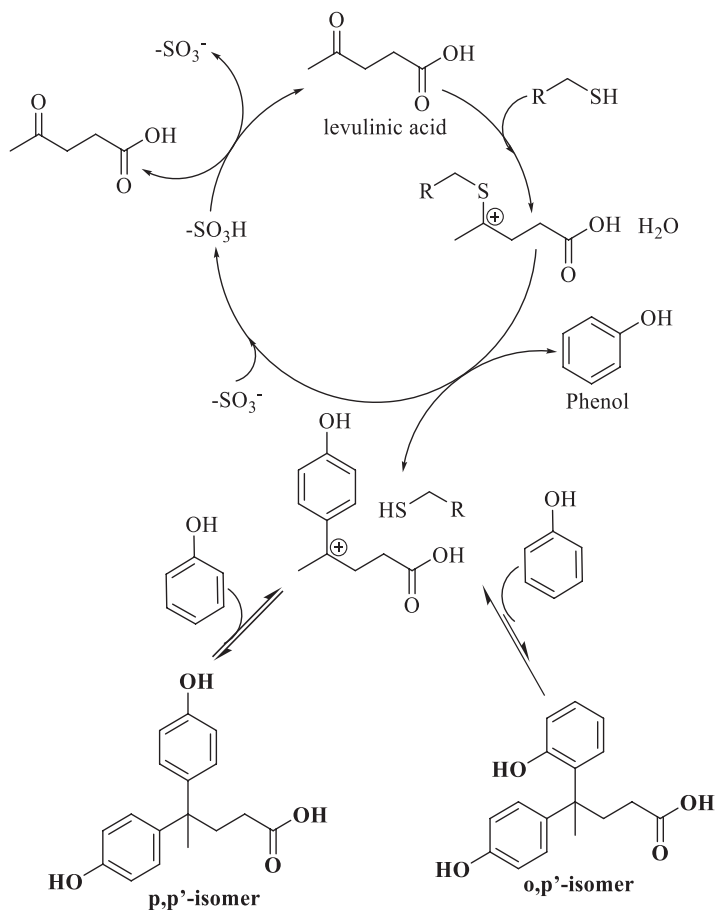
Scheme 8 Mechanism for formation of diphenolic acid using sulfonic acid-functionalized catalyst with thiol promoter
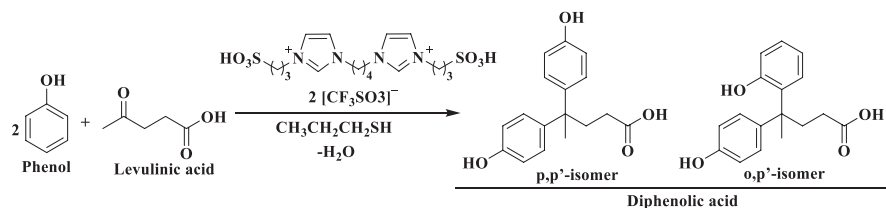
Scheme 9 Ionic liquid-catalysed diphenolic acid formation using propanethiol

High yield of DPA has been reported using Bronsted acidic ionic liquids (BAILs) as catalyst [90]. The combination of ionic liquid and propanethiol showed 91% yield of DPA including high selectivity of p,p'-DPA isomer (ratio of $p,p'/o,p'$ is >100) at 60 °C for 48 h (Scheme 9). The catalytic system is also applied for the preparation of diphenolic esters by reacting alkyl levulinates with phenol. The alkyl levulinates, methyl, ethyl and n-butyl, gave 57%, 58% and 75% yield of corresponding diphenolic esters, and diphenolic acid was observed as the side product. Interestingly, high yield of diphenolic esters was observed using levulinic acid as the reactant in a suitable alcoholic medium. Methanol, ethanol and n-butanol resulted in 87%, 83% and 86% yield of the corresponding diphenolic esters, and a minor yield of diphenolic acid (2–6%) was reported. The catalytic system had good stability and was recyclable for four reaction cycles, with a minor decrease in the product yield.

Recently, Shen et al. reported different acid catalysts for this conversion such as [BSMim]OAc, as [BSMim]CF$_3$SO$_3$, [BSMim]HSO$_4$, [Bpy]HSO$_4$, [AMim]Br, [BMin]Cl, NH$_3$SO$_3$H, p-TSA and HCl at 60 °C, 24 h, LA to phenol (1:4) ratio, 50 mol% of catalyst and 1 mol% ethanethiol w.r.t LA. Among them, [BSMim]CF$_3$SO$_3$ and [BSMim]HSO$_4$ resulted in 100% selectivity for p,p'-DPA with 81 and 75% conversion of LA. At optimized condition, [BSMim]HSO$_4$ showed 93% conversion with desired p,p'-DPA as the only product [91].

Preparation of 4,4-Bis(5-Methylfuran-2-yl) Pentanoic Acid and Esters

Zhang research group disclosed the acid-catalysed preparation of γ,γ-di-2-methylfuran pentanoic acid (4,4-bis(5-methylfuran-2-yl) pentanoic acid) and its esters from levulinic acid and its derivatives (angelica lactone and ethyl levulinate) with 2-methylfuran by hydroxyalkylation-alkylation (HAA) (Schemes 10 and 11) [92, 93]. Nafion-212 resin showed good catalytic activity towards the desired product. At reaction conditions (50 °C for 1 h), angelica lactone showed high yield of HAA product with 81.3%, wherein 12.0% and 4.8% yield of HAA product was reported from ethyl levulinate and levulinic acid. The reusability of Nafion-212 resin was investigated for six reaction cycles with marginal decrease after the third run, attributed to handling loss of the catalyst.

Hydroxyalkylation

Ethyl-levulinate   2-methylfuran

Alkylation

2-methylfuran

ethyl 4,4-bis(5-methylfuran-2-yl)pentanoate
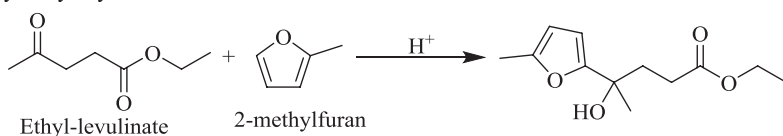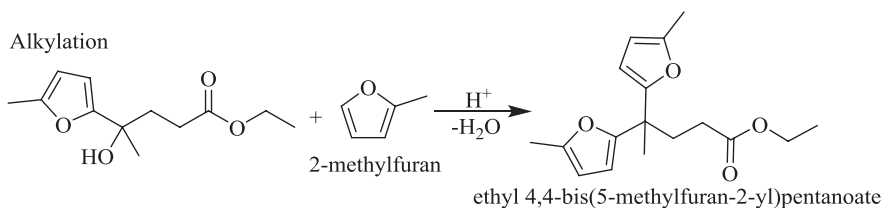
Scheme 10 Hydroxyalkylation-alkylation of ethyl levulinate with 2-methylfuran

The product from HAA reaction, i.e. 4,4-bis(5-methylfuran-2-yl)pentanoic acid, is converted into 4,4-bis(5-methyl-tetrahydrofuran-2-yl)pentan-1-ol intermediate by hydrogenation over 5% Pd/C catalyst. The substituted pentanol is converted into liquid alkanes ((C_9–C_{15} diesel range alkanes (81–82%), C_5–C_8 gasoline range alkenes (10–11%) and C_1–C_4 alkanes (1–2%)) through hydrodeoxygenation using again 5% Pd/C catalyst under continuous flow (Scheme 12) [92].

Preparation of (4,4-Bis(5-Methylthiophen-2-yl)pentanoic Acid

Our group reported the preparation of (4,4-bis(5-methylthiophen-2-yl)pentanoic acid denoted as bisthiophenic acid-methyl (BTA-M)) from levulinic acid with 2-methylthiophene for the first time using solid acid catalysts (Scheme 13). Among the catalysts used such as zeolites, clay and resins, the resin catalysts (Indion-190 and Amberlyst-15) were more active. Indion-190, an inexpensive resin catalyst, showed 98% selectivity and 99% conversion (based on LA) of BTA-M under optimized solvent-free reaction conditions, i.e. levulinic acid to 2-methylthiophene molar ratio is 2.5, 30 wt% of Indion-190 catalyst w.r.t LA, 110 °C for 6 h. The recyclability of Indion-190 for the preparation of BTA-M was demonstrated for three reaction cycles with a slight decrease in the conversion of reactants.

Preparation of alkyl 4,4-bis(5-methylthiophen-2-yl)pentanoate (bisthiophenic alkyl esters-methyl (BTAE-M)) from levulinic esters (methyl, ethyl and butyl) with 2-methylthiophene using Indion-190 catalyst was also attempted (Scheme 13). In the presence of methyl and ethyl levulinates, high conversion (99 and 94%) and good selectivities of related products methyl 4,4-bis(5-methylthiophen-2-yl)pentanoate (96%) and ethyl 4,4-bis(5-methylthiophen-2-yl)pentanoate (95%) were observed. Under similar conditions, butyl levulinate showed less conversion (13%) with poor selectivity of butyl 4,4-bis(5-methylthiophen-2-yl)pentanoate (38%).
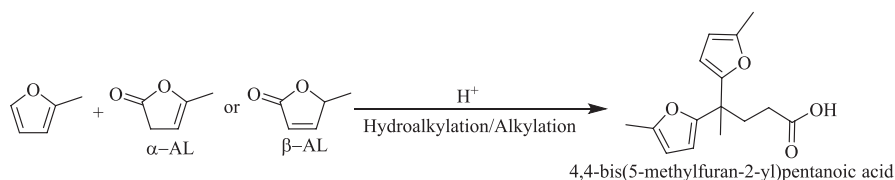
Scheme 11 Hydroxyalkylation-alkylation of angelica lactone with 2-methylfuran

This poor conversion may be due to the bigger size of butyl levulinate, which is sterically precluded from interacting with the acidic active sites of the catalyst.

The applications of BTA-M and BTAE-M were explored in various domains. We tested BTA-M compound as lubricant, plasticizer and antioxidant and antibacterial agent. Surprisingly, the molecule showed good applicability in the field of polymers as plasticizing agent. Moreover, the compound has good antioxidant property.

3 5-Hydroxymethylfurfural

5-Hydroxymethylfurfural (HMF) is an organic compound which was first identified in 1875 as an intermediate product during the synthesis of LA from sugar under sulphuric acid treatment. Mainly, HMF is considered as a platform chemical for the synthesis of bio-based fuel additives and polyester building blocks.

3.1 Preparation of 5-Hydroxymethylfurfural

In principle, HMF preparation Fructose dehydration to HMF conversion mechanism is simple, i.e. removal of three water molecules from hexose using an acid catalyst. However, practically synthesizing HMF is quite complicated because of the side reactions under acidic medium, i.e. hydration of HMF to LA with formic acid as a byproduct and homo-polymerization of HMF into poly-furanics which result in poor yield of HMF. According to the literature, cellulose or starch can be converted to HMF in three steps as follows:

1. Acid-catalysed hydrolysis of cellulose or starch into glucose monomeric units.
2. Acid-catalysed isomerization of glucose to fructose.
3. Acid-catalysed dehydration of fructose to HMF.

The key to achieve good yields of HMF is to choose the best catalyst, and the reaction condition simultaneously should suppress the formation of byproducts.
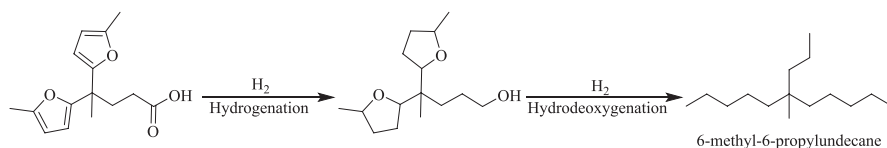
Scheme 12 Liquid alkanes from obtained 4,4-bis(5-methylfuran-2-yl)pentanoic acid through hydrogenation followed hydrodeoxygenation

3.1.1 Catalytic systems reported for Fructose Dehydration to HMF

According to the literature, there are two dehydration mechanistic pathways, resulting in cyclic and acyclic intermediates [94]. However, cyclic pathway is well accepted around the scientific community (Scheme 14). Many catalysts were reported for this conversion including mineral/organic acids, metal salts/oxides, heteropolyacids, functionalized carbon materials, ion-exchange resins, clay and zeolites. The summarized reports of each type of catalytic materials are discussed in the following sections.

Mineral and Organic Acids

Mineral acid (HCl, H_3PO_4, H_2SO_4)-catalysed homogenepus catalytic reactions are reported in batch and continuous flow conditions (Table 3, entries 1–5) [95–100]. High HMF conversion rate was observed regardless of the nature of the acid, and it is well known that H^+ ions are responsible for the dehydration reaction. Using mineral acid catalysts, the difference in the selectivity of HMF is observed by varying medium and anions associated with the acids [95].

In continuous micro-reactor system using HCl catalyst, 96% conversion of fructose with 85% selectivity of HMF in mixed solvents (MIBK/2-butanol + H_2O + DMSO) was reported (Table 3, entry 1). H_2SO_4 and HCl showed excellent yield of HMF, i.e. 95 and 97% in the presence of ionic liquid (Table 3, entries 2 and 3). 67% yield of HMF was observed with H_3PO_4 as catalyst in [BMIM]Cl ionic liquid (Table 3, entry 4). Fructose in DMSO medium using formic acid catalyst afforded maximum yield of HMF (99%) (Table 3, entry 5). Practical problems observed in making HMF using mineral acids as catalyst are corrosion of reactor vessel and product separation.

Metal Salts

Lewis acidic metal chlorides were found to be excellent materials for acid-catalysed dehydration of fructose for HMF production. $AlCl_3$, catalysts from lanthanide group, chromium chloride, zinc chloride, lithium chloride, niobium chloride, indium chloride and cupric chloride were also employed as catalysts in DMSO, water, sulfolane and ionic liquids like [BMIM]Cl and [EMIM]Cl solvents (Table 4, entries

Where
R= H or Alkyl (methyl, ethyl, and butyl)
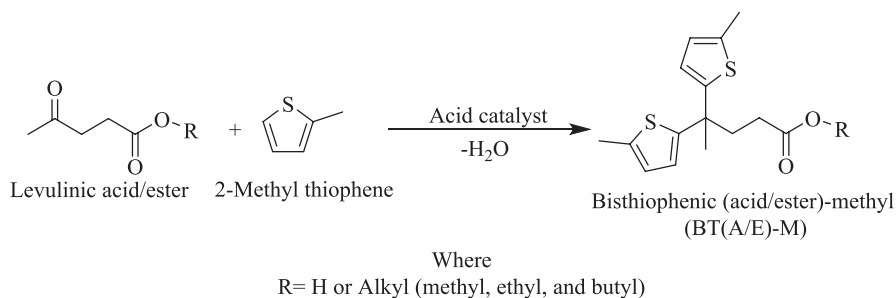
Scheme 13 Preparation of BT(A/E)-M from levulinic acid and its esters with 2-Met using acid catalysts
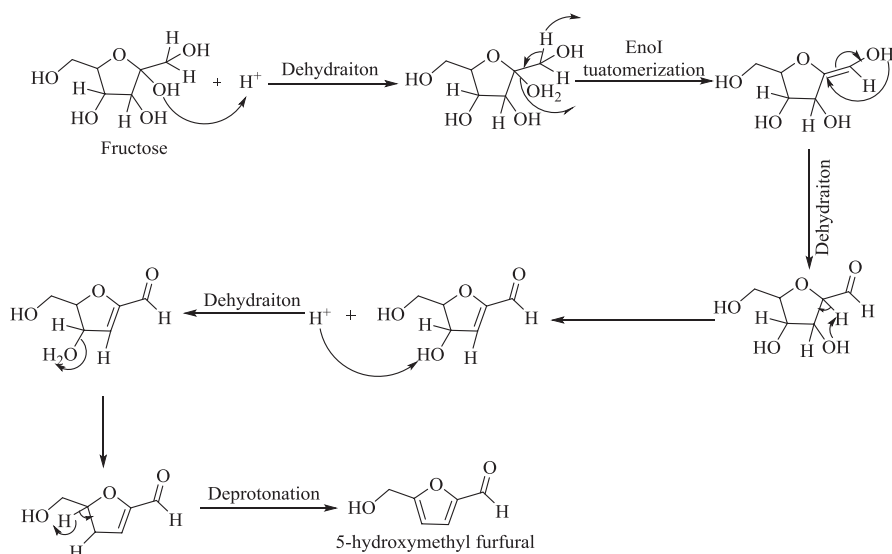
Scheme 14 Proposed mechanism for the dehydration of fructose to HMF using acid catalyst

1–9) [101–109]. The highest yield of HMF was observed with LaCl$_3$ and CrCl$_3$ (92.6 and 96%). Other metal salts afforded good to moderate yield of HMF and some of them were recyclable, e.g. AlCl$_3$ and InCl$_3$.

In a noticeable study, our group reported that the synergism among alumina, metal salt and solvent played an important role in the direct conversion of glucose to HMF. Alumina helped in the isomerization of glucose to fructose, while copper chloride and solvent promoted fructose dehydration to HMF (Scheme 15). Using this catalytic system, several carbohydrates were chosen for the preparation of HMF such as glucose, fructose, galactose, cellobiose, sucrose and starch (Table 4, entries 10 and 11) [110]. Reaction at higher glucose concentration (50 wt% w.r.t to DMSO) was carried out at 140 °C. The HMF yield was 52% with the retention of efficiency even at high substrate concentration.

Table 3 Fructose dehydration to HMF using homogeneous mineral and organic acid catalysts

Entry	Wt. of fructose	Catalyst	Solvent	Temp (°C)	Time	Conv. (%)	Sel. (%)	Yield (%)	References
1	30 wt%	HCl (0.1 M)	MIBK/2-butanol + H_2O + DMSO	185	1 min	96	85	82	[96]
2	1 g	H_2SO_4 (40μL, 0.75 mmol)	[BMIM]Cl (20 g)	120	30 min	100	95	95	[97]
3	0.4 g	HCl (0.2 mmol)	[BMIM]Cl (4.0 g)	80	8 min	–	–	97	[98]
4	180 mg	H_3PO_4 (1 mmol)	[BMIM]Cl (10 mmol)	80	1 h	–	–	67.2	[99]
5	3.6 g	10 mol% HCOOH	DMSO (8 ml)	150	8 h	–	–	99	[100]

Metal Oxides

Inexpensive metal oxides were extensively studied for fructose dehydration in different solvent systems (Table 5). Armaroli et al. reported niobium phosphate as heterogeneous catalyst for this dehydration reaction in water as solvent medium. Although the conversion level is low, selectivity (100%) towards HMF was excellent, and the catalyst was reusable for four cycles (Table 5, entry 1) [111]. Carniti group demonstrated fructose to HMF dehydration reaction in a continuous flow reactor system using silica-niobia mixed metal oxide catalyst (Table 5, entry 2) [112, 113]. The mentioned fixed-bed reactor system was operational up to several hundred hours, but the selectivity and yields were very low. At high temperature (175 °C), silicoaluminophosphate catalyst yielded 80% HMF at 1 h and was reusable up to five cycles (Table 5, entry 3) [114]. Binary mixtures of solvents (water +2-butanol) was reported using tantalum hydroxide (treated with 1 M phosphoric acid) as a catalyst at 160 °C and afforded 90% yield of HMF (Table 5, entry 4). Catalyst recyclability experiments were done by washing the used catalyst several times with water followed by oven drying overnight and used for further reaction cycles [115]. Saha research group discussed self-assembled mesoporous titania microspheres for this dehydration reaction in binary solvent system, i.e. dimethylacetamide and 10% lithium chloride with 74.2% yield of HMF (Table 5, entry 5). Lewis acidic TiO_2 is responsible for the glucose to fructose conversion, and lithium chloride was responsible for fructose dehydration [116]. Sulphated zirconia (prepared by impregnation with H_2SO_4) reported moderate HMF yield (72.8%) from fructose in acetone-DMSO medium under microwave irradiation (Table 5, entry 6) [117].

Table 4　Fructose dehydration to HMF using metal salt catalysts

Entry	Wt. of fructose	Catalyst	Solvent	Temp (°C)	Time	Conv. (%)	Sel. (%)	Yield (%)	Reuse	References
1	5 wt%	AlCl$_3$ 50 mol%	DMSO	140	5 min	–	–	70.1	5	[101]
2	0.20 M	LaCl$_3$ (50 mol%)	DMSO	120	2 h	–	–	92.6	–	[102]
3	2 g	ZnCl$_2$ (63 g) + HCl (405 mg)	H$_2$O (37 mL)	120	40 min	97.3	55	53.3	–	[103]
4	0.1 g	LiCl (100 mg)	Sulfolane (1.40 g)	100	2 h	–	–	67	–	[104]
5	1.0 g	InCl$_3$ (30 mg)	H$_2$O (20 mL)	180	10 min	100	76.5	76.5	3	[105]
6	1.0 g	InCl$_3$ (30 mg)	H$_2$O (20 mL)	180	10 min	100	76	76	–	[106]
7	0.180 g	NbCl$_5$ (0.20 mmol)	[BMIM]Cl (10.0 mmol)	80	30 min	–	–	79	–	[107]
8	50 mg	CuCl$_2$ (0.20 mmol)	[EMIM]Cl (500 mg)	80	3 h	90	93	84	–	[108]
9	1.00 g	CrCl$_3$·6H$_2$O (0.39 mmol)	[BMIM]–[HSO$_4$] (0.70 g)	100	3 h	–	–	96	–	[109]
10	0.9 g	γ-Al$_2$O$_3$ (0.3 g) and CuCl$_2$ (0.05 mmol)	DMSO (3 g)	120	3 h	–	–	67	5	[110]
11	0.9 g Glucose	γ-Al$_2$O$_3$ (0.3 g) and CuCl$_2$ (0.05 mmol)	DMSO (3 g) and H$_2$O (0.45 g)	120	3 h	–	–	57	–	
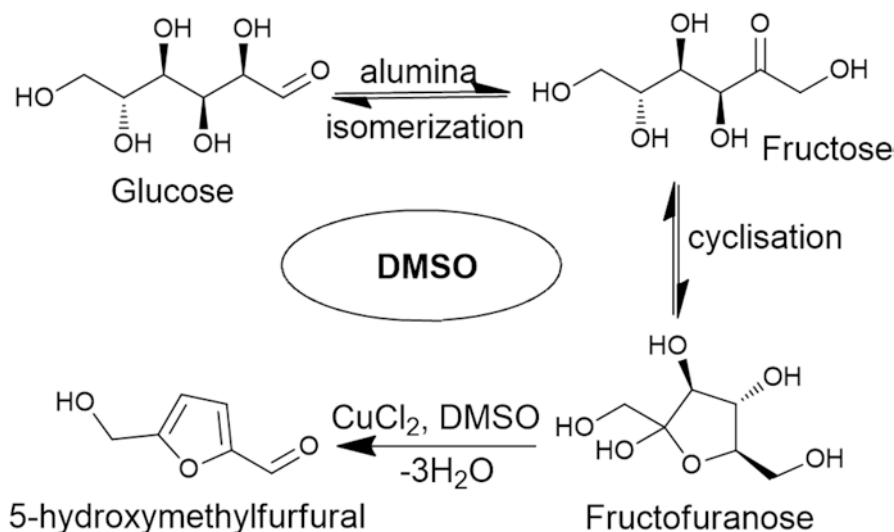
Scheme 15 Conversion of glucose to HMF using combination of Al_2O_3 and $CuCl_2$ in DMSO medium

Heteropolyacid (HPA)-Based Catalysts

Heteropolyacids are a class of strong acids having certain metal or non-metal-based oxo-anionic clusters in the system. Due to their excellent physicochemical properties, Keggin structure, thermal stability and high acidity, they have been extensively reported as catalysts for acid-catalysed organic transformations including dehydration reactions [118–120]. Xiao et al. demonstrated that $H_3PW_{12}O_{40}$ and $H_4SiW_{12}O_{40}$ are highly efficient catalysts for this dehydration reaction using 1-butyl-3-methylimidazolium chloride [BMIM]Cl as a solvent. HMF was obtained with 99% yield in only 5 min at 80 °C under microwave irradiation condition (Table 6, entry 1) [121].

Jiang group reported a novel water-tolerant $C_{16}H_3PW_{11}CrO_{39}$ catalyst, prepared from cetyltrimethyl ammonium salt of transition metal $(Cr^{(III)})$-substituted polyoxometalate (C16-cetyltrimethyl ammonium). The novel catalyst showed moderate performance even at high concentration of fructose (30 wt%) (Table 6, entry 2) [122]. The high catalytic activity at concentrated fructose solution is due to the coexistence of Lewis and Bronsted acidic sites and also the hydrophobic groups present in the catalyst.

Wang research group found an economic and environmental friendly method for obtaining HMF from fructose using $Cs_{2.5}H_{0.5}PW_{12}O_{40}$ catalyst in a biphasic system (water + MIBK). Seventy-four per cent yield of HMF with 94.75% conversion of fructose at 115 °C for 1 h was reported, and the catalyst was reported to be effective up to high concentrations of fructose (50 wt%) as well (Table 6, entry 3) [123]. Silver ion exchanged phosphotungstic acid $(Ag_3PW_{12}O_{40})$ also proved to be an excellent catalytic system for fructose dehydration to HMF (Table 6, entry 4) [124].

Table 5 Fructose dehydration to HMF using heterogeneous metal oxides

Entry	Wt. of fructose	Catalyst	Solvent	Temp (°C)	Time	Conv. (%)	Sel. (%)	Yield (%)	Reuse	References
1	6 wt%	Niobium phosphate (0.7 g)	H_2O	100	0.5 h	28.8	100	28.8	4	[111]
2	0.1 mL/min (0.3 M)	Silica-niobia oxides	H_2O	100	20–40 min	≈72	≈21	≈15	100 h	[112]
3	0.5 g	Silicoaluminophosphate (0.143 g)	H_2O (5 mL) + MIBK (25 mL)	175	1 h	90	89	80	5	[114]
4	1.2 g	Tantalum hydroxide	H_2O + 2-butanol	160	100 min	94	96	90	15	[115]
5	0.1 g	TiO_2 (50 mg)	DMA-LiCl (10%), 2 g	130	2 min	–	–	74.2	5	[116]
6	0.1 g	Sulphated zirconia (0.02 g)	Acetone (3.5 g) + DMSO (3.5 g)	180	20 min	93.6	77.8	72.8	–	[117]

Table 6 Fructose dehydration to HMF using heteropolyacid catalysts

Entry	Wt. of fructose	Catalyst	Solvent	Temp (°C)	Time	Conv. (%)	Sel (%)	Yield (%)	Reuse	References
1	0.5 g	$H_3PW_{12}O_{40}$ or $H_4SiW_{12}O_{40}$ (0.1 mmol)	[BMIM]cl (0.6 g)	80	5 min	>99	99	99	10	[121]
2	0.6 g	$C_{16}H_3PW_{11}Cr$ (0.1 mmol)	H_2O (2 mL)	130	1.5 h	90.3	45	40.6	6	[122]
3	0.6 g	$Cs_{2.5}H_{0.5}PW_{12}O_{40}$ (128 mg)	H_2O (2 mL) + MIBK (6 mL)	115	1 h	78	94.7	74.0	6	[123]
4	2.4 g	$Ag_3PW_{12}O_{40}$	H_2O (8 mL) + MIBK-18 mL	120	1 h	83	93.8	77.7	6	[124]
5	0.5 g	$[MIMPS]_3PW_{12}O_{40}$ (0.25 g)	Sec-butanol (100 mL)	120	2 h	99.7	98.8	99.1	6	[125]
6	0.120 g	Sn-silicotungstic acid	DMSO (2 mL)	120	2 h	98	98	98	3	[126]

To overcome the difficulty in separation and large usage of ionic liquids (ILs), HPA-ILs composites were developed for this acid-catalysed dehydration reaction. Such a system was reusable at least five times (Table 6, entry 5) [125]. Ganji recently reported tin-loaded silicotungstic acid (Sn-STA-2) by hydrothermal microwave treatment which showed good conversion and yield of HMF in DMSO medium. The surface acidity of the catalyst (Sn-STA-2) plays a crucial role for optimum catalytic activity (Table 6, entry 6) [126].

Ion-Exchange Resins

Ion-exchange resins are insoluble solid matrix/support normally in the form of 0.5–1 nm size beads or balls. The appearance varies from yellow, brown and faded black colour, made from organic polymeric substrate. Predominantly, two main classes of ion-exchange resins are available, styrene-based sulfonic acid resins and Dow-type resins [127, 128]. The resin catalysts show high catalytic activity towards many acid-catalysed reactions. Hence, the researchers explored them for the dehydration of fructose to HMF. A comparative study was done by Nijhuis group with acidic heterogeneous catalysts like alumina, aluminosilicate, zirconium phosphate, niobic acid, ion-exchange resin, Amberlyst-15 and mordenite (MOR)-zeolite for fructose dehydration to 5-hydroxymethylfurfural (HMF) in aqueous medium. It was reported that the order of Bronsted acidity contributing to the dehydration reaction is Amberlyst-15 > MOR>$ZrPO_4$ > SiO_2-Al_2O_3 > Nb_2O_5 > Al_2O_3. The authors concluded that HMF selectivity correlates with the presence of Bronsted acidity in Amberlyst-15 and zeolite-MOR catalysts, whereas Lewis acidity is responsible for the decreased HMF selectivity due to the initial condensation of fructose to humins over Lewis acidity (Table 7, entry 1) [129].

Mu group extensively studied fructose dehydration in low boiling solvents using Amberlyst-15 acidic resin catalyst and yielded approximately 50% HMF (Table 7, entry 2) in THF medium and in binary mixture of solvents (THF and methanol).

Table 7 Fructose dehydration to HMF using resin catalysts

Entry	Wt. of fructose	Catalyst	Solvent	Tem. (°C)	Time	Conv. (%)	Sel. (%)	Yield (%)	Reuse	References
1	20 g	Amberlyst-15 (4 g)	H_2O (300 mL)	135	400 m	≈31	≈54	≈17	–	[129]
2	0.25 g	Amberlyst-15 (0.29 g)	THF (10 mL)	120	20 m	98	49	48	11	[130]
3	9 g	Amberlyst-15 (10 g)	Dioxane (100 mL)	100	3 h	98	82	80	5	[131]
4	0.38 g	Amberlyst-70 (0.20 mmol H^+)	DMSO (5.0 g)	140	1 h	100	93	93	3	[132]
5	0.4 g	Amberlyst-15 (0.1 g)	DMSO (3 mL)	120	1 h	100	82	82	7	[133]

Table 8 Fructose dehydration to HMF using functionalized carbon materials

Entry	Wt. of fructose	Catalyst	Solvent	Temp (°C)	Time	Conv. (%)	Sel. (%)	Yield (%)	Reuse	References
1	0.5 g	Glu-TsOH (0.4 g)	DMSO (6 mL)	130	1.5 h	99.9	91.2	91.2	5	[134]
2	0.180 g	Cellulose sulphuric acid (50 mg)	DMSO (3 mL)	100	45 min	100	93.6	93.6	6	[135]
3	0.150 g	CNT-PSSA 15 mg	DMSO (1.5 mL)	120	30 min	>99	89	89	3	[136]
4	0.33 M	Carbon-silica composite	Ethanol-water	170	1 h	78	55	43	–	[137]
5	0.09 g	Graphene oxide (8 mg)	DMSO + 2-proponal (4:1)	120	6 h	100	90	90	4	[138]

Table 9 Fructose dehydration to HMF using clay and zeolitic materials

Entry	Wt. of fructose	Catalyst	Solvent	Temp (°C)	Time	Conv. (%)	Sel. (%)	Yield (%)	Reuse	References
1	3.5 g	Mordenite (Si/Al = 11) (1 g)	H_2O (35 mL) + MIBK (175 ml)	165	1 h	76	91	69	–	[139]
2	3.5 g	Mordenite (Si/Al = 11) (1 g)	H_2O (35 mL) + MIBK (175 mL)	165	2 h	93	78	73	–	[140]
3	0.218 g	Zeolite microspheres (18 mg)	DMSO-8 g	120	5 h	100	77	77	–	[141]
4	5 wt%	Sn-mont (0.2 g) + NaCl (0.37 g)	H_2O-(1 mL + THF 5 mL)	160	3 h	n.d.	n.d.	78	6	[142]
5	0.18 g	K-10 clay-Al (120 mg) DMSO	DMSO- (5 mL)	120	3 h	n.d.	n.d. n.d.	93.2	6	[143]
6	1.2 g	Natural clay, attapulgite 100 mg	2-butanol, water	160	2.5 h	n.d.	n.d.	96.3	4	[144]

HMF along with 5-methoxymethylfurfural (MMF) were obtained with an increase in the total yield to 65%. Using methanol as solvent, etherification was initiated as HMF was converted into MMF with 37% yield (Table 7, entry 2) [130]. Commercially attractive process for the production of HMF from high fructose corn syrup was developed by Jeong *et al.* They found 1,4-dioxane to be a promising solvent media after screening various solvents using Amberlyst-15 a solid acid catalyst. HMF yield was 80% with the reusability of the catalyst up to five times and solvent recycled after simple distillation (Table 7, entry 3) [131]. Morales group reported high sulfonic acid-loaded acidic resin as a heterogeneous catalyst for the dehydration of fructose to HMF in DMSO, yielding 93% of HMF in 1 h (Table 7, entry 4). The authors also studied this reaction with glucose as a starting material, which yielded 33% HMF in 24 h. In this case, DMSO as a solvent played an important role in dehydrating glucose to anhydroglucose which facilitated the production of HMF by reducing side reaction [132].

A study done by our group showed the influence of DMSO and dimethylformamide (DMF) on the recyclability of Amberlyst-15 catalyst for the dehydration of fructose to HMF. In case of DMSO as a solvent, stable activity of the catalyst is noted, whereas in DMF, significant loss of activity is observed up on recycling. The loss of activity in DMF is due to the neutralization of acidic sites by the formation of ammonium ions which was inferred from FT-IR and CHNS studies. To regenerate the catalytic activity, dilute acid treatment was required (Table 7, entry 5) [133].

Functionalized Carbon Materials

High stability of carbon materials and complementary properties on hydrophobicity have resulted in the use of mainly sulfonated carbonaceous materials as solid catalysts for fructose dehydration to HMF. Wang group reported a carbon-based solid acid, prepared from glucose and *p*-toluenesulfonic acid (TsOH), and used for catalytic dehydration of fructose into HMF (91.2% yield). The catalyst was active in DMSO at 130 °C for 1.5 h (Table 8, entry 1). Moreover, this catalyst showed a good reusability for five reaction cycles [134]. Huang et al. reported cellulose-sulphuric acid as catalyst, prepared from cellulose treated with chlorosulfonic acid. The recyclable solid acid catalyst revealed high yield (93.6%) of HMF in DMSO for 45 min (Table 8, entry 2) [135].

A series of sulfonic acid-functionalized carbon materials (C-SO₃H), including poly(*p*-styrenesulfonic acid)-grafted carbon nanotubes (CNT-PSSA), poly(*p*-styrenesulfonic acid)-grafted carbon nanofibers (CNF-PSSA), benzenesulfonic acid-grafted CMK-5 (CMK-5-BSA) and benzenesulfonic acid-grafted carbon nanotubes (CNT-BSA), was studied for this conversion. Among these functionalized carbons, CNT-PSSA showed exceptional catalytic activity and afforded 89% HMF yield (Table 8, entry 3). This excellent catalytic activity is due to the high Bronsted acid strength which is confirmed by potentiometric acid-base titration and ion chromatography [136].

Russo et al. adopted a simple synthetic procedure for the preparation of carbon-silica composite activated with SO₃H groups by acid treatment with different acid
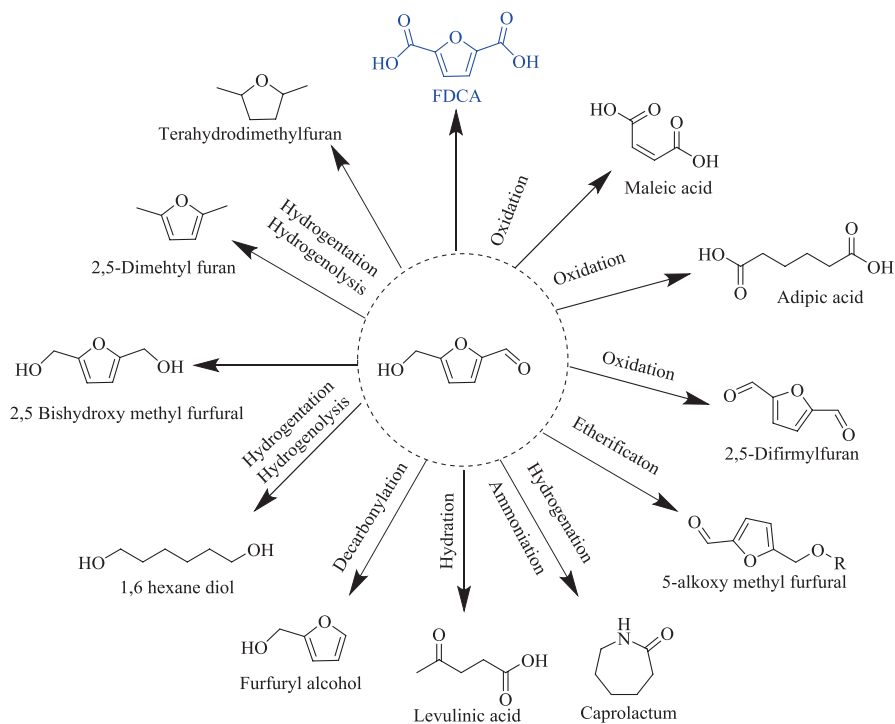
Scheme 16 Organic transformations of HMF
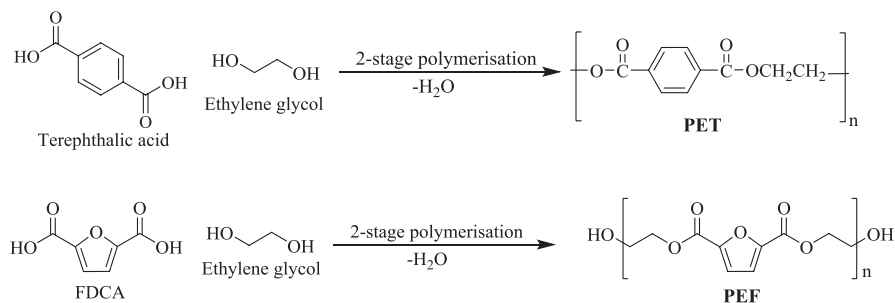
Scheme 17 Preparation of PET (from terephthalic acid) and PEF (from FDCA)

concentration. The reaction carried out in the binary solvent mixture (ethanol-water) at 170 °C for 1 h resulted in fructose conversion up to 78% with 43% yield of HMF (Table 8, entry 4) [137]. The authors claimed that increase in the ratio of surface activating agent and mass of carbon precursor eventually increases the acid strength of the catalyst, and this is also accompanied by the creation of mesoporosity which increases the accessibility of the reactants towards the active sites. Zhu research group reported graphene oxide as a catalyst for this conversion. In this work, a series of co-solvents were employed with DMSO. 20 vol% 2-proponal (with DMSO

80 vol%) binary solvent system yielded 90% HMF (Table 8, entry 5). The authors revealed that a small number of sulfonic groups and abundance of oxygen-containing groups (alcohols, epoxides, carboxylates) play a synergic role in maintaining the high performance of graphene oxide [138].

Clay and Zeolitic Materials

Zeolites are microporous aluminosilicates widely used as commercial adsorbents, more particularly in gas adsorption and bearing worldwide application as industrial catalysts. Zeolites have large open cage-like structure that form channels, having large pore size and high surface area which greatly allow the reactants into the zeolite framework and result in good catalytic activity. This property of zeolites culminated in their classification under the materials known as "molecular sieves". Zeolites are more advantageous over other solid acid catalysts, having advantages like easy separation compared to homogenous catalysts, catalyst regeneration upon high temperature treatment and stable at high temperature in aqueous condition compared to ion-exchange resin catalysts. Some highlighted results of fructose dehydration investigated using zeolite catalysts and listed in Table 9.

Moreau *et al.* performed dehydration of fructose into 5-hydroxymethylfurfural in a batch mode in the presence of H-form of zeolites as catalysts at 165 °C and in a binary solvent mixture consisting of water and methylisobutylketone (1:5 by volume). The catalytic activity observed depended on both the acidic sites and structural properties of the catalyst used. Good selectivity towards HMF was achieved using mordenite-zeolite catalyst with the Si/Al ratio—11 (Table 9, entries 1 and 2). The high selectivity obtained was correlated by shape-selective properties of catalyst which can be reused for several runs after thermal treatment without considerable loss in activity [139, 140].

Zhang group discussed the preparation of novel zeolite microspheres for the dehydration of fructose to HMF. They adopted a simple synthetic procedure named polymerization-induced colloid aggregation (im-PICA) for the preparation of zeolite microspheres (ZMSs) with a hierarchical porous structure and uniform particle size. As expected, these zeolite microspheres afforded good yield of HMF (77%)
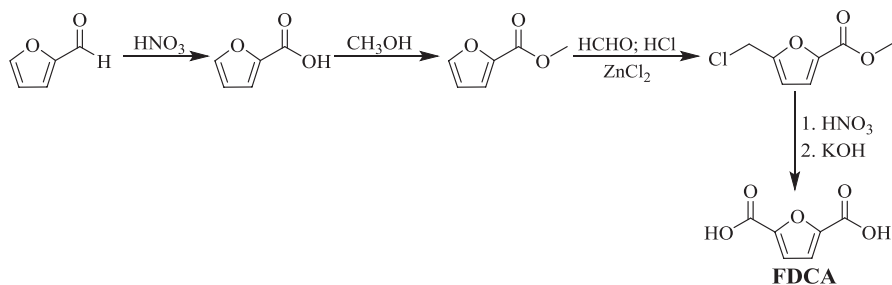
Scheme 18 Preparation of FDCA from furfural
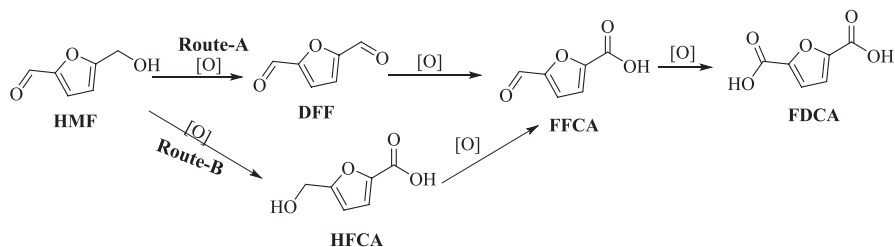
Scheme 19 Oxidation reaction network of HMF to possible products

(Table 9, entry 3) [141]. The catalytic activity of Sn-montmorillonite (mont) was explored towards this conversion in DMSO-THF binary mixture of solvents, and the HMF yield was 78% in 1 h at 160 °C from fructose (Table 9, entry 4) [142]. The aluminium-exchanged montmorillonite-K-10 clay was found to be an efficient catalyst for the dehydration of fructose to HMF in DMSO solvent with 93.2% yield at 120 °C in 3 h (Table 9, entry 5) [143]. Yang et al. provided a green and economic pathway for the conversion of fructose to HMF using natural clay attapulgite (ATP) in a 2-butanol-water system. The highest activity was observed with phosphoric acid-treated attapulgite (ATP-P) catalyst. This excellent activity was attributed to the appropriate amount of Bronsted acidic sites which brought the HMF yield of 96.3% (Table 9, entry 6) [144].

3.2 Applications of 5-Hydroxymethylfurfural

HMF is a multifunctional molecule which can undergo many organic transformations, for example, oxidation, hydrogenation, etherification, hydrodeoxygenation, hydration, decarboxylation, hydrogenation-hydrogenolysis and esterification, with several high value-added products as mentioned in Scheme 16. Thus, HMF is known as the "sleeping giant" in the field of biomass and is a common building platform reported in the survey by DOE and EU.

Among the applications FDCA conversion of HMF, the selective oxidation product FDCA is attractive in the present scenario as it is a precursor for polyethylene furanoate (PEF), a suitable alternative for the replacement of fossil-based terephthalic acid (TPA)-derived polyethylene terephthalate (PET) for making plastics (Scheme 17) [145]. Unfortunately, HMF is not stable for long periods under ambient conditions, though pure HMF remains stable up to 8 months under freezing conditions. Presence of small impurity promotes the formation of dimer and oligomers.

Table 10 Oxidation of HMF using non-Ru-supported catalysts

Entry	Catalyst	Solvent	Base	T (°C)/t (h)	HMF con. (%)	FDCA yield (%)	DFF yield (%)	References
Non-noble catalysts								
1	Cu-MnO$_2$	MeOH	–	140/5	75	–	51	[146]
2	g-C$_3$N$_3$-TiO$_2$	ACN	–	RT/4	52	–	42 S	[147]
3	MnO$_2$	H$_2$O	NaHCO$_3$	100/24	99	91	–	[148]
4	MnO$_x$-CeO$_2$	H$_2$O	KHCO$_3$	100/21	98	91	–	[149]
5	Mn$_{0.5}$Co$_{0.50}$	EtOH	Na$_2$CO$_3$	140/2	42	–	98 S	[150]
6	V$_2$O$_5$/CP	DMSO	–	140/5	100	–	80	[151]
7	Co/Mn/Br	H$_2$O/OAc	–	160/0.5	99	83	–	[152]
8	Fe$_3$O$_4$@C@Pt	H$_2$O	Na$_2$CO$_3$	90/10	100	100	–	[153]
9	CuOCeO$_2$	H$_2$O	–	110/3	99	–	99 FFCA	[154]
10	NNC-900	H$_2$O	K$_2$CO$_3$	80/48	100	80	–	[155]
11	Mn$_{0.75}$/Fe$_{0.25}$	H$_2$O	NaOH	90/24	99	21	79 FFCA	[156]
12	Fe$_3$O$_4$-CoO$_x$	DMSO	–	80/12	97	68	–	[157]
13	Fe^{III}-POP-1	H$_2$O	–	100/10	100	79		[158]
14	1 wt% V$_2$O$_5$/H-beta	DMSO	–	125/3	84	–	82	[159]
15	Holey 2D Mn$_2$O$_3$	H$_2$O	NaHCO$_3$	100/24	100	99	–	[160]
Noble metals								
16	Pt-Bi/C	H$_2$O	2 equiv. Na$_2$CO$_3$	100/6	100	99	–	[161]
17	Pd/PVP	H$_2$O	1.25 equiv. NaOH	90/6	99	90	–	[162]
18	Au/HY	H$_2$O	5 equiv. NaOH	60/6	99	99	–	[163]
19	5 wt% Bi-Pt/C	H$_2$O	NaHCO$_3$	100/3	98	98	–	[161]

3.2.1 History of FDCA Synthesis

FDCA was first produced from the dehydration of mucic acid in the presence of strong acid (48% HBr) by Fitting *et al*. This conversion is industrially un-attractive due to high cost of starting material, long reaction time and relatively high reaction temperature. Further, a process was developed from xylose-derived furfural. Unfortunately, this pathway was also aborted due to the multistep synthesis including a number of intermediates (Scheme 18). Thus, the researchers strived to look for the alternative, efficient and economical pathway for the production of FDCA [145].

Table 11 Selective oxidation of HMF to FDCA using Ru-supported catalysts

Entry	Catalyst	Solvent	T(°C)/t(h)	HMF conv. (%)	FDCA yield (%)	References
1	Ru(OH)x/CeO$_2$	H$_2$O	140/20/18	–	60	[164]
2	Ru/C	H$_2$O	140/1	99.9	23.7	[165]
3	Ru/γ-Al$_2$O$_3$	H$_2$O	140/1	32.4	0	
4	Pd/C	H$_2$O	140/1	35.1	0	
5	Pt/C	H$_2$O	140/1	100	56.3	
6	Ru/CTF	H$_2$O	140/1	100	41.4	
7	Ru/CTF	H$_2$O	140/3	100	77	
8	Ru/C + NaOH	H$_2$O	120/5	100	69	[166]
9	Ru/C + K$_2$CO$_3$	H$_2$O	120/5	100	80	
10	Ru/C + Na$_2$CO$_3$	H$_2$O	120/5	100	93	
11	Ru/C + HT	H$_2$O	120/5	100	90	
12	Ru/C + CaCO$_3$	H$_2$O	120/5	100	95	
13	Ru/C	H$_2$O	120/10	100	88	
14	Ru/MnCo$_2$O$_4$	H$_2$O	120/10	100	99.1	[167]
15	Ru/CoMn$_2$O$_4$	H$_2$O	120/10	100	82.2	
16	Ru/MnCo$_2$CO$_3$	H$_2$O	120/10	99.9	69.9	
17	Ru/MnO$_2$	H$_2$O	120/10	98.8	31.1	
18	Ru/CoO	H$_2$O	120/10	91.1	17.8	
19	ZrP-Ru	H$_2$O	110/12	14	11	[168]
20	ZrP-Ru	MeCN	110/12	19	20	
21	ZrP-Ru	Ethanol	110/12	20	4[a]	
22	ZrP-Ru	DMSO	110/12	39	27[a]	
23	ZrP-Ru	MIBK	110/12	55	19[a]	
24	ZrP-Ru	Toluene	110/12	91	26[a]	
25	ZrP-Ru	p-Cl toluene	110/12	95	28[a]	
26	ZrP-Ru + K$_2$CO$_3$	p-Cl toluene	150/6	100	34[a]	
27	Ru/ZrO$_{2\,H}$-SBA	H$_2$O	120/16	97	87[a]	[169]
28	Ru/ZrO$_{2\,H}$-aero	H$_2$O	120/16	100	97[a]	
29	Ru/MgAlO	H$_2$O	140/4	100	99	[170]
30	Ru/MgO	H$_2$O	140/4	80	58	
31	Ru/La$_2$O$_3$	H$_2$O	140/4	4.6	0.8	
32	Ru/CeO$_2$	H$_2$O	140/4	89	7.0	
33	Ru/ZrO$_2$	H$_2$O	140/4	100	0	
34	Ru/HAP	H$_2$O	120/1	100	>99	[171]
35	Pt/CNT	H$_2$O	100/12	100	98	[172]
36	Pd/CNT	H$_2$O	100/12	100	96	
37	Ru/CNT	H$_2$O	100/12	100	93	
38	Co/CNT	H$_2$O	100/12	97	96[b]	
39	Ni/CNT	H$_2$O	100/12	97	92[b]	

Table 11 (continued)

Entry	Catalyst	Solvent	T(°C)/t(h)	HMF conv. (%)	FDCA yield (%)	References
40	CNT	H_2O	100/12	86	86[c]	

[a]Selectivity of FDCA
[b]DFF
[c]FFCA

3.2.2 Selective Oxidation of 5-Hydroxymethylfurfural to 2,5-Furandicarboxylic Acid

Several furanic derivatives can be obtained via catalytic oxidation of HMF, including 2,5-diformylfuran (DFF), 5-formyl-2-furancarboxylic acid (FFCA), 5-hydroxy methyl-2-furancarboxylic acid (HFCA) and 2,5-furandicarboxylic acid (FDCA). Among these multiple oxidation products, an efficient and selective preparation of FDCA is a challenging task. The reaction scheme of HMF to FDCA is mentioned in Scheme 19.

Selective oxidation of HMF to FDCA is advantageous because it is a one-pot synthesis. Conversion of HMF to FDCA was demonstrated using several homogeneous catalysts such as $KMnO_4$, HNO_3, $Co(OAc)_2$, $Mn(OAc)_2$, $Zn(OAc)_2$, $CuCl_2$, etc. [145]. Working with homogeneous catalyst has some drawbacks like reduced FDCA yield, side products, cumbersome separation and purification of product from reaction mixture, use of additives and reusability of the catalyst.

Oxidation of HMF to FDCA was demonstrated extensively using various heterogeneous catalysts with molecular oxygen (O_2), air, H_2O_2, t-BuOOH and $KMnO_4$ as oxidants, but researchers mostly prefer molecular oxygen due to its high oxidation potential, low cost and environmentally benign nature. Non-noble mono-metal or its mixed metal oxide heterogeneous catalysts from Mn, Co, Fe, Ce, Cu and Li are reported for this oxidation reaction with base or under base-free conditions (Table 10, entry 1-15). Among the non-noble metal-containing catalysts, Fe, Mn and Ce metal oxides were exclusively reported for this conversion in organic, aqueous and ionic liquid medium with moderate to good yields of FDCA. For further improvement in FDCA selectivity, researchers developed many noble metal (Au, Rh, Pt, Pd and Ru) catalytic systems under base or base-free aqueous medium using O_2/air oxidant (Table 10, entry 16-19 and Table 11). Even though good yields were achieved using Rh and Pt, these expensive materials increased the cost of the end product. Au, Pd and a combination of these metals as catalysts showed high activity using base additive at mild reaction conditions and short time as compared with base-free reaction set-ups. Moreover, according to the recent analysis, the Pd metal price raised by 400%, and this precious metal is now $1351.40 for 25 g, and hence more expensive than platinum ($792.30).

Recently, Ru-based catalysts are becoming attractive towards this oxidation, as there are several advantages behind it: stability in aqueous medium, high selectivity

of FDCA at relatively milder reaction conditions (preferably low O_2/air pressure), base-free and availability of multiple Ru species such as Ru(0), oxide and hydroxide. Moreover, the price of Ru is comparatively less than other noble metals. Important findings for the HMF oxidation to FDCA using Ru metal-supported catalysts preferably under aqueous base-free medium are covered in the following section.

3.2.2.1   Preparation of FDCA from Selective Oxidation of HMF over Supported Ru Catalysts and its activity comparison with other metal catalysts

Gorbanev *et al*. studied $Ru(OH)_x$ catalyst on different oxide supports such as TiO_2, Al_2O_3, Fe_3O_4, ZrO_2, CeO_2, MgO, La_2O_3, hydrotalcite, hydroxyapatite and MgO. La_2O_3 for conversion of HMF into FDCA in aqueous medium, under base-free condition with low to moderate oxygen pressure [164]. ZrO_2- and Al_2O_3-supported catalysts induced the formation of formic acid as side product. Fe_3O_4 and hydroxyapatite supports showed good selectivity of the desired product; however, in both cases, the observed mass balance of the reaction was low, due to the formation of solid humins in the course of the reaction. Even though good selectivity of FDCA was achieved using basic Mg oxide supports such as MgO, $MgO.La_2O_3$ and hydrotalcite, the authors found leaching of Mg in the reaction medium. Compared with TiO_2, CeO_2 support showed high conversion and selectivity; at 140 °C, 2.5 bar O_2 for 18 h, $Ru(OH)_x/CeO_2$ afforded 60% yield of FDCA and 10% of 5-hydroxymethyl-2-furan-carboxylic acid (Table 11, entry 1), and no other side products (levulinic acid and formic acid) were detected using CeO_2 support. Recyclability of $Ru(OH)_x/CeO_2$ system was also demonstrated for three cycles by the authors.

Palkovits research group introduced Ru supported on covalent triazine framework (CTF) catalysts for this oxidation. The catalytic activity of Ru/CTF was compared with conventional catalysts such as Ru/C, Pt/C, Ru/γ-Al_2O_3 and Pd/C under base-free aqueous medium using synthetic air as the oxidant (20 bar) (Table 11, entries 2–6) [165]. Ru/γ-Al_2O_3 and Pd/C exhibited low conversion of HMF and no discernable yield of FDCA. Pt/C catalyst was very active for FDCA formation (56%) but less mass balance was reported for the reaction; formation of polymeric/oligomeric products of FDCA could be the reason behind. In the case of Ru-based catalysts, mass balance is generally good, and side products DFF and FFCA are formed in addition to FDCA. Ru/CTF showed 41.4% yield of FDCA which is higher than Ru/C (23.7%) catalyst under similar reaction conditions. High surface area (2071 m²/g) and high polarity related to hydrophilicity seem to have positive effects in this conversion. Interestingly, the authors observed high yield of FDCA (77%) by treating Ru/CTF catalyst with DMSO before reaction with a reaction time of 3 h (Table 11, entry 7). Ru/CTF has good reusability and was found to be stable compared to conventional Ru/C.

Yi *et al*. investigated HMF to FDCA over commercially available Ru/C catalyst [166]. Initially, the reaction was conducted with strong and weak base additives, and

the authors observed that weak base such as $CaCO_3$ is attractive and showed high yield (95%) of FDCA under O_2 pressure (2 bar) (Table 11, entries 8–12). Moreover, a clear solution was obtained in the presence of weak bases, while a brownish coloured solution was obtained for strong bases (NaOH or KOH) owing to the degradation of HMF and promotion of side reactions. Ru/C catalyst was applied in the absence of base as well. At optimized reaction condition (120 °C, 5 bar O_2 for 10 h), the catalyst afforded 88% yield of FDCA with complete conversion of HMF (Table 11, entry 13). Recyclability for Ru/C was also examined, and after each reaction, the catalyst was washed with methanol before being used, that showed good activity and stability for three reaction cycles. From the control experiments, the authors proposed the reaction path, following the Route-A mechanism (Scheme 16) via intermediate DFF and FFCA.

Mishra *et al*. discussed supported Ru catalysts for air oxidation of HMF to FDCA in aqueous medium and absence of base. In this work, supports were chosen from various Mg- and Co-based oxides such as $MnCo_2O_4$, $CoMn_2O_4$, $MnCo_2CO_3$, MnO_2 and CoO [167]. Among them, Ru/$MnCo_2O_4$ exhibited the highest selectivity for FDCA (99.1% yield) at relatively milder reaction conditions (120 °C, 24 bar air for 10 h) (Table 11, entries 14–18). The appropriate acidic sites in Ru/$MnCo_2O_4$ catalyst was confirmed by NH_3-TPD, Bronsted acid sites (10.7 mmol/g) and Lewis acid-coordinated NH_3 (7.3 mmol/g), i.e. a total of 18 mmol/g aided in the selective formation of FDCA. Moreover, $MnCo_2O_4$ support is a crystalline cubic system, whereas others have distorted spinel structures (e.g. $CoMn_2O_4$ is body-centred tetragonal phase). Generally, the spinel system has more adsorption affinity of oxygen. Additionally, using $MnCo_2O_4$ support had high surface area (151.1 m^2/g) and high Ru dispersion % (39.2) which were beneficial for its higher activity. Ru/$MnCo_2O_4$ was reused for five cycles with similar conversion and selectivity. ICP analysis precluded even traces of leached Ru metal in the solution.

Yang *et al*. investigated the effect of reaction parameters and solvents towards HMF oxidation using Ru^{III}-incorporated zirconium phosphate (ZrP-Ru) catalyst [168]. Various solvents were used for this study including H_2O, MeCN, ethanol, methanol, DMSO, MIBK, toluene and *p*-chlorotoluene. Among these, DMSO, toluene and *p*-chlorotoluene resulted in high selectivity of FDCA (Table 11, entries 19–25). In the case of alcohol solvents, etherified product was predominant which could be attributed to the Lewis acidity of Zr. Addition of base and increasing the temperature of the reaction improved the selectivity of FDCA (Table 11, entry 26). The decrease in selectivity of FDCA may be associated with the feed pattern of O_2 pressure, as the authors flushed the reaction set-up with oxygen under atmospheric pressure at a flow rate of 20 mL/min.

Pichler *et al*. demonstrated different ZrO_2-supported ruthenium catalysts for this conversion in aqueous basic medium using O_2 gas as the oxidant (10 bar) [169]. The high surface area-containing catalysts such as Ru/ZrO_2 H-SBA and Ru/ZrO_2 H-aero showed high catalytic activity and 97% and 100% conversion of HMF with 87% and 97% selectivity of FDCA (Table 11, entries 27 and 28). The high activity of these supports is associated with high surface area; for Ru/ZrO_2 H-SBA the surface area is 256 m^2/g and 239 m^2/g for Ru/ZrO_2 H-aero. The experiments show that the

size of the ruthenium particles is crucial for the catalytic performance; larger surface area leads to the formation of small Ru particles (0.8 nm for Ru/ZrO$_{2 \text{ H-}}$aero, 1.0 nm for Ru/ZrO$_{2 \text{ H-SBA}}$) which were found to be more active than bigger Ru particles observed in other synthesized and commercial (monoclinic and tertragonal) ZrO$_2$ supports. Ru/ZrO$_{2 \text{ H-}}$aero catalyst was tested for reusability studies, and a decrease in activity was observed with increasing reaction cycles, but no loss in the carbon balance and no leaching of Ru metal was observed.

Antonyraj *et al*. studied different oxide supports such as MgO, MgAlO, La$_2$O$_3$, CeO$_2$ and ZrO$_2$ [170]. Among these supports, MgAlO (prepared by co-precipitation under low supersaturation followed by calcination)-supported Ru catalyst showed better activity and afforded 99% yield of FDCA which is higher as compared with other supported Ru catalysts (Table 11, entries 29–33). Because of the high surface area (200 m^2/g) and appropriate basic property (6.09 mmol/g) of MgAlO, it was found to be highly active. In the case of other supports including MgO, their observed surface area was less than 100 m^2/g. Even though La$_2$O$_3$ support has strong basic sites, the catalyst showed poor conversion due to the less surface area (13 m^2/g) and surface acidity. In the case of CeO$_2$ and ZrO$_2$, less surface area and no basic property resulted in poor selectivity towards FDCA. The authors also studied the reusability of both catalysts, i.e. Ru/MgO and Ru/MgAlO supports were found to be dissolved during the reaction, but Ru/MgO showed good catalytic activity/stability for five reaction cycles.

Gao *et al*. studied highly dispersed ruthenium nanoparticles on hydroxyapatite (HAP) solid support for the aerobic oxidation of HMF to FDCA in aqueous medium under base-free condition [171]. A systematic study done by the authors includes the effect of HMF/Ru molar ratio, oxygen pressure, reaction temperature, kinetic study, catalyst stability upon reuse, surface acidity and basicity, morphology and dispersion and valence state of surface Ru. At optimized condition (HMF/Ru molar ratio: 25, 120 °C, 10 bar O$_2$ for 1 h), Ru/HAP showed >99% yield of FDCA (Table 11, entry 34). The temperature was varied from 60 to 120 °C. At 60 °C, only FFCA intermediate was observed, which clearly showed that Ru/HAP catalyst is capable of converting other oxidized intermediates such as DFF and HMFCA to FFCA at this temperature. Upon increasing the temperature to 120 °C, >99 yield of FDCA from FFCA intermediate was reported. The authors disclosed that well-dispersed Ru^0 and acidic-basic sites located in the HAP support were essential to drive this base-free oxidation process. The catalyst was reusable up to five cycles, and after five cycles, slight deactivation was observed which can be reversed by reducing the catalyst under H$_2$ at 350 °C.

Sharma *et al*. demonstrated metal (Pt/Pd/Ru/Co/Ni)-functionalized carbon nanotubes (CNT) for base-free aerobic oxidation of HMF to FDCA in aqueous medium [172]. The noble metal-based catalysts such as Pt/CNT, Pd/CNT and Ru/CNT showed high yield, i.e. 98, 96 and 95%, respectively, of FDCA under relatively mild reaction condition, i.e. 100 °C, 30 bar O$_2$ for 12 h (Table 11, entries 35–37). The screened non-noble metals such as Ni and Co-loaded CNT were selective towards DFF (Table 11, entries 38 and 39). In the absence of metal, simple-functionalized CNT material gave 86% yield of FFCA (Table 11, entry 40). In this article, the

authors clearly explained the mechanism of HMF to FDCA using metal-supported functionalized CNT (M/CNT) catalyst. Initially, the hydroxyl group of HMF is adsorbed on the surface of M/CNT catalyst, followed by C–H activation. Two hydrogen atoms (H of CH_2 and OH) were abstracted by the support and removed by oxygen molecule favouring the formation of DFF. The functional groups on the CNT interacted with the aldehyde group (of DFF) which undergo hydrolysis and form FFCA intermediate. Finally, FFCA easily converts into FDCA with similar hydrolysis mechanism as mentioned above. This work also successfully investigated the adsorption behaviour of substrate and product on CNT surface. Among these catalysts, noble metals have more selectivity and activity towards FDCA formation because of their excellent ability to attract the β-H atom from the methyl side chain of HMF. The catalyst ability for the attraction of β-H group is in the order Pt > Pd > Ru on CNT; accordingly, FDCA product selectivity also varied.

4 Conclusion and Challenges

4.1 Conclusions

The importance of biomass conversion and primary building blocks of carbohydrates is discussed at the beginning of this chapter. The application and importance of levulinic and furan-based molecules were explained with pertinent examples. A brief outline of levulinic acid synthesis and its catalytic conversion to various valuable products such as γ-valerolactone, arylated-γ-lactones and 4,4-disubstituted pentanoic acid/esters was covered. Prior art on hydrocyclization of levulinic acid to γ-valerolactone in the presence of different hydrogen sources using layered double hydroxide-based catalysts is discussed along with their catalytic performances. Preparation of arylated-γ-lactones (levulinic acid and aromatics) was introduced in this chapter using various homogeneous and heterogeneous (zeolite) catalysts. The acid-catalysed conversion of levulinic acid with aromatics into 4,4-disubstituted pentanoic acid/esters is disclosed such as diphenolic acid, γ,γ-di-2-methylfuran pentanoic acid (4,4-bis(5-methylfuran-2-yl)pentanoic acid) and (4,4-bis(5-methylthiophen-2-yl)pentanoic acid). The possible applications of 4,4-disubstituted pentanoic acid/esters were also mentioned.

A brief discussion on 5-hydroxymethylfurfural (HMF) synthesis preferably from fructose dehydration has been covered using various acid catalysts including mineral/organic acids, metal salts, metal oxides, heteropolyacids, ion-exchange resins, functionalized carbon materials, clay and zeolitic materials. We focused on the performance of mentioned catalysts by considering conversion of fructose, yield of HMF, stability, reusability, etc.. Finally, brief outline of the results of selective oxidation of 5-hydroxymethylfurfural into 2,5-furandicarboxylic acid is discussed with emphasis on Ru-based catalyst for this conversion under base-free aqueous medium using O_2/air as the oxidant.

4.2 Challenging Tasks

- Several processes have been demonstrated for the synthesis of γ-valerolactone. However, the problem lies with its applicability. It is studied as fuel blender and precursor for polymers. But the high cost of Gvl starting material such as levulinic acid (2–3$/kg) is the bottleneck for its use in the abovementioned fields. So, finding the application of Gvl, as a solvent in agrochemical formulations, as an electrolyte in electrochemical cells and as alternative high boiling liquids, may be economically viable and might result in impactful research.
- Finding the suitable application for novel arylated-γ-lactones and 4,4-disubstituted pentanoic acid/esters, which are emerging areas in biorefinery, is also relevant but challenging.
- Even though maximum possible selectivity of HMF has been achieved from fructose, HMF separation from the reaction medium and obtaining the desired purity are still challenging tasks for researchers. Also, the relatively higher cost for fructose compared to other sugar starting materials creates a problem in its exploration for bulk scale synthesis of HMF. HMF production directly from cellulose is highly desirable and has been presently reported in moderate yields. Its implementation requires a cost-competitive process. While using cellulose as a starting material for HMF synthesis, the side reactions, i.e. the formation of levulinic acid and poly-furanics (humins), has to be suppressed at optimal condition and catalyst. Thus, there is a scope for development in this area.
- Selective oxidation of HMF to FDCA was reported at a maximum concentration of 3–5 wt% in aqueous medium which is not viable at the industrial scale. Thus, for this conversion, high concentration of HMF has to be studied with high selectivity of FDCA by implementing technical/reaction tools.

References

1. Sasaki M, Adschiri T, Arai K (2003) Production of cellulose II from native cellulose by near- and supercritical water solubilization. J Agric Food Chem 51:5376–5381
2. Li C, Zhao X, Wang A, Huber GW, Zhang T (2015) Catalytic transformation of lignin for the production of chemicals and fuels. Chem Rev 115:11559–11624
3. Achyuthan KE, Achyuthan AM, Adams PD, Dirk SM, Harper JC, Simmons BA, Singh AK (2010) Supramolecular self-assembled chaos: polyphenolic lignin's barrier to cost-effective lignocellulosic biofuels. Molecules 15:8641–8688
4. Delidovich I, Hausoul PJ, Deng L, Pfutzenreuter R, Rose M, Palkovits R (2016) Alternative monomers based on lignocellulose and their use for polymer production. Chem Rev 116:1540–1599
5. Gauthier C, Chiche B, Finiels A, Geneste P (1989) Influence of acidity in friedel-crafts acylation catalyzed by zeolites. J Mol Catal 50:219–229
6. Rackemann DW, Doherty WOS (2011) The conversion of lignocellulosics to levulinic acid. Biofuels Bioprod Biorefin 5:198–214

 7. Stocker M (2008) Biofuels and biomass-to-liquid fuels in the biorefinery: catalytic conversion of lignocellulosic biomass using porous materials. Angew Chem 47:9200–9211
 8. Bevilaqua DB, Rambo MKD, Rizzetti TM, Cardoso AL, Martins AF (2013) Cleaner production: levulinic acid from rice husks. J Clean Prod 47:96–101
 9. Yang Z, Kang H, Guo Y, Zhuang G, Bai Z, Zhang H, Feng C, Dong Y (2013) Dilute-acid conversion of cotton straw to sugars and levulinic acid via 2-stage hydrolysis. Ind Crop Prod 46:205–209
10. Victor A, Pulidindi IN, Gedanken A (2014) Levulinic acid production from Cicer arietinum, cotton, Pinus radiata and sugarcane bagasse. RSC Adv 4:44706–44711
11. Morone A, Apte M, Pandey RA (2015) Levulinic acid production from renewable waste resources: bottlenecks, potential remedies, advancements and applications. Renew Sust Energ Rev 51:548–565
12. Tabasso S, Montoneri E, Carnaroglio D, Caporaso M, Cravotto G (2014) Microwave-assisted flash conversion of non-edible polysaccharides and post-harvest tomato plant waste to levulinic acid. Green Chem 16:73–76
13. Li J, Jiang Z, Hu L, Hu C (2014) Selective conversion of cellulose in corncob residue to levulinic acid in an aluminum trichloride–sodium chloride system. ChemSusChem 7:2482–2488
14. Peng L, Lin L, Zhang J, Zhuang J, Zhang B, Gong Y (2010) Catalytic conversion of cellulose to levulinic acid by metal chlorides. Molecules 15:5258–5272
15. Upare PP, Yoon J-W, Kim MY, Kang H-Y, Hwang DW, Hwang YK, Kung HH, Chang J-S (2013) Chemical conversion of biomass-derived hexose sugars to levulinic acid over sulfonic acid-functionalized graphene oxide catalysts. Green Chem 15:2935–2943
16. Hegner J, Pereira KC, DeBoef B, Lucht BL (2010) Conversion of cellulose to glucose and levulinic acid via solid-supported acid catalysis. Tetrahedron Lett 51:2356–2358
17. Weingarten R, Kim YT, Tompsett GA, Fernández A, Han KS, Hagaman EW, Conner WC Jr, Dumesic JA, Huber GW (2013) Conversion of glucose into levulinic acid with solid metal(IV) phosphate catalysts. J Catal 304:123–134
18. Ramli NAS, Amin NAS (2015) Fe/HY zeolite as an effective catalyst for levulinic acid production from glucose: characterization and catalytic performance. Appl Catal B Environ 163:487–498
19. Suacharoen S, Tungasmita DN (2013) Hydrothermolysis of carbohydrates to levulinic acid using metal supported on porous aluminosilicate. J Chem Technol Biotechnol 88:1538–1544
20. Szabolcs A, Molnar M, Dibo G, Mika LT (2013) Microwave-assisted conversion of carbohydrates to levulinic acid: an essential step in biomass conversion. Green Chem 15:439–445
21. Shen Y, Sun J-K, Yi Y-X, Wang B, Xu F, Sun RC (2015) One-pot synthesis of levulinic acid from cellulose in ionic liquids. Bioresour Technol 192:812–816
22. Ren H, Girisuta B, Zhou Y, Liu L (2015) Selective and recyclable depolymerization of cellulose to levulinic acid catalyzed by acidic ionic liquid. Carbohydr Polym 117:569–576
23. Ren H, Zhou Y, Liu L (2013) Selective conversion of cellulose to levulinic acid via microwave-assisted synthesis in ionic liquids. Bioresour Technol 129:616–619
24. Sun Z, Xue L, Wang S, Wang X, Shi J (2016) Single step conversion of cellulose to levulinic acid using temperature-responsive dodeca-aluminotungstic acid catalysts. Green Chem 18:742–752
25. Saravanamurugan S, Riisager A (2013) Zeolite catalyzed transformation of carbohydrates to alkyl levulinates. ChemCatChem 5:1754–1757
26. Wang G, Zhang Z, Song L (2014) Efficient and selective alcoholysis of furfuryl alcohol to alkyl levulinates catalyzed by double SO3H-functionalized ionic liquids. Green Chem 16:1436–1443
27. Zhang Z, Dong K, Zhao ZK (2011) Efficient conversion of furfuryl alcohol into alkyl levulinates catalyzed by an organic-inorganic hybrid solid acid catalyst. ChemSusChem 4:112–118
28. Demma Carà P, Ciriminna R, Shiju NR, Rothenberg G, Pagliaro M (2014) Enhanced heterogeneous catalytic conversion of furfuryl alcohol into butyl levulinate. ChemSusChem 7:835–840

29. Huang YB, Yang T, Zhou MC, Pan H, Fu Y (2016) Microwave-assisted alcoholysis of furfuryl alcohol into alkyl levulinates catalyzed by metal salts. Green Chem 18:1516–1523

30. Zhu SH, Cen YL, Guo J, Chai JC, Wang JG, Fan WB (2016) One-pot conversion of furfural to alkyl levulinate over bifunctional Au-H4SiW12O40/ZrO2 without external H2. Green Chem 18:5667–5675

31. Timokhin BV, Baransky VA, Eliseeva GD (1999) Levulinic acid in organic synthesis. Russ Chem Rev 68:73–84

32. Luo W, Bruijnincx PCA, Weckhuysen BM (2014) Selective, one-pot catalytic conversion of levulinic acid to pentanoic acid over Ru/H-ZSM5. J Catal 320:33–41

33. Upare PP, Lee J-M, Hwang YK, Hwang DW, Lee J-H, Halligudi SB, Hwang J-S, Chang J-S (2011) Direct hydrocyclization of biomass-derived levulinic acid to 2-methyltetrahydrofuran over nanocomposite copper/silica catalysts. ChemSusChem 4:1749–1752

34. Mizugaki T, Nagatsu Y, Togo K, Maeno Z, Mitsudome T, Jitsukawa K, Kaneda K (2015) Selective hydrogenation of levulinic acid to 1,4-pentanediol in water using a hydroxyapatite-supported Pt-Mo bimetallic catalyst. Green Chem 17:5136–5139

35. Wright WRH, Palkovits R (2012) Development of heterogeneous catalysts for the conversion of levulinic acid to gamma-valerolactone. ChemSusChem 5:1657–1667

36. Lange J-P, Price R, Ayoub PM, Louis J, Petrus L, Clarke L, Gosselink H (2010) Valeric biofuels: a platform of cellulosic transportation fuels. Angew Chem Int Ed 49:4479–4483

37. Zhao Y, Fu Y, Guo QX (2012) Production of aromatic hydrocarbons through catalytic pyrolysis of gamma-valerolactone from biomass. Bioresour Technol 114:740–744

38. Bond JQ, Alonso DM, Wang D, West RM, Dumesic JA (2010) Integrated catalytic conversion of gamma-valerolactone to liquid alkenes for transportation fuels. Science 327:1110–1114

39. Alonso DM, Bond JQ, Dumesic JA (2010) Catalytic conversion of biomass to biofuels. Green Chem 12:1493–1513

40. Manzer LE (2004) Catalytic synthesis of α-methylene-γ-valerolactone: a biomass-derived acrylic monomer. Appl Catal A Gen 272:249–256

41. Van de Vyver S, Roman-Leshkov Y (2013) Emerging catalytic processes for the production of adipic acid. Cat Sci Technol 3:1465–1479

42. Lange J-P, Vestering JZ, Haan RJ (2007) Towards 'bio-based' nylon: conversion of [gamma]-valerolactone to methyl pentenoate under catalytic distillation conditions. Chem Commun 33:3488–3490

43. Alonso DM, Wettstein SG, Mellmer MA, Gurbuz EI, Dumesic JA (2013) Integrated conversion of hemicellulose and cellulose from lignocellulosic biomass. Energy Environ Sci 6:76–80

44. Horváth IT (2008) Solvents from nature. Green Chem 10:1024–1028

45. Duan Z-Q, Hu F (2012) Highly efficient synthesis of phosphatidylserine in the eco-friendly solvent γ-valerolactone. Green Chem 14:1581–1583

46. Stradi A, Molnar M, Ovari M, Dibo G, Richter FU, Mika LT (2013) Rhodium-catalyzed hydrogenation of olefins in γ-valerolactone-based ionic liquids. Green Chem 15:1857–1862

47. Strappaveccia G, Ismalaj E, Petrucci C, Lanari D, Marrocchi A, Drees M, Facchetti A, Vaccaro L (2015) A biomass-derived safe medium to replace toxic dipolar solvents and access cleaner heck coupling reactions. Green Chem 17:365–372

48. Strappaveccia G, Luciani L, Bartollini E, Marrocchi A, Pizzo F, Vaccaro L (2015) γ-Valerolactone as an alternative biomass-derived medium for the Sonogashira reaction. Green Chem 17:1071–1076

49. Pongrácz P, Bartal B, Kollár L, Mika LT (2017) Rhodium-catalyzed hydroformylation in γ-valerolactone as a biomass-derived solvent. J Organomet Chem 847:140–145

50. Fegyverneki D, Orha L, Láng G, Horváth IT (2010) Gamma-valerolactone-based solvents. Tetrahedron 66:1078–1081

51. Gundekari S, Srinivasan K (2019) Screening of solvents, hydrogen source, and investigation of reaction mechanism for the hydrocyclisation of levulinic acid to γ-valerolactone using Ni/SiO2-Al2O3 catalyst. Catal Lett 149:215–227

52. Osatiashtiani A, Lee AF, Wilson K (2017) Recent advances in the production of gamma-valerolactone from biomass-derived feedstocks via heterogeneous catalytic transfer hydrogenation. J Chem Technol Biotechnol 92:1125–1135

53. Liguori F, Moreno-Marrodan C, Barbaro P (2015) Environmentally friendly synthesis of gamma-valerolactone by direct catalytic conversion of renewable sources. ACS Catal 5:1882–1894

54. Tang X, Zeng X, Li Z, Hu L, Sun Y, Liu S, Lei T, Lin L (2014) Production of γ-valerolactone from lignocellulosic biomass for sustainable fuels and chemicals supply. Renew Sust Energ Rev 40:608–620

55. Dutta S, Yu IKM, Tsang DCW, Ng YH, Ok YS, Sherwood J, Clark JH (2019) Green synthesis of gamma-valerolactone (GVL) through hydrogenation of biomass-derived levulinic acid using non-noble metal catalysts: a critical review. Chem Eng J 372:992–1006

56. Xue ZM, Liu QL, Wang JF, Mu TC (2018) Valorization of levulinic acid over non-noble metal catalysts: challenges and opportunities. Green Chem 20:4391–4408

57. Yu ZH, Lu XB, Liu C, Han YW, Ji N (2019) Synthesis of gamma-valerolactone from different biomass-derived feedstocks: recent advances on reaction mechanisms and catalytic systems. Renew Sust Energ Rev 112:140–157

58. Yan K, Chen A (2013) Efficient hydrogenation of biomass-derived furfural and levulinic acid on the facilely synthesized noble-metal-free Cu–Cr catalyst. Energy 58:357–363

59. Yan K, Liao J, Wu X, Xie X (2013) A noble-metal free Cu-catalyst derived from hydrotalcite for highly efficient hydrogenation of biomass-derived furfural and levulinic acid. RSC Adv 3:3853–3856

60. Yan K, Chen A (2014) Selective hydrogenation of furfural and levulinic acid to biofuels on the ecofriendly Cu–Fe catalyst. Fuel 115:101–108

61. Long X, Sun P, Li Z, Lang R, Xia C, Li F (2015) Magnetic Co/Al2O3 catalyst derived from hydrotalcite for hydrogenation of levulinic acid to γ-valerolactone. Chin J Catal 36:1512–1518

62. Zhang J, Chen J, Guo Y, Chen L (2015) Effective upgrade of Levulinic acid into γ-valerolactone over an inexpensive and magnetic catalyst derived from hydrotalcite precursor. ACS Sustain Chem Eng 3:1708–1714

63. Gupta SSR, Kantam ML (2018) Selective hydrogenation of levulinic acid into γ-valerolactone over Cu/Ni hydrotalcite-derived catalyst. Catal Today 309:189–194

64. Li W, Fan GL, Yang L, Li F (2016) Highly efficient vapor-phase hydrogenation of biomass-derived Levulinic acid over structured nanowall-like nickel-based catalyst. ChemCatChem 8:2724–2733

65. Hussain SK, Kumar VV, Pethan RN, Putra KB, Chary KVR (2018) Synthesis of γ-Valerolactone from Levulinic acid and formic acid over Mg-Al Hydrotalcite like compound. ChemistrySelect 3:6186–6194

66. Jiang K, Sheng D, Zhang ZH, Fu J, Hou ZY, Liu XY (2016) Hydrogenation of levulinic acid to γ-valerolactone in dioxane over mixed MgO-Al2O3 supported Ni catalyst. Catal Today 274:55–59

67. Gundekari S, Srinivasan K (2017) In situ generated Ni(0)@boehmite from NiAl-LDH: an efficient catalyst for selective hydrogenation of biomass derived levulinic acid to γ-valerolactone. Catal Commun 102:40–43

68. Ma MW, Liu H, Cao JJ, Hou P, Huang JH, Xu XL, Yue HJ, Tian G, Feng SH (2019) A highly efficient Cu/AlOOH catalyst obtained by in situ reduction: catalytic transfer hydrogenation of ML into γ-GVL. Mol Catal 467:52–60

69. Gundeboina R, Gadasandula S, Velisoju VK, Gutta N, Kotha LR, Aytam HP (2019) Ni-Al-Ti hydrotalcite based catalyst for the selective hydrogenation of biomass-derived levulinic acid to γ-valerolactone. Chemistryselect 4:202–210

70. Liu M, Li S, Fan G, Yang L, Li F (2019) Hierarchical flower-like bimetallic NiCu catalysts for catalytic transfer hydrogenation of ethyl levulinate into γ-valerolactone. Ind Eng Chem Res 58:10317–10327

71. Swarna Jaya V, Sudhakar M, Naveen Kumar S, Venugopal A (2015) Selective hydrogenation of levulinic acid to γ-valerolactone over a Ru/Mg-LaO catalyst. RSC Adv 5:9044–9049

72. Bal R, Pendem C, Bordolol A, Konthala L, Narayan S, Manoj K, Saran S (2018) Process for the production of γ-Valerolactone. US patent 10,005,747 B2

73. Kannan Srinivasan SG (2019) Process for the preparation of γ-Valerolactone by catalytic hydrogenation of levulinic acid using Ru-based catalysts. US patent 10,221,149 B2

74. Mitta H, Seelam PK, Chary KVR, Mutyala S, Boddula R, Inamuddin AAM (2018) Efficient vapor-phase selective hydrogenolysis of bio-Levulinic acid to γ-valerolactone using Cu supported on hydrotalcite catalysts. Glob Challenges 2:1800028

75. Yonezawa N, Koike M, Kameda A, Naito S, Hino T, Maeyama K, Ikeda T (2002) Chemospecificity in arylations of δ- and γ-ketocarboxylic acids with P2O5–MsOH, TfOH, and related acidic media. Synth Commun 32:3169–3180

76. Makiko H, Yumi M, Hiroshi Y (2011) Oxygen-containing cyclic compound and method for producing the same. JP 2011201847 A

77. Jansen JC, Creyghton EJ, Njo SL, van Koningsveld H, van Bekkum H (1997) On the remarkable behaviour of zeolite Beta in acid catalysis. Catal Today 38:205–212

78. Zhao Z, Xu S, Hu MY, Bao X, Peden CHF, Hu J (2015) Investigation of aluminum site changes of dehydrated zeolite H-Beta during a rehydration process by high-field solid-state NMR. J Phys Chem C 119:1410–1417

79. Galletti AMR, Antonetti C, De Luise V, Martinelli M (2012) A sustainable process for the production of γ-valerolactone by hydrogenation of biomass-derived levulinic acid. Green Chem 14:688–694

80. Singh AP (1992) Preparation of bisphenol-a over zeolite catalysts. Catal Lett 16:431–435

81. Darbre PD (2015) Chapter 1 – what are endocrine disrupters and where are they found? In: Darbre PD (ed) Endocrine disruption and human health. Academic Press, Boston, pp 3–26

82. Bozell JJ, Moens L, Elliott DC, Wang Y, Neuenscwander GG, Fitzpatrick SW, Bilski RJ, Jarnefeld JL (2000) Production of levulinic acid and use as a platform chemical for derived products. Resour Conserv Recycling 28:227–239

83. Bader AR, Kontowicz AD (1954) γ,γ-Bis-(p-hydroxyphenyl)-valeric acid. J Am Chem Soc 76:4465–4466

84. Yu X, Guo Y, Li K, Yang X, Xu L, Guo Y, Hu J (2008) Catalytic synthesis of diphenolic acid from levulinic acid over cesium partly substituted wells–dawson type heteropolyacid. J Mol Catal A Chem 290:44–53

85. Guo Y, Li K, Yu X, Clark JH (2008) Mesoporous H3PW12O40-silica composite: efficient and reusable solid acid catalyst for the synthesis of diphenolic acid from levulinic acid. Appl Catal B Environ 81:182–191

86. Guo Y, Li K, Clark JH (2007) The synthesis of diphenolic acid using the periodic mesoporous H3PW12O40-silica composite catalysed reaction of levulinic acid. Green Chem 9:839–841

87. Li K, Hu J, Li W, Ma F, Xu L, Guo Y (2009) Design of mesostructured H3PW12O40-silica materials with controllable ordered and disordered pore geometries and their application for the synthesis of diphenolic acid. J Mater Chem 19:8628–8638

88. Van de Vyver S, Helsen S, Geboers J, Yu F, Thomas J, Smet M, Dehaen W, Román-Leshkov Y, Hermans I, Sels BF (2012) Mechanistic insights into the kinetic and regiochemical control of the thiol-promoted catalytic synthesis of diphenolic acid. ACS Catal 2:2700–2704

89. Van de Vyver S, Geboers J, Helsen S, Yu F, Thomas J, Smet M, Dehaen W, Sels BF (2012) Thiol-promoted catalytic synthesis of diphenolic acid with sulfonated hyperbranched poly(arylene oxindole)s. Chem Commun 48:3497–3499

90. Liu H-F, Zeng F-X, Deng L, Liao B, Pang H, Guo Q-X (2013) Bronsted acidic ionic liquids catalyze the high-yield production of diphenolic acid/esters from renewable levulinic acid. Green Chem 15:81–84

91. Shen Y, Sun J, Wang B, Xu F, Sun R (2014) Catalytic synthesis of diphenolic acid from levulinic acid over Bronsted acidic ionic liquids. Bioresources 9:3264–3275

92. Wang W, Li N, Li S, Li G, Chen F, Sheng X, Wang A, Wang X, Cong Y, Zhang T (2016) Synthesis of renewable diesel with 2-methylfuran and angelica lactone derived from carbo-hydrates. Green Chem 18:1218–1223

93. Li G, Li N, Wang Z, Li C, Wang A, Wang X, Cong Y, Zhang T (2012) Synthesis of high-quality diesel with furfural and 2-methylfuran from hemicellulose. ChemSusChem 5:1958–1966

94. De Melo FC, De Souzaa RF, Coutinhob PLA, De Souza MO (2014) Synthesis of 5-hydroxy-methylfurfural from dehydration of fructose and glucose using ionic liquids. J Braz Chem Soc 25(12)

95. Cinlar B, Wang T, Shanks BH (2013) Kinetics of monosaccharide conversion in the presence of homogeneous Bronsted acids. Appl Catal A Gen 450:237–242

96. Tuercke T, Panic S, Loebbecke S (2009) Microreactor process for the optimized synthesis of 5-hydroxymethylfurfural: a promising building block obtained by catalytic dehydration of fructose. Chem Eng Technol 32:1815–1822

97. Sievers C, Musin I, Marzialetti T, Olarte MB, Agrawal PK, Jones CW (2009) Acid-catalyzed conversion of sugars and furfurals in an ionic-liquid phase. ChemSusChem 2:665–671

98. Li C, Zhao ZK, Wang A, Zheng M, Zhang T (2010) Production of 5-hydroxymethylfurfural in ionic liquids under high fructose concentration conditions. Carbohydr Res 345:1846–1850

99. Ray D, Mittal N, Chung WJ (2011) Phosphorous pentoxide mediated synthesis of 5-HMF in ionic liquid at low temperature. Carbohydr Res 346:2145–2148

100. Thananatthanachon T, Rauchfuss TB (2010) Efficient route to hydroxymethylfurans from sugars via transfer hydrogenation. ChemSusChem 3:1139–1141

101. De S, Dutta S, Saha B (2011) Microwave assisted conversion of carbohydrates and biopoly-mers to 5-hydroxymethylfurfural with aluminium chloride catalyst in water. Green Chem 13:2859–2868

102. Seri K, Inoue Y, Ishida H (2000) Highly efficient catalytic activity of lanthanide(III) ions for conversion of saccharides to 5-hydroxymethyl-2-furfural in organic solvents. Chem Lett 29:22

103. Deng T, Cui X, Qi Y, Wang Y, Hou X, Zhu Y (2012) Conversion of carbohydrates into 5-hydroxymethylfurfural catalyzed by ZnCl2 in water. Chem Commun 48:5494–5496

104. Caes BR, Raines RT (2011) Conversion of fructose into 5-(hydroxymethyl)furfural in sulfo-lane. ChemSusChem 4:353–356

105. Shen Y, Sun J, Yi Y, Wang B, Xu F, Sun R (2014) 5-Hydroxymethylfurfural and levulinic acid derived from monosaccharides dehydration promoted by InCl3 in aqueous medium. J Mol Catal A Chem 394:114–120

106. Shen Y, Xu YF, Sun JK, Wang B, Xu F, Sun RC (2014) Efficient conversion of monosaccha-rides into 5-hydroxymethylfurfural and levulinic acid in InCl3-H2O medium. Catal Commun 50:17–20

107. Mittal N, Nisola GM, Chung W-J (2012) Facile catalytic dehydration of fructose to 5-hydroxy-methylfurfural by niobium pentachloride. Tetrahedron Lett 53:3149–3155

108. Pidko EA, Degirmenci V, Hensen EJM (2012) On the mechanism of lewis acid catalyzed glucose transformations in ionic liquids. ChemCatChem 4:1263–1271

109. Eminov S, Wilton-Ely JDET, Hallett JP (2014) Highly selective and near-quantitative conver-sion of fructose to 5-hydroxymethylfurfural using mildly acidic ionic liquids. ACS Sustain Chem Eng 2:978–981

110. Sampath G, Srinivasan K (2017) Remarkable catalytic synergism of alumina, metal salt and solvent for conversion of biomass sugars to furan compounds. Appl Catal A Gen 533:75–80

111. Tiziana Armaroli GB, Carlini C, Giuttari M, Sbrana G, Galletti AMR (2000) Acid sites characterization of niobium phosphate catalysts and their activity in fructose dehydration to 5-hydroxymethyl-2-furaldehyde. J Mol Catal A Chem 151:233–243

112. Carniti P, Gervasini A, Marzo M (2010) Silica–niobia oxides as viable acid catalysts in water: effective vs. intrinsic acidity. Catal Today 152:42–47

113. Carniti P, Gervasini A, Marzo M (2011) Absence of expected side-reactions in the dehydration reaction of fructose to HMF in water over niobic acid catalyst. Catal Commun 12:1122–1126

114. Bhaumik P, Dhepe PL (2013) Influence of properties of SAPO's on the one-pot conversion of mono-, di- and poly-saccharides into 5-hydroxymethylfurfural. RSC Adv 3:17156

115. Yang F, Liu Q, Yue M, Bai X, Du Y (2011) Tantalum compounds as heterogeneous catalysts for saccharide dehydration to 5-hydroxymethylfurfural. Chem Commun 47:4469–4471

116. De S, Dutta S, Patra AK, Bhaumik A, Saha B (2011) Self-assembly of mesoporous TiO2 nanospheres via aspartic acid templating pathway and its catalytic application for 5-hydroxy-methyl-furfural synthesis. J Mater Chem 21:17505

117. Qi X, Watanabe M, Aida TM, Smith RL Jr (2009) Sulfated zirconia as a solid acid catalyst for the dehydration of fructose to 5-hydroxymethylfurfural. Catal Commun 10:1771–1775

118. Timofeeva MN (2003) Acid catalysis by heteropoly acids. Appl Catal A Gen 256:19–35

119. Kozhevnikov IV (1998) Catalysis by heteropoly acids and multicomponent polyoxometalates in liquid-phase reactions. Chem Rev 98:171–198

120. Yunxiang Qiao ZH (2009) Polyoxometalate–based solid and liquid salts for catalysis. Curr Org Chem 13:1347–1365

121. Xiao Y, Song Y-F (2014) Efficient catalytic conversion of the fructose into 5-hydroxymeth-ylfurfural by heteropolyacids in the ionic liquid of 1-butyl-3-methyl imidazolium chloride. Appl Catal A Gen 484:74–78

122. Zheng H, Sun Z, Yi X, Wang S, Li J, Wang X, Jiang Z (2013) A water-tolerant C16H3PW11CrO39 catalyst for the efficient conversion of monosaccharides into 5-hydroxy-methylfurfural in a micellar system. RSC Adv 3:23051

123. Zhao Q, Wang L, Zhao S, Wang X, Wang S (2011) High selective production of 5-hydroxy-methylfurfural from fructose by a solid heteropolyacid catalyst. Fuel 90:2289–2293

124. Fan C, Guan H, Zhang H, Wang J, Wang S, Wang X (2011) Conversion of fructose and glucose into 5-hydroxymethylfurfural catalyzed by a solid heteropolyacid salt. Biomass Bioenergy 35:2659–2665

125. Qu Y, Huang C, Zhang J, Chen B (2012) Efficient dehydration of fructose to 5-hydroxy-methylfurfural catalyzed by a recyclable sulfonated organic heteropolyacid salt. Bioresour Technol 106:170–172

126. Ganji P (2020) Synthesis and catalytic performance of SnxSTA by microwave-assisted hydrothermal synthesis for fructose to HMF. Biomass Conv Bioref 10:823–830

127. Harmer MA, Sun Q (2001) Solid acid catalysis using ion-exchange resins. Appl Catal A Gen 221:45–62

128. Barbaro P, Liguori F (2009) Ion exchange resins: catalyst recovery and recycle. Chem Rev 109:515–529

129. Ordomsky VV, van der Schaaf J, Schouten JC, Nijhuis TA (2012) Fructose dehydration to 5-hydroxymethylfurfural over solid acid catalysts in a biphasic system. ChemSusChem 5:1812–1819

130. Zhu H, Cao Q, Li C, Mu X (2011) Acidic resin-catalysed conversion of fructose into furan derivatives in low boiling point solvents. Carbohydr Res 346:2016–2018

131. Jeong J, Antonyraj CA, Shin S, Kim S, Kim B, Lee K-Y, Cho JK (2013) Commercially attractive process for production of 5-hydroxymethyl-2-furfural from high fructose corn syrup. J Ind Eng Chem 19:1106–1111

132. Morales G, Melero JA, Paniagua M, Iglesias J, Hernández B, Sanz M (2014) Sulfonic acid heterogeneous catalysts for dehydration of C6-monosaccharides to 5-hydroxymethylfurfural in dimethyl sulfoxide. Chin J Catal 35:644–655

133. Sampath G, Kannan S (2013) Fructose dehydration to 5-hydroxymethylfurfural: remarkable solvent influence on recyclability of Amberlyst-15 catalyst and regeneration studies. Catal Commun 37:41–44

134. Wang J, Xu W, Ren J, Liu X, Lu G, Wang Y (2011) Efficient catalytic conversion of fructose into hydroxymethylfurfural by a novel carbon-based solid acid. Green Chem 13:2678–2681

135. Liu B, Zhang Z, Huang K (2013) Cellulose sulfuric acid as a bio-supported and recyclable solid acid catalyst for the synthesis of 5-hydroxymethylfurfural and 5-ethoxymethylfurfural from fructose. Cellulose 20:2081–2089

136. Liu R, Chen J, Huang X, Chen L, Ma L, Li X (2013) Conversion of fructose into 5-hydroxy-methylfurfural and alkyl levulinates catalyzed by sulfonic acid-functionalized carbon materials. Green Chem 15:2895–2903

137. Russo PA, Antunes MM, Neves P, Wiper PV, Fazio E, Neri F, Barreca F, Mafra L, Pillinger M, Pinna N, Valente AA (2014) Solid acids with SO3H groups and tunable surface properties: versatile catalysts for biomass conversion. J Mater Chem A 2:11813–11824

138. Wang H, Kong Q, Wang Y, Deng T, Chen C, Hou X, Zhu Y (2014) Graphene oxide catalyzed dehydration of fructose into 5-hydroxymethylfurfural with isopropanol as cosolvent. ChemCatChem 6:728–732

139. Moreau C, Durand R, Pourcheron C, Razigade S (1994) Preparation of 5-hydroxymethylfurfural from fructose and precursors over H-form zeolites. Ind Crop Prod 3:85–90

140. Moreau C, Durand R, Razigade S, Duhamet J, Faugeras P, Rivalier P, Ros P, Avignon G (1996) Dehydration of fructose to 5-hydroxymethylfurfural over H-mordenites. Appl Catal A Gen 145:211–224

141. Shi Y, Li X, Hu J, Lu J, Ma Y, Zhang Y, Tang Y (2011) Zeolite microspheres with hierarchical structures: formation, mechanism and catalytic performance. J Mater Chem 21:16223–16230

142. Wang J, Ren J, Liu X, Xi J, Xia Q, Zu Y, Lu G, Wang Y (2012) Direct conversion of carbohydrates to 5-hydroxymethylfurfural using Sn-Mont catalyst. Green Chem 14:2506–2512

143. Liu B, Gou Z, Liu A, Zhang Z (2015) Synthesis of furan compounds from HMF and fructose catalyzed by aluminum-exchanged K-10 clay. J Ind Eng Chem 21:338–339

144. Yang F, Weng J, Ding J, Zhao Z, Qin L, Xia F (2019) Effective conversion of saccharides into hydroxymethylfurfural catalyzed by a natural clay. Attapulgite Renew Energy 151:829–836

145. Sajid M, Zhao X, Liu D (2018) Production of 2,5-furandicarboxylic acid (FDCA) from 5-hydroxymethylfurfural (HMF): recent progress focusing on the chemical-catalytic routes. Green Chem 20:5427–5453

146. Tong X, Yu L, Chen H, Zhuang X, Liao S, Cui H (2017) Highly efficient and selective oxidation of 5-hydroxymethylfurfural by molecular oxygen in the presence of Cu-MnO2 catalyst. Catal Commun 90:91–94

147. Krivtsov I, García-López EI, Marcì G, Palmisano L, Amghouz Z, García JR, Ordóñez S, Díaz E (2017) Selective photocatalytic oxidation of 5-hydroxymethyl-2-furfural to 2,5-furandicarboxyaldehyde in aqueous suspension of g-C3N4. Appl Catal B Environ 204:430–439

148. Hayashi E, Komanoya T, Kamata K, Hara M (2017) Heterogeneously-catalyzed aerobic oxidation of 5-hydroxymethylfurfural to 2,5-furandicarboxylic acid with MnO2. ChemSusChem 10:654–658

149. Han X, Li C, Liu X, Xia Q, Wang Y (2017) Selective oxidation of 5-hydroxymethylfurfural to 2,5-furandicarboxylic acid over MnOx–CeO2 composite catalysts. Green Chem 19:996–1004

150. Gui Z, Saravanamurugan S, Cao W, Schill L, Chen L, Qi Z, Riisager A (2017) Highly selective aerobic oxidation of 5-hydroxymethyl furfural into 2,5-diformylfuran over Mn-Co binary oxides. ChemistrySelect 2:6632–6639

151. Cui M, Huang R, Qi W, Su R, He Z (2017) Cascade catalysis via dehydration and oxidation: one-pot synthesis of 2,5-diformylfuran from fructose using acid and V2O5/ceramic catalysts. RSC Adv 7:7560–7566

152. Zuo X, Venkitasubramanian P, Busch DH, Subramaniam B (2016) Optimization of Co/Mn/Br-Catalyzed oxidation of 5-Hydroxymethylfurfural to enhance 2,5-furandicarboxylic acid yield and minimize substrate burning. ACS Sustain Chem Eng 4:3659–3668

153. Zhang Y, Xue Z, Wang J, Zhao X, Deng Y, Zhao W, Mu T (2016) Controlled deposition of Pt nanoparticles on Fe3O4@carbon microspheres for efficient oxidation of 5-hydroxymethylfurfural. RSC Adv 6:51229–51237

154. Ventura M, Aresta M, Dibenedetto A (2016) Selective aerobic oxidation of 5-(Hydroxymethyl) furfural to 5-formyl-2-furancarboxylic acid in water. ChemSusChem 9:1096–1100

155. Nguyen CV, Liao Y-T, Kang T-C, Chen JE, Yoshikawa T, Nakasaka Y, Masuda T, Wu KCW (2016) A metal-free, high nitrogen-doped nanoporous graphitic carbon catalyst for an effective aerobic HMF-to-FDCA conversion. Green Chem 18:5957–5961

156. Neațu F, Marin RS, Florea M, Petrea N, Pavel OD, Pârvulescu VI (2016) Selective oxidation of 5-hydroxymethyl furfural over non-precious metal heterogeneous catalysts. Appl Catal B Environ 180:751–757

157. Wang S, Zhang Z, Liu B (2015) Catalytic conversion of fructose and 5-hydroxymethylfurfural into 2,5-furandicarboxylic acid over a recyclable Fe3O4–CoOx magnetite nanocatalyst. ACS Sustain Chem Eng 3:406–412

158. Saha B, Gupta D, Abu-Omar MM, Modak A, Bhaumik A (2013) Porphyrin-based porous organic polymer-supported iron(III) catalyst for efficient aerobic oxidation of 5-hydroxymethyl-furfural into 2,5-furandicarboxylic acid. J Catal 299:316–320

159. Sádaba I, Gorbanev YY, Kegnaes S, Putluru SSR, Berg RW, Riisager A (2013) Catalytic performance of zeolite-supported vanadia in the aerobic oxidation of 5-hydroxymethylfurfural to 2,5-diformylfuran. ChemCatChem 5:284–293

160. Bao L, Sun F-Z, Zhang G-Y, Hu T-L (2020) Aerobic oxidation of 5-hydroxymethylfurfural to 2,5-furandicarboxylic acid over holey 2D Mn2O3 nanoflakes from a Mn-based MOF. ChemSusChem 13:548–555

161. Ait Rass H, Essayem N, Besson M (2013) Selective aqueous phase oxidation of 5-hydroxymethylfurfural to 2,5-furandicarboxylic acid over Pt/C catalysts: influence of the base and effect of bismuth promotion. Green Chem 15:2240–2251

162. Siyo B, Schneider M, Pohl M-M, Langer P, Steinfeldt N (2014) Synthesis, characterization, and application of PVP-Pd NP in the aerobic oxidation of 5-hydroxymethylfurfural (HMF). Catal Lett 144:498–506

163. Xu J, Liu J, Ma J, Cai J, Du Z, Ma H (2015) Advances in catalytic synthesis of bio-based dicarboxylic acid. Sci Sin Chim 45:526–532

164. Gorbanev YY, Kegnæs S, Riisager A (2011) Effect of support in heterogeneous ruthenium catalysts used for the selective aerobic oxidation of HMF in water. Top Catal 54:1318–1324

165. Artz J, Palkovits R (2015) Base-free aqueous-phase oxidation of 5-hydroxymethylfurfural over ruthenium catalysts supported on covalent triazine frameworks. ChemSusChem 8:3832–3838

166. Yi G, Teong SP, Zhang Y (2016) Base-free conversion of 5-hydroxymethylfurfural to 2,5-furandicarboxylic acid over a Ru/C catalyst. Green Chem 18:979–983

167. Mishra DK, Lee HJ, Kim J, Lee H-S, Cho JK, Suh Y-W, Yi Y, Kim YJ (2017) MnCo2O4 spinel supported ruthenium catalyst for air-oxidation of HMF to FDCA under aqueous phase and base-free conditions. Green Chem 19:1619–1623

168. Wang F, Yuan Z, Liu B, Chen S, Zhang Z (2016) Catalytic oxidation of biomass derived 5-hydroxymethylfurfural (HMF) over Ru III -incorporated zirconium phosphate catalyst. J Ind Eng Chem 38:181–185

169. Pichler CM, Al-Shaal MG, Gu D, Joshi H, Ciptonugroho W, Schuth F (2018) Ruthenium supported on high-surface-area zirconia as an efficient catalyst for the base-free oxidation of 5-hydroxymethylfurfural to 2,5-furandicarboxylic acid. ChemSusChem 11:2083–2090

170. Antonyraj CA, Huynh NTT, Lee KW, Kim YJ, Shin S, Shin JS, Cho JK (2018) Base-free oxidation of 5-hydroxymethyl-2-furfural to 2,5-furan dicarboxylic acid over basic metal oxide-supported ruthenium catalysts under aqueous conditions. J Chem Sci 130:156

171. Gao T, Yin Y, Fang W, Cao Q (2018) Highly dispersed ruthenium nanoparticles on hydroxyapatite as selective and reusable catalyst for aerobic oxidation of 5-hydroxymethylfurfural to 2,5-furandicarboxylic acid under base-free conditions. Mol Catal 450:55–64

172. Sharma P, Solanki M, Sharma RK (2019) Metal-functionalized carbon nanotubes for biomass conversion: base-free highly efficient and recyclable catalysts for aerobic oxidation of 5-hydroxymethylfurfural. New J Chem 43:10601–10609

Solid Acid-Catalyzed Esterification of Levulinic Acid for Production of Value-Added Chemicals

Kalpana C. Maheria, Aayushi Lodhi, Henilkumar Lankapati, and Rishav Krishna

Abstract In view of the growing threat of climate change, there is a need to put intense research efforts to reverse global warming effects. Use of inexpensive and abundantly available lignocellulose as a carbon source for reducing societal dependence on fossil fuels and anthropogenic CO_2 emissions is vital in the current scenario. There is a need to emphasize on gradual shift from petroleum-based technologies toward renewable feedstock-based technologies for value-added chemical synthesis. Catalytic conversion of low-cost biomass into diversified industrially significant platform chemicals is of great research interest. Lignocellulose-derived levulinic acid (LA) is increasingly gaining attention among industrialists and academicians owing to its useful properties and potential industrial applications. Notable chemicals that are synthesized/derived from LA include levulinate esters, γ-valerolactone, acrylic acid, 1,4-pentanediol, β-acetylacrylic acid, α-angelica lactone, 2-methyltetrahydrofuran, δ-aminolevulinic acid, etc. Among these, levulinate esters find useful applications as plasticizing agents, fragrance chemicals, solvents, intermediates in organic process industries, oxygenate additives in fuels, etc. Levulinate esters are generally obtained by esterification reaction in the presence of suitable acid catalysts, either in homogeneous (liquid acid) and heterogeneous (solid acid) medium. The solid acid catalysts are mostly favored over liquid acids to avoid issues related to handling, separation, regeneration, and disposal due to the corrosive and toxic nature of liquid acids. This chapter presents a brief account on several value-added chemicals that are derived from LA and discussion on homogeneously and heterogeneously catalyzed esterification reaction of LA to yield various valuable levulinate esters. Zeolite-/mesozeolite-catalyzed esterification of LA to synthesize *n*-butyl levulinate and pentyl levulinate has been covered in detail. Zeolites as a heterogeneous catalyst are important in the development of cleaner technologies. This effort will serve as an aid for industrialists and academicians who are working in the area of conceptualizing LA biorefineries.

K. C. Maheria (✉) · A. Lodhi · H. Lankapati · R. Krishna
Department of Chemistry, Sardar Vallabhbhai National Institute of Technology, Surat, Gujarat, India

1 Biomass-Derived Scaffolds

The design and efficient synthesis of versatile molecules marks as a leading research front in today's time. The reaction products—the prime focus—have shared the importance equivocally with the method of production and the side products generated in the process. The "method" of production has imbibed in it an important attribute, viz., the source. Wherein terminologies like environmental degradation and climate change have caught the eye of the world, all associated sectors need to adapt and evolve urgently. The sources mentioned here need to be environmentally compatible at the first place. Naturally available sources come to the mind in a go and upon proper research and enlightenment have taken the frontline of modern research.

Deriving viable chemicals from biologically alive things or part thereof is one such subclass to this horizon of research. The "biomass" enriched with molecular dexterity can be scientifically exploited for the better good—extracting or synthetically converting to numerous derivatives [1].

It has been established till now that this source-class has advantages in versatile domains, and at this point, it becomes important to gist out a few of the *n*-numbered benefits it withholds.

- Environmentally Benign—This point is listed out the first and therefore the primal importance. The source comes from the environment itself and hence should be environmentally aligned and friendly.
- Biological Compatibility—Biomass is compatible to organic matter and also is the biomass-derived product.
- Noncarcinogenic—Most of the bio-derived scaffolds as well as the side products involved in their production process are noncarcinogenic, enhancing their usability.

However, forming an unbiased reference certifies biomass with a few barriers, a low content of energy, discrete availability, seasonality, high content of moisture, and collection costs [1, 2]. In addition, available biomass is highly scarce. As an alternative raw material, on the other hand, biomass would be a preferable resource as chemical manufacturing needs far lower volumes of biomass to fulfill the demand [2–4].

In the current scenario, research toward the conversion of biomass having rich lignocellulose content to produce fuels, chemicals, and energy due to the rapidly increasing global energy consumption and environmental concerns has garnered considerable interest [5–7]. Meeting energy demands in the future will require alternatives and adequate substitution to the prevailing technologies based on fossil fuels with renewable and sustainable carbon-neutral technologies utilizing

lignocellulosic biomass as an important feedstock and raw material. To economically utilize biomass, we should not just aim for a single component but also the other components present. Biomass, in general, is composed of mainly three components: cellulose, lignin, and hemicellulose [8, 9]. All these three components of lignocellulose biomass have signification potential and approaching for one at a time would waste two of the other active components.

The biochemical industry has constantly been driving a dedicated emphasis on the production of some chemical intermediates that can prove to be the building blocks for the subsequent design and synthesis of a family of end-user-centric chemicals. These chemicals, called the "platform chemicals," are the promising candidates that can be transformed into commercially important chemicals. The US Department of Energy (2004) report has made a remarkable amount of reference on the identification of these promising bio-derived platform molecules and presented the well-known list of 12 highly valued building blocks [10]. In their own words, they defined these platform chemicals as follows: "Building block chemicals, as considered for this analysis, are molecules with multiple functional groups that possess the potential to be transformed into new families of useful molecules." Platform chemicals have the potential to create high-value commercial products. However, by merely being intermediaries, they will not add value to the industrial chain. That value can actually be substantiated by transforming these intermediates into high-value end products which can properly be adopted by the end users. Glucose monomers are end products of cellulose (biomass precursor) hydrolysis. And various value-added compounds can be derived from this glucose and the end product obtained based on the type of catalyst selected and reaction conditions adapted. Few of them are sorbitol via hydrogenation reaction, gluconic acid via oxidation, fructose through isomerization, and 5-hydroxymethylfurfural (5-HMF). The latter can be further converted into levulinic acid (LA) through hydration and formic acid through hydrolysis [11].

LA is an important platform chemical produced from a biomass-based feedstock for several petrochemical operations. An extensive literature is available on useful properties and prospective industrial applications of LA and its derivatives [11–13].

2 Levulinic Acid: An Introduction

In the current scenario, LA is gaining considerable attention as it is sourced from biomass and is an essential feedstock for the current petrochemical operations/processing. 4-Oxypentanoic acid, popularly known as levulinic acid, is one of the 12 platform organic chemicals that can be efficaciously derived from biomass and utilized for the economical production of biofuels [11]. The significance of LA is mainly attributed to the presence of carboxylic acid and ketone functional groups in them which can lead to various value-added adducts via several organic reactions.

On the molecular level, conversion of lignin-rich biomass to levulinic acid follows a complicated scheme of reactions involving several byproducts and

intermediates [14]. Cellulose and hemicellulose, two major constituents of biomass, belong to a class of polymers which are carbohydrate-based and can be hydrolyzed to low weight sugars using acid catalysis. The catalytic decomposition of the six-membered sugar fragments (e.g., glucose) produces 5-hydroxymethyl-2-furalde-hyde as an intermediate. This is then subsequently rehydrated giving levulinic acid and formic acid as final products (Scheme 1).

As mentioned in the preceding paragraph, the presence of both the ketone and a carboxylic acid group in the molecule at the same time helps in deriving numerous potent chemicals, to name a few, levulinate esters, acrylic acid, γ-valerolactone, 1,4-pentanediol, α-angelica lactone, β-acetylacrylic acid, δ-aminolevulinic acid, 2-methyl THF, etc. [15]. They have many end-user applications; for instance, 2-methyl-THF (2-MTHF) and levulinic esters may find use as gasoline and bio-diesel additives, respectively. δ-Aminolevulinate, a popularly known herbicide, and various other bisphenol derivatives may substitute bisphenol A with added

Scheme 1 One of the many methods for the derivation of LA from polysaccharides in biomass
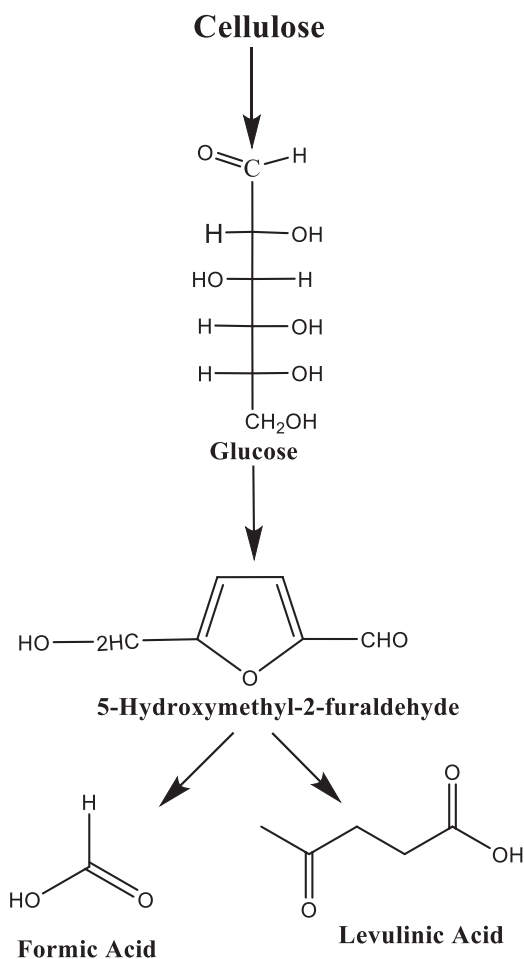
properties [16]. Ethyl levulinate, the product of the esterification reaction between LA and ethanol, is utilized as an oxygenating additive in fuels [17]. Another levulinate ester, *n*-butyl levulinate, is an important intermediate in the organic processing industries for purposes such as solvents, odorous substances, and plasticizing agents [18].

Another important derivative is the γ-valerolactone (GVL) [19], which is a sustainable liquid and is produced by the catalytic hydrogenation of LA [20]. GVL has successfully been used for the synthesis of pentane-1,4-diol, ionic liquids, butene isomers, adipic acid, alkanes, transportation fuels, and polymers [19, 21–25].

Considering the commercial aspects of the levulinic acid, it is reported that DIBANET project (Development of Integrated Biomass Approaches NETwork) focuses on the utilization of organic waste and residues to produce ethyl levulinate and on the production of δ-aminolevulinic acid (DALA) and methyltetrahydrofuran (MTHF) from biologically defined processes. DIBANET aims to promote the collaboration of seven and six universities, respectively, from Latin America and Europe. The budget of the project was €3.7 million. Therefore, it could be concluded that there is a remarkable interest to scale up to the desired production because of its significant potential for both research and industrial applications.

3   Levulinic Acid as a Platform Chemical for Value-Added Products

The presence of dual functional groups like ketone and carboxylic acid made levulinic acid an important platform for the productions of useful value-added products. It is the most important class of gamma-keto acids, which can be derived from the biomass and can undergo various chemical reactions to produce value-added products, such as animal feed, textile dye, coating material, pharmaceuticals, food flavoring agents, polymers, herbicides, anti-freezing agents, etc. [12, 26, 27]. Due to such kind of properties, the US National Renewable Energy Laboratory (NREL) has considered it as the most promising building block for various organic transformations [28].

Levulinic acid can be used to produce γ-valerolactone by hydrogenation reaction. Further hydrogenation of γ-valerolactone gives 1,4-pentanediols, and subsequent hydrogenation affords 2-methyltetrahydrofuran (2-MTHF), which can be used in the lithium rechargeable batteries as the source of electrolyte [29]. Alkyl levulinates can be produced by the esterification reaction of the levulinic acids with various alcohols, which can be utilized as the oxygenated fuels and solvent additives [29] (Scheme 2).

Some of the potentially interesting derivatives of levulinic acid are explained as follows:
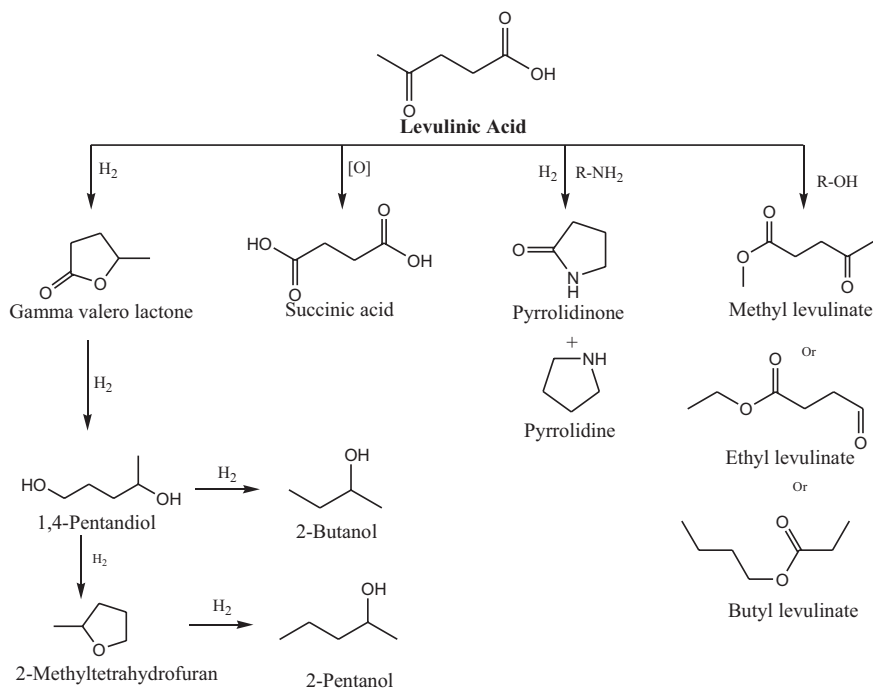
Scheme 2 Few products derived from levulinic acid

3.1 Synthesis of GVL from LA

Hydrogenation reaction of LA gives γ-valerolactone, which is found to be the most sustainable intermediate product and can be further applied to produce renewable biofuels. Horvath et al. [30] have first proposed the potential use of GVL as renewable biofuel, due to its excellent energy carrier property. They have reported two-step process involving Shvo catalyst and GVL as solvent. In the first step, they have applied sulfuric acid as homogeneous acid catalyst for the conversion of fructose into LA. Formic acid is also produced during this step which will further act as an H-donor to convert levulinic acid into GVL. Homogeneous catalyst system has the drawback of separation of the catalyst from the reaction mixture, and hence research in LA conversion through heterogeneously catalyzed system is highly in demand nowadays. Various metal-based catalyst systems have been studied, and among them, Ru-based catalyst system is found to be more efficient for LA conversion with 72% yield of GVL at 800 psi H_2 and about 150 °C temperature [31, 32]. Lin et al. have also found similar observation and confirmed that the catalytic activity of the Ru/C is far better than the compared catalysts, i.e., Raney Ni, Urushibara Ni, and Pd/C [33]. In α-hydrogenation of LA, LA conversion of 92% is observed with 99% selectivity of GVL using Ru/C catalyst in methanol. However, this system which is suffering in terms of reusability of the catalyst due to the leaching of Ru decreases

the conversion gradually. GVL can further be catalytically converted into valuable chemicals and fuels such as 1,4-pentanediol, 2-methyltetrahydrofuran, valeric biofuels, 5-nonanone, and α-methylene-γ-valerolactone (Scheme 3).

3.2 Synthesis of 1,4-Pentanediol and 2-Methyltetrahydrofuran from LA

The use of GVL as a liquid fuel is restricted due to its high solubility in water. Hence, researchers are now focusing on converting GVL to another useful product, which can be further utilized as a biofuel additive. The hydrogenation of GVL produces other useful fuel additives like 1,4-pentanediol (1,4-PDO) and 2-methyltetrahydrofuran (2-MTHF). Palkovits et al. [34] have reported the catalytic hydrogenation reaction of GVL to produce 2-MTHF in a solvent-free reaction condition using Ru/C as heterogeneous catalyst. The conversion of GVL is found to be about 99% with 43% yield of 2-MTHF at 190 °C and 24-h reaction time. Du et al. have reported the conversion of GVL to 2-MTHF with 98% conversion and 93% selectivity over an inexpensive Cu catalyst. They have also reported that if the reaction is carried out at low temperature in the presence of calcined Cu catalyst and H_2 instead of air, the formation of 1,4-pentanediol is observed [35] (Scheme 4).

Direct conversion of LA into 2-MTHF in the presence of noble metal catalysts using 1,4-dioxane and water as a solvent system is reported by Elliott and Frye [35]. The conversion proceeds via the formation of GVL and 1,4-PDO as the reaction intermediates. The literature is also available for the conversion of LA into 2-MTHF via GVL using both homogeneous and heterogeneous catalyst systems. Leiner et al. have reported the homogeneous catalyst system based on Ru with acidic additives to produce 2-MTHF from LA. The best performance, i.e., 92% yield of 2-MTHF, was observed for the $Ru(acac)_3$/triphos catalyst with cooperation of NH_4PF_6 and acidic ion liquid additives at 10 MPa H_2 and 160 °C reaction temperature [36].
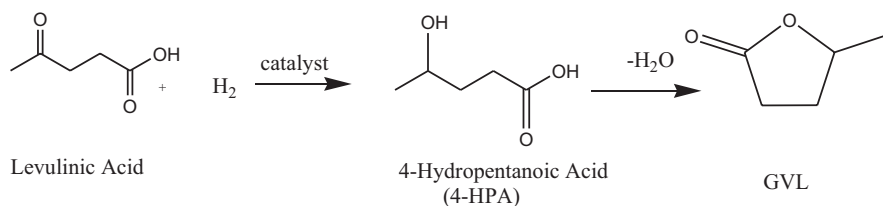
Scheme 3 Synthesis of GVL from levulinic acid
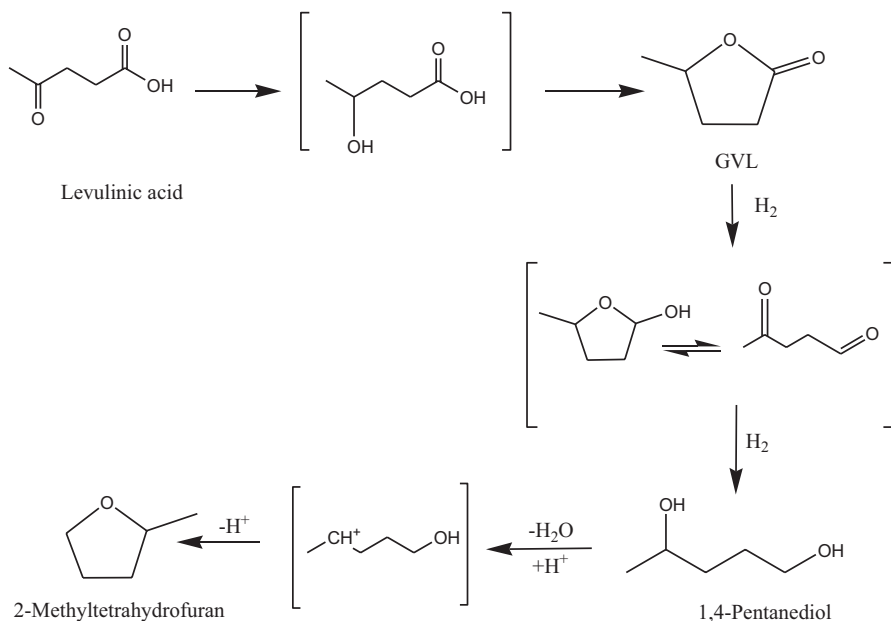
Scheme 4 Synthesis of 1,4-PDO and 2-MTHF from levulinic acid

3.3   Synthesis of Valeric Biofuels from LA

As shown above, GVL and LA as well can be converted to other useful value-added products. Similar to 1,4-PDO and 2-MTHF, GVL and, ultimately, LA can be converted into liquid hydrocarbon fuels like alkanes by applying selective catalytic pathways. The reaction path goes away in two different steps, in which the first step involves the ring opening reaction of GVL and generation of pentanoic acid. While in the second step, the reaction of pentanoic acid with dicarboxylic acid leads to the formation of butenes. Butenes can be further applied as a precursor for the synthesis of C8 alkanes.

Lange et al. [37] have introduced valeric biofuels, which are the new derivatives of LA and are fully compatible as transportation fuels. In the report, GVL is first converted into pentanoic acid over Pt/ZSM-5 as the bifunctional metal acid catalyst. By the use of Pt-based bifunctional catalyst, a yield of up to 90% of pentanoic acid is achieved. Further, pentanoic acid is converted to valerate ester by esterification reaction in the presence of solid acid catalyst and alcohols. Zaccheria et al. have reported the simple one-step process for the production of pentylvalerate from GVL using Cu-supported SiO_2-ZrO_2 catalyst [38] (Scheme 5).
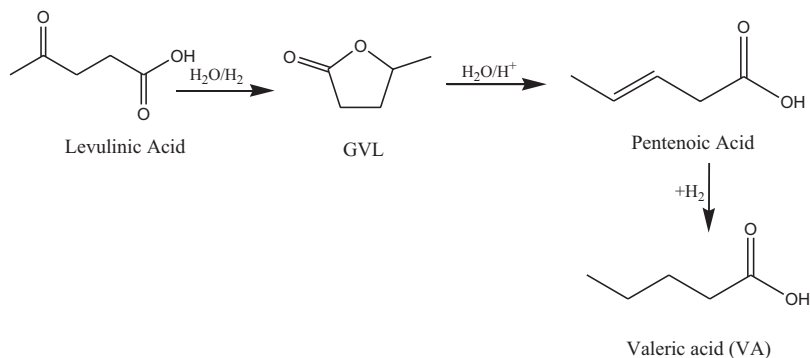
Scheme 5 Synthesis of GVL from levulinic acid

3.4 Synthesis of Succinic Acid from LA

Succinic acid is one of the top 12 value-added products derived from the biomass because it possesses dicarboxylic group at positions 1 and 4. It is another significant value-added chemical that can be obtained from LA. It has various applications and can be used as a fuel additive, polymer, solvent, food/cosmetic/pharmaceuticals, etc. Zeikus [39] was the first to recognize the industrial significance of succinic acid. Succinic acid serves as a pH regulator and flavoring agent and has many medicinal applications [40] such as a antimicrobial agent and vitamin additive and for the production of antibiotics and amino acid synthesis [41]. Succinic acid is also one of the useful precursors for the industrially important chemicals, such as 1,4-butyrolactone, pyrrolidinone, tetrahydrofuran, and g-butyrolactone [42]. Moreover, succinic acid can be produced from LA by oxidation reaction. Dunlop et al. patented the process of oxidation of LA over V_2O_5 as catalyst at higher temperature which is around 360–400 °C [43]. Ru-based magnetic nanoparticles have been efficiently utilized by Parvulescu et al. for the production of succinic acid from LA. One-step conversion of LA to SA has been reported by Kawasumi et al. [44] using I_2/t-BuOK system with 3% H_2O_2. They achieved 83% yield within 1-h room temperature. Dutta et al. have also reported the synthesis of SA through oxidation using H_2O_2 in trifluoroacetic acid. They got 62% yield of SA within 2 h at 90 °C [45] (Scheme 6).

3.5 Synthesis of Pyrrolidinones from LA

Pyrrolidinones are one of the value-added chemicals derived from levulinic acid, which serve as the platform to produce other high value-added chemicals. They are also useful for various industrial applications, such as organic solvents and as precursors in the production of surfactants, and in various pharmaceutical products
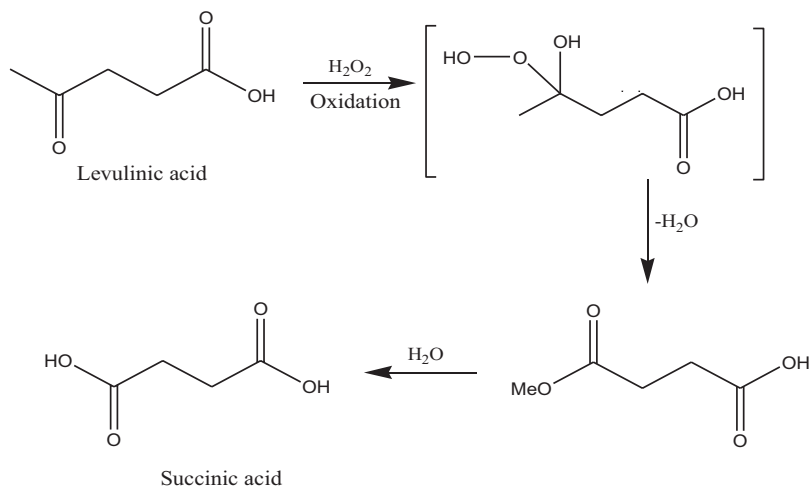
Scheme 6 Synthesis of SA from levulinic acid

[46–48]. The presence of carboxylic groups along with the presence of ketone in the structure of LA provides the possible environment for its conversion into pyrrolidinones via catalytic tandem reductive amination and amidation reactions. The reaction proceeds through the formation of imine, which further gives γ-amino pentanoic acid as an intermediate. Finally, pyrrolidinone is produced via amidation of γ-amino pentanoic acid. Many reports are available for both catalytic systems, i.e., homogeneous and heterogeneous for the transformation of LA into pyrrolidinone. Fu et al. have reported the homogeneous catalyst system based on Ru and formic acid as hydrogen donor [49]. Sun et al. [50] have designed very efficient heterogeneous solid acid catalyst NHC-Ru, which shows excellent activity even after 37 catalytic recycles (Scheme 7).

In heterogeneous catalytic system, the catalysts loaded with metals and metal oxides over the supports show noticeable improved catalytic activity for the reaction of reductive amination. Rode et.al have carried out the synthesis of pyrrolidinones over ZrO_2-supported Au catalyst with formic acid as hydrogen donor [51]. Siddiki and coworkers [52] have developed TiO_2-supported Pt-based catalyst. They have proposed that the Pt sites surrounded by TiO_X species enhance the chemoselectivity of the catalyst and exhibited higher catalytic performance with ~98% yield of pyrrolidinone in the reductive amination process [50]. Other metal alloy-based catalysts were developed by Esposito et al., and they have applied it in the continuous flow reactor. It was observed that there is not any variation found in the activity of catalyst FeNi even after 52.5 h [53]. Further text of the chapter is focused on levulinate esters, the most important levulinic acid-derived value-added chemical.
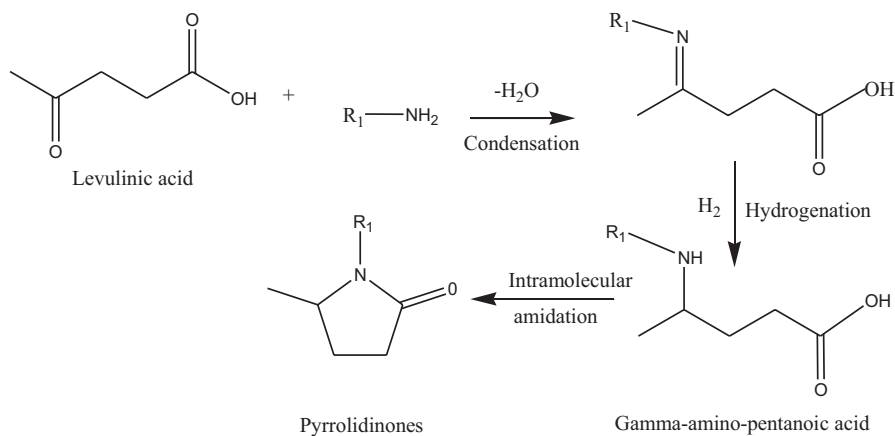
Scheme 7 Synthesis of pyrrolidinones from levulinic acid

3.6 Levulinic Acid-Derived Levulinic Esters: Properties and Applications

Levulinic esters, like methyl levulinates, ethyl levulinates, and *n*-butyl levulinates, can be efficiently produced from the esterification reaction of levulinic acid with various alcohols. Levulinic esters are the most promising and versatile compounds which are regarded as the alternate energy source and a promising replacement of fossil fuels. Various organic transformations (condensation, addition, etc.) are realized in synthetic pathways of biochemicals, due to the presence of keto ester groups of levulinic esters, creating possibility for them to be used as significant platform chemicals in the list of futuristic biorefinery. They can be used as an important intermediate in flavoring and fragrance industries, plasticizer, solvent biofuel additives, etc. In recent times, the utilization of the long alkyl-chain levulinate as the green solvent is explored widely, due to its low cytotoxicity and mutagenicity properties [54]. Levulinates possess remarkable fuel blending properties like low toxicity, stable flash point, higher lubricant property, and moderate flow properties, and because of these properties, they can be efficiently utilized as additives for diesel and gasoline [55]. Grove and co-workers have studied the properties of the diesel blends with various levulinates and other esters as well [56].The study carried out by Lake and Burton for the blend of ultralow sulfur diesel, biodiesel, and ethyl levulinate in a turbocharged engine (3.1 L) indicates possibilities of utilization of ethyl levulinate as the fuel blend. The study shows that the particulate matter and oxides of nitrogen emission were reduced in the EL blend (80% ULSD +13.33% biodiesel +6.47% ethyl levulinate) as compared to the 20% biodiesel blend [57]. Similar kinds of studies have been carried out by Janssen and coworkers; they have investigated the combustion study of the higher blend ratio of BL (60–80%) with *n*-tetradecane, in the single-cylinder diesel engine [58]. They observed soot-free

combustion with this high blend but found incompatibility of the fuel with high butyl levulinate blend with the hoses and sealed engine fuel system. They have also studied a 10% ethyl levulinate blend with diesel fuel and observed reduction in the particulate matter emission up to 50% [59].The blending octane numbers for methyl levulinate, ethyl levulinate, and iso-/secondary butyl levulinate were found to be 106.5, 107.5, and 102.5 [54]. The internal molecule organization, specifically hydrogen bond network, makes alkyl levulinates more compressible. Esters derived from levulinic acid possess very low vapor pressures as compared to the most commonly utilized solvent. Chlorinated solvents show more than 400 kPa vapor pressure, at 100 °C, while methyl, ethyl, and butyl levulinates show very less, i.e., 5.96, 4.69, and 1.56 kPa vapor pressure, respectively. Due to such kind of properties, Bayarri Ferrer et al. have claimed the degreasing efficiency of alkyl levulinates equivalent to the industrially utilized harmful trichloroethylene [60]. They have also reported the VOC classification, cytotoxicity, and mutagenicity data for butyl and pentyllevulinates. According to the reported data, they have confirmed the potential of alkyl levulinate to be utilized as the green solvent [61].

4 Esters and Esterification Reaction: Chemistry

Esters are naturally occurring and vital organic compounds. They are responsible for the fragrant odor of flowers and many fruits (e.g., methyl butanoate in pineapples, isopentyl acetate in banana oil). These pleasant smelling liquids are constitutional parts of animal fats and biologically significant molecules. Esters are commonly made by a nucleophilic acyl substitution reaction between a carboxylic acid and an alcohol. It involves initial protonation of carboxylic acid followed by nucleophilic attack of ROH, an excess of the latter normally being employed to get ester product as it facilitates shifting of equilibrium in the desired direction. Esters result from simply heating a carboxylic acid in methanol or ethanol solution containing a small amount of mineral acid catalyst, as per discovery made by Fischer and Speier in 1895 [62]. In this nucleophilic acyl substitution reaction, free carboxylic acids are hard to be attacked by most nucleophiles, but use of strong mineral acid such as HCl and H_2SO_4 boosts its reactivity. The mineral acid facilitates protonation of oxygen atoms of the carbonyl group, thereby generating positive charge on carboxylic acid, thus making it much more reactive toward nucleophilic attack by alcohol to yield tetrahedral intermediate. Transfer of proton from one oxygen to another generates second tetrahedral intermediate and converts the –OH group into a good leaving group. In the final step, protonated ester is formed by subsequent loss of water, and the final deprotonation step leads to regeneration of acid catalyst to form free ester product. Overall, Fischer esterification is nothing but is simply a substitution of an –OH group by –OR′. The reaction steps involved are all reversible, and one can get either ester or carboxylic acid based on proper selection of reaction conditions. The use of excess alcohol leads to ester formation, whereas the use of excess water leads to carboxylic acid formation via acidic hydrolysis (initial protonation of ester being followed by nucleophilic attack by water).

5   Catalysis for Production of Levulinic Esters

Usually, a catalyst is a substance that increases the rate of reaction without being consumed in the chemical reaction, and the phenomenon occurring when a catalyst acts is termed as catalysis. The word "catalysis" was first coined by Berzelius in 1836, which originates from two words, the prefix cata-, meaning down, and the verb lysein, meaning to split or break [63]. He probably used the term "catalysis" to denote breaking down of the normal forces that are preventing the reaction of molecules. The catalyst primarily influences a chemical reaction, which is already thermodynamically feasible or lowers the reaction temperature at which the reaction achieves a given rate. Catalyst does not alter the equilibrium constant. The progress of catalyzed chemical reaction occurs through new and more energetically favored reaction pathway. Such phenomenon of lowering of activation energy is basic principle of catalysis and applied to all class of catalysis [63].

As far as esterification reaction of levulinic acid with primary alcohols is concerned, the reaction occurs even at room temperature; however, the rate is very slow, which can be accelerated either by using higher temperature and catalyst to get equilibrium conversion within reasonable time period. Conventionally, alkyl levulinates can be obtained by levulinic acid esterification in the presence of mineral acid catalysts such as H_2SO_4, HCl, or H_3PO_4 [64]. A variety of catalysts have been reported for the esterification of levulinic acid to yield levulinate esters that include homogeneous, heterogenized homogeneous catalysts, heterogeneous catalysts, enzymatic catalysts, supported catalysts, etc. An overview of several types of catalysts that are reported for synthesis of levulinic esters is provided herein, in the subsequent text.

In the homogeneous system, it is convenient to manipulate acidic strength by adding acid/water/native solvent. Varkolu et al. [65] demonstrated synthesis of various levulinates via esterification over environmentally benign bio-glycerol-derived carbon-sulfonic acid catalyst. Negus et al. [66] prepared ethyl levulinate using p-toluenesulfonic acid (PTSA) and other mineral acid (HCl, H_2SO_4, HNO_3) homogeneous catalysts. The authors obtained better results with H_2SO_4 and PTSA due to their higher acid strength among all studied catalysts.

In the last two decades, ionic liquids (ILs) have emerged as versatile green building blocks and have wide applications in the area of separation, materials, catalysis, green solvents etc. The use of IL for lignocellulose conversion into value-added chemicals and fuel products is of great research interest. ILs are molten salts at room temperature having wide applications in the area of green chemistry due to its bifunctional role as green solvent and catalyst. Mostly, the IL framework consists of a combination of cation and anion, wherein, IL cation is organic and IL anion is inorganic/organic [67]. The salient properties of ILs that are responsible for increasing the popularity of these materials are good thermal stability, broad liquid state range, non-volatility, better slvation ability, wide electrochemical window, nonflammability, and higher ionic conductivity. They can be a robust reaction medium for organic synthesis due to their better solubilizing and stabilizing behavior to reactive

intermediates [67, 68]. Khiratkar et al. used ionic liquid-based phase-transfer cata-
lyst (sulfonic acid-functionalized benzimidazolium-based poly-IL) for the synthesis
of ethyl levulinate, while Bhanage and coworkers have used imidazole-based IL
(1-methyl-imidazolium hydrogen sulfate) as both a catalyst and a solvent for the
synthesis of levulinates [69].

It is worthy to mention that homogeneous catalysis shows excellent catalytic
activity in esterification reaction. However, major drawbacks associated with such
homogeneous system are difficulty in isolation, corrosiveness of reactor, high reac-
tion temperature, waste disposal, toxicity, non-reusability, non-regeneration, etc.
Such practical difficulties necessitate the need for replacement of such conventional
homogeneous toxic and corrosive acid catalysts with recyclable strong solid acid
(heterogeneous) catalysts in synthetic organic reactions. Thus, the development of
cost-effective and robust solid acid catalyst via energy-efficient synthetic protocols
to improve the yield of levulinic esters is currently of great research interest.

6 Solid Acids as Catalysts for Esterification of Levulinic Acid

According to the name, the solid acid catalysts are the solid materials which work
similar to the liquid catalyst. They provide active surface having active hydrogen
ions and act as a hydrogen donor to produce reaction intermediates, which is further
converted to the desired products by giving back the hydrogen ions [70]. The impor-
tant properties of solid acid catalysts consist of their acidity in terms of Brønsted
and Lewis, the strength of these acid sites in terms of NH_3-TPD, and the surface
properties, i.e., morphology, surface area, and pore size [71].

Reactions of LA with various alcohols using several solid acid catalysts have
been reported, such as various metal oxide (SnO_2, ZrO_2, Nb_2O_5, TiO_2, etc.)-sup-
ported catalysts, various zeolites (HBEA, HZSM-5, H-Y, HMOR, MCM-22, etc.)
(Scheme 8), metal organic frameworks, ion exchange resins, graphene oxides, etc.
[72–77]. The subsequent text covers discussion on major class of heterogeneous
catalysts that are currently in practice for esterification of levulinic acid.

6.1 Metal Organic Frameworks (MOFs)

Porous materials have grabbed significant levels in modern science and technology.
They are strategic materials and have contributed significantly in the area of petro-
leum, catalysis, gas separation, or nuclear storage. Currently, intense research has
been generated for the discovery of new porous materials with larger pores, in order
to cope up with the demand of industry for obtaining special dimensions and shapes.
Metal organic frameworks, abbreviated as MOFs, are such collection of compounds
which contain metal ions linked through molecular species, which first appeared in
the literature in 1997. However, co-ordinatively bridged metal centers with organic
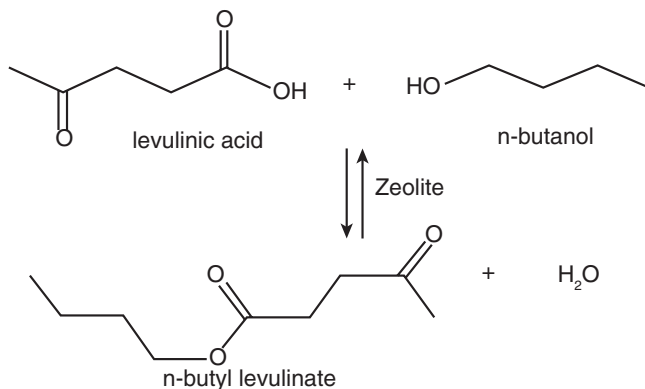
Scheme. 8 Solid acid-catalyzed esterification of levulinic acid

ligand concept were first reported in 1991. They are three-dimensional porous hybrid materials made up of organic units (multidentate hydrophobic linkers) and metal ions (metal-ions-oxo clusters) [78–80]. These organic structures have the potential for manipulation, through varying the metal ions, their counter-anions, organic linkers, and mixed organic linkers and through the control of the architectures and functionalization of the pores [81, 82]. Various combinations of organic unit and metal ion-oxo-cluster generates a library of MOFs. High variability and possibility of modifications are two salient features of MOFs which enables one to design tailor-made MOFs for desired end-use applications [72, 73, 79]. In the last decade, the design and synthesis of such supramolecular assemblies have attracted considerable attention due to their potential applications as smart optoelectronics, magnetic, heterogeneous catalysis, sensors, and gas storage and in separation, due to their inherently high surface areas, uniform and tuneable pore sizes, and ample possibilities for functionalization [80, 83–87]. MOFs may be produced to act as highly selective molecular sieves, sensors, or catalysts. Incorporation of guest species generates sensing capabilities of MOFs. The guest species can be removed and reintroduced reversibly without collapse of the framework [88].

Catalysis is often regarded as a desirable attribute of MOFs. Kim and coworkers [85] studied the enantiopure Zn-based MOFs involving coordination linkages with pyridinium functional groups and demonstrated catalytic activity in transesterification reaction.

An esterification reaction can also be well executed using Brønsted acidity of MOFs, which is attributed to the functional groups present in them. Because of improved mass transport and structure tunability, these materials have tremendous possibilities from the point of view of designing a highly active heterogeneous catalyst for targeted applications [89]. UiO-66 MOF whose nominal composition is $Zr_6O_4(OH)_4(BDC)_6$ (BDC = 1,4-benzene dicarboxylate). This MOF is made of 12-coordinated $Zr_6O_4(OH)_4$ metal clusters (Zr6 nodes linked with benzene dicarboxylate linkers). [90–92]. From catalysis perspective, favorable porosity and

extraordinary high surface area of the MOF improve mass transfer due to enhanced accessibility of active sites, thus increasing the catalytic activity. In particular, the exposed Zr sites exhibit excellent catalytic behavior which offers an advantage of efficiently catalyzing various acid-catalyzed reactions [93]. UiO-66,35, MOFs exhibited robust mechanical, thermal, and chemical stabilities. In addition, versatile synthesis methods and ease of functionalization are other key favorable factors of these MOFs.

Literature is available on use of UiO-66-(COOH) (Zr-based MOF) as a heterogeneous catalyst for levulinic acid esterification with ethanol [94]. The authors have mentioned that, the excellent activity of this MOF, for this reaction stem from synergistic effect between the Lewis acidic Zr clusters and Brønsted acidity due to organic functionality (–COOH groups) within the framework. Such proven Brønsted acidity enables this material to be used as active acid catalytic material for the esterification of biomass-derived acids with alcohols [72, 73, 91, 95]. The authors have mentioned, based on computational studies, that the Zr sites form coordination bonds with carbonyl groups of levulinic acid, while the free carboxylic group forms H-bond with the substrate, facilitating the removal of –OH group from levulinic acid. The author confirmed reusability of catalyst across five runs [94].

Further, the scope exists for applications of MOFs in upgradation of lignocellulosic biomass and biomass-derived platform chemicals, and this area holds much potential for further development. However, there are issues associated with control of orientation of building blocks in the solid state and prediction of resulting framework structure [96]. Due to weak coordination bonding, MOFs are expected to be less thermally stable. Thermal stability can be improved by appropriate combination of ligand and metals, and an introduction of chelate effect can also be beneficial to enhance stability of porous MOFs.

6.2 Ion-Exchange Resins

Resins are organo-polymeric materials that exhibit high surface area, high ion-exchange capacities, and characteristic functional groups which determine the nature of resultant resins [76, 77, 97, 98]. Several types of organic transformations are catalyzed by acid or base, which can be preferentially carried out with ion-exchange resins/solids. Easy separation, ease of continuous operations, loss of valuable reactant, reusability of resin, non-corrosiveness to the reactor, and elimination of removal acid/base from the product mixture and liquid effluent are some of the merits of using ion-exchange solids/resins [99]. One can design tailor-made resins to get selective product with proper choice of monomers and manipulate the degree of cross-linking. However, one has to look into thermodynamic aspects of sorption of reactants and products as it also affects the selectivity problem to a larger extent.

The degree of cross-linking, stiffness, swelling, functionality type, etc. are significant as they largely affect the activity of resins. The swelling property of resin is associated with the flexibility and stiffness of resin which in turn depends on the

amount of cross-linker. Higher cross-linking causes more stiffness and lesser swelling. The gel type Dowex 50Xx2 affords higher yield than macroporous resins in polar media (e.g., esterification of levulinic acid with alcohol) due to swelling which causes enlargement of the pore size, recurrence of new pores, and subsequent improvement in mass transfer of reactants and surface area. Trombettoni et al. [77] used cationic sulfonated resins (Aquivion mP90, micronized pellets of perfluorosulfonic polymer) for esterification of levulinic acid with long-chain alcohols. Ramli et al. [98] have made use of Amberlyst-15 resin as a solid acid catalyst for alkyl levulinate compounds. SO_3H and SO_4 functional groups present in Amberlyst-15 were found to play a crucial role in esterification of levulinic acid. Tejero et al. [76] have carried out an esterification of levulinic acid with butanol by employing Dowex 50Wx2, a gel-type resin. Several other resin-based catalysts such as Amberlyst-based resins, Purolite, Dowex, and polystyrene-supported PTSA are reported for levulinate synthesis. In esterification reaction, the resin which prevents adsorption of byproduct (water molecules) from its own surface performs better and offers higher yield. Adsorption of water declines the catalytic activity and slows down the reaction in the case of resins like Amberlyst and polystyrene-supported PTSA [77, 100]. Amberlyst-70 is found efficient among all macroporous Amberlyst catalysts for levulinate synthesis and found to exhibit exceptional thermal stability and flexibility among all Amberlyst resins [76]. Use of Amberlyst-15 and Amberlyst-70 type of resins, in the reaction medium, is very simple and is less expensive than other resin-based catalysts; hence, they are widely used. So far, inorganic ion-exchange resins like tetravalent metal acid salts are not much explored for levulinic acid esterification reaction.

Resins play a vital role in maintaining appropriate flexibility, hydrophobicity, and porosity in reaction media. However, they could not withstand high boiling stiffness and disintegrate at high temperatures. Moreover, high cost, sluggish thermostability, tendency to form H-bonds, and destabilization of active groups are some of the major challenges associated with such materials [71, 101–103].

6.3   Zirconia

Zirconia (ZrO_2) is the metal oxide-based solid acid catalyst, specifically zirconium metal, which of great interest as it possesses higher catalytic activity with typical characteristic porosity. Such porosity provides easy access to the long-chain and bulky molecules and facilitates smooth mass transport on the pore surfaces [104–108]. It also possesses semiconducting nature, anticorrosion property, and reducing nature [109]. Both Brønsted and Lewis acidities are available in zirconia [109, 110]. Various zirconia-based catalysts have been explored for the synthesis of levulinate esters. Su et al. have synthesized zirconia-supported phosphotungstic heterogeneous solid acid catalyst which is utilized for the production of methyl levulinate from LA. The yield of 99 mol% methyl levulinate was observed at 65 °C, 1:7 LA to methanol ratio in 3-h reaction time [107].

6.4   Carbonaceous Materials

Carbonaceous material is one of the important classes of solid acid catalysts derived from the partial pyrolysis process followed by sulfonation of the carbon-based materials at specified temperature. These types of materials have advantages like high catalyst dispersion ability, high thermal stability, high adsorption capacity, reusability, and easy separation from the reaction mixture [69, 111–116]. Such kind of solid acid catalyst has the ability to hold various protonic sites and shows very good catalyst activity in the various organic reactions like esterification, hydration, and hydrolysis [117]. Carbonaceous materials can be derived by stepwise procedure, pyrolysis, sulfonation, and carbonization [118]. In the second step, sulfonation is carried out by means of mineral acids like sulfuric acid of the carbon materials [119–121], which is further subjected to hydrothermal carbonization process to get the catalytic material [122–124]. Li et al. have synthesized such kind of carbonaceous catalyst using loofah sponge as renewable biomass source and applied for the esterification of ethanol to produce ethyl levulinate. The conversion of LA is obtained up to 91% using this catalyst with satisfactory reusability [112].

Yang et al. [55] have evaluated the catalytic performance of various solid acid catalysts and compared with the carbonaceous solid acid catalysts. Zeolites H-ZSM-5 and H-BEA and resins Amberlyst-15 and Nafion-212 were compared with carbonaceous solid acid catalysts such as GC400 (glucose-derived amorphous carbon) and AC400 (commercial grade activated carbon). It was observed that under optimized reaction conditions, i.e., LA/n-butanol ratio of 1:5, 10% catalyst, 4-h reaction time, and 100 °C temperature, GC400 displayed a much higher catalytic efficiency toward esterification among the studied catalysts (sulfonated active carbon, HZSM-5, Nafion-212). The authors concluded that the high acid (–SO_3H) density and acid strength along with weak acid sites linked on the surface of catalysts (due to –COOH and phenolic –OH) are responsible factors behind the higher catalytic activity of GC400. This fact is found in accordance with the reported literature wherein, the authors (Fernandes et al.) have performed comparative catalytic screening of catalysts [zeolites (ZSM-5, Beta, USY, Mordenite, and MCM-22) (SnO_2, ZrO_2, Nb_2O_5, TiO_2)] for LA esterification reaction. They observed lower activity of zeolite than sulphated oxides, which is attributed to the formation of transition state inside the channel structure rather than acidity of microporous zeolite. Author has mentioned that the same reason is responsible for the activity gap between H-BEA and HZSM-5 i.e. the gap is due to different pore structure [74].

6.5   Solid-Supported Reagents

Solid-supported reagents comprise polymeric/non-polymeric solid supports (alumina, silica, zeolite, etc.) on which reagents (in dissolved form) are supported. In such cases, problems of removal of the products may arise, but if the chemical

reagent is covalently linked to solid support [62], the product can be easily separated from the reaction mixture. Usually, porous support is preferable as it provides higher surface area. Thus, insoluble support provides powerful means to facilitate synthesis. There are several examples of some reactions which are difficult to carry out in homogeneous medium or offer very poor yields which can be effectively carried out with solid-supported reagents under mild reaction conditions with high selectivity.

Silica gel-supported reagents are reported to recover valuable scaffolds [62]. Silica is a low-cost significant inorganic porous solid which is the widely accepted support due to its high surface area and chemical and mechanical stability and the feasibility of surface functionalization [29, 100, 125–129]. Moreover, they possess excellent mechanical stability. Pasquale et al. [29] performed a study of the catalytic activity toward synthesis of ethyl levulinate via esterification of levulinic acid with ethanol over silica-based catalyst. Yang and coworkers [129] studied the synthesis of alkyl levulinates over perchloric acid-decorated nano-porous silica. Enumula et al. demonstrated [125] the use of tungsten oxide-based silica catalyst in alkyl levulinate under continuous mode vapor-phase conditions. Malero et al. [127] performed the synthesis of ethyl levulinates over sulfonic mesoporous silica catalyst. Furthermore, they could reuse the catalyst up to three runs without its regeneration. Ramli et al. [100] carried out the synthesis of methyl levulinate and obtained 69% yield over sulfated silica under mild conditions. Chermahini and Nazeri [128] used Al-MCM-41 as the solid acid catalyst for the synthesis of isobutyl and butyl levulinates. Maggi et al. [126] have successfully utilized silica-supported sulfonic acid catalysts for ethyl levulinate and achieved excellent yield and selectivity for ethyl levulinate. Tungsten oxide-based SBA-16 silica catalyst was found to exhibit better acidity and afforded subsequent yield of levulinate ester, owing to dispersion of dynamic acidic sites of tungsten oxide over larger surface area of SBA-16 [125]. The authors concluded that sulfonic acid mesostructured silica exhibits promising catalytic features such as higher surface area and higher hydrophobicity which lead to higher activity and better recyclability than various homogeneous sulfonic acid catalysts under study (H_2SO_4, PTSA, propylsulfonic acid). It is noteworthy to mention that the silica-based catalyst leads to form the H– bonding in polar solvent (like alcohol in esterification of levulinic acid with alcohol), leading to dissolution of the active functionality of silica-supported catalyst, consequently causing decrease in activity and reusability of the catalyst [29].

Heteropolyacids (HPAs) are well-known as acid catalysts in view of their significant high acidity, redox properties, catalytic activity, pseudo-liquid behavior, and physicochemical properties [130]. HPAs are well-known for its Brønsted acidity. Especially, in organic media, the molar catalytic activity of HPAs is extremely higher as compared to mineral acid like sulfuric acid [131–133]. This feature makes possible to carry out the catalytic reaction through "chemie douce" approach, i.e., a soft chemical route involving lower catalyst concentration and/or at a lower temperature. Moreover, no side reactions occur during HPAs-assisted sulfonation, chlorination, nitration, etc. which are obvious with mineral acids [131, 132]. However, these solid acids are lacking in terms of surface area, thermal stability, uneven

dispersion of the positive charges, solubility in the polar solvent, and porosity. They exhibit very low surface area (typically 1–10 $m^2 g^{-1}$) and low porosity (<0.1$cm^3 g^{-1}$). To overcome these difficulties, these salts are supported on various supports such as titania, zirconia, mesoporous silica, etc. and exchanging the HPAs protons with suitable metal cations [29, 134, 135]. To avoid the leaching issue, hydrophobic graphene-anchored HPAs compounds are reported, which furnish well acidity and are considered as good graphene-based compounds anchored onto HPAs. The HPAs-supported catalysts furnish well acidity and are regarded as good candidates for better conversion of the levulinate compounds, due to their improved surface area and free dynamic active sites required to facilitate the reaction.

Quereshi et al. have prepared zirconia-supported Keggin silicotungstic acid to produce ethyl levulinate from LA and get more than 90 mol% ethyl levulinate at 110 °C in 30 min using a microwave reactor [136]. Pasha and Raj [137] synthesized Zr exchanged phosphotungstic acid with retention of Keggin's structure of TPA and applied to the esterification reaction of LA and ethanol. The authors have successfully demonstrated the use of zirconia to enhance the catalytic activity of the HPAs. Wu et al. [138] have studied extensively porous 3D graphene aerogel-anchored tungstophosphoric acid catalyst for the synthesis of ethyl levulinate. Shimizu et al. [139] prepared Cs^+, Ag^+ Al^{3+},Ti^{4+}, Y^{3+}, Zr^{4+}, Sn^{4+}, and Hf^{4+} salts of tungstophosphoric acid. Among the studied catalysts, Zr0.75TPA has been found to be the best catalyst for the conversion of LA to ethyl levulinate with a yield of 91% in 2 h and at 120 °C. The catalyst also showed five-time reusability. Zhou et al. [140] have assessed the catalytic activity of silver or ammonium co-doped phosphotungstic acid for the synthesis of ethyl levulinate. The catalytic activity of Al-MCM-41 and zirconia-supported dodeca-tungstophosphoric acid for the synthesis of hexyl levulinate and ethyl levulinate, respectively, is also reported [98, 141, 142]. These catalysts displayed excellent recyclability.

Zheng et al. [143] and Wu et al. [144] have undertaken catalytic studies of tungstophosphoric acid supported on graphene oxide and MCM-41 catalysts, respectively, in esterification of LA to synthesize ethyl levulinate. Luan et al. [145] demonstrated the synthesis of alkyl levulinates (ethyl, methyl, and isobutyl levulinates) using organic salt of $H_4SiW_{12}O_{40}$. Dharne and Bokade [18] performed the synthesis of butyl ester from levulinic acid over dodeca-tungstophosphoric acid-treated clay (K − 10). $H_4SiW_{12}O_{40}$ catalyst is reported for the synthesis of several levulinates by Vilanculo et al. [146]. Numerous catalysts are reported for such as heteropolyacid-supported silicalites, heteropolyacid-supported STA-AlSBA-15, and tungstosilicic acid $H_4SiW_{12}O_{40}$-SiO_2 for an efficient synthesis of alkyl levulinates [147–149]. In all cases, the heteropolyacid-supported catalysts performed better than the sole support (Al-SBA15/silica/K10/MCM-41/Al-MCM-41/desilicated H-ZSM-5, etc.).

Several sulfated metal oxides (SnO_2, ZrO_2, Nb_2O_5, TiO_2) have also been used as solid acid catalysts for esterification reactions including zeolites. Since the last decade, we have been working in the area of zeolite-/mesozeolite-catalyzed organic transformations including an esterification reaction of levulinic acid for the

synthesis of *n*-butyl levulinate. Further text of the chapter provides insight of our related research efforts, starting with a brief introduction to zeolites.

7　Synthesis of Levulinic Esters Using Zeolites as Solid Acid Catalysts

Zeolites are inorganic crystalline materials of aluminum and silicates having an intricate and delicate porous structure. These materials are distinguished in terms of the framework "corner atoms" and have cavities and channels in their design. Different constituent atoms and their subsequent arrangements lead to a plethora of structures which are formally attributed with a nomenclature by the Structure Commission of the International Zeolite Association (IZA-SC) [150]. The famously known sieves, viz., zeolites, MOFs, aluminophosphates, as well as a few other silicates, fall under this category. Although each of these materials is equally important and finds relevant applications in various fields [151, 152], the likes of zeolites and silicates are many in the recent times [153].

Zeolites are naturally occurring three-dimensional microporous aluminosilicates interlinked by oxygen atoms and possessing specific sized molecular pores, cavities, and channels.

Henceforth, they are widely used as ion-exchange materials, adsorbents, and solid acid catalysts in various industrial sectors, like oil refining plants, petroleum industry, water purification, wastewater treatment plants, and perfumery industry, and in effluent treatment. Due to the presence of uniform molecular cavities, pores, and channel system, they allow entry of selective molecules which in turn depends on the size of channels, pores, and cavities [69, 154–159]. The constituent atoms can be replaced by a variable number of other elements imparting interesting properties and the same applicability. The channels and cavities possess a diameter in the range of 0.3–1.3 nm, depending upon the structure. Generally, the values of internal surface area and pore volume are 800 m^2 g^{-1} and 0.35 cm^3 g^{-1}, respectively [160, 161].

A comprehensive insight into the formation, mechanistic growth, as well as structures of the zeolitic materials has been elaborately presented by Barrer and Richard [162]. They present the growth and crystallization mechanism as a bottom-up phenomenon wherein small preformed framework building blocks known as the secondary building units (SBUs) condense into the three-dimensional microporous structures [150]. The synthesis strategy of microporous zeolites involves the precursors, viz., alumina and silica polycondensed using the sol-gel process. The method often involves the use of structure-directing materials commonly termed as templates. The templates bring about a horizon of crystalline structures that can be synthesized and put forward into applications. The templates used are mostly organics of amines, quaternary ammonium cations, cyclic ethers, and coordination compounds (or the organometallics) [163]. A perfect highly ordered porous structure

imparts the properties of sieving and selective catalysis. Moreover, the presence of compensating cations in its structure adds the properties of ion exchangeability and catalysis.

Zeolites have established themselves as efficient catalysts for various industrial and laboratory-scale reactions. This catalytic activity is expressed by the Brønsted as well as Lewis acid sites present in their framework [164]. The pores (of varied ring sizes) of zeolites can always act as encapsulating agents for guest species of adequate sizes. These species can be treated and reacted inside these pores, given the catalytically active sites present in their structure. They also endow the advantages of high thermal stability and easy availability of the precursors for production [165]. Zeolites contain ambient number of Brønsted acid sites. The number of these sites will be equivalently proportional to the number of aluminum atoms present in the zeolitic framework. These sites can be highly active as proton donors to a number of catalytic reactions. Substitution of silicon atoms with high valence metals like tin, titanium, and zirconium can help produce Lewis acid sites into the zeolitic framework. Reactions which require Lewis acidity can be run inside the pores of these catalysts. A relevant example that requires Lewis acidity is the aldol condensation of keto esters generating diacid esters as products. Also, zeolites can be modified to introduce both Lewis and Brønsted acidities to their overall framework. These come handy in reactions which require both of these catalytic sites in different steps.

The most fundamental and conventional catalytic activity shown by a zeolite is that of ZSM-5 for the selective formation of the *para*-isomer of xylene [166]. The catalytic activity of zeolites owes to the presence of both Lewis and Brønsted acidic sites in their three-dimensional framework. The cavities in these porous materials can effectively embed small molecules and can henceforth act as reactors. Moreover, the heterogeneous nature of the catalyst adds the benefits of easy separation and reusability. The refining and petrochemical industry depends heavily on zeolites as catalysts for carrying out several important chemical processes [167, 168]. To name a few, cracking, cyclization, isomerization, dehydrogenation, and transalkylation are some of the reactions applying zeolites as catalysts [165]. The channels present in their structures imply properties of proton and ion conduction to these materials.

Although microporous zeolites have several advantages attributed to their name, a pore size of 2 nm is considerably small. Also, the accessibility to these pores is tough and is limited only to small molecules. To address these problems in virtue, the design of materials having bigger cavities is critically being looked upon.

The strategies commonly applied for the design of these materials having "mesopores" may be one of the following:

1. Pre-synthesis strategy—Supramolecular aggregates like surfactants and block copolymers have sizes in the dimensions of a few nanometers. Their use as a template for the structural development of large pored zeolitic materials is obvious. A research group at Mobil Oil Corporation was the first one to adopt this strategy [169], and henceforth, they did prepare the mesoporous silica which is today famously known as the MCM.

Surfactant molecules of different chain lengths can help design zeolitic pores of varying dimensions [170]. The same is the case with the block copolymers. These templating molecules can then be subsequently removed after the utility using various methods (preferably a calcination treatment).

2. Post-synthesis strategy—The removal of silicon and/or aluminum atoms present within the framework leads to an effective increase in the void size. Respectively called as desilication and dealumination, they can efficiently be carried forward by the treatment of varying alkali and acid concentrations, respectively (Fig. 1).

In case of conventional zeolites, being its crystal size in micrometer range, they suffer lack of external surface, thereby external active sites and whatever active sites available are located inside the microporosity of zeolite; hence, the accessibility to these pores is tough and is limited only to small molecules. This feature limits to utilization of potential of zeolites to a fuller extent. One of the solutions to this shortcoming is reduction of crystal size to enhance the external surface, i.e., formation of nanozeolites. These nanozeolites (pore size <100 nm) with high external surface area and narrow pore size distribution have wide applicability as film preparation/coating materials.

The porosity of zeolite need not be uniform and highly ordered always. Instead of the conventional uniformity setup, different pore systems with varying dimensions can be imbibed into the zeolitic material. Building such a "multimodal" system helps build hybrid composite materials with several added features and properties. Trends in the development of less hindered and more active cavities have led to the development of the multiple porosity containing zeolites (usually micro- or mesoporous) and are often termed as the "hierarchical zeolites." They serve to increase external surface and accessibility to pores. These materials possess secondary porosity along with typical and uniform microporosity of zeolites. This secondary porosity may comprise of varied porosity range from supermicropore to mesopores/marcropores. Mostly, it lies in mesopore range depending upon the method of synthetic modification involved in making of hierarchical zeolites. General post-synthetic approaches for hierarchical zeolites are depicted in Fig. 2 [171–173]. Synthetic strategies are classified into major top-down (demetallation) and bottom-up approaches (use of soft and hard templates/template-free) [174].
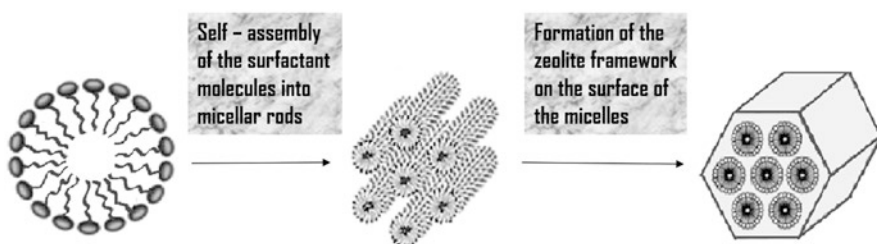
Fig. 1 The use of surfactant molecules as templates for the synthesis of zeolite nanorods

The procedure of dealumination used for making hierarchical zeolites involves severe acid treatments that can severely damage the zeolite framework. Moreover, the process involves the reduction in the number of interconnecting channels from the external surface to the pores leading to a serious accessibility drawback [173]. Henceforth, the process of desilication for the generation of mesoporosity is often preferred over the dealumination one. It is reported that hierarchical zeolites prepared by desilication offer better mesopore accessibility and preserved acidity as compared to those by dealumination [175]. Ogura et al. in their studies concluded that desilication process could be a promising approach for creation of uniform mesoporous framework structure with zeolitic acidity [176]. During desilication, base treatment causes leaching of Si species from zeolite framework, creating interconnected mesopores that are accessible from the external surface of zeolite.

The use of templates is regarded as less energy efficient and environmentally benign with high temperature requirement for toxic organic template removal and greenhouse gas emission during its combustion. Zhijie Wu and coworkers have recently reviewed green synthesis of hierarchical zeolites [177].

Hierarchical zeolites possess several advantages over microporous zeolites, such as improved mass transport of reactants, facilitated by mesopores, due to enhanced accessibility of the acid sites, and due to shorter diffusion path length of hierarchical materials, products retained for lesser time in micropores, thus causing reduction in probability of side reactions which consequently increases preference toward primary products and enhances the catalyst's life by improving the transport of coke precursors out of the catalyst. Also, they are far better over individual mesoporous
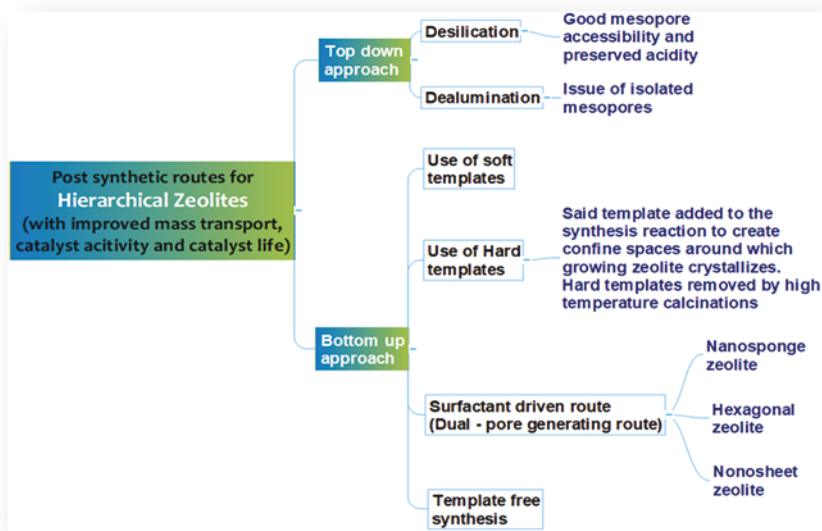
Fig. 2 General post-synthetic routes for hierarchical/mesozeolites

materials in terms of hydrothermal stability (due to introduction of zeolite building blocks on the surface of mesoporous walls), which leads to improved reusability of the catalyst in many organic reactions' regeneration cycles, and zeolitic acidity, which creates new possibilities for applications of mesoporous zeolites in the catalytic reactions demanding strong acidity [171]. Due to such positive attributes, hierarchical zeolites are preferable and gaining attention as heterogeneous catalysts/ supports to execute various organic transformations involving demanding acidity and bulkier entities (which is generally the case with fine chemical synthesis) over conventional zeolites due to their improved catalytic activity. One can envisage the wide utility of mesozeolites and their functionalized derivatives for biomass-derived chemical synthesis. Verboekend and Pérez-Ramírez [178] have provided in-depth discussion on the catalyst design aspect of mesoporous zeolites for catalytic applications from the point of view of synthesis-property-function relationship. They suggested that the functionalization of mesopores can exposed zeolites to novel applications; however, one has to think of large-scale synthesis of mesozeolites/ hierarchical zeolites in which the shape of the catalyst is a key factor, as each size has its different role to play. Activity, intracrystalline mass transport, and practical implementation for mesozeolite synthesis are key functions of micropores, mesopores, and shape-geometry, respectively. Further, the authors suggested that, for large-scale industrial success, one has to look into the economic aspect critically while keeping in mind both the production cost and advantage in catalysis which demands for close collaborations between inventors and industrial partners.

Zeolites have extensively been used for the preparation of numerous ester derivatives, an important one being alkyl levulinates. Since the last decade, our research group has been engaged on research related to the development of environmentally benign methods for the synthesis of complex drug molecules via multicomponent reactions and the conversion of biomass-based derivatives into value-added chemicals, especially esterification of biomass-derived levulinic acid to produce *n*-butyl levulinates using hierarchical zeolite catalysts.

Initially, attempts have been made for the development of mesozeolite BEA (via desilication approach using alkali-treated zeolite precursors) and employing them in biologically active drug-like molecules [derivatives of dihydopyridinones (DHPMs), dialkylpyrimidinones (DAPMs), amino alkyl naphthols (AANs), etc.]. In this research, the success of mesozeolites is realized as improved catalytic activity is observed in case of the synthesis of bulkier products as compared to parent zeolite H-BEA catalyst. In the subsequent research, several mesoporous zeolites (meso-ZSM-5 and meso-H-BEA) have been developed after employing a series of synthetic modifications in terms of change in reaction conditions, use of varied templates [surfactants: [cetyltrimethylammonium bromide (CTAB), tetradecyltrimethylammonium bromide (TTAB)], rice husk, pH, stirring period, etc.], etc. [179, 180]. The resulting hierarchical materials were characterized for their morphology (by SEM/TEM/low- and wide-angle XRD, ^{27}Al and ^{29}Si-MAS-NMR), thermal stability (by TG-DTA), elemental analysis (by ICP-AES), surface area (by BET), pore volume (by BJH), acidity (by NH_3-TPD), etc. using several sophisticated analytical techniques [181, 182].

Maheria et al. demonstrated a study of the effect of different protozeolites of varied catalytic characteristics on % LA conversion into *n*-butyl levulinate. This butyl ester is one of the value-added chemicals as mentioned earlier in the text and finds its wide applications as a reaction intermediate in bio-based chemical synthesis, a plasticizing agent, a solvent, and an odorous substance. One hundred percent selectivity and higher % LA conversion was obtained in case of H-BEA zeolite owing to its three-dimensional structure along with its moderate acidity and medium pore size. The order of catalytic activity was found as H-BEA > H-Y > H-ZSM-5 > H-MOR [183].

Subsequent research was focused on generating hierarchical zeolites (meso-H-ZSM-5 and meso-H-BEA) and applying them as solid acid catalysts in levulinic acid esterification reaction to synthesize *n*-butyl levulinate [179, 180, 182]. Morawala et al. synthesized mesozeolite BEA using controlled desilication by sol-gel method with the help of rice husk, CTAB, and microporous zeolite BEA precursor. Zeolite BEA derivatives have been synthesized with rice husk and CTAB (designated as MCRK) and with only CTAB surfactant (designated as MCCK). The bimodal porosity of mesozeolite BEA is confirmed by XRD, BET surface area, solid-state NMR, and thermal (TGA) analysis. Both mesozeolites were found to exhibit higher thermally stability as compared to the parent zeolite. MCRK was found more thermally stable as compared to MCCK and parent H-BEA, which may be due to thicker walls (due to introduction of zeolite building units into the mesopore walls) of MCRK and MCCK. They concluded that use of rice husk has contributed toward increasing the thermal stability of the compounds. Also, upon analysis of spent catalysts, the authors have observed enhanced ability of mesozeolite to retain acidity after converting microporous structure of zeolite H-BEA into hierarchical structure. Further, the surface area of both mesoporous materials was found higher as compared to parent microporous H-BEA. Both hierarchical zeolites performed better than parent microporous zeolite BEA in LA esterification to generate *n*-butyl levulinate. Higher % LA conversion (95.6%) and selectivity (91%) were observed in the case of MCRK as compared to parent H-BEA and MCCK due to higher acidity and lower Si/Al ratio of MCRK. The authors observed the preferential order of activity as MCRK > MCCK > parent H-BEA (18) > Al-MCM-41 [182].

Further, an attempt was made to synthesize mesoporous zeolite BEA using TTAB surfactant as structure-directing agent via desilication approach. Further, catalysis efficiency of synthesized mesozeolite BEA (MTCK) was studied toward synthesis of *n*-butyl levulinate from LA esterification. An optimization study was undertaken using the Box-Behnken method. The material was characterized by using usual catalyst characterization techniques. MTCK was found to exhibit improved surface area and acidity and possess bimodal porosity. XRD and BET surface area analysis confirmed the creation of mesopores within microporous zeolite H-BEA. The authors obtained a 99.4% LA conversion, 91.51% yield, and 99% selectivity of *n*-butyl levulinate, over micromeso-MTCK catalyst under reaction condition of 120 °C reaction temperature and 13% catalyst concentration. At optimized process parameters (by BBD), an optimum of 99.44% LA conversion was obtained. From response surface methodology analysis, reaction time parameter is

found as the most influential parameter in the esterification of LA with *n*-butanol over MTCK catalyst. The catalyst reusability study was performed up to four catalytic runs, and the catalyst was found reusable without any significant loss of its activity. The authors claimed that the green protocol developed for LA esterification to synthesize *n*-butyl levulinate can also be further explored in green conversion of other biomass-derived scaffolds into other value-added chemicals [180].

Many other researchers are working on esterification of levulinic acid with various alcohols to synthesize alkyl levulinates. Several reports exist on use of various zeolite-based catalysts for alkyl levulinate synthesis. Some examples of use of hierarchical zeolites BEA with a secondary porosity were reported [159] and Nandiwale et al. [157]-synthesized ZSM-5 mesozeolites through a post-synthetic extraction of framework silicon with NaOH. Newly introduced mesoporosity was found to contribute in enhancing the catalytic activity of these materials in the esterification of levulinic acid with ethanol. Hierarchical ZSM-5 zeolite obtained by desilication has also been used as support to incorporate a second acid functionality, like dodecatungstophosphoric acid [184]. The study revealed that modified desilicated H-ZSM-5 gives higher yield as compared to the parent H-ZSM-5 zeolite, due to the increase of higher surface area after desilication. Modification through desilication involves the extraction of silicon selectively, thus enhancing the surface area, generating mesoporosity, and increasing the mass transfer at the catalytic active sites [154, 157, 184].

8   Concluding Remarks and Outlook

LA provides remarkable potential for the development of several linear as well as heterocyclic systems and an economical alternative to the carbon-derived fossil fuels for designing novel derivatives. Researches in the field promise a larger objective of conversion of biological residues and wastes into sophisticated synthesized valuable chemicals. LA, however, having a potential for dozens of other molecules, has had the authors inclined toward the class of molecules—levulinate esters— which are being used in numerous industries in today's time and promise of greater utilization in several other undiscovered applications. The conversion is an esterification reaction with alcohol molecules, requiring the presence of an acid catalyst.

Catalyzing the above-said reaction has seen a groundbreaking research with scientists bringing out several moieties for undergoing the strenuous transformation with an optimum yield. Research has yielded featured materials like MOFs, zirconia, heteropolyacids, zeolites, and even carbonaceous and supported catalytic entities for the aforementioned purpose [93, 180, 182, 183, 185, 186]. Special focus has been on zeolites, which possess sized pores which can be engineered using processes like dealumination, desilication, as well as the merging of two or more zeolite molecules with a high yield and affinity toward the reactant molecules.

The monitoring of the reaction however becomes a bit difficult and hard to handle, requiring the confirmation of the same using several spectroscopic techniques,

given that the boiling points of the reactants and the product near each other with a narrow margin. This situation becomes tedious in the case of lower molecular weight alcohols which are in actuality very near in boiling point to levulinic acid. Also, the generation of the zeolites sometimes requires high-temperature transformations for several hours making the processes highly energetic ones [182]. Decreasing the same using alternative methods is another aspect of research scientists are working upon. The process of desilication is often favored over dealumination for several reasons proposed in the chapter. Stability of the catalyst is a property that forms a primal importance, as the regeneration of catalyst goes through intensive temperatures as mentioned above. Frutiful results have show that zeolite catalysts have high stability due to which they can withstand temperatures as high as 823 K with an almost the same activity even after two catalytic cycles [182].

Hierarchical zeolites have also been introduced in this chapter, showing a promising future with multimode porosity, high acidity, high catalytic activity, high stability, and optimum yields [187]. This blend shows manifold active sites in the moieties with adequate pore sizes for the reacting molecules. Several pathways for their generation were also brought into notice of the readers for further synthesis pursuits.

With an emphasis on lignocellulose biomass-derived economically viable chemicals instead of the hydrocarbon-based one, increased research in the field is a call of the hour. Given the manifold advantages of the translational processes involved outweighing the equally important challenges, several associated industrial sectors in a larger front will be impacted. Henceforth, further research work employing the development and design of efficacious solid acid catalysts for the purpose as well as the understanding of important processes for the decomposition of biomasses into important derivatives is necessary for an enhanced economical and commercial production of the value-added chemicals being referred to in this chapter.

References

1. Laurijssen J, Marsidi M, Westenbroek A et al (2010) Resources, conservation and recycling paper and biomass for energy? The impact of paper recycling on energy and CO2 emissions. Resour Conserv Recycl 54:1208–1218. https://doi.org/10.1016/j.resconrec.2010.03.016
2. Urbaniec K, Bakker RR (2015) Biomass residues as raw material for dark hydrogen fermentation – a review. Int J Hydrog Energy 40:3648–3658. https://doi.org/10.1016/j.ijhydene.2015.01.073
3. Matti Parikka (2004) Global biomass fuel resources. 27:613–620. https://doi.org/10.1016/j.biombioe.2003.07.005
4. Singh P, Sulaiman O, Hashim R et al (2013) Using biomass residues from oil palm industry as a raw material for pulp and paper industry: potential benefits and threat to the environment. Environ Dev Sustain 15:367–383. https://doi.org/10.1007/s10668-012-9390-4
5. Sheldon RA, Sheldon R (2014) Green and sustainable manufacture of chemicals from biomass: state of the art several books on catalysis as well. Green Chem 16:950–963. https://doi.org/10.1039/c3gc41935e

6. Van Haveren J, Scott EL, Sanders J (2008) Bulk chemicals from biomass. Biofuels Bioprod Biorefin 2:41–57. https://doi.org/10.1002/bbb

7. Zhang Y, Bi P, Wang J et al (2015) Production of jet and diesel biofuels from renewable lignocellulosic biomass. Appl Energy 150:128–137. https://doi.org/10.1016/j.apenergy.2015.04.023

8. Raveendran K, Ganesh A, Khilar KC (1996) Pyrolysis characteristics of biomass and biomass components. Fuel 75:987–998. https://doi.org/10.1016/0016-2361(96)00030-0

9. Vassilev SV, Baxter D, Andersen LK, Vassileva CG (2010) An overview of the chemical composition of biomass. Fuel 89:913–933. https://doi.org/10.1016/j.fuel.2009.10.022

10. Werpy T, Petersen G (2004) Top value added chemicals from biomass: volume I -- results of screening for potential candidates from sugars and synthesis gas full record other related research. US Department of Energy (US). https://doi.org/10.2172/15008859

11. Muranaka Y, Suzuki T, Sawanishi H, et al (2014) Effective production of levulinic acid from biomass through pretreatment using phosphoric acid, hydrochloric acid, or ionic liquid 53, 11611−11621. https://doi.org/10.1021/ie501811x

12. Morone A, Apte M, Pandey RA (2015) Levulinic acid production from renewable waste resources: bottlenecks, potential remedies, advancements and applications. Renew Sust Energ Rev 51:548–565. https://doi.org/10.1016/j.rser.2015.06.032

13. Pileidis FD, Titirici M-M (2016) Levulinic acid biorefineries: new challenges for efficient utilization of biomass. ChemSusChem 9:562–582. https://doi.org/10.1002/cssc.201501405

14. Pradipta MSA, Purnamasari NR, Pradana YS (2019) Levulinic acid synthesis from Indonesian sugarcane bagasse using two-step acid catalyzed treatment. AIP Conf Proc 2085:20065. https://doi.org/10.1063/1.5095043

15. Leonard RH (1956) Levulinic acid as a basic chemical raw material. Ind Eng Chem 48:1330–1341. https://doi.org/10.1021/ie50560a033

16. Sasaki K, Watanabe M, Tanaka T, Tanaka T (2002) Biosynthesis, biotechnological production and applications of 5-aminolevulinic acid. Appl Microbiol Biotechnol 58:23–29. https://doi.org/10.1007/s00253-001-0858-7

17. Windom BC, Lovestead TM, Mascal M et al (2011) Advanced distillation curve analysis on ethyl levulinate as a diesel fuel oxygenate and a hybrid biodiesel fuel. Energy Fuel 25:1878–1890. https://doi.org/10.1021/ef200239x

18. Dharne S, Bokade VV (2011) Esterification of levulinic acid to n-butyl levulinate over heteropolyacid supported on acid-treated clay. J Nat Gas Chem 20:18–24. https://doi.org/10.1016/S1003-9953(10)60147-8

19. Marosvölgyi-Haskó D, Lengyel B, Tukacs JM et al (2016) Application of γ-valerolactone as an alternative biomass-based medium for aminocarbonylation reactions. ChemPlusChem 81:1224–1229. https://doi.org/10.1002/cplu.201600389

20. Wright WRH, Palkovits R (2012) Development of heterogeneous catalysts for the conversion of levulinic acid to g-valerolactone. ChemSusChem 5:1657–1667. https://doi.org/10.1002/cssc.201200111

21. Bond JQ, Alonso DM, Wang D, et al (2010) Integrated catalytic conversion of g-Valerolactone to liquid alkenes for transportation fuels. 1110–1115 https://doi.org/10.1126/science.1184362

22. Fegyverneki D, Orha L, Láng G, Horváth IT (2010) Gamma-valerolactone-based solvents. Tetrahedron 66:1078–1081. https://doi.org/10.1016/j.tet.2009.11.013

23. Orha L, Tukacs JM, Gyarmati B, Szilágyi A, Kollár L, LTM (2018) Modular synthesis of γ-valerolactone-based ionic liquids and their application as alternative media for copper-catalyzed ullmann-type coupling reactions. ACS Sustain Chem Eng, vol 6, p 5097. https://doi.org/10.1021/acssuschemeng.7b04775

24. Xue Z, Zhao X, Sun R, Mu T (2016) Biomass-derived γ-valerolactone-based solvent systems for highly efficient dissolution of various lignins: dissolution behavior and mechanism study. ACS Sustain Chem Eng 4:3864–3870. https://doi.org/10.1021/acssuschemeng.6b00639

25. Zhang Z (2016) Synthesis of g-valerolactone from carbohydrates and its applications. ChemSusChem 9:156–171. https://doi.org/10.1002/cssc.201501089

26. Kang M, Kim SW, Kim JW et al (2013) Optimization of levulinic acid production from Gelidium amansii. Renew Energy 54:173–179. https://doi.org/10.1016/j.renene.2012.08.028
27. Rackemann DW, Doherty WOS (2011) The conversion of lignocellulosics to levulinic acid. Biofuels Bioprod Biorefin 5:198–214. https://doi.org/10.1002/bbb.267
28. Bozell JJ, Petersen GR (2010) Technology development for the production of biobased products from biorefinery carbohydrates - The US Department of Energy's "top 10" revisited. Green Chem 12:539–554. https://doi.org/10.1039/b922014c
29. Pasquale G, Vázquez P, Romanelli G, Baronetti G (2012) Catalytic upgrading of levulinic acid to ethyl levulinate using reusable silica-included Wells-Dawson heteropolyacid as catalyst. Catal Commun 18:115–120. https://doi.org/10.1016/j.catcom.2011.12.004
30. Horváth IT, Mehdi H, Fábos V et al (2008) γ-Valerolactone-a sustainable liquid for energy and carbon-based chemicals. Green Chem 10:238–242. https://doi.org/10.1039/b712863k
31. Tang X, Zeng X, Li Z et al (2014) Production of γ-valerolactone from lignocellulosic biomass for sustainable fuels and chemicals supply. Renew Sust Energ Rev 40:608–620. https://doi.org/10.1016/j.rser.2014.07.209
32. Yan K, Yang Y, Chai J, Lu Y (2015) Catalytic reactions of gamma-valerolactone: a platform to fuels and value-added chemicals. Appl Catal B Environ 179:292–304. https://doi.org/10.1016/j.apcatb.2015.04.030
33. Yan ZP, Lin L, Liu S (2009) Synthesis of γ-valerolactone by hydrogenation of biomass- derivedLevulinic acid over Ru/C catalyst. Energy Fuels 23:3853–3858. https://doi.org/10.1021/ef900259h
34. Al-Shaal MG, Dzierbinski A, Palkovits R (2014) Solvent-free γ-valerolactone hydrogenation to 2-methyltetrahydrofuran catalysed by Ru/C: a reaction network analysis. Green Chem 16:1358–1364. https://doi.org/10.1039/c3gc41803k
35. Elliott DC, Frye JG (1999) Hydrogenated 5-carbon compound and method of making, United States Patent, Patent Number US005883266A
36. Geilen FMA, Engendahl B, Harwardt A et al (2010) Selective and flexible transformation of biomass-derived platform chemicals by a multifunctional catalytic system. Angew Chem Int Ed 49:5510–5514. https://doi.org/10.1002/anie.201002060
37. Lange JP, Price R, Ayoub PM et al (2010) Valeric biofuels: a platform of cellulosic transportation fuels. Angew Chem Int Ed 49:4479–4483. https://doi.org/10.1002/anie.201000655
38. Zhu R, Jiang JL, Li XL et al (2017) A comprehensive study on metal triflate-promoted hydrogenolysis of lactones to carboxylic acids: from synthetic and mechanistic perspectives. ACS Catal 7:7520–7528. https://doi.org/10.1021/acscatal.7b01569
39. Zeikus JG (1980) Chemical and fuel production by anaerobic bacteria. Annu Rev Microbiol 34:423–464
40. Akhtar J, Idris A, Abd Aziz R (2014) Recent advances in production of succinic acid from lignocellulosic biomass. Appl Microbiol Biotechnol 98:987–1000. https://doi.org/10.1007/s00253-013-5319-6
41. McKinlay JB, Vieille C (2008) 13C-metabolic flux analysis of Actinobacillus succinogenes fermentative metabolism at different NaHCO3 and H2 concentrations. Metab Eng 10:55–68. https://doi.org/10.1016/j.ymben.2007.08.004
42. Song H, Lee SY (2006) Production of succinic acid by bacterial fermentation. Enzym Microb Technol 39:352–361. https://doi.org/10.1016/j.enzmictec.2005.11.043
43. Dunlop AP, Riverside, and Smith S (1954) Prepration of succinic acid, United states patent office, Patent No. 2,676,186
44. Kawasumi R, Narita S, Miyamoto K et al (2017) One-step conversion of Levulinic acid to succinic acid using I 2/t - BuOK system: the Iodoform reaction revisited. Sci Rep 7:17967. https://doi.org/10.1038/s41598-017-17116-4
45. Dutta S, Yu IKM, Tsang DCW et al (2019) Green synthesis of gamma-valerolactone (GVL) through hydrogenation of biomass-derived levulinic acid using non-noble metal catalysts: a critical review. Chem Eng J 372:992–1006. https://doi.org/10.1016/j.cej.2019.04.199

46. Manzer LE (2004) Production of 5-methyl-n-aryl-2- pyrrolidone and 5-methyl-n-alkyl 2-pyr-rolidone by reductive amination of levulinic acid with nitro compounds, United States, Patent, Patent No. US 6,818,593 B2

47. Manzer LE, Hutchenson KW (2007) Production of 5-methyl-dihydro-furan-2-one from levu-linic acid in supercritical media, European Patent Office, EP 1636203 B1

48. Werpy T, Frye JG, Wang Y, Zacher H (2003) Methods of making pyrrolidones, United States Patent, Patent No. US 6,603,021 B2

49. Huang Y, Dai J, Deng X, et al (2011) Ruthenium-catalyzed conversion of levulinic acid to pyrrolidines by reductive amination ChemSusChem. 4 1578–1581. https://doi.org/10.1002/cssc.201100344

50. Sun Z, Chen J, Tu T (2017) NHC-based coordination polymers as solid molecular catalysts for reductive amination of biomass levulinic acid. Green Chem 19:789–794. https://doi.org/10.1039/C6GC02591A

51. Hengne AM, Kamble SB, Rode CV (2013) Single pot conversion of furfuryl alcohol to levu-linic esters and γ-valerolactone in the presence of sulfonic acid functionalized ILs and metal catalysts. Green Chem 15:2540–2547. https://doi.org/10.1039/C3GC41098F

52. Siddiki SMAH, Touchy AS, Jamil MAR et al (2018) C-methylation of alcohols, ketones, and indoles with methanol using heterogeneous platinum catalysts. ACS Catal 8:3091–3103. https://doi.org/10.1021/acscatal.7b04442

53. Chieffi G, Braun M, Esposito D (2015) Continuous reductive amination of biomass-derived molecules over carbonized filter paper-supported FeNi alloy. ChemSusChem 8:3590–3594. https://doi.org/10.1002/cssc.201500804

54. Hayes DJ (2009) An examination of biorefining processes, catalysts and challenges. Catal Today 145:138–151. https://doi.org/10.1016/j.cattod.2008.04.017

55. Yang J, Li G, Zhang L, Zhang S (2018) Efficient production of n-butyl levulinate fuel additive from levulinic acid using amorphous. Catalyst. https://doi.org/10.3390/catal8010014

56. Christensen E, Williams A, Paul S et al (2011) Properties and performance of levulinate esters as diesel blend components. Energy Fuel 25:5422–5428. https://doi.org/10.1021/ef201229j

57. Lake MA, Pleasant M, Burton SW, Cary (2010) Diesel fuel compositions containing levu-linate ester. Patent application publication (10) Pub No. US 2010/0313467 A1

58. Janssen A, Pischinger S, Muether M (2010) Potential of cellulose-derived biofuels for soot free diesel combustion. SAE Int J Fuels Lubr 3:70–84

59. Janssen A, Muether M, Kolbeck A, et al (2018) The impact of different biofuel compo-nents in diesel blends on engine efficiency and emission performance, https://doi.org/10.4271/2010-01-2119

60. Bayarri Ferrer N (2013) Degreasing compositions derived from levulinic acid (a compound obtainable from biomass) and process for degreasing metal surfaces, European Patent Office, Patent No. EP 2540871 A1

61. Démolis A, Essayem N, Rataboul F (2014) Synthesis and applications of alkyl levulinates. ACS Sustain Chem Eng 2:1338–1352. https://doi.org/10.1021/sc500082n

62. McMurry J (1988) Organic chemistry, 2nd edn. Brooks, Cole Publishing, Pacific Groove

63. Bond GC (1987) heterogeneous Catalysis: Principles and applications. United states, https://www.osti.gov/biblio/5847708

64. Takeuchi Y, Jin F, Tohji K, Enomoto H (2008) Acid catalytic hydrothermal conversion of carbohydrate biomass into useful substances. J Mater Sci 43:2472

65. Varkolu M, Moodley V, Potwana FSW et al (2017) Esterification of levulinic acid with eth-anol over bio-glycerol derived carbon–sulfonic-acid. React Kinet Mech Catal 120:69–80. https://doi.org/10.1007/s11144-016-1105-7

66. Negus MP, Mansfield AC, Leadbeater NE (2015) The preparation of ethyl levulinate facili-tated by flow processing: the catalyzed and uncatalyzed esterification of levulinic acid. J Flow Chem 5:148–150. https://doi.org/10.1556/1846.2015.00005

67. Khiratkar AG, Balinge KR, Krishnamurthy M et al (2018) Sulphonic acid-functionalized Benzimidazolium based poly ionic liquid catalyzed esterification of levulinic acid. Catal Lett 148:680–690. https://doi.org/10.1007/s10562-017-2284-1

68. Kalghatgi SG, Bhanage BM (2019) Green syntheses of levulinate esters using ionic liquid 1-methyl imidazolium hydrogen sulphate [MIM][HSO4] in solvent free system. J Mol Liq 281:70–80. https://doi.org/10.1016/j.molliq.2019.02.053

69. Badgujar KC, Badgujar VC, Bhanage BM (2020) A review on catalytic synthesis of energy rich fuel additive levulinate compounds from biomass derived levulinic acid. Fuel Process Technol 197:106213. https://doi.org/10.1016/j.fuproc.2019.106213

70. Thomas JM (2013) Solid acid catalysts. J Chem Inf Model 53:1689–1699. https://doi.org/10.1017/CBO9781107415324.004

71. Gupta P, Paul S (2014) Solid acids : green alternatives for acid catalysis. Catal Today 236:153. https://doi.org/10.1016/j.cattod.2014.04.010

72. Cirujano FG, Corma A, Llabrés i Xamena FX (2015) Zirconium-containing metal organic frameworks as solid acid catalysts for the esterification of free fatty acids: synthesis of biodiesel and other compounds of interest. Catal Today 257:213–220

73. Cirujano FG, Corma A, Llabrés i Xamena FX (2015) Conversion of levulinic acid into chemicals: synthesis of biomass derived levulinate esters over Zr-containing MOFs. Chem Eng Sci 124:52–60. https://doi.org/10.1016/j.ces.2014.09.047

74. Fernandes DR, Rocha AS, Mai EF et al (2012) Applied catalysis a : general levulinic acid esterification with ethanol to ethyl levulinate production over solid acid catalysts. Appl Catal A Gen 425–426:199–204. https://doi.org/10.1016/j.apcata.2012.03.020

75. Nakhate AV, Yadav GD (2016) Synthesis and characterization of sulfonated carbon-based graphene oxide monolith by solvothermal carbonization for esterification and unsymmetrical ether formation. ACS Sustain Chem Eng 4:1963–1973. https://doi.org/10.1021/acssuschemeng.5b01205

76. Tejero MA, Ramírez E, Fité C et al (2016) Esterification of levulinic acid with butanol over ion exchange resins. Appl Catal A Gen 517:56–66. https://doi.org/10.1016/J.APCATA.2016.02.032

77. Trombettoni V, Bianchi L, Zupanic A et al (2017) Efficient catalytic upgrading of levulinic acid into alkyl levulinates by resin-supported acids and flow reactors. Catalysts 7. https://doi.org/10.3390/catal7080235

78. Guo T, Qiu M, Qi X (2019) Selective conversion of biomass-derived levulinic acid to ethyl levulinate catalyzed by metal organic framework (MOF)-supported polyoxometalates. Appl Catal A Gen 572:168–175. https://doi.org/10.1016/j.apcata.2019.01.004

79. Gupta SSR, Kantam ML (2019) Catalytic conversion of furfuryl alcohol or levulinic acid into alkyl levulinates using a sulfonic acid-functionalized hafnium-based MOF. Catal Commun 124:62–66. https://doi.org/10.1016/j.catcom.2019.03.003

80. Seo JS, Whang D, Lee H et al (2000) A homochiral metal-organic porous material for enantioselective separation and catalysis. Nature 404:982–986. https://doi.org/10.1038/35010088

81. Abrahams BF, Hoskins BF, Michall D, Robson R (1994) Assembly of porphyrin building blocks into network structure with large channels. Nature 369:727–729

82. Yaghi OM, Li G (1995) Mutually interpenetrating sheets and channels in the extended structure of [Cu(4,4′-bpy)Cl]. Angew Chem Int Ed 34:207–209. https://doi.org/10.1002/anie.199502071

83. Evans OR, Lin W (2001) Crystal engineering of nonlinear optical materials based on interpenetrated Diamondoid coordination networks. Chem Mater 13:2705–2712. https://doi.org/10.1021/cm010301n

84. Kahn O (2000) Chemistry and physics of Supramolecular magnetic materials. Acc Chem Res 33:647–657. https://doi.org/10.1021/ar9703138

85. Kim J, Chen B, Reineke TM et al (2001) Assembly of metal-organic frameworks from large organic and inorganic secondary building units: new examples and simplifying principles for complex structures. J Am Chem Soc 123:8239–8247. https://doi.org/10.1021/ja010825o

86. Kitagawa S, Mitsuru K (1998) Functional micropore chemistry of crystalline metal complex-assembled compounds. Bull Chem Soc Jpn 71:1739–1753

87. Lin W, Wang Z, Ma L (1999) A novel Octupolar metal−organic NLO material based on a chiral 2D coordination network. J Am Chem Soc 121:11249–11250. https://doi.org/10.1021/ja9928327

88. Link AJ, Tirrell DA (2003) Cell surface labeling of Escherichia coli via copper(I)-catalyzed [3+2] Cycloaddition. J Am Chem Soc 125:11164–11165. https://doi.org/10.1021/ja036765z

89. Bai Y, Dou Y, Xie LH et al (2016) Zr-based metal-organic frameworks: design, synthesis, structure, and applications. Chem Soc Rev 45:2327–2367. https://doi.org/10.1039/c5cs00837a

90. Cavka JH, Jakobsen S, Olsbye U et al (2008) A new zirconium inorganic building brick forming metal organic frameworks with exceptional stability. J Am Chem Soc 130:13850–13851. https://doi.org/10.1021/ja8057953

91. Ling S, Slater B (2016) Dynamic acidity in defective UiO-66. Chem Sci 7:4706–4712. https://doi.org/10.1039/C5SC04953A

92. Serrano-Ruiz JC, Wang D, Dumesic JA (2010) Catalytic upgrading of levulinic acid to 5-nonanone. Green Chem 12:574–557. https://doi.org/10.1039/b923907c

93. Cirujano FG, Corma A, Llabrés FX (2014) Conversion of levulinic acid into chemicals: synthesis of biomass derived levulinate esters over Zr-containing MOFs. Chem Eng Sci 124:1–9. https://doi.org/10.1016/j.ces.2014.09.047

94. Wang F, Chen Z, Chen H et al (2019) Interplay of Lewis and Brønsted acid sites in Zr-based metal-organic frameworks for efficient esterification of biomass-derived levulinic acid. ACS Appl Mater Interfaces 11:32090–32096. https://doi.org/10.1021/acsami.9b07769

95. Klet RC, Liu Y, Wang TC et al (2016) Evaluation of Brønsted acidity and proton topology in Zr- and Hf-based metal–organic frameworks using potentiometric acid–base titration. J Mater Chem A 4:1479–1485. https://doi.org/10.1039/C5TA07687K

96. Herbst A, Janiak C (2017) MOF catalysts in biomass upgrading towards value-added fine chemicals. CrystEngComm 19:4092–4117. https://doi.org/10.1039/c6ce01782g

97. Kokare MB, V R, Mathpati CS (2018) Response surface optimization, kinetic study and process design of n-butyl levulinate synthesis. Chem Eng Res Des 137:577–588. https://doi.org/10.1016/j.cherd.2018.07.036

98. Ramli NAS, Zaharuddin NH, Amin NAS (2017) Esterification of renewable levilinic acid to levulinate esters using Amberlyst 15 as a solid acid catalyst. J Teknol https://doi.org/10.11113/jt.v79.8095

99. M. M. Sharma (1990) CSIR distinguished lectures selectivity engineering, New Delhi

100. Ramli NAS, Hisham NI, Amin NAS (2018) Esterification of levulinic acid to levulinate esters in the presence of sulfated silica catalyst. Sains Malaysiana 47(6):1131–1138

101. Berty JM (ed) (1999) Studies in surface science and catalysis. In: Experiments in catalytic reaction engineering. Elsevier, Amsterdam, pp 261–268

102. Hu L, Lin L, Wu Z et al (2015) Chemocatalytic hydrolysis of cellulose into glucose over solid acid catalysts. Appl Catal B Environ 174–175:225–243. https://doi.org/10.1016/j.apcatb.2015.03.003

103. Yamaguchi A, Sato O, Mimura N, Shirai M (2016) Catalytic production of sugar alcohols from lignocellulosic biomass. Catal Today 265:199–202. https://doi.org/10.1016/j.cattod.2015.08.026

104. Fang S, Qingyin W, Daiyu S, Xianghuan Z, Mei W, Yihang G (2013) Pore morphology-controlled preparation of ZrO_2-based hybrid catalysts functionalized by both organosilica moieties and Keggin-type heteropoly acid for the synthesis of levulinate esters. J Mater Chem A 1(42):13209–13221. https://doi.org/10.1039/c3ta12412f

105. Kuwahara Y, Kaburagi W, Nemoto K, Fujitani T (2014) Applied catalysis a: general esterification of levulinic acid with ethanol over sulfated Si-doped ZrO_2 solid acid catalyst: study of the structure – activity relationships. Appl Catal A Gen 476:186–196. https://doi.org/10.1016/j.apcata.2014.02.032

106. Kuwahara Y, Kaburagi W, Nemoto K, Fujitani T (2014) Esterification of levulinic acid with ethanol over sulfated Si-doped ZrO2 solid acid catalyst: study of the structure–activity relationships. Appl Catal A Gen 476:186–196. https://doi.org/10.1016/j.apcata.2014.02.032

107. Su F, Ma L, Song D et al (2013) Design of a highly ordered mesoporous H3PW12O40/ZrO2–Si(Ph)Si hybrid catalyst for methyl levulinate synthesis. Green Chem 15:885–890. https://doi.org/10.1039/C3GC36912A

108. Unlu D, Ilgen O, Durmaz Hilmioglu N (2017) Reactive separation system for effective upgrade of levulinic acid into ethyl levulinate. Chem Eng Res Des 118:248–258. https://doi.org/10.1016/j.cherd.2016.12.009

109. Yamaguchi T (1994) Application of ZrO2 as a catalyst and a catalyst support. Catal Today 20:199–217. https://doi.org/10.1016/0920-5861(94)80003-0

110. Samaranch B, Ramírez de la Piscina P, Clet G et al (2007) Synthesis and characterization of Ta2O5−ZrO2 systems: structure, surface acidity, and catalytic properties. Chem Mater 19:1445–1451. https://doi.org/10.1021/cm062704z

111. Budarin VL, Clark JH, Luque R, Macquarrie DJ (2007) Versatile mesoporous carbonaceous materials for acid catalysis. Chem Commun:634–636. https://doi.org/10.1039/B614537J

112. Li N, Jiang S, Liu Z et al (2019) Preparation and catalytic performance of loofah sponge-derived carbon sulfonic acid for the conversion of levulinic acid to ethyl levulinate. Catal Commun 121:11–14. https://doi.org/10.1016/j.catcom.2018.12.007

113. Liu C, Zhang K, Liu Y, Wu S (2019) Esterification of levulinic acid into ethyl levulinate catalyzed by sulfonated bagasse-carbonized solid acid. Bioresources 14:2186–2196. https://doi.org/10.15376/biores.14.1.2186-2196

114. Pileidis FD, Tabassum M, Coutts S, Ttitirici MM (2014) Esterification of levulinic acid into ethyl levulinate catalysed by sulfonated hydrothermal carbons. Chin J Catal 35:929–936. https://doi.org/10.1016/S1872-2067(14)60125-X

115. Zainol MM, Amin NAS, Asmadi M (2017) Effects of thermal treatment on carbon cryogel preparation for catalytic esterification of levulinic acid to ethyl levulinate. Fuel Process Technol 167:431–441. https://doi.org/10.1016/j.fuproc.2017.07.028

116. Zainol MM, Amin NAS, Asmadi M (2019) Kinetics and thermodynamic analysis of levulinic acid esterification using lignin-furfural carbon cryogel catalyst. Renew Energy 130:547–557. https://doi.org/10.1016/j.renene.2018.06.085

117. Nakajima K, Hara M (2012) Amorphous carbon with SO3H groups as a solid Brønsted acid catalyst. ACS Catal 2:1296–1304. https://doi.org/10.1021/cs300103k

118. Hara M, Yoshida T, Takagaki A et al (2004) A carbon material as a strong protonic acid. Angew Chem Int Ed 43:2955–2958. https://doi.org/10.1002/anie.200453947

119. Okamura M, Takagaki A, Toda M et al (2006) Acid-catalyzed reactions on flexible polycyclic aromatic carbon in amorphous carbon. Chem Mater 18:3039–3045. https://doi.org/10.1021/cm0605623

120. Suganuma S, Nakajima K, Kitano M et al (2008) Hydrolysis of cellulose by amorphous carbon bearing SO3H, COOH, and OH groups. J Am Chem Soc 130:12787–12793. https://doi.org/10.1021/ja803983h

121. Toda M, Takagaki A, Okamura M et al (2005) Biodiesel made with sugar catalyst. Nature 438:178. https://doi.org/10.1038/438178a

122. Hu B, Yu S-H, Wang K et al (2008) Functional carbonaceous materials from hydrothermal carbonization of biomass: an effective chemical process. Dalton Trans 40:5414–5423. https://doi.org/10.1039/B804644C

123. Mahajan A, Gupta P (2019) Carbon - based solid acids : a review. Environ Chem Lett 18:299. https://doi.org/10.1007/s10311-019-00940-7

124. Sun X, Li Y (2004) Ga2O3 and GaN semiconductor hollow spheres. Angew Chem Int Ed 43:3827–3831. https://doi.org/10.1002/anie.200353212

125. Enumula SS, Gurram VRB, Chada RR et al (2017) Clean synthesis of alkyl levulinates from levulinic acid over one pot synthesized WO3-SBA-16 catalyst. J Mol Catal A Chem 426:30–38. https://doi.org/10.1016/j.molcata.2016.10.032

126. Maggi R, Shiju NR, Santacroce V et al (2016) Silica-supported sulfonic acids as recyclable catalyst for esterification of levulinic acid with stoichiometric amounts of alcohols. Beilstein J Org Chem 12:2173–2180. https://doi.org/10.3762/bjoc.12.207

127. Melero JA, Morales G, Iglesias J et al (2013) Efficient conversion of levulinic acid into alkyl levulinates catalyzed by sulfonic mesostructured silicas. Appl Catal A Gen 466:116–122. https://doi.org/10.1016/j.apcata.2013.06.035

128. Najafi Chermahini A, Nazeri M (2017) Esterification of the levulinic acid with n-butyl and isobutyl alcohols over aluminum-containing MCM-41. Fuel Process Technol 167:442–450. https://doi.org/10.1016/j.fuproc.2017.07.034

129. Yang F, Tang J (2019) Catalytic upgrading of renewable levulinic acid to levulinate esters using perchloric acid decorated nanoporous silica gels. ChemistrySelect 4:1403–1409. https://doi.org/10.1002/slct.201803608

130. Drago RS, Dias JA, Maier TO (1997) An acidity scale for Brönsted acids including H3PW12O40. J Am Chem Soc 119:7702–7710. https://doi.org/10.1021/ja9639123

131. Costa VV, da Silva Rocha KA, Oliveira LCA et al (2016) Heteropoly acid catalysts for the synthesis of fragrance compounds from bio-renewables: acetylation of nopol and terpenic alcohols. RSC Adv 6:43217–43222. https://doi.org/10.1039/C6RA02266A

132. Kuwahara Y, Kango H, Yamashita H (2017) Catalytic transfer hydrogenation of biomass-derived levulinic acid and its esters to γ-valerolactone over sulfonic acid-functionalized UiO-66. ACS Sustain Chem Eng 5:1141–1152. https://doi.org/10.1021/acssuschemeng.6b02464

133. Taylor P, Heravi MM, Fard MV, Faghihi Z (2013) Green chemistry letters and reviews heteropoly acids-catalyzed organic reactions in water : doubly green reactions. Green Chem Lett Rev 6:282–300. https://doi.org/10.1080/17518253.2013.846415

134. Bennardi DO, Romanelli GP, Sathicq ÁG et al (2011) Wells–Dawson heteropolyacid as reusable catalyst for sustainable synthesis of flavones. Appl Catal A Gen 404:68–73. https://doi.org/10.1016/j.apcata.2011.07.011

135. Vázquez PG, Blanco MN, Cáceres CV (1999) Catalysts based on supported 12-molybdophosphoric acid. Catal Lett 60:205–215. https://doi.org/10.1023/A:1019071410838

136. Quereshi S, Ahmad E, Pant KK, Dutta S (2019) Synthesis and characterization of zirconia supported silicotungstic acid for ethyl levulinate production. Ind Eng Chem Res 58:16045–16054. https://doi.org/10.1021/acs.iecr.9b01659

137. Pasha N, Raj NL (2019) Zirconium exchanged phosphotungstic acid catalysts for esterification of levulinic acid to ethyl levulinate. Catal Lett 149:2500–2507. https://doi.org/10.1007/s10562-019-02862-z

138. Wu M, Zhang X, Su X et al (2016) 3D graphene aerogel anchored tungstophosphoric acid catalysts: characterization and catalytic performance for levulinic acid esterification with ethanol. Catal Commun 85:66–69. https://doi.org/10.1016/j.catcom.2016.07.023

139. Shimizu K, Niimi K, Satsuma A (2008) Polyvalent-metal salts of heteropolyacid as catalyst for Friedel-Crafts alkylation reactions. Appl Catal A Gen 349:1–5. https://doi.org/10.1016/j.apcata.2008.03.042

140. Zhou X, Li ZX, Zhang C et al (2016) Efficient conversion of renewable levulinic acid to n-butyl levulinate catalyzed by ammonium and silver co-doped phosphotungstic acid. J Mol Catal A Chem 417:71–75. https://doi.org/10.1016/j.molcata.2016.03.006

141. Ramli NAS, Sivasubramaniam D, Amin NAS (2017) Esterification of levulinic acid using ZrO2-supported phosphotungstic acid catalyst for ethyl levulinate production. Bioenergy Res 10:1105–1116. https://doi.org/10.1007/s12155-017-9872-1

142. Wu M, Zhao Q, Li J et al (2016) Esterification of levulinic acid into hexyl levulinate over dodecatungstophosphoric acid anchored to Al-MCM-41. J Exp Neurosci 11:1331. https://doi.org/10.1080/17458080.2016.1214985

143. Zheng X-C, Li N, Wu M et al (2017) Synthesis of biofuel via levulinic acid esterification over porous solid acid consisting of tungstophosphoric acid and reduced graphene oxide. Res Chem Intermed 43:6651–6664. https://doi.org/10.1007/s11164-017-3012-6

144. Wu M, Jie QZ, Su LX (2016) Tungstophosphoric acid-based mesoporous materials anchored to MCM-41 : characterization and catalytic performance in esterification of levulinic acid with ethanol. J Porous Mater 23:1329. https://doi.org/10.1007/s10934-016-0192-1

145. Luan Q, Liu L, Gong S et al (2018) Clean and efficient conversion of renewable levulinic acid to levulinate esters catalyzed by an organic-salt of H4SiW12O40. Process Saf Environ Prot 117:341–349. https://doi.org/10.1016/j.psep.2018.05.015

146. Vilanculo CB, de Andrade Leles LC, da Silva MJ (2020) H4SiW12O40-catalyzed levulinic acid esterification at room temperature for production of fuel bioadditives. Waste Biomass Valor 11:1895–1904. https://doi.org/10.1007/s12649-018-00549-x

147. Lucas N, Gurrala L, Athawale A (2019) Heteropolyacids supported on mesoporous AlSBA-15 as efficient catalysts for esterification of levulinic acid. J Porous Mater 26:1335. https://doi.org/10.1007/s10934-019-00734-w

148. Manikandan K, Cheralathan KK (2017) Heteropoly acid supported on silicalite–1 possessing intracrystalline nanovoids prepared using biomass – an efficient and recyclable catalyst for esterification of levulinic acid. Appl Catal A Gen 547:237–247. https://doi.org/10.1016/j.apcata.2017.09.007

149. Yan K, Wu G, Wen J, Chen A (2013) One-step synthesis of mesoporous H4SiW12O40-SiO2 catalysts for the production of methyl and ethyl levulinate biodiesel. Catal Commun 34:58–63. https://doi.org/10.1016/j.catcom.2013.01.010

150. Baerlocher C, McCusker LB, Olson DH (2007) Atlas of zeolite framework types. Elsevier science, 6th Edition, ISBN No. 978-0-444-53064-6

151. Larsen SC (2007) Nanocrystalline zeolites and zeolite structures: synthesis, characterization, and applications. J Phys Chem C 111:18464–18474. https://doi.org/10.1021/jp074980m

152. Zhang Z, Wagner VE (2017) Antimicrobial coatings and modifications on medical devices, Springer, Cham, ISBN978-3-319-57492-9. https://doi.org/10.1007/978-3-319-57494-3

153. Vermeiren W, Gilson J-P (2009) Impact of zeolites on the petroleum and petrochemical industry. Top Catal 52:1131–1161. https://doi.org/10.1007/s11244-009-9271-8

154. Maheria KC, Kozinski J, Dalai A (2013) Esterification of levulinic acid to n -butyl levulinate over various acidic zeolites. Catal Lett 143:1220–1225. https://doi.org/10.1007/s10562-013-1041-3

155. Nandiwale KY, Bokade VV (2015) Esterification of renewable levulinic acid to n-butyl levulinate over modified H-ZSM-5. Chem Eng Technol 38:246–252. https://doi.org/10.1002/ceat.201400326

156. Nandiwale KY, Bokade VV (2016) Optimization by box-Behnken experimental design for synthesis of n-hexyl levulinate biolubricant over hierarchical H-ZSM-5: an effort towards agricultural waste minimization. Process Saf Environ Prot 99:159–166. https://doi.org/10.1016/j.psep.2015.11.003

157. Nandiwale KY, Niphadkar PS, Deshpande SS, Bokade VV (2014) Esterification of renewable levulinic acid to ethyl levulinate biodiesel catalyzed by highly active and reusable desilicated H-ZSM-5. J Chem Technol Biotechnol 89:1507–1515. https://doi.org/10.1002/jctb.4228

158. Nandiwale KY, Yadava SK, Bokade VV (2014) Production of octyl levulinate biolubricant over modified H-ZSM-5: optimization by response surface methodology. J Energy Chem 23:535–541. https://doi.org/10.1016/S2095-4956(14)60182-0

159. Patil CR, Niphadkar PS, Bokade VV, Joshi PN (2014) Esterification of levulinic acid to ethyl levulinate over bimodal micro–mesoporous H/BEA zeolite derivatives. Catal Commun 43:188–191. https://doi.org/10.1016/j.catcom.2013.10.006

160. Guth JL, Kessler H (1999) Synthesis of aluminosilicate zeolites and related silica – based materials. In: Puppe JW (ed) Catalysis and zeolites – fundamentals and applications, 1st Edition. Springer, Germany.

161. Puppe JW (1999) Catalysis and zeolites. Catal Zeolites. https://doi.org/10.1007/978-3-662-03764-5
162. Barrer RM (Richard M (1982) Hydrothermal chemistry of zeolites. Academic, London
163. Pérez-Page M, Yu E, Li J et al (2016) Template-based syntheses for shape controlled nanostructures. Adv Colloid Interf Sci 234:51–79. https://doi.org/10.1016/j.cis.2016.04.001
164. Ch Deka R (1998) Acidity in zeolites and their characterization by different spectroscopic methods. NISCAIR-CSIR, New Delhi
165. Millini R, Zou X, K Strohmaier WS (2017) Zeolites in catalysis: properties and applications. Royal Society of Chemistry, London
166. Zhang J, Qian W, Kong C, Wei F (2015) Increasing Para-xylene selectivity in making aromatics from methanol with a surface-modified Zn/P/ZSM-5 catalyst. ACS Catal 5:2982–2988. https://doi.org/10.1021/acscatal.5b00192
167. Choudary NV, Newalkar BL (2011) Use of zeolites in petroleum refining and petrochemical processes: recent advances. J Porous Mater 18:685–692. https://doi.org/10.1007/s10934-010-9427-8
168. Yilmaz B, Müller U (2009) Catalytic applications of zeolites in chemical industry. Top Catal 52:888–895. https://doi.org/10.1007/s11244-009-9226-0
169. Kresge CT, Leonowicz ME, Roth WJ, Vartuli JC, Beck JS (1992) Ordered mesoporous molecular sieves synthesized by a liquid-crystal template mechanism. Nature 359:710–713
170. Ciesla U, Schuth F (1999) Ordered mesoporous materials. Microporous Mesoporous Mater 27:131–149
171. Ivanova II, Knyazeva EE (2013) Micro-mesoporous materials obtained by zeolite recrystallization: synthesis, characterization and catalytic applications. Chem Soc Rev 42:3671–3688. https://doi.org/10.1039/c2cs35341e
172. Na K, Somorjai GA (2015) Hierarchically nanoporous zeolites and their heterogeneous catalysis: current status and future perspectives. Catal Lett 145:193–213. https://doi.org/10.1007/s10562-014-1411-5
173. Serrano DP, Escola JM, Pizarro P (2013) Synthesis strategies in the search for hierarchical zeolites. Chem Soc Rev 42:4004–4035. https://doi.org/10.1039/c2cs35330j
174. Zhang K, Ostraat ML (2016) Innovations in hierarchical zeolite synthesis. Catal Today 264:3–15. https://doi.org/10.1016/j.cattod.2015.08.012
175. Suárez N, Pérez-Pariente J, Mondragón F, Moreno A (2019) Generation of hierarchical porosity in beta zeolite by post-synthesis treatment with the cetyltrimethylammonium cationic surfactant under alkaline conditions. Microporous Mesoporous Mater 280:144–150. https://doi.org/10.1016/j.micromeso.2019.02.001
176. Ogura M, Shinomiya SY, Tateno J et al (2000) Formation of uniform mesopores in ZSM-5 zeolite through treatment in alkaline solution. Chem Lett 29:882–883. https://doi.org/10.1246/cl.2000.882
177. Pan T, Wu Z, Yip ACK (2019) Advances in the green synthesis of microporous and hierarchical zeolites: a short review. Catalysts 9:1–18. https://doi.org/10.3390/catal9030274
178. Verboekend D, Pérez-Ramírez J (2011) Design of hierarchical zeolite catalysts by desilication. Cat Sci Technol 1:879–890. https://doi.org/10.1039/c1cy00150g
179. Morawala D, Dalai A, Maheria K (2019) Rice husk mediated synthesis of meso-ZSM-5 and its application in the synthesis of n-butyl levulinate. J Porous Mater 26:677–686. https://doi.org/10.1007/s10934-018-0664-6
180. Morawala DH, Lathiya DR, Dalai AK, Maheria KC (2019) TTAB mediated synthesis of Meso-H-BEA and its application in the production of n-butyl levulinate. Catal Today 348:177. https://doi.org/10.1016/j.cattod.2019.10.009
181. Kalpana C, Maheria SRM (2014) Synthesis, characterization of mesoporous zeolite BEA and its application in multicomponent reactions. J Catal Catal 1:1–24
182. Morawala DH, Dalai AK, Maheria KC (2019) Synthesis of n-butyl levulinate using mesoporous zeolite H-BEA catalysts with different catalytic characteristics. Catal Lett 150:1049. https://doi.org/10.1007/s10562-019-03005-0

183. Maheria KC, Kozinski J, Dalai A (2013) Esterification of levulinic acid to n-butyl levu-
     linate over various acidic zeolites. Catal Lett 143:1220–1225. https://doi.org/10.1007/
     s10562-013-1041-3
184. Nandiwale KY, Sonar SK, Niphadkar PS et al (2013) Catalytic upgrading of renewable lev-
     ulinic acid to ethyl levulinate biodiesel using dodecatungstophosphoric acid supported on
     desilicated H-ZSM-5 as catalyst. Elsevier B.V., Amsterdam
185. Joshi SS, Zodge AD, Pandare KV, Kulkarni BD (2014) Efficient conversion of cellulose to
     levulinic acid by hydrothermal treatment using zirconium dioxide as a recyclable solid acid
     catalyst. Ind Eng Chem Res 53:18796–18805. https://doi.org/10.1021/ie5011838
186. Wang J, Jaenicke S, Chuah GK (2014) Zirconium-beta zeolite as a robust catalyst for the
     transformation of levulinic acid to γ-valerolactone via Meerwein-Ponndorf-Verley reduction.
     RSC Adv 4:13481–13489. https://doi.org/10.1039/c4ra01120a
187. Holm MS, Taarning E, Egeblad K, Christensen CH (2011) Catalysis with hierarchical zeo-
     lites. Catal Today 168:3–16. https://doi.org/10.1016/j.cattod.2011.01.007

C(*sp*³)–H Bond Hetero-functionalization of Aliphatic Carboxylic Acid Equivalents Enabled by Transition Metals

Aniket Gupta, Sreedhar Gundekari, and Sukalyan Bhadra

Abstract Aliphatic carboxylic acids and their common derivatives such as amides and esters, particularly embracing heteroatom-based substituents, are widespread among natural and synthetic complex molecular frameworks, ratified drugs, and various tailored materials. Conventional synthetic processes to access these compounds comprise multistep protocols that are virtually inconvenient and unsafe, generating large mass of wastes within the synthetic sequence. The straightforward transition metal-catalyzed installation of a heteroatom-based function via transforming a selective C–H bond of an aliphatic carboxylic acid equivalent has recently materialized as an attractive substitute to those multistep processes. In the latter case, the carboxylate group, either directly or in the form of an interconvertible directing group, controls the highly selective metal-promoted hetero-functionalization process in the alkyl chain residue through extraordinarily ordered transition states.

The current chapter summarizes the advances in the field of transition metal-enabled C(*sp*³)–H bond hetero-functionalization of aliphatic carboxylic acids and their synthetic equivalents. Due to substantial progress in recent years, only frequently employed transition metals, including palladium, nickel, copper, iron, and cobalt, which promoted reactions have been described. The chapter has been divided into two key subtopics: (1) directed C(*sp*³)–H hetero-functionalization approaches, in which the carboxylic acid or a promptly adaptable carboxylate equivalent actively binds to the metal catalyst and brings it close to the cleavable C(*sp*³)–H bond to facilitate further functionalization, and (2) non-directed C(*sp*³)–H hetero-functionalization approaches, in which the carboxylic acid equivalents passively control the metal-promoted C(*sp*³)–H functionalization. Gratifyingly, both approaches lead to regiospecific functionalization of carboxylic acid synthons at either proximal-selective α-C–H bonds or distal β-, γ-, and even δ-C–H bonds with

A. Gupta · S. Gundekari · S. Bhadra (✉)

Inorganic Materials and Catalysis Division, Academy of Scientific and Innovative Research (AcSIR), Ghaziabad, India

CSIR-Central Salt and Marine Chemicals Research Institute, Bhavnagar, Gujarat, India
e-mail: sbhadra@csmcri.res.in

various heteroatom-based substituents, e.g., O-, N-, S-, Se-, halogen-, B-, Si-, and recently Ge-based groups.

Keywords Hetero-functionalization · C–H bond cleavage · Carboxylic acid esters · Bidentate · Monodentate

1 Introduction

Aliphatic carboxylic acid equivalents/derivatives, particularly embracing heteroatom-based substituents positioned at diverse carbon centers (e.g., α-, β-, γ-, δ-, etc.) in the alkyl residue, possess tremendous applications in fine chemicals and pharmaceutical industries [1–13]. Traditional methods to access those elegant molecules demand multistep synthetic protocols employing practically inconvenient and frequently hazardous operational conditions that produce large quantity of non-disposable chemical wastes. The concept of transition metal-catalyzed direct functionalizations by cleaving of a specific C–H bond has recently emerged as an attractive tool for installing heteroatom-based groups onto an aliphatic carboxylic acid substrate under mild and environmentally benign conditions [14–21]. However, the latter class of transformation holds several fundamental challenges owing to the robust nature and intrinsic inertness of aliphatic C–H bonds (BDE = ~90−100 kcal/mol, pKa = ~45−60, etc.). The decisive cleavage with succeeding functionalization of a specific C−H bond of alkanes in the presence of numerous chemically identical C–H bonds also seems extremely intricate [15]. Two independent approaches are generally conceived to realize the transition metal-catalyzed C–H bond functionalization of carboxylic acid derivatives directly [22–25]: (1) a directed approach in which the carboxylate counterpart pre-associates with the metal catalyst to hold it in the proximity of the cleavable C(sp^3)–H bond, thereby promoting the hetero-functionalization process at the distal-selective β-, γ-, and/or even δ-positions, and (2) a non-directed C(sp^3)–H hetero-functionalization approach, which commonly proceeds through the formation of a stabilized enol or carbon-centered radical intermediate typically resulting in α-functionalized carboxylic acid synthons. The present chapter sketches the advances in the field of transition metal-catalyzed C(sp^3)–H bond hetero-functionalization of aliphatic carboxylic acid equivalents. Due to considerable progress in recent years, only frequently employed transition metals, including palladium, iridium, nickel, copper, iron, and cobalt, which promoted reactions have been described.

2 Directed C(sp^3)–H Hetero-functionalization Approaches

In directed hetero-functionalization approaches, the carboxylate equivalent of the substrate serves as a polar chelating metal template that assists to form a five- or six-membered metallacycle intermediate via the selective activation of the β- or

γ-C–H bond, respectively [26]. Due to the weak coordinating nature of free carboxylic acid groups, they are often converted into relatively stronger chelating directing groups, e.g., mono- and bidentate N-donor functional groups, that facilitate the building of exceptionally ordered metallacycle transition states. Consecutively, the C–heteroatom bond realization generally takes place at the reductive elimination step to furnish the targeted heteroatom-substituted products (Scheme 1).

2.1 Hetero-functionalization of Free Carboxylic Acids

Free carboxylic acids are known to coordinate to transition metals, however, in a rather weak manner [27]. Nevertheless, the first hetero-functionalization of aliphatic carboxylic acids appeared in the literature as early as in 1991. A Pt^{2+}/Pt^{4+} catalyst system was employed to oxidize the C(*sp*³)–H bonds of aliphatic carboxylic acids in aqueous solution to obtain various lactones via intramolecular C–O bond formations [28]. The reactivity trends of various C(*sp*³)–H bonds of aliphatic carboxylic acids were as follows: α-C–H ≪ β-C–H < γ-C–H ≥ δ-C–H ~ ε-C–H bonds to give a mixture of lactones and the subsequent ring-opened hydroxy acid products. Thus butanoic acid when subjected to the C–H oxidation process resulted in a mixture of γ-C–H activation product (γ-butyrolactone) (16%), β-C–H activation product (β–butyrolactone) (2%), and the ring cleavage product of γ-butyrolactone (γ–hydroxy butanoic acid) (8%) (Scheme 2). The reaction preferentially proceeds through the involvement of a less-strained six-membered platinacycle species as obtained by the γ-C–H activation of butanoic acid. The β-butyrolactone was obtained as the kinetically controlled product. Furthermore, in the presence of β-, γ-, and/or δ-C–H bonds, no lactonization took place at α-C–H bonds in the substrate, indicating the intermediacy of a metallacycle species.

However, the prerequisite of high platinum loading and the nonselective product formation appeared as a major restriction of this Pt-based system. The true catalytic variant of this Pt^{2+}-based system was developed by utilizing $CuCl_2$ as the terminal oxidant. Thus, the catalytic system enables the C−H bond lactonization of α-amino acids, e.g., L-valine, in water medium to produce hydroxyvaline isomers, which can be isolated in the form of *N*-Boc-lactones in moderate yield (Scheme 3) [29]. Since

Scheme 1 Hetero-functionalization of aliphatic carboxylate equivalents via directed approach
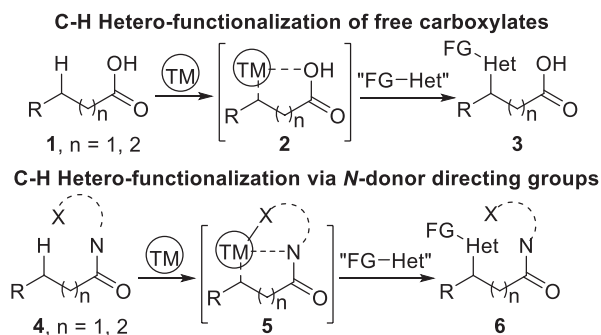
Scheme 2 The first directed lactonization of aliphatic acids
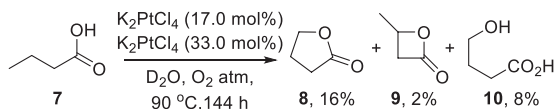
amino acids are known to pre-associate with a metal ion in a bidentate manner, the selectivity of this Pt-catalyzed C–H lactonization process was much higher compared to a simple aliphatic carboxylic acid.

Whereas Pt^{2+}-based system was proved to efficiently catalyze the direct lactonization, the examples of site-selective hydroxylation of carboxylic acids are limited. A finding by De Vos demonstrated that the γ-hydroxylation of *n*-butanoic acid can be achieved by a Pt^{2+} catalyst system, in which molecular oxygen acts as the terminal oxidant [30–32]. In this reaction, FeCl$_2$ was used as the co-catalyst, and *ortho*-substituted pyridine derivatives were used as additives to enhance the catalytic activity of the Pt^{2+} species. The selectivity towards γ-hydroxybutyric acid could be further improved by using boric acid as a protecting agent, thereby precluding the over-oxidation of the terminal primary hydroxy group (Scheme 4).

While Pt^{2+} catalysts were explored for lactonization and/or hydroxylation of carboxylic acids through intramolecular C–O bond formation, van Gemmeren et al. described that a Pd-based catalyst system is capable of enabling the intermolecular β-acetoxylation of various aliphatic carboxylic acids in the presence of acetic anhydride as the external acetoxylating agent (Scheme 5) [33]. In this reaction, in situ-prepared carboxylate salts from the acid substrate and conventional bases showed deleterious effect compared to pre-synthesized sodium carboxylate salt as the substrate. Interestingly, the sodium salt of the functioning solvent, HFIP, was found to serve as a "traceless" base to free carboxylic acid substrates giving the best result in terms of both reactivity and selectivity. In all cases the acetoxylation took place regioselectively at the terminal methyl (β-C–H) groups. A simple alteration of the catalyst system provided access to a range of β-oxyacylated derivatives of pivalic acid (Scheme 5).

2.2 Hetero-functionalization of Carboxylic Acid Equivalents via Monodentate Directing Groups

Due to modest chelating ability of carboxylic acids towards transition metals, the scope of direct hetero-functionalization of those compounds is rather narrow and limited to only C–O bond formations. Nevertheless, the coordinating ability of carboxylates is enhanced by protecting them as an amide having an N-based polar chelating functionality, e.g., pyridine. In a subsequent synthetic step, after the desired hetero-functionalization process, the N-donor functional group can be removed to obtain the heteroatom-decorated carboxylic acid. However, these sequential hetero-functionalizations of aliphatic carboxylic acids constitute step- and energy-intensive processes.
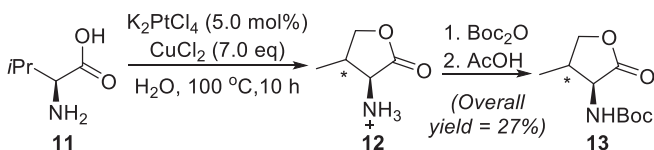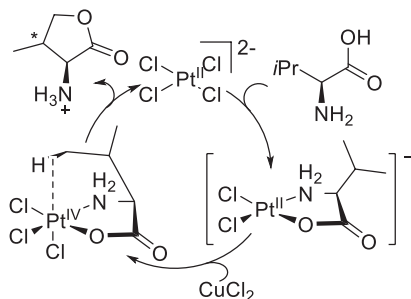
Scheme 3 Lactonization of L-valine via Pt catalysis

C–O bond formation: In 2005, Yu et al. developed a C(*sp*³)–H acetoxylation of methyl groups of aliphatic carboxylic acids via transforming them into strongly chelating 2-substituted 4,4-dimethyloxazolines [34]. The acetoxylation took place swiftly with Ac_2O, at the β-position with respect to the oxazoline ring using MeCOOOtBu as an inexpensive oxidant through a trinuclear Pd intermediate containing five-membered palladacycles (Scheme 6). When chiral oxazoline was used as the directing auxiliary, the β-acetoxylation proceeded in diastereoselective fashion. Notably in the latter case, lauroyl or benzoyl peroxide was employed in place of MeCOOOtBu as the oxidant.

C–N bond formation: The strongly electron-withdrawing monodentated *N*-arylamide directing group enables the intermolecular β-C-H amination of carboxylic acids in the presence of Pd(allyl)Cl_2 and electron-deficient P[3,5-$(CF_3)_2C_6H_3]_3$ ligand system [35]. The amination technique was applied for the structural modification of a drug molecule gemfibrozil **24** (Scheme 7). In this reaction, the oxidative addition of the *O*-benzoyl hydroxylamine to Pd⁰ triggers the catalytic cycle that affords the C-N coupled product at the reductive elimination step without using further external oxidant (Scheme 8) [36, 37]. The reaction was highly monoselective in terms of amines, as the newly assembled amino substituent inhibits the palladium catalyst from activating the second methyl group due to bidentate chelation. The *N*-arylamide auxiliary can be cleaved to achieve the corresponding β-amino acid.

C–B bond formations: Diversely substituted borylated carboxylic acids/equivalents function as fundamentally important synthetic intermediate for preparing drug scaffolds. Direct borylation of aliphatic carboxylic acid amides by activating a C(*sp*³)-H bond can be attained using palladium catalysts; however, it possessed significant challenges due to the following reasons: (1) reductive elimination of a C–B bond from the borylated palladium complex demands strategic ligand design

Scheme 4 γ-Hydroxylation of *n*-butanoic acid using molecular O_2 as the oxidant

$$\text{14} \xrightarrow[\substack{H_2SO_4/H_2O,\ O_2\ (20\ \text{bar}),\\ 150\ ^\circ C,\ 6\ h}]{\substack{K_2PtCl_4\ (1.0\ \text{mol\%})\\ FeCl_2\ (5.0\ \text{mol\%})\\ H_3BO_3\ (1.0\ \text{eq})}} \text{15, 47\%}$$
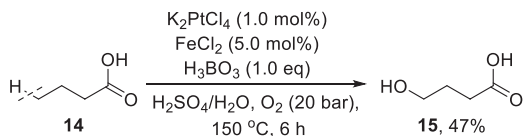
[38–41] and (2) the resulting C–B bonds are often reactive and may undergo further transmetallation leading to deborylated and/or β-hydride eliminated products [42, 43]. Yu et al. developed a palladium-catalyzed, ligand-enabled procedure for the C(sp^3)-H β-borylation of alkyl carboxylic acids using a monodentate fluorinated directing group [44]. The palladium-based system, comprising an electron-rich and sterically less hindered quinoline ligand, when combined with tetrabutylammonium tetrafluoroborate (TEABF$_4$) exhibited superior results in terms of both yield and selectivity (Scheme 9). The β-borylated products can be further transformed into the corresponding β-hydroxylated compounds through a subsequent reaction step (Scheme 10).

The enantioselective variant of the Pd-catalyzed β-C(sp^3)−H borylation of cycloalkane carboxylic acid amides was achieved by using a mono-*N*-protected amino acid (MPAA) ligand, namely, acetyl-protected aminomethyl oxazoline (APAO). Modification in the oxazoline ligand core enables the enantioselective borylation of various weakly coordinating cycloalkane carboxamides, e.g., cyclopropanes, cyclobutanes, and cyclohexanes in excellent enantioselectivity [45]. Thus, while the borylation of cyclobutanes was operational by employing an (*S,R*)-oxazoline ligand **30**, that of cyclopropane and cyclohexane derivatives were realized by using **31** and **32**, respectively, as optimal ligands (Scheme 11). The borylated cyclohexanes were successively oxidized into the corresponding diastereo- and enantio-enriched alcohols. The absolute configuration of the products is in accord with the involvement of the transition state as shown in Fig. 1. The functional groups in the ligand framework exhibit a synergistic interplay to preferably form the five-membered palladacycle **40** over **41**.

Although the palladium-catalyzed borylation of cyclopropane carboxylic acid amides led to the formation of highly enantio-enriched monoborylated cyclopropane **36**, the scope of the transformation is inadequate as the bis-borylated cyclopropane ring-opened product **37** was always identified as the by-product. Nevertheless, by altering the palladium system with an iridium catalyst in conjunction with a chiral bidentate boryl ligand, the desired ring borylation of cyclopropyl amides was successfully achieved in high yield and enantioselectivity (Scheme 12) [46]. The stereochemical outcome of the reaction was justified by comparing the two proposed complexes (1*R*,2*S*)-**45** and (1*S*,2*R*)-**45** in the stereoselective oxidative addition step (Fig. 2).

In an independent report, the borylation of 2-alkyl-1,3-azoles at the β-C-H bond with regard to the azole ring in the 2-alkyl side chain was achieved by means of silica-supported monophosphine-iridium catalyst [47]. The borylation strategy was equally effective for both primary and secondary C(sp^3)-H bonds of alicyclic and acyclic substituents attached with the azole ring (oxazoles, thiazoles, and imidazoles). However, benzazoles bearing sterically less congested alkyl chains often
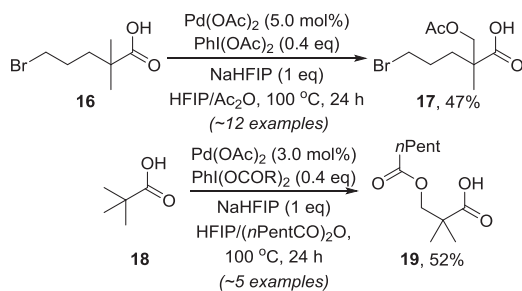
Scheme 5 Direct intermolecular acyloxylation of carboxylic acids
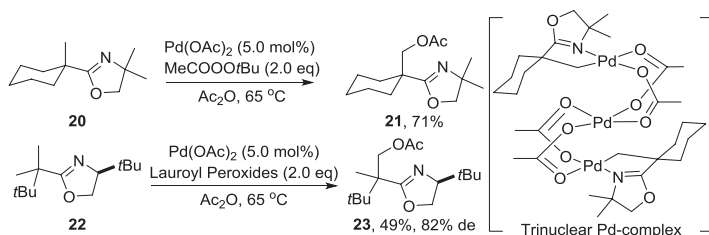
Scheme 6 Oxazoline-directed C(sp^3)–H acetoxylation of methyl groups
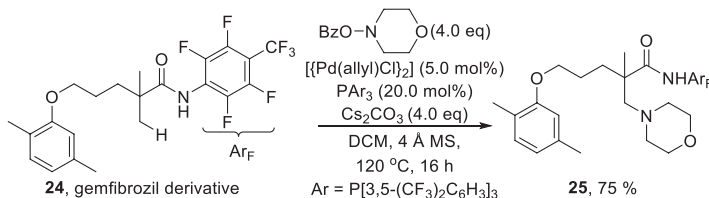
Scheme 7 β-Amination of gemfibrozil amide using a monodentate DG

resulted in a mixture of monoborylated and *geminal* bis-borylated products. The monoborylated compound **47** can be converted into a tertiary amine through a subsequent reaction step (Scheme 13).

C–halogen bond formations: Halogenated carboxylic acids and amides act as vital building blocks as they can be further transformed into useful synthetic compounds relying on dehalogenation and C–halogen bond activation strategies. The iodination of β-C–H groups with respect to a σ-chelating oxazoline auxiliary was achieved by molecular I_2 in the presence of Pd(OAc)$_2$/PhI(OAc)$_2$ system [48]. Thus, the cyclopropane substrate prepared from (*R*)-*tert*-leucinol was iodinated as a single stereoisomer that can be transformed into the corresponding carboxylic acid ester in outstanding enantioselectivity (99% ee) upon a hydrolysis/esterification sequence (Scheme 14). One of the unique advantages of this catalytic system is the recyclability of the Pd catalyst that precipitates as PdI$_2$ at the end of the reaction and can be further reused.

Scheme 8 Proposed catalytic cycle for the β-amination of monodentate carboxamides

L = P[3,5-(CF$_3$)$_2$C$_6$H$_3$]$_3$
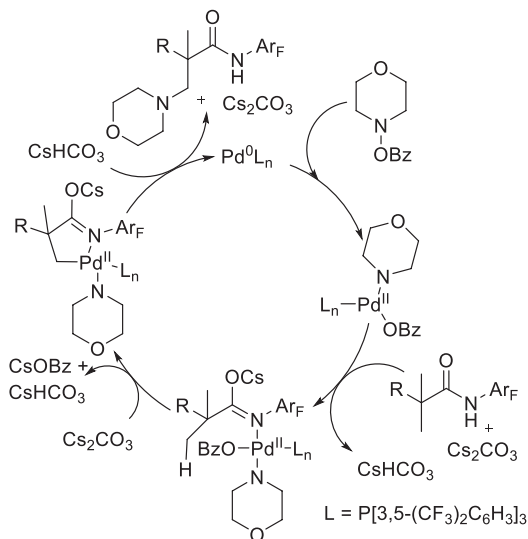
Scheme 9 Pd-catalyzed β-borylation of carboxylic acid amides

Pd(OAc)$_2$ (10.0 mol%)
L (20.0 mol%)
AcOH (20.0 mol%)
KHCO$_3$ (2.0 equiv),
TEABF$_4$ (50.0 mol%)

CH$_3$CN, 80 °C, O$_2$, 15 h

27, 71%

Plausible reaction mechanism
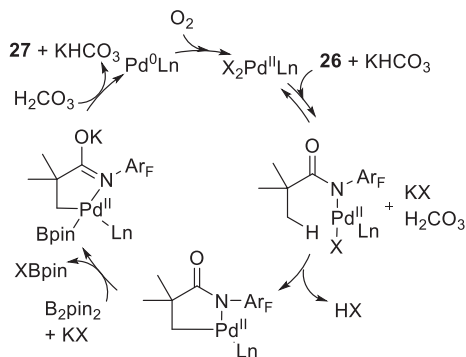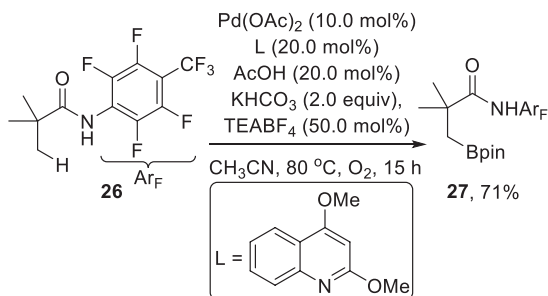
Developments along this direction show alkyl carboxamides, having electron-withdrawing *N*-aryl groups, can be fluorinated, brominated, as well as iodinated at β-C(*sp^3*)–H bonds using palladium/electron-rich ligand systems. It is worth mentioning that the presence of a more acidic α-proton decreases the Thorpe–Ingold

Scheme 10 Transformation of β-borylated products
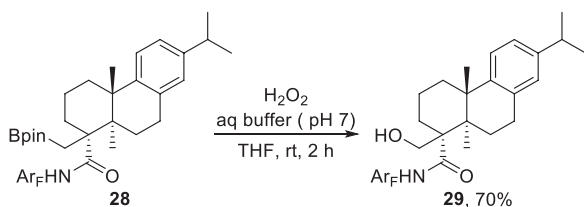
Scheme 11 Pd-catalyzed enantioselective direct borylation of cycloalkane carboxylic acids
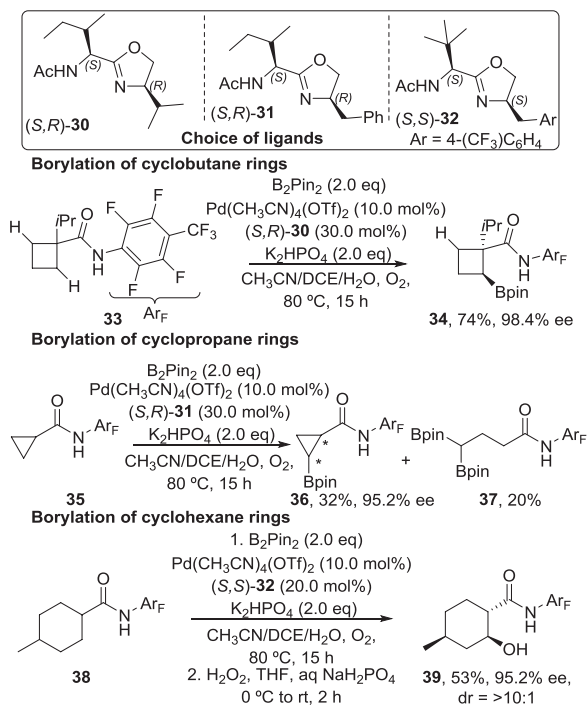
Fig. 1 Predicted stereochemical model for borylation of cyclobutane rings
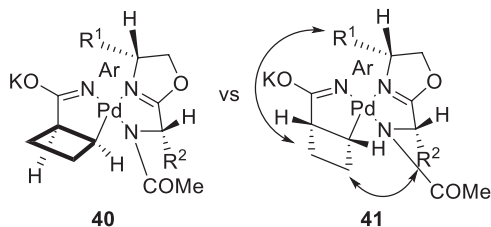
effect, thereby decelerating the formation of metallacycle intermediate, and that in the halogenated product is prone to undergo dehalogenation [49]. Nonetheless, these reaction systems efficiently enable halogenation, e.g., β-fluorination, β-bromination, and β-iodination of α-unsubstituted/protonated carboxamides (Scheme 15) [50, 51].
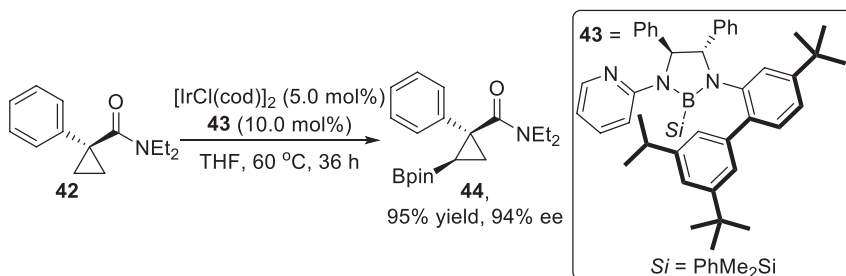
Scheme 12 Highly regio- and enantioselective C–H borylation of cyclopropane carboxamides
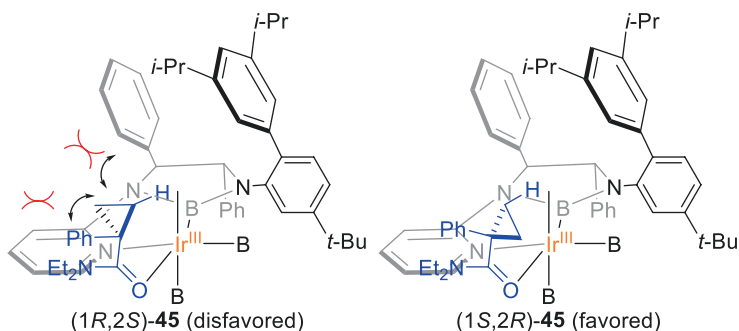
Fig. 2 Predicted stereochemical model for the borylation of cyclopropane
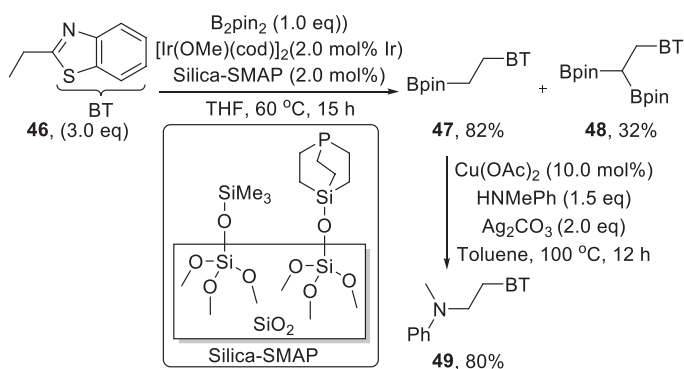
Scheme 13 β-Borylation of benzazoles via iridium catalysis
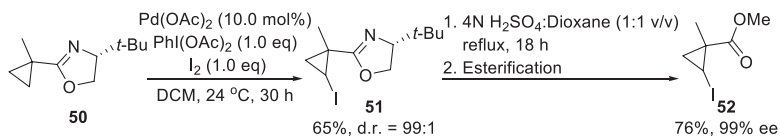
Scheme 14 C–H iodination of cyclopropane ring under the assistance of monodentate oxazoline group

2.3 Hetero-functionalization of Carboxylic Acid Equivalents via Bidentate Directing Groups

Since the influential work by Daugulis on 8-aminoquinoline-directed C–H bond functionalization of arenes under palladium catalysis, the bidentate directing group-assisted C–H functionalization has emerged as a fascinating area of research in organic chemistry [52]. A series of N,N-, N,O-, and N,S-bidentate directing groups were developed for the hetero-functionalization of aliphatic carboxylic acids [14, 53–55]. Due to stronger chelating aptitude of bidentate directing groups towards transition metals compared to that of monodentate counterparts, the formation of metallacycle intermediates is thermodynamically more favored. In addition, simple installation and cleavage of those directing groups augment the practical applicability of the catalytic approaches [54, 55].

C–O bond formation: The directed C(sp^3)–H bond oxy-functionalization under the assistance of a bidentate chelating group is one of the most explored hetero-functionalization approaches for carboxylic acids. In 2005, Corey et al. reported the first example of a palladium-catalyzed direct acetoxylation of α-amino acids via transforming them into 8-aminoquinoline-derived amides [56]. Common α-amino acids, including leucine, alanine, β-phenylalanine, etc., were acetoxylated with acetic anhydride at the β-carbon center with regard to the 8-aminoquinoline amide giving an expedient entry to β-hydroxy- and β-acetoxy-α-amino acids that serve as versatile building blocks for numerous bioactive compounds (Scheme 16) [57–60]. The rate of this C–H oxidation process was notably enhanced by the presence of Mn^{2+} that was believed to form $Mn_3O(OAc)_7$ under oxidative condition, hence acting as a Lewis acid to ease the palladacycle **60** formation.

A copper-catalyzed strategy for the acetoxylation of methyl groups in simple carboxamides was also described with the aid of 8-aminoquinoline directing auxiliary. Hence, $Cu(OAc)_2$ in conjunction with AgOAc promotes the β-acetoxylation of terminal methyl groups in respect to the bidentate 8-aminoquinolinyl amide substituent (Scheme 17) [61]. However, a mixture of mono- and bis-acetoxylated products was resulted for substrates bearing two chemically alike methyl groups at β-position. The cleavage of the chelating auxiliary can be performed under mild reaction condition to afford the primary amide.

The C(sp^3)–H acetoxylation of carboxylic acids was also reported to proceed under the influence of another bidentate coordinating substituent, *S*-methyl-*S*-2-pyridylsulfoximine (MPyS) [62, 63]. In this case the five-fused five-membered palladacycle intermediate is formed via the coordination of the directing group through pyridyl and sulfoximine nitrogens to the palladium center. Gratifyingly, the reaction condition was tuned to obtain mono-acetoxylated products at room temperature and bis-acetoxylated products at an elevated temperature (70 °C) (Scheme 18). The free β-hydroxy carboxylic acids can be accessed via the removal of the exquisite *S*-methyl-*S*-2-pyridylsulfoximine (MPyS) auxiliary from the acetoxylated carboxamides.
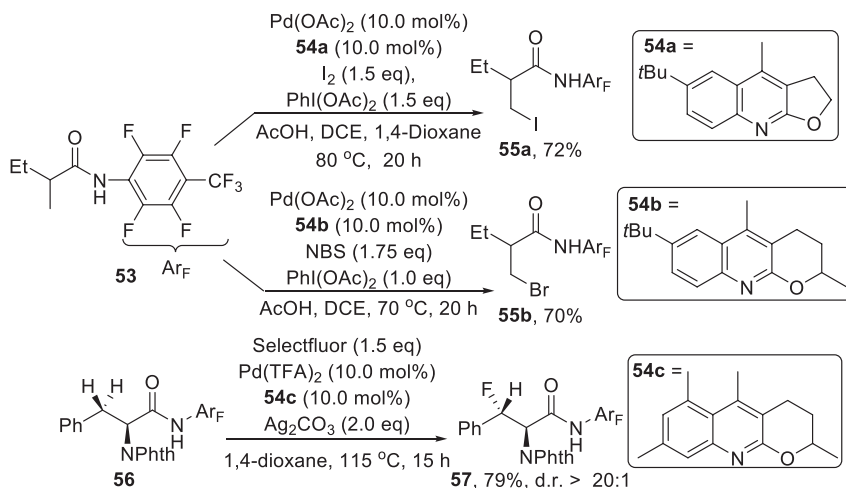
Scheme 15 Pd-catalyzed β-halogenation in the presence of α-protons
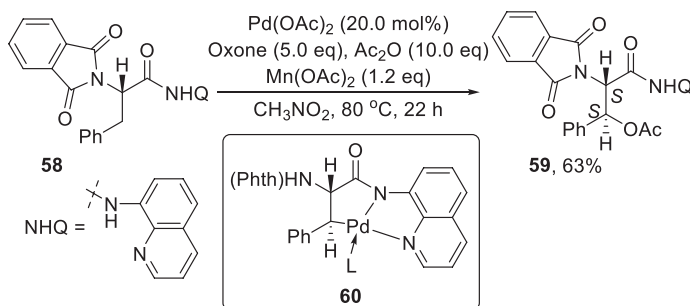
Scheme 16 Direct β-acetoxylation of α-amino acids

While the scope of direct acetoxylation methods consists of ample examples in terms of both acid substrates and chelating directing groups, that of C(sp^3)–H alkoxylations is rather sporadic. The first alkoxylation of inactivated methylene C–H bonds with alcohols was accomplished by using a Pd-based catalyst system incorporating hypervalent iodine (I^{3+}) reagents as the oxidant [64]. Of note, the catalytic activation of a methylene C–H bond is a difficult task owing to more steric demand and a more facile β-hydride elimination in comparison to methyl groups. For the targeted alkoxylation, the active alkoxylating I^{3+} agent **70** was generated by mixing MeOH with Dess–Martin periodinane (DMP) (I^{5+}). The use of an alcohol as the solvent, in the presence of **70**, allows for attaching the corresponding alkoxy group at the β-position of 8-aminoquinoline-derived aliphatic carboxamides (Scheme 19). The late-stage derivatization of few anti-inflammatory drugs, e.g., ibuprofen, naproxen, flurbiprofen, ketoprofen, etc., was realized by using the alkoxylation technique (Scheme 20).
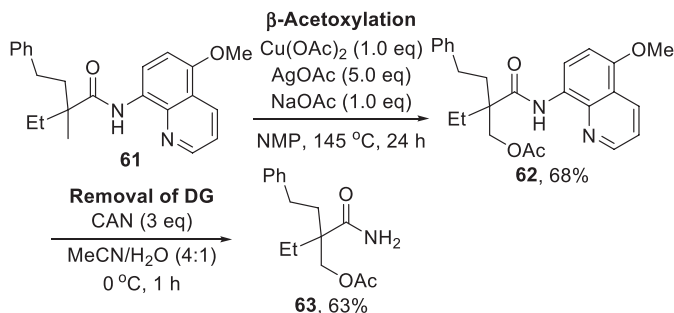
Scheme 17 Copper-catalyzed acetoxylation of methyl groups
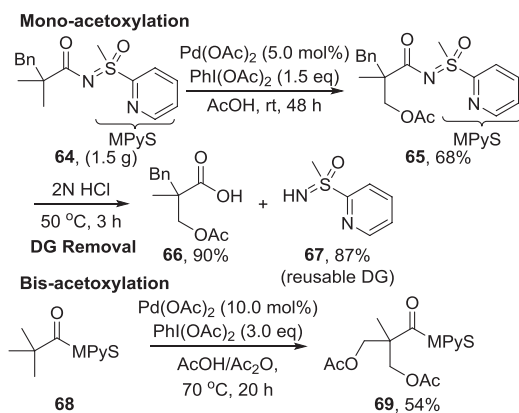
Scheme 18 Use of sulfoximine directing group for acetoxylation of methyl groups

By utilizing this approach, both symmetrical and unsymmetrical acetals were accessed via geminal double alkoxylation at the β-carbon center [65]. The installation of the second alkoxy group, however, was found tricky and required Ag_2CO_3 as the crucial additive to promote the desired twofold alkoxylation giving a series of symmetrical acetals by using an alcohol as the solvent. This protocol constitutes a complementary route to acetals without making use of aldehyde substrates. However, the optimized reaction condition for symmetrical acetals could not be applied for accessing unsymmetrical acetals as premixing of two dissimilar alcohols always led to the symmetrical acetal from the relatively active alcohol. Instead, the second alcohol had to be employed into the reaction vessel after completion of the first alkoxylation step. Thus in a sequence, after realizing the first monoalkoxylation with R^1OH, the alcohol solvent was removed and the second alcohol R^2OH along with the oxidant was introduced in the same reaction vessel to conduct the second alkoxylation to furnish unsymmetrical acetal products (Scheme 21).

The directed approach for the alkoxylation of C(*sp³*)–H bonds was also expanded to other bidentate directing groups. A pyridine-based auxiliary among various

Scheme 19 β-Acetoxylation of unactivated methylene C(sp^3)–H bonds
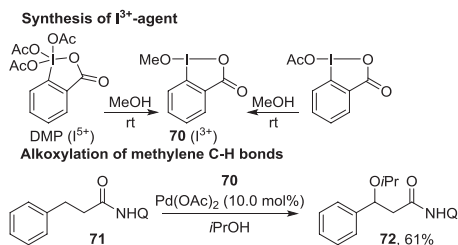
Scheme 20 Late-stage modification of ibuprofen
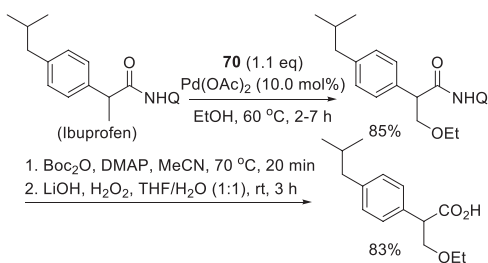
N-donor directing groups, holding *gem*-dimethyl substituents at the benzylic site next to the pyridine ring, promotes the palladium-catalyzed methoxylation process at considerably faster rate (Scheme 22) [66]. This is possibly attributed to the fact that the formation of the metallacycle intermediate is accelerated through entropic restraint and bond angle compression by the *gem*-dimethyl substituents.

Notably, the typically used Pd(OAc)$_2$/PhI(OAc)$_2$ catalyst system enables the β-C(sp^3)–H alkoxylation of PIP-decorated amides in the presence of a 1:1 combination of *m*-xylene and an alcohol. The PIP group can be detached from the β-alkoxylated products under mild condition to form the corresponding carboxylic acids (Scheme 23).

However, relatively little prospect has been made in building C(sp^3)−O bonds via directed approach by means of a chiral auxiliary. Along this track, an intramolecular etherification was realized in stereoselective manner with the aid of a privileged chiral bidentate group in the absence of an optically active ligand. The reaction yields numerous sterically demanding cyclic ethers and oxaspirocyclic compounds in highly diastereoselective manner (up to dr = 39:1) (Scheme 24) [67, 68]. Mechanistic investigation and DFT calculations indicate that only low levels of diastereoselectivity were persuaded at the C–H metalation–deprotonation step and were markedly enhanced at the reductive elimination step.

C–S and C–Se bond formation: Synthesis of chalcogenated acids, particularly thioether-substituted carboxylic acids/equivalents, via chelation-assisted direct functionalization of a C–H bond is a rather new-fangled approach. The major hitches associated with thiolating a C–H bond is originated due to the catalyst poisoning effect by the sulfur agent [69]. Nevertheless, the catalyst retarding effect can be minimized with the use of dichalcogenides. For example, 8-aminoquinoline-derived amides were thiolated at the β-carbon centers by using disulfides

Scheme 21 Synthesis of acetals via double alkoxylation of C–H bonds

Synthesis of symmetrical acetals

Pd(OAc)$_2$ (7.5 mol%)
70 (3.5-4.0 eq)
Ag$_2$CO$_3$ (1.0 eq)
OH, 80 °C, 4 h

73 → **74**, 66%
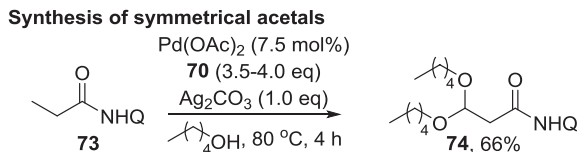
Synthesis of unsymmetrical acetals

1. Pd(OAc)$_2$ (15.0 mol%)
70 (1.5-2.0 eq),
Ag$_2$CO$_3$ (0.5 eq)
R^{1}OH, 80 °C, 4 h

2. Pd(OAc)$_2$ (7.5 mol%)
70 (2.0-2.5 eq),
Ag$_2$CO$_3$ (0.5 eq)
R^{2}OH/*m*-xylene (1:1)
120 °C, 4 h

73 → **75**, 56%
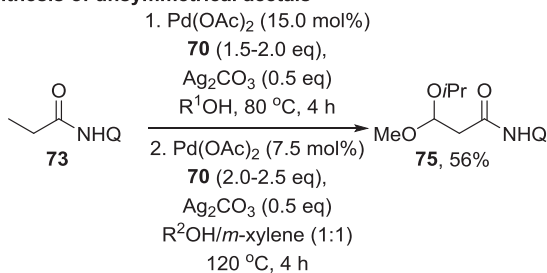
Scheme 22 Identification of N-donor directing group for the alkoxylation

Pd(OAc)$_2$ (10.0 mol%)
PhI(OAc)$_2$ (3.0 eq)
MeOH, 90 °C, 24 h

76 → **77**

DG =

77a, 0%   **77b**, 0%

77c, 0%   **77d**, 0%   PIP **77e**, 50%
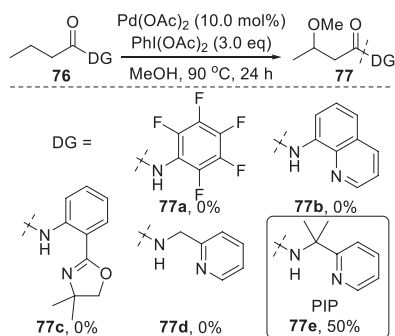
Scheme 23 PIP-directed alkoxylation of C(*sp³*)–H bonds

Pd(OAc)$_2$ (10.0 mol%)
PhI(OAc)$_2$ (1.5 eq)
MeOH:*m*-Xylene (1:1),
90 °C, 24 h

78 → **79**, 90%

1. AcOH/Ac$_2$O, NaNO$_2$,-15 °C
2. LiOH, 30% H$_2$O$_2$, THF-H$_2$O
3. Na$_2$SO$_3$

80, 87%
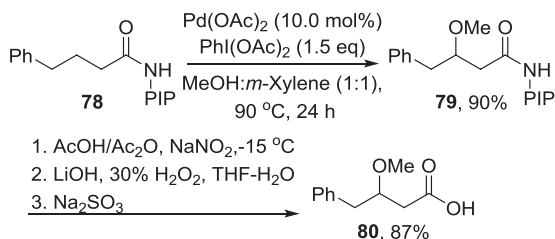
(Scheme 25). Nickel-based catalyst systems permitted the required transformation by oxidizing β-C–H bonds of methyl groups with high monoselectivity [70, 71]. These thiolations proceed via the formation of a five-fused five-membered nickelacycle intermediate, and commonly the C–S bond formations occur at the reductive elimination step. Subsequently, the 8-aminoquinoline auxiliary was simply removed by hydrolysis to furnish the corresponding thioether-substituted acid that can be further derivatized.

Scheme 24 Chiral auxiliary-directed C(sp^3)–O bond formation
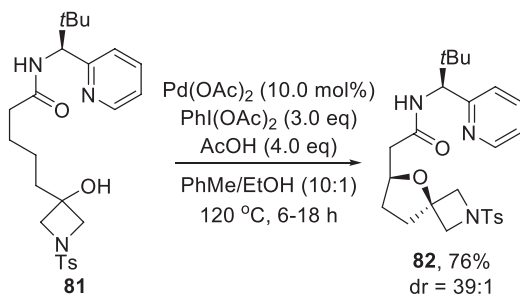
Scheme 25 Nickel-catalyzed direct thioetherification of carboxamides
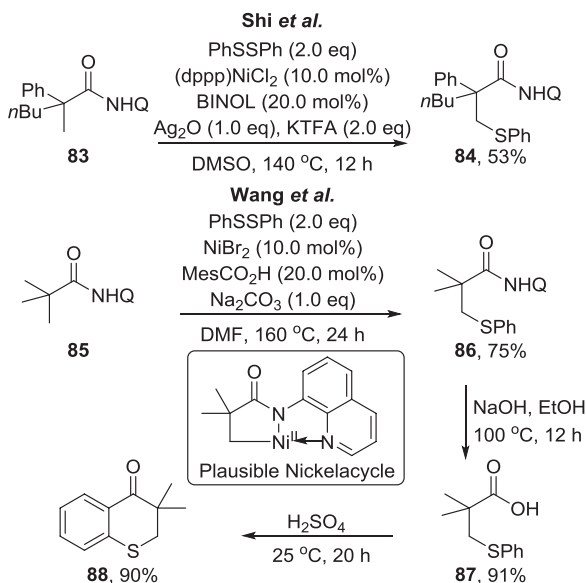
In another report, it was demonstrated that even free thiophenols can be employed for the direct thioetherification of β-C–H bonds of terminal methyl groups in 8-aminoquinoline-derived carboxamides (Scheme 26) [72].

Not only arylthiolations, 8-amidoquinolines also direct the palladium-catalyzed arylsulfonylation of C(sp^3)–H bonds with sodium sulfinates as the S-coupling counterpart to provide an extensive range of aryl alkyl sulfones (Scheme 27) [73]. The sulfur atom in sodium sulfinate, being soft in nature, prefers to coordinate to the palladium catalyst over oxygen atoms and thus reductively eliminates arylsulfonyl-ated products. Several complex molecules, including a cholic acid derivative, underwent late-stage sulfonylations under the operative condition.

Direct trifluoromethylthiolation also proceeded swiftly with the electrophilic SCF$_3$ agent **95** to afford the β-thiolated carboxamide products (Scheme 28) [74]. The reaction relies on a higher-valent Pd^{IV} intermediate formed in situ by oxidizing the trifluoromethylthiolating agent [75, 76].

Scheme 26 Nickel-catalyzed arylthiolation with free thiophenol

89

SH / F (4.0 eq)
Ni(OTf)$_2$ (20.0 mol%)
LiO*t*Bu (7.0 eq)
DMF, 120 °C

90, 80%

91

PhSO$_2$Na (2.0 eq)
Pd(OAc)$_2$ (10.0 mol%)
MesCO$_2$H (20.0 mol%)
Ag$_2$CO$_3$ (2.0 eq)
DCM, 90 °C

92, 44%

93, Cholic acid derivative

Sulfinylation Condition

NHQ = 8-Aminoquinolinyl

94, 43%
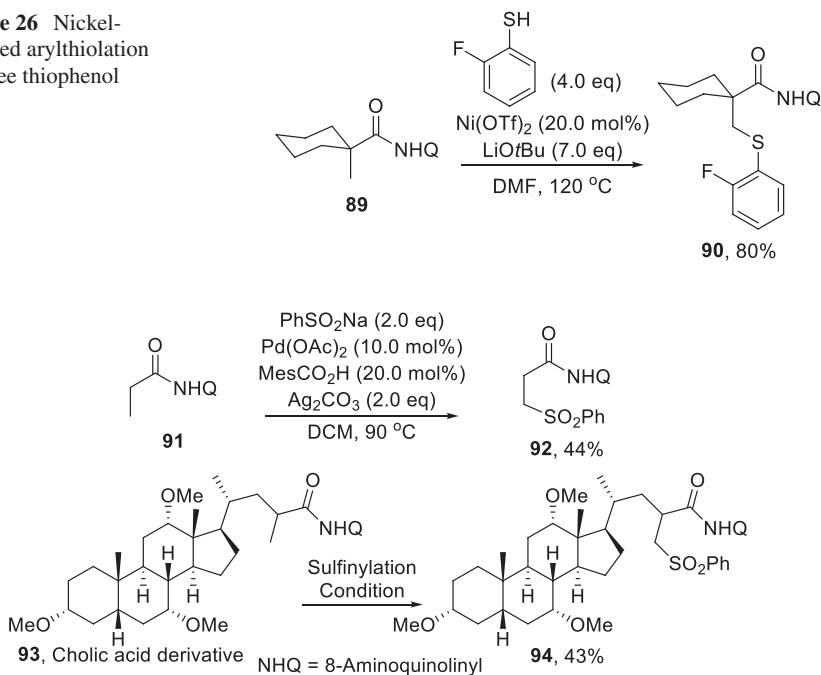
Scheme 27 Sulfonylation of terminal β-C–H bonds of carboxamides

All these regioselective β-C(*sp*³)–S bond formations depend on the thermodynamic steadiness of a five-membered metallacycle intermediate. The chalcogenation at γ-position would require an analogous C–H activation strategy that proceeds through a six-membered metallacycle intermediate and is however challenging due to constitutional and conformational constraints. A Pd^{II}-catalyzed approach was introduced for the regiospecific γ-thioarylation of aliphatic carboxylic acids controlled by 8-aminoquinoline directing group. This γ-thioarylation technique was also applied to structurally modify common α-amino acids, e.g., valine, isoleucine, *tert*-leucine, etc. A similar mechanism also operates for the arylselenylation of 8-amidoquinolines giving an appropriate entry to selenoether-decked carboxylates (Scheme 29) [77].

C–N bond formation: Given the abundance of nitrogen-rich aliphatic carboxylic acid equivalents in natural and synthetic organic compounds, the installation of an amine-based functional group via C–H bond activation of aliphatic carboxylic acid precursors under transition metal catalysis has received significant interest. The first example of a C(*sp*³)-H group activating amination of aliphatic carboxylic acid amides was mediated by bidentate 8-aminoquinoline (AQ) and 2-pyridylmethyl amine (PM) directing groups. The amination proceeds intramolecularly at the γ-position with respect to the directing group under palladium catalysis [78]. Both AQ and PM directing groups gave comparable outcome; however, slightly higher temperature was required in the case of using PM as the directing group (90 °C vs.
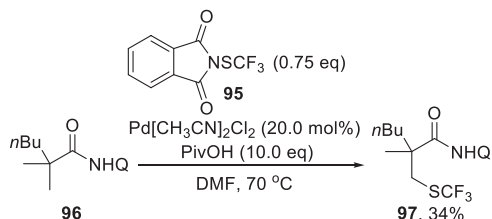
Scheme 28 Trifluoromethylthiolation of primary C(sp^3)–H bonds
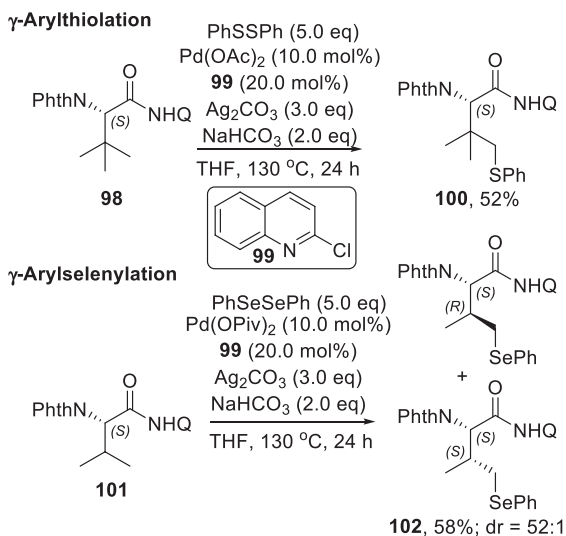
Scheme 29 γ-Chalcogenation of C(sp^3)–H bonds directed by a bidentate group

110 °C). A protocol for the facile cleavage of the quinolinyl directing group was also illustrated (Scheme 30).

Subsequently, the bidentate ligation by the directing groups has been profoundly utilized for intra- as well as intermolecular amination reactions of aliphatic carboxylic acid amides. While majority of the intramolecular C–N bond-forming reactions led to β-lactam cores, the intermolecular version provided β-aminated products. For instance, Shi et al. developed a palladium-catalyzed monoarylation/amidation sequence for *N*-protected amino acids delivering chiral α-amino-β-lactam scaffolds by means of 2-(pyridin-2-yl)isopropyl (PIP) directing group (Scheme 31) [79].

However, the PIP auxiliary cannot be removed from the resulting highly functionalized β-lactam moieties. This has restricted the general synthetic practicality of this sequential amidation method. When the PIP group was replaced with 8-aminoquinoline, the sequential monoarylation/amidation under a slightly modified catalytic condition also provided similar class of α-amino-β-lactam motifs from which the directing group can be removed [80]. Thus, upon the ring cleavage, the
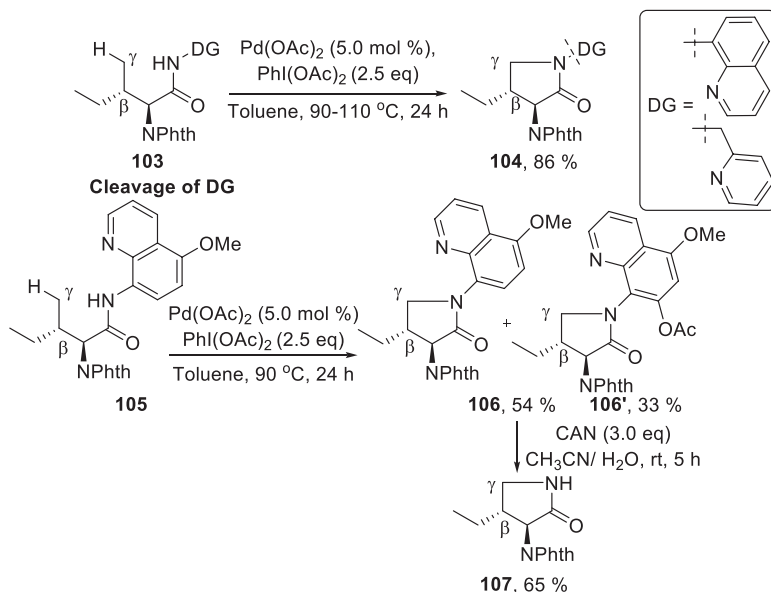
Scheme 30 Intramolecular amination of γ-C(sp^3)–H bonds

β-lactam can be further converted into orthogonally protected *anti*-α,β-diamino acids (Scheme 32).

In another report, it has been documented that pentafluoroiodobenzene, being an electron-withdrawing agent, can act as a crucial component of the Pd^{II}/Pd^{IV}-based catalytic cycle for the 8-aminoquinoline-directed intramolecular lactamization by not only regulating the steric and electronic nature of intermediates in favor of the C−N bond formation but also as an oxidant to the Pd^{II}-metallacycle species (Scheme 33) [81, 82].

This fine-tuning of the catalytic system by the addition of C_6F_5I has enabled the straightforward synthesis of β-lactams with 5/4, 6/4, 7/4, or 8/4 cis-fused ring systems including the key fragment of the β-lactamase inhibitor MK-8712 (Scheme 34) [82].

Earth abundant, first row transition metals, e.g., copper, nickel, and cobalt, can also effectively catalyze the oxidation of methyl and methylene protons of 8-aminoquinoline-derived carboxylic amides. The β-lactam ring is constructed via the activation of a β-C(sp^3)–H bond through the formation of five-fused five-membered metallacycle, similar to a palladacycle intermediate. The copper-catalyzed intramolecular amidation of 8-aminoquinoline-derived carboxamides to β-lactams was accomplished by employing either silver carbonate or duroquinone as the stoichiometric oxidant (Scheme 35) [83, 84]. The C(sp^3)–H lactamization took place favorably at the terminal β-methyl group or at internal β-benzylic
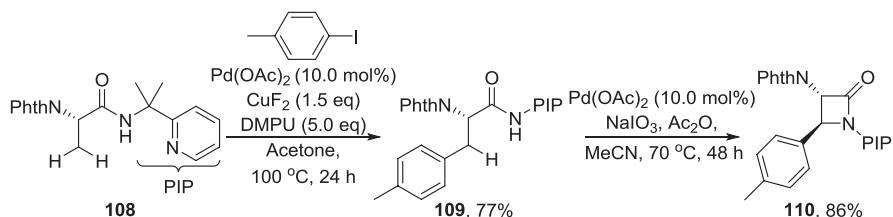
Scheme 31 Synthesis of β-lactam cores via sequential β-arylation/amination of carboxamides
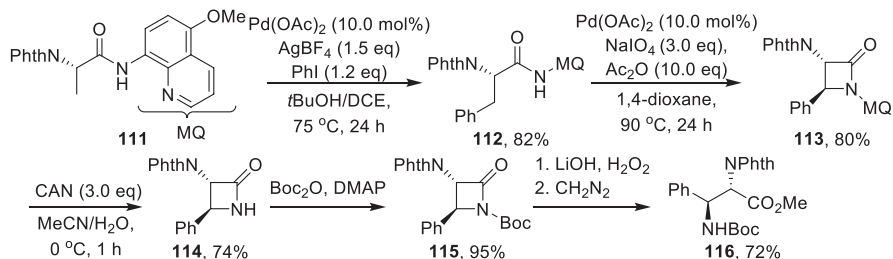
Scheme 32 Palladium-catalyzed β-lactam synthesis and further derivatization
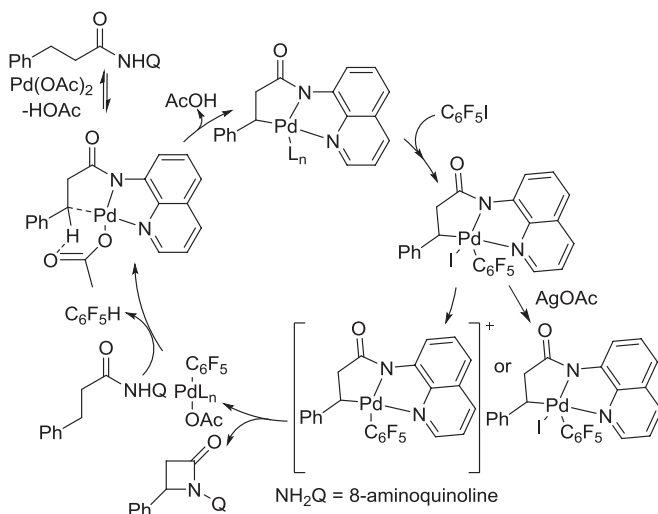
Scheme 33 Influence of C$_6$F$_5$I in controlling the C–N bond formations

position of the alkane residue giving practically useful synthetic yields. The copper-catalyzed reaction system follows the reactivity trend as β-benzylic > β-methyl > β-ring > β-linear carbon centers. However, the substrate scope is slightly narrower than the existing Pd-catalyzed intramolecular amidation protocol.

The copper-based catalytic cycle can also successfully operate to produce β-lactams in the presence of oxygen as the terminal oxidant. This Cu-catalyzed
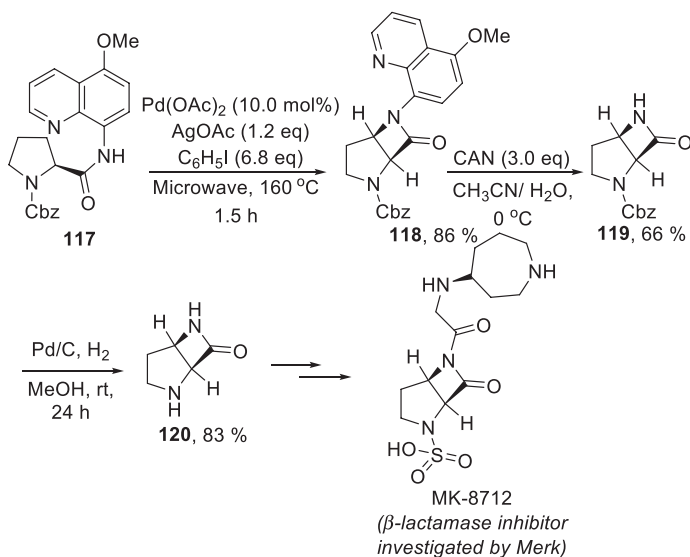
Scheme 34 Synthesis of a key fragment of β-lactamase inhibitor MK-8712 via C(sp^3)–H lactamization
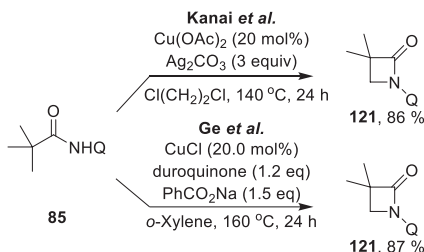
Scheme 35 Copper-catalyzed β-lactamization of 8-aminoquinoline-derived carboxamides

aerobic lactamization is particularly beneficial in terms of product economy and waste minimization (water is the only by-product) (Scheme 36) [85]. Contrary to the copper-catalyzed protocols that operate through employing silver carbonate or duroquinone as the oxidant, the aerobic system is highly site-selective for the oxidation of β-methyl groups even in the presence of a β-benzylic C–H bond. The *N*-quinolyl auxiliary can be elegantly disintegrated by further converting it into 5-methoxyquinolyl motif via coupling with a Ni-catalyzed methoxylation strategy (Scheme 37) [86–88].

A nickel-based catalyst system was also developed relying on the assumption that in the presence of an external single-electron oxidant, the Ni^{II} catalyst can undergo a Ni^{II}/Ni^{III} catalytic cycle in which the higher-valent Ni^{III} intermediate reductively eliminates the C–N cross-coupled product [89–91]. Thus, a catalyst system, consisting of Ni(dme)$_2$I$_2$ as the Ni^{II} source and TEMPO as the single-electron

oxidant, was found crucial for the highly selective lactamization process via β-C–H activation of methyl groups of 8-aminoquinoline-functionalized carboxamides. However, the scope of the reaction is limited to substrates having quaternary α-carbon centers (Scheme 38) [92].

In another independent Ni-catalyzed approach, an analogous C–H β-lactamization was attained under the assistance of 5-chloroquinoline-derived carboxamide in the presence of molecular iodine as the stoichiometric additive [93]. In this case, two reaction pathways were suggested for the formation of the β-lactam ring (Scheme 39). The first possibility involves a common C–N bond reductive elimination step from higher-valent cyclometallated Ni^{III} (**128**) or Ni^{IV} intermediate (**129**). The other route can be a stepwise mechanism in which a direct β-iodination of the aliphatic amide takes place followed by a ready intramolecular cyclization leading to the β-lactam ring. Interestingly, when the preformed β-iodinated amide **131** was subjected to amidation even in the absence of the Ni catalyst, molecular iodine, and other additives, the cyclized β-lactam product was predominated, indicating an indirect evidence for the stepwise pathway to be operational for the lactamization process.

A cobalt-based catalytic system was also introduced for the C–H β-lactam synthesis from 8-aminoquinolinyl amides. The catalyst system, comprising Co(OAc)$_2$,

Scheme 36 Synthesis of β-lactams via copper-catalyzed aerobic oxidation of methyl groups
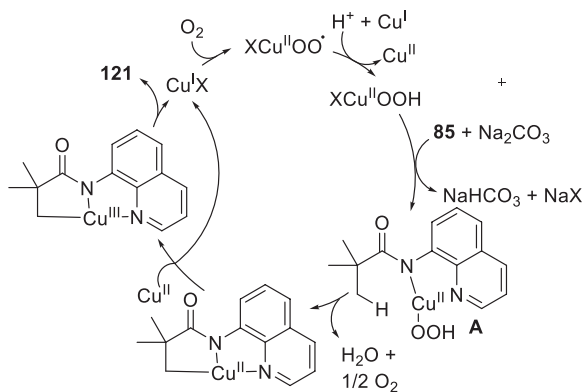
Scheme 37 Removal of the N-quinolyl protection from the β-lactam cores
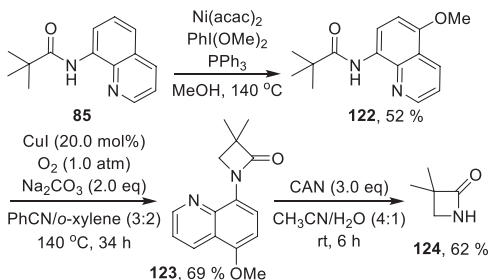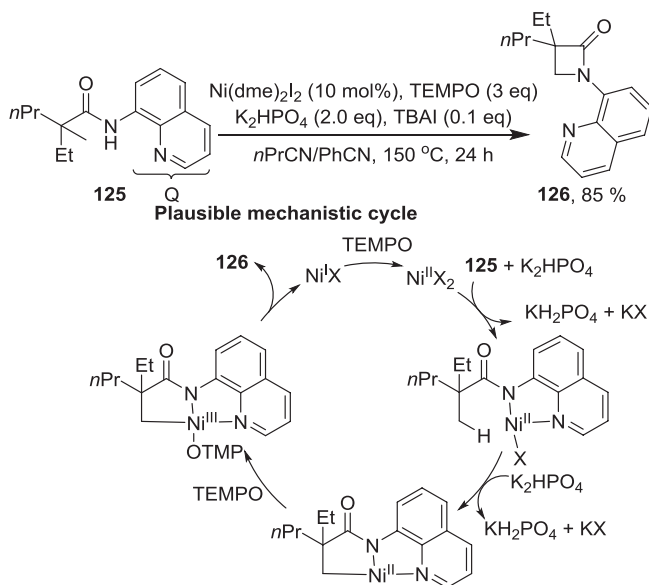
Scheme 38 Nickel-catalyzed β-lactam synthesis using TEMPO as a single-electron oxidant
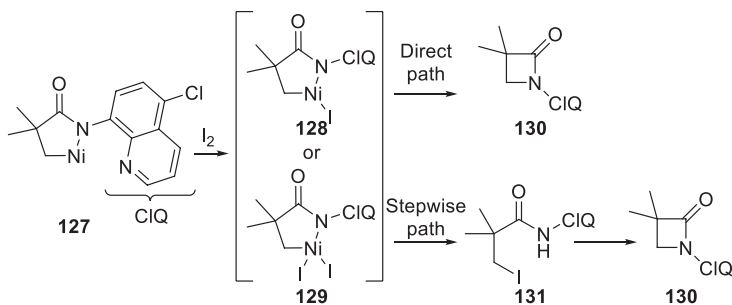
Scheme 39 Proposed reaction pathway for the iodine-mediated C–H lactamization reaction

Ag$_2$CO$_3$, and PhCO$_2$Na, operates in highly selective fashion to activate β-methyl groups even in the presence of more reactive β-benzylic groups [94]. However, the presence of γ-benzylic protons led to γ-lactams as the major product. However, when an aromatic ring was present at the α-carbon, the *ortho*-protons of the ring underwent activation under cobalt catalysis to provide indolin-2-one derivative as the predominant product (Scheme 40).

The cobalt system also promotes the intermolecular amination reaction via the C–N bond formation between 8-aminoquinoline-derived amides as the C–H substrate and α,α-disubstituted amides as the N source (Scheme 41) [94]. This
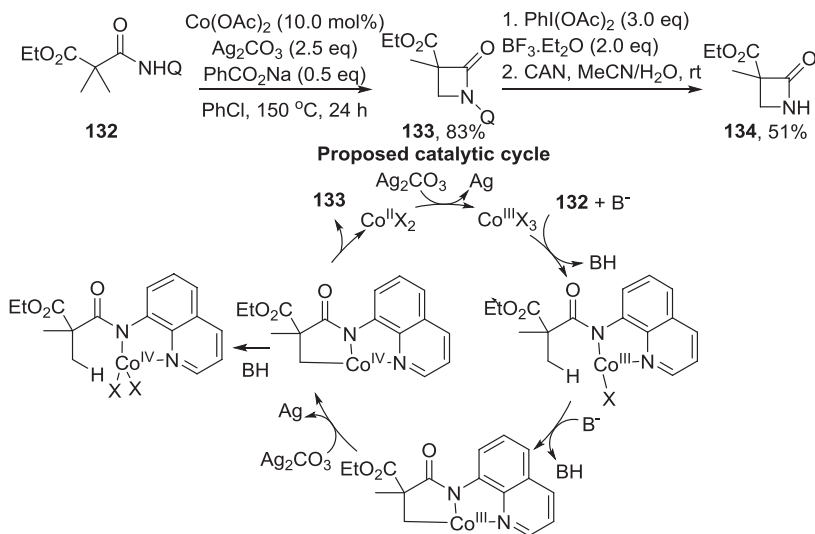
Scheme 40 Cobalt-catalyzed β-lactam synthesis by directed C–H functionalization

cobalt-catalyzed methodology constitutes the only example of oxidative β-amidation of aliphatic carboxylic acid amides.

The directed C–H amination of aliphatic carboxylic acid synthons through intermolecular C–N bond formation was also reported to proceed by using electrophilic N sources. Qin et al. reported that the hydroxylamine derivative **137** can be used as the amine source for the palladium-catalyzed amination of aliphatic carboxylic acid amides by means of a bidentate 2-aminothioether as the coordinating directing group (Scheme 42) [95]. This reaction proceeds via the oxidative addition of the N–O bond into Pd^{II} metallacycle intermediate, forming the Pd^{IV} species that leads to construct the new C–N bond after reductive elimination.

Another isolated example demonstrates that Pd(OAc)$_2$ can catalyze the intermolecular amination of 2-(pyridin-2-yl)isopropyl (PIP)-derived aliphatic carboxylic amides using diethyl azodicarboxylate (DEAD) as the N source under the influence of the bidentate chelation assistance of PIP group [96]. The diethoxycarbonyl hydrazine and the directing group were cleaved giving β-amino acid methyl ester (Scheme 43).

C–Si and C–Ge bond formations: Organosilicon compounds serve as highly significant synthetic intermediates in numerous organic transformations and are known to possess potential applicability in material sciences. However, successful examples for direct silylation via activation of unreactive C(sp^3)–H bonds of aliphatic carboxylic acid equivalents are only sporadic, presumably due to the reluctant migratory aptitude of the bulky silyl group to be transferred to the transition metal catalyst through transmetallation. The well-established bidentate directing group, 8-aminoquinoline, was employed to control the site-selective intermolecular silylation of unactivated aliphatic acids by utilizing commonly engaged Pd(OAc)$_2$/Ag$_2$CO$_3$ system (Scheme 44) [97]. However, while the protocol suffers from narrow
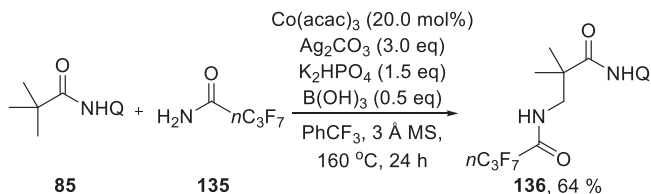
Scheme 41 Cobalt-catalyzed intermolecular C–H amination of carboxylic acid amides
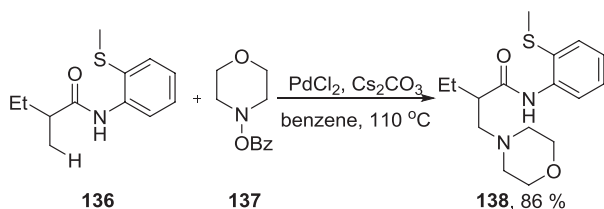
Proposed mechanism
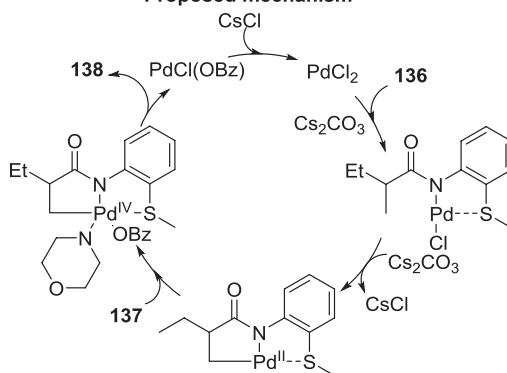
Scheme 42 Pd-catalyzed intermolecular electrophilic amination of carboxylic acid amides
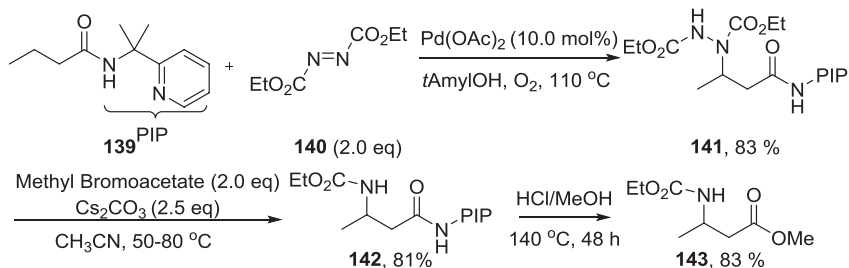
Scheme 43 Pd-catalyzed intermolecular amination with DEAD
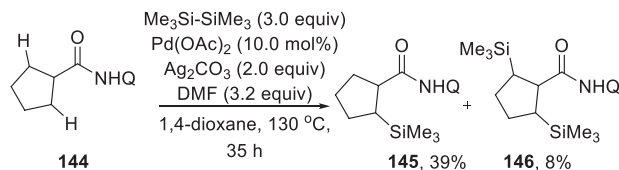
Scheme 44 8-Aminoquinoline-directed C(sp^3)–H silylation of aliphatic carboxamides
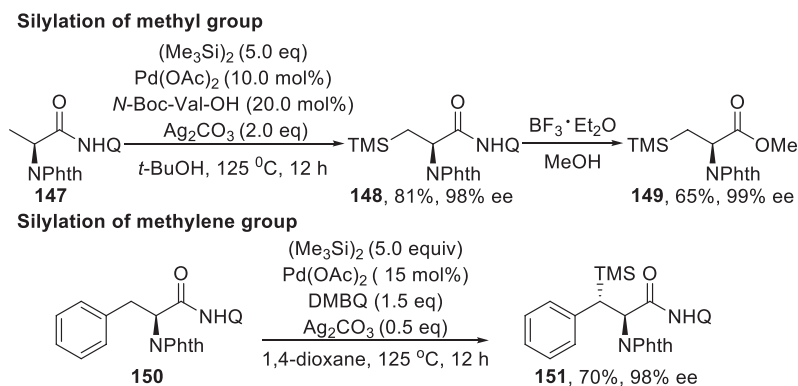
Scheme 45 Oxidative β-silylation of α-amino acids

substrate scope, poor product yields, and modest selectivity by giving a combination of mono- and bis-silylated products, this has constituted a novel opportunity in palladium-catalyzed C–H silylation reaction of aliphatic carboxylates.

Relying on a palladium-catalyzed protocol, *N*-phthaloyl-protected α-amino acids were directly converted into β-silyl-α-amino acids with 97–99% retention of stereoselectivity in the presence of hexamethyldisilane as the Si source [98]. Both methyl and methylene C–H bonds can be silylated using this approach (Scheme 45).

By applying a slightly modified reaction condition, bioactive molecules (−)-santonin can be silylated at the β-C–H bond (Scheme 46).

Further improvement of the palladium-based catalyst system was made by replacing the silver-based oxidant with *p*-benzoquinone (BQ) to realize the β-C–H bond silylation of simple aliphatic carboxylic amide substrates derived from 8-aminoquinoline (Scheme 47) [99].

Recently Maiti et al. have disclosed the first C–H silylation and germenylation at a more distal γ-position of the aliphatic carboxylic acid equivalents via the involvement of thermodynamically less stable six-membered palladacycle intermediate [100]. The preference for the six-membered palladacycle formation over the five-membered analogue was deliberately established by generating steric hindrance at the β-position. The Pd(OPiv)$_2$/Ag$_2$CO$_3$ catalyst system gave the best results in terms of both yield and selectivity in the presence of 2-chloroquinoline as the exogenous ligand (Scheme 48).
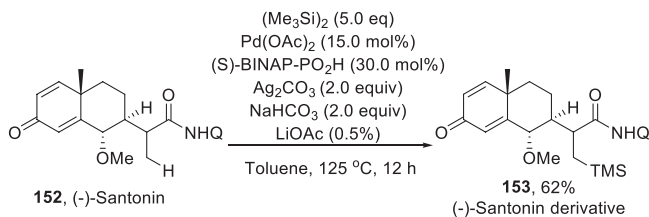
Scheme 46 Structural modification of (−)-santonin
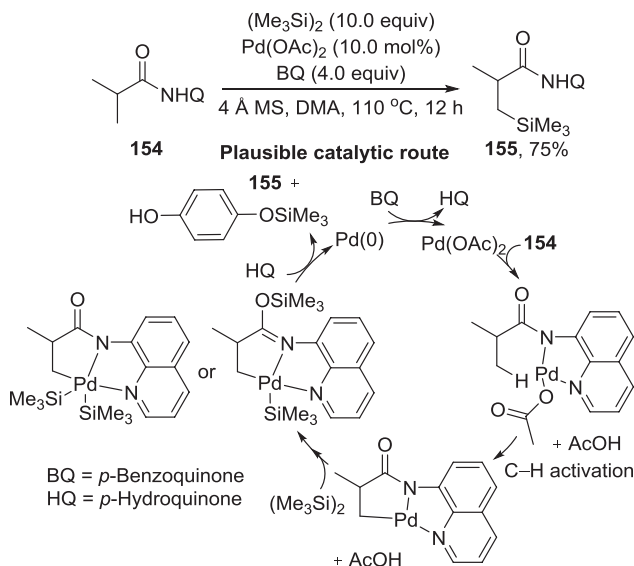
Scheme 47 Silylation of carboxylic amides using BQ as the oxidant

Further, mechanistic investigation including isolation of a Pd^{II} intermediate and DFT calculations were in support of the involvement of the six-membered palladacycle intermediate **159** (Fig. 3).

C–halogen bond formations: While direct halogenation at an alkyl C–H bond of carboxylic acids/equivalents gives access to further amendable halogenated products, there are several associated pitfalls with this transformation. Major problems embrace (1) C–halogen bond-forming reductive elimination, (2) likelihood of metal insertion at the C-halogen bond of the product, and (3) ready nucleophilic displacement of the halogen in the product [101–104]. However, these problems can be minimized by accomplishing those reactions under the assistance of a bidentate chelating directing group.

A Pd^{II}/Pd^{IV} catalytic cycle-based halogenation strategy allows the chlorination and bromination at the β-C–H bonds of aliphatic carboxylic acids by means of installing a *S*-methyl-*S*-2-pyridyl-sulfoximine (MPyS) directing group [105]. The reasonably strong chelating property of MPyS with the Pd catalyst facilitates the formation of a [5,5]-fused cyclopalladium^{II} intermediate, which is oxidized to a Pd^{IV}
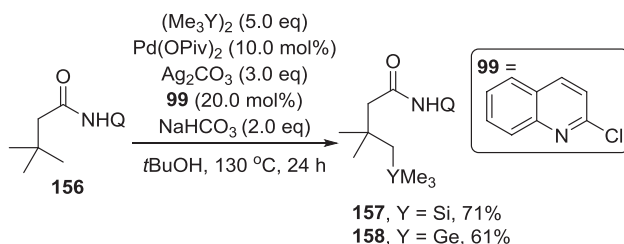
Scheme 48 Maiti's γ-silylation/germenylation of aliphatic carboxamides

species by N-halophthalimide. Finally, the desired halo-compound is produced within an acetate-driven reductive elimination step. Thus, further metal insertion at the C-halogen bond of the product is prevented (Scheme 49).

The classical and versatile 8-aminoquinoline group was also utilized as the directing auxiliary to functionalize β-C–H group of aliphatic acids with halogen partners. However, quinoline ring chlorinated products were often formed due to the background electrophilic aromatic substitution reaction. To prevent the latter, 5-chloro-8-aminoquinoline can be used as the directing group to give the desired β-halogenated product at the alkyl side chain (Scheme 50) [106]. In addition, the post-functionalization of various drug molecules leading to further manipulable bioactive substrates was also achieved by using 5-chloro-8-aminoquinoline as the directing group.

However, under acidic condition simple 8-aminoquinoline can also be used as the directing group for the β-C(sp^3)–H mono- and dichlorination of α,α-dialkyl-substituted propanamides under palladium catalysis [107]. Fine-tuning of the Pd source is required to the selective formation of mono- or bis-chlorinated aliphatic carboxylic acid derivative (Scheme 51).

8-Aminoquinoline is also known to efficaciously direct the β-fluorination of carboxylic acids to furnish fluorinated building blocks of high medicinal significance. In general, electrophilic fluorinating agents, such as N-fluorobenzenesulfonimide (NFSI), Selectfluor, N-fluoropyridinium salts, etc., are used to transfer "F+ ion" to the palladium catalyst, and the N–F bond is then constructed from a Pd^{IV}–F intermediate complex via reductive elimination, in which the latter is believed as a key step in all directed fluorination reactions. Hence, the unactivated β-C(sp^3)–H bonds of carboxylic amides were fluorinated using Pd(OAc)₂/Ag₂O/pivalic acid catalyst system in the presence of NFSI as the fluorinating agent (Scheme 52) [108]. In this reaction, pivalic acid (PivOH) facilitates the reductive elimination of C–F bond by precluding the competitive C–N bond formation from the active FPd^{IV}N(SO₂Ph)₂ species **173**.

In a comparative study, quinoxaline among various N-chelating functional groups, including pyrimidine, pyrazine, quinoline, quinazoline, and 8-aminoquinoline, showed better performance for the β-fluorination of carboxylic acids. It was also observed that the reactivity of 8-aminoquinoline-derived amides can be improved by using quinoxaline as a stoichiometric ligand. Mechanistic

Fig. 3 Plausible Pd intermediate

159
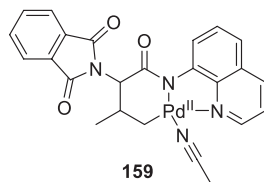
Scheme 49 MPyS directed halogenation of C(*sp*³)–H bonds

Pd(OAc)₂ (10.0 mol%)
AcOH (2.5 eq),
NBP (1.5 eq)
DCE, 60-65 °C; 15 h
161, 74%

Pd(OAc)₂ (10.0 mol%)
AcOH (2,5 eq),
NCP (1.5 eq)
DCE, 60-65 °C; 20 h

NBP = N-Bromophthalimide
NCP = N-Chlorophthalimide
162, 77%

160 MPyS

Probable Pd^II/Pd^IV cycle

X= Br, Cl

NXP

Pd(OAc)₂ (10.0 mol%)
NCS (2.5 eq)
AcOH, rt, 48 h
164, 52%

Pd(OAc)₂ (10.0 mol%)
NIS (2.0 eq)
AcOH, rt, 24 h
165, 45%

163 ClQ

Post functionalization of bio-molecules

166

1. Chlorination
2. NaN₃ (1.0 eq),
Cu(OAc)₂ (20.0 mol%)
DMF, 80 °C, 0.5 h

167, 65%

Scheme 50 Halogenation of C(*sp*³)–H bonds by 5-chloro-8-aminoquinoline directing group
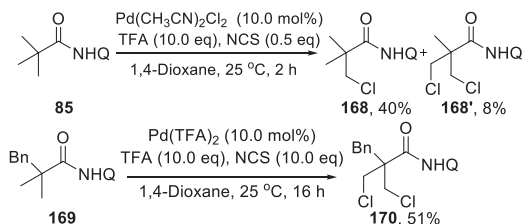
Scheme 51 Mono- and bis-chlorination using 8-aminoquinoline directing group
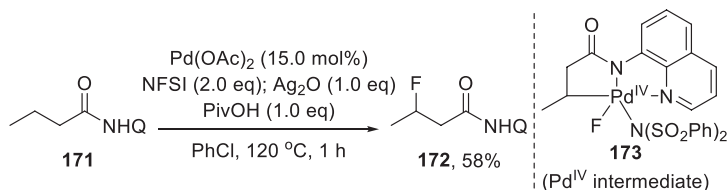
Scheme 52 8-Aminoquinoline-directed b-fluorination of C(sp^3)–H bonds
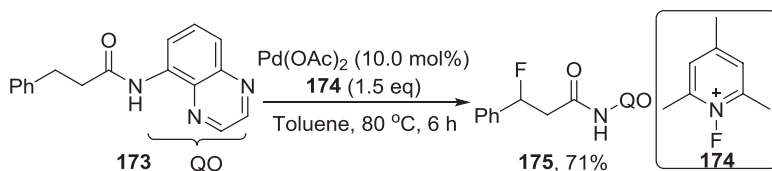
Scheme 53 Quinoxaline-directed β-fluorination of carboxamides

considerations suggest that quinoxaline alters the rate-determining step by dropping the activation energy of the Pd^{II} to Pd^{IV} oxidation step leading to greater formation of the desired fluorinated product. Remarkably, the prerequisite of an external ligand can be circumvented when quinoxaline is used as the directing group in the palladium-catalyzed fluorination reaction (Scheme 53) [109].

Independent research in this line unveils that palladium-catalyzed site- and dia-stereoselective β-fluorination of α-amino acids can be achieved by employing 2-(pyridine-2-yl)isopropyl amine (PIP) as the chelating directing group. Both ben-zylic and methylene C–H bonds of α-amino acids were regiospecifically converted into the corresponding β-fluorinated product in satisfactory synthetic yields (Scheme 54) [110, 111].
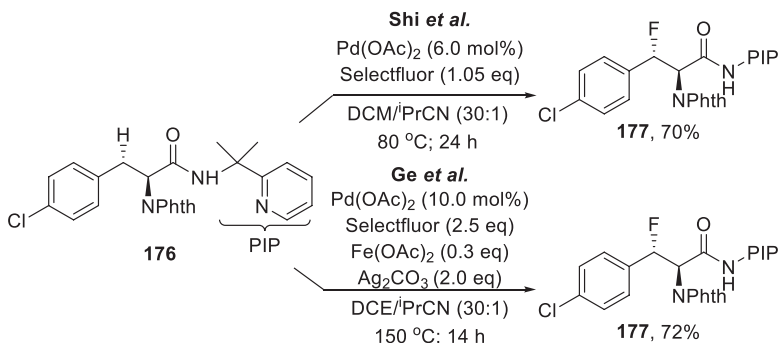
Scheme 54 PIP group-directed stereoselective β-fluorination of α-amino acids

3   Non-directed C(sp^3)–H Hetero-functionalization Approaches

Whereas the mainstream of C(sp^3)–H hetero-functionalization of aliphatic carboxylic acid synthons relies on transition metal-catalyzed directed approaches, only a handful of non-directed strategies were disclosed. In the latter class of approaches, the transition metal catalyst does not expedite the formation of a metallacycle intermediate via chelation assistance; rather, it promotes the hetero-functionalization through the formation of either an enol or a stabilized radical intermediate from the carboxylate equivalent. It is noteworthy to mention that these approaches commonly lead to α-hetero-functionalization of aliphatic carboxylates, with few exception of β-functionalization(s). However, few instances of non-directed approaches proceed through a transient interplay between the substrate and the metal catalyst.

3.1   Hetero-functionalization of Carboxylic Acid Esters and Amides

In general, simple carboxylic acid esters and amides, in the presence of an α-proton, form enol ester/amide that undergoes swift metal-assisted activation/hetero-functionalization process at the α-position. Furthermore, these substrates can stabilize an in situ-generated radical at the α-position and are therefore prone to α-hetero-functionalization through non-directed strategy.

C–N bond formations: A straightforward oxidative α-amination approach of carboxylic esters with secondary amines has been developed under copper catalysis. In this reaction, the promptly formed enol ester undergoes bromination with CuBr$_2$ at the α-position via a Cu-bound enolate intermediate. Ready nucleophilic replacement of the α-bromo substituent by a secondary amine produces the α-amino ester product (Scheme 55) [112].

Scheme 55 Copper-catalyzed non-directed α-amination of carboxy esters
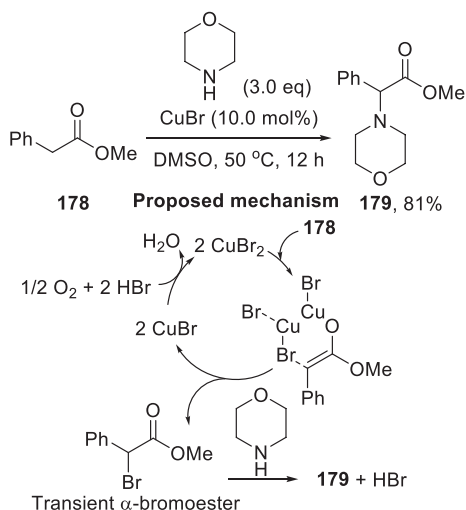
Another copper-based catalyst system was deployed to enable the highly chemoselective α-amination of *N*-acylpyrazoles which serve as the protected form of aliphatic carboxylic acids. A series of acids were aminated at the α-position via acylpyrazoles by means of a hypervalent iodine nitrenoid precursor, PhI=NTs [113]. Systematic mechanistic studies indicate that the weak amide conjugation and concurrent bidentate coordination promote the chemoselective enolization of acylpyrazole to react with the highly active in situ-generated copper nitrenoid species leading to the α-aminated product (Scheme 56). Importantly, this amination technique allowed the late-stage functionalization of many bioactive compounds including a TBS-protected lithocholic acid derivative into an analogous α-amino acid derivative (Scheme 57).

Apart from acylpyrazoles, 2-alkyl-substituted β-keto esters also undergo copper-catalyzed amination and aziridination with the hypervalent iodine nitrenoid precursor **181** towards the formation of α-acyl-β-amino acid and 2,2-diacyl aziridine derivatives, respectively (Scheme 58) [114]. In cases of both amination and aziridination reactions, the copper catalyst triggers the β-keto ester to selectively form the enol via bidentate coordination in a manner similar to acylpyrazoles, thereby reacting with the copper nitrenoid species.

A copper-based system, consisting of CuCl/P(*t*Bu)₃, was shown to activate di-*tert*-butyldiaziridinone to generate a nitrogen coupling partner in situ for the synthesis of hydantoin derivatives via an α-amination of ester and subsequent ring closer sequence (Scheme 59) [115]. However, this amination protocol was less effective for bulkier esters derived from ethyl or *tert*-butyl alcohols.

Likewise, palladium catalysts are also reported to enable C(sp^3)–H amination of a tailored substrate **190** in which the enol functionality can be further stabilized via chelation assistance. The reaction involves an intramolecular reductive cyclization of nitroarenes through nitrosoarene intermediate in the presence of carbon
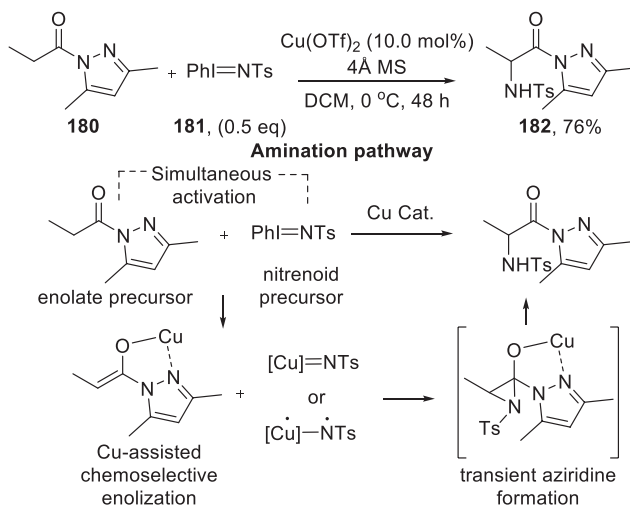
Scheme 56 α-Amination of *N*-acylpyrazoles with metal nitrenoid species
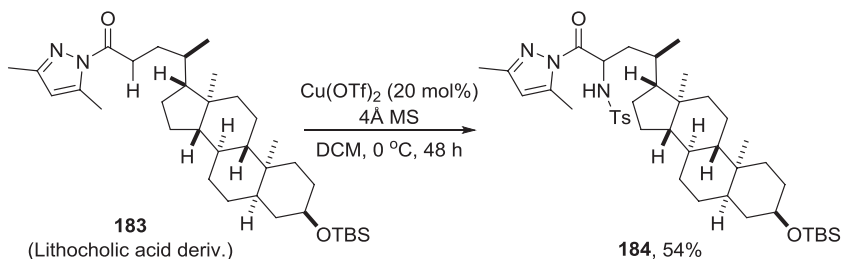
Scheme 57 α-Amination of lithocholic acid derivative

Scheme 58 Amination and aziridination of β-keto esters
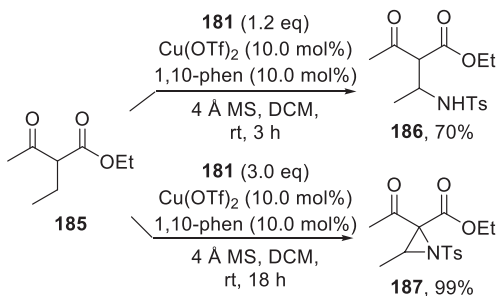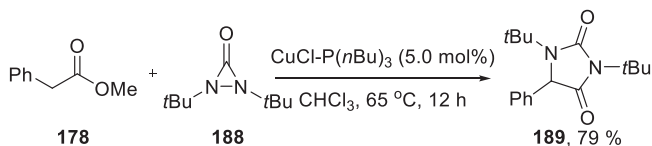
Scheme 59 Synthesis of hydantoin derivatives via copper-catalyzed α-amination
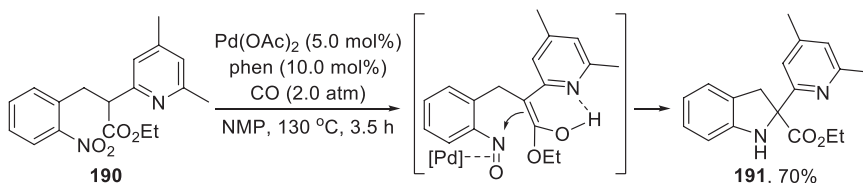
Scheme 60 Palladium-catalyzed intramolecular amination of nitroarenes
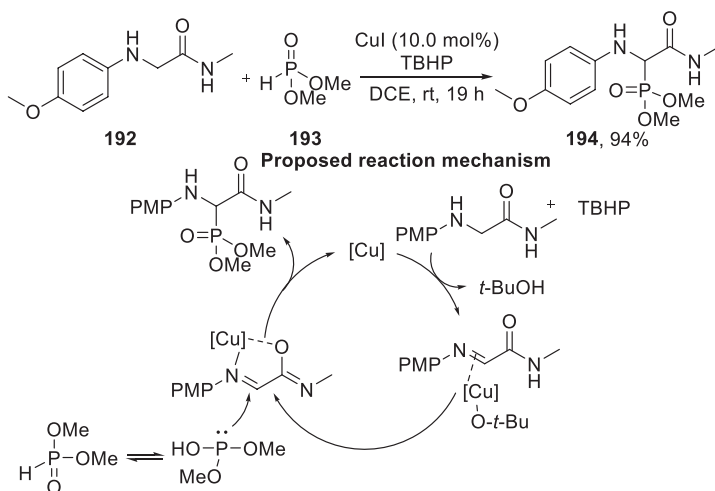
Scheme 61 Copper-catalyzed α-phosphorylation of glycine derivatives

monoxide as the terminal reductant leading to the benzopyrrolidine heterocycles (Scheme 60) [116].

C–P bond formation: A copper-catalyzed protocol was also established to enable the α-phosphorylation of glycine derivatives under mild reaction condition (Scheme 61) [117]. Substituent attached with the amine part of glycine plays a crucial role in this α-phosphorylation reaction by lowering the oxidation potential of the substrate and stabilizing the intermediates involved. It was proposed that in the presence of the Cu catalyst and *tert*-butyl hydroperoxide (TBHP), the glycine derivative forms an imino amide intermediate that can be further stabilized by the copper catalyst

Scheme 62 Iron-catalyzed α-thiolation of carboxamides

195
(PMP = *p*-Methoxyphenyl)

196, 48%

197

198, 48%
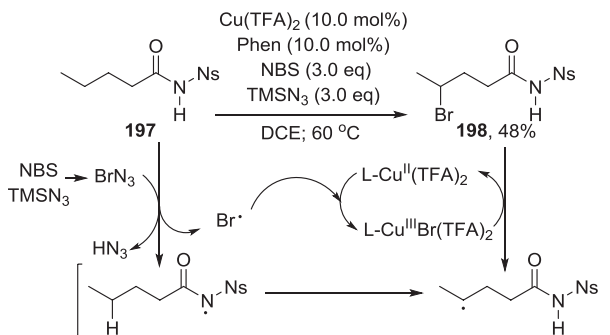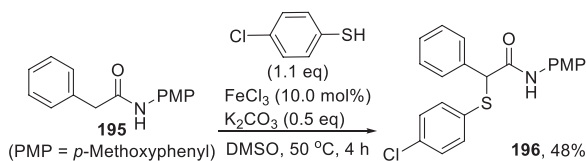
Scheme 63 Copper-catalyzed radical γ/δ-bromination of carboxamides

through chelation assistance and consequently undergoes phosphorylation with phosphonates to afford α-phosphorylated products.

C–S bond formation: In general, C-centered radicals at the α-position with regard to an amide or ester are further stabilized due to the delocalization with the carboxy functional group. Xu et al. reported that an iron catalyst, e.g., FeCl₃, under a base-mediated condition generates an α-carbo-radical from **195** via single-electron transfer (SET) mechanism. These radicals can react with in situ-generated disulfides from thiophenols to deliver α-thiolated acid amides (Scheme 62) [118].

C–Br bond formation: Bromination at γ and/or δ-carbon centers of aliphatic carboxamides was achieved by Yu et al. through a copper-promoted radical H-abstraction in the presence of *N*-bromosuccinimide (NBS) (Scheme 63). The extent of γ- vs. δ-bromination is however dictated by the steric demand exerted by substituents attached with that particular carbon center. During the course of the reaction, an azidyl radical is proposed to be formed to initiate the N–H proton abstraction. The N-radical thus formed is further converted via hydrogen abstraction to a methylene C-radical which undergoes a copper-assisted bromination process forming the final brominated product (Scheme 63) [119].

3.2 Hetero-functionalization of Carboxylic Acids via Benzazoles

Similar to enols, a radical intermediate can also be stabilized at the α-position of a carboxylate equivalent. These radical intermediates can be scavenged with a heteroatom-based radical species under transition metal catalysis to form a new C–heteroatom bond at the α-position with respect to the carboxy-equivalent functional group.

C–O bond formation: Phenylacetic acids can be methoxylated at the α-carbon through converting into 2-benzylbenzazoles as their synthetic equivalents using methanol as the oxy-nucleophile. The methoxylation proceeds via palladium catalyzed facile tautomerization of the 2-alkylbenzazole system to its enamine-type form. Hence, the requisite α-methoxylation was accomplished by using the commonly employed $Pd(OAc)_2/PhI(OAc)_2$ system by dehydrogenative C–O coupling strategy (Scheme 64) [120]. The benzoxazole auxiliary can be successively removed to access α-methoxyacetic acids that constitute backbone of numerous bioactive compounds and are extensively used as NMR anisotropy reagents.

The catalytic cycle begins with the tautomerization of 2-alkylazole to the enamine-type congener that accelerates the realization of a carbopalladated intermediate via an imine–enamine tautomerization/palladation array in a fashion similar to as observed by Yoshikai and Glorius et al. independently [121, 122]. The Pd^{II} intermediate then undergoes oxidation to form the putative Pd^{IV} intermediate in the presence of $PhI(OAc)_2$ and methanol. The methoxyalkane product is finally obtained in the reductive elimination step (Scheme 65).

C–S/Se bond formation: An analogous direct α-chalcogenation of alkanoic acids has been also developed via the synthesis of corresponding benzazoles [123]. While

Scheme 64 α-Methoxylation of phenylacetic acids via benzoxazoles

419
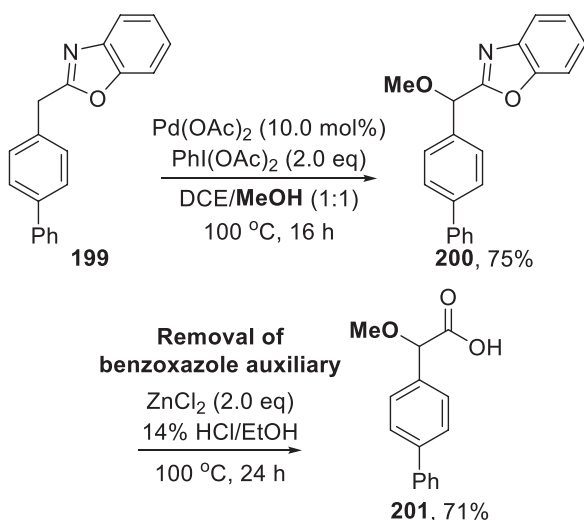
Scheme 65 Mechanistic interpretation of the α-methoxylation

199' **199** (facile tautomerization) (R = *p*-PhC$_6$H$_4$)

MeOH, HY, Pd^{II}Y$_2$, Pd^{II}Y(OMe), **200**, (MeO)$_2$YPd^{IV}, YPd^{II}, PhI + 2 AcOH, PhI(OAc)$_2$ + 2 MeOH, HY
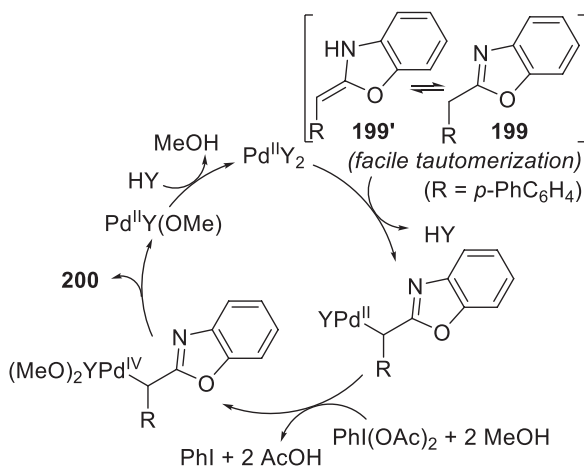
Scheme 66 α-Chalcogenation of aliphatic carboxylic acids and further derivatization

α-Thiolation of alkanoic acids

202 (1.26 g) + SH (Br, Br) → CuI (10.0 mol%), K$_3$PO$_4$ (2.0 eq), DMSO, 90 °C, 10 h → **203**, (1.45 g, 61%)

ZnCl$_2$ (2.0 eq), HCl, EtOH, 100 °C, 24 h

NaOH (6.0 eq), EtOH, 100 °C

204, 84%

1. (COCl)$_2$, DCM, 25 °C, 3 h
2. ArNH$_2$, *i*Pr$_2$NEt, DCM, 25 °C, 16 h

205, 82%

α-Selenylation of alkanoic acid

206 + Ph$_2$Se$_2$ → CuI (10.0 mol%), K$_3$PO$_4$ (2.0 eq), DMSO, 25 °C, 10 h → **207**, 70%
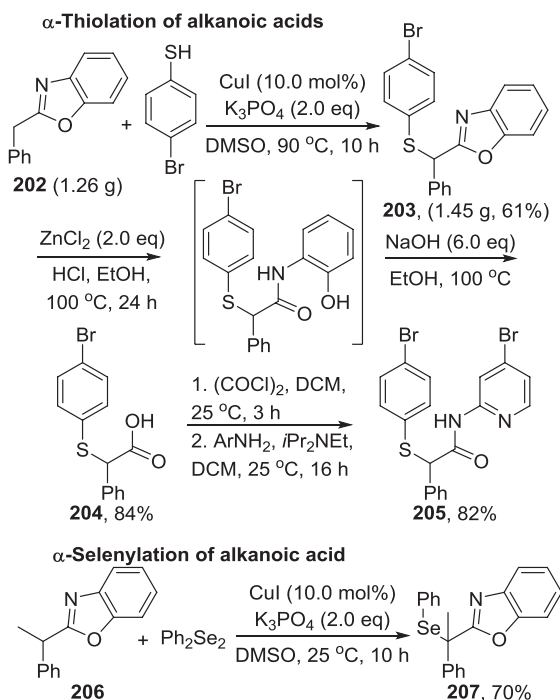
the thiolation was achieved by employing an array of free arene thiols, the required selenylation was realized upon using diphenyldiselenide. The requisite catalyst system is composed of CuI, DMSO, and a base, precisely K$_3$PO$_4$, to promote the chalcogenation process in a unique mechanism giving an expedient entry to practically important variety of thio- and selenoethers. It is worth mentioning that during the chalcogenation, DMSO plays crucial roles as a solvent as well as an oxidant to the
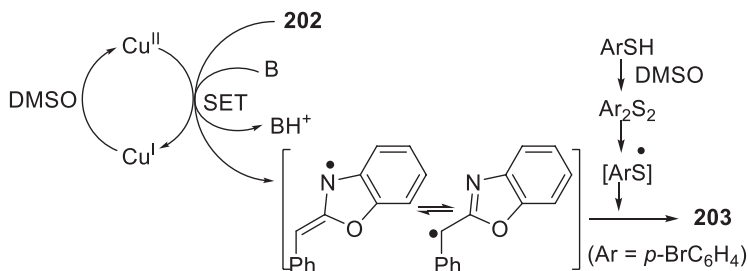
Scheme 67 Proposed mechanistic outline for the α-chalcogenation
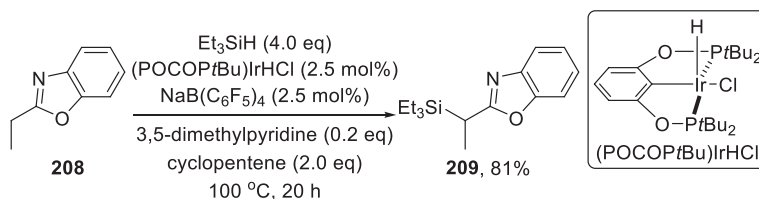
Scheme 68 Iridium-catalyzed silylation of 2-alkylbenzoxazoles

Cu^I catalytic species. When necessitates, the benzoxazole auxiliary can be released to obtain α-thiolated carboxylic acids that are required to constitute bioactive compounds such as a sphingosine 1-phosphate antagonist **205** (Scheme 66).

Extensive mechanistic investigation, including radical trapping experiments and EPR studies, is in agreement with a base-enabled single-electron transfer (SET) process from 2-alkylazole to the Cu^{II} intermediate which is initially formed by the oxidation with DMSO. The thus formed C-cantered radical rapidly undergoes thiolation in the presence of in situ-generated disulfide leading to α-thiolated products (Scheme 67).

C–Si bond formation: The benzoxazole auxiliary was also utilized to enable the silylation of a C(sp^3)–H bond adjacent to the azole ring. The silylation is catalyzed by a cationic iridium complex, generated in situ by reacting (POCOPtBu)IrHCl and NaB(C_6F_5)$_4$ (Scheme 68) [124]. Albeit the reaction may proceed in the absence of a hydrogen acceptor, the addition of an acceptor gave superior result. The silyl group is transferred in the form of an electrophilic silicon species as an active intermediate.

4 Conclusion and Perspective

The number of available methodologies for the direct hetero-functionalization of carboxylic acid equivalents particularly via C(sp^3)–H bond functionalization by a transition metal catalyst has been sufficiently amplified in recent years to access proximal-selective α-functionalized acids or distal-selective β-, γ-, and even

δ-functionalized acids with various commonly used heteroatoms. Nevertheless, there are several restrictions and challenges to meet in the near future. These not only include development of alternative more attractive and environment-friendly catalytic procedures, but also various other factors need to be addressed. For example, as discussed in this chapter, majority of the catalytic hetero-functionalization approaches involve carboxylic acid equivalents including amides/esters/azoles; however, the use of a free carboxylic acid group is rather limited to mostly lactonization (intramolecular C–O bond formation). Furthermore, the synthesis of optically active stereogenic centers by using these hetero-functionalization approaches is underdeveloped and needs to be established. Applications of organo- and photocatalysts in the hetero-functionalization of carboxylic acids also remain in their infancy [125–129]. Although these issues remained to be solved, we sincerely believe that the various techniques thus far available for the direct hetero-functionalization of C(*sp*³)–H bonds of substrates bearing carboxy-equivalent groups will be applied to broad sectors of academia and industry in the near future.

References

1. Hansch C, Sammes PG, Taylor JB (eds) (1990) Comprehensive medicinal chemistry: the rational design, mechanistic study & therapeutic application of chemical compounds. Pergamon Press, Oxford, pp 12–27
2. Harada N, Watanabe M, Kuwahara S, Sugio A, Kasai Y, Ichikawa A (2000) 2-Methoxy-2-(1-naphthyl)propionic acid, a powerful chiral auxiliary for enantioresolution of alcohols and determination of their absolute configurations by the 1H NMR anisotropy method. Tetrahedron Asymmetry 11:1249–1253
3. Fraústo da Silva JR, RJP W (eds) (2001) The biological chemistry of the elements. Oxford University Press, New York
4. Kasai Y, Watanabe M, Harada N (2003) Convenient method for determining the absolute configuration of chiral alcohols with racemic 1H NMR anisotropy reagent, MαNP acid: Use of HPLC-CD detector. Chirality 15:295–299
5. Seco JM, Quiñoá E, Riguera R (2004) The assignment of absolute configuration by NMR. Chem Rev 104:17–118
6. Carballeira NM, Miranda C, Orellano EA, González FA (2005) Synthesis of a novel series of 2-methylsulfanyl fatty acids and their toxicity on the human K-562 and U-937 leukemia cell lines. Lipids 40:1063–1067
7. Mellah M, Voituriez A, Schulz E (2007) Chiral sulfur ligands for asymmetric catalysis. Chem Rev 107:5133–5209
8. Deaton DN, Gao EN, Graham KP, Gross JW, Miller AB, Strelow JM (2008) Thiol-based angiotensin-converting enzyme 2 inhibitors: P1 modifications for the exploration of the S1 subsite. Bioorg Med Chem Lett 18:732–737
9. Maji B, Mayr H (2012) Structures and reactivities of O-methylated breslow intermediates. Angew Chem Int Ed 51:10408–10412

10. Ilardi EA, Vitaku E, Njardarson JT (2014) Data-mining for sulfur and fluorine: an evaluation of pharmaceuticals to reveal opportunities for drug design and discovery. J Med Chem 57:2832–2842

11. Labeeuw O, Levoin N, Billot X, Danvy D, Calmels T, Krief S, Ligneau X, Berrebi-Bertrand I, Robert P, Lecomte JM, Schwartz JC, Capet M (2016) Synthesis and evaluation of a 2-benzothiazolylphenylmethyl ether class of histamine H4 receptor antagonists. Bioorg Med Chem Lett 26:5263–5266

12. Carballeira NM, Montano N, Morales C, Mooney J, Torres X, Díaz D, Sanabria-Rios DJ (2017) 2-Methoxylated FA display unusual antibacterial activity towards clinical isolates of methicillin-resistant staphylococcus aureus (CIMRSA) and escherichia coli. Lipids 52:535–548

13. Zimmermann SC, Duvall B, Tsukamoto T (2019) Recent progress in the discovery of allosteric inhibitors of kidney-type glutaminase. J Med Chem 62:46–59

14. Daugulis O, Roane J, Tran LD (2015) Bidentate, monoanionic auxiliary-directed functionalization of carbon–hydrogen bonds. Acc Chem Res 48:1053–1064

15. He J, Wasa M, Chan KSL, Shao Q, Yu JQ (2017) Palladium-catalyzed transformations of alkyl C–H bonds. Chem Rev 117:8754–8786

16. Baudoin O (2011) Transition metal-catalyzed arylation of unactivated C(sp3)–H bonds. Chem Soc Rev 40:4902–4911

17. Dastbaravardeh N, Christakakou M, Haider M, Schnürch M (2014) Recent advances in palladium-catalyzed C(sp3)–H activation for the formation of carbon–carbon and carbon–heteroatom bonds. Synthesis 46:1421–1439

18. He G, Wang B, Nack WA, Chen G (2016) Syntheses and transformations of α-amino acids via palladium-catalyzed auxiliary-directed sp3 C–H functionalization. Acc Chem Res 49:635–645

19. Alberico D, Scott ME, Lautens M (2007) Aryl− aryl bond formation by transition-metal-catalyzed direct arylation. Chem Rev 107:174–238

20. Wencel-Delord J, Glorius F (2013) C–H bond activation enables the rapid construction and late-stage diversification of functional molecules. Nat Chem 5:369–375

21. Ackermann L (2014) Carboxylate-assisted ruthenium-catalyzed alkyne annulations by C–H/Het–H bond functionalizations. Acc Chem Res 47:281–295

22. Jazzar R, Hitce J, Renaudat A, Sofack-Kreutzer J, Baudoin O (2010) Functionalization of organic molecules by transition-metal-catalyzed C(sp3)–H activation. Chem Eur J 16:2654–2672

23. Lyons TW, Sanford MS (2010) Palladium-catalyzed ligand-directed C−H functionalization reactions. Chem Rev 110:1147–1169

24. Bhadra S, Yamamoto H (2018) Substrate directed asymmetric reactions. Chem Rev 118:3391–3446

25. Mulzer J (1999) Basic principles of asymmetric synthesis. In: Jacobsen EN, Pfaltz A, Yamamoto H (eds) Comprehensive asymmetric catalysis, vol 1. Springer, Berlin, pp 42–79

26. Kapdi A, Maiti D (eds) (2017) Strategies for palladium-catalyzed non-directed and directed C bond H bond functionalization. Elsevier, Amsterdam

27. Uttry A, van Gemmeren M (2020) Direct C(sp3)–H activation of carboxylic acids. Synthesis 52: 479-488

28. Kao LC, Sen A (1991) Platinum(II) catalysed selective remote oxidation of unactivated C–H bonds in aliphatic carboxylic acids. J Chem Soc Chem Commun 1242–1243

29. Dangel BD, Johnson JA, Sames D (2001) Selective functionalization of amino acids in water: a synthetic method via catalytic C−H bond activation. J Am Chem Soc 123:8149–8150

30. Janssen M, de Vos DE (2019) PtII-catalyzed hydroxylation of terminal aliphatic C(sp3)−H bonds with molecular oxygen. Chem Eur J 25:10724–10734

31. Goldshleger NF, Tyabin MB, Shilov AE, Shteinman AA (1969) Zh Fiz Khim 43:2174

32. Goldshleger NF, Eskova VV, Shilov AE, Shteinman AA (1972) Zh Fiz Khim 46:1353–1354

33. Ghosh KK, Uttry A, Koldemir A, Ong M, van Gemmeren M (2019) Direct β-C(*sp*³)–H acetoxylation of aliphatic carboxylic acids. Org Lett 21:7154–7157
34. Giri R, Liang J, Lei JG, Li JJ, Wang DH, Chen X, Naggar IC, Guo C, Foxman BM, Yu JQ (2005) Pd-catalyzed stereoselective oxidation of methyl groups by inexpensive oxidants under mild conditions: a dual role for carboxylic anhydrides in catalytic C-H bond oxidation. Angew Chem Int Ed 44:7420–7424
35. He J, Shigenari T, Yu JQ (2015) Palladium(0)/PAr₃-catalyzed intermolecular amination of C(*sp*³)–H bonds: synthesis of β-amino acids. Angew Chem Int Ed 54:6545–6549
36. Wasa M, Engle KM, Yu JQ (2009) Pd(0)/PR₃-catalyzed intermolecular arylation of sp³ C−H bonds. J Am Chem Soc 131:9886–9887
37. Tan Y, Hartwig JF (2010) Palladium-catalyzed amination of aromatic C−H bonds with oxime esters. J Am Chem Soc 132:3676–3677
38. Fürstner A, Seidel G (2002) Microwave-assisted synthesis of pinacol boronates from aryl chlorides catalyzed by a palladium/imidazolium salt system. Org Lett 4:541–543
39. Billingsley KL, Barder TE, Buchwald SL (2007) Palladium-catalyzed borylation of aryl chlorides: Scope, applications, and computational studies. Angew Chem Int Ed 46:5359–5363
40. Billingsley KL, Buchwald SL (2008) An improved system for the palladium-catalyzed borylation of aryl halides with pinacol borane. J Org Chem 73:5589–5591
41. Molander GA, Trice SLJ, Dreher SD (2010) Palladium-catalyzed, direct boronic acid synthesis from aryl chlorides: A simplified route to diverse boronate ester derivatives. J Am Chem Soc 132:17701–17703
42. Dai HX, Yu JQ (2012) Pd-catalyzed oxidative ortho-C–H borylation of arenes. J Am Chem Soc 134:134–137
43. Zhang LS, Chen G, Wang X, Guo QY, Zhang XS, Pan F, Chen K, Shi ZJ (2014) Direct borylation of primary C–H bonds in functionalized molecules by palladium catalysis. Angew Chem Int Ed 53:3899–3903
44. He J, Jiang H, Takise R, Zhu RY, Chen G, Dai HX, Murali Dhar TG, Shi J, Zhang H, Cheng PTW, Yu JQ (2016) Ligand-promoted borylation of C(*sp*³)–H bonds with palladium(II) catalysts. Angew Chem Int Ed 55:785–789
45. He J, Shao Q, Wu Q, Yu JQ (2017) Pd(II)-Catalyzed enantioselective C(*sp*³)–H borylation. J Am Chem Soc 139:3344–3347
46. Shi Y, Gao Q, Xu S (2019) Chiral bidentate boryl ligand enabled iridium-catalyzed enantioselective C(*sp*³)–H borylation of cyclopropanes. J Am Chem Soc 141:10599–10604
47. Murakami R, Iwai T, Sawamura M (2016) Site-selective and stereoselective C(*sp*³)-H borylation of alkyl side chains of 1,3-azoles with a silica-supported monophosphine-iridium catalyst. Synlett 27:1187–1192
48. Giri R, Chen X, Yu JQ (2005) Palladium-catalyzed asymmetric iodination of unactivated C–H bonds under mild conditions. Angew Chem Int Ed 44:2112–2115
49. He J, Li S, Deng Y, Fu H, Laforteza BN, Spangler JE, Homs A, Yu JQ (2014) Ligand-controlled C(*sp*³)–H arylation and olefination in synthesis of unnatural chiral α–amino acids. Science 343:1216–1220
50. Zhu RY, Saint-Denis TG, Shao Y, He J, Sieber JD, Senanayake CH, Yu JQ (2017) Ligand-enabled Pd(II)-catalyzed bromination and iodination of C(*sp*³)–H bonds. J Am Chem Soc 139:5724–5727
51. Zhu RY, Tanaka K, Li GC, He J, Fu HY, Li SH, Yu JQ (2015) Ligand-enabled stereoselective β-C(*sp*³)–H fluorination: Synthesis of unnatural enantiopure anti-β-fluoro-α-amino acids. J Am Chem Soc 137:7067–7070
52. Zaitsev VG, Shabashov D, Daugulis O (2005) Highly regioselective arylation of sp³ C−H bonds catalyzed by palladium acetate. J Am Chem Soc 127:13154–13155
53. Rouquet G, Chatani N (2013) Catalytic functionalization of C(*sp*²)–H and C(*sp*³)–H bonds by using bidentate directing groups. Angew Chem Int Ed 52:11726–11743
54. Castro LCM, Chatani N (2015) Nickel catalysts/N,N′-bidentate directing groups: an excellent partnership in directed C–H activation reactions. Chem Lett 44:410–421

55. Liu J, Chen G, Tan Z (2016) Copper-catalyzed or-mediated C–H bond functionalizations assisted by bidentate directing groups. Adv Synth Catal 358:1174–1194

56. Reddy BVS, Reddy LR, Corey EJ (2006) Novel acetoxylation and C−C coupling reactions at unactivated positions in α-amino acid derivatives. Org Lett 8:3391–3394

57. Caldwell CG, Bondy SS (1990) A convenient synthesis of enantiomerically pure (2S,3S)- or (2R,3R)-3-hydroxyleucine. Synthesis 34–36

58. Panek JS, Masse CE (1998) An improved synthesis of (4S,5S)-2-phenyl-4-(methoxycarbonyl)-5-isopropyloxazoline from (S)-phenylglycinol. J Org Chem 63:2382–2384

59. MacMillan JB, Molinsky TF (2002) Lobocyclamide B from Lyngbya confervoides. configuration and asymmetric synthesis of β-hydroxy-α-amino acids by (−)-Sparteine-mediated aldol addition. Org Lett 4:1883–1886

60. Saravanan P, Corey EJ (2003) A short, stereocontrolled, and practical synthesis of α-methylomuralide, a potent inhibitor of proteasome function. J Org Chem 68:2760–2764

61. Wang Z, Kuninobu Y, Kanai M (2014) Copper-mediated direct C(sp^3)–H and C(sp^2)–H acetoxylation. Org Lett 16:4790–4793

62. Rit RK, Yadav MR, Sahoo AK (2012) Pd(II)-catalyzed primary-C(sp^3)–H acyloxylation at room temperature. Org Lett 14:3724–3727

63. Rit RK, Yadav MR, Ghosh K, Sahoo AK (2015) Reusable directing groups [8-aminoquinoline, picolinamide, sulfoximine] in C(sp^3)–H bond activation: present and future. Tetrahedron 71:4450–4459

64. Shan G, Yang X, Zong Y, Rao Y (2013) An efficient palladium-catalyzed C-H alkoxylation of unactivated methylene and methyl groups with cyclic hypervalent iodine (I3+) oxidants. Angew Chem Int Ed 52:13606–13610

65. Zong Y, Rao Y (2014) Developing Pd(II) catalyzed double sp^3 C–H alkoxylation for synthesis of symmetric and unsymmetric acetals. Org Lett 16:5278–5281

66. Chen FJ, Zhao S, Hu F, Chen K, Zhang Q, Zhang SQ, Shi BF (2013) Pd(II)-catalyzed alkoxylation of unactivated C(sp^3)–H and C(sp^2)–H bonds using a removable directing group: efficient synthesis of alkyl ethers. Chem Sci 4:4187–4192

67. Jerhaoui S, Djukic JP, Wencel-Delord J, Colobert F (2017) Stereoselective sulfinyl aniline-promoted Pd-catalyzed C−H arylation and acetoxylation of aliphatic amides. Chem Eur J 23:15594–15600

68. Kim Y, Kim S, Kang D, Sohn T, Jang E, Baik M, Hong S (2018) Stereoselective construction of sterically hindered oxaspirocycles via chiral bidentate directing group-mediated C(sp^3)–O bond formation. Chem Sci 9:1473–1480

69. Hegedus LL, McCabe RW (eds) (1984) Catalyst poisoning. Marcel Dekker, New York

70. Yan SY, Liu YJ, Liu B, Liu YH, Zhang ZZ, Shi BF (2015) Nickel-catalyzed direct thiolation of unactivated C(sp^3)–H bonds with disulfides. Chem Commun 51:7341–7344

71. Wang X, Qiu R, Yan C, Reddy VP, Zhu L, Xu X, Yin SF (2015) Nickel-catalyzed direct thiolation of C(sp^3)–H bonds in aliphatic amides. Org Lett 17:1970–1973

72. Ye X, Petersen JL, Shi X (2015) Nickel-catalyzed directed sulfenylation of sp^2 and sp^3 C–H bonds. Chem Commun 51:7863–7866

73. Rao WH, Zhan BB, Chen K, Ling PX, Zhang ZZ, Shi BF (2015) Pd(II)-catalyzed direct sulfonylation of unactivated C(sp^3)–H bonds with sodium sulfinates. Org Lett 17:3552–3555

74. Xiong HY, Besset T, Cahard D, Pannecoucke X (2015) Palladium(II)-catalyzed directed trifluoromethylthiolation of unactivated C(sp^3)–H bonds. J Org Chem 80:4204–4212

75. Topczewski JJ, Sanford MS (2015) Carbon–hydrogen (C–H) bond activation at PdIV: a Frontier in C–H functionalization catalysis. Chem Sci 6 :70–76

76. Canty AJ, Ariafard A, Yates BF, Sanford MS (2015) Computational study of intramolecular arene palladation at a palladium(IV) center. Organometallics 34:1085–1090

77. Guin S, Deb A, Dolui P, Chakraborty S, Singh VK, Maiti D (2018) Promoting highly diastereoselective γ-C–H chalcogenation of α-amino acids and aliphatic carboxylic acids. ACS Catal 8:2664–2669

78. He G, Zhang SY, Nack WA, Li Q, Chen G (2013) Use of a Readily Removable Auxiliary Group for the Synthesis of Pyrrolidones by the Palladium-catalyzed intramolecular amination of unactivated γ C(sp³)-H bonds. Angew Chem Int Ed 52:11124–11128

79. Zhang Q, Chen K, Rao W, Zhang Y, Chen FJ, Shi BF (2013) Stereoselective synthesis of chiral α-amino-β-lactams through palladium(II)-catalyzed sequential monoarylation/amidation of C(sp³)-H Bonds. Angew Chem Int Ed 52:13588–13592

80. Ling PX, Fang SL, Yin XS, Zhang Q, Chen K, Shi BF (2017) Palladium-catalyzed sequential monoarylation/amidation of C(sp³)–H bonds: stereoselective synthesis of α-amino-β-lactams and anti-α,β-diamino acid. Chem Commun 53:6351–6354

81. Sun WW, Cao P, Mei RQ, Li Y, Ma YL, Wu B (2014) Palladium-catalyzed unactivated C(sp³)–H bond activation and intramolecular amination of carboxamides: A new approach to β-lactams. Org Lett 16:480–483

82. Zhang SJ, Sun WW, Cao P, Dong XP, Liu JK, Wu B (2016) Stereoselective synthesis of diazabicyclic β-lactams through intramolecular amination of unactivated C(sp³)–H bonds of carboxamides by palladium catalysis. J Org Chem 81:956–968

83. Wang Z, Ni J, Kuninobu Y, Kanai M (2014) Copper-catalyzed intramolecular C(sp³)-H and C(sp²)-H amidation by oxidative cyclization. Angew Chem Int Ed 53:3496–3499

84. Wu X, Zhao Y, Zhang G, Ge H (2014) Copper-catalyzed site-selective intramolecular amidation of unactivated C(sp³)-H bonds. Angew Chem Int Ed 53:3706–3710

85. Wang C, Yang Y, Qin D, He Z, You J (2015) Copper-catalyzed intramolecular dehydrogenative amidation of unactivated C(sp³)–H bonds using O₂ as the sole oxidant. J Org Chem 80:8424–8429

86. Desai LV, Malik HA, Sanford MS (2006) Oxone as an inexpensive, safe, and environmentally benign oxidant for C−H bond oxygenation. Org Lett 8:1141–1144

87. Wang GW, Yuan TT (2010) Palladium-catalyzed alkoxylation of N-methoxybenzamides via direct sp² C−H bond activation. J Org Chem 75:476–479

88. Suess AM, Ertem MZ, Cramer CJ, Stahl SS (2013) Divergence between organometallic and single-electron-transfer mechanisms in copper(II)-mediated aerobic C–H oxidation. J Am Chem Soc 135:9797–9804

89. Aihara Y, Chatani N (2014) Nickel-catalyzed direct arylation of C(sp³)–H bonds in aliphatic amides via bidentate-chelation assistance. J Am Chem Soc 136:898–901

90. Wu XS, Zhao Y, Ge HB (2014) Nickel-catalyzed site-selective alkylation of unactivated C(sp³)–H bonds. J Am Chem Soc 136:1789–1792

91. Li ML, Dong JX, Huang XL, Li KZ, Wu Q, Song FJ, You JS (2014) Nickel-catalyzed chelation-assisted direct arylation of unactivated C(sp³)–H bonds with aryl halides. Chem Commun 50:3944–3946

92. Wu X, Zhao Y, Ge H (2014) Nickel-catalyzed site-selective amidation of unactivated C(sp³)-H bonds. Chem Eur J 20:9530–9533

93. Aihara Y, Chatani N (2016) Nickel-catalyzed reaction of C–H bonds in amides with I₂: ortho-iodination via the cleavage of C(sp²)–H bonds and oxidative cyclization to β-lactams via the cleavage of C(sp³)–H bonds. ACS Catal 6:4323–4329

94. Wu X, Yang K, Zhao Y, Sun H, Li G, Ge H (2015) Cobalt-catalysed site-selective intra- and intermolecular dehydrogenative amination of unactivated sp³ carbons. Nature Commun 6:6462. https://doi.org/10.1038/ncomms7462

95. Gou Q, Liu G, Liu ZN, Qin J (2015) PdII-catalyzed intermolecular amination of unactivated C(sp³)-H bonds. Chem Eur J 21:15491–15495

96. Bai HY, Ma ZG, Yi M, Lin JB, Zhang SY (2017) Palladium-catalyzed direct intermolecular amination of unactivated methylene C(sp³)–H bonds with azodiformates via bidentate-chelation assistance. ACS Catal 7:2042–2046

97. Kanyiva KS, Kuninobu Y, Kanai M (2014) Palladium-catalyzed direct C–H silylation and germanylation of benzamides and carboxamides. Org Lett 16:1968–1971

98. Liu YJ, Liu YH, Zhang ZZ, Yan SY, Chen K, Shi BF (2016) Divergent and stereoselective synthesis of β-silyl-α-amino acids through palladium-catalyzed intermolecular silylation of unactivated primary and secondary C-H bonds. Angew Chem Int Ed 55:13859–13862

99. Pan JL, Li QZ, Zhang TY, Hou SH, Kang JC, Zhang SY (2016) Palladium-catalyzed direct intermolecular silylation of remote unactivated C(sp³)–H bonds. Chem Commun 52:13151–13154

100. Deb A, Singh S, Seth K, Pimparkar S, Bhaskararao B, Guin S, Sunoj RB, Maiti D (2017) Experimental and computational studies on remote γ-C(sp³)–H silylation and germanylation of aliphatic carboxamides. ACS Catal 7:8171–8175

101. Wheelaghan OR, Ortuño MA, Díez J, Garrido SEG, Maya C, Lledos A, Conejero S (2012) Characterization of a paramagnetic, mononuclear Pt(III)–alkyl complex intermediate in carbon–halogen bond coupling reactions. J Am Chem Soc 134:15261–15264

102. Kaspi AW, Goldberg I, Vigalok A (2010) Reagent-dependent formation of C−C and C−F bonds in Pt complexes: An unexpected twist in the electrophilic fluorination chemistry. J Am Chem Soc 132:10626–10627

103. Roy AH, Hartwig JF (2004) Reductive elimination of aryl halides upon addition of hindered alkylphosphines to dimeric arylpalladium(II) halide complexes. Organometallics 23:1533–1541

104. Canty AJ (1992) Development of organopalladium(IV) chemistry: fundamental aspects and systems for studies of mechanism in organometallic chemistry and catalysis. Acc Chem Res 25:83–90

105. Rit RK, Yadav MR, Ghosh K, Shankar M, Sahoo AK (2014) Sulfoximine assisted Pd(II)-catalyzed bromination and chlorination of primary β-C(sp³)–H bond. Org Lett 16:5258–5261

106. Yang X, Sun Y, Sun T, Rao Y (2016) Auxiliary-assisted palladium-catalyzed halogenation of unactivated C(sp³)–H bonds at room temperature. Chem Commun 52:6423–6426

107. Xiong HY, Cahard D, Pannecoucke X, Besset T (2016) Pd-catalyzed directed chlorination of unactivated C(sp³)–H bonds at room temperature. Eur J Org Chem 3625–3630

108. Zhu Q, Ji D, Liang T, Wang X, Xu Y (2015) Efficient palladium-catalyzed C–H fluorination of C(sp³)–H bonds: Synthesis of β-fluorinated carboxylic acids. Org Lett 17:3798–3801

109. Sun H, Zhang Y, Chen P, Wu YD, Zhang X, Huang Y (2016) Ligand-assisted palladium(II)/(IV) oxidation for sp³ C–H Fluorination. Adv Synth Catal 358:1946–1957

110. Zhang Q, Yin XS, Chen K, Zhang SQ, Shi BF (2015) Stereoselective synthesis of chiral β-fluoro α-amino acids via Pd(II)-catalyzed fluorination of unactivated methylene C(sp³)–H bonds: Scope and mechanistic studies. J Am Chem Soc 137:8219–8226

111. Miao J, Yang K, Kurek M, Ge H (2015) Palladium-catalyzed site-selective fluorination of unactivated C(sp³)–H bonds. Org Lett 17:3738–3741

112. Evans RW, Zbieg JR, Zhu S, Li W, MacMillan DWC (2013) Simple catalytic mechanism for the direct coupling of α-carbonyls with functionalized amines: A one-step synthesis of plavix. J Am Chem Soc 135:16074–16077

113. Tokumasu K, Yazaki R, Ohshima T (2016) Direct catalytic chemoselective α-amination of acylpyrazoles: A concise route to unnatural α-amino acid derivatives. J Am Chem Soc 138:2664–2669

114. TMU T, Tejo C, DLY T, PWH C (2012) Copper(II) triflate catalyzed amination and aziridination of 2-alkyl substituted 1,3-dicarbonyl compounds. J Am Chem Soc 134:7344–7350

115. Zhao B, Du H, Shi Y (2008) A Cu(I)-catalyzed C−N α-amination of esters. Direct synthesis of hydantoins. J Am Chem Soc 130:7220–7221

116. Ford RL, Alt I, Jana N, Driver TG (2019) Intramolecular Pd-catalyzed reductive amination of enolizable sp³-C–H bonds. Org Lett 21:8827–8831

117. Zhi H, Ung SPM, Liu Y, Zhao L, Li CJ (2016) Phosphorylation of glycine derivatives via copper(I)-catalyzed Csp³−H bond functionalization. Adv Synth Catal 358:2553–2557

118. Huang LS, Han DY, Xu DZ (2019) Iron-catalyzed cross-dehydrogenative coupling of oxindoles with thiols/selenols for direct C(sp³)−S/Se bond formation. Adv Synth Catal 361:4016–4021

119. Liu T, Myers MC, Yu JQ (2017) Copper-catalyzed bromination of C(sp³)−H bonds distal to functional groups. Angew Chem Int Ed 56:306–309
120. Kumar J, Gupta A, Bhadra S (2019) PdII-catalyzed methoxylation of C(sp³)–H bonds adjacent to benzoxazoles and benzothiazoles. Org Biomol Chem 17:3314–3318
121. Wei Y, Deb I, Yoshikai N (2012) Palladium-catalyzed aerobic oxidative cyclization of N-aryl imines: Indole synthesis from anilines and ketones. J Am Chem Soc 134:9098–9101
122. Shi Z, Suri M, Glorius F (2013) Aerobic synthesis of pyrroles and dihydropyrroles from imines: Palladium(II)-catalyzed intramolecular C–H dehydrogenative cyclization. Angew Chem Int Ed 52:4892–4896
123. Gupta A, Rahaman A, Bhadra S (2019) Direct α-chalcogenation of aliphatic carboxylic acid equivalents. Org Lett 21:6164–6168
124. Hirano M, Fukumoto Y, Matsubara N, Chatani N (2018) A cationic iridium-catalyzed C(sp³)–H silylation of 2-alkyl-1,3-azoles at the α-position in the 2-alkyl group leading to 2-(1-silylalkyl)-1,3-azoles. Chem Lett 47:385–388
125. Dohi T, Takenaga N, Goto A, Maruyama A, Kita Y (2007) Direct lactone formation by using hypervalent iodine(III) reagents with KBr viaselective C−H abstraction protocol. Org Lett 9:3129–3132
126. Liu H, Feng W, Kee CW, Zhao Y, Leow D, Pan Y, Tan CH (2010) Organic dye photocatalyzed α-oxyamination through irradiation with visible light. Green Chem 12:953–956
127. Koike T, Yasu Y, Akita M (2012) Visible-light-driven oxidation of 1,3-dicarbonyl compounds via catalytic disproportionation of TEMPO by photoredox catalysis. Chem Lett 41:999–1001
128. Im H, Kang D, Choi S, Shin S, Hong S (2018) Visible-light-induced C–O bond formation for the construction of five- and six-membered cyclic ethers and lactones. Org Lett 20:7437–7441
129. Gonçalves CR, Lemmerer M, Teskey CJ, Adler P, Kaiser D, Maryasin B, González L, Maulide N (2019) Unified approach to the chemoselective α-functionalization of amides with heteroatom nucleophiles. J Am Chem Soc 141:18437–18443

Carbohydrates to Chemicals and Fuel Additives over ModifiedPolyoxometalate Catalysts

B. Srinivasa Rao, P. Krishna Kumari, and N. Lingaiah

Abstract The quest to produce chemicals and transportation fuels from sources other than conventional non-renewable fossil resources has shifted the focus and direction of research activities towards the utilization of cleaner renewable feedstock. Renewable resources like biomass are ever-abundant and also have an added advantage of being carbon rich that can be leveraged for the production of various chemicals. Biomass is the source of carbohydrates which are the major precursor to produce fine chemicals and fuel additives. The catalytic conversion of biomass-derived carbohydrates to chemicals and fuel additives has been an extensive topic of research lately. Among various fine chemicals derived from biomass, 5-hydroxymethylfurfurl, 5-ethoxymethylfurfurl, alkyl levulinates and gamma valerolactone are some value-added chemicals with immense potential. The preparation of these chemicals derived from biomass requires catalysts with specific active sites with desirable acid/base properties. A majority of these chemicals can be formed by acid catalysis of carbohydrates. This chapter mainly focuses on the conversion of carbohydrates to value-added chemicals over modified heteropoly acid catalysts with sufficient Bronsted/Lewis acidity. Supported and metal-exchanged heteropoly molybdate and tungstate catalysts are synthesized and utilized for the conversion of biomass-derived carbohydrates to chemicals. The activity of these catalysts is discussed on the basis of their acidic sites, surface properties and structural features. Operating conditions such as reaction temperature, reaction time, feed concentration, catalysts concentration, solvent volume and the type of reactor used are also briefly discussed in this chapter.

Keywords Biomass conversion · Heteropoly acid · 5-Hydroxymethylfurfural · Alkyl levulinates · 5-Ethoxymethylfurfural

B. S. Rao · P. K. Kumari · N. Lingaiah (✉)
Department of Catalysis and Fine Chemicals, CSIR-Indian Institute of Chemical Technology, Hyderabad, Telangana, India
e-mail: nakkalingaiah@iict.res.in

1   Introduction

The global industrialization has changed the picture of the world's energy consumption. Most of the energy needs of the people are globally catered by fossil fuel resources. The market worth of world's energy is about 1.5 trillion dollars and still directed by fossil fuels. The World Energy Outlook (WEO) states that energy produced through fossil fuels will remain as the chief source and is projected to meet ~84% of energy requirement up to 2030. Crude oil, gas and coal are the leading supplies for energy. Ever-increasing consumption of these resources led to the carbon dioxide emissions and depletion of the fossil fuel reservoirs. The continuous consumption leads to the dwindling of the resources [1–3]. All over the globe, the fossil fuel reserve depletion times for coal, gas and crude oil are nearly 109, 54, and 53 years, respectively [4]. These reports are alarming for the energy demands of the future generations.

The quest to produce transportation fuels and chemicals from resources other than fossil resources switched over the ongoing research activities towards renewable resources. The main theme is to produce clean energy, transportation fuels and chemicals in a sustainable approach from biomass, wind, nuclear, solar and hydroelectric resources. Except biomass, other renewable resources are familiar for the production of electricity. To compete with the fossil fuel resources in terms of the production of transportation fuels and chemicals, biomass is the outstanding renewable resource as it is carbon rich and the most abundant feedstock. Moreover, the carbon dioxide released during the consumption of biomass-derived transportation fuels can be utilized for the production of feedstock via photosynthesis and thereby maintain the carbon neutrality.

2   Lignocellulosic Biomass

During the past decades, researchers tried to produce biofuels and chemicals from sugars, starches and vegetable oils. These are called first-generation biofuels and have created several problematic issues. The competition between food and fuel arises due to the need of fertile land and high economic inputs for the cultivation and conservation of the crops. Both the economic and environmental (eutrophication and acidification) complications are associated with the production of first-generation biofuels [5, 6]. However, the production of biofuels and chemicals from biomass is still encouraging due to utilization of the most abundant lignocellulosic biomass. The major sources for the lignocellulosic biomass are from agricultural, forestry and dedicated energy crops. These are second-generation biofuel feedstocks [7, 8]. Figure 1 shows the first- and second-generation feedstocks for biofuels. The global production of plant biomass amounts to about 200*10^9 tons/year, of that over 90% is lignocellulose, in which potentially accessible biomass remains only about 8–20*10^9 tons.
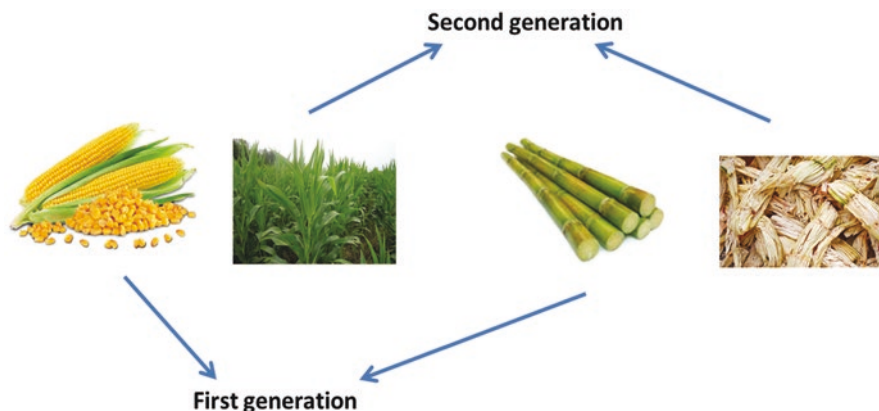
Fig. 1 Feedstocks of the first- and second-generation biofuels
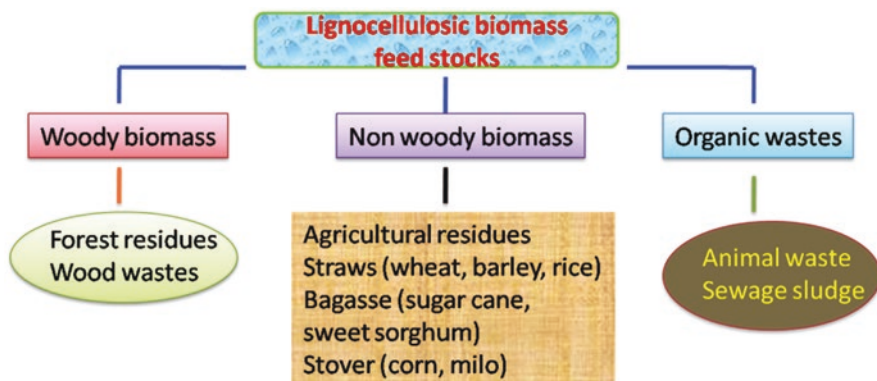
Fig. 2 Feedstocks of lignocellulosic biomass

Interestingly, lignocellulosic biomass (LB) can be obtained along with the non-agricultural lands, food (e.g. straw and corn) and degraded soils eliminating the unwanted issues. The advantageous features for utilization of lignocellulosic biomass are due to widespread and easy availability of raw materials. Its utility could concede the creation of valuable biofuels and chemicals, along with electricity and heat. These are steering to better environmental, energy and economic accomplishment through the development of biorefinery concepts. The feedstocks for the lignocellulosic biomass can be classified into three categories depending upon their origin. The feedstocks for lignocellulosic biomass are shown in Fig. 2. They are woody biomass, non-woody biomass and organic waste.

The major compositions of the LB are cellulose, hemicellulose and lignin. The structural organization of the LB is shown in Fig. 3. The cellulose present in the linear conformation facilitates the packing of plentiful cellulose strands into crystalline fibrils. Hemicellulose is bound non-covalently to the cellulose fibrils' surface [9].
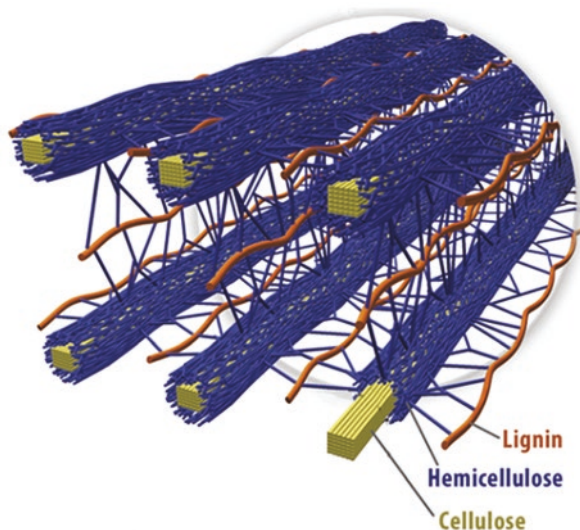
Fig. 3 The structural organization of the lignocellulosic biomass

It works as an amorphous matrix material to hold the firm cellulose fibrils in place. Lignin caters structural reinforcement, waterproofing and resilience to biological and physical attack compared to the all-carbohydrate cell walls of immature plant tissues [10].

The average contribution of these fractions towards the lignocellulosic biomass is cellulose (35–50%), hemicellulose (20–25%) and lignin (15–25%). However, the compositions of these fractions may vary due to the difference in the plant material and construction of the cell wall [11]. The detailed information about the composition of the LB is shown in Table 1. The differences in these compositions influence the biomass destruction process. For example, the composition differences of lignin result in difficulty in delignification of softwood compared to the hardwood and grasses [12].

2.1 Cellulose

Cellulose was first isolated from timber that was consecutively treated with HNO_3 and NaOH solutions by Anselme Payen in the year 1839. Cellulose has a distinct, rigid structure that assists essential function in plants. Its molecules are combined by hydrogen bonds and are arrayed parallel to one another, leading to the formation of lengthy cable-like structure that unites with other cellulose moieties. This built the strong support structure that leads plants to stand upright. It is a crystalline linear homopolymer of D-glucopyranose units. The only monomer in cellulose is the glucose molecule which is connected through β-1, 4-glycosidic bonds composed of

Table 1 Agricultural and other lignocellulosic residues' composition (wt %)

Material	Cellulose	Hemicellulose	Lignin	Ash	Extractives
Algae	20–40	20–50	–	–	–
Cotton	80–95	5–20	–	–	–
Grasses	25–40	25–50	10–30	–	–
Hardwoods	45	30	20	0.6	5
Hardwood barks	22–40	2–38	30–55	0.8	–
Softwoods	42	27	28	0.5	3
Softwood barks	18–38	15–33	30–60	0.8	–
Wheat straw	37–41	27–32	13–15	11–14	–
Corn stover	38–40	28	7–21	3.6–7	–
Bagasse	32–48	19–24	23–32	1.5–5	–
Rice straw	28–36	23–28	12–14	14–20	–
Barley straw	31–45	27–38	14–19	2–7	
Sorghum straw	32	24	13	12	–

Fig. 4 Structural representation of cellulose
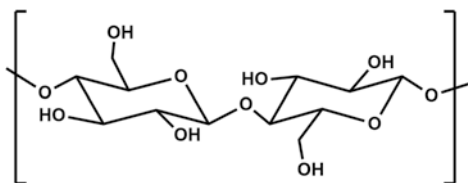
800–1700 units. The structure of cellulose is shown in Fig. 4. The conversion of cellulose by thermal decomposition leads to the different products at different temperatures. At lower temperature of 200–280 °C, cellulose dehydrates into dried cellulose which leads to formation of charcoal and gas products [13]. Cellulose splits into flammable volatile products like tar at higher temperatures. One of the transitional products of cellulose in this conversion is laevoglucose that can be further degraded into low molecular compounds and tar-like products. The conversion of cellulose to glucose can be achieved via enzymatic hydrolysis or acidic hydrolysis.

2.2 Hemicellulose

Hemicellulose is a polysaccharide present in the plant fibre materials. The name hemicellulose is suggested by Schulz et al. (1891) due to its resemblance with the semi-finished products and precursor molecules of cellulose [14]. Hemicellulose functions as a storage polysaccharide and in grouping with lignin and cellulose molecules increases the resistance to enzymatic degradation of the cell wall and maintains the insolubility property. The structure and content of hemicellulose are different in various plants. Considerable divergences also exist in hemicellulose composition and content between the roots, stem, bark and branches of the plant.

Hemicellulose is a heteropolymer of pentoses (xylose and arabinose) and hexoses (glucose, galactose and mannose) and sugar acids (acetic). The structural forms of hemicellulose are shown in Fig. 5. The composition of the hemicellulose in softwoods is rich with mannose and glucose, whereas hardwoods consist higher proportions of xylose units. Hemicellulose is more highly acetylated in hardwoods than in softwoods [15]. Hemicellulose is in amorphous nature with 100–200 units of basic sugar monomers. The monomers of the hemicellulose are connected by β-1,4 linkage. As the hemicellulose is hetero-polysaccharide, upon hydrolysis it gives furfural and 5-hydroxymethyl furfural from pentoses and hexoses, respectively.

2.3 Lignin

Lignin is an amorphous compound with a three-dimensional network composed of complicated randomly linked phenyl propane units. The structure of the lignin is quite complex and varied from one plant material to another and even changes in the extraction stage resulting in different structural relations in the lignin [16]. The lignin constitutes with three major monomers coumaryl alcohol, sinapyl alcohol and coniferyl alcohol as shown in Fig. 6. Lignin is divided into three types based on the monomer: *p*-phenyl monomer (H type) obtained from coumaryl alcohol, guaiacyl monomer (G type) from coniferyl alcohol and syringyl monomer (S type) from sinapyl alcohols which are linked through the random coupling of C–C and C–O bonds. The coupling modes that exist among each basic unit include β-O-4, β-5 and β-1. In lignin the existing ether bonds are phenol-ether, alkyl-ether, dialkyl, diaryl ether bonds and so on. Majority of the phenyl propane moieties of lignin are attached to the adjoining structural units by ether bonds, and a minute part only exists in free phenolic hydroxyl form [17].

Lignin is a white or nearly colourless substance. Its colour is a result of preparation and separation process. The solubility of lignin is directed by the hydroxyls and other polar groups present in its structure, and these led to strong intra- and
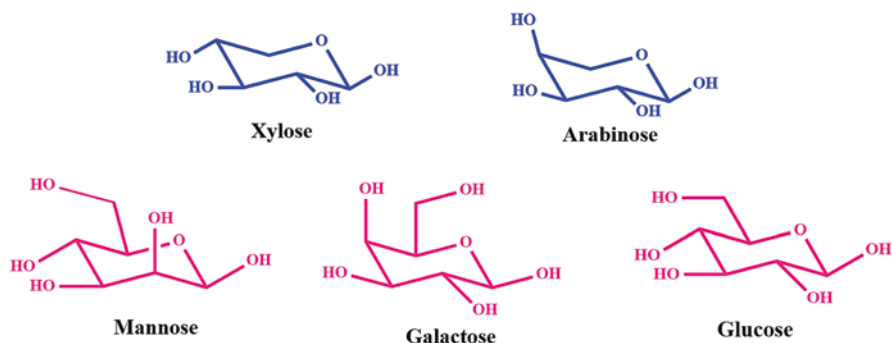
Fig. 5 Basic sugar monomers of the hemicellulose
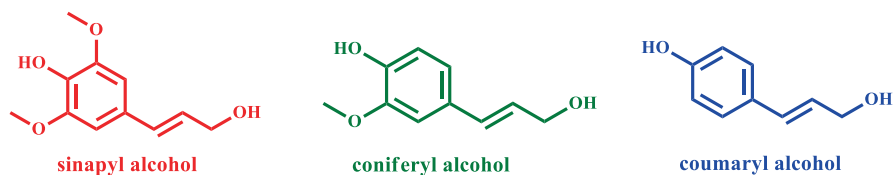
Fig. 6   Basic monomer units of the lignin

intermolecular hydrogen bonds. These properties made lignin as insoluble in any solvent. The processing of lignin by condensation or degradation led it to be divided into insoluble and soluble ones with an amorphous and morphological structure, respectively. The phenolic hydroxyl and carboxyl groups' presence in lignin is responsible for its solubility in alkaline medium. Separated Braun's and organosolv lignin are dissolved in various organic solvents such as DMSO, dioxane, methanol, ethanol, acetone and pyridine. The complexity in the structural arrangement of lignin results in the resistance to the selective conversion into the products. Most of the lignin is converted into bio oil by pyrolysis approach [18].

3   Conversion of Lignocellulosic Biomass to Chemicals

The US Department of Energy has proposed several notable platform chemicals that can be obtained from biomass to maintain the sustainability with techno-economic feasibility. Biomass is rich source for the synthesis of important platform chemicals and fuel additives like 5-hydroxymethylfurfural (HMF), 5-ethoxymethylfurfural (EMF), alkyl levulinates (AL) and γ-valerolactone (GVL). These chemicals can be yielded directly either from biomass or its derivatives in the presence of a proper catalyst. The catalyst can be homogeneous, heterogeneous or ionic liquids having Bronsted and Lewis acidity or a combination of both. The function of the catalyst is not only to increase the rates of reactions but also to enhance the product selectivity and yield.

The conversion of cellulosic biomass via hydrolysis techniques can be accomplished by the use of mineral acids. The hydrolysis techniques are capable of yielding the selective formation of renewable chemicals and fuels in successive operations. The acid hydrolysis of cellulose gives glucose which further undergoes isomerization to fructose. Acid treatment of carbohydrates in the presence of aqueous media will give levulinic acid. Dehydration of fructose yields HMF and further etherification gives the product EMF. Rehydration followed by deformylation of these furan derivatives yields alkyl levulinates which further undergo hydrogenation to yield GVL. Acid treatment of hemicellulose produces xylose as a major product. Hydrolysis of xylose gives furfural as major product which on hydrogenation yields furfuryl alcohol. The alcoholysis of furfuryl alcohol results in the formation of alkyl levulinates. The schematic representations of the possible transformations from cellulosic biomass are presented in Fig. 7.
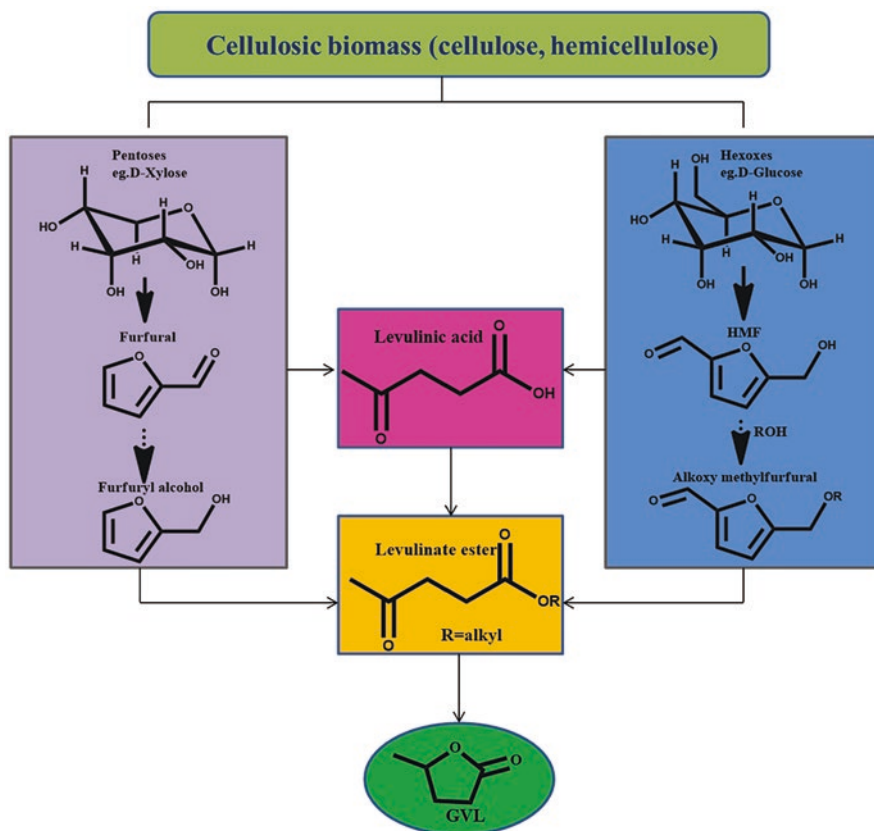
Fig. 7 Possible conversion of cellulosic biomass to chemicals

4   Catalysts for the Conversion of Biomass to Chemicals

A number of techniques have been developed for the transformation of biomass to value-added chemicals. Earlier researchers utilized corrosive and strong homogeneous acids such as HCl and H_2SO_4 as active catalysts for converting biomass to sugars and its commodity chemicals [18]. Recently, sulfonic acid-functionalized carbon, mesoporous silica materials [14, 15], zeolites [13], porous alumino-silicates [19], aryl sulfonic acid-containing hollow mesoporous carbon spheres [20] and ionic liquids with sulfonic acid functionalization [21, 22] have been explored for the making of 5-ethoxymethyl furfural and alkyl levulinates from carbohydrates. However, many of these catalysts have concerns such as separation, reusability and environmental compatibility. In order to overthrow these disputes, the use of environmentally benevolent heterogeneous catalyst is a perfect approach. Among the different heterogeneous catalysts, heteropoly acids are widely used as oxidation and acid catalysts. There are promising catalytic systems to be used in biomass valorization.

5   Heteropoly Acid Catalysts

Heteropoly acids (HPAs) also called polyoxometalate compounds are known as acid and oxidation catalysts [23, 24]. HPAs have more benefits as these catalysts are economically and environmentally desirable. These are strong Bronsted acid catalysts with acidity close to superacid region. They are competent oxidants with reversible multi-electron redox transformations under trivial conditions. These are progressively becoming important in applied catalysis. Explorative work has been made by Japanese and Russian research groups since the 1970s [25, 26]. In the last two decades, the expansive usage of HPAs in catalysis has been established in a wide range of synthetically attractive organic transformations of different substances [27].

5.1   Classification of Heteropoly Acids

Heteropoly compounds, including their salts, are composed of heteropoly anions and counter ions, e.g. protons or metal cations. A heteropoly anion contains metal (e.g. tungsten, molybdenum or vanadium) atoms that are termed as addenda atoms, oxygen atoms and an element from the p-block of periodic table, generally like silicon, phosphorus or arsenic (heteroatom) as central atom. Heteropoly compounds have many types such as Keggin, Dowson and Anderson based on their structure and different amount of hetero and addenda atoms. The Keggin-type ones are widely used in catalysis, due to their moderate thermal stability, strong acidity and high oxidizing ability. Table 2 shows different types of heteropolyoxometalates with their general chemical formula. Among them, only Keggin heteropoly acid catalysts are discussed in this chapter.

5.2   Keggin Heteropoly Ion

Keggin heteropoly ions are a class of polyoxometalates. Keggin heteropoly anions are represented as $X_nM_{12}O_{40}^{(8-n)-}$, where X = heteroatom. The addenda and heteroatom ratio for Keggin HPAs is 12 (M/X = 12). These are well-known and studied widely for various applications among which catalytic applications are important

Table 2 Different types of heteropolyoxometalates

Formula	Heteroatom (X)	Structure
$[X_n^+M_{12}O_{40}]^{(8-n)-}$	P^{5+}, Si^{4+}, As^{5+}, Ge^{4+}	Keggin
$[X_n^+M_{11}O_{39}]^{(12-n)-}$	P^{5+}, Si^{4+}, As^{5+}, Ge^{4+}	Lacunary Keggin
$[X_2^{5+}M_{18}O_{62}]^{6-}$	P^{5+}, As^{5+}	Dawson
$[X_n^+M_6O_{24}]^{n-}$	I^{7+}, Te^{6+}	Anderson

due to their moderately high thermal stability and redox and acidic properties. The heteroatom X is mostly either P^{5+} or Si^{4+}, and many other metals have been reported to act as heteroatom, and M is usually W^{6+} or Mo^{6+}.

5.3 Structure of Keggin Heteropoly Acids

The first heteropoly anion $[PMo_{12}O_{40}]^{3-}$ was reported in 1826 by Berzelius. Several conjectures were created on the structure of HPAs, particularly by Alfred Werner followed by Linus Pauling. A century later in 1933, J.F. Keggin from the University of Manchester did powder X-ray diffraction studies on 12-tungstophosphoric acid ($H_3PW_{12}O_{40}$), and its structure was determined, which is known as the Keggin structure [28]. Figure 8 shows the ball and stick representation of Keggin anion.

The primary structure of $H_3PW_{12}O_{40}$ is well-recognized Keggin unit (KU), in which the central P atom is in tetrahedral coordination (PO_4) and surrounded by 12 metal oxygen octahedral (WO_6) units [29]. The negative charge of the Keggin ion is neutralized by three protons. Oxygen atoms exist in four types in a KU. In the Keggin unit four central oxygen atoms (Oa), 12 oxygen atoms that bridge 2 W atoms sharing a central oxygen atom (edge-sharing Oc), 12 oxygen atoms that bridge tungsten atoms not sharing a central oxygen atom (Ob) and 12 terminal oxygen atoms (Od) bound to each W atom.

The examples of Keggin heteropoly acids are:

- $H_3PMo_{12}O_{40}$: 12-molybdophosphoric acid (MPA)
- $H_3PW_{12}O_{40}$: 12-tungstophosphoric acid (TPA)
- $H_4SiMo_{12}O_{40}$: 12-silicomolybdic acid (SMA)
- $H_4SiW_{12}O_{40}$: 12-silicotungstic acid (STA)

Fig. 8 Ball and stick representation of Keggin anion
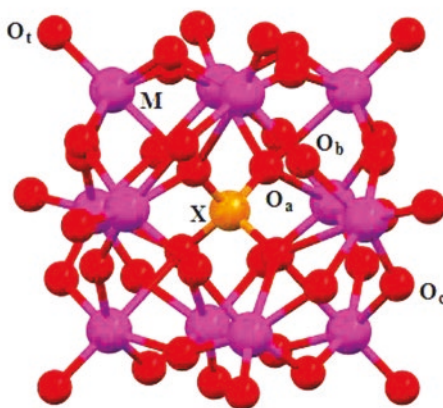
HPAs based on P and Si central atoms and Mo and W as addenda atoms are commonly available. The Keggin structure is flexible and has five geometrical rotational isomers, also known as Baker-Figgis isomers. These ions are known to exist in α form, and this term is frequently used in several applications including heterogeneous catalysis [30].

Generally, heteropoly acids and their salts form ionic crystals composed of heteropoly anions known as primary structure; counter cations such as H^+, H_3O^+ and $H_5O_2^+$; hydration water; and other molecules are secondary structure. The hierarchical structure of solid HPAs is essential for the understanding of its catalytic activity, and the substructures are denoted as primary, secondary and tertiary structure [31]. The primary structure of the heteropoly acid is its anion $[PW_{12}O_{40}]^{3-}$ that exist in Keggin structure. The arrangement of primary structure together with counter cations forms the secondary structure (e.g. $Cs_{2.5}H_{0.5}PW_{12}O_{40}$). The secondary structure is flexible and relies on the amount of hydration water, counter cation and heteropoly anion. The aggregates of secondary structures in three-dimensional manner give the tertiary structure. It explains the formation of solid particles and links to properties like surface area, pore structure, particle size and distribution of protons in particles [32]. This hierarchical structure of HPAs plays a crucial role in understanding and designing these as heterogeneous catalysts. This appears to be a simple idea, but helps enormously in the research on HPA-based catalysis.

5.4   Acidic Properties of Keggin Heteropoly Acids

In aqueous solution, HPAs are strong acids. Their acidity is comparable to that of common acids such as H_2SO_4, HNO_3 and HCl and hence is sometimes called superacids [33]. The protons present in the secondary structure of HPAs are considered as mobile protons. Thus, the high mobility of these protons makes HPAs as superacids. The acid strength of HPAs varies in a wide range depending on polyanion structure and its constituent elements (both heteroatoms and addenda atoms), on the extent of hydration and reduction. Among the Keggin-type HPAs, MPA is stronger acid and its acidity is close to that of superacid [34].

5.5   Modification of Keggin Heteropoly Acids

HPAs have been identified as efficient acid and oxidation catalysts. Bulk forms of Keggin HPAs have limited number of catalytic applications since they are associated with certain drawbacks [35]. HPAs have low surface areas less than 10 m^2/g, which hinder approachability to their strong acidic sites. Due to their relatively low specific surface area, catalytic activity of HPAs is limited in gas-phase reactions. Solubility of HPAs in polar solvents is another limitation. These are highly soluble in alcohols, water and ethers which cause them to be leached during catalytic

reactions involving polar molecules as reactants or products. Furthermore, the thermal stability of pure heteropoly acids is very low and cannot be used in vapour-phase reactions. In order to overcome these shortcomings and extend their catalytic applications in a wide range, these materials have to be modified.

HPAs can be modified in the following ways:

1. By exchange of HPA protons with various metal cations
2. By supporting them on suitable solid supports

1. Metal-Exchanged Keggin Heteropoly Acids

HPAs can be modified by replacing the protons partially or fully with metal ions in secondary structure without altering the primary structure. Metal-exchanged Keggin HPAs, indicated by formula $M^1_X H_{Y-X} M^2 M^3_{12} O_{40}$, where $M^1 = Cs^+$, Rb^+, etc., $M^2 = P$ or Si, $M^3 = W$ or Mo, $x = 2.5$ and $y = 3$ or 4 if M^2 is P or Si, respectively, are produced by partially exchanging the protons of heteropoly acids. Figure 9 represents the exchange of Cs ion with the protons of heteropolytungstate. The HPAs modified by this way can be used as catalysts [36, 37]. Metal-exchanged heteropoly acids can be classified into two groups: A and B [38]. Group A are the HPAs whose protons are replaced with small ions like Na^+ and Cu^{2+}. These group A HPAs possess low surface area (1–15 m^2/g), high solubility in water and absorption capability of polar or basic molecules. Group B are the HPAs with large cations like Cs^+ and Rb^+, and these solids have properties such as high surface area up to 50–200 m^2/g, insoluble in water and incapable to absorb molecules.

Exchange of protons with metal ions would enhance the HPAs' stability and surface area. The catalytic behaviour of metal-exchanged HPAs has received considerable interest, because of their multifunctional nature [39]. Various metal ions like Cu^{2+}, Fe^{3+}, Ag^+, Al^{3+} and Sn^{4+} have been used to exchange the protons of different Keggin HPAs [40–42]. The structure of HPA is stable even after modifying its protons with diverse metal ions. Acidic properties of HPAs rely on
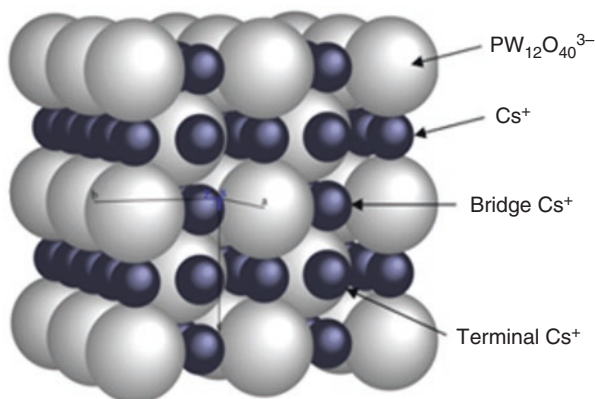
Fig. 9 Exchange of Cs ions with the protons of TPA

the number of protons exchangeable in Keggin secondary structure. It is known that partially exchanged HPAs display high acidity than fully exchanged or parent acid owed to high protons' mobility [43].

Partial exchange of protons of HPAs with cations of large size such as Cs^+, Rb^+, NH_4^+ and K^+ results in conversion of a water-soluble acid with low surface area (<5 m^2/g) into a water-insoluble acid salt with surface area more than 100 m^2/g [44]. Heteropoly salts are more stable than the parent acid. However, the relative stability depends upon the counter cation [45]. The acidic Cs salt of TPA ($Cs_{2.5}H_{0.5}PW_{12}O_{40}$) is stable better than parent $H_3PW_{12}O_{40}$. This salt was not decomposed at high temperature >500 °C, while the parent acid decomposes at lower temperatures (about 300 °C). In metal-substituted HPAs, polar solvents like water and alcohol can easily diffuse and exit in bulk, which leads to expansion or contraction of the distance between the Keggin anions in the crystal lattice. In case of non-polar molecules like hydrocarbons cannot enter into the bulk. This specific character of the Keggin structure, few reactions undergo in bulk and this state is called pseudo liquid phase. Non-polar molecules are incompetent to be absorbed in the bulk of HPA and interact only with the surface [34]. Some of the HPA salts of metal ions (M^{n+}) of $PW_{12}O_{40}^{3-}$ ($M_{3/n}PW_{12}O_{40}$) exhibit Lewis acidity [46, 47], due to the presence of metal cation which acts as electron pair acceptor, distinct from the characteristic Bronsted acidity of HPAs.

2. Supported Keggin Heteropoly Acids

The second type of modification of HPAs is to support on high surface area acidic or neutral supports like zirconia, silica, titania, niobia, ceria, tin oxide and mesoporous materials (SBA-15, MCM-41, HMCM-41). When HPA is supported on support with acidic sites, a deep interaction between heteropoly acid and surface of oxide results in the formation of species such as $[\equiv M\text{-}OH_2]_n^+ [H_{3-n}PW_{12}O_{40}]_n^{-3}$. Therefore, one can overcome the solubility problem. On the other hand, support enhances the surface area of active HPA. The number of active sites of solid material is also enhanced along with stability and thereby its catalytic activity. Basic supports are not suggestible because HPAs readily decompose on basic supports. As the supported samples are heterogeneous, these can be simply separable from the reaction mixture in liquid-phase applications, and stability increases in high-temperature gas-phase reactions [36]. Figure 10 shows the representation of HPAs supported on acidic supports.

6   Conversion of Carbohydrates to 5-Hydroxymethylfurfural

5-Hydroxymethylfurfural, a dehydration product from hexoses, is judged as a biorenewable platform chemical. The high functionality of HMF allows it to be converted to various important biofuel molecules as shown in Fig. 11 such as ethyl levulinate, 5-ethoxymethylfurfural and 2,5-dimethylfuran (DMF) and valuable chemicals such as levulinic acid, 2,5-diformylfuran (DFF), 2,5-furandicarboxylic acid, adipic acid and caprolactone.
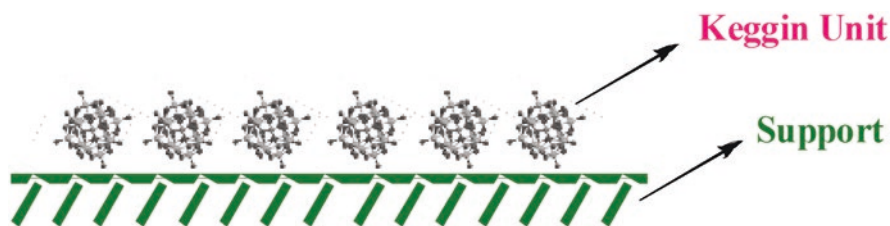
Fig. 10 Schematic representation of supported HPAs
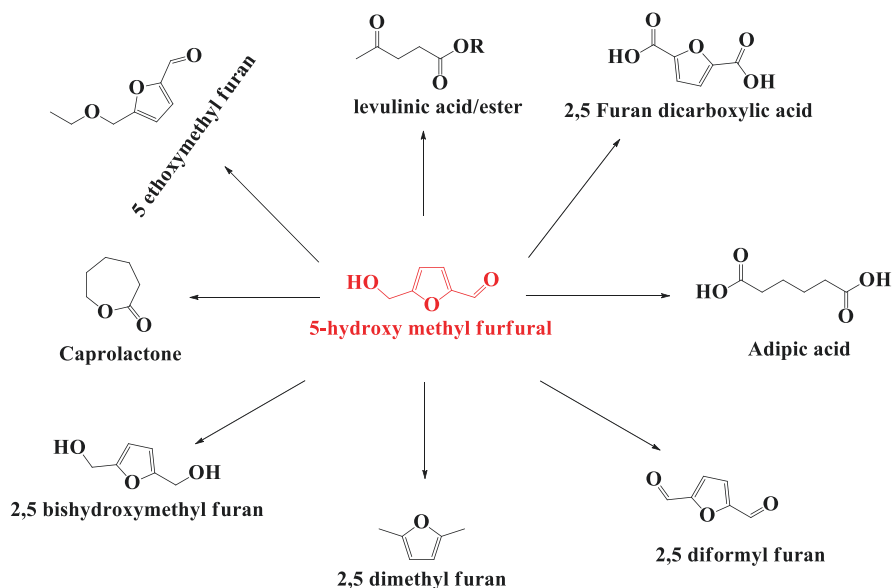
Fig. 11 HMF conversion to fuels/value-added chemicals

6.1 Conversion of Carbohydrates to HMF over Modified Heteropoly Acid Catalysts

Carbohydrates derived from biomass are the platform compounds to derive fine chemical and fuel additives. These are the starting compounds in realization of biomass valorization. Glucose and fructose are the main compounds used as feed to prepare many desired commodity chemicals. In the recent past, dehydration of fructose to HMF reaction has been studied using mineral and organic acids [48, 49]. HMF yields which varied from 24 to 97% were attained over these acids. Recently, solid catalysts with both Bronsted and Lewis acidity have been significantly used for the preparation of HMF from fructose.

Modified HPA catalysts are explored as solid catalysts for conversion of carbohydrates. Heteropoly acid salts Cs-exchanged heteropoly tungstate [50] and

Ag-exchanged heteropoly tungstate [51] were prepared and examined for the dehydration of fructose. These catalysts gave 74 and 77.7% of HMF yield in the presence of water/MIBK, respectively. Roy et al. reported Zn_xTPA/γ-Al_2O_3 via microwave-assisted hydrothermal method for fructose conversion to HMF [52].

Shun Zhao et al. reported bifunctional surfactant combined with heteropoly tungstate catalyst for one-pot transformation of cellulose to HMF [53]. Yongshui et al. reported sulphate-functionalized ionic liquid containing heteropoly tungstate catalyst for fructose dehydration [54]. This catalyst showed an exceptional activity with 99% of HMF yield in 2-butanol. Direct conversion of glucose to HMF was disclosed by Lei Hu and co-workers [55]. They used the combination of boric acid and tungstophosphoric acid as catalyst in ionic liquid solvent. This catalyst gave 52% HMF within 30 min of reaction time at 120 °C. Direct conversion of glucose to HMF was reported over ionic liquid-exchanged HPW [MimAM]$H_2PW_{12}O_{40}$ catalyst [56]. In this report the maximum yield of 53% HMF was attained in THF/water and NaCl mixture. Song-Bai Yu et al. successfully converted sucrose into HMF using different ILs and heteropoly acid catalysts in DMSO/H_2O mixture [57]. Among the combinations [Hmim][HSO_4]/$Cs_{2.3}H_{0.7}PW_{12}O_{40}$ showed better HMF yield of 91% from sucrose at 180 °C. Glucose and fructose are also examined with this catalyst combination. Gomes et al. reported fructose conversion to HMF over HPW dispersed on MCM-41. Around 80% HMF was observed in 1 h at 120 °C [58].

Our group reported Al-exchanged heteropoly tungstate (AlTPA) supported on SnO_2 catalyst for fructose dehydration to HMF in DMSO [59]. The results suggested that the activity of the catalyst is guided by the acidity of the catalyst, which varied with calcination temperature of the catalyst. 20%AlTPA/SnO_2 catalyst calcined at 400 °C showed 100% fructose conversion with around 90% yield of HMF. We also reported heteropoly tungstate supported on Ta_2O_5 catalyst for HMF synthesis from fructose. The maximum yield of 85% HMF was achieved with 20%TPA/Ta_2O_5 calcined at 300 °C [60]. The active catalyst in this study was assessed with different oxide supports such as Nb_2O_5, SiO_2 and ZrO_2, and the results are displayed in Table 3. All these catalysts showed moderate HMF yields. In order to know the activity difference in these catalysts, all the catalysts were characterized by NH_3-TPD analysis to know their acidity. The 20%TPA/Ta_2O_5 catalyst had more acidity than other catalysts, and it showed best activity. These results clearly indicate the dehydration of fructose was unambiguously proportionate to acidity of the catalyst. The support nature also played an important role.

Mesoporous ZrO_2-supported molybdophosphoric acid catalyst was also reported by our group [61]. A high HMF yield of 80% within a reaction time of 30 min at 120 °C was achieved. The reason to get good yields in less reaction time is dependent on the dispersion of MPA on mesoporous ZrO_2. The dispersion increased the accessibility of active sites of the catalyst.

The above-discussed catalytic systems for the transformation of carbohydrates to HMF were summarized in Table 4.

Table 3 Effect of reaction temperature on fructose dehydration

Catalyst	HMF conv. (%)	Acidity (mmol/g)
20%TPA/Ta$_2$O$_5$	85	0.41
20%TPA/Nb$_2$O$_5$	65	0.13
20%TPA/SiO$_2$	63	0.10
20%TPA/ZrO$_2$	60	0.09

Reaction conditions: fructose (0.36 g), dimethyl sulfoxide (5 g), catalyst weight (0.05 g), reaction temperature (120 °C), reaction time (3 h)

Table 4 Literature review on HMF synthesis over modified heteropoly acid catalysts

S. no.	Feed	Catalyst	Temperature (°C)	Time (h)	HMF yield (%)	Refs.
1	Fructose	Zn$_{0.5}$TPA/ɣ-Al$_2$O$_3$	120	2	88	[52]
2	Fructose	Cs$_{2.5}$H$_{0.5}$PW$_{12}$O$_{40}$	115	1	74	[50]
3	Cellulose	Cr[(DS)H2PW12O40]3	150	2.5	57	[53]
4	Sucrose	Cs$_{2.3}$H$_{0.7}$PW$_{12}$O$_{40}$	180	3	92	[57]
5	Fructose	[MIMPS]$_3$PW$_{12}$O$_{40}$	120	2	99	[54]
6	Glucose	[MimAM]$_2$PW$_{12}$O$_{40}$	160	7.5	54	[56]
7	Glucose	TPA/boric acid in [BMIM]Cl	140	0.66	52	[55]
8	Fructose	HPW/MCM-41	120	1	80	[58]
9	Fructose	Ag$_3$PW$_{12}$O$_{40}$	120	1	78	[51]
10	Fructose	Mesoporous Zr-MPA	120	0.5	80	[61]
11	Fructose	AlTPA/SnO$_2$	120	4	86	[59]
12	Fructose	TPA/Ta$_2$O$_5$	120	3	85	[60]

7 Conversion of Carbohydrates to 5-Ethoxymethylfurfural

Alkoxymethyl furfurals are used as flavours in tobacco in early 1960, and they remained unmapped until they were recently explored as additive for diesel fuel. Among alkoxymethyl furfurals, 5-ethoxymethylfurfural (EMF) is considered as an exceptional additive for diesel as it has high energy density (8.7 kWh L^{-1}), as good as that of diesel fuel (9.7 kWh L^{-1}) and gasoline (8.8 kWh L^{-1}). EMF has high boiling point (508 K) than gasoline, ethanol, DMF and 2-MF, which helps in improving the fuel's density, stability and flow properties [62]. EMF is a favourable biofuel recognized as an alternative energy source. The preparation of EMF in high scale is not easy as it requires selective catalyst and huge production cost. Therefore the synthesis of EMF in industrial scale is a big challenge present in front of researchers.

Basically EMF is synthesized from carbohydrates which are the major compounds derived from biomass. The preparation of EMF from carbohydrates was a multistep transformation as carbohydrates are initially transformed into HMF and then the separated HMF on ethanolysis is converted into EMF. A considerable yield of EMF had been obtained from 5-chloromethylfurfural (CMF), which was

produced by the reaction of carbohydrates with concentrated hydrochloric acid. Alternatively, some synthetic strategies such as the formation of EMF from HMF in presence of ethanol had also been reported. These synthesis approaches for EMF are illustrated in Fig. 12.

7.1 Synthesis of 5-Ethoxymethyl Furfural from Carbohydrates Using Modified Heteropoly Acid Catalysts

Hexoses present in cellulosic biomass (cellulose and hemicellulose) are the major sources for the preparation of EMF. The EMF synthesis from carbohydrates was a multistep process. In this, firstly, carbohydrates are converted into HMF and subsequently to EMF. In many studies HMF was chosen as starting compound in order to establish the optimum reaction conditions for EMF synthesis as HMF is an intermediate product in EMF synthesis from carbohydrates. Different catalysts such as soluble organic acids, metal salts, ion exchange resins and zeolites are examined for EMF synthesis. Many research groups have explored to realize suitable solid acid catalysts and compared their activities with common homogeneous acid catalysts. Different types of traditional acid catalysts such as H_2SO_4 [63], HCl [64] and soluble metal salts are disclosed for the one-pot conversion of fructose to EMF. Mineral acid H_2SO_4 showed 70% EMF yield which is much more compared to HCl (40%). Liu et al. [65] got relatively high EMF yield of 72% with $AlCl_3$ as a catalyst for the
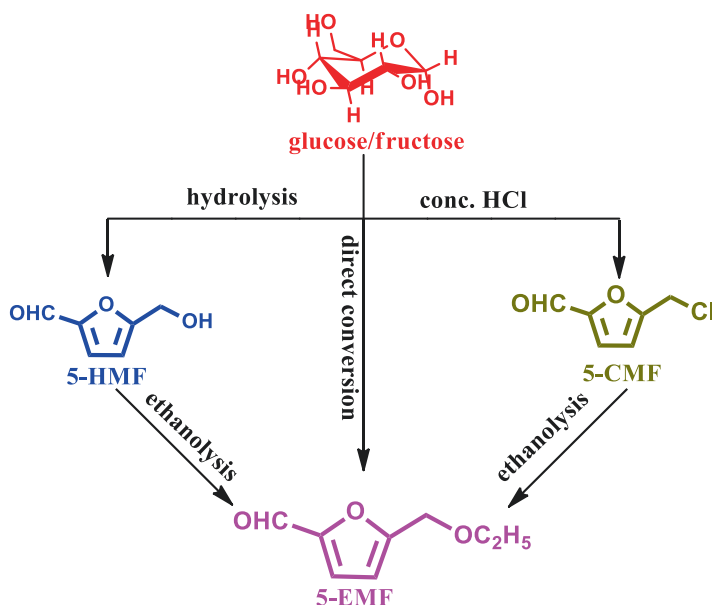
Fig. 12 General synthesis approach of 5-EMF

dehydrative etherification of fructose to EMF. Different inorganic salts were tested for fructose conversion to EMF [66]. Among all, $SnCl_4 \cdot 5H_2O$ and $FeCl_3$ showed acceptable activity with moderate EMF yields.

Many researchers reported solid acid catalysts for EMF preparation from fructose. Christopher M. Lew et al. disclosed Sn-beta and Amberlyst-15 combination catalyst for dehydrative etherification of carbohydrates with less EMF yields at 90 °C [67]. Polymer modified with H_2SO_4 catalysts were evaluated for conversion of fructose to EMF by Song Yang and co-workers [68]. About 72% of EMF was obtained at 110 °C in 10 h of reaction time. Sulphated organic polymer exhibited 89% conversion with 67% EMF yield [69]. A magnetically separable catalyst was prepared and used for EMF synthesis from various carbohydrates. About 63% EMF yield was attained from fructose [62]. Sulfonic acid-functionalized silica catalyst (silica-SO_3H) was also used as solid acid catalyst by Zhang et al. [70].

HAPs-based catalysts are attractive compared to other catalysts for transformation of carbohydrates to EMF in place of traditional homogeneous catalysts. Yang et al. used heteropoly tungstate as able catalyst for converting fructose, inulin and sucrose to EMF [62]. They got 65% of EMF yield from fructose in ethanol solvent under microwave irradiation. The EMF yield was improved from 65 to 76% when THF was added as co-solvent. Sucrose and inulin were converted to EMF with 33 and 62% yields, respectively, at their optimum reaction conditions. In this report they observed that increase in reaction time resulted in the formation of EL. Wang et al. [71] developed $Fe_3O_4@SiO_2$-HPW for fructose conversion with 54.8% of EMF yield. Poly(VMPS)-HPA catalyst exhibited better performance with EMF yield up to 72.8% under the optimized reaction conditions [72]. Ag-exchanged heteropolytungstate was used for HMF and fructose conversion to EMF by Ren et al. [73]. They got a good EMF yield of 70% when fructose was used as a feed and 88% yield from HMF. Heteropoly tungstate supported on K-10 clay was developed by Zhang et al. for the etherification of HMF and dehydrative etherification of fructose with noticeable EMF yield of 91 and 61%, respectively [74]. Silicotungstic acid and phosphotungstic acids are supported on MCM-41 [75, 76] and used for EMF synthesis from fructose and HMF. TPA/MCM-41 catalyst showed a high activity for HMF etherification with 83% of EMF yield. The yield of EMF (43%) was moderate in direct conversion of fructose. STA/MCM-41 catalyst was used for HMF etherification and reported a maximum of 91% EMF yield. Mesoporous SBA-15-supported phosphotungstic acid catalysts were prepared by Rode et al. [77], and their catalytic activity was carried out for the conversion of fructose to HMF and EMF. HMF was the major product when the lower loading of HPW on SBA-15 was used as catalyst. 5%HPW/SBA-15 catalyst showed 78% fructose conversion with 70% of HMF yield. With increasing the loading of HPW to 20%, HMF was converted to EMF, and a maximum of 67% EMF was achieved.

Our group studied Ta-modified heteropoly tungstate supported on SnO_2 catalysts for the etherification of both HMF and fructose [78]. Thirty percent TaTPA/SnO_2 resulted in 90% EMF yield from HMF and 67% from fructose. Modification of heteropoly tungstate with Ta ions introduced Lewis acidity to the heteropoly acid, and it is driven towards high activity even if fructose is used as starting material. The

reaction of fructose was conducted for longer reaction time to know the reaction pathway. Figure 13 indicates the influence of time on fructose conversion to EMF. Fructose conversion to EMF was increased with increase in time. Ethyl levulinate yield was increased with time as the formed EMF was further converted to ethyl levulinate.

We also evaluated mesoporous niobium phosphate-supported tungstophosphoric acid catalysts for the synthesis of EMF from HMF [79]. The catalyst with 25%TPA/NbP showed about 95% HMF conversion with EMF yield of 89%. In this report, activity of 25%TPA/NbP catalyst was compared with different metal oxide supports. All these results are shown in Table 5. Total acidity of the catalysts was calculated by NH_3 temperature-programmed desorption analysis. Among all the catalysts, NbP-supported catalyst showed high acidity. Different heteropoly acids are also supported on NbP, and the maximum acidity was achieved with TPA-containing catalyst. These results clearly indicate the activity was dependent on the acidity of the catalysts which is dependent on the nature of support also.

The detailed study in the preparation of EMF from carbohydrates and HMF over modified heteropoly acid catalysts is summarized in Table 6.
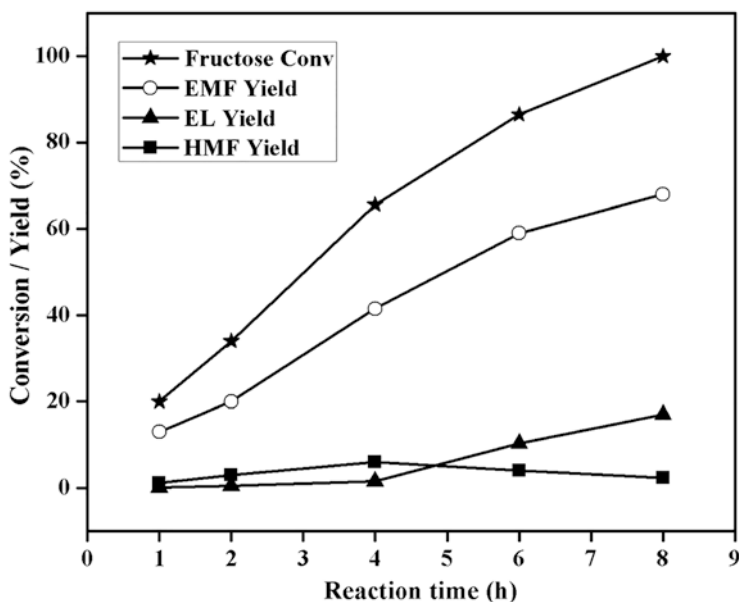
Fig. 13 Influence of time on fructose conversion to EMF. Reaction conditions: fructose (0.180 g), ethanol (6 mL), catalyst weight (0.1 g), temperature (120 °C)

Table 5 Activity results of TPA supported on different supports

Catalyst	HMF conv. (%)	EMF yield (%)	EL yield (%)	Acidity (mmol/g)
25 wt% TPA/ZrO$_2$	35	34	1	0.13
25 wt% TPA/Nb$_2$O$_5$	43	41	2	0.41
25 wt% TPA/SiO$_2$	60	56	4	0.57
25 wt% TPA/NbP	95	89	6	1.69
25%STA/NbP	82	77	4	0.93
25%MPA/NbP	65	62	3	0.53

Reaction conditions: HMF (0.126 g), catalyst wt% (3.76), ethanol (2 g), temperature (120 °C), time (60 min)

Table 6 Literature review on modified heteropoly acid catalysts for EMF synthesis

S. no.	Feed	Catalyst	Temp. (°C)	Time (h)	EMF yield (%)	Refs.
1	Fructose	PWA/SBA-15	100	24	67	[77]
2	Fructose	K-10-Clay-HPW	100	24	62	[74]
3	Fructose	Fe$_3$O$_4$@SiO$_2$-HPW	100	11	54	[71]
4	HMF	Ag$_1$H$_2$PW	100	10	88.7	[72]
5	HMF	STA/MCM-41	90	2	84.1	[75]
6	HMF	HPW /MCM-41	100	12	83.4	[76]
7	Fructose	H$_3$PW$_{12}$O$_{40}$	130	0.5	65	[62]
8	Fructose	Poly(VMPS)-HPA	110	10	73	[72]
9	Fructose	TaTPA/SnO$_2$	120	8	67	[78]
10	HMF	TPA/NbP	120	1	89	[79]

8 Conversion of Carbohydrates to Alkyl Levulinates

Alkyl levulinates (AL) are the biomass-derived chemicals with two functional groups keto and ester. Different types of AL are shown in Fig. 14. The importance of these functional groups made these AL as versatile chemicals in the synthetic organic chemistry. Besides the functional groups, their physical properties (Table 7) are also helpful to gain much interest as solvents and fragrance and flavouring agents.

The lower esters (methyl, ethyl and propyl) contain pleasing melon-like odours and butyl and amyl esters have only pale, but still have pleasant odours. The taste of esters is strongly burning and bitter [80]. AL are green solvents which help to minimize the adverse effects of conventional solvents according to the green chemistry principles. The solvents are characterized by their physical properties like density, thermal conductivity, refractive index, viscosity, surface tension, dipole moment, vapour pressure, hydrogen bond donor and hydrogen bond acceptor capability [81]. Alkyl levulinates possess most of these properties, and more research is still needed to explore the other properties of the alkyl levulinates at different conditions. The internal hydrogen bonding between the molecules of alkyl levulinates imparts compressibility to them resulting in lower vapour pressure which is a characteristic feature of the industrial solvents. Alkyl levulinates are used as flavouring
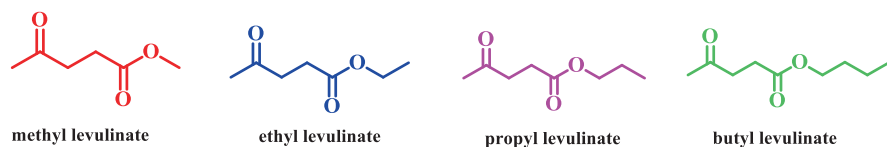
Fig. 14 Chemical structures of alkyl levulinates

Table 7 Physical properties of alkyl levulinates

Alkyl levulinate	Boiling point (°C)	Refractive index	Specific gravity at 25 °C	Surface tension (dyne/cm)	Vapour pressure at 100 °C (kPa)	Solubility in water (mL/100 mL)
Methyl	196	1.4233	1.0495	38.8	5.96	Miscible
Ethyl	205.8	1.4228	1.0111	35.7	4.69	12.5
n-Propyl	221.2	1.4257	0.9896	34.2	–	2.8
n-Butyl	237.8	1.4290	0.9730	34.4	1.56	0.93

agents for food materials and as fragrance agents in the manufacture of candles, cosmetics and soaps [82]. Alkyl levulinates are also used as plasticizers, coalescent solvents and latex coatings [83].

Three different routes are possible for the preparation of AL from carbohydrates as displayed in Fig. 15. The route one is the levulinic acid esterification with alcohol using acid catalysts. Secondly, alcoholysis of furfuryl alcohol to AL. In addition to these, the third route is directly from carbohydrates. Preparation of AL from furfuryl alcohol is more favourable among these three routes because of easy availability and high reactivity of alcoholysis reaction compared to other routes.

8.1   Conversion of Carbohydrates and Their Derived Chemicals to Alkyl Levulinates over Modified Heteropoly Acid Catalysts

Solid acid catalysts are desirable candidates for the conversion of FAL into AL. The first solid acid-catalysed conversion was reported by Lange et al. They studied the conversion of FAL into alkyl levulinates over various acidic catalysts such as H_2SO_4, zeolites and acidic ion exchange resins. They found that resins with accessibility for both the alcohol and FAL catalysed the reaction with higher yields of AL [84]. Hengne et al. examined various ionic liquids functionalized with acidic anions for the synthesis of alkyl levulinates. The MIm acidic anion increased the Bronsted acidity of [BMIm-SH][HSO$_4$] catalyst and thereby yield of the alkyl levulinate [85]. Wang et al. disclosed the synthesis of AL by using ionic liquids functionalized with double SO$_3$H group as catalyst and found that the acidity and the molecular structure influence strongly the activity of ionic liquids [86].
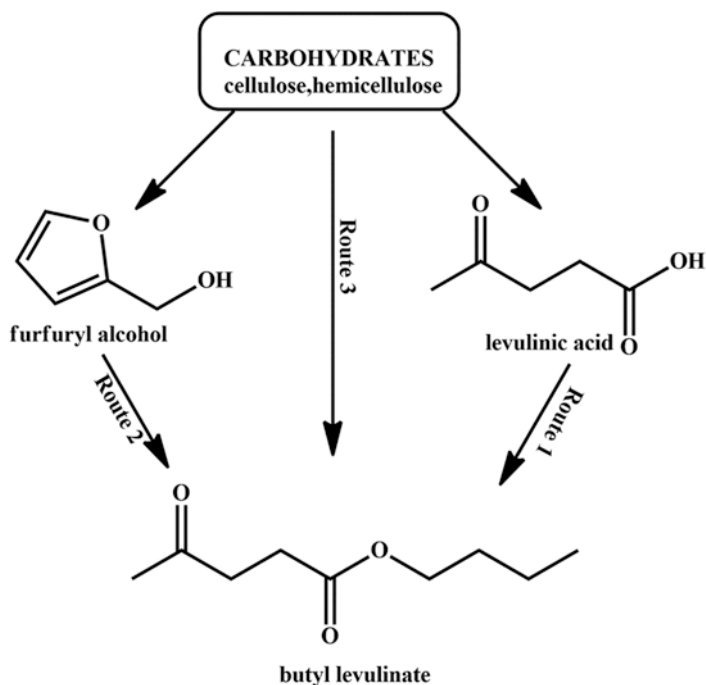
Fig. 15 Possible ways for the preparation of butyl levulinate from biomass derivatives

Bokade et al. reported the acid-treated K-10-supported tungstophosphoric acid for the levulinic acid conversion to butyl levulinate. This catalyst showed 97% of levulinic acid conversion with almost 100% selectivity [87]. Zhang et al. synthesized an ionic liquid and heteropoly acid-containing ([MIMBS]$_3$PW$_{12}$O$_{40}$) catalyst and demonstrated its activity towards the synthesis of butyl levulinate [88]. Mesoporous ZrO$_2$-supported heteropoly acid catalysts were prepared, and their activity for levulinic acid esterification with methanol was tested [89]. Mesoporous STA/SiO$_2$ catalyst was used for the synthesis of different AL from levulinic acid. 20%STA/SiO$_2$ catalyst exhibited better activity with 73 and 67% yields of methyl and ethyl levulinates, respectively [90]. Tungstophosphoric acid dispersed on desilicated HZSM-5 catalyst was reported for esterification of levulinic acid with ethanol [91]. 15%TPA/D-HZSM-5 catalyst showed 94% levulinic acid conversion with 100% of ethyl levulinate selectivity. Different metal-modified heteropoly acid catalysts were used for direct synthesis of ethyl levulinate from carbohydrates by Shiqiang Zhao et al. Different carbohydrates such as cellulose, glucose, fructose, inulin and sucrose were used as feeds for preparation of alkyl levulinates. Among them high ethyl levulinate yield of 64% was observed with fructose over

potassium-modified heteropoly tungstate catalyst. Ethyl levulinate yield was increased to 69% with addition of toluene as co-solvent [92].

We reported the butyl levulinate synthesis from furfuryl alcohol over Zn-modified heteropoly tungstate supported on niobia catalysts [93]. About 94% butyl levulinate yield was achieved with $20\%Zn_1TPA/Nb_2O_5$ catalyst. The catalyst activities explained based on the presence of new Lewis acidic sites in heteropoly tungstate generated with the introduction of Zn ions into their secondary structure. Partially Zn-exchanged catalyst was more effective than completely exchanged catalyst, since it has both Bronsted and Lewis acidity. The catalyst with both Bronsted and Lewis acidic sites is responsible for high conversion and yield. Lewis acidic sites are useful for the etherification of furfuryl alcohol, and Bronsted acidity was involved in ring opening to get butyl levulinate. All the reaction conditions were optimized over the active catalyst. The product butyl levulinate yield was dependent on the amount of active component supported on Nb_2O_5. Figure 16 shows the dependence of Zn_1TPA loading on Nb_2O_5. Even though the lower loading catalysts (5–15% Zn_1TPA/Nb_2O_5) show 100% furfuryl alcohol conversion, the butyl levulinate yield was low. The intermediate ether was not fully converted to butyl levulinate for the catalysts with low amount of Zn_1TPA. The product yield was also low at higher loadings of active component on support. The dark brown colour solid was observed in the reaction mixture when high loading catalysts (25 and 30%) were used. The high acidity of the catalyst is the reason to produce furfuryl alcohol polymers so the butyl levulinate yield was lower than the optimum 20% Zn_1TPA/Nb_2O_5 catalyst.

We reported the direct conversion of carbohydrates and their derived chemicals to ethyl levulinate over Ti-exchanged tungstophosphoric acid catalysts [94]. A series of Ti-exchanged TPA catalysts were prepared, characterized and evaluated for the synthesis of alkyl levulinates. Table 8 reveals the activity of $Ti_{0.75}TPA$ catalyst for the preparation of EL from various starting materials. $Ti_{0.75}TPA$ catalyst showed 92–98% yield of ethyl levulinate from carbohydrate-derived chemicals such as furfuryl alcohol, 5-hydroxymethyl furfural and levulinic acid. However, moderate yields of 63 and 21% of ethyl levulinate were achieved from fructose and glucose, respectively. Diverse alkyl levulinates were also synthesized from furfuryl alcohol. High EL yield of 97 and 98% was reached within 30 min when furfuryl alcohol and levulinic acid were used as feed, respectively. During 5-HMF alcoholysis, about 92% EL yield was obtained in 360 min, whereas 21 and 63% yield of EL was observed with glucose and fructose used as starting materials. These results validated that the $Ti_{0.75}TPA$ was an effective catalyst for the preparation of EL from carbohydrates (glucose, fructose) and their derived chemicals (LA, 5-HMF, FAL).

The details about the use of modified heteropoly acid catalysts towards the preparation of alkyl levulinates from variety of starting materials are shown in Table 9.
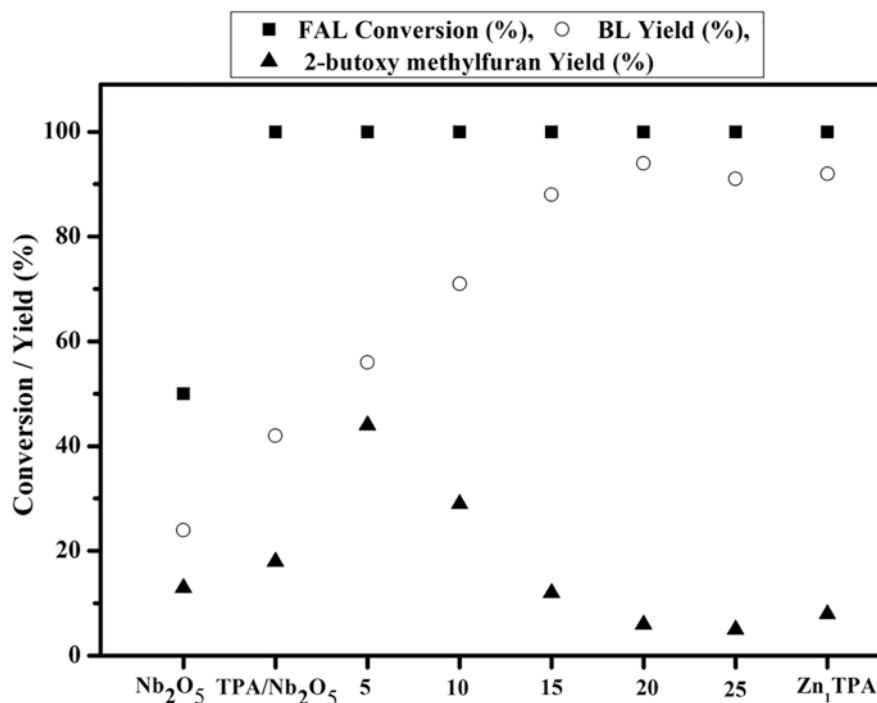
Fig. 16 Furfuryl alcohol alcoholysis activity of the catalysts as a function of Zn_1TPA content on niobia (5–25%), Nb_2O_5, TPA/Nb_2O_5 and Zn_1TPA. Reaction conditions: furfuryl alcohol (0.098 g), butanol (6 mL), temperature (110 °C), catalyst weight (0.3 g), time (5 h)

Table 8 Synthesis of EL from different substrates

S. no.	Feed	Time (min)	Conv. (%)	EL yield (%)
1	Glucose[a]	360	100	21
2	Fructose[a]	360	100	63
3	5-HMF[b]	360	100	92
4	LA[b]	30	100	98
5	FAL[b]	30	100	97

Reaction conditions: [a]Carbohydrate (4 mmol), ethanol (16 mL), catalyst loading (2.25 wt%), reaction temperature (120 °C). [b]Substance (1 mmol), ethanol (4 mL), catalyst loading (2.25 wt%), reaction temperature (120 °C)

9 Synthesis of γ-Valerolactone

γ-Valerolactone (GVL) is a versatile molecule with industrial interest. Naturally it is found in fruits, and it is a colourless liquid. It is a stable compound at normal conditions and has a sweet, herbaceous odour, which makes it suitable for the production of perfumes and food additives. The vapour pressure of GVL is low

Table 9 Heteropoly acid-based catalysts for alkyl levulinate synthesis

S.no.	Feed	Catalyst	Temp. (°C)	Time (h)	Product	Yield (%)	Refs.
2	LA	DTPA/K10	120	4h	BL	97	[91]
3	LA	$[H_3PW_{12}O_{40}/ZrO_2Si(Ph)Si]$	65	3h	ML	99	[89]
4	LA	$H_4SiW_{12}O_{40}$–SiO_2	65	6h	ML EL	73 67	[90]
5	LA	DTPA/DH-ZSM-5(97)	78	4h	EL	94	[91]
6	Fructose	K-HPW-1	150	2h	EL	66	[92]
9	Furfuryl alcohol	$([MIMBS]_3PW_{12}O_{40}]$	110	12h	BL	93	[88]
10	Furfuryl alcohol	$ZnTPA/Nb_2O_5$	110	5	BL	94	[93]
11	Glucose Fructose HMF LA Furfuryl alcohol	TiTPA	140 140 120 120 120	6 6 6 0.5 0.5	EL EL EL EL EL	63 21 92 97 98	[94]

compared to the other oxygenates and alcohols. It is a stable liquid and does not form peroxides under neutral conditions. These properties made GVL as a sustainable fuel additive and solvent. Moreover, GVL can be stored and transported in larger scale, and it is biodegradable [95]. All the products from cellulose deconstruction are soluble in GVL, so it can be utilized as a biphasic solvent system in biorefineries [96]. Luterbacher reported the use of GVL as effective solvent in thermo-catalytic preparation of soluble sugars with high yields from corn stover and wood.

Among the biomass-derived chemicals, GVL became one of the prominent chemicals in the last decade because of its excellent properties as green solvent and fuel additive. It is also a useful precursor for the preparation of high-value biopolymers and liquid alkanes [97, 98]. Currently GVL production is based on a multistep process involving the selective fractionation and depolymerization of the lignocellulosic biomass. The derived monosaccharides from biomass are converted to levulinic acid (LA) by acid-catalysed transformation. GVL is obtained by the hydrogenation of LA.

In general, GVL was obtained by LA and its esters' hydrogenation. Hydrogenation of LA can be conceded by two methods: (1) metal-catalysed hydrogenation with molecular H_2 and (2) catalytic transfer hydrogenation (CTH) with hydrogen donors such as alcohols, formic acid, etc. Conventional hydrogenation carried over expensive noble metal catalysts at high H_2 pressure. However, CTH approach proceeds over simple and cheap metal oxide catalysts with alcohols as H-donors. Figure 17 shows the graphical representation of conventional and CTH approach for GVL synthesis.

Hydrogenation of LA and its esters by CTH via Meerwein-Ponndorf-Verley (MPV) reaction in alcohol as alternative to conventional hydrogenation has been widely covered in literature [99, 100]. Most of the reports for GVL preparation are dedicated on the use of LA and/or its esters. This methodology needs a source of pure LA which is generally derived from furfural. Recently, researchers thought to prepare GVL directly in one pot from furfural instead of LA to avoid isolation and further hydrogenation of LA. This one-pot approach can be conceived by the collective action of acid (Bronsted) and reduction (Lewis/base) sites. Roman-Leshkov and his co-workers firstly disclosed catalytic integrated process for the preparation of GVL from furfural in a single pot using both Lewis and Bronsted catalysts in the form of physical mixture [101]. Weibin Fan et al. revealed an integrated process for GVL preparation from furfural using Au/ZrO$_2$ and ZSM-5 as combined catalysts with 80% yield [102]. Winoto et al. used Zr-Al-β-zeolite catalyst containing both Bronsted and Lewis acid sites for the selective conversion of furfural to GVL. About 95% of GVL yield was obtained over this catalyst within 24 h of reaction time [103]. More recently, Jungho Jae et al. studied Sn-Al-zeolite catalyst using 2-butanol as H-donor and reported moderate yield of GVL up to 60% at 180 °C during CTH of furfural [103]. In another study, Juan A. Melero et al. achieved GVL with 34% yield directly from xylose using Zr-Al-β-zeolite catalyst at 190 °C within 10 h [104], and the same catalyst yielded 72% GVL using FA as feed within 24 h [105].

Our group reported a series of catalysts containing metal oxide and heteropolytungstate on H-β-zeolite [106]. In this study we screened various metal oxides such as Al$_2$O$_3$, SnO$_2$, TiO$_2$ and Nb$_2$O$_5$. The catalyst activity was evaluated for the conversion of furfural to GVL, and the results are presented in Fig. 18.

In these catalysts, GVL yield was related on the nature of metal oxide exist in M-TPA/β-zeolite catalyst. The furfural conversion and GVL yield were low (20–50%) for the catalysts containing Nb, Ti and Sn oxides. However, the catalysts with Zr and Al oxides exhibited high conversion with exceeding GVL yield up to 90%. The activity order of these catalysts is as follows: Zr-T-zeolite > Al-T-zeolite > Sn-T-zeolite > Ti-T-zeolite > Nb-T-zeolite catalysts, where T is tungstophosphoric acid. The difference in activities was defended in terms of the catalysts'
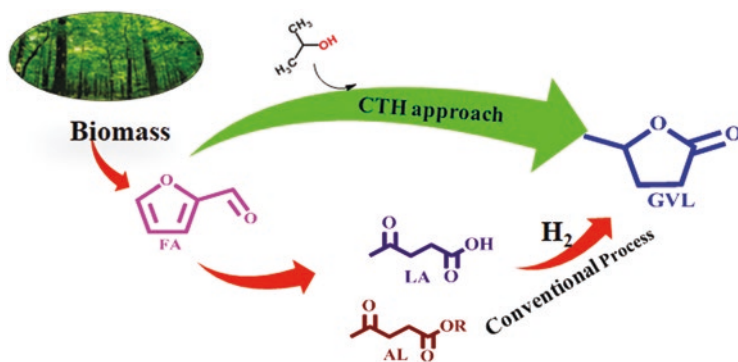
Fig. 17 Different pathways for the synthesis of GVL
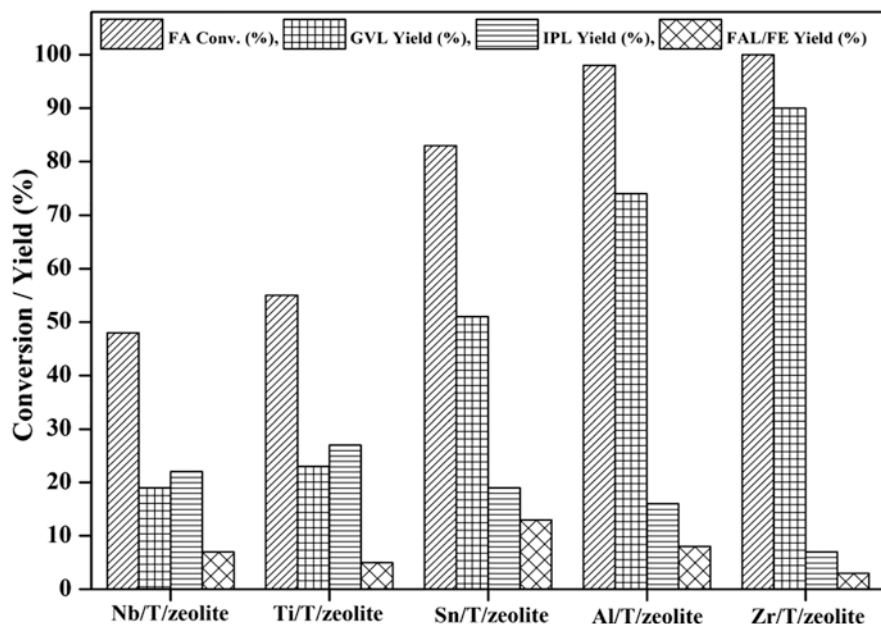
Fig. 18 Conversion of furfural to GVL over various metal oxide-5%TPA/β-zeolite catalysts. Reaction conditions: furfural (0.196 g), 2-propanol (20 mL), temperature (170 °C), catalyst weight (7.5 g cat./L), time (10 h)

characteristics and nature of acidity. The catalysts with low Lewis-to-Bronsted acid sites ratio (Sn, Ti, Nb-T-zeolite) displayed less conversion of furfural with limited GVL yield, while catalysts both Zr-T-zeolite and Al-T-zeolite possess high Lewis-to-Bronsted acid ratio and gave high yield of GVL. These Zr- and Al-containing catalysts also showed the presence of minimum amount of basic sites. Further, the characterization of catalysts by FT-IR indicated that the interaction of 2-propanol (H-donor) with basic sites of these catalysts was significant. Therefore, the Zr-T-zeolite catalyst's high conversion and yield was mainly related to the presence of high amount of Lewis acidity with sufficient amount of Bronsted acidity. The existence of few base sites in this catalyst which improved the interaction with 2-propanol is also another reason for high GVL yield. Further all the above-discussed catalysts were summarized in Table 10.

10   Conclusion

Conversion of biomass to chemicals and fuel additives has been an intense research topic as biomass is considered as a better alternative for the fossil resources. Among the chemicals, HMF and its derivatives like EMF and alkyl levulinates have been recognized as value-added chemicals. All these chemicals can be formed over acid catalysis from carbohydrates. The selectivity of the value-added chemical depends

Table 10 Activity profiles of different reported catalysts for GVL preparation

S. no	Catalyst	Feed	Temp. (°C)	Time (h)	GVL yield (%)	Refs.
1	Au/ZrO$_2$ + ZSM-5	Furfural	120	24	80	[102]
2	Zr-Al-β zeolite	Furfural	120	24	95	[103]
3	Sn-Al-β zeolite	Furfural	180	6	60	[103]
4	Zr-Al-β zeolite	xylose	190	10	34	[104]
5	Zr-Al-β zeolite	Furfural	170	24	72	[105]
6	ZrO$_2$-TPA-β zeolite	Furfural	170	10	90	[106]

on the type of catalysts having Bronsted/Lewis acidity. Heteropoly acid catalysts are desirable candidates for the conversion of biomass as these possess strong Bronsted acidity. Lewis acidity was generated with the modifications in heteropoly acids. The catalyst with more Bronsted acidity is effective for the dehydrating step, and Lewis acidic catalyst is needed in isomerization step in the transformation of carbohydrates to chemicals/fuel additives. This chapter reviewed the modification possible for heteropoly acids to use as heterogeneous catalysts in conversion of cellulosic biomass. The role of modified heteropoly acids in the realization of biomass valorization is also summarized. Reaction temperature, time, catalyst weight and the feed to solvent ratio which are the other parameters that can affect the product yield are discussed.

References

1. Shafiee S, Topal E (2009) When will fossil fuel reserves be diminished? Energy Policy 37:181
2. International Energy Agency (2014) World energy outlook
3. Goldemberg J (2006) The promise of clean energy. Energy Policy 34:2185
4. (2015) BP Statistical Review of World Energy, 64th edition
5. Cherubini F, Bird ND, Cowie A, Jungmeier G, Schlamadinger B (2009) Resour Conserv Recycl 253(8):434
6. Zah R, Boni H, Gauch M, Hischier R, Lehmann M, Wager P (2007) Life cycle assessment of energy products: environmental assessment of biofuels. EMPA, Bern
7. Spatari S, Bagley DM, MacLean HL (2010) Bioresour Technol 101(2):654
8. Gonzalez-Garcıa S, Gasol CM, Gabarrell X, Rieradevall J, Moreira MT, Feijoo G (2009) Renew Sustain Energy Rev 13((9):2613
9. O'Sullivan AC (1997) Cellulose 4:173
10. U.S. Department of Energy Genome Programs image gallery. http://genomics.energy.gov. Accessed 22 Feb 2011
11. Saini JK, Saini R, Tewari L (2015) Biotech 5:337
12. Boerjan W, Ralph J, Baucher M (2003) Annu Rev Plant Biol 54:519
13. Gao J, Tang LG (1996) Cellulose science. Science Press, Beijing
14. Zhang P, Hu HR, Shi SL (2006) Application of hemicellulose. Tianjin Pap Mak 2:16
15. Fengel D, Wenger G (1989) Wood chemistry, ultra structure, reactions. Walter De Gruyter, Berlin

16. Jiang TD (2001) Lignin. Chemical Industry Press, Beijing
17. Tao YZ, Guan YT (2003) J Cell Sci Technol 11(1):42
18. Hendriks ATWM, Zeeman G (2009) Bioresour Technol 100:10
19. Van Steen E, Claeys M (2008) Chem Eng Technol 31:655
20. Tijm PJA, Waller FJ, Brown DM (2001) Appl Catal A 221:275
21. Williams PT, Besler S (1996) Renew Energy 7:233
22. Kraus GA, Guney T (2012) Green Chem 14:1593
23. Hill CL, McCartha P, Coord CM (1995) Chem Rev 143:407
24. Kozhevnikov IV, Matveev KI (1983) Appl Catal 5:135
25. Misono M (1987) Catal Rev Sci Eng 29:269
26. Y. Ono J M Thomas, K I Zamaraev, Perspectives in catalysis, Oxford: Blackwell Science (1992) 431.
27. Zhang J, Sun M, Han Y (2014) RSC Adv 4:35463
28. Keggin JF (1934) Proc R Soc A 144:75
29. Pope MT, Muller A (1991) Angew Chem Int Ed Engl 30:34
30. Weinstock IA, Cowan JJ, Barbuzzi EMG, Zeng H, Hill CL (1999) J Am Chem Soc 121:4608
31. Misono M, Sakata K, Yoneda Y, Lee WY (1980) Proceedings of 7th international congress on catalysis, Tokyo, p 1047
32. Misono M (1992) Proceedings of 10th international congress on catalysis, Budapest. Elsevier, p 69
33. Misono M, Okuhara T (1993) Chemtech. 23:23
34. Mizuno N, Misono M (1998) Chem Rev 98:199
35. Herrera JE, Kwak JH, Hu JZ, Wang Y, Peden CHF (2008) Top Catal 49:259
36. Liu S, Kurth DG, Bredenkotter B, Volkmer D (2002) J Am Chem Soc 124:12279
37. Okuhara T (2003) Appl Catal A Gen 256:213
38. Koyano G, Ueno K, Misono M (1999) Appl Catal A Gen 181:267
39. Suzuki S, Kogai S, Ono Y (1984) Chem Lett:699
40. Rath D, Rana S, Parida KM (2010) Ind Eng Chem Res 49:8942
41. Nagaraju P, Pasha N, Sai Prasad PS, Lingaiah N (2007) Green Chem 9:1126
42. Gurgul J, Zimowska M, Mucha D, Socha RP, Matachowski L, Mol J (2011) Catal A Chem 351:1
43. Parry EP (1963) J Catal 2:371
44. Soled S, Miseo S, Mc Vicker G, Gates WE, Gutierrez A, Paes J (1997) Catal Today 36:441
45. Kozhevnikov IV (2002) Catalysts for fine chemical synthesis: catalysis by polyoxometalates, vol 2. Wiley, New York
46. Shimizu KI, Niimi K, Satsuma A (2008) Appl Catal A Gen 349:1
47. Baba T, Watanabe H, Ono Y (1983) J Phys Chem 87:2406
48. Yang Y, Hu CW, Abu-Omar MM (2012) Green Chem 14:509
49. Pagan-Torres YJ, Wang TF, Gallo JMR, Shanks BH, Dumesic JA (2012) ACS Catal 2:930–934
50. Zhao Q, Wang L, Zhao S, Wang X, Wang S (2011) Fuel 90:2289
51. Fan C, Guan H, Zhang H, Wang J, Wang S, Wang X (2011) Biomass Bioenergy 35:2659–2665
52. Parameswaram G, Roy S (2018) RSC Adv 8:28461
53. Zhao S, Cheng M, Li J, Tian J, Wang X (2011) Chem Commun 47:2176
54. Qu Y, Huang C, Zhang J, Chen B (2012) Bioresour Technol 106:170
55. Hua L, Sun Y, Lin L, Liu S (2012) Biomass Bioenergy 47:289
56. Zhao P, Zhang Y, Wang Y, Cui H, Song F, Sun X, Zhang L (2018) Green Chem 20:1551
57. Yu SB, Zang HJ, Yang XL, Zhang MC, Xie R, Yu PF (2017) Chin Chem Lett 28:1479
58. Filipe NDC, Mendesb FMT, Souzaa MMVM (2017) Catal Today 279:296
59. Raveendra G, Srinivas M, Sai Prasad PS, Lingaiah N (2013) Int J Adv Eng Sci Appl Math 5(4):232
60. Raveendra G, Srinivas M, Pasha N, Rao AVP, Prasad PSS, Lingaiah N (2015) React Kinet Mech Catal 115:663

61. Pasha N, Kumari PK, Vamsikrishna N, Lingaiah N, Subhashini NJP, Shivaraj (2019) Indian J Chem 58A:313
62. Yang Y, Abu-Omar MM, Hu C (2012) Appl Energy 99:80
63. Balakrishnan M, Sacia ER, Bell AT (2012) Green Chem 14:1626
64. Lai L, Zhang Y (2011) ChemSusChem 4:1745
65. Liu B, Zhang Z, Huang K, Fang Z (2013) Fuel 113:625
66. Liu J, Tang Y, Wu K, Bi C, Cui Q (2012) Carbohydr Res 350:20
67. Li H, Saravanamurugan S, Yang S, Riisager A (2016) Green Chem 18:726
68. Che P, Lu F, Zhang J, Huang Y, Nie X, Gao J (2012) Bioresour Technol 119:433
69. Jia X, Ma J, Che P, Lu F, Miao H, Gao J (2013) J Energy Chem 22:93
70. Liu B, Zhang Z (2013) RSC Adv 3:12313
71. Wang S, Zhang Z, Liu B, Li J (2013) Catal Sci Technol 3:2104
72. Li H, Zhang Q, Yang S (2014) Int J Chem Eng. https://doi.org/10.1155/2014/481627
73. Ren Y, Liu B, Zhang Z, Lin J (2015) J Ind Eng Chem 21:1127
74. Liu A, Liu B, Wang Y, Ren R, Zhang Z (2014) Fuel 117:68
75. Che P, Lu F, Zhang J, Huang Y, Nie X, Gao J, Xu J (2012) Bioresour Technol 119:433
76. Liu A, Zhang Z, Fang Z, Liu B, Huang K (2014) J. Ind. Eng. Chem. 20:1977
77. Patil CR, Rode CV (2018) Fuel 217:38
78. Kumari PK, Rao BS, Padmakar D, Pasha N, Lingaiah N (2018) Mol Catal 448:108
79. Kumari PK, Rao BS, Lakshmi DD, Paramesh NRS, Sumana C, Lingaiah N (2019) Catal Today 325:53
80. Gerald JC, Mary LD (1933) Ind. Eng. Chem. 25(9):967
81. Reichardt C (2007) Org Process Res. Dev 11:105
82. Yontz DJ (2011) U.S. Patent US20110274643A1
83. Rieth LR, Leibig CM, Pratt J, Jackson M (2012) Patent WO2012021826A2
84. Lange JP, van de Graaf WD, Haan RJ (2009) ChemSusChem 2:437
85. Hengne AM, Kamble SB, Rode CV (2013) Green Chem 15:2540
86. Wang G, Zhang Z, Song L (2014) Green Chem 16:1436
87. Dharne S, Bokade VV (2011) J Natural Gas Chem 20:18
88. Zhang Z, Dong K, Zhao Z (2011) ChemSusChem 4:112
89. Su F, Ma L, Song D, Zhang X, Guo Y (2013) Green Chem 15:885
90. Yan K, Wu G, Wen J, Chen A (2013) Catal Commun 34:58
91. Nandiwale KY, Sonar SK, Niphadkar PS, Joshi PN, Deshpande SS, Patil VS, Bokade VV (2013) Appl Catal A Gen 460–461:90
92. Zhao S, Xu G, Chang C, Fang S, Liu Z, Du F (2015) Catalysts 5:1897
93. Rao BS, Kumari PK, Lakshmi DD, Lingaiah N (2017) Mol Catal 427:80
94. Rao BS, Kumari PK, Lakshmi DD, Lingaiah N (2018) Catal Today 309:269
95. Horvath T, Mehdi H, Fabos V, Boda L, Mika LT (2008) Green Chem 10:238
96. Wettstein SG, Alonso DM, Chong Y, Dumesic JA (2012) Energy Environ Sci 5:8199
97. Yan K, Yang Y, Chai J, Lu Y (2015) Appl Catal B Environ 179:292
98. Bond JQ, Alonso DM, Wang D, West RM, Dumesic JA (2010) Science 327:1110
99. Gilkey MJ, Xu B (2016) ACS Catal 6:1420
100. Osatiashtiani A, Lee AF, Wilson K (2017) J Chem Technol Biotechnol 92:1125
101. Bui L, Luo H, Gunther WR, Roman-Leshkov Y (2013) Angew Chem Int Ed 52:8022
102. Zhu S, Xue Y, Guo J, Cen Y, Wang J, Fan W (2016) ACS Catal 6:2035
103. Winoto HP, Ahn BS, Jae J (2016) J Ind Eng Chem 40:62
104. Meleroa JA, Moralesa G, Iglesiasa J, Paniaguaa M, Lopez-Aguado C, Wilson K, Osatiashtiani A (2017) Green Chem 19:5114
105. Melero JA, Morales G, Iglesias J, Paniagua M, Lopez-Aguado C (2018) Ind Eng Chem Res 57:11592
106. Rao BS, Kumari PK, Koley P, Tardio J, Lingaiah N (2019) Mol Catal 466:52
107. Alonso DM, Bond JQ, Dumesic JA (2010) Green Chem. 12:1493

Catalytic Conversion of Biomass-Derived Glycerol to Value-Added Chemicals

Check for updates

Kushanava Bhaduri ⓘ**, Anindya Ghosh, and Biswajit Chowdhury** ⓘ

Abstract In the scenario of fossil fuel depletion, the promotion of renewable energy like biodiesel has intensified research. Due to this, another significant challenge has emerged which is to deal with the surplus by-product glycerol. In order to address the issue, production of value-added chemicals from glycerol is an efficient alternative pathway. Thus the renewability, bioavailability and exclusive structure of glycerol make it an appropriately attractive starting material for producing a broad number of crucial chemicals. Here in this chapter, we have reviewed the catalytic conversion of glycerol in terms of oxidation, dehydration, carbonylation, esterification and acetalization and kept our focus on products like acrylic acid, acrolein, glycerol carbonate, glycerol acetins and solketal, respectively. Recent studies regarding catalysts, reaction parameters and plausible pathways are discussed in detail.

Keywords Glycerol · Acrylic acid · Glycerol oxidation · Glycerol dehydration · Glycerol carbonylation

1 Introduction

1.1 Biomass and Biomass Conversion

In the twenty-first century, the increasing energy demand, depleting fossil fuels and abnormal change of climate are the huge obstacle faced by humankind. The whole world mainly depends on one single source, that is, non-renewable fossil carbon, which fulfilled the global need of chemicals, fuels and daily commodities for maintaining a living standard of seven billion people. So, it is quite obvious fate that excessive combustion of fossil carbon and its derivatives is the major reason for the upsurge in the atmospheric greenhouse gas levels and hence causing global

K. Bhaduri · A. Ghosh · B. Chowdhury (✉)
Department of Chemistry, Indian Institute of Technology (ISM), Dhanbad, Dhanbad, Jharkhand, India
e-mail: biswajit72@iitism.ac.in

warming [1]. Renewable energy sources as an alternative to contemporary fossil fuels are the most encouraging solutions for moving towards a more sustainable future for humankind. The biomass valorization, which is an abundant non-fossil carbon source, has significantly attracted a lot of scrutinies as it possesses the ability to provide vast range of value-added chemicals and high-energy-density fuels. Right after crude oil, coal and natural gas, biomass is the largest source of energy which has been used to produce heat and power. Researchers are expecting that within two decades, worldwide demand of petroleum will increase by over 30% [2]. So the centre of interest is shifted to find an alternative, multiple and more flexible, less greenhouse-emitting energy backbone for a long-term solution not only to fulfil the demand but also to substitute the petroleum feedstock. In this context hydrogen, solar and biomass energy are the promising sources to replace petroleum reserves. The future success of these newborn technologies fully depends on the understanding of process implementation and chemical mechanism at the fundamental level. Among similar preferred sources, biomass is an abundant and the cost-effective carbon source which has the potential to produce liquid hydrocarbon fuel and provides huge amount of renewable feedstock without production of higher amount of greenhouse gases through subsequent regrowth of biomass [3]. They can be easily processed and incorporated without disturbing the existing infrastructure to the transportation and the internal combustion engine [4]. Despite all other complexity, researchers are trying to produce biodiesel and chemicals from biomass as it has several advantages including engine performance, price, non-toxicity, biodegradability and biocompatibility. Hence competent valorization of biomass is not only helpful to produce advantageous fuels and chemicals but also helps to reduce net emission of CO_2. Therefore, the share of biofuel is predicted to reach at about 9% in the transport sector by 2030 [4]. The application of naturally abundant biomass feedstock for the production of chemicals can boost the foundation of green chemistry within the context of sustainability. Renewable energy origins like solar, geothermal, wind and biomass are acknowledged to be feasible surrogates to traditional oil [5]. However, the energy sourced from biomass is recognized to have more sustainability specially for the transportation category. Biofuel is the common name of fuel generated from biomass. Among the various biofuels, biodiesel is the subject of the most researches, and it is still in momentum despite all the rigorous developments. The immense interest of various researches, industrialists and governments throughout the world may be attributed to the fundamental advantages of it. The main reasons are its biodegradability, non-toxicity, renewability, inbuilt oxygen content, higher cetane number, higher combustion with regulated emissions, full carbon cycle and raw material availability [6, 7]. Biodiesel is the mono alkyl ester of fatty acids retrieved from animal fat or vegetable oil by the transesterification or esterification with alcohol in the existence of a catalyst (Scheme 1).

From the forecast of the International Energy Agency (IEA), the maximal oil production of the world will be achieved between 1996 and 2035. According to some experts, current oil may totally diminish by 2050. According to the European
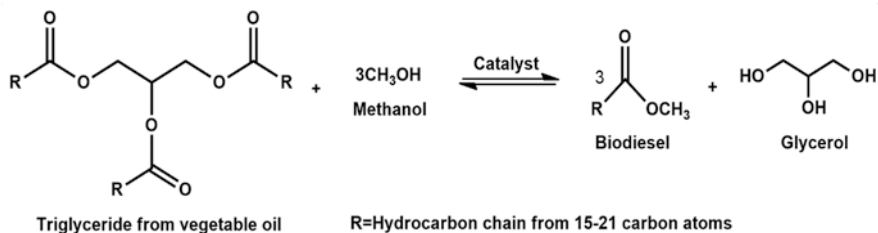
Scheme 1 Conversion scheme of triglyceride to biodiesel and glycerol
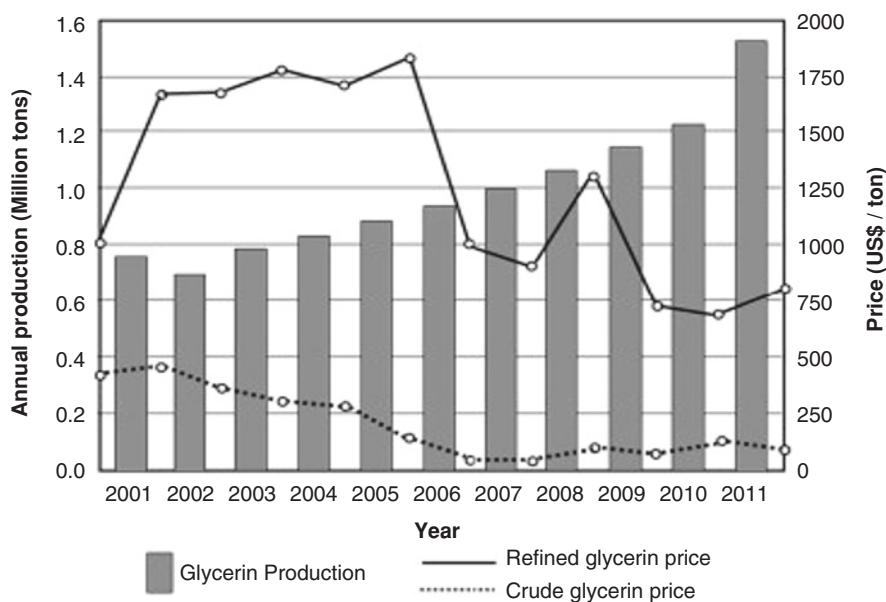
Fig. 1 Global glycerol production and prices (Reproduced with permission from ref. [8], © Elsevier (2013))

Union (EU) directive, conventional fuels must add at least 5.75% biofuels by 2010, with a possible increment of 20% by 2020. Production of biodiesel in EU representative countries was estimated at 1.93 in 2004 and 10.37 in 2013 and surging up to 11.58 in 2016 (Fig. 1). The biodiesel production in the United States upsurged from 250 million gallons in the year 2006 to 2.89 billion gallons in 2016 [8, 9, 10]. All the efforts have been put worldwide to boost energy efficiency and cut down greenhouse gas emissions. The high biodiesel production is accompanied by large-scale volumes of waste, in which glycerol is the major one. For every 100 kg of biodiesel production, 10 kg of glycerol is generated [10].

1.2   Glycerol as Biomass: Current Availability and Market

The applications of glycerol can be found back to the initial civilized society of humans where vegetable oil and animal fat hydrolysis were done in alkaline medium to manufacture soap [11]. At the time of World War I, glycerol usage was on a high, overpassing the soap-making industry for nitroglycerin production which is a base for preparing dynamite and cordite [12].

During World War II, production of glycerol feedstock has moved to petroleum-based origins. The annual production of glycerol globally reached around 1.6 million metric tons which is expected to triple by 2024 [11]. The upsurge in the production of glycerol in the last decade is largely due to the boom in biofuel production sector. Biodiesel is nothing but the fatty acid esters, obtained from vegetable oils or animal lipids by transesterification with methanol or ethanol [13, 14]. Generally, glycerol is obtained as main by-product during biodiesel production, and approximately 10 wt% glycerol is produced from the total production of biodiesel. The United States and the European nations have both decided that they will supply 1.3 billion and 17.4 million tons of biomass per annum [2, 3]. According to a report published in 'Roadmap for Biomass Technologies', 20% of transportation oil will come from biomass by 2030 [3]. As a consequence, biodiesel progress would be suffered by the overabundance of glycerol in the market, which also effects on its commercial value. However, the high price of starting materials, low oxidation stability and poorer cold flow properties hinder its commercialization improvement [4].

1.3   Various Ways of Glycerol Conversion

The usage of glycerol for the production of value-added chemicals is very important from an industrial point of view as not only glycerol formation occurs in large amounts amid biodiesel formation but also glycerol being non-toxic, biodegradable and biosustainable chemical. Nowadays the lower worth of glycerol can project towards advanced markets in fine chemicals, polymers, biofuel additives, etc. The multifunctional properties of glycerol can be tuned by various different reaction routes. It is very obvious that a hefty number of valuable chemicals can be produced from glycerol. In this chapter we have discussed about the most important catalytic conversion processes to transform glycerol into valuable chemicals.

Glycerol conversion can be done via various different methodologies like oxidation, dehydration, hydrogenolysis, carbonylation, esterification, etherification, acetalization, reforming, etc. The oxygenated products derived from glycerol mainly include glyceric acid, acrylic acid, dihydroxyacetone, tartronic acid, hydroxypyruvic acid, etc. The dehydration of glycerol results in the main product acrolein followed by some other by-products like hydroxyacetone, acetol, 3-hydroxypropanal, etc. The hydrogenolysis of glycerol results in the formation of 1,2 propylene glycol, 1,3 propylene glycol and ethylene glycol. The carbonylation of glycerol has many

pathways like reacting glycerol with carbon dioxide, reacting with urea and reacting with di-alkyl carbonate which is also the transesterification pathway, all leading to glycerol carbonate formation. The esterification of glycerol yields monoacetin, diacetin and triacetin which mainly act as biofuel additives. The etherification of glycerol results in glycerol monoethers, diethers and triethers. In the glycerol acetalization reaction, it is reacted with ketones and/or aldehyde to achieve products like glycerol solketal and acetal. The reforming of glycerol results in hydrogen formation. In this chapter we have discussed glycerol oxidation, dehydration, carbonylation, esterification and acetalization and mainly kept our focus on products like acrylic acid, acrolein, glycerol carbonate, glycerol esters and solketal (Scheme 2).

2 Catalytic Oxidation of Glycerol

Vigorous attempts have been made to take advantage of glycerol as an alternative fuel. On the other hand, glycerol, as a sustainable feedstock, can be employed for generation of some C_3 derivatives as glycerol oxidation products including glyceraldehydes, glyceric acid, 1,3-dihydroxyacetone, hydroxypyruvic acid,
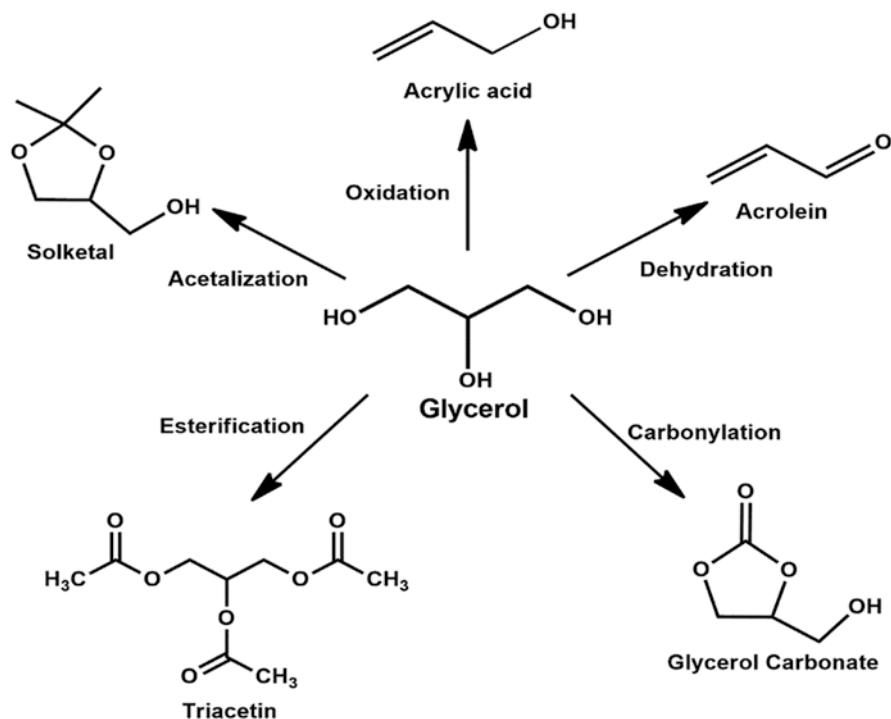
Scheme 2 Glycerol to important value-added products

pyruvaldehyde, pyruvic acid, lactic acid, acrylic acid, tartronic acid and mesoxalic acid [15–18]. Usual glycerol oxidation typically initiates with two types of reactions: dehydration (i.e. cleavages of C-H and C-O bonds) succeeded by additional dehydrogenation and oxidation (i.e. formation of C-H and C-O bonds) and dehydrogenation (i.e. cleavages of C-H and O-H bonds). The pathway of C-O bond cleavage differentiates the initial dehydration and dehydrogenation. The C-O bond cleavage requires reaction temperature 300–400 °C for dehydration [19, 20] and <100 °C for dehydrogenation [21, 22].

2.1 Glycerol Oxidation via Dehydration

In an economic viewpoint, glycerol conversion via dehydration becomes more attractive since more than 60% oxygen content of glycerol can be simply removed without hydrogen consumption under mild condition [23]. The existence of primary and secondary hydroxyl groups with different reactivity induces the selectivity problems in glycerol conversion. Commercial oxidation processes of glycerol using hydrogen peroxide as an oxidant produce dihydroxyacetone and glycerol aldehyde [24, 25] as an intermediate for serine and glyceric acid [26, 27] in liquid phase. To conquer the reactivity/selectivity problem, it is better to synthesize glycerol derivatives, e.g. esters or acetals, which allow the subsequent oxidation of a particular type of carbon atom only [28].

Acrylic acid, the simplest unsaturated carboxylic acid, is a monomer for polyacrylic acid which is widely used for production of hygiene products like diaper, elastomers, plastics, paints, adhesives and coatings [29]. Using biomass resources like glycerol for production of acrylic acid (via gas phase or liquid phase) has been extensively investigated. A wide category of solid acid catalysts, such as zeolites, metal oxides, phosphates and heteropolyacids, have been extensively evaluated for glycerol dehydration [30]. Those acid catalysts failed to meet the industry demands since they suffered from heavy coke deposition leading to fast deactivation.

2.2 Glycerol Oxidation into Acrylic Acid via Allyl Alcohol as an Intermediate

Recently, some reports claimed that acrylic acid can be prepared from glycerol via two steps: deoxydehydration (DODH) of glycerol to allyl alcohol followed by selective oxidation of obtained allyl alcohol into acrylic acid. Recently, Lee's group reported that a high yield of ~87% of acrylic acid can be synthesized from glycerol by using Au-deposited CeO_2 [31, 32]. They studied the effects of different morphologies of CeO_2 (like rods, cubes and octahedra) as support as well as the particle size of the Au as active phase. The liquid phase DODH of glycerol is carried out
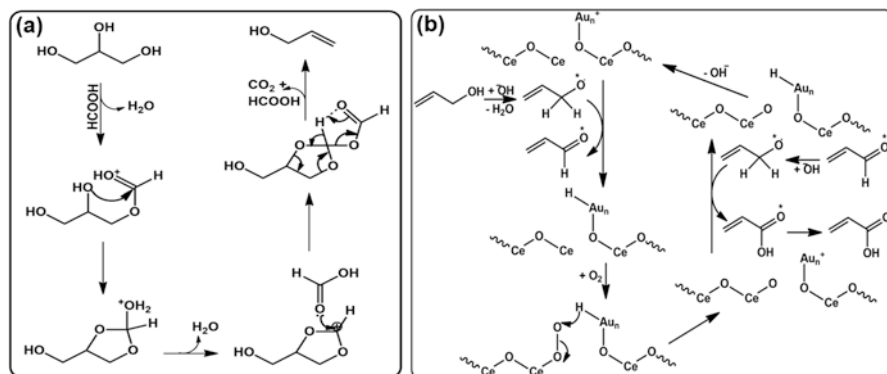
Scheme 3 Mechanism for the DODH of glycerol to allyl alcohol in formic acid medium (**a**). Catalytic oxidation mechanism for acrylic acid from allyl alcohol over Au/CeO$_2$ (**b**) proposed by Yang et al. [32]

using formic acid as the hydrogen donor and the catalyst, shown in Scheme 3a. Among Cu-, Au-, Pd- and Pt-deposited CeO$_2$ supports, only Au catalyst is very active in the allyl alcohol oxidation to form acrylic acid at 25 °C. Au/CeO$_2$-octahedral, among different shapes of CeO$_2$ such as cubic, rod, octahedral and commercial, exhibited the highest yield towards acrylic acid due to its highest BET surface area (110 m^2/g), lowest size of Au (2.2 nm), highest oxygen storage capacity (OSC) and highest amount of oxidic Au species. They suggest that both oxidic as well as metallic Au are responsible for the selective oxidation of allyl alcohol via the formation of acrolein as an intermediate and as shown in Scheme 3b a basic medium is essential for the formation of acrylic acid.

The different reaction parameters such as reaction temperature, allyl alcohol concentration and oxygen pressure also affect the selective oxidation of allyl alcohol into acrylic acid. With increase in the oxygen pressure up to 10 bar, the production of acrylic acid significantly increases by suppressing the yield for 3-hydroxypropionic acid (3-HPA). The higher reaction temperature can also accelerate the production of 3-HPA and glyceric acid, whereas at lower temperature, more allyl alcohol is selectively oxidized into acrylic acid. General selective oxidation desires dilute reactant solution. With increase in the concentration of allyl alcohol, the production of the dimers and hydrated species increases.

2.3 Glycerol Oxidation into Acrylic Acid via Acrolein as an Intermediate

The two-step tandem reaction is the best known way for the production of acrylic acid from glycerol. Over an acid catalyst, glycerol dehydrated into acrolein which is followed by the oxidation of obtained acrolein into acrylic acid. Andrushkevich
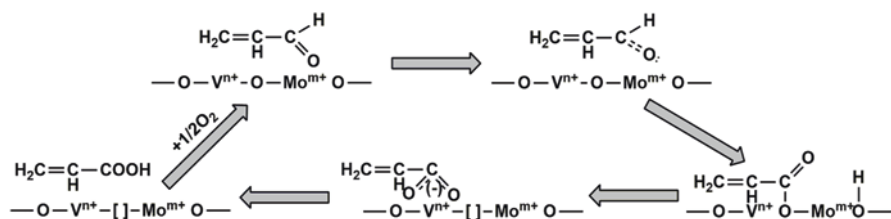
Scheme 4 Catalytic oxidation mechanism for the conversion of acrolein to acrylic acid using Mo-V oxide catalyst proposed by Andrushkevich [34]

investigated the three efficient catalysts, Mo-V catalyst, Mo-Co oxide catalyst and V-W system for conversion of acrolein to form acrylic acid [33]. It is revealed that the efficient catalyst must have the presence of ions with amphoteric features such as Mo^{4+} and V^{4+} and the existence of Mo^{6+} ions. The catalytic oxidation mechanism for the conversion of acrolein to acrylic acid is proposed in Scheme 4. Martins' group have also studied the performance of Mo-V mixed oxides in the catalytic oxidation of glycerol to acrylic acid at different heat-treated conditions [35]. They found that the Mo-V mixed oxides showed superior activity, compared to the pure MoO_3 and V_2O_5 oxides. The Mo-V mixed oxides were heat-treated under different gas-flow compositions (100% N_2, 20% O_2 in N_2 and 100% O_2). The Mo-V mixed oxide, heat-treated under 100% N_2 and 20% O_2, showed similar selectivity for acrylic acid, as the pure oxides, while the catalyst, heat-treated under 100% O_2, gave better selectivity of 33.5% towards acrylic acid. Zhang's group have also executed an efficient process for the production of acrylic acid from glycerol with 10% O_2/He via gas phase catalytic oxidation at atmospheric pressure using Mo-V-W-O catalyst at a temperature range 300–400 °C [34]. The V^{4+}/V^{5+} species may be responsible for the redox cycle in the MoVW oxide and high selectivity of acrolein, whereas addition of Mo stabilized valence states of V and incorporation of W improved stability of the catalyst and enhanced selectivity for acrylic acid. Acrylic acid, the key intermediate to acrylic acid, rapidly oxidized with increase in temperature up to 340 °C, reaching 87% selectivity for acrylic acid. In contrast, further rise in temperature decreased the selectivity for acrylic acid because of over-oxidation, by increasing the amount of CO, CO_2 and acetic acid.

2.4 Glycerol Oxidation into Acrylic Acid via Propylene as an Intermediate

The production of acrylic acid from glycerol via propylene as the intermediate is also a promising path. Glycerol can be converted into propylene using a stacked catalyst of HZSM-5 (at the bottom layer) and Ir/ZrO₂ (at the top layer) and gained 85% of yield for propylene under 30 bar H_2 pressure at 250 °C [36]. High pressure
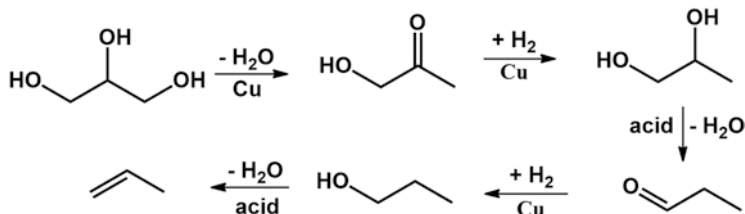
Scheme 5 Route for the hydrogenolysis of glycerol to propylene
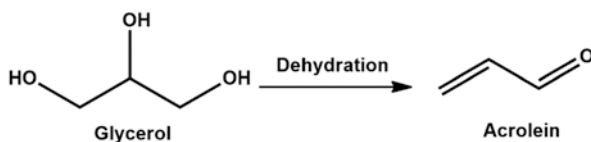
Scheme 6 Dehydration of glycerol to acrolein

of H_2 increases glycerol conversion, while the selectivity for propylene decreases because of again hydrogenation of obtained propylene into propane. Sato et al. studied the hydrogenolysis of glycerol into propylene over WO_3 modified Cu/Al_2O_3 under ambient H_2 pressure [37]. Further addition of SiO_2-Al_2O_3 under the catalyst bed of WO_3-Cu/Al_2O_3 converts the 1-propanol to obtain 84.8% of selectivity for propylene with full conversion. The multistep formation of propylene via dehydration and hydrogenation over the stacked catalyst is shown in Scheme 5.

3 Catalytic Dehydration of Glycerol

Acrolein which is produced from the dehydration of glycerol is one of the most valuated chemicals derived from glycerol valorization (Scheme 6). Acrolein is one of the simplest unsaturated aldehydes which is also known as acrylic aldehyde or 2-propenal. It is used for the manufacturing of acrylic acid, 1,3 propanediol, pyridines, glutaraldehyde, superabsorbent polymers, fragrances, flavours, etc. which have compelling part in food and chemical industry. Acrolein at present is produced via selective oxidation of propylene, while at the same time, glycerol dehydration for acrolein production has also been investigated extensively. Production of acrolein by gas phase dehydration of glycerol can be dated long back ago in 1933 by Schering-Kahlbaum AG [38]. They patented the gas phase glycerol dehydration at 573–873 K with around 80 mol.% yield for acrolein. However, in the past high glycerol cost forced the process to remain undeveloped until the last two decades ago when glycerol started to become cheaper as biodiesel production was surging.

3.1 Efficient Catalyst Systems for Gas Phase Glycerol Dehydration to Acrolein

Various types of catalyst systems have been widely reported for the glycerol dehydration reaction like heteropolyacids, zeolites, metal oxides and phosphate catalysts. The catalytic performance of some reported catalysts for the dehydration reaction of glycerol to acrolein is summarized in Table 1. To catalyse dehydration of glycerol to form acrolein, the use of heteropolyacids is a very good option. Among widely used common HPA catalysts is the tungstophosphoric acid. Chai et al. used zirconia-supported HPA catalysts for glycerol dehydration to acrolein [57, 59]. The results obtained by them showed zirconia-supported HPA is more effective than silica-supported HPA.

Katryniok et al. explored glycerol dehydration to acrolein over silicotungstic acid supported on zirconia-grafted SBA-15 [74]. The interaction between the support and HPA was modified by the grafting. The synergy between the zirconia and HPA eventually reduced the strength of Brønsted acidic site and thus increased catalyst stability. An acrolein yield of 69% could be seen after 24 h time on stream study. Dubois et al. scrutinized metal-substituted silicotungstic (SiW) and phosphotungstic (PW) acid salts [75]. Among the various metals used for substitution are calcium (Ca), rubidium (Rb), caesium (Cs), bismuth (Bi), zirconium (Zr), iron (Fe) and lanthanum (La). The caesium-substituted $Cs_{2.5}H_{1.5}SiW_{12}O_{40}$ catalyst exhibited the highest acrolein yield of 93%. Another important aspect demonstrated by the authors was the oxygen co-feed in the reaction which helped to increase the acrolein yield. The study performed by Alhanash et al. which also included caesium salts of PW acids achieved an acrolein yield of around 98%, but its longevity was small [76]. Atia et al. [62] prepared an array of supported silicotungstic acid from selected silica and aluminosilicate supports. Alkaline metals were used to adjust the Brønsted acidic sites. It was found that the unmodified supported HSiW catalysts displayed the highest activity which was the indication about the strong connection of activity with acidity (Brønsted). Kim et al. [77] explored dehydration of glycerol to acrolein with silicotungstic acid (HSiW) using various different metal oxides (SiO_2, TiO_2, ZrO_2, γ-Al_2O_3, CeO_2, MgO, etc.) as supports. The use of zirconia-supported HSiW resulted in highest selectivity of 58.1% for acrolein. All the studies on heteropolyacids proved them as potential candidates for glycerol dehydration reactions. Fast deactivation was one drawback of this catalyst.

Zeolites are also largely reported for glycerol dehydration reaction. Two well-acknowledged zeolite segment catalysts (β-zeolite and ZSM-5) were patented by Dubois et al. for glycerol dehydration [78]. β-Zeolite and HZSM-5 exhibited 57% and 39% acrolein yield, respectively. Zuang et al. used MCM-based and ZSM-based catalysts for glycerol dehydration and obtained 70–85% acrolein yield [79]. In another patent by Okuno and co-workers [80], various metallo-silicate catalysts with MFI structure were used for this reaction which actually reached up to 63% acrolein yield. Zhou et al. [81] synthesized micro- and mesoporous ZSM-5 catalyst in a dual template method which gave highest acrolein yield of 73.6%. In another

Table 1 Performance of some catalysts for glycerol dehydration to acrolein as reported in literature

Catalyst	Temperature (°C)	TOS (h)	Total flow (ml)	Catalyst amt. (g)	Conversion (%)	Selectivity (%)	Reference
NbWAI	305	3	15	0.8	100	72	[39]
NbWZr	305	3	15	0.8	100	72.1	[40]
Ta_2O_5	315	9–10	30	0.82	39	75	[41]
Nb/SiZr5	325	2	15	0.5	77	45	[42]
ZrNbO	300	8	75	7.5	88	60	[43]
ZrSiWO-2.5	300	8	75	6.96	100	63	[44]
WO_3/ZrSi	325	2	15	0.5	99	42	[45]
VPO/ZrP	300	1–2	16	0.2	100	60	[46]
VPO	320	2	30	0.5	100	70	[47]
WO_3/ZrP	300	10	10	0.2	100	82	[48]
Nano-ZSM5	320	10	–	0.5	91	83	[49]
MCM-22	320	2	30	0.1	99.8	50.1	[50]
ZrNbP0.2	325	2	15	0.5	100	56	[51]
mSAPO-40	320	2.5	30	0.3	100	80	[52]
1-Fe/AlPO4-450	280	10	75	0.1	100	40	[53]
SAPO-40	350	2.5	30	0.3	100	75	[54]
FeP-H	260	5	20	0.8	100	92	[55]
Al_2O_3-PO_4	280	1	100	0.2	100	42	[56]
30PWZ-AN-650	315	9–10	30	0.71	70	70	[57]
20wtPTA/Y--zeolite	275	3	10	0.3	100	79	[58]
10PWZ-AN-650	315	9–10	30	0.61	79	69	[59]
Cs-STA-1	300	5	100	–	66	87	[60]
Q6-SiW-30	325	5	–	0.3	100	74	[61]
Li/HSiW/AS5	300	2	30	0.3	99	73.4	[62]
HSiW/Al_2O_3	300	2	30	0.5	100	66	[63]
HSiW/ZrO_2	300	3	20	0.5	92	69	[64]
30HZ-20A	320	3	20	0.5	97	88	[65]
17-$NiSO_4$	340	10	20	1.0	90	70	[66]
M-Al_2O_3	280	2	–	0.5	80	74	[67]
Sepiolite	320	3	20	0.2	92	59	[68]
WO_3/ZrO_2@SiC	250	10	30	14.0	100	71	[69]
SBA-SO_3H	300	3	30	0.3	100	92	[70]
H-ZSM-5(75)	320	10	15	0.15	81	86	[71]
SZ11-2	300	2	30	0.1	95	60	[72]
Nano-MFI-Zeolite	320	12	20	0.25	99	86	[73]

interesting study, Kim et al. [82] prepared various H-zeolites which include H-ferrierite, H-Y, H-β, HZSM-5 and H-mordenite with different Si and Al ratios. Among these H-ferrierite showed highest selectivity for acrolein of 77% at favourable conditions. For this catalyst the selectivity of acrolein has a monotonal increase with increase in reaction temperatures. On the other side, the conversion of glycerol is seen to increase while having longer contact time, but acrolein selectivity is found to decrease gradually. In an interesting study by Possato et al. [83], they have tried to escalate the conversion of glycerol by applying the desilication methodology where they have tried to minimize diffusion limitations by secondary pore formation in zeolite catalysts. They observed increase in conversion of glycerol due to the weakened surface acidity and an increase in accessibility of the active sites by glycerol. Longer catalyst stability and very few blocked micropores are the main convenience in this method. Qureshi et al. [71] synthesized nano-H-ZSM-5 catalyst with short channels. The Si and Al ratio is varied, and the catalyst with Si/Al = 75 showed the best results at 81% glycerol conversion with 86% of acrolein selectivity at 10 h time on stream at 320 °C temperature. Ding et al. [72] developed microstructured ZSM-11 catalyst by direct growth on sinter-locked stainless steel microfibres. It exhibited very good reactivity and stability over other reported zeolites. It reached up to a glycerol conversion of 95% with 60% selectivity towards acrolein. The formation of coke was suppressed due to enhanced diffusion through zeolite pores at high flow of carrier gas. Also a new nanosheet MFI zeolite with different Si/Al molar ratio was prepared, and it could achieve a glycerol conversion of 99% with 86.6% acrolein selectivity for 12 h TOS [73].

Various types of mixed oxides, metal pyrophosphates and phosphates are also extensively used in glycerol dehydration into acrolein. Chai et al. [84] used Nb_2O_5 catalyst for glycerol dehydration reaction at 315 °C where effect of different calcination temperatures, acidity, catalyst structure and crystal structure was studied. Glycerol conversion of 88% with 51 mol.% selectivity for acrolein was observed. Suprun et al. [56] explored gas phase glycerol dehydration over aluminium phosphate ($AlPO_4$), titanium phosphate ($TiPO_4$) and silica-alumina phosphates (e.g. SAPO-11 and SAPO-34). The glycerol conversion was found to be dependent on the acidity and textural characteristics of the catalyst. The catalyst SAPO-34 could achieve 59% conversion of glycerol with 72% acrolein selectivity, but its drawback was fast deactivation. Wang et al. [85] probed different types of vanadium phosphate catalysts where various reaction parameters could be varied to ultimately achieve 66% acrolein selectivity at complete conversion of glycerol. The oxygen flow in the reaction ended up giving good results. In another study on vanadium pyrophosphate oxides, Wang et al. did some temperature study on the catalysts and found out that morphology, crystallinity and acidity changed with it. The catalyst treated at temperature 1073 K exhibited 64% selectivity for acrolein at 100% glycerol conversion. Deleplanque et al. [55] synthesized iron phosphates in hydrothermal methods which could obtain an acrolein yield of 92%, and the catalyst showed activity up to 25 h. Dubois [86] performed glycerol dehydration on potassium (K)-, strontium (Sr)- and caesium (Cs)-doped phosphate catalyst, where Cs-catalyst obtained 72% acrolein yield. In a different study by Lauriol-Garbey et al. [43], they

synthesized different niobium-zirconium mixed oxide catalysts for this reaction. They investigated the relation between acidity-basicity and the catalytic activity. Niobium oxide supported on zirconia proved to be the best one with 98% conversion of glycerol and 72% selectivity for acrolein. Again in another research by Lauriol-Garbey and their co-workers, studied the effect of SiO_2 doping on WO_3/ZrO_2 catalyst for glycerol dehydration at 573 K [44]. From different characterization techniques, it was revealed that modification with silica formed large mesopores limiting the production of undesirable coke. The catalyst exhibited 78% acrolein selectivity at total conversion of glycerol, and also it showed stable catalytic activity even after 100 h time on stream. WO_3/TiO_2 catalysts prepared by Ulgen and Hoelderich [87] achieved around 85% selectivity towards acrolein at almost total glycerol conversion. They observed that using oxygen could inhibit formation of by-products. Due to gradual deactivation rate and being inexpensive, titania-supported tungsten oxide is a good catalyst for glycerol dehydration. Cavani et al. [88] synthesized sulphated zirconia catalyst for this reaction and also used co-feeding of oxygen. They could achieve 49% glycerol conversion with 42% selectivity towards acrolein. Liu et al. [89] prepared Cr-, Cu- and La-modified aluminium phosphate (AlPO) catalysts for dehydration at 443 K in gas phase. The meso-LaCuCrAlPO catalyst showed very good catalytic activity results of 80% selectivity towards acrolein with 99% glycerol conversion at 613 K. Massa et al. [40] synthesized monoclinic zirconia-supported niobium and tungsten oxide for this reaction. The tungsten oxide supported zirconia showed 78% yield for acrolein at 100% conversion for glycerol. Though oxygen flow decreased the deactivation rate a little, it had no serious effect on acrolein yield. Gu et al. [66] prepared different supported nickel sulphate catalysts for gas phase glycerol dehydration where $17NiSO_4$–623 catalyst achieved up to 70 mol.% selectivity for acrolein with more than 90% conversion of glycerol during 10 h time on stream. Also in this case, oxygen co-feed did not help to improve acrolein yield, but it could reduce the catalyst deactivation. Tao et al. [41] scrutinized the activity of tantalum oxide (Ta_2O_5) catalyst prepared in different calcination temperatures for glycerol dehydration. Acrolein selectivity of 75% was obtained at 40% glycerol conversion using Ta_2O_5–350 at 623 K temperature. The catalyst showed excellent long-life stability even after 100 h time on stream. Apart from the above heteropolyacids, zeolites, metal oxides and phosphates, recently some interesting catalyst systems have been reported for glycerol dehydration to acrolein. Huang et al. [67] synthesized a metal-organic framework-mediated alumina catalyst and tested for glycerol dehydration reaction. The M-Al_2O_3 catalyst achieved a conversion of about 80% with nearly 74% acrolein selectivity for a long 200 h time on stream. Zhou et al. [68] synthesized acid-activated sepiolite catalyst for glycerol dehydration reaction and achieved an acrolein yield of 52% at 320 °C. In a different and new investigation, Xie et al. prepared microwave-absorbing catalyst WO_3/ZrO_2@SiC and performed microwave-assisted catalytic dehydration of glycerol. The acrolein selectivity could reach over 70% with complete glycerol conversion at 250 °C with microwave heating [69].

3.2   *Liquid Phase Dehydration of Glycerol to Acrolein*

In some recent years, supercritical water reforming of glycerol has gained much consideration for producing valued chemicals like acrolein. Ott et al. [90] assessed the effect of zinc sulphate (Zn-SO$_4$) catalyst in supercritical water condition and in continuous high-pressure tubular reactor. At 25 MPa pressure and 633 K reaction temperature, 50% glycerol conversion could be achieved with 75 mol.% selectivity towards acrolein. Liquid phase dehydration of glycerol was investigated at elevated temperature and atmospheric pressure by Suzuki et al. [91] and Yoshimi et al. [92] where they used potassium bisulphate (KHSO$_4$), magnesium sulphate (MgSO$_4$) and phosphorus alumina (5 wt% H$_3$PO$_4$/Al$_2$O$_3$) as catalysts. KHSO$_4$ achieved 80% acrolein yield with 97% conversion of glycerol. Shen et al. [93] performed liquid phase glycerol dehydration to acrolein in semi-batch reactor using silicotungstic, phosphotungstic and phosphomolybdic acids. The best yield for acrolein (78.6%) was obtained over silicotungstic acid catalysts. In another study by Shen et al. [94], they prepared Brønsted acidic ionic liquid (BAIL) catalysts for liquid phase glycerol dehydration. An acrolein yield of 57.4% with complete conversion of glycerol could be achieved. The acidity of the catalyst was the main reason for its activity. The above are some worthy mentions for liquid phase glycerol dehydration, but it is quite evident that liquid phase glycerol dehydration is not as effective like gas phase glycerol dehydration.

3.3   *Reaction Mechanism*

From Scheme 7, the glycerol dehydration mechanism can be seen on Lewis and Brønsted acidic sites which leads to formation of acrolein and acetol, respectively, as suggested by Alhanash et al. [76]. For the Brønsted acidic sites, the dehydration begins with the secondary hydroxyl group protonation of glycerol and the release of the H$_3$O$^+$ by the secondary intermediate to form 1,3-dihydroxypropane, and then keto-enol rearrangement gives 3-hydroxypropionaldehyde, which finally generates acrolein followed by a further dehydration. On the other case, over Lewis acidic sites, the generation of an intermediate 2,3-dihydroxypropane takes place by the concerted deportation of the terminal OH group of glycerol to the Lewis acidic site, and the H$^+$ shifts from the internal carbon atom to the bridging 'O'-atom. After that the final acetol is formed by further tautomerization of 2,3-dihydroxypropene. The proposed mechanism by Alhanash et al. is supported by the study performed by Foo et al. [95] in which they did glycerol dehydration over Nb$_2$O$_5$ along with DFT calculations. They also came to the same conclusion that acrolein formation is favoured by Brønsted acid sites and acetol formation is favoured by Lewis acid sites. The glycerol dehydration study investigated by Wang et al. [96] suggested that there is a cooperation between the Brønsted and Lewis acid sites.
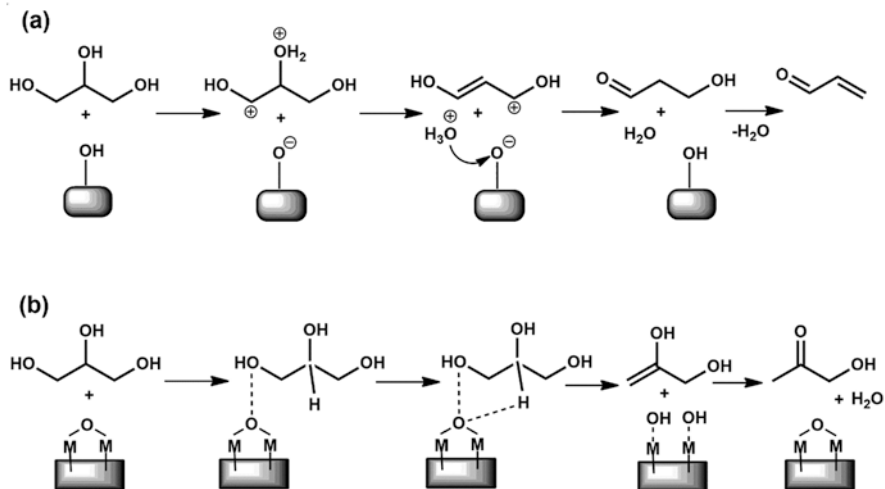
Scheme 7 The reaction mechanism for dehydration of glycerol over (**a**) Brønsted acid sites and (**b**) Lewis acid sites as suggested by Alhanash et al. [76]

3.4 Effects of Physicochemical Properties of the Catalyst on Acrolein Yield

The two main properties of the catalyst which significantly affect glycerol dehydration to acrolein are the acidic property and the textural property. The general consideration is that Brønsted acidic sites facilitate acrolein formation. Chai et al. [97] studied an array of catalysts with different acid strengths for the glycerol dehydration reaction. According to their observation, catalysts with very strong acid sites achieved lower acrolein yields (40–50%) due to severe deposition of coke, while catalysts with strong acid sites found to be most effective in terms of acrolein yield (60–70%). On the other hand, catalysts having moderate or weak acid sites could attain low acrolein yield due to their low selectivity (30%). This simply indicates that catalysts with very strong acidity lead to serious deposition of coke. The textural properties of the catalyst are also associated with formation of coke which eventually leads to deactivation. In an investigation by Sato's group, they prepared heteropolyacid supported on SiO_2 with different pore sizes of 3, 6, and 10 nm [61]. It was observed that the catalyst with largest pore size demonstrated durable catalytic performance, whereas the silica with small pore size results in fast deactivation. The observation was supported by Atia et al. [23] where they did the same type of study with Al_2O_3-supported heteropolyacids. It was concluded that open and interconnected mesopores in catalyst are more stable than closed and small mesopores which tend to deactivate early due to the heavy production and transfer limitations of coke formed in the pores.

## 3.5	Methods for Inhibiting Catalyst Deactivation

Although high yield of acrolein has been achieved over a large number of catalyst systems, deactivation remains a serious problem for this reaction. The prime reason for deactivation mainly applies to the coke formation which is caused by glycerol/acrolein polycondensation. According to the investigation led by Chai et al. [98], the co-feed of O_2 with a molar ratio of $N_2/O_2 = 9/1$ effectively maintains the catalytic activity up to 10 h. On the other side, high concentration of O_2 feed results in formation of acetaldehyde, thus decreasing the acrolein yield. From various studies it can be found that the oxygen feed decreases the carbon species which are adsorbed and can be transformed to coke. On the other hand, high O_2 concentration escalates the selectivity towards oxidative decomposition products like acetic acid and acetaldehyde, so the true concentration of the O_2 feed is very decisive. The alteration of solid acid catalysts with the doping of precious metals can result in higher catalytic activity than unmodified catalysts. According to Ma et al. [99], Pd-doped $H_3PW_{12}O_{40}$/Zr-MCM-41 is more effective than doping with Pt. It is studied that doping with Pd escalates the Brønsted acidic sites and reduces the amount of Lewis acid sites which eventually contributes to the stable and selective production of acrolein from the dehydration of glycerol.

## 4	Catalytic Carbonylation of Glycerol

Glycerol carbonate (glycerine carbonate or 4-hydroxymethyl 2-oxo-1,3-dioxolane) has gained great interest over the last two decades owing to its versatile reactivity and as a way for waste glycerol valorization. The main uses of glycerol are as solvents, carrier in pharmaceutical preparations, carrier in lithium and lithium-ion batteries, solid laundry detergent compositions, building ecocomposites, polymers (hyperbranched polyethers, polycarbonates, polyurethanes, non-isocyanate polyurethanes), chemical intermediates and beauty and personal care. Glycerol carbonate is acknowledged as a green substitute for crucial petroderivative compounds like ethylene carbonate or propylene carbonate. Glycerol carbonate is synthesized by the reaction of glycerol using urea or dimethyl carbonate or by direct reaction with carbon dioxide which ultimately results in the chemical fixation of CO_2 in glycerol (Schemes 8, 9, 10, 11, and 12).

## 4.1	Glycerol Carbonate from Direct Carboxylation of Glycerol with CO_2

Direct carboxylation of glycerol with CO_2 seems the most superior process as this has the potential to transform two waste products into value-added chemical. Among the first catalysts to be reported for the direct carboxylation of glycerol with CO_2 are

Scheme 8 Synthesis of glycerol carbonate from glycerol by direct carboxylation with carbon dioxide
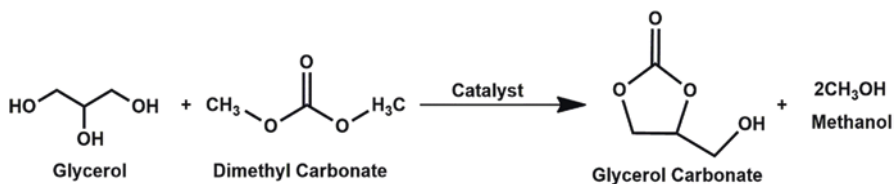
Scheme 9 Synthesis of glycerol carbonate from glycerol via transesterification with dimethyl carbonate.
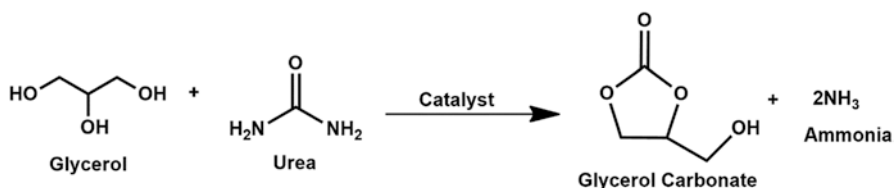
Scheme 10 Synthesis of glycerol carbonate from glycerol via glycerolysis of urea

the Sn-catalysts [100, 101]. Addition of methanol as an alcoholic solvent helped to improve the yield from 7% to 35%. The findings of thermodynamic estimations indicated that this reaction is thermodynamically limited, which also explains the reported low yields of the reaction. An alternate synthetic procedure was suggested by Ochoa-Gomez et al. Among the three steps in this procedure, first, CO_2 capture takes place which will act as carbonation source and then glycerol to 3-chloro-1,2 propanediol synthesis followed by converting it into glycerol carbonate with the carbonation source [102]. They also synthesized glycerol carbonate in another successive study where along with 3-chloro-1,2-propanediol and carbon dioxide, triethylamine was used both as solvent and CO_2 fixing and activating agent, where they could achieve glycerol carbonate yield of 90% [103]. Another work of direct carboxylation was reported by Aresta et al. [100, 104] where transition metal alkoxides (Sn-catalysts) were used. Among different Sn-based catalysts, n-Bu$_2$Sn(OMe)$_2$ was found to be superior in catalytic activity. All the above findings certainly indicate that there is still lot of room for modification to produce glycerol carbonate from glycerol and CO_2 more effectively and energy efficiently.
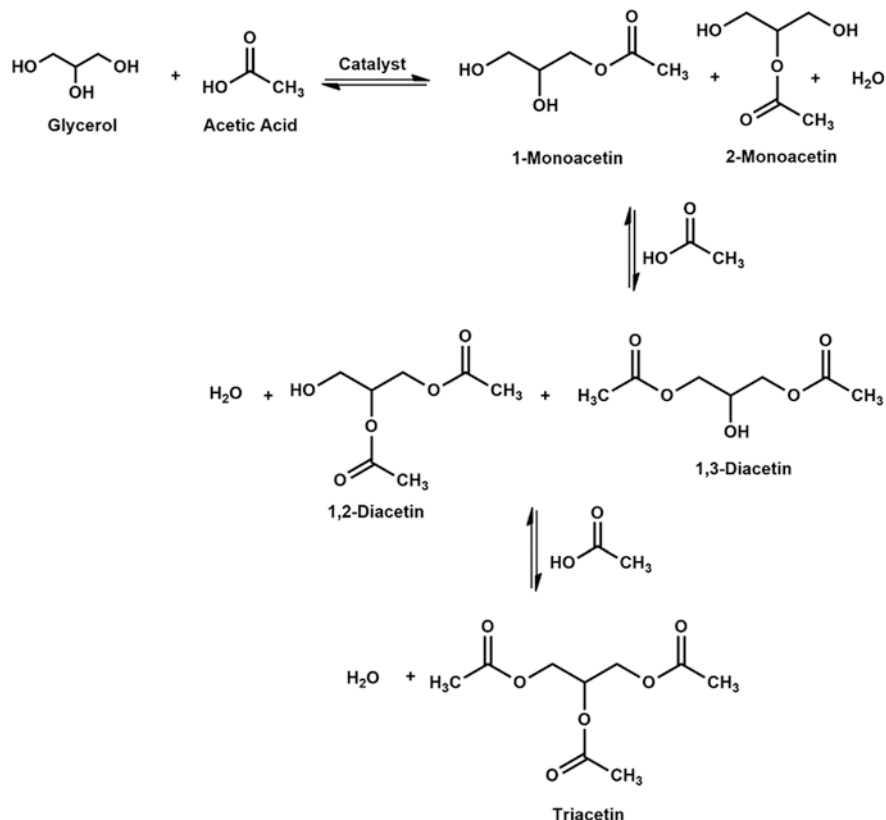
Scheme 11 Synthesis of acetin by esterification of glycerol with acetic acid
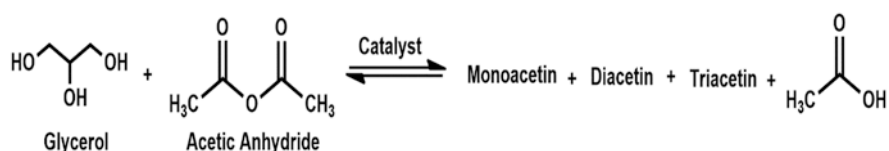
Scheme 12 Synthesis of acetin by esterification of glycerol with acetic anhydride

4.2 Glycerol Carbonate from Transcarbonation of Glycerol with Alkyl Carbonates

Transcarbonation, which is quite comparable to transesterification, is the exchange between carbonate sources and alcohols. In order to convert one carbonate into another, nucleophilic attack by the oxygen atom of the alcohol hydroxl group to the carbon atom from the carbonate group takes place. Therefore, it is quite obvious to prepare glycerol carbonate via the transcarbonation route. Among the other reported

carbonate sources, phosgene, alkyne carbonate and dialkyl carbonate are used in many literatures. Though transcarbonation involving phosgene seems to be a simplistic way for the production of organic carbonate, the handling issues regarding this toxic gas make its applications very limited. Alkyne carbonate systems like propylene carbonate or ethylene carbonate can be employed to prepare glycerol carbonate from transcarbonation of glycerol. Chemical equilibrium calculations revealed that cyclic carbonate preparations by glycerol transcarbonation were thermodynamically favourable for the production of glycerol carbonate [105]. While taking ethylene carbonate, it involves a two-step reaction: first ethylene carbonate is synthesized from carbon dioxide and ethylene oxide and then glycerol carbonate formation takes place via transcarbonation between glycerol and ethylene carbonate [106]. Among the various catalytic systems reported, zeolites, basic oxides and mixed oxides derived from hydrotalcites are worth mentioning. Reduced pressure is usually applied to facilitate the chemical equilibrium for the glycerol carbonate formation. Increasing temperature has a negative effect on chemical equilibrium in this reaction, so most of reported reaction temperatures are lower than previous synthetic routes. Similar to ethylene carbonate, propylene carbonate is also used to prepare glycerol carbonate where abolishing the propylene glycol by-product under reduced pressure is an important step [107]. Dimethyl carbonate is extensively used as a carbonate source to synthesis of glycerol carbonate by the transcarbonation glycerol as it is quite environment friendly and can be prepared from urea and methanol. A large number of catalysts have been reported for this reaction: uncalcined Mg-Al HT, Mg/Al/Zr mixed oxide, NaOH/γ-Al$_2$O$_3$, Mg-Al mixed oxide, Mg-Al LDO, Mg-La mixed oxide, CaO, hydrotalcite, KF-HAP, Mg/Zr/Sr mixed oxide, N-heterocyclic carbenes, Ti-SBA-1 and K$_2$CO$_3$ [108–121]. Performance of some catalysts in glycerol carbonylation with dimethyl carbonate as reported in literature is summarized in Table 2.

Apart from the basic catalysts, some enzymes like lipase (Novozym 435) exhibited promising results towards glycerol carbonate synthesis [122]. Glycerol transcarbonation using alkyl carbonate is reversible in nature, so high mole ratio of alkyl carbonate to glycerol will promote the chemical equilibrium towards the formation of glycerol carbonate. Chemical equilibrium calculations also showed that increase in temperature should increase the chemical equilibrium for the formation of glycerol carbonate [105]. Diethyl carbonate can also be used similar to dimethyl carbonate as carbonate source. Nonetheless some of these methods involve the use of some organic solvents like THF, DMSO, DMF, benzene, etc., and the not easily recoverable or homogeneous nature of the catalysts has unfavourable ecological impacts.

4.3 Glycerol Carbonate from Glycerol and Urea

One of the most promising ways for glycerol carbonate production is from glycerol using urea as a carbonating agent. The main utility for this route of preparation besides having biomass glycerol as raw material is ammonia which is produced as

Table 2 Performance of some catalysts in glycerol carbonylation with dimethyl carbonate as reported in literature

Catalyst	Temperature (°C)	Time (h)	GC yield (%)	Reference
Uncalcined Mg-Al HT	100	1	75	[108]
Mg/Al/Zr mixed oxide	75	1.5	94	[109]
NaOH/γ-Al$_2$O$_3$	78	1	97	[110]
HTC-Ni	100	2	55	[111]
Mg-Al LDO	100	2	66	[112]
Mg-La mixed oxide	85	1.5	81	[113]
CaO	75	0.5	94	[114]
CaO	95	1.5	95	[115]
Hydrotalcite	170	2.5	72	[116]
KF-HAP	78	1	99	[117]
Mg/Zr/Sr mixed oxide	90	1.5	56	[118]
N Heterocyclic carbenes	RT	20 min	95	[119]
Ti-SBA-15	87	4	82	[120]
K$_2$CO$_3$	75	3	97	[121]

by-product can be re-employed for urea production which makes it a very efficient process. The glycerol carboxylation has been reported with numerous heterogeneous catalysts like Zn-Sn mixed oxide, γ-zirconium phosphate, Sm$_{0.66}$TPA, Zn-exchanged zeolites, Cu-Mn mixed oxide, Co$_3$O$_4$/ZnO, Sn-W mixed oxide, ZnSn(OH)$_6$, La$_2$O$_3$, Zn$_1$TPA, Zn/MCM-41, Au-supported ZSM-5, Ta-TPA, WO$_3$-TiO$_2$, Sn(OH)$_2$ [123–138], etc. which have resulted in very high yield of glycerol carbonate. Performance of some catalysts in glycerol carbonylation with urea as reported in literature is summarized in Table 3. The use of Sn-beta, Au/Fe$_2$O$_3$ and ZnAlO catalysts resulted in good conversion of glycerol but with reduced selectivity towards glycerol carbonate, while in the cases of Sm$_{0.66}$TPA, SW21, Zn$_1$TPA, Co$_3$O$_4$/ZnO, La$_2$O$_3$ and Zn/MCM-41 catalysts, the reverse was noticed. ZrP and Ta$_{0.4}$TPA catalysts exhibited 80% and 71% conversion of glycerol, respectively, with maintaining a very good selectivity towards glycerol carbonate. The Zn$_2$Sn-CoPre-600, ZnSn(OH)$_6$ and Zn-Y catalyst exhibited very good conversion and selectivity because of the presence of bifunctional, i.e. both acidic and basic, sites in them.

In literature two hypotheses were proposed regarding the reaction mechanism of urea glycerolysis, where firstly urea was converted to isocyanic acid followed by urea directly attacking glycerol. Li et al. proposed that at the time of using metal oxide as catalysts, they confirmed the formation of isocyanic acid (O=C=N stretching) [137]. Keeping in accordance with this observation, a mechanism was suggested where first urea gets activated and with a loss of ammonia molecule to form isocyanic acid (HNCO) which would react with glycerol to form carbamate followed by the carbonate. In another study by Aresta et al. where they used γ-zirconium phosphate as catalyst, no isocyanic acid formation was observed [127]. According to their study, there is direct reaction between glycerol and urea after which release of ammonia takes place and then carbamate formation. Eventually the reaction between glycerol and urea produces high quantity of by-product ammonia which in a way limits its implementation to the industry. To counter with this issue, a positive

Table 3 Performance of some catalysts in glycerol carbonylation with urea as reported in literature

Catalyst	Temperature (°C)	Time (h)	Conversion (%)	Selectivity (%)	GC yield (%)	Reference
SW21	140	4	52.1	95.3	49.7	[128]
Zr-P	140	3	80	100	80	[127]
Au/Fe$_2$O$_3$	150	4	80	48	38.4	[139]
2.5% Au/ Nb$_2$O$_5$	150	4	66	32	21	[139]
Zn/MCM-41 (im)	145	5	75	98	73	[123]
Sm$_{0.66}$TPA	140	4	49.5	85.4	42.3	[125]
Zn$_1$TPA	140	4	69.2	99.7	68.8	[140]
Co$_3$O$_4$/ZnO	145	4	69	97	66.9	[129]
15% WO$_3$/TiO$_2$	140	4	100	73	73	[136]
Ta$_{0.4}$TPA	140	4	71	100	71	[132]
Sn(OH)$_2$	140	4	87	85	74	[135]
ZnAlO	140	4	91	70	64	[133]
Cu-Mn	140	6	91	99	90	[134]
Zn-Y	150	3	94.6	98	92.7	[130]
ZnSn(OH)$_6$	165	5	98.0	99.6	97.6	[131]
La$_2$O$_3$	140	4	68.9	98.1	67.6	[124]
Zn$_2$Sn-CoPre-600	155	4	96	99.6	95.6	[126]

and possible way out would be to combine both the units which produce glycerol carbonate and can consume the by-product ammonia. Li et al. also proposed that in order to selectively prepare cyclic carbonates by using diols and urea, it could be seen that catalysts having both acidic and basic properties are much favourable [137]. Shanbhag et al. showed that catalysts with optimum acid-base sites can deliver remarkable results for glycerol carbonylation reaction [126]. According to Marakatti et al., Lewis acid sites along with their conjugate bases are reasons for better catalytic activity for the synthesis of glycerol carbonate. A bunch of study reported by Lingaiah et al. on glycerol carbonylation also stated the fact about the presence of Lewis acid-base pair for selective synthesis of glycerol carbonate. Chemical equilibrium calculations demonstrated that elevated temperature and reduced pressure facilitate the glycerol carbonylation reaction with urea [105]. From ecological and energy point of view, this synthetic route is the most advantageous involving biobased reactants and notably not involving any organic solvents.

5 Catalytic Esterification of Glycerol

The esterification of glycerol is another widely studied pathway to convert glycerol into value-added chemicals. Esterification of glycerol with an acetyl source results in mono-, di- and tri-acetyl esters which are commonly termed as monoacetin

(MAG), diacetin (DAG) and triacetin (TAG). Among the various uses of these products, MAG is normally used in cryogenics (resists freezing), solvents in dye industry, raw material for biodegradable polyester production, explosive production, humectant to retain moisture in cosmetics, etc. DAG is used as solvent and plasticizers, softening agents, raw material for biodegradable polyester production, cryogenics processes, etc. TAG is primely used as additive for fuel blend which improves the efficiency for burning. Blending of TAG with biodiesel improves the performance of direct-injection diesel engine. Apart from the above important use, it is also used as antimicrobial agent and emulsifying agent in pharmaceuticals [138, 141]. In terms of acylation agent, acetic acid (AcOH) and acetic anhydride (Ac_2O) have been widely used. For the production of TAG, Ac_2O is a more thermodynamically preferable alternative than AcOH as the reaction between glycerol and Ac_2O goes ahead exothermally and results in negative Gibbs free energy, while the reverse is observed for acetylation of glycerol with AcOH. The acetylation of glycerol with Ac_2O over zeolite beta and K-montmorillonite can yield 100% TAG under mild reaction conditions [142]. However, the use of Ac_2O generates elevated heat of reaction, sometimes violent reactions, and apart from this, no effective changes can be seen for thermodynamic parameters even at different ambient temperature conditions. Furthermore, Ac_2O is used as a raw material to produce narcotics which restricts its use in many countries. So the use of Ac_2O as an acylation agent has become costlier and tough in comparison to AcOH which is cheap and readily available. Along with this, exclusively synthesizing TAG cuts down the production of other two analogues (MAG and DAG) that have important application to industry.

Esterification is generally carried out involving mineral acids (homogeneous catalyst) to structure glycerol esters (MAG, DAG and TAG). These mineral acids like hydrofluoric acid, hydrochloric acid and sulphuric acid are highly toxic, corrosive and hazardous, and their usage brings in recovery difficulties and high-energy multistep processes [143]. The disposal of these acids is another challenging task which might lead to environmental problems. So the use of friendly heterogeneous catalysts is more justified as they can be designed accordingly to attain high yield and effortless regeneration. The catalyst systems used for glycerol esterification include heteropolyacids, mixed oxides, ion-exchange resins, ionic liquids, acid-functionalized zeolites, carbon-based catalysts, etc. The catalytic activity of various catalysts employed for glycerol esterification with acetic acid is summarized in Table 4.

5.1   Route of the Esterification of Glycerol with Acetic Acid

The esterification of glycerol with acetic acid is a reversible equilibrium reaction for synthesizing acetylated esters which proceeds in three successive steps. Firstly, the protons present within the catalyst get attached to the acetic acid oxygen lone pair electron, and then nucleophilic attack of the hydroxyl group takes place by electrophiles which releases water to form MAG. Secondly more acetylation by a second

Table 4 Performance catalysts in the esterification of glycerol with acetic acid as reported in literature

Catalyst	Temperature (°C)	Time (h)	Gly: AcOH	Conversion (%)	Selectivity (%)			Reference
					MAG	DAG	TAG	
Ar-SBA-15	125	4	1:9	90	15	85		[144]
Amberlyst-35	105	4	1:6	100	49.1	25.9	25.0	[142]
SBAH-15(15)	110	3	1:6	100	14	67	19	[145]
MP-TaMCF	150	4	1:9	91	13	53	34	[146]
Amberlyst-70	105	10	1:6	100	0	9.4	85.4	[147]
SCZ	120	1	1:6	100	25.8	57.7	16.5	[148]
HS₁W/ZrO₂	120	4	1:10	100	6.4	61.3	32.3	[149]
Ag₁PW	120	15 min	1:10	96.8	48.4	46.4	5.2	[150]
TPA₃/MCM-41	100	6	1:6	87	25	60	15	[138]
MTZ	120	3	1:6	100	52.03	40.45	7.52	[151]
Carbon catalyst	110	3	1:3	99	12	88		[152]
3%Y/SBA-3	110	2.5	1:4	100	11	34	55	[153]
AC-SA5	120	3	1:8	91	38	28	34	[154]
Sulphonated carbon Catalyst	120	2	1:5	98.4	32.8	54.5	12.7	[155]
MP(5)/NbSBA-15-32	150	4	1:9	94	11	51	38	[156]
GO	120	1	1:10	98.5	15.5	60	24.5	[157]
Sb₂O₅	120	1	1:6	96.8	33.2	54.2	12.6	[158]
SHTC	115	10	1:9	98	5	38	57	[159]
[(HSO3-P)₂im][HSO₄]	100	1:8	30 min	95	43.1	51.4	5.5	[160]
Cs-PWA	85	2	1:8	98	27	58	15	[161]
PW-in-S2	120	7	1:16	87	36	59	4	[141]
[H-NMP][H-SO₄]	100	30 min	1:6	99	20.8	60.3	18.9	[162]

nucleophilic attack on the hydroxyl group of the MAG that is formed produces DAG which again releases water as a by-product. Finally, the remaining oxygen lone pair electrons of the last hydroxyl group in DAG experience a third nucleophilic attack to produce TAG followed by more water. Normally three moles of water molecule are formed as a result of the consecutive esterification steps in the formation of TAG.

5.2 Effects of Different Reaction Parameters: Reaction Temperature, Catalyst Loading, Molar Ratio and Reaction Time

In the presence of an acid catalyst, glycerol acetylation with acetic acid comprises a three-step reversible equilibrium reaction from monoacetin to triacetin. The reaction insights and behaviour under optimum conditions have been thoroughly discussed by many researchers in order to develop thermodynamic and kinetic models. By developing these models with the help of experimental and mechanistic data, the consequences of various reaction parameters over reaction rate were demonstrated [163]. Thermodynamic parameters like activation energy and Gibbs free energy were estimated under different reaction conditions. Esterification of glycerol with acetic acid pursues first-order rate law kinetics, and the mathematical expression can be revealed by applying the Langmuir-Hinshelwood-Hougen-Watson model, where the rate-determining step is the surface reaction. Further thermodynamic investigation demonstrated that Gibbs free energies corresponding to the formation of MAG and DAG were rather low than TAG which justifies the reduced selectivity of TAG. However, if high acetic acid amount is used compared to glycerol, the reaction equilibrium can be shifted to obtain satisfactory value of TAG. The quantitative relation between the reactant amount and the formed product amount can be easily found out from the balanced equation of the three successive steps for esterification of glycerol with acetic acid. However, this provides no information regarding the reaction rate. Study on chemical kinetics reveals the rate of the reaction is dependent on various parameters which include reaction temperature, reactant concentrations and catalyst loading. This reveals the insights about the correct parameter that should be subjected to modification in order to achieve high yield. The study conducted by Ghoreish et al. [164] revealed the increase in temperature from 50 to 110 °C increased the conversion of glycerol with high selectivity towards DAG and TAG. According to their study, high temperature enhances the conversion of glycerol as well as DAG and TAG formation, whereas the MAG formation is enhanced by low temperatures. Another study involving silicotungstic acids supported on zirconia revealed rising temperature (60–120 °C) increased conversion of glycerol (54.4–100%) linearly with a gradual increment in DAG and TAG at the consumption of MAG under endothermic condition [149]. Khayoon et al. [153] investigated yttrium-functionalized SBA-3 catalyst in the temperature range of 90 °C to 110 °C

and found out conversion of glycerol increased from 65% to 100% at 110 °C where no further increment in conversion could be observed above 110 °C. However, temperature upsurge had no effect on the yield of TAG. This finding is a clear indication that equilibrium is attained and optimum temperature is reached. In another study over polymer-supported WO_3 catalyst, it showed increasing temperature (50–110 °C) increased conversion of glycerol (58.8–98%) along with TAG selectivity (5–70%). Based on the catalyst system, the optimum temperature should be taken, for example, ion-exchange resins are not much thermally stable at temperatures above 120 °C and are prone to be deactivated which results in low catalytic activity [142]. Based on the above investigations, we can summarize that with increasing temperature, rate also increases, that is, the glycerol conversion increases with gradual upsurge in DAG and TAG selectivity at the cost of MAG.

Different investigations showed increment in catalyst loading facilitates the acetylation of MAG and DAG to TAG. This probably may have emerged from the increment in number of accessible active acid sites in reaction mixture. In the glycerol esterification with acetic acid over sulphated activated carbon, it was observed that an increase in catalyst loading (0.2–0.8 g) causes linear increment in conversion of glycerol and selectivity of TAG. Further increment in catalyst amount resulted in no significant surge in conversion or selectivity which indicates the saturation. In a similar way, in another investigation involving zirconia-supported silicotungstic acid, it showed that on increasing the amount of catalyst from 0.1 to 0.2 g, conversion of glycerol escalated from 97.7% to 100% and on further increasing the amount of catalyst (0.3 g), it resulted in higher selectivity for DAG and TAG. However, catalyst loading over 0.3 g exhibited no significant effect on either conversion or selectivity. According to Zhu et al. [149] and Ghoreishi et al. [165], acetylation does not mainly depend on catalyst as the production of MAG can equally proceed without the presence of catalyst. Therefore, an increased catalyst amount in general promotes higher selectivity towards DAG and TAG. This also confirms the fact that a three-step glycerol esterification actually takes place.

The molar ratio of the reactants is an influencing parameter for this reaction. From the equation stoichiometry, it is evident that 3 mol of acetic acid is needed to react completely with 1 mol glycerol for the production of TAG. So the excess amount of acetic acid facilitates DAG and TAG formation. Acetic acid in excessive amount moves the equilibrium towards higher selectivity of DAG and TAG. In an observation by Popova et al. [166], excess glycerol to acetic acid molar ratio (1:10) increased the DAG and TAG selectivity and lowered the reaction time for reaching equilibrium. While in other reports involving Amberlyst resin, it was showed that high amount of acetic acid lags the formation of product and reaction equilibrium [166]. Mufrodi et al. [167] showed that the conversion of glycerol increased from 0.28% to 98.5% upon increasing the molar ratio of glycerol to acetic from 1:1 to 1:6 accompanied by increase in selectivity for DAG and TAG at the price of MAG. All these studies suggest that the increase in amount of acetic acid increases conversion of glycerol as well as formation of acetyl ester.

The influence on reaction time was reviewed to investigate the time for reaching equilibrium. According to Ghoreishi et al. [165], there is a linear relationship

between the glycerol conversion rate and increase in time in a 10 h reaction. Selectivity for TAG reached 70% at 10 h time and selectivity for DAG reached 50% at 6 h, while the MAG selectivity gradually decreased. Zhu et al. [149] showed that conversion of glycerol reached 93% within 30 min and 100% within 2 h over silico-tungstic catalyst supported on zirconia, while selectivity of MAG was higher than TAG at 30 min. As the time progressed, yield for DAG and TAG increases. So it is quite clear that increment in reaction time increases glycerol conversion as well as selectivity towards DAG and TAG, but this also depends on the catalyst system and reaction conditions chosen during the esterification reaction.

6 Catalytic Acetalization of Glycerol

Production of cyclic acetals and ketals from glycerol with aldehydes and ketones is another strategy to promote the concept of circular economy in between biodiesel production and glycerol upgradation. The glycerol acetalization with aldehydes or ketones yields five- and six-membered cyclic acetals or ketals. These cyclic oxygenated compounds are one of the major potential fuel additive candidates. Such additives are also known as anti-knocking agent, used in the formulation of diesel, gasoline and biodiesel as they can significantly enhance fuel rating and cold flow properties besides achieving the required flash point and oxidation stability for long-term biodiesel storage [14, 168–170]. In addition, theses additives can effectively cut down the emission of hydrocarbons, carbon monoxide, unregulated aldehydes, etc. released by the uncontrolled combustion of diesel fuel. Among various fuel additives, solketal is the most effective, synthesized by the acetalization of glycerol with acetone. Melero et al. [171] performed an experiment with different oxygenated compounds obtained from glycerol, including triacetin, solketal, a mixture of glycerol esters and mixture of tert-butylated glycerol. There they showed that the solketal and tert-butylated glycerol are able to reduce viscosity and density of the fuel effectively. Apart from that, blending of solketal with biodiesel meets its established requirements for maximum pour point at a temperature −4 to −7 °C, higher than the other additives. Based on several literature reports, glycerol acetalization process can be classified into three generations (Scheme 13): (a) first-generation glycerol acetalization, (b) second-generation glycerol acetalization and (c) third-generation glycerol acetalization.

Amin et al. [172] recently showed the annual operation cost of a plant through a pie chart where 432 tons of glycerol is consumed with the production of 620.9 tons of solketal per year and solketal production cost was 12.29 US$/kg (Fig. 2). Therefore, more attention and investigation should be needed to minimize its cost of production.

Glycerol acetalization reaction with acetone is acid-catalysed reversible reaction where water is formed as co-product along with formation of five- and six-membered cyclic ketals [14]. Therefore, hydrophobic acid catalyst is highly desirable for getting maximum glycerol conversion and five-membered selectivity. In this reaction,

six-membered product appears as minor one because there is the presence of 1, 3-axial interaction. However, this type of effect can be minimized in five-membered ring by ring contraction and appeared as kinetically most stable product [169]. There are two types of possible reaction mechanism for the formation of solketal:
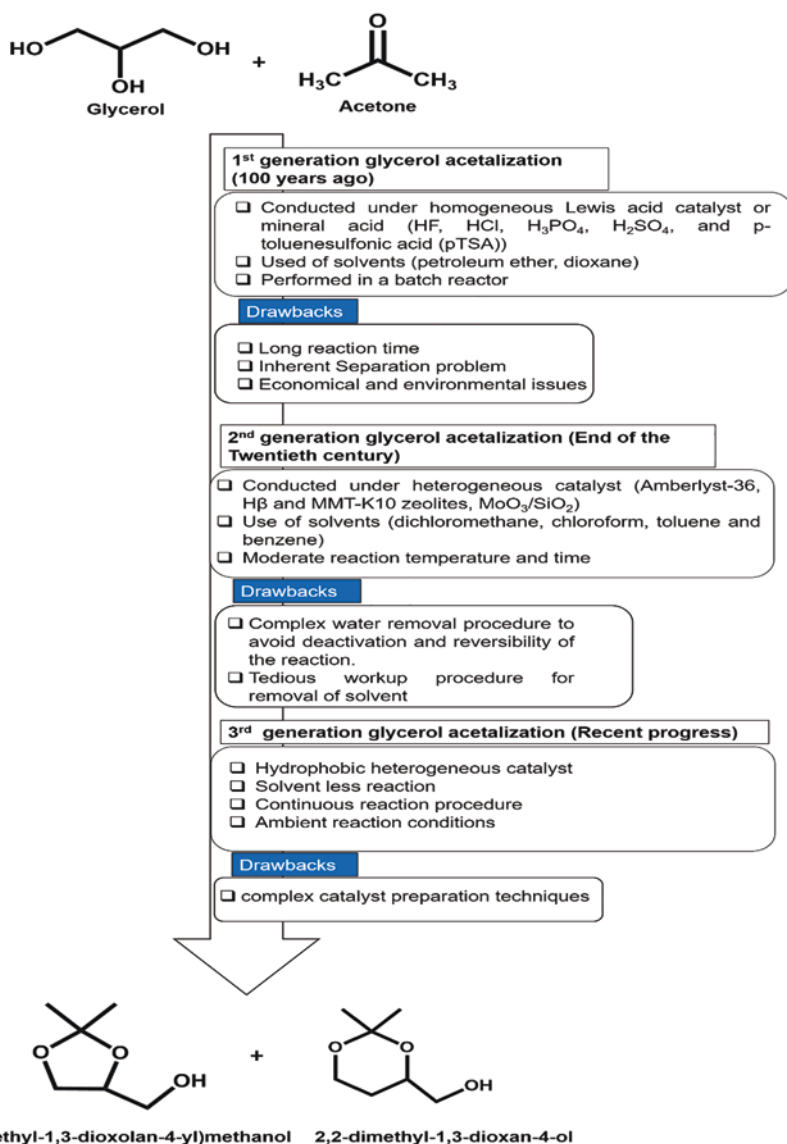
Scheme 13 Generation-wise classification of glycerol acetalization

(a) Ketal mechanism: selective solketal formation takes place via carbenium inter-
    mediate initiated by Brønsted acid sites (Scheme 14) [168].
(b) Meerwein-Ponndorf-Verley reduction/Oppenauer oxidation (MPVO reaction):
    dihydroxyacetone and 2-propanol may have been formed along with formation
    of solketal over Lewis acid sites (Scheme 15) [174].

Here a comprehensive literature survey is summarized on zeolite, metal oxide
and carbon-based catalyst for glycerol acetalization reaction. Besides that, we have
discussed several factors that are responsible for altering glycerol conversion and
selectivity.

Zeolite catalyst: Zeolites are the crystalline aluminium silicate with well-defined
frameworks and pores in the molecular dimension of 0.3–1.5 nm [175]. They are
unique class of materials, found very active towards various chemical reactions
especially catalytic fuel upgradation in oil refinery and several chemical transfor-
mations in petrochemical industry as they have tunable porosity and acidity and
high thermal stability [173, 175, 176]. The nanocrystalline zeolite beta and Y are the
most active than the other forms of zeolites as they possess high surface area, lower
diffusion path length and exposed sites [177]. Despite achieving a lot of success
using zeolites, the major problem lies in catalytic application which is the molecular
transport to and from active sites situated within the micropores which slows down
the reaction rate and forces the catalyst deactivation. However controlled reduction
of zeolite crystal can minimize the diffusion problem, but filtration of those small
crystals during preparation is very difficult due to the colloidal nature of the zeolite
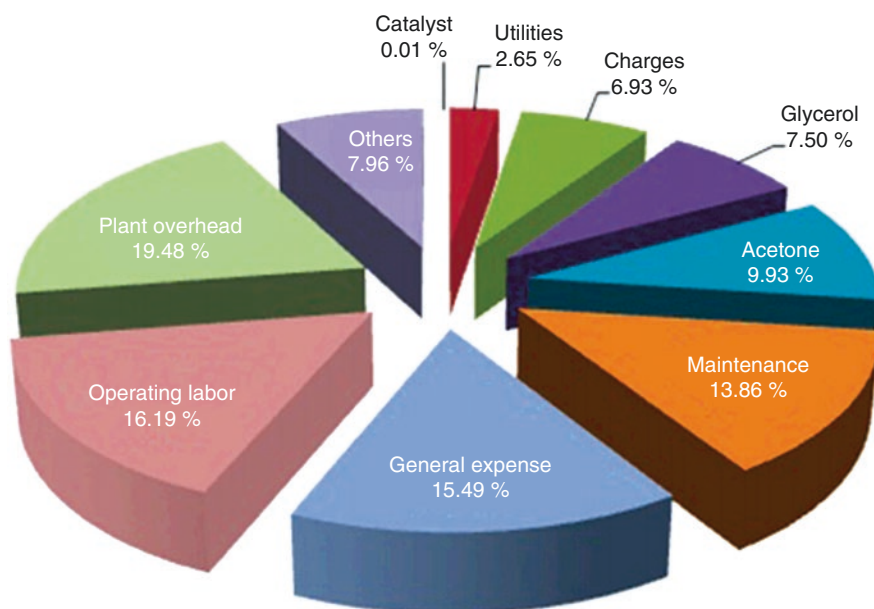
Fig. 2 Annual operation cost of glycerol to solketal production plant (Reproduced from Reference
[173] Copyright © 2018 Talebian-Kiakalaieh, Amin, Najaafi and Tarighi)
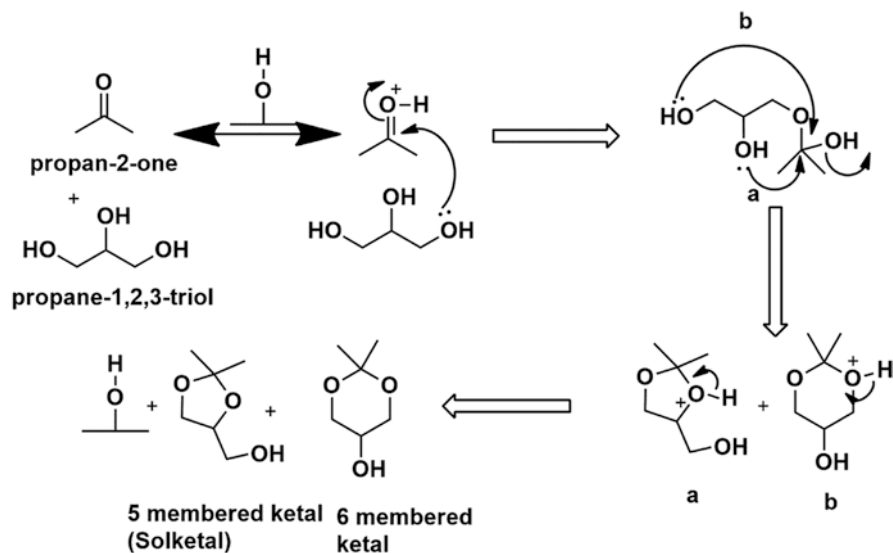
Scheme 14 Glycerol acetalization over Brønsted acid sites
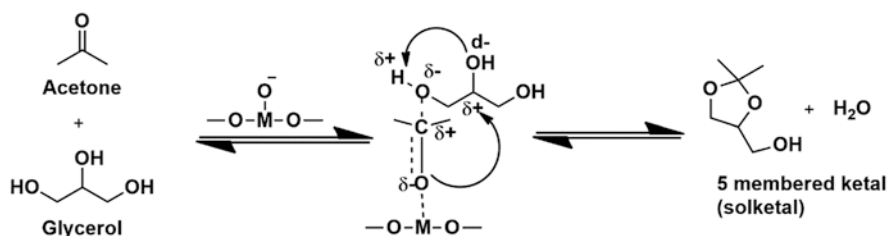
Scheme 15 Glycerol acetalization over Lewis acid sites

crystal [176]. Recently, hierarchical architecture porosity has been introduced to improve transport problem either through adaptation of hard template route or through dealumination process. The term 'hierarchical' signifies that the mesopores are linked to the micropores and to the external surface. This type of system easily transports the reactant to the active sites through the mesopores and maintains the shape selectivity through small pores [173, 175–177].

The glycerol acetalization over zeolite catalyst mainly depends on its pore size and concentration of acid sites. The glycerol acetalization is lower over medium pore zeolite (H-ZSM-5) and dual pore zeolite (H mordenite) due to the diffusion limitation, but moderate conversion of zeolite H-Y is mainly due to the combination of acidity and three-dimensional large pore structure [178]. However, zeolite beta came with better activity than other zeolites because of its shorter path length and smaller crystallite size (Fig. 3). The smaller crystallite size favours the diffusion process. For this reason, larger zeolite beta crystal does not show better

performance towards glycerol acetalization reaction [178]. More better performances are obtained towards glycerol acetalization reaction when hierarchical structure is created inside the zeolite framework [179]. As a result, faster diffusion of the reactants to active sites took place. The selectivity of the product can be controlled by the organic acid treatment of zeolite beta catalyst. Basically, acidity of the zeolite is associated with the aluminium content; the higher is the content of aluminium, the higher is the Bronstead as well as Lewis acidity. When zeolite beta is treated with different organic acids such as phenoldisulfonic acid, methanesulfonic acid and paratoluenesulfonic acid, aluminium gets removed from the edge as well as framework of the zeolites [180], which causes reduction of acidity but increase in surface area and pore volume, but it depends on how much amount of aluminium gets out from zeolite beta. Each organic acid shows different ability towards dealumination process and follows the order of phenoldisulfonic acid → methanesulfonic acid → paratoluenesulfonic acid. So, it is obvious that the paratoluenesulfonic acid-treated sample exhibits highest amount of acid sites and lowest surface area. Interestingly, there is not any change in structure upon acid treatment. Among acid-treated zeolite beta, phenoldisulfonic acid showed 100% selectivity towards five-membered ketal (solketal) because it has the highest surface area and pore volume due to which six-membered rings can be easily converted to five-membered rings through rearrangement. Even concentration of phenoldisulfonic acid has significant effect on solketal selectivity. During acid treatment, decreasing the concentration of phenoldisulfonic acid reduces pore volume and surface area but increases acid amount to a greater extent. On the contrary, decrease in acid concentration decreases the volume space acidity factor (VSA) which restricts rearrangement of six-membered to five-membered ring (solketal) and eventually lowers the selectivity of
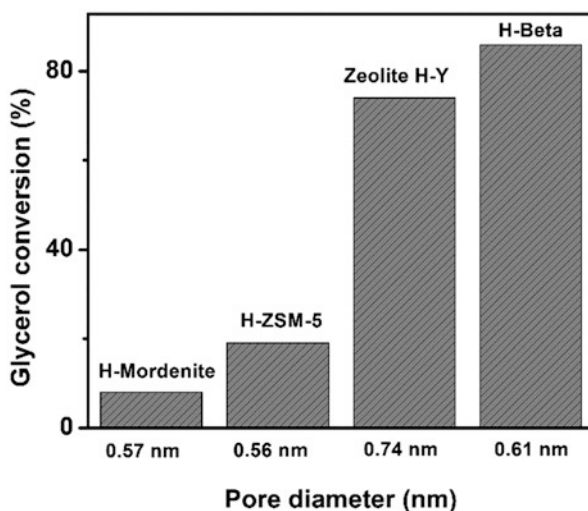
Fig. 3 Glycerol acetalization with acetone over different-sized zeolites

five-membered ring (Table 5). Basically, VSA is the volume required for the rearrangement through accessing the available acid sites. Therefore, higher pore volume is the crucial factor to reach the acid sites and show highest selectivity. Not only pore volume and acidity but hydrophobicity plays important role towards product selectivity. The dealumination causes decrease in hydrophobicity by the increase in silica content. High silica content preserves the acid sites by expelling out and preventing diffusion of water through the pore which eventually impairs the reverse reaction rate that means slowing down hydrolysis of six-membered and five-membered rings. The more the dealumination, more is the silica amount, the better is the hydrophobicity and consequently better is the selectivity. Sometime acidity of zeolite beta has been increased by anchoring with silicotungstates to obtain high selectivity because large pore along with strong acidity facile the ring transformation [181].

Carbon catalyst: In moving forwards towards green and sustainable chemistry, carbon-based materials have been advocated as an emerging material due to their high surface area, tunable porosity, chemical inertness, high electrical conductivity, surface hydrophobicity, easy accessibility and straightforward surface functionalization [182–184]. The carbon material obtained from residual biomass through thermal treatment can be able to minimize carbon footprint of a biomass transformation process [183]. The surface chemistry of the carbon materials is very interesting and can be altered according to the reaction conditions, either through oxidation with acid or through introduction of heteroatoms. These functional groups decide the chemical properties of the carbon surface whether it will be acidic or basic depending upon their type and quantity. Generally, oxygen functionalities are responsible for acidity, whereas nitrogen groups are responsible for basicity of the carbon material (Fig. 4). The surface functionalization can be achieved at low-temperature (473–573 K) or high-temperature (573–1073 K) hydrothermal treatment either by adding activating agent with carbon precursor or by taking functional group containing precursor directly [184]. Oxidation with acid causes generation of carboxylic, lactone, carbonyl, phenol and quinone groups at the edge or the defect sites. These kinds of functional groups play a decisive role for the dispersion in

Table 5 Physicochemical properties of acid-treated zeolite beta catalyst and catalytic performances towards glycerol acetalization reaction

Catalyst	Glycerol conversion (%)	Selectivity (5 membered) (%)	Si/Al ratio	Acidity (pyridine IR), mmol/g	Pore volume, cm³/g	VSA, cm³/mmol
P$_{BEA}$ (0.1)	72	83	48	0.992	0.345	0.347
P$_{BEA}$ (0.25)	75	86	63	0.953	0.364	0.381
P$_{BEA}$ (0.5)	76	95	84	0.928	0.392	0.422
P$_{BEA}$ (1)	80	100	96	0.878	0.412	0.469

[a]P$_{BEA}$ () = phenoldisulfonic acid-treated zeolite beta (concentration)

polar solvent but show a negative impact for catalytic biomass transformation process where water is formed as a co-product.

Generally, oxidation can be done by fuming H_2SO_4 or HNO_3 to prepare highly acid carbon material [184, 186]. Using of H_2SO_4 causes incorporation of $-SO_3H$ groups along with generation of oxygen functionalities on the surface. These types of materials are ideal for glycerol acetalization reaction as they possess predominantly Brønsted acid sites with excellent Hammett acid strength (H_0) in the range of $-8 < H0 \leq -11$ [186]. However, HNO_3 treatment generates a large number of oxygen functionalities as it is a stronger oxidizing agent than H_2SO_4, but sometimes pyrrole-pyridine nitrogen groups are also generated inside the carbon matrix which are not expected as catalytic sites for glycerol acetalization reaction. There are mainly two factors responsible for glycerol acetalization reaction over carbon-based solid acid catalyst. First factor is acidity of the carbon catalyst where acetalization is done over untreated carbon, H_2SO_4-treated carbon and HNO_3-treated carbon catalyst. It has been observed that the untreated carbon catalyst displayed poor glycerol conversion than H_2SO_4- and HNO_3-treated carbon catalyst as it exhibits lower amount of acid sites in the form of carboxyl groups, lactones and phenolic hydroxyl
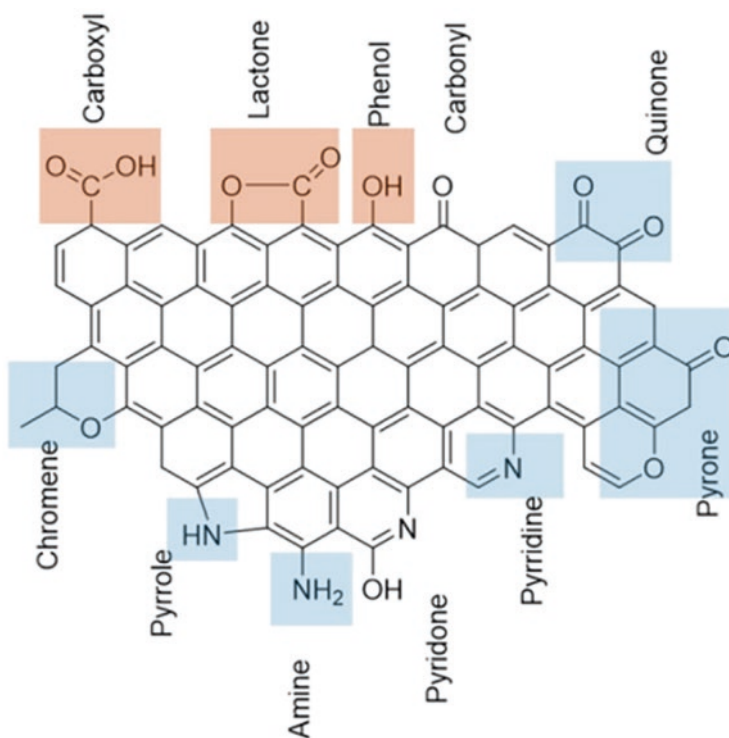
Fig. 4 Different functional groups on carbon surface. Acid groups are highlighted in red, and base groups are highlighted in blue (Reproduced with permission from Reference [185] Copyright © (2017) American Chemical Society)

groups [14]. An oxidizing treatment with HNO_3 leads to increase in the population of acid sites, which is much higher than the H_2SO_4-treated catalyst as HNO_3 is the strong oxidizing agent. Notably, after this treatment, HNO_3-treated catalyst is not able to reach the acetalization performances shown by H_2SO_4-treated catalyst. The better performances of H_2SO_4-treated catalyst are related to the generation of strongly acidic $-SO_3H$ groups on the surface. The effect of acid treatment is more pronounced when we move forwards to the higher concentration [14, 187]. The HNO_3 treatment with high concentration is accompanied by the reduction of pore volume and surface area along with formation of a large number of acid sites [14]. However, surface area and pore volume are preserved even after treatment with high concentration of H_2SO_4 with the generation of a greater number of $-SO_3H$. Therefore, H_2SO_4-treated carbon catalyst appeared as a better candidate for glycerol acetalization reaction.

The second factor which influences the glycerol acetalization is the hydrophobicity of the surface. Carbon surface is generally hydrophobic in nature, but incorporation of heteroatoms alters their hydrophobicity. As we know, the HNO_3 treatment forms a large number of oxygen functionalities whose concentration is significantly higher than the H_2SO_4-treated sample; that's why H_2SO_4-treated sample is more hydrophobic and responsible for the highest activity towards glycerol acetalization through protecting acid sites from water. Despite having high amount of strong acid (-SO_3H) sites on the carbon surface, it won't be able to perform well in glycerol acetalization reaction as higher concentration of $-SO_3H$ group makes the surface hydrophilic which favours the reverse reaction as well as diffusion of water to the pores [14, 187]. Taking this into account, a balance is necessary in between hydrophobicity and acidity for obtaining maximum glycerol conversion.

Metal oxide catalyst: The metal oxides are the most vibrant catalyst in the field of heterogeneous catalysis as they cover majority of the reactions and serve as prominent candidate since 1950. The oxide surface consists of defects and environments (kinks, steps, terraces), which control the catalytic performances. The salient features for controlling catalytic activity are the point and extended defect structure, crystalline phase, atomic compositions and electronic defects. Apart from this, porous structure, electrical conductivity, thermal stability, diffusion acting on sintering and lattice oxygen anion mobility are also taken into consideration [188]. Solid acid oxide catalyst is being used in petroleum industry when the green chemistry concept is made to stop harmful effect of a chemical process on the environment. A large number of solid acid oxide catalysts have been used for acetalization reaction such as ZrO_2, promoted ZrO_2 [189], promoted SnO_2 [168, 170], Nb_2O_5 [190], modified niobium oxyhydroxide [191], Nb_2O_5-Al_2O_3 [192] and phosphate [193] catalyst as they are acidic as well as have excellent water tolerance power. When glycerol acetalization is done over ZrO_2 and promoted ZrO_2 (WOx/ZrO_2, MoOx/ZrO_2, SO_4^{2-}/ZrO_2), glycerol conversion follows the order of SO_4^{2-}/ZrO_2 → MoOx/ZrO_2 → WOx/ZrO_2 → ZrO_2 [189]. The highest activity may be due to the highest surface area and large number of available acid sites. It has also been noticed that all promoted ZrO_2 displayed >80% glycerol conversion, unlike the case of ZrO_2 (10%). This may be due to the greater number of acid sites on the promoted ZrO_2 catalyst

[189]. Similarly, pure SnO_2 showed lower glycerol conversion than the promoted (molybdenum and tungsten) SnO_2 prepared by wet impregnation method [168]. Promotion of Mo and W induces surface area, acid sites, redox property as well as lattice defect. Metal oxide can be prepared by thermal treatment to obtain better physicochemical properties, but pure metal oxide suffers due to the agglomeration or sintering of particles at higher temperature which leads to the formation of larger crystallites. In the case of mixed oxide, the cooperative nature of the cations resists the agglomeration and sintering process, and their mutual interactions can stop the individual crystallization and particle growth which is responsible for obtaining higher surface of mixed oxide than pure oxide. The incorporation of Mo and W leads to generation of excess positive or negative on Sn-O-M (M = Mo, W) bond which causes an improvement of acid amount into the SnO_2. Additionally, promoted sample is mainly enriched with Brønsted acidic site rather than Lewis acidic sites; that's why it follows ketal mechanism and resulting formation of solketal as a selective product. A further improvement of glycerol conversion is observed when SO_4^{2-} is added into the SnO_2 [170]. This observation could be due to the existence of surface superacid sites along with improvement of surface area. However, the catalyst suffers during regeneration because of the loss of sulphur content which actually provides Brønsted acid sites and helps to improve surface area by decreasing crystallite size.

Niobium-based catalyst is also active towards glycerol acetalization [190–192]. Recently, it has been found that the glycerol acetalization performance changes with changing the niobium precursor for preparing same niobium oxyhydroxide catalyst [191]. For the glycerol acetalization, three niobium oxyhydroxide catalysts can be prepared with two different niobium precursor (ammonium niobium oxalate (NH_4-$[NbO(C_2O_4)_2(H_2O)](H_2O)n$) or niobium chloride ($NbCl_5$)) and CTAB. It was obtained that the ammonium niobium oxalate precursor has the larger CTAB incorporation capacity into the niobium oxyhydroxide than the niobium chloride precursor which causes reduction of surface area but improvement of the surface hydrophobicity of the former precursor. The CTAB is likely to bind with surface hydroxyl group resulting in decreasing of surface acidity of niobium oxyhydroxide catalyst prepared from ammonium niobium oxalate or niobium chloride precursor with CTAB. The niobium oxyhydroxide catalyst prepared without surfactant exhibits higher acidity than the CTAB-containing catalyst but suffers due to the lack of hydrophobicity. So, acidity with hydrophobicity is essential for obtaining better glycerol conversion. However, niobium oxyhydroxide catalyst prepared from niobium chloride precursor could not perform well despite having high surface area as its hydrophobicity and acidity are lower than the catalyst prepared from ammonium niobium oxalate precursor (Table 6).

Effect of various reaction parameters: Glycerol acetalization is an exothermic reaction. A high temperature can shift the reaction equilibrium towards the reactant side resulting in a decrease in glycerol conversion. So, moderate temperature (room temperature to 353 K) is highly desirable for getting maximum conversion. On the other hand, the yield of a product is highly dependent on the molar ratio of the reactants. As we know, the lower acetone concentration in acetalization favours the

reverse reaction; likewise, higher concentration ruins its activity through saturation. Therefore, it is necessary to maintain an optimum glycerol and acetone molar ratio. Apart from this, reaction time also plays crucial role in glycerol acetalization reaction. Prolonged reaction time can reduce glycerol conversion through the hydrolysis of five-membered or six-membered ring [194]. Thus, reaction time must be optimized depending on the catalyst.

7 Prospect and Conclusion

The usage of petroleum chemicals and fuels continues to create pollution hazard which has a huge impact on the environment. Recently emerging researches for more sustainable alternatives are interestingly growing very fast, and even commercialization of some processes has already taken place. In recent times a large number of countries in the world have already adopted biodiesel as fuel or fuel additive. The prime by-product in this biodiesel production is glycerol which is growing at a

Table 6 Some recently reported metal oxide, carbon and zeolite catalysts for glycerol acetalization with acetone

Catalyst	Reaction temperature (K)	Glycerol/ acetone	Catalyst loading (wt% w.r.t glycerol), wt%	Reaction time, h	Glycerol conversion (%)	Solketal selectivity (%)	Reference
ZrO_2	RT	1:6	5 wt%	1.5	10	97	[189]
WOx/ZrO_2	RT	1:6	5 wt%	1.5	80	97	[189]
$MoOx/ZrO_2$	RT	1:6	5 wt%	1.5	88	97	[189]
$SO4^{2-}/ZrO_2$	RT	1:6	5 wt%	1.5	98	97	[189]
MO_3/SnO_2	RT	1:1	5 wt%	1.5h	71	96	[168]
SO_4^{2-}/SnO_2	RT	1:1	5 wt%	4	95	96	[170]
Nb_2O_5	343	1:1.5	6.4 wt %	6	80	92	[190]
$Nb_2(OH)$	343	1:2	200 mg	1	65	95	[191]
Nb_2O_5-Al_2O_3	323	1:4	2.7 wt %	6	84	98	[192]
Activated carbon-SO_3H	RT	1:4	3 wt%	6	97	98	[14]
Acidic carbon	RT	1:4	3 wt%	4	80	95	[187]
H-beta zeolite	RT	1:2	5 wt%	2	88	98.5	[178]
Hierarchical MFI zeolites	343	1:1	1 wt%	–	80	100	[179]

good rate, and its valorization has become a necessity and already taking place via various methodologies. This is to act effectively against the future consequences of the by-product and also to mitigate the production cost of biodiesel. Glycerol can be effectively converted into various valued products by several different reaction pathways. These products consist of important chemicals, fuels and fuel additives. This chapter presents recent studies for the conversion of glycerol into useful chemicals and fuels. Among the various catalytic processes discussed for the glycerol conversion are oxidation, dehydration, carbonylation, esterification and acetalization which result in acrylic acid, acrolein, glycerol carbonate, glycerol esters, solketal, etc. Different catalyst systems, reaction parameters, reaction mechanism and catalyst shortcomings are also adequately discussed. The challenges that still remain are the deactivation of the catalyst, low selectivity to a particular desired product, usage of harsh reaction conditions, prolonged reaction time and catalyst separation difficulty. Surmounting the crude glycerol impurity still remains another big challenge for its efficient usage in the industry. To deal with the challenges, the global scientific community should explore new process technologies, novel catalysts with high tolerance, improvement of activation methods, reactor system improvement and overcoming intrinsic weaknesses related to a catalyst. Finally, if some of the hurdles can be conquered, the production and usage of biodiesel will become more effective and sustainable, as well as undoubtedly glycerol will become an enormous feedstock that will potentially succeed conventional petroleum-based fuels and chemicals.

References

1. Sudarsanam P, Peeters E, Makshina EV, Parvulescu V, Sels BF (2018) Advances in porous and nanoscale catalysts for viable biomass conversion. Chem Soc Rev 48:2366–2421
2. Wang T, Noltea MW, Shanks BH (2013) Catalytic dehydration of C_6 carbohydrates for the production of hydroxymethylfurfural (HMF) as a versatile platform chemical. Green Chem 16:548–572
3. Chheda JN, Huber GW, Dumesic JA (2007) Liquid-phase catalytic processing of biomass-derived oxygenated hydrocarbons to fuels and chemicals. Angew Chem Int Ed 46:7164–7183
4. Christensen CH, Rass-Hansen J, Marsden CC, Taarning E, Egeblad K (2008) The Renewable Chemicals Industry. ChemSusChem 1:283–289
5. Yang CY, Fang Z, Li B, Long YF (2012) Review and prospects of Jatropha biodiesel industry in China. Renew Sust Energ Rev 16:2178–2190
6. Knothe G, Razon LF (2017) Biodiesel fuels. Prog Energy Combust Sci 58:36–59
7. Fan X, Burton R (2009) Recent development of biodiesel feedstocks and the applications of glycerol: a review. Open Fuels Energ Sci J 2:100–109
8. Quispe CAG, Coronado CJR, Carvalho JA Jr (2013) Glycerol: production, consumption, prices, characterization and new trends in combustion. Renew Sust Energ Rev 27:475–493

9. Liu H, Su L, Shao Y, Zou L (2012) Biodiesel production catalyzed by cinder supported CaO/KF particle catalyst. Fuel 97:651–657

10. Nda-Umar UI, Ramli I, Taufiq-Yap YH, Muhamad EN (2018) An overview of recent research in the conversion of glycerol into biofuels, fuel additives and other bio-based chemicals. Catalysts 9:15

11. Liu B, Gao F (2018) Navigating glycerol conversion roadmap and heterogeneous catalyst selection aided by density functional theory: a review. Catalysts 8:44

12. Carlson TR, Tompsett GA, Conner WC, Huber GW (2009) Aromatic production from catalytic fast pyrolysis of biomass-derived feedstocks. Top Catal 52(3):241–252

13. Mallesham B, Sudarsanam P, Raju G, Reddy BM (2012) Design of highly efficient Mo and W-promoted SnO_2 solid acids for heterogeneous catalysis: acetalization of bio-glycerol. Green Chem 15:478–489

14. Rodrigues R, Gonçalves M, Mandelli D, Pescarmona PP, Carvalho WA (2014) Solvent-free conversion of glycerol to solketal catalysed by activated carbons functionalised with acid groups. Cat Sci Technol 4:2293–2301

15. Ribeiro LS, Rodrigues EG, Delgado JJ, Chen X, Pereira MFR, Orfao JJM (2016) Pd, Pt, and Pt-Cu catalysts supported on carbon nanotube (CNT) for the selective oxidation of glycerol in alkaline and base-free conditions. Ind Eng Chem Res 55:8548–8556

16. Georgios D, Harun T (2017) Effect of post-treatment on structure and catalytic activity of CuCo-based materials for glycerol oxidation. ChemCatChem 9:610–619

17. Deng X, Dodekatos G, Pupovac K, Weidenthaler C, Schmidt WN, Schuth F, Tuysuz H (2018) Pseudomorphic generation of supported catalysts for glycerol oxidation. ChemCatChem 7:3832–3837

18. Mallat T, Baiker A (2004) Oxidation of alcohols with molecular oxygen on solid catalysts. Chem Rev 104:3037–3058

19. Silva TQ, dos Santos MB, Santiago AA, Santana DO, Cruz FT, Andrade HM, Mascarenhas AJ (2017) Gas phase glycerol oxidative dehydration over bifunctional V/H-zeolite catalysts with different zeolite topologies. Catal Today 289:38–46

20. Liu R, Wang T, Cai D, Jin Y (2014) Highly efficient production of acrylic acid by sequential dehydration and oxidation of glycerol. Ind Eng Chem Res 53:8667–8674

21. Lei J, Duan X, Qian G, Zhou X, Chen D (2014) Size effects of Pt nanoparticles supported on carbon nanotubes for selective oxidation of glycerol in a base-free condition. Ind Eng Chem Res 53:16309–16315

22. Dou J, Zhang B, Liu H, Hong J, Yin S, Huang Y, Xu R (2016) Carbon supported Pt9Sn1 nanoparticles as an efficient nanocatalyst for glycerol oxidation. Appl Catal B Environ 180:78–85

23. Atia H, Armbruster U, Martin A (2008) Dehydration of glycerol in gas phase using heteropolyacid catalysts as active compounds. J Catal 258:71–82

24. McMorn P, Roberts G, Hutchings GJ (1999) Oxidation of glycerol with hydrogen peroxide using silicalite and aluminophosphate catalysts. Catal Lett 63:193–197

25. Carrettin S, McMorn P, Johnston P, Griffin K, Kiely CJ, Hutchings GJ (2003) Oxidation of glycerol using supported Pt, Pd and Au catalysts. Phys Chem Chem Phys 5:1329–1336

26. Ketchie WC, Murayama M, Davis RJ (2007) Promotional effect of hydroxyl on the aqueous phase oxidation of carbon monoxide and glycerol over supported Au catalysts. Top Catal 44:307–317

27. Abbadi A, Bekkum H (1996) Selective chemo-catalytic routes for the preparation of β-hydroxypyruvic acid. Appl Catal A 148:113–122

28. Deutsch J, Martin A, Lieske H (2007) Investigations on heterogeneously catalysed condensations of glycerol to cyclic acetals. J Catal 245:428–435

29. Diallo MM, Mijoin J, Laforge S, Pouilloux Y (2016) Preparation of Fe-BEA zeolites by isomorphous substitution for oxidehydration of glycerol to acrylic acid. Catal Commun 79:58–62

30. Sun D, Yamada Y, Sato S, Ueda W (2017) Glycerol as a potential renewable raw material for acrylic acid production. Green Chem 19:3186–3213
31. Kim M, Lee H (2017) Highly selective production of acrylic acid from glycerol via two steps using Au/CeO2 catalysts. ACS Sustain Chem Eng 5:11371–11376
32. Yang S, Kim M, Yang S, Kim DS, Lee WJ, Lee H (2016) Production of acrylic acid from biomass-derived allyl alcohol by selective oxidation using Au/ceria catalysts. Cat Sci Technol 6:3616–3622
33. Andrushkevich TV (1993) Heterogeneous catalytic oxidation of acrolein to acrylic acid: mechanism and catalysts. Catal Rev Sci Eng 35:213–259
34. Li X, Zhang Y (2016) Highly efficient process for the conversion of glycerol to acrylic acid via gas phase catalytic oxidation of an allyl alcohol intermediate. ACS Catal 6:143–150
35. Rasteiro LF, Vieira LH, Possato LG, Pulcinelli SH, Santilli CV, Martins L (2017) Hydrothermal synthesis of Mo-V mixed oxides possessing several crystalline phases and their performance in the catalytic oxydehydration of glycerol to acrylic acid. Catal Today 296:10–18
36. Yu L, Yuan J, Zhang Q, Liu YM, He HY, Fan KN, Cao Y (2014) Propylene from renewable resources: catalytic conversion of glycerol into propylene. ChemSusChem 7:743–747
37. Sun D, Yamada Y, Sata S (2015) Efficient production of propylene in the catalytic conversion of glycerol. Appl Catal B 174:13–20
38. Schwenk E, Gehrke M, Aichner F (1933) (Schering-Kahlbaum AG), US Patent 1916743
39. Massa M, Andersson A, Finocchio E, Busca G (2013) Gas-phase dehydration of glycerol to acrolein over Al2O3-, SiO2-, and TiO2-supported Nb- and W-oxide catalysts. J Catal 307:170–184
40. Massa M, Andersson A, Finocchio E, Busca G, Lenrick F, Wallenberg LR (2013) Performance of ZrO₂-supported Nb- and W-oxide in the gas-phase dehydration of glycerol to acrolein. J Catal 297:93–109
41. Tao L, Yan B, Liang Y, Xu B (2013) Sustainable production of acrolein: catalytic performance of hydrated tantalum oxides for gas-phase dehydration of glycerol. Green Chem 157:696–705
42. García-Sancho C, Cecilia JA, Moreno-Ruiz A, Mérida-Robles JM, Santamaría-González J, Moreno-Tost R, Maireles-Torres P (2015) Influence of the niobium supported species on the catalytic dehydration of glycerol to acrolein. Appl Catal B Environ 179:139–149
43. Lauriol-Garbey P, Millet JMM, Loridant S, Bellière-Baca V, Rey P (2011) New efficient and long-life catalyst for gas-phase glycerol dehydration to acrolein. J Catal 281:362–370
44. Lauriol-Garbey P, Loridant S, Bellière-Baca V, Rey P, Millet JMM (2011) Gas phase dehydration of glycerol to acrolein over WO₃/ZrO₂ catalysts: improvement of selectivity and stability by doping with SiO₂. Catal Commun 16:170–174
45. Cecilia JA, García-Sancho C, Mérida-Robles JM, González JS, Moreno-Tost R, Maireles-Torres P (2016) WO₃ supported on Zr doped mesoporous SBA-15 silica for glycerol dehydration to acrolein. Appl Catal A Gen 516:30–40
46. Rajan NP, Rao GS, Pavankumar V, Chary KVR (2014) Vapour phase dehydration of glycerol over VPO catalyst supported on zirconium phosphate. Cat Sci Technol 4:81–92
47. Feng X, Yao Y, Su Q, Zhao L, Jiang W, Ji W, Au CT (2015) Vanadium pyrophosphate oxides: the role of preparation chemistry in determining renewable acrolein production from glycerol dehydration. Appl Catal B Environ 164:31–39
48. Rao GS, Rajan NP, Sekhar MH, Ammaji S, Chary KVR (2014) Porous zirconium phosphate supported tungsten oxide solid acid catalysts for the vapour phase dehydration of glycerol. J Mol Catal A Chem 395:486–493
49. Beerthuis R, Huang L, Shiju NR, Rothenberg G, Shen W, Xu H (2018) Facile synthesis of a novel hierarchical ZSM-5 zeolite: a stable acid catalyst for dehydrating glycerol to acrolein. ChemCatChem 10:211–221
50. Carriço CS, Cruz FT, dos Santos MB, Oliveira DS, Pastore HO, Andrade HMC, Mascarenhas AJS (2016) MWW-type catalysts for gas phase glycerol dehydration to acrolein. J Catal 334:34–41

51. García-Sancho C, Cecilia JA, Mérida-Robles JM, González JS, Moreno-Tost R, Infantes-Molina A, Maireles-Torres P (2018) Effect of the treatment with H₃PO₄ on the catalytic activity of Nb₂O₅ supported on Zr-doped mesoporous silica catalyst. Case study: glycerol dehydration. Appl Catal B Environ 221:158–168

52. Fernandes A, Ribeiro MF, Lourenço JP (2017) Gas-phase dehydration of glycerol over hierarchical silicoaluminophosphate SAPO-40. Catal Commun 95:16–20

53. Lopez-Pedrajas S, Estevez R, Navarro R, Luna D, Bautista FM (2016) Catalytic behaviour of mesoporous metal phosphates in the gas-phase glycerol transformation. J Mol Catal A Chem 421:92–101

54. Lourenço JP, Fernandes A, Bertolo RA, Ribeiro MF (2015) Gas-phase dehydration of glycerol over thermally stable SAPO-40 catalyst. RSC Adv 5:10667–10674

55. Deleplanque J, Dubois JL, Devaux JF, Ueda W (2010) Production of acrolein and acrylic acid through dehydration and oxydehydration of glycerol with mixed oxide catalysts. Catal Tod 157:351–358

56. Suprun W, Lutecki M, Haber T, Papp H (2009) Acidic catalysts for the dehydration of glycerol: activity and deactivation. J Mol Catal A Chem 309:71–78

57. Chai SH, Wang HP, Liang Y, Xu BQ (2008) Sustainable production of acrolein: gas-phase dehydration of glycerol over 12-tungstophosphoric acid supported on ZrO₂ and SiO₂. Green Chem 10:1087–1093

58. Viswanadham B, Nagaraju N, Rohitha CN, Vishwanathan V, Chary KVR (2017) Synthesis, characterization and catalytic dehydration of glycerol to acrolein over phosphotungstic acid supported Y-zeolite catalysts. Catal Lett 148:397–406

59. Chai SH, Wang HP, Liang Y, Xu BQ (2009) Sustainable production of acrolein: preparation and characterization of zirconia-supported 12-tungstophosphoric acid catalyst for gas-phase dehydration of glycerol. Appl Catal A Gen 353:213–222

60. Haider MH, Dummer NF, Zhang D, Miedziak P, Davies TE, Taylor SH, Willock DJ, Knight DW, Chadwick D, Hutchings GJ (2012) Rubidium- and caesium-doped silicotungstic acid catalysts supported on alumina for the catalytic dehydration of glycerol to acrolein. J Catal 286:206–213

61. Tsukuda E, Sato S, Takahashi R, Sodesawa T (2007) Production of acrolein from glycerol over silica-supported heteropoly acids. Catal Commun 8:1349–1353

62. Atia H, Armbruster U, Martin A (2011) Influence of alkaline metal on performance of supported silicotungstic acid catalysts in glycerol dehydration towards acrolein. Appl Catal A Gen 393:331–339

63. Liu L, Wang B, Du Y, Borgna Y (2015) Supported H₄SiW₁₂O₄₀/Al₂O₃ solid acid catalysts for dehydration of glycerol to acrolein: evolution of catalyst structure and performance with calcination temperature. Appl Catal A Gen 489:32–41

64. Talebian-Kiakalaieh A, Amin NAS (2015) Supported silicotungstic acid on zirconia catalyst for gas phase dehydration of glycerol to acrolein. Catal Today 256:315–324

65. Talebian-Kiakalaieh A, Amin NAS, Zakaria ZY (2016) Gas phase selective conversion of glycerol to acrolein over supported silicotungstic acid catalyst. J Ind Eng Chem 34:300–312

66. Gu Y, Liu S, Li C, Cui Q (2013) Selective conversion of glycerol to acrolein over supported nickel sulfate catalysts. J Catal 301:93–102

67. Huang L, Qin F, Huang Z, Zhuang Y, Ma J, Xu H, Shen W (2017) Metal organic framework-mediated synthesis of small-sized γ-alumina as highly active catalyst for dehydration of glycerol to acrolein. ChemCatChem 10:381–386

68. Zhou CH, Li GL, Zhuang XY, Wang PP, Tong DS, Yang HM, Lin CX, Li L, Zhang H, Ji SF, Yu WH (2017) Roles of texture and acidity of acid-activated sepiolite catalysts in gas-phase catalytic dehydration of glycerol to acrolein. Mol Catal 434:219–231

69. Xie Q, Li S, Gong R, Zheng G, Wang Y, Xu P, Duan Y, Yu S, Lu M, Ji W, Nie Y, Ji J (2019) Microwave-assisted catalytic dehydration of glycerol for sustainable production of acrolein over a microwave absorbing catalyst. Appl Catal B Environ 243:455–462

70. Lourenço JP, Macedo MI, Fernandes A (2012) Sulfonic-functionalized SBA-15 as an active catalyst for the gas-phase dehydration of glycerol. Catal Commun 19:105–109

71. Qureshi BA, Lan X, Arslan MT, Wang T (2019) Highly active and selective nano H-ZSM-5 catalyst with short channels along b-axis for glycerol dehydration to acrolein. Ind Eng Chem Res 58:12611–12622

72. Ding J, Wang L, Zhang Z, Zhao S, Zhao J, Lu Y, Huang J (2019) Microstructured ZSM-11 catalyst on stainless steel microfibers for improving glycerol dehydration to acrolein. ACS Sustain Chem Eng 7:16225–16232

73. Shan J, Li Z, Zhu S, Liu H, Li J, Wang J, Fan W (2019) Nanosheet MFI zeolites for gas phase glycerol dehydration to acrolein. Catalysts 9:121

74. Katryniok B, Paul S, Capron M, Lancelot C, Belli'ere-Baca V, Rey P, Dumeignil F (2010) A long life catalyst for glycerol dehydration to acrolein. Green Chem 12:1922–1925

75. Dubois JL, Magatani Y, Okumura K (2009) (Arkema), Process for manufacturing acrolein from glycerol, WO 2009127889 and WO 2009128555

76. Alhanash A, Kozhevnikova EF, Kozhevnikov IV (2010) Gas-phase dehydration of glycerol to acrolein catalysed by caesium heteropoly salt. Appl Catal A Gen 378:11–18

77. Kim YT, Jung KD, Park ED (2010) Gas-phase dehydration of glycerol over supported silico-tungstic acids catalysts. Bull Kor Chem Soc 31(11):3283–3290

78. Dubois JL, Duquenne C, Hoelderich W (2006) (Arkema), Process for preparing acrolein from glycerol or glycerin, WO patent 087083

79. Zhuang A, Zhang C, Wen S, Zhao X, Wu T (2008) (Shanghai Huayi Acrylic Acid Co), Method for preparing acroleic acid by using glycerol as raw material, CN 101225039

80. Okuno M, Matsunami E, Takahashi T, Kasuga H, Okada M, Kirishik M (2007) (Nippon Catalytic Chem. Ind.), Production method of acrolein, WO 2007132926

81. Zhou CJ, Huang CJ, Zhang WG, Zhai HS, Wu HL, Chao ZS (2007) Synthesis of micro and mesoporous ZSM-5 composites and their catalytic application in glycerol dehydration to acrolein. Stud Surf Sci Catal 165:527–530

82. Kim YT, Jung KD, Park ED (2011) A comparative study for gas-phase dehydration of glycerol over H-zeolites. Appl Catal A Gen 393:275–287

83. Possato LG, Diniz RN, Garetto T, Pulcinelli SH, Santilli CV, Martins LA (2013) comparative study of glycerol dehydration catalyzed by micro/mesoporous MFI zeolites. J Catal 300:102–112

84. Chai SH, Wang HP, Liang Y, Xu BQ (2007) Sustainable production of acrolein: gas phase dehydration of glycerol over Nb$_2$O$_5$ catalyst. J Catal 250:342–349

85. Wang F, Dubois JL, Ueda W (2010) Catalytic performance of vanadium pyrophosphate oxides (VPO) in the oxidative dehydration of glycerol. Appl Catal A Gen 276:25–32

86. Dubois JL (2009) Arkema France, Process for manufacturing acrolein from glycerol, FR2921361 A1;WO2009044081 A1

87. Ulgen A, Hoelderich WF (2011) Conversion of glycerol to acrolein in the presence of WO$_3$/TiO$_2$ catalysts. Appl Catal A Gen 400:34–38

88. Cavani F, Guidetti S, Marinelli L, Piccinini M, Ghedini E, Signoretto M (2010) The control of selectivity in gas-phase glycerol dehydration to acrolein catalysed by sulfated zirconia. Appl Catal B Environ 100:197–204

89. Liu SY, Zhou CJ, Liu Q, Liu GC, Huang CJ, Chao ZS (2008) Synthesis of mesoporous La-Cu-, and Cr-doped aluminophosphates and their catalytic behavior in the dehydration of glycerol. ChemSusChem 1:575–578

90. Ott L, Bicker M, Vogel H (2006) Catalytic dehydration of glycerol in sub- and supercritical water: a new chemical process for acrolein production. Green Chem 8(2):214–220

91. Suzuki N, Takahashi M (2006) (KAO Corp.), Method for producing acrolein, JP patent 2006290815

92. Yoshimi Y, Masayuki Y, Torakichi A, Takanori A (2009) (Showa Denko), Method for producing acrolein, JP patent 2009179569

93. Shen L, Yin H, Wang A, Feng Y, Shen Y, Wu Z, Jiang T (2012) Liquid phase dehydration of glycerol to acrolein catalyzed by silicotungstic, phosphotungstic, and phosphomolybdic acids. Chem Eng J 180:277–283

94. Akizuki M, Oshima Y (2012) Kinetics of glycerol dehydration with WO_3/TiO_2 in supercritical water. Ind Eng Chem Res 51:12253–12257

95. Foo GS, Wei D, Sholl DS, Sievers C (2014) Role of Lewis and Brønsted acid sites in the dehydration of glycerol over Niobia. ACS Catal 4:3180–3192

96. Yun D, Yun YS, Kim TY, Park H, Lee JM, Han JW, Yi J (2016) Mechanistic study of glycerol dehydration on Brønsted acidic amorphous aluminosilicate. J Catal 2016(341):33–43

97. Chai S, Wang H, Liang Y, Xu B (2007) Sustainable production of acrolein: investigation of solid acid–base catalysts for gas-phase dehydration of glycerol. Green Chem 9:1130–1136

98. Chai S, Tao L, Yan B, Vedrine JC, Xu B (2014) Sustainable production of acrolein: effects of reaction variables, modifiers doping and ZrO_2 origin on the performance of WO_3/ZrO_2 catalyst for the gas-phase dehydration of glycerol. RSC Adv 4:4619–4630

99. Ma T, Yun Z, Xu W, Chen L, Li L, Ding J, Shao R (2016) Pd-$H_3PW_{12}O_{40}$/Zr-MCM-41: an efficient catalyst for the sustainable dehydration of glycerol to acrolein. Chem Eng J 4:343–352

100. Aresta M, Dibenedetto A, Nocito F, Pastore C (2006) A study on the carboxylation of glycerol to glycerol carbonate with carbon dioxide: the role of the catalyst, solvent and reaction conditions. J Mol Catal A Chem 257:149–153

101. George J, Patel Y, Pillai SM, Munshi P (2009) Methanol assisted selective formation of 1,2-glycerol carbonate from glycerol and carbon dioxide using $^nBu_2SnO$ as a catalyst. J Mol Catal A Chem 304:1–7

102. Gómez-Jiménez-Aberasturi O, OchoaGómez JR, Pesquera-Rodríguez A, Ramírez-López C, Alonso-Vicario A, Torrecilla-Soria J (2010) Solvent-free synthesis of glycerol carbonate and glycidol from 3-chloro-1,2-propanediol and potassium (hydrogen) carbonate. J Chem Technol Biotechnol 85:1663–1670

103. Ochoa-Gómez JR, Gómez-Jiménez-Aberasturi O, Ramírez-López CA, Nieto-Mestre J, Maestro-Madurga B, Belsué M (2011) Synthesis of glycerol carbonate from 3-chloro-1,2-propanediol and carbon dioxide using triethylamine as both solvent and CO2 fixation–activation agent. Chem Eng J 175:505–511

104. Aresta M, Dibenedetto A, Pastore C (2006) Direct carboxylation of alcohols to organic carbonates: comparison of the group 5 element alkoxides catalytic activity: an insight into the reaction mechanism and its key steps. Catal Today 115:88–94

105. Li J, Wang T (2011) Chemical equilibrium of glycerol carbonate synthesis from glycerol. J Chem Thermodyn 43:731–736

106. Behr A, Eilting J, Irawadi K, Leschinski J, Lindner F (2008) Improved utilisation of renewable resources: new important derivatives of glycerol. Green Chem 10:13–30

107. Ochoa-Gómez JR, Gómez-Jiménez-Aberasturi O, Ramírez-López C, Belsué M (2012) A brief review on industrial alternatives for the manufacturing of glycerol carbonate, a green chemical. Org Process Res Dev 16:389–399

108. Takagaki A, Iwatani K, Nishimura S, Ebitani K (2010) Synthesis of glycerol carbonate from glycerol and dialkyl carbonates using hydrotalcite as a reusable heterogeneous base catalyst. Green Chem 12:578–581

109. Malyaadri M, Jagadeeswaraiah K, Prasad PSS, Lingaiah N (2011) Synthesis of glycerol carbonate by transesterification of glycerol with dimethyl carbonate over Mg/Al/Zr catalysts. Appl Catal A General 401:153–157

110. Bai R, Wang Y, Wang S, Mei F, Li T, Li G (2013) Synthesis of glycerol carbonate from glycerol and dimethyl carbonate catalysed by NaOH/γ-Al2O3. Fuel Process Technol 106:209–214

111. Liu P, Derchi M, Hensen EJM (2014) Promotional effect of transition metal doping on the basicity and activity of calcined hydrotalcite catalysts for glycerol carbonate synthesis. Appl Catal B Environ 144:135–143

112. Liu P, Derchi M, Hensen EJM (2013) Synthesis of glycerol carbonate by transesterification of glycerol with dimethyl carbonate over MgAl mixed oxide catalysts. Appl Catal A Gen 467:124–131
113. Simanjuntak FSH, Widyaya VT, Kim CS, Ahn BS, Kim YJ, Lee H (2013) Synthesis of glycerol carbonate from glycerol and dimethyl carbonate using magnesium–lanthanum mixed oxide catalyst. Chem Eng Sci 94:265–270
114. Simanjuntak FSH, Kim TK, Lee SD, Ahn BS, Kim HS, Lee H (2011) CaO-catalyzed synthesis of glycerol carbonate from glycerol and dimethyl carbonate: isolation and characterization of an active Ca species. Appl Catal A Gen 401:220–225
115. Ochoa-Gomez JR, Gomez-Jimenez-Aberasturi O, Maestro-Madurga B, Pesquera-Rodriguez A, Ramirez-Lopez C, Lorenzo-Ibarreta L, Torrecilla-Soria J, Villaran-Velasco MC (2009) Synthesis of glycerol carbonate from glycerol and dimethyl carbonate by transesterification: catalyst screening and reaction optimization. Appl Catal A Gen 366:315–324
116. Yadav GD, Chandan PA (2014) A green process for glycerol valorization to glycerol carbonate over heterogeneous hydrotalcite catalyst. Catal Today 237:47–53
117. Bai R, Wang S, Mei F, Li T, Li G (2011) Synthesis of glycerol carbonate from glycerol and dimethyl carbonate catalyzed by KF modified hydroxyapatite. J Ind Eng Chem 17:777–781
118. Parameswaram G, Srinivas M, Hari Babu B, Prasad PSS, Lingaiah N (2013) Transesterification of glycerol with dimethyl carbonate for the synthesis of glycerol carbonate over Mg/Zr/Sr mixed oxide base catalysts. Cat Sci Technol 3:3242–3249
119. Hervert B, McCarthy PD, Palencia H (2014) Room temperature synthesis of glycerol carbonate catalysed by N-heterocyclic carbenes. Tetrahedron Lett 55:133–136
120. Devi P, Das U, Dalai AK (2018) Production of glycerol carbonate using a novel Ti-SBA-15 catalyst. J Chem Eng 346:477–488
121. Rokicki G, Rakoczy P, Parzuchowski P, Sobiecki M (2005) Hyperbranched aliphatic polyethers obtained from environmentally benign monomer: glycerol carbonate. Green Chem 7:529–539
122. Kim S, Kim YH, Lee H, Yoon D, Song B (2007) Lipase-catalyzed synthesis of glycerol carbonate from renewable glycerol and dimethyl carbonate through transesterification. J Mol Catal B Enzym 49:75–78
123. Kondawar SE, Potdar AS, Rode CV (2015) Solvent-free carbonylation of glycerol with urea using metal loaded MCM-41 catalysts. RSC Adv 5:16452–16460
124. Wang L, Ma Y, Wang Y, Liu S, Deng Y (2011) Efficient synthesis of glycerol carbonate from glycerol and urea with lanthanum oxide as a solid base catalyst. Catal Commun 12:1458–1462
125. Kumar CR, Jagadeeswaraiah K, Prasad PSS, Lingaiah N (2012) Samarium-exchanged heteropoly tungstate: an efficient solid acid catalyst for synthesis of glycerol carbonate from glycerol and benzylation of anisole. ChemCatChem 4:1360–1367
126. Manjunathan P, Ravishankar R, Shanbhag GV (2016) Novel bifunctional Zn–Sn composite oxide catalyst for the selective synthesis of glycerol carbonate by carbonylation of glycerol with urea. ChemCatChem 8:631–639
127. Aresta M, Dibenedetto A, Nocito F, Ferragina C (2009) Valorization of bio-glycerol: new catalytic materials for the synthesis of glycerol carbonate via glycerolysis of urea. Catalogue 268:106–114
128. Jagadeeswaraiah K, Kumar CR, Prasad PSS, Loridant S, Lingaiah N (2014) Synthesis of glycerol carbonate from glycerol and urea over tin-tungsten mixed oxide catalysts. App Catal A 469:165–172
129. Rubio-Marcos F, Calvino-Casilda V, Banares MA, Fernandez JF (2010) Novel hierarchical Co$_3$O$_4$/ZnO mixtures by dry nanodispersion and their catalytic application in the carbonylation of glycerol. J Catal 275:288–293
130. Marakatti VS, Halgeri AB (2015) Metal ion-exchanged zeolites as highly active solid acid catalysts for the green synthesis of glycerol carbonate from glycerol. RSC Adv 5:14286–14293
131. Sandesh S, Shanbhag GV, Halgeri AB (2014) Zinc hydroxystannate: a promising solid acid–base bifunctional catalyst. RSC Adv 4:974–977

132. Babu MS, Srivani A, Parameswaram G, Veerabhadram G, Lingaiah N (2015) Understanding the role of tantalum in heteropoly tungstate catalysts for the synthesis of glycerol carbonate from glycerol and urea. Catal Lett 145:1784–1791

133. Nguyen-Phu H, Shin EW (2018) Investigating time-dependent Zn species over Zn-based catalysts in glycerol carbonylation with urea and their roles in the reaction mechanism. Appl Catal A 561:28–40

134. Luo W, Sun L, Yang Y, Chen Y, Zhou Z, Liua J, Wang F (2018) Cu-Mn composite oxides: a highly efficient and reusable acid-base catalysts for the carbonylation reaction of glycerol with urea. Cat Sci Technol 8:6468–6477

135. Chaves DM, Da Silva MJ (2019) A selective synthesis of glycerol carbonate from glycerol and urea over Sn(OH)$_2$: a solid and recyclable in situ generated catalyst. New J Chem 43:3698–3706

136. Jagadeeswaraiah K, Kumar CR, Rajashekar A, Srivani A, Lingaiah N (2016) The role of tungsten oxide species supported on titania catalysts for the synthesis of glycerol carbonate from glycerol and urea. Catal Lett 146:692–700

137. Li Q, Zhang W, Zhao N, Wei W, Sun Y (2006) Synthesis of cyclic carbonates from urea and diols over metal oxides. Today 115:111–116

138. Patel A, Singh S (2014) A green and sustainable approach for esterification of glycerol using 12-tungstophosphoric acid anchored to different supports: kinetics and effect of support. Fuel 118:358–364

139. Hammond C, Sanchez JAL, Rahim MHA, Dimitratos N, Jenkins RL, Carley AF, He Q, Kiely CJ, Knight DW, Hutchings GJ (2011) Synthesis of glycerol carbonate from glycerol and urea with gold-based catalysts. Dalton Trans 40:3927–3937

140. Jagadeeswaraiah K, Kumar CR, Prasad PSS, Lingaiah N (2014) Incorporation of Zn2+ ions into the secondary structure of heteropoly tungstate: catalytic efficiency for synthesis of glycerol carbonate from glycerol and urea. Cat Sci Technol 4:2969–2977

141. Ferreira P, Fonseca IM, Ramos AM, Vital J, Castanheiro JE (2009) Esterification of glycerol with acetic acid over dodecamolybdophosphoric acid encaged in USY zeolite. Catal Commun 10:481–484

142. Liao X, Zhu Y, Wang SG, Li Y (2009) Producing triacetylglycerol with glycerol by two steps: esterification and acetylation. Fuel Process Technol 90:988–993

143. Zhou L, Nguyen TH, Adesina A (2012) The acetylation of glycerol over amberlyst-15: kinetic and product distribution. Fuel Process Technol 104:310–318

144. Melero JA, Grieken RV, Morales G, Paniagua M (2007) Acidic mesoporous silica for the acetylation of glycerol: synthesis of bioadditives to petrol fuel. Energy Fuel 21:1782–1791

145. Khayoon MS, Hameed BH (2012) Synthesis of hybrid SBA-15 functionalized with molybdophosphoric acid as efficient catalyst for glycerol esterification to fuel additives. Appl Catal A Gen 433–434:152–161

146. Stawicka K, Trejda M, Ziolek M (2013) The production of biofuels additives on sulphonated MCF materials modified with Nb and Ta—towards efficient solid catalysts of esterification. Appl Catal A Gen 467:325–334

147. Kale S, Umbarkar SB, Dongare MK, Eckelt R, Armbruster U, Martin A (2015) Selective formation of triacetin by glycerol acetylation using acidic ion-exchange resins as catalyst and toluene as an entrainer. Appl Catal A Gen 490:10–16

148. Reddy PS, Sudarsanam P, Raju G, Reddy BM (2012) Selective acetylation of glycerol over CeO$_2$–M and SO$_4^{2-}$/CeO$_2$–M (M = ZrO$_2$ and Al$_2$O$_3$) catalysts for synthesis of bioadditives. J Ind Eng Chem 18:648–654

149. Zhu S, Zhu Y, Gao X, Mo T, Zhu Y, Li Y (2013) Production of bioadditives from glycerol esterification over zirconia supported heteropolyacids. Bioresour Technol 130:45–51

150. Zhu S, Gao X, Dong F, Zhu Y, Zheng H, Li Y (2013) Design of a highly active silver-exchanged phosphotungstic acid catalyst for glycerol esterification with acetic acid. J Catal 306:155–163

151. Reddy PS, Sudarsanam P, Raju G, Reddy BM (2010) Synthesis of bio-additives: acetylation of glycerol over zirconia-based solid acid catalysts. Catal Commun 11:1224–1228
152. Okoye PU, Abdullah AZ, Hameed BH (2017) Synthesis of oxygenated fuel additives via glycerol esterification with acetic acid over bio-derived carbon catalyst. Fuel 209:538–544
153. Khayoon MS, Triwahyono S, Hameed BH, Jalil AA (2014) Improved production of fuel oxygenates via glycerol acetylation with acetic acid. J Chem Eng 243:473–484
154. Khayoon MS, Hameed BH (2011) Acetylation of glycerol to biofuel additives over sulfated activated carbon catalyst. Bioresour Technol 102:9229–9235
155. Tao ML, Guan HY, Wang XH, Liu YC, Louh RF (2015) Fabrication of sulfonated carbon catalyst from biomass waste and its use for glycerol esterification. Fuel Process Technol 138:355–360
156. Trejda M, Stawicka K, Dubinska A, Ziolek M (2012) Development of niobium containing acidic catalysts for glycerol esterification. Catal Today 187:129–134
157. Gao X, Zhu S, Li Y (2015) Graphene oxide as a facile solid acid catalyst for the production of bioadditives from glycerol esterification. Catal Commun 62:48–51
158. Hu W, Zhang Y, Huang Y, Wang J, Gao J, Xu J (2015) Selective esterification of glycerol with acetic acid to diacetin using antimony pentoxide as reusable catalyst. J Energy Chem 24:632–636
159. Calle CDL, Fraile JM, García-Bordejé E, Pires E, Roldán L (2015) Biobased catalyst in biorefinery processes: sulphonated hydrothermal carbon for glycerol esterification. Cat Sci Technol 5:2897–2903
160. Liu X, Ma H, Wu Y, Wang C, Yang M, Yana P, Welz-Biermann U (2011) Esterification of glycerol with acetic acid using double SO3H-functionalized ionic liquids as recoverable catalysts. Green Chem 13:697–701
161. Sandesh S, Manjunathan P, Halgeri AB, Shanbhag GV (2015) Glycerol acetins: fuel additive synthesis by acetylation and esterification of glycerol using cesium phosphotungstate catalyst. RSC Adv 5:104354–104362
162. Keogh J, Tiwari MS, Manyar H (2019) Esterification of glycerol with acetic acid using nitrogen-based Brønsted-acidic ionic liquids. Ind Eng Chem Res 58:17235–17243
163. Zhou L, Al-Zaini E, Adesina A (2013) Catalytic characteristics and parameters optimization of the glycerol acetylation over solid acid catalysts. Fuel 103:617–625
164. Ghoreishi KB, Yarmo MA (2013) Sol-gel sulfated silica as a catalyst for glycerol acetylation with acetic acid. J Sci Technol 5:65–78
165. Ghoreishi KB, Yarmo MA, Nordin NM, Samsudin MW (2013) Enhanced catalyst activity of WO$_3$ using polypyrrole as support for acidic esterification of glycerol with acetic acid. J Chem 2013:264832
166. Popova M, Szegedi Á, Ristić A, Tušar NN (2014) Glycerol acetylation on mesoporous KIL-2 supported sulphated zirconia catalysts. Cat Sci Technol 4:3993–4000
167. Mufrodi Z, Rochmadi R, Sutijan S, Budiman A (2014) Synthesis acetylation of glycerol using batch reactor and continuous reactive distillation column. Eng J 18:29–40
168. Mallesham B, Sudarsanam P, Raju G, Reddy BM (2013) Design of highly efficient Mo and W-promoted SnO$_2$ solid acids for heterogeneous catalysis: acetalization of bio-glycerol. Green Chem 15:478
169. Priya SS, Selvakannan PR, Chary KVR, Kantam ML, Bhargava SK (2017) Solvent-free microwave-assisted synthesis of solketal from glycerol using transition metal ions promoted mordenite solid acid catalysts. Mol Catal 434:184–193
170. Mallesham B, Sudarsanam P, Reddy BM (2014) Eco-friendly synthesis of bio-additive fuels from renewable glycerol using nanocrystalline SnO$_2$-based solid acids. Cat Sci Technol 4:803–813
171. Melero JA, Vicente G, Morales G, Paniagua M, Bustamante J (2010) Oxygenated compounds derived from glycerol for biodiesel formulation: influence on EN 14214 quality parameters. Fuel 89:2011–2018

172. Talebian-Kiakalaieh A, Amin NAS, Najaafi N, Tarigh SA (2018) Review on the catalytic acetalization of bio-renew glycerol to fuel additives. ront Chem 6:573
173. Groen GC, Zhu W, Brouwer S, Huynink SJ, Kapteijn F, Moulijn JA, Pérez-Ramírez JA (2007) Direct demonstration of enhanced diffusion in mesoporous zsm-5 zeolite obtained via controlled desilication. J Am Chem Soc 129:355–360
174. Li L, Korányi TI, Sels BF, Pescarmona PP (2012) Highly-efficient conversion of glycerol to solketal over heterogeneous Lewis acid catalysts. Green Chem 14:1611–1619
175. Christense CH, Johannsen K, Schmidt I, Christensen CH (2003) Catalytic benzene alkylation over mesoporous zeolite single crystals: improving activity and selectivity with a new family of porous materials. J Am Chem Soc 125:13370–13371
176. Tao Y, Kanoh H, Kaneko K (2003) ZSM-5 monolith of uniform mesoporous channels. J Am Chem Soc 125:6044–6045
177. Taufiqurrahmi N, Mohamed AR, Bhatia S (2011) Nanocrystalline zeolite beta and zeolite y as catalysts in used palm oil cracking for the production of biofuel. J Nanopart Res 13:3177–3189
178. Manjunathan P, Maradur SP, Halgeri AB, Shanbhag GV (2015) Room temperature synthesis of solketal from acetalization of glycerol with acetone: effect of crystallite size and the role of acidity of beta zeolite. J Mol Catal A Chem 396:47–54
179. Kowalska-Kus J, Frankowski AHM, Nowinska K (2017) Solketal formation from glycerol and acetone over hierarchical zeolites of different structure as catalysts. J Mol Catal A Chem 426:205–212
180. Venkatesha BYS, Prakash BSJ (2016) Dealuminated BEA zeolite for selective synthesis of five-membered cyclic acetal from glycerol under ambient conditions. RSC Adv 6:18824–18833
181. Narkhede N, Patel A (2016) Sustainable valorisation of glycerol via acetalization as well as carboxylation reactions over silicotungstates anchored to zeolite Hß. Appl Catal A 515:464–465
182. Liu L, Zhu YP, Su M, Yuan ZY (2015) Metal-free carbonaceous materials as promising heterogeneous catalysts. ChemCatChem 7:2765–2787
183. Cao Y, Mao S, Li M, Chen Y, Wang Y (2017) Metal/porous carbon composites for heterogeneous catalysis: old catalysts with improved performance promoted by n-doping. ACS Catal 7:8090–8112
184. De S, Balu AM, Waal J, Luque R (2015) Biomass-derived porous carbon materials: synthesis and catalytic applications. ChemCatChem 7:1608–1629
185. Donoeva B, Masoud N, Jongh PE (2017) Carbon support surface effects in the gold-catalyzed oxidation of 5 hydroxymethylfurfural. ACS Catal 7:4581–4591
186. Nakajima K, Hara M (2012) Amorphous carbon with SO3H groups as a solid Brønsted acid catalyst. ACS Catal 2:1296–1304
187. Gonçalves M, Rodrigues R, Galhardo TS, Carvalho WA (2016) Highly selective acetalization of glycerol with acetone to solketal over acidic carbon-based catalysts from biodiesel waste. Fuel 181:46–54
188. Védrine JC (2017) Heterogeneous catalysis on metal oxides. Catalysts 7:341
189. Reddy PS, Sudarsanam P, Mallesham B, Raju G, Reddy BM (2011) Acetalisation of glycerol with acetone over zirconia and promoted zirconia catalysts under mild reaction conditions. J Ind Eng Chem 17:377–381
190. Nair GS, Adrijanto E, Alsalme A, Kozhevnikov IV, Cooke DJ, Brown DR, Shiju NR (2012) Glycerol utilization: solvent-free acetalisation over niobia catalysts. Cat Sci Technol 2:1173–1179
191. Souza TE, Portilho MF, Souza PMTG, Souza PP, Oliveira LCA (2014) Modified niobium oxyhydroxide catalyst: an acetalization reaction to produce bio-additives for sustainable use of waste glycerol. ChemCatChem 6:2961–2969

192. Rodrigues R, Mandelli D, Gonçalves NS, Pescarmona PP, Carvalho WA (2016) Acetalization of acetone with glycerol catalyzed by niobium-aluminum mixed oxides synthesized by a sol–gel process. J Mol Catal A Chem 422:122–130

193. Gadamsetti S, PethanRajan N, G S R, Chary KVR (2015) Acetalization of glycerol with acetone to bio fuel additives over supported molybdenum phosphate catalysts. J Mol Catal A Chem 410:49–57

194. Churipard SR, Manjunathan P, Chandra P, Shanbhag GV, Ravishankar R, Rao PVC, Ganesh GS, Halgeri AB, Maradur SP (2017) Remarkable catalytic activity of a sulfonated mesoporous polymer (MP-SO3H) for the synthesis of solketal at room temperature. New J Chem 41:5745–5751

Catalytic Conversion of Alcohols into Value-Added Products

R. Vinayagamoorthi, B. Viswanathan, and K. R. Krishnamurthy

Abstract Alcohols belong to an important class of oxygenates, containing highly versatile hydroxyl (–OH) functional group(s) which are capable of undergoing a variety of chemical transformations, yielding fuels, fuel additives and a wide range of highly useful chemicals and chemical intermediates. Production of methanol, bioethanol and other higher alcohols in plenty, through various biomass conversion processes, has rendered them renewable and carbon-neutral in character and highly useful as platform chemicals. Novel catalytic processes for the conversion of aliphatic C_1-C_4 alcohols to C_2-C_4 olefins/building block chemicals, like ethylene, propylene, isobutene and butadiene, and oxygenates like aldehydes, esters and ethers and gasoline range hydrocarbons have been developed. Catalytic coupling of ethanol to higher alcohols followed by dehydration, oligomerization and hydrogenation to yield jet fuel and middle distillates results in the production of low-carbon renewable/sustainable fuels. Steam reforming and aqueous phase reforming of alcohols to produce hydrogen is yet another process option available for the transformation of alcohols that has several advantages over conventional, non-renewable methane steam reforming. Significant progress has been reported in the catalytic α-alkylation of ketone esters and amides with alcohols and aldol condensation of alcohols with other oxygenates like acetone/ketones. Catalytic upgradation of biomass-derived glycerol, furfuryl alcohol and sugar-derived alcohols like sorbitol, mannitol and xylitol results in a range of value-added products. The origin of such processes, process chemistry, development of catalysts, recent advances and future trends are covered in this chapter.

Keywords Biomass conversion · Biofuels · Sugar alcohols · Furfuryl alcohol · Glycerol

R. Vinayagamoorthi · B. Viswanathan · K. R. Krishnamurthy (✉)
National Centre for Catalysis Research (NCCR), Indian Institute of Technology Madras, Chennai, Tamil Nadu, India

1 Introduction

In the journey towards clean energy and environmental sustainability, identification of biomass as an alternate, renewable and sustainable resource and the advent of biomass conversion processes for the production of fuels and chemicals are the two important milestones [1–5]. Abundant availability of various types of biomass [6–8] and the development of a series of biomass conversion processes, through homogeneous, heterogeneous and enzymatic catalytic routes, have opened up a new avenue of research, full of challenges and enormous opportunities [9–12]. Through sustained research efforts, spread over more than three decades, a well-defined road map in this vital area has been drawn up. Emergence of the concept of *biorefinery* [13–15], akin to the petroleum refining/petrochemical plants based on fossil resources [16, 17], was the first step in this direction. As the nodal entity, biorefinery provides a structured approach, oriented towards the development of biomass conversion processes for practical applications. Different types of lignocellulosic biomass, which are useful as feedstock for the biorefinery, in general, consist of three major components [18], namely, cellulose (34–54%), hemicellulose (19–34%) and lignin (11–30%). Being complex in character, it is necessary that the biomass is first converted into relatively simple and active intermediates or platform chemicals, which can undergo further transformations in a facile manner, into value-added products with wider applications (Fig. 1).

In an effort to drive focused research work in the area of biomass conversion, the US Department of Energy (DOE) in 2004 identified a set of 12 platform chemicals,
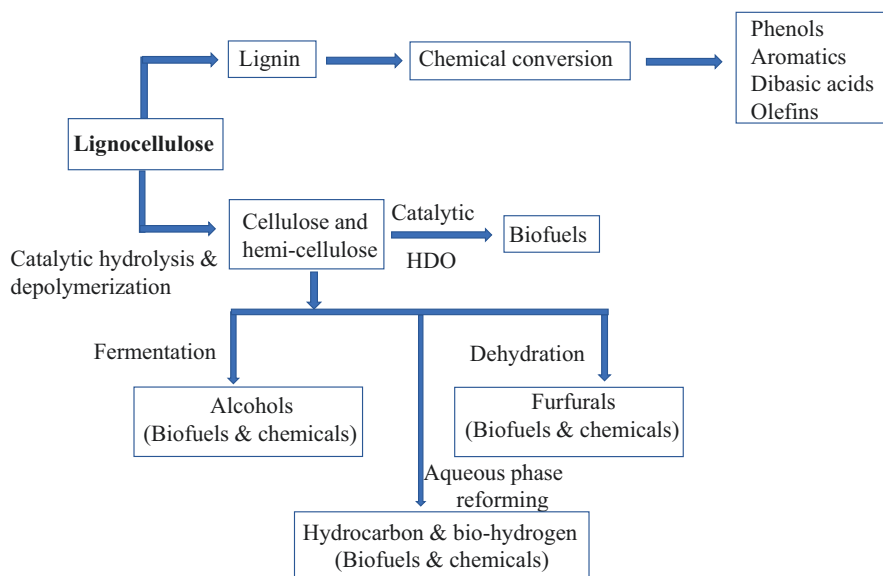
Fig. 1 Primary processing of biomass in biorefinery (Adapted from Kohli et al. [19])

namely, succinic, fumaric and maleic acids, 2,3-furan dicarboxylic acid, hydroxy propionic acid, aspartic acid, glucaric acid, glutamic acid, itaconic acid, levulinic acid, 3-hydroxy-butyrolactone, *glycerol, sorbitol and xylitol/arabinitol*, based on the importance of the final products derived from them, by utilizing the existing conversion processes [20]. With the development of novel catalysts and processes specifically for biomass conversion, a greater number of platform chemicals were identified, and the list was subsequently updated in 2010 to include *ethanol*, *furfural*, hydroxy methyl furfural, 2,5-furan dicarboxylic acid, lactic acid and isoprene, besides those considered in the earlier list [21]. Development of sustainable chemistry/processes now revolves around these platform chemicals for conversion to end products, which were otherwise being produced from fossil resources. *It is pertinent to note that as many as five biomass-derived alcohols are considered as platform chemicals.* Both sugar/starch-based and lignocellulosic feedstock-based biorefineries that follow biochemical (fermentation), thermochemical (gasification of biomass to syngas) and hybrid syngas-biochemical routes [22–25] produce a range of alcohols, rendering them as abundantly available, low-cost and carbon-neutral platform chemicals. In this scenario, several novel catalytic processes for the conversion of alcohols into biofuels and value-added products have emerged. Salient features of such bio-alcohols-based processes, process chemistry, development of catalysts and future trends are described in this chapter.

2 Chemistry of Alcohols

Alcohols (R-OH) belong to an important class of oxygenates, containing highly versatile hydroxyl (–OH) functional group(s) which are capable of undergoing a variety of chemical transformations involving cleavage of O-H or R-O bonds [26]. Variations in the molecular structure (primary, secondary and tertiary alcohols) and nature (mono-, di-, tri- and polyhydric alcohols) (Fig. 2) govern their reactivity and product selectivity for various reactions like oxidation, reduction, esterification, dehydration, dehydrogenation, nucleophilic substitution, etherification and cyclization. With the growing importance of biomass conversion processes, several other reactions of alcohols, like aldol condensation with aldehydes and ketones, acetalization, alcohol coupling and aromatization reactions are being pursued [27]. Based on the carbon number, alcohols can be divided broadly into different groups, C_1–C_2 alcohols (methanol and ethanol), C_3–C_5 alcohols (1-propanol,1-butanol, 1-pentanol) and C_6–C_{22} long-chain alcohols (2-ethyl hexanol, 1-decanol) and sugar alcohols (sorbitol, mannitol). Besides their applications as fuels/fuel additives, alcohols, in general, are used as feedstocks for numerous processes related to a wide spectrum of industrial sectors, chemical, petrochemical, polymers, pharmaceutical, fine chemicals and agro-chemicals, detergents, personal care products, lubricants and industrial solvents for various applications (inks, paints, coatings, etc.).

Fig. 2 Types of alcohols

$$CH_3OH \qquad CH_3CH_2OH$$

Methanol   Ethanol

$$CH_3CH_2CH_2OH \qquad CH_3CHOHCH_3$$

Propanol   Isopropyl alcohol

$$
\begin{array}{cc}
CH_2OH & CH_2OH \\
| & | \\
CH_2OH & CHOH \\
 & | \\
 & CH_2OH
\end{array}
$$

Ethylene glycol   Glycerol

Sorbitol
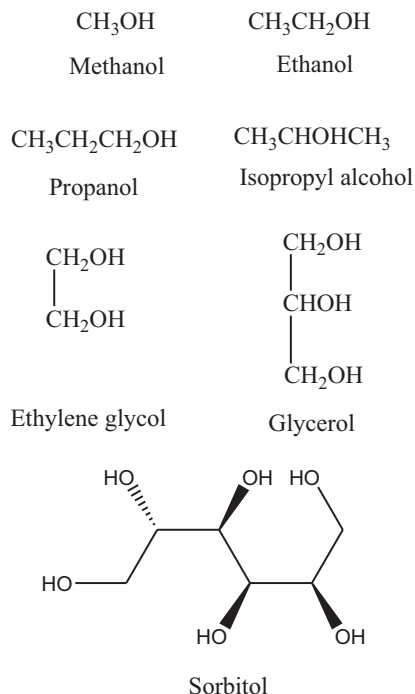
3   Production and Applications of Alcohols

Methanol, with an estimated annual consumption of 97 MMT (million metric tons) during 2019 [28], is one of the most important bulk chemical and raw materials used for the production of a number of value-added chemicals (Fig. 3). Leading global companies engaged in methanol production are BASF SE, Methanex Corporation, Mitsubishi Chemical, Mitsui & Co., Ltd. and Petroliam Nasional Berhad (Petronas). Current industrial process for the manufacture of methanol is based on fossil-derived (natural gas, coal) syngas (CO + H_2) as raw material, mostly through the low-pressure process developed by ICI (now Johnson Matthey) operating at 35–54 bar pressure and in the temperature range of 200–300 °C [29]. Details on 100 years of history of industrial methanol synthesis process and catalysts, the developments starting from the wood-based process and the classical high-pressure BASF catalytic process down to the recent ones, major products from different methanol conversion processes and their applications and its fuel characteristics and applications as fuel/fuel additives have been covered in exhaustive reviews [29–31].

As on date, investigations on fundamental aspects and development of superior methanol synthesis catalysts/process continue to be active areas of research. Such studies are highly relevant, especially in the current context, wherein the emphasis is on the use of the most abundant greenhouse gas (GHG) CO_2 in the place of CO
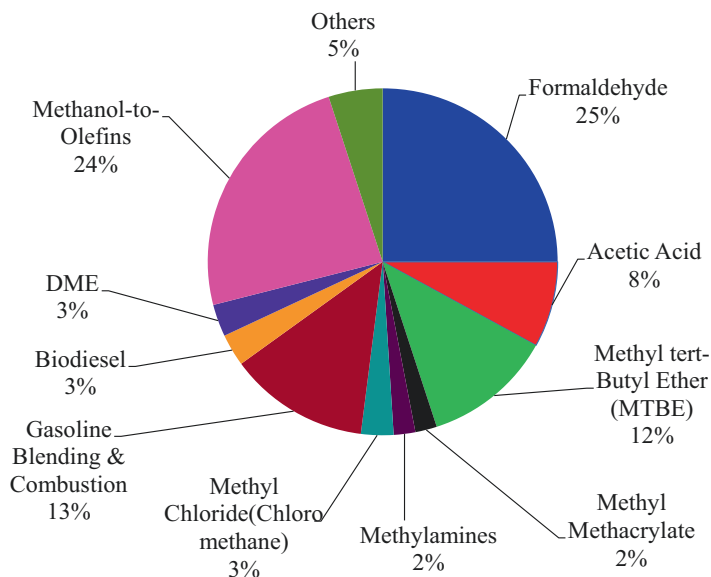
Fig. 3 Consumption pattern for methanol, product-wise in 2019 [28]

Table 1 Novel processes under development for the synthesis of renewable methanol

Company/process	Raw material
BioMCN, Netherlands	Crude glycerine, green gas, biomass, CO_2
Enerkem, Canada	Municipal solid waste
Carbon Recycling International, Iceland	CO_2 from geothermal power station and renewable H_2 by electrolysis using geothermal and hydroelectricity
Chemrec AB, Sweden	Gasification of black liquor from paper/pulp industry
Vamlandsmetanol, Sweden	Gasification of forest residue biomass
Maverick Synfuels	Biomass-derived syngas

and moving towards developing sustainable, low-carbon processes, using renewable biomass resources. The basic attributes of *green/renewable methanol* are (1) use of renewable carbon source/waste product, (2) the hydrogen used is not produced from fossil fuel sources and (3) the energy used is generated from renewable sources [32–34]. Table 1 gives a list of such efforts for developing processes that utilize syngas derived from renewable biomass resources, utilize carbon oxides from industrial waste gases and municipal solid wastes and use renewable hydrogen by electrolysis [35]. The first three processes are in the advanced stage of development. Compared to fossil-based, renewable methanol production results in 65–90% reduction in CO_2 emission, depending on the feedstock and process.

Synthesis of methanol via enzymatic routes, by oxidation of methane by methylotrophs (*Methylosinus trichosporium*) and ammonia-oxidizing bacteria (*Nitrosomonas* spp.), both using the enzyme methane monooxygenase, has been

reported [36–40]. However, the maximum methanol concentration of 1.1 g/L makes it unviable economically. Tyurin and Kiriukhin [41] could achieve more than 70 g/L methanol from a 20% CO_2/80% H_2 gas mixture in continuous fermentation using an acetogenic *Clostridium*. The process could be a totally sustainable one, when CO_2 from any waste gas stream and renewable hydrogen from water via photovoltaic-powered electrolysis are used.

With the addition of a number of renewable resources as raw materials, the cost of methanol as feedstock for chemicals and fuels is set to become competitive and hence the products there from (Fig. 4). With the continued growth of petrochemicals, increasing demand for blending in transportation fuels/additives and use as alternative fuel, consumption of methanol is expected to grow. Besides, utilization of methanol for production of ethylene and propylene by MTO process has increased significantly, from 6% in 2011 [42] to 24% in 2019 [28], indicating a shift away from energy-intensive steam cracking process and fossil-based resources for ethylene and propylene production.

Ethanol—Unlike methanol and most of the other alcohols, almost all ethanol is manufactured worldwide by fermentation process that has undergone several improvements over the years to increase the efficiency and lower the cost of production [43–46]. Broadly, three bio-based feedstocks, namely, (1) sugars (i.e. sugar cane, molasses, fruits, etc.), (2) starches (i.e. grains such as maize, root crops such as cassava) which are to be first hydrolysed to fermentable sugars, and (3) cellulose (i.e. woody material, agricultural waste, black liquor from pulp and paper) which again needs to be converted to sugars by the pretreatment with mineral acids (e.g. acid or enzymatic hydrolysis), are being used. Historical developments in the processes for the production of ethanol through the first-, second-, third- and fourth-generation bioethanol, utilizing different feedstocks/routes, have been covered extensively in literature [47–51]. A simplified representation of the bioethanol
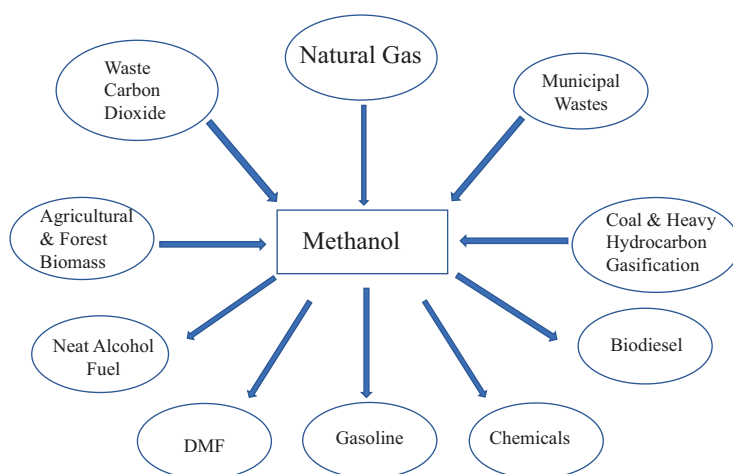
Fig. 4 Methanol – raw materials and major products

manufacturing processes through the generations and the primary process steps involved therein are given in Fig. 5 [49].

Global ethanol production has increased steadily from around 75 billion litres in 2007–2009 to 160 billion litres in 2019 [52] with coarse grains and sugar cane being the major feedstock and the USA and Brazil making up >80% of global production (Fig. 6). Corn/grains and sugar cane are food based and specific to the USA and Brazil. Amongst the feedstocks used for bioethanol production, non-food lignocellulosic biomass is the most promising one, due to its abundancy, low cost and availability of appropriate process technology. However, the cellulosic process for the production of bioethanol is complex in nature involving several steps, and hence its price as biofuel is not competitive in comparison with fossil fuels and its utilization as raw material for the production of bio-derived ethylene. Recently an attractive strategy [53] to lower the cost has been proposed, wherein besides ethanol, other value-added chemicals could be produced as co-products.

Of recent, fermentation processes that use syngas derived from biomass, industrial wastes and municipal solid wastes are being explored vigorously due to the potential advantages in cost and low-carbon character [54]. Gas fermentation technologies at pilot scale and demonstration plants have been set up by companies Coskata, INEOS Bio and LanzaTech [55, 56] with the ultimate objective of commercial production. Availability of bioethanol in plenty from various biomass resources and development of processes for ethanol conversion to building block chemicals and key chemical intermediates (Fig. 7) have rendered it as a highly valuable and versatile platform chemical [56].
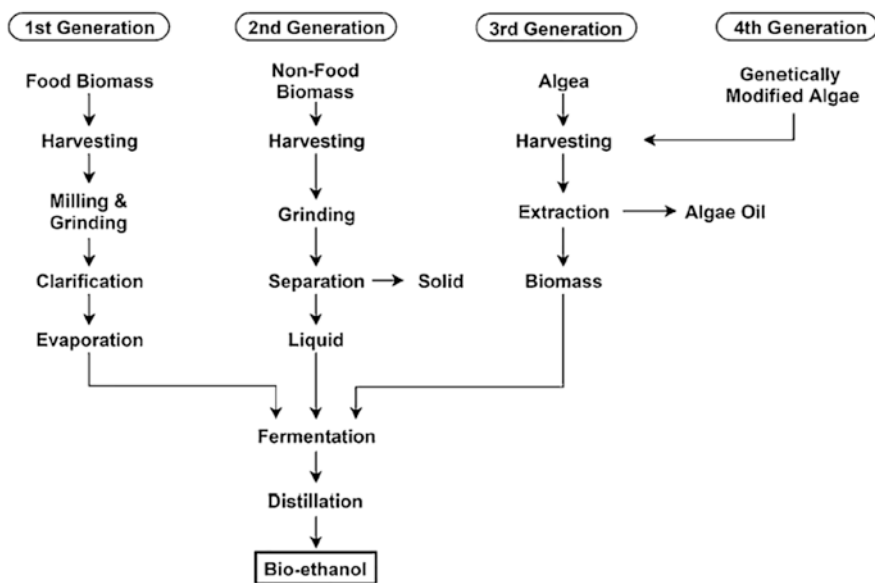
Fig. 5 Process steps involved in the production of bioethanol (Reproduced from Alalwan et al. [49])
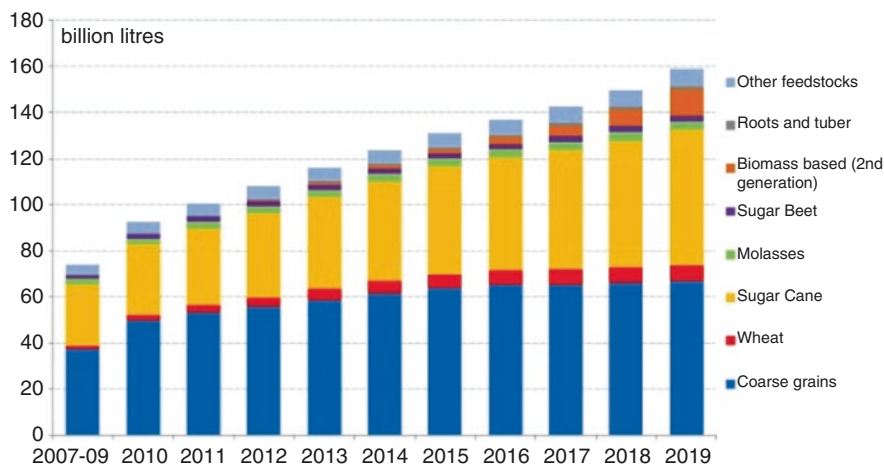
Fig. 6 Global ethanol production (2007–2019) [52]
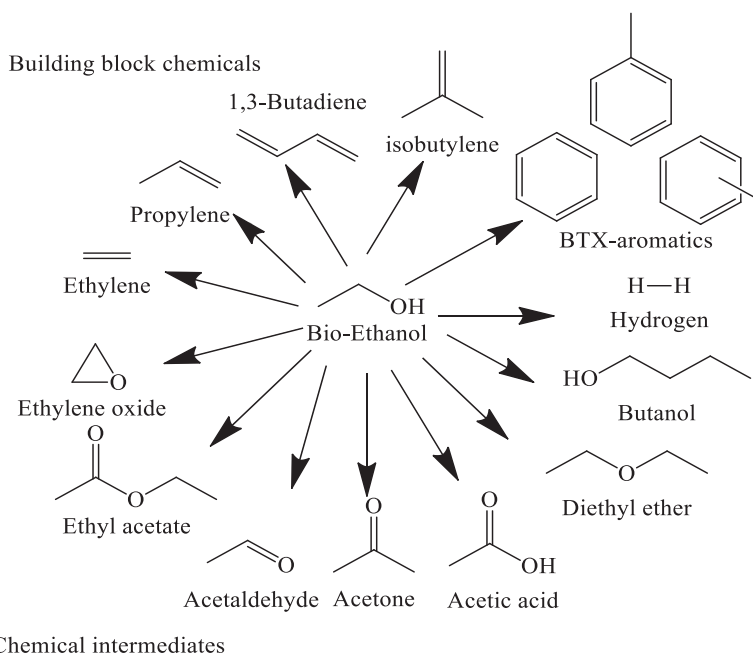
Fig. 7 Bioethanol—a versatile platform chemical (Adapted from Kuhz et al. [56])

Amongst *C₃ alcohols*, *1-propanol* is produced by hydrogenation of propanal, which, in turn, is manufactured from ethylene by hydroformylation process [57]. Attempts have been made for the production by microbial routes [58], and the best yield 10.8 g/L has been realized for the process using a recombinant *E. coli* as host

[59]. 1-Propanol finds applications [57] as a solvent, antimicrobial agent and chemical intermediates for the production of value-added products.

There are two different routes for the manufacture of *isopropanol*, (1) indirect hydration of propylene with H_2SO_4 via a mixture of mono- and di-isopropyl sulphate esters and (2) direct hydration of propylene over an acidic heterogeneous catalyst [56]. Its applications include use as a solvent in inks and surfactants, as a chemical intermediate and as a cleaning fluid [57]. Microbial processes for isopropanol production, including *Clostridium beijerinckii*, engineered *E. coli* and engineered *Clostridium acetobutylicum* [60, 61], have been reported.

C_4 alcohols, namely, *1-butanol (n-butanol)*, *2-butanol (secondary butanol)*, *2-methyl propanol (isobutanol) and 2-methyl 2-propanol (tertiary butyl alcohol)*, are highly versatile in terms of applications as solvents, in manufacturing of chemical intermediates and as fuel additives. Details on the manufacturing of *1-butanol, 2-butanol and 2-methyl propanol* by conventional chemical as well as microbial routes and typical applications have been described by Kunz et al. [56]. *2-Methyl 2-propanol* (tertiary butyl alcohol) is produced by hydration of isobutylene [62]. Its reaction with methanol/ethanol results in methyl tertiary butyl ether (MTBE)/ethyl tertiary butyl ether (ETBE), useful as octane booster and oxygenate for blending with gasoline. Tertiary butyl hydroperoxide (TBHP) is another useful chemical intermediate.

Amongst C_4 alcohols, *1-butanol* has the unique distinction of being highly useful raw material/chemical and the most efficient gasoline additive. 1-Butanol is considered as the next-generation biofuel [63, 64] with several advantages over ethanol (Table 2), such as higher energy density (29.2 vs. 19.6 MJ/L), lower volatility and solubility in water and non-corrosive nature. Besides, butanol blends well with gasoline and with higher air-to-fuel ratio results in more efficient combustion [65–69]. 1-Butanol finds widespread applications in chemical industry, in the manufacture of butyl acrylate, butyl acetate, glycol ethers and plasticizers and as solvent in the manufacture of coatings, paintings, engineering plastics, super absorbent polymers, adhesives and sealants. With the increase in the consumption of 1-butanol for these applications, its market has been expanding over the years. n-Butanol market, estimated at US$ 3.89 billion in 2016, is projected to touch US$ 5.58 billion by 2022, at a CAGR of 5.9% [70].

Currently, 1-butanol is produced from propylene by the oxo process [71, 72], which is based on the use of the raw material derived from non-renewable resources. Availability of bioethanol in plenty and at low cost has triggered global research

Table 2 Fuel characteristics of 1-butanol vs. other fuels (Adapted from Gautam and Martin [65])

Fuel	Energy density (MJ/L)	Air-to-fuel ratio	Energy content/ Btu/US gallon	Research octane number	Water solubility (%)
Gasoline	32	14.6	114,000	81–89	Negligible
Diesel	35.5	14.7	130,000	nd	Negligible
Butanol-1	29.2	11.12	105,000	78	7
Ethanol	19.6	8.94	84,000	96	100

efforts on the development of sustainable chemical catalytic processes for the conversion of bioethanol to 1-butanol via classical Guerbet chemistry [73, 74]. A number of reviews covering in detail the development of both homogeneous and heterogeneous processes and catalysts for the conversion of ethanol to 1-butanol have been published [56, 75–77]. Several types of heterogeneous catalysts, based on MgO, Mg−Al-O mixed oxides, Cu/CeO$_2$, basic zeolites, hydroxyapatite, solid acid-supported Cu and alumina- and carbon-supported metal catalysts, in batch and continuous-flow mode, under different reaction conditions, have been explored [77]. 1-Butanol yields in the range 20–30% could be obtained with heterogeneous catalysts [77] along with the formation of C$_{4+}$ alcohols. With Ru-based homogeneous catalysts, n-butanol selectivity as high as 94%, but at very low ethanol conversion of 22% (21% yield of butanol), has been reported [78]. Thus, achieving high yields of 1-butanol remains a challenge. Increase in demand for 1-butanol has led to the revival of one of the oldest known fermentation processes, ABE (acetone-butanol-ethanol) process for production of 1-butanol, using different strains of *Clostridium* sp. with glucose, starch, molasses, corn stover, rice straw and cranny grass as feedstocks [79–81]. Different types of biomass feedstocks, microorganisms, biomass pretreatment methods, extraction methods, genetic engineering techniques like cell recycle and cell immobilization and strategies to minimize product inhibition have been adopted to improve butanol yield [82–84]. Using starch-based packing peanuts as substrate for continuous production with *C. beijerinckii* BA101strains, 18.9 g/L of butanol could be produced from 80.0 g/L of the substrate within 110 h, indicating the crucial role played by the selection of substrate and microbial strain [85].

C$_2$, *C$_3$* and *C$_4$ diols* are highly useful chemical intermediates which can be transformed into a number of value-added products. *Mono ethylene glycol* (MEG) is manufactured by hydrolysis of ethylene oxide, which in turn is produced by catalytic oxidation of ethylene. Major application of MEG is as the monomer in the manufacture of polyester fibre and polyethylene terephthalate (PET), PTA being the other monomer. Other minor applications include anti-freeze and coolants, solvents and chemical intermediates (Fig. 8).

With the growing emphasis on sustainable products, bio-based PET is being manufactured, using bio-MEG produced using ethylene obtained by dehydration of bioethanol. *PlantBottle*, made from PET using bio-MEG and PTA, was introduced by Coca Cola [56, 87] in 2009. Global market for bio-based PET (containing 30% bio-MEG and 70% PTA) is expected to touch 5.8 million tons by 2020 and consequently help in moving towards sustainable packaging applications. Global sustainable packaging market on the same lines is expected to grow from US$ 200.00 billion in 2014 to US$ 267.00 billion in 2020, with a CAGR of 4.9%.

*C$_3$ diols***,** namely, *1,2 and 1,3 propane diols* are valuable monomers for the production of polyesters, polycarbonates and polyurethanes, besides having applications as anti-freezing agents, additive in nutrition products, solvents and component of hydraulic fluids [56]. 1,3-Propane diol (1,3 PDO) on polymerization with terephthalic acid yields commercial polyesters, SORONA® (from DuPont) and CORTERRA® (from Shell), which are used in the manufacture of high-quality carpet and textile fibres. While 1,2-PDO is produced by selective hydrolysis of

Fig. 8 Applications of mono ethylene glycol [86]
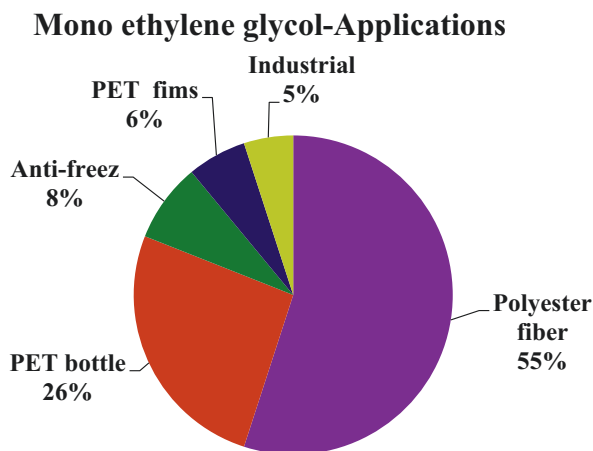
propylene oxide in presence of ion-exchange resin catalysts at 150–180 °C [88, 89], 1,3-PDO is manufactured [90–92] either by Shell process from ethylene oxide or acrolein by DuPont process. Several microbial processes for the production of both 1,2- and 1,3-propane diols [56] using a variety of microorganisms and feedstocks (glucose, glycerol, sugars) have been reported. Notable amongst them is DuPont/ Tate & Lyle process [93], in which two conversions, glucose to glycerol by recombinant *E. coli* and conversion of glycerol to 1,3-PDO by *Klebsiella* strains, are combined. The process was first commercialized in 2006, and the capacity was expanded to 65,000 MTA. Similarly, microbial process for the conversion of glycerol to 1,2-PDO using *E. coli* [94] as the microorganism was developed.

Emergence of biomass conversion processes to fuels and chemicals and the large-scale availability of biodiesel-derived *glycerol* as an important platform molecule paved way for the development of sustainable processes for the production of a number of important chemicals and chemical intermediates from glycerol [91, 95–97].

Catalytic processes for the hydrogenolysis of glycerol to yield selectively either 1,2- or 1,3-PDOs have been reported [98–102]. Nakagawa and Tomishige [98] investigated hydrogenolysis of glycerol on four different types of catalysts, namely, non-noble metal catalysts, noble metal catalysts with an acid as an additive, noble metal catalysts combined with a base and metal oxide-modified noble metal catalysts, and observed that only metal oxide-modified noble metal catalysts were selective for 1,3-PDO while the other three catalysts displayed high selectivity for 1,2-PDO. Accordingly, Arundhathi et al. [100] observed that hydrogenolysis of glycerol on Pt-WO$_x$/AlOOH yields 1,3-PDO with 66% selectivity. Reaction pathways leading to the formation of 1,2- or 1,3-propane diol have been proposed by Nakagawa and Tomishige [98]. Selection of suitable catalyst and reaction conditions for glycerol hydrogenolysis leads to the formation of 1,2- or 1,3-propanediol (Fig. 9).
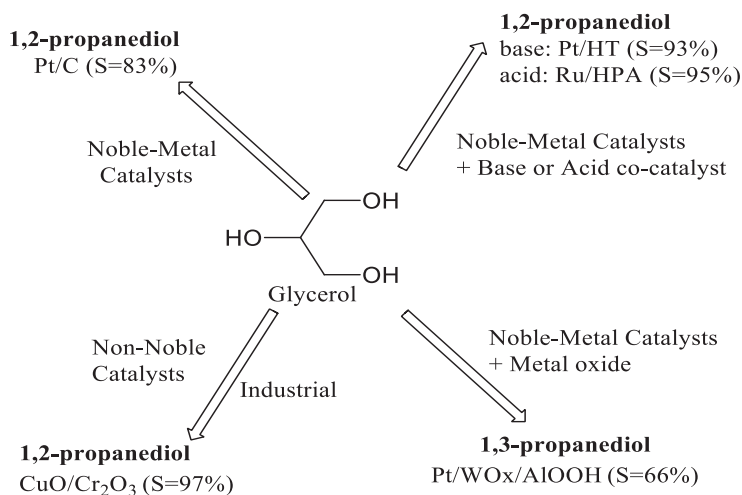
Fig. 9 Selective hydrogenolysis of glycerol to 1,2- and 1,3-propanediols (Adapted from Kuhz et al. [56])

Of the four isomers of *butane diol (BDO)*, 2*,3- and 1,4-BDO* have a wide range of applications, while *1,2- and 1,3-BDO* have relatively limited range of use. While 1,2-BDO is used for the production of polyester resins and plasticizers, the main application of 1,3-BDO is as solvent for food flavouring agents and as co-monomer for some of the polyurethane and polyester resins [103–105].

Amongst the C_4 diols, *2,3-BDO* is perhaps one of the most useful bio-based feedstock chemical intermediates, with applications on several sectors. *2,3-BDO* on dehydration yields 1,3-butadiene, the monomer for synthetic rubber production or methyl ethyl ketone (MEK), useful as solvent and fuel additive. 2,3-BDO itself can serve as an "octane booster" for gasoline and, due to its lower freezing point (−60 °C), anti-freeze agent as well. Diacetyl, a highly valued flavouring agent that protects against bacterial attack, is made by dehydrogenation of 2,3-BDO [106]. Esters of 2,3-BDO and maleic acid are used for polyurethane/maleimide with cardiovascular applications [107]. 2,3-BDO esters are also useful for pharmaceuticals and cosmetics applications. Though 2,3-BDO is produced by chemo-catalytic route via butene-chlorohydrin pathway [56, 108], manufacturing by biotechnological routes using renewable biomass feedstocks and biomass wastes has recently become prominent. Several reviews covering significant developments in the microbial production of 2,3-BDO have been published [109–112]. 1,4-BDO is produced through Reppe chemistry by reaction between acetylene and formaldehyde to form 1,4-butyene diol, which is subsequently hydrogenated to yield 1,4-BDO. Hydroformylation of propylene, hydrogenation of maleic anhydride and dichloro-butene process from 1,3-butadiene or the 1,3-butadiene-acetic acid are the other processes for the manufacture of 1,4-BDO [109, 113]. With the identification of succinic acid as one of the platform chemicals from the biomass refinery, synthesis of 1,4-BDO by reduction of succinic acid as a sustainable process has gained

prominence. Microbial routes for 1,4-BDO using engineered *E. coli* microorganisms have been developed up to demonstration scale [114–116]. Major applications of 1,4-BDO include synthesis of gamma butyrolactone, use as solvents and in the manufacture of plastics, fibres and polyurethanes.

C4 and C5 alcohols and diols are highly valuable chemical intermediates used as monomers in the production of polyesters, polyurethanes and polyethers, as fuel additives to boost gasoline octane number and as versatile solvents for various applications. Several process options for the synthesis of C_{5+} *alcohols/higher alcohols/fatty alcohols* are available. Some of the processes developed earlier include [56, 117]:

- Hydrogenation of fatty acids and fatty acid esters derived from vegetable and animal fats and oils.
- Conversion of ethylene with Al alkyls, Al $(CH_2CH_3)_3$ to a mixture of linear, primary alcohols (Ziegler process).
- Hydroformylation of olefins with CO and H_2 to a mixture of branched and unbranched aldehydes and subsequent hydrogenation to the corresponding alcohols.
- Oxidation of paraffins with boric acid to linear, secondary alcohols.
- Condensation of primary alcohols C_2–C_4 with basic catalysts to α-branched and linear, dimeric alcohols based on Guerbet chemistry [118].

Of recent, advances in the development of biomass conversion processes have brought into focus more process options:

– Oligomerization of ethylene derived from bioethanol and bio-methanol conversion through MTO to higher carbon number olefins followed by oxo synthesis and hydrogenation [119–121].
– Condensation of biomass-derived methanol and ethanol to higher alcohols via Guerbet chemistry [118, 122], self-condensation and cross-condensation reactions.

Biomass-derived platform chemicals/intermediates have been used as raw materials for the sustainable production of C_4–C_5 alcohols and diols. A comprehensive review by Sun et al. [123] describes in detail the processes and catalysts developed and other features for the synthesis of C_4–C_5 alcohols and diols from various biomass-based raw materials, like succinic acid, dialkyl succinates, γ-butyrolactone, levulinic acid and alkyl levulinates, γ-valerolactone and furfural and its derivatives.

Since many years, *syngas* has been another rich source for the production of higher alcohols and versatile in application, since it can be obtained from different raw materials, both fossil and biomass based, with several syngas conversion options therein. An extensive review, by Luk et al. [124], covering various process options for the conversion of syngas to higher alcohols, the catalysts and structure-activity correlations therein and the process features, (Fig. 10) along with the details on the applications of C_6–C_{22} long-chain alcohols [125] as feedstocks and chemical intermediates and in polymers, surfactants and detergent industries, has been published.
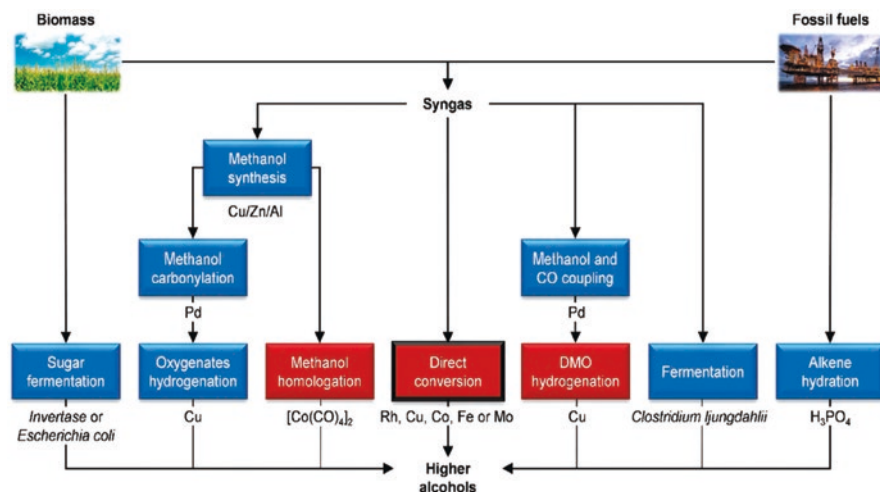
Fig. 10 Syngas conversion to higher alcohols—Process options (Reproduced from Luk et al. [124])

While the classical routes for higher alcohols like direct conversion of syngas and indirect routes like methanol homologation, methanol-CO coupling and methanol carbonylation are still relevant (Fig. 10), several novel routes like alkene hydration, sugar fermentation [126, 127] and, more recently, direct syngas fermentation are emerging as viable and more efficient routes with low carbon footprint. Diender et al. have reported [128] production of C_4–C_6 fatty acids and alcohols from a mixture of syngas and CO, using co-culture consisting of *Clostridium autoethanogenum* and *Clostridium kluyveri*.

Sugar alcohols/polyols/polyhydric alcohols, with the general formula $H_2(CH_2O)_{n+1}$, are well-known biomass-derived chemicals with widespread applications as chemical intermediates and platform chemicals (sorbitol, xylitol and arabinitol) [20, 21]. Mannitol and erythritol are the other two important sugar alcohols [56]. Besides their main use as artificial sweeteners in food, beverages and confectionary, sugar alcohols find applications in polymers, pharma and cosmetics industries [22]. Global consumption of sugar alcohols is projected to grow from 1.6 million metric tons in 2017 to 1.9 million metric tons by 2022 at a CAGR of 3.4% [56, 129]. Sugar alcohols are produced, in general, through hydrogenation or fermentation of mono- or disaccharides [130–132]. While sorbitol and mannitol are synthesized by hydrogenation of sucrose, glucose and fructose [131], xylitol can be produced by hydrogenation of xylose and erythritol by fermentation of glucose [22, 133–135]. Cellulose and hemicellulose, the two major components in biomass, are hydrolysed to glucose, mannose and xylose, which undergo further hydrogenation to yield sugar alcohols as shown in Scheme 1. An extensive review of the catalytic processes for the conversion of glucose, mannose and xylose to sorbitol, mannitol and xylitol, respectively, has been presented by Zada et al. [136]. Detailed studies
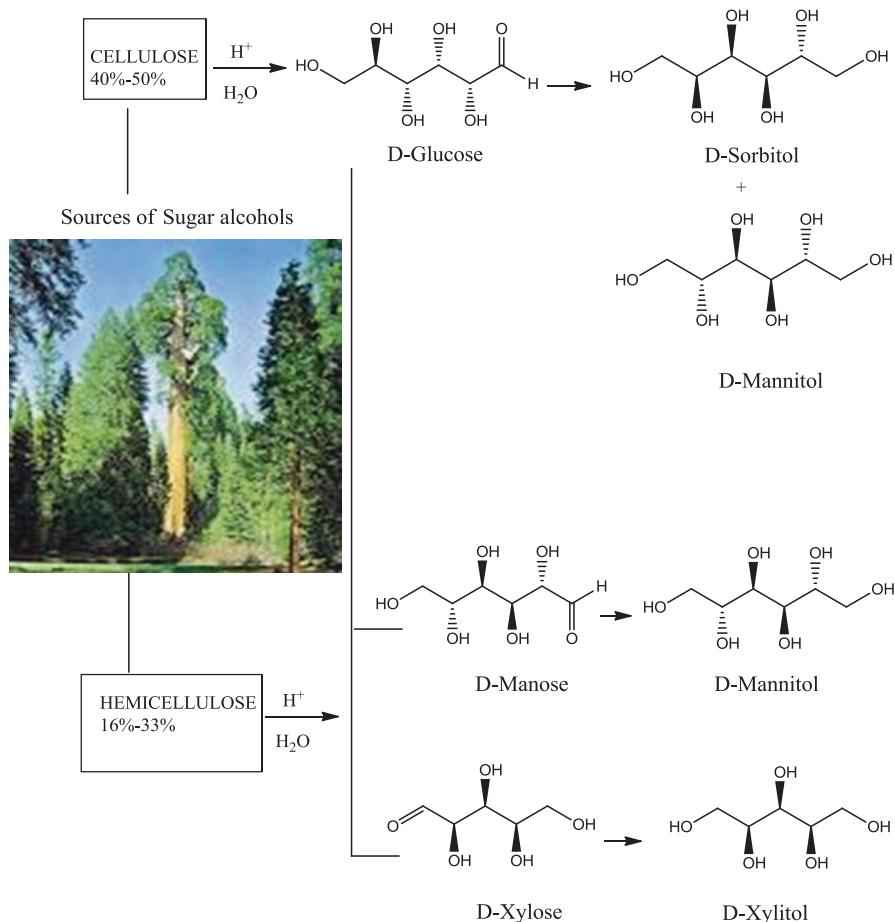
Scheme 1 Conversion of cellulosic biomass into sugar alcohols (Reproduced from Zada et al. [136])

on a number of noble metal, non-noble metal and bimetallic catalysts on various supports, along with the activity, selectivity and yield data, have been covered in the review. Different types of catalysts for the production of sugar alcohols by hydrogenation and hydrogenolysis of mono- and disaccharides have been described in another review by Ruppert et al. [92]. Erythritol, a C_4 sugar alcohol, is obtained from pentose sugars (xylose and arabinose) by selective cleavage of C-C bond. Several homogeneous and heterogeneous catalysts have been explored [136] for this process which requires mild reaction conditions (<180 °C temperature and <60 bar hydrogen pressure) to minimize side reactions and achieve selective C-C bond cleavage to yield erythritol [137, 138]. Several microbial processes for the production of sugar alcohols have been described in a review by Kunz et al. [56].

4 Value-Added Products from Alcohols

Abundant availability of nearly complete range alcohols, at low cost, derived mostly from renewable biomass resources, has provided a great impetus for the development of a number of catalytic processes for their conversion into value-added products. Processes for the manufacture of whole range of chemicals that include building block chemicals (olefins and aromatics), oxygenates (aldehydes, ketones, acids, ethers, esters, amides) and fuels (gasoline, diesel, jet fuel and fuel additives) with alcohols as feedstocks have been explored, thus making them as the most versatile group of platform molecules. Salient features of such processes and advances therein are described in the following pages. However, well-established applications of alcohols like conversion of methanol to formaldehyde, acetic acid and MTBE are not covered.

4.1 Conversion of Methanol to C_2–C_3 Olefins

Global demand for ethylene and propylene is estimated as 152 MMT (million metric tons) and 102 MMT, respectively, in 2017 and is projected to reach 185 MMT and 127 MMT by 2022 [139]. Building block olefins like ethylene and propylene along with 1,3-butadiene and butenes (1-, 2- and iso-) are the raw materials for commodity petrochemicals and polymers, and the current dominant route for manufacturing is by highly energy-intensive thermal steam cracking (SC), using non-renewable fossil-based raw materials, ethane/propane or naphtha.

Methanol to olefins (MTO) process developed by UOP-Hydro [140] provided the first commercially viable alternative route for SC process. Based on the tailor-made SAPO-34 catalyst [141–143], the process operates in the temperature range 340–540 °C at 0.1–0.3 MPa pressure, in a fluidized bed reactor (Fig. 11) coupled with catalyst regenerator, considering the deactivation characteristics of the catalyst [144]. Appropriate pore size (3.8 Å), to minimize the formation of higher carbon number products, and optimized acidity, to control the formation of paraffins by hydride transfer, are the key catalyst characteristics responsible for 75–80% carbon-based combined selectivity towards ethylene and propylene. By varying the process conditions, maximization of ethylene or propylene yield could be achieved. Besides ethylene and propylene, small amounts of C_4–C_{6+} olefins are generated. In the advanced version of the process, Olefins Cracking (OC) process technology, developed by Total Petrochemicals [145], which involves routing the by-product C_4–C_{6+} olefins stream through a catalyst bed for further cracking to ethylene and propylene, was integrated with MTO process. This additional process step increases the overall yield of ethylene and propylene and reduces by-products' formation.

With further modifications in the catalyst formulation to maximize propylene, propylene/ethylene ratio >2 (Fig. 12) could be achieved [146]. Similar MTO processes, D-MTO and D-MTO-II (from Dalian Institute of Chemical Physics, DICP,
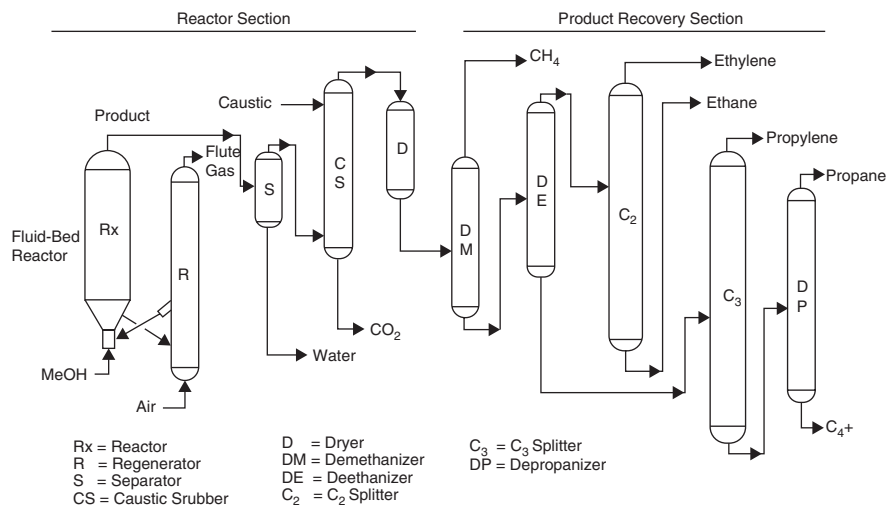
Fig. 11 Simplified process flow diagram for UOP-Hydro MTO process (Reproduced from Keil [144])
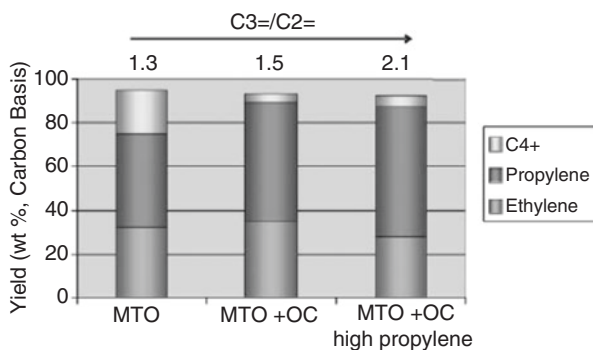
Fig. 12 Increase in propylene/ethylene ratio by integration with OC technology and catalyst optimized for high propylene (Reproduced from Chen et al. [146])

China) and S-MTO (from SINOPEC, China), have been developed and proven on commercial scale [147, 148].

Extensive research work on the mechanism of MTO process under different process conditions (temperature and LHSV) and using $C^{13}H_3OH$ for tracing the reaction pathway by Dahl and Kolboe [149] resulted in the proposal of *hydrocarbon pool mechanism* for the process (Fig. 13).

Comprehensive reviews [147, 148, 150, 151] tracing the first discovery of the MTO process by researchers from Mobil Corporation on ZSM-5 catalysts [152] and the discovery of SAPO-34 catalyst by Union Carbide scientists and further in-depth research work on the catalyst and process development by UOP-Hydro that finally
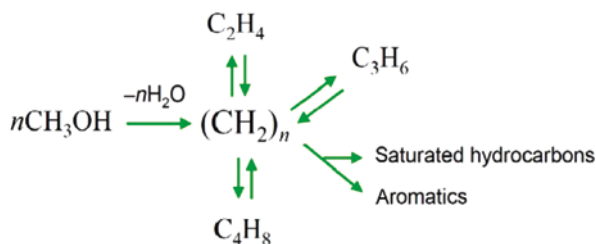
Fig. 13 Hydrocarbon pool mechanism for MTO process. Reproduced from Dahl et al. [149]

lead to the commercialization of the process and the intricacies in the synthesis of SAPO-34 with appropriate structure and topology have been published. MTO process has several advantages in comparison with gas/naphtha steam cracking like:

– Lower reaction temperature.
– Easier separation and purification of products.
– Relatively less capital investment.
– Feedstock flexibility.

Raw material (syngas) for methanol could be obtained from different resources: biomass or coal, waste gases, etc. Since methanol could be obtained from syngas derived from coal gasification, the process is named as CTO (*coal to olefins*), and a commercial plant based on this technology with 0.6 MMTA capacity for ethylene/propylene has been set up by China Shenhua Energy, China [148].

Another process for the conversion of methanol into building block chemicals is the *methanol to propylene (MTP)* process technology developed by Lurgi AG [153].

In the late 1990s, availability of natural gas in plenty led to setting up MegaMethanol plants (5000 MT/day) by Lurgi [154]. With the knowledge base available at that point of time on MTO process using ZSM-5 catalyst [149, 152], Lurgi developed MTP processes to selectively produce propylene, by using suitably modified ZSM-5 catalyst. The process [153, 155] uses a series of adiabatic fixed bed reactors (Fig. 14), wherein methanol is converted to dimethyl ether (DME) at near thermodynamic equilibrium in the pre-reactor. Feed consisting of methanol, DME and water pass through five to six reactors loaded with highly selective and stable ZSM-5 catalyst at 1.3–1.6 bar pressure and 400–450 °C temperature along with recycle olefin stream and steam, to ensure stability of the catalyst. >99% conversion of methanol and DME is achieved with carbon-based propylene selectivity of >70% along with some quantity of gasoline as by-product. After 500–600 h of operation, the catalyst needs regeneration in situ, by controlled coke burning. According to the established material balance, with 1.67 MTA of methanol as feed, 474,000 MT of propylene and 185,000 MT of gasoline could be produced. The first commercial plant using MTP process technology was established in 2011 in China followed by two more plants, and now it is considered as proven technology for on-purpose propylene production [156]. A techno-economic evaluation [157] of MTO vs. MTP has shown that both processes are equally viable, subject to variations in natural
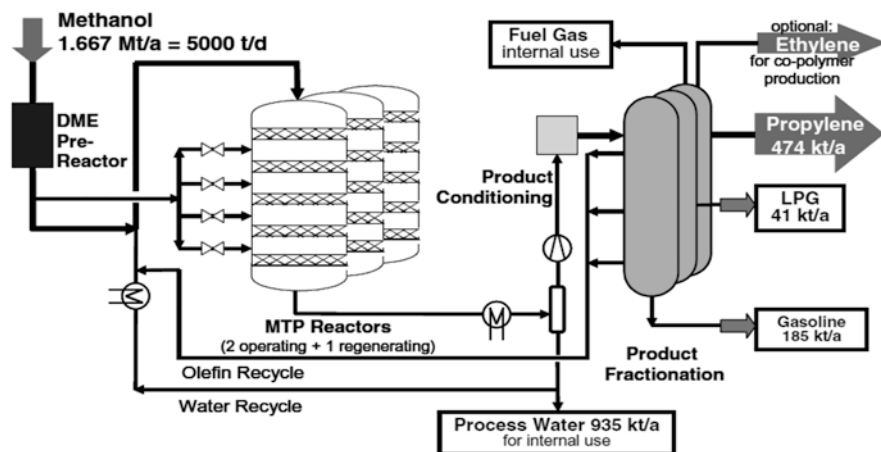
Fig. 14 Process flow diagram for methanol To propylene (MTP) plant (Adopted from Koempel et al. [153])

gas/methanol and products' prices, and MTP has slight advantage in terms of lower CO_2 emission (MT/MT of propylene). Though CTO process may have some advantage due to low-cost coal as raw material, high emission of chemical as well as energy-related CO_2 renders the process environmentally unfriendly [158].

4.2 Conversion of Ethanol to Ethylene

MTO, MTP and CTO processes utilize methanol produced from non-renewable resources. Availability of large quantities of bioethanol at low cost has resulted in the development of catalytic processes for the production of *C_2–C_4 olefins from bioethanol*. Production of *ethylene by catalytic dehydration of ethanol/bioethanol* was established long ago [159, 160], but biomass-derived ethylene as feedstock for petrochemicals was not cost-effective vis-à-vis ethylene from steam cracking [161]. Abundance of bioethanol from different biomass resources (corn, sugar cane and cellulosic biomass) revived the interest in bioethanol conversion to ethylene.

Ethanol dehydration being endothermic in nature (45.7 kJ/mole) requires reaction temperatures in the range 300–500 °C. While acetaldehyde is formed by dehydrogenation at higher temperatures, diethyl ether is formed at temperatures below the optimum. Besides, the product water also influences the reaction. Hence, controlling reaction temperature and maintaining optimum contact time are needed to minimize side reactions.

In practice, isothermal and adiabatic fixed bed and fluidized bed reactors have been considered [163, 164]. Different types of catalysts, like modified alumina, modified HZSM-5, SAPO-34, MCM-41 and modified heteropoly acid catalysts, have been explored, mainly to minimize by-products' formation and improve the

Table 3 Selected catalysts for dehydration of ethanol to ethylene (Adopted from Fan et al. [162])

Catalysts	Ethylene selectivity, %	Ethanol conversion, %	Reaction temp., °C	LHSV[a]/ WHSV[b]/ GHSV[c], h^{-1}	Lifespan, stability
TiO_2 /γ-Al_2O_3	99.4	100	360–500	26–234[a]	400 h, stable
0.5% La-2% P-HZSM-5	99.9	100	240–280	2[b]	Very stable
Nano-CAT	99.7	100	240	1[b]	630 h, very stable
$Ag_3 PW_{12}O_{40}$	99.2	100	220	6000[c]	Stable in 9% humidity
TPA-MCM-41	99.9	98	300	2.9[b]	Very stable
STA-MCM-41	99.9	99	250	2.9[b]	Stable
TRC-92	99.0	70	280	2.9[b]	Very stable
SynDol (Halcon) (SD, USA)	96.8	99	450	26–234[a]	Very stable

[a]Liquid hourly space velocity (LHSV)
[b]Weight hourly space velocity (WHSV)
[c]Gas hourly space velocity (GHSV)

stability of the catalyst [162]. A list of catalysts that display nearly 100% ethanol conversion with ~99% selectivity for ethylene is presented in Table 3.

Commercial plants, which are in operation for the production of ethylene from bioethanol are America Halcon Scientific Design Inc., USA (with Synthol catalyst, Al_2O_3-MgO/SiO_2); British Petroleum (Hummingbird process, heteropoly acid catalyst); Axens (Atol process); Chematur; Braskem, Brazil; and Dow Chemical [162, 164–166]. Though the processes could be operated with very high efficiency, cost of ethylene from bioethanol is higher in comparison with ethylene from steam cracking (SC) process due to higher cost of bioethanol and very high energy efficiency realized in mega-scale ethylene plants based on SC.

4.3 Conversion of Bioethanol-Derived Ethylene to C_3, C_4 Olefins

As illustrated by Hulea [165], well-established olefins conversion processes like dimerization, metathesis, oligomerization, isomerization, cracking and aromatization could be applied for the conversion of bio-based ethylene to value-added products (Fig. 15).

Both homogeneous and heterogeneous catalysts have been studied extensively [167, 168] for the *dimerization of ethylene to 1-butene*, an important co-monomer in the manufacture of commodity polyolefins, like linear low-density polyethylene (LLDPE). Commercial process for the manufacture of 1-butene, the *AlphaButol* technology developed by Axens and SABIC, is based on highly selective (93%)
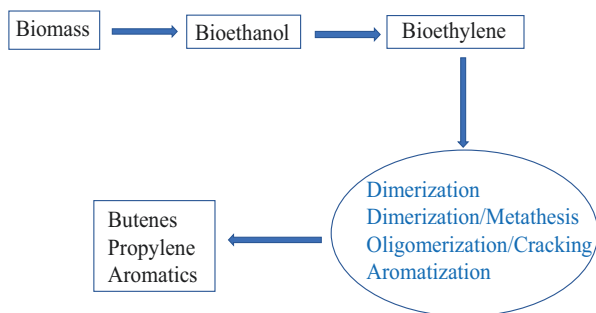
Fig. 15 Process options for the conversion of biobased ethylene to value-added products (Reproduced from Hulea [165])

homogeneous catalyst $Ti(OBu)_4$ with $AlEt_3$ as the co-catalyst. Metal complexes based on Ni, Ti, Zr, Cr, Co and Fe with different co-catalysts in homogeneous medium have been explored for selective *dimerization and oligomerization of ethylene* [168–171]. Such homogeneous catalyst systems, though highly active and selective under mild reaction conditions, require the use of aluminoxane activators or co-catalysts in large amounts and use of solvents/reactants in bulk liquid phase. Besides, many of the metal complexes are not air stable and undergo structural degradation and deactivation, requiring complex regeneration procedures, thus limiting their applications in large-scale continuous mode processes. In order to circumvent such limitations and realize the specific advantages that heterogeneous catalysts offer on these aspects, several types of catalysts in heterogeneous phase, like (a) metal complexes immobilized on polymers and oxides, (b) metal-organic framework (MOF) and covalent organic framework (COF) materials and (c) nickel and palladium supported on inorganic porous materials, have been explored [165]. Nickel metal complexes supported on polymers and inorganic supports like alumina, silica and other zeolites like $AlPO_4$ and Al-MCM-41 display good activity and selectivity for ethylene dimerization, but stability of the active phase during the process and loss of selectivity due to acid-catalysed side reactions on the support that lead to deactivation are the issues. Similarly, metal complexes supported on MOF and COF materials with well-defined chemical environments to promote dimerization and oligomerization are found to be highly active and selective, but the deactivation due to heavier oligomers/polymer formation is the challenge.

In this context, nickel and palladium supported on inorganic porous materials exhibit exceptional performance in ethylene dimerization and oligomerization [168, 172, 173].

Zeolites, sulphated alumina, amorphous silica-alumina and mesostructured MCM-41, MCM-48, SBA-15 and MCM-22 are the supports on which nickel is incorporated by ion exchange as envisaged in the illustration (Fig. 16). Exchangeable Na^+ ions are first exchanged with NH_4^+ ions followed by ion exchange with Ni^{2+} ions and then calcined in air at 550 °C. On thermal treatment, isolated Ni^+ and dehydrated Ni^{2+} species are formed which act as oligomerization sites, and the support

provides the acid sites. Such high-temperature treatment ensures thermal stability of the catalyst at temperatures up to 160 °C and pressures up to 40 bar. Besides the reaction could be carried out in liquid phase in slurry mode—gas-solid-liquid – or continuous-flow mode. Mesoporous character of the support leads to facile diffusion of the reactant and products resulting in lower deactivation and higher activity. Besides the chemical nature and acidity, the texture and topology of the mesoporous supports influence the oligomerization activity [174].

For example, Agirrezabal-Telleria and Iglesia [175] observed that Ni-MCM-41 is a very active and selective dimerization catalyst at sub-ambient temperature (243–258 K) with 93% selectivity for 1-butene and TOF > 10 s^{-1} with very little deactivation. The high catalyst activity and stability as well as the C_4 selectivity were attributed to the presence of the ethylene in liquid phase within MCM-41 channels.

Conversion of *ethylene to propylene* is an important process in petrochemical industry considering the supply-demand gap for propylene. Several proven *on-purpose* processes like dehydrogenation of propane, methanol to olefins (MTO) and methanol to propylene (MTP) are available for on-purpose propylene production. Conversion of ethylene to propylene could be achieved through different processes:

1. Metathesis of ethylene and butenes.
2. Direct conversion of ethylene by dimerization and metathesis.
3. Direct conversion of ethylene by oligomerization and cracking.

Metathesis is based on supported Re, W and Mo catalysts, and the process technology is offered by ABB Lummus, BASF and Atofina, Mitsui Chemicals, BP Chemical and Sinopec [176, 177].

Direct conversion of ethylene to propylene actually involves three steps, the first being partial conversion of ethylene to 1-butene by dimerization and then isomerization of 1-butene to 2-butene followed by metathesis of remaining ethylene with 2-butenes to yield propylene. Though two-stage processes and single-pot processes have been attempted [165] a cascade process involving two different catalysts is found to be promising (Fig. 17). Andrei and co-workers [178, 179] devised a
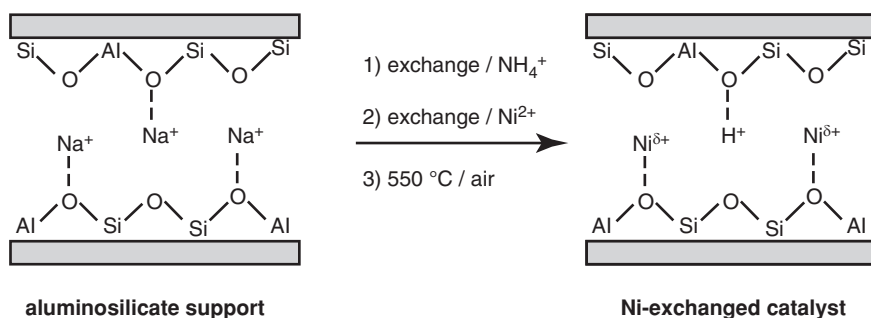
Fig. 16 Ion exchange of Ni^{2+} with the surface Na^{+} ions on zeolite matrix (Reproduced from Hulea [165])
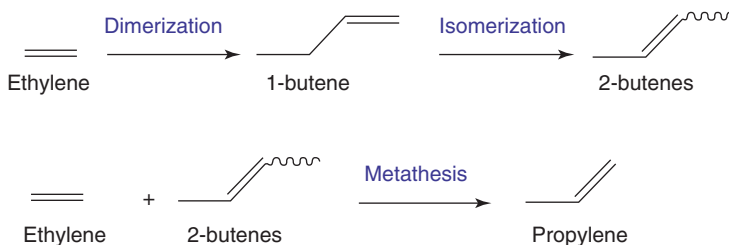
Fig. 17 Cascade process for the conversion of ethylene to propylene (Reproduced from Hulea [165])

cascade process with two different air-stable catalysts, Ni-AlSBA-15 for dimerization and isomerization and MoO_3-SiO_2-Al_2O_3 for metathesis reactions. Both catalysts were loaded in a single reactor, and under identical process conditions, at 80 °C and 30 bar, propylene yield of 48 mmol/g of catalyst per hr. could be realized [178, 179].

For the direct conversion by oligomerization and cracking, ZSM-5 and SAPO-34 were found to be most appropriate [180, 181]. While ZSM-5 with strong acid sites and medium-sized pores (0.55 nm) displayed lower selectivity for propylene, on SAPO-34, with smaller pores (0.38 nm) and weaker acidity, 80% selectivity for propylene could be achieved. The process requires high temperature 450–600 °C to enable the cracking of oligomers. Since the catalysts are acidic in nature and microporous, deactivation by coking is a serious challenge to be tackled.

4.4 Conversion of Ethanol to C_3–C_4 Olefins

Two types of catalysts, zeolites and mixed metal oxide catalysts, have been explored for the conversion of ethanol to C_3–C_4 olefins, and the results have been summarized in a review by Sun and Wang [166]. On ZSM-5 reaction follows MTG pathway, involving the formation of ethylene, which undergoes oligomerization, cracking and aromatization to form products with broad carbon number range. Moderation of acidity of ZSM-5 and optimization of reaction temperature and residence time are crucial to minimize the formation of higher carbon number products and improve selectivity towards C_3–C_4 olefins. Studies in this direction by Song et al. [182] on ZSM-5 with different SAR values indicated that selectivity for C_3–C_4 olefins (at 673 K, 0.1 MPa pressure) was maximum (40%) at SAR −80 due to moderation of acidity. On NiO/MCM-41 (Si/Ni = 23) catalyst at 400 °C, complete conversion of ethanol with propylene selectivity of 30% was reported by Mizuno et al. [183]. Reaction pathway involved the formation of ethylene, which undergoes dimerization, isomerization and metathesis to form propylene. Iwamoto et al. [184] observed that on scandium-modified indium oxide catalyst, propylene selectivity of 60% could be achieved at 550 °C following a different reaction pathway, involving

condensation and ketonization of acetaldehyde to acetone which is converted to propylene by dehydration of isopropyl alcohol formed by reduction of acetone. Though the metal oxide catalysts display better stability vis-à-vis zeolites, achieving higher C_3–C_4 olefins selectivity remains a challenge.

4.5 Conversion of Ethanol to Isobutene

Two processes, based on mixed metal oxide catalysts, are available for the conversion of ethanol to isobutene [166]. The first one is a two-step process involving formation of acetone from ethanol in the first step followed by its conversion to isobutene in the second step according to the equations:

$$2CH_3CH_2OH + H_2O \rightarrow CH_3COCH_3 + CO_2 + 4H_2 \tag{1}$$

$$3CH_3COCH_3 \rightarrow 2i - C_4H_8 + CO_2 + H_2O \tag{2}$$

The first step involves base-catalysed dehydrogenation of ethanol to yield acetaldehyde, which on aldol condensation and de-carbonylation results in acetone formation [185, 186]. An alternative route [187] consists of oxidation of acetaldehyde to acetic acid, which can undergo ketonization to acetone. Amongst the different catalysts explored [166], Cu supported on $La_2Zr_2O_7$ catalyst [188] displayed 72% carbon selectivity for acetone (96% of theoretical yield) at 400 °C, with water/ethanol mole ratio of 9:1 The second step for the conversion of acetone to isobutene is a complex process, involving three molecules of acetone and many reactions, like condensation, dehydration and decomposition, probably requiring Bronsted or Lewis acid-base pair sites [189, 190], where acetone condensation reaction is initiated. Condensation is envisaged between two acetone molecules, one in gas phase and the other adsorbed on Lewis acid sites, while it occurs through two molecules adsorbed on Bronsted acid sites [191]. Such a complex pathway involving two types of acid sites with varying strengths results in further conversion of isobutene and formation of mesityl oxide intermediates, and higher reaction temperatures lead to formation of aromatics [166]. Zeolite β [192] with moderate acidity displays 87% isobutene selectivity at 400 °C and better stability in comparison with ZSM-5 [193]. Zhu et al. observed that use of nanosize zeolites helps to control the rate of deactivation, possibly by promoting facile diffusion and reducing residence time of reactants and intermediates within the pores [194].

In contrast, the one-step process developed by Zhu et al. [195] uses $Zn_xZr_yO_z$ mixed oxide catalyst with balanced acidity-basicity characteristics. It was observed that addition of ZnO moderated strong acid sites present in ZrO_2, favouring dehydrogenation of ethanol to acetaldehyde against dehydration to ethylene [196, 197]. Aldol condensation of acetaldehyde followed by ketonization leads to the formation of acetone. Presence of weak Bronsted acid sites brings out further conversion of acetone, via diacetone alcohol and mesityl oxide, to the final product isobutene. The

process thus follows a cascade reaction pathway, involving dehydrogenation, condensation, dehydration and decomposition reactions, taking place in a sequential manner, yielding isobutene with >80% selectivity in a single step, along with valuable hydrogen as by-product. Overall reaction is expressed as:

$$3CH_3CH_2OH + H_2O \rightarrow i-C_4H_8 + 2CO_2 + 6H_2 \tag{3}$$
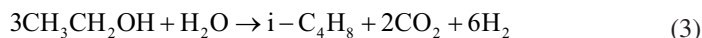
While complete conversion of ethanol is achieved, the product distribution and isobutene selectivity are dependent on ethanol concentration and space velocity [197]. Accordingly, maximum isobutene selectivity is achieved at lower ethanol concentration and higher space velocity (Fig. 18), the conditions that help in controlling side reactions.

4.6 Conversion of Ethanol to 1,3-Butadiene

Global demand for 1,3-butadiene (BD) was estimated to be ~12.3 MMT in 2018 (Fig. 19) and is projected to touch ~14 MMT by 2025 [198]. Major applications for BD are in the manufacturing of styrene butadiene rubber (SBR), polybutadiene rubber (PBR), acrylonitrile butadiene styrene (ABS), adiponitrile, polychloroprene elastomers, nitrile rubbers and others. Steam cracking of naphtha, dehydrogenation of butane and dehydration of ethanol are the established conventional routes for butadiene production. While the demand for BD is growing steadily, there is some
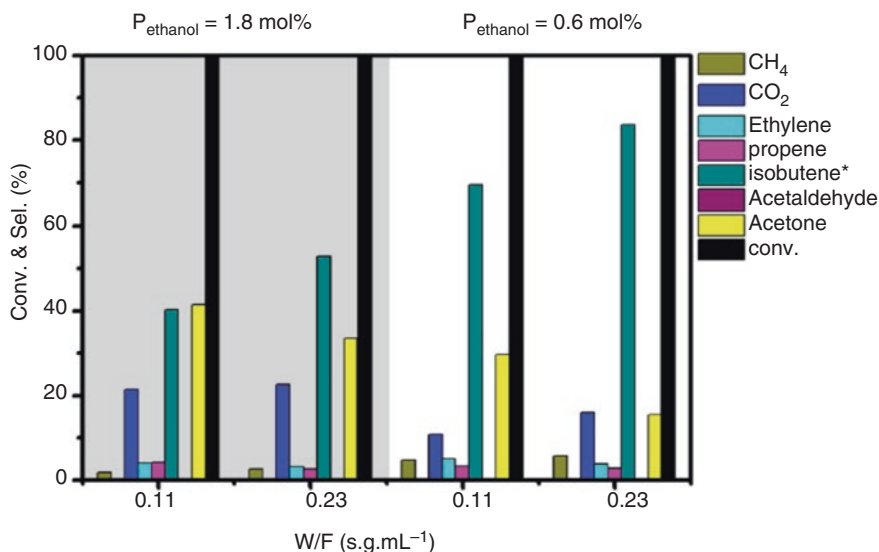
Fig. 18 Conversion of ethanol to isobutene on $Zn_1 Zr_{10}O_x$ mixed oxide catalyst as a function of space velocity and ethanol concentration (Reproduced from Sun et al. [196])

uncertainty in the feedstock scenario, since most of the recent steam crackers are C_2/C_3 gas/shale gas based. Hence, production of BD from readily available low-cost bioethanol and other biomass-derived chemical intermediates has been gaining ground. Accordingly, scientific investigations on catalysts and processes for ethanol to butadiene (ETB) process are on the rise (Fig. 20). A complete life cycle analysis of GHG effect on ETB process vs. naphtha-based one has shown 155% reduction in emissions in the bio-based process [200], thus making it highly relevant in the current context of environmental sustainability of chemical processes.

Historically, two ETB processes have been described. The first one is a single-step process, on ZnO-Al$_2$O$_3$ catalyst, at 400 °C, discovered by Sergey Lebedev in 1929 [201–203] according to the reaction:
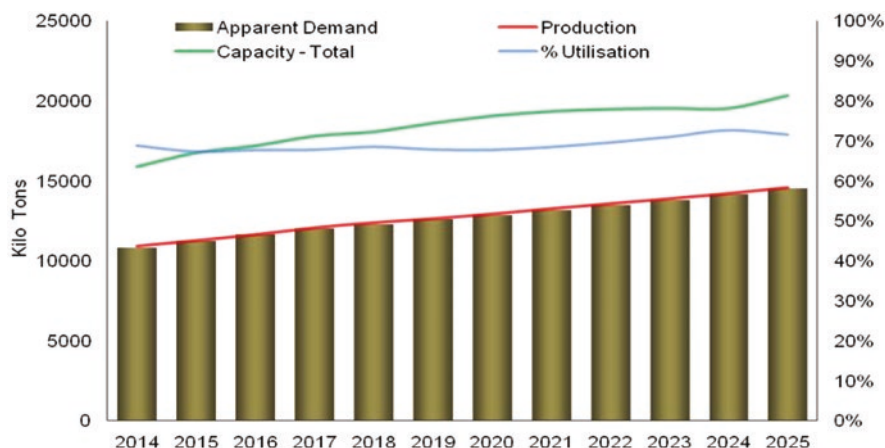
Fig. 19 Global demand/production of 1,3-butadiene [198]
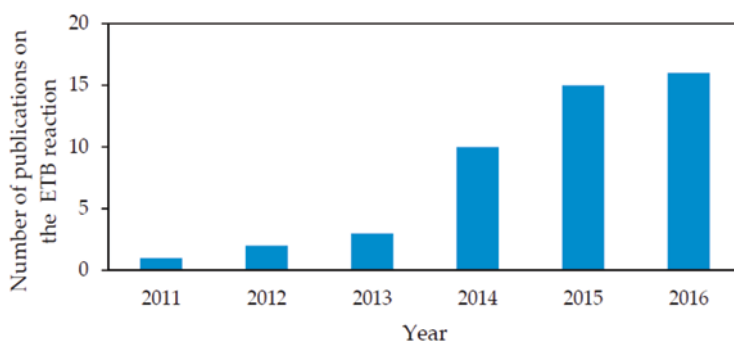
Fig. 20 Number of publications dedicated to ethanol to butadiene in the recent years (Reproduced from Pomalaza et al. [199])

$$2CH_3CH_2OH \rightarrow CH_2 = CH - CH = CH_2 + 2H_2O + \tag{4}$$
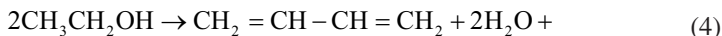
and the other, by Ivan Ostromislensky [204], consists of two steps, the first step being partial dehydrogenation of ethanol to acetaldehyde and the second involving reaction between ethanol and acetaldehyde:

$$CH_3CH_2OH \rightarrow +CH_3CHO + H_2 \tag{5}$$

$$CH_3CH_2OH + CH_3CHO \rightarrow CH_2 = CH - CH = CH_2 + 2H_2O \tag{6}$$
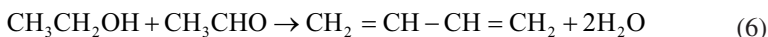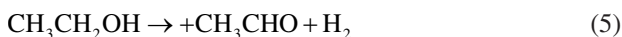
Reaction pathways involved in both processes are the same. While Lebedev process [201–203], carried out at 400–450 °C, was based on metal oxide catalysts, Ostromislensky [204] process used tantalum oxide-promoted silica catalyst at 325–350 °C. Commercial production plants based on these processes were in operation till the 1960s, when naphtha-based BD production route became more competitive. Ethanol conversion of 45% with BD selectivity of 55% could be realized in Union Carbide and Chemicals plant [205]. Many by-products, diethyl ether, acetic acid, ethyl acetate, n-butanol, 1-butene, ethylene and hexadiene, were formed in the process. Progress in research related to the different catalyst formulations (mono-, bi- and trimetallic), especially the crucial role of preparation methods, nature of supports, process improvements and understanding of the reaction pathways/mechanism for the conversion of ethanol to BD have been covered extensively in several reviews [199, 206–210].

Though different mechanistic pathways have been proposed for ETB process over the years [199, 207], the generally accepted one (Scheme 2) for the single-step process involves dehydrogenation of ethanol to acetaldehyde as the first step, which on aldol condensation yields acetaldol. Meerwein-Ponndorf-Verley (MPV) reduction of acetaldol by another molecule of ethanol gives 1,3-butanediol that subsequently dehydrates to form BD [211, 212]. In the two-step process (Scheme 3), dehydrogenation of ethanol (on copper catalysts) yields acetaldehyde in the first step. In the second step, acetaldehyde forms acetaldol followed by dehydration to crotonaldehyde. MPV reduction of crotonaldehyde by ethanol results in crotyl alcohol, which on dehydration gives BD [213, 214].

Fripiat et al. [215, 216] observed that on silver supported on sepiolite catalyst, selectivity for ethylene and BD increased with ethanol conversion and hence suggested that the process follows Prins reaction pathway. Cavani et al. proposed a different mechanism based on carbanion formation [217]. However, formation of by-products and studies using C^{13}-labelled acetaldehyde supported the mechanism involving MPV reduction [211, 212]. Based on the accepted mechanistic pathway, acidity, basicity and redox characteristics are the functionalities required for conversion of ethanol to BD.

However, developing catalyst formulations that possess the right combination of the active components in required proportions remains a challenge. Details on the development of different types of catalysts for single- and two-step ETB processes have been reviewed from time to time [199, 207–209]. Based on the voluminous
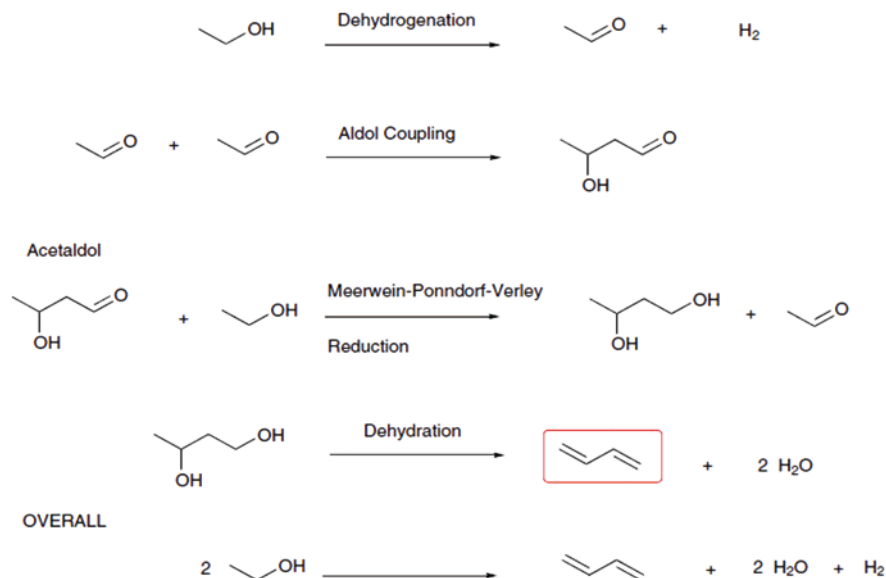
Scheme 2 Reaction pathway for single-step ETB process (Reproduced from Kagan et al. [211] and Vinogradova et al. [212])
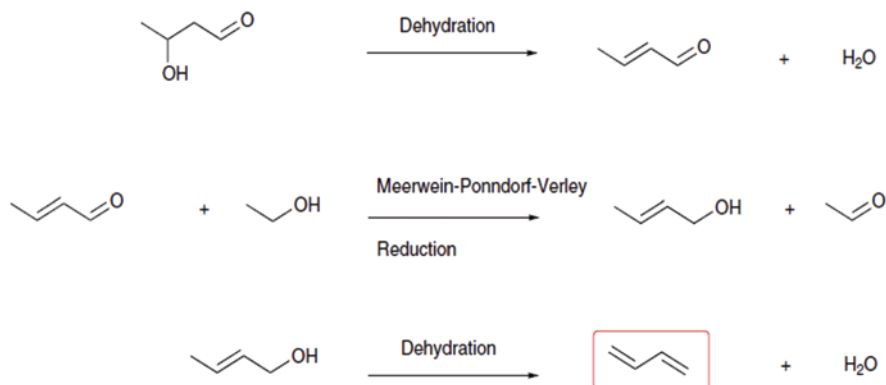
Scheme 3 Reaction pathway for two-step ETB process (Reproduced from Kagan et al. [211] and Vinogradova et al. [212])

literature data [199, 206–210], the catalysts investigated so far could be broadly classified into:

- Mixed metal oxide catalysts based on alumina.
- $MgO + SiO_2$ mixed oxides.
- Metal oxide (Cr_2O_3, ZnO, Ta_2O_5, NiO, CuO) and metal (Ag, Au)-promoted $MgO + SiO_2$.

Table 4 Selected catalyst systems for ETB process

Catalyst systems	Reaction temp., °C	BD yield, %	References
$MgO/SiO_2/Cr_2O_3$ (3/2/0.11)	415	41.9	[218]
$MgO/SiO_2/Cr_2O_3$ (59/39/2)	425	39.0	[219]
Mg/sepiolites	300	33.4	[220]
$NiO/MgO/SiO_2$ (10/27.9/62.1)	280	53.0	[221]
MgO/SiO_2(1/1)	350	42.0	[222]
MgO/SiO_2(1/1) + 0.1% K_2O	350	70.0	[222]
MgO/SiO_2(1/1) + 0.1% Na_2O	350	87.0	[222]
MgO/SiO_2 (0.83/1)	350	16.0	[223]
Zr (1.5%), Zn(0.5%)/SiO_2	375	11.5	[210]
Cu (1%), Zr(1.5%), Zn (0.5%)/SiO_2	375	30.1	[210]
5% CuO-MgO/SiO_2 (2/1)	350	58.2	[224]
5% ZnO-MgO/SiO_2 (2/1)	350	52.4	[224]
5% Ag-MgO/SiO_2 (2/1)	350	56.3	[224]
$ZnO.Al_2O_3$ (60:40) fixed bed	425	55.8	[225]
$ZnO•Al_2O_3$ (60:40) fluidized bed	425	72.8	[226]

- Silica-based bimetallic Zr-Zn and trimetallic Zr-Zn-CuO.
- Sepiolite and zeolite (BEA, Al-MCM-41) based.

Table 4 gives a list of selected catalyst compositions and BD yields from the literature [208]. Besides the variations in composition, methods of preparation (wet kneading, sol-gel, hydrothermal), calcination/activation of the catalysts and pore size of the supports are known to influence the activity and selectivity [210, 227, 228]. Though BD selectivity of 50–80% could be achieved, corresponding alcohol conversion levels are lower, and hence there is a need to develop catalysts capable of performing at high ethanol concentrations to obtain higher BD productivity. Current volume productivity of BD in the range from 50 to 400 g BD per hour per litre catalyst volume needs to be improved for commercial application. On-stream stability of the catalyst/catalyst life also needs improvements. Besides fixed bed reactors, other reactor configurations like fluidized bed reactors and the intricacies involved in recycling unreacted ethanol, etc. are to be explored.

A comparative evaluation of naphtha-based and bioethanol-based processes for BD production has been made by Patel et al. [229] in 2012, based on the descriptors for techno-economic viability, sustainability index and life cycle analysis. The descriptors used are economic constraints, environmental impact of raw materials, process costs and environmental aspects, EHS (Environment Health and safety) hazards and risk aspects. After assigning the weightage for each parameter, the integrated score for both processes is presented in Fig. 21. Overall score for bioethanol-based process is lower (0.81), and hence it has a slight edge over naphtha-based (0.9) process. Processing costs and EHS hazards are lower with bio-based process, while risk aspects and environmental impact of raw materials are nearly equal. Economic constraints are higher with bio-based process. However, GHG emission, in terms of kg of CO_2 per kg of BD, is 2.45 for bioethanol-based process vs. 3.98 for
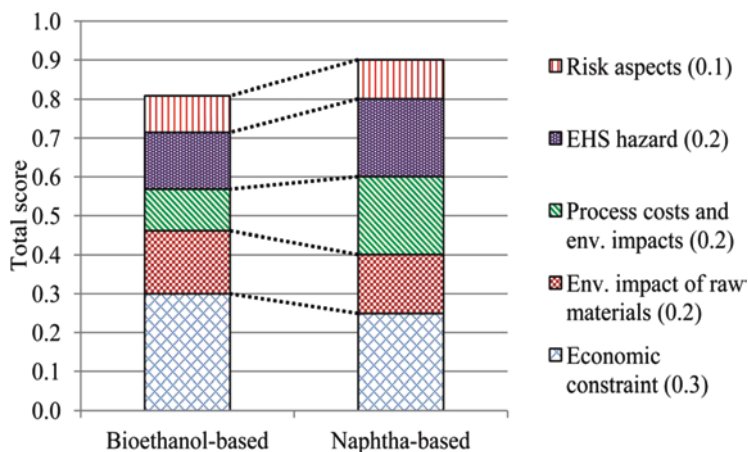
Fig. 21 Comparative evaluation of naphtha-based and bioethanol-based processes (Reproduced from Patel et al. [229])

naphtha-based. Similar advantage in sustainability for bio-based BD process in terms of GHG emissions has been reported by Shylesh et al. [200] in 2016.

Techno-economic analysis of the two-step process carried out by Burla et al. [205] in 2012, based on the conversions and selectivity values achieved in the old Union Carbide plant, has shown that 200,000 MTA BD plant is viable when ethanol and BD prices are favourable and unprofitable when ethanol price becomes >US$ 3.0 per gallon. There is no doubt that ETB process could be a viable one in near future, due to favourable process economics and sustainability. Hence research efforts, especially towards development of catalysts with higher productivity and stability and process improvements, could gain more attention from the researchers and support from the industry.

4.7 Conversion of Alcohols to Fuels

4.7.1 Alcohols to Gasoline

Alcohols, especially methanol and ethanol, find significant applications in the fuel/energy sector, for blending directly with gasoline, as fuel additives/octane-boosting agents, for production of biofuels and biodiesel and, more recently, for conversion into middle distillate range fuels (diesel, jet fuel). Around 31% methanol demand (Fig. 3) is for fuels, for blending with gasoline (13%) and in the manufacture of MTBE (12%), biodiesel (3%) and DME (3%). Utilization of methanol for the production of MTBE and other octane-boosting agents, biodiesel and DME is well-established and understood.

Discovery of *methanol to gasoline* (MTG) on ZSM-5 catalysts in the 1970s by Mobil Corporation opened up a new avenue for direct conversion of methanol [230]

to gasoline, to start with. Elucidation of the mechanistic pathways in the MTG process, with methanol and ethanol as feed, by Derouane et al. [231] and Chang et al. [232] and the development of fixed bed reactor process [233, 234] paved way for further improvements in the process. With a better understanding of the catalytic action by ZSM-5 zeolites and the process steps involved, Tabak and Yurchak [235] proposed the integration of MTG process with two other major front-end catalytic processes, namely, methanol synthesis from syngas and syngas production from basic raw materials, coal, gas and biomass. Such a process configuration rendered MTG process more flexible and versatile, capable of producing a range of fuels and chemicals as illustrated in Scheme 4, by suitable optimization of the process conditions. While the use of methanol provided an alternative to route to crude oil-derived gasoline, the pioneering work on ZSM-5 catalysts and demonstration of the other processes (Scheme 4) by Mobil research group [235] for olefins (ethylene, propylene) and middle distillate production provided the scientific basis for the development of several novel and important processes, years later, CTL (Coal to Liquids), GTL (Gas to Liquid) and BTL (Biomass to Liquid) processes, to be followed by MTO and MTP processes. A recent development in this direction is the conversion of ethanol to jet fuels which would be discussed later.

Based on the experience gained in the 14,500 BPD Synfuel MTG plant in New Zealand, CTL process, consisting coal gasification, methanol synthesis plants along with MTG plant with second generation catalyst, [236] was envisaged by Exxon Mobil Research and Engineering (EMRE) and Uhde. The first 2500 BPD CTL plant based on MTG process was established at JAMG, Shanxi Province, China, in 2009 [237]. By 2014, eight such plants were licensed. EMRE-MTG process [238] consists of three units, syngas, methanol and MTG process (Fig. 22), which also includes heavy gasoline treatment unit for removal of durene. Durene with melting point of 79 °C could cause problems in the fuel supply lines and hence is to be minimized to <2% in product gasoline.

Two more processes for MTG have been developed, one by Haldor Topsoe's TIGAS [238] (Haldor Topsoe Improved GASoline) process and the other by Primus STG+ [239]. TIGAS mostly resembles EMRE-MTG process except that methanol production unit is integrated with MTG unit and is based on proprietary GSK-10 catalyst for MTG conversion. It is claimed TIGAS process is licensed to three plants in China and two are in planning stage [238].

Improvements in Primus' proprietary STG+™ process [239] over EMRE-MTG and TIGAS processes include recycling unconverted hydrocarbons in a single-loop process so that the gasoline yield increases and up to 70% of natural gas is getting

Scheme 4 Processes for the production of fuels and chemicals from methanol (Reproduced from Tabak et al. [235])
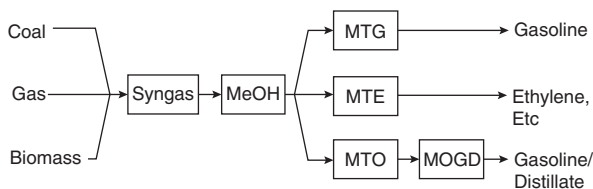
converted directly to high-quality gasoline. Besides, there is no need for separate durene reduction unit. It is further claimed that the Primus process is more energy efficient, requires lower investment cost and amenable for easy scale up.

Sector wise utilization of ethanol (Fig. 23) shows that nearly 50% of the demand is in automobile sector as fuel additive, for blending with gasoline, the other major application being in the food and beverages industry [240]. In contrast to methanol share (Fig. 3) of 64% for chemicals (including 24% for MTO), the usage of ethanol in chemical industry is around ~30%, only, including chemicals, personal care products, pharmaceuticals and others.

Catalytic conversion of *Ethanol to Gasoline* (ETG) has been studied extensively [166], though its large-scale application, like MTG process, is yet to emerge. However, of recent, few processes for conversion of ethanol to diesel and jet fuels
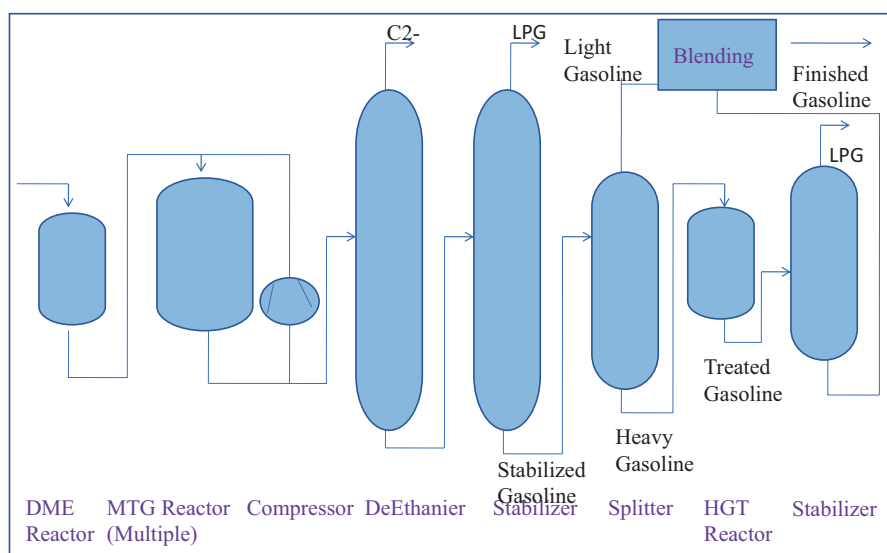
Fig. 22 Simplified process flow diagram for EMRE-MTG process [236]

Fig. 23 Sector-wise utilization of ethanol [240]
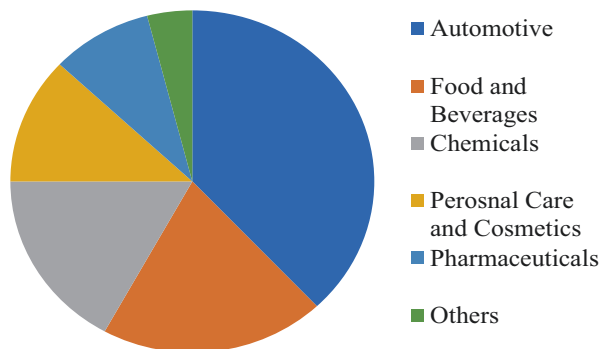
have progressed towards commercial application [241]. ETG process follows nearly the same mechanistic pathway that is proposed for MTG process, and accordingly the product distribution in both cases is similar. Detailed identification and structural analysis of the reaction intermediates trapped inside the pores of ZSM-5 during ETG process have been investigated by Johansson et al. [242]. It is suggested that various types of cyclic organic intermediates (poly-alkylated benzenes) located within the pores form the *hydrocarbon pool* which undergo alkylation-dealkylation and cracking, depending upon the acidity of the zeolite and reaction temperature, thus giving rise to different products.

The transformations occurring in ETG process are similar to those proposed for MTG and illustrated in Scheme 5.

When compared to MTG process, predominantly ethyl-substituted aromatics are found in hydrocarbon pool within the pores in ETG process, but the product stream in ETG, however, contains only methyl-substituted aromatics. Besides, no durenes are observed in ETG [166].

In general, acidity of ZSM-5 as dictated by Si/Al (SAR) ratio, reaction temperature, space velocity and addition of water influence ethanol conversion, product distribution/selectivity and catalyst stability. Major reason for deactivation of ETG catalysts is coke formation, and addition of water retards coke formation and hence less deactivation and improvements in liquid yield [243]. Formation of aromatics/liquid hydrocarbons is favoured with ZSM-5 catalysts with lower SAR [244]. As reported by Talukdar et al. [245], ZSM-5 with SAR-20 yielded full range (olefins and aromatics) products with high liquid yields, while the catalyst with SAR-103 resulted in high yields of light olefins (C_3–C_4) even with ethanol containing 50% water. Investigations by Madeira et al. [246] on ZSM-5 catalysts with SAR values in the range 16–500 have shown that the catalyst with SAR-40 displays the best activity, stability and highest selectivity towards long-chain hydrocarbons and have attributed it to the balance between Bronsted acid sites (active sites) and hydrocarbon radicals (coke species responsible for blocking active sites). Another strategy frequently adopted to moderate acidity and deactivation is by modification/ion exchange with metal ions. Introduction of Ni [247], Ga and Zn [248] ions leads to improvements in catalyst life and increase in liquid hydrocarbon yields. Partial substitution of Al^{3+} in the framework by Fe^{3+} also leads to improvements in liquid yields and stability. Modifications with trimethyl phosphite increase weak acid sites, and accordingly, only ethers appear as products [249]. Besides strong acidity, porosity of ZSM-5 [250] and optimum water content in ethanol [244, 245] are the other parameters that affect the catalyst performance and hydrocarbon yield pattern.

Scheme 5 Representation of hydrocarbon pool mechanism proposed for MTG/ETG processes (Reproduced from Johansson et al. [242])
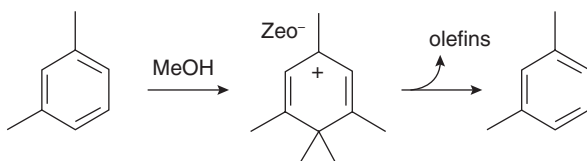
4.7.2 Ethanol to Jet Fuels and Middle Distillates

Transportation sector accounts for 25% of global total energy demand for the movement of people and goods. The consumption pattern for different types of fuels is given in Fig. 24 [251].

According to International Energy Outlook 2016 [252], the total energy consumption in passenger and freight modes of transportation, using all types of fuels, is increasing (Fig. 25) continuously from ~100 quadrillion Btu in 2012 towards the projected consumption of ~150 quadrillion Btu by 2040 [252]. Considering the need for sustainable energy resources and minimization of the environmental
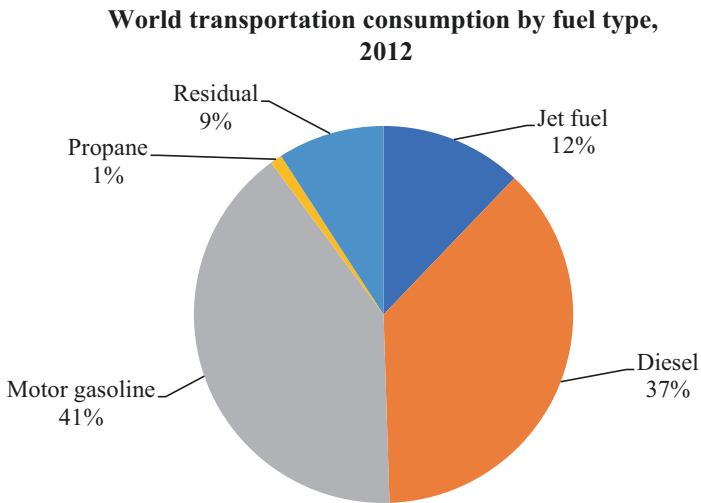
Fig. 24 World fuel consumption for transportation—types of fuels (Total—103 quadrillion Btu) [251]
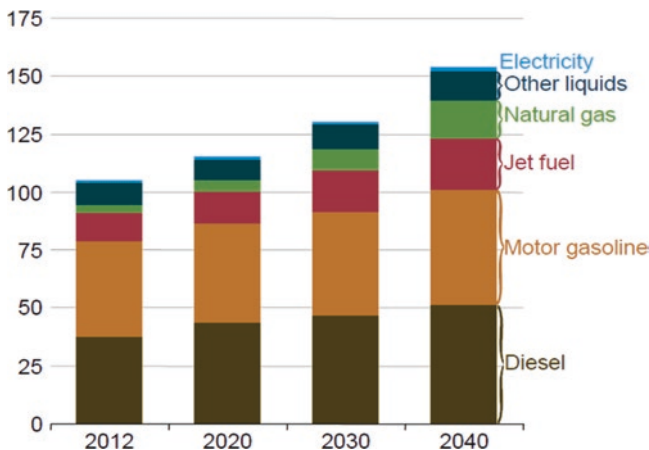
Fig. 25 Global energy consumption in transport sector (in quadrillion Btu) 2012–2040 [252]

impacts, relentless efforts are on to derive these fuels from renewable resources. Significant progress has been achieved in the utilizations of bio-fuels (bio-ethanol, biobutanol, biodiesel, gasoline through MTG process, bio-jet fuels etc.), though overall contribution of bio-fuels in global total energy consumption (in 2017) remains low at 13% [253]. Bio-ethanol, besides its application for blending with gasoline, can be converted into value-added fuels in middle distillate range and jet fuels by different catalytic processes. Jet fuel constitutes around 12% of the global transportation fuels consumption and its contribution towards emission of green-house gases (GHG) is 2%. In order to comply with the Paris Climate Control Accord, 2015, airlines industry is aiming to become carbon-neutral by 2020 and by 2050 reduce emissions by 50% with respect to 2005 emissions level, by gradual replacement of fossil-derived jet fuels with low-carbon bio-based fuels. In this context, besides bioethanol, several process technologies (Table 5) for production of bio-jet fuels have emerged depending on the type of bio-resources used [254]. A number of multinational companies have developed process technologies (Table 6) for the conversion of different types of biomass/renewable feedstocks to bio-jet fuel [255]. While a few of them have gone through ASTM certification process for blending with petroleum-based jet fuel, others are under consideration for certification. Nearly all types of raw materials (Table 6), fossil-based (coal, natural gas), biomass, cellulosic biomass, starch, sugars and bio-renewables like vegetable oils, recycled oil and animal fat have been explored for production of bio-jet fuel. Fermentation, hydrolysis, oligomerization, hydrotreatment and thermal decomposition are the conversion processes employed. Most of the processes listed in the table are in the advanced stage of development, and several airlines have entered into contracts for the supply of bio-jet fuels manufactured by applying these processes [256], for conducting flight trials after mixing with petroleum-derived jet fuel as per ASTM norms.

Compared to the different raw materials used for bio-jet fuels production, bio-ethanol is better placed with respect to abundant availability and relatively lower cost and hence continues to receive global attention. Recently, a number of SAJF

Table 5 Process technologies for the production of bio-jet fuels (Adapted from Wei-Cheng et al. [254])

Technologies	Production processes
Alcohol to jet (ATJ)	Ethanol to jet
	n-butanol to jet
	Isobutanol to jet
	Methanol to jet
Oil to jet (OTJ)	Hydro-processed renewable jet
	Catalytic hydro-thermolysis
	Hydrotreated depolymerized cellulosic jet
Gas to jet (GTJ)	Fischer-Tropsch synthesis (FT)
	Gas fermentation
Sugar to jet (STJ)	Direct sugar to hydrocarbons (DSHC)
	Catalytic upgrading

Table 6 Bio-based jet fuel production processes—status on development and application [255]

Production process	Developer/manufacturer	Raw materials	Aromatic content	ASTM review stage and max. mixing proportions
FT-SPK	Sasol, Shell, Syntroleum	Coal, natural gas, biomass	Low	(2009)—50% approved
HEFA	Honeywell UOP, Neste Oil, Dynamic Fuels, EERC	Vegetable oil, animal fat, recycled vegetable oil	Low	(2011)—50% approved
SIP	Amyris, Total	Sugar	Low	(2014)—50% approved
ATJ-SPK	Gevo, Cobalt, Honeywell UOP, LanzaTech, Swedish Biofuels, Byogy	Starch, sugar, cellulose-based biomass	Low	(2016)—50% approved
FT-SKA	Sasol	Coal, natural gas, biomass	High	Under review by committee
HDO-SK	Virent	Starch, sugar cellulose-based biomass	Low	Investigation report submitted
HDO-SKA	Virent	Starch, sugar cellulose-based biomass	High	Investigation report under review
HDCJ	Honeywell UOP, Licella, KiOR	Cellulose-based biomass	High	Supplement to investigation report received
CH	Chevron Lummus Global, Applied Research Associates, Blue Sun Energy	Vegetable oil, animal fat, recycled vegetable oil	Low	Investigation report under review

FT-SPK Fischer-Tropsch synthetic paraffinic kerosene, *HEFA* hydrotreated esters and fatty acids, *SIP* synthesized isoparaffins, *SKA* synthetic paraffinic kerosene with high aromatics, *HDO* hydro-deoxygenation, *HRJ* hydrotreated renewable jet

(Sustainable Alternative Jet Fuel) processes using ethanol, methanol, n-butanol and isobutanol have been developed. These processes differ in terms of biomass raw materials used and the processes followed for conversion of biomass to alcohols, types of alcohols and processes adopted for conversion of alcohols to jet fuel. Some of the ATJ/SAJF processes which are in various stages of development are described in the following pages.

Lanza-PNNL Process

LanzaTech Inc. and PNNL (Pacific Northwest National Laboratory) have collaborated to develop a hybrid process, LT-PNNL [257], for the conversion of three different biomass raw materials, wood, corn stover and bagasse, to jet fuel, distillate and value-added chemical, butadiene (BD), following a multistage integrated
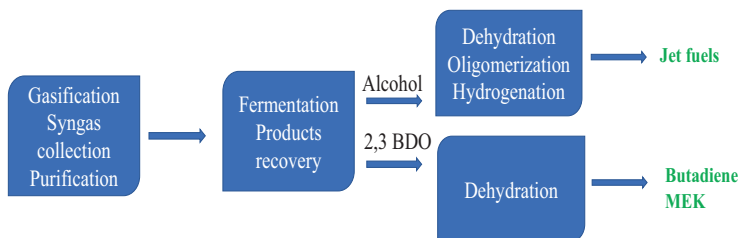
Fig. 26 Block diagram for Lanza-PNNL process for conversion of biomass-derived ethanol to jet fuel and value-added chemicals (Adapted from Ref. [257])

process, as depicted in Fig. 26. The first stage consists of thermochemical conversion of biomass into syngas. The process, that uses highly energy-efficient plasma to convert biomass into clean syngas with consistent composition, was developed by LanzaTech Inc. The process includes collection, compression and purification of syngas. In the second stage, syngas is fed to the bioreactor, wherein it undergoes microbial fermentation process [258] developed by NREL (National Renewable Energy Laboratory), to yield two products, ethanol and 2,3-butanediol (2,3-BDO). The next stage for the conversion of ethanol to jet fuel, involving a series of three catalytic steps, (1) dehydration of ethanol to ethylene, (2) ethylene oligomerization to jet fuel range olefins and (3) olefins hydrogenation, was developed by PNNL [259].

Since direct oligomerization of ethylene is a slow process with lower selectivity/yields towards olefins in the desired carbon number range, a two-stage oligomerization process was developed. In the first stage, ethylene undergoes oligomerization to C_4–C_{10} olefins, which go through further oligomerization in the second stage, to yield jet fuel range olefins [259, 260]. Separation of the fermentation co-product, 2,3-butane diol, and its catalytic conversion to butadiene (BD) were achieved by stepwise catalytic dehydration, first to methyl vinyl carbinol, followed by second dehydration step, to yield 70% BD with 98% purity [257, 261]. Optionally, BDO can be converted to methyl ethyl ketone (MEK). Some of the additional features of the LT-PNNL process are [257]:

- Industrial waste gas streams containing carbon oxides (i.e. steel plant) can be used for ethanol production by fermentation.
- Fermentation process can be optimized for the production of ethanol and BDO in desired proportions, depending on the requirements.
- The process was demonstrated on lab scale with 2000 h of continuous run, producing 400 gallons of jet fuel and 400 gallons of diesel.
- Jet fuel produced meets the specifications designated for "Alcohol to Jet Synthetic Paraffinic Kerosene" (ATJ-SPK) in ASTM D7566, *Standard Specification for Aviation.*

Turbine Fuel Containing Synthesized Hydrocarbons, which specifies requirements for alternative jet fuels

- Co-production of 2,3-BDO/BD reduces overall cost of production.

ORNL-Vertimass Process

Oak Ridge National Laboratory (ORNL) has developed highly versatile process and catalyst [262] for single-step conversion of dilute ethanol from fermentation stream to highly value-added product stream consisting of blend stocks suitable for jet fuel, middle distillate or gasoline. The process is capable of using feedstocks containing 5–100% ethanol in water without external supply of hydrogen and under mild conditions, at low pressure, 60 psi, 350 °C and optimum space velocity (LHSV). Pilot-scale evaluation of the process is to be undertaken by TechnipFMC, and the lab-scale process has been licensed to Vertimass for exploring commercial venture [263–266]. V-, V-In- and Ga-exchanged mono- and bimetallic ZSM-5 catalysts, under optimized process conditions, display C_3–C_{16} hydrocarbon selectivity >80% (Fig. 27) with 100% conversion of ethanol. Light hydrocarbons ($C_2 + C_3$) formation is <5% [267–269]. Metal-exchanged zeolite catalyst in combination with a benzene alkylation catalyst helps to bring down benzene content to <0.68% in the product stream [270], in accordance with environmental regulations.

In order to gain mechanistic insights into the process, studies have been conducted using deuterium-labelled reactants, C_2H_5OD and D_2O and in situ DRIFTS studies [267]. It is observed that with C_2H_5OD as reactant, deuterium is incorporated in product hydrocarbons, but with 70% ethylene and 30% D_2O, deuterium incorporation is not observed. But with 70% ethanol and 30% D_2O, deuterium is incorporated in all hydrocarbons except ethylene. Based on these results and DRIFTS studies, Chaitanya et al. [267] concluded that ethylene is not the intermediate in this process and the reaction proceeds via hydrocarbons pool mechanism.

It is proposed that, unlike LT-PNNL multistep process, which involves ethanol dehydration to ethylene and oligomerization of ethylene to higher carbon number olefins followed by hydrogenation, ONRL-Vertimass process on metal-exchanged zeolite catalysts follows a *consolidated alcohol dehydration-oligomerization* (CADO) pathway to yield, in single step, hydrocarbon blend stocks, suitable for jet

Fig. 27 Ethanol conversion on V-ZSM-5 catalyst as a function of temperature at LHSV-2.93 h^{-1} (Reproduced from Narula et al. [267])
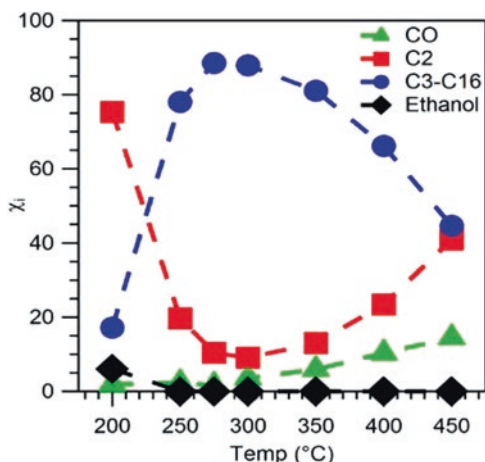
fuel, diesel and gasoline. Product stream composition could be varied depending on market demands by suitable optimization of the process conditions. The lab-scale process has been demonstrated by 200 h continuous run, and the product composition and fuel characteristics have been established. However, long-term stability of the catalyst and ASTM-D-7566 certification are yet to be established. Techno-economic and life cycle analysis [271] of ONRL-Vertimass vs. LT-LNNL processes has shown that the former one is cost-efficient, is viable for blending when oil is at US$100 per barrel and can reduce GHG emissions by 40–96%. Vertimass along with Bioenergy Technology Office of the US Department of Energy would jointly work for further improvements in the process and catalysts and to establish commercial viability.

C$_4$ Bio-alcohols-Based Processes

Two C$_4$ bio-alcohol-based processes, one by Gevo, Inc., using bio-isobutanol and the other by *Cobalt Biofuels* (now Cobalt Technologies) using bio-1-butanol, for conversion to jet fuel, have been developed. Sugars extracted from biomass undergo fermentation by Gevo Integrated Fermentation Technology (GIFT) using specific microorganisms to yield isobutanol [272], which is dehydrated to isobutylene. On oligomerization using acidic catalysts like Amberlyst 35, iso-butylene is converted to C$_8$–C$_{16}$ olefins, which are subsequently hydrogenated to jet fuels [273]. Jet fuel blend from Gevo process has secured certification as per ASTM-D-7566 for blending with commercial aviation fuel. Airliner Delta has entered into an agreement with Gevo, Inc., for offtake of 10 mill gallons per year of bio-jet fuel [274].

CLJ-5 bio-jet fuel developed by *Cobalt Biofuels* is based on 1-butanol obtained by fermentation of C$_5$–C$_6$ sugars extracted from cellulosic biomass [275–277]. Bio-1-butene produced by dehydration of bio-1-butanol undergoes oligomerization followed by hydrogenation to yield jet fuels. Oligomerization is achieved by using metallocene catalyst, bis-cyclopentadienyl zirconium dichloride, with MAO as co-catalyst [278]. The process has been demonstrated at pilot scale, and the jet fuel product meets all specifications for blending with JP-5 and other aviation fuels.

Other Processes Based on Ethanol/Alcohols

Conversion of *ethanol to butanol and higher alcohols through Guerbet chemistry* has opened up another route for ethanol to jet fuel (ETJ) production [241], wherein C$_4$–C$_6$ alcohols could undergo sequential dehydration, oligomerization and hydrogenation to yield jet fuels. With Cu/MgO-Al$_2$O$_3$ catalyst, PNNL [279] could achieve 44% ethanol conversion and 75% C$_4$+ alcohol selectivity at 300–350 °C and WHSV 0.1–0.2 h^{-1}. However, achieving higher ethanol conversion with high selectivity for C$_{4+}$ alcohols and longer life has been a challenge for ethanol coupling processes. Hence many options for [241] ETJ process are being explored as illustrated in Fig. 28. A combination of two methanol conversion steps, the first through MTO
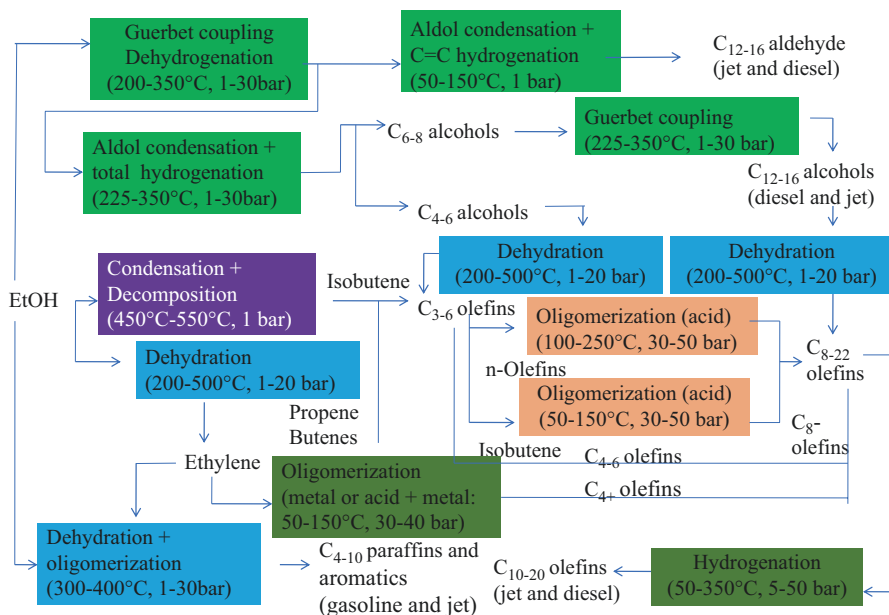
Fig. 28 Various pathways and catalytic processes available for the conversion of ethanol to jet fuel, middle distillates and gasoline (Reproduced from Eagan et al. [241])

(via C_2–C_4 olefins oligomerization and hydrogenation) and the second through DME (via MTG/MOGD), has been envisaged by Bradin [280] for methanol to jet fuel (MTJ) process.

An integrated process involving biomass-derived syngas conversion to a mixture of oxygenates, containing C_1–C_5 alcohols, acetic acid and acetaldehyde, followed by oligomerization and hydrogenation to jet fuel/distillates has been explored by Dagle et al. [281] from PNNL. A systematic review of bio-jet fuel conversion technologies, covering the developments in each case, published by Wang et al. [282], shows that this area has tremendous potential.

5 Aqueous Phase Reforming of Alcohols

Hydrogen is recognized as the clean and efficient source and carrier of energy. Currently, hydrogen is produced by steam reforming, which utilizes non-renewable fossil resources (natural gas, oil, coal) and is highly energy intensive with a large carbon footprint as well. Renewable biomass-based hydrogen production processes like gasification and pyrolysis, though carbon-neutral, are again energy-intensive. In this context, aqueous phase reforming (APR) of biomass feedstocks, developed by Dumesic et al. [283], has emerged as a viable and sustainable route for the production of hydrogen. Unlike steam reforming, APR is carried out at lower

temperature (at <500 K compared to 773–1073 K required for vapour phase steam reforming process) and pressure of 20–25 bar, to maintain water in liquid state, thus eliminating energy required for evaporation. Besides, APR includes water-gas shift reaction (WGS) that involves the formation of additional hydrogen to lower CO content, along with the conversion of CO to CO_2 [284].

Aqueous solutions containing 5–20 wt% of any type of biomass intermediates/ platform chemicals, like cellulose, C_5–C_6 sugars, polyols and C_1–C_4 aliphatic alcohols, could be used as feed, rendering APR as a highly versatile process for the production of fuels and chemicals from biomass [285, 286]. APR is a carbon-neutral process, which can be integrated with other biological, thermal, chemical or fermentation processes [287] without the need for external hydrogen source. A recent Scopus survey (Fig. 29) brings out a quick indication of the level of global research activity in APR, with all types of biomass feedstocks, in terms of number of publications, in the past two decades.

Transformation of alcohols under APR process conditions is represented by the following reactions/equations:

$$C_nH_{2n+2}O_n + nH_2O \rightarrow nCO_2 + (2n+1)H_2 \tag{7}$$
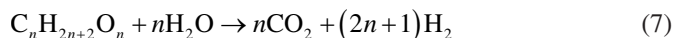
C-C bond breaking could lead to the formation of CO, which can undergo water-gas shift reaction to yield hydrogen.

$$CO + H_2O \rightarrow CO_2 + H_2 \tag{8}$$

Side reactions involving CO_2 are possible, especially at lower reaction temperatures, leading to the formation of alkanes via methanation and Fischer-Tropsch reactions:
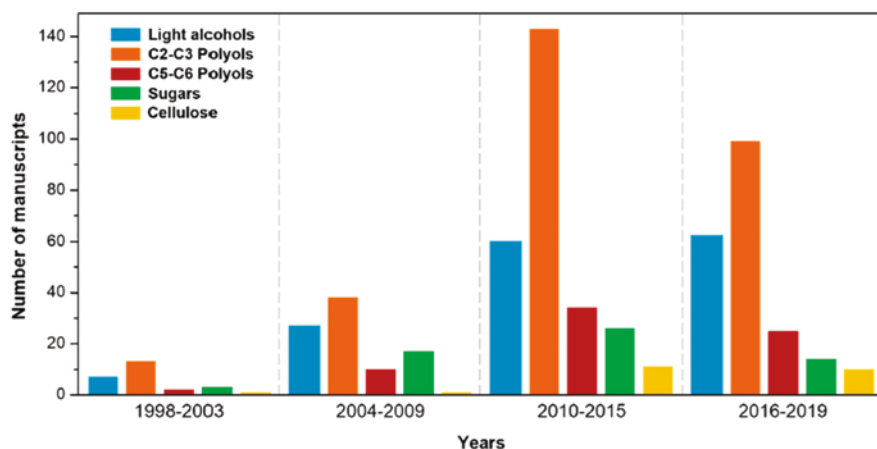
Fig. 29 Trend of the peer- reviewed manuscripts contain "X aqueous phase reforming" (with X = methanol, ethanol, EG, glycerol, sorbitol, etc.) in abstract, keywords and title (Adapted from Scopus® (accessed on Oct 4, 2019) (Reproduced from Fasolini et al. [286]))

$$3H_2 + CO \rightarrow CH_4 + H_2O \tag{9}$$

$$4H_2 + CO_2 \rightarrow CH_4 + 2H_2O \tag{10}$$

$$nCO + 2nH_2 \rightarrow \left[-CH_2-\right]n + nH_2O \tag{11}$$
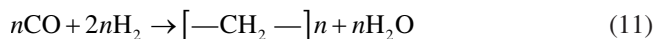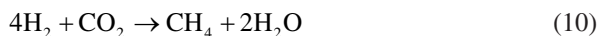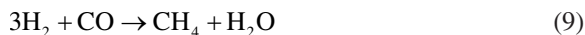
Mechanistic pathways followed during reforming of alcohols towards the formation of hydrogen and alkanes have been investigated in detail by Davda et al. [288] with *ethylene glycol* as the substrate, as illustrated in Scheme 6. Preferred pathway involves initial dehydrogenation, followed by the C-C bond cleavage of the adsorbed intermediate to yield CO, which undergoes water-gas shift reaction forming hydrogen and CO_2. Cleavage of C-O bond is not desirable since it would lead to the formation of acids. Thus, dehydrogenation and C-C bond cleavage are the two essential catalytic functionalities required for hydrogen production. While supported metal catalysts, in general, are suitable for these surface transformations, side reactions, methanation and F-T synthesis reactions involving the products, CO_2 and H_2, are also possible depending on process conditions. Reforming of two polyols, ethylene
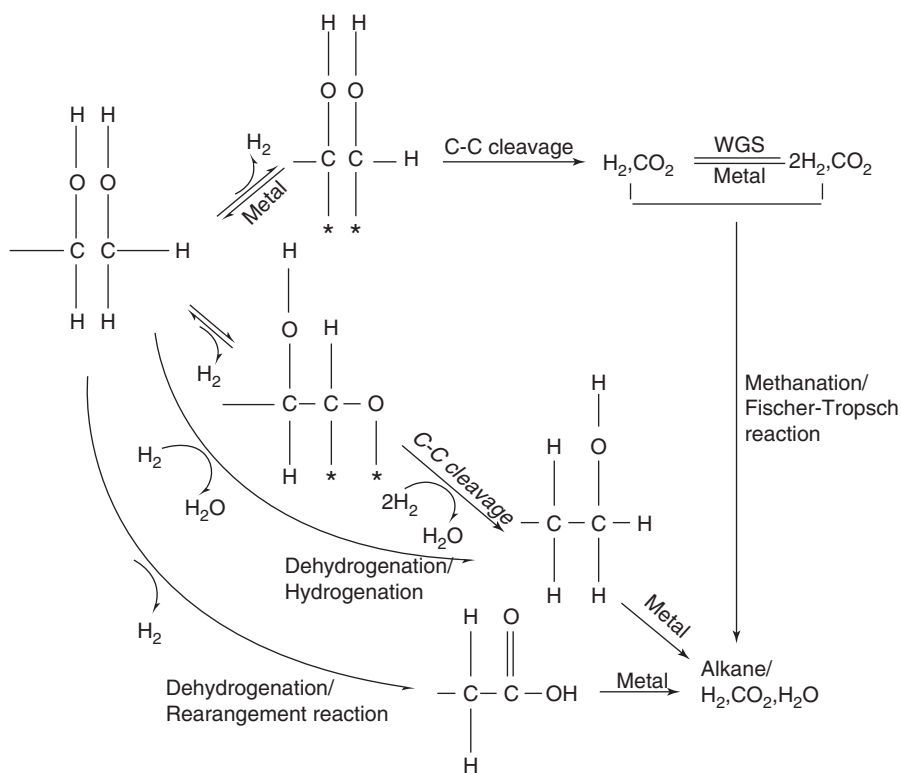
Scheme 6 Reaction pathways during aqueous phase reforming of ethylene glycol (Reproduced from Davda et al. [288])

glycol and glycerol, has been investigated extensively, and comprehensive reviews covering noble (Pt) and non-noble (Ni) monometallic and bimetallic (Pt-Re, Pt-Mn, Pt-Ni and Ni-Sn) catalysts on various supports and the influence of process conditions have been published [287, 289].

In the case of ethylene glycol, the order of activity on silica-supported metal catalysts was observed to be Pt ~ Ni > Ru > Rh > Pd > Ir, with Pt and Pd displaying high selectivity for H_2 formation while Ni and Rh for alkanes [288]. Amongst the supports investigated, alumina, silica, activated carbon (AC), mesoporous carbon (CMK-3) and pseudo-boehmite (Catapal B) for monometallic Pt and bimetallic Pt-Re and Pt-Mn catalysts [290–292], CMK-3 and AC exhibited higher conversion and selectivity for H_2 and better hydrothermal stability compared to silica and alumina supports. Kim et al. [291] have investigated several bimetallic catalysts supported on CMK-3 and observed that Pt-Re displayed high conversion (44.2%) but higher alkane selectivity (19.8%), while Pt-Mn exhibited lower conversion (39.7%) and lower alkane selectivity (2.9%) with higher hydrogen production rate, 26.8 cm^3/g/min vis-à-vis 19.8 cm^3/g/min for Pt-Re catalyst. Higher activity observed with bimetallic Pt-Mn and Pt-Ni catalysts is attributed to alloy formation [291, 293]. According to Bai et al. [294], addition of basic components, MgO and CeO_2, to alumina-supported Pt-Re catalysts resulted in 100% conversion and nearly 100% H_2 selectivity. Increase in Pt dispersion by addition of CeO_2 and moderation of alumina acidity by MgO are proposed to be responsible for high activity and selectivity. Choice of support, tuning support characteristics, metal loading and the active phase composition are thus crucial to achieve higher conversion as well as selectivity.

Similar studies on supported metal catalysts, especially on Pt-based mono- and bimetallic catalysts, on different supports, have been reported for aqueous phase reforming of *glycerol* as well [287, 289]. One significant observation [295, 296] is that larger Pt particles lead to a decrease in H_2 and CO_2 formation and C-C bond cleavage is favoured by small Pt particles as against C-O bond cleavage and hydrogenation reactions, thus highlighting the importance of catalyst preparation methods to achieve higher metal dispersion. Though nickel-based mono- and bimetallic (Pt-Ni) catalysts were active for APR of glycerol, deactivation of catalysts was a major concern, and several strategies, like changes in method of preparation (solgel, combustion synthesis), choice of supports and promoter elements, have been adopted to improve the stability of the catalyst [289]. Wen et al. [297] observed that for Pt-based catalysts, basic supports (MgO, CeO_2) resulted in higher conversion and selectivity, while neutral (AC) and acidic supports (alumina, silica, HUSY) increased the formation of alkanes. An exhaustive review by Fasolini et al. [298] covering the catalysts and process features in steam reforming and aqueous phase reforming of glycerol brings out the latest developments on these two processes. Highly efficient catalysts for both glycerol steam reforming (Ni/La$_2$O$_3$-Al$_2$O$_3$ catalyst with 100% conversion and 99.7% H_2 yield [299]) and aqueous phase reforming (Pt-Ni-Ce/Al$_2$O$_3$ catalyst with 96% conversion and 96% yield [300]) have been reported.

Though many methods for reforming of *ethanol* like steam reforming, oxidative reforming and autothermal catalytic reforming are known, all of them involve

higher reaction temperatures and tedious hydrogen purification processes due to high CO contents [291, 301].

Tokarev et al. [302] reported nearly complete conversion (98.3%) of 10% ethanol in water, during APR on Pt/Al$_2$O$_3$ catalyst at 225 °C and 29.3 bar pressure, in continuous-flow mode and observed hydrogen production of 0.15 mmol/min and stable activity. Addition of 10% sorbitol or 10% glycerol to aqueous ethanol solution resulted in increase of hydrogen production to 0.71 and 0.30 mmol/min, respectively, along with methane and CO formation. In the case of alumina (prepared by solution combustion synthesis—SCS)-supported Ni (10% w/w loading) catalyst for ethanol reforming, Roy et al. [303] observed that surface modification of the catalyst by non-thermal RF plasma treatment resulted in improvement in the ethanol conversion from 81.2% on unmodified catalyst to 85.9% on modified one at 225 °C, which displayed no deactivation for 144 h. Hydrogen yield was also higher, at 381 μmol/min for modified catalyst in comparison with 334 μmol/min for unmodified one. Roy et al. [303] attributed the superior performance of plasma-treated catalyst to an increase in Ni metal dispersion, stronger metal-support interaction and increase in acidity. Detailed studies on the influence of preparation methods for Ni/Al$_2$O$_3$ [304, 305] and Ru/TiO$_2$ [306] catalysts on the performance for ethanol reforming process have also been reported. Nickel supported on Mg-Al hydrotalcites with basic character and higher surface area and pore volume displays higher ethanol reforming activity compared to Ni/Al$_2$O$_3$ [307]. Though *n-butanol* has higher hydrogen content (13.5% w/w) compared to ethanol (13%) and methanol (12.5%), n-butanol conversions are low, 5.77% on Ni/CeO$_2$ and 2.77% on Ni/Al$_2$O$_3$ at 488 K [308]. Both noble metal (Pt, Pd) and non-noble metal (Ni) catalysts have been explored for reforming of *sorbitol and xylitol* [289]. Higher hydrogen yield and hydrogen selectivity were observed for xylitol in comparison with sorbitol, since its longer carbon chain leads to higher alkane formation.

Comparative evaluation of the APR activity of different alcohols has been reported albeit with some contradictions. While Shabaker et al. [309] reported similar APR rates for methanol and ethylene glycol on Pt/Al$_2$O$_3$, with higher hydrogen production rate for methanol, Liu et al. [310] reported higher ethylene glycol reforming rates with higher hydrogen selectivity compared to methanol, on Pt catalysts on five different supports.

According to Cortright et al. [283], amongst different alcohols, maximum selectivity for hydrogen production was observed with methanol, with lowest CO$_2$ production, since it has lowest number of carbon atoms (Table 7).

These studies reveal that C-C bond cleavage is not the decisive step in APR process and the reaction mechanism varies with the type and molecular structure of the substrate alcohol.

Table 7 APR reaction data for different alcohols on Pt-based catalysts

Feedstock	Concentration, %	Carbon in liquid/ gas phase effluents, %	Hydrogen selectivity, %	Alkane selectivity, %	CO₂ in gas phase effluent, %
Methanol	12.5	6.5/94	99	1.7	25
Ethylene glycol	9.7	11/90	96	4	29
Glycerol	8.6	17/83	75	19	29.7
Sorbitol	7.6	29/61	66	15	35

Temperature, 498 K; pressure, 2.9 MPa (Adapted from Cortright et al. [283])

6 Value Added Products from Sugar Alcohols: Sorbitol, Mannitol and Xylitol

Sorbitol is a versatile platform chemical with highly reactive hydroxyl groups, which undergo a variety of transformations like dehydration, hydrogenolysis, oxidation and aqueous phase reforming to yield value-added products with many applications [136, 311]. An illustration of the applications of sorbitol and its derivatives in pharma, medicinal, cosmetics, food, confectionary, bioplastics and elastomers industries, brought out by Kobayashi and Fukuoka [312], is presented in Scheme 7. Isosorbide (1,4:3,6-dianhydrohexitol) is one such derivative of sorbitol, with multiple applications (Scheme 7) with a market size of US$ 396 million in 2018 which is projected to grow at CAGR of 8.5% during 2019–2025 [313]. A number of isosorbide-based biopolymers like polyethylene isosorbide terephthalate (PEIT), polycarbonate, isocyanate-free polyurethane [314], polyisosorbide succinate and isosorbide diesters are produced from isosorbide. Hence, production of isosorbide from sorbitol by acid-catalysed stepwise dehydration (Scheme 8) and directly from cellulose has been the subject of extensive investigations. Different types of solid acid catalysts like supported metal catalysts, zeolites, heteropoly acids, metal phosphates and ion-exchange resins have been explored for the conversion of sorbitol to isosorbide [136, 311]. Otomo et al. [315] could achieve isosorbide selectivity of 80% with zeolite β catalyst with SAR-75. Sulphonic acid-functionalized silica, modified with optimum loading of (3-mercapto-propyl) trimethoxy silane (MPTS) catalysts displayed better performance, with 100% sorbitol conversion and 84% yield of isosorbide [316]. Direct conversion of cellulose to isosorbide, using a combination of Amberlyst 70 ion-exchange catalyst (for cellulose hydrolysis to glucose and dehydration of sorbitol to isosorbide) and 4% Ru/C (for hydrogenation of glucose to sorbitol) to get 55.8% yield of isosorbide in single-pot process, has been reported by Yamaguchi et al. [317].

Besides the applications indicated in Scheme 7, catalytic conversion of sorbitol to alkanes via aqueous phase reforming and hydrogenolysis to ethylene glycol and 1,2- and 1,3-propylene glycols are the other important and well-known applications of sorbitol [136, 312].

Mannitol is useful in the synthesis of surfactants, resins and biofuels [318, 319], and mannitol-boric acid complex is used in the preparation of dry electrolytic capacitors. Mannitol has several crucial applications in the field of medicines [136]: (1) as a powerful osmotic diuretic, enhancing the urination to prevent renal failure by removing toxic materials from the body, (2) for reducing the brain swelling, (3) in enhancing the drugs' transport across the blood-brain barrier for the treatment of acute brain diseases and (4) as a common vasodilator for the treatment of hypertension.

Xylitol is yet another platform chemical which is used in food, bakery and confectionary industries. Though not widely used in the chemical industry due to its
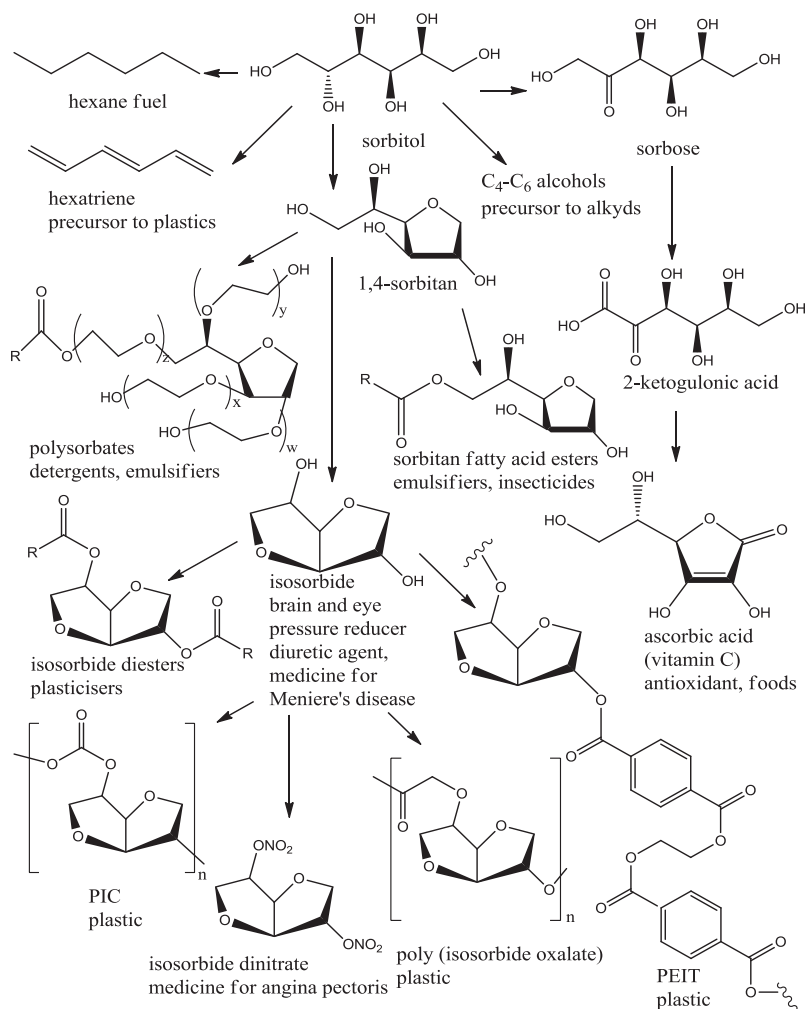
Scheme 7 Applications of sorbitol and its derivatives (Reproduced from Kobayashi and Fukuoka [312])
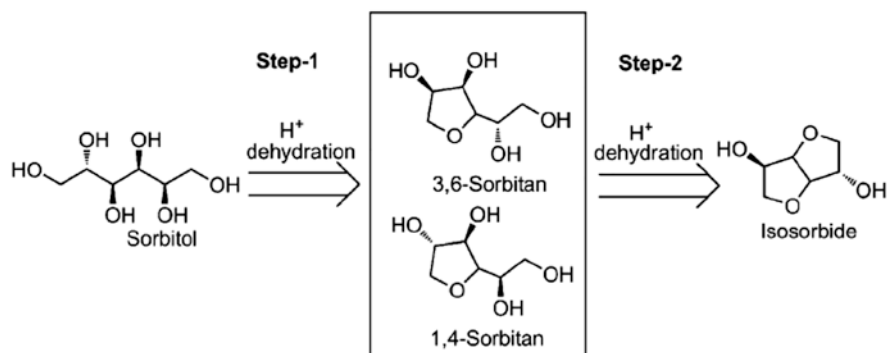
Scheme 8 Stepwise dehydration of sorbitol to isosorbide (Reproduced from Zada et al. [136])

inert nature, it is an active ngredient in several pharmaceutical, dental and oral care products [136].

Catalytic conversion of xylitol to value-added products, ethylene glycol and propylene glycol, proceeds through dehydrogenation, retro-aldol condensation and re-hydrogenation pathways [320, 321]. An illustration of the major applications of mannitol, xylitol and arabitol, another sugar alcohol, according to Kobayashi and Fukuoka [312], is presented in Scheme 9.

7   Conversion of Glycerol into Value-Added Products

Applications of glycerol as a versatile platform chemical, capable of undergoing a variety of sustainable chemical transformations towards a wide range of value-added chemicals, fuels and fuel additives, have been reviewed comprehensively [91, 95–99]. Some of the unique features of glycerol that make it as the most useful raw material are:

- Abundance and low cost.
- Utilization as crude glycerol.
- Amenable to chemo- as well as bio-catalytic conversions.
- Highly reactive functional groups.
- Wide spectrum of products based on types of catalysts/reaction conditions.

A summary of value-added products from glycerol (Fig. 30), through different catalytic processes, types of catalysts and developments therein, reported up to 2009, has been published by Bozell and Petersen [21]. Two recent comprehensive reviews by Nda-Umar et al. [322] and Cognet and Aroua [323] on this topic cover the latest developments in the processes, catalysts and other features for the production of many glycerol derivatives indicated in Fig. 30. Non-combustion routes like steam reforming, partial oxidation, autothermal reforming and aqueous phase
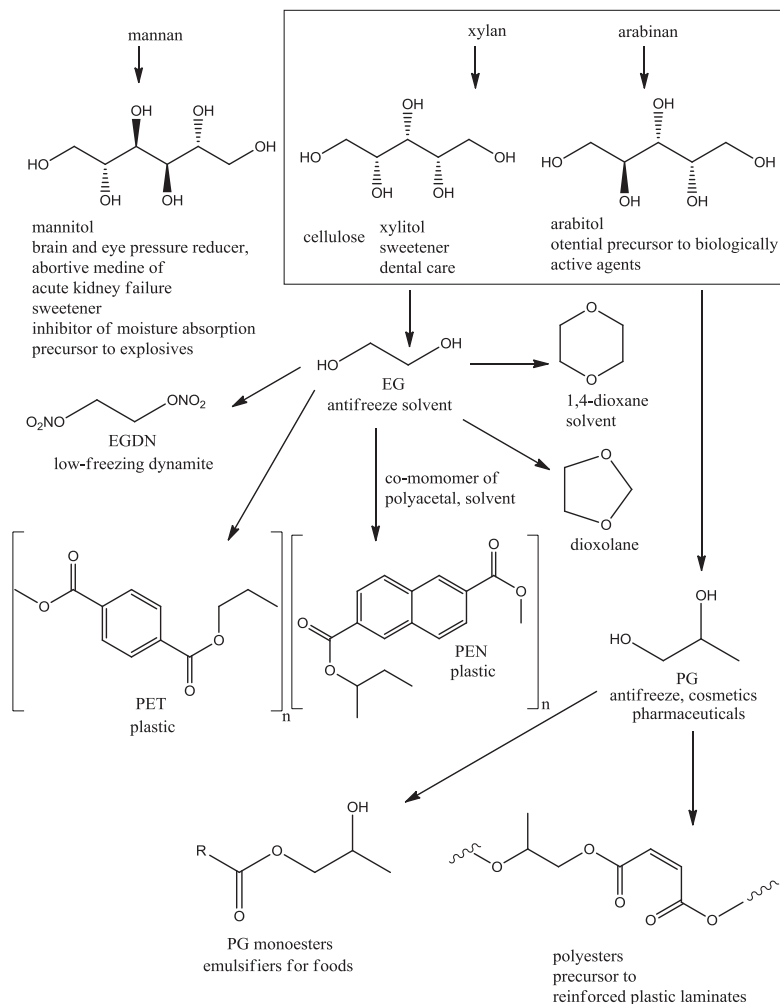
Scheme 9 Applications of mannitol, xylitol and arabitol (Reproduced from Kobayashi and Fukuoka [312])

reforming and supercritical water reforming are available for the conversion of *glycerol into hydrogen and syngas* [322]. Both nickel- and platinum-based catalysts supported on modified (especially with ceria) alumina have been explored for steam reforming [322]. 10%Ni/5%CeO$_2$-Al$_2$O$_3$ at 650 °C displayed 85.7% selectivity for hydrogen in continuous-flow packed bed reactor [324]. For APR of glycerol, 71.9% yield of hydrogen could be obtained on 1.44% Pt/Al$_2$O$_3$ at 225 °C, pressure = 2.3 MPa time = 3 h, with 100 mg of catalyst [325].

Though glycerol conversion and hydrogen production in APR process are, in general, less in comparison with steam reforming, utilization of crude glycerol in APR is less energy-intensive since vaporization is not required. Hence further
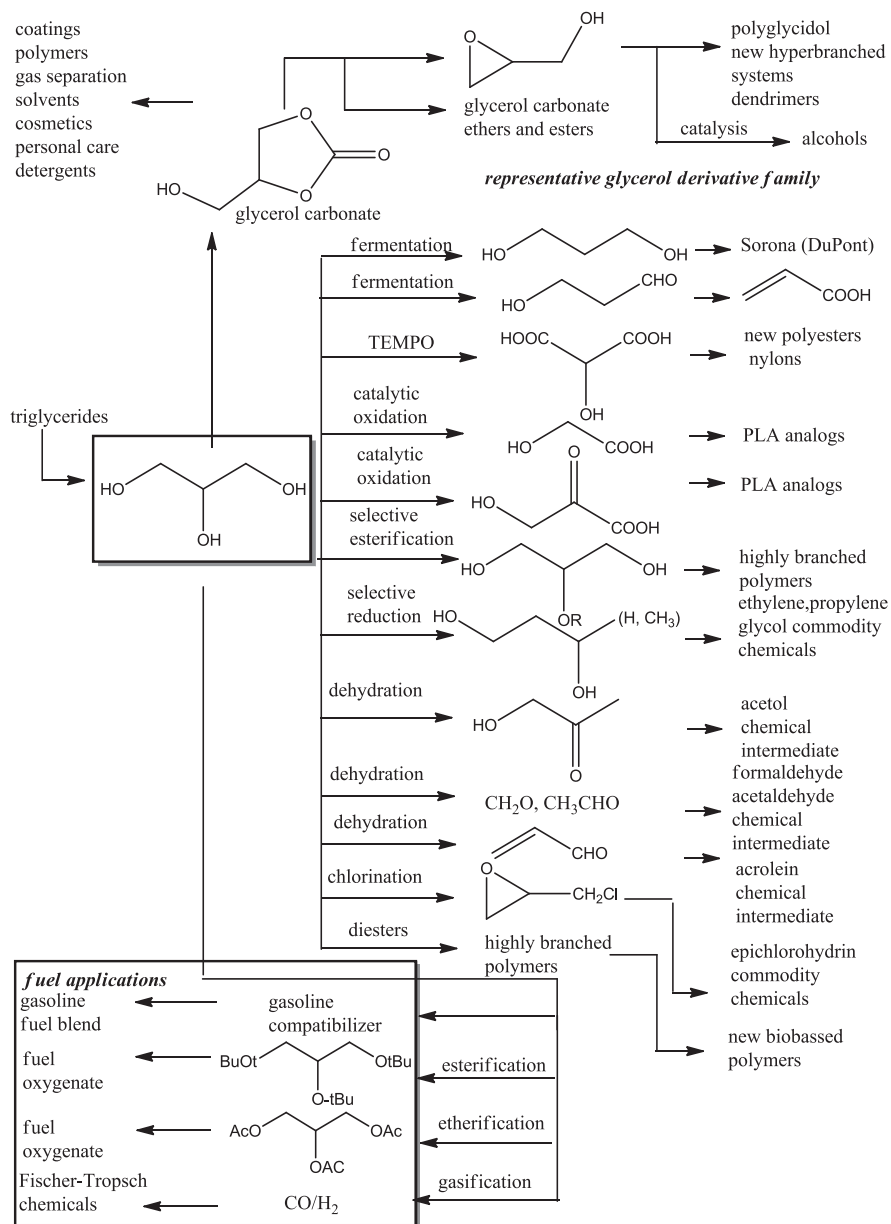
Fig. 30 Summary of the processes for conversion of glycerol into value-added chemicals, fuels and fuel additives (Reproduced from Bozell and Petersen [21])

improvements in catalysts for APR of glycerol is required. Conversion of glycerol to syngas by microwave plasma and supercritical water gasification of glycerol result in syngas production, which is to be converted further to yield hydrogen. These processes however require higher temperatures (500–650 °C) and low concentration of glycerol, 5–20% w/w [322].

Fuel additives, when blended with gasoline or diesel, help to improve viscosity and cold flow properties, anti-knock characteristics and octane rating and reduce emission of harmful exhaust gases (NOx) and particulates. They also ensure thermal stability and clean combustion of the fuel and prevent corrosion of engines. Some of the fuel additives that can be obtained from glycerol are *acetin (glycerol esters)*, *glycerol ethers*, *solketal and acetal*.

Esterification of glycerol with acetic acid or acetic anhydride using homogeneous and heterogeneous catalysts [326, 327] and transesterification of glycerides or glycerol with methyl acetate [328, 329] are known. Being a trihydric alcohol, acetylation of glycerol could lead to the formation of mono-, di- and triacetins, as illustrated in Scheme 10 [322]. While mono- and diacetins find applications in cosmetics, medicines and food industries and as monomers in the production of biodegradable polyesters, it is the triacetins which are useful as fuel additives. Esterification is basically an acid-catalysed reaction, and almost all types of heterogeneous acidic catalysts, starting from ion-exchange resins (Amberlyst-15), clays (K10-montmorillonite), zeolites (H-beta, HZSM-5, HSUY), niobic acid, heteropoly acids, sulfonic acid-functionalized mesoporous SBA-15, zirconia-based mixed metal oxides and sulphated zirconia-based catalysts, have been explored as catalysts. A list of such catalysts, reported recently, has been compiled by Nda-Umar et al. [322], and few examples are covered here. Though acetic acid is commonly employed as acetylating agent, use of acetic anhydride is advantageous due to better accessibility of acylium ion from the anhydride compared to the intermediate from acetic acid. Due to this reason, on H-beta and K10, with acetic anhydride, 100% selectivity for triacetin was achieved in 20 min at low temperature of 60 °C [330].
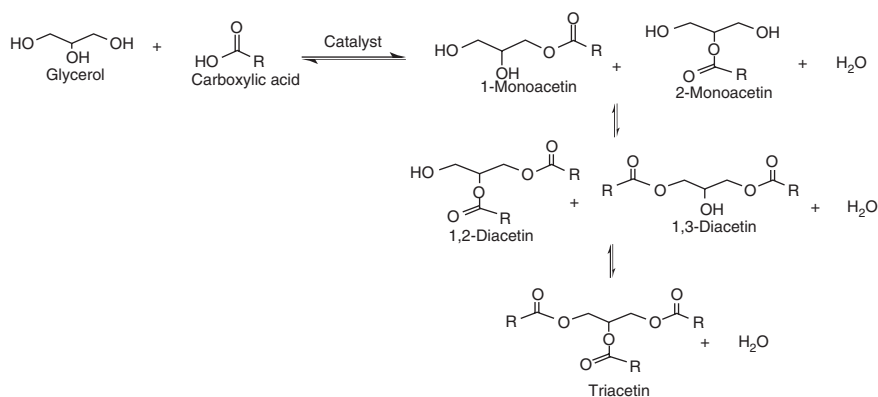
Scheme 10 Conversion of glycerol to acetins by esterification with carboxylic acid (Reproduced from Nda-Umar et al. [322])

On Amberlyst-15, with acetic acid as acylating agent, 90% glycerol conversion and 31%, 54% and 13% selectivity towards mono-, di- and triacetins could be realized. However, with acetic anhydride, on the same catalyst, 100% selectivity for triacetin was observed in 80 min at 60 °C. Iron oxide nanoparticles supported on mesoporous SBA-15 were highly active for glyceride formation with levulinic acid in the place of acetic acid, displaying >99% conversion of glycerol and 71% diacetin and 28% triacetin selectivity [331]. Sandesh et al. [332] have reported simultaneous synthesis of biodiesel and acetins using methyl acetate, on a series of novel solid basic catalysts, based on metal hydroxy stannates, MSn $(OH)_6$ with M = Mg, Zn, Sr and Ca. The catalyst with higher basicity, CaSn $(OH)_6$, exhibited glycerol conversion of 78.2%, with 67.3 monocetins and 32.6% diacetins selectivity. While complete conversion of glycerol could be realized, major research efforts are directed towards achieving desired acetin selectivity, by employing different catalysts and process conditions [322].

Glycerol ethers are useful as oxygenated fuel additives and solvents. Glycerol ethers are obtained by etherification of glycerol with olefins/alcohols (isobutene/ tertiary butyl alcohol). Similar to acetins, glycerol mono-, di- and tri-ethers are formed. Different types of zeolites, clays, ion-exchange resins and supported heteropoly acids have been employed as catalysts [322]. Carbon supports derived from bio-resources like sugar cane bagasse, coconut husk and coffee grounds, after functionalization with sulphonic acid, proved to be highly effective for etherification of glycerol. 81.8% glycerol conversion with 60.5% selectivity to mono-ether and 21.8% to di- and tri-ethers could be obtained with carbon derived from sugar cane bagasse [333]. A comparative evaluation of ion-exchange resins (Amberlyst-15 and Amberlyst-35) and zeolites (Beta-BEA and USY and MOR) has shown that though the resin catalysts exhibit higher glycerol conversion at a lower temperature (75 °C) than zeolite-based catalysts (90–110 °C), the latter group of catalysts display higher stability, forming preferentially di- and tri-tertiary butyl glycerol. More than 95% glycerol conversion with 45% and 54% selectivity for di- and tri-tertiary butyl glycerol is realized on nanosize BEA catalyst, due to relatively larger-sized pores [334].

Glycerol formals are formed by reaction between glycerol and aldehyde or ketone as illustrated in Scheme 11.

Solketal is a highly useful fuel additive, known for reducing particulate emission and gum formation and improving cold flow characteristics and oxidation stability [335, 336]. More than 90% yield of solketal is obtained by condensation of glycerol
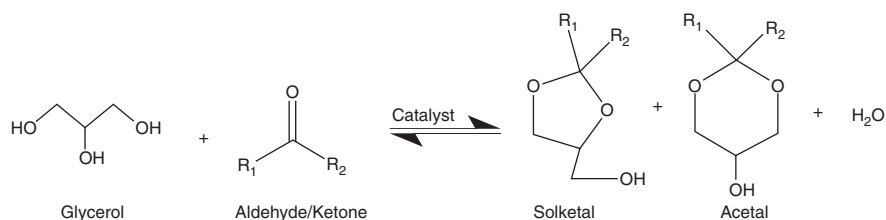
Scheme 11 Conversion of glycerol to solketal and acetal (Reproduced from Nda-Umar et al. [322])

and acetone using p-toluene sulfonic acid as the catalyst, with glycerol/acetone ratio of 1:6 [337]. Formation of ketals with several types of ketones besides acetone like butanone, cyclopentanone, 4-methyl-2-pentanone and 3,3-dimethyl-2-butanone was investigated by De Torres et al. [338]. In the condensation of glycerol and cyclopentanone, at a molar ratio 1:1 and at 60 °C temperature, 81.4% solketal was obtained with fluorosulfonic resins (NR-50 and SAC-13) and K10-montmorillonite as catalysts over a reaction time of 2 h. Condensation of glycerol with acetone in continuous-flow mode using several heterogeneous catalysts (Amberlyst wet, zeolite, Amberlyst dry, zirconium sulphate, montmorillonite and polymax) was investigated by Nanda et al. [339]. Under optimized process conditions of 25 °C, acetone/crude glycerol molar ratio of 4 and WHSV of 2 h^{-1}, maximum yield of 94 ± 2% solketal could be obtained [340] on Amberlyst wet catalyst, which could be regenerated and reused for another 24 h cycle, without any loss of activity.

Similarly, formation of *acetals* by condensation of glycerol with aldehydes, using different types of acidic catalysts, has been studied extensively [322]. Like ketals, acetals are useful as fuel additives and solvents in paint and pesticide industries. Umbarkar et al. [341] have studied acetalization of glycerol with different aldehydes on well-characterized mesoporous MoO_3/SiO_2. Maximum conversion of 72% benzaldehyde with 60% selectivity to acetal was observed on 20% w/w MoO_3/SiO_2 at 100 °C in 8 h. Recent developments in the catalysts and features in the processes for acetalization of glycerol have been covered in a review by Amin et al. [342].

Glycerol could be converted into a number of *value-added chemicals/chemical intermediates* (Fig. 30) through chemo- and bio-catalytic routes as described in several reviews [21, 91, 95–99, 322, 323]. Apparently simple conversion like dehydration of *glycerol to acrolein* has been the subject of intensive studies, mainly devoted to the development of catalysts that display maximum selectivity at optimum conversion and reasonable life/regenerability. Though Cs salt of heteropoly tungstic acid supported on silica displayed 100% glycerol conversion and 98% selectivity for acrolein, the stability of the active phase (leaching) was the challenge [343]. Similarly, on supported $NiSO_4$ catalyst, 90% glycerol conversion and 70% selectivity to acrolein could be achieved, but the catalyst was prone to deactivation due to oxidation and loss of sulphur [344]. Multicomponent catalyst with W-Zr-Al active phase, supported on hexagonal mesoporous silica (HMS) (MUICat-5), displayed excellent stability, higher glycerol conversion (86%) but moderate acrolein selectivity of 60% [345]. Though zeolite-based catalysts are active at high GHSV (1438 h^{-1}), selectivity for acrolein is low [346]. A compilation of catalysts for dehydration of glycerol from recent literature is presented in the review by Nda-Umar et al. [322]. Some of the strategies for extending the catalyst life and reactor design aspects are discussed in another monograph by Cognet and Aroua [323].

Glycerol carbonate (GC) is the other glycerol derivative with widespread applications in the manufacture of polyurethanes, polyesters, polycarbonates and polyamides and useful as substitute for fossil-derived ethylene carbonate or propylene carbonate. It is also used as solvent in the paint, battery and detergent industries as well as in the synthesis of very valuable intermediates such as glycidol. GC is

prepared by three routes, by reacting glycerol with urea or dimethyl carbonate or by directly reacting it with carbon dioxide under supercritical conditions [322]. Transesterification of glycerol with ethylene carbonate over basic oxide catalysts (MgO, CaO) and mixed metal oxides of Al-Mg, Li-Al and Al-Ca-MO with hydrotalcite structure at 35 °C results in high conversion and >98% selectivity to GC [347]. Ionic liquid catalysts like 1-n-butyl-3-methylimidazolium-2-carboxylate could yield 93% GC in 5 h. With the ionic liquid 1-ethyl-3-methylimidazolium acetate as catalyst, glycerol conversion of 93.5%, selectivity of 94.9% and GC yield of 88.7% were obtained at optimum conditions of 120 °C, 0.5 mol.% catalyst loading, diethyl carbonate/glycerol molar ratio of 2 and reaction time of 2 h [348]. There was no deactivation even after the catalyst was used three times, which was attributed to excellent interaction between the ionic liquid and the reactant.

1,3-Propane diol is a versatile chemical intermediate and highly useful monomer for the production of polyesters (polytetramethylene terephthalate, PTT), polyethers, polyurethanes and many other value-added chemicals [322]. Hydrogenolysis of C-O bond in glycerol results in the formation of 1,2-propane diol (1,2-PDO) and 1,3-propane diol (1,3-PDO), with the selectivity for specific diol determined by the type of catalyst and the reaction conditions adopted. Hydrogenolysis, which involves dehydration as the first step, can result in the formation of hydroxy acetone, which on further hydrogenation leads to 1,2-PDO. If, on the other hand, the dehydration leads to the formation of 3-hydroxy propanal, its further hydrogenation results in 1.3-PDO [349]. Since formation of hydroxy acetone is favoured thermodynamically, 1,2-PDO is formed with high selectivity on many types of catalysts, noble metal, non-noble metal or noble metals in combination with acidic/basic components [98–102]. However, 1,3-PDO with high selectivity of 66% is observed only with noble metal- mixed oxide catalysts, like Pt-WO_x/AlOOH with moderated acidity [100]. Though a large number of other catalyst systems, mono- and bimetallic catalysts with different supports, have been explored [322, 349], maximum 1,3-PDO selectivity of 52% could be realized. On Ir-ReO_x/SiO_2 catalyst, Nakagawa et al. [349] could observe 1,3-PDO selectivity of 65% but at lower glycerol conversion of 22.6%. Thus, achieving high conversion of glycerol with high selectivity for 1,3-PDO on heterogeneous catalysts remains a challenge. Biochemical conversion of glycerol to 1,3-PDO, using different microorganisms like *Bacillus*, *Lactobacillus*, *Klebsiella*, *Citrobacter*, *Ilyobacter*, *Enterobacter and Clostridium*, in batch and continuous mode processes, has been reported [350].

Glycerol as biochemical feedstock has gained prominence when it replaced glucose as the raw material for the enzymatic conversion to 1,3-PDO [21]. With glycerol as the feedstock, 1,3-PDO yields approaching to the theoretical yield (g of 1,3-PDO per g of feed) of 67% could be achieved with genetically modified *Clostridium acetobutylicum* with concentrations of over 84 g L^{-1} at a rate of 1.7 g L^{-1} h^{-1}. In contrast, with glucose as feedstock, the yield was 30–40% only [351, 352]. Fermentation of *crude glycerol* with *Clostridium acetobutylicum* [353] and *Klebsiella pneumoniae* [354] resulted in the same level of PDO concentration and productivity realized with purified glycerol, thus paving way for the utilization of crude glycol as economically viable bio-resource for the production of 1,3-PDO.

Utilization of crude glycerol as biochemical feedstock for 1,3-PDO has brought into focus the production of several other important chemicals/chemical intermediates through enzymatic processes. Microbial processes with crude glycerol as feedstock have been reported for the production of hydrogen, methanol, ethanol, n-butanol, glyceric acid, citric acid, polyunsaturated fatty acids, lactic acid, succinic acid and biopolymers like poly hydroxy alkanoate (PHA), poly hydroxy butyrate (PHB) and acrylates. Development of microbial processes for these chemicals, types of microorganisms employed and the process conditions adopted have been covered in detail in the reviews by Dobson et al. [355] and Garlapati et al. [356].

Oligomerization of glycerol to polyglycerol and conversion to olefins (ethylene, propylene and butadiene) are the other processes that utilize glycerol as raw material [322].

Though a number of processes have been developed and patented [322] for the conversion of glycerol to value-added chemicals, fuels and fuel additives, only few of them have reached commercial scale. Epichlorohydrin from glycerol (Dow, Solvay) via dichloro propanol [21], 1,3-PDO using recombinant *Escherichia coli* (DuPont) and polyglycerols by Sakamato Japan have been successful on commercial scale. Tremendous opportunities as well as challenges remain in glycerol conversion processes, requiring continuous research efforts to improve process efficiency, selectivity, catalyst stability and reduction in the cost of production, to enable viability on commercial scale.

8   Conversion of Furfuryl Alcohol into Fuels and Chemicals

Furfuryl alcohol (FOL) is one amongst the most important derivatives of furfural (FAL), another abundant biomass intermediate and a versatile platform chemical [357]. More than 65% of FAL is utilized for the manufacture of FOL by catalytic hydrogenation, which has been studied extensively [357, 358]. Major applications of FOL derivatives towards production of value-added chemicals/fuels are illustrated in Fig. 31.

An important derivative of FOL is *levulinic acid* (LA, 4-oxopentanoic acid), which is one amongst the 12 platform chemicals identified by US DOE in 2004, with tremendous application potential. Global market for LA during the period 2019–2024 is projected to grow at CAGR of 4.9%, to touch US$ 34.5 Mill. by 2024 [359]. As many as 16 different application segments for LA have been listed by Bozell et al. [360]. LA can be produced from lignocellulosic biomass via the Biofine process [361] and also from FOL by acid-catalysed ring opening in H_2O [362]. LA with two active functional groups (keto and carboxyl) undergoes a range of chemical transformations (Fig. 32) yielding highly useful chemicals and fuels. Salient features of these transformations brought out by different catalysts have been covered in the reviews by Bozell et al. [360], Mariscal et al. [357] and Xue et al. [363].

Delta-aminolevulinic acid (DALA), another derivative of LA, is useful as biodegradable broad-spectrum herbicide/insecticide and for cancer treatment [360].
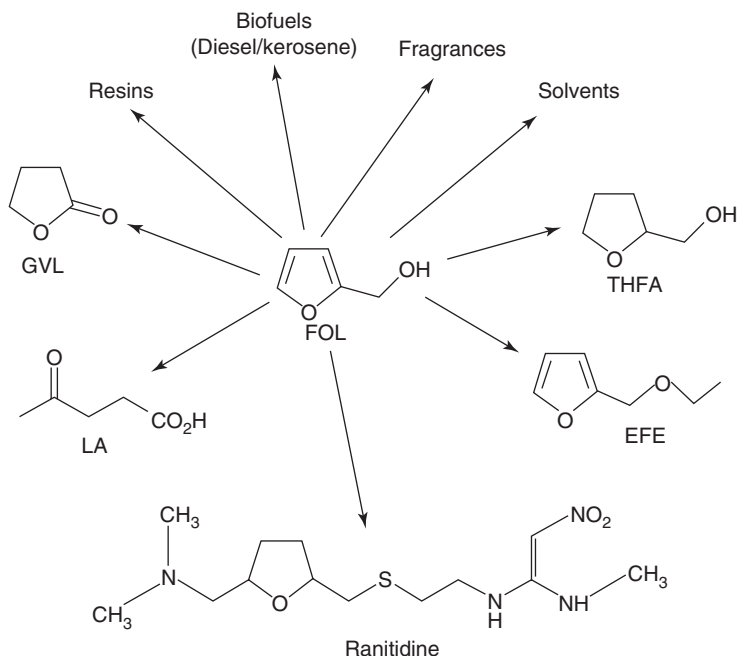
Fig. 31 Value-added products from furfuryl alcohol (Reproduced from Mariscal et al. [357])
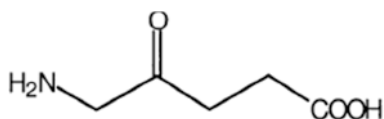
Delta-aminolevulinic acid (DALA).

Other derivatives like methyltetrahydrofuran, γ-valerolactone (GVL) and esters of levulinic, valeric and pentanoic acids find applications as fuels and fuel additives [357].

Alkyl levulinates (AL) or esters of levulinic acid, especially with ethanol and butanol, belong to a class of highly efficient bio-based fuel additives for blending with gasoline and diesel, due to low sulphur content and toxicity, high lubricity, good flow properties and flash point stability [357, 364]. Several routes based on solid acid catalysts for synthesis of AL from different raw materials like (1) levulinic acid, (2) mono- and disaccharides (glucose, fructose, sucrose), (3) polysaccharides and biomass and (4) furfuryl alcohol have been investigated in detail and been covered extensively in the reviews by Ahmad et al. [364] and Demolis et al. [365]. Ionic liquids [IL]-based and sulfonic acid-functionalized catalysts are reported to be promising candidates for these processes [364]. Though direct synthesis of AL from cellulosic biomass is possible, due to its complex structure, the process involves several steps like depolymerization, solvolysis, dehydration and

alcoholysis and requires relatively severe process conditions and hence lower selectivity/yields in comparison with those from LA or FOL.

Etherification of FOL with ethanol yields (Scheme 12) *ethyl furfuryl ether* (EFE), an efficient fuel additive. Synthesis of EFE using ZSM-5 and zeolite beta catalysts and its blending characteristics with gasoline up to 30% w/w have been reported by Haan and Lange [366, 367].

Especially with ZSM-5 (SAR-30) catalyst, and ethanol/FOL molar ratio of 7.5:1, EFE yield of 50% could be achieved with 80% conversion of FOL at 398 K by Lange et al. [368]. Though some amount of (<10 mol.%) useful side products like LA and angelica lactone could be observed, formation of ~20 mol.% of heavier products points out the need for further improvements in the process, in terms of
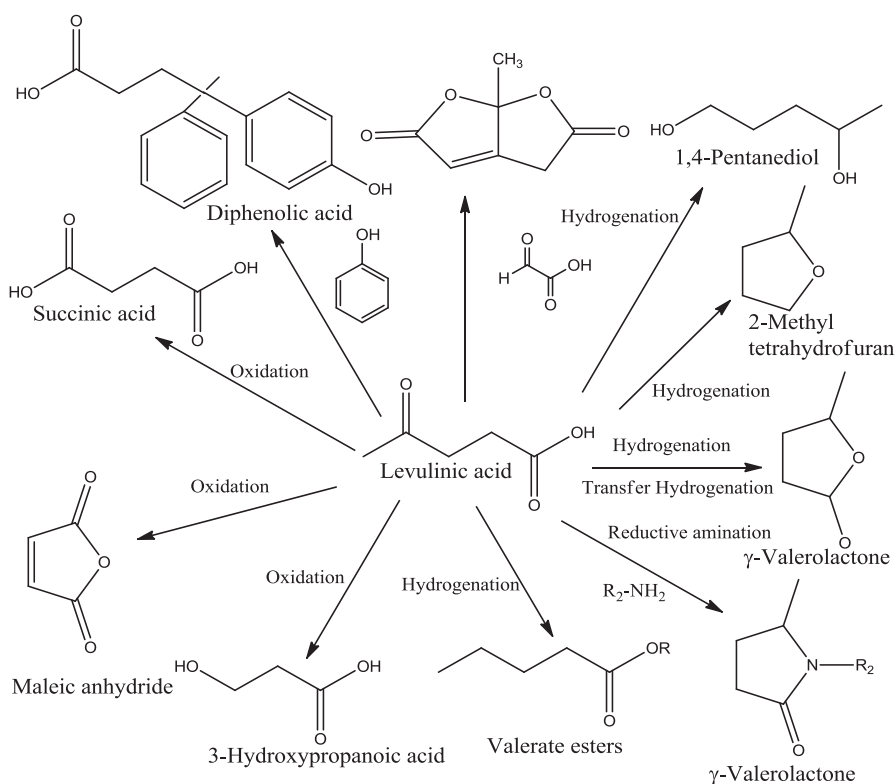
Fig. 32 Chemical transformations of levulinic acid to value-added chemicals and fuels (Reproduced from Xue et al. [363])

Scheme 12 Etherification of furfuryl alcohol to ethyl furfuryl ether
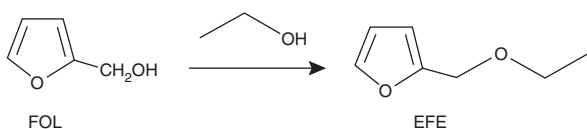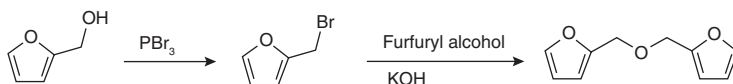
Scheme 13 Synthesis of DFE from FOL

alternative more selective catalysts and optimization of process conditions and arresting the deactivation of catalysts. *2,2′-Difurfuryl ether* (DFE), a well-known flavouring agent in the food industry, is obtained from FOL, by conventional two-step process [369] involving bromination of FOL followed by etherification (Scheme 13).

DFE is also formed as by-product during oligomerization of FOL [370] and by direct etherification using polyoxometallate catalysts [369].

By carrying out appropriate modifications in the catalyst formulations and optimization of process conditions (to achieve ring/side-chain or total hydrogenation), three more useful derivatives of FOL, namely, tetrahydro furfuryl alcohol (THFOL), methyl furan (MF) and methyltetrahydrofuran (MTF), with specific individual applications as chemicals and fuels [357, 358, 368], could be obtained.

Highly controlled *oligomerization and polymerization* of FOL yield a range of useful materials/composites [371–373]. Oligomerization of FOL (in homogeneous phase with H_2SO_4 or Amberslyst-15 ion-exchange catalyst in heterogeneous phase) followed by hydrogenation on Ni/Al_2O_3 catalyst (Scheme 14) results in C_9–C_{20} hydrocarbons useful as diesel/kerosene range blends [357, 374] and fuels.

Besides being the raw material for the manufacture of numerous chemicals and fuels, the most important application of FOL, in terms of consumption volume (~88%), is for the manufacture of resins. Exothermic condensation polymerization of FOL in the presence of aqueous acid solution proceeds in two modes, the first one being alkylation at C_5 position of the furan heterocycle (forming a methylene bridge, with head-to-tail structure) and the second involving the condensation of two −OH groups (etherification, with head-to-head structure) as depicted in Fig. 33. However, on elimination of formaldehyde from ether linkages, head-to-head configuration transforms into head-to-tail structure. The resinification process, besides being highly exothermic, is also autocatalytic, requiring efficient heat removal and careful control of pH, to avoid any possible explosion [375]. Inorganic (H_2SO_4 HCl and HNO_3) and organic (p-toluene sulfonic, dodecyl benzene sulfonic, formic, lactic, maleic and oxalic) acids and Lewis acids $SnCl_4$ and $TiCl_4$ have been employed as catalysts for resinification of FOL. This is followed by curing process, wherein conjugated polyfurfuryl chains undergo interchain Diels-Alder condensation leading to cross-linking [357]. When solid acid catalysts are used, they get incorporated in the resin matrix, forming polymer-based nanocomposites (PNC) with improved properties [376]. Such cross-linked polymers of FOL possess excellent chemical, thermal, corrosion resistance and mechanical properties, thus rendering them highly useful for applications in foundry industry and for coatings, wood protection, fibre-reinforced plastics, adhesives and binders, low-flammability materials, membranes and fabrication of electronic materials. Hazards due to emission of formaldehyde, generally associated with formaldehyde-based resins, are avoided with the use of FOL-based resins.
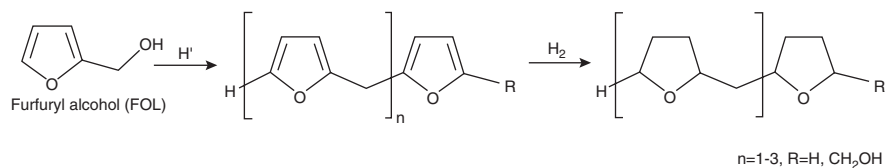
Scheme 14 Oligomerization-hydrogenation of FOL to diesel/kerosene blends [357]
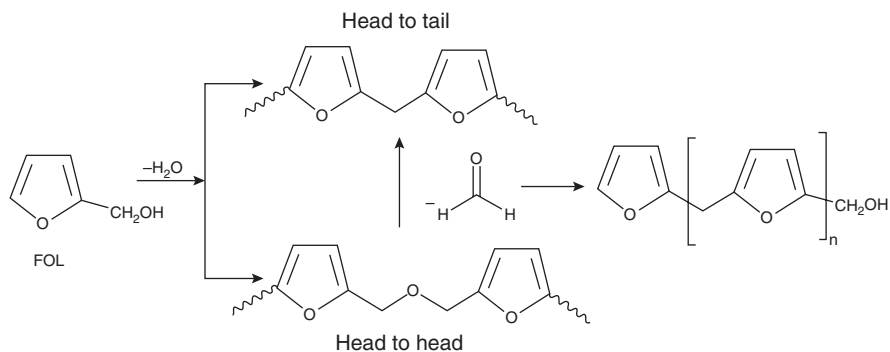
Fig. 33 Acid-catalysed condensation polymerization of FOL [357]

9 Miscellaneous Conversions of Alcohols

Oxygenates of alcohols, namely, aldehydes, ketones, acids, ethers and esters, are important class of derivatives, useful mainly as solvents, raw materials and intermediates for the synthesis of value-added products. Depending on the type of catalysts (usually supported metal/metal oxide) and the process conditions, different oxygenated products are formed. Dehydration, dehydrogenation, oxidative dehydrogenation, etherification, oxidation and esterification are the typical reactions involved. Synthesis and applications of oxygenates from ethanol have been studied extensively and reviewed [166, 377, 378]. Simplest of all is the conversion of ethanol to diethyl ether (DEE) by vapour phase acid-catalysed dehydration of ethanol. On gamma alumina [379], DEE with 80% selectivity is obtained, while on heteropoly acid catalyst [380], nearly 100% selectivity could be achieved. While monofunctional supported copper catalysts are active for acetaldehyde formation via dehydrogenation, supported gold catalysts, on the other hand, catalyse oxidative dehydrogenation of ethanol to yield acetaldehyde [377]. A bi-functional redox-acidic catalyst [Cu/ZrO$_2$] further transforms acetaldehyde into ethyl acetate by reaction with ethanol. It is proposed that a pair of Cu^0/Cu^{+1} sites present at metal/support interface facilitate further reaction of acetaldehyde and ethanol to ethyl acetate [381]. Both liquid phase (supported Au catalysts) and vapour phase (supported Mo-V-Nb catalysts) oxidation of ethanol to acetic acid have been reported. Cu-doped Au/NiO is found to be highly active at 120 °C in aqueous phase oxidation of ethanol

to acetic acid with >90% selectivity [377]. However, the process is not viable on industrial scale, wherein carbonylation of methanol with CO in homogeneous phase, with Rh/Ir complexes (Monsanto/CATIVA processes), is the preferred route.

Alkylation with alcohols is a well-known reaction, and catalytic alkylation of aromatics with alcohols is a well-established process in petrochemical industry. Recently *alpha-alkylation* reactions of various substrates with alcohols via hydrogen borrowing cycle are being pursued extensively [382]. Scheme 15 presented below describes the mechanistic pathway involved in the process, which starts with the transfer of hydrogen from alcohol A to the metal M, resulting in the formation of aldehyde B and metal hydride C. Base-catalysed aldol condensation of aldehyde B with the substrate carbonyl compound D leads to the formation of αβ-unsaturated ketone E, which undergoes hydrogenation through metal hydride to yield the alpha-alkylated product F. The process, resulting in the formation of C-C bonds via C-alkylation in presence of various transition metal catalysts and a base, has widespread applications in synthetic organic chemistry and been studied extensively. Different types of carbonyl substrates, like aldehydes, ketones, esters, amides [383], nitriles, acetonitrile, acetamides, methyl pyrimidines and methyl quinolines [382], with appropriate catalysts, undergo alpha-alkylation with alcohols. Besides the traditional transition metal-based catalysts, homogeneous catalysts, for instance, Mn-based pincer complexes [383] and Os- and Ir-based complexes, and heterogeneous catalysts, especially supported transition metal catalysts and Pd and Ni
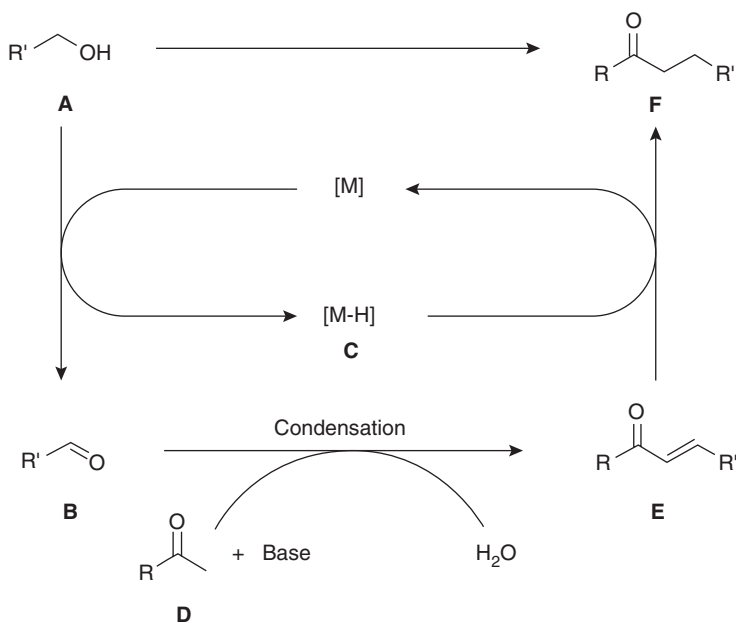
Scheme 15 Alpha-alkylation of typical carbonyl compound with alcohol (Reproduced from Ref. [382], Obora Y)

nanoparticles immobilized on inorganic supports, have been explored for alpha-alkylation [382]. Typical examples of such conversions are presented for illustration.

Shimizu et al. [384] have reported selective C-3 alkylation of oxindole (1 mmol) with 1-octanol (1.1 mmol) using 1% Pt supported on CeO$_2$ catalyst in mesitylene as solvent (1.5 g) at 170 °C for 24 h (Scheme 16) which could achieve 99% yield of alkylated product.

Alkylation of acetophenone (1 mmol) with benzyl alcohol (1.2 mmol) on nanoscale Pd particles supported on AlO(OH) catalyst in presence of K$_3$PO$_4$ (3 mmol) at 80 °C in Ar atmosphere results in 92% yield of alkylated product in 8 h (Scheme 17).

N-alkylation of amines and nitroarenes is another important step in synthetic organic chemistry. Dimethyl carbonate (DMC), dimethyl sulphate (DMS), methyl iodide (MI) and methanol are commonly used as methylation reagents. Comparative evaluation of these reagents on green chemistry metrics (atom economy, mass index) has shown that both DMC and methanol provide safer and greener reactions [387]. Hence methanol/alcohols are preferred reagents for N-alkylation of amines and O-methylation of phenols. Another desirable criterion is the selective N-monomethylation vs. overalkylation. Recently, Fu et al. [388] have developed an active and reusable Ir@YSMCNs nano catalyst (iridium nanoparticles encapsulated within yolk-shell-structured mesoporous carbon nanospheres) which is highly effective for selective mono N-methylation of amines and nitroarenes. The reaction follows again the hydrogen borrowing cycle, with methanol acting as hydrogen donor, as depicted in Scheme 18. On Ir@YSMCNs catalyst (0.5 g, 4% Ir loading), in presence of t-BuOK (1 mol. eq.) as base and 2 mmol of aniline in methanol (15 ml) at 170 °C, 92% conversion of aniline with 97% selectivity for N-mono methyl aniline could be achieved.

Under optimized reaction conditions (2 mmol of nitrobenzene in 15 ml methanol, 2 mmol of t-BuOK, 0.15 g catalyst with 4% Ir loading and at 170 °C), complete conversion of nitrobenzene with 97% selectivity towards N-monomethylated aniline could be realized in 30 h. Nitro compounds with different substituents could undergo facile conversion with high yields of N-monomethylated anilines on Ir@
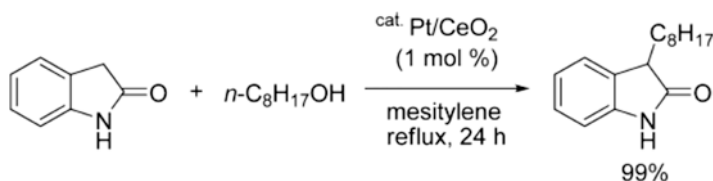
Scheme 16 Selective alpha-alkylation of oxindole (Reproduced from Shimizu et al. [384])
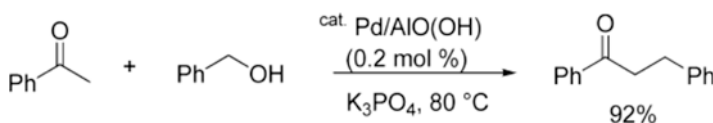
Scheme 17 Alpha-alkylation of acetophenone (Reproduced from Kwon et al. [385, 386])

Scheme 18 Mechanism proposed for N-monomethylation of nitroarenes and amines with methanol via borrowed hydrogen cycle pathway (Reproduced from Fu et al. [388])
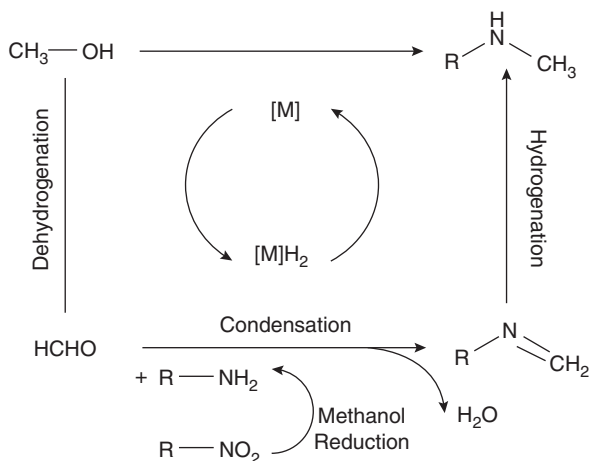
YSMCNs catalyst under optimized reaction conditions. In both cases [385, 386, 388], though hydrogen borrowing is envisaged, the actual step could be hydride/hydrogen transfer.

Jiang et al. [389] have reported the application of reusable, commercial 5% Pd/carbon catalysts for selective N-mono methylation of various aniline substrates with high yields, in presence of a base CH_3ONa under mild reaction conditions. Besides methanol, other alcohols also could be used as alkylation reagents, thus rendering alcohols as highly efficient alkylation reagents.

10   Future Trends

Currently, the global energy scenario is in the midst of a paradigm shift, with the emphasis on the generation of clean energy through environmentally sustainable processes. The chemical industry, on its part, is on the lookout for low-carbon energy, renewable feedstocks and more efficient as well as sustainable process technologies. The existing fossil resources as the raw material inventory for the refineries/chemical industries are gradually getting replaced with renewable bio-sources, carbon oxides from industrial waste gases and solid wastes [32–35, 53–56, 390]. Accordingly, the chemical process slate is also changing its face. In this context, production of bio-methanol/ethanol and other alcohols from renewable resources through chemo/bio-catalytic processes and their subsequent conversion to fuels and other value-added products have reached commercial status already, though limited in number, as of now.

Besides the technological challenges associated with conversion of bio-based feedstocks, the cost of production through sustainable routes has been a major limiting factor in this endeavour. The cost of production of ammonia, methanol, olefins (ethylene, propylene) and aromatics (benzene, toluene, xylenes), which together

account for nearly two thirds of GHG emissions from the chemical industry, would be significantly higher, if alternative renewable feedstocks were to be used as of now [391]. Comparison of cost of production of fuels and chemicals from fossil vs. renewable resources has been a subject of in-depth study from time to time, since the early 1980s [392, 393]. However, it remains only indicative, due to the wild variations/shocks (Fig. 34) in the price of crude oil, which is governed by several extraneous factors other than availability, exploration and production issues, like climate conditions/control, various types of geo-political environments/compulsions/tensions, frequent demand-supply imbalances and, of recent, a global pandemic. In the year 2007, Rass-Hansen et al. [393] have indicated the relative cost of some selected chemicals (Fig. 35) derived from fossil and renewable resources, based on the cost of the raw materials prevalent at that time. It is observed that the cost of production of ethanol, ethylene and acetic acid from renewable resources is lower vis-à-vis the cost from fossils, possibly due to high crude oil price in 2007. The scenario is bound to change with the volatility in crude oil price.

As we move on into the future, the societal benefits due to clean environment, low-carbon energy and sustainable chemical processes may outweigh the indicative cost differentials, with technological innovations taking the centre space. Hence, the major future research focus in the area of alcohol conversion processes would be towards improving overall process efficiency. Some of the key areas that need further investigations/improvements/innovations are:

- Further reduction in the cost of production of bioethanol from lignocellulosic biomass is needed to remain competitive vis-à-vis raw materials/fuels from fossil sources [163, 164, 394–396]. Especially the pretreatment and fractionation of biomass into major components/active intermediates/platform molecules continue to be challenging and add to the cost. Strategies to co-produce value-added products along with ethanol from biomass [53] are to be pursued vigorously to reduce the cost.
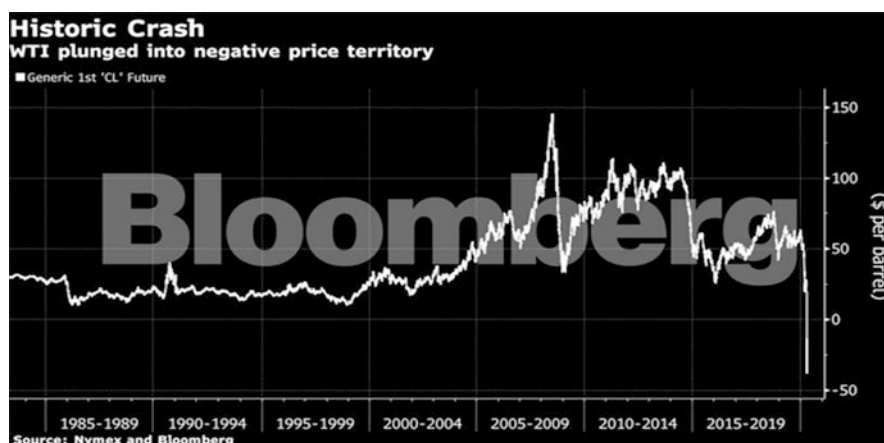
Fig. 34 Fluctuations in crude oil price (26 April 2020)
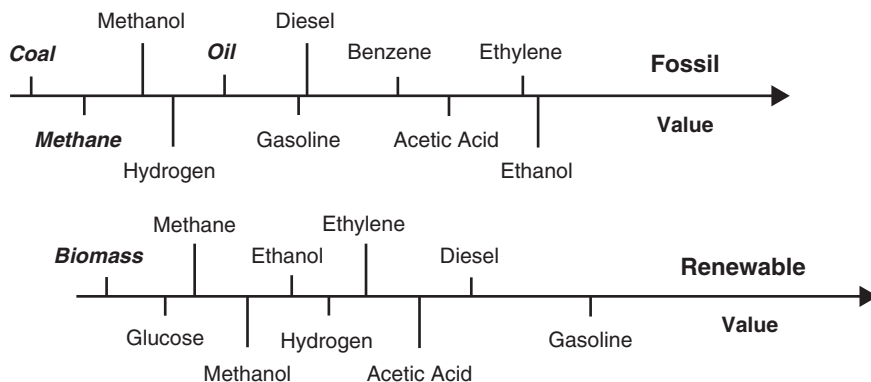
Fig. 35 Relative cost of selected chemicals derived from either fossil or renewable sources [393]

- A closely related area of concern is the separation and purification of products. In many biomass conversions by chemo- as well as bio-catalytic routes, a number of side products are formed, and developing innovative and more efficient separation and purification technique for maximum recovery of desired product(s) could boost the process efficiency.

- Though production of acetone, butanol and ethanol (ABE) process has been in practice for a number of years now, the high cost of hydrolytic enzymes and the need for expensive pretreatment steps are still the challenges that have to be addressed. The success and adaptability of ABE and other enzymatic processes for 1-butanol and other alcohols depend on the choice of microorganism species, their genetic manipulation and process optimization along with substrate. Recent developments in these aspects have led to renewed interest in bio-catalytic processes for the production of alcohols [397–399].

- Developing active, selective and stable catalysts for alcohol/biomass conversion processes has been a challenge, especially to maximize selectivity and retard deactivation. Amongst the different possible reaction pathways, the desirable one needs to be catalysed, by incorporation of requisite catalytic functionalities. Highly reactive molecule like glycerol can undergo several transformations, as illustrated in Fig. 30. To maximize the yield of a specific product, both metal and acidic/basic sites need to be fine-tuned, which requires a thorough understanding of the reaction pathways and generation of appropriate active sites. In-depth characterization of used/deactivated/spent catalysts could provide vital clues to understand the process of deactivation and devise means of arresting the same. Such an approach needs more in-depth studies on the reaction kinetics and mechanism, supported by advanced in situ spectroscopic investigations and computational approaches.

- A number of alcohol conversion processes like ethanol to propylene/isobutene/aromatics; various conversions of glycerol, sugar alcohols and furanics; and aqueous phase reforming process require more systematic studies to develop

catalysts with higher selectivity and stability and improvements in overall process efficiency.

- Though the process for the conversion of ethanol to 1,3-butadiene (BD) has successfully met all the criteria for sustainability, the process economics is not favourable since BD production rate (grams of BD produced per hour per unit weight of the catalyst) is to be improved, which requires the development of superior catalysts [200, 205, 207, 229]. In this respect, 90% conversion of ethanol with 70% selectivity and high productivity rate of 0.4 g BD/g of catalyst/hr. on Ag/ZrO$_2$-SiO$_2$ reported by Dagle et al. [400] is noteworthy.

- Development of single-pot conversion processes, especially for versatile chemicals like levulinic acid/alkyl levulinates [364, 365], GVL and other furan derivatives, fuels and fuel additives [357], which utilize biomass intermediates and neat platform chemicals as raw materials, is the right approach. Synthesis of these chemicals directly from lignocellulosic biomass, though challenging, would be desirable. Designing multi-functional catalysts with appropriate active sites and a re-look on separation and purification steps are the key issues.

- Processes based on aldol condensation of alcohols with aldehydes and ketones and self- and cross-aldol condensation of alcohols (Guerbet alcohols) are highly important steps in C-C bond formation [27, 241] and synthesis of highly useful fuels and chemicals and, in general, in many biomass conversion processes. Dual functional catalysts involving metal (for dehydrogenation and hydrogenation) and acid-base sites (for aldol condensation) are required. There are still questions regarding the role of the key intermediates in these reactions, and the exact nature of the acid-base sites responsible for generation of critical intermediates is yet to be established. Various supports like hydroxyapatite, hydrotalcites, γ-Al$_2$O$_3$ and MgO with several modifiers and reducible of the metal ions (Ni. Cu, Ru, Pd) have been explored for the conversion of ethanol to butanol [73–78]. However, the mode of functioning of the catalysts is not clear, though the general consensus is that low ratio of acid-base sites of the support may favour this reaction. Similarly, the criterion to be used for identifying the ease of reducibility of metal ions is yet to specified [401].

- Several promising processes have been developed for the conversion of alcohols to jet fuels and middle distillates/diesel [241, 282]. As the demand for these types of fuels is set to increase, the future research focus in this area would be towards a better understanding of oligomerization and aldolization chemistries that constitute the backbone for these routes. Studies in these and related areas would be helpful in improving the process efficiency.

11   Summary and Conclusions

Tremendous potential of biomass as feedstock for fuels and chemicals was visualized as early as 1981 by Lipinsky [392], when the biomass conversion processes were at primitive stage.
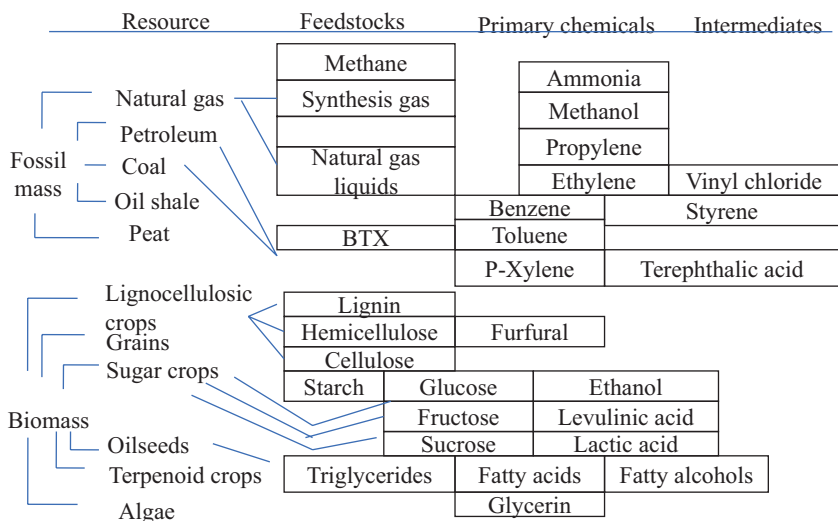
Fig. 36 Relationship between resources, feedstocks, primary chemicals and intermediates (Reproduced from Lipinsky [392])

The relationship (Fig. 36) between the two major resources, fossil and biomass, and their transformation into feedstocks, primary chemicals and intermediates, as envisaged at that stage, included biomass-derived *ethanol*, *glycerol*, *levulinic acid*, *lactic acid and furfural*, which were identified later, as versatile platform molecules, in 2010 [20, 21]. Since then, the development of processes for economically viable production of different types of alcohols through sustainable routes and a wide range of alcohol conversion processes have received global attention. Besides the traditional biomass resources, carbon oxides from industrial waste gases, solid wastes and other renewables [32–35, 257] have been explored as feedstocks for alcohols, thus enormously improving their availability at lower cost through low-carbon sustainable routes.

Alcohols with highly reactive R-O and O-H linkages are amenable for several types of catalytic transformations, yielding a range of fuels and chemicals. A compilation of major alcohol conversion processes developed over a period of time and the typical product slates in each case is presented in Fig. 37. A brief account of the origin of these processes, catalysts used therein, recent developments and future directions for research has been covered in this chapter.

Nearly, all types of fuels derived from fossil resources could now be produced from alcohols, besides highly efficient and new range of bio-based fuel additives, like alkyl levulinates and furfural/furan/furfuryl alcohol derivatives. Amongst the building block chemicals, production of ethylene and propylene in *on-purpose* mode, through MTO and MTP processes, has been well-established on commercial scale. Three *renewable methanol* production processes, developed by Carbon Recycling Institute (CRI), BioMCN and Enerkem, have successfully completed
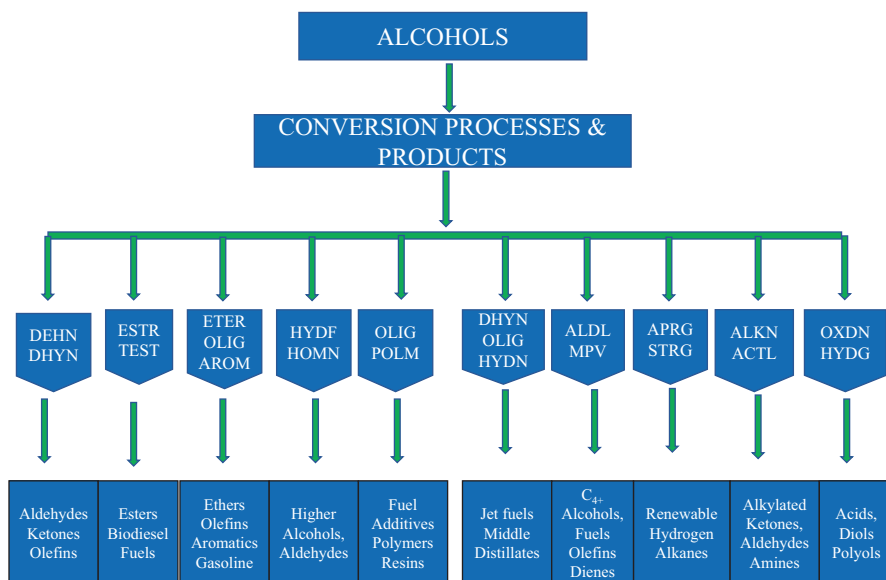
Fig. 37 Conversion processes and products from alcohols. *DEHN/DHYN* dehydrogenation/dehydration, *ESTR/TEST* esterification/trans-esterification, *ETER/OLIG/AROM* etherification/oligomerization/aromatization, *COPL/HOMN* coupling/homologation with CO, *OLIG/POLM* oligomerization/polymerization, *DHYN-OLIG-HYDN* dehydration-oligomerization-hydrogenation, *ALDL/MPV* aldolization Meewrwein Pondorrf Varley reaction, *APRG/STRG* aqueous phase reforming/steam reforming, *ALKN/NALK* alkylation/N-alkylation, *OXDN/HYDG* oxidation/hydrogenolysis

pilot/demonstration stage runs, and commercial-scale plants are under planning [32–35]. Once *renewable methanol* is available on commercial scale, MTO and MTP processes could, in the near future, become viable low-carbon alternatives to the olefins production by conventional steam cracking process. Similar developments could be envisaged for MTG and ETG processes as well, with the emphasis on improving the stability of the catalysts. 1,3-Butadiene from ethanol is another process with high promise, wherein the productivity rate is to be improved.

ASTM approval for the blending of bio-jet fuels produced by catalytic conversion of alcohols/other renewables (Lanza-PNNL and other processes) is a significant milestone in the area of biofuels. This development is expected to help the aviation industry in realizing the objective of reducing emissions by 50% (with respect to 2005 emission levels) by 2050, by substituting fossil-derived jet fuels with low-carbon bio-based fuels.

Alcohols have proven to be one of the most important sources for fuels and chemicals. Recent developments, as exemplified in this chapter, underpin the pivotal role that the catalytic transformations of alcohols could play, in building low-carbon sustainable society. Developments in large-scale production of renewable hydrogen from water, via photovoltaic-powered electrolysis, could greatly contribute towards improving the sustainability of processes based on alcohols. Such a

scenario is bound to motivate sustained and more focused research efforts in this area, especially towards addressing the issues enlisted earlier and simultaneously seeking new avenues for growth.

References

1. Huber GW, Iborra S, Corma A (2006) Synthesis of transportation fuels from biomass: chemistry, catalysts, and engineering. Chem Rev 106:4044–4098. https://doi.org/10.1021/cr068360d
2. Corma A, Iborra S, Velty A (2007) Chemical routes for the transformation of biomass into chemicals. Chem Rev 107:2411–2502. https://doi.org/10.1021/cr050989d
3. Alonso DM, Bond JQ, Dumesic JA (2010) Catalytic conversion of bi omass to biofuels. Green Chem 12:1493–1513. https://doi.org/10.1039/C004654J
4. Huber GW, Chheda JN, Barrett CJ, Dumesic JA (2005) Production of liquid alkanes by aqueous-phase processing of biomass-derived carbohydrates. Science 308:1446–1450. https://doi.org/10.1126/science.1111166
5. Climent MJ, Corma A, Iborra S (2011) Converting carbohydrates to bulk chemicals and fine chemicals over heterogeneous catalysts. Green Chem 13:520–540. https://doi.org/10.1039/C0GC00639D
6. Demirbaş A (2001) Biomass resource facilities and biomass conversion processing for fuels and chemicals. Energy Convers Manag 42(11):1357–1378. https://doi.org/10.1016/S0196-8904(00)00137-0
7. Fang Z, Smith RL Jr, Qi X (2019) Resources in biomass and biorefineries, vol 9. Springer, New York, NY
8. Zhou C-H, Xia X, Lin CX, Tonga DS, Beltramini J (2011) Catalytic conversion of ligno-cellulosic biomass to fine chemical and fuels. Chem Soc Rev 40:5588–5617. https://doi.org/10.1039/C1CS15124J
9. Hayes DJ (2009) An examination of biorefining processes, catalysts and challenges. Catal Today 145:138–151. https://doi.org/10.1016/j.cattod.2008.04.017
10. Fernando S, Adhikari S, Chandrapal C, Murali N (2006) Biorefineries: current status, challenges and future direction. Energy Fuel 20:1727–1737. https://doi.org/10.1021/ef060097w
11. Pileidis FD, Titirici MM (2016) Levulinic acid biorefineries: new challenges for efficient utilization of biomass. ChemSusChem 9:562–582. https://doi.org/10.1002/cssc.201501405
12. Serrano-Ruiz JC, Dumesic JA (2011) Catalytic routes for the conversion of biomass into liquid hydrocarbon transportation fuels. Energy Env Sci 4:83–99. https://doi.org/10.1039/C0EE00436G
13. Kamm B, Kamm M (2004) Principles of biorefineries. Appl Microbiol Biotechnol 64:137–145. https://link.springer.com/article/10.1007/s00253-003-1537-7
14. Kamm B, Gruber PR, Kamm M (2006) Biorefineries-industrial processes and products. Weinheim, Wiley-VCH Verlag GmbH &Co. K GaA
15. Kamm B (2007) Production of platform chemicals and synthesis gas from biomass. Angew Chem Int Ed 46:5056–5058. https://doi.org/10.1002/anie.200604514
16. De Jong E, Jungmeier G (2015) Biorefinery concepts in comparison to petrochemical refineries. In: Pandey A, Hofer R, Taherzadeh M, Nampoothiri M, Larroche C (eds) Industrial biorefineries and white biotechnology, 1st edn. Elsevier, Amsterdam, pp 3–33

17. Bozell JJ (2010) Connecting biomass and petroleum processing with a chemical bridge. Science 329:522–523. https://doi.org/10.1126/science.1191662
18. Somerville C, Youngs H, Taylor C, Davis SC, Long SP (2010) Feedstock for lignocellulosic biofuels. Science 329:790–791. https://doi.org/10.1126/science.1189268
19. Kohli K, Prajapati R, Sharma BK (2019) Bio-based chemicals from renewable biomass for integrated biorefineries. Energies 12:233. https://doi.org/10.3390/en12020233
20. Werpy T, Petersen G, Aden A, Bozell J, Holladay J, White J, Manheim A et al (2004) Results of screening for potential candidates from sugars and synthesis gas. In: Werpy T, Petersen G (eds) Top value-added chemicals from biomass – vol. 1. Pacific Northwest National Laboratory, National Renewable Energy Laboratory and Department of Energy, Washington, DC
21. Bozell JJ, Petersen GR (2010) Technology development for the production of biobased products from biorefinery carbohydrates-the US Department of Energy's "Top 10" revisited. Green Chem 12:539–554. https://doi.org/10.1039/B922014C
22. Gallezot P (2012) Conversion of biomass to selected chemical products. Chem Soc Rev 41:1538–1558. https://doi.org/10.1039/C1CS15147A
23. Langeveld H, Sanders J, Meeusen M (eds) (2010) The biobased economy: biofuels, materials and chemicals in the post-oil era. Earthscan, New York, NY
24. Sudhakar T, Tao L, Michael AG (2018) An overview of biorefinery derived platform chemicals from a cellulose and hemicellulose biorefinery, us environmental protection agency. Clean Technol. Environ Policy 20(7):1615–1630. https://doi.org/10.1007/s10098-018-1568-5
25. Mohammadi M, Najafpour GD, Younesi H, Lahijani P, Uzir MH, Mohamed AR (2011) Bioconversion of synthesis gas to second generation biofuels. A review. Renew Sust Energ Rev 15:4255–4273
26. Quellette A, Rawn D (2014) Journal of organic chemistry – structure, mechanism and synthesis. Elsevier, Amsterdam
27. Wu L, Moteki T, Gokhale AA, Flaherty DW, Toste FD (2016) Production of fuels and chemicals from biomass: condensation reactions and beyond. Chemistry 1:32–58. https://doi.org/10.1016/j.chempr.2016.05.002
28. Methanol Institute-Methanol Market Survey Asia (MMSA) (2020) World supply-demand summary, Jan 2020. Accessed 7 Feb 2020
29. Dalena F, Senatore A, Basile M, Knani S, Basile A, Iulianelli A (2018) Advances in methanol production and utilization, with particular emphasis toward hydrogen generation via membrane reactor technology. Membranes 8:98. https://doi.org/10.3390/membranes8040098
30. Sheldon D (2017) Methanol production – a technical history. Johnson Matthey Technol Rev 61(3):172–182. https://doi.org/10.1595/205651317X695622
31. Bertau M, Offermanns H, Plass L, Schmidt F, Wernicke H-J (2014) Methanol: the basic chemical and energy feedstock of the future. Asinger's vision today. Springer, Berlin. https://doi.org/10.1007/978-3-642-39709-7
32. Olah GA (2005) Angew Chem Int Ed 44(18):2636–2639. https://doi.org/10.1002/anie.200462121
33. Olah GA, Goeppert A, Prakash GKS (2018) Beyond oil and gas: the methanol economy. Wiley-VCH, Weinheim
34. Roode-Gutzmer QI, Kaiser D, Bertau M (2019) Renewable methanol synthesis. Chem Bio Eng Rev 6:209–236. https://doi.org/10.1002/cben.201900012
35. Hobson C, Marques C (2018) Renewable methanol report. Methanol Institute, Washington, DC. http://www.mefco2.eu/news/mapping-out-renewable-methanol-around-the-world.php
36. Straathof AJJ (2014) Transformation of biomass into commodity chemicals using enzymes or cells. Chem Rev 114(3):1871–1908. https://doi.org/10.1021/cr400309c
37. Ge X, Yang L, Sheets JP, Yu Z, Li Y (2014) Biological conversion of methane to liquid fuels: status and opportunities. Biotechnol Adv 32(8):1460–1475. https://doi.org/10.1016/j.biotechadv.2014.09.004

38. Hwang IY, Lee SH, Choi YS, Park SJ, Na JG, Chang IS, Kim C, Kim HC, Kim YH, Lee JW, Lee EY (2014) Biocatalytic conversion of methane to methanol as a key step for development of methane-based biorefineries. J Microbiol Biotechnol 24(12):1597–1605. https://doi.org/10.4014/jmb.1407.07070

39. Duan C, Luo M, Xing X (2011) High-rate conversion of methane to methanol by Methylosinus trichosporium OB3b. Bioresour Technol 102(15):7349–7353. https://doi.org/10.1016/j.biortech.2011.04.096

40. Chandran K (2012) Methods and systems for biologically producing methanol. WO 2012/078845 A1

41. Tyurin M, Kiriukhin M (2013) Selective methanol or formate production during continuous CO2 fermentation by the acetogen biocatalysts engineered via integration of synthetic pathways using Tn7-tool. World J Microbiol Biotechnol 29(9):1611–1623. https://doi.org/10.1007/s11274-013-1324-2

42. Johnson D (2012) Global methanol market review. http://www.ptq.pemex.com/productosyservicios/eventosdescargas/Documents/Foro%20PEMEX%20Petroqu%C3%ADmica/2012/PEMEX_DJohnson.pdf. Accessed 23 Mar 2016

43. Rosillo-Calle F, Walter A (2006) Global market for bioethanol: historical trends and future prospects. Energy Sustain Dev 10(1):20–32. https://doi.org/10.1016/s0973-0826(08)605049

44. Kosaric N, Duvnjak Z, Farkas A, Sahm H, Bringer-Meyer S, Goebel O, Mayer D (2011) Ethanol. Ullmann's encyclopedia of industrial chemistry. doi:https://doi.org/10.1002/14356007.a09_587.pu-2

45. Mussatto SI, Dragone G, Guimaraes PM, Silva JP, Carneiro LM, Roberto IC, Vicente A, Domingues L, Teixeira JA (2010) Technological trends, global market, and challenges of bio-ethanol production. Biotechnol Adv 28(6):817–830. https://doi.org/10.1016/j.biotechadv.2010.07.001

46. Demirbas¸ A (2005) Bioethanol from cellulosic materials: a renewable motor fuel from biomass. Energy Sources 27(4):327–337. https://doi.org/10.1080/00908310390266643

47. Ralph EH, Sims WM, Saddler JN, Taylor M (2010) An overview of second generation biofuel technologies. Bioresour Technol 101:1570–1580. https://doi.org/10.1016/j.biortech.2009.11.046

48. Robak K, Balcerek M (2018) Review of second generation bioethanol production from residual biomass. Food Tech BioTech 56(2):174–187. https://doi.org/10.17113/ftb.56.02.18.5428

49. Alalwan AA, Alminshid AH, Aljaafari HAS (2019) Promising evolution of biofuel generations. Subject review. Renew Energy Focus 28:127–139. https://doi.org/10.1016/j.ref.2018.12.006

50. Abdullah B, Muhammad SAFS, Shokravic Z, Ismail S, Kassime KA, Mahmood AN, Azize MMA (2019) Fourth generation biofuel: a review on risks and mitigation strategies. Renew Sust Energ Rev 107:37–50. https://doi.org/10.1016/j.rser.2019.02.018

51. Li K, Liu S, Liu X (2014) An overview of algae bioethanol production. Int J Energy Res 38(8):965–977. https://doi.org/10.1002/er.3164

52. Doutton JA. e-Education Institute, Penn State University, Pennsylvania

53. Rosales-Calderon O, Arantes V (2019) A review on commercial scale high value products that can be produced alongside cellulosic ethanol. Biotechnol Biofuels 12:240. https://doi.org/10.1186/s13068-019-1529-1

54. Bengelsdorf FR, Straub M, Dürre P (2013) Bacterial synthesis gas (syngas) fermentation. Environ Technol 34(13–14):1639–1651. https://doi.org/10.1080/09593330.2013.827747

55. LanzaTech (2015) LanzaTech executive summary. http://www.lanzatech.com/wp-content/uploads/2015/03/2-pager-2015.pdf. Accessed 1 Feb 2017

56. Kuhz H, Kuenz A, Preuße U, Willke T, Vorlop (2017) K-D Products components. Alcohols Adv Biochem Eng Biotechnol 2017:1–34. https://doi.org/10.1007/10_2016_74

57. Papa AJ (2011) Propanols. Ullmann's encyclopedia of industrial chemistry. doi:https://doi.org/10.1002/14356007.a22_173.pub2

58. Ammar EM, Wang Z, Yang ST (2013) Metabolic engineering of Propionibacterium freuden-reichii for n-propanol production. Appl Microbiol Biotechnol 97(10):4677–4690. https://doi.org/10.1007/s00253-013-4861-6

59. Choi YJ, Lee J, Jang YS, Lee SY (2014) Metabolic engineering of microorganisms for the production of higher alcohols. MBio 5(5):e01524–e01514. https://doi.org/10.1128/mBio.01524-14

60. Jang YS, Kim B, Shin JH, Choi YJ, Choi S, Song CW, Lee J, Park HG, Lee SY (2012) Bio-based production of C2-C6 platform chemicals. Biotechnol Bioeng 109(10):2437–2459. https://doi.org/10.1002/bit.24599

61. Inokuma K, Liao JC, Okamoto M, Hanai T (2010) Improvement of isopropanol produc-tion by metabolically engineered Escherichia coli using gas stripping. J Biosci Bioeng 110(6):696–701. https://doi.org/10.1016/j.jbiosc.2010.07.010

62. Sada M et al (1981) US patent 4307257, 22 Dec 1981

63. Harvey BG, Meylemans HA (2011) The role of butanol in the development of sustainable fuel technologies. J Chem Technol Biotechnol 86:2–9. https://doi.org/10.1002/jctb.2540

64. Xue C, Zhao XQ, Liu CG, Chen LJ, Bai FW (2013) Prospective and development of buta-nol as an advanced biofuel. Biotechnol Adv 31:1575–1584. https://doi.org/10.1016/j.biotechadv.2013.08.004

65. Gautam M, Martin DW (2000) Combustion characteristics of higher-alcohol/gasoline blends. Proc Inst Mech Eng A J Power Energy 214:497–511. doi:10.1243%2F0957650001538047

66. Thompson R, Behnam M, Swana J, Yang Y (2011) An analysis of net energy production and feed-stock availability for biobutanol and bioethanol. Bioresour Technol 102:2112–2117. https://doi.org/10.1016/j.biortech.2010.08.051

67. Singh SB, Dhar A, Agarwal AK (2015) Technical feasibility study of butanol as gasoline blends for powering medium-duty transportation spark ignition engine. Renew Energy 76:706–716. https://doi.org/10.1016/j.renene.2014.11.095

68. Derre P (2007) Biotechnol J Rep 2:1525–1534

69. Ndaba B, Chiyanzu I, Marx S (2015) n-Butanol derived from biochemical and chemical routes: a review. Biotechnol Rep 8:1–9. https://doi.org/10.1016/j.btre.2015.08.001

70. n-Butanol market by application (butyl acrylate, butyl acetate, glycol ethers, direct solvents, plasticizers), and region (Asia Pacific, North America, Europe, Middle East & Africa, South America)—Global Forecast to 2022: a report (CH1543) 2018

71. Hahn HD, Dambkes G, Rupprich N, Bahl H, Frey GD (2013) Butanols. Ullmann's encyclo-pedia of industrial chemistry. doi:10.1002/14356007.a04_463.pub3

72. Spivey JJ, Groppi G, Cristiani C, Forzatti P (1997) Preparation and characterization of hexaaluminate materials for high-temperature catalytic combustion. Catalysis 13:209. https://doi.org/10.1039/9781847553256

73. Guerbet MCR (1899) Acad Sci Paris 128:1002–1004

74. Guerbet MCR (1909) Acad Sci Paris 149:129–132

75. Kozlowski J T, Davis RJ (2013) Heterogeneous catalysts for the Guerbet coupling of alco-hols. ACS Catal 3:1588–1600. https://pubs.acs.org/doi/10.1021/cs400292f

76. Aitchison H, Wingad RL, Wass DF (2016) Homogeneous ethanol to butanol catalysis. ACS Catal Guerbet Renewed 6:7125–7132. https://doi.org/10.1021/acscatal.6b01883

77. Wu X, Fang G, Tong Y, Jiang D, Liang Z, Leng W, Liu L, Tu P, Wang H, Ni J, Li X (2018) Catalytic upgrading of ethanol to n-butanol: progress in catalyst development. ChemSusChem 11:71–85. https://doi.org/10.1002/cssc.201701590

78. Dowson GRM, Haddow MF, Lee J, Wingad RL, Wass DF (2013) Catalytic conversion of ethanol into an advanced biofuel: unprecedented selectivity for n-butanol. Angew Chem Int Ed 52:9005–9008. https://doi.org/10.1002/anie.201303723

79. Jang YS, Malaviya A, Cho C, Lee J, Lee SY (2012) Butanol production from renew-able biomass by Clostridia. Bioresour Technol 123:653–663. https://doi.org/10.1016/j.biortech.2012.07.104

80. Garncarek Z, Kociolek-Balawejder E (2009) Biobutanol. Perspectives of the production development. Przem Chem 88(6):658–666

81. Li J, Baral N, Jha A (2014) Acetone–butanol–ethanol fermentation of corn stover by Clostridium species: present status and future perspectives. World J Microbiol Biotechnol 30(4):1145–1157. https://doi.org/10.1007/s11274-013-1542-7

82. Jain S, Yadav MK, Kumar A (2014) In: Babu V, Thapliyal A, Patel GK (eds) Production of butanol: a biofuel in biofuels production. Scrivener Publishing LLC, Beverly, MA, pp 255–284

83. Rathour RK, Ahuja V, Bhatia RK, Bhatt AK (2018) Biobutanol: new era of biofuels. Int J Energy Res 2018:1–14. https://doi.org/10.1002/er.4180

84. Kolesinska B, Fraczyk J, Binczarski M, Modelska M, Berlowska J, Dziugan P, Hubert Antolak H, Kaminski ZJ, Witonska IA, Kregiel D (2019) Butanol synthesis routes for biofuel production: trends and perspectives. Materials 12:350. https://doi.org/10.3390/ma12030350

85. Ezeji T, Groberg M, Qureshi N, Blaschek HP (2003) Continuous production of butanol from starch-based packing peanuts. Appl Biochem Biotechnol 105–108:375–382. https://doi.org/10.1385/abab:106:1-3:375

86. https://www.plasticsinsight.com/resin-intelligence/resin-prices/mono-ethylene-glycolmeg. Accessed on 16th Feb 2020

87. Bio PET (2020) Market size, share, forecast, industry report. Plastics industry. Radiant Insights Inc, San Francisco, CA

88. Sullivan CJ, Anja K, Vorlop K, Dieter (2018) Propanediols. In: Ullmann's encyclopedia of industrial chemistry. Wiley, Weinheim. https://doi.org/10.1002/14356007.a22_163.pub23

89. Alain C, Gilles L (1989) Petrochemical processes. Volume 2: major oxygenated, chlorinated and nitrated derivatives. Editions Technip, New York, NY, p 26. ISBN:9782710805632

90. Feng J, Xu B (2014) Reaction mechanisms for the heterogeneous hydrogenolysis of biomass derived glycerol to propanediols. Prog React Kinet Mech 39:1–15. https://doi.org/10.3184/97809059274714x13874723178485

91. Zheng Y, Chen X, Shen Y (2008) Commodity chemicals derived from glycerol, an Important biorefinery feedstock. Chem Rev 108:5253–5277. https://doi.org/10.1021/cr068216s

92. Ruppert AM, Weinberg K, Palkovits R (2012) Hydrogenolysis goes bio: from carbohydrates and sugar alcohols to platform chemicals. Angew Chem 51:2564–2601. https://doi.org/10.1002/anie.201105125

93. Nakamura CE, Whited GM (2003) Metabolic engineering for the microbial production of 1,3-propanediol. Curr Opin Biotechnol 14: 454–459. https://www.ncbi.nlm.nih.gov/pubmed/14580573

94. Saxena RK, Anand P, Saran S, Isar J, Agarwal L (2010) Microbial production and applications of 1,2-propanediol. Indian J Microbiol 50:2–11. https://doi.org/10.1007/s12088-010-0017-x

95. Behr A, Eilting J, Irawadi K, Leschinski J, Lindner F (2008) Improved utilisation of renewable resources: new important derivatives of glycerol. Green Chem 10:13. https://doi.org/10.1039/b710561d

96. Zhou CH, Beltramini JN, Fan YX, Lu GQ (2008) Chemo selective catalytic conversion of glycerol as a bio-renewable source to valuable commodity chemicals. Chem Soc Rev 37:527–549. https://doi.org/10.1039/b707343g

97. Pagliaro M, Rossi M (2010) The future of glycerol, vol 2. RSC Green Chemistry Series Royal Society of Chemistry, London

98. Nakagawa Y, Tomishige K (2011) Heterogeneous catalysis of the glycerol hydrogenolysis. Cat Sci Technol 1:179. https://doi.org/10.1039/c0cy00054j

99. Lee CS, Aroua MK, Daud WMAW, Cognet P, Pe're's-Lucchese Y, Fabre PL, Reynes O, Latapie L (2015) A review: conversion of bio-glycerol into 1,3-propanediol via biological and chemical method. Renew Sust Energ Rev 42:963–972. 10.1016/j.rser.2014.10.033

100. Arundhathi R, Mizugaki T, Mitsudome T, Jitsukawa K, Kaneda K (2013) Highly selective hydrogenolysis of glycerol to 1,3-propanediol over a boehmite-supported platinum/tungsten catalyst. ChemSusChem 6(8):1345–1347. https://doi.org/10.1002/cssc.201300196

101. Martin A, Armbruster U, Gandarias I, Arias PL (2013) Glycerol hydrogenolysis into propane-diols using in situ generated hydrogen – a critical review. Eur J Lipid Sci Technol 115:9–27. https://doi.org/10.1002/ejlt.201200207

102. Chaminand J, La D, Gallezot P, Marion P, Pinel C, Cc R (2004) Glycerol hydrogenolysis on heterogeneous catalysts. Green Chem 6(8):359. https://doi.org/10.1039/b407378a

103. Ji XJ, Huang H (2014) Bio-based butanediols production: the contributions of catalysis, met-abolic engineering, and synthetic biology. In: Bisaria VS, Kondo A (eds) Bioprocessing of renewable resources to commodity bioproducts. Wiley, Hoboken, NJ, pp 261–288

104. Zeng AP, Sabra W (2011) Microbial production of diols as platform chemicals: recent pro-gresses. Curr Opin Biotechnol 22(6):749–757. https://doi.org/10.1016/j.copbio.2011.05.005

105. Grafje H, K€ornig W, Weitz HM, Reiß W, Steffan G, Diehl H, Bosche H, Schneider K, Kieczka H (2000) Butanediols, butenediol, and butynediol. In: Ullmann's encyclopedia of industrial chemistry. https://doi.org/10.1002/14356007.a04_455

106. Bartowsky EJ, Henschke PA (2004) The 'buttery' attribute of wine – diacetyl desirabil-ity, spoilage and beyond. Int J Food Microbiol 96(3):235–252. https://doi.org/10.1016/j.ijfoodmicro.2004.05.013

107. Petrini P, Ponti SD, Fare S, Tanzi MC (1999) Polyurethane-maleamides for cardio-vascular applications: synthesis and properties. J Mater Sci Mater Med 10:711–714. https://doi.org/10.1023/A:1008970904334

108. Myszkowski J, Zielinski AZ (1965) Synthe'se de la butyle'ne-chlorhydrine et sa conversion enme'thyle'thylce'tone, oxyde de butyle'ne et butyle'ne-glycol. Chim Ind 93:3

109. Celinska E, Grajek W (2009) Biotechnological production of 2,3-butanediol – current state and prospects. Biotechnol Adv 27:715–725. https://doi.org/10.1016/j.biotechadv.2009.05.002

110. Harden A, Walpole GS (1906) Chemical action of Bacillus lactis aerogenes (Escherich) on glucose and mannitol: production of 2, 3-butyleneglycol and acetyl methyl carcinol. Proc Royal Soc B Bio 77:399–405. https://doi.org/10.1098/rspb.1906.0028

111. Fulmer EI, Christensen LM, Kendali AR (1933) Production of 2,3-butylene glycol by fer-mentation. Ind Eng Chem 25:798–800. https://doi.org/10.1021/ie50283a019

112. Ji XJ, Huang H, Ouyang PK (2011) Microbial 2,3-butanediol production: a state-of-the art review. Biotechnol Adv 29:351–364. https://doi.org/10.1016/j.biotechadv.2011.01.007

113. Sampat BG (2011) 1,4-Butanediol: a techno-commercial profile. Chem Weekly 2011:205–211

114. Burk MJ (2010) Sustainable production of industrial chemicals from sugars. Int Sugar J 112 (1333):30–35 https://www.genomatica.com/_uploads/pdfs/ISJ_markburke.pdf

115. Burk MJ, Van Dien SJ, Burgard AP, Niu W (2015) Composition and methods for the biosyn-thesis of 1,4-butanediol and its precursors. US 8969054 B2

116. Genomatica (2015) Commercial-scale production, customer validation, licenses. http://www.genomatica.com/products/genobdoprocess/. Accessed 14 Apr 2015

117. Dittmeyer R, Keim W, Kreysa G, Oberholz A (2005) Chem Tech Prozesse Prod 5:55–68. https://doc1.bibliothek.li/aao/FLMA135383.pdf

118. O'Lenick AJ (2001) Guerbet chemistry. J Surfactant Deterg 4:311–315. https://doi.org/10.1007/s11743-001-0185-1

119. Ott J, Gronemann V, Pontzen F, Fiedler E, Grossmann G, Kersebohm DB, Weiss G, Witte C (2012) Methanol. Ullmann's encyclopedia of industrial chemistry. doi:https://doi.org/10.1002/14356007.a16465.pub3

120. Morschbacker A (2009) Bio-ethanol based ethylene. Polym Rev 49:79–84. https://doi.org/10.1080/15583720902834791

121. Forestie're A, Olivier-Bourbigou H, Saussine L (2009) Oligomerization of mono olefins by homogeneous catalysts. Oil Gas Sci Technol Rev l'IFP 64:649–667. https://doi.org/10.2516/ogst/2009027

122. Olson ES, Sharma RK, Aulich TR (2004) Higher-alcohols biorefinery. Appl Biochem Biotechnol 113–116:913–932. https://doi.org/10.1007/978-1-59259-837-3_74

123. Sun D, Sato S, Ueda W, Primo A, Garcia H, Corma A (2016) Production of C_4 and C_5 alco-hols from biomass derived materials. https://doi.org/10.1039/C6GC00377J

124. Luk HT, Mondelli C, CurullaFerre D, Stewart JA, Pe'rez-Ramı'rez J (2017) Status and prospects in higher alcohols synthesis from syngas. Chem Soc Rev 46:1358–1426. https://doi.org/10.1039/c6cs00324a

125. Nexant Inc. (2015) Petrochemical market dynamics oxo alcohols. Nexant Inc., Louisville, CO

126. Lamsen EN, Atsumi S (2012) Recent progress in synthetic biology for microbial production of C3-C10 alcohols. Front Microbiol 3:196. https://doi.org/10.3389/fmicb.2012.00196

127. Zhao J, Lu C, Chen C-C, Yang S-T (2013) In: Yang S-T, El-Enshasy HA, Thongchul N (eds) Bioprocessing technologies in biorefinery for sustainable production of fuels, chemicals, and polymers, 1st edn. John Wiley & Sons, Inc., pp 235–261

128. Diender M, Alfons JMS, Sousa DZ (2016) Biotechnol Biofuels 9:82. https://doi.org/10.1186/s13068-016-0495-0

129. Polyols (sugar alcohols) – a global market overview industry experts. Report code: FB007, Jan 2017

130. Moon HJ, Jeya M, Kim IW, Lee JK (2010) Biotechnological production of erythritol and its applications. Appl Microbiol Biotechnol 86:1017–1025. https://doi.org/10.1007/s00253-010-2496-4

131. Zhang J, Li J-BWS-B, Liu Y (2013) Advances in the catalytic production and utilization of sorbitol. Ind Eng Chem Res 52:11799–11815. https://doi.org/10.1021/ie4011854

132. Ghosh S, Sudha ML (2012) A review on polyols: new frontiers for health-based bakery, products. Int J Food Sci Nutr 63:372–379. https://doi.org/10.3109/09637486.2011.627846

133. Tathod A, Kane T, Sanil ES, Dhepe PL (2014) Solid base supported metal catalysts for the oxidation and hydrogenation of sugars. J Mol Catal A Chem 388-389:90–99. https://doi.org/10.1016/j.molcata.2013.09.014

134. May A, Pastore GM, Park YK (1993) Microbial transformation of sucrose and glucose to erythritol, Biotechnol Lett, 15:383–388 https://link.springer.com/article/10.1007/BF00128281

135. Van der Klis F, Gootjes L, van Haveren J, van Es DS, Bitter JH (2015) Selective terminal C–C scission of C5-carbohydrates. Green Chem 17:3900–3909. https://doi.org/10.1039/C5GC01012H

136. Zada B, Chen M, Chen C, Yan L, Xu Q, Li W, Guo Q, Fu Y (2017) Recent advances in catalytic production of sugar alcohols and their applications. Sci China Chem 60:853–859. https://doi.org/10.1007/s11426-017-9067-1

137. Fabre L, Gallezot P, Perrard A (2001) Catal Commun 2:249–253. https://doi.org/10.1016/S1566-7367(01)00042-5

138. Fabre L, Gallezot P, Perrard A (2002) Catalytic hydrogenation of arabinonic acid and lactones to arabitol. J Catal 208:247–254. https://doi.org/10.1006/jcat.2002.3567

139. Dickson D, Hussain A, Kumpf B (2019) The future of petrochemicals: growth surrounded by uncertainty. Deloitte Consulting LLP, London. https://www2.deloitte.com/content/dam/Deloitte/us/Documents/energy-resources/the-future-of-petrochemicals.pdf. Accessed 21 Feb 2020

140. Vora BV, Marker TL, Barger PT, Nilsen HR, Kvisle S, Fuglerud T (1997) Economic route for natural gas conversion to ethylene and propylene. Stud Surf Sci Catal 107:87

141. Kaiser S (1985) U.S. Patent 4,499,327

142. Kaiser SW (1985) Arab J Sci Eng 10:361

143. Lewis JMO (1998) In: Ward JW (ed) Catalysis. Elsevier, Amsterdam, p 199

144. Keil F (1999) Methanol-to-hydrocarbons: process technology. Microporous Mesoporous Mater 29:49–66. https://doi.org/10.1016/S1387-1811(98)00320-5

145. Gregor J, Vermeiren W (2003) Proceedings of the fifth EMEA petrochemicals technology conference, 25–26 Jun Paris, Jun 2003

146. Chen JQ, Bozzano A, Glover B, Fuglerud T, Kvisle S (2005) Recent advancements in ethylene and propylene production using the UOP/Hydro MTO process. Catal Today 106:103–107. https://doi.org/10.1016/j.cattod.2005.07.178

147. Yang M, Fan D, Wei Y, Tian P, Liu Z (2019) Recent progress in methanol- to-olefins (MTO) catalysts. Adv Mater 31(50):1902181. https://doi.org/10.1002/adma.201902181

148. Gogate MR (2019) Methanol-to-olefins process technology: current status and future prospects. Pet Sci Technol 37(5):559–565. https://doi.org/10.1080/10916466.2018.1555589

149. Dahl IM, Kolboe S (1996) On the reaction mechanism for hydrocarbon formation from methanol over SAPO-34: 2. Isotopic labeling studies of the co-reaction of propene and methanol. J Catal 161(1):304–309. https://doi.org/10.1006/jcat.1996.0188

150. Xu, S, Zhi, Y, Han, J, Zhang, W, Wu, X, Sun, T, Wei, Y, Liu, Z, Advances in catalysis for methanol-to-olefins conversion, Adv Catal, 61:38–118 doi:10.1016/bs.acat.2017.10.002 2017

151. Tian P, Wei Y, Ye M, Liu Z (2015) Methanol-to-olefins (MTO): from fundamentals to commercialization. ACS Catal 5(3):1922–1938. https://doi.org/10.1021/acscatal.5b00007

152. Chang CD (1984) Methanol conversion to light olefins. Catal Rev Sci Eng 26(3–4):323–344. https://doi.org/10.1080/01614948408064716

153. Koempel, H, Liebner, W (2007) Lurgi's methanol to propylene (MTP®), report on a successful commercialisation, in Natural gas conversion VIII F.B. Noronha, Schmal M, EF Sousa-Aguiar Amsterdam, Elsevier.V:262–267

154. Streb S, Göhna H (2000) Mega methanol. Paving the way for new downstream industries. World methanol conference, Copenhagen, 8–10 Nov 2000

155. Rothaemel M, Holtmann HD (2001) MTP, methanol to propylene – Lurgi's way, DGMK-conference "creating value from light olefins – production and conversion, Hamburg, 10–12 Oct 2001

156. Rothaemel M (2016) Methanol-to-propylene (MTP®): a proven technology for on-purpose propylene production NGCS 11 conference, Tromso, Norway, 6–9 Jun. doi:10.13140/RG.2.2.31772.49283

157. Jasper S, Mahmoud M, El-Halwagi A (2015) Techno-economic comparison between two methanol-to-propylene processes. PRO 3:684–698. https://doi.org/10.3390/pr3030684

158. Amghizar I, Laurien A, Vandewalle KM, Van Geem Guy MB (2017) New trends in olefin production. Engineering 3:171–178. https://doi.org/10.1016/J.ENG.2017.02.006

159. Adkins H, Perkins PP (1925) Dehydration of alcohol over alumina. J Am Chem Soc 47:1163–1167. https://doi.org/10.1021/ja01681a036

160. Kochar NK, Merims R, Padia AS (1981) Ethylene from ethanol. Chem Eng Prog 6:66–70

161. Fathi-Afshar F, Rudd DF (1980) Biomass ethanol as a chemical feedstock in the United States. Biotechnol Bioeng XXII:677–679

162. Fan D, Dai D-J, Wu H-S (2013) Ethylene formation by catalytic dehydration of ethanol with industrial considerations. Materials 6:101–115. https://doi.org/10.3390/ma6010101

163. Tsao U, Zasloff H.B (1979) Production of ethylene from ethanol, US patent, 4134926A

164. Mohsenzadeh A, Zamani A, Mohammad TJ (2017) Bio-ethylene production from ethanol: a review and techno-economical evaluation. Chem Bio Eng Rev 4:1–18. https://doi.org/10.1002/cben.201600025

165. Hulea V (2018) Toward platform chemicals from bio-based ethylene: heterogeneous catalysts and processes. ACS Catal 8:3263–−327. https://doi.org/10.1021/acscatal.7b04294

166. Sun J, Wang Y (2014) Recent advances in catalytic conversion of ethanol to chemicals. ACS Catal 4:1078–1090. https://doi.org/10.1021/cs4011343

167. Al-Ali AlMa'adeed M, Krupa I (2016) Polyolefin compounds and materials: fundamentals and industrial applications. Springer, Berlin

168. Al-Jarallah AM, Anabtawi JA, Siddiqui MAB, Aitani AM, Alsa'doun AW (1992) Part 1 dimerization of ethylene to butene-1. Catal Today 14:1–−121. https://doi.org/10.1016/0920-5861(92)80128-A

169. McGuinness DS (2011) Olefin oligomerization via metallacycles: dimerization, trimerization, tetramerization, and beyond. Chem Rev 111:2321–2341. https://doi.org/10.1021/cr100217q

170. Olivier-Bourbigou H, Forestière A, Saussine L, Magna L, Favre F, Hugues F (2010) Olefin oligomerization for the production of fuels and petrochemicals. Oil Gas Eur Mag, 36:97−102. https://www.osti.gov/etdeweb/biblio/21327984

171. Svejda SA, Brookhart M (1999) Ethylene oligomerization and propylene dimerization using cationic (α-diimine) nickel(II) catalysts. Organometallics 18:65–74. https://doi.org/10.1021/om980736t

172. Finiels A, Fajula F, Hulea V (2014) Nickel-based solid catalysts for ethylene oligomerization. A review. Cat Sci Technol 4:2412–2426. https://doi.org/10.1039/C4CY00305E

173. Skupinska J (1991) Oligomerization of alpha-olefins to higher oligomers. Chem Rev 91:613–648. https://doi.org/10.1021/cr00004a007

174. Andrei RD, Popa MI, Fajula F, Hulea V (2015) Heterogeneous oligomerization of ethylene over highly active and stable Ni-AlSBA-15 mesoporous catalysts. J Catal 323:76–−84. https://doi.org/10.1016/j.jcat.2014.12.027

175. Agirrezabal-Telleria I, Iglesia E (2017) Stabilization of active, selective, and regenerable Ni-based dimerization catalysts by condensation of ethene within ordered mesopores. J Catal 352:505–514. https://doi.org/10.1016/j.jcat.2017.06.025

176. Mol JC (2004) Industrial applications of olefin metathesis. J Mol Catal A Chem 213:39–−45. https://doi.org/10.1016/j.molcata.2003.10.049

177. Lwin S, Wachs IE (2014) Olefin metathesis by supported metal oxide catalysts. ACS Catal 4:2505–2520. https://doi.org/10.1021/cs500528h

178. Andrei RD, Popa MI, Cammarano C, Hulea V (2016) Nickel and molybdenum containing mesoporous catalysts for ethylene oligomerization and metathesis. New J Chem 40:4146–4152. https://doi.org/10.1039/C5NJ02586A

179. Andrei RD, Popa MI, Fajula F, Cammarano C, AlKhudhair A, Bouchmella K, Mutin PH, Hulea V (2015) Ethylene to propylene by one-pot catalytic cascade reactions. ACS Catal 5:2774–2777. https://doi.org/10.1021/acscatal.5b00383

180. Lin B, Zhang Q, Wang Y (2009) Catalytic conversion of ethylene to propylene and butenes over H-ZSM-5. Ind Eng Chem Res 48:10788−10795. https://doi.org/10.1021/ie901227p

181. Oikawa H, Shibata Y, Inazu K, Iwase Y, Murai K, Hyodo S, Kobayashi G, Baba T (2006) Highly selective conversion of ethylene to propene over SAPO-34 as a solid acid catalyst. Appl Catal A 312:181–185. https://doi.org/10.1016/j.apcata.2006.06.045

182. Song ZX, Takahashi A, Mimura N, Fujitani T (2009) Production of propylene from ethanol over ZSM-5 zeolites. Catal Lett 131:364–369. https://doi.org/10.1007/s10562-009-0071-3

183. Mizuno S, Kurosawa M, Tanaka M, Iwamoto M (2012) One-path and selective conversion ethanol to propene on scandium-modified indium oxide catalysts. Chem Lett 41:892–894. https://doi.org/10.1246/cl.2012.892

184. Iwamoto M (2011) One step formation of propene from ethene or ethanol through metathesis on nickel ion-loaded silica. Molecules 16:7844–7863. https://doi.org/10.3390/molecules16097844

185. Nishiguchi T, Matsumoto T, Kanai H, Utani K, Matsumura Y, Shen WJ, Imamura S (2005) Catalytic steam reforming of ethanol to produce hydrogen and acetone. Appl Catal A 2005(279):273–277. https://doi.org/10.1016/j.apcata.2004.10.035

186. Murthy RS, Patnaik P, Sidheswaran P, Jayamani M (1988) Conversion of ethanol to acetone over promoted iron oxide catalysis. J Catal 109:298–302. https://doi.org/10.1016/0021-9517(88)90212-6

187. Nakajima T, Nameta H, Mishima S, Matsuzaki I, Tanabe KJ (1994) A highly active and highly selective oxide catalyst for the conversion of ethanol to acetone in the presence of water vapour. Mater Chem 4:853–−858. https://doi.org/10.1039/JM9940400853

188. Bussi J, Parodi S, Irigaray B, Kieffer R (1998) Catalytic transformation of ethanol into Acetone using copper pyrochlore catalysts. Appl Catal A 172:117–129. https://doi.org/10.1016/S0926-860X(98)00106-9

189. Xu T, Munson EJ, Haw JF (1994) Toward a systematic chemistry of organic reactions in zeolites: in situ NMR studies of ketones. J Am Chem Soc 116:1962–1972. https://doi.org/10.1021/ja00084a041

190. Zaki MI, Hasan MA, Pasupulety L (2001) Surface reactions of acetone on Al_2O_3, TiO_2, ZrO_2, and CeO: IR spectroscopic assessment of impacts of the surface acid−base properties. Langmuir 17:768–774. https://doi.org/10.1021/la000976p

191. Panov AG, Fripiat JJ (1998) Acetone condensation reaction on acid catalysts. J Catal 178:188–197. https://doi.org/10.1006/jcat.1998.2142

192. Hutchings GJ, Johnston P, Lee DF, Warwick A, Williams CD, Wilkinson M (1994) The conversion of methanol and other O-compounds to hydrocarbons over zeolite β. J Catal 147:177–185. https://doi.org/10.1006/jcat.1994.1128

193. Masuda T, Fujikata Y, Mukai SR, Hashimoto K (1998) Changes in catalytic activity of MFI-type zeolites caused by dealumination in a steam atmosphere. Appl Catal A 172:73–83. https://doi.org/10.1016/S0926-860X(98)00120-3

194. Zhu KK, Sun JM, Liu J, Wang LQ, Wan HY, Hu JZ, Wang Y, Peden CHF, Nie ZM (2011) Solvent evaporation assisted preparation of oriented nanocrystalline mesoporous MFI zeolites. ACS Catal 1:682–−690. https://doi.org/10.1021/cs200085e

195. Zhu KK, Sun JM, Zhang H, Liu J, Wang Y (2012) J Nat Gas Chem 21:215–−232

196. Sun J, Zhu K, Gao F, Wang C, Liu J, Peden CHF, Wang YJ (2011) Direct conversion of bio-ethanol to isobutene on nanosized ZnxZryOz mixed oxides with balanced acid-base sites. J Am Chem Soc 133:11096–11099. https://doi.org/10.1021/ja204235v

197. Liu C, Sun J, Smith C, Wang Y (2013) A study of ZnxZryOz mixed oxides for direct conversion of ethanol to isobutene. Appl Catal A 467:91–97. https://doi.org/10.1016/j.apcata.2013.07.011

198. Global Butadiene Market Overview (2020) Prismane consulting. https://www.openpr.com/news/1831666/global-butadiene-market-overview. Accessed 25 Feb 2020

199. Pomalaza G, Capron M, Ordomsky V, Dumeignil V (2016) Recent breakthroughs in the conversion of ethanol to butadiene. Catalysts 6:203. https://doi.org/10.3390/catal6120203

200. Shylesh S, Gokhale AA, Scown CD, Kim D, Christopher R, Ho CR, Bell AT (2016) From sugars to wheels: the conversion of ethanol to 1,3-butadiene over metal-promoted magnesia-silicate, catalysts. ChemSusChem 9:1462–1472. https://doi.org/10.1002/cssc.201600195

201. Lebedev SV (1929) FR 665917

202. Lebedev SV (1930) GB 331482

203. Lebedev SV (1933) Zhurnal Obshchei Khimii 3:698

204. Ostromislenskiy J (1915) J Russ Phys Chem Soc 47:1472–1506

205. Jonathan B, Ross F, Philip L, Peter T (2012) Two-step production 1,3-butadiene from ethanol. Senior Design Rep (CBE) 42. http://repository.upenn.edu/cbe_sdr/42

206. Ezinkwo GO, Tretyakov VP, Aliyu A, Ilolov AM (2014) Fundamental issues of catalytic conversion of bio-ethanol into butadiene. Chem Bio Eng Rev 1:194–203. https://doi.org/10.1002/cben.201400007

207. Makshina EV, Dusselier M, Janssens W, Degrève J, Jacobs PA, Sels BF (2014) Review of old chemistry and new catalytic advances in the on-purpose synthesis of butadiene. Chem Soc Rev 43:7917–7953. https://doi.org/10.1039/C4CS00105B

208. Angelici C, Weckhuysen BM, Bruijnincx PCA (2013) Chemo catalytic conversion of ethanol into butadiene and other bulk chemicals. ChemSusChem 6:1595–1614. https://doi.org/10.1002/cssc.201300214

209. Jones M (2014) Catalytic transformation of ethanol into 1,3-butadiene. Chem Cent J 8:53. https://doi.org/10.1186/s13065-014-0053-4

210. Jones M, Keir C, Iulio C, Robertson R, Williams C, Apperley D (2011) Investigations into the conversion of ethanol into 1,3-butadiene. Cat Sci Technol 1:267–272. https://doi.org/10.1039/C0CY00081G

211. Kagan MY, Lyubarskii GD, Podurovskaya OM, Izv Akad (1947) Nauk SSSR, Ser Khim, pp 173–181

212. Vinogradova OM, Keier NP, Roginskii SZ (1957) Dokl. Akad Nauk SSSR 112:1075–1078
213. Toussaint WJ, Dunn JT (1947) US 2,421,361
214. Toussaint W.J, Dunn J. T, Jackson D. R (1947) Ind Eng Chem, 39, 120–125. https://pubs.acs.org/doi/pdf/10.1021/ie50446a010
215. Delacaillerie JBD, Gruver V, Fripiat JJ (1995) Modification of the surface properties of natural phyllosilicate sepiolite by secondary isomorphic substitution. J Catal 151:420–430. https://doi.org/10.1006/jcat.1995.1044
216. Gruver V, Sun A, Fripiat J. J, (1995) Catalytic properties of aluminated sepiolite in ethanol conversion. Catal Lett 34:359–364. https://link.springer.com/article/10.1007/BF00806885
217. Chieregato A, Ochoa JV, Cavani F (2016) Olefins from biomass. In: Chemicals and fuels from bio-based building blocks. Wiley-VCH Verlag GmbH & Co. KGaA, Weinheim, pp 1–32
218. Natta G, Rigamonti R (1947) Chim Ind 29:95
219. Corson, B. B, Jones H.E, Welling C.E, Hinckley J.A, Stahly E.E (1950) Butadiene from ethyl alcohol, Ind Eng Chem, 42:359. https://pubs.acs.org/doi/pdf/10.1021/ie50482a039
220. Kitayama Y, Michishita A (1981) Catalytic activity of fibrous clay mineral sepiolite for butadiene formation from ethanol. J Chem Soc Chem Commun 9:401–402. https://doi.org/10.1039/C39810000401
221. Kitayama Y, Satoh M, Kodama, T (1996) Preparation of large surface area nickel magnesium silicate and its catalytic activity for conversion of ethanol into buta-1,3-diene Catal Lett36:95 https://link.springer.com/article/10.1007/BF00807211
222. Ohnishi R, Akimoto T, Tanabe K (1985) Pronounced catalytic activity and selectivity of $MgO–SiO_2–Na_2O$ for synthesis of buta-1,3-diene from ethanol. J Chem Soc Chem Commun 22:1613–1614. https://doi.org/10.1039/C39850001613
223. Kvisle S, Aguero A, Sneeden RPA (1988) Transformation of ethanol into 1,3-butadiene over magnesium oxide/silica catalysts. Appl Catal 43:117–131. https://doi.org/10.1016/S0166-9834(00)80905-7
224. Makshina EV, Janssens W, Sels BF, Jacobs PA (2012) Catalytic study of the conversion of ethanol into 1,3-butadiene. Catal Today 198:338–344. https://doi.org/10.1016/j.cattod.2012.05.031
225. Bhattacharyya, S, K, Ganguly, N. D (1962) One-step catalytic conversion of ethanol to butadiene in the fixed bed. II binary- and ternary-oxide catalysts J Appl Chem, 12:105–110. https://doi.org/10.1002/jctb.5010120302
226. Bhattacharyya, S. K, Avasthi, B. N (1963) One-step catalytic conversion of ethanol to Butadiene in a fluidized bed, Ind Eng Chem Process Des Dev, 2, 45–51. https://pubs.acs.org/doi/pdf/10.1021/i260005a010
227. Chung SH, Angelici C, Hinterding SOM, Weingarth M, Baldus M, Houben K, Weckhuysen M, Bruijnincx PCA (2016) On the role of magnesium silicates in wet-kneaded silica-magnesia catalysts for the Lebedev ethanol-to-butadiene process. ACS Catal 6:4034–4045. https://doi.org/10.1021/acscatal.5b02972
228. Angelici C, Velthoen MEZ, Weckhuyse BM, Bruijnincx PCA (2015) Influence of acid– base properties on the Lebedev ethanol-to-butadiene process catalyzed by $SiO_2 – MgO$ materials. Cat Sci Technol 5:2869–2879. https://doi.org/10.1039/C5CY00200A
229. Patel AD, Meesters K, den Uil H, de Jong E, Blok K, Patel MK (2012) Sustainability assessment of novel chemical processes at early stage: application to biobased processes. Energy Environ Sci 5:8430. https://doi.org/10.1039/c2ee21581k
230. Chang CD, Silvestri AJ (1977) The conversion of methanol and other o-compounds to hydrocarbons over zeolite catalysts. J Catal 47:249–259
231. Derouane EG, Nagy JB, Dejaifve P, Van hoof JHC, Ben P, Spekman BP, Vedrine JC, Naccache C (1978) Elucidation of the mechanism of conversion of methanol and ethanol to hydrocarbons on a new type of synthetic zeolite. J Catal 53:40–55. https://doi.org/10.1016/0021-9517(78)90006-4

232. Chang CD, Lang W, Smith R (1979) The conversion of methanol and other O- compounds to hydrocarbons over zeolite catalysts: II. Pressure effects. J Catal 56:69–173. https://doi.org/10.1016/0021-9517(79)90103-9

233. Chang, C. D, James, C.W, Kuo, J.C.W, Lang, W.H, Solomon M, Jacob, S.M, Wise, J.J. Silvestri, A. J, (1978) Process studies on the conversion of methanol to gasoline, Ind Eng Chem Process Des Dev, 17, 255–260. https://pubs.acs.org/doi/pdf/10.1021/i260067a008

234. Yurchak S (1988) Development of Mobil's fixed-bed methanol-to-gasoline (MTG) process. Stud Surf Sci Catal 36:251–272. https://doi.org/10.1016/S0167-2991(09)60521-8

235. Tabak S, Yurchak S (1990) Conversion of methanol over ZSM-5 to fuels and chemicals. Catal Today 6:307–327. https://doi.org/10.1016/0920-5861(90)85007-B

236. Tabak S, Heinritz-Adrian M, Brandl A, McGihon R, Brandl A (2008) An alternative route for coal to liquid fuel-applying the exxon mobil methanol to gasoline (MTG) process, gasification technologies conference, 5–8 Oct, Washington, DC

237. Helton T, Hindman M (2014) Methanol to gasoline technology – an alternative for liquid fuel production-GTL technology forum, Texas, USA, 30–31 Jul 2014

238. Udessen H (2013) TIGAS—Topsoe improved gasoline synthesis, 16th IMPCA-2013 Asian methanol conference, 30 Oct to 1 Nov 2013

239. Gal E, Fang H, Qin H, Boyajian G, Li N (2015) Comparison of STG+ with other GTL Technologies. PGE_White-paper-GTL-Comparison-V32. www.primusge.com www.chem-winfo.com. Accessed 29 Feb 2020

240. ID:MRFR/CnM/5385-HCR-March 2020. https://www.marketresearchfuture.com/reports/ethanol-market-7304. Accessed 1 Mar 2020

241. Eagan, N. M, Kumbhalkar M.D, Buchanan, J. S, Dumesic, J. A, Huber, G.W (2019) Chemistries and processes for the conversion of ethanol into middle distillate fuels, Nat Rev Chem, 3, 223–249. https://www.nature.com/articles/s41570–019–0084-4

242. Johansson R, Hruby SL, Rass-Hansen J, Christensen CH (2009) The hydrocarbon pool in ethanol-to-gasoline over HZSM-5 catalysts. Catal Lett 127:127–132. https://doi.org/10.1007/s10562-008-9711-2

243. Aguayo AT, Gayubo AG, Atutxa A, Olazar M, Bilbao J (2002) Kinetic Modelling of the Transformation of Aqueous Ethanol into Hydrocarbons on a HZSM-5 Zeolite. J Ind Eng Chem Res 41:4216-−4224. https://doi.org/10.1021/ie001115e

244. Costa E, Uguina A, Aguado J, Hernandez PJ (1985) Ethanol to gasoline process: effect of variables, mechanism, and kinetics. Ind Eng Chem Process Des Dev 1985(24):239–244. https://doi.org/10.1021/i200029a003

245. Talukdar AK, Bhattacharyya KG, Sivasanker S (1997) HZSM-5 catalysed conversion of aqueous ethanol to hydrocarbons. Appl Catal A 148:357-−371. https://doi.org/10.1016/S0926-860X(96)00240-2

246. Madeira FF, Ben Tayeb K, Pinard L, Vezin H, Maury S, Cadran N (2012) Ethanol Transformation into hydrocarbons on ZSM-5 zeolites: Influence of Si/Al ratio on catalytic performances and deactivation rate. Study of the radical species role. Appl Catal A 443:171-−180. https://doi.org/10.1016/j.apcata.2012.07.037

247. Gayubo AG, Alonso A, Valle B, Aguayo AT, Olazar M, Bilbao J (2010) Hydrothermal stability of HZSM-5 catalysts modified with Ni for the transformation of bioethanol into hydrocarbons. Fuel 89:3365-−3372. https://doi.org/10.1016/j.fuel.2010.03.002

248. Saha SK, Sivasanker S (1992) Influence of Zn- and Ga-doping on the conversion of ethanol to hydrocarbons over ZSM-5. Catal Lett 15:413–418. https://doi.org/10.1007/BF00769166

249. Tynjala P, Pakkanen TT, Mustamaki S (1998) Modification of ZSM-5 Zeolite with Trimethyl Phosphite. 2. Catalytic Properties in the Conversion of C1−C4 Alcohols. J Phys Chem B 102:5280–5286. https://doi.org/10.1021/jp9806720

250. Viswanadham N, Saxena SK, Kumar J, Sreenivasulu P, Nandan D (2012) Catalytic performance of nano crystalline H-ZSM-5 in ethanol to gasoline (ETG) reaction. Fuel 95:298–304. https://doi.org/10.1016/j.fuel.2011.08.058

251. https://www.maritime-executive.com/article/transport-uses-25-percent-of-world-energy. Accessed 6 Mar 2020
252. International energy outlook-2016 DOE/EIA-0484(2016) I May 2016 www.eia.gov/forecasts/ieo/pdf/0484(2016).pdf
253. Global bioenergy statistics-2019, World Biofuel Association, p 12
254. Wei-Cheng W, Ling T (2016) Bio-jet fuel conversion technologies. Renew Sust Energ Rev 53:801–822. https://doi.org/10.1016/j.rser.2015.09.016
255. US Energy Information Administration (2015) The flight paths for biojet fuel. US Energy Information Administration, Washington, DC, p 20585. https://www.eia.gov/workingpapers/pdf/flightpaths_biojetffuel.pdf
256. Han GB, Jang JM, Hwei-Ahn M, Jung BH (2019) Recent application of bio-alcohol: bio-jet fuel. Inetch Open. https://doi.org/10.5772/intechopen.89719
257. Harmon L, Hallen R, Lilga MA, Heijstra B, Palou-Rivera I, Handler R (2017) A hybrid catalytic route to fuels from biomass syngas OSTI. GOV. doi:https://doi.org/10.2172/142374
258. Humbird RD, Tao L, Kinchin C, Hsu D, Aden A, Schoen P (2011) Process design and economics for biochemical conversion of lignocellulosic biomass to ethanol: dilute-acid pre-treatment and enzymatic hydrolysis of corn stover. Report no. NREL/TP-5100-47764. http://www.nrel.gov/docs/fy11osti/47764.pdf
259. Brooks KP, Snowden-Swan LJ, Jones SB, Butcher MG, Lee GSJ, Anderson DM, Frye JG, Holladay JE, Owen J, Harmon L, Burton F, Palou-Rivera I, Plaza J, Handler R, Shonnard D (2016) Low-carbon aviation fuel through the alcohol to jet pathway. In: Chuck C (ed) Biofuels for aviation: feedstocks, technology and implementation. Academic, Cambridge, MA, p 390
260. Lilga MA (2016) Systems and processes for conversion of ethylene feedstocks to hydrocarbon fuels. WO 2016067032, WO 2016067033 (2016); US9,663,416 (2017)
261. Lilga MA, Frye J, Lee S, Albrecht K (2016) Conversion of 2,3 butane-diol to butadiene, U.S. Patent No. 9:434,569 B2
262. Narula CK, Li Z, Casbeer E, Geiger RA, Szybist JP, Keller M, Davison BH, Theiss T. Direct catalytic upgrading of current dilute alcohol fermentation streams to hydrocarbons for fungible fuels. www.energy.gov-2015/04-biochemical_conversion_davison_0315
263. Wyman CE. Novel vertimass catalyst for conversion of ethanol and other alcohols into fungible gasoline, jet, and diesel fuel blend stocks. https://energy.gov/sites/prod/files/2015/07/f24/wyman_bioenergy_2015
264. Hannon JR. Ethanol conversion to fungible gasoline, diesel, and jet fuel blend stocks and high value chemical coproducts (BTEX). www.energy.gov-sites-files-2017/10-hannon_bioeconomy_2017
265. Wyman CE, Hannon J (2016) R systems and methods for reducing energy consumption in production of ethanol fuel by conversion to hydrocarbon fuels US20160362612A1, 15 Dec, 2016
266. Wyman CE, Hannon JR (2019) Systems and methods for improving yields of hydrocarbon fuels from alcohols, US/2019/00119579A1, 25 Apr 2019
267. Narula, C.K, Li, Z, Casbeer, E.M, Geiger, R. A, Debusk, M.M, Keller, M, Buchanan, M.V, and Davison, B.H, Heterobimetallic zeolite, InV-ZSM-5, enables efficient conversion of biomass derived ethanol to renewable hydrocarbons, Sci Rep, 5, 16039. doi: 10.1038/srep16039
268. Narula CK, Davison BH, Keller M (2017) Zeolitic catalytic conversion of alcohols to hydrocarbons, U.S 9533921, 3 Jan 2017
269. Narula CK, Davison BH (2015) Catalytic conversion of alcohols having at least three carbon Atoms to hydrocarbon blend-stock, U.S. 9181493, 10 Nov 2015
270. Narula CK, Davison BH, Keller M. Catalytic conversion of alcohols to hydrocarbons with low benzene content, U.S. 9278892, 8 Mar, US9434658, 5 Sep 2016
271. Hannon JR. Technoeconomic and life-cycle analysis of single-step catalytic conversion of wet ethanol into fungible fuel blend stocks. www.pnas.org/cgi/doi/10.1073/pnas.1821684116

272. Johnston G 2017 Alcohol to jet-iso-butanol—ICAO seminar on alternate fuels, ICAO Head Quarters, Montreal, 8–9 Feb 2017

273. Matthew WP, Taylor JD. Renewable jet fuel blendstock from iso-butanol, US 8975461, 10th Mar 2015; US Pat. Appl. 2011/0288352, 24 Nov 2011

274. Green car Congress, Dec 19th 2019 – Delta enters off-take agreement with Gevo for 10 million gallons per year of sustainable aviation fuel

275. Wright ME (2012) Biomass to alcohol to jet/diesel-APAN Community. community.apan.org›intelligent-evolution-components-attachments, Aus. Brief, final.pdf

276. Cobalt and the Naval Air Warfare Center team up to produce a renewable jet fuel from bio N-butanol from naval-air-warfare-center-team-up-to-produce-a-renewable-jet-fuel-from-bio-n-butanol-143461676.html. http://www.prnewswire.com/news-releases/cobalt-and-the-

277. Naval Air Warfare Center awards contract to Albemarle for processing Cobalt Technologies bio n-butanol to renewable jet fuel using alcohol-to-jet process – Green car Congress, 20 Mar 2012

278. Michael E, Wright ME, Benjamin GH (2008) Quintana RL Highly Efficient Zirconium-catalyzed Batch Conversion of1-Butene: A New Route to Jet Fuels. Energy Fuel 22:3299–3302. https://doi.org/10.1021/ef800380b

279. Ruddy D, Dagle R Li Z (2019) Liquid fuels via upgrading of indirect liquefaction intermediates. WBS: 2.3.1.100/304/305. www.energy.gov, 2019/03

280. Bradin D 2014 Process for producing renewable jet fuel compositions, WO 2014/008337 Al, 9 Jun

281. Dagle VL, Smith C, Flake AKO, Gray MJ, Ramaswamy KK, Dagle RA (2016) Integrated process for the catalytic conversion of biomass-derived syngas into transportation fuels. Green Chem 18:1880–1891. https://doi.org/10.1039/c5gc02298c

282. Wang W-C, Tao L, Markham J, Zhang Y, Tan E, Batan L, Warner E, Biddy M (2016) Review of biojet fuel conversion technologies, technical report NREL/TP-5100-66291, July. National Renewable Energy Laboratory, Golden, CO. www.nrel.gov/publications

283. Cortright R, Davda R, Dumesic J (2002) Hydrogen from catalytic reforming of biomass-derived hydrocarbons in liquid water. Nature 418(6901):964–976. https://doi.org/10.1038/nature01009

284. Davda R, Shabaker J, Huber G, Cortright RJ, Dumesic JA (2005) A review of catalytic issues and process conditions for renewable hydrogen and alkanes by aqueous-phase reforming of oxygenated hydrocarbons over supported metal catalysts. Appl Catal B Environ 56:171–186. https://doi.org/10.1016/j.apcatb.2004.04.027

285. Hoang, T. M. C, Vikla, A.K.K Seshan K 2016 Aqueous-phase reforming of sugar derivatives: challenges and opportunities, in Dmitry Murzin and Olga Simakova Biomass sugars for non-fuel applications, RSC Green Chemistry The Royal Society of Chemistry London 44, pp. 54–88

286. Fasolini A, Cucciniello R, Paone E, Mauriello F, Tabanelli TA (2019) Short overview on the hydrogen production via aqueous phase reforming (APR) of cellulose, C_6-C_5 sugars and polyols. Catalysts 9:917. https://doi.org/10.3390/catal9110917

287. Vaidya PD, Lopez-Sanchez JA (2017) Review of hydrogen production by catalytic aqueous-phase reforming. Chem Select 2:6563–6576. https://doi.org/10.1002/slct.201700905

288. Davda R, Shabaker J, Huber G, Cortright RJ, Dumesic JA (2003) Aqueous phase reforming of ethylene glycol on silica-supported metal catalysts. Appl Catal B Environ 43:13–26. https://doi.org/10.1016/S0926-3373(02)00277-1

289. Chen G, Li W, Chen H, Yan B (2015) Progress in the aqueous-phase reforming of different biomass-derived alcohols for hydrogen production. J Zhejiang Univ Sci A (Appl Phys Eng) 16(6):491–506. https://doi.org/10.1631/jzus.A1500023

290. Kim TW, Kim HD, Jeong KE, Chae H-J, Jeong S-Y, Lee C-H, Kim C-U (2011) Catalytic production of hydrogen through aqueous-phase reforming over platinum/ordered mesoporous carbon catalysts. Green Chem 13(7):1718–1728. https://doi.org/10.1039/c1gc15235a

291. Kim HD, Park HJ, Kim TW, Jeong K-E, Chae H-J, Jeong S-Y, Lee C-H, Kim C-U (2012) Hydrogen production through the aqueous phase reforming of ethylene glycol over supported Pt-based bimetallic catalysts. Int J Hydrog Energy 37(10):8310–8317. https://doi.org/10.1016/j.ijhydene.2012.02.160

292. Kim HD, Park HJ, Kim TW, Jeong K-E, Chae H-J, Jeong S-Y, Lee C-H, Kim C-U (2012) The effect of support and reaction conditions on aqueous phase reforming of polyol over supported Pt-Re bimetallic catalysts. Catal Today 185(1):73–80. https://doi.org/10.1016/j.cattod.2011.08.012

293. Huber GW, Shabaker JW, Evans ST, Dumesic JA (2006) Aqueous-phase reforming of ethylene glycol over supported Pt and Pd bimetallic catalysts. Appl Catal B Environ 62:226–235. https://doi.org/10.1016/j.apcatb.2005.07.010

294. Bai Y, Lu CS, Ma L, Chen P, Zheng YF, Li XN (2006) Hydrogen production by aqueous-phase reforming of ethylene glycol over Pt catalysts supported on γ-Al2O3 modified with Ce and Mg. Chin J Catal 27(3):275–280

295. Wawrzetz A, Peng B, Hrabar A, Jentys A, Lemonidou AA, Lercher JA (2010) Towards understanding the bifunctional hydrodeoxygenation and aqueous phase reforming of glycerol. J Catal 269(2):411–420. https://doi.org/10.1016/j.jcat.2009.11.027

296. Barbelli ML, Pompeo F, Santori GF, Nichio NN (2013) Pt catalyst supported on α-Al$_2$O$_3$ modified with CeO$_2$ and ZrO$_2$ for aqueous-phase-reforming of glycerol. Catal Today 213:58–64. https://doi.org/10.1016/j.cattod.2013.02.023

297. Wen G, Xu Y, Ma H, Xu Z, Tian Z (2008) Production of hydrogen by aqueous-phase reforming of glycerol. Int J Hydrog Energy 33(22):6657–6666. https://doi.org/10.1016/j.ijhydene.2008.07.072

298. Fasolini A, Cespi D, Tabanelli T, Cucciniello R, Cavani F (2019) Hydrogen from renewables: a case study of glycerol reforming. Catalysts 9:722. https://doi.org/10.3390/catal9090722

299. Seretis A, Tsiakaras P (2016) Hydrogenolysis of glycerol to propylene glycol by in situ produced hydrogen from aqueous phase reforming of glycerol over SiO$_2$– Al$_2$O$_3$ supported nickel catalyst. Fuel Process Technol 142:135–146

300. Iriondo A, Barrio VL, Cambra JF, Arias PL, Guemez MB, Navarro RM, Sánchez-Sánchez MC, Fierro JLG (2008) Hydrogen production from glycerol over nickel catalysts supported on Al$_2$O$_3$ modified by Mg, Zr, Ce or La. Top Catal 49:46–58. https://doi.org/10.1007/s11244-008-9060-9

301. Haryanto A, Fernando S, Murali N, Adhikari S (2005) Current status of hydrogen production techniques by steam reforming of ethanol: a review. Energy Fuel 19:2098–2106. https://doi.org/10.1021/ef0500538

302. Tokarev A, Kirilin A, Murzina E, Eranen K, Mikkola JP (2010) The role of bio-ethanol in aqueous phase reforming to sustainable hydrogen. Int J Hydrog Energy 35:12642–12649. https://doi.org/10.1016/j.ijhydene.2010.07.118

303. Roy B, Loganathan K, Pham H, Datye AK, Leclerc CA (2010) Surface modification of solution combustion synthesized Ni/Al$_2$ O$_3$ catalyst for aqueous-phase reforming of ethanol. Int J Hydrog Energy 35:11700–11708. https://doi.org/10.1016/j.ijhydene.2010.07.167

304. Roy B, Martinez U, Loganathan K, Datye AK, Leclerc CA (2012) Effect of preparation methods on the performance of Ni/Al$_2$ O$_3$ catalysts for aqueous-phase reforming of ethanol: Part I catalytic activity. Int J Hydrog Energy 37:8143–8153. https://doi.org/10.1016/j.ijhydene.2012.02.056

305. Roy B, Artyushkova K, Pham H, Li L, Leclerc CA (2012) Effect of preparation method on the performance of the Ni/Al$_2$O$_3$ catalysts for aqueous-phase reforming of ethanol: Part II characterization. Int J Hydrog Energy 37:18815–18826. https://doi.org/10.1016/j.ijhydene.2012.09.098

306. Nozawa T, Mizukoshi Y, Yoshida A, Naito S (2014) Aqueous phase reforming of ethanol and acetic acid over TiO2 supported Ru catalysts. Appl Catal B Environ 146:221–226. https://doi.org/10.1016/j.apcatb.2013.06.017

307. Cruz IO, Ribeiro NF, Aranda DA, Souza MMVM (2008) Hydrogen production by aqueous-phase reforming of ethanol over nickel catalysts prepared from hydrotalcite precursors. Catal Commun 9:2606–2611. https://doi.org/10.1016/j.catcom.2008.07.031

308. Roy B, Sullivan H, Leclerc CA (2011) Aqueous-phase reforming of n-BuOH over Ni/Al$_2$O$_3$ and Ni/CeO$_2$ catalysts. J Power Sources 196:10652–10657. https://doi.org/10.1016/j.jpowsour.2011.08.093

309. Shabaker JW, Davda RR, Huber GW, Cartwright RD (2003) Aqueous-phase reforming of methanol and ethylene glycol over alumina-supported platinum catalysts. J Catal 215:344–352. https://doi.org/10.1016/S0021-9517(03)00032-0

310. Liu XH (2011) Aqueous-phase reforming of ethylene glycol to hydrogen on supported platinum catalysts. Ph.D. thesis. East China University of Science and Technology, Shanghai

311. Rose M, Palkovits R (2012) Isosorbide as a renewable platform chemical for versatile applications—quo vadis? ChemSusChem 5:167–176. https://doi.org/10.1002/cssc.201100580

312. Kobayashi H, Fukuoka A (2013) Synthesis and utilisation of sugar compounds derived from lignocellulosic biomass. Green Chem 15:1740–1763. https://doi.org/10.1039/c3gc00060e

313. Grand View Research Inc. (2020) Market research report—isosorbide market size, share and trend analysis. Grand View Research Inc., San Francisco, CA. Accessed 22 Mar 2020

314. Besse V, Auvergne R, Carlotti S, Boutevin G, Otazaghine B, Caillol S, Pascault JP, Boutevin B (2013) Synthesis of isosorbide-based polyurethanes: an isocyanate free method. React Funct Polym 73:588–594. https://doi.org/10.1016/j.reactfunctpolym.2013.01.002

315. Otomo R, Yokoi T, Tatsumi T (2015) Synthesis of isosorbide from sorbitol in water over high-silica aluminosilicate zeolites. Appl Catal A Gen 505:28–35. https://doi.org/10.1016/j.apcata.2015.07.034

316. Shi J, Shan Y, Tian Y, Wan Y, Zheng Y, Feng Y (2016) Hydrophilic sulfonic acid-functionalized micro-bead silica for dehydration of sorbitol to isosorbide. RSC Adv 6:13514–13521. https://doi.org/10.1039/x0xx00000x

317. Yamaguchi A, Sato O, Mimura N, Shirai M (2015) One-pot conversion of cellulose to isosorbide using supported metal catalysts and ion-exchange resin. Catal Commun 67:59–63. https://doi.org/10.1016/j.catcom.2015.04.009

318. Xu Y, Tian Z, Wen G, Xu Z, Qu W, Lin L (2006) Production of CO$_x$-free hydrogen by alkali enhanced hydrothermal catalytic reforming of biomass-derived alcohols. Chem Lett 35:216–217. https://doi.org/10.1246/cl.2006.216

319. Soetaert W, Buchholz K, Vandamme E (1995) Production of D-mannitol and D-lactic acid by fermentation by Leuconostoc mesenteroides Agro Food Ind Hi Tech, 6: 41–44. https://lib.ugent.be/catalog/pug01:256408

320. Clark IT (1958) Hydrogenolysis of sorbitol. Ind Eng Chem 50:1125–1126. https://doi.org/10.1021/ie50584a026

321. Sun J, Liu H (2011) Selective hydrogenolysis of biomass-derived xylitol to ethylene glycol and propylene glycol on supported Ru catalysts. Green Chem 13:135–142. https://doi.org/10.1039/c0gc00571a

322. Nda-Umar UI, Ramli I, Taufiq-Yap YH, Muhamad EN (2019) An overview of recent research in the conversion of glycerol into biofuels, fuel additives and other bio-based chemicals. Catalysts 9:15. https://doi.org/10.3390/catal9010015

323. Cognet P, Aroua MK (eds) (2020) From glycerol to value-added products. Frontiers Media SA, Lausanne. https://doi.org/10.3389/978-2-88963-577-1

324. Demsash HD, Mohan R (2016) Steam reforming of glycerol to hydrogen over ceria promoted nickel–alumina catalysts. Int J Hydrog Energy 41:22732–22742. https://doi.org/10.1016/j.ijhydene.2016.10.082

325. Menezes AO, Rodrigues MT, Zimmaro A, Borges LE, Fraga MA (2011) Production of renewable hydrogen from aqueous-phase reforming of glycerol over Pt catalysts supported on different oxides. Renew Energy 36:595–599. https://doi.org/10.1016/j.renene.2010.08.004

326. Rahmat N, Abdullah AZ, Mohamed AR (2010) Recent progress on innovative and potential technologies for glycerol transformation into fuel additives: a critical review. Renew Sust Energ Rev 14:987–1000. https://doi.org/10.1016/j.rser.2009.11.010

327. García JI, García-Marín H, Pires E (2014) Glycerol based solvents: synthesis, properties and applications. Green Chem 16:1007–1033. https://doi.org/10.1039/C3GC41857J

328. Usai E, Gualdi E, Solinas V, Battistel E (2010) Simultaneous enzymatic synthesis of FAME and triacetyl glycerol from triglycerides and methyl acetate. Bioresour Technol 101:7707–7712. https://doi.org/10.1016/j.biortech.2010.05.044

329. Morales G, Paniagua M, Melero JA, Vicente G, Ochoa C (2011) Sulfonic acid- functionalized catalysts for the valorization of glycerol via transesterification with methyl acetate. Ind Eng Chem Res 50:5898–5906. https://doi.org/10.1021/ie102357c

330. Silva LN, Gonçalves VL, Mota CJ (2010) Catalytic acetylation of glycerol with acetic anhydride. Catal Commun 11:1036–1039. https://doi.org/10.1016/j.catcom.2010.05.007

331. Gonzalez-Arellano C, De S, Luque R (2014) Selective glycerol transformations to high value-added products catalysed by aluminosilicate-supported iron oxide nanoparticles. Catal Sci Technol 4:4242–4249. https://doi.org/10.1039/C4CY00714J

332. Sandesh S, Kristachar PKR, Manjunathan P, Halgeri AB, Shanbhag GV (2016) Synthesis of biodiesel and acetins by transesterification reactions using novel CaSn (OH)$_6$ heterogeneous base catalyst. Appl Catal A Gen 523:1–11. https://doi.org/10.1016/j.apcata.2016.05.006

333. Gonçalves M, Souza VC, Galhardo TS, Mantovani M, Figueiredo FVC, Mandelli D, Carvalho WA (2013) Glycerol conversion catalyzed by carbons prepared from agro industrial wastes. Ind Engg Chem Res 52:2832–2839. https://doi.org/10.1021/ie303072d

334. Viswanadham N, Saxena SK (2013) Etherification of glycerol for improved production of oxygenates. Fuel 103:980–986. https://doi.org/10.1016/j.fuel.2012.06.057

335. Cornejo A, Barrio I, Campoy M, Lázaro J, Navarrete B (2017) Oxygenated fuel additives from glycerol valorization. Main production pathways and effects on fuel properties and engine performance: a critical review. Renew Sust Energ Rev 79:1400–1413. https://doi.org/10.1016/j.rser.2017.04.005

336. Mota CJ, da Silva CXA, Rosenbach N Jr, Costa J, da Silva FV (2010) Glycerin derivatives as fuel additives: the addition of glycerol/acetone ketal (solketal) in gasolines. Energy Fuel 24:2733–2736. https://doi.org/10.1021/ef9015735

337. Vicente G, Melero JA, Morales G, Paniagua M, Martín E (2010) Acetalization of bio-glycerol with acetone to produce solketal over sulfonic mesostructured silicas. Green Chem 12:899–907. https://doi.org/10.1039/B923681C

338. De Torres M, Jimenez-Oses G, Mayoral JA, Pires E, Santos M (2012) Glycerol ketals: synthesis and profits in biodiesel blends. Fuel 94:614–616. https://doi.org/10.1016/j.fuel.2011.11.062

339. Nanda MR, Yuan Z, Qin W, Ghaziaskar HS, Poirier M-A, Xu CC (2014) A new continuous-flow process for catalytic conversion of glycerol to oxygenated fuel additive: catalyst screening. Appl Energy 123:75–81. https://doi.org/10.1016/j.apenergy.2014.02.055

340. Nanda MR, Yuan Z, Qin W, Ghaziaskar HS, Poirier M-A, Xu CC (2014) Catalytic conversion of glycerol to oxygenated fuel additive in a continuous flow reactor: process optimization. Fuel 128:113–119. https://doi.org/10.1016/j.fuel.2014.02.068

341. Umbarkar SB, Kotbagi TV, Biradar AV, Pasricha R, Chanale J, Dongare MK, Mamede A-S, Lancelot C, Payen E (2009) Acetalization of glycerol using mesoporous MoO$_3$ /SiO$_2$ solid acid catalyst. J Mol Catal A Chem 310:150–158

342. Amin T-K, Amin NAS, Najaafi N, Tarighi S (2018) A review on the catalytic acetalization of bio-renewable glycerol to fuel additives. Front Chem 6:573. https://doi.org/10.3389/fchem.2018.00573

343. Ma T, Ding J, Shao R, Xu W, Yun Z (2017) Dehydration of glycerol to acrolein over Wells–Dawson and Keggin type phospho tungstic acids supported on MCM-41 catalysts. Chem Eng J 316: 797–806. http://doi:10.1016/j.cej.2017.02.018

344. Gu Y, Liu S, Li C, Cui Q (2013) Selective conversion of glycerol to acrolein over supported nickel sulfate catalysts. J Catal 301:93–102. https://doi.org/10.1016/j.jcat.2013.01.019

345. Yadav GD, Sharma RV, Katole SO (2013) Selective dehydration of glycerol to acrolein: development of efficient and robust solid acid catalyst MUICaT-5. Ind Eng Chem Res 52:10133–10144. https://doi.org/10.1021/ie401098n

346. Jia C-J, Liu Y, Schmidt W, Lu A-H, Schüth F (2010) Small-sized HZSM-5 zeolite as highly active catalyst for gas phase dehydration of glycerol to acrolein. J Catal 269:71–79. https://doi.org/10.1016/j.jcat.2009.10.017

347. Climent MJ, Corma A, De Frutos P, Iborra S, Noy M, Velty A, Concepción P (2010) Chemicals from biomass: synthesis of glycerol carbonate by transesterification and carbonylation with urea with hydrotalcite catalysts – the role of acid–base pairs. J Catal 269:140–149. https://doi.org/10.1016/j.jcat.2009.11.001

348. Ishak ZI, Sairi NA, Alias Y, Aroua MKT, Yusoff R (2016) Production of glycerol carbonate from glycerol with aid of ionic liquid as catalyst. Chem Eng J 297:128–138. https://doi.org/10.1016/j.cej.2016.03.104

349. Nakagawa Y, Tamura M, Tomishige K (2014) Catalytic materials for the hydrogenolysis of glycerol to 1,3-propanediol. J Mater Chem A 2014(2):6688–6702. https://doi.org/10.1039/c3ta15384c

350. Leoneti AB, Aragão-Leoneti V, De Oliveira SVWB (2012) Glycerol as a by-product of biodiesel production in Brazil: alternatives for the use of unrefined glycerol. Renew Energy 45:138–145. https://doi.org/10.1016/j.renene.2012.02.032

351. Cameron DC, Altaras NE, Hoffman ML, Shaw AJ (1998) Metabolic engineering of propanediol pathways. Biotechnol Prog 14:116–125. https://doi.org/10.1021/bp9701325

352. Gonzalez-Pajuelo M, Meynial-Salles I, Mendes F, Soucaille P, Vasconcelos I (2006) Microbial conversion of glycerol to 1,3-propanediol: physiological comparison of a natural producer, clostridium butyricum VPI 3266, and an engineered strain, clostridium acetobutylicum DG1(pSPD5). Appl Environ Microbiol 72:96–101. https://doi.org/10.1128/AEM.72.1.96-101.2006

353. Gonz'alez-Pajuelo M, Meynial-Salles I, Mendes F, Andrade JC, Vasconcelos I, Soucaille P (2005) Metabolic engineering of *Clostridium acetobutylicum* for the industrial production of 1,3-propanediol from glycerol. Metab Eng 7:329–336. https://doi.org/10.1016/j.ymben.2005.06.001

354. Mu Y, Teng H, Zhang DJ, Wang W, Xiu ZL (2006) Microbial production of 1,3-propanediol by *Klebsiella pneumoniae* using crude glycerol from biodiesel preparations. Biotechnol Lett 28:1755–1759. https://doi.org/10.1007/s10529-006-9154-z

355. Dobson R, Gray V, Rumbold K (2012) Microbial utilization of crude glycerol for the production of value-added products. J Ind Microbiol Biotechnol. https://doi.org/10.1007/s10295-011-1038-0

356. Garlapati VK, Shankar U, Budhiraja A (2016) Bioconversion technologies of crude glycerol to value added industrial products. Biotechnol Rep 9:9–14. https://doi.org/10.1016/j.btre.2015.11.002

357. Mariscal R, Maireles-Torres P, Ojeda M, Sadaba I, Lopez Granados M (2016) Furfural: a renewable and versatile platform molecule for the synthesis of chemicals and fuels. Energy Environ Sci 9:1144–1189. https://doi.org/10.1039/C5EE02666K

358. Wang Y, Zhao, Rodríguez-Padrón D, Len C (2019) Recent advances in catalytic hydrogenation of furfural. Catalysts 9:796. https://doi.org/10.3390/catal9100796

359. Prescient and Strategic Intelligence Pvt. Ltd. Report published in Global Newswire, 7th Nov 2019

360. Bozell JJ, Moens L, Elliot DC, Wang Y, Neuenscwander GG, Fitzpatrick SW, Bilski RJ, Jarnefeld JL (2000) Production of levulinic acid and use as a platform chemical for derived products. Resources, Conservation and Recycling 28:227–239. PII:S0921-3449(99)00047-6

361. Hayes DJ, Fitzpatrick S, Hayes MHB, Ross JRH (2008) The biofine process: production of levulinic acid, furfural, and formic acid from lignocellulosic feedstocks. In: Kamm B, Gruber PR, Kamm M (eds) Biorefineries – industrial processes and products. Wiley-VCH, Weinheim

362. Gonzalez Maldonado GM, Assary RS, Dumesic JA, Curtiss LA (2012) Experimental and theoretical studies of the acid-catalyzed conversion of furfuryl alcohol to levulinic acid in aqueous solution. Energy Environ Sci 5:6981–6989. https://doi.org/10.1039/C2EE03465D

363. Xue Z, Liu Q, Wang J, Mu T (2018) Valorization of levulinic acid over non-noble metal catalysts: challenges and opportunities. Green Chem 20:4391–4408. https://doi.org/10.1039/x0xx00000x

364. Ahmad E, Alam MI, Pant KK, Ali Haider M (2018) Catalytic and mechanistic insights into the production of ethyl levulinate from bio renewable feedstocks. Green Chem 18:4804–4823. https://doi.org/10.1039/C6GC01523A

365. Demolis A, Essayem N, Rataboul E (2014) Synthesis and applications of alkyl levulinates. ACS Sust Chem Eng 2:1338–1352. https://doi.org/10.1021/sc500082n

366. Haan RJ, Lange J-P (2011) US Patent Appl., 20110035991A1

367. Haan RJ, Lange J-P (2009) World Patatent, WO 2009077606 A2

368. Lange J-P, Heide E, Buijtenen J, Price R (2012) Furfural-a promising platform for lignocellulosic biofuels. ChemSusChem 5:150–166. https://doi.org/10.1002/cssc.201100648

369. Yang S, Hao Y, Wang J, Wang H, Zheng Y, Tian H, Liu Y, Sun B (2017) Selective catalytic dehydration of furfuryl alcohol to 2,2′-difurfuryl ether using a polyoxometalate catalyst. Sci Rep 7:12954. https://doi.org/10.1038/s41598-017-13472-3

370. Meng Q, Zheng H, Zhu Y, Li Y (2016) Study on the reaction pathway in decarbonylation of biomass-derived 5-hydroxymethylfurfural over Pd-based catalyst. J Mol Catal A Chem 421:76–82. https://doi.org/10.1016/j.molcata.2016.05.012

371. Kim T, Assary RS, Pauls RE, Marshall CL, Curtiss LA, Stair PC (2014) Thermodynamics and reaction pathways of furfuryl alcohol oligomer formation. Catal Commun 46:66–70. https://doi.org/10.1016/j.catcom.2013.11.030

372. Yi B, Rajagopalan R, Foley HC, Kim UJ, Liu X, Eklund PC (2006) Catalytic polymerization and facile grafting of poly (furfuryl alcohol) to single-wall carbon nanotube: preparation of nanocomposite carbon. J Am Chem Soc 128:11307–11313. https://doi.org/10.1021/ja063518x

373. Kumar R, Rajesh A (2012) Process for preparing polyfurfuryl alcohol products, WO 2012/123902 Al, 20 Sep 2012

374. van Buijtenen J, Lange JP, Price RJ (2011) United States Pat., 2011/0173877

375. Moreau C, Belgacem MN, Gandini A (2004) Recent catalytic advances in the chemistry of substituted furans from carbohydrates and in the ensuing polymers. Top Catal 27:11–30. https://doi.org/10.1023/B:TOCA.0000013537.13540.0e

376. Pranger LA, Nunnery GA, Tannenbaum R (2012) Mechanism of the nanoparticle-catalyzed polymerization of furfuryl alcohol and the thermal and mechanical properties of the resulting nanocomposites. Compos Part B 2012(43):1139–1146. https://doi.org/10.1016/j.compositesb.2011.08.010

377. Takei T, Iguchi N, Haruta M (2010) Synthesis of acetaldehyde, acetic acid, and others by the dehydrogenation and oxidation of ethanol. Catal Surv Jpn 15:80–88. https://doi.org/10.1007/s10563-011-9112-1

378. Gallo JMR, Bueno JMC, Schuchardt U (2014) Catalytic transformations of ethanol for biorefineries. J Braz Chem Soc 25:2229–2243. https://doi.org/10.5935/0103-5053.20140272

379. Pease RN, Yung CC (1924) The catalytic dehydration of ethyl alcohol and ether by alumina. J Am Chem Soc 46:390–340

380. Varisli D, Dogu T, Dogu G (2007) Ethylene and diethyl-ether production by dehydration reaction of ethanol over different heteropoly acid catalysts. Chem Eng Sci 62:5349–5352. https://doi.org/10.1016/j.ces.2007.01.017

381. Sato AG, Volanti DP, de Freitas IC, Longo E, Bueno JMC (2012) Site-selective ethanol conversion over supported copper catalysts. Catal Commun 26:122–126. https://doi.org/10.1016/j.catcom.2012.05.008

382. Obora Y (2014) Recent advances in α-alkylation reactions using alcohols with hydrogen borrowing methodologies. ACS Catal 4:3972–3981. https://doi.org/10.1021/cs501269d

383. Chakraborty S, Daw P, David YB, Milstein D (2018) Manganese-catalyzed α-alkylation of ketones, esters, and amides using alcohols. ACS Catal 8:10300−10305. https://doi.org/10.1021/acscatal.8b03720

384. Chaudhari C, Siddiki SMAH, Kon K, Tomita A, Tai Y, Shimizu K (2014) Cat Sci Technol 4:1064–1069. https://doi.org/10.1039/C3CY00911D

385. Kwon MS, Kim N, Seo SH, Park IS, Cheedrala RK, Park J (2005) Recyclable palladium catalyst for highly selective a alkylation of ketones with alcohols. Angew Chem Int Ed 44:6913–6915. https://doi.org/10.1002/anie.200502422

386. Kwon MS, Kim N, Park CM, Lee JS, Kang KY, Park J (2005) Palladium nanoparticles entrapped in aluminum hydroxide: dual catalyst for alkene hydrogenation and aerobic alcohol oxidation. Org Lett 7:1077–1079. https://doi.org/10.1021/ol047381w

387. Selva M, Perosa A (2008) Green chemistry metrics: comparative evaluation of dimethyl carbonate, methyl iodide, dimethyl sulfate and methanol as methylating agents. Green Chem 10:457–464. https://doi.org/10.1039/B713985C

388. Fu A, Liu Q, Jiang M, Xu G (2019) Selective N-mono methylation of amines and nitroarenes using methanol over an encapsulated iridium nano catalyst. Asian J Org Chem 8:1–6. https://doi.org/10.1002/ajoc.201900140

389. Jiang L, Guo F, Wang Y, Jiang J, Duan Y, Hou Z (2019) Selective *N*-mono methylation of anilines with methanol catalyzed by commercial Pd/C as an efficient and reusable catalyst. Asian J Org Chem 8:1–5. https://doi.org/10.1002/ajoc.201900509

390. Nanda S, Dalai AK, Kozinski JA (2014) Butanol and ethanol production from lignocellulosic feed stock: biomass pretreatment and bioconversion. Energy Sci Eng 2:138–148. https://doi.org/10.1002/ese3.41

391. Bazzanella AM, Ausfelder F (2017) Low carbon energy and feedstock for the European chemical industry. DECHEMA Gesellschaft für Chemische Technik und Biotechnologie e.V, Frankfurt. ISBN:978-3-89746-196-2

392. Lipinski ES (1981) Chemicals from biomass: petrochemical substitution options. Science 212:1465–1471. https://doi.org/10.1126/science.212.4502.1465

393. Rass-Hansen J, Falsig H, Jørgensen B, Christensen CH (2007) Bio-ethanol: fuel or feedstock? J Chem Technol Biotechnol 82:329. https://doi.org/10.1002/jctb.1665

394. Dale BE, Anderson JE, Brown RC, Csonka S, Dale VH, Herwick G et al (2014) Take a closer look: biofuels can support environmental, economic and social goals. Environ Sci Technol 48:7200–7203. https://doi.org/10.1021/es5025433

395. Balan V, Chiaramonti D, Kumar S (2013) Review of US and EU initiatives toward development, demonstration, and commercialization of lignocellulosic biofuels. Biofuels Bioprod Biorefin 7:732–759. https://doi.org/10.1002/bbb.1436

396. Balan V (2014) Current challenges in commercially producing biofuels from lignocellulosic biomass. Biotechnology 463074:463074. https://doi.org/10.1155/2014/463074

397. Karimi K, Tabatabaei M, Horvath IS, Kumar R (2015) Recent trends in acetone, butanol and ethanol (ABE) production. Biofuel Res J 8:301–308. https://doi.org/10.18331/BRJ2015.2.4.4

398. Biswas S, Katiyar R, Gurjar BR, Pruthi V (2017) Role of different feedstocks on the butanol production through microbial and catalytic routes. Int J Chem Engg 2017:20160215. https://doi.org/10.1515/ijcre-2016-0215

399. Tsvetanova F, Petrova P, Petrov K (2018) Microbial production of 1-butanol – recent advances and future prospects. J Chem Technol Metall 53:683–696. https://www.researchgate.net/publication/325554503

400. Dagle VL, Flake MD, Lemmon TL, Lopez JS, Kovarik L, Dagle RA (2018) Effect of the SiO_2 support on the catalytic performance of $Ag/ZrO_2/SiO_2$ catalysts for the single-bed production of butadiene from ethanol. Appl Catal B Environ 236:576–587. https://doi.org/10.1016/j.apcatb.2018.05.055

401. Cimino S, Lisi L, Romannucci S (2018) Catalysts for conversion of ethanol to butanol: effect of acid-base and redox properties. Catal Today 304:58–63. https://doi.org/10.1016/j.cattod.2017.08.035

Steam Reforming of Methanol, Ethanol and Glycerol over Catalysts with Mesoporous Supports: A Comparative Study

S. Bepari, R. Abrokwah, V. Deshmane, and D. Kuila

Abstract Hydrogen generation via steam reforming of alcohols (SRA) has gained tremendous attention among green energy industries, research scientists and government policy makers. A variety of mesoporous heterogeneous catalysts used to produce hydrogen from alcohols like methanol (SRM), ethanol (SRE) and glycerol (SRG) are discussed. Siliceous mesoporous supports, e.g. SBA-15, MCM-41, MCM-48 and KIT-6, have proven to be substantially thermally stable compared to metal oxide supports such as TiO_2, Al_2O_3 and CeO_2. While Cu-based catalysts are commonly used for SRM, Ni- and Co-based catalysts are preferred for SRE and SRG reactions. Addition of promoters like group 1 and 2 metals to these monometallic catalysts significantly improves reducibility of the metal oxides as well as the basicity of the catalysts that minimize deactivation of catalysts by coking. Synergistic effects of bimetallic catalysts such as Cu-Ni, Pd-Ni and Ni-Co to increase hydrogen selectivity and long-term stability of the catalysts are discussed. Hydrogen selectivity and feed conversion of 100% can be attained depending on the reaction conditions like temperature, feed flow rate, type of catalyst, catalyst loading and alcohol/water molar ratio.

Keywords Mesoporous · N_2 adsorption-desorption · Hydrogen · Steam reforming

S. Bepari · R. Abrokwah · V. Deshmane
Department of Chemistry, Joint School of Nanoscience and Nanoengineering, North Carolina
A&T State University, Greensboro, NC, USA

D. Kuila (✉)
Department of Chemistry, Joint School of Nanoscience and Nanoengineering, North Carolina
A&T State University, Greensboro, NC, USA

Department of Nanoengineering, Joint School of Nanoscience and Nanoengineering, North
Carolina A&T State University, Greensboro, NC, USA
e-mail: dkuila@ncat.edu

1 Introduction

Due to limited fossil fuel sources, climate change and environmental concerns, researchers are motivated to develop renewable energy sources for the full replacement of fossil fuel. Among all energy sources, hydrogen is now gaining attention because it can be used in fuel cell applications to generate electricity [1, 2]. Hydrogen is considered a clean source of energy that can be consumed without emitting carbon-based environmental pollutants [3, 4]. Also, hydrogen has an energy density of 143 MJ/kg, which is more than any known hydrocarbon-based fuels [5, 6]. Currently, 90% of hydrogen is obtained from reforming of nonrenewable sources—natural gas and other fossil fuels—which are not sustainable [3, 7].

Storage and transportation of hydrogen, which is flammable, are the major challenges to commercialize hydrogen as a standard fuel for vehicles. One of the convenient ways to overcome this issue is the use of metal hydrides like MgH_2, $NaAlH_4$, LiH and hydrides of some transition metals to capture hydrogen. The main problems of the metal hydrides are their regeneration after the hydrogen is released, diffusion and leakage of H_2 during storage and transportation [8]. On-site production and use of H_2 are possible solutions to mitigate the storage problem [6]. Utilization of hydrogen in different sectors such as rocket engines [9], petrochemical industry [10], ammonia production [11], fertilizer [10], and Fischer-Tropsch synthesis [12–14] has globally bolstered future demands of hydrogen. Other popular industrial applications of hydrogen include metal production and fabrication, methanol synthesis, food processing and electronic applications [6].

Water electrolysis, hydrocarbon reforming, photocatalysis and biocatalysis are different routes to produce H_2 [15–17]. Steam reforming of hydrocarbons is currently used to produce highly purified H_2 [18–21]. Worldwide H_2 production mainly comprises 48% from steam reforming of methane, 30% from reforming of naphtha/oil, 18% from coal gasification and 3.9% from electrolysis of water [22]. The major drawback of methane steam reforming is the high temperature required for reforming effective in the range of 800–1000 °C [23]. The steam reforming of alcohols such as ethanol, methanol and glycerol is favoured commercially because it provides a much less endothermic (200–700 °C), less energy-intensive, hence lower capital cost route to produce hydrogen compared to fossil fuels [4, 24]. Steam reforming of alcohols also generates less greenhouse gases relative to fossil fuels. This ensures that the amount of CO_2 released into the atmosphere is low enough to be consumed by green plants via photosynthesis [25].

For steam reforming of methanol, ethanol and glycerol, researchers aim to control the effective way to cleave C–H, C–C and C–O bonds [25] in order to free the hydrogen atoms. While the C–H and C–O bonds are broken in steam reforming of methanol, the C–C bond is broken for higher alcohols—ethanol and glycerol, and the process is more complex. Several catalysts with different supports have been used for steam reforming of these three alcohols. Metals such as Cu, Ni, Co and Fe have been used extensively for methanol steam reforming [26–28]. Among these catalysts, Cu-based catalysts are more effective in methanol steam reforming (SRM) due to its higher activity and selectivity [29–34]. However, these catalysts suffer

deactivation due to thermal sintering [35] and have triggered the search for other catalysts. Group 8–10 catalysts have been reported by different groups to be promising with similar activity and high selectivity as observed with copper catalysts [36–38]. In the case of ethanol steam reforming (SRE) and glycerol steam reforming (SRG), many noble metals (e.g. Pd, Ru, Rh and Pt) and non-noble metals (e.g. Ni and Co) have been investigated [39–49]. In order to minimize catalyst deactivation rates via sintering, catalyst supports like SiO_2, γ-Al_2O_3, ZrO_2, CeO_2, TiO_2, MgO and La_2O_3 have been used to immobilize the metal active sites in the steam reforming reactions [50–54].

Mesostructured supports with pore sizes of 2–50 nm have been extensively studied and employed for drug delivery, sensors, adsorbents, molecular sieves and heterogeneous catalysis. Generally, silica-based mesoporous frameworks (e.g. MCM-41, MCM-48, SBA-15, KIT-6, FSM-16, zeolites) are more thermally stable than the nonsiliceous metal oxides (e.g. TiO_2, Al_2O_3, CeO_2) and mesoporous carbon. Mesostructures are synthesized via either exotemplating in which the mesoporous material is prepared within the channels of a porous supramolecular template or endotemplating where by inorganic compounds are tethered on a template already coated on a well-ordered porous material [55]. Compared to homogeneous catalysts, supported heterogeneous catalysts are usually less reactive, are more expensive to synthesize, requires large amounts to be used and have regeneration cost due to occasional blocking of catalyst active sites. However, supported heterogeneous catalysts are more widely preferred within the green energy research community and green energy production industry because:

1. They are environmentally friendly and safe to handle as the active sites (e.g. acids and bases) are anchored to the supports unlike aqueous phase homogeneous acids/bases that could be very corrosive and hazardous.
2. They can be easily separated from reaction medium, can be reactivated and are reusable.
3. They have high selectivity for desired products due to the ability of tailored pore structure and shapes to control the chemistry and molecular diffusion of reactants and products.
4. Their large surface areas provide strong adsorption sites for the metal catalysts, thereby retarding or inhibiting sintering during reactions [56, 57].

This chapter provides an in-depth outlook of different mesoporous supported catalysts and their activities for methanol, ethanol and glycerol steam reforming reactions.

2 Steam Reforming of Methanol (SRM)

Methanol has the highest carbon-to-hydrogen ratio compared to all hydrocarbons [25]. It is easy to perform methanol steam reforming studies compared to methane due to the presence of –OH group. It can be used for on-board fuel cell applications

due to lack of C–C bond that helps to activate it at lower temperature (300–400 °C) compared to that of methane (>700 °C) [58]. There is an advantage of less CO and coke formation during SRM reaction. This makes methanol a good candidate for hydrogen production for different applications including on-board fuel cells to power electric cars [25].

2.1 Reaction Mechanism for Steam Reforming of Methanol (SRM)

The main methanol steam reforming is [25]:

$CH_3OH + H_2O \leftrightarrow CO_2 + 3H_2$ ($\Delta H = +49.7$ kJ/mol).

Other side reactions are:

$CH_3OH \leftrightarrow CO + 2H_2$ ($\Delta H = +90.2$ kJ/mol) (methanol decomposition).

$CO + H_2O \leftrightarrow CO_2 + H_2$ ($\Delta H = -41.2$ kJ/mol) (water-gas shift reaction).

$2CO \rightarrow C + CO_2$ ($\Delta H = -171$ kJ/mol) (Boudouard reaction).
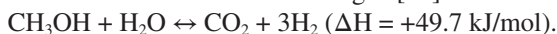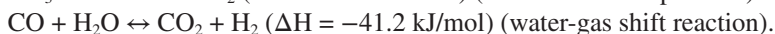
Excess amount of carbon formation is prevented by increasing the water-to-methanol molar ratio higher than the stoichiometry ratio [59]. Typically, methanol first decomposes to give CO and H_2. Then CO reacts with water to generate CO_2 and H_2 via the exothermic water-gas shift reaction (shown above). Another reaction pathway during SRM is the formation of formaldehyde due to dehydrogenation of methanol followed by reaction of formaldehyde and water to produce formic acid. Finally, formic acid decomposes to CO_2 and H_2 [60]. However, this reaction pathway depends on the structural and elemental composition of the catalysts.

$CH_3OH \leftrightarrow HCHO + H_2$ (methanol to formaldehyde formation).

$HCHO + H_2O \leftrightarrow HCOOH + H_2$ (formaldehyde to formic acid formation).

$HCOOH \leftrightarrow CO_2 + H_2$ (formic acid decomposition reaction).
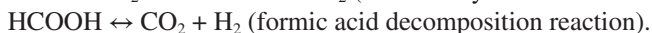
2.2 Overview of Mesoporous Supports for Steam Reforming of Alcohols

2.2.1 Identification of Mesoporous Structures

N_2 adsorption-desorption analysis is the most crucial characterization technique that is widely used for mesoporous catalysts. The low-angle XRD analysis is frequently used to confirm whether the mesoporous materials have short- or long-range ordered mesopores. The mesostructures that have long-range ordered pores with good periodicity exhibit resolved low−/small-angle XRD diffraction peaks between 2-theta 2θ values of 2–10°, while the more amorphous inorganic frameworks which have short-medium-range ordered pores usually show weaker intensity XRD patterns at $2\theta = 20$–25°. Generally, the type of isotherm and shape of hysteresis loop (based on IUPAC nomenclature) are used to determine the morphology of mesoporous

catalysts. For example, a type H3 hysteresis is observed in structures with slit-like pores. Several computational models are used to calculate textural characteristics of the mesoporous catalysts. The Brunauer-Emmett-Teller (BET) equation from the adsorption isotherm is the most widely accepted model to calculate the surface area, while the nonlocal density functional theory (NLDFT) and Barrett-Joyner-Halenda (BJH) are the most popular models for quantification of the pore size and its distribution.

Table 1 shows the N_2 adsorption-desorption isotherm analysis results of selected catalysts with mesoporous supports.

Eswaramoorthi and Dalai [61] studied mesoporous silica (SBA-15)-supported Pd-Zn catalyst for MSR. Hydrothermal and conventional impregnation methods were used for the synthesis of the mesoporous support and catalyst. The N_2 adsorption-desorption isotherm of support and catalyst are type IV in nature as per IUPAC classification and exhibit H1-type hysteresis loop. This type of hysteresis loop is characteristic of large-pore mesoporous materials with narrow-pore size distribution [67]. They also observed that capillary condensation occurred due to sharp inflection in the relative pressure (P/P_0) between 0.6 and 0.7. Mesoporous Cu-CeO$_2$-ZrO$_2$ support was prepared by nanocasting method using MCM-48 as template [62]. The specific surface area decreases with the incorporation of Cu because it blocks

Table 1 N_2 adsorption-desorption analysis results of different mesoporous supported catalysts

Catalysts	Metals (wt%)	BET surface area (m²/g)	Average pore diameter (nm)	Pore volume (cc/g)	References
SBA-15	–	818	10.3	1.85	[61]
Pd-Zn/SBA-15	Pd (4.5) Zn (6.75)	524	10.07	1.13	[61]
CeO$_2$-ZrO$_2$	–	260	–	–	[62]
Cu-Ce$_{0.75}$Zr$_{0.25}$O$_2$	Cu (9)	165	–	–	[62]
MCM-41	–	1039.2	3.2	0.75	[33]
Cu-MCM-41	Cu (10)	795.7	3.7	0.62	[33]
KIT-6	–	703	5.95	0.91	[63]
Ce-Cu/KIT-6 (CT)	Cu (10) Ce (2)	560	5.28	0.71	[63]
Al$_2$O$_3$	–	338	4.7	0.43	[64]
Pd-Zn/Al$_2$O$_3$	Pd (2) Zn (20)	245	3.9	0.31	[64]
TiO$_2$	–	146.6	3.59	0.71	[65]
Pd-TiO$_2$	Pd (10)	99.7	3.32	0.081	[65]
SBA-15	–	767.4	4.1	0.8218	[66]
CuZnCeZr-SBA-15	Cu (10) Ce (2) Zr (2) Zn (5)	523.6	4.3	0.5527	[66]
MCM-41	–	1039.2	3.3	0.75	[34]
Cu-MCM-41	Cu (15)	662.4	3.78	0.62	[34]

the mesoporous support pore which inhibits N_2 adsorption during BET analysis [68]. Similar type of behavior was observed for Cu-MCM-41 [33]. All isotherms were type IV with H1 hysteresis loop based on IUPAC classification. Capillary condensation was observed between the relative range of 0.6 to 0.8 for KIT-6 and Ce-Cu/KIT-6 [63]. This result showed the existence of large channel-like pores that fall between a narrow range (0.6–0.8) [69]. Same type of isotherm was observed for Pd-Zn on mesoporous alumina synthesized by impregnation method [64]. After addition of Pd and Zn, the surface area decreases due to pore blockage of the support. Steep inflection, observed between the relative pressure range of 0.45 to 0.7, suggests the mesoporosity of the materials. Deshmane et al. [34] used mesoporous TiO_2-supported Pd catalyst for methanol steam reforming. All the isotherms belong to type IV. H2-type hysteresis loop often attributed to disordered and nonuniform pore size distribution was observed for mesoporous TiO_2 support. The hysteresis loop changed from H2 to H4 type (indicative of a combination of narrow-slit mesopores and inner micropores) after incorporation of metal into the support. Tajrishi et al. [66] prepared SBA-15-supported Cu-Ce-Zr-Zn catalyst and found the same type of isotherm observed by Eswaramoorthi and Dalai [61]. After addition of metals, the isotherm was preserved, but the pore size of the nanocatalysts was less uniform and ordered, compared with that of SBA-15 [70]. MCM-41 and Cu-loaded MCM-41 catalysts were synthesized by Deshmane et al. [34] where the pores were blocked upon addition of Cu (Fig. 1). Small pores are blocked first which increases the pore size [71]. Similar kind of phenomena was reported by Abrokwah et al. [33].

2.2.2 Comparison of SRM Activity of Different Mesoporous Supported Catalysts.

Table 2 shows the activities of Cu- and Pd-based mesoporous supported catalysts for the methanol steam reforming. Cu-based catalyst is very common in methanol steam reforming [73–75]. Apart from Cu-based catalysts, Pd can also be used in SRM [76, 77].

Eswaramoorthi and Dalai [61] and Tajrishi et al. [66] investigated Pd- and Cu-based SBA-15 (mesoporous silica) catalysts for SRM. Both catalysts showed good catalytic activity in SRM. However, Cu-based catalyst containing Ce and Zr yielded better methanol conversion and hydrogen selectivity at the same reaction temperature. So, it can be concluded that other metals, Ce and Zr, play an important role in Cu dispersion. Mesoporous Ce-Zr supported Cu-based catalyst, and its activity in SRM was also studied by Jampa et al. [62]. The catalyst showed good catalytic activity in terms of methanol conversion and hydrogen selectivity. Different Cu loading (10 and 15 wt%) on the same mesoporous silica (MCM-41)-supported catalysts were synthesized by Abrokwah et al. [33] and Deshmane et al. [34]. The optimum metal loading of 15% Cu showed the best catalyst activity at a fixed temperature, indicating that the Cu loading plays an important role in catalyst activity. Another type of mesoporous silica (KIT-6)-supported Cu-based catalyst, prepared by Taghizadeh et al. [63] yielded 100% H_2 selectivity and 92.2% methanol conversion. They reported that the catalyst activity increased due to the incorporation of Ce into the catalyst. Mesoporous TiO_2 supported Pd catalyst showed 98% methanol conversion and 95% H_2 selectivity [65]. They reported that good catalytic activity depends on metal-support interactions. Abrokwah et al. [33] studied time on stream of different metals supported MCM-41 catalysts for 40 h at 300 °C (Fig. 2). They found that Cu-supported catalyst gave promising results based on the analysis.
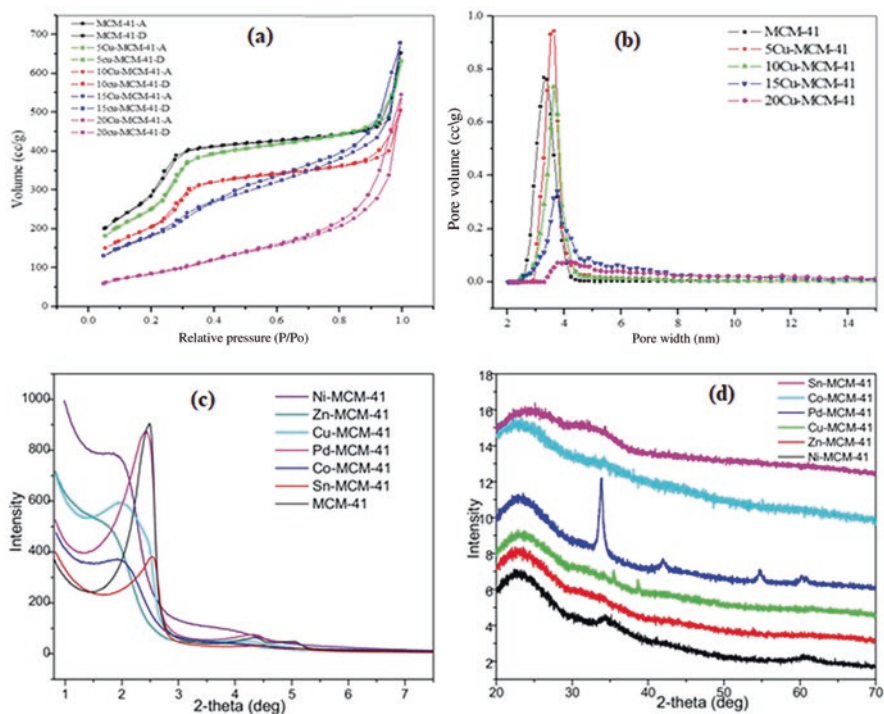
Fig. 1 (**a**) N_2 adsorption-desorption isotherms and (**b**) pore size distribution of different Cu-MCM-41 samples [34]: (**c**) Small angle XRD and (**d**) Wide Angle XRD patterns of calcined M-MCM-41catalysts [33]

3 Steam Reforming of Ethanol (SRE)

Fermentation of biomass such as sugar cane, corn and switchgrass is the technique to produce ethanol [16, 78]. Ethanol steam reforming as a source of hydrogen has been extensively studied in recent years [40, 79]. It is a highly endothermic process [25].

3.1 Reaction Mechanism for Steam Reforming of Ethanol (SRE)

The overall ethanol steam reforming can be expressed as [6, 25]:

$$C_2H_5OH + 3H_2O \leftrightarrow 2CO_2 + 6H_2 \ (\Delta H = +174 \text{ kJ/mol}).$$
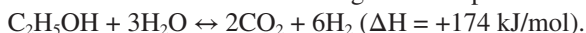
Other side reactions with the main SRE reaction depends on operating conditions and the type of catalyst. Undesirable side reactions produced products which limit the production of hydrogen [80, 81]:

Table 2 MSR activity of different mesoporous catalysts

Catalysts	Metal (wt%)	Temperature (°C)	CH_3OH conversion (%)	H_2 selectivity (%)	References
Pd-Zn/SBA-15	Pd (4.5) Zn (6.75)	300	65	85	[61]
$Cu-Ce_{0.75}Zr_{0.25}O_2$	Cu (9)	300	100	60	[62]
Cu-MCM-41	Cu (10)	350	82.3	99.5	[33]
Ce-Cu/KIT-6 (CT)	Cu (10) Ce (2)	300	92.2	99.2	[63]
Pd-TiO$_2$	Pd (10)	350	98	95	[65]
CuZnCeZr-SBA-15	Cu (10) Ce (2) Zr (2) Zn (5)	300	91	88.2	[66]
Cu-MCM-41	Cu (15)	350	96.4	100	[34]
Cu-MCM-41	Cu (10)	300	69.9	100	[72]
Pd-MCM-41	Pd (10)	300	69.0	98.5	[72]
Sn-MCM-41	Sn (10)	300	39.1	74.8	[72]
Zn-MCM-41	Zn (10)	300	35.6	98.5	[72]
Ni-MCM-41	Ni (10)	300	22.1	99.6	[72]
Co-MCM-41	Co (10)	300	14.4	98.2	[72]

C_2H_5OH decomposition to CH_4, CO, H_2: $C_2H_5OH \rightarrow CH_4 + CO + H_2$ ($\Delta H = +49$ kJ/mol).

C_2H_5OH dehydration to C_2H_4: $C_2H_5OH \rightarrow C_2H_4 + H_2O$ ($\Delta H = +45$ kJ/mol).

C_2H_5OH dehydrogenation to C_2H_4O: $C_2H_5OH \rightarrow C_2H_4O + H_2$ ($\Delta H = +68$ kJ/mol).

C_2H_4O decomposition to CH_4 and CO or steam reforming of C_2H_4O:

$C_2H_4O \rightarrow CH_4 + CO$.

$C_2H_4O \rightarrow H_2O + 3H_2 + CO$.

Water-gas shift reaction: $CO + H_2O \leftrightarrow CO_2 + H_2$ ($\Delta H = -41.2$ kJ/mol).

Methane steam reforming: $CH_4 + H_2O \leftrightarrow CO + 3H_2$ ($\Delta H = +206.2$ kJ/mol).

Methanation:

$CO + 3H_2 \leftrightarrow CH_4 + H_2O$ ($\Delta H = -251$ kJ/mol).

$CO_2 + 4H_2 \leftrightarrow CH_4 + 2H_2O$.

Deposition of carbon:

$CH_4 \rightarrow C + 2H_2$ (Methane decomposition).

$2CO \rightarrow CO_2 + C$ (Boudouard reaction) ($\Delta H = -171$ kJ/mol).

$C_2H_4 \rightarrow 2C + 2H_2$ or polymerization to coke.

Acetone may form due to aldol condensation in some cases:

$2C_2H_5OH + H_2O \leftrightarrow CH_3COCH_3 + CO + 4H_2$.
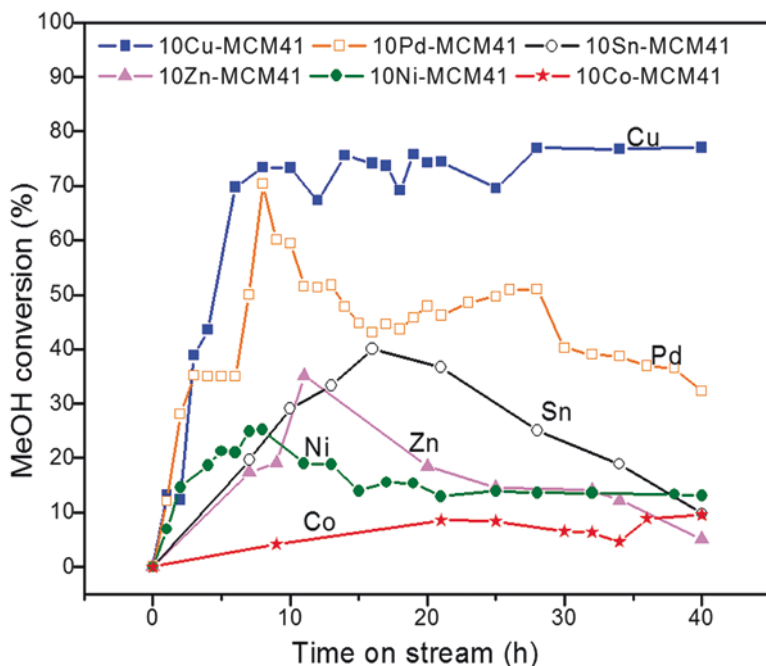
Fig. 2 Time-on-stream studies of different metals supported MCM-41 catalysts (reaction conditions: 300 °C, 1 atm, methanol/water molar ratio of 1:3 and a GHSV of 2838 h^{-1} at STP) [33]

3.2   SRE with Different Mesoporous Supported Catalysts

3.2.1   Comparison of Different Mesoporous Supported Catalysts Based on Catalyst Characterization

Table 3 shows the N$_2$ adsorption-desorption isotherms of different mesoporous supported catalysts used for ethanol steam reforming.

3.2.2   Comparison of the Activities of Catalysts Supported by Different Mesoporous Supports

The additional methyl group (–CH$_3$) in ethanol makes ethanol steam reforming reaction more complex than methanol steam reforming [25]. The main advantage of ethanol over methanol for steam reforming is that it is cheap, non-toxic and an abundant feedstock due to its ability to be readily obtained from thermochemical and biochemical processing of biomass. Table 4 shows the activity of different mesoporous supported (e.g. MC—mesoporous carbon) catalysts in steam reforming of ethanol (SRE).

Table 3 N_2 adsorption-desorption data of different mesoporous supported catalysts

Catalysts	Metals (wt%)	BET surface area (m²/g)	Average pore diameter (nm)	Pore volume (cc/g)	References
MC-Ni-Co	–	229	8.12	0.52	[82]
MC-Ni-Co/Zr	Zr (2)	480	5.91	0.524	[82]
MC-Ni-Co/Y	Y (2)	296	5.29	0.39	[82]
Ni/SBA-15	Ni (10)	403.4	16.4	1.34	[83]
Ni-La/SBA-15	Ni (10) La (5)	388.6	15.3	1.301	[83]
Ni-La-Ce/ SBA-15	Ni (10) La (5) Ce (5)	394.7	15	1.310	[83]
NiOMC	Ni (9.2)	156	3.5	0.73	[84]
SBA-15	–	657	5.5	0.56	[85]
Ni/SBA-15	Ni (6)	298	4.5	0.44	[85]
Ni-Au/SBA-15	Ni (6) Au (1.2)	398	4.8	0.55	[85]
MCM-41	–	1176	2.42	0.9401	[86]
Ni/MCM-41	Ni (10)	496.2	1.86	0.6416	[86]
Co/MCM-41	Co (10)	427.9	1.67	0.5986	[86]
Ni-Co/ MCM-41	Ni (9) Co (1)	481.7	1.95	0.6516	[86]
Zr-SBA-15	–	670	6.6	1.3	[87]
Ni/Zr-SBA-15	Ni (6)	515	5.7	1.1	[87]
Zr-MCM-41	–	595	3.4	1.1	[87]
Ni/Zr-MCM-41	Ni (6)	338	3.4	0.7	[87]
Co/0.5CaO-Al₂O₃	Co (15)	155	13.5	0.52	[81]

The activity of different Ni-Co-MC catalysts with promoters (Zr and Y) was studied at 375 °C by Gharahshiran et al. [82]. The highest ethanol conversion and hydrogen selectivity were achieved for yttria-promoted catalyst. The smaller crystallite size and dispersion on support played an important role to increase the catalytic activity. Nickel embedded on mesoporous carbon (NiOMC) catalyst showed good catalytic activity and stability for a longer period at 450 °C. Hydrogen selectivity of 65% and 100% ethanol conversion were obtained with this catalyst [84]. He et al. [85] studied Ni/SBA-15 and Ni-Au/SBA-15 catalysts for ethanol steam reforming. They found that both the catalysts showed promising catalytic activity at temperature 550 °C. However, Au-promoted catalyst gave better results compared to the unpromoted catalyst. Activities of mesoporous silica (MCM-41)-supported monometallic (Ni, Co) and bimetallic (Ni-Co) catalysts were investigated in the temperature range of 420–500 °C by Nejat et al. [86]. The catalysts showed the highest activity at 490 °C. The bimetallic catalyst was more promising for SRE reaction. They observed that the increase of Ni amount with the decrease of Co amount in bimetallic catalyst increased ethanol conversion and yield of hydrogen.

Table 4 Activity in SRE of different mesoporous supported catalysts

Catalysts	Metals (wt%)	Temperature (°C)	C_2H_5OH conversion (%)	H_2 selectivity/ yield (%)	References
MC-Ni-Co	–	375	10	30	[82]
MC-Ni-Co/Zr	Zr (2)	375	46	25	[82]
MC-Ni-Co/Y	Y (2)	375	51	38	[82]
NiOMC	Ni (9.2)	450	100	65	[84]
Ni/SBA-15	Ni (6)	550	100	80	[85]
Ni-Au/SBA-15	Ni (6) Au (1.2)	550	100	82	[85]
Ni/MCM-41	Ni (10)	490	70	55	[86]
Co/MCM-41	Co (10)	490	62	25	[86]
Ni-Co/MCM-41	Ni (9) Co (1)	490	90	80	[86]
Co/0.5CaO-Al$_2$O$_3$	Co (15)	450	100	74.6	[81]
Ni-Al$_2$O$_3$-ZrO$_2$	Ni (15)	500	100	124.9	[88]
Cu-Ni-Al$_2$O$_3$-ZrO$_2$	Cu (0.2) Ni (15)	450	100	86.6	[89]
P123 assisted-Ni-Al$_2$O$_3$-ZrO$_2$	Ni (15)	500	100	126	[90]
Ni-Al$_2$O$_3$-ZrO$_2$	Ni (15)	500	100	128	[91]
Ni-Al$_2$O$_3$-ZrO$_2$	Ni (15)	500	100	115	[91]

Mesoporous xerogel support CaO-Al$_2$O$_3$ with Co-based catalyst was used in SRE by Han et al. [81]. They investigated with different Ca/Al molar ratio and measured the catalyst activity at 450 °C. They concluded that Ca/Al molar ratio (0.5) gave maximum ethanol conversion (100%) and hydrogen (74.6%) yield. The variation of basicity of different catalysts for the variation of Ca/Al molar ratio was the key factor of all catalyst's activity. Ni-Al$_2$O$_3$-ZrO$_2$ xerogel catalyst with different Ni loading (5, 10, 15, 20 and 25) was synthesized and introduced for SRE by Han et al. [88, 91]. Among all catalysts studied, 15 wt% Ni exhibited maximum hydrogen yield. The group reported that the catalyst showed promising stability over longer time on stream (2100 min) at 500 °C (Fig. 3).

Different amounts of Cu loading (0, 0.1, 0.2, 0.3 and 1.0 wt%) with fixed Ni (15 wt%) and Zr/Al molar ratio (0.2) catalysts were prepared by Han et al. [89] for SRE. 0.2 wt% Cu-loaded catalyst gave a maximum hydrogen yield (86.6%) with complete ethanol conversion at 450 °C. Han et al. [90] synthesized mesoporous Ni-Al$_2$O$_3$-ZrO$_2$ xerogel catalysts with fixed Ni loading (15 wt%) and Zr/Al molar ratio 0.2. They varied the P-123 concentration (0, 6, 12, 18 and 24 mM) during synthesis of the catalysts. Twelve millimetre-concentrated P123-assisted Ni-Al$_2$O$_3$-ZrO$_2$ catalyst produced the highest hydrogen yield (126%) with complete ethanol conversion at 500 °C. So, P-123 concentration played an important role in catalyst activity. Ni-Al$_2$O$_3$-ZrO$_2$ and Ni/Al$_2$O$_3$-ZrO$_2$ catalysts were developed by sol-gel and incipient wet-impregnation method, and the catalysts activity for ethanol steam
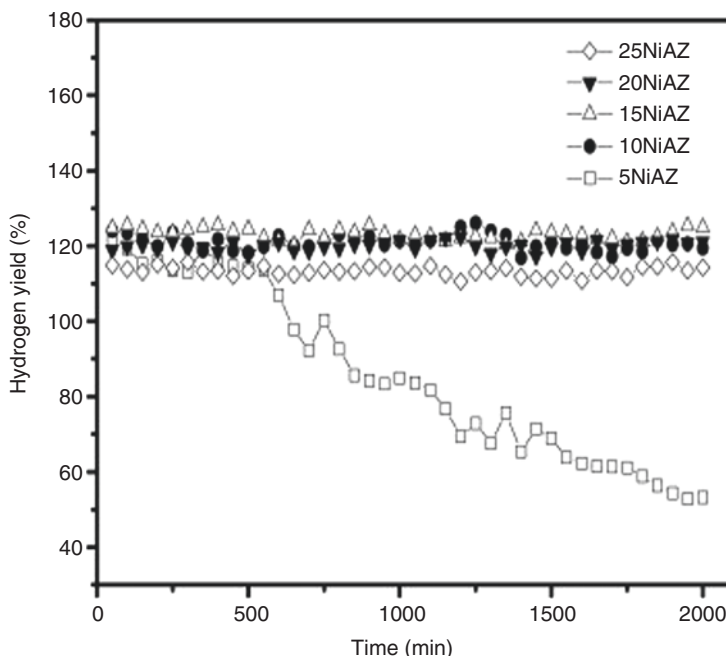
Fig. 3 Steam reforming of ethanol: hydrogen yield with time on stream of different Ni-loaded Ni-Al$_2$O$_3$-ZrO$_2$ catalysts at 500 °C [91]

reforming reaction was investigated [91]. Their results also revealed that the catalyst prepared by sol-gel method gave better catalytic activity in terms of hydrogen yield at 500 °C. They inferred that high surface area, high reducibility and high nickel dispersion of Ni-Al$_2$O$_3$-ZrO$_2$ catalyst were the key factors of its superior catalytic activity.

4 Steam Reforming of Glycerol (SRG)

In recent years, biodiesel has been reported as a promising alternative to diesel automobiles, and its consumption is expected to quadruple from 2010 to 2035 worldwide (43 metric tons/year) [92]. The main problem of biodiesel industry is the cost of overall production, which can be offset by conversion of its by-products like glycerol into energy and value-added chemicals [93].

Based on the reaction stoichiometry, 10 wt% of vegetable oil is converted to glycerol during transesterification reaction [79]. Unfortunately, a large amount of glycerol is sold at a low price. A small amount of glycerol can be used in food, beverage and pharmaceuticals to produce value-added chemicals [94]. Steam reforming of glycerol (SRG) is a versatile technique and commercially viable to produce renewable hydrogen to maintain a cleaner and healthier environment [95].

4.1   Reaction Mechanism for Steam Reforming of Glycerol (SRG)

The overall glycerol steam reforming process is endothermic in nature. The process is mainly a combination of glycerol decomposition and water-gas shift reaction [94]:

$C_3H_8O_3 + 3H_2O \leftrightarrow 3CO_2 + 7H_2$ (ΔH = +123 kJ/mol).

$C_3H_8O_3 \leftrightarrow 3CO + 4H_2$ (ΔH = +245 kJ/mol).

$CO + H_2O \leftrightarrow CO_2 + H_2$ (ΔH = −41 kJ/mol).
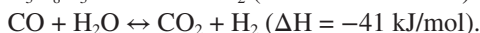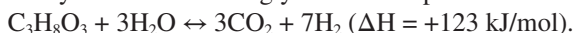
Additionally, other side reactions also occur based on catalyst activity and reaction operating conditions. Methane is formed from CO, CO_2 and H_2 by two exothermic reactions:

$CO + 3H_2 \leftrightarrow CH_4 + H_2O$ (ΔH = −206 kJ/mol).

$CO_2 + 4H_2 \leftrightarrow CH_4 + 2H_2O$ (ΔH = −165 kJ/mol).

A key function of steam reforming catalysts is the cleavage of C–C and O–H bonds in the oxygenated hydrocarbon reactant leading to H_2 and CO and facilitate the water-gas shift reaction to convert CO to CO_2, as opposed to cleavage of C–O bonds leading to alkanes [96].

4.2   SRG with Different Mesoporous Supported Catalysts

4.2.1   Comparison of Different Mesoporous Supported Catalysts Based on Catalyst Characterization

Table 5 shows the N_2 adsorption-desorption analysis results of different mesoporous supported catalysts.

4.2.2   Comparison of Different Mesoporous Supported Catalysts Activity

Glycerol, the by-product of the biodiesel industry, has received wide attention because it contains high H_2 compared to methanol and ethanol [101]. Theoretically, seven moles of H_2 can be produced from glycerol steam reforming reaction [99]. Table 6 shows the different mesoporous supported catalysts activity for glycerol steam reforming reaction.

SRG reaction was carried out with two directly synthesized catalysts (1Ni-2Al$_2$O$_3$-2ZrO$_2$ and 1Ni-2SiO$_2$-2ZrO$_2$) and one impregnated catalyst (Ni/SBA-16) at 600 °C by Lee and Lee [102]. They mainly found H_2, CO and CO_2 and very less amount of CH_4 as products in the SRG reaction. All the catalysts showed good catalytic activity at that temperature. However, in comparison to catalyst activity, directly synthesized catalyst was superior to the impregnated catalyst. They reported that enhanced Ni dispersion was the key factor to give better activity of 1Ni-2Al$_2$O$_3$-2ZrO$_2$ and 1Ni-2SiO$_2$-2ZrO$_2$ catalysts. Calles et al. [97] investigated a

Table 5 N_2 adsorption-desorption data of different mesoporous supported catalysts

Catalysts	Metals (wt%)	BET surface area (m²/g)	Average pore diameter (nm)	Pore volume (cc/g)	References
SBA-15	–	581	8.7	1.00	[97]
Ni/SBA-15	Ni (6.8)	545	8.3	0.91	[97]
Ni/Mg/SBA-15	Ni (6.7) Mg (6.0)	313	7.4	0.62	[97]
Ni/Ca/SBA-15	Ni (6.5) Ca (7.1)	291	7.3	0.58	[97]
SBA-15	–	581	8.7	1.00	[98]
Co/SBA-15	Co (7)	539	8.2	0.86	[98]
Co/Zr/SBA-15	Co (7) Zr (8.5)	458	7.9	0.72	[98]
Co/Ce/SBA-15	Co (7) Ce (8.5)	478	7.8	0.73	[98]
Co/La/SBA-15	Co (7) La (8.5)	421	7.8	0.69	[98]
SBA-15	–	703.97	5.07	0.89	[99]
Co-Ni-SBA-15 (OP)	Ni (5) Co (10)	706.57	4.89	0.68	[99]
Co-Ni-SBA-15 (IMPG)	Ni (5) Co (10)	565.7	5.13	0.72	[99]
Al_2O_3	–	188.3	8.1	0.66	[100]
Ni/Al_2O_3	Ni (5)	183.5	8.75	0.53	[100]
Ni/Al_2O_3	Ni (10)	176.6	8.0	0.47	[100]
Ni/Al_2O_3	Ni (15)	158.3	7.8	0.39	[100]
Ni/Al_2O_3	Ni (20)	143.3	7.4	0.36	[100]

time-on-stream study (up to 5 h) of all catalysts. Promoted catalysts showed a promising activity when compared to the unpromoted catalyst. Especially, Ca-promoted catalyst maintained greater than 95% conversion throughout the 5-h time-on-stream study. This behaviour of the catalyst is attributed to higher thermal stability of Ni due to stronger metal support interaction. Different promoters (Zr, La and Ce) with Co-based SBA-15-supported catalysts were utilized for SRG by Carrero et al. [98]. Promoted catalysts gave nearly 100% glycerol conversion than unpromoted catalyst at 600 °C. They observed that Co crystal size obtained from XRD for the promoted catalyst was less than that of unpromoted catalyst. So, low crystal size particles were easy to reduce. This was the main reason of superior catalytic activity of promoted catalysts. Recently, Al-Salihi et al. [99] investigated the catalyst activity based on a time-on-stream study at 650 °C. All the catalysts showed glycerol conversion in the range of 90–100% except for Ni-SBA-15 catalyst (Fig. 4). Bimetallic catalyst maintained complete conversion, and no sign of deactivation of catalysts was observed during the reaction period of 40 h. Ni-SBA-15 catalyst yielded 85% conversion, and it slowly dropped to 10% at the end of reaction. Addition of MgO

Table 6 Catalyst activity in SRG of different mesoporous supported catalysts

Catalysts	Metals (wt%)	Temperature (°C)	$C_3H_8O_3$ conversion (%)	H_2 selectivity/ yield (%)	References
1Ni-2Al$_2$O$_3$-2ZrO$_2$	Ni (11.4)	600	93	72	[102]
1Ni-2SiO$_2$-2ZrO$_2$	Ni (9.9)	600	73	70	[102]
Ni/SBA-16	Ni (10)	600	63	62	[102]
Ni/SBA-15	Ni (6.8)	600	46	52.6	[97]
Ni/Mg/SBA-15	Ni (6.7) Mg (6.0)	600	97.5	53.2	[97]
Ni/Ca/SBA-15	Ni (6.5) Ca (7.1)	600	98.4	53.0	[97]
Co/SBA-15	Co (7)	600	90	57.1	[98]
Co/Zr/SBA-15	Co (7) Zr (8.5)	600	100	75.2	[98]
Co/Ce/SBA-15	Co (7) Ce (8.5)	600	100	68.2	[98]
Co/La/SBA-15	Co (7) La (8.5)	600	100	73.5	[98]
Co-SBA-15	Co (15)	650	85	75	[99]
Ni-SBA-15	Ni (15)	650	10	40	[99]
Co-MgO-SBA-15	Co (10) Mg (5)	650	100	70	[99]
Ni-MgO-SBA-15	Ni (10) Mg (5)	650	82	70	[99]
Co-Ni-SBA-15	Ni (5) Co (10)	650	100	75	[99]
Co-Ni-SBA-15 (IMPG)	Ni (5) Co (10)	650	100	52	[99]
Ni/Al$_2$O$_3$	Ni (5)	650	87	96.25	[100]
Ni/Al$_2$O$_3$	Ni (10)	650	90	98.5	[100]
Ni/Al$_2$O$_3$	Ni (15)	650	95	100	[100]
Ni/Al$_2$O$_3$	Ni (20)	650	88	98.75	[100]

in Ni-SBA-15 catalyst increased conversion up to 85% for the first 28 h, and after that it dropped to 80% at the end of reaction. The hydrogen selectivity of all the catalysts was around 70–80% except Ni-SBA-15 and Co-Ni-SBA-15 (IMPG) catalyst.

The effect of different Ni loading was investigated in SRG by Senseni et al. [100]. Glycerol conversion increased with the increase of Ni loading up to 15%. Then glycerol conversion decreased. This was attributed to lower Ni dispersion or bigger Ni crystal size at higher nickel loading [103]. However, H_2 selectivity did not vary too much with the increase of Ni loading over the mesoporous γ-Al$_2$O$_3$ support.
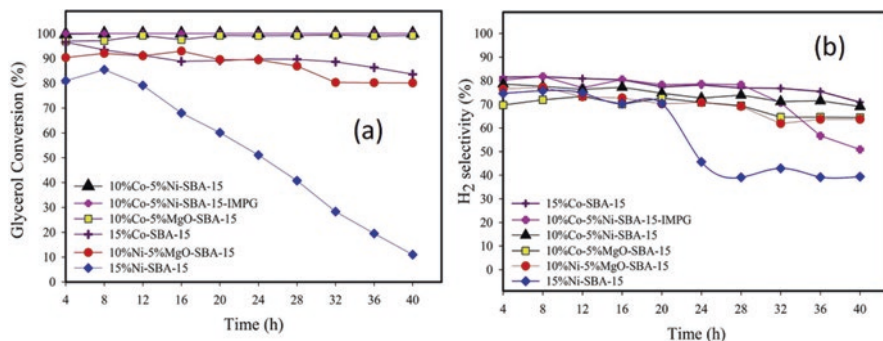
Fig. 4 Time-on-stream studies of all catalysts at 650 °C: (**a**) glycerol conversion and (**b**) H_2 selectivity [99]

5 Conclusions

This book chapter provides an in-depth summary of mesoporous catalysts widely used to produce hydrogen via steam reforming of methanol, ethanol and glycerol. The main characterization techniques used to identify these mesostructures are N_2 adsorption-desorption textural property analysis and XRD patterns which confirms whether the structure has short-, medium- or long-range ordered mesoporosity. Unlike ethanol and glycerol that are reformed at high temperature (400–700 °C), methanol reforming is performed at relatively low temperature (<300 °C), making it more commercially viable in terms of energy consumption and safety costs. However, ethanol reforming is very popular because ethanol is a more available feedstock and glycerol has the highest hydrogen-to-carbon ratio. While Cu-based catalysts are commonly used for SRM, Ni- and Co-based catalysts are preferred for SRE and SRG. Promoters like group 1 and 2 metals significantly improve (1) catalyst activity by reducing the crystal sizes of the metals, thereby improving reducibility of the metal oxides and (2) increasing the basicity of the catalyst which minimizes coking and increases the shelf-life of the catalyst. Depending on the type of support used, bimetallic catalysts like Cu-Ni, Pd-Ni and Ni-Co have been shown to increase hydrogen selectivity and catalyst stability. Generally, the siliceous mesoporous supports (e.g. SBA-15, MCM-41, MCM-48, KIT-6) exhibit substantially better stability than the crystalline metal oxides (e.g. TiO_2, Al_2O_3, CeO_2).

References

1. Ni M, Leung DYC, Leung MKH, Sumathy K (2006) An overview of hydrogen production from biomass. Fuel Process Technol 87:461–472

2. Jones SD, Hagelin-Weaver HE (2009) Steam reforming of methanol over CeO_2- and ZrO_2-promoted cu-ZnO catalysts supported on nanoparticle Al_2O_3. Appl Catal B 90:195–204

3. Das D, Veziroglu TN (2001) Hydrogen production by biological processes: a survey of literature. Int J Hydrog Energy 26:13–28

4. Contreras JL, Salmones J, Colin-Luna JA, Nuno L, Quintana B, Cordova I, Zeifert B, Tapia C, Fuentes GA (2014) Catalysts for H_2 production using the ethanol steam reforming (a review). Int J Hydrog Energy 39:18835–18853

5. Mazloomi K, Gomes C (2012) Hydrogen as an energy carrier: prospects and challenges. Renew Sust Energ Rev 16:3024–3033

6. Bepari S, Kuila D (2020) Steam reforming of methanol, ethanol, and glycerol over nickel-based catalysts-a review. Int J Hydrog Energy 45:18090–18113

7. Schwengber CA, Alves HJ, Schaffner RA, Silva FA, Sequinel R, Bach VR, Ferracin RJ (2016) Overview of glycerol reforming for hydrogen production. Renew Sust Energ Rev 58:259–266

8. Olah GA, Geoppert A, Surya Prakash GK (1999) Beyond oil and gas: the methanol economy, 2nd edn. Wiley-VCH, Weinheim

9. Cecere D, Giacomazzi E, Ingenito A (2014) A review on hydrogen industrial aerospace applications. Int J Hydrog Energy 39:10731–10747

10. Ramachandran R, Menon RK (1998) An overview of industrial use of hydrogen. Int J Hydrog Energy 23:593–598

11. Kammert J, Moon J, Cheng Y, Daemen L, Irle S, Fung V, Liu J, Page K, Ma X, Phaneuf V, Tong J, Ramirez-Cuesta AJ, Wu Z (2020) Nature of reactive hydrogen for Ammonia synthesis over a Ru/ C12A7 Electride catalyst. J Am Chem Soc 142:7655–7667

12. Mohammad N, Bepari S, Aravamudhan S, Kuila D (2019) Kinetics of Fischer–Tropsch synthesis in a 3-D printed stainless steel microreactor using different mesoporous silica supported co-Ru catalysts. Catalysts 9:872

13. Mohammad N, Abrokwah RY, Stevens-Boyd RG, Aravamudhan S, Kuila D (2020) Fischer-tropsch studies in a 3d-printed stainless steel microchannel microreactor coated with cobalt-based bimetallic-mcm-41 catalysts. Catal Today 358:303–315

14. Bepari S, Stevens-Boyd RG, Mohammad N, Li X, Abrokwah R, Kuila D Composite mesoporous SiO_2-Al_2O_3 supported Fe, FeCo and FeRu catalysts for Fischer-Tropsch studies in a 3-D printed stainless-steel microreactor. Mater Today DOI: https://doi.org/10.1016/j.matpr.2020.04.582, (2020)

15. Taboada E, Angurell I, Llorca J (2014) Dynamic photocatalytic hydrogen production from ethanol-water mixtures in an optical fiber honeycomb reactor loaded with au/TiO_2. J Catal 309:460–467

16. Ni M, Leung MKH, Leung DYC, Sumathy K (2007) A review and recent developments in photocatalytic water-splitting using TiO_2 for hydrogen production. Renew Sust Energ Rev 11:401–425

17. Marone A, Izzo G, Mentuccia L, Massini G, Paganin P, Rosa S, Varrone C, Signorini A (2014) Vegetable waste as substrate and source of suitable microflora for bio-hydrogen production. Renew Energy 68:6–13

18. Gallucci F, Basile A (2008) Palladium membrane reactor for steam reforming reaction: a comparison between deferent fuels. Int J Hydrog Energy 33:1671–1687

19. Sun J, Qiu X, Wu F, Zhu W, Wang W, Hao S (2004) Hydrogen from steam reforming of ethanol in low and middle temperature range for fuel cell application. Int J Hydrog Energy 29:1075–1081

20. Ribeirinha P, Alves I, Vidal Vazquez F, Schuller G, Boaventura M, Mendes A (2017) Heat integration of methanol steam reformer with a high-temperature polymeric electrolytic membrane cell. Energy 120:468–471

21. Ribeirinha P, Abdollahzadeh M, Sousa JM, Boaventura M, Mendes A (2017) Modelling of a high-temperature polymer electrolyte membrane fuel cell integrated with a methanol steam reformer cell. Appl Energy 202:6–19

22. Ewan BCR, Allen RWK (2005) A figure of merit assessment of the routes to hydrogen. Int J Hydrog Energy 30:809–819

23. Basile A, Lulianelli A, Longo T, Liguori S, De FM (2011) Pd-based selective membrane State-of-the Art [Chapter 2]. In: Marrwlli L, De Falco M, Laquaniello G (eds) Handbook of Membrane reactors for hydrogen production processes. Springer, London/Dordrecht/Heidelberg/New York, pp 21–55

24. Goltsov VA, Veziroglu TN, Goltsova LF (2006) Hydrogen civilization of the future–a new conception of the IAHE. Int J Hydrog Energy 31:153–159

25. Liu Z, Senanayake SD, Rodriguez JA (2019) Catalysts for the steam reforming of ethanol and other alcohols. In: Ethanol. https://doi.org/10.1016/B978-0-12-811458-2.00005-5

26. Hyber GW, Iborra S, Corma A (2006) Synthesis of transition fuels from biomass: chemistry, catalysts, and engineering. Chem Rev 106:4044–4098

27. Lytkina AA, Zhilyaeva NA, Ermilova MM, Orekhova NV, Yaroslavtsev AB (2015) Inference of the support structure and composition of Ni-cu-based catalysts on hydrogen production by methanol steam reforming. Int J Hydrog Energy 40:9677–9684

28. Sengodan S, Lan R, Humphreys J, Du DW, Xu W, Wang HT, Tao SW (2018) Advances in reforming and partial oxidation of hydrocarbons for hydrogen production and fuel cell applications. Renew Sust Energ Rev 82:761–780

29. Papavasiliou J, Avgouropoulos G, Ioannides T (2009) Steady-state isotopic transient kinetic analysis of steam reforming of methanol over Cu-based catalysts. Appl Catal B 88:490–496

30. Takahashi K, Takezawa N, Kobayashi H (1982) The mechanism of steam reforming of methanol over a copper-silica catalyst. Appl Catal 2:363–366

31. Breen JP, Ross JRH (1999) Methanol reforming for fuel-cell applications: development of zirconia-containing Cu–Zn–Al catalysts. Catal Today 51:521–533

32. Jiang CJ, Trimm DL, Wainwright MS, Cant NW. Kinetic study of steam reforming of methanol over copper-based catalysts(1993) Appl Catal A Gen 93:245–255

33. Abrokwah RY, Deshmane VG, Kuila D (2016) Comparative performance of M-MCM-41 (M: cu, co, Ni, Pd, Zn and Sn) catalysts for steam reforming of methanol. J Mol Catal A Chem 425:10–20

34. Deshmane VG, Abrokwah RY, Kuila D (2015) Synthesis of stable cu-MCM-41 nanocatalysts for H_2 production with high selectivity via steam reforming of methanol. Int J Hydrog Energy 40:10439–10452

35. Karim AM, Conant T, Datye AK (2008) Controlling ZnO morphology for improved methanol steam reforming reactivity. Phys Chem Chem Phys 10:5584–5590

36. Ranganathan ES, Bej SK, Thompson LT (2005) Methanol steam reforming over Pd/ZnO and Pd/CeO$_2$ catalysts. Appl Catal A Gen 289:153–162

37. Conant T, Karim AM, Lebarbier V, Wang Y, Girgsdies F, Schlogl R, Datye A (2008) Stability of bimetallic Pd–Zn catalysts for the steam reforming of methanol. J Catal 257:64–70

38. Suwa Y, Ito SI, Kameoka S, Tomishige K, Kunimori K (2004) Comparative study between Zn–Pd/C and Pd/ZnO catalysts for steam reforming of methanol. Appl Catal A Gen 267:9–16

39. Liguras DK, Kondarides DI, Verykios XE (2003) Production of hydrogen for fuel cells by steam reforming of ethanol over supported noble metal catalysts. Appl Catal B 43:345–354

40. Haryanto A, Fernando S, Murali N, Adhikari S (2005) Current status of hydrogen production techniques by steam reforming of ethanol: a review. Energy Fuel 19:2098–2106

41. Sun J, Qiu XP, Wu F, Zhu WT (2005) H_2 from steam reforming of ethanol at low temperature over Ni/Y$_2$O$_3$, Ni/La$_2$O$_3$ and Ni/ Al$_2$O$_3$ catalysts for fuel-cell application. Int J Hydrog Energy 30:437–445

42. Bepari S, Pradhan NC, Dalai AK (2017) Selective production of hydrogen by steam reforming of glycerol over Ni/Fly ash catalyst. Catal Today 291:36–46

43. Bepari S, Basu S, Pradhan NC, Dalai AK (2017) Steam reforming of ethanol over cerium-promoted Ni-Mg-Al hydrotalcite catalysts. Catal Today 291:47–57

44. Cheng CK, Foo SY, Adesina AA (2011) Steam reforming of glycerol over Ni/Al$_2$O$_3$ catalyst. Catal Today 178:25–33

45. Surendar M, Sagar TV, Babu BH, Lingaiah N, Rao KSR, Prasad PSS (2015) Glycerol steam reforming over La-Ce-Co mixed oxide-derived cobalt catalysts. RSC Adv 5:45184–45193

46. Pompeo F, Santori GF, Nichio NN (2011) Hydrogen production by glycerol steam reforming with Pt/SiO$_2$ and Ni/SiO$_2$ catalysts. Catal Today 172:183–188

47. Chiodo V, Freni S, Galvagno A, Mondello N, Frusteri F (2010) Catalytic features of Rh and Ni supported catalysts in the steam reforming of glycerol to produce hydrogen. Appl Catal A Gen 381:1–7

48. A. Ebshish, Z. Yaakob, Y.H. Taufiq-Yap, A. Bshish, A. Shaibani, Catalytic steam reforming of glycerol over cerium and palladium-based catalysts for hydrogen production. J Fuel Cell Sci Technol 10, 021003 (1–6) (2013)

49. Sundari R, Vaidya PD (2012) Reaction kinetics of glycerol steam reforming using a Ru/Al$_2$O$_3$ catalyst. Energy Fuel 26:4195–4204

50. Frusteri F, Freni S, Chiodo V, Spadaro L, Di Blasi O, Bonura G, Cavallaro S (2004) Steam reforming of bio-ethanol on alkali-doped Ni/MgO catalysts: hydrogen production for MC fuel cell. Appl Catal A Gen 270:1–7

51. Fatsikostas AN, Verykios XE (2004) Reaction network of steam reforming of ethanol over Ni-based catalysts. J Catal 225:439–452

52. Yang Y, Ma J, Wu F (2006) Production of hydrogen by steam reforming of ethanol over a Ni/ZnO catalyst. Int J Hydrog Energy 31:877–882

53. Pompeo F, Santori G, Nichio NN (2010) Hydrogen and/or syngas from steam reforming of glycerol. Study of platinum catalysts. Int J Hydrogen Energy 35:8912–8920

54. Khzouz M, Wood J, Pollet B, Bujalski W (2013) Characterization and activity test of commercial Ni/Al$_2$O$_3$, cu/ZnO/Al$_2$O$_3$ and prepared Ni–cu/Al$_2$O$_3$ catalysts for hydrogen production from methane and methanol fuels. Int J Hydrog Energy 38:1664–1675

55. D. Zhao, Y. Wan, W. Zhou, Ordered mesoporous materials. (John Wiley & Sons; 2012, New York), pp. 1–22. ISBN 9783527647866, https://doi.org/10.1002/9783527647866

56. Taguchi A, Schuth F (2005) Ordered mesoporous materials in catalysis. Microporous Mesoporous Mater 77:1–45

57. K. Wilson, A. F. Lee, Heterogeneous catalysts for clean technology: spectroscopy, design, and monitoring. (John Wiley & Sons; 2013, New York) pp. 2–7. ISBN 9783527326358, https://doi.org/10.1002/9783527658985

58. Pakhare D, Spivey J (2014) A review of dry (CO$_2$) reforming of methane over noble metal catalysts. Chem Soc Rev 43:7813–7837

59. Iulianelli A, Ribeirinha P, Mendes A, Basile A (2014) Methanol steam reforming for hydrogen generation via conventional and membrane reactors: a review. Renew Sust Energ Rev 29:355–368

60. Sa S, Silva H, Brandao L, Sousa JM, Mendes A (2010) Catalysts for methanol steam reforming—a review. Appl Catal B 99:43–57

61. Eswaramoorthi I, Dalai AK (2009) A comparative study on the performance of mesoporous SBA-15 supported Pd-Zn catalysts in partial oxidation and steam reforming of methanol for hydrogen production. Int J Hydrog Energy 34:2580–2590

62. Jampa S, Jamieson AM, Chaisuwan T, Luengnaruemitchai A, Wongkasemjit S (2017) Achievement of hydrogen production from autothermal steam reforming of methanol over Cu-loaded mesoporous CeO$_2$ and Cu-loaded mesoporous CeO$_2$-ZrO$_2$ catalysts. Int J Hydrog Energy 42:15073–15084

63. Taghizadeh M, Akhoundzadeh H, Rezayan A, Sadeghian M (2018) Excellent catalytic performance of 3D-mesoporous KIT-6 supported Cu and Ce nanoparticles in methanol steam reforming. Int J Hydrog Energy 43:10926–10937

64. Lenarda M, Moretti E, Storaro L, Patrono P, Pinzari F, Rodriguez-Castellon E, Jimenez-Lopez A, Busca G, Finocchio E, Montanari T, Frattini R (2006) Finely dispersed Pd-Zn catalyst supported on an organized mesoporous alumina for hydrogen production by methanol steam reforming. Appl Catal A Gen 312:220–228

65. Deshmane VG, Owen SL, Abrokwah RY, Kuila D (2015) Mesoporous nanocrystalline TiO_2 supported metal (cu, co, Ni, Pd, Zn, and Sn) catalysts: effect of metal-support interactions on steam reforming of methanol. J Mol Catal A Chem 408:202–213

66. Tajrishi OZ, Taghizadeh M, Kiadehi AD (2018) Methanol steam reforming in a microchannel reactor by Zn-, Ce- and Zr- modified mesoporous cu/SBA-15 nanocatalyst. Int J Hydrog Energy 43:14103–14120

67. Zhao D, Sun J, Li Q, Stucky GD (2000) Morphological control of highly ordered mesoporous silica SBA-15. Chem Mater 12:275–279

68. Araujo VD, Bellido JDA, Bernardi MIB, Assaf JM, Assaf EM (2012) CuO-CeO_2 catalysts synthesized in one-step: characterization and PROX performance. Int J Hydrog Energy 37:5498–5507

69. Kleitz F, Berube F, Guillet-Nicolas R, Yang C-M, Thommes M (2010) Probing adsorption, pore condensation, and hysteresis behavior of pure fluids in three-dimensional cubic mesoporous KIT-6 silica. J Phys Chem C 114:9344–9355

70. Wan H, Li X, Ji S, Huang B, Wang K, Li C (2007) Effect of Ni loading and $Ce_xZr_{1-x}O_2$ promoter on Ni based SBA-15 catalysts for steam reforming of methane. J Nat Gas Chem 16:139–147

71. Panpranot J, Goodwin JG Jr, Sayari A (2002) Synthesis and characteristics of MCM-41 supported CoRu catalysts. Catal Today 77:269–284

72. Abrokwah RY, Dade W, Owen SL, Deshmane V, Rahman M, Kuila D (2016) Effects of mesoporous supports and metals on steam reforming of alcohols [Chapter 6]. In: Nanda S, Sarangi PK, Vo D-VN (eds) Fuel processing and energy utilization. Taylor and Francis, New York, pp 93–108. ISBN 9780429489594. https://doi.org/10.1201/9780429489594

73. Peppley BA, Amphlett JC, Kearns LM, Mann RF (1999) Methanol–steam reforming on Cu/ZnO/Al_2O_3. Part 1: the reaction network. Appl Catal A Gen, 179:21–29

74. Gunter MM, Ressler T, Jentoft RE, Bems B (2001) Redox behavior of copper oxide/zinc oxide catalysts in the steam reforming of methanol studied by *in situ* x-ray diffraction and absorption spectroscopy. J Catal 203:133–149

75. Yao C-Z, Wang L-C, Liu Y-M, Wu G-S, Cao Y, Dai W-L, He H-Y, Fan K-N (2006) Effect of preparation method on the hydrogen production from methanol steam reforming over binary Cu/ZrO_2 catalysts. Appl Catal A Gen 297:151–158

76. Chin Y-H, Dagle R, Hu J, Dohnalkova AC, Wang Y (2002) Steam reforming of methanol over highly active Pd/ZnO catalyst. Catal Today 77:79–88

77. Heggen M, Penner S, Friedrich M, Dunin-Borkowski RE, Armbruster M (2016) Formation of ZnO patches on ZnPd/ZnO during methanol steam reforming: a strong metal−support interaction effect. J Phys Chem C 120:10460–10465

78. Huber GW, Iborra S, Corma A (2006) Synthesis of transportation fuels from biomass: chemistry, catalysts, and engineering. Chem Rev 106:4044–4098

79. Vaidya PD, Rodrigues AD (2009) Glycerol reforming for hydrogen production: a review. Chem Eng Technol 32:1463–1469

80. Velu S, Satoh N, Gopinath C, Suzuki K (2002) Oxidative reforming of bio-ethanol over CuNiZnAl mixed oxide catalysts for hydrogen production. Catal Letters 82:145–152

81. Han SJ, Song JH, Yoo J, Park S, Kang KH, Song IK (2017) Sorption-enhanced hydrogen production by steam reforming of ethanol over mesoporous Co/CaO-Al_2O_3 xerogel catalysts: effect of Ca/Al molar ratio. Int J Hydrog Energy 42:5886–5898

82. Gharahshiran VS, Yousefpour M, Amini V (2020) A comparative study of zirconia and yttria promoted mesoporous carbon-nickel-cobalt catalysts in steam reforming of ethanol for hydrogen production. Mol Catal 484:110767

83. Moogi S, Lee I-G, Park J-Y (2019) Effect of La_2O_3 and CeO_2 loadings on formation of nickel-phyllosilicate precursor during preparation of Ni/SBA-15 for hydrogen-rich gas production from ethanol steam reforming. Int J Hydrog Energy 44:29537–29546

84. Chiou JYZ, Kung H-Y, Wang C-B (2017) Highly stable and active Ni-doped ordered mesoporous carbon catalyst on the steam reforming of ethanol application. J Saudi Chem Soc 21:205–209

85. He S, He S, Zhang L, Li X, Wang J, He D, Lu J, Luo Y (2015) Hydrogen production by ethanol steam reforming over Ni/SBA-15 mesoporous catalysts: effect of Au addition. Catal Today 258:162–168

86. Nejat T, Jalalinezhad P, Hormozi F, Bahrami Z (2019) Hydrogen production from steam reforming of ethanol Ni-Co bimetallic catalysts and MCM-41 as support. J Taiwan Inst Chem Eng 97:216–226

87. Arslan A, Gunduz S, Dogu T (2014) Steam reforming of ethanol with zirconia incorporated mesoporous silicate supported catalysts. Int J Hydrog Energy 37:5498–5507

88. Han SJ, Bang Y, Yoo J, Kang KH, Song JH, Seo JG, Song IK (2013) Hydrogen production by steam reforming of ethanol over mesoporous $Ni-Al_2O_3-ZrO_2$ aerogel catalyst. Int J Hydrog Energy 38:15119–15127

89. Han SJ, Song JH, Bang Y, Yoo J, Park S, Kang KH, Song IK (2016) Hydrogen production by steam reforming of ethanol over mesoporous $Cu-Ni-Al_2O_3-ZrO_2$ xerogel catalysts. Int J Hydrog Energy 41:2554–2563

90. Han SJ, Bang Y, Yoo J, Park S, Kang KH, Choi JH, Song JH, Song IK (2014) Hydrogen production by steam reforming of ethanol over P123-assisted mesoporous $Ni-Al_2O_3-ZrO_2$ xerogel catalysts. Int J Hydrog Energy 39:10445–10453

91. Han SJ, Bang Y, Yoo J, Seo JG, Song IK (2013) Hydrogen production by steam reforming of ethanol over mesoporous $Ni-Al_2O_3-ZrO_2$ xerogel catalysts: effect of nickel content. Int J Hydrog Energy 38:8285–8292

92. Gupta M, Kumar N (2012) Scope and opportunities of using glycerol as an energy source. Renew Sust Energ Rev 16:4551–4556

93. Almeida JRM, Favaro LCL, Quirino BF (2012) Biodiesel biorefinery: opportunities and challenges for microbial production of fuels and chemicals from glycerol waste. Biotechnol Biofuels 5:48

94. Sad ME, Duarte HA, Vignatti C, Padro CL, Apesteguia CR (2015) Steam reforming of glycerol: hydrogen production optimization. Int J Hydrog Energy 40:6097–6106

95. Dou B, Song Y, Wang C, Chen H, Xu Y (2014) Hydrogen production from catalytic steam reforming of biodiesel byproduct glycerol: issues and challenges. Renew Sust Energ Rev 30:950–960

96. Alcala R, Mavrikakis M, Dumesic JA (2003) DFT studies for cleavage of C-C and C-O bonds in surface species derived from ethanol on Pt (111). J Catal 218:178–190

97. Calles JA, Carrero A, Vizcaino AJ, Garcia-Moreno L (2014) Hydrogen production by glycerol steam reforming over SBA-15-supported nickel catalysts: effect of alkaline earth promoters on activity and stability. Catal Today 227:198–206

98. Carrero A, Vizcaino AJ, Calles JA, Garcia-Moreno L (2017) Hydrogen production through glycerol steam reforming using Co catalysts supported on SBA-15 doped with Zr, Ce and La. J Energy Chem 26:42–48

99. Al-Salihi S, Abrokwah R, Dade W, Deshmane V, Hossain T, Kuila D (2020) Renewable hydrogen from glycerol steam reforming using Co-Ni-MgO based SBA-15 nanocatalysts. Int J Hydrog Energy 45:14183–14198

100. Senseni AZ, Meshkani F, Rezaei M (2016) Steam reforming of glycerol on mesoporous nanocrystalline Ni/Al_2O_3 catalysts for H_2 production. Int J Hydrog Energy 41:20137–20146

101. Silva JM, Soria MA, Madeira LM (2015) Challenges and strategies for optimization of glycerol steam reforming process. Renew Sust Energ Rev 42:1187–1213

102. Lee D, Lee HC (2012) A direct synthesis of nickel nanoclusters embedded on multicomponent mesoporous metal oxides and their catalytic properties for glycerol steam reforming to hydrogen. Int J Hydrog Energy 37:18773–18781

103. Sadanandam G, Ramya K, Kishore DB, Durgakumari V, Subrahmanyam M, Chary KVR (2014) A study to initiate development of sustainable Ni/γ-Al$_2$O$_3$ catalyst for hydrogen production from steam reforming of biomass-derived glycerol. RSC Adv 4:32429–32437

Catalytic Production of High-Value Chemicals from High Volume Non-food Biomass

Md. Imteyaz Alam

Abstract Growing population and energy crises with depletion in fossil resources have necessitated efforts to find a sustainable solution. With circular production and abundant availability, biomass is regarded as an effective renewable option to produce chemicals and fuels. Every year, over 40 million tons of non-food biomass such as sugarcane bagasse, wheat straw, paddy straw, and wood shavings are produced. Many of them are thrown or burned in the open air leading to environmental pollution. Converting these discarded biomasses into chemicals and fuels could minimize waste disposal issues and reduce dependency on fossil fuels without competing with the demand for increased food production, which the world is facing due to shrinking landholdings and growing population. Indeed, it has the potential to reduce environmental issues associated with climate change and employment generation in rural areas. Herein, recent advances in non-food biomass conversion processes via chemo-catalytic routes are discussed. This chapter will not only give a better understanding of the current catalytic process on biomass but also provide proper direction in the development of successful biorefinery for a sustainable future.

Keywords Biomass · Catalysis · 5-Hydroxymethyl furfural · Biofuel · Acid catalyst

1 Introduction

The past century has witnessed a close network between petrochemical and everyday needs. A variety of simple molecules derived from fossil resources are employed to produce complex chemicals that are used as polymers, drugs, pharmaceuticals, fuels, solvents, and flavors in the chemical industry. The growing concerns on environmental pollution with marked depletion in fossil feedstocks have prompted researchers to investigate the sustainable process and related technologies for providing solutions to alternate energy and climate change by deriving chemicals and

M. I. Alam (✉)
WowChemE M&C Pvt. Ltd, Delhi, India

fuels from alternative (nonfossil) feedstocks. At present, only 13% energy, 10% chemicals, and below 2% organic materials are estimated to be produced from nonfossil resources [1]. Interestingly, the progress in bio- and chemo-catalytic process has accelerated the development of novel pathways to obtain commodity chemicals from biomass as biorenewable feedstocks [2–6]. Biomass is usually a plant- and animal-sourced carbonaceous material produced by activities such as food, feed, crop residue, manure, and wood shavings. As shown in Fig. 1, the plant biomass typically constitutes cellulose, hemicellulose, and lignin (collectively called lignocellulose). It may undergo suitable bio- or chemo-catalysis and result in reactive intermediates or platform chemicals. It can be upgraded to the myriad of industrial molecules via the process of isomerization, dehydration, hydrogenation, ring-opening and decarboxylation, condensation, and hydrodeoxygenation [3, 7–11]. It was year 2004 when US Department of Energy (DOE) released a list of top 12 biomass-derived chemical building blocks with their high potential to substitute petroleum-derived molecules. Among them, 5-hydroxymethyl furfural (HMF) and furfural (Fur) have shown a significant potential to derive various necessary chemicals (e.g., furfuryl alcohol, levulinic acid), fuels (dimethyl furan, long-chain hydrocarbons, ethyl levulinate), and solvents (tetrahydrofuran, γ-valerolactone). Thus, the HMF and Fur have direct applications in biorefinery as intermediate for making a variety of useful chemicals and fuels.

The transformation of biomass into platform chemicals (Fur or HMF) proceeds via three main steps. In the first step, lignocellulosic biomass gets hydrolyzed to yield monomeric sugars such as xylose and glucose (aldose). In the second step, these aldoses (xylose or glucose) get isomerized into ketoses (xylulose or fructose),
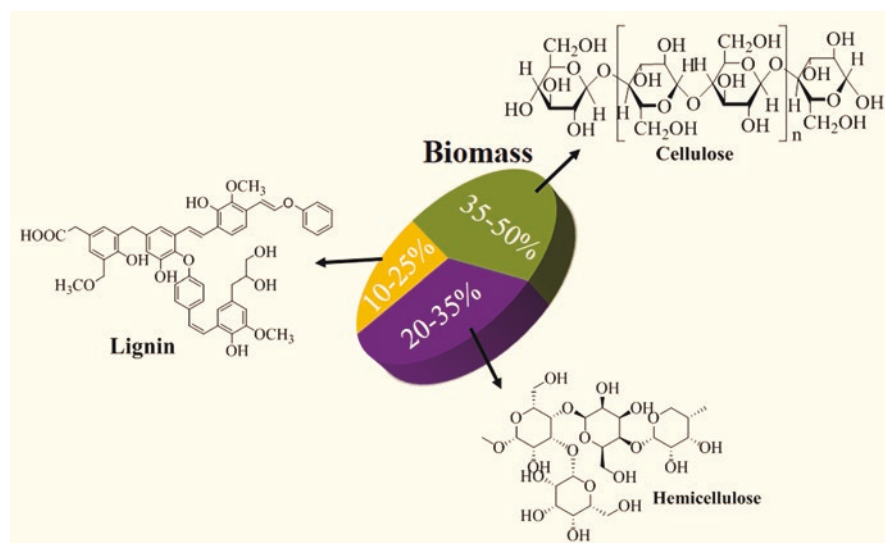
Fig. 1 Schematic illustration showing major constituents of lignocellulosic biomass (cellulose, hemicellulose, and lignin)

which subsequently transformed into related products, Fur or HMF, by the removal of three molecules of water. In order to produce HMF, various sources such as monosaccharaides (e.g., glucose, xylose), disaccharides (e.g., inulin, sucrose), polysaccharide (e.g., cellulose, starch), and untreated biomass (e.g., maize corn, agricultural residues) have been used.

To convert these feedstocks, approaches based on enzymes, mineral acids, transition metal catalysts, ionic liquids, and metal salts have been suitably applied. However, the limitation such as the use of the corrosive chemicals (mineral acids), difficult product separation (e.g., in enzyme catalysis), and high cost of the catalyst makes such process difficult for commercialization.

Moreover, the existing method of utilizing edible biomass (e.g., maize corn and potato tuber) to produce Fur may create competition with the food that could aggravate food prices. An approach based on non-food feedstock (as summarized in Table 1) is advantageous for future commercialization.

Nevertheless, the key issues with the raw lignocellulosic biomass are the complex structure of biomass with a strong H-bonding network and the inability to meet or solubilize in conventional solvents. This is the ubiquitous reason for using model compounds as a reactant for studying conversion processes besides the exploration of natural lignocellulosic biomass. To turn the complex structure of lignocellulose

Table 1 Summary of results showing the catalytic conversion of untreated biomass into HMF

Entry	Substrate	T (°C), t (min)	Catalyst	Solvent	% HMF yield	Refs.
1.	Foxtail grass	120, 2	[DMA][CH_3SO_3]	DMA-LiCl	58	[12]
2.	Red nutsedge	120, 2	[DMA][CH_3SO_3]	DMA-LiCl	35	[12]
3.	Sugarcane bagasse	140, 5	$Zr(O)Cl_2$/$CrCl_3^+$ [BMIM]cl	DMA-LiCl	42	[13]
4.	*Phragmites communis*	120, 120	$CrCl_2$/$RuCl_3$	[EMIM]cl	41	[14]
5.	Corn Stover	180, 30	$AlCl_3 \cdot 6H_2O$	H_2O-NaCl/THF	19	[15]
6.	Pinewood	180, 30	$AlCl_3 \cdot 6H_2O$	H_2O-NaCl/THF	35	[15]
7.	Poplar	180, 30	$AlCl_3 \cdot 6H_2O$	H_2O-NaCl/THF	26	[15]
8.	Switchgrass	160, 60	$AlCl_3 \cdot 6H_2O$	H_2O-NaCl/THF	13	[16]
9.	Corn Stover	140, 120	$CrCl_3^+$ [EMIM]cl	DMA-LiCl	48	[17]
10.	Rice straw	200, 60	$CrCl_3 \cdot 6H_2O$	[C_4mim]cl	47	[18]
11.	Wheat straw	160, 60	$FePO_4$ + NaH_2PO_4	Water-NaCl/THF	44	[19]
12.	Jerusalem artichoke		Nb_2O_5 + H_3PO_4	H_2O:2-butanol	22	[20]
13.	Jerusalem artichoke		$FeCl_2$, H_2O_2	H_2O:2-butanol	46	[21]
14.	Girasol tuber		HCl	Extraction: HCl	55	[22]
15.	Potato tuber			[OMIM][cl], ethylacetate	30	[21]
16.	Mushroom	140, 10	[DMA][CH_3SO_3]	DMA-LiCl	44	[23]
17.	Mushroom	140, 10	[BBIM-SO_3][NTf_2]	DMA-LiCl	46	[23]

into a valuable product, the use of strong acid/alkali is substantial, but there are certain limitations. For instance, in a conventional viscose process on cellulose regeneration, CS_2 with strong alkalis and mineral acid is used, which releases H_2S and SO_2 into the environment leading to air pollution. To overcome environmental problems and achieve better dissolution with high reactivities, a variety of new solvents have been employed. *N*-Methylmorpholine-*N*-oxide,*N*,*N*-dimethylformamide/ dinitrogen tetroxide (DMF-N_2O_4), molten salt hydrates (LiClO$_4$·3H$_2$O, LiSCN·2H$_2$O), *N,N*-dimethylacetamide/lithium chloride (DMA-LiCl), *N*-methylmorpholine-*N*-oxide (NMMO), and dimethyl sulfoxide tetrabutylammonium (DMSO/TBAF) are few examples. However, some serious drawbacks such as the requirement of harsh conditions, low dissolving power, high processing cost due to difficult solvent recovery, and comparatively higher toxicity are still existing, which limits the overall applicability for industrial uses. It is to note that converting sugars like mono- and disaccharides into HMF/fur requires less energy than the lignocellulose due to the absence of lignin and strong H-bonding network within the structure. For further understanding about the trends in HMF production from sugar molecules, readers may refer previously published literature [8, 13, 24]. Since the focus of this chapter is the utilization of raw biomass for chemicals and fuels, discussion on mono- and disaccharide-mediated HMF production has been avoided. This chapter is aimed to summarize the recent developments in raw biomass conversion over the use of various catalysts, including ionic liquids under mild thermal conditions. Further, discussion proposed a progressive pathway toward HMF/Fur production starting from raw biomass and the need for combined bio- and chemocatalytic approach for producing high-value molecules for fuel and chemical industries.

2   Transformation of Lignocellulosic Biomass

With the increasing demand for food, energy, and materials, the United Nations has estimated the global population to increase from 7.7 billion to 9.1 billion by 2050 [25]. One compound that has attracted attention from both academic and industrial researchers is Fur, a triple dehydration product (furanic heterocycle molecule with aldehyde functionality). The furfural is directly derived from hemicellulosic biomasses by hydrolysis and subsequent dehydration of pentose sugars in suitable acid catalysts under the desired solvent medium. It is an inefficient, high-cost production of furfural and non-scalability. The focus is yet to be established on the future possibilities for economically and environmentally feasible technologies based on recyclable solvent catalysts to minimize the use of high boiling solvents and mineral acid. In this direction, the conversion of hemicellulosic biomass into furfural via hydrolysis followed by dehydration would create a high impact in furfural synthesis. Further valorization in such a scalable quantity can be used as a future platform chemical to produce second-generation biofuels and build block chemicals.

3   Ionic Liquid for Lignocellulose Conversion

It was 1934 when Graenacher [26] first discovered molten *N*-alkyl pyridinium chloride for dissolution and cellulose modification. Inspired with the pioneering work of the Graenacher, in 2002, Swatloski et al. found dialkyl imidazolium-based ionic liquid (IL) that is capable enough to dissolve cellulose up to 10–25 wt%. In general, ILs are salts in the liquid state at a temperature below 373 K and exhibit unique physicochemical properties, including low vapor pressure, high thermal stability, better solvation capacities, and non-flammabilities. Brønsted acidic ionic liquids (BAILs) contain free proton (H^+), which is advantageous to use over the traditional chemicals owing to its unique performance and tunable properties. Since the breaking of the lignocellulose's glycosidic linkage is the key step for turning them into HMF/Fur via monomer formation, the ILs are considered to be useful to disrupt the H-bonding network even at low concentrations. An enhanced effect of the ionic liquid-assisted cellulose dissolution was demonstrated under microwave irradiation [27]. Subsequently, several ILs with acidic hydrogen on anion (e.g., 1-butyl-3-methylimidazolium hydrogen sulfate), cation (e.g., *N*-methyl-2-pyrrolidonium methyl sulfonate $[NMP] + [CH_3SO_3]$), and acidic functional groups have been used for BAIL-mediated/-catalyzed HMF production [28–31]. Tao et al. have demonstrated the catalytic performance of SO_3H-functionalized BAILs for C_6 and C_5 sugar conversion [29]. Varying the chain length with different anions (HSO_4^-, $CF_3SO_3^-$, CF_3COO^-, and CH_3COO^-) of the ILs, the yields of furfural/HMF were found to be varied due to change in their acidic strengths. But, to perform these challenging and multistep processes in a single step, several catalytic systems have been studies to produce HMF from raw biomass. Including agricultural residues such as wheat straw, paddy straw, reed from *Phragmites communis*, corn stover, the husk of *Xanthoceras sorbifolium*, sugarcane bagasse, weeds, potato tuber, poplar, pinewood, etc. as feedstock (listed in Table 1) [12, 13, 15, 16, 32–35]. Among these catalysts, Brønsted acidic ionic liquids (ILs), *N*-methyl-2-pyrrolidonium methyl sulfonate $[NMP] + [CH_3SO_3]$- and *N,N*-dimethylacetamide methyl sulfonate $[DMA] + [CH_3SO_3]$-, have been reported as superior catalyst, giving maximum 58 and 52 wt% of HMF. The reaction was reported to be conducted in DMA-LiCl solvent using the one-pot conversion of Foxtail weed biomass under mild reaction conditions [12]. These acidic IL catalysts were also observed to effectively convert carbohydrate-rich weed biomass into EMF [12]. This development leads to reduce the use of ILs in bulk quantity and minimize the use of mineral acids and chlorinated metal salts. The results with acidic ILs have further motivated to explore the catalytic activity of –SO_3H-functionalized 1-butylimidazolium ILs with trifluoromethanesulfonate (OTf-) and bis((trifluoromethyl)sulfonyl)amide (NTf2-) counter ions for the transformation of non-food mushroom biomass into HMF. It is to note that the yield and selectivity of desired chemicals are directly related to the carbohydrate content in the feedstock used. The higher the sugar content in the biomass, the greater will be the possibility for high conversion and desired product yield. So, the selection criteria of biomass for their transformation are (1) presence of high

carbohydrate content [36–39]; (2) non-food values, so that they do not compete with the food (3); and abundant availability for sustainable supply and rapid growth rate.

Since acidity plays a key role in biomass to HMF/furfural production, many techniques have been used to establish a tool to measure acidity, but the accuracy of the results relies solely on the measurement procedure [40, 41]. For example, the results were observed to be sensitive to impurities when the UV-Vis probe was used [41]. Iglesia and his co-workers have reported a computational method using ab initio DFT calculation to measure deprotonation energy (DPE) of the heteropoly acids. They have established a trend between the activity of various heteropoly acids and their corresponding DPEs in acid-catalyzed reactions. These findings were consistent with the experimental observations, as reported in the activity-acidity plot [42, 43]. Lower values of the DPE of heteropoly acid were suggested to show higher acidic content, resulting in the high activity of the catalysts. Most recently, Alam et al. have studied the role of Brønsted acidity of the ILs in HMF and EMF formation [23]. The study includes DPEs of SO_3H-functionalized ILs containing different cations (DMA^+, NMP^+, and $BBIM\text{-}BuSO_3H^+$); anions, e.g., $[(CH_3SO_3^-) (OTh^-)]$, $[(CF_3SO_3^-) (OTf^-)]$, $[(CH_3SO_3)_2N^- (NTh_2^-)]$, and $[(CF_3SO_3)_2N^- (NTf_2^-)]$; and their corresponding activities in terms of HMF yield. Computationally measured values of DPEs were observed to be linearly correlated to experimentally obtained HMF yield.

3.1 Determination of HMF Yields

HMF and some of its derivatives can be analyzed through UV-Visible spectroscopy [24, 44], ^{1}HNMR spectroscopy [8, 9, 24], HPLC [7], and GC [33]. For ^{1}H NMR spectroscopic analysis, HMF was extracted from the reaction mixture with ethyl acetate or dimethyl ether. Upon rotary evaporation, resultant HMF was obtained.

UV-Vis method: The UV-Vis spectrum of pure HMF solution shows a distinct peak at 284 nm and the corresponding extinction coefficient (e) value of 1.66×10^4 $M^{-1}cm^{-1}$. The percentage of HMF in each reaction product can be calculated from the measured absorbance values at 284 nm wavelength and the extinction coefficient value [24]. The yield of HMF was calculated in wt% concerning the total mass of the starting substrates.

^{1}H NMR method: To quantify HMF yield by ^{1}H NMR method, a known concentration of mesitylene as internal standard and HMF product solution were charged in a glass tube. The resultant mixture was solubilized in solvents like chloroform-d or DMSO-d_6. Remember that the solvent's peak should not merge with the corresponding product or internal standard. The percentage of HMF yield was typically measured by the integrated values of the aldehydic peak of HMF ($d = 9.58$ ppm) and aromatic protons of mesitylene ($d = 6.79$ ppm) as reported by Saha and co-workers [23, 24].

3.2 DFT Calculation to Measure Deprotonation Energy

Density Functional Theory (DFT) is a key tool to study and understand chemical reactions computationally. Since acidity plays a crucial role in biomass conversion processes, measuring DPE of the acidic ILs can give better ideas about reactivity trends to screen catalyst [23]. DFT calculations were performed in Material Studio 8 (Biovia, San Diego, USA) based on DMol3 [45] module using DNP (double numerical plus polarization) numerical basis set and generalized gradient approximation (GGA) PW91 functional [46]. Previous studies with PW91 functional have shown to correlate with experimental trends [9, 47–49]. Energy, force, and atom displacement convergence criterion of 0.0001 eV, 0.05 eV/Å, and 0.005 Å, respectively, were used for the geometry optimization. Mulliken charges were obtained using the "population analysis" property tab as implemented in DMol3. DPEs of the ILs were obtained using the formula, where and are the energy of IL, deprotonated IL, and proton, respectively.

Humin is a viscous dark black or brown material produced as a byproduct in biorefinery under acid treatments or hydrothermal reactions of lignocellulosic biomass, which is the key barrier in obtaining desired chemicals efficiently in an economical way. The exact mechanism of its formation is debatable. Generally it is considered to form via hydrothermal carbonization [50–52] or the acid-catalyzed dehydration of C5 and C6 sugars as a co-product with the HMF, Fur, and/or LA [53]. HMF and Fur is reported to be the most possible intermediate for humin formation, which takes place via uncontrolled self or cross condensation with the other reactive intermediates in aqueous medium [54–56]. Since the accurate structure of humin is still unknown, it is proposed to be consisting of oxygen containing heterocyclic ring with aliphatic chains or functional groups such as carbonyl, hydroxyl, ketone, and/ or ester. Moreover, these functionalities are supposed to be dependent on the feedstock used and reaction conditions such as time, temperature, pH, and solvents [57, 58]. So far, there is no clear evidence to exclude or substantiate the mechanism of humin formation from the desired product, and therefore understanding the complete reaction route is important so that humin formation could be suppressed. Being polymeric in nature and with the presence of diverse functional groups, humin has numerous opportunities to either transform it into chemicals, materials, and fuels, or use directly to explore options as a catalyst support in catalyst industry, monomers or resins in polymer industries, and other products. Sustainable use of humin may create market opportunities for various products with regard to the circular economy of the industrial processes and environmental viewpoint.

4 Conclusions

The increasing population and gradual depletion of fossil fuels have caused an imbalance in the demand and supply of energy and products. Lignocellulosic biomass, including plant residues, has a tremendous potential to be used as a

sustainable source to produce fuels and chemicals. Acid catalysts are essential to cleave strong glycosidic linkages of the biomass for its depolymerization into monomeric sugars and its subsequent dehydration to yield high-value chemicals such as HMF, furfural, and LA. With high acidity and tunable properties, BAILs are reported as a viable option as reaction medium and the catalyst as well. In order to correlate activity trends of different BAILs, DPE calculated from ab initio DFT simulation could be the simplest way. Furthermore, UV-Vis and NMR spectroscopic method are reported as significant tools to quantify HMF yield. In summary, this chapter provides a brief account of the recent advances in converting a variety of raw biomass, including agricultural residues (e.g., sugarcane bagasse, rice straw), grasses, corn stover, mushrooms, etc., into HMF and correlation between acidity of the ionic liquids with the yield.

References

1. Galkin KI, Ananikov VP (2019) When will 5-Hydroxymethylfurfural, the "sleeping Giant" of sustainable chemistry, awaken? ChemSusChem 12(13):2976–2982. https://doi.org/10.1002/cssc.201900592
2. Alam MI, Gupta S, Ahmad E, Haider MA (2015) Integrated bio- and chemocatalytic processing for biorenewable chemicals and fuels. In: Saha B, Fan M, Wang J (eds) Sustainable catalytic processes, pp 157–177. https://doi.org/10.1016/B978-0-444-59567-6.00006-6
3. Alam MI, Saha B (2015) Catalysis for production of sustainable chemicals and fuels from biomass. In: Saha B, Fan M, Wang J (eds) Sustainable catalytic processes, 1st edn, pp 99–123. https://doi.org/10.1016/B978-0-444-59567-6.00004-2
4. Becker J, Wittmann C (2015) Advanced biotechnology: metabolically engineered cells for the bio-based production of chemicals and fuels, materials, and health-care products. Angew Chem Int Ed 54(150):3328–3350. https://doi.org/10.1002/anie.201409033
5. Corma A, Iborra S, Velty A (2007) Chemical routes for the transformation of biomass into chemicals. Chemical Review 107:2411–2502
6. Straathof AJJ (2014) Transformation of biomass into commodity chemicals using enzymes or cells. Chem Rev 114:1871–1908. https://doi.org/10.1021/cr400309c
7. Ahmad E, Alam MI, Pant KK, Haider MA (2019) Insights into the synthesis of ethyl Levulinate under microwave and nonmicrowave heating conditions [research-article]. Ind Eng Chem Res 58(35):16055–16064. https://doi.org/10.1021/acs.iecr.9b01137
8. Alam MI, De S, Singh B, Saha B, Abu-Omar MM (2014) Titanium hydrogenphosphate: an efficient dual acidic catalyst for 5-hydroxymethylfurfural (HMF) production. Appl Catal A Gen 486:42–48. https://doi.org/10.1016/j.apcata.2014.08.019
9. Alam MI, Gupta S, Bohre A, Ahmad E, Khan TS, Saha B, Haider MA (2016a) Development of 6-amyl-α-pyrone as a potential biomass-derived platform molecule. Green Chem 18(24):6431–6435. https://doi.org/10.1039/c6gc02528e
10. Alam MI, Khan TS, Haider MA (2019) Alternate biobased route to produce δ-Decalactone: elucidating the role of solvent and hydrogen evolution in catalytic transfer hydrogenation. ACS Sustain Chem Eng 7(3):2894–2898. https://doi.org/10.1021/acssuschemeng.8b05014
11. Gupta S, Alam MI, Khan TS, Haider MA (2019) Mechanistic approaches toward rational Design of a Heterogeneous Catalyst for ring-opening and deoxygenation of biomass-derived cyclic compounds [review-article]. ACS Sust Chem Eng 7(12):10165–10181. https://doi.org/10.1021/acssuschemeng.9b00734
12. Alam MI, De S, Dutta S, Saha B (2012) Solid-acid and ionic-liquid catalyzed one-pot transformation of biorenewable substrates into a platform chemical and a promising biofuel. RSC Adv 2:6890–6896. https://doi.org/10.1039/c2ra20574b

13. Dutta S, De S, Alam I, Abu-Omar MM, Saha B (2012) Direct conversion of cellulose and lignocellulosic biomass into chemicals and biofuel with metal chloride catalysts. J Catal 288:8–15. https://doi.org/10.1016/j.jcat.2011.12.017

14. Kim B, Jeong J, Lee D, Kim S, Yoon H-J, Lee Y-S, Cho JK (2011) Direct transformation of cellulose into 5-hydroxymethyl-2-furfural using a combination of metal chlorides in imidazolium ionic liquid. Green Chem 13(6):1503. https://doi.org/10.1039/c1gc15152e

15. Yang Y, Hu C, Abu-omar MM (2012a) Conversion of carbohydrates and lignocellulosic biomass into 5-hydroxymethylfurfural using AlCl3·6H2O catalyst in a biphasic solvent system. Green Chem 14:509–513. https://doi.org/10.1039/c1gc15972k

16. Yang Y, Hu C, Abu-omar MM (2012b) Synthesis of furfural from xylose , Xylan , and biomass using AlCl3·6 H2O in biphasic media via xylose isomerization to Xylulose. ChemSusChem 5:405–410. https://doi.org/10.1002/cssc.201100688

17. Binder J, Raines R (2009) Simple chemical transformation of lignocellulosic biomass into furans for fuels and chemicals. J Am Chem Soc 131:1979. https://doi.org/10.1021/ja808537j

18. Zhang Z, Zhao ZK (2010) Microwave-assisted conversion of lignocellulosic biomass into furans in ionic liquid. Bioresour Technol 101(3):1111–1114. https://doi.org/10.1016/j.biortech.2009.09.010

19. Xia H, Xu S, Yang L (2017) Efficient conversion of wheat straw into furan compounds, bio-oils, and phosphate fertilizers by a combination of hydrolysis and catalytic pyrolysis. RSC Adv 7:1200–1205. https://doi.org/10.1039/c6ra27072g

20. Yang F, Liu Q, Bai X, Du Y (2011) Conversion of biomass into 5-hydroxymethylfurfural using solid acid catalyst. Bioresour Technol 102(3):3424–3429. https://doi.org/10.1016/j.biortech.2010.10.023

21. Seo Y, Han J (2014) Direct conversion from Jerusalem artichoke to hydroxymethylfurfural (HMF) using the Fenton reaction. Food Chem 151:207–211. https://doi.org/10.1016/j.foodchem.2013.11.067

22. Yi YB, Lee JW, Choi YH, Park SM, Chung CH (2012) Simple process for production of hydroxymethylfurfural from raw biomasses of girasol and potato tubers. Biomass Bioenergy 39:484–488. https://doi.org/10.1016/j.biombioe.2012.01.011

23. Alam MI, De S, Khan TS, Haider MA, Saha B (2018) Acid functionalized ionic liquid catalyzed transformation of non-food biomass into platform chemical and fuel additive. Ind Crop Prod 123(July):629–637. https://doi.org/10.1016/j.indcrop.2018.07.036

24. De S, Dutta S, Saha B (2011) Microwave assisted conversion of carbohydrates and biopolymers to 5-hydroxymethylfurfural with aluminium chloride catalyst in water. Green Chem 13(10):2859. https://doi.org/10.1039/c1gc15550d

25. World Population Prospects 2019: Highlights (2019). Retrieved from https://www.un.org/development/desa/publications/world-population-prospects-2019-highlights.html

26. Graenacher, C. (1934). Patent No. US Patent 1943176. Switzerland

27. Swatloski RP, Spear SK, Holbrey JD, Rogers RD (2002) Dissolution of cellose with ionic liquids. J Am Chem Soc 124(18):4974–4975. https://doi.org/10.1021/ja025790m

28. Ding ZD, Shi JC, Xiao JJ, Gu WX, Zheng CG, Wang HJ (2012) Catalytic conversion of cellulose to 5-hydroxymethyl furfural using acidic ionic liquids and co-catalyst. Carbohydr Polym 90(2):792–798. https://doi.org/10.1016/j.carbpol.2012.05.083

29. Tao F, Song H, Chou L (2011) Hydrolysis of cellulose in SO3H-functionalized ionic liquids. Bioresour Technol 102(19):9000–9006. https://doi.org/10.1016/j.biortech.2011.06.067

30. Tao F, Song H, Yang J, Chou L (2011) Catalytic hydrolysis of cellulose into furans in MnCl2-ionic liquid system. Carbohydr Polym 85(2):363–368. https://doi.org/10.1016/j.carbpol.2011.02.040

31. Zakrzewska ME, Bogel-łukasik E, Bogel-łukasik R (2011) Ionic liquid-mediated formation of 5-Hydroxymethylfurfural s a promising biomass-derived building block. Chem Rev 111:397–417

32. Binder JB, Raines RT, Binder JB, Raines RT (2009) Simple chemical transformation of lignocellulosic biomass into furans for fuels and chemicals. J Am Chem Soc 131:1879–1985. https://doi.org/10.1021/ja808537j

33. De S, Dutta S, Saha B (2012) One-pot conversions of lignocellulosic and algal biomass into liquid fuels. ChemSusChem 5(9):1826–1833. https://doi.org/10.1002/cssc.201200031

34. Kim B, Jeong J, Shin S, Lee D, Kim S, Yoon H (2010) Facile single-step conversion of macroalgal polymeric carbohydrates into biofuels. ChemSusChem 3:1273–1275. https://doi.org/10.1002/cssc.201000192

35. Zhao S, Cheng M, Li J, Tian J, Wang X (2011) One pot production of 5-hydroxymethylfurfural with high yield from cellulose by a Brønsted-Lewis-surfactant-combined heteropolyacid catalyst. Chem Commun 47(7):2176–2178. https://doi.org/10.1039/c0cc04444j

36. Beluhan S, Ranogajec A (2011) Chemical composition and non-volatile components of Croatian wild edible mushrooms. Food Chem 124(3):1076–1082. https://doi.org/10.1016/j.foodchem.2010.07.081

37. Berna E, Jaworska G (2010) Comperision of amino acid content in forzen P ostreatus and A bisporus mushrooms. Acta Sci Pol, Technol Aliment 9(3):295–303

38. Kalac P (2009) Chemical composition and nutritional value of European species of wild growing mushrooms : a review. Food Chem 113:9–16. https://doi.org/10.1016/j.foodchem.2008.07.077

39. Yong-jun Z, Jie-min H, Li-yun Z, Hui J, Jia L (2012) Effect of extraction method on functional properties of dietary fibre from auricularia auricula. Appl Mech Mater 140:314–318. https://doi.org/10.4028/www.scientific.net/AMM.140.314

40. Johnson KE, Pagni RM, Bartmess J (2007) Brønsted acids in ionic liquids: fundamentals, organic reactions, and comparisons. Monatshefte Fur Chemie 138(11):1077–1101. https://doi.org/10.1007/s00706-007-0755-6

41. Mihichuk LM, Driver GW, Johnson KE (2011) Brønsted acidity and the medium: fundamentals with a focus on ionic liquids. ChemPhysChem 12(9):1622–1632. https://doi.org/10.1002/cphc.201100087

42. Macht J, Janik MJ, Neurock M, Iglesia E (2007) Catalytic consequences of composition in polyoxometalate clusters with keggin structure. Angew Chem Int Ed 46(41):7864–7868. https://doi.org/10.1002/anie.200701292

43. Macht J, Janik MJ, Neurock M, Iglesia E (2008) Mechanistic consequences of composition in acid catalysis by polyoxometalate keggin clusters. J Am Chem Soc 130(31):10369–10379. https://doi.org/10.1021/ja803114r

44. Dutta S, De S, Patra AK, Sasidharan M, Bhaumik A, Saha B (2011) Microwave assisted rapid conversion of carbohydrates into 5-hydroxymethylfurfural catalyzed by mesoporous TiO2 nanoparticles. Appl Catal A Gen 409–410:133–139. https://doi.org/10.1016/j.apcata.2011.09.037

45. Delley B (2006) The conductor-like screening model for polymers and surfaces. Mol Simul 32(2):117–123. https://doi.org/10.1080/08927020600589684

46. Perdew J, Wang Y (1992) Accurate and simple analytic representation of the electron-gas correlation energy. Phys Rev B 45(23):13244–13249

47. Chia M, Haider MA, Pollock G, Kraus GA, Neurock M, Dumesic JA (2013) Mechanistic insights into ring-opening and decarboxylation of 2-Pyrones in liquid water and tetrahydrofuran. J Am Chem Soc 135(15):5699–5708. https://doi.org/10.1021/ja312075r

48. Gupta S, Alam MI, Khan TS, Sinha N, Haider MA (2016) On the mechanism of retro-Diels-Alder reaction of partially saturated 2-Pyrones to produce biorenewable chemicals. RSC Adv 6:60433–60445. https://doi.org/10.1039/C6RA11697C

49. Khan TS, Gupta S, Alam I, Haider MA (2016) Reactivity descriptor for the retro Diels–Alder reaction of partially saturated 2-pyrones : DFT study on substituents and solvent effects. RSC Adv 6:101697–101706. https://doi.org/10.1039/C6RA22303F

50. Titirici MM, Thomas A, Yu SH et al (2007) A direct synthesis of mesoporous carbons with bicontinuous pore morphology from crude plant material by hydrothermal carbonization. Chem Mater 19:4205–4212. https://doi.org/10.1021/cm0707408

51. Titirici MM, White RJ, Brun N et al (2015) Sustainable carbon materials. Chem Soc Rev 44:250–290. https://doi.org/10.1039/c4cs00232f

52. Chuntanapum A, Matsumura Y (2009) Formation of tarry material from 5-HMF in subcritical and supercritical water. Ind Eng Chem Res 48:9837–9846. https://doi.org/10.1021/ie900423g
53. Farmer TJ, Mascal M (2015) Platform molecules. In: Clark J, Deswarte F (eds) Introduction to chemicals from biomass, 2nd edn. Wiley, Chichester, pp 89–155
54. Galkin KI, Krivodaeva EA, Romashov LV et al (2016) Critical influence of 5-hydroxymethylfurfural aging and decomposition on the utility of biomass conversion in organic synthesis. Angew Chemie Int Ed 55:8338–8342. https://doi.org/10.1002/anie.201602883
55. Patil SKR, Heltzel J, Lund CRF (2012) Comparison of structural features of humins formed catalytically from glucose, fructose, and 5-hydroxymethylfurfuraldehyde. Energy Fuels 26:5281–5293. https://doi.org/10.1021/ef3007454
56. Van Zandvoort I, Wang Y, Rasrendra CB et al (2013) Formation, molecular structure, and morphology of humins in biomass conversion: influence of feedstock and processing conditions. ChemSusChem 6:1745–1758. https://doi.org/10.1002/cssc.201300332
57. Wang S, Lin H, Zhao Y et al (2016) Structural characterization and pyrolysis behavior of humin by-products from the acid-catalyzed conversion of C6 and C5 carbohydrates. J Anal Appl Pyrolysis 118:259–266. https://doi.org/10.1016/j.jaap.2016.02.009
58. Van Zandvoort I, Koers EJ, Weingarth M et al (2015) Structural characterization of 13C-enriched humins and alkali-treated 13C humins by 2D solid-state NMR. Green Chem 17:4383–4392. https://doi.org/10.1039/c5gc00327j

Efficient Nanocomposite Catalysts for Sustainable Production of Biofuels and Chemicals from Furanics

Mallesham Baithy, Deepak Raikwar, and Debaprasad Shee

Abstract In recent decade, the depletion of the finite fossil fuels and their consumptions related to environmental concerns have spearheaded the development of alternative routes for the production of energy and chemicals from renewable sources in sustainable manner and without causing a harmful effect to the environment. The biomass is the only organic carbon bearing renewable resource with the potential to produce energy and chemicals in a sustainable manner. The efficient transformation of biomass into biofuels and valued chemicals can take place from thermo-physical and thermo-chemical processes by various catalysts. The biomass-derived furfural and 5-hydroxymethylfurfural (HMF) are important furanic platform molecules, which can be further catalytically converted to biofuels/fuel additives and chemicals in integrated biorefinery. Hence, the carefully formulated various heterogeneous catalysts are expected to play a pivotal role for the development of green valorization processes of biomass-derived furfural and 5-hydroxymethylfurfural into valued chemicals and advanced biofuels/fuel additives under relatively mild conditions. The valorization processes can involve many types of reactions such as hydrogenation of the C=O bond, hydrogenation of the furan ring, oxidation, amination, condensation, and coupling. For these reactions, the catalytic materials have been classified into two subgroups such as metal and mixed metal oxide-based nanocomposite materials to discuss their physicochemical properties and active sites toward selective transformation of furfural and HMF into the desired products using appropriate references.

Keywords Biomass conversion · Biofuels · Furfural · 5-Hydroxymethylfurfural · Furanics

M. Baithy · D. Raikwar · D. Shee (✉)
Department of Chemical Engineering, Indian Institute of Technology Hyderabad,
Kandi, Sangareddy, Telangana, India
e-mail: dshee@che.iith.ac.in

1 General Introduction

1.1 *Biomass-Derived Platform Chemicals*

The lignocellulosic biomass is the most significant renewable feedstock consisting of lignin and carbohydrates, which could be effectively converted into biofuels and fine chemicals in integrated biorefinery. The biomass-derived platform molecules, furfural (FUR) and 5-hydroxymethylfurfural (HMF), are synthesized from dehydration of five- and six-membered carbon sugars, respectively. Both these platform molecules have been identified as important platform molecules for their efficient transformation into sustainable products such as biofuels, bio-based chemicals, and bio-polymers (Fig. 1) [1, 2]. The hydrogenation, oxidation, amination, and condensation of FUR and HMF produce a variety of biofuels and fine chemicals such as 2,5-dimethylfuran, 2,5-diformylfuran, and 2,5-furandicarboxylic acid (2,5-FDCA), furfuryl alcohol, tetrahydrofuran, 2-methyltetrahydrofuran, maleic anhydride, 1,5-pentanediol, and intermediates for fine chemicals [3–11]. Hence, these platform molecules have exhibited a great prospect in alternative to the fossil-derived compounds for the production of industrial important biofuels/fuel-additive and bio-based chemicals.
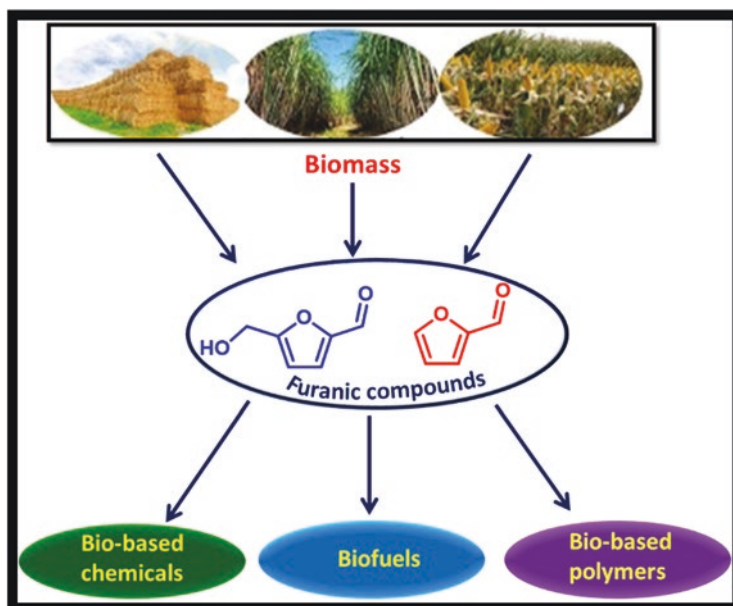
Fig. 1 Schematic diagram for the production and its transformation of HMF and FUR into biofuels, bio-based chemicals, and bio-polymers

1.1.1 Furfural

Furfural is a promising biomass-derived platform molecule produced from the lignocellulosic biomass, which can be further transformed into biofuels and biochemicals. Because of the highly functionalized molecular structure, FUR represents as a preferred feedstock material for the sustainable production of a variety of valuable oxygenated products. The catalytic transformation of furfural from C_4 to C_{13} products by various catalytic nanocomposites is discussed. For example, the C_5 products are mostly produced through sequential hydrogenation and hydrogenolysis, whereas most of the C_4 products are produced with selective catalytic oxidation as the first step [1]. The physicochemical properties of the FUR and HMF compounds are listed in Table 1.

1.1.2 5-Hydroxymethylfurfural (HMF)

HMF is a highly oxygenated platform molecule in comparison with that of most petrochemical products. However, it is known to be toxic in nature for few microorganisms [12]. Thus, the catalytic transformation of HMF into value-added chemicals and biofuels is an important challenge. HMF is multifunctionalized platform molecule, and various reactions could be proceeded in the selective catalytic conversions. In addition, the HMF molecule has an aldehyde group, a hydroxyl group, and a furan ring which offers a great potential for the production of various valuable chemicals and fuels. In this chapter, we mainly focused on selective catalytic transformation of HMF into valuable products over the highly active nanocomposite materials as heterogeneous catalysts. Also, the different catalytic reactions were described, including hydrogenation, condensation, oxidation, and amination.

Table 1 Physicochemical properties of the furfural and HMF compounds

Property	Furfural	5-Hydroxymethylfurfural
Molecular formula	$C_5H_4O_2$	$C_6H_6O_3$
Molecular weight	96.08 g mol^{-1}	126.11 g mol^{-1}
Density	1.16 g cm^{-3} at 20 °C	1.29 g cm^{-3} at 20 °C
Vapor pressure	2.6 mmHg (0.35 kPa) at 20 °C	0.001 mmHg at 25 °C
Boiling point	162 °C	115 °C
Melting point	37 °C	32 °C
Flash point	62 °C	79.44 °C
Appearance	Colorless to yellow oily Liquid; turns black in air	Low-melting white solid
Odor	Almond-like pungent odor	Buttery, caramel

1.2   Nanocomposite Materials

Nanocomposites are a broad range of multiphase materials with at least one of the phases having size in the range between 1 and 100 nm, or structures were in the nano-scale repeat distances between the various phases that made up the nanocomposite material. The main idea behind it is to use various components with their dimensions in nm range to develop and create new materials with extraordinary flexibility and enhancement in their characteristic properties:

- Nanocomposite materials consisting of two different phases like nanocrystalline phase and matrix phase: the phase might be inorganic-inorganic, inorganic-organic, and organic-organic.
- Nanocomposite means nanosized particles such as metals, metal oxides, semi-conductors, dielectric materials, etc. and surrounded in different matrix materials including ceramics, metal oxides, glass, polymers, etc.

Figure 2 shows the flow chart for the classification of nanocomposite materials. The characteristic properties of the various types of the nanocomposite materials are listed below.

1. *Metal-based nanocomposites materials:*

    - Increased hardness, strength, and super plasticity.
    - Lowered melting point.
    - Uniformly distributing the active sites throughout the catalyst.
    - Increased electrical resistivity due to increased disordered grain surfaces.
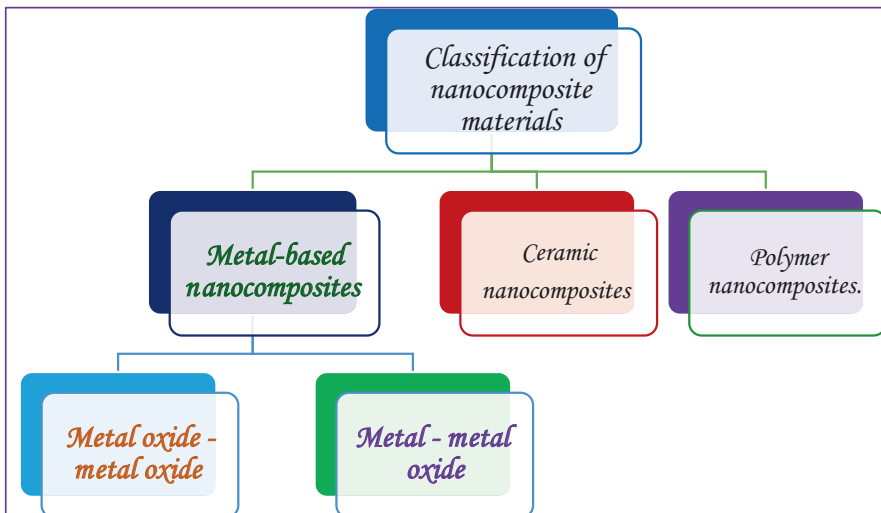
Fig. 2   Flow chart for the classification of nanocomposite materials

- Increased miscibility of the non-equilibrium components in alloying and solid solution.
- Improved magnetic properties such as coercivity, super paramagnetization, saturation magnetization, and magnetocaloric properties.

2. *Ceramic-based nanocomposites:*

- Increase in the strength, hardness, and abrasion by refining particle size.
- Enhance ductility, toughness, formability, and super plasticity by nanophase.
- Change electrical conduction and magnetic properties by increasing the disordered grain boundary interface.

3. *Polymer-based nanocomposites:*

- Electrical, optical, magnetic, and catalytic properties arising from the inorganic materials and enhanced thermal and mechanical stability originating from the polymeric matrix.

Nanocomposites are multiphase solid materials, which are used as highly active materials with at least one of the phases such as 1D, 2D, or 3Ds of lower than that of 100 nm in size. In brief, it can be usually taken as the solid combination of a two or more components such as bulk matrix and nano-dimensional phase(s) differing in physicochemical properties because of the variations in structure and chemistry. Hence, the nanocomposites have different physicochemical properties (e.g., catalytic, thermal, mechanical, optical, electrochemical, and electrical) from the individual component materials. Moreover, these materials have been extensively applied in various industries including chemical catalysts, cosmetics, medical devices, drug delivery, electronics, magnetics, and optoelectronics [13–21]. These nanosized catalysts have better catalytic performances in the chemical industries. Generally, various effective catalytic applications of these materials are determined by their structure, composition, particle size, and other parameters [22–27]. This area is a one of the major challenges in the integration of two dissimilar components/materials with different structures to produce a unique hybrid catalytic system with various functionalities for real-time application (Fig. 2) [28–31]. Therefore, in this chapter we will discuss highly efficient nanocomposite catalysts for production of biofuels and chemicals from furanic compounds.

Currently, the catalytic transformations were rapidly developing research area in the worldwide which consists of chemical methodologies (~90%) and chemical production (~60%) [32, 33]. For this, we have to satisfy the crucial demand for high catalytic performance with the characteristic properties such as better activity, excellent selectivity, and outstanding stability. Catalysis (especially heterogeneous catalysis) has been undertaking broad examinations and innovative advances convoyed by abundant ability in nanoscience and nanotechnology [34]. The main advantages of heterogeneous catalysis over other catalyses like the homogeneous one are easy separation of catalyst from the reaction mixture, recyclability of used catalysts, minimization of waste production, etc., which have been well-described in standard textbooks of catalysis. Further, single-component heterogeneous

catalysts have also been broadly studied, and some of them had successfully been used in chemical industries [35]. Recently, the author reported that the research interest drastically increases toward the single-site heterogeneous catalysts on atomic and/or molecular scales [35]. In these catalysts, the active sites are spatially separated from other active sites and uniformly spread over a large surface area of another component, and each site has the same energy of interaction between the site and incoming reactants. A suitable component not only affords a high specific surface area to stabilize small nanoparticles in the durable catalysis but also reduces hybrid intersections with rich redox reactions on two-phase interface [36]. Additionally, most general techniques for the synthesis of various metal-based nanocomposite materials are listed below:

- Spray pyrolysis.
- Liquid metal infiltration.
- Rapid solidification.
- Vapor techniques (PVD, CVD).
- Electrodeposition.
- High-energy ball milling.
- Chemical methods.

Table 2 shows the various metal-based nanocomposite materials that were prepared by different methodologies with their advantages and limitations. These meta-based nanocomposites are very attractive catalysts for selective transformation of the various transformations, which are mainly due to the controllable integration of the different materials between the noble and non-noble metals (e.g., Ru, Au, Pd, Pt, Cu, Ni, Fe, etc.) and metal oxides including TiO_2, CeO_2, ZrO_2, SnO_2, Al_2O_3, MgO, Fe_2O_3, etc. into single nanostructures has recently considered as attractive research topic. They not only mix the function of individual components but also get more unique collective and synergetic catalytic physicochemical properties when compared to that of single-component materials. Usually, these nanocomposite catalysts are easily synthesized using chemical methodologies such as sol-gel, colloidal, impregnation, coprecipitation, deposition-precipitation, etc. [17, 26, 27, 37–43]. To design high-performance catalysts, there are several many approaches that have been taken and generally classified into four categories based on earlier reports [36]:

- Confinement of metal NPs into microporous and mesoporous supports.
- Modification of the supports.
- Replacement of mono-component metal NPs with alloy NPs.
- Encapsulation of metal NPs into supports with a core-shell structure.

In this chapter, we discuss different catalytic processes for the transformation of furanic compounds into biofuels and value-added chemicals over a variety of nanocomposite (metal-metal oxide, mixed metal oxide, and their combination) materials as heterogeneous catalysts. Furthermore, describe the different strategies for upgrading HMF and FUR to liquid biofuels and valuable chemicals from various catalytic reactions, such as hydrogenation, oxidation, condensation, amination, and its reaction mechanisms.

Table 2 Advantages and limitations of processing methods for metal-based nanocomposites

Entry	Methods	Nanocomposite	Advantages	Limitations
1.	Spray pyrolysis	Fe/MgO, W/Cu	Effective preparation of ultra-fine, spherical and homogeneous powders in multicomponent systems, reproductive size and quality.	High cost associated with producing large quantities of uniform, nanosized particles.
2.	Liquid infiltration	Pb/cu, Pb/Fe, W/Cu/Nb/Cu, Nb/Fe, Al-C60	Short contact times between matrix and reinforcements; moulding into different and near net shapes of different stiffness and enhanced wear resistance; rapid solidification; both lab scale and industrial scale production.	Use of high temperature, segregation of reinforcements, formation of undesired products during processing.
3.	Rapid solidification process (RSP)	Al/Pb, Al/X/Zr (X = Si, Cu, Ni), Fe alloy	Simple; effective.	Only metal-metal nanocomposites; induced agglomeration and nonhomogeneous distribution of fine particles.
4.	RSP with ultrasonics	Al/SiC	Good distribution without agglomeration, even with fine particles.	–
5.	High-energy ball milling	Cu-Al$_2$O$_3$	Homogeneous mixing and uniform distribution.	–
6.	Chemical processes (sol-gel, colloidal, etc.)	Ag/Au, Fe/SiO$_2$, Au/Fe/Au	Simple; low processing temperature; versatile; high chemical homogeneity; rigorous stoichiometry control; high purity products.	Weak bonding, low wear resistance, high permeability and difficult control of porosity.
7.	CVD/PVD	Al/Mo, Cu/W, Cu/Pb	Capability to produce highly dense and pure materials; uniform thick films; adhesion at high deposition rates; good reproducibility	Optimization of many parameters; cost; relative complexity.

2 Production of Fuels (or Fuel Additives) and Chemicals from Furanics

The catalytic transformation of biomass-derived building block platform compounds is essential for the production of fuels and value-added chemicals. Among the identified biomass derivatives, furanics such as furfural (FUR) and 5-hydroxymethyl furfural (HMF) are known as platform compounds that can be subsequently converted into a wide range of biofuels and biochemicals. FUR and HMF are obtained from sugars by dehydration. The catalytic transformation of furan ring and −CHO or hydroxymethyl group through hydrogenation, condensation, oxidation, dehydration, decarbonylation, polymerization, amination, nitration, or opening ring reactions can yield a variety of high-value-added products, important building blocks for both the production of liquid hydrocarbon fuels, fuel additives, and valuable chemicals.

2.1 Hydrogenation of Furanics

2.1.1 Furfural

The catalytic hydrogenation of FUR has been extensively studied to produce an attractive and wide range of compounds with potential uses as chemicals, biofuels, or fuel additives. Various types of products such as furfuryl alcohol (FA), 2-methyl furan (MF), tetrahydrofurfuryl alcohol (THFOL), tetrahydrofuran, 2-methyl tetrahydrofuran (2-MTHF), lactones, levulinates, cyclopentanone, or diols can be obtained by the hydrogenation of FUR, directly or by further transformation. The reaction route for converting FUR via hydrogenation can be divided into (1) hydrogenation without opening the furan ring and (2) hydrogenation with the opening of the furan ring. The activity as well as selectivity pattern is directly related to the catalytic conditions and the nature of the active phase.

There have been several attempts to use a supported catalyst based on noble metals such as Pt, Pd, Ru, and Ir (Table 3) [44–48]. However, the high cost, high H_2 pressure, and poor selectivity due to over hydrogenation with some noble metal catalysts exclude them from their large-scale application. Thus, one of the biggest challenges is the development of inexpensive catalysts for the selective reduction of C=O bond in FUR under ambient H_2 pressure. Over the past few years, catalysts based on non-noble metals were developed with advanced modification to make their properties and activity comparable to noble metals. In particular, catalysts based on non-noble metals (Ni [49], Co [50, 51], Cu [52]), metal oxides [53–56], and mixed metal oxides [53] have been investigated for the hydrogenation of FUR (Table 3). Among the various alternatives, Cu, Ni, and Co catalysts show a great promise for replacing noble metal catalysts, taking the advantage of low cost and high H_2 activation activity. However, they suffer from poor selectivity for

Table 3 Summary of hydrogenation of FUR with different catalysts

Reaction condition	Reactant	Product	Catalyst	Performance		Refs.
				Conversion (%)	Yield (%)	
413 K, 3 h, 3 MPa H_2	FUR	FAL	5 wt% Pd/MCM-41	~50	~30	[44]
275 K, 1 h, 8 MPa H_2	FUR	FAL	4 wt% Ir/SiO_2	14	13.4	[48]
463 K, 5 h, H_2 flow = 10 mL min^{-1}	FUR	FAL	2.5 wt% Ni-Sep-a	84	85	[49]
423 K, 6 h, 0.5 MPa N_2	FUR	FAL	Co-N-C-700	100	99.9	[51]
383 K, 2.5 h, 2 MPa H_2	FUR	FAL	$Cu_{0.4}Mg_{5.6}Al_2$	100	99.5	[52]
423 K, 6 h	FUR	FAL	Co_3O_4-Al_2O_3	76	74	[53]
443 K, 0.5 h	FUR	FAL	NiO	98.9	94.4	[54]
393 K, 3 h	FUR	FAL	NiO(P)-300	97.3	94.2	[55]
298 K, 12 h, 0.1 MPa H_2	FUR	FAL	Pd_1Ag_1/C	99	94	[58]
443 K, 3 h, N_2 atm	FUR	FAL	Cu-Pd/C	100	98.1	[59]
453 K, 5 h, 2 MPa H_2	FUR	FAL	Cu_1Co_5	100	38.1	[60]
423 K, 2 h, 2 MPa H_2	FUR	FAL	$Fe_{50}Ni_{50}$/SiO_2	100	74	[61]
453 K, 3 h, 3 MPa H_2	FUR	FAL	Ni-In(2.0)/AlOH	96	92	[62]
373 K, 5 h, 2 MPa H_2	FUR	FAL	Ni_3Sn_2	100	99	[63]
393 K, 12 h, 1.5 MPa H_2	FUR	FAL	$NiCu_{0.33}$/C	96.7	90.7	[64]
283 K, 2 h, 5 MPa H_2	FUR	FAL	Pd/Ni/Ni$(OH)_2$/C	100	90.7	[65]
423 K, 1 h, 3 MPa H_2	FUR	FAL	1.0% Pd/$MgAlO_x$(2)	62.9	30.5	[66]
393 K, 1 h, 0.5 MPa H_2	FUR	FAL	Pt@MT-450	97	93.1	[67]
453 K, 4 h, 2 MPa N_2	FUR	FAL	Ru-Fe_3O_4/CNTs	99.4	99.4	[68]
443 K, 6 h, He atm	FUR	FAL	HT_MgFe-3	97	90	[69]
503 K, 4 h	FUR	2-MF	$CuNi_2Al$	100	64.8	[70]
453 K, 4 h, 0.1 MPa N_2	FUR	2-MF	$Cu_{2.5}$Zn−Al-600	99	72	[71]
523 K, W/F = 0.1 h, H_2/FU = 25, 1 atm	FUR	2-MF	5 wt% Ni-2wt%Fe/SiO_2	96.3	37.6	[72]
473 K, 14 h, 9 MPa H_2	FUR	2-MF	Cu-Fe (Cu^{2+}/Fe^{3+} = 2)	100	51.1	[73]
473 K, 2 h, 3.5 MPa H_2	FUR	2-MF	Cu(5%)−Ni(0.5%)/TiO_2	99	87	[74]

unsaturated alcohols due to thermodynamically and kinetically favorable hydrogenation of C=C bonds rather than C=O bond. The addition of a secondary metal to the active phase is a desirable approach to promote the activity and selectivity and reduce the cost of the catalysts [57–60]. Following a similar methodology, various studies have been conducted to improve the FA hydrogenation performance over inexpensive Ni by designing its electronic structures. For example, Ni-based alloys, such as Ni-Fe, Ni-In, Ni-Sn, Cu-Ni, and Ni-Pd, exhibit better catalytic performance than with their single metal counterpart [61–65]. The catalyst support also plays an important role in the hydrogenation of FUR reaction [44, 66]. Supports often include Lewis acids, basic metal oxides, and base metal carbonates, which assist in

polarizing the carbonyl group of FUR and can actively take part in reaction pathways [66].

The use of liquid organic solvents as hydrogen donors (e.g., alcohols and acids) further reduces the process complexity and cost and improves the safety concerns regarding the handling high-pressure hydrogen gas. Several supported noble and non-noble metal catalysts have been reported for the CTH of FUR to FA (Table 3) [67–69]. Rodiansono et al. developed a very stable nanosized bimetallic Ni-In alloy catalyst supported over amorphous alumina (Ni-In(x)/AA) for the selective hydrogenation of FUR to FA [62]. Ni-In(2.0)/AA showed the best catalytic performance due to the presence of Ni_2In alloy as the main phase, and 96% FUR conversion with 92% FA yield was obtained at 453 K after 3 h under 3 MPa H_2 pressure in the presence of isopropanol as a solvent. In a recent study, Yang et al. reported the selective hydrogenation of FUR on non-noble intermetallic compound (Ni_3Sn_1, Ni_3Sn_2, and Ni_3Sn_4) derived from a layered double hydroxide precursor [63]. The Ni_3Sn_2 sample exhibited optimal catalytic behavior, and complete conversion of FUR with 99% selectivity for FA was attained at 373 K after 3 h under 2 MPa H_2 pressure using isopropanol as a solvent. It was observed that the introduction of Sn to Ni suppresses the highly active C=C hydrogenation on pristine Ni while at the same time accelerates C=O hydrogenation to produce FA. The combined experimental and theoretical results suggested that the specific geometric and electronic properties of Ni_3Sn_2 induces a vertical adsorption configuration of FUR molecules via activation of the C=O group, leading to high selectivity for FA.

A reaction mechanism for the hydrogenation of FUR to FA over Ni_3Sn_2 catalyst is given in Fig. 3. The hydrogenation reaction mechanism proceeds via five steps:
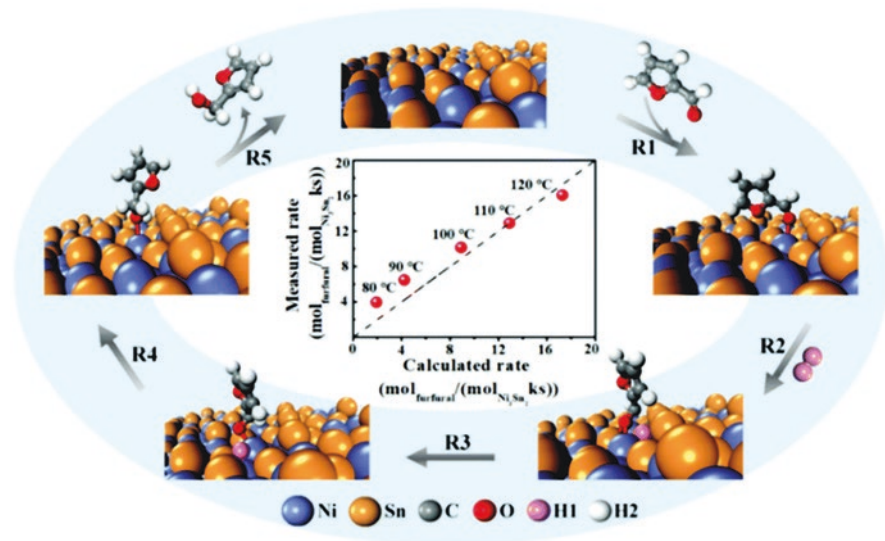
Fig. 3 A schematic illustration of the reaction mechanism of FUR hydrogenation to FA on $Ni_3Sn_2(101)$. H1, H atom from a H_2 molecule; H2, H atom from a FUR molecule

Step 1: The activation of the FUR molecule carried out by the adsorption on the Ni_3Sn_2 active site through the terminal oxygen atom of carboxide attaching to the top site of the metallic Ni.

Step 2: Dissociation of molecular H_2 produces active hydrogen atoms on the adjacent Ni species.

Step 3: Firstly, active H atom of a bridge site attacks the carbon atom of carboxide with the formation of an alkoxide intermediate.

Step 4: The alkoxide intermediate undergoes sequential hydrogenation at the oxygen atom to produce FA.

Step 5: FA desorbs from the surface of the nanocomposite.

Furthermore, Shi et al. investigated the performance of SiO_2-supported Ni-based bimetallic catalyst for the hydrogenation of FUR to FA using isopropanol as a solvent [61]. Bimetallic Ni-Fe nanoparticles in the bimetallic catalyst exhibited better performance with 97–100% FUR conversion at 423 K under 20 MPa H_2 pressure after 120 min. Furthermore, depending on the process conditions, the type of supported metal catalyst, and the solvent, FUR hydrogenation produced numerous products [57]. In Fig. 3, the inset shows a parity plot between the measured and calculated rates of FUR hydrogenation over the range of 80–120 °C.

The selective hydrogenation of FUR could also produce potential fuel components such as 2-methylfuran (2-MF) via direct hydrogenation of aldehyde group or by second step hydrogenation [70–74]. 2-MF is an excellent liquid fuel additive with relatively high energy density, boiling points, and octane numbers and can be partially blended with engine gasoline. Yan et al. reported 51% yield of 2-MF with an inexpensive Cu-Fe nanocomposite with Cu^{2+}/Fe^{3+} ratio of 2 under the conditions of 493 K and 90 bar initial H_2 pressure after 14 h [73]. It was observed that the acidic center present on the Cu-Fe catalyst is responsible for the dehydration of FUR to MF. In another study, Seemala et al. explored the effect of bimetallic Cu-Ni nanoparticle composition with varying Ni loading (0, 0.5, 1.5, 3, 5, and 10 wt %) at a constant Cu loading of 5 wt% and support (Al_2O_3 and TiO_2) on the HDO of FUR [74]. It has been observed that TiO_2-supported Cu-Ni bimetallic nanoparticles promote the formation of Cu-rich near-surface alloys containing predominantly dispersed Ni species. Alternatively, in Cu-Ni bimetallic particles supported on Al_2O_3 support, Cu and Ni are evenly distributed throughout the particles, and there exists segregation of Ni and Cu domains at the particle surfaces. As a result of the support-induced changes in the compositional structure of the bimetallic Cu-Ni nanoparticle surfaces, TiO_2 as support primarily resulted in the formation of 2-MF, while FA and THFOL were the main products with Al_2O_3 as support. A maximum 2-MF yield of 87% with 99% FUR conversion was reported over Cu(5%)-Ni(5%)/TiO_2 at 473 K after 2 h under 35 bar initial H_2 pressures in the presence of 1,4-dioxane as a solvent. In a recent study, Zhang et al. investigated the CTH of FUR to 2-MF and 2-MTHF over Al_2O_3-supported Cu and Ni bimetallic catalyst in the presence of isopropanol as a H-donor solvent [70]. Under optimal conditions, a 64.8% yield of 2-MF and a 17.7% yield of 2-MTHF (82.5% yield in total) were achieved at a temperature of 503 K for 4 h over $CuNi_2Al$. In addition, 2-MTHF could also be selectively formed with 51.2% yield at 523 K after 9 h with $CuNi_2Al$. Niu et al. reported inexpensive
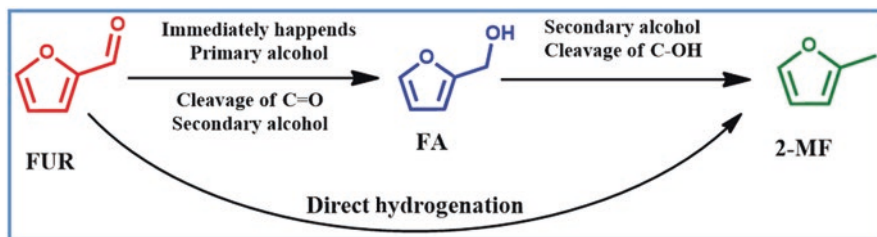
Fig. 4 Proposed mechanism for the CTH of FUR to 2-MF over the nanocomposite catalyst

CuZnAl catalyst for the CTH of FUR to 2-MF using isopropanol as a H-donating solvent [71]. Based on the calcination/reduction temperature and Cu/Zn mole ratio, the higher performance of the catalyst was related to the presence of Cu^0, Cu^+, and preserved $CuAl_2O_3$ phases on the surface of the catalyst. From Fig. 4, FA is immediately produced as intermediate, which can be further hydrogenated into 2-MF by using suitable CuZnAl catalysts.

2.1.2   5-Hydroxymethyl Furfural (HMF)

5-Hydroxymethylfurfural (HMF) is a very important and versatile platform compound derived from the dehydration biomass-derived carbohydrates. The various products obtained by hydrogenation of HMF typically includes 2,5-dimethylfuran (DMF); 5-methylfurfural (MF); 5-methylfurfuryl alcohol (MFA); 2,5-(dimethyl) tetrahydrofuran; 2,5-dihydroxymethylfuran; 5-hydroxymethyltetrahydrofurfural; 2,5-bis(hydroxymethyl)tetrahydrofuran; and ring-opened products, respectively [75–80]. In principle, the hydroxyl group can be removed by hydrogenolysis, while the carbonyl group and furan ring can be saturated by hydrogenation. Furthermore, the furan ring could be opened to form aliphatic compounds. These various conversion routes make it difficult to selectively convert HMF to specific compounds. Therefore, in order to achieve the selective conversion of HMF, it is important to develop a catalyst with excellent hydrogenation performance.

Among various hydrogenation products of HMF, DMF is particularly attractive due to its interesting properties such as a high-octane number (i.e., 119), high energy density, and low oxygen content. Many chemical routes and catalysts for DMF production have already been developed. The reaction pathway and product distribution strongly depend on the reaction conditions and the type of catalyst employed. Noble metals are reported to be high-performing catalysts for HMF hydrogenation in comparison with non-noble metal-based catalysts [Table 4]. The catalytic hydrogenation of 5-HMF to 2,5-DMF has been less explored over non-noble metals. Among the non-noble metals, catalysts based on Ni, Co, Cu, and Fe have been reported for hydrogenation of 5-HMF [81–83]. Yang et al. reported the synthesis of Co-graphene ($Co_{1.0}$/rGO) nanocomposite materials with Co species on the graphene surface in the form of single Co atoms/Co clusters and CoO nanoparticles [76]. The

Table 4 Summary of hydrogenation of HMF with different catalysts

Reaction condition	Reactant	Product	Catalyst	Performance		Refs.
				Conversion (%)	Yield (%)	
443 K, 4 h, 2 MPa H_2	HMF	DMF	Cu-Fe (1:2)	97	90.2	[75]
473 K, 1 h, 2 MPa H_2	HMF	DMF	$Co_{1.0}$/rGO	100	94.1	[76]
393 K, 4 h, 1.5 MPa H_2	HMF	DMF	PtIr-CMK-3	98	84.2	[91]
403 K, 24 h, 0.7 MPa H_2	HMF	DMF	11.8%Co-(ZnO-$ZnAl_2O_4$)	99.9	74.2	[82]
513 K, 6 h, N_2 atm	HMF	DMF	Cu/Al_2O_3	100	73.9	[83]
353 K, 2 h, 3 MPa H_2	HMF	DMF	Au/Fe(10)	100	96	[85]
423 K, 3 h, 2 MPa H_2	HMF	DMF	Fe-Pd/C	100	85	[84]
453 K, 0.2 mL min^{-1}, 1.5 MPa H_2	HMF	DMF	10Cu-1Pd/RGO	100	>95	[86]
453 K, 2 h, 1.5 MPa H_2	HMF	DMF	Ru-Co/SiO_2	100	96	[87]
393 K, 7 h, 1.5 MPa H_2	HMF	DMF	Cu−Pd@C	96.5	96.5	[88]
453 K, 6 h, 1 MPa H_2	HMF	DMF	5% Ni/WO_3	>99	95	[92]
483 K, 24 h, N_2 atm	HMF	DMF	2%Ni-20%Co/C	99	90	[89]
493 K, 5 h, 3 MPa H_2	HMF	DMF	CuZnO(P)-r2(ox)	100	94	[93]
493 K,6 h, 3 MPa H_2	HMF	DMF	Cu-Co/Al_2O_3	NA	87	[94]
403 K, 6 h, 1 MPa H_2	HMF	DMF	5Ni-7MoS_2/mAl_2O_3	100	95	[90]

combination of strong interfacial effects, synergistic effect between Co/C and CoO$_x$ and modulation effect of rGO enabled efficient hydrogenation of HMF to DMF requiring a pre-reduction step. Using ethanol as a solvent, a high DMF yield of 94.1% with 100% HMF conversion was obtained at 473 K after 1 h under 2 MPa H_2 pressure. Zhang et al. developed a Cu-based catalyst with different supports (Al_2O_3, ZnO, ZrO_2, and CeO_2) for the in situ hydrogenation of HMF to DMF in the presence of methanol as an H-donating solvent [83]. The high catalytic performance of Cu/Al_2O_3 was attributed to the highest activity for the in situ H_2 production from methanol, smallest Cu crystallite size, and the strongest acidity. However, a monometallic catalyst often does not efficiently obtain the desired target product. Therefore, bimetallic catalysts and modified supports were often used for the selective hydrogenolysis of HMF to DMF.

To further minimize costs and achieve high catalytic activity, the combination between noble metal and a second (transition) metal is highly explored as it can reduce noble metal loading and maximize activity/selectivity to DMF through electronic and geometric interactions. For example, a bimetallic combination of Au-FeO$_x$, Fe-Pd, Pd-Cu, and Ru-Co was used for the hydrogenation of HMF to DMF [84–87]. In the recent work reported by Talpade et al., 85% selectivity for DMF with 100% HMF conversion was obtained by using Fe-Pd/C in THF under optimal conditions [84]. Furthermore, Sarkar et al. reported the formation of DMF from HMF with a yield of 96.5% at 393 K after 7 h under 15 bar initial H_2 pressure in the presence of Cu-Pd bimetallic nanoparticles embedded in carbon matrix (Cu-Pd@C-B) as a catalyst [88], whereas Mhadmhan et al. used isopropanol as the

H-donor solvent and 10Cu-1Pd/RGO as a catalyst, afforded an excellent DMF yield of 95% with 96% HMF conversion at 453 K under 15 bar H_2 pressure and a flowrate of 0.2 mL min^{-1} [86]. The presence of Pd-Cu alloy was found to be associated with the higher activity and stability of the catalyst. Yang et al. developed carbon-supported Ni-Co bimetallic catalyst (2%Ni-20%Co/C) for the CTH of HMF to DMF with a yield of 90% at 483 K after 24 h in the presence of formic acid as the H_2 source [89]. The high catalytic activity was attributed to the specific structural properties in the form of hybrid nanomorph exhibiting oxophilic nature and Lewis acidity of Fe, whereas the high selectivity toward DMF was due to the Brønsted acidity of CuO and its affinity for the C–O bond.

A reaction mechanism was also proposed for the hydrogenation of HMF to DMF over metal-metal nano-hybrid catalyst (i.e., Cu-Fe catalyst) (Fig. 5). The initial activation of 5-HMF occurs through the –C=O group by the Lewis acidity and oxophilic nature of Fe by attacking its electron-rich oxygen. As a result, the H_2 molecule which dissociates on the metallic Cu of the Cu-Cu-Fe$_2$O$_4$ nanomorph attacks the electrophilic carbon of the –C=O group giving BHMF as an initial reaction intermediate. This enhances the rapid dehydration of BHMF into DMF via MFAL. Furthermore, Han et al. recently developed ordered mesoporous alumina supported Ni-Mo sulfide catalyst (Ni-MoS$_2$/mAl$_2$O$_3$) by evaporation-induced self-assembly method for catalyzing the selective hydrogenolysis of HMF to DMF [90]. The yield of DMF could reach to 95% DMF over 5Ni-7MoS$_2$/mAl$_2$O$_3$ under the mild reaction conditions of 403 K for 6 h at a H_2 pressure of 1 MPa using isopropanol as the H-donating solvent. The characterization results and DFT calculation suggests that the active site was a coordinated unsaturated site located at S-edge and the intrinsic activity of coordinated unsaturated site was directly related to the proportion of Mo replaced by Ni.

2.2 Oxidation of Furanics

2.2.1 Furfural

The selective oxidation of FUR can produce various C4-oxygenated products, such as acid anhydrides (malic anhydride (MAN)), dicarboxylic acids (succinic (SA), malic (MA), and fumaric acids (FAc)), and furanone (FU) (Fig. 6). Among them, MAN is an attractive value-added chemical used in the manufacture of lubricant, unsaturated polyester resins, surface coatings, plasticizers, co-polymers, coatings, and pharmaceuticals. Several renewable routes for the catalytic oxidation of FUR to MAN have been reported. Supported vanadium oxide catalysts have been studied for decades for the gas-phase oxidation of FUR to MAN in the presence of air or oxygen, where MAN yields in the range of 15–90% have been described. Alonso-Fagúndez et al. reported a considerably high yield of 73% for MAN at 100% FUR conversion during the vapor-phase oxidation of FUR in the presence of VO$_x$/Al$_2$O$_3$ as a solid catalyst for under the conditions of 593 K and 5.7 kPa O$_2$ [5]. When
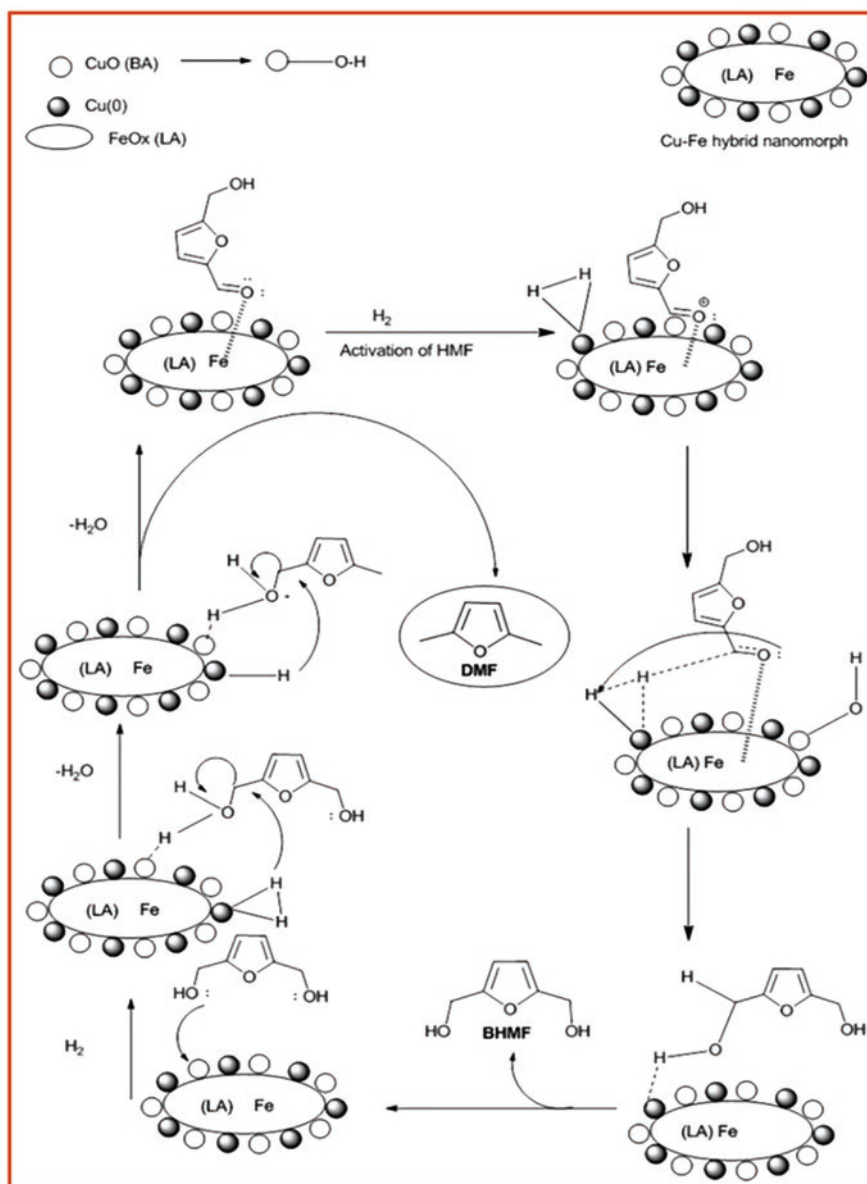
Fig. 5 Proposed mechanism for the hydrogenation of HMF to DMF over the Cu-Fe hybrid nanomorph catalyst (adopted from ref. [75])
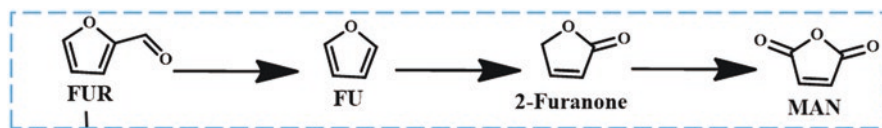
Fig. 6 Various products obtained during the oxidation of FUR

Table 5 Summary of oxidation of FUR with different catalysts

Reaction condition	Reactant	Product	Catalyst	Performance Conversion (%)	Yield (%)	Refs.
593 K, 5.7 kPa O_2	FUR	MAN	VO_x/Al_2O_3	100	73	[5]
383 K, 14 h, 20 atm O_2	FUR	MAN	$H_5PV_2Mo_{10}O_{40}$ and $Cu(CF_3SO_3)_2$	98.7	54	[95]
633 K, 21% O_2/N_2 atm	FUR	MAN	VPO_{HT}	100	90	[96]
573 K, 1.68 kPa O_2	FUR	MAN	V_2O_5/γ-Al_2O_3	100	55	[97]
343 K, 1 h	FUR	MA	VZPK1 (0.25 Zr/V ratio loading)	81.2	29.2	[98]
373 K, 4 h	FUR	MA	TS-1 and acetic acid	100	62	[100]
403 K, 4 h, 0.275 MPa O_2	HMF	DFF	Ru/γ-Al_2O_3	99	96	[101]
383 K, 2.0 MPa O_2	HMF	DFF	Ru/C	100	96	[102]
383 K, 4 h, 2.0 MPa O_2	HMF	DFF	Ru/OMC-P0.56	100	88	[103]
383 K, 2 h, 1.0 MPa O_2	HMF	DFF	Ru_1/NiO	91.1	74	[104]
413 K, 6 h, in air	HMF	DFF	$NH_4 \cdot V_3O_8/Fe_3O_4$	95.5	79.1	[105]
353 K, 5 h, TBHP	HMF	DFF	Co_xO_y-N@TiO_2	91	36.4	[106]
413 K, 2 h, 3 MPa air	HMF	DFF	$Mn_{0.50}$-$Co_{0.50}$-O	42.6	41.7	[107]
343 K, 8 h, 0.4 MPa O_2	HMF	DFF	Cu/NG_4, TEMPO	99.8	99.2	[108]
363 K, 1 h, 0.8 MPa O_2	HMF	DFF	MnO_x microtubes	50.4	50.4	[109]
383 K, 10 h, 0.2 MPa O_2	HMF	DFF	$MgO \cdot MnO_2 \cdot CeO_2$	98.8	94	[110]
373 K, 15 h, 0.9 MPa O_2	HMF	DFF	$MgO \cdot CeO_2$	97.8	95.8	[111]
373 K, 12 h, 1 MPa O_2	HMF	DFF	Cs/MnO_x	98.4	94.7	[112]
393 K, 7 h, in air	HMF	DFF	$10V_2O_5$@Cu−MOR(125)	>99.9	91.5	[113]
373 K, 6 h, 1 MPa O_2	HMF	DFF	FeCo/C(500)	100	>99	[114]

vanadium oxide catalysts are used, the active sites are reduced by FUR and reoxidized by oxygen, and the reoxidation of the reduced catalyst has been identified as the rate-determining step. In 2014, Lan et al. found that 54% yield of MAN and 7.5% yield of 5-acetoxyl-2(5H)-furanone were obtained at 98.7% conversion of FUR over $H_5PV_2Mo_{10}O_{40}$ and $Cu(CF_3SO_3)_2$ as catalysts [95]. Furthermore, Li et al. synthesized a vanadium phosphorous oxide (VPO_{HT})-based plate catalyst via a hydrothermal method with glucose as a reducing agent for the gas-phase oxidation of FUR to MAN [96]. They found that developed catalyst has predominantly 200 exposed crystal planes responsible for the remarkable activity, selectivity, and stability. VPO_{HT} gave 90% MAN yield at 633 K in 21% O_2/N_2 atm and demonstrated stable activity up to 25 h time on stream (Table 5). Recently, Santander et al. investigated the gas-phase oxidation of FUR over vanadium supported on SiO_2, γ-Al_2O_3, ZrO_2, and TiO_2, where they demonstrated that catalytic properties during the oxidation reaction depend both on the nature of the support and dispersion of vanadium [97]. Among the different supported catalysts, V_2O_5/γ-Al_2O_3 and V_2O_5/SiO_2 displayed higher activity with 49% and 36% MAN yield at 573 and 593 K.

MA is another important intermediate of C_4 compounds in the chemical industry. Different methods have been reported for the green oxidation of FUR to MA either in gas or liquid phase. Recently, Rezaei et al. developed a VZPK catalyst by stabilizing a mixture of vanadium and zirconium supported over KIT-6 to oxidize FUR to MA in the presence of H_2O_2. A 29.2% MA yield at 81.2% FUR conversion was obtained in the presence of VZPK1 (0.25 Zr/V ratio loading) at 343 K after 1 h with 3:1 (H_2O_2/FUR mole ratio) in acetonitrile as the solvent [98].

2.2.2 5-Hydroxymethyl Furfural (HMF)

Based on the position and degree of HMF oxidation, various high-value derivatives, such as 5-hydroxymethylfuroic acid (HMFCA); 2,5-diformylfuran (DFF); 5-formyl-2-furancarboxylic acid (FFA) [99]; 2,5-furandicarboxylic acid (FDCA); maleic anhydride (MA); and maleic acid (MAc), can be selectively produced.

The selective oxidation of HMF to DFF remains a great challenge that requires the controlled oxidation of its primary hydroxyl group while leaving the aldehyde group intact. Recently, to improve the selectivity of DFF, considerable efforts have been devoted to the design of highly active and selective heterogeneous catalyst. Among noble metals, γ-Al_2O_3-supported Ru catalyst was reported to convert 99% of HMF with 97% DFF selectivity at 403 K after 4 h and 40 psi O_2 pressure in toluene as a solvent [101], whereas Nie et al. reported that Ru/C achieved 96% DFF yield with complete HMF conversion under the conditions of 383 K and 2.0 MPa O_2 in toluene [102]. Other Ru-based catalysts have also gained excellent yield and selectivity for DFF during the oxidation of HMF [103, 104, 115]. Non-noble metal catalyst based on V, Co, Cu, and Mn and mixed oxides were also developed for the oxidation of HMF to DFF [105–112]. Zhang et al. synthesized a vanadium oxide supported Cu-MOR zeolites ($10\%V_2O_5$@Cu-MOR(125)) for the oxidation HMF, where 91.5% yield for DDF was achieved at 393 K for 7 h in DMSO with
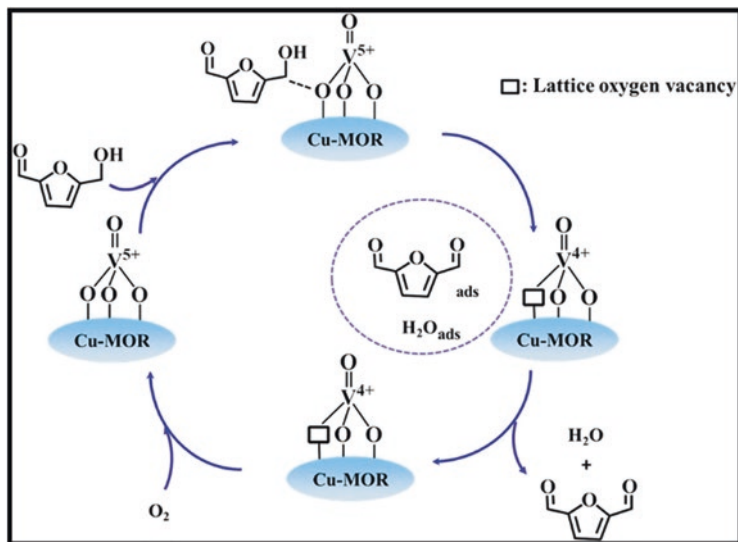
Fig. 7 Possible reaction mechanism for aerobic oxidation of HMF to DFF over $10V_2O_5@$ Cu-MOR(125) catalyst [111]

atmospheric O_2 (1 bar) [113]. The remarkable performance of the catalyst was associated with a strong interaction between framework Cu species and V guest which promoted both the activity and the stability of the supported V active sites. The catalyst followed Mars-van Krevelen mechanism during the oxidation of HMF to DFF (Fig. 7). According to the reaction mechanism, HMF is adsorbed on the catalyst surface and oxidized to generate DFF mainly by lattice oxygen (V^{5+}−$O^{2−}$). The formed V^{4+}−γ (γ denotes the lattice oxygen vacancy) transition active site is further reoxidized with O_2 to regenerate V^{5+}−$O^{2−}$ species. More recently, magnetic Fe_3O_4-supported $NH_4·V_3O_8$ catalyst ($NH_4·V_3O_8/Fe_3O_4$) converted HMF to DFF with a conversion of 95.5% with 82.9% selectivity under optimal reaction conditions of 413 K after 6 h in DMSO with air as oxidant [105].

Fang et al. used non-noble Fe-Co-based bimetallic catalysts derived from a metal-organic framework (MIL-45b) to convert HMF to DFF [114]. Complete HMF conversion with a DFF yield of >99% was achieved using FeCo/C at 373 K after 6 h under 1 MPa O_2 in toluene (Table 5). It is proposed that the oxidation reaction proceeds according to Mars-van Krevelen mechanism, where the lattice oxygen of FeCo oxides facilitated HMF oxidation to DFF (instead of HMFCA) and was later replenished with O_2 molecules. Moreover, weak adsorption of DFF on the catalysts might also inhibit the over oxidation of DFF, leading to the high observed selectivity to DFF. The catalyst has magnetic properties and can be recycled up to six times without significant activity losses. Lv et al. reported a HMF conversion of 99.8% with a DMF yield of 99.2% using Cu-incorporated pyridinic nitrogen-dominated nitrogen-doped graphene (Cu/NG) as a catalyst and 2,2,6,6-tetramethyl-piperidin-1-oxyl (TEMPO) as co-catalyst under the conditions of 343 K after 8 h and 0.4 MPa

O_2 in acetonitrile [108]. Yuan et al. disclosed the selective oxidation of HMF catalyzed by reusable cesium-doped manganese dioxide (Cs/MnOx) catalyst with a DFF yield of 94.7% at 98.4% HMF conversion at 373 K within 12 h under 10 bar O_2 in *N,N*-dimethylformamide [112]. The higher catalytic activity of the Cs/MnOx catalyst was explained by the higher oxidation state of Mn, stronger basicity, larger amount of defects, larger surface area, and more abundant pores.

2.3 Amination of Furanics

Reductive amination of carbonyl compounds derived from biomass has received great attention for the synthesis of value-added N-containing compounds, which are important building blocks for the preparation of synthetic organic intermediates in pharmaceuticals and agrochemicals. The reductive amination of carbonyl compounds in the presence of amine source (ammonia, primary or secondary amines) and reducing agent (hydrogen) is one of the most suitable protocols for the synthesis of the variety of amines. Among them, more valuable primary amines are generated in two steps: (1) condensation of the carbonyl compound with ammonia, followed by elimination of water to form an imine over an acid or base catalyst (although this can also occur without a catalyst), and (2) hydrogenation of the imine to give the final primary amine catalyzed by a hydrogenation catalyst. However, the selectivity for primary amines in reductive amination remains difficult to control since primary amines are more nucleophilic than ammonia and easily react with aldehydes to form secondary amines. In addition, undesired hydrogenation of the carbonyl groups and unsaturated bonds also limits selectivity for the corresponding primary amines.

2.3.1 Reductive Amination of Furfural

The reductive amination of FUR over metal catalysts with NH_3 in the presence of H_2 can convert its carbonyl functionality to an amine such as furfurylamine (FAM). FAM is one of the primary amines used to prepare drugs, fibers, and pesticides. The reaction network proposed in the literature for the synthesis of FAM involves (Fig. 8):

1. Hydrogenation of alcohol.
2. Reaction with ammonia resulting in the formation of reactive intermediates (including primary imine) or react with FAM to form Schiff base-type intermediate.
3. Hydrogenation of secondary imine to the secondary amine.
4. It can decompose to the primary amine and primary imine in the presence of ammonia. From nitrile reduction reactions, it is known that primary imines and primary amines can couple to form secondary imines and subsequently form secondary/tertiary amines. A generally accepted mechanistic suggestion con-
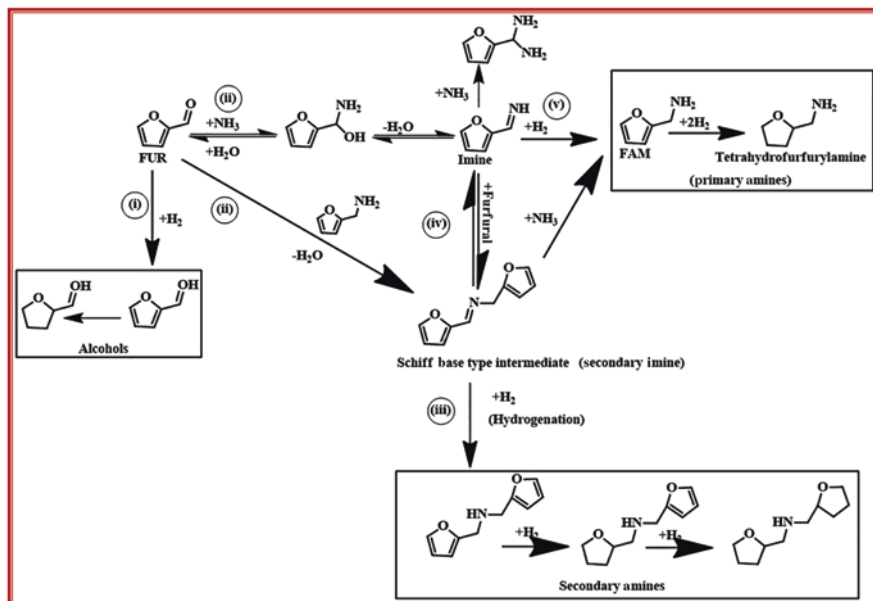
Fig. 8 Proposed reaction network for the reductive amination of FUR

necting the two sides of the equilibrium in step 4 is the formation of a secondary gem-diamine intermediate.

5. The primary imine can also be hydrogenated to the primary amine.

Chatterjee et al. investigated the reductive amination of FUR using noble metals (Rh, Pt, Pd) supported on activated carbon, mesoporous silica (MCM-41), and Al_2O_3 [116]. High FAM selectivity (92%) and complete FUR conversion were achieved with Rh/Al_2O_3 catalyst under the optimal reaction conditions. Notably, the hydrogenation of imines to FAM was observed as a main pathway, whereas the conversion of the Schiff base-type intermediate to FAM and secondary amines is a minor one. Furthermore, Dong et al. reported HZSM-5 ($SiO_2/Al_2O_3 = 46$)-modified noble metals (Ru, Pt, Pd, and Rh) catalysts for the reductive amination of FUR [117]. With Ru/HZSM-5(46), 75% FAM yield was achieved within 15 min at 373 K under 3 MPa H_2 and NH_3 (7 M in MeOH) and could be recycled up to five times without loss in activity (Table 6). Recently, Zhou et al. reported a 98.9% FAM yield over Raney Co catalyst under the conditions of 393 K for 2 h under 0.1 MPa pressures for NH_3 and H_2 and with the possibility to reuse more than eight times [118]. They observed that the Schiff base intermediate was mainly undergone hydrogenolysis to produce FAM and hydrogenation of the Schiff base intermediate to secondary amine was the minor pathway. The superior performance of Raney Co in FAM synthesis was ascribed to its high hydrogenolysis efficiency of the Schiff base intermediate and its low hydrogenation efficiency of the Schiff base, carbonyl group, and furan ring. Gould et al. revealed that the performance of non-noble Ni/

Table 6 Summary of reductive amination of furanics over different nanocomposite catalysts

Reaction condition	Reactant	Product	Catalyst	Performance		Refs.
				Conv. (%)	Yield (%)	
353 K, 2 h, 2 MPa H_2, 28% aq. NH_3	FU	FAM	Rh/Al_2O_3	100	92	[116]
373 K, 15 min, 3 MPa H_2, NH_3 sol.	FU	FAM	Ru/ HZSM-5(46)	NA	75	[117]
393 K. 2 h, 0.1 MPa NH_3 and 1 MPa H_2	FU	FAM	Raney Co	100	98.9	[118]
403 K, 10 h, 5.17 MPa H_2, 1 mL NH_4OH	FU	FAM	Ni/SiO_2 and Co/ SiO_2	100	90–94	[119]
363 K, 10 h, 4 MPa CO, amines (0.5 mmol)	HMF	BHMF	Au/TiO_2-R	>99	93	[120]
323 K, 2 h, 5 MPa H_2, aniline (0.24 mmol)	HMF	Amine	UiO-67/PpPDA/ Pd	100	94.5	[121]
373 K, 6 h, 0.1 MPa H_2, NH_3	HMF	FAA	$Ni_6Al_1O_x$	100	98	[122]
373 K, 4 h, 2 MPa H_2, aq. NH_3 (5 mL)	HMF	AMF	Ni/SBA-15	NA	89.8	[123]

SiO_2 and Co/SiO_2 catalysts for the reductive amination of FUR was similar to noble metal Ru/SiO_2 catalyst with FAM yield of 94, 93, and 90% under the conditions of 750 psi H_2 and 403 K for 10 h [119].

2.3.2 Reductive Amination of HMF

The reductive amination of HMF can produce N-substituted-5-(hydroxymethyl)-2-furfuryl amines with pharmaceutical functions such as calcium antagonistic activity, cholinergic agent, antimuscarinic agent, and carcinogenesis inhibitors. Zhu et al. used rutile titania-supported gold (Au/TiO_2-R) catalyst to catalyze the reductive amination of HMF using Co and water as inexpensive reductant [120]. The yield of 2,5-bis-(hydroxymethyl)furan (BHMF) reached to 93% within 2.5 h at 333 K under 20 bar CO in the presence of water/methanol (1:1). Recently, García-Ortiz et al. investigated the reductive amination of HMF in the presence of Pd/C as a catalyst using various amines and ammonia as an amine source, as well as nitro-benzene in the one-pot reaction, where N-substituted-5-(hydroxymethyl)-2-furfuryl amines were obtained in excellent yield [124]. Furthermore, Karve et al. reported active palladium-functionalized MOF/polymer composite (UiO-67/PpPDA/Pd) for the reductive amination of HMF with different aliphatic and aromatic amines exhibiting electron-withdrawing or electron-donating groups [121]. A 94.5% yield for the desired amine was obtained at 323 K under 5 MPa H_2 after 2 h in the presence of aniline as a substrate and ethanol as a solvent (Table 6). Also, the catalyst showed high recyclability of up to 15 cycles, which was associated with the addition of polymer poly-para-phenylenediamine (PpPDA), which prevents the aggregation

and leaching of Pd nanoparticles. Among non-noble catalysts, Yuan et al. developed the Ni_6AlO_x catalyst by coprecipitation method for the reductive amination of HMF with ammonia, reaching a 99% yield for 5-aminomethyl-2-furylmethanol (FAA) under the reaction conditions of 373 K, 6 h under 1 bar H_2 [122]. In a more recent study, Chen et al. reported the direct reductive amination of HMF over Ni/SBA-15 using aqueous ammonia at 373 K after 4 h under 20 bar H_2 pressure, which obtained a yield of 89.5% for 5-(aminomethyl)-2-furanmethanol (AMF) [123].

According to the proposed reaction pathway over Ni/SBA-15, the two types of intermediate compounds were observed in the reaction mixture, the terminal (compound 1) and internal imine groups (compound 2) (Fig. 9). Compound 2 possesses a bulkier structure as compared to compound 1 which leads to a serious steric effect for hydrogenation reaction, limiting the formation of compound 3. The moderate catalytic activity of hydrogenating nickel catalysts enhances the selectivity for compound 1, thereby generating AMF. On the other hand, due to the higher nucleophilicity of primary amine (AMF) than ammonia, a further reaction of AMF with HMF generates by-products such as compound 2, followed by catalytic hydrogenation to form compound 3. Interestingly, the presence of an appropriate amount of water in the reaction medium promotes the hydrolysis of AMF to form ammonium ion, which reduces the nucleophilicity of AMF and inhibits its further conversion.

2.4　Condensation Reactions of Furanics

2.4.1　Aldol Condensation of Furfural

Aldol condensation reaction is widely used in organic synthesis processes of producing α, β unsaturated compounds from carbonyl group at low temperature. Aldol condensation of FUR and ketones provides an attractive route for the production of oxygenated precursors for liquid hydrocarbons of chain length and molecular weight appropriate for diesel and jet fuels. The oxygenated precursors can subsequently be transformed to high-quality diesel and jet fuel range liquid hydrocarbons
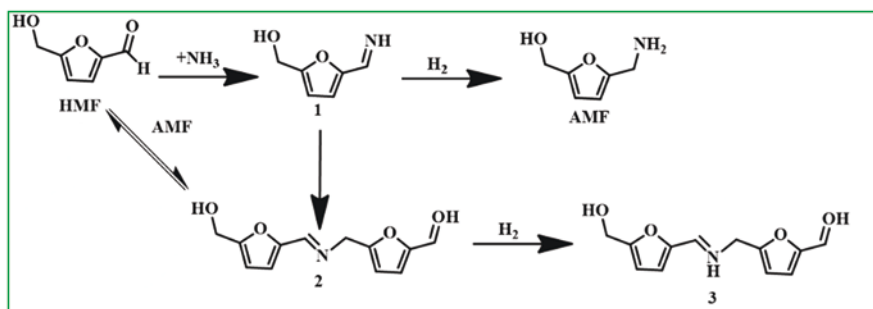
Fig. 9　Proposed reaction network for the reductive amination of HMF

via hydrogenation and hydrodeoxygenation reactions. Moreover, furfurylidene ketone-based compounds produced by aldol condensation reaction of FUR and acetone are widely used in the food industry, (e.g., alcohol-free drinks, gelatins, ice candies as aromas) and as monomers to produce furan-derived resins [125]. The various linear cyclic ketones are employed for aldol condensation reaction. The desired products from the condensation of FUR and ketones are shown in Fig. 10. FUR reacts with acetone to produce furfural acetone monomer 4-(2-furyl)-3-butene-2-one (FAc, C_8) followed by condensation with another FUR to produce furfural acetone dimer 1,5-bis (2-furanyl)-1,4-pentadiene-3-one (F_2Ac, C_{13}). Aldol condensation of FUR and ketones is often performed using homogeneous base catalysts. However, homogeneous base catalysts have serious drawbacks of difficulty in catalyst regeneration and corrosion of equipment. Recently, heterogeneous base catalysts have gained great attention due to ease of catalyst regeneration and non-corrosiveness nature. For the development of sustainable and green process, aldol condensation reaction is carried out either in nontoxic and inexpensive solvents (e.g., water) or in solvent-free condition. The latter option limits the utilization of toxic and hazardous solvents and minimizes the generation of waste [125]. The different types of heterogeneous base catalysts used for aldol condensation reaction are discussed below, and performance of the few catalysts is tabulated in Table 7.

The family of hydrotalcite (HT) solid materials have layered or laminar structure similar to that of the mineral hydrotalcite [126]. The chemical composition of hydrotalcite material is not restricted to only Mg and Al atoms. The HTs are commonly designated as layered double hydroxides with the chemical formula of $[M^{2+}_n M^{3+}_m(OH)_{2(n+m)}]^{m+}[A^{x-}]_{m/x} \cdot yH_2O$, where M^{2+} and M^{3+} are divalent and trivalent metal cations, respectively [126]. The isomorphic substitution of M^{2+} atoms in the brucite-like layers with M^{3+} atoms results in the generation of a net-positive charge in HT crystal lattice which is counterbalanced by extra-framework charge anions A^{x-}. Carbonate groups generally make up the positive framework charge in the as-prepared HTs. Thermal activation of HTs leads to the formation of well-dispersed mixed oxide materials. The occurrence of M^{2+}-O^{2-} acid-base pairs (Lewis basicity) in the thermally activated mixed oxides ascertains their unique catalytic properties in many organic reactions, such as condensations, transesterifications, alkylations, etc. The basic mixed oxide catalysts prepared from hydrotalcite (HT) precursors exhibit superior catalytic performance in aldol condensation reaction due to their tunable physicochemical properties [126, 127]. The physicochemical properties of reconstructed Mg-Al HT were correlated with the catalytic performance in aldol condensation reaction of FUR and acetone by Kikhtyanin et al. [126]. The
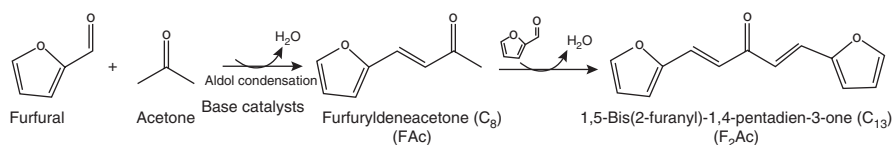
Fig. 10 Reaction pathway for aldol condensation of furfural and acetone

Table 7 Summary of aldol condensation of furfural using different catalysts

Entry	Substrates	Reaction condition	Catalyst	Performance		Refs.
				Conv. (%)	Sel. (%)	
1.	FUR and Ac (1:40)	50 °C, 7 h, 0.15 g	La_xMg_yMO-H ($x = 1$, $y = 1$–4)	96	C_8:98	[125]
2.	FUR and Ac (1:10)	50 °C, 1 bar, 6 h, 2 g cat	Zn_2Al, Mg_2Al, and ZnMgAl	100	C_8:60 C_{13}:35	[127]
3.	FUR and Ac (1:10)	100 °C, 2 h, 2.0 g cat	Mg-Al	95	C_8 and C_{13}: >90%	[129]
4.	FUR and Ac (1:1)	52 °C, 10 bar, 24 h, 0.5 g cat	MgO-ZrO_2, MgO-Al_2O_3, CaO-ZrO_2	81.4	C_8:14.7 C_{13}:61.5	[131]
5.	FUR and Ac (1:2, 1, 0.5)	50 °C, 1 bar, 6 h, 0.2 g cat	$MgF_{2-x}(OH)_x$	34	C_8:36 C_{13}:48	[134]
6.	FUR and Ac (1:10)	160 °C, 3 h, 0.1 g cat	P/CeO_2 180-900	96	C_8:54.3 C_{13}:14.1	[135]
7.	FUR and cyclopentanone (2:1)	60 °C, 2 h, 0.2 g cat	Mg-Zr, Mg-Al, Co-Al and KF/Al_2O_3	100	C_{15}:98	[137]
8.	FUR and Ac (1:10)	100 °C, 1 h, 2.0 g cat	HBEA	38.5	FAc: 79.5 F2Ac: 3.7 $(FAc)_2$: 16.8	[139]
9.	FUR and Ac (1:10)	160 °C, 2 h, 0.1 g cat	Sn-Beta	99	FAc:40 F_2Ac: 22	[140]
10.	FUR and Ac (1:10)	100 °C, 1 h, 1.0 g cat	Fe-BTC	26.2	FAc: 71 F_2Ac: 20 $(FAc)_2$: 1	[141]
11.	FUR and Ac (1:10)	100 °C, 1 h, 2.0 g cat	K-BEA	77.8	FAc:67.2 F_2Ac: 17.6	[143]
12.	FUR and Ac (1:10)	160 °C, 1 h, 0.2 g cat	K-Sn-MFI	100	C_8:75 C_{13}:10	[144]
13.	FUR and Ac (1:2)	85 °C, 8 h, 1.06 g cat	MgO/NaY	99.6	FAc:42.2 F_2Ac: 57.1	[145]
14.	FUR and Ac (1:0.8)	80 °C, 2 h, 1.0 g cat	Ca/ZSM-5	99.1	FAc:38.4 F_2Ac: 60.2	[146]
15.	FUR and Ac (1:10)	140 °C, 5 h, 2.0 g cat	Pd/Co-Al	98.9	FAc:69.2 F_2Ac: 30.8	[150]

reconstructed Mg-Al HTs were prepared by using different rehydration and drying time. The Mg-Al mixed oxide regain its HT structure within a few seconds of contact with water. The calcination of as-prepared HT followed by rehydration of Mg-Al mixed oxide led to the more than 90% replacement of carbonate groups with Brønsted basic characteristic hydroxyl group. Consequently, the reconstructed HT exhibits higher aldol condensation activity than the as-prepared Mg-Al catalyst. In a different study, the authors showed the impact of acidic impurities in furfural on the catalytic performance of solid base catalysts [128]. FUR often undergoes air

oxidation to form furoic acid even if stored in a closed tank. Some portions of added base catalysts were utilized to neutralize the acid impurities, which may demonstrate no activity of the strong base catalyst in certain condition. The authors proposed that distillation is an effective way to remove acid impurities in as-received FUR. Thus, a detailed monitoring of acid impurities in furfural is critical while evaluating the performance of solid base catalysts and their stability in aldol condensation. Hora et al. investigated the effect of pretreatment methods of the HT-based catalysts (Mg-Al) on their activity and selectivity of targeted products in aldol condensation [129]. They have considered calcination and rehydration procedures (ex situ vs. in situ and liquid vs. gas phase) as pretreatment methods for their studies and determined the impact of calcination temperature and rehydration procedures on the yield of desired aldol condensation products. The ex situ rehydration of the calcined Mg-Al catalysts showed remarkably lower activity, except the catalyst with Mg/Al molar ratio of 2. However, in situ rehydration improved the catalyst activity only for Mg/Al molar ratio of 3. The activity of these catalysts was determined to a significant extent by the ratio of HT and MgO phase. Comparison of structural data indicates that the catalysts displaying poor crystallinity are greatly influenced by the rehydration procedure, while the catalysts with well-developed hydrotalcite structure are more resistance to ex situ rehydration procedure. The Mg-Al catalyst with molar ratio of 3 exhibits best performance in aldol condensation reaction with 95% FUR conversion and more than 90% selectivity of C_8–C_{13} products. In a different study, the effect of preparation method and activation temperature of Mg-Zr mixed oxide on catalytic performance for aqueous-phase aldol condensation of FUR with acetone was reported by Sadaba et al. [130]. It was demonstrated that the preparation method requires a high-temperature activation in oxidizing environment, which generates cubic $Mg_xZr_{1-x}O_{2-x}$ mixed oxide and MgO. The formation of cubic MgO phase greatly enhanced the FUR/acetone aldol condensation. Smoláková et al. showed the influence of acid-base properties of HT precursor-derived mixed oxide catalysts on the activity and selectivity in aldol condensation reaction [127]. The basicity of the mixed oxides was strongly reckoned on the preparation of parent HT precursors. The total amount of basic sites of different catalysts increased in the following order $Zn_2Al < Mg_1Zn_1Al < Mg_2Al$. The FUR conversion and selectivity to longer carbon chain C_{13} (F_2Ac) product were observed to follow the similar trend of the total amount of basic sites. The higher activity of Mg_2Al catalyst was also because of its higher surface area. However, the selectivity of C_8 (FAc) at iso-conversion follows the opposite trend. More specifically, the presence of medium strength basic sites was responsible for higher activity as strong basic sites promote transesterification reaction. Faba et al. studied aqueous-phase aldol condensation reaction with acetone using three different mixed oxide base catalysts (Mg-Zr, Mg-Al and mesoporous Ca-Zr nano oxide) with different basic site distribution [131]. They also reported that the Mg-Zr mixed oxide catalysts with the highest amount of medium-strength basic sites showed the best performance in terms of activity and selectivity for the C_{13} (F_2Ac) fraction, whereas the Ca-Zr mixed oxide showed poor performance because of the higher rate of retro-aldolization reaction. Sádaba et al. demonstrated a systematic investigation to identify the

different phases formed during preparation of series of MgO-ZrO$_2$ mixed oxides by coprecipitation method and their catalytic activity in aldol condensation of FUR with acetone [132]. Two different phases (a cubic Mg$_x$Zr$_{1-x}$O$_{2-x}$ and c-MgO) were identified, and formation of these phases depends on the nominal Mg/(Mg + Zr) atomic ratio. The cubic Mg$_x$Zr$_{1-x}$O$_{2-x}$ solid solution was obtained below the nominal atomic ratio of 0.5, and a mixture of c-Mg$_x$Zr$_{1-x}$O$_{2-x}$ and c-MgO was formed above nominal atomic ratio of 0.5. The Zr-O-Zr sites are inactive for the condensation reaction. Two different active sites, Mg-O-Mg and Mg-O–Zr, exist on the surface of c-MgO. With the increase in Mg amount in the solid, Mg-O-Zr sites are replaced with the Mg-O-Mg sites and make the later active sites predominant at the higher Mg concentration. The maximum concentration of Mg-O-Zr species was formed in the 0.5MgZr catalyst. The relative intrinsic catalytic activity (per mol of Mg) of identified active sites follows the following trend: Mg-O-Zr sites on MgO > Mg-O-Mg sites on MgO ≈ Mg-O-Zr sites on Mg$_x$Zr$_{1-x}$O$_{2-x}$. The overall activity of the catalysts is the combined activity of these sites that are existed in different proportions in the catalysts depending on the nominal atomic ratio. Desai and Yadav prepared LaMg mixed oxide catalysts of varying mole ratio and studied for solvent-free crossed aldol condensation reaction [125]. LaMg mixed oxide catalysts were prepared by combustion and hydrothermal process, and the latter synthesis process provides higher surface area and higher amount of medium to strong basic sites. La$_1$Mg$_3$ catalyst prepared by hydrothermal process exhibits superior catalytic performance in aldol condensation due to the presence of moderate to strong basic sites. About 96% conversion of FUR with 98% selectivity of C$_8$ (FAc) fraction was obtained at 150 °C in 7 h.

Natural dolomite has also been used as solid base catalyst for aldol condensation reaction. Dolomite is an abundant sedimentary carbonate rock consisting of alternate planner structures of Ca^{2+}and Mg^{2+} ions generating a nonideal basic chemical compound of formula CaMg(CO$_3$)$_2$. O'Neill et al. studied aldol condensation of FUR using activated dolomite as solid base catalyst [133]. Activation of dolomite by calcination and hydration generates catalytically active Ca and Mg hydroxides with enhanced surface area and surface basicity. The activated dolomite is more selective to C$_{13}$ (F$_2$Ac) product due to the higher heat of adsorption of C$_8$ (FAc) product.

Various nanosized magnesium hydroxide fluorides, MgF$_{2-x}$(OH)$_x$, as different base catalysts were demonstrated for aldol condensation reaction of FUR and acetone to produce C$_{13}$ (F$_2$Ac) fuel precursor with high yield [134]. The tunable acid-base properties and high surface area make these catalysts appropriate for such type of reaction. Also, this class of catalytic material does not require activation before reaction, which is often performed in case of metal oxide base catalyst due to the presence of carbonate species on the catalyst surface. The presence of fluoride stabilizes the basic sites even at low temperature. The optimum amount of MgF$_2$ (Lewis acid sites) and Mg(OH)$_2$ (medium-strength basic sites) determines the performance of the nanocomposite catalysts, and MgF$_{1.5}$(OH)$_{0.5}$ exhibits the best performance for producing C$_{13}$ (F$_2$Ac) fuel precursors. The effect of different crystal structures of cerous phosphate as solid acid catalysts on their catalytic performance

for aldol condensation of FUR and acetone was reported by Li et al. [135]. The physicochemical properties of cerous phosphate were greatly influenced by the different crystal structures, which are played an important role on catalyst performance. The distribution of different crystal structures can be varied by tuning the synthesis condition (hydrothermal synthesis temperature) and pretreatment conditions (calcination temperature). The increase in calcination temperature to 900 °C of cerous phosphate catalyst with monoclinic crystal structure increases the catalytic performance for condensation reaction due to the presence of the higher amount of acid sites and relatively stable textural properties. However, opposite trend was observed for cerous phosphate catalyst with hexagonal crystal structure. The FUR conversion and aldol product yield increased to 96% and 68.4% (C_8:54.3, C_{13}:14.1), respectively, for cerous phosphate with the monoclinic structure after calcination at 900 °C.

Yang et al. reported the solvent-free synthesis of diesel and jet fuel range alkanes by aldol condensation of 2-pentanone and 2-heptanone followed by HDO of condensation product [136]. Various solid base catalysts were employed for the condensation reaction, and the activity sequence of these catalysts is CaO > MgAl-HT > KF/Al_2O_3 > CoAl-HT > $MgO–ZrO_2$ > MgO. The higher activity of CaO (98.3% conversion, 86.7% yield) was due to the stronger basicity of the material. Ao et al. performed aldol condensation reaction of FUR and cyclopentanone to produce C_{15} (2,5-bis(furan-2-ylmethylidene)cyclopentan-1-one) fuel precursor with high yield [137]. Various HT-based mixed oxide catalysts (Mg-Zr, Mg-Al, and Co-Al) and KF/Al_2O_3 were studied for the condensation reaction. It was demonstrated that KF/Al_2O_3 exhibits superior performance compared to HT-based catalysts because of the presence of strong basic sites, which were generated by strong interaction of KF salt with the support. The authors have studied the condensation reaction using various solvents and demonstrated their effect on the targeted product solubility and yield. It was reported that the targeted product was highly soluble in THF, and product yield was about 98%. However, cost of solvent and environmental aspect (green process) should be considered as other important parameters while choosing the appropriate solvent. Chen et al. demonstrated the two-step synthesis process of C_9–C_{10} branched alkanes by aldol condensation of FUR and 3-pentanone and 5-nonanone and followed by hydrodeoxygenation of condensation product [138]. 5-Nonanone is less reactive than the 3-pentanone because of the greater steric effect of alkyl group of 5-nonanone. Different types of solid base catalysts such as MgO, CaO, $MgO-ZrO_2$, $MgO-La_2O_3$, MgAl hydrotalcite, LiAl hydrotalcite, and KF/Al_2O_3 were employed for the condensation reaction. Among these catalysts, CaO and KF/Al_2O_3 catalysts showed higher activity in aldol condensation of FUR and 3-pentanone. The authors have used different SiO_2-supported monometallic and bimetallic catalysts for HDO of aldol condensation products to produce jet fuel range branched alkanes (Fig. 11). $Ni-Cu/SiO_2$ catalyst showed superior HDO activity compared to other catalysts.

Recently pure and modified zeolites and metal organic frameworks (MOFs) have been studied for aldol condensation of FUR. Zeolites are reusable heterogeneous catalysts of high stability, surface area, and activity. Pure zeolites of different
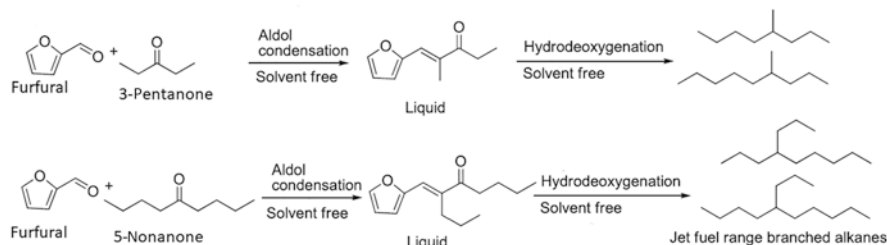
Fig. 11 Illustration of solvent-free synthesis of jet fuel range branched alkanes [138]

structural types and textural properties were considered for aldol condensation of FUR and acetone. Kikhtyanin et al. studied aldol condensation reaction using HZSM5, HBEA, HMOR, and HSDUSY [139]. Among these zeolites HBEA was found to be the best for aldol condensation reaction due to the presence of wide pores and three-dimensional crystalline framework. The Brønsted acid sites are responsible for the transformation of FUR and acetone to FAc. However, further transformation of FAc to (FAc)$_2$ was different than the basic catalysts and was formed via dimerization of the olefinic FAc on the acid sites. During the reaction, the activity of the studied zeolites decreases due to the deposition of heavy carbonaceous species inside the micropores of the zeolites. However, catalytic activity was completely restored after calcination at a temperature of 530 °C. The different Sn-containing MFI (Sn-MFI) and BEA Lewis acid zeolites were also studied for aldol condensation of FUR and acetone [140]. Both of these zeolites were active for the aldol condensation reaction and produces aldol products with different selectivity. The Sn-Beta catalyst produced both aldol products, FAc and F$_2$Ac, with selectivities of 40% and of 22%, respectively. Contrarily, only FAc was produced over Sn-MFI catalyst. The difference in selectivity was attributed to the different pore geometries of Sn-Beta and Sn-MFI, resulting in shape-selective aldol condensation reaction of FUR and acetone. Additionally, the addition of water also influenced the product selectivity and led to the formation of FAc exclusively over Sn-Beta. In a different study, different metal organic frameworks (Cu-BTC, Fe-BTC, Mg-formate, and ZIF-8) possessing Lewis acid sites were investigated for aldol condensation of FUR and acetone [141]. It was reported that the MOF with exclusively Lewis acid sites showed poor catalytic activity for aldol condensation. A fairly good activity of Fe-BTC MOF was attributed to the presence of weak Brønsted acid sites, which were formed due to the existence of structural defects or due to the interaction of Fe^{3+} cation with surrounding water molecules resulting in the formation of H$^+$ ions. The formation of (FAc)$_2$ confirms the presence of Brønsted acid sites. The zeolites modified and/or ion exchanged with alkali metals are reported as active for the aldol condensation reactions. Kikhtyanin et al. reported the effect of chemical composition and textural properties of zeolites on the performance in aldol condensation reactions of FUR and acetone [142]. They have prepared a series of K-mollified Y and USY zeolites of different Si/Al ratio. The K-impregnated low-alumina-content Y zeolite showed higher selectivity to FAcOH and F$_2$Ac, whereas K-Y (2.5)

produced FAc (>85%) as the primary product. The residual acid sites in low Si/Al Y zeolites caused fast dehydration of FAcOH forming FAc, whereas strong basic sites of K-impregnated and high Si/Al ratio zeolites promote second condensation step to produce F_2Ac. In case of USY zeolite, K_2O species were formed by thermal activation due to the presence of a lower amount of ion-exchangeable proton sites in mesoporous and defective crystalline framework of USY. The K_2O species as the strong basic sites in K-impregnated USY causes higher activity in aldol condensation and occurrence of the second condensation step. Kikhtyanin et al. also studied the aldol condensation reaction of FUR and acetone using K-containing BEA zeolite prepared by ion exchange and combined ion exchanged and impregnation methods [143]. The K-BEA zeolite prepared by ion-exchanged method showed low activity than the K-BEA zeolite prepared by combined ion-exchanged and impregnation method. The strong basic sites were formed by the combined ion-exchanged and impregnation method due to the formation of K_2O cluster on the zeolite. The strong basic sites exhibit higher activity for aldol condensation reaction. Moreover, this K-BEA zeolite limits the deposition of carbonaceous species and offers better catalyst stability during reaction. Li et al. studied the aldol condensation of FUR and acetone using K-promoted Sn-MFI zeolites [144]. The basicity of Sn-MFI increases by addition of K resulting in remarkable change in production distribution. The pure Sn-MFI produces only C_8 (FAc) aldol product, whereas both C_8 (FAc) and C_{13} (F_2Ac) aldol products were formed with K-promoted Sn-MFI catalysts (Table 7). Moreover, the addition of K improves the water resistance capability of K-promoted Sn-MFI zeolite than the parent Sn-MFI zeolite. The K-promoted Sn-MFI promotes the formation of C_{18} product in the presence of water. Xiao-ming et al. studied the aldol condensation reaction of FUR and acetone using MgO/NaY catalyst to produce jet fuel intermediates [145]. The performance of MgO/NaY catalysts depends on the MgO loading, and 20% MgO/NaY showed higher activity with condensation product yield of 98.6% at 99.6% FUR conversion. The selectivity of F_2Ac enhances with the increase of FUR-to-acetone ratio with a slight decline of the reaction rate. This catalyst deactivates gradually due to the formation of inactive $Mg(OH)_2$. However, the spent catalyst showed good regeneration capability after heat treatment. CaO-loaded HZSM-5 (Ca/ZSM-5) catalyst was also studied for aldol condensation of FUR and acetone in the presence of lower dosages of water [146]. The catalyst activity was related to the formation of CaO species. The Ca/ZSM-5 catalyst showed no activity in the absence of water. The excess water favors the formation of FAc and inhibits the formation of F_2Ac. Highest yields of FAc (38.4 mol%) and F_2Ac (60.2 mol%) were obtained with acetone-to-FUR mole ratio of 0.8:1 and water content of 29.7 wt%. The catalyst deactivated due to the leaching of CaO from the Ca/ZSM-5 catalyst, and the catalyst activity was restored appreciably by reloading of CaO.

Tandem catalysis empowers multiple consecutive reactions to be performed in one pot and one step at similar or identical conditions. This strategy is an example of effective process intensification for chemical process by removing expensive separation steps and enhancing energy efficiency [147]. The tandem reactions require a catalytic material of two or more types of active sites to facilitate

individual reaction steps. Moreover, the distribution of different types of active sites are tailored for a specific reaction. Cho et al. demonstrated the performance of zeolite-encapsulated Pt nanoparticles for tandem aldol condensation reaction and hydrogenation aldol condensation products [148]. HZSM-5-encapsulated Pt nanoparticle showed higher selectivity for tandem reaction of aldol condensation and hydrogenation of the aldol products. A combined yield of FAc hydrogenated products of 87%. In contrast, Pt nanoparticle supported on HZSM-5 promotes the FUR conversion by hydrogenation, decarbonylation, and hydrodeoxygenation. Moreover, the encapsulated Pt nanoparticles offer superior resistance against sintering and leaching. The authors further demonstrated the tailoring of types of acid sites of Pt@ZSM-5 and choosing of appropriate solvent composition to manipulate the product distribution in tandem catalysis [148]. The tandem reaction of aldol condensation of FUR with acetone was studied in cyclohexane and EtOH solvents. Pt@HZSM-5 with Brønsted acid sites which are in intracrystalline mesopores selectively promotes the tandem aldol condensation of FUR and acetone and subsequent hydrogenation of aldol products by restricting the access of FUR to Pt sites. A total yield of 69% for hydrogenated aldol products was obtained. The Pt@ NaZSM-5 catalyst possesses both the Lewis acid sites and Brønsted acid sites in zeolitic micropores and intracrystalline mesopores and promotes the hydrogenation of FUR resulting in the formation of valeric acid and ethyl valerate. It was also reported that the concentration of ethyl alcohol influences the formation and selectivity of different products. Faba et al. demonstrate the performance of Pd catalyst supported on various basic mixed oxides, M_xN_yO (M = Mg, Ca; N = Zr, Al) for aldolization-hydrogenation reaction of FUR and acetone [149]. The catalyst (Ca-Zr) with lower concertation of basic sites showed poor performance for aldol reaction, whereas the catalyst (Pd/Mg-Al) with medium-strength basic sites showed higher activity. It was also reported that the selectivity of the desired product (F_2Ac) was related to the concentration of medium-strength basic sites. Xu et al. demonstrated the aldol condensation reaction followed by hydrogenation of aldol products using mesoporous Pd/cobalt-aluminate catalyst [150]. The bifunctional catalyst was efficient for the aldol condensation reaction, and ~ 99% FUR conversion was achieved (Table 7).

2.4.2 Reaction Mechanism

The base catalyzed aldol condensation proceeds with the abstraction of α-hydrogen from ketone (e.g., acetone) forming carbanion as shown in Fig. 12 [131, 133]. The ease of abstraction of hydrogen depends on the basicity of the active site and acidity of the hydrogen. Then, the carbanion formed consecutively attacks the carbonyl group of adsorbed FUR molecule. The FUR molecule adsorbs on acid sites by coordinating with the oxygen of the carbonyl group. An unstable β-hydroxyl ketone intermediate is formed due to the nucleophilic attack of carbanion. This unstable intermediate is readily dehydrated to form C_8 (FAc) and water molecule. The dehydration of hydroxy ketone intermediate and desorption of product regenerate active
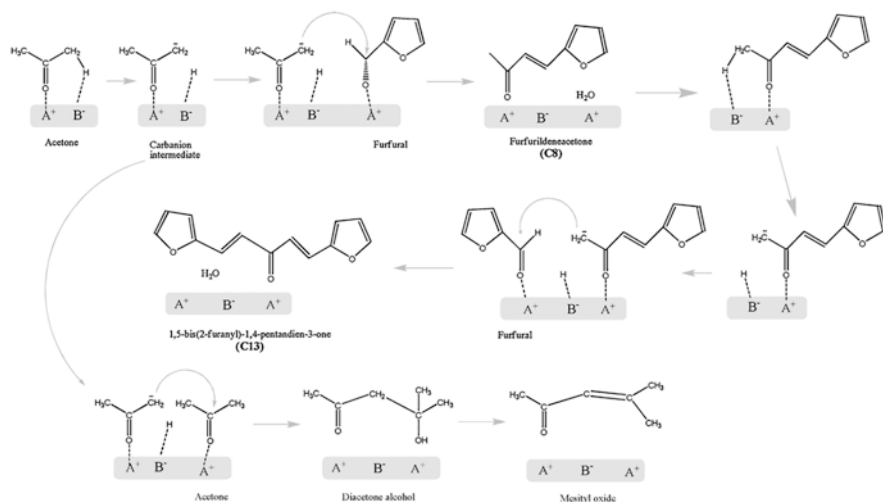
Fig. 12 Reaction mechanism of furfural and acetone aldol condensation reaction [131]

sites of the catalyst surface. In parallel self-condensation reaction pathway, the carbanion intermediate may attack another acetone molecule resulting in the formation of diacetone alcohol and mesityl oxide. In the similar way, the abstraction of α-hydrogen of C_8 product generates a carbanion intermediate that consecutively attacks the carbonyl group of another adsorbed FUR molecule followed by dehydration reaction resulting in the formation of C_{13} (F_2Ac) product. In case of cyclic ketone, the reaction proceeds in similar way as discussed above [137].

2.4.3 Aldol Condensation of 5-HMF

5-Hydroxymethylfurfural (5-HMF) possesses an aldehyde group and cannot undergo self-aldol condensation reaction due to the absence of α-hydrogen in its structure. However, 5-HMF can condense with other aldehydes and ketones (acetone). A general reaction pathway for the condensation of 5-HMF is shown in Fig. 13. Chheda and Dumesic presented a comprehensive overview for the production of liquid alkanes from biomass-derived carbohydrates which includes dehydration of carbohydrates and aldol condensation and hydrogenation of furfurals [151]. They demonstrated the aldol condensation reaction of HMF and acetone using various base catalysts and mixed oxide catalysts and combination of mixed oxide and metal catalysts. Among the various catalysts considered for condensation reaction, Mg-Al mixed oxide exhibited higher activity for aldol condensation, and MgO/ZrO_2 and MgO/TiO_2 also showed good activity for the condensation reaction. The optimum temperature for aldol condensation reaction was 353K, and further increase in reaction temperature decreases the yield of dimer product. The 5-HMF to acetone mole ratio plays a significant role in product selectivity. The presence of excess
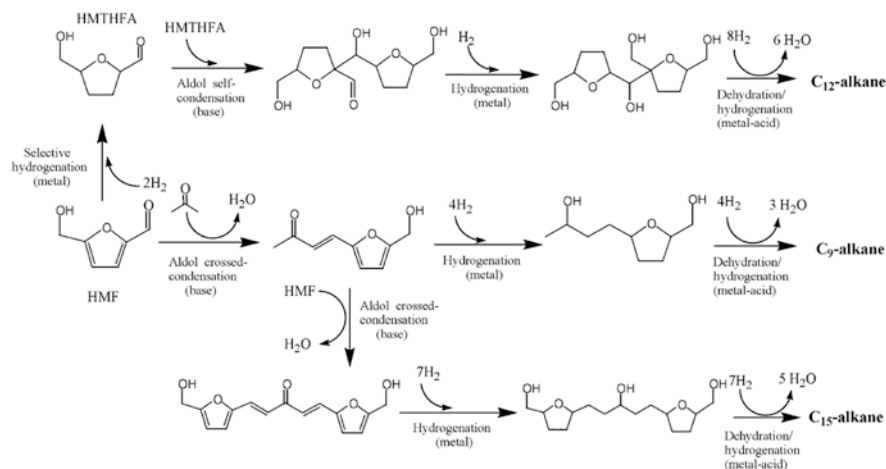
Fig. 13 Reaction pathways for the transformation of 5-HMF to diesel and jet fuel range alkanes

Table 8 Summary of aldol condensation of 5-HMF using different catalysts

Entry	Substrates	Reaction condition	Catalyst	Performance		Refs.
				Conv. (%)	Sel. (%)	
1.	HMF and Ac (1:1)	53 °C, 10 bar, 26 h, Org/Cat =6	5 wt% Pd/ MgO-ZrO$_2$	79	HAc: 18 H$_2$Ac:61	[152]
2.	HMF and Ac (1:10)	50 °C, 24 h, 50 mg cat	Mg-La (3:1)	100	HAc: 89	[154]
3.	HMF and Ac (2:1)	50 °C, 10 bar, 24 h, 0.5 g cat	Mg-Zr	68	HAc: 43.4 H$_2$Ac:16.1	[155]
4.	HMF and Ac (1:20)	130 °C, 6 h, 0.25 g cat	Hie-FAU-ZIF-8-15C	68.3	HAc: 67%	[156]
5.	HMF and Ac (1:258)	160 °C, 10 bar, 10 h, 0.15 g cat	Al$_{0.66}$-DTP@ ZIF-8	98	HAc: 84 H$_2$Ac:11	[157]
6.	HMF and Ac (1:20)	60 °C, 24 h, 100 mg cat	Zr(CO$_3$)$_x$ and Pd/Zeolite-β	100	HAc:92 (C9:40 and ethoxynonane: 60)	[158]
7.	HMF and Ac (1:20)	130 °C, 48 h, 0.5 g cat	NaX-NS	61	HAc:89.67 H2Ac:2.01	[159]
8.	HMF and Ac	140 °C, 7 h, HMF/cat = 2 (w/w)	Cu/MgAl$_2$O$_4$	100	HAc:78 H$_2$Ac:7	[160]

acetone leads to the formation of monomer species, whereas relatively lower concentration of acetone causes formation of dimer products. The same research group also demonstrated sequential aldol condensation and hydrogenation of 5-HMF using bifunctional catalyst, Pd/MgO-ZrO$_2$ [152]. The bifunctional catalysts transformed 5-HMF and acetone to water-soluble intermediates which can be further processed to produce liquid alkanes (Table 8). The Pd/MgO-ZrO$_2$ catalyst loses its activity after the cycle of aldol condensation and hydrogenation. However, the catalyst activity and selectivity of dimer were completely restored after calcination at

873 K. Huber et al. performed crossed aldol condensation reaction with acetone using mixed Mg-Al oxide catalyst at room temperature [153]. The aldol products were then hydrogenated and dehydrogenated to produce alkanes, and more than 40% carbon selectivity of C_9 product and 25% carbon selectivity of C_8 product were achieved. Bohre et al. studied the aldol condensation reaction of 5-HMF and acetone using series of basic magnesium and lanthanum (Mg-La) mixed oxides of different Mg/La molar ratio for the production of green diesel and jet fuel intermediates [154]. Among the various Mg-La catalysts, Mg-La catalyst of Mg/Al molar ratio of 3 (ML-3) exhibits superior catalyst activity, and 99% 5-HMF conversion and 89% yield of C_9 (HAc) product was achieved. The higher activity of ML-3 mixed oxide was attributed to the higher basic strength, moderate surface area, and strong interaction between Mg and Al in mixed oxide. Cueto et al. demonstrated the catalytic performance of basic mixed oxides (Mg-Al and Mg-Zr) for aqueous-phase 5-HMF and acetone aldol condensation [155]. MgZr showed the superior performance for aldol condensation reaction and selectivity of dimer aldol product (H_2Ac) was higher for this catalyst (Table 8). The high activity of this catalyst was attributed to the presence of optimum concentration of medium-strength acid-base sites. The stronger basic site promotes the retro-aldolization reaction which was identified as an important side reaction.

Suttipat et al. developed a highly efficient composite of hierarchical faujasite nanosheets and zeolite imidazolate framework-8 (Hie-FAU-ZIF-8) by stepwise deposition of ZIF-8 on modified zeolite surface and tested this nano-composite catalyst for the aldol condensation of 5-HMF and acetone [156]. The designed hierarchical nano-composite showed excellent acid-base catalytic properties for aldol condensation reaction with a yield of HAc of 66.8% in comparison to the isolated FAU and ZIF-8 (Table 8). The stepwise deposited Hie-FAU-ZIF-8 nano-composite develops a synergistic effect between the Na^+-stabilized zeolite framework and ZIF-8 catalytic functions, which causes higher activity and selectivity to target product. Malkar et al. reported a novel composite catalyst of aluminum-exchanged heteropoly acid (HPA) encapsulated inside the cage of ZIF-8 (Al0.66-DTP@ZIF-8) (DTP = dodecatungstophosphoric acid; ZIF = zeolitic imidazolate framework) for selective synthesis of HAc product by aldol condensation of 5-HMF and acetone [157]. The higher concentration of acid sites in HPA moiety and the smaller pore diameter of ZIF-8 in Al0.66-DTP@ZIF-8 composite catalyst lead to the selective formation of the HAc aldol product at high 5-HMF conversion of 98% in 10 h (Table 8). Bohre et al. reported a composite solid base ($Zr(CO_3)_x$) and bifunctional metal acid catalyst (Pd/Zeolite β) for the production of biofuel from 5-HMF in two steps [158]. The zirconium carbonate exhibits high catalytic activity and water tolerance for aldol condensation reaction of 5-HMF and acetone. Ninety-two percent yield of HAc aldol product was achieved at 100% 5-HMF conversion in the first step (Table 8). The bifunctional Pd/zeolite-β catalyst quantitatively converted the aldol product in ethanol to n-nonane and 1-ethoxynonane with 40 and 56% selectivity, respectively. The amine-grafted hierarchical FAU zeolite nanosheets with basic sites were also tested for aldol condensation of 5-HMF and acetone [159]. In this study, the synergistic effects of hierarchical porosity and the basicity of various

alkaline metals and amine surface modification on HMF conversion and selectivity of HAc and coke resistance of a nanosheet zeolite were demonstrated. Among the various alkaline metal exchange zeolites, NaX-NS showed the best performance in terms of HMF conversion and selectivity to HAc (Table 8). Pupovac and Palkovits reported copper supported on mesoporous magnesium aluminate as noble metal-free base bifunctional catalysts for sequential aldol condensation of 5-HMF and acetone and hydrogenation of aldol product [160]. The magnesium aluminate showed higher activity for aldol condensation reaction (100% HMF conversion) compared to zinc- and cobalt-based aluminates. The higher activity was correlated with the higher concentration of surface basic sites on magnesium aluminate. The $Cu/MgAl_2O_4$ catalyst selectively hydrogenates only the C-O, and furan ring remains unaffected during hydrogenation.

2.4.4 Claisen-Schmidt Condensation of Furfural and 5-HMF

The chalcones with structure of 1,3-diphenyl-2-propen-1-one belong to the flavo-noid family and are widespread in plants. Naturally occurring and synthetic chal-cones are associated with several biological activities such as antioxidant, anti-inflammatory, antibacterial, antihyperglycemic, antifungal, antimalarial, anti-cancer, etc. [161, 162]. The furan-based chalcones or furanochalcones are produced by the Claisen-Schmidt condensation between FUR derivatives and acetophenones using various base catalysts.

Arias et al. described the synthesis of furanochalcones by Claisen-Schmidt con-densation reaction of 5-HMF and various substituted acetophenones using different solid acid catalysts (MgO, Al/Mg mixed oxide (HTc) and hydrated A/Mg mixed oxide (HTr)) [161]. The calcined HTc possesses Lewis acid sites, whereas hydrated HTr is associated with Brønsted acidity. These three catalysts showed high activity for the condensation reaction in the absence of solvent. However, this catalyst deac-tivates very fast in the absence of solvent due to the adsorption of HMF and furano-chalcones on the catalyst surface. The polarity of solvent plays a significant role in catalyst stability, activity, and product selectivity. The condensation reaction per-formed in the presence of high-polarity solvent mixture such as ethanol-water exhibited high 5-HMF conversion and selectivity of furanochalcones using HTc and HTr mixed oxide catalysts. However, MgO deactivates fast in water-based solvent mixture due to the formation of inactive $Mg(OH)_2$. Yadav et al. demonstrated the Claisen-Schmidt condensation reaction of FUR and acetophenone using various solid base catalysts [162]. The following solid base catalysts were studied for the condensation reaction: CaO, 15w% Al_2O_3 supported on CaO, MgO, and SrO, hydrated hydrotalcite (HHT), and calcined hydrotalcite (CHT) with different ratios of Mg/Al. Among these solid base catalysts, 15w% Al_2O_3/CaO showed superior activity giving maximum FUR conversion of 98.5% within 2 h of reaction (Table 9). Other catalysts showed poor activity for condensation reaction. The 15w% Al_2O_3/CaO showed marginal deactivation after recycling for three times.

Table 9 Summary of Claisen-Schmidt condensation of furfural and 5-HMF using different catalysts

Entry	Substrates	Reaction condition	Catalyst	Performance Conv. (%)	Sel. (%)	Yield (%)	Refs.
1.	HMF and AcPh (1:1)	90 °C, 5 h, EtOH:H2O:1:1	HTc	99	100	99	[37]
2.	FUR and AcPh (1:2)	120 °C, 2 h	15 w% Al_2O_3/CaO	98.5	100	98.5	[38]

3 Conclusions

Nanocomposite materials have developed as green and sustainable nano-catalysts to offer new opportunities for the growth of the chemical industry. Thus, the majority of the developments toward a better understanding of metal-based nanocomposites in terms of their catalytic role in a particular reaction are discussed in this chapter. The metal-metal oxide nanocomposite catalysts are successfully described for the selective transformation of the furanics to biofuels and value-added chemicals. The nanocomposites exhibited an enhanced physicochemical and structural properties due to the combination of different types of components, formation of the active site, the superior catalytic activity, and selectivity toward the desired product. Especially, these materials have shown a high specific surface area, smaller particle size, more numbers of acid-base sites, high thermal stability, and recyclability. We also illustrated the general reaction pathways for the selective transformation of the furanics into the desired product.

References

1. Li X, Jia P, Wang T (2016) Furfural: a promising platform compound for sustainable production of C_4 and C_5 chemicals. ACS Catal 6:7621–7640
2. Nakagawa Y, Tamura M, Tomishige K (2013) Catalytic reduction of biomass-derived furanic compounds with hydrogen. ACS Catal 3:2655–2668
3. Perez RF, Fraga MA (2014) Hemicellulose-derived chemicals: one-step production of furfuryl alcohol from xylose. Green Chem 16:3942–3950
4. Biswas P, Lin J-H, Kang J, Guliants VV (2014) Vapor phase hydrogenation of 2-methylfuran over noble and base metal catalysts. Appl Catal A Gen 475:379–385
5. Alonso-Fagúndez N, Granados ML, Mariscal R, Ojeda M (2012) Selective conversion of furfural to maleic anhydride and furan with VO x/Al_2O_3 catalysts. Chem Sus Chem 5:1984–1990

6. Xu W, Wang H, Liu X, Ren J, Wang Y, Lu G (2011) Direct catalytic conversion of furfural to 1,5-pentanediol by hydrogenolysis of the furan ring under mild conditions over Pt/Co_2AlO_4 catalyst. Chem Commun 47:3924–3926

7. Thananatthanachon T, Rauchfuss TB (2010) Efficient production of the liquid fuel 2,5-dimethylfuran from fructose using formic acid as a reagent. Angew Chemie Int Ed 49:6616–6618

8. Lichtenthaler FW (2002) Unsaturated O- and N-Heterocycles from Carbohydrate Feedstocks. Acc Chem Res 35:728–737

9. Kaye S, Fox JM, Hicks FA, Buchwald SL (2001) The use of catalytic amounts of cucl and other improvements in the benzyne route to biphenyl-based phosphine ligands. Adv Synth Catal 343:789–794

10. Mallesham B, Sudarsanam P, Raju G, Reddy BM (2013) Design of highly efficient Mo and W-promoted SnO2 solid acids for heterogeneous catalysis: Acetalization of bio-glycerol. Green Chem 15:478–489

11. Mallesham B, Sudarsanam P, Reddy BM (2014) Eco-friendly synthesis of bio-additive fuels from renewable glycerol using nanocrystalline SnO_2-based solid acids. Cat Sci Technol 4:803–813

12. Klinke HB, Thomsen AB, Ahring BK (2004) Inhibition of ethanol-producing yeast and bacteria by degradation products produced during pre-treatment of biomass. Appl Microbiol Biotechnol 66:10–26

13. Kango S, Kalia S, Celli A, Njuguna J, Habibi Y, Kumar R (2013) Surface modification of inorganic nanoparticles for development of organic-inorganic nanocomposites-A review. Prog Polym Sci 38:1232–1261

14. Cai S, Wang D, Niu Z, Li Y (2013) Progress in organic reactions catalyzed by bimetallic nanomaterials. J Catal 34:1964–1974

15. Katta L, Sudarsanam P, Mallesham B, Reddy BM (2012) Preparation of silica supported ceria-lanthana solid solutions useful for synthesis of 4-methylpent-1-ene and dehydroacetic acid. Cat Sci Technol 2:995–1004

16. Sudarsanam P, Mallesham B, Prasad AN (2013) Synthesis of bio–additive fuels from acetalization of glycerol with benzaldehyde over molybdenum promoted green solid acid catalysts. Fuel Process Technol 106:539–545

17. Sudarsanam P, Mallesham B, Durgasri DN, Reddy BM (2014) Physicochemical characterization and catalytic CO oxidation performance of nanocrystalline Ce-Fe mixed oxides. RSC Adv 4:11322–11330

18. Sudarsanam P, Mallesham B, Rangaswamy A, Rao BG, Bhargava SK, Reddy BM (2016) Promising nanostructured gold/metal oxide catalysts for oxidative coupling of benzylamines under eco-friendly conditions. J Mol Catal A Chem 412:47–55

19. Sudarsanam P, Hillary B, Mallesham B, Rao BG, Amin MH, Nafady A, Alsalme AM, Reddy BM, Bhargava SK (2016) Designing CuOx nanoparticle-decorated CeO_2 nanocubes for catalytic soot oxidation: role of the nanointerface in the catalytic performance of heterostructured nanomaterials. Langmuir 32:2208–2215

20. Mallesham B, Govinda Rao B, Reddy BM (2016) Production of biofuel additives by esterification and acetalization of bioglycerol. Comptes Rendus Chim 19:1194–1202

21. Navgire ME, Gogoi P, Mallesham B, Rangaswamy A, Reddy BM, Lande MK (2016) β-Cyclodextrin supported MoO_3–CeO_2 nanocomposite material as an efficient heterogeneous catalyst for degradation of phenol. RSC Adv 6:28679–28687

22. Motl NE, Smith AF, Desantis CJ, Skrabalak SE (2014) Engineering plasmonic metal colloids through composition and structural design. Chem Soc Rev 43:3823–3834

23. Leung KCF, Xuan S, Zhu X, Wang D, Chak CP, Lee SF, Hob WKW, Chung BCT (2012) Gold and iron oxide hybrid nanocomposite materials. Chem Soc Rev 41:1911–1928

24. Mallesham B, Sudarsanam P, Reddy BM (2014) Production of biofuel additives from esterification and acetalization of bioglycerol over SnO_2-based solid acids. Ind Eng Chem Res 53:18775–18785

25. Sudarsanam P, Mallesham B, Reddy PS, Großmann D, Grünert W, Reddy BM (2014) Nano-Au/CeO$_2$ catalysts for CO oxidation: influence of dopants (Fe, La and Zr) on the physicochemical properties and catalytic activity. Appl Catal B Environ 144:900–908

26. Mallesham B, Sudarsanam P, Reddy BVS, Reddy BM (2016) Development of cerium promoted copper-magnesium catalysts for biomass valorization: selective hydrogenolysis of bioglycerol. Appl Catal B Environ 181:47–57

27. Mallesham B, Sudarsanam P, Reddy BVS, Rao BG, Reddy BM (2018) Nanostructured Nickel/Silica catalysts for continuous flow conversion of levulinic acid to γ-valerolactone. ACS Omega 3:16839–16849

28. Sasmal AK, Pal J, Sahoo R, Kartikeya P, Dutta S, Pal T (2016) Superb dye adsorption and dye-sensitized change in Cu$_2$O–Ag crystal faces in the dark. J Phys Chem C 120:21580–21588

29. Sasmal AK, Dutta S, Pal T (2016) A ternary Cu$_2$O-Cu-CuO nanocomposite: a catalyst with intriguing activity. Dalt Trans 45:3139–3150

30. Pal J, Ganguly M, Dutta S, Dutta S, Mondal C, Negishi Y, Pal T (2014) Hierarchical Au–CuO nanocomposite from redox transformation reaction for surface enhanced raman scattering and clock reaction. Cryst Eng Comm 16:883–893

31. Sasmal AK, Mondal C, Sinha AK, Gauri SS, Pal J, Aditya T, Ganguly M, Dey S, Pal T (2014) Fabrication of superhydrophobic copper surface on various substrates for roll-off, self-cleaning, and water/oil separation. ACS Appl Mater Interfaces 6:22034–22043

32. Zaera F (2010) The new materials science of catalysis: toward controlling selectivity by designing the structure of the active site. J Phys Chem Lett 1:621–627

33. Zhong CJ, Maye MM (2001) Core–Shell assembled nanoparticles as catalysts. Adv Mater 13:1507–1511

34. Lee I, Albiter MA, Zhang Q, Ge J, Yin Y, Zaera F (2011) New nanostructured heterogeneous catalysts with increased selectivity and stability. Phys Chem Chem Phys 13:2449–2456

35. Shi J (2013) On the synergetic catalytic effect in heterogeneous nanocomposite catalysts. Chem Rev 113:2139–2181

36. Ray C, Pal T (2017) Retracted article: recent advances of metal–metal oxide nanocomposites and their tailored nanostructures in numerous catalytic applications. J Mater Chem A 5:9465–9487

37. Rao BG, Sudarsanam P, Mallesham B, Reddy BM (2016) Highly efficient continuous-flow oxidative coupling of amines using promising nanoscale CeO$_2$-M/SiO$_2$ (M = MoO$_3$ and WO$_3$) solid acid catalysts. RSC Adv 6:95252–95262

38. Reddy PS, Sudarsanam P, Mallesham B, Raju G, Reddy BM (2011) Acetalisation of glycerol with acetone over zirconia and promoted zirconia catalysts under mild reaction conditions. J Ind Eng Chem 17:377–381

39. Sudarsanam P, Hillary B, Deepa DK, Amin MH, Mallesham B, Reddy BM, Bhargava SK (2015) Highly efficient cerium dioxide nanocube-based catalysts for low temperature diesel soot oxidation: the cooperative effect of cerium- and cobalt-oxides. Cat Sci Technol 5:3496–3500

40. Mallesham B, Rangaswamy A, Rao BG, Rao TV, Reddy BM (2020) Solvent-free production of glycerol carbonate from bioglycerol with urea over nanostructured promoted SnO$_2$ catalysts. Catal Letters 150:3626–3641

41. Guzman J, Carrettin S, Fierro-Gonzalez JC, Hao Y, Gates BC, Corma A (2005) CO oxidation catalyzed by supported gold: cooperation between gold and nanocrystalline rare-earth supports forms reactive surface superoxide and peroxide species. Angew Chemie Int Ed 44:4778–4781

42. Zorn K, Giorgio S, Halwax E, Henry CR, Grönbeck H, Rupprechter G (2011) CO oxidation on technological Pd−Al$_2$O$_3$ catalysts: oxidation state and activity. J Phys Chem C 115:1103–1111

43. Oh S-H, Hoflund GB (2006) Chemical state study of palladium powder and ceria-supported palladium during low-temperature CO oxidation. J Phys Chem A 110:7609–7613

44. Yi Z, Xu H, Hu D, Yan K (2019) Facile synthesis of supported Pd catalysts by chemical fluid deposition method for selective hydrogenation of biomass-derived furfural. J Alloys Compd 799:59–65

45. Bhogeswararao S, Srinivas D (2015) Catalytic conversion of furfural to industrial chemicals over supported Pt and Pd catalysts. J Catal 327:65–77

46. Durndell LJ, Zou G, Shangguan W, Lee AF, Wilson K (2019) Structure-reactivity relations in ruthenium catalysed furfural hydrogenation. Chem Cat Chem 11:3927–3932

47. Kurchenko YV, Simakova IL, Demidova YS, Panchenko VN, Timofeeva MN (2019) Hydrogenation of furfural to furfuryl alcohol in the presence of Ru-Containing catalysts based on new zeolite-like materials. Catal Ind 11:130–137

48. Nakagawa Y, Takada K, Tamura M, Tomishige K (2014) Total hydrogenation of furfural and 5-Hydroxymethylfurfural over supported Pd–Ir alloy catalys. ACS Catal 4:2718–2726

49. Guerrero-Torres A, Jiménez-Gómez CP, Cecilia JA, García-Sancho C, Franco F, Quirante-Sánchez JJ, Maireles-Torres P (2019) Ni supported on sepiolite catalysts for the hydrogenation of furfural to value-added chemicals: influence of the synthesis method on the catalytic performance. Top Catal 62:535–550

50. Wang Y, Lu Y, Cao Q, Fang W (2020) A magnetic CoRu–CoO$_X$ nanocomposite efficiently hydrogenates furfural to furfuryl alcohol at ambient H$_2$ pressure in water. Chem Commun 56:3765–3768

51. Xu L, Nie R, Lyu X, Li Y, Wang J, Lu X (2020) Selective hydrogenation of furfural to furfuryl alcohol without external hydrogen over N-doped carbon confined Co catalysts. Fuel Process Technol 197:106205

52. Zhou X, Feng Z, Guo W, Liu J, Li R, Chen R, Huang J (2019) Hydrogenation and hydrolysis of furfural to furfuryl alcohol, cyclopentanone, and cyclopentanol with a heterogeneous copper catalyst in water. Ind Eng Chem Res 58:3988–3993

53. Ramos R, Peixoto AF, Arias-Serrano BI, Soares OSGP, Pereira MFR, Kubička D, stina Freire C (2020) Catalytic transfer hydrogenation of furfural over Co$_3$O$_4$−Al$_2$O$_3$ hydrotalcite-derived catalyst. Chem Cat Chem 12:1467–1475

54. He J, Schill L, Yang S, Riisager A (2018) Catalytic transfer hydrogenation of bio-based furfural with NiO nanoparticles. ACS Sustain Chem Eng 6:17220–17229

55. He J, Nielsen MR, Hansen TW, Yang S, Riisager A (2019) Hierarchically constructed NiO with improved performance for catalytic transfer hydrogenation of biomass-derived aldehydes. Cat Sci Technol 9:1289–1300

56. Nguyen-Huy C, Lee J, Seo JH, Yang E, Lee J, Choi K, Lee H, Kim JH, Lee MS, Joo SH, Kwak JH, Lee JH, An K (2019) Structure-dependent catalytic properties of mesoporous cobalt oxides in furfural hydrogenation. Appl Catal A Gen 583:117125

57. Stucchi M, Alijani S, Manzoli M, Villa A, Lahti R, Galloni MG, Lassi U, Pratia L (2020) A Pt-Mo hybrid catalyst for furfural transformation. Catal Today 357:122–131

58. Wu ZL, Wang J, Wang S, Zhang YX, Bai GY, Ricardez-Sandoval L, Wang GC, Zhao B (2020) Controllable chemoselective hydrogenation of furfural by PdAg/C bimetallic catalysts under ambient operating conditions: an interesting Ag switch. Green Chem 22:1432–1442

59. Du J, Zhang J, Sun Y, Jia W, Si Z, Gao H, Tang X, Zeng X, Lei T, Liu S, Lin L (2018) Catalytic transfer hydrogenation of biomass-derived furfural to furfuryl alcohol over in-situ prepared nano Cu-Pd/C catalyst using formic acid as hydrogen source. J Catal 368:69–78

60. Nguyen-Huy C, Lee H, Lee J, Kwak JH, An K (2019) Mesoporous mixed CuCo oxides as robust catalysts for liquid-phase furfural hydrogenation. Appl Catal A Gen 571:118–126

61. Shi D, Yang Q, Peterson C, Lamic-Humblot AF, Girardon JS, Griboval-Constant A, Stievano L, Sougrati MT, Briois V, Bagot PAJ, Wojcieszak R, Paul S, Marceau E (2019) Bimetallic Fe-Ni/SiO$_2$ catalysts for furfural hydrogenation: identification of the interplay between Fe and Ni during deposition-precipitation and thermal treatments. Catal Today 334:162–172

62. Rodiansono AMD, Mujiyanti DR, Santoso UT, Shimazu S (2018) Novel preparation method of bimetallic Ni-In alloy catalysts supported on amorphous alumina for the highly selective hydrogenation of furfural. Mol Catal 445:52–60

63. Yang Y, Chen L, Chen Y, Liu W, Feng H, Wang B, Zhang X, Wei M (2019) The selective hydrogenation of furfural over intermetallic compounds with outstanding catalytic performance. Green Chem 21:5352–5362

64. Tang F, Wang L, Dessie Walle M, Mustapha A, Liu YN (2020) An alloy chemistry strategy to tailoring the d-band center of Ni by Cu for efficient and selective catalytic hydrogenation of furfural. J Catal 383:172–180

65. Ruan L, Zhang H, Zhou M, Zhu L, Pei A, Wang J, Yang K, Zhang C, Xiao S, Chen BH (2020) A highly selective and efficient Pd/Ni/Ni(OH)2/C catalyst for furfural hydrogenation at low temperatures. Mol Catal 480:110639

66. Mironenko RM, Talsi VP, Gulyaeva TI, Trenikhin MV, Belskaya OB (2019) Aqueous-phase hydrogenation of furfural over supported palladium catalysts: effect of the support on the reaction routes. React Kinet Mech Catal 126:811–827

67. Zhang S, Yang X, Zheng K, Xiao R, Hou Q, Liu B, Ju M, Liu L (2019) In-situ hydrogenation of furfural conversion to furfuryl alcohol via aqueous-phase reforming of methanol. Appl Catal A Gen 581:103–110

68. Li F, Zhu W, Jiang S, Wang Y, Song H, Li C (2020) Catalytic transfer hydrogenation of furfural to furfuryl alcohol over Fe3O4 modified Ru/Carbon nanotubes catalysts. Int J Hydrog Energy 45:1981–1990

69. Maderuelo-Solera R, López-Asensio R, Cecilia JA, Jiménez-Gómez CP, García-Sancho C, Moreno-Tost R, Maireles-Torres P (2019) Catalytic transfer hydrogenation of furfural to furfuryl alcohol over calcined MgFe hydrotalcites. Appl Clay Sci 183:105351

70. Zhang Z, Pei Z, Chen H, Chen K, Hou Z, Lu X, Ouyang P, Fu J (2018) Catalytic in-situ hydrogenation of furfural over bimetallic Cu–Ni alloy catalysts in isopropanol. Ind Eng Chem Res 57:4225–4230

71. Niu H, Luo J, Li C, Wang B, Liang C (2019) Transfer hydrogenation of biomass-derived furfural to 2-methylfuran over CuZnAl catalysts. Ind Eng Chem Res 58:6298–6308

72. Sitthisa S, An W, Resasco DE (2011) Selective conversion of furfural to methylfuran over silica-supported Nisingle bondFe bimetallic catalysts. J Catal 284:90–101

73. Yan K, Chen A (2014) Selective hydrogenation of furfural and levulinic acid to biofuels on the ecofriendly Cu–Fe catalyst. Fuel 115:101–108

74. Seemala B, Cai CM, Kumar R, Wyman CE, Christopher P (2018) Effects of Cu–Ni bimetallic catalyst composition and support on activity, selectivity, and stability for furfural conversion to 2-methyfuran. ACS Sustain Chem Eng 6:2152–2161

75. Solanki BS, Rode CV (2019) Selective hydrogenation of 5-HMF to 2,5-DMF over a magnetically recoverable non-noble metal catalyst. Green Chem 21:6390–6406

76. Yang F, Mao J, Li S, Yin J, Zhou J, Liu W (2019) Cobalt–graphene nanomaterial as an efficient catalyst for selective hydrogenation of 5-hydroxymethylfurfural into 2,5-dimethylfuran. Cat Sci Technol 9:1329–1333

77. Sun G, An J, Hu H, Li C, Zuo S, Xia H (2019) Green catalytic synthesis of 5-methylfurfural by selective hydrogenolysis of 5-hydroxymethylfurfural over size-controlled Pd nanoparticle catalysts. Cat Sci Technol 9:1238–1244

78. Hu L, Li T, Xu J, He A, Tang X, Chu X, Xu J (2018) Catalytic transfer hydrogenation of biomass-derived 5-hydroxymethylfurfural into 2,5-dihydroxymethylfuran over magnetic zirconium-based coordination polymer. Chem Eng J 352:110–119

79. Sun K, Shao Y, Li Q, Liu Q, Wu W, Wang Y, Hu S, Xiang J, Liu Q, Hu X (2019) Cu-based catalysts for hydrogenation of 5-hydroxymethylfurfural: understanding of the coordination between copper and alkali/alkaline earth additives. Mol Catal 474:110407

80. Chen S, Ciotonea C, De Oliveira VK, Jérôme F, Wojcieszak R, Dumeignil F, Marceau E, Royer S (2020) Hydroconversion of 5-Hydroxymethylfurfural to 2,5-Dimethylfuran and 2,5-Dimethyltetrahydrofuran over non-promoted Ni/SBA-15. Chem Cat Chem 12:2050–2059

81. Lange JP, Van Der Heide E, Van Buijtenen J, Price R (2012) Furfural—a promising platform for lignocellulosic biofuels. Chem Sus Chem 5:150–166

82. An Z, Wang W, Dong S, He J (2019) Well-distributed cobalt-based catalysts derived from layered double hydroxides for efficient selective hydrogenation of 5-hydroxymethyfurfural to 2,5-methylfuran. Catal Today 319:128–138

83. Zhang Z, Wang C, Gou X, Chen H, Chen K, Lu X, Ouyanga P, Fu J (2019) Catalytic in-situ hydrogenation of 5-hydroxymethylfurfural to 2,5-dimethylfuran over Cu-based catalysts with methanol as a hydrogen donor. Appl Catal A Gen 570:245–250

84. Talpade AD, Tiwari MS, Yadav GD (2019) Selective hydrogenation of bio-based 5-hydroxy-methyl furfural to 2,5-dimethylfuran over magnetically separable Fe-Pd/C bimetallic nano-catalyst. Mol Catal 465:1–15

85. Ohyama J, Hayashi Y, Ueda K, Yamamoto Y, Arai S, Satsuma A (2016) Effect of FeOx modi-fication of Al_2O_3 on its supported Au catalyst for hydrogenation of 5-Hydroxymethylfurfural. J Phys Chem C 120. 15129–151362–9

86. Mhadmhan S, Franco A, Pineda A, Reubroycharoen P, Luque R (2019) Continuous flow selective hydrogenation of 5-hydroxymethylfurfural to 2,5-dimethylfuran using highly active and stable Cu–Pd/Reduced graphene oxide. ACS Sustain Chem Eng 7:14210–14216

87. Esen M, Akmaz S, Koç SN, Gürkaynak MA (2019) The hydrogenation of 5-hydroxymethyl-furfural (HMF) to 2,5-dimethylfuran (DMF) with sol–gel Ru-Co/SiO2 catalyst. J Sol-Gel Sci Technol 91:664–672

88. Sarkar C, Koley P, Shown I, Lee J, Liao YF, An K, Tardio J, Nakka L, Chen KH, Mondal J (2019) Integration of interfacial and alloy effects to modulate catalytic performance of metal–organic-framework-derived Cu–Pd nanocrystals toward Hydrogenolysis of 5-Hydroxymethylfurfural. ACS Sustain Chem Eng 7:10349–10362

89. Yang P, Xia Q, Liu X, Wang Y (2017) Catalytic transfer hydrogenation/hydrogenolysis of 5-hydroxymethylfurfural to 2,5-dimethylfuran over Ni-Co/C catalyst. Fuel 187:159–166

90. Han W, Tang M, Li J, Li X, Wanga J, Zhou L, Yang Y, Wang Y, Ge H (2020) Selective hydro-genolysis of 5-hydroxymethylfurfural to 2,5-dimethylfuran catalyzed by ordered mesoporous alumina supported nickel-molybdenum sulfide catalysts. Appl Catal B Environ 268:118748

91. Ledesma B, Juárez J, Mazarío J, Domine M, Beltramone A (2021) Bimetallic platinum/irid-ium modified mesoporousA (2016) effect of FeOx modification of Al_2O_3 on its supported Au catalyst for hydrogenation of 5-Hydroxymethylfurfural. J Phys Chem C 120:15129–15136

92. Siddiqui N, Roy AS, Goyal R, Khatun R, Pendem C, Chokkapu AN, Bordoloi A, Bal R (2018) Hydrogenation of 5-hydroxymethylfurfural to 2,5 dimethylfuran over nickel sup-ported tungsten oxide nanostructured catalyst. Sustain Energy Fuels 2:191–198

93. Brzezińska M, Keller N, Ruppert AM (2020) Self-tuned properties of CuZnO catalysts for hydroxymethylfurfural hydrodeoxygenation towards dimethylfuran production. Cat Sci Technol 10:658–670

94. Srivastava S, Jadeja GC, Parikh JK (2018) Optimization and reaction kinetics stud-ies on copper-cobalt catalyzed liquid phase hydrogenation of 5-hydroxymethylfurfural to 2,5-Dimethylfuran. Int J Chem React Eng 16:1–16

95. Lan J, Chen Z, Lin J, Yin G (2014) Catalytic aerobic oxidation of renewable furfural to maleic anhydride and furanone derivatives with their mechanistic studies. Green Chem 16:4351–4358

96. Li X, Ko J, Zhang Y (2018) Highly efficient gas-phase oxidation of renewable furfu-ral to maleic anhydride over plate vanadium phosphorus oxide catalyst. Chem Sus Chem 11:612–618

97. Santander P, Bravo L, Pecchi G, Karelovic A (2020) The consequences of support identity on the oxidative conversion of furfural to maleic anhydride on vanadia catalysts. Appl Catal A Gen 595:117513

98. Rezaei M, Najafi Chermahini A, Dabbagh HA, Saraji M, Shavar A (2019) Furfural oxidation to maleic acid with H2O2 by using vanadyl pyrophosphate and zirconium pyrophosphate supported on well-ordered mesoporous KIT-6. J Environ Chem Eng 7:102855

99. Serrano A, Calviño E, Carro J, Sánchez-Ruiz MI, Cañada FJ, Martínez AT (2019) Complete oxidation of hydroxymethylfurfural to furandicarboxylic acid by aryl-alcohol oxidase. Biotechnol Biofuels 12:217

100. Lou Y, Marinkovic S, Estrine B, Qiang W, Enderlin G (2020) Oxidation of furfural and furan derivatives to maleic acid in the presence of a simple catalyst system based on acetic acid and TS-1 and hydrogen peroxide. ACS Omega 5:2561–2568

101. Antonyraj CA, Jeong J, Kim B, Shin S, Kim S, Lee KY, Cho JK (2013) Selective oxidation of HMF to DFF using Ru/γ-alumina catalyst in moderate boiling solvents toward industrial production. J Ind Eng Chem 19:1056–1059

102. Nie J, Xie J, Liu H (2013) Efficient aerobic oxidation of 5-hydroxymethylfurfural to 2,5-diformylfuran on supported Ru catalysts. J Catal 301:83–91

103. Ren HF, Luo X, Zhang K, Cai Q, Liu CL, Dong WS (2020) Selective aerobic oxidation of 5-hydroxymethylfurfural to 2,5-dimethylfuran over heteroatom-doped ordered carbon supported Ru catalysts. J Porous Mater 27:1003–1012

104. Liu Y, Gan T, He Q, Zhang H, He X, Ji H (2020) Catalytic oxidation of 5-Hydroxymethylfurfural to 2,5-Diformylfuran over atomically dispersed ruthenium catalysts. Ind Eng Chem Res 59:4333–4337

105. Lai J, Zhou S, Cheng F, Guo D, Liu X, Xu Q, Yin D (2020) Efficient and selective oxidation of 5-Hydroxymethylfurfural into 2, 5-Diformylfuran catalyzed by magnetic vanadium-based catalysts with air as oxidant. Catal Letters 150:1301–1308

106. Ning L, Liao S, Sun Y, Yu L, Tong X (2018) The efficient oxidation of biomass-derived 5-Hydroxymethyl furfural to produce 2,5-Diformylfuran over supported cobalt catalysts. Waste and Biomass Valori 9:95–101

107. Gui Z, Saravanamurugan S, Cao W, Schill L, Chen L, Qi Z, Riisager A (2017) Highly selective aerobic oxidation of 5-Hydroxymethyl furfural into 2,5-Diformylfuran over Mn–Co binary oxides. Chemistry Select 2:6632–6639

108. Lv G, Chen S, Zhu H, Li M, Yang Y (2018) Pyridinic-nitrogen-dominated nitrogen-doped graphene stabilized Cu for efficient selective oxidation of 5-hydroxymethfurfural. Appl Surf Sci 458:24–31

109. Ma Y, Zhang T, Chen L, Cheng H, Qi Z (2019) Self-developed fabrication of manganese oxides microtubes with efficient catalytic performance for the selective oxidation of 5-Hydroxymethylfurfural. Ind Eng Chem Res 58:13122–13132

110. Nocito F, Ventura M, Aresta M, Dibenedetto A (2018) Selective oxidation of 5-(Hydroxymethyl) furfural to DFF using water as solvent and oxygen as oxidant with earth-crust-abundant mixed oxides. ACS Omega 3:18724–18729

111. Ventura M, Lobefaro F, de Giglio E, Distaso M, Nocito F, Dibenedetto A (2018) Selective aerobic oxidation of 5-Hydroxymethylfurfural to 2,5-Diformylfuran or 2-Formyl-5-furancarboxylic acid in water by using MgO·CeO₂ mixed oxides as catalysts. Chem Sus Chem 11:1305–1315

112. Yuan Z, Liu B, Zhou P, Zhang Z, Chi Q (2018) Aerobic oxidation of biomass-derived 5-hydroxymethylfurfural to 2,5-diformylfuran with cesium-doped manganese dioxide. Cat Sci Technol 8:4430–4439

113. Zhang W, Xie J, Hou W, Liu Y, Zhou Y, Wang J (2016) One-pot template-free synthesis of cu–MOR zeolite toward efficient catalyst support for aerobic oxidation of 5-Hydroxymethylfurfural under ambient pressure. ACS Appl Mater Interfaces 8:23122–23132

114. Fang R, Luque R, Li Y (2016) Selective aerobic oxidation of biomass-derived HMF to 2,5-diformylfuran using a MOF-derived magnetic hollow Fe–Co nanocatalyst. Green Chem 18:3152–3157

115. Pérez-Bustos HF, Lucio-Ortiz CJ, de la Rosa JR, de Haro del Río DA, Sandoval-Rangel L, Martínez-Vargas DX, Maldonado CS, Rodriguez-González V, Garza-Navarro MA, Morales-Leala FJ (2019) Synthesis and characterization of bimetallic catalysts Pd-Ru and

Pt-Ru supported on γ-alumina and zeolite FAU for the catalytic transformation of HMF. Fuel 239:191–201

116. Chatterjee M, Ishizaka T, Kawanami H (2016) Reductive amination of furfural to furfuryl-amine using aqueous ammonia solution and molecular hydrogen: an environmentally friendly approach. Green Chem 18:487–496

117. Dong C, Wang H, Du H, Peng J, Cai Y, Guo S, Zhang J, Samart C, Ding M (2020) Ru/HZSM-5 as an efficient and recyclable catalyst for reductive amination of furfural to furfu-rylamine. Mol Catal 482:110755

118. Zhou K, Chen B, Zhou X, Kang S, Xu Y, Wei J (2019) Selective synthesis of furfurylamine by reductive amination of furfural over raney cobalt. Chem Cat Chem 11:5562–5569

119. Gould NS, Landfield H, Dinkelacker B, Brady C, Yang X, Xu B (2020) Selectivity control in catalytic reductive amination of furfural to furfurylamine on supported catalysts. Chem Cat Chem 12:2106–2115

120. Zhu MM, Tao L, Zhang Q, Dong J, Liu YM, He HY, Cao Y (2017) Versatile CO-assisted direct reductive amination of 5-hydroxymethylfurfural catalyzed by a supported gold cata-lyst. Green Chem 19:3880–3887

121. Karve VV, Sun DT, Trukhina O, Yang S, Oveisi E, Luterbacher J, Queen WL (2020) Efficient reductive amination of HMF with well dispersed Pd nanoparticles immobilized in a porous MOF/polymer composite. Green Chem 22:368–378

122. Yuan H, Li JP, Su F, Yan Z, Kusema BT, Streiff S, Huang Y, Titus MP (2019) Reductive amination of furanic aldehydes in aqueous solution over versatile NiyAlOx catalysts. ACS Omega 4:2510–2516

123. Chen W, Sun Y, Du J, Si Z, Tang X, Zeng X, Lin L, Liu S, Lei T (2018) Preparation of 5-(Aminomethyl)-2-furanmethanol by direct reductive amination of 5-Hydroxymethylfurfural with aqueous ammonia over the Ni/SBA-15 catalyst. J Chem Technol Biotechnol 93:3028–3034

124. García-Ortiz A, Vidal JD, Climent MJ, Concepción P, Corma A, Iborra S (2019) Chemicals from biomass: selective synthesis of N-substituted furfuryl amines by the one-pot direct reductive amination of furanic aldehydes. ACS Sustain Chem Eng 7:6243–6250

125. Desai DS, Yadav GD (2019) Green synthesis of furfural acetone by solvent-free aldol con-densation of furfural with acetone over La2O3–MgO mixed oxide catalyst. Ind Eng Chem Res 58:16096–16105

126. Kikhtyanina O, Tišler Z, Velvarská R, Kubička D (2017) Reconstructed Mg-Al hydrotalcites prepared by using different rehydration and drying time: Physico-chemical properties and catalytic performance in aldol condensation. Appl Catal A Gen 536:85–96

127. Smoláková L, Frolich K, Kocík J, Kikhtyanin O, Čapek L (2017) Surface properties of Hydrotalcite-based Zn(Mg) Al oxides and their catalytic activity in aldol condensation of furfural with acetone. Ind Eng Chem Res 56:4638–4648

128. Kikhtyanin O, Korolova V, Spencer A, Dubnová L, Shumeiko B, Kubička D (2020) On the influence of acidic admixtures in furfural on the performance of MgAl mixed oxide catalysts in aldol condensation of furfural and acetone. Catal Today (In press). https://doi.org/10.1016/j.cattod.2020.04.022

129. Horaa L, Kelbichová V, Kikhtyanin O, Bortnovskiy O, Kubička D (2014) Aldol condensation of furfural and acetone over Mgsingle bondAl layered double hydroxides and mixed oxides. Catal Today 223:138–147

130. Sádaba I, Ojeda M, Mariscal R, Richards R, Granados ML (2011) Mg–Zr mixed oxides for aqueous aldol condensation of furfural with acetone: effect of preparation method and activa-tion temperature. Catal Today 167:77–83

131. Faba L, Díaz E, Ordó˜nez S (2012) Aqueous-phase furfural-acetone aldol condensation over basic mixed oxides. Appl Catal B Environ 113–114: 201–211

132. Sádaba I, Ojeda M, Mariscal R, Fierro JLG, Granados ML (2011) Catalytic and structural properties of co-precipitated Mg–Zr mixed oxides for furfural valorization via aqueous aldol condensation with acetone. Appl Catal B Environ 101:638–648

133. O'Neill RE, Vanoye L, De Bellefon C, Aiouache F (2014) Aldol-condensation of furfural by activated dolomite catalyst. Appl Catal B Environ 144:46–56

134. Xu M, Célérier S, Comparot JD, Rousseau J, Corbet M, Richard F, Clacens JM (2019) Upgrading of furfural to biofuel precursors via aldol condensation with acetone over magnesium hydroxide fluorides $MgF_{2-x}(OH)_x$. Cat Sci Technol 9:5793–5802

135. Li W, Su M, Yang T, Zhang T, Ma Q, Li S, Huang Q (2019) Preparation of two different crystal structures ofcerous phosphate as solid acid catalysts: theirdifferent catalytic performance in the aldolcondensation reaction between furfural andacetone. RSC Adv 9:16919–16928

136. Yang J, Li N, Li S, Wang W, Li L, Wang A, Wang X, Conga Y, Zhang T (2014) Synthesis of diesel and jet fuel range alkanes with furfural and ketones from lignocellulose under solvent free conditions. Green Chem 16:4879–4884

137. Ao L, Zhao W, Guan Y, Wang D, Liu K, Guo TT, Fan X, Wei X (2019) Efficient synthesis of C15 fuel precursor by heterogeneously catalyzed aldol-condensation of furfural with cyclopentanone. RSC Adv 9:3661–3668

138. Chen F, Li N, Li S, Yang J, Liu F, Wang W, Wang A, Cong Y, Wang X, Zhang T (2015) Solvent-free synthesis of C9 and C10 branched alkanes with furfural and 3-pentanone from lignocellulose. Catal Commun 59:229–232

139. Kikhtyanin O, Kelbichová V, Vitvarová D, Kubům M, Kubička D (2014) Aldol condensation of furfural and acetone on zeolites. Catal Today 227:154–162

140. Su M, Li W, Zhang T, Xin HS, Li S, Fan W, Ma L (2017) Production of liquid fuel intermediates from furfural via aldol condensation over Lewis acid zeolite catalysts. Cat Sci Technol 7:3555–3561

141. Kikhtyanina O, Kubička D, Čejka J (2015) Toward understanding of the role of Lewis acidity in aldol condensation of acetone and furfural using MOF and zeolite catalysts. Catal Today 243:158–162

142. Kikhtyanina O, Ganjkhanlou Y, Kubička D, Bulánek R, Čejka J (2018) Characterization of potassium-modified FAU zeolites and their performance in aldol condensation of furfural and acetone. Appl Catal A Gen 549:8–18

143. Kikhtyanina O, Bulánek R, Frolich K, Čejka J, Kubička D (2016) Aldol condensation of furfural with acetone over ion-exchanged and impregnated potassium BEA zeolites. J Mol Catal A Chem 424:358–368

144. Li W, Su M, Zhanga T, Ma Q, Fan W (2019) Production of liquid fuel intermediates from furfural via aldol condensation over potassium-promoted Sn-MFI catalyst. Fuel 237:1281–1290

145. Xiao-ming H, Qing Z, Tie-jun W, Qi-ying L, Long-long M, Zhang Q (2012) Production of jet fuel intermediates from furfural and acetone by aldol condensation over MgO/NaY. J Fuel Chem Technol 40:973–978

146. Fang X, Wang Z, Song W, Li S (2020) Aldol condensation of furfural with acetone over Ca/ZSM-5 catalyst with lower dosages of water and acetone. J Taiwan Inst Chem Eng 108:16–22

147. Cho HJ, Kim D, Li J, Su D, Xu B (2018) Zeolite-encapsulated Pt nanoparticles for tandem catalysis. J Am Chem Soc 140:13514–13520

148. Cho HJ, Kim D, Li J, Su D, Xu B (2020) Selectivity control in tandem catalytic furfural upgrading on zeolite-encapsulated Pt nanoparticles through site and solvent engineering. ACS Catal 10:4770–4779

149. Faba L, Díaz E, Ordóñez S (2011) Performance of bifunctional Pd/MxNyO (M = Mg, Ca; N = Zr, Al) catalysts for aldolization–hydrogenation of furfural–acetone mixtures. Catal Today 164:451–456

150. Xu W, Liu X, Ren J, Zhang P, Wang Y, Guo Y, Guo Y, Lu G (2010) A novel mesoporous Pd/cobalt aluminate bifunctional catalyst for aldol condensation and following hydrogenation. Catal Commun 11:721–726

151. Chheda JN, Dumesic JA (2007) An overview of dehydration, aldol-condensation and hydrogenation processes for production of liquid alkanes from biomass-derived carbohydrates. Catal Today 123:59–70

152. Barrett CJ, Chheda JN, Huber GW, Dumesic JA (2006) Single-reactor process for sequential aldol-condensation and hydrogenation of biomass-derived compounds in water. Appl Catal B Environ 66:111–118
153. Huber GW, Chheda JN, Barrett CJ, Dumesic JA (2005) Production of liquid alkanes by aqueous-phase processing of biomass-derived carbohydrates. Science 308:1446–1450
154. Bohre A, Alam MI, Avasthi K, Ruiz-Zepeda F, Likozar B (2020) Low temperature transformation of lignocellulose derived bioinspired molecules to aviation fuel precursor over magnesium–lanthanum mixed oxide catalyst. Appl Catal B Environ 276:119069–119080
155. Cueto J, Faba L, Díaz E, Ordóñez S (2017) Performance of basic mixed oxides for aqueous-phase 5-hydroxymethylfurfural-acetone aldol condensation. Appl Catal B Environ 201:221–231
156. Suttipat D, Wannapakdee W, Yutthalekha T, Ittisanronnachai S, Ungpittagul T, Phomphrai K, Bureekaew S, Wattanakit C (2018) Hierarchical FAU/ZIF-8 hybrid materials as highly efficient acid-base catalysts for aldol condensation. ACS Appl Mater Interfaces 10:16358–16366
157. Malkar RS, Daly H, Hardacre C, Yadav GD (2019) Aldol condensation of 5-Hydroxymethylfurfural to fuel precursor over novel aluminum exchanged-DTP@ZIF-8. ACS Sustain Chem Eng 7:16215–16224
158. Bohre A, Saha B, Abu-Omar MM (2015) Catalytic upgrading of 5-Hydroxymethylfurfural to drop-in biofuels by solid base and bifunctional metal–acid catalysts. Chem Sus Chem 8:4022–4029
159. Yutthalekha T, Suttipat D, Salakhum S, Thivasasith A, Nokbin S, Limtrakul J, Wattanakit C (2017) Aldol condensation of biomass-derived platform molecules over amine-grafted hierarchical FAU-type zeolite nanosheets (Zeolean) featuring basic sites. Chem Commun 53:12185–12188
160. Pupovac K, Palkovits R (2013) Cu/MgAl2O4 as bifunctional catalyst for aldol condensation of 5-Hydroxymethylfurfural and selective transfer hydrogenation. Chem Sus Chem 6:1–9
161. Arias KS, Climent MJ, Corma A, Iborra S (2016) Chemicals from biomass: synthesis of biologically active furanochalcones by claisen–schmidt condensation of biomass-derived 5-hydroxymethylfurfural (HMF) with acetophenones. Top Catal 59:1257–1265
162. Yadav GD, Yadav AR (2014) Novelty of claisen–schmidt condensation of biomass-derived furfural with acetophenone over solid super base catalyst. RSC Adv 4:63772–63778

Waste Valorization of Water Hyacinth Using Biorefinery Approach: A Sustainable Route

Priti V. Ganorkar, G. C. Jadeja, Jigisha K. Parikh, and Meghal A. Desai

Abstract The concept of biorefinery can pave way for shifting to the circular economy by developing unified and multipurpose processes that convert biomass or waste into value-added products. One such waste is water hyacinth, which has the profound effect on the aquatic life as well as poses a challenge across the world for its control. It is the proliferative aquatic weed adversely affecting the environment. However, it has been found that the plant can become a useful source of various chemicals and fuel if used judiciously. Some important groups of phytochemicals like organic acids, sterols, phenolic components, etc. are present in roots, stems, leaves, petioles and flowers of this plant and are known for antioxidant, antibacterial, antifungal and anticancer activities. All these extractives have potential applications in food, pharmaceutical and promoting functional foods. Apart from phytochemicals, water hyacinth is extensively utilized in making fuel, sorbent, biopolymer, carbon fibre, composites, vermicompost and supercapacitor. The concept of biorefinery can be implemented in the effective utilization of water hyacinth due to its potential use in various fields. This review article focuses on various aspects of utilization of water hyacinth, thereby projecting it as a potential biorefinery candidate.

1 Introduction

An ever-increasing demand for food, energy and water is a serious challenge the world is facing today with the burgeoning human population [1]. The anthropogenic climatic change is known for several serious effects on the environment. While actual collection of waste is ~60% in developing countries like India, Pakistan and

P. V. Ganorkar · G. C. Jadeja · J. K. Parikh (✉) · M. A. Desai (✉)
Chemical Engineering Department, Sardar Vallabhbhai National Institute of Technology, Surat, Gujarat, India

Bangladesh, most of the waste is not handled properly and thrown to open area or discarded in drains. The disposal of organic wastes to the open dumpsites severely affects the environmental, economic and social life. The expenditure towards managing the solid waste all over the world is expected to grow up to approx. US $375.5 billion by 2025 [2].

As per the report of the European Commission [3], 'The bioeconomy encloses the production of renewable biological resources and utilization of waste streams to derive useful products, such as food, bio-based products and bioenergy'. A proper utilization of waste is done by converting it into value-added products and its potential to replace fossil resources.

Annual municipal solid waste (MSW) generation is about 1.3 billion tonnes worldwide and is projected to reach around 2.2 billion tonnes annually by 2025 [3]. The organic fraction of municipal solid waste (OFMSW) and food supply chain waste (FSCW) has the potential of being converted to high-value-added compounds by using extraction and recovery methods and to produce fuel and chemicals. The extraction of high-value components from various FSCW has been achieved by employing various physical, chemical and biochemical processes [3]. Various bioactive compounds such as polyphenols, carotenoids, vitamins, antioxidants, flavonoids, fibre and pectin are generally used as additives in food industries, in pharmaceutical applications and for production of functional foods.

The concept of biorefinery can be used for shifting to the circular economy by developing unified and multipurpose processes upon using biomass or waste to derive useful products [4]. Biorefinery mainly focuses on the treatment of the biomass which includes organic residue, some energy-generating crops and aquatic biomass using physical, chemical or mechanical means so that a variety of products including phytochemicals and biofuels can be obtained. The sustainability of biorefinery encompasses the maximum use of biomass and minimum formation of waste [5].

In the case of countries which are at the developing stage, the waste biorefinery concept is very relevant for minimizing the economic investment and environmental burden generated due to energy fulfilment need and current waste disposal techniques. Waste biorefinery concept has gained importance in such nations as a sustainable alternative to prevailing waste management options and to produce thermal energy, electricity, fuel, valuable materials and chemicals for enabling the circular economies.

There are three types of biorefineries:

Phase I biorefinery: Single feedstock is used to obtain major product by using single process.
Phase II biorefinery: Single feedstock is utilized to obtain multiple major products by using multiple processes.
Phase III biorefinery: Multiple feedstocks are utilized to obtain multiple major products by using multiple processes.

Waste biorefinery approach includes the waste sources like municipal waste, animal waste, forestry waste, agricultural waste and industrial waste to generate

valuable products. Biorefineries are classified as agricultural, cereal, oil seeds, lignocellulosic, green, forestry and industrial- and municipal-based biorefineries, according to their ability to provide a variety of products such as fuel, energy, chemicals, materials, etc. [2, 6]. For obtaining such products, conversion processes such as biological conversion (anaerobic digestion, fermentation, enzymatic operation, aerobic digestion/composting, etc.), thermochemical conversion (liquefaction, pyrolysis, gasification, combustion, etc.), chemical conversion (hydrolysis, solvent extraction, supercritical conversion, transesterification, refuse derived fuel, etc.), and physical conversion (mechanical extraction, briquetting of biomass, distillation, etc.) are employed either alone or in combination [7, 8].

Along with sustainable waste management, waste biorefineries focus on significant economic and environmental benefits. Economic advantages include extraction of various forms of energy and useful products from raw material having no cost and elimination of requirement of landfill, thereby no requirement of land and no expenditure on landfill and new avenues for business development. Environmental benefits are reduced greenhouse gas release compared to prevailing treatment methods and conservation of natural resources like land, soil and ground water and fossil fuel [2].

Water hyacinth is among the category of the most proliferative macrophytes and has an adverse impact on aquatic environment. However, if utilized sensibly water hyacinth can become an important resource for biorefinery. Utilization of water hyacinth has been explored for phytoremediation, ethanol production, sorption of dyes and heavy metals, reinforcement for composites, supercapacitor electrode, generation of fuel, controlled drug release, preparation of biomanure, etc. [9]. Sindhu et al. [10] have pointed out the generation of valuable products such as enzyme, organic acids, fuel, biopolymer, carbon fibre, composites, biofertilizers, fish/animal feed, xylitol, vermicompost, supercapacitor electrode, etc. from this aquatic plant. Sharma et al. [11] focussed on the origin of water hyacinth, its distribution, ecology, biology and control measure along with its applications. Phytochemicals present in water hyacinth, threats posed by this plant and its control measures have been reported by Patel [12] along with its applications. The review on energy by Rezania et al. [13] has covered the utilization of water hyacinth as a co-fuel, briquette biomass, phytoremediation, composting and fertilizer, animal feed, furniture, etc. Malik [14] has given details on reproduction of this plant, its environmental implications and how to mitigate this issue. It also includes the application of water hyacinth as phytoremediation agent, power alcohol production, biogas production, compost, fish and animal feed. However, details regarding operating parameters for a specific process/application and its outcome were not given due importance. Further, cause-and-effect diagram can become instrumental in understanding the real scenario for a given application.

This chapter attempts to provide comprehensive representation of the work done till date which will help the readers to explore water hyacinth for a varied spectrum of applications. It includes the distribution of water hyacinth and its control measures in brief. Applications of water hyacinth for various products have been described in detail along with cause-and-effect diagram, also known as fishbone diagram or Ishikawa diagram.

2 Water Hyacinth

Aquatic weeds are generating a huge amount of biomass in the aquatic environment. Some of the well-known aquatic weed species such as *Eichhornia crassipes* (also known as water hyacinth), *Pistia stratiotes* and *Salvinia auriculata* are rapidly growing plants [15]. *Eichhornia crassipes* (Mart.) Solms belongs to the pickerel-weed family (Pontederiaceae) and is seen in the tropical and subtropical regions. It was first seen in Zimbabwe (1937). Afterwards its presence was seen in the Incomati River in Mozambique (1946) and the Zambezi river and some important rivers in Ethiopia (1956). In West Africa it was first found between 1997 and 2000. In Nigeria, almost all rivers are affected by the water hyacinth [16]. It has reached River Nile Delta in Egypt and also found in southwards. European countries like France, Hungary, the Netherlands, Belgium, Italy,the Czech Republic and Romania are also badly affected by this aquatic weed. In Asia, it is found in dense mat on freshwater wetlands of the Mekong Delta. It has also been observed in the Sundarbans forest of Bangladesh [17] and the Kaziranga National Park, India. A freshwater lake, Deepor Beel, formed by the Brahmaputra river, Assam (India), is highly affected because of this invasive plant [12]. In southern China, the weed has disturbed the economic, environmental and social life [18]. A catastrophic imbalance has been caused by water hyacinth in the Sacramento-San Joaquin River Delta in California [19]. It has origin from Amazon basin, but it spreads in lakes and is slowly moving to rivers as it prefers nutrient-enriched water to grow. It further proliferates by human activities throughout the world in Africa, Asia, Australia and North America [20] and the countries lying between 40°N and 40°S which include India, South Africa and the USA. The optimum range of pH to grow water hyacinth is 6–8, and temperature varies in the range of 1–40 °C, whereas the optimum growth is observed at 25–27.5 °C. The growth rate of water hyacinth depends mainly on nitrogen present in water bodies, and it increases with an increase in nitrogen content. It has attractive purple or blue flowers along with oval glossy leaves and bulbous petioles and used as an ornamental plant in many countries. *Eichhornia crassipes* is among the top ten worse aquatic weeds [21], and International Union for Conservation of Nature (IUCN) has listed it in 100 unwieldy invasive plants [22].

Water hyacinth has the potential to grow rapidly, and excessive growth of this weed destructs the biodiversity. Water hyacinth can cause oxygen depletion, as dense mat blocks the oxygen transfer from air to water and dissolved oxygen content in the water decreases dominantly apart from depleting the water body of nutrients. The low content of dissolved oxygen catalyses the manumission of phosphorous residing in the alluvium that is responsible for eutrophication, thereby further accelerating the growth of water hyacinth or algal bloom [23]. It can damage the navigation, fish production, power generation and irrigation [14]. The fisherman faces the problems because of low fish population, difficulty during access and loss of fishing equipment. In many rivers water hyacinth has negatively affected the navigation and water distribution system for agriculture. Water hyacinth dense mat slows the water flow in the irrigation channels leading to severe flooding. Many hydropower plants

are suffering from it as continuous removal of weed from water bodies before entering the turbine is expensive. The biomass generated after death of water hyacinth lowers the quality of drinkable water, and therefore the purification cost to get potable water is increased [12]. Water hyacinth provides breeding environment to the pest. The dense mat of water hyacinth is favourable for disease causing organisms like *Anopheles* mosquito responsible for malaria [24]. Water hyacinth provides cover for reptiles and poisonous snakes [12].

3 Water Hyacinth Control

Control of water hyacinth is very necessary as it adversely affects the aquatic life and environment. Control methods generally applied for removal of water hyacinth include mechanical, chemical and biological control. In mechanical control method, various machines are used to perform the operations such as cutting, shearing, shredding, crushing, pressing, lifting, conveying and transporting of the weed for the maximum removal. However, the use of mechanical means like heavy machines during these operations is very expensive [14]. Chemical herbicides like paraquat, diquat, glyphosate, amitrole and 2,4-dichlorophenoxyacetic acid (2, 4-D) have been utilized for controlling water hyacinth. But the long-term use of these herbicides deteriorates the water quality which is dangerous for aquatic life. In biological control, the weevils decrease potency of water hyacinth upon reducing the growth rate, controlling its reproduction as well as formation of flowers and seeds [25]. However, the growth of this invasive weed is difficult to control as it spreads rapidly either by vegetative propagation or by seeds [26]. Hence, water hyacinth should be further utilized for value-added products after its eradication under the concept of biorefinery. Biorefinery provides sustainable waste management along with generation of significant economic and environmental benefits [2]. Water hyacinth can be controlled by utilizing it for value-added products which is the emerging trend.

4 Potential Applications of Water Hyacinth

In spite of the fact that the water hyacinth is a notorious aquatic species, various researchers have found the potential of it for numerous applications. Water hyacinth is perennially available in huge amount despite of the attempts to curtail its growth; thus, there will be a continuous and steady supply for wide spectrum of its utility. Value-added products from *Eichhornia crassipes* include fuel [27], ethanol [28] and biopolymer [29]; biohydrogen, biobutanol, sorbent for heavy metals [30] and dyes [31], composites [32], enzymes [33], fuel with higher heating value (HHV or HCV) [34] and brick manufacturing [35]; and ultracapacitor electrode [36]. Some important extractives like organic acids, sterols and phenolic components from various morphological parts such as roots, stems, leaves, petioles and flowers of water

hyacinth have exhibited antioxidant, antibacterial, antifungal and anticancer activities. All these extractives have potential applications in food, pharmaceutical and promoting functional food. Each part of water hyacinth is useful in numerous applications. Figure 1 provides an overview regarding the utilization of various parts of water hyacinth in numerous fields. Cause-and-effect diagram has been prepared for different applications of water hyacinth such as phytochemical extraction, bioethanol production, biogas production, heavy metal and dye removal and bio-oil production. This diagram displays method required, machine applied, material utilized and measurement technique adopted to achieve defined goal.

4.1   Water Hyacinth as a Source of Phytochemicals

Various phytochemicals such as sterols, shikimic acid and polyphenols have been successfully extracted from different parts of water hyacinth. The recovery of valuable compounds improves the commercial value of natural resources and thereby supports the concept of biorefinery. Figure 2 presents the fishbone diagram for phytochemical extraction from water hyacinth.

Phytochemicals from various sources of plant materials have been efficiently isolated using solvents under supercritical conditions [37]. Carbon dioxide is a preferred solvent as its critical temperature is near room temperature (~31 °C) and critical pressure is moderate (~74 bar). Also, it possesses higher diffusivity and is cheap,
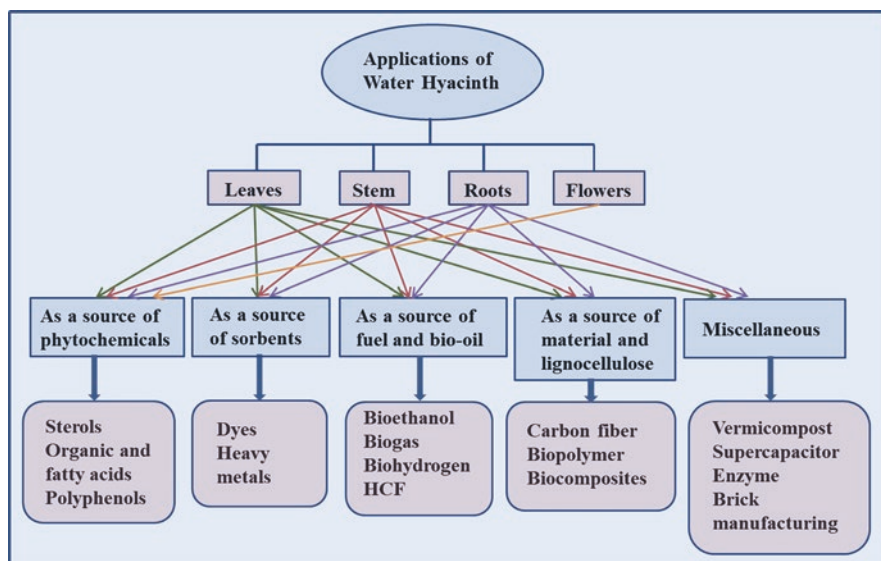
Fig. 1   Applications of water hyacinth
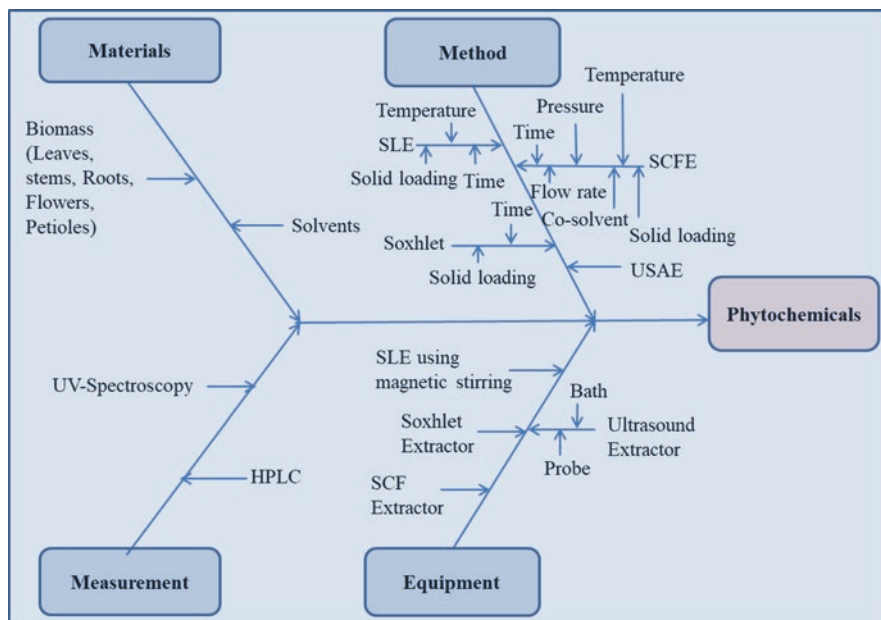
Fig. 2 Cause-and-effect diagram for phytochemicals extracted from water hyacinth

nontoxic and environment-friendly in nature. To increase the solvating power, CO_2 is used with other polar solvents to increase the polarity [38].

A variety of chemicals like glycolipids, phospholipids, triglycerols, phenalenone, sterols and phenolic compounds such as flavonoids and quinones have been identified in the extract of different parts of water hyacinth. These compounds have shown antimicrobial action, antiproliferative activity against malignant cells, cure against inflammation and antioxidant activity [39]. Table 1 provides details about various phytochemicals extracted from different parts of water hyacinth.

The extraction of lipophilic and polar components from roots, stem, leaves and flowers has been carried out [42] along with antioxidant activity. After Soxhlet extraction using dichloromethane, the extract was analysed for lipophilic components. Solid-liquid extraction followed by Soxhlet extraction for 1:100 g/mL of biomass sample was performed with the solvent mixture of methanol/water/acetic acid having 47.5:47.5:5.0 (v:v:v) proportion for 24 h to identify the polar components. A total of 29 components were analysed in the lipophilic extract of water hyacinth. The total mass of extract obtained was in the range of 22.42–39.17% (wt); amongst them glycerol, hexadecanoic acid, linoleic acid, linolenic acid, cholesterol, methyl cholesterol, stigmasterol and β-sitosterol were found in significant amount. These lipophilic compounds are classified into four groups of families as sterols (ST), fatty acids (FA), long-chain aliphatic alcohols (LCAA) and aromatic compounds, and the concentration of these compounds was in the range of 9.80–22.55% (wt), 7.42–13.13% (wt), 0.17–1.26% (wt) and 0.15–0.40% (wt), respectively. The most

Table 1 Water hyacinth as a source of phytochemicals

Sr. no.	Targeted phytochemicals	Plant part	Parameter	Results	References
1.	Sterols	Leaves and stalks	Supercritical fluid extraction: Solid loading, 30 g Pressure, 200–300 bar Temperature, 50 °C Solvent, CO_2 Flow rate, 7.5 g/min Co-solvent, 0.0–5.0% (wt) ethanol	Total yield, 1.25% (wt) ethanol at 250–300 bar and 5.0% (wt) Total sterol concentration, 38.26% (wt) Stigmasterol concentration, 26.35% (wt) at 300 bar and 2.5% (wt)	Martins et al. [40]
2.	Stigmasterol	Leaves and stalks	Supercritical fluid extraction: Solid loading, 70 g Pressure, 200 bar Temperature, 40–60 °C Time, 6 h Solvent, CO_2 Co-solvent, 0–10% (wt) ethanol	Total yield, 0.73% (wt) Stigmasterol yield, 0.22% (wt) Stigmasterol concentration, 30.6 kg/100 kg extract at 60 °C and 0% (wt) ethanol. Addition of ethanol led to increased yield up to 1.88% (wt) with an extended time of extraction	de Melo et al. [41]

Table 1 (continued)

Sr. no.	Targeted phytochemicals	Plant part	Parameter	Results	References
3.	Polar and lipophilic components	Roots, stalks, leaves and flowers	Solid loading, 10 g Soxhlet extraction: Time, 8 h Solvent, dichloromethane Solid-liquid extraction (SLE): Time, 24 h Solid-liquid ratio, 1:100 biomass after Soxhlet extraction (g): solvent (mL) Solvent, methanol/water/ acetic acid (47.5:47.5:5.0 v:v:v) Temperature, RT	Yield from stalk Soxhlet, 2.65% (wt) SLE, 28.84% (wt) Total, 31.49% (wt)	Silva et al. [42]
4.	Shikimic acid	Aerial parts and roots	Solid loading, 1 g Time, 20 min (magnetic stirring at RT and 45 °C; sonication at RT and 45 °C) Solvent, methanol and water (2 × 25 mL)	Significant yield was obtained for sonication at room temperature (1.450% (wt)) using methanol for aerial parts	Cardoso et al. [43]
5.	Phenolic compounds	Petioles, leaves and flowers	Solid loading, 5 g Volume of solvent, 50 mL Solvent, ethanol; water Temperature, RT Time, overnight	Higher extraction yield was found for flower 25.5% (wt) with water	Surendraraj et al. [44]
6.	8-Phenylphenalenones	Roots and leaves	Solid loading, 870 g Temperature, RT Solvent, acetone	Structure elucidation 8-phenylphenalenones Total amount extracted, 7.2 mg/g	Hölscher and Schneider [45]

abundant amount among all the compounds in the lipophilic extract was sterols with β-sitosterol and stigmasterol with the concentration of 67–80% (wt). The leaves and stalk contained higher amount of stigmasterol with 13.45% and 15.15%, respectively, while flowers had β-sitosterol in abundant quantity. Extract from leaves (4.86 mg$_{AAE}$/g$_{biomass}$ (mg ascorbic acid equivalent per gram biomass)) has exhibited better antioxidant action compared to the extracts obtained from stalks and roots, i.e. 2.04 mg$_{AAE}$/g$_{biomass}$ and 0.11 mg$_{AAE}$/g$_{biomass}$, respectively. Among all the parts, leaves possessed the highest value of phenolic compounds followed by the stalks and roots.

The total phenolic compounds (TPC) have been extracted from petioles, leaves and flowers by Surendraraj et al. [44]. The biomass was extracted with 96% ethanol as well as distilled water at room temperature overnight. The extraction yield with water was found more as compared to ethanol. The highest extraction yield of 25.5% (wt) was obtained for flowers with water. Phenolic contents of various sections of water hyacinth were in the range of 0.84–6.66 mg$_{GAE}$/g of dried sample. TPC have been obtained in a higher amount in flowers compared to other parts of the plant. The ethanolic extract of *Eichhornia crassipes* showed the presence of α-tocopherol in significant amount in petioles, δ- tocopherol in leaves and γ-tocopherol in petioles. A total of 11 phenolic acids were identified from the water and ethanolic extract such as benzoic phenolic types (gallic, protocatechuic, gentisic, p-hydroxybenzoic, vanillic and salicylic acid) and cinnamic phenolic types (chlorogenic, syringic, caffeic, p-coumaric and ferulic acid). Protocatechuic and gentisic acids have been found in greater amount in ethanolic extract of petioles, leaves and flowers. Flowers have a significant amount of protocatechuic acid (53.94 mg/g extract) and gentisic acid (137.26 mg/g extract) [44]

Recovery of shikimic acid in purer form from the aerial parts and roots was carried out using methanol and water as solvents. The techniques are used for extraction such as magnetic stirring and sonication at room temperature as well as 45 °C and Soxhlet extraction. The maximum yield of shikimic acid (1.45%) and (2.70%) was obtained for aerial part of water hyacinth using sonication at room temperature and Soxhlet extraction, respectively [43].

4.2 Water Hyacinth as a Source of Sorbent for Heavy Metals and Dyes

Aquatic plants can control the pollution caused due to heavy metals and pesticides in freshwater. Since the conditions are favourable in tropical and subtropical regions, *Eichhornia crassipes* is produced in huge quantity and has gained importance for this purpose. Apart from adsorbing or accumulating heavy metals, water hyacinth is capable of converting reactively toxic compounds to inert and nontoxic compounds [46]. Powder and adsorbents made from various parts of this plant have been assessed for removal of harmful compounds. Different parameters such as
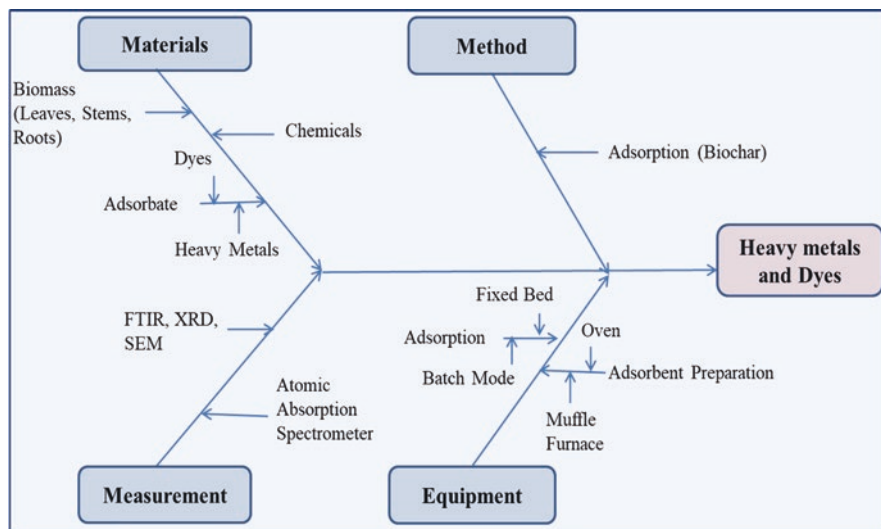
Fig. 3 Cause-and-effect diagram for heavy metal and dye removal by water hyacinth

adsorbent concentration, time employed, temperature and pH of effluent have been studied. Figure 3 shows cause-and-effect diagram for adsorption of noxious compounds using water hyacinth. The results obtained based on these studies conducted for heavy metal and dye removal are given in Table 2.

Biochar was made by pyrolysis of water hyacinth powder for 5 h at 350 °C. Pristine biochar and biochar coated with nanoscale zero valent iron (nZVI) were utilized towards adsorbing Cd (II) in batch and continuous mode. Batch experiments were carried out in 25 mL Erlenmeyer flask using concentration of Cd (II) in the range of 0.01–200 ppm, 0.01 g biochar and pH at 7. For continuous operation, fixed bed was formed using 1 g of dry nZVI/biochar composite. Langmuir isotherm has been employed for assessment purpose. The solution containing Cd (II) was allowed to pass through the bed. The highest removal of Cd (II) was 56.62 mg/g for nZVI/biochar composite which was 2.2-folds than that of the virgin one [59].

Artificial wetland system (AWS) was developed for biodegradation of organic compounds and removal of heavy metals using *Eichhornia crassipes* as biofilter [60]. Water hyacinth was used as biological filter for biodegradation of organic compounds (malathion, piroxicam and 2,4-dichlorophenoxyacetic acid (2,4-D)) and heavy metals (Pb, Ni, Zn and Cd) from water. AWS was constructed by polyethylene material with an objective to be used in batch as well as continuous mode for 20 consecutive days. The concentration of these organic compounds was analysed after every 2 days. The highest removal of malathion, 2,4-D and piroxicam was achieved to be 67.6%, 58.3% and 99.1%, respectively. Water hyacinth has absorbed 1.8–16.6 g of COD/kg DM (dry mass of water hyacinth), and 45.8% removal of BOD was achieved. AWS loaded with water hyacinth has removed 15.5, 5.4, 16.5 and 13.5 mg/kg dry biomass of Pb, Ni, Zn and Cd, respectively in 48 h.

Table 2 Water hyacinth as a source of sorbent for heavy metals and dyes

Sr. no.	Plant part	Response	Parameters	Results	References
1.	Petioles and leaves	Pb^{2+}, Ni^{2+}, Zn^{2+}	Chemical treatment of adsorbent: Temperature, 25 °C Time, 2 h NaOH concentration, 0.1 mol/L HNO_3 concentration, 10% Volume of NaOH and HNO_3, 25 mL Washing in Soxhlet extractor: Temperature, 90 °C pH, 7 Drying: Temperature, 100 ± 2 °C Time, 5 h Initial concentration of solution, 50–600 mg/L pH, 5 ± 0.2	Single-element adsorption capacity for alkali-treated adsorbent, 28.6 ± 3.9 mg/g, 18.9 ± 1.6 mg/g and 76.8 ± 4.7 mg/g for Ni^{2+}, Zn^{2+} and Pb^{2+}, respectively, at 25 °C	Neris et al. [30]
2.	Water hyacinth trunk	Methylene blue (MB)	Carbonization: Temperature, 600 °C Time, 1 h Sulphonation with concentrated H_2SO_4: Time, 3 h Adsorption: Adsorbent amount, 0.0625–0.125 g Adsorbate initial concentration, 80–120 mg/L Adsorbate volume, 25 mL Time, 5 min–12 h pH, 1–12	Adsorption capacity, 18.517 mg/g (without sulphonation) and 19.480 mg/g (with sulphonation)	Nurhadi et al. [47]

Sr. no.	Plant part	Response	Parameters	Results	References
3.	Water hyacinth (WH) Water lettuce (WL) *Myriophyllum spicatum* (MS)	COD, total nitrogen (TN) Ammonium nitrogen (NH_4^+-N) Total phosphorus (TP)	Static experiment: Temperature, 25–36 °C Influent concentration: COD, 60–72 mg/L TN, 16.57–17.25 mg/L NH_4^+-N, 11.8–13.68 mg/L TP, 1.59–1.89 mg/L Dynamic experiment: Temperature, 14–26 °C Hydraulic retention time (HRT), 10, 20, 30 days Influent concentration: COD, 89 mg/L TN, 24.65 mg/L NH_4^+-N, 21.31 mg/L TP, 2.94 mg/L	Removal efficiencies (%) using WH, WL and MS: COD, 68.21,61.70 and 62.55 TN, 87, 77 and 77 NH_4^+-N, 96, 93 and 93 TP, 84, 88 and 80.55, respectively, after 20 days in static mode In dynamic mode nutrient removal efficiency was enhanced by increased HRT	Lu et al. [48]
4.	Whole plant	Formaldehyde (HCHO)	Water hyacinth wastewater ratio, 0.6:10 *Eupatorium odoratum* L. extract concentration, 0.5 ppm Lab scale study: Plant weight, 70 ± 5 g Temperature, 10–40 °C Time, 10 days Initial concentration of HCHO, 100, 200, 300 ppm Pilot scale study: Plant weight, 200 ± 20 g Temperature, 10–30 °C Time, 12–144 h Initial concentration of HCHO, 200 ppm	HCHO removal efficiency: Lab scale, 100% at 20 °C in 8 days for 100 ppm Pilot scale, 100% up to the third recycling in 144 h	Gong et al. [49]

Sr. no.	Plant part	Response	Parameters	Results	References
5.	Water hyacinth biochar	Cr (IV)	Carbonization temperature, 500–800 °C ZnO content, 10–50% (wt) Contact time, 0.17–14 h	Cr (IV) removal efficiency, 95% with biochar loaded with 30% (wt) ZnO and carbonization temperature of 700 °C in 14 h	Yu et al. [50]
6.	Water hyacinth	Methylene blue	Initial concentration of MB, 100–600 mg/L pH, 2–10 Adsorbent dose, 10–100 mg Contact time, 30 min–24 h	MB removal, 320 mg/g at acidic pH, contact time of 2 h and 50 mg adsorbent dose	Siswoyo et al. [31]
7.	Shoot	Cr and Cu	Temperature, 28 ± 2 °C Time, 3 h Influent concentration in standard solution (SS): Cr, 472.56 mg/L Cu, 482.06 mg/L Influent concentration in tannery effluent (TE): Cr, 10.4749 mg/L Cu, 2.445 mg/L	The removal efficiency of Cr and Cu, 99.98% and 99.96% for SS and 98.83% and 99.59% for TE, respectively	Sarkar et al. [51]
8.	Roots	Pb, Zn, Cu and Cd	Time, 30 min–4 h pH, 1–7 Root powder concentration, 5–40 g/L Initial metal concentration: Single-metal system, 5–25 mg/L Multimetal system, 15–25 mg/L	Pb (98.33%), Cd (95.16%) and Zn (93.5%) were removed at pH -5, root powder concentration, 20 g/L; initial metal concentration of Pb and Zn, 25 mg/L; Cu and Cd, 20 mg/L in single-metal system Order of metal adsorption, Pb > Cd > Zn > Cu	Li et al. [52]
9.	Stem and leaves	Uranium U(VI)	Temperature, 25–45 °C Time, 10–160 min pH, 2–7 Initial U(VI) concentration, 50–300 mg/L Bioadsorbent concentration, 1.2 g/L	Adsorption capacity of U(VI), 142.85 mg/g at pH 5.5, and equilibrium was achieved within 30 min at 25 °C and initial U(VI) concentration of 150 mg/L	Yi et al. [53]

Sr. no.	Plant part	Response	Parameters	Results	References
10.	Rice husk (RH), palm leaf (PL) and water hyacinth (WH)	Cu(II), Co(II) and Fe(III) ions	Temperature, 25 °C Time, 0.5–4 h pH, 7 and 9 Initial metal ion concentration, 300–500 ppm Initial bioadsorbent concentration, 0.1–1 g/L	Adsorption efficiency (%) using RH, PL and WH bioadsorbent for Cu(II), 99.6, 98.8 and 99.2, respectively; for Co(II), 99.1, 98.8 and 99.4, respectively; for Fe(III), 97.8, 97.5 and 98.6, respectively, at time (4 h), pH (9) and initial bioadsorbent concentration (1 g/L)	Sadeek et al. [54]
11.	Roots, stems and leaves	Cr(VI), phenol	Temperature, 30 °C Time, 16 days for Cr(VI) and 14 days for phenol Initial Cr(VI) concentration, 5–20 mg/L Initial phenol concentration, 10–40 mg/L	At initial concentration of 5 mg/L, 99% Cr(VI) was removed in 16 days. At initial concentration of 10 mg/L, 99.8% phenol was removed At initial concentration of 5 mg/L and 10 mg/L, 99% of Cr(VI) and phenol was removed by binary solution of Cr(VI) and phenol in 7 and 11 days, respectively	Gupta and Balomajumder [55]
12.	Leaves	Methylene blue and crystal violet	Temperature, 30 °C Time, 5 hpH, 3–10 Initial influent concentration: Methylene blue, about 0.1–2.8 mg/L Crystal violet, about 1.2–4.5 mg/L	Removal of 97% for methylene blue and 93% for crystal violet was observed at pH 10 and initial concentration of methylene blue and crystal violet 2.8 mg/L and 4.5 mg/L, respectively	Mahamadi and Mawere [56]
13.	Roots, stem and leaves	Cr(VI)	Solid loading, 0.2–0.6 g Temperature, 25 °C Time, 450 min pH, 1–5 Initial Cr(VI) concentration—10–30 mg/L	Removal up to 73–89% of the metal with solid loading of 0.2 g, initial concentration of 10 mg/L and pH of 1	Mohanty et al. [57]
14.	Whole plant	Methylene blue	Temperature, 27 °C Time,160 min pH, 3.7–4.4 Initial methylene blue concentration, 97.2–1187.2 mg/L	Removal of methylene blue of 99% at initial methylene blue concentration of 97.2 mg/L	El-Khaiary [58]

4.3   Water Hyacinth as a Source of Fuel

Due to increase in energy demand with increase in population all over the world and depletion of fossil fuel, the researchers have focussed on the renewable energy sources. Over-exploitation of crude oil and coal and ever-increasing demand of energy necessitate the finding of alternative fuel sources. Bioethanol, biogas, biohydrogen and high calorific fuel (HCF) are considered as important renewable energy sources, and lignocellulosic biomass can be utilized for producing such renewable products. Minimization of waste like water hyacinth by utilizing this biomass for production of renewable energy source can become critical benefaction in achieving sustainable development goals. Three stages such as pre-treatment, hydrolysis and fermentation are involved in producing bioethanol from water hyacinth [10]. Figures 4 and 5 represent cause-and-effect diagram for bioethanol and biogas production, respectively, from *Eichhornia crassipes*.

Eichhornia crassipes is regarded as the potential source of biogas. The production of biohydrogen is eco-friendly, and anaerobic microorganisms are used from organic waste [13]. In addition, combustion of biohydrogen produces water and heat and has a higher energy output, i.e. 122 kJ/g. Details of work conducted in this field are summarized in Table 3.

Production of biohydrogen followed by biomethane from waste of *Saccharum officinarum* and *Eichhornia crassipes* in batch and continuous operations was achieved by Kumari and Das [73]. Sugarcane bagasse (SCB) was pre-treated with solution having 1% w/v caustic soda and 2.5% v/v H_2O_2. Hydrolysis of SCB was done with aqueous solution containing citrate buffer which was supplied with cellulase from *Trichoderma reesei*. By pre-treatment and hydrolysis, lignin was reduced to $89 \pm 3\%$ (w/w). Biohydrogen was produced by mixing 10 g/L hydrolysed SCB with varying concentration (5–25 g/L) of water hyacinth (WH) in batch mode. The cumulative gas production of 111.6 ± 1.9 mL/g COD and biohydrogen production of 72.5 ± 1.3 mL/g COD with SCB-WH ratio of 1:2 was observed for batch mode. In continuous process, maximum biohydrogen yield of 303 mL/g COD in 8 h of hydraulic retention time was observed, while 142 mL/g COD biomethane yield was observed in 240 h of hydraulic retention period.

Gao et al. [74] have focussed on the influence of ionic liquid with co-solvent on morphology of plant material as well as quality and quantity of biogas generated from *Eichhornia crassipes*. Ionic liquid (1-N-butyl-3-methylimidazolium) [Bmim]Cl and dimethyl sulfoxide (DMSO) as co-solvent were used for delignifying the biomass. Pre-treatment by [Bmim]Cl/DMSO has decreased the crystallinity of biomass structure, and porosity of the surface was increased. Removal of lignin in the range of 27.1–60.4% has assisted in the increase in biomass production in the range of 16.3–97.6% upon treating the biomass at 120 °C for 120 min. [Bmim]Cl/DMSO recovery has been found to be 90% employing two-phase aqueous solution having K_3PO_4.

Anaerobic digestion of *Eichhornia crassipes* was accomplished to enhance methane production using microwave pre-treatment [75]. Pre-treatment was carried out at microwave power of 500 W, temperature of 100 °C, 20.1 g/L substrate concentration and 15 min operational time. Using microwave pre-treatment, methane production was 221 mL/g-sub which was 38.3% higher than the conventional method.

Varanasi et al. [76] have studied the biohydrogen production, biomethanation and bioelectricity generation from water hyacinth. Biohydrogen was produced in batch process carried out in a reactor of 500 mL volume at pH of 6.5 and temperature 37 °C with the maximum cumulative H_2 production (904 ± 40.69 mL/L) and yield (41.38 ± 2.06 L/kg COD). Biomethanation of water hyacinth has been performed in double-jacketed batch reactor having 500 mL volume. Anaerobic environment was maintained by sparging N_2 for 5 min. Temperature was maintained at 37 °C and stirring speed at 280 rpm. The maximum cumulative methane production was achieved to be 796.73 ± 18.62 mL/L with 35.69 ± 1.24 L/kg COD yield. Microbial fuel cell (MFC) was incorporated to produce electricity. Carbon felt coated with WO_3 catalyst as anode and carbon ink-coated anion exchange membrane as cathode were used in the polyacrylic MFC chamber. The batch time for MFC was 72 h, and the internal resistance was 17–20 Ω. The maximum power densities in two-stage and three-stage process were obtained as 18.15 ± 0.54 and 16.28 ± 0.65 W/m^3, respectively. The combined system comprising of three stages was able to provide the highest energy (60%) in the form of hydrogen, methane and electricity with 94% of overall COD removal.

Biohydrogen was produced from water hyacinth in batch and continuous process by Ruen-ngam and Jaruyanon [77] using a batch reactor. The processing conditions were temperature in the range of 400–500 °C at 50 °C of interval, pressure variation from 21.2 to 26.8 MPa and 5–30 min variation in reaction time. Biomass ratio was varied from 2.5% to 15%. The continuous system used for gas production was operated at 0.51 L/h, while maintaining temperature and pressure conditions closed to supercritical water ($T = 374$ °C, $P = 22$ MPa). The H_2 production rate in continuous system was 0.96 mol/min which could recover energy equivalent to 2.08 Wh/g biomass or 11.43 kWh/mole glucose. The H_2 yield was 2.7 times higher in continuous system than the batch system.

Water hyacinth was used for producing hydrogen using cellulose and xylanase enzyme [78]. Sodium chlorite ($NaClO_2$) was added in acidic fermentation process for lignin deterioration. The concentration of $NaClO_2$ was varied from 0 to 20 mg/L. The maximum hydrogen yield of 119.6 ± 7.8 mL/g TVS (total volatile solids) at $NaClO_2$ concentration of 8 mg/L was obtained which was much more as compared to 39.7 ± 2.5 mL/g TVS (without $NaClO_2$). A higher concentration of $NaClO_2$ (more than 8 mg/L) has caused the death of anaerobes in the fermentation media showing an adverse impact on performance of the process.
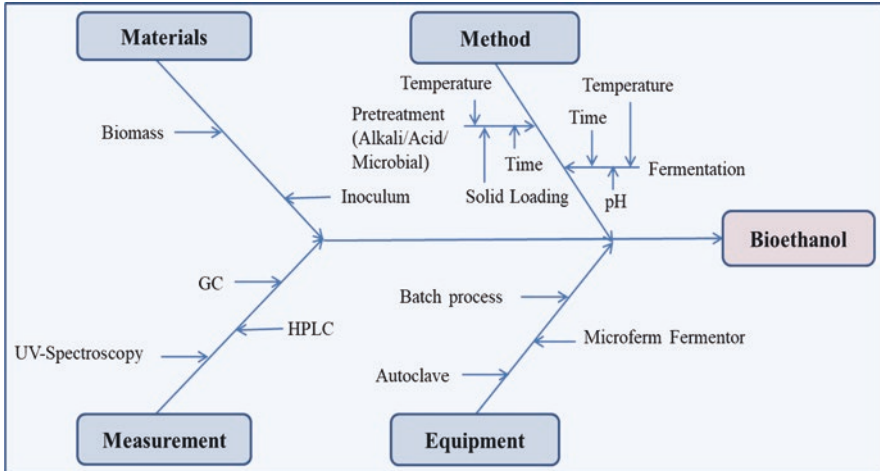
Fig. 4 Cause-and-effect diagram for bioethanol production from water hyacinth
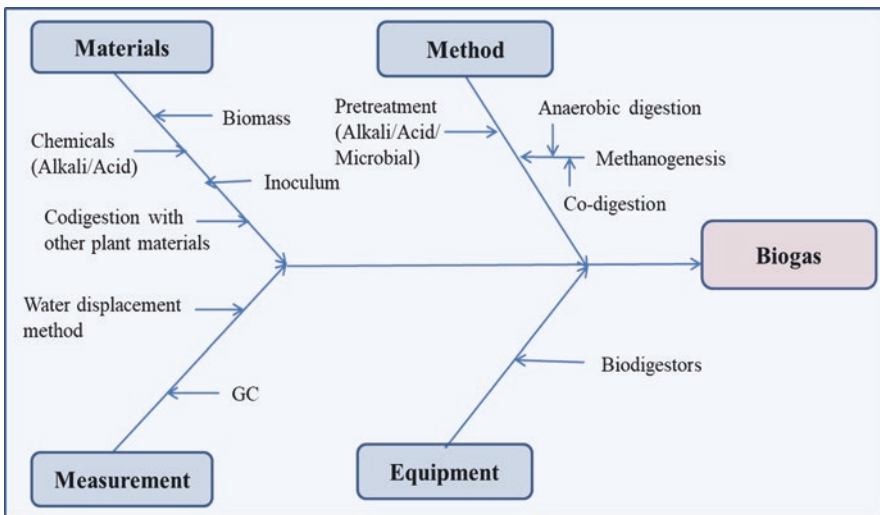
Fig. 5 Cause-and-effect diagram for biogas production from water hyacinth

4.4 Water Hyacinth as a Source of Material

Eichhornia crassipes has been successfully used for production of biopolymer, carbon fibre and composites. Carbon fibre is generally used as a source for composites [10]. Commercially, carbon fibres are made from organic polymers like rayon, polyacrylonitrile or petroleum pitches which further depend upon petrochemicals and refineries. High cost of these organic polymers is another limitation. To produce

Table 3 Water hyacinth as a source of fuel

Sr. no.	Raw material	Microorganism/ inoculum	Parameters	Results	References
Bioethanol					
1.	Water hyacinth	*Aspergillus terreus* F-98 *Candida tropicalis* (fungus)	Acid hydrolysis with H_2SO_4: Temperature, 119.27 °C Time, 16.11 min Biomass amount, 7.56% (w/v) H_2SO_4 concentration, 4.66% (v/v) Chemical hydrolysis with H_2SO_4, HCl, NaOH and KOH: Autoclave temperature, 121 °C Time, 20 min Biomass amount, 4 g Fungal hydrolysis: Autoclave temperature, 121 °C Incubation temperature, 30 °C Autoclave Time, 20 min Incubation time, 10 days Biomass amount, 4 g Bioethanol production (batch fermenter): Temperature, 30 °C Time, 60 h pH, 5.5	Bioethanol production, 14 g/L	Madian et al. [28]

Table 3 (continued)

Sr. no.	Raw material	Microorganism/ inoculum	Parameters	Results	References
2.	Water hyacinth	Cellic C Tech 3 (enzyme) *Saccharomyces cerevisiae* (yeast)	Biomass pre-treatment 1: Solid loading, 30 g Volume of solvent, 2000 mL Solvent, water, hydrogen peroxide, acetic acid Solvent concentration, 1.7 mol/L Steam explosion, 2.5 kgf/cm^2/h Biomass pre-treatment 2: Solvent, acetone/ water (20% v/v) Time, 15 min Drying temperature, 50 °C to achieve humidity less than 5% SSF and SHF: Solid loading, 5 g pre-treated biomass Volume of water, 200 mL Temperature, 32 °C Shaking speed, 120 rpm SSF Time, 0–72 h pH, 4.8 SHF Time, 0–144 h pH, 5	Bioethanol production, 0.39 mL Yield, 0.078 mL/g For hydrogen peroxide pre-treatment in 78 h using SHF	Roberta et al. [61]

(continued)

Table 3 (continued)

Sr. no.	Raw material	Microorganism/ inoculum	Parameters	Results	References
3.	Water hyacinth	*Phanerochaete chrysosporium* (fungus) *Saccharomyces cerevisiae*	Solid-liquid ratio, 1:20 Pre-treatment with microbe (*Phanerochaete chrysosporium*): Temperature, 30 °C Time, 60 h Shaking speed, 150 rpm Pre-treatment with acid (1% H_2SO_4) and alkali (4% NaOH): Time, 1 h Temperature, 100 °C Bioethanol production: Temperature, 30 °C Time, 6–30 h Shaking speed, 120 rpm *Saccharomyces cerevisiae* concentration, 6 g/L	Bioethanol production, 1.40 g/L in 24 h	Zhang et al. [62, 63]

Table 3 (continued)

Sr. no.	Raw material	Microorganism/ inoculum	Parameters	Results	References
4.	Water hyacinth	*Saccharomyces cerevisiae*	Pre-treatment with 4% H_2SO_4: Solid loading, 10% (w/v) Temperature, 121 °C for 15 min Time, 1 h for pre-treatment SSF: Solid loading, 10 g pre-treated biomass in 90 mL fermentation medium Temperature, 30 °C Time, 72 h Shaking speed, 200 rpm pH, 5	Bioethanol production, 5.1 ± 1.2 g/L Yield, 0.42 g_p/g_s (gram ethanol per gram of sugar consumed) for 60 h of fermentation using the mixture of all enhancer	Rezania et al. [64]
5.	Water hyacinth	*Trichoderma reesei* *Pichia stipites* **Fusarium oxysporum**	Solid loading, 10% (w/v) Pre-treatment with (0.5% w/v) $Ca(OH)_2$: Temperature, 100 °C Time, 3 h SHF: Temperature, 35 °C Time, 48 h pH, 6 Shaking speed, 200 rpm SSF: Microbial biomass, 5–25% Temperature, 25–45 °C Time, 24–72 h pH, 6	Yield, 0.411 g/g at 35 °C and 60 h for SSF using co-culture fermentation (*T. reesei* and *P. stipites*) with microbial biomass of 3.12 g DCW/L (gram dry cell weight per L) for solid loading of 100 g/L	Pothiraj et al. [65]

Biogas

Table 3 (continued)

Sr. no.	Raw material	Microorganism/ inoculum	Parameters	Results	References
6.	Water hyacinth (leaves, stem and roots) Banana peels	Cow dung	Water hyacinth pre-treatment: Temperature, 90 °C Time, 1 h Anaerobic co-digestion: Time, 50 days Leaves/stem/roots ratio, 13:69:45 Mixing ratio, 1–2.5 F/M ratio, 1 Inoculum, 50 g	Biogas production: (1) 170 ± 10 mL for untreated water hyacinth with optimum mixing ratio of 2 on the 16th day (2) 197 ± 10 mL for pre-treated water hyacinth with mixing ratio of 1.5 on the 11th day	Barua et al. [27]
7.	Water hyacinth	Cow dung	Leaves/stem/root ratio 13:69:45 Microbial pre-treatment: Dose, 10^9 CFU/ mL Time, 4 days Anaerobic treatment: Time, 50 days Food/ microorganism (F/M) ratio, 0.5–2.5 Cow dung, 50 g	Biogas production, 156 ± 11 mL CH_4/g VS (volatile solids) for F/M ratio 1.5	Barua and Kalamdhad [66]
8.	Water hyacinth and minimal salt media (MSM)	Cow dung	Leaves/stem/root ratio, 13:69:45 Microbial pre-treatment: Dose, 10^8– 10^{10} CFU/mL Time, 4 days Anaerobic treatment: F/M ratio, 1.5 Time, 80 days	Pre-treatment with microbe: Cumulative biogas production, 3737 ± 21 mL using in 50 days and microorganism dose of 10^9 Without pre-treatment: Cumulative biogas production, 3038 ± 21 mL in 50 days	Barua et al. [67]

Table 3 (continued)

Sr. no.	Raw material	Microorganism/ inoculum	Parameters	Results	References
9.	Fresh water hyacinth, sun dried (wilted) water hyacinth	–	Anaerobic digestion in lab-scale digester: Plant weight (fresh), 4 kg Time, 12 days Anaerobic digestion of sun-dried water hyacinth: Substrate-to-sludge VS ratio, 0.5 Time, 1 day Co-digestion: Water hyacinth biomass: waste ratio, 1:1 Temperature, ambient Time, 15 days	Biogas production: Fresh water hyacinth, 141 ± 6 mL/g VS Wilted water hyacinth, 142.8 ± 10 mL/g VS Water hyacinth + municipal sewage sludge, 148 ± 5 mL/g VS Water hyacinth + food waste, 394 ± 12 mL/g VS	Priya et al. [68]
10.	Water hyacinth (WH) and morning glory (MG)	Cow dung	Temperature, 25–35 °C Time, 17 weeks pH, 6–9 MG/WH, 100:0, 70:30, 50:50, 30:70, 0:100	MG/WH ratio of 50/50 gave highest biogas yield of 0.29 L/kg VS fed per day Co-digestion had a significant effect on TBC (total bacteria count) and not on biogas production	Adanikin et al. [69]
11.	Water hyacinth (WH) and sheep waste (SW)	–	Temperature, 30–37 °C Time, 60 days WH/SW/Water, 8:0:92, 2:18.01:79.99, 3:15.01:81.90, 4:12.01:83.90, 5:9.01:86.0, 0:24.02:75.97	For WH/SW/Water ratio of 4:12.01:83.90, the highest biogas yield of 0.36 L/g VS was obtained	Patil et al. [70]
12.	Water hyacinth and channel grass	Cattle manure	Temperature, 35 °C Time, 21 days	Biogas production from water hyacinth of 15.4–23.65 L/kg dry weight and from channel grass of 22.8–29.9 L/kg dry weight	Singhal and Rai [71]

Biohydrogen and HCF

(continued)

Table 3 (continued)

Sr. no.	Raw material	Microorganism/ inoculum	Parameters	Results	References
13.	Water hyacinth stem	–	Hydrolysis with H_2SO_4: Temperature, 30 ± 2 °C Time, 5.32–8.68 h pH, 5.5 H_2SO_4 concentration, 0.32–3.68% (v/v) Shaking speed, 165.91–334.09 rpm	Maximum hydrogen production, 127. 6 mmol H_2/L at 7.73 h, 1.3% (v/v) H_2SO_4 concentration and 264.41 rpm	Pattra and Sittijunda [72]
14.	Water hyacinth plant	–	Temperature, 300–450 °C Time, 10 min Heating rate, 60 K/min Plant weight, 3 g with 15% water	The maximum yield, 12.6% of HCF High heating value (HHV) 43.8 MJ/kg at 350 °C	Lu et al. [34]

low-cost material for engineering, natural fibres from water hyacinth have been used because of the presence of a higher cellulose fraction and lesser cellulose diameter and can be reinforced with polymer composites. Table 4 shows studies on biopolymer, carbon fibre and composite.

4.5 Water Hyacinth as a Source of Lignocelluloses

The reuse and recycling of agro-industrial lignocellulosic wastes are considered under phase II biorefinery in which single biomass produces multiple products such as bio-based products (food, feed, chemicals) and bioenergy (biofuels, power, heat) which are produced using integrated and sustainable processes [80].

Biocomposite from water hyacinth fibre (WHF) pulp and tapioca starch has been prepared by Asrofi et al. [81]. Water hyacinth fibre was treated with 25% NaOH solution at temperature about 130 °C and 2 bar pressure for 6 h followed by neutralization and solar drying. The dried pulp was homogenized with water, tapioca powder and glycerol and then gelatinized. The mould thus prepared was tested for tensile strength (6.68 MPa) and tensile modulus (210.95 MPa). This method was improved by Asrofi et al. [81] upon incorporating sonication at 40 kHz with 100% amplitude and 250 W which has resulted in 83% increase in tensile strength and 108% increase in tensile modulus.

Chonsakorn et al. [82] have studied the effect of different extraction methods for improving the quality of fibre from raw *Eichhornia crassipes*. The methods include

mechanical extraction, chemical extraction using NaOH solution, mechanical and chemical extraction, extraction with water at boiling point, natural alkali extraction using ash from banana stem and retting extraction. Water hyacinth contained 72.17% cell walls which further consisted of 52.63% lignocelluloses. Mechanical extraction has shown the highest elongation of fibre, whereas chemical extraction method with 10% NaOH at 37 °C for 1 h was found superior as it was able to generate uniform surface texture with the maximum number of split fibres upon completion of the method.

Cellulose nanofibres from water hyacinth have been isolated by Thiripura Sundari and Ramesh [83] using different chemical and mechanical treatments. Bleaching and processing with alkaline and sodium chlorite solution were the chemical methods employed to separate cellulose, hemicellulose and lignin. Mechanical methods like ball milling, cryocrushing and ultrasound treatment of chemically treated fibres were performed to obtain the desired particle size of fibre. The microfibres have been subjected to cryocrushing using liquid nitrogen to produce nanofibres from stem bundle which were further sonicated for 15 min to form individual nanofibres. The nanofibres with 20–100 nm diameter as per scanning electron microscopy and 25 nm as per transmission electron microscopy have been obtained by this method.

Microwave pre-treatment under acidic conditions led to hydrolysis of hemicellulose into monosaccharide such as xylose, galactose and arabinose, while some fractions of cellulose and lignin were hydrolysed into glucose and propiolic acid, respectively [84]. A higher content of cellulose has been obtained after degradation of lignocellulosic biomass. Microwave pre-treatment of 10 g/L input with 1% H_2SO_4 at 140 °C for 15 min and hydrolysis with cellulase enzyme reducing sugar yield of 48.3 g/100 g WH have been achieved. Hydrolysis of *Eichhornia crassipes* into fermentable sugars is desirable for production of clean biofuels (e.g. ethanol and hydrogen).

Nguyen Thi et al. [85] have employed subcritical water (SCW) pre-treatment for cellulose recovery from water hyacinth and compared with pre-treatment using H_2SO_4 and untreated biomass. Recovery of cellulose, hemicellulose and lignin from untreated biomass was 25%, 11% and 2.5%, respectively. The SCW pre-treatment was carried out at 165 °C, 30 min, 50 bar with water to dried biomass ratio of 10:1 mL/g for which cellulose content of 68.2% was obtained. Pre-treatment with 1% H_2SO_4 under same operating conditions has provided 69.4% cellulose content. Though the cellulose content was more using H_2SO_4 pre-treatment, SCW pre-treatment is environment-friendly. Cellulose recovery and removal of lignin have promoted the bioethanol production.

Devi et al. [86] have prepared cellulose nanocrystals (CNCs) by acid hydrolysis of compost made with water hyacinth (120 kg), cow dung (15 kg) and sawdust (15 kg). Compost was treated with alkali (NaOH) and bleaching chemicals (H_2O_2 and NaClO) for gradual removal of hemicellulose and lignin followed by acid hydrolysis (H_2SO_4) to hydrolyse cellulose and prepare CNCs. CNCs were obtained with mixed morphology of cone, rectangular with diameter of ~30–50 nm and length ~200–300 and spherical shaped CNCs with diameter of 20–30 nm.

Table 4 Water hyacinth as a source of material

Sr. no.	Material	Raw material	Parameters	Results	References
1.	Carbon fibre	Water hyacinth	Liquid tar production: Pyrolysis temperature, 450–600 °C Carbon fibre production: Carbonization temperature, 900 °C	Yield of carbon fibre, 29% with axial modulus of 42.1 GPa and tensile strength of 600.7 Mpa at 550 °C	Soenjaya et al. [79]
2.	Composite	Water hyacinth stem, polyester	Temperature, 22 °C Time, 20 days WH fibre percentages, 5–20 wt%	Water hyacinth having concentration in the range of 5–10% (wt) has provided better mechanical properties	Flores Ramirez et al. [32]
3.	Biopolymer poly(3-hydroxybutyrate) (PHB)	Water hyacinth, *Cupriavidus necator* (bacteria)	Temperature, 22.5–32.5 °C Time, 96 h Nitrogen source, 0.5–2.5 g/L Carbon source, 25–45 g/L pH, 6–8	PHB production, 4.3 ± 0.4 g/L at pH 7, temperature 27 °C with carbon source 35 g/L and nitrogen source 2 g/L	Radhika and Murugesan [29]

Silver nanoparticles (Ag-NPs) were synthesized by extracting cellulose from water hyacinth [87]. Silver nanoparticles were prepared by adding 1 M of silver nitrate solution in 45 mL solution of cellulose (0.5 g/100 mL) at 75 °C at different pH (4, 8 and 11). The average particle mean diameter was obtained 5.69 ± 5.89, 4.53 ± 1.36 and 2.68 ± 0.69 nm at different pH 4, 8 and 11, respectively.

4.6   Water Hyacinth as a Source of Bio-oil

Pyrolysis has been extensively used for producing bio-oil from water hyacinth by many researchers. Various factors affecting bio-oil production are presented in Ishikawa diagram (Fig. 6).

Wauton and Ogbeide [88] have studied the characteristics of bio-oil obtained from *Eichhornia crassipes*. The biomass has been heated to 450 °C at a rate of 50 °C/min. The particle size of plant material was 0.6 mm, while the inert gas flow-rate was maintained at 100 cm³/min. Characteristic properties of bio-oil were noted as 2.93 pH, 58.58% water content, 220 °C flash point, 1004.3 kg/m³ density, 19.8 cSt

viscosity and +15 °C pour point. Calorific value of the oil was 28.35 MJ/kg, much higher (~63%) than the feedstock.

Various processing conditions have been assessed to observe their influence on catalytic pyrolysis of *Eichhornia crassipes* to produce bio-oil, and its composition was reported by Gulab et al. [89]. The oil production was optimized by considering various parameters like temperature (150–450 °C), time (60–100 min) and 5% (wt) catalyst (aluminium, copper) concentration. Under optimum process conditions (450 °C, 60 min and copper as a catalyst), 31.6% (wt) bio-oil was produced.

Zhang et al. [62, 63] have employed by two-stage microwave-assisted catalytic fast pyrolysis (MACFP) in series. Production of bio-oil has been optimized by varying temperature from 500 to 750 °C at 750 W of microwave power. Ce-doped γ-Al_2O_3/ZrO_2 composite mesoporous catalyst (CAZ) in packed bed was used along with MACFP to minimize the coke formation and boost hydrocarbon generation. The highest yield of oil was achieved to be 20.5% (wt) at 650 °C.

Lin et al. [90] assessed the influence of chromium containing polluted *Eichhornia crassipes* on pyrolysis in fixed bed to produce bio-oil. Water hyacinth was treated with different concentration of chromium 0.5–2.5% (wt) before pyrolysis. Pyrolysis was done at different temperatures 300–600 °C. The maximum bio-oil yield value for chromium-treated water hyacinth was 63.1% (wt). Thus, chromium might have played a role as a catalyst to improve the yield. The acid value and high heating value (HHV) for chromium-treated water hyacinth pyrolitic bio-oil were found to be 85.04 mg KOH/g and 26.72 MJ/kg, respectively. The best results were obtained at 500 °C and chromium concentration of 2.5% (wt). The yield of bio-oil for chromium-treated biomass was increased by 23.2% compared to untreated biomass.

4.7 Miscellaneous Applications

4.7.1 Vermicompost

Vermicompost is generally prepared from the vegetables and foods using worms like earth worms, white worms and red wigglers. Vermicompost is extensively used as an organic fertilizer and soil conditioner [10]. Compost was made by adding layers of water hyacinth and cow dung. Vermicompost made from water hyacinth has been successfully used for maturing of the angiosperm *Crossandra undulaefolia* with fruitful outcomes. The factors regarding plant growth like plant height, number of leaves, root length, shoot-root ratio and flowering have been tested, and the positive impact of vermicompost on the growth of plant has been observed [91].

4.7.2 Supercapacitor Electrode

Water hyacinth was successfully employed for the preparation of carbon microsphere used for supercapacitor electrode. Water hyacinth was hydrolysed into sugar using dilute sulphuric acid solution (0.25 M) at 20 bar and 130 °C for 2 h. The

resultant sugar solution further carbonized at 40 bar by varying temperature (160–200 °C) and time (6–10 h) to produce carbon microsphere. The conversion of carbon microsphere has been 0.1019 g/g dry WH when processed at 200 °C for 10 h. The product was then activated using KOH solution and microwave radiation to get a better porosity and specific surface area. A higher specific surface area and electrochemical stability have been obtained at 1:1 impregnation ratio (KOH/carbon) [36].

4.7.3   Enzyme

Eichhornia crassipes was employed as a substrate for production of cellulase, and *Aspergillus niger* was used as a microbe. The maximum cellulose activity of 1.035 IU/mL and 0.535 IU/mL with moisture content of 75% and 80%, respectively, at pH 5 and temperature 30 °C has been observed after 7 days of incubation period [33]. The production of cellulase enzyme using *Trichoderma reesei* and water hyacinth as a substrate has also been studied. The cellulose activity of 0.22 IU/mL after 15 days of incubation period at pH 6 and temperature 30 °C was obtained [92].

4.7.4   Brick Manufacturing

Goel and Kalamdhad [35] employed water hyacinth in brick manufacturing. The binary mix of 10% (wt) water hyacinth with rest soil was used and set at firing temperature of 900 °C. Durability of brick improved at this temperature. Water hyacinth
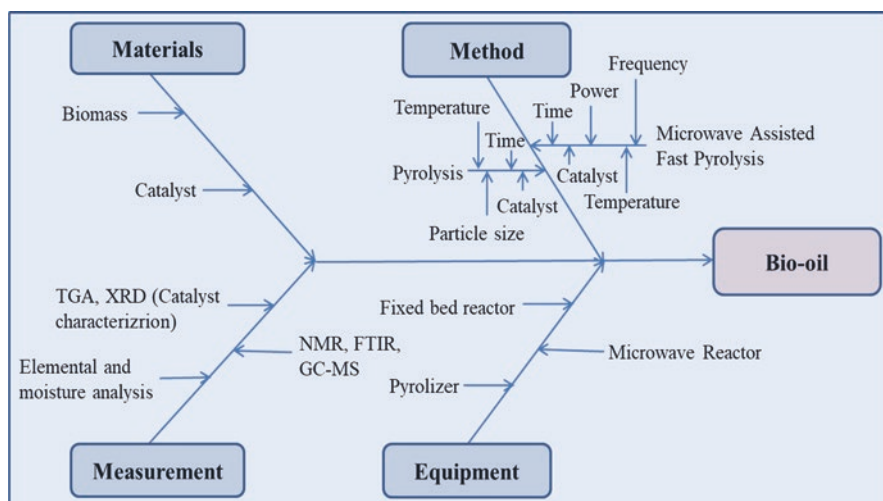
Fig. 6 Cause-and-effect diagram for bio-oil production from water hyacinth

contains different fluxing agents such as K_2O, Fe_2O_3, CaO, MgO and TiO_2 which reduce firing temperature required for brick production. Porosity of brick increased with more inclusion of water hyacinth. Water absorption capacity of brick increases with higher porosity. Brick with 10% inclusion of water hyacinth absorbed less than 25% of water. Therefore, water hyacinth blended brick can be used as a moderate weather resistant.

5 Biorefinery Approach

For extraction of various value-added compounds such as sterols, organic and fatty acids and polyphenols from water hyacinth, different extraction methods like super-critical fluid extraction (SFE) [40, 41], solvent extraction [44] and ultrasound assisted extraction (USAE) [43] have been employed. Sterols have been extracted from water hyacinth by SFE using CO_2 as a solvent which is eco-friendly solvent. With some possible modifications in solubilization capacity of supercritical CO_2, it is possible to extract a variety of useful constituents with very high degree of separation from solvent without the issue of residual solvent [93], thereby making SFE a green extraction process. Using USAE, shikimic acid has been successfully extracted. USAE is based on cavitation phenomenon in which due to collapse of cavitation bubbles high thermal energy and pressure are released, thereby generating micro jets and shock waves that affect the cell morphology. Hence, cell structure experiences the damage which enhances the extraction efficiency by increasing the solvent diffusion rate. The use of sonication, due to intensification in aqueous media, reduction in extraction time and low energy consumption, makes the process a greener one [93]. In solvent extraction, water has been used as a solvent making the process sustainable. By pyrolysis process, biochar and bio-oil have been made from *Eichhornia crassipes*. Adsorbents like biochar have effectively removed heavy metals like Cd (II) [59] and dyes. After removing lignocelluloses, water hyacinth has been utilized to produce bioethanol and biogas. Minimization of waste like water hyacinth by utilizing it for production of renewable energy source may assist in creating self-sufficient system. Three stages such as pre-treatment, hydrolysis and fermentation are involved in producing bioethanol from *Eichhornia crassipes* [10]. Biogas was produced by pre-treatment (acid/alkali/microbial) followed by methanogenesis.

Water hyacinth grows rapidly, and to control growth of this invasive weed is not economically viable. Instead of control, sensible utilization of water hyacinth as feedstock for various value-added products minimizes the dependency on fossil fuels. The integrated biorefinery concept can be successfully implemented to water hyacinth upon incorporating extraction of phytochemicals followed by production of lignocellulose materials and finally biofuel production. Phase II biorefinery can be implemented for water hyacinth biomass valorization. The complete utilization of water hyacinth feedstock supports financial and ecological advantages. The

economic gains are in terms of easy and free availability of water hyacinth in river and lakes, and usability product of one process as raw material for other.

6   Conclusions

Though considered as a major source of waste-generating material, water hyacinth can be successfully employed for a variety of applications like a source of phytochemicals, alcohol, sorbents, fuel, material and others. Lipophilic extracts of *Eichhornia crassipes* roots, stalks, leaves and flowers contain the compounds like sterol, fatty acids, long-chain aliphatic alcohols and aromatic compounds. Polar extractives have shown the presence of phenolic components and very strong antioxidant activity. Shikimic acid, from fatty acid family, is one of the important compounds found in water hyacinth, and higher yield was obtained from aerial parts of water hyacinth. Thus, if water hyacinth is utilized cautiously, it can become the useful source for various chemicals and fuels and bolster the circular economy. The research on water hyacinth to useful products has been developed only on academic basis, and no technologies have been developed on commercial scale. There is a need to commercialize various application routes of this weed to useful products for sustainable and economic development.

References

1. Amulya K, Dahiya S, Venkata Mohan S (2016) Building a bio-based economy through waste remediation. Bioremediat Biocon 2016:497–521
2. Nizami AS, Rehan M, Waqas M (2017) Waste biorefineries: enabling circular economies in developing countries. Bioresour Technol 241:1101–1117
3. Maina S, Kachrimanidou V, Koutinas A (2017) A roadmap towards a circular and sustainable bioeconomy through waste valorization. Curr Opin Green Sustain Chem 8:18–23
4. Thi NBD, Kumar G, Lin CY (2015) An overview of food waste management in developing countries: current status and future perspective. J Environ Manage 157:220–229
5. Moncada BJ, Aristizábal MV, Cardona ACA (2016) Design strategies for sustainable biorefineries. Biochem Eng J 116:122–134
6. Naik SN, Goud VV, Rout PK et al (2010) Production of first and second generation bioenergy: a comprehensive review. Renew Sustain Energy Rev 14:578–597
7. Ismail IMI, Nizami AS (2016) Waste-based biorefineries in developing countries an imperative need of time. Paper presented at The Canadian Society for Civil Engineering: 14th international environmental specialty conference in London, ON, 1–4 June
8. Ouda OKM, Raza SA, Nizami AS et al (2016) Waste to energy potential: a case study of Saudi Arabia. Renew Sustain Energy Rev 61:328–340
9. Guna V, Ilangovan M, Anantha Prasad MG et al (2017) Water hyacinth: a unique source for sustainable materials and products. Sustain Chem Eng 5:4478–4490
10. Sindhu R, Binod P, Pandey A (2017) Water hyacinth a potential source for value addition: an overview. Bioresour Technol 230:152–162

11. Sharma A, Aggarwal NK, Saini A et al (2016) Beyond biocontrol: water hyacinth-opportunities and challenges. J Environ Sci Technol 9:26–48

12. Patel S (2012) Threats, management and envisaged utilizations of aquatic weed *Eichhornia crassipes*: an overview. Rev Environ Sci Biotechnol 11:249–259

13. Rezania S, Ponraj M, Din MFM (2015a) The diverse applications of water hyacinth with main focus on sustainable energy and production for new era: an overview. Renew Sustain Energy Rev 41:943–954

14. Malik A (2007) Environmental challenge vis a vis opportunity: the case of water hyacinth. Environ Int 33:122–138

15. Pereira LAM, Nakamura RYM, de Souza GFS (2012) Aquatic weed automatic classification using machine learning techniques. Comput Electron Agric 87:56–63

16. Borokini TI, Babalola FD, Dana E (2012) Management of invasive plant species in Nigeria through economic exploitation: lessons from other countries. Manag Biol Invasions 3:45–55

17. Biswas SR, Choudhury JK, Nishat A, Rahman MM (2007) Do invasive plants threaten the Sundarbans mangrove forest of Bangladesh? For Ecol Manage 245:1–9

18. Choo TP, Lee CK, Low KS et al (2006) Accumulation of chromium (VI) from aqueous solutions using water lilies (*Nymphaea spontanea*). Chemosphere 62:961–967

19. Khanna S, Santos MJ, Ustin SL, Haverkamp PJ (2011) An integrated approach to a biophysiologically based classification of floating aquatic macrophytes. Int J Remote Sens 32:1067–1094

20. Dagno K, Lahlali R, Diourte M, Jijakli MH (2012) Fungi occurring on water hyacinth [*Eichhornia crassipes* (Martius) Solms-Laubach] in niger river in Mali and their evaluation as mycoherbicides. J Aquat Plant Manag 50:25–32

21. Shanab SMM (2012) Biological activities and anticorrosion efficiency of water hyacinth (*Eichhornia crassipes*). J Med Plant Res 6:3950–3962

22. Téllez TR, EMR L, Granado GL (2008) The water hyacinth, *Eichhornia crassipes*: an invasive plant in the Guadiana River Basin (Spain). Aquat Invasions 3:42–53

23. Bicudo DDC, Fonseca BM, Bini LM et al (2007) Undesirable side-effects of water hyacinth control in a shallow tropical reservoir. Freshw Biol 52:1120–1133

24. Minakawa N, Sonye G, Dida GO et al (2008) Recent reduction in the water level of Lake Victoria has created more habitats for *Anopheles funestus*. Malar J 7:119

25. Venter N, Hill MP, Hutchinson SL (2013) Weevil borne microbes contribute as much to the reduction of photosynthesis in water hyacinth as does herbivory. Biol Control 64:138–142

26. Sullivan P R, Wood R (1976) Water hyacinth (*Eichhornia crassipes* (Mart.) Solms) seed longevity and the implications for management. Eighteenth Australasian weeds conference, pp 37–40

27. Barua VB, Rathore V, Kalamdhad AS (2019) Anaerobic co-digestion of water hyacinth and banana peels with and without thermal pretreatment. Renew Energy 134:103–112

28. Madian HR, Sidkey NM, Elsoud MMA et al (2019) Bioethanol production from water hyacinth hydrolysate by Candida tropicalis Y-26. Arab J Sci Eng 44(1):33–41

29. Radhika D, Murugesan AG (2012) Bioproduction, statistical optimization and characterization of microbial plastic (poly 3-hydroxy butyrate) employing various hydrolysates of water hyacinth *(Eichhornia crassipes)* as sole carbon source. Bioresour Technol 121:83–92

30. Neris JB, Luzardo FHM, Santos PF et al (2019) Evaluation of single and tri-element adsorption of Pb 2 +, Ni 2 + and Zn 2 + ions in aqueous solution on modified water hyacinth (*Eichhornia crassipes*) fibers. J Environ Chem Eng 7:102885

31. Siswoyo E, Adrian A R, Tanaka S (2018) Bioadsorbent based on water hyacinth modified with citric acid for adsorption of methylene blue in water. MATEC web of conferences vol. 154 EDP Sciences

32. Flores Ramirez N, Sanchez Hernandez Y, Cruz de Leon J et al (2015) Composites from water hyacinth (*Eichhornea crassipes*) and polyester resin. Fibers Polym 16:196–200

33. Amriani F (2016) Physical and biophysical pretreatment of water hyacinth biomass for cellulase enzyme production. Chem Biochem Eng Q 30:237–244

34. Lu W, Wang C, Yang Z (2009) The preparation of high caloric fuel (HCF) from water hyacinth by deoxy-liquefaction. Bioresour Technol 100:6451–6456
35. Goel G, Kalamdhad AS (2018) A practical proposal for utilisation of water hyacinth: recycling in fired bricks. J Clean Prod 190:261–271
36. Kurniawan F, Wongso M, Ayucitra A et al (2015) Carbon microsphere from water hyacinth for supercapacitor electrode. J Taiwan Inst Chem Eng 47:197–201
37. Lang Q, Wai CM (2001) Supercritical fluid extraction in herbal and natural product studies – a practical review. Talanta 53:771–782
38. Herrero M, Mendiola JA, Cifuentes A, Ibáñez E (2010) Supercritical fluid extraction: recent advances and applications. J Chromatogr A 1217:2495–2511
39. Aboul-Enein AM, Al-Abd AM, Shalaby E et al (2011) *Eichhornia crassipes* (Mart) solms. Plant Signal Behav 6:834–836
40. Martins PF, De Melo MMR, Sarmento P et al (2016) Supercritical fluid extraction of sterols from *Eichhornia crassipes* biomass using pure and modified carbon dioxide. Enhancement of stigmasterol yield and extract concentration. J Supercrit Fluids 107:441–449
41. de Melo MMR, Silva RP, Silvestre AJD et al (2016) Valorization of water hyacinth through supercritical CO_2 extraction of stigmasterol. Ind Crop Prod 80:177–185
42. Silva RP, de Melo MMR, Silvestre AJD et al (2015) Polar and lipophilic extracts characterization of roots, stalks, leaves and flowers of water hyacinth (*Eichhornia crassipes*), and insights for its future valorization. Ind Crop Prod 76:1033–1038
43. Cardoso SF, Lopes LMX, Nascimento IR (2014) *Eichhornia crassipes*: an advantageous source of shikimic acid. Braz J Pharmacogn 24:439–442
44. Surendraraj A, Farvin KHS, Anandan R (2013) Antioxidant potential of water hyacinth (*Eichornia crassipes*): *in vitro* antioxidant activity and phenolic composition. J Aquat Food Prod Technol 22:11–26
45. Hölscher D, Schneider B (2005) The biosynthesis of 8-phenylphenalenones from *Eichhornia crassipes* involves a putative aryl migration step. Phytochemistry 66(1):59–64
46. Rezania S, Ponraj M, Talaiekhozani A et al (2015b) Perspectives of phytoremediation using water hyacinth for removal of heavy metals, organic and inorganic pollutants in wastewater. J Environ Manage 163:125–133
47. Nurhadi M, Widiyowati II, Wirhanuddin W (2019) Kinetic of adsorption process of sulfonated carbon- derived from *Eichhornia crassipes* in the adsorption of methylene blue dye from aqueous solution. Bull Chem React Eng Catal 14(1):17–27
48. Lu B, Xu Z, Li J et al (2018) Removal of water nutrients by different aquatic plant species: an alternative way to remediate polluted rural rivers. Ecol Eng 110:18–26
49. Gong Y, Zhou X, Ma X et al (2018) Sustainable removal of formaldehyde using controllable water hyacinth. J Clean Prod 181:1–7
50. Yu J, Jiang C, Guan Q (2018) Enhanced removal of Cr (VI) from aqueous solution by supported ZnO nanoparticles on biochar derived from waste water hyacinth. Chemosphere 195:632–640
51. Sarkar M, Rahman AKML, Bhoumik NC (2017) Remediation of chromium and copper on water hyacinth (*E. crassipes*) shoot powder. Water Resour Ind 17:1–6
52. Li Q, Chen B, Lin P et al (2016) Adsorption of heavy metal from aqueous solution by dehydrated root powder of long-root *Eichhornia crassipes*. Int J Phytoremediation 18:103–109
53. Yi ZJ, Yao J, Chen HL et al (2016) Uranium biosorption from aqueous solution onto *Eichhornia crassipes*. J Environ Radioact 154:43–51
54. Sadeek SA, Negm NA, Hefni HHH (2015) Metal adsorption by agricultural biosorbents: adsorption isotherm, kinetic and biosorbents chemical structures. Int J Biol Macromol 81:400–409
55. Gupta A, Balomajumder C (2015) Removal of Cr(VI) and phenol using water hyacinth from single and binary solution in the artificial photosynthesis chamber. J Water Process Eng 7:74–82
56. Mahamadi C, Mawere E (2013) High adsorption of dyes by water hyacinth fixed on alginate. Environ Chem Lett 12:313–320

57. Mohanty K, Jha M, Meikap BC et al (2006) Biosorption of Cr(VI) from aqueous solutions by *Eichhornia crassipes*. Chem Eng J 117:71–77

58. El-Khaiary MI (2007) Kinetics and mechanism of adsorption of methylene blue from aqueous solution by nitric-acid treated water-hyacinth. J Hazard Mater 147:28–36

59. Chen L, Li F, Wei Y et al (2018) High cadmium adsorption on nanoscale zero - valent iron coated *Eichhornia crassipes* biochar. Environ Chem Let 17(1):589–594

60. Rodríguez-Espinosa PF, Mendoza-Pérez JA, Tabla-Hernandez J et al (2018) Biodegradation and kinetics of organic compounds and heavy metals in an artificial wetland system (AWS) by using water hyacinths as a biological filter. Int J Phytoremediat 20(1):35–43

61. Roberta G, Bronzato F, Ziegler SM et al (2018) Water hyacinth second-generation ethanol production: a mitigation alternative for an environmental problem. J Nat Fibers 16:1201–1208

62. Zhang B, Zhong Z, Li T et al (2018a) Bio-oil production from sequential two-step microwave-assisted catalytic fast pyrolysis of water hyacinth using Ce-doped γ-Al2O3/ZrO2 composite mesoporous catalyst. J Anal Appl Pyrolysis 132:143–150

63. Zhang Q, Wei Y, Han H et al (2018b) Enhancing bioethanol production from water hyacinth by new combined pretreatment methods. Bioresour Technol 251:358–363

64. Rezania S, Din MF, Taib SM (2017) Ethanol production from water hyacinth *(Eichhornia crassipes)* using various types of enhancers based on the consumable sugars. Waste Biomass Valori 9(6):939–946

65. Pothiraj C, Arumugam R, Gobinath M (2014) Sustaining ethanol production from lime pre-treated water hyacinth biomass using mono and co-cultures of isolated fungal strains with *Pichia stipitis*. Bioresour Bioprocess 1:27

66. Barua VB, Kalamdhad AS (2018) Anaerobic biodegradability test of water hyacinth after microbial pretreatment to optimise the ideal F/M ratio. Fuel 217:91–97

67. Barua VB, Goud VV, Kalamdhad AS (2018) Microbial pretreatment of water hyacinth for enhanced hydrolysis followed by biogas production. Renew Energy 126:21–29

68. Priya P, Nikhitha SO, Anand C et al (2018) Biomethanation of water hyacinth biomass. Bioresour Technol 255:288–292

69. Adanikin BA, Ogunwande GA, Adesanwo OO (2017) Evaluation and kinetics of biogas yield from morning glory (*Ipomoea aquatica*) co-digested with water hyacinth (*Eichhornia crassipes*). Ecol Eng 98:98–104

70. Patil JH, AntonyRaj MAL, Shankar BB (2014) Anaerobic co-digestion of water hyacinth and sheep waste. Energy Procedia 52:572–578

71. Singhal V, Rai JPN (2003) Biogas production from water hyacinth and channel grass used for phytoremediation of industrial effluents. Bioresour Technol 86:221–225

72. Pattra S, Sittijunda S (2015) Optimization of factors affecting acid hydrolysis of water hyacinth stem (*Eichhornia crassipes*) for bio-hydrogen production. Energy Procedia 79:833–837

73. Kumari S, Das D (2019) Biohythane production from sugarcane bagasse and water hyacinth: a way towards promising green energy production. J Clean Prod 207:689–701

74. Gao J, Chen L, Yan Z et al (2013) Effect of ionic liquid pretreatment on the composition, structure and biogas production of water hyacinth *(Eichhornia crassipes)*. Bioresour Technol 132:361–364

75. Zhao BH, Chen J, Yu HQ (2017) Optimization of microwave pretreatment of lignocellulosic waste for enhancing methane production: hyacinth as an example. Front Environ Sci Eng 11:1–9

76. Varanasi JL, Kumari S, Das D (2017) Improvement of energy recovery from water hyacinth by using integrated system. Int J Hydrogen Energy 43:1303–1318

77. Ruen-ngam D, Jaruyanon P (2018) New batch and continuous systems for converting hydrogen from water hyacinth. Chem Eng Commun 2018:1–13

78. Elsamadony M, Tawfik A (2018) Maximization of hydrogen fermentative process from delignified water hyacinth using sodium chlorite. Energy Convers. Manag 157:257–65

79. Soenjaya SA, Handoyo N, Soetaredjo FE (2015) Preparation of carbon fiber from water hyacinth liquid tar. Int J Ind Chem 6:1–7

80. Liguori R, Amore A, Faraco V (2013) Waste valorization by biotechnological conversioninto added value products. Appl Microbiol Biotechnol 97(14):6129–6147
81. Asrofi M, Abral H, Kurnia YS et al (2018) Effect of duration of sonication during gelatinization on properties of tapioca starch water hyacinth fiber biocomposite. Int J Biol Macromol 108:167–176
82. Chonsakorn S, Srivorradatpaisan S, Mongkholrattanasit R (2019) Effects of different extraction methods on some properties of water hyacinth fiber. J Nat Fibers 16(7):1015–1025
83. Thiripura Sundari M, Ramesh A (2012) Isolation and characterization of cellulose nanofibers from the aquatic weed water hyacinth – *Eichhornia crassipes*. Carbohydr Polym 87:1701–1705
84. Xia A, Cheng J, Song W (2013) Enhancing enzymatic saccharification of water hyacinth through microwave heating with dilute acid pretreatment for biomass energy utilization. Energy 61:158–166
85. Nguyen Thi BT, Ong LK, Nguyen Thi DT (2017) Effect of subcritical water pretreatment on cellulose recovery of water hyacinth (*Eichhornia crassipe*). J Taiwan Inst Chem Eng 71:55–61
86. Devi RR, Dhar P, Kalamdhad A et al (2015) Fabrication of cellulose nanocrystals from agricultural compost. Compost Sci Util 23:104–116
87. Mochochoko T, Oluwafemi OS, Jumbam DN et al (2013) Green synthesis of silver nanoparticles using cellulose extracted from an aquatic weed; water hyacinth. Carbohydr Polym 98:290–294
88. Wauton I, Ogbeide SE (2019) Characterization of pyrolytic bio-oil from water hyacinth (*Eichhornia crassipes*) pyrolysis in a fixed bed reactor. Biofuels. https://doi.org/10.1080/17597269.2018.1558838
89. Gulab H, Hussain K, Malik S et al (2018) Effect of process conditions on bio-oil composition and production from catalytic pyrolysis of water hyacinth biomass. Waste Biomass Valori 10(9):2595–2609
90. Lin H, Rong C, Jiu B et al (2017) Effects of chromium on pyrolysis characteristic of water hyacinth (*Eichornia crassipes*). Renew Energy 115:676–684
91. Gajalakshmi S, Abbasi SA (2002) Effect of the application of water hyacinth compost/vermicompost on the growth and flowering of *Crossandra undulaefolia*, and on several vegetables. Bioresour Technol 85:197–199
92. Deshpande P, Nair S, Khedkar S (2009) Water hyacinth as carbon source for the production of cellulase by Trichoderma reesei. Appl Biochem Biotechnol 158:552–560
93. Rombaut N, Tixier AS, Bily A (2014) Green extraction processes of natural products as tools for biorefinery. Biofuels Bioprod Biorefin 8(4):530–544

Furfural and Chemical Routes for Its Transformation into Various Products

Nayan J. Mazumdar, Rupam Kataki, and K. K. Pant

Abstract Vegetable biomass is basically made up of C_6 and C_5 sugars which constitutes of cellulose, hemicellulose and lignin along with other energy storage products like lipids and starches. The global interest and need to reduce the dependency on crude oil for energy have motivated and directed the researchers and scientists to explore the field of biomass as a source of energy especially for transportation fuels for vehicles. Gradual development of technology has shifted the interest to derive the conventional petroleum-based chemicals from biomass components with functional groups. Henceforth catalytic reactions, various chemical routes via heterogeneous catalysis, homogeneous processes, enzyme reactions for transformation and conversion of lignocellulosic biomass to various bio-based value-added chemicals have been extensively and widely explored, with special interests on developing environmentally friendly processes involving mineral acids, bases, etc.

Chemical transformation of sugars, which are made up of monosaccharide and disaccharides (glucose, fructose, xylose), is the most important and explored reaction pathway due to its availability in biomass primary compounds. Three important nonpetroleum-based chemicals, i.e. furfural (FUR), 5-hydroxymethylfurfural (5-HMF) and levulinic acid (LA), are derived via thermal dehydration of pentose and hexose sugars. FUR is one of the important chemicals derived from biomass and also one of the key derivatives for producing significant nonpetroleum-derived chemicals. The annual production of FUR is about 300,000tTonne/year. FUR is commercially produced by hydrolysis of pentosan polymers in biomass to pentose sugars (xylose) which undergo acid catalysis under high temperatures and successive dehydration. Furfuryl alcohol (FAL) is one such important product produced from catalytic hydrogenation of FUR. Cannizzaro reaction of FUR further produces furoic acid (FuA) which is an important feedstock for organic synthesis and an intermediate compound in the production of medicines and perfumes. Further,

N. J. Mazumdar (✉)
Department of Chemical Engineering, IIT Delhi, New Delhi, Delhi, India

Department of Energy, Tezpur University, Tezpur, Assam, India

R. Kataki
Department of Energy, Tezpur University, Tezpur, Assam, India

K. K. Pant
Department of Chemical Engineering, IIT Delhi, New Delhi, Delhi, India

hydroxymethylation of FUR with formaldehyde is the commercial method for producing hydroxymethylfurfural (HMF). Commercial production of furan and tetrahydrofuran (THF) is also via catalytic decarbonylation and successive hydrogenation of FUR.

The different kinds and types of catalysts used in these processes of hydrogenation, alkylation and reduction by various researchers over the period of time also need to be properly combined in a single source, so as to create an updated library of various reaction pathways done so far with FUR to produce various kinds of value-added chemicals.

Keywords C5 sugars · Xylan · Furfural · Furfural hydrogenation · Resinification

1 Introduction

History: In year 1831, Johann Wolfgang Döbereiner successfully isolated an oily substance which was yellow in colour, through the reaction of carbohydrates by sulphuric acid and manganese oxide. In 1845, George Fownes prepared a similar substance when he experimented with bran in acid medium for digestion and named the product obtained as furfural, which had a molecular formula $C_5H_4O_2$. In 1922, Quaker Oats Company of Iowa which was located at Cedar Rapids started commercial mass production of the chemical furfural in their cereal production industry with a production rate of several tonnes per month [1]. The usage and applications of furfural in the oil-refining industry and phenol resins gradually necessitated the increase in synthesis of furfural in the years 1930s to 1940s. Commercial availability of furfuryl alcohol by the process of high-pressure reduction was also started by Quaker Oats in 1934, which is presently the largest product derived from furfural. Du Pont in 1949 discovered Nylon 66 by a new process using furfural which led to exponential increase of the production of furfural in the 1950s. It was eventually abandoned by Du Pont in 1961, when one of the important intermediates, tetrahydrofuran, started to be manufactured from C_4 hydrocarbons (Reppe process). Tetrahydrofurfuryl alcohol which is soluble in water was produced by using furfuryl alcohol as precursor in 1955 for commercial uses. In 1958, resins manufactured from furfural and its derivatives found wide usage in the foundry industry after a new process which involves furan was introduced for the production of casting moulds. Subsequently in 1985 furfuryl alcohol was used as a key intermediate for producing ranitidine, an antiulcer drug.

Some chemicals derived from furfural:

- Furfuryl alcohol.
- Tetrahydrofurfuryl alcohol.
- Furfural resins.
- Levulinic acid.
- γ-Valerolactone.

- 1,5-Pentanediol-derived biofuels.
- 2-Methyl tetrahydrofuran.
- 2-Methylfuran.
- Furan.
- Cyclopentanone.
- Furfurylidene ketone.
- Furfuryl amine.
- Furoic acid.
- Succinic acid.

Sustainable production and synthesis of fuels and chemicals are very much important and necessary for the development of modern-day society. A variety of factors, like increased demand for the fuels and chemicals which is related to the exponential global rise in population, the gradual slump in the fossil fuel reserves and growing environmental concerns, are directly responsible for the increased requirement. The European Parliament in 2008 declared a notion for mandatory increase of present energy efficiency by 20%, and renewable energy should contribute at least 20% of the total energy that will be expended in the end of year 2020 [2]. The USA and China have already started working on different policies to reach this goal. Food crops such as sugarcane and wheat, which are being used for development of biofuels, have been criticised due to its influence on the food economy and environment. Without subsidies they fail to compete with conventional fossil fuels, and reduction of greenhouse gases is very limited by the use of these biofuels. Hence the new field of research and development in lignocellulosic biomass (nonedible) has opened up with tremendous possibilities. These second-generation biofuels are sustainable from economical and geopolitical point of view without having any disadvantages as the previous first-generation fuels. They have emerged as one of the most feasible and promising platforms aimed at producing ecologically clean and supportable chemicals and biofuels [3].

Presently, the process of bioethanol production from carbohydrates which are biomass derivatives is commercially feasible. In addition to this, the production of bio-based chemicals is also very much feasible from the commercial point. Over recent years, these chemicals have carved themselves a niche amidst the competition from the conventional crude oil industry derivatives. They have a wide variety of chemical routes like gasification, fermentation, pyrolysis, etc. for transforming into chemicals, which is very much broad and wide [4].

In this context, furfural (FUR) has been advocated as one of the topmost value-added chemicals to be derived from biomass. It is also one of the key platform chemicals to be produced from bio-refineries. Furfural is produced from agricultural residues produced from food crops and wood. Production of furfural from petroleum derivatives based on the raw materials like 1,3-dienes via catalytic oxidation is not economically feasible and sustainable. Presently, China is the largest producer of furfural with almost 70% total production capacity. Other countries like South Africa and Dominican Republic also contribute to approximately 20, 32 kTon/year, respectively. These nations together contribute to almost 90% of the total FUR being produced in the whole world [5].
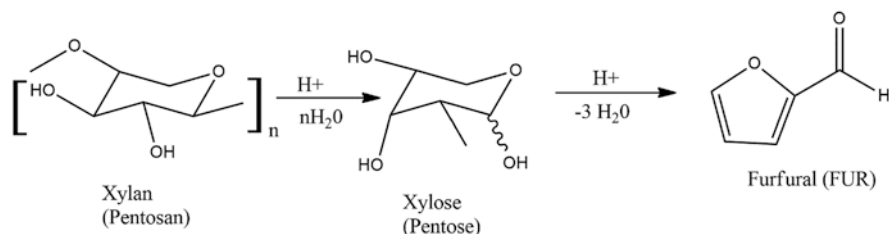
Fig. 1 Reaction scheme of conversion of Xylan to FUR [2]

Presently FUR is being manufactured industrially by the conversion of pentose sugars via acid catalysis of biomass. Initially hydrolysis of C_5 polysaccharides to monosaccharaides of xylose is done and further dehydrated to FUR (Fig. 1).

The presence of an aldehyde (-CHO) and the aromatic ring in furfural makes it capable for high chemical reactivity, and FUR undergoes different aldehyde reactions, for example, acetalisation reaction, acylation reaction and condensation reactions. Furfural also undergoes some reduction reactions from alcohols, amines, etc. Presently, FUR is being used as a chemical feedstock for producing furfuryl alcohol, furan, methyl furan, furfurylamine, etc. One of the most important applications of FUR is production of tetrahydrofuran and methylfuran, which is used widely as an important solvent in the industry [6].

Acid hydrolysis of lignin is also a constantly analysed area for production of a variety of value-added chemicals like furfural, furfuryl alcohol, levulinic acid and ethyl levulinate [7]. Out of all the products obtained from FUR, 2-methylfuran has wide usage as a flavouring substance and as an alternative fuel. It has a molecular weight of 82.1 g/mol and has a boiling point of 63 °C. It has an appearance of colourless to light yellow and is highly flammable. It has wide applications in the perfume industry and personalised care industry. The traditional route of converting pentose sugar derived from hemicellulose to furfural which is transformed into furfuryl alcohol via metal-doped catalysed hydrogenation eventually serves as a precursor to form ethyl levulinate which is one of the most valuable platform chemicals derived from biomass [8]. Furfural is one of the most critical petroleum derivatives.

All the chemicals that can be synthesised from FUR are shown in Fig. 2.

2 Furfural Properties

2.1 Properties

2.1.1 Physical Properties

Furfural also known as 2-furaldehyde and furfuraldehyde has the structure of $C_5H_4O_2$ and molecular weight of 96.08. It has an odour similar to almonds, and it is
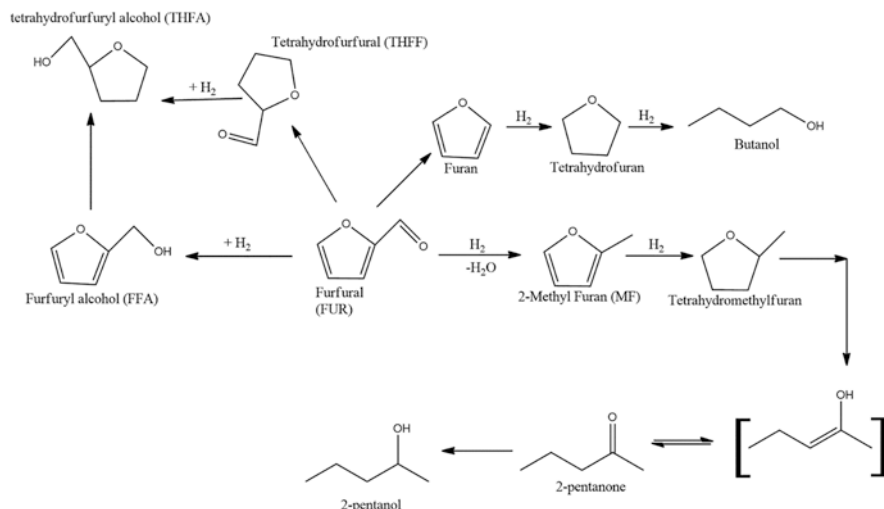
Fig. 2 Reaction pathway of furfural hydrogenation [9]

used as an extractant to remove aromatics from lubricating oils and diesel [1]. It forms an azeotropic mixture with H_2O at 1 atm pressure (65 wt% water and boiling point 97.85 °C). Table 1 lists the general properties of furfural.

2.1.2 Chemical Properties

Aldehydes react widely to form various by-products by undergoing acylation reaction, aldol condensations, acetalisation, reduction, amination reactions, oxidation, Knoevenagel condensations and decarbonylation which can be performed with furfural. The furan ring in furfural is less vulnerable to hydrolytic ring opening due to the presence of the carbonyl group which provides the electron-withdrawing effect of the carbonyl group and also helps in Diels-Alder reactions.

Alkylation (arylation): Furfural reacts with chlorinated hydrocarbons to undergo Friedel-Crafts alkylations. The 5-position being the most vulnerable for the alkylation reaction eventually leads furfural to develop resin-like properties [1]. Furfural also undergoes alkylation via oxidative coupling by usage of Pd acetate as catalyst which acts as an alkylating driving force. This reaction generates moderate yield percentage and Pd-based turnover numbers when acrylic esters are used. Using photochemical aryl coupling of furfural and 5-bromofurfural, 5,5-diformyl-2,20-di-furan is formed. Synthesis of this reaction in the presence of an acid medium yields high amount of 5,5-diformyl-2,20-di-furan [10].

Table 1 Furfural: physical
properties

Molecular weight	96.08
Boiling point at 101.3 kPa	161.7 °C
Freezing point	−36.5 °C
Density at 20 °C	1.1598 g/cm³
Solubility in water (25 °C)	8.3 wt%
Flash point	61.7 °C
Heat of vaporisation (liquid)	42.8 kJ/mol
Heat of combustion (liquid)	2344 kJ/mol
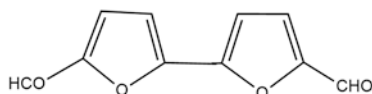
5,5-Diformyl-2,2'-difuran

Cannizzaro reactions: Furfural undergoes Cannizzaro reaction with KOH solution as medium to yield equimolar percentages to form potassium furan-2-carboxylate and furfuryl alcohol. Microwave-assisted reactions under solvent-free conditions can also be performed for Cannizzaro reactions of furfural [11]. Presently furfural undergoing Cannizzaro reaction is widely performed for commercially producing furoic acid.

Acetalisation and acylation: Furfural undergoes acetalisation reaction like other aldehydes with various alcohols. Recent use of montmorillonite clays exchanged with cerium and aluminosilicates which are mesoporous in size yielded good results and were found to be efficient for the formation of acetals from furfural [12].
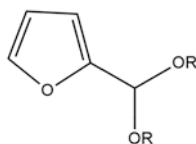
Furfuryl acetal

Acid anhydrides are also used for acylation of furfural [13, 14]. Formation of furfuryl diacetate is done with ethanoic anhydride and SnCl₂ as catalyst. Recently acid catalysts such as H-Nafion, ferric chloride and silica reacted in microwave conditions and silica-supported Wells-Dawson heteropoly acid have been applied for furfural acylation [15].
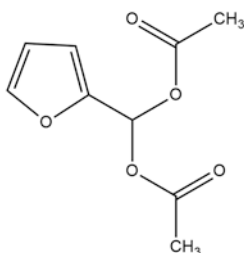
Furfuryl diacetate

Condensation reactions: Aldol reaction of furfural is done with sodium hydroxide or potassium hydroxide along with aldehydes which reacts as alkaline catalysts [16]. Condensation reaction of $C_5H_4O_2$ (furfural) with benzene-acetaldehyde which gives 2-phenyl-3-(2-furyl)propenal can be considered a typical example of furfural condensation reaction.
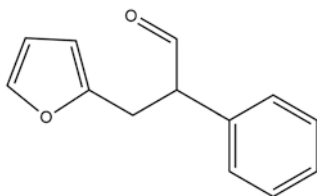
2-Phenyl-3-(2-furyl)-propenal

This reaction is known as Knoevenagel condensation when the active α-hydrogen atom is replaced with an ester, acid or organic compound having $-C≡N$ functional group [17]. Recently microwave-assisted and solvent-free methods with heterogeneous catalysts have garnered attention [18].

Reduction and reductive amination: Reduction of furfural is by far the most widely used principle reaction in the industry presently. Products obtained from furfural reduction are furfuryl alcohol, tetrahydrofurfuryl alcohol, furfurylamine and tetra-hydrofurfurylamine [1].

Oxidation: The presence of the aldehyde group in furfural helps in catalytic oxidation of furfural in the presence of air and H_2O_2 and oxygen. At temperatures of around 320 °C, furfural undergoes oxidation with O_2 to produce acid anhydride of maleic acid ($C_2H_2(CO)_2O$) with a yield of around 25% using MoO_3–V_2O_5 as catalysts [19].
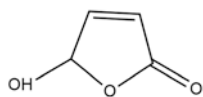
5-hydroxy-2(5H)-furanone

Almost 80% yield of 5-hydroxy-2(5H)-furanone is obtained via photooxidation of furfural ($C_5H_4O_2$) along with single di-oxygen, 5-hydroxy-5H-furan-2-one being a very adaptable compound used in organic synthesis along with being a key ingredient in many active compounds [20]. The primary usage of 5-hydroxy-5H-furan-2-one is majorly as a potent pesticide and insecticide.

Halogenation and nitration: 5-Chloro-2-furfuraldehyde and 5-nitrofurfural are formed by the halogenations and nitration of furfural at the 5-position. Bromine reacts with furfuryl diacetate to form 5-bromo-2-furfuraldehyde. Furfural undergoes nitration with fuming HNO_3 in ethanoic anhydride in temperature of −10 °C [21]. Subsequently 5-nitro-2-furfuraldehyde is formed via hydrolysis of the nitrated furfural. Manufacturing of a wide variety of antimicrobial nitrofuran pharmaceuticals requires key components as 5-nitro-2-furaldehyde and 5-nitro-2-furaldehyde diacetate.
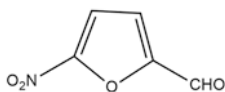
5-nitro-2-furfuraldehyde

Grignard reaction: Secondary furfuryl alcohol results in the reaction between 2-furaldehyde and Grignard compound (R-Mg-X). It is widely used in the production of 5-methyl-2-furanmethanol which is the antecedent for maltol production [1].
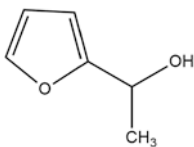
α-methylfurfuryl alcohol

Resinification: Furfural reacts very sensitively to resinification and when heated experiences symmetrical aldol condensation in the presence of both acid and alkaline mediums. Furfural undergoes the formation of di-furyl ketonic aldehyde (P) and then trifurylic dialdehyde (Q) in the initial stages of polymerisation [22].

Trifurylic dialdehyde yields black cross-linked polymer which results in further polymerisation.
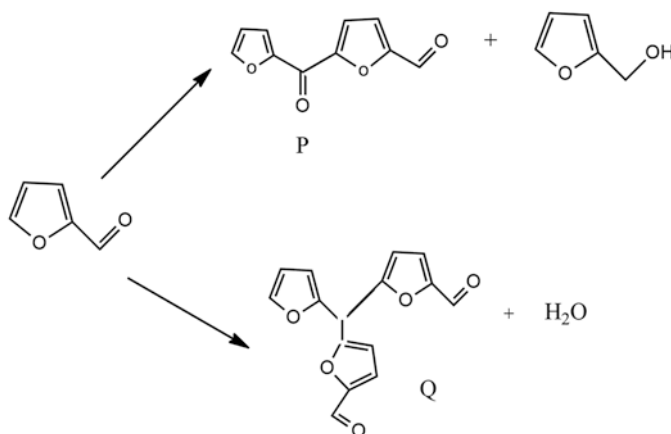
Furfural (FUR), $C_5H_4O_2$, has high chemical reactivity due to the presence of an aldehyde group and an aromatic ring. Due to this reason, FUR undergoes different types of aldehyde reactions like Knoevenagel condensations, aldol condensation, acylation, acetalisation, etc. FUR also takes part in Grignard reactions, alcohol reductions, reductive amination to amines, decarbonylation and oxidation reactions to form carboxylic acids. Due to the presence of the aromatic furan ring, FUR also undergoes reactions like hydrogenation, nitration, alkylation, oxidation and halogenation. FUR is currently used as the most relevant platform chemical feedstock for producing chemicals like furfuryl alcohol, heterocyclic compounds like furans, 2-methylfuran, furfurylamine, furoic acid, etc.

Since the early twentieth century, which is termed as the golden age of furan chemistry, FUR has been used widely as a solvent and to manufacture phenol-FUR resins. In recent times FUR is being viewed as a feedstock for production of biofuels and bio-based chemicals, which is evident from the rising number of research publications from the last 5 years on catalytic transformation of furfural to other chemicals [23]. For the literature review of this report, the research work which dealt with FUR conversion to direct production of biofuels or indirectly from any other chemicals obtained from FUR was studied and reviewed. Mechanisms and work done on potential furanic chemicals and compounds which have direct implementation and applications in the industry and are derived from FUR were also studied and noted in this review.

Hydrogenation reaction is widely used for FUR conversion because of its industrial feasibility and ease of commercialisation. Biofuels and value-added chemicals like tetrahydromethylfuran, furfuryl alcohol, methylfuran, tetrahydrofurfuryl alcohol, cyclopentanone, etc. are derived from the process. For industrial synthesis of FUR, catalytic hydrogenation is performed which is either gas or liquid phase.

Although the gaseous-phase hydrogenation in the presence of copper (Cu) catalyst of furfural is the favoured route for conversion of FUR to biofuels, in this report we tried to explore the field of liquid-phase hydrogenation which is much more feasible from lab-scale perspective. From economical perspective, the liquid-phase hydrogenation requires much less as compared to the gas-phase process. In the gaseous-phase hydrogenation of FUR, the use of an evaporator system for FUR feeding, which consists of a packed column, in addition to that a circulating pump, heaters, and supply of continuous H_2 gas under high pressure must be maintained.

Hydrogenation of 2-furaldehyde was initially started in year 1928 by a company called the Quaker Oats Company, by using bimetallic catalyst of nickel (Ni) supported on magnesium oxide (MgO) which required absolute control to prevent total conversion of FUR and to prevent side-step reactions forming tetrahydrofurfuryl alcohol as product [2]. One of the most widely catalyst was reduced copper (Cu) and chromite (Cr), which was used under high temperature and pressure, yielding more than 90% of furfuryl alcohol production from FUR. Further addition of basic metal oxides as calcium oxide (CaO) and barium oxide (BaO) resulted in an improved furfuryl alcohol yield and high selectivity even at low H_2 pressures. From industrial perspective, the use of chromium catalysts was very much feasible and successful. But from the environmental concern, the main drawback being excess toxicity of chromium led to more research in the field of catalysts for designing a catalyst which is cost-effective, environmentally safe and environmentally friendly. It was seen that the hydrogenation of furfural was producing chemicals like furfuryl alcohol and subsequent furanic chemicals with selectivity close to 100%. But the use of high hydrogen pressure adds to the risk of operation. Hence various metals like nickel (Ni) and copper (Cu) were mostly under different experimental conditions. By using these multicomponent systems, almost full conversion of furfural to furfuryl alcohol was attained [24].

With the current effort focussed on developing economically viable, inexpensive and environmentally sustainable new technologies, H_2O-organic solvent biphasic systems such as poly(styrene sulphonic) acid for xylose dehydration to furfural were used [23]. The mechanism behind such an approach was to utilise the coefficient of partition of FUR between the organic solvent and H_2O. Due to the absence of a catalyst in the inhibition phase of degradation reaction, FUR exhibits higher affinity towards the organic phase. A large variety of catalysts such as sulfonated metal oxides, sulfonic ion-exchange resins, zeolites and zeotypes, sulfonic acid-modified mesoporous silicas, Keggin heteropoly acids, mesoporous niobium phosphate, etc. have been tried and tested in the recent years. Reaction kinetics of the liquid-phase selective hydrogenation have been also studied with catalysed synthesised by platinum metal doped over carbon (Pt/C) [25]. The Langmuir-Hinshelwood dual-site mechanism is adequately followed which have separate active sites associated with hydrogen adsorption and for furfural and furfuryl alcohol. Furfural and hydrogen adsorption together forms the rate determining step. The copper (Cu)-doped catalysts are deactivated, and by atomic layer deposition via sintering and leaching, it is used for selective liquid-phase hydrogenation [26]. Reducing an aldehyde by oxidising it in the presence of a secondary alcohol, which is also known as

the Meerwein-Ponndorf-Verley (MPV) reduction, is the basis of catalytic transfer hydrogenation (CTH) [27].

In an ex situ reaction mechanism as shown in Fig. 3a, the hydrogen required for the MPV reduction is provided externally generally by passing H_2 gas under high pressure. As the reaction proceeds, the hydrogen firstly attaches itself to the catalyst surface, and when Furfural interacts with the catalyst, the hydrogen detaches itself from the catalyst surface and reacts with the aldehyde ($-CHO$) transforming the double bond into a single bond and converting it to an alcohol.

In an in situ mechanism, as proposed by López-Asensio et al., the MPV reaction takes place with the help of heterogeneous catalysts such as metal oxides, zeolites, etc. They demonstrated the use of alumina which have co-existing Lewis acid sites and Bronsted acid sites, which carries forwards the hydrogenation. As shown in Fig. 3b, due to the presence of Lewis acid sites, the C=O aldehyde bond undergoes de-protonation, and the proposed mechanism depicts the formation of a temporary intermediate six-member structure. The availability of alumina and its low toxicity makes it an excellent and attractive choice for hydrogenation. In in situ mechanism, the hydrogen required for the FUR conversion is directly supplied from the secondary alcohol, which acts as a solvent. Hence, it removes the use of high-pressure H_2 supply, which is very dangerous and risky from safety point of view.

CTH process does not require the supply of external hydrogen, and the tendency to form by-products like methylfuran, tetrahydromethylfuran and furan is reduced. This acts as one of the prime and most important advantages and benefits of this process. The alcohol used as a solvent can be chosen with the corresponding aldehyde or ketone that is going to form after the reaction. Table 1 lists the performances of various kinds of catalysts used in the selective furfural hydrogenation.

Hydrogen (H_2) acts as a reducing mediator in liquid-phase hydrogenation, and it has been already proposed as an efficient substitute to convert functional groups like ketones (R-($C=O$)-R') or aldehydes ($-CHO$) to alcohols (R-OH). The use of hydrogen at high pressure can be avoided via this process. The Meerwein-Ponndorf-Verley (MPV) reduction helps in the reduction of aldehydes or ketones by alcohols in existence of a Lewis acid or basic catalyst [29]. Acidic Lewis sites activates the C=O bond of aldehyde and ketones, whereas the alcohol suffers deprotonation. With this hypothesis López-Asensio et al. used commercially available alumina (Al_2O_3) because it is easily available and has an affordable market price and is not toxic as well as environment-friendly. Also it also explains the greater catalytic reactivity of hydrotalcites compared to pure basic oxides, which holds good for
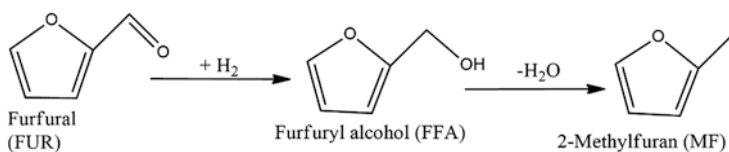
Fig. 3 (**a**) Ex situ mechanism of FUR reaction [28]. (**b**) In situ mechanism of FUR conversion
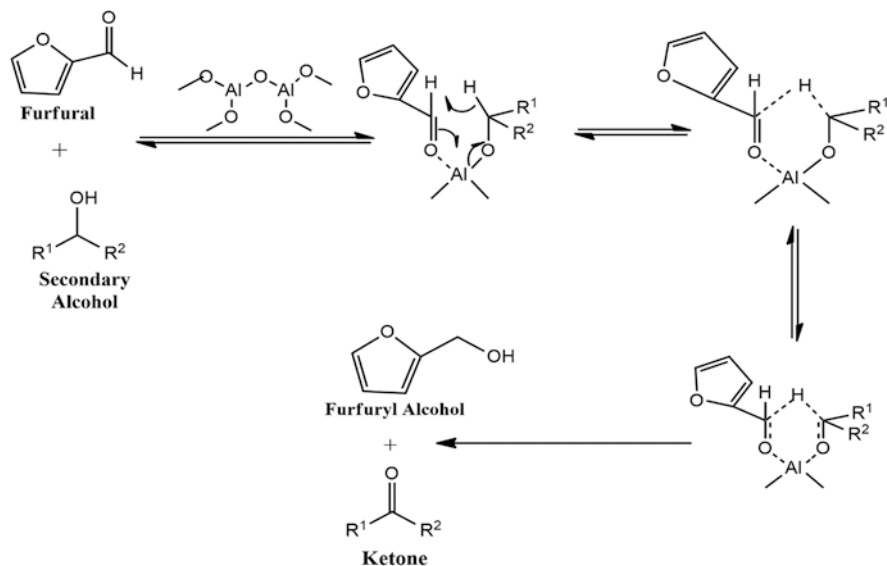
Fig. 21.3 (continued)

alumina as well. Higher temperature is required for high conversion in the case of alumina; on the contrary, lower reactivity of the Lewis acid sites helps in selective yield of furfuryl alcohol instead of converting all the way to MTHF, 2-MF, etc. [29]. Similarly, He et al. came up with low-cost mixed metal oxides by applying them widely with catalysis in addition with renewables due to their adjustable physico-chemical properties [30]. They introduced solid catalysts with magnetic properties due to easy separation and recycling of the catalyst from the liquid mixture by applying an external magnetic field. They used bifunctional magnetic $Al_7Zr_3@$ Fe_3O_4 oxide catalysts and observed conversion of furfural up to ~100% but at a very high temperature of 180 °C [30]. Interestingly, readily available potassium fluoride (KF) was able to give a yield of 76% of furfuryl alcohol by converting 76% of FUR at room temperature in just 5 min [31]. This was probably due to the high nucleo-philicity of fluoride, which would have been favourable for FUR conversion. But the toxicity and corrosive nature of fluoride do make this process neither a favour-able nor a sustainable one. Due to their lower stabilisation possibility of silicon atoms, using polyhydrosiloxane (which is very expensive) may have led to high conversion of FUR to furfuryl alcohol [31]. Bimetallic systems of catalysts were also used for hydrogenation of furfural by controlled surface reaction to reduce unwanted side reactions [32]. Vetere et al. tried using Pt, Rh and Ni catalysts pro-moted with tin and got FUR conversion of 31% at 100 °C with selectivity of furfuryl alcohol of 97% with Ni being an attractive option due to its low cost.

Merlo et al. tried with Pt-based bimetallic catalyst for furfural conversion. They got the highest conversion of 100% FUR with the lowest Sn/Pt atomic ratio. It was concluded that Pt-Sn systems were more active than the monometallic catalyst. And

the use of Pt-based system was also highly selective, yielding only the desired product. But the use of elevated pressure (1 MPa) of hydrogen gas was still to be taken care of [6]. Co-Cu/SBA-15 as catalysts were used for FUR conversion with fixed copper loading of 10% by Srivastava et al. [33]. Mesoporous silica associated with bimetallic catalyst was tried in this experiment. SBA-15 being hydrothermally stable and having high surface area will prove advantageous in the FUR conversion. Furthermore, solid interaction between cobalt and copper will help enhance the constancy of copper in the bimetallic catalyst combination [32]. One hundred percent FUR conversion was achieved at 170 °C. Villaverde et al. used Cu-Mg-Al as catalysts for FUR conversion and at 110 °C got approximately 64% conversion of FUR. The intimate interaction between Cu^0 atoms and Mg^{2+} cations entangled in a spinal-like matrix is the probable reason of the highest activity of Cu-Mg-Al with furfuryl alcohol selectivity of 99% [33]. Novel Cu-Zn-Cr-Zr catalysts were developed and experimented by Sharma et al. for FUR conversion. One hundred percent conversion of FUR with 96% furfuryl alcohol yield was obtained. This was probably due to delineation of the constituent metals in the catalyst. On the one hand, Zn increases the activity of FUR conversion; on the other hand, Zr contributes in the selectivity of furfuryl alcohol. It was found that Zr loading in the catalyst increased the acidity of the catalyst and helps dispersing the metallic Cu as well. Cu/TiO_2 was used in the presence of green solvent cyclopentyl methyl ether (CPME) to achieve 100% FUR conversion and 99% selectivity of furfuryl alcohol in a microwave reactor. One of the probable causes is being the dielectric microwave heating, which could increase the temperature of the active sites of the catalysts above the bulk temperature. And TiO_2 having a high dielectric constant receives and absorbs the irradiation and getting super-heated and increasing the conversion rate [34]. Cu supported on $MgO-Al_2O_3$ in the presence of isopropanol generated 100% furfural conversion with 89.3% furfuryl alcohol yield. The results were due to the Cu loading in the catalyst which influenced the catalyst's acidity, especially the Lewis acid. With the increase of Cu loading, weak and high basic strength sites increased. The physicochemical properties of Cu were important for the CTH of FUR, which occurred at the surfaces of metallic sites.

3   Applications and Commercial Features of Furfural

Uses: Out of the total furfural production in the world, 60–70% is utilised for manufacturing of 2-furanmethanol or furfuryl alcohol. The remaining part is used as:

- Aromatic extractants from lubricating oils.
- Solvent used for purification of C_4 and C_5 hydrocarbons.
- Reactive solvent and wetting agent.
- Used as a chemical feed for deriving other furanic compounds.
- Used as an insecticide.

2-Furaldehyde or furfural is widely used as a solvent in the petrochemical industry. Initial refining industrial plant established in 1933 by Texaco, the Indian Refining Company, led to production of several high-valued lubricating oils along with producing benzene, toluene, xylene and other polar compounds, mercaptans and compounds derived from crude oil with the help of furfural for extraction. Furfural found wide usage as decolorising compound in refining wood rosin [21]. After the development of butadiene purification technology which was used to manufacture synthetic rubber by the USA during World War II, the demand of furfural increased. Since furfural undergoes extractive distillation with buta-1,3-diene and 2-methylbuta-1,3-diene and can be alienated from saturated C_4 and C_5 hydrocarbons. In addition to the synthesis of furfuryl alcohol, furfural is also widely used as a chemical feedstock for a lot of other five-member furanic compounds such as furan, 2-methylfuran, acetyl-furan, 1-(2-furyl)methylamine and furoic acid. Furfural has also been introduced in South Africa as an insecticide to protect the plants. Toxicity of the present insecticide and pesticides (e.g. methyl bromide) although effective in removing pests has adverse health effects upon humans that occurs due to prolong exposure. Furfural is much less toxic and effective as a pesticide in controlling worms in the soil.

Economic aspects: World production of furfural in 2003 was 200,000 tonnes, and the market is projected to reach 423,372 tonnes by 2024. It has been estimated that the furfural market size is projected to grow from USD 551 million in 2019 to USD 700 million by 2024 at a compound annual growth rate (CAGR) of 4.9%. The last two decades have seen the monopoly of China in the furfural-producing industry. Presently, furfural activities are established basically in the developing countries where cheap labour and low operational costs along with favourable climatic conditions and fertile land are available. Furfural production is evolving in nations like the Dominican Republic, China, Thailand, India, Argentina, Brazil, Mexico, the USA, Tunisia and South Africa. At present China being the largest producer of furfural across the globe contributes to around 70% of the total production. The rest of the countries contribute for approximately 280 kTon of the global production capacity of furfural.

Conclusion: Viability of furfural-based bio-refinery, which will initially require large investments, might initially face potential technological hindrance but will be very much dependent on present and future returns and incentives. Well-designed policies and regulatory mandates regarding biomass-derived platform chemicals and value-added chemicals are required for ensuring economic viability and success of furfural-based bio-refineries. Furfural-based bio-refineries would be competitive with the crude oil-derived products and chemicals. In spite of the unsteady and volatile oil market, the use of low-risk and well-designed technologies is very much needed for meeting the societal demands. Bio-refineries will clearly be a feasible solution in the future and a competitive option because of the depleting crude oil reserves and increasing price of manufacturing. However, increasing focus on environmental norms and energy security and management rather than commercial and economic viability should really carry forwards the research and development of furfural-based bio-refineries.

References

1. Hoydonckx HE et al (2012) Ullmanns Encycl Ind Chem 16:285–313
2. Mariscal R, Maireles-Torres P, Ojeda M, Sádaba I, López Granados M (2016) Energy Environ Sci 9(4):1144–1189
3. Huber GW, Iborra S, Corma A (2006) Chem Rev 106(9):4044–4098
4. Axelsson L, Franzén M, Ostwald M, Berndes G, Lakshmi G, Ravindranath NH (2012) Biofuels Bioprod Biorefin 6(3):246–256
5. Alonso DM, Bond JQ, Dumesic JA (2010) Green Chem 12(9):1493–1513
6. Merlo AB, Vetere V, Ruggera JF, Casella ML (2009) Catal Commun 10(13):1665–1669
7. Ahmad E, Pant KK (2018) Lignin conversion: a key to the concept of lignocellulosic biomass-based integrated biorefinery. In: Bhaskar T, Pandey A, Mohan SV, Lee D-J, Khanal SK (eds) Waste biorefinery. Elsevier, Amsterdam, pp 409–444
8. Ahmad E, Alam MI, Pant KK, Haider MA (2016) Green Chem 18(18):4804–4823
9. Corma Canos A, Iborra S, Velty A (2007) Chem Rev 107(6):2411–2502
10. Taljaard B, Burger GJ (2002) Adv Synth Catal 344:1111–1114
11. Yoshizawa K, Toyota S, Toda F (2001) Tetrahedron Lett 42:7983–7985
12. Wang C, Li M (2002) Synth Commun 32(22):3469–3473
13. Li T, Gao Y (1998) Synth Commun 28:4665–4671
14. Pereira C, Gigante B, Marcelo-Curto MJ (1995) Synthesis 09:1077–1078
15. Romanelli GP, Bennardi D, Ruiz DM, Baronetti G, Thomas HJ, Autino JC (2004) Tetrahedron Lett 45:8935–8939
16. Kantom ML et al (1998) Chem Commun 1:1033–1034
17. Loupy A et al (2001) J Chem Soc Perkin Trans 1:1220–1222
18. Kwon PK et al (1997) Synth Commun 27:4091–4100
19. Milas NA, Walsh WL, Am J (1935) Chem Soc 57:1389–1390
20. Esser P, Pohlmann B, Scharf HD (1994) Angew Chem 106:2093–2108
21. Dunlop AP, Peters FN (1953) ACS monograph series: the furans. Reinhold Publishing Corp., New York, NY, pp 152–156
22. Gandini A, Belgacem MN (1997) Prog Polym Sci 22:1203–1379
23. Granados ML, Alba-Rubio AC, Sádaba I, Mariscal R, Mateos-Aparicio I, Heras Á (2011) Green Chem 13(11):3203–3212
24. Lee SP, Chen YW (1999) Ind Eng Chem Res 38(7):2548–2556
25. Vaidya PD, Mahajani VV (2003) Ind Eng Chem Res 42(17):3881–3885
26. O'Neill BJ et al (2013) Angew Chem Int Ed 52(51):13808–13812
27. Corma A, Domine ME, Nemeth L, Valencia S (2002) J Am Chem Soc 124(13):3194–3195
28. Yan K, Liao J, Wu X, Xie X (2013) RSC Adv 3(12):3853–3856
29. López-Asensio R, Cecilia JA, Jiménez-Gómez CP, García-Sancho C, Moreno-Tost R, Maireles-Torres P (2018) Appl Catal A Gen 556:1–9
30. He J, Li H, Riisager A, Yang S (2018) ChemCatChem 10(2):430–438
31. Wu W et al (2018) Catal Commun 105:6–10
32. Vetere V, Merlo AB, Ruggera JF, Casella ML (2010) J Braz Chem Soc 21(5):914–920
33. Srivastava S, Mohanty P, Parikh JK, Dalai AK, Amritphale SS, Khare AK (2015) Chin J Catal 36(7):933–942
34. Romano PN, de Almeida JMAR, Carvalho Y, Priecel P, Falabella Sousa-Aguiar E, Lopez-Sanchez JA (2016) ChemSusChem 9(24):3387–3392

A Sustainable Process for the Synthesis of Alkylpyrazines by Dehydrocyclization of Crude Glycerol and Ethylenediamine over Metal Chromite Catalysts

Reema Sarkari, Vankudoth Krishna, Chatla Anjaneyulu, Velisoju Vijay Kumar, Enumula Siva Sankar, Gutta Naresh, and Akula Venugopal

Abstract Dehydrocyclization of ethylenediamine and crude glycerol was examined over ZnO-doped Cr_2O_3 catalyst. The 10 wt%-loaded Zn/Cr_2O_3 catalyst demonstrated a maximum rate of 2-methylpyrazine (2MP) production under the optimized reaction conditions. The prepared catalysts were investigated by various techniques such as PXRD, UV-DRS, XPS, FT-IR, and Raman spectroscopic analyses. Moreover, a correlation between Zn (wt%) loadings and the 2MP rate was established.

Keywords Alkylpyrazines · Dehydrocyclization · Glycerol · Ethylenediamine · Chromite catalysts

1 Introduction

1.1 Synthesis of 2-Methylpyrazine Over the $ZnCr_2O_4$ Catalysts

In recent decades, R&D has been focused on alternative fuels, specifically the production of biodiesel from inedible oils and renewable resources. Among various biofuels, many challenges were posed to technologists from the economic and environmental point of view on biodiesel production as a large amount of crude glycerol was found, which became a more significant concern for commercialization. Recovery and safe disposal of biodiesel coproducts such as glycerol have become an important issue in order to minimize the overall cost of biodiesel production.

R. Sarkari · V. Krishna · C. Anjaneyulu · V. V. Kumar · E. S. Sankar · G. Naresh
A. Venugopal (✉)
Catalysis and Fine Chemicals Department, CSIR – Indian Institute of Chemical Technology, Hyderabad, Telangana, India
e-mail: akula.iict@gov.in; akula@iict.res.in

Several routes were proposed and currently being utilized to convert such crude glycerol to produce a variety of industrially important chemical additives [1]. Therefore, the utilization of crude glycerol for the production of alkylpyrazines is the main topic in this book chapter.

To the best of our knowledge, we have developed a route for the first time to synthesize 2-methylpyrazine (2MP) via vapor-phase reaction by using ethylenediamine (EDA) and crude glycerol by dehydrocyclization over a mixed oxide catalyst composed of $ZnO\text{-}ZnCr_2O_4$ (Zn-Cr) derived from HTlc (as shown in Scheme 1) [2].

2MP is a key intermediate substance for the synthesis of 2-amidopyrazine is a well-known antitubercular and bacteriostatic drug. Commercially, 2MP was prepared by dehydrocyclization of EDA and 1,2-propylene glycol (PG) over Pd-promoted Zn-Cr catalyst (as shown in Scheme 2) [3].

In our previous reports, the effect of the acid-base properties of the Zn-Cr catalyst was investigated for product distributions during the synthesis of Zn-Cr HT precursors by changing their pH [4]. It was noticed that the acid-base characteristics of Zn-Cr catalyst significantly affect the 2MP selectivity. The Zn-Cr catalyst precursor synthesized at pH = 7 and exhibited enhanced selectivity toward pyrazine due to more acidic nature via the cyclization of EDA. In contrast, the catalyst that contains both weak acidity and basicity sites showed high 2MP selectivity. In comparison, high specific rate of 2MP was observed over the Zn-Cr catalyst prepared at pH $\sim$9 [5]. Under these experimental conditions, it is also quite possible that the ethylenediamine undergoes intermolecular cyclization to form pyrazine as a by-product (Scheme 3).

In our previous studies, the effect of catalyst calcination temperature on physicochemical characteristics of Zn-Cr catalyst and their influence on reaction
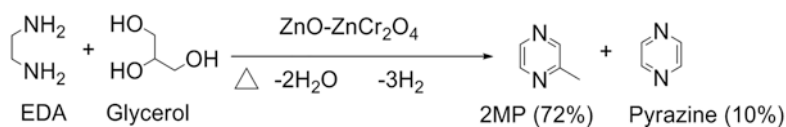
Scheme 1 Synthesis of 2MP via glycerol dehydrocyclization over Zn-Cr catalysts
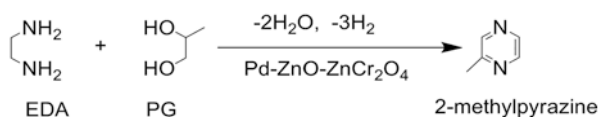
Scheme 2 Synthesis of 2MP by using EDA and PG over Pd-based Zn-Cr catalyst

Scheme 3 Intermolecular cyclization of EDA to form pyrazine
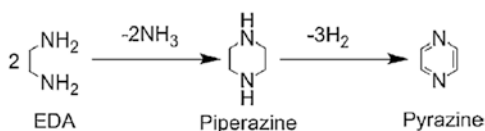
mechanism and product distribution was investigated [6]. The obtained results indicated the catalysts calcined at lower-temperature produced mixed oxides of ZnO-ZnCr$_2$O$_4$ are active and selective for 2MP synthesis. Moreover, 2MP selectivity remarkably depends upon catalyst crystallite size and acid-base strength. The mixed oxide catalyst characterization results showed that low-temperature treated catalyst produced higher 2MP yields, whereas the high-temperature one was more selective toward 2-pyrazinylmethanol. Based on the detailed experiments, a linear correlation was drawn between the rate of 2-pyrazinylmethanol and calcination temperature, which might be due to a decrease in the surface –OH groups on the Zn-O-Cr surface. In addition, the Zn-Cr mixed oxide catalyst activities were rationalized with poisoning studies using 2,6-dimethylpyridine (interacts with Brønsted acid site selectively) and pyridine (blocks both Lewis and Brønsted acid sites) to see the influence acid-base sites on 2MP rate [7].

1.2 Synthesis of 2,6-Dimethylpyrazine Over the CuCr$_2$O$_4$ Catalysts

In the previous section, a detailed investigation was discussed in the synthesis of 2-methylpyrazine (2MP). It has been established that under the reaction conditions, intermolecular cyclization of ethylenediamine is quite possible. Dehydrocyclization of 1,2-propanediamine and glycerol produced 2,6-dimethyl pyrazine (2,6-DMP) (as shown in Scheme 4) [8–13].

   In this section, a detailed overview is given on the applications and synthesis of 2,6-DMP from 1,2-propanediamine and (1,2-PDA) glycerol using the Cu-Cr catalysts under almost a similar protocol. 2,6-DMP is used in producing different agrochemicals, food flavoring agent, and as a ligand for catalyst synthesis. In 2014, Krishna et al. found a new methodology using solid acid-base catalyst to synthesize 2,6-DMP selectively from crude glycerol with 1,2-PDA under continuous-flow conditions at atmospheric pressure. This methodology was also useful for the selective synthesis of different alkylpyrazines with reduced by-products, as these solid acid-base catalysts gained more interest from both the environmental and economic views to explore crude bio-glycerol.

   In this reference, in our group, we have explored various chromite catalysts and found different product distribution over mixed oxides of M$_x$O$_y$–MCr$_2$O$_4$ (M = Cu, Fe, Ni, Co, Mg, and Ni) synthesized from their respective HT precursors [8]. In this investigation, it was concluded that the catalysts with both acid and base functionalities in close proximity with that of metal sites were effective for the selective
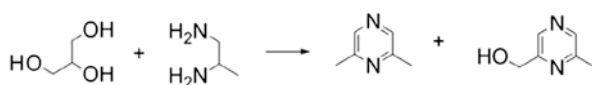
Scheme 4 Synthesis of 2,6-DMP by using 1,2-propanediamine and glycerol

synthesis of 2,6-DMP from 1,2-PDA and glycerol. The Cu-Cr-O catalyst performed better in 2,6-DMP production although methanol and KOH were present in the reaction mixture. The interaction (solid-solid) in Cu_xO_y–$CuCr_2O_4$ due to CuO resulted in easily reducible species (Cu-Cr from Cu-Cr-O) was the main reason for high activity over this catalyst. It was also found to be more selective toward 2,6-DMP as the individual bulk oxides showed less activity in comparison to CuO-$CuCr_2O_4$.

In the following study, the influence of acid-base sites and metallic copper species was investigated on the activity of Cu-Cr catalysts [9]. A detailed study was conducted on the role of acid-base sites (Lewis and Brønsted) on the product distribution using formic acid and pyridine as probe molecules for adsorbed IR spectroscopy combined with N_2O pulse titration experiments to estimate the Cu active metal surface area. The N_2O titration measurements determined that the rate of 2,6-DMP formation was linearly proportional to the active metal surface area with Cu_2Cr_1 sample displaying the highest activity for 2,6-DMP. In addition, the selectivity of 2,6-DMP was dependent on both copper chromite and Cu^0 species.

To see the effect of preparation method, $CuCr_2O_4$ catalyst was synthesized by various methods, namely, mechanical mixing, sol-gel, and co-precipitation [10]. It was observed that a high quantity of Cu particles interacted with Cr_2O_3 in $CuCr_2O_4$ resulted from the sol-gel method with a low ratio of Cu^{2+}/Cu^0 exhibited better dehydrocyclization activity with high 2,6-DMP selectivity. Besides, dehydrocyclization activities were examined under catalyst poisoning conditions to highlight the influence of acidic and basic sites (Lewis) responsible for the 2,6-DMP selectivity. The HCOOH adsorbed IR spectroscopic data, and the N_2O pulse titration results demonstrated that there is a higher proportion of basicity on the $CuCr_2O_4$ surface (synthesized by the sol-gel method) than on $CuCr_2O_4$ that is synthesized by mechanical mixing and co-precipitation routes. The sol-gel-derived $CuCr_2O_4$ catalyst was also found to be stable even when crude glycerol was used as the reactant that was received from the biodiesel plant. The Cu impregnated on Cr_2O_3 exhibited segregated CuO and Cr_2O_3 species that showed 2,6-DMP with high selectivity. It was found that fine-tuning of surface acid-base sites could result in the desired products with high selectivity in the dehydrocyclization process.

In the subsequent study, the Cu-Cr catalyst was calcined at different temperature (from 400 to 750 °C) to study the role of copper dispersion and acid-base properties on the product distribution [11]. The modified (with Na, K and Cs) Cu-Cr catalyst studied their behavior in the vapor-phase synthesis 2,6-DMP from1,2-PDA and glycerol. The results indicated that K-modified Cu-Cr sample efficiently minimizes the by-product formation. The influence of calcination temperatures had a significant impact on the activity of Cu-Cr catalyst and found that 550 °C could be an optimum temperature where a stable CuO-$CuCr_2O_4$ was observed. Whereas at 400 °C calcination temperature, CuO-$CuCr_2O_4$ exhibited low activity due to the less number of Cu active sites available on the surface. The results also showed that the dehydrocyclization rate was declined over CuO-$CuCr_2O_4$ sample calcined at high temperatures (>550 °C) due to low surface area of catalyst when calcined at high temperature mostly due to sintering. On contrary, 2,6-DMP rate decreased

significantly with the increase in calcination temperature to 750 °C. These results emphasize that at high calcination temperatures, a significant drop in catalyst active sites consequently on 2,6-DMP synthesis rate is observed.

In the later investigation, $CuCr_2O_4$ catalyst prepared by the sol-gel method was further modified with different promoters such as zinc, zirconium, and magnesium to study their effect on product distribution in the synthesis of 2,6-DMP from crude glycerol and 1,2-PDA [12]. Among them, it was noticed that the Zn-promoted Cu-Cr catalyst exhibited a higher rate of 2,6-DMP formation. A detailed investigation on the acid-base sites indicated that the stable activity of Zn-modified $CuCr_2O_4$ catalyst was mainly due to stabilization of Cu^0 species and improved Lewis acidity. In addition, Zn addition (up to 5 wt%) resulted in highly dispersed copper on the catalyst surface with improved activity and stability. In this study, it was found that strong basicity with a pair of weak to moderate acid sites (Lewis) is crucial for the desired selectivity of 2,6-DMP.

Finally, in a recent investigation, a nano-crystalline $ZnO\text{-}ZnCr_2O_4$ and mixed oxide hydrotalcite precursor material were prepared at different pH (8, 10, and 12) and evaluated to convert the crude bio-glycerol to 2,6-DMP [13]. Different aspects such as the nature and strength of acid-base properties were discussed, and it was found that the $ZnO\text{-}ZnCr_2O_4$ catalyst with high ratio of Lewis to Brønsted basic sites was key to selective 2,6-DMP synthesis. The $ZnO\text{-}ZnCr_2O_4$ catalyst that prepared a pH of 10 demonstrated highest activity compared to other catalysts that were mainly due to finely dispersed $ZnO\text{-}ZnCr_2O_4$ particles on the surface. It was also found that the presence of strong acidity resulted in lower activity. It can be concluded that conversion of aqueous (crude) glycerol with corresponding amines to synthesize alkyl pyrazines entails weak Lewis acidity in conjunction with a pair of strong basic sites. In this investigation, a comparative study is made in parenthesis to the recent reports on dehydrocyclization of glycerol, and diamine compounds in reference to 2MP rates are discussed.

2 Experimental

2.1 Preparation of Catalysts

Zn supported on Cr_2O_3 catalysts was prepared with different loadings of ZnO loadings via wet impregnation method. In this method, 2, 5, 7, 10, and 15 wt% of ZnO loadings on Cr_2O_3 support was prepared. In a typical experiment, Cr_2O_3 was dispersed in double-distilled water and taken in a beaker, and then the desired quantity of $Zn(NO_3)_2 \cdot 6H_2O$ was added portion-wise while continuous stirring and heating at 80 °C and oven-dried for 12 h at 100 °C, subsequently calcined at 450 °C in static air. Catalysts with 2, 5, 7, 10, and 15 wt% loadings of ZnO were denoted as $2ZnO/Cr_2O_3$, $5ZnO/Cr_2O_3$, $7ZnO/Cr_2O_3$, $10ZnO/Cr_2O_3$, and $15ZnO/Cr_2O_3$, respectively.

2.2 Characterization of Catalysts

The BET surface areas of the catalysts were estimated by using N_2 adsorption-desorption method at $-196\ ^{\circ}C$ in an Autosorb 3000 equipment. Powder XRD patterns were recorded using a Rigaku MiniFlex X-ray diffractometer instrument using Ni-filtered Cu K_{α} radiation ($\lambda = 0.15406$ nm) with a scan rate of 2° min^{-1} between $2\theta = 20^{\circ}$ and 80°. Raman spectroscopic analysis of the catalysts was carried out using a Horiba Jobin Yvon lab ram HR Raman spectrometer with beam excitation of $\lambda = 632.81$ nm. The UV-Vis spectra in diffuse reflectance mode were obtained in UV-Vis spectrophotometer (UV-2000 from Shimadzu) consisting of $BaSO_4$ reference and an integrating sphere in the range of 800–185 nm with a slit width of 2 nm and sampling interval of 0.5 nm at ambient temperature. The Fourier transform infrared (FTIR) spectra of the catalyst samples were analyzed by diluting the samples with KBr as pressed wafers using IR spectrometer (Thermo Nicolet Nexus 670) from 4000 to 400 cm^{-1} region. The surface elemental analyses of the catalysts were obtained from X-ray photoelectron (XPS; Kratos Axis Ultra Imaging) spectrometer, equipped with multichannel detector and Mg anode. Background correction (Shirley-type) was done by referencing the obtained spectra with C 1 s at a binding energy of 284.8 eV.

2.3 Activity Tests

The dehydrocyclization activities were conducted using $-18/+23$ sieved (BSS) catalyst particles. The carbon mass balance was calculated based on the inlet and outlet concentration of the organic moiety. In a typical measurement, prior to the reaction, about 0.2 g of calcined catalyst (sieved particles $-18/+25$ BSS) was treated in 5% H_2/Ar at $400\ ^{\circ}C$ for 5 h. A 20 wt% aqueous glycerol solution was used, and the glycerol to EDA mole ratio of 1:1 with a flow rate of the reaction mixture of 2 mL h^{-1} along with N_2 as carrier gas at a flow rate of 1800 cc h^{-1} was maintained. The reaction mixture contained a glycerol flow rate = 88.2 cc h^{-1}, EDA flow rate = 87.4 cc h^{-1}, H_2O flow rate = 1806.2 cc h^{-1}, and N_2 flow rate = 1800 cc h^{-1}. The collected samples (after 6 h) were analyzed by gas chromatography (Shimadzu, GC-17A) equipped with a flame ionization detector (FID) using ZB-5 capillary column.

3 Results and Discussion

3.1 Powder XRD Analysis

The XRD patterns of various loadings of ZnO on Cr_2O_3 are presented in Fig. 1. It shows that $2ZnO/Cr_2O_3$, $5ZnO/Cr_2O_3$, and $7ZnO/Cr_2O_3$ samples displayed Cr_2O_3 phase prominently, and no ZnO and $ZnCr_2O_4$ phases were detected. The catalysts

with higher loadings of ZnO (10ZnO/Cr$_2$O$_3$ and 15ZnO/Cr$_2$O$_3$) have both ZnO and ZnCr$_2$O$_4$ phases along with Cr$_2$O$_3$. Diffraction signals at $2\theta = 35.7°$, 30.3°, 63.1°, 57.4°, and 43.4° corresponding "d" values of 0.251, 0.294, 0.147, 0.160, and 0.208 nm are confirmed as ZnCr$_2$O$_4$ phase [ICDD #: 22-1107]. Diffraction lines at $2\theta = 36.2°$, 31.7°, 34.4°, 56.6°, and 62.8° with "d" values of 0.247, 0.281, 0.260, 0.162, and 0.147 nm are due to the presence of ZnO phase [ICDD #: 89-0510] [14, 15]. Diffraction signals due to Cr$_2$O$_3$ [ICDD #: 85-0730] are appeared at $2\theta = 33.6°$, 36.1°, 24.4°, 54.8°, 41.5°, and 50.2° with "d" values of 0.265, 0.247, 0.362, 0.167, 0.216, and 0.181 nm [2, 16]. All the diffraction lines are in good correlation with standard ICDD data.

3.2 FTIR Analysis

The FTIR spectra of various loadings of ZnO on Cr$_2$O$_3$ are shown in Fig. 2. The vibrational bands observed at 410, 445, 566, and 626 cm^{-1} are characteristic of chromium oxide with Cr^{+3} oxidation state, and results are consistent with reported literature [14–19]. The signal at 930 cm^{-1} is characteristic vibration of CrO$_4$ tetrahedra due to Cr^{6+} ions [19, 20]. The intensity of this band is decreased upon increasing the ZnO loading on Cr$_2$O$_3$. Absorption bands at 410 and 445 cm^{-1} were present in all the samples except in 15ZnO/Cr$_2$O$_3$. However, a new band located at 507 cm^{-1} is found over 15ZnO/Cr$_2$O$_3$. The spinel structure of ZnCr$_2$O$_4$ is considered to be originated from CrO$_6$ octahedral and ZnO$_4$ tetrahedral. ZnCr$_2$O$_4$ spinels are expected to have four phonon bands centered at 185, 367, 497, and 615 cm^{-1}. Among these, the two high-frequency IR bands originated due to F$_{1u}$ symmetry of the ZnCr$_2$O$_4$ spinel, and they depend on position and shape on the chemical nature and stoichiometry of
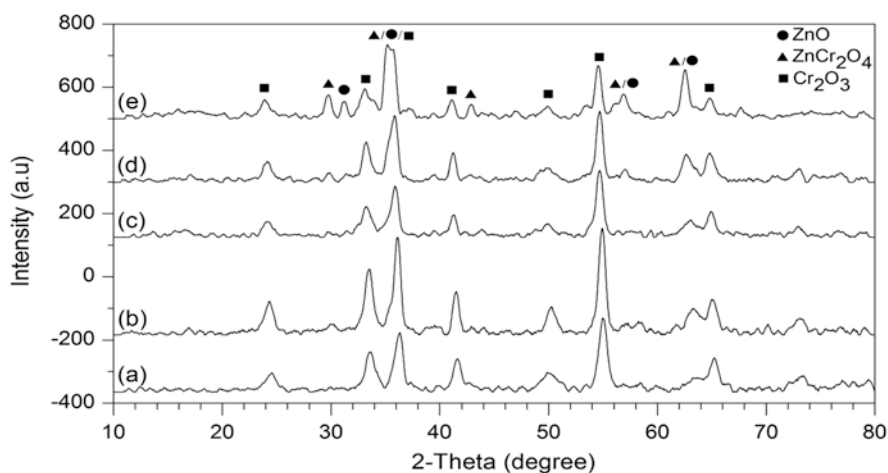
Fig. 1 XRD patterns of various loadings of ZnO on Cr$_2$O$_3$ (**a**) 2ZnO/Cr$_2$O$_3$, (**b**) 5ZnO/Cr$_2$O$_3$, (**c**) 7ZnO/Cr$_2$O$_3$, (**d**) 10ZnO/Cr$_2$O$_3$, and (**e**) 15ZnO/Cr$_2$O$_3$
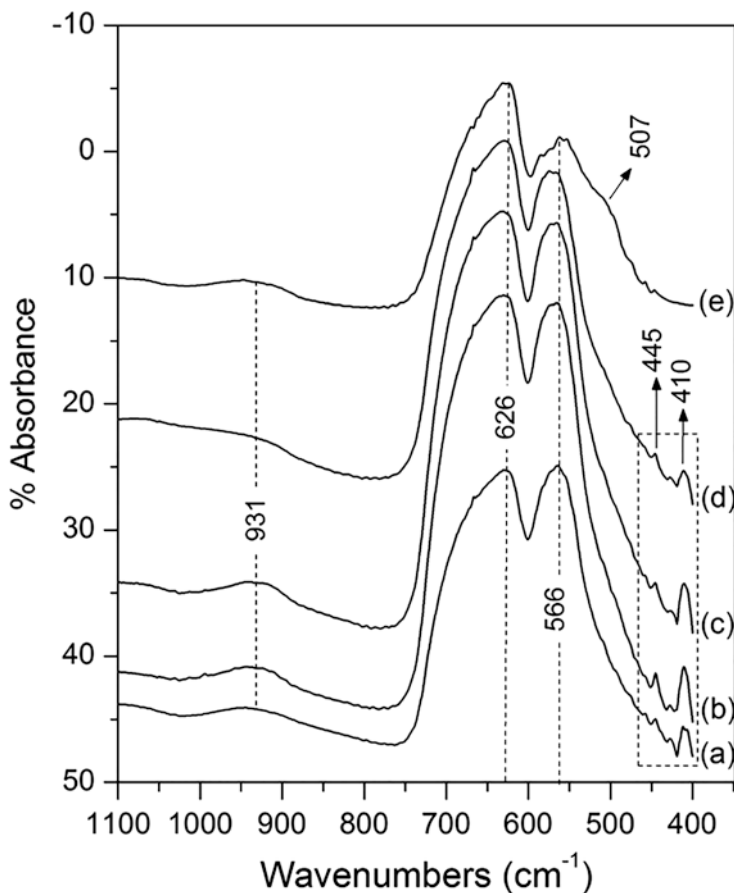
Fig. 2 FTIR spectra of various loadings of ZnO on Cr_2O_3 (**a**) $2ZnO/Cr_2O_3$, (**b**) $5ZnO/Cr_2O_3$, (**c**) $7ZnO/Cr_2O_3$, (**d**) $10ZnO/Cr_2O_3$, and (**e**) $15ZnO/Cr_2O_3$

the octahedral Cr species, which are related to vibrations of lattice octahedral groups [20]. The absorption band around 500 cm^{-1} appeared only in catalyst $15ZnO/Cr_2O_3$, thus indicating the presence of $ZnCr_2O_4$ phase in this catalyst. The formation of the $ZnCr_2O_4$ phase in the $15ZnO/Cr_2O_3$ sample is further evidenced by the XRD analysis (Fig. 1) of the sample.

3.3 Raman Spectroscopy

Raman spectra of different loadings of ZnO supported on Cr_2O_3 are reported in Fig. 3. About seven Raman-active modes, namely, two A_{1g} and five E_g modes, are due to D_{3d} point group such as Cr_2O_3 [21, 22]. XRD analysis showed the presence of only the Cr_2O_3 phase in $2ZnO/Cr_2O_3$, $5ZnO/Cr_2O_3$, and $7ZnO/Cr_2O_3$ samples,

while Raman spectra show the presence of $ZnCr_2O_4$ phase too. $ZnCr_2O_4$ spinel consists of ZnO_4 tetrahedra and CrO_6 octahedra. The close cubic-packed arrangement of oxide species combines CrO_6 octahedra involving two opposite corners of ZnO_4 tetrahedra. $ZnCr_2O_4$ belongs to space group O_h^7. In factor group analysis, one A_{1g}, one E_g, and three F_{2g} Raman active modes are predicted [20, 23]. Raman active band
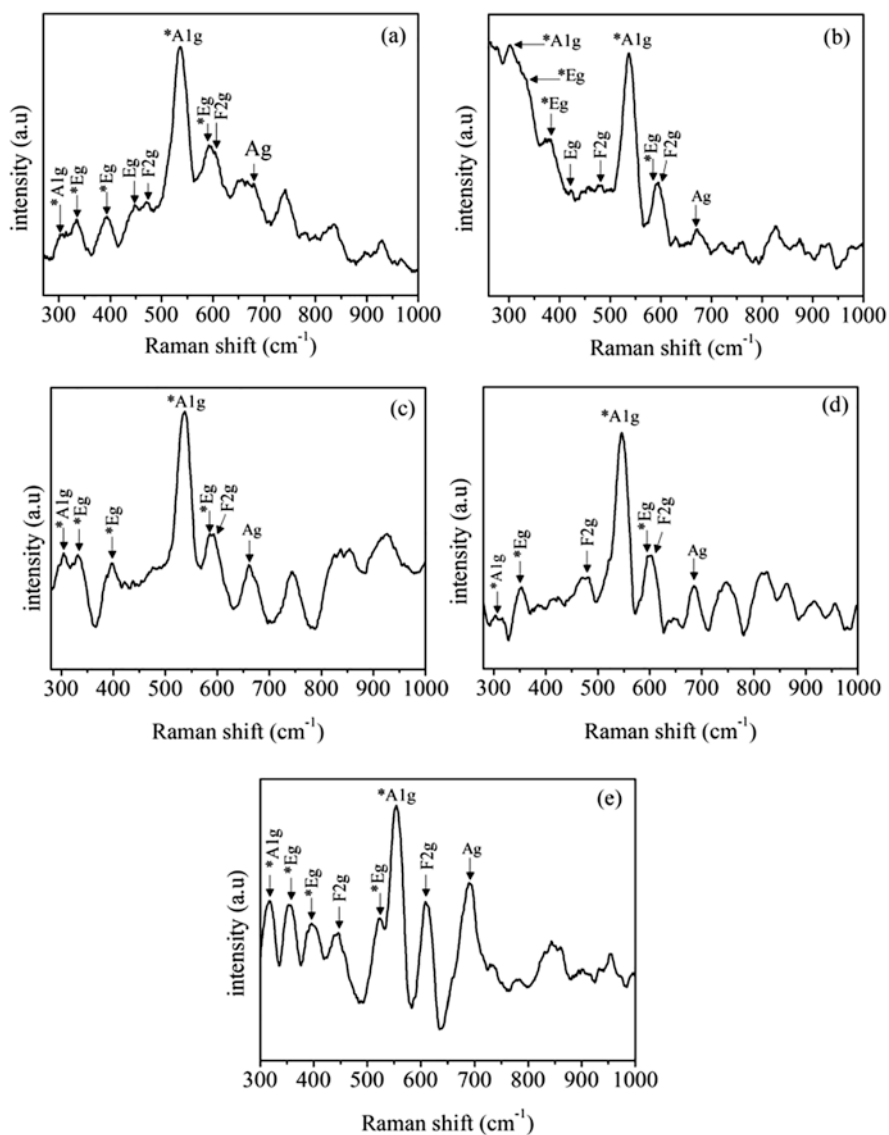
Fig. 3 Raman spectra of various loadings of ZnO on Cr_2O_3 (**a**) $2ZnO/Cr_2O_3$, (**b**) $5ZnO/Cr_2O_3$, (**c**) $7ZnO/Cr_2O_3$, (**d**) $10ZnO/Cr_2O_3$, and (**e**) $15ZnO/Cr_2O_3$. Modes indicated with asterisk mark are due to Cr_2O_3 species, while without asterisk mark are due to $ZnCr_2O_4$ species

Table 1 An overview of Raman active modes of different loadings of ZnO on Cr_2O_3

Crystallite phase	Raman active modes	McCarty et al. [18]	Shim et al. [21]	Wang et al. [23]	Venu-gopal et al. [5]	wt% of ZnO present on ZnO/Cr_2O_3				
						2	5	7	10	15
Cr_2O_3 (indicated by asterisk mark in Fig. 3)	A_{1g}	304	298	na	na	306	312	303	313	316
	E_g	353	354	na	na	338	338	335	350	355
	E_g	401	397	na	na	395	390	391	382	398
	E_g	529	531	na	na	510	512	511	520	525
	A_{1g}	553	556	na	na	537	537	534	548	554
	E_g	616	618	na	na	592	599	592	605	609
$ZnCr_2O_4$	E_g	na	na	430	427	439	418	438	420	400
	F_{2g}	na	na	511	506	482	485	483	476	446
	F_{2g}	na	na	605	595	618	620	622	645	663
	A_g	na	na	687	675	680	679	670	687	689

at A_{1g} of Cr_2O_3 appears around 537–550 cm^{-1} as the most dominant peak. The second strong peak is E_g Raman active mode of Cr_2O_3 around 592–609 cm^{-1}. It is clear that two F_{2g} Raman active modes and one E_g mode originated due to $ZnCr_2O_4$ are more prominent in 10ZnO/Cr_2O_3 and 15ZnO/Cr_2O_3 (Table 1).

3.4 UV-DRS Analysis

To understand the coordination states and chemical environment of Cr species, the fresh calcined samples of ZnO supported on Cr_2O_3 analyzed by UV-DR and the spectra are presented in Fig. 4 [5]. As well-known, the Cr oxidation states vary between +2 and +6. Typically, Cr^{3+} (d^3) and Cr^{6+} (d^0) ions are stable with octahedral and tetrahedral symmetries, respectively. The d–d transitions and charge transfer of Cr species were characterized between 200 and 800 nm region. Fresh catalysts did not show any absorption bands around 270 and 360 nm wavelength, which could have originated from charge transfer ($O^{2-} \rightarrow Cr^{6+}$) transitions of chromate species ($ZnCrO_4$). Thus, suggesting chromate species are not present in the fresh samples. Figure 4 shows two typical characteristic d–d transitions for Cr^{3+} at 407 nm ($A_{2g} \rightarrow T_{1g}$) and 535 nm ($A_{2g} \rightarrow T_{2g}$). There is a red shift in d–d transitions to 411 and 538 nm with an increase in ZnO loadings. These changes might indicate toward Cr^{3+}oligomerization essentially in the form of dimers [24, 25]. UV-DR spectra of reduced samples are presented in Fig. 5. The signal intensity is slightly lowered as the Cr/Zn ratio decreased at higher ZnO loading. The Cr (III) species in the samples at a higher Cr/Zn ratio also suggests the presence of abroad signal at 600 nm can be assigned to d–d transitions of Cr^{3+}in octahedral symmetry ($A_{2g} \rightarrow T_{2g}$) [26]. Weak band at about 456 nm was due to d–d transition of Cr^{3+} ($A_{2g} \rightarrow T_{1g}$) that was noticed for reduced catalyst samples. Upon increasing ZnO loading, a blue shift from 466 to 457 nm is found, which is probably due to increased ZnO content [3]. The bands at 465 nm and 600 nm appeared in reduced samples were absent in their fresh form (Fig. 4).
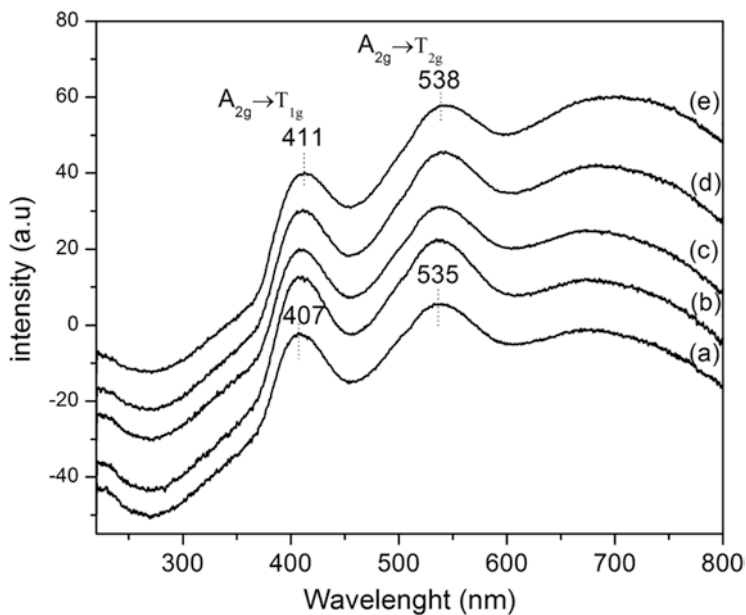
Fig. 4 UV-DR spectra of fresh calcined catalysts of various loadings of ZnO on Cr_2O_3 (**a**) 2ZnO/Cr_2O_3, (**b**) 5ZnO/Cr_2O_3, (**c**) 7ZnO/Cr_2O_3, (**d**) 10ZnO/Cr_2O_3, and (**e**) 15ZnO/Cr_2O_3
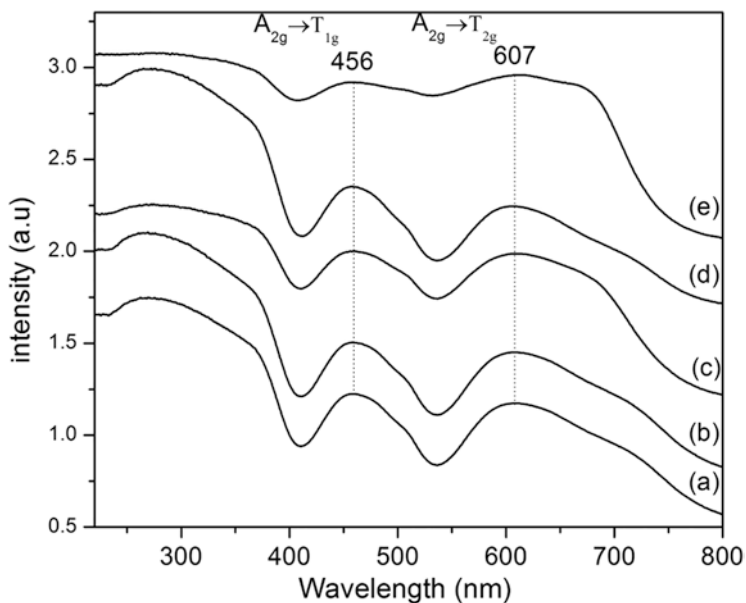
Fig. 5 UV-DR spectra of reduced samples (**a**) 2ZnO/Cr_2O_3, (**b**) 5ZnO/Cr_2O_3, (**c**) 7ZnO/Cr_2O_3, (**d**) 10ZnO/Cr_2O_3, and (**e**) 15ZnO/Cr_2O_3

3.5 XPS Analysis of ZnO Supported on Cr₂O₃ Samples

XPS patterns of various ZnO-loaded Cr_2O_3 samples are presented in Fig. 6. The fresh calcined spectra show Cr 2p peak in the range 576.2–577.8 eV, attributed to Cr^{3+} species [27–32]. Binding energy values of 1022.2 and 1021.5 eV are due to the presence of $ZnCr_2O_4$ and ZnO, respectively [33, 34]. The XP spectra of O1s, lines in the region 530.0–533.3 eV, are due to the presence of two types of oxygen-containing species. These results clearly confirm the presence of Cr_2O_3 and $ZnCr_2O_4$ species in the near-surface region. It is also found that at higher ZnO loadings (in 10 wt% ZnO and 15 wt% ZnO), both Cr $2p_{3/2}$ and Zn $2p_{3/2}$ showed slightly higher BE values when compared to lower loadings of ZnO. This shift is probably because of the formation of $ZnCr_2O_4$ at higher ZnO loadings.

3.6 Activity Measurements

Dehydrocyclization was carried out on various loadings of ZnO supported on Cr_2O_3 catalysts at 375 °C, and the results are presented in Fig. 7. The specific rate of 2MP and pyrazine was calculated by normalizing the rate of the products with surface areas of the corresponding samples. It shows that 10 wt% ZnO loading on Cr_2O_3 exhibited a better selectivity toward 2MP with a rate of 1.85 mmol s^{-1} g^{-1} (Table 2).
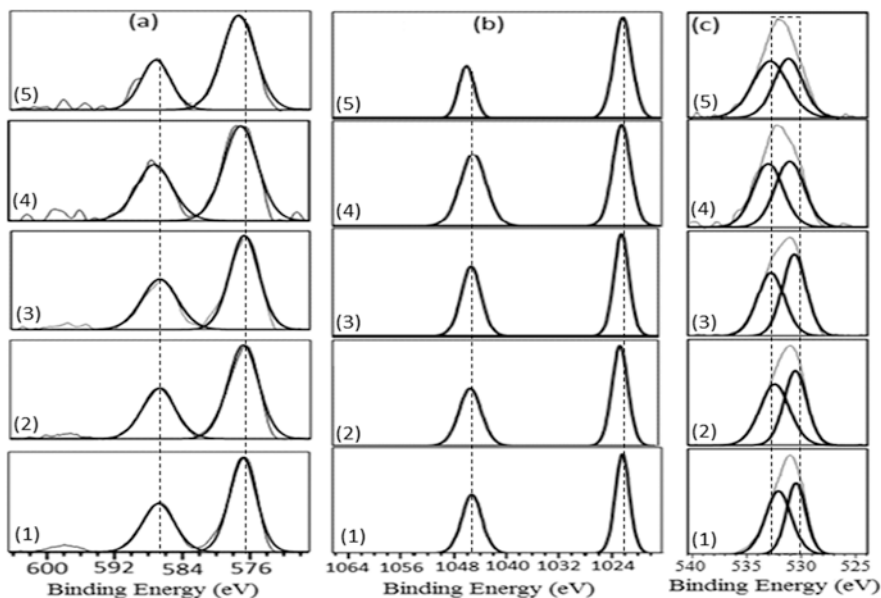
Fig. 6 XPS analysis of (**a**) Cr 2p, (**b**) Zn 2p, and (**c**) O1s spectra of various loadings of ZnO (wt%) on Cr_2O_3: (1) 2.0, (2) 5.0, (3) 7.0, (4) 10.0, and (5) 15.0 catalysts

At lower loadings of ZnO, the catalysts showed better EDA conversion (>60%) than the glycerol conversion (<20%) with a pyrazine formation rate of 0.85 mmol s^{-1} g^{-1} and 2MP ~0.21 mmol s^{-1} g^{-1}.

The higher rate of pyrazine synthesis was explained due to a high EDA conversion by the intermolecular cyclization of EDA, which is predominant than the dehydrocyclization at lower loadings of ZnO (Scheme 3). As the loading of ZnO is increased, the selectivity toward pyrazine is decreased, and the 2-methylpyrazine selectivity is increased. Further, increase in ZnO loading 10–15 wt%, 2-methylpyrazine rate is slightly decreased from 1.85 to 1.65 mmol s^{-1} g^{-1}, which is probably due to formation of large-sized clusters of ZnO.

Upon increasing the ZnO loading, the specific rate of 2MP is increased up to 10 wt% ZnO loading, indicating an optimum loading of ZnO on Cr_2O_3 for the 2MP formation (Fig. 8). Powder XRD analysis indicated the formation of the $ZnCr_2O_4$
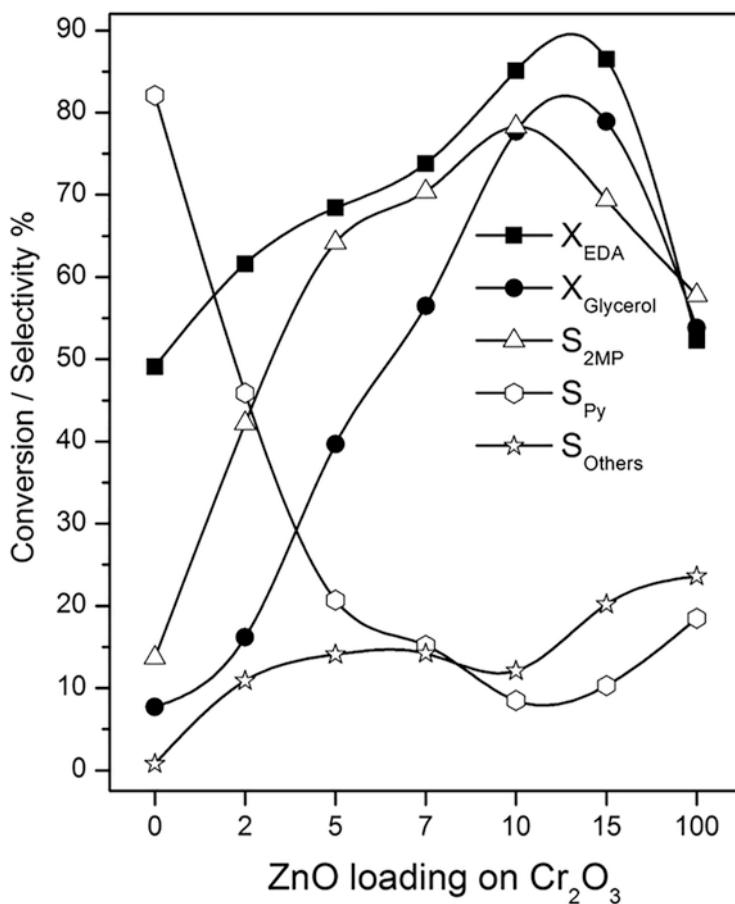
Fig. 7 Influence of various ZnO loadings on Cr_2O_3 in EDA and glycerol conversion at 375 °C

Table 2 Physicochemical characteristics of the various loadings of ZnO on Cr_2O_3

Sample ZnO/Cr$_2$O$_3$ (wt%)	Rate (mmol s^{-1} g^{-1})		Crystallite[a] size (nm)			S_{BET}[b] (m^{2}g^{-1})	Carbon[c] content (wt%)
	r_{2MP}[d]	$r_{pyrazine}$[e]	ZnO	ZnCr$_2$O$_4$	Cr$_2$O$_3$		
2	0.21	0.85	nf	nf	15.6	64.4	1.98
5	0.77	0.43	nf	nf	16.6	37.0	1.69
7	1.20	0.34	nf	nf	16.6	34.3	1.45
10	1.85	0.22	15.4	17.6	17.8	38.5	1.34
15	1.65	0.22	22.5	20.5	16.6	38.2	0.98

[a]Calculated using the Scherrer equation

[b]BET surface areas of the calcined catalysts

[c]Obtained from the analysis of the used catalysts after 6 h of reaction time

[d]Rate of 2MP is calculated with 2MP yield from glycerol conversion

[e]Pyrazine rate measured from its yield from EDA conversion
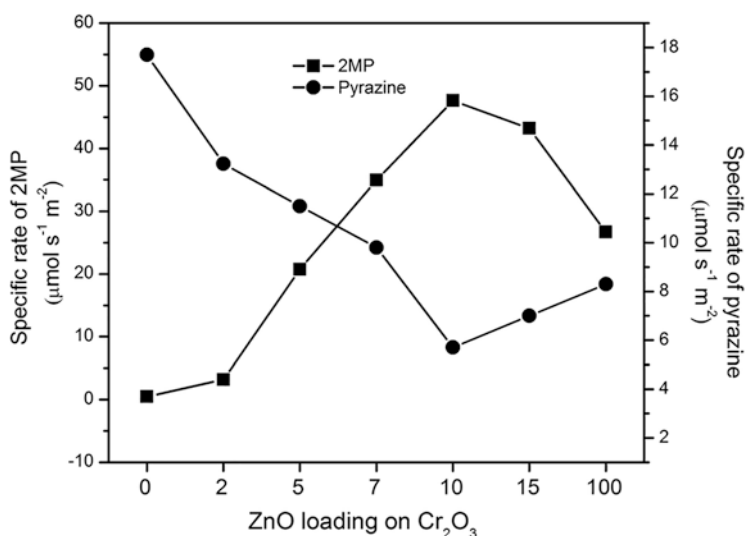
Fig. 8 Comparison of specific rates of 2-methylpyrazine and pyrazine over various ZnO loadings on Cr_2O_3 in the EDA and glycerol conversion at 375 °C

phase starts appearing at a 10 wt% ZnO loading. However, it cannot be ruled out the zinc chromite phase at lower loadings as they may either smaller in crystallite size or in a lower concentration.

As discussed earlier, the presence of strong acid sites leads to carbon deposition on the catalyst surface. The elemental analysis of the used (after 6 h of continuous operation) catalysts showed a decrease in carbon deposition with an increase in the ZnO loading on Cr_2O_3 (Fig. 9).
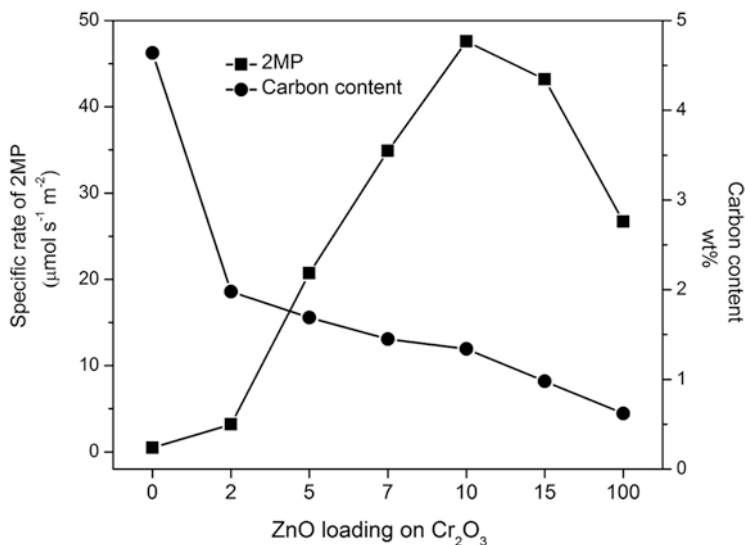
Fig. 9 Comparison of specific rate of 2-methylpyrazine and carbon deposited on catalyst surface after reaction over various ZnO loadings on Cr_2O_3 in the dehydrocyclization of EDA and glycerol at 375 °C

4 Conclusions

Catalytic conversion of crude glycerol for the synthesis of alkyl pyrazines was established over various Zn and Cu chromite catalysts. A combination of acid-base pairs was involved in the dehydrocyclization process. A detailed investigation on structure-activity relationship was emphasized using bulk and surface characterization techniques. Finally, the role of ZnO and Cr_2O_3 on product selectivity was discussed by conducting a series of experiments on ZnO/Cr_2O_3 catalysts for dehydrocyclization reaction, which indicated a 10 wt% loading of ZnO on Cr_2O_3 showed better 2MP rates. The catalysts with lower loadings of ZnO showed the formation of pyrazine by intermolecular cyclization reaction. Upon increasing the ZnO loadings, the crystallite size was increased, which may be a reason for the decreased activity of 15 wt% ZnO/Cr_2O_3 catalyst. Thus it can be concluded that the presence of ZnO and $ZnCr_2O_4$ phases with appropriate crystallite size is important for the dehydrocyclization reaction of EDA and glycerol for the synthesis of 2-methylpyrazine.

References

1. Clayton Zhou CH, Beltramini JN, Fan YX, Max Lu GQ (2008) Chemo selective catalytic conversion of glycerol as a bio-renewable source to valuable commodity chemicals. Chem Soc Rev 37:527–549

2. Sarkari R, Anjaneyulu C, Krishna V, Kishore R, Sudhakar M, Venugopal A (2011) Vapor phase synthesis of methylpyrazine using aqueous glycerol and ethylenediamine over $ZnCr_2O_4$ catalyst: elucidation of reaction mechanism. Catal Commun 12:1067–1070

3. Forni L (1988) Structural analysis of $ZnO/ZnCr_2O_4/Pd$ catalyst. J Catal 111:199–209

4. Venugopal A, Sarkari R, Naveen Kumar S, Kotesh Kumar M, John SS, Reddy JK, Padmasri AH (2014) Effective utilization of glycerol for the synthesis of 2-methylpyrazine over ZnO-$ZnCr_2O_4$ catalyst. J Chem Sci 126(2):387–393

5. Venugopal A, Sarkari R, Anjaneyulu C, Krishna V, Kotesh Kumar M (2012) Synthesize 2-methylpyrazine using aqueous glycerol and ethylenediamine over zinc oxide–zinc chromite catalysts: Structure–activity relationship. Appl Catal A 441:108–118

6. Sarkari R, Krishna V, Sudhakar M, Rao TV, Padmasri AH, Srinivas D, Venugopal A (2016) The effects of thermal treatment of ZnO–$ZnCr_2O_4$ catalyst on the particle size and product selectivity in dehydrocyclization of crude glycerol and ethylenediamine. Kinet Catal 57:602–609

7. Venugopal A, Sarkari R, Anjaneyulu C, Krishna V, Kumar MK, Narender N, Padmasri AH (2014) Influence of acid-base sites on ZnO–$ZnCr_2O_4$ catalyst during dehydrocyclization of aqueous glycerol and ethylenediamine for the synthesis of 2-methylpyrazine: kinetic and mechanism studies. Appl Catal A Gen 469:398–409

8. Krishna V, Kumar SN, Reema S, Padmasri AH, Chary KVR, Venugopal A (2014) Bio-glycerol utilization: Synthesis of 2,6-dimethylpyrazine over M_xO_y–MCr_2O_4 (M = Mg, Fe, Co, Ni, Cu and Zn) catalysts. Appl Catal A Gen 488:275–284

9. Krishna V, Naresh G, Kumar VV, Sarkari R, Padmasri AH, Venugopal A (2016) Synthesis of 2,6-dimethylpyrazine by dehydrocyclization of aqueous glycerol and 1,2-propanediamine over CuCrO catalyst: rationalization of active sites by pyridine and formic acid adsorbed IR studies. Appl Catal B Environ 193:58–66

10. Krishna V, Naresh G, Kumar VV, Suresh M, Padmasri AH, Venugopal A (2017) $CuCr_2O_4$ derived by the sol–gel method as a highly active and selective catalyst for the conversion of glycerol to 2,6-dimethylpyrazine: a benign and eco-friendly process. Cat Sci Technol 7:3399–3407

11. Krishna V, Naresh G, Kumar SN, Beltramini J, Padmasri AH, Venugopal A (2017) Alkali promoted Cu-Cr-O catalyst for the dehydrocyclization of crude glycerol and 1,2-propanediamine: Effect of thermal treatment on the activity and product selectivity. Curr Catal 6:135–143

12. Krishna V, Kumar VV, Naresh G, Kumar SN, Padmasri AH, Sreedhar I, Venugopal A (2017) Zn-modified $CuCr_2O_4$ as stable and active catalyst for the synthesis of 2,6-dimethylpyrazine: valorization of crude glycerol obtained from a biodiesel plant. Ind Eng Chem Res 56:11664–11671

13. Krishna V, Padmasri AH, Sarkari R, Kumar VV, Naresh G, Kumar SN, Rohita CN, Venugopal A (2017) The role of Lewis acid–base pair sites in ZnO–$ZnCr_2O_4$ catalysts for cyclization via dehydrogenative condensation of crude glycerol and 1,2-propanediamine for the synthesis of 2,6-dimethylpyrazine. New J Chem 41:9875–9883

14. Cheng R, Borca CN, Dowben PA, Stadler S, Idzerda YU (2001) Potential phase control of chromium oxide thin films prepared by laser-initiated organometallic chemical vapor deposition. Appl Phys Lett 78:521–523

15. Steger WE, Landmesser H, Boettcher U, Schubert E (1990) Infrared spectra of amorphous oxides. J Mol Struct 217:341–346

16. Forni L, Oliva C, Vatti FP, Tugarinov VY, Vishniakov AV (1993) Structural analysis and catalytic activity of sol-gel-prepared Zn-Cr-O. J Mater Sci 28:3291–3297

17. Carta G, Natali M, Rossetto G, Zanella P, Salmosa G, Restello S, Rigato V, Kaciulis S, Mezzi A (2005) Chem Vap Depos 11:375–380

18. McCarty KF, Boehme DR (1989) J Solid State Chem 79:19–27
19. Ivanova T (2008) J Phys Conf Ser 13:12030
20. Marinković ZV, Stanojević RN, Stojanović B (2007) Spectroscopic study of spinel $ZnCr_2O_4$ obtained from mechanically activated ZnO–Cr_2O_3 mixtures. J Eur Ceram Soc 27:903–907
21. Shim SH, Duffy TS, Jeanloz R, Yoo CS, Iota V (2004) Raman spectroscopy and x-ray diffraction of phase transitions in Cr_2O_3 to 61 GPa. Phys Rev B 69:144107
22. Tatsuyama C, Fan HY (1980) Raman scattering and phase transitions in V_2O_3 and $(V_{1-x} Cr_x)_2O_3$. Phys Rev B 21(7):2977
23. Wang Z, Lazor P, Saxena SK, Artioli G (2002) High-pressure Raman spectroscopic study of spinel ($ZnCr_2O_4$). J Solid State Chem 165:165–170
24. Michorczyk P, Ogonowski J, Zenczak K (2011) Activity of chromium oxide deposited on different silica supports in the dehydrogenation of propane with CO_2 – a comparative study. J Mol Catal A Chem 349:1–12
25. Delgado RR, Vidaurre MA, De Pauli CP, Ulibarri MA, Avena MJ (2004) J Colloid Interface Sci 280:431–441
26. Simard F, Sedran UA, Sepulveda J, Figoli NS, de Lasa HI (1995) $ZnOCr_2O_3$+ZSM-5 catalyst with very low Zn/Cr ratio for the transformation of synthesis gas to hydrocarbons. Appl Catal A 125:81–98
27. Allen GC, Tucker PM (1976) Multiplet splitting of X-ray photoelectron lines of chromium complexes. The effect of co-valency on the 2p core level spin-orbit separation. Inorg Chim Acta 16:41–45
28. Allen GC, Curtis MT, Hooper AJ, Tucker PH (1973) X-Ray photoelectron spectroscopy of chromium–oxygen systems. J Chem Soc Dalton Trans 16:1675–1683
29. Cimino A, De Angelis BA, Lucchetti A, Minelli G (1976) The characterization of CrO_x-SiO_2 catalysts by photoelectron spectroscopy (XPS), X-ray and optical measurements. J Catal 45:316–325
30. Okamoto Y, Fuiji M, Imanaka T, Teranishi S (1976) X-Ray photoelectron spectroscopic studies of catalysts—chromia–alumina catalysts. Bull Chem Soc Jpn 49:859–863
31. Jagannathan K, Srinivasan A, Rao CNR (1981) An XPS study of the surface oxidation states of metals in some oxide catalysts. J Catal 69:418–427
32. Best SA, Squires RG, Walton RA (1977) The X-ray photoelectron spectra of heterogeneous catalysts: II The chromia-silica catalyst system. J Catal 47:292–299
33. Hoflund GB, Epling WS, Minahan DM (1999) Reaction and surface characterization study of higher-alcohol synthesis catalysts XII: K- and Pd-promoted Zn/Cr/Mn spinel. Catal Today 52:99–109
34. Parhi P, Manivannan V (2008) Microwave metathetic approach for the synthesis and characterization of $ZnCr_2O_4$. J Eur Ceram Soc 28:1665–1670

The Role of Group VIII Metals in Hydroconversion of Lignin to Value-Added Chemicals and Biofuels

A. Sreenavya, P. P. Neethu, and A. Sakthivel

Abstract Biomass utilization originating from inedible farming and forest waste, as a renewable feedstock for liquid biofuels and viable products, will have important environmental and social impacts in the future. Lignocellulose, the main nonedible component of biomass, is a primordial element abundantly rich in cellulosic compounds and lignins. The conversion of cellulose and hemicellulose to biofuels and valuable platform chemicals (such as levulinic acid, formic acid, furfural, γ-valerolactone and other derivatives) has long been studied, and great progress has been made in their industrial production. Lignin being a unique raw material has gained enormous attention in the recent years being an important source for sustainable and viable products. The successful conversion of lignin into value-added chemicals involves three main processes: (1) decomposition of lignocellulose, (2) depolymerization (3) upgradation to the desirable chemicals. The choice of catalyst in either homo- or heterogeneous systems is crucial for the effective depolymerization of lignin and upgrading to desirable chemicals. Hydro-processing (hydrogenolysis, hydrogenation, hydrodeoxygenation and hydro-demethoxylation) is a highly preferred, practical method for the depolymerization leading to production of valuable products and drugs. These reactions generally occur over metals, namely, platinum, palladium, ruthenium and nickel. This chapter aims to present a holistic analysis of the role of Group VIII metals in conversion of lignin and lignin-based aromatic monomers. This simplified summary will be useful to researchers for developing heterogeneous catalyst towards effective production of industrially sound products.

Keywords Biomass conversion · Lignin · Biofuels · Hydroprocessing · Group VIII metals catalysis · Hydrodeoxygenation

A. Sreenavya · P. P. Neethu · A. Sakthivel (✉)
Inorganic Materials & Heterogeneous Catalysis Laboratory, Department of Chemistry, School of Physical Sciences, Central University of Kerala, Kasaragod, Kerala, India
e-mail: sakthivelcuk@cukerala.ac.in

1 Introduction

Global climatic change caused by the increased anthropogenic activities has not only brought the world into the cusp of energy crisis but also challenged the environmental sustainability [1]. A viable alternative should meet certain essential criteria; it should be renewable, be attainable year around and essentially be a nonedible food crop. The most plausible solution for viable production of energy and chemicals is utilization of nonedible plant-based lingo-cellulosic biomass as sustainable energy crops [2]. Biomass is a prime renewable carbonaceous, cost-effective energy feedstock with potentials of high diversity and production [3]. Biomass-based energy is made of three essential biopolymers, namely, cellulose, hemicellulose and lignin, that results in a robust, highly oxygenated and a heterogeneously composite end product [4, 5]. Of the abovementioned, cellulose (C5) and hemicellulose (C6) are topics of industrial research as they are promising sources for essential products and bio-based fuels. In comparison with cellulose and hemicellulose, the complex phenylpropanoid structures and high thermal stability of lignin limit its commercial use. Being a low-cost product, lignin is immensely used for energy generation in biorefineries [5]. Besides, it is the most abundant naturally occurring aromatic polymer and is a promising renewable feedstock for chemicals and fuels due to the presence of key functional moieties (phenyl, hydroxyl, methoxy and allyl groups). The molecular structure of lignin is composed of three blocks, namely, phenyl propane building blocks (Fig. 1) such as sinapyl alcohol, coniferyl alcohol and *p*-coumaryl alcohol [5, 7].

Effective depolymerization of lignin and subsequent upgradation can deliver a wide variety of chemicals and fuels; hence it is a sensible choice to boost the cost-effectiveness and sustainability of the biorefinery process [2]. Production of bio-based chemicals and fuels from lignin requires three interconnected biorefinery processes: lignocellulose fractionation, lignin depolymerization and upgrade to desirable chemicals [2]. Of the several conversion methods tested, heterogeneous catalysis is the most recent methodology adopted for the transformation of biological feedstocks into value-added products [4].

Lignin degradation is quite challenging due to its intricate three-dimensional structure; hence they are subjected to different catalytic processes which would result in simple yet very useful monomers such as aromatics, phenolics, etc. [7].

Fig. 1 Building components of lignin (monolignols) (Extracted from [6] with due perusal from the American Chemical Society)

p-coumaryl alcohol　Coniferyl alcohol　Sinapyl alcohol
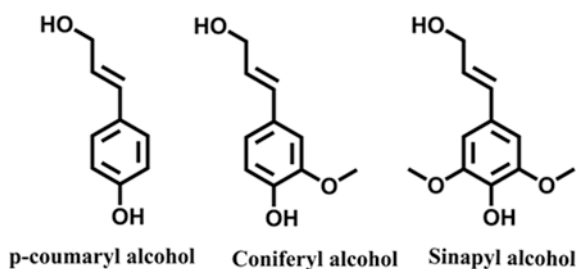
There are three vital thermochemical routes to transform lignin to fuel, namely, gasification, pyrolysis/liquefaction and hydrolysis [8]. Conventionally, pyrolysis is a slow, irreversible thermal decomposition of biomass to bio-oil. Rapid thermal decomposition of lignin yields bio-based oil rich in oxygenated chemicals (Fig. 2), notably phenolics [10].
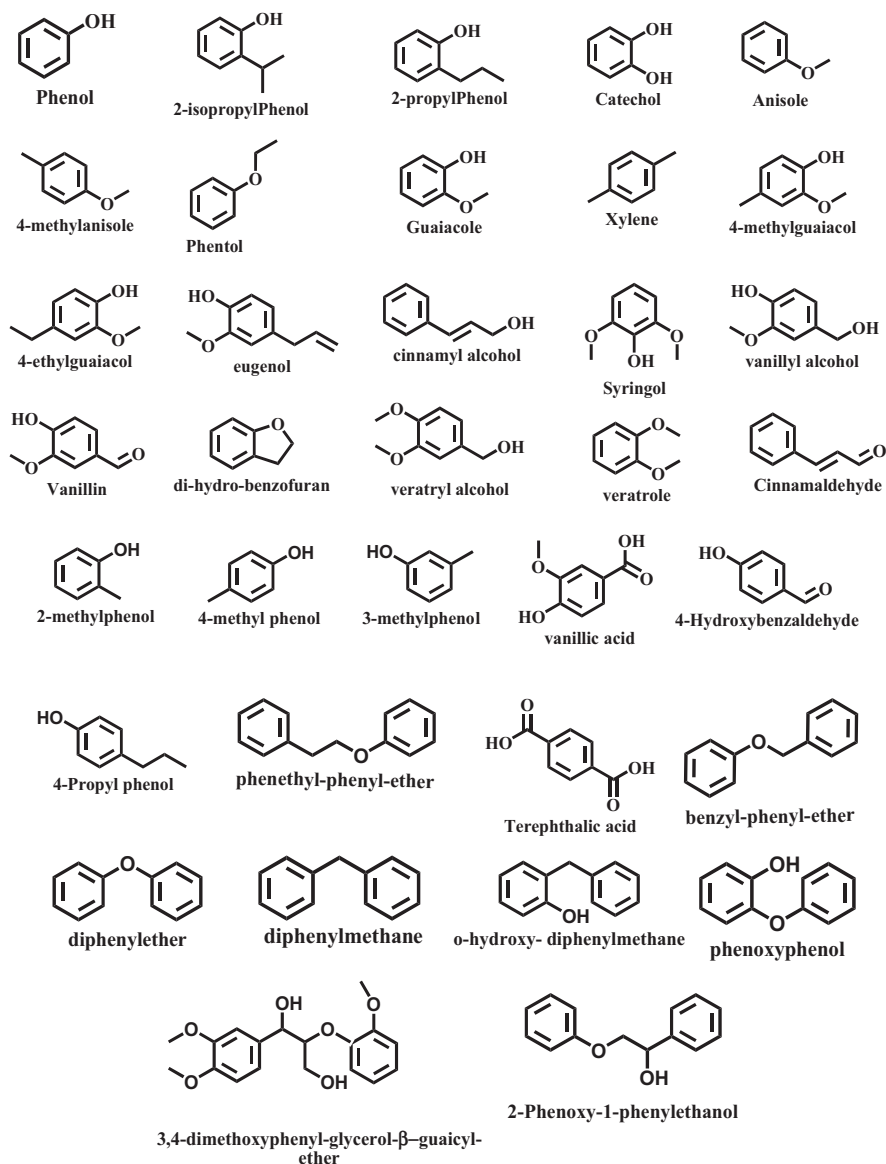
Fig. 2 Structure of lignin model and lignin derived compounds (Adapted from [9] with due consent from Elsevier)

The oil that is produced from lignin cannot be as such used in transportation vehicles owing to the high oxygen content, which results in many drawbacks like lesser heating value, stability, pH and elevated viscosity [11]. Thus, in order to use this bio-oil as a biofuel, it needs to be upgraded through a proper channel. Catalytic hydro-processing (hydrogenation, hydrogenolysis, hydrocracking, hydrodeoxygenation and dehydration) is the established successful method of converting lignin-based oil as usable fuels and other chemicals. Micro-porous zeolites, mesoporous silicates and metal-derived nanoparticles or amphiprotics ($-SO_3H$ and $-NH_2$) are widely used in the process [4].

It is well established that Group VIII metals in the periodic table possess significantly useful catalytic properties, particularly for hydrogenation and related reactions, due to the presence of unpaired 'd' electrons and the ease of thermochemical reduction. Group VIII metals are broadly classified into (1) base metals such as Fe, Co and Ni (occupants of the first line) and (2) platinum group metals such as ruthenium, rhodium, palladium, osmium and platinum (second and third line) [12]. This chapter presents a comprehensive summary of Group VIII metal-containing heterogeneous catalysts and their pivotal role in production of lignin-based chemicals and fuels in a viewpoint to provide an insight for the researchers to design sturdy and specific catalytic models for lignin valorization.

2 Pyrolysis of Biomass Using Iron Based Catalyst

This is the thermochemical treatment of organic compounds where physical separation of products occurs in anaerobic environment at higher temperature. Catalytic pyrolysis involves both pyrolysis and catalytic upgrade in the single unit and used effectively for production of hydrocarbons from biomass. Iron (Fe)-based catalysts are widely used in the industry and catalysis due to their low price, availability and less toxicity. Iron-based catalysts are constantly used by researchers for both oxidative and reductive lignin cleavages.

Lignin conversion using zeolites to hydrocarbons is a critical reaction due to its rapid deactivation accompanied with adsorption of phenolic compounds and reduced reactivity. Bio-wastes of palm kernel shells are an affluent source of lignin (~50%) and were explored for production of hydrocarbons using Fe/HBeta catalyst (Daud et al. [13]). Deoxygenation of lignin-based phenolic compounds is catalysed at the active Fe site by the hydrogenolysis reaction. In their study a maximum aromatic hydrocarbon yield of 5.13 wt% was achieved when Fe/HBeta was used as the catalyst and H_2 as the carrier gas. The performance of HBeta and HZSM-5 was compared with the wastes of palm kernel shells. The study extrapolated two key factors that had a significant impact on the catalysis deactivation at the zeolitic acid sites: (1) pore size of the catalyst and (2) stability of the zeolite acid sites. Further, the reactivity of lignin and cellulose over a zeolite catalyst was compared. The yield of aromatics from lignin significantly increased upon the incorporation of Fe to the

HBeta structure. However, similar changes were not observed in the conversion of cellulose.

HZSM-5 catalysts are used by researchers for the catalytic pyrolysis of lignin to hydrocarbons (Scheme 1). Mullen et al. evaluated the performance of the catalyst HZSM modified by loading with Fe in pyrolytic conversion of cellulose, cellobiose, lignin and switchgrass. Gas chromatography-mass spectrometry (GC-MS) integrated with small-scale pyrolysis reactor was used to study the separated fractions [14]. Of the different Fe catalyst concentrations tested (1.4, 2.8 or 4.2 wt%), maximum aromatic hydrocarbon was obtained at 1.4% of iron. The product selectivity changed by following the introduction of iron. The study also identified that Fe-containing catalyst exhibited more sensitivity for benzene and naphthalene as compared to HZSM-5. Interestingly other compounds p-xylene, ethylbenzene and trimethylbenzene showed reduced sensitivity.

Bifurcation of C_β-O bonds in lignin model compounds [guaiacylglycerol-β-guaiacyl ether (GG) and veratrylglycerol-β-guaiacyl ether (VG)] in an ionic water solution with metal chlorides was experimented by Ekerdt et al. It was identified that lysis of C_β-O in GG was pronounced when metal chlorides (iron III chloride, copper chloride and aluminium chloride) along with in situ HCl was used as an acid catalyst [15]. Tong et al. performed the further studies on lignin depolymerization with a Fe-based catalyst. Fenton's reagent catalysed the lignin depolymerization in
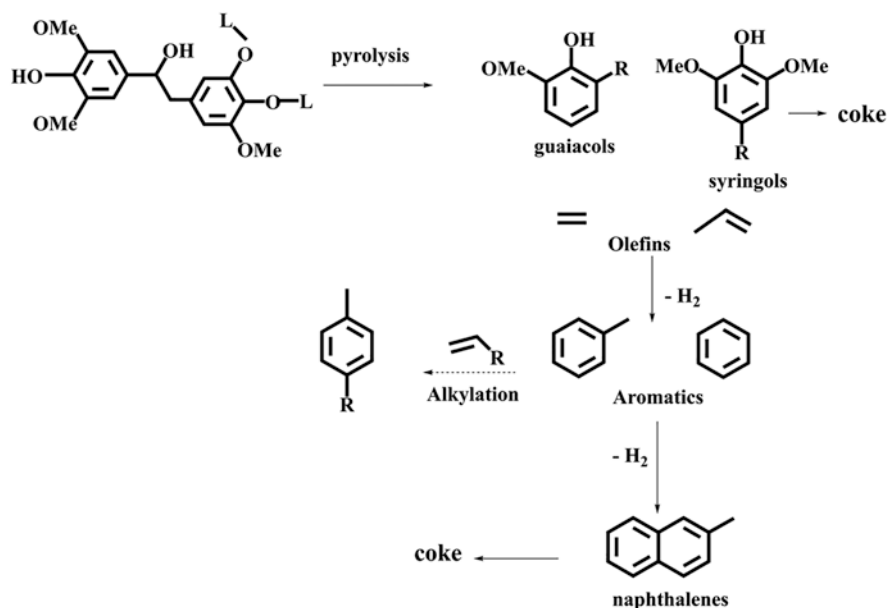
Scheme 1 Catalytic pyrolysis of lignin-based compounds for production of aromatic hydrocarbons against (Fe) H-ZSM-5. Thickened arrows are indicative of enhanced production in limited Fe concentration, while thin arrows indicate pathways with excess of Fe (Presented from [14] with due consent from the American Chemical Society)

supercritical ethanol environment at 250 °C in 7 MPa pressure [16]. The products of lignin depolymerization were monomers of aromatic compound, phenolics, ethers acids and its derivatives. Thermal degradation of the modified lignin was carried out using gas chromatography-integrated-mass spectrometry-integrated pyrolytic reactor (Py-GC-MS), and the impact of various Fenton reaction conditions was studied. The experiments revealed that Fenton's reagent has a positive impact on lignin depolymerization in terms of β-ether bond cleavage.

Bolm et al. conducted experiments on lignin models using $FeCl_3$-derived catalysts in DMSO [17]. The catalytically active species used was the methyl radical produced by H_2O_2 in DMSO. The results suggested that bifurcation of C_β-O bonds produced oxidative depolymerization of lignin, and the end products were methoxyphenol and benzaldehyde derivatives, respectively. Low-cost Fe complexes from $FeCl_3$ were employed to catalyse degradation of resorcinol.

Phenol from lignin compounds is a bi-step reaction in which depolymerization is succeeded by its cleavage in hydrogen-free environment at 623 K for 2 h where silica/alumina acted as a catalyst in a H2O/butyl alcohol medium. Successively the slurry liquid (lignin source) was catalytically dissolved at 673 K using Fe_2O_3 catalyst in a fixed bed reactor. The experiment was carried out in a pressurized system to prevent the yield of robust compounds. The prime routes in which the lignin compounds are depolymerized are by hydrolysis of aryl ether bonds. The following studies focused on the impact of the various parameters on the end product. Every step of the process was investigated through similar substitutes ($C_9H_{12}O$ and 4-methylguaiacol) [18]. The slurry liquid has two phases, water and 1-butanol. The second step was carried out in 1-butanol phase with a number of catalysts, namely, cerium (IV) oxide-zirconium dioxide and aluminium oxide-iron oxide. Using the lattice oxygen present in the iron oxide, the organics adsorbed on the catalysts undergo oxidative decomposition.

The impregnation of metal in biomass can change the pyrolysis mechanism. Pyrolysis of metal-impregnated biomass caused a notable reduction in coke concentration and an increase in H_2 [19]. Nickel salts (Ni) and Fe change the pyrolysis mechanism of cellulose, hemicellulose and lignin. The biomass was saturated with nickel and ferrous wherein Fe impregnation accelerated the production of char and tar concentration got reduced. In comparison with Fe, Ni is more efficient in rearranging the aromatic ring and therefore leads to greater hydrogen production. The pyrolysis catalysis was performed at 600 °C, the resultant liquids analysed quantitatively by GC–MS.

3   Hydrodeoxygenation of Biomass-Based Pyrolysis Oil Using Iron Based Catalysts

Bio-based oil produced by pyrolysis is utilized by further subjecting it to hydrodeoxygenation (HDO). It is a process of extracting out the excess oxygen as water using H_2 catalyst between temperatures 300 and 600 °C [20]. HDO of pyrolysis oil

is positively aided using Fe-based catalysts [21]. Among various metal-based catalysts (Fe, Ni, Co, Cu) used for hydrodeoxygenation of guaiacol, Fe is the most promising one for hydrogen economy.

Dufour et al. investigated lignin hydrolysis to aromatic compounds employing guaiacol and studied effects of gaseous concentration, catalyst loading and supports [silica or activated carbon (AC)]. Fe/AC at 10 wt% had an enhanced specificity for phenol and cresol as compared to Fe/SiO_2 [22]. The study aimed to do comparative study of guaiacol vs. Fe/SiO_2 HDO on pyrolysis reaction under different gaseous atmospheres (carbon monoxide, carbon dioxide, methane and H_2O).

Dufour et al. compared the HDO of guaiacol and aromatics with iron-based catalysts in his work [23]. The authors conducted experiments with packed bed reactors at 673 K and performed vapour-phase reactions where uncondensed lignin pyrolysis vapours were used. The Fe/SiO_2 catalyst selectively yields benzene and phenols as the hydrodeoxygenation products. A series of experiments were carried out for guaiacol catalysis using intricate compositions (H_2, H_2O, CO and CO_2), and the kinetic models were predicted for the resultant products.

Fe-based catalysts are highly useful in clarifying tar from biomass. In a study by Guan et al., tar extracted from lignin sources was steam reformed with Fe-loaded calcined scallop shell (CS) with enhanced impact of potassium on the catalysis reaction. When K_2CO_3 was incorporated as a K precursor, mesoporous structures coupled with pompom-like Fe-based particles on the scallop shell (CS) were observed which was not in the case of KOH and KNO_3, respectively [24].

4   Cobalt-Based Catalysts for Lignin Valorization

Liu et al. screened an array of cobalt (Co)-type catalyst and type specified each of them for HDO of lignin-based phenols to cyclohexanol using various supports (ZrO_2, SiO_2, Al_2O_3 and CeO_2). Cyclohexanols are important feedstocks for the industrial production of polymers, spices and medicines. Of the different tested catalysts, Co/TiO_2 exhibited higher hydrodeoxygenation (HDO) reaction resulting in a maximum of 99.9% $C_9H_{19}O$ selectivity under 1 MPa H_2 at 200 °C for 2 h. The effect of temperature gradient, H_2 pressures and reaction times on eugenol conversion by Co/TiO_2 was further studied. The catalyst yielded a maximum of 99% propyl-cyclohexanol from eugenol by HDO using non-noble metal-based catalyst in the simplest experimental conditions (180 °C for 8 h at 0.4 MPa H_2) [25]. Bu et al. came up with an advanced method of using microwave for pyrolysis of lignin utilizing co-modified ZSM-5 catalysts. The experiment design was developed using Response Surface Methodology (CCD model) where the key factors, namely, ketones, furans, phenols and guaiacols, were optimized using factorial designs against the gas variables H_2 and CO [26].

5 Role of Nickel-Based Catalysts in Production of Viable Products from Lignin

Of the various metals tested (Ni, Fe and Co), Ni catalyst exhibited maximum specificity and high yield for lignin valorization and subsequent yield of renewable energy crops. These catalysts are having an upper hand not only by being efficient, but they also catalyse the reaction with lesser tar yield and O_2 and are also cost-effective. These factors thus contribute to the good-quality oil and gas and are thus largely applied for biomass gasification processes. In certain cases, to enhance H_2 yield and avoid tar formation, extra metals are included in Ni-Al catalyst during the reaction process [1]. In another finding reported by Wu et al., the effect of Zn/Ca on pyrolysis reaction with Ni-Al catalyst was evaluated in the H_2 yield from the sources of lignin, cellulose and hemicellulose. It was unraveled that Ni catalyst enhanced the product yield notably when splurged in to the system in steamed conditions, and thus Ni-Zn-Al accelerated the lignin pyrolysis by 50 wt% [27].

Akubo et al. experimented on steam clarification of cellulose, hemicellulose and lignin from agricultural waste using 10 wt% Ni-based alumina catalysts ($NiAl_2O_3$). The results affirmed that incorporation of catalyst in the steam clarification notably enhanced the syngas production with special mention of H_2 gas. Interestingly of the various source crops tested in the study, lignin yielded maximum H_2 gas as compared to others [28].

Schmitt and coworkers carried out the upgradation of beech wood pyrolysis oil and isolated the heavy phase under different temperature and pressure conditions using the Ni-Cr catalyst. The HDO reaction produced, upgraded resultant products with an elevated carbon and reduced O2 concentration at an increased temperature range of 275–325 °C [29].

Ben and Ragauskas worked on softwood craft lignin with nickel chloride and zeolite Socony Mobil-5-hydrated aluminium silicate catalyst. The results proved to be significantly reduced O_2 content in bio-oil by supporting the breakdown of methoxy and carboxyl groups and ether bonds [30]. It is to be understood that biomass catalysis to gaseous and other products (syngas) is the model ideal route. However enormous amounts of tar (aromatic hydrocarbons with high molecular mass) is produced in the process of gasification which may be condensed and cause damage to various parts of the reactor. The development of an effective catalyst to improve the syngas yield is of great importance, and significant measures have been directed towards the formulation of a cost-effective Ni-based catalyst possessing coke resistance capacity with a view to obtain higher performance. In this regard, Ma and coworkers developed a unique Ni-based catalyst enabled by iron slag for the catalysis of the pine sawdust, and the nature of its volatile content was critically cross-evaluated with Al-Ni catalysts. The study identified that Fe slag Ni-based catalyst with Ni loading of 1.8% can extract ~90% of the tar or more at 800 °C that more resembles the pyrolysis yield of Al-Ni-based catalysts [31].

Catalytic hydro-treatment is a plausible route to convert oil to intermediates possessing improved properties. Wang et al. performed catalyst screening for the H_2

treatment of pyrolysis oil with nickel compounds and compared the findings with ruthenium catalyst. Additionally, heterogeneous nickel catalyst was formulated with molybdenum, copper and palladium (bi-metallic) or their combination (tri-metallic) as promoters in SiO_2, SiO_2-ZrO_2 and SiO_2-Al_2O_3 matrices [32]. The results of the catalytic hydro-treatment of pyrolysis liquids indicated that nickel leads to an elevated hydrogen/carbon ratio in resultant products compared with the Ru/C catalysts. The produced oil is thus indicative of a high thermal stability and low coke formation upon heating. Thus, the oil obtained using Ni-based catalysts is preferred over those obtained using Ru/C catalysts. The H/C ratio of the produced oil varied with Ni-based catalysts with different promoters. Among all Ni-based catalysts, monometallic Ni-based catalysts yielded the lowest H/C ratio. The copper is introduced to nickel catalyst contributed to elevated H/C ratio, and addition of Pd had a similar effect, as it is a profound hydrogenation catalyst. Mo-upgraded catalysts showed comparable results with negligible tar by-products. In addition to the H/C ratio, charring tendency is another important parameter essential to evaluate pyrolysis products. To further assess the standards, char formation, the residue was heated to 900 °C in an inert atmosphere, and the residue formation was measured. Molybdenum resulted in oil products with least remnants (0.7–1.4 wt%), which is the maximum in nickel and nickel-copper catalysts. It can be concluded that Ni-Mo and Ni-Pd are ideal complexes for the hydro-conversion of pyrolysis liquid organic products with desirable traits like low tar formation and increased hydrogen/carbon ratio. Pd-promoted Ni catalysts showed the highest carbon balance in the product phase; however, the fact that Pd is immensely expensive than Mo makes Mo a good promoter for nickel compounds. The performance of ruthenium catalysts is lesser to that of nickel catalyst as far as traits of the products are concerned [32].

6 Hydrogenolysis of Lignin-Derived Molecules

Hydrogenolysis/hydrodeoxygenation (HDO) of lesser mass lignin crops using various catalytic systems is a popular method used to study lignin valorization (Scheme 2). The oil obtained by pyrolytic catalysis is complicated to use, since it is thermally unstable, is highly viscous and possesses a low heating value. Reductive depolymerization is an alternative approach to attain essential compounds from lignin substrates that belongs to the family of phenyl propanoid polymers interlinked by carbon-carbon or carbon-oxygen-carbon bonds. The representative molecules (Fig. 2) are attained from lignin depolymerization and contain similar linkages; thus, their reactivity in different catalytic systems will provide minute details of lignin polymer degradation [6, 34]. Many researchers have examined a number of catalytic compounds for the decomposition of lignin. Among these, Ni-based catalysts are not only promising but also cost-effective in lignin depolymerization. Yagadri and coworkers formulated a panel of mesopore range silica KIT-6-supported over nickel by water-based fixation protocol and subsequently studied hydrogenolysis of lignin-derived diphenyl ether under atmospheric pressure. Among the tested
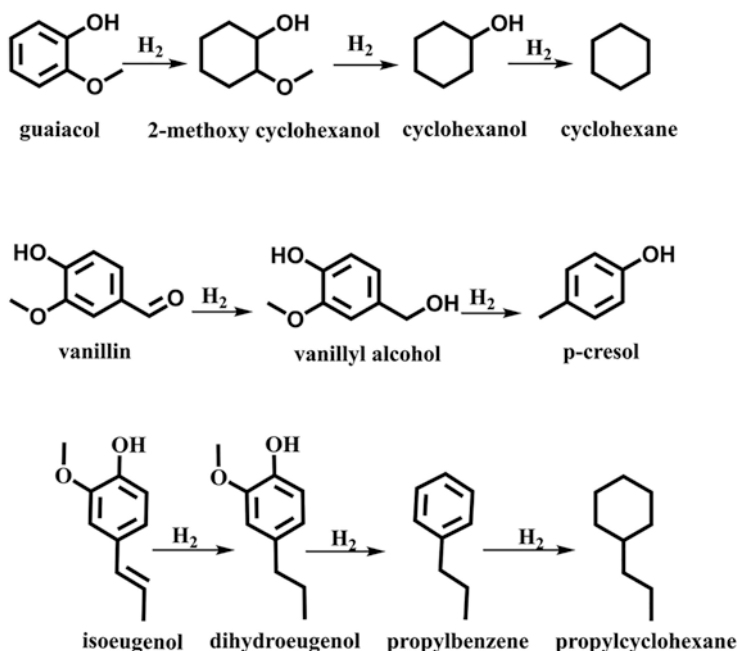
Scheme 2 Hydrodeoxygenation of guaiacol, vanillin and isoeugenol (Taken from [33] with due consent from Springer)

substances, nickel-mesoporous silica supported catalyst shows higher activity and specificity attributed with the uniform dispersal of nickel into the porous channel. The 20 wt% Ni/KIT-6 showed consistent selectivity for aromatics (benzene and phenol) during the hydrogenolysis of DPE. A time-on-stream study showed that the catalyst endured a reduced DPE transformation, because of the blockage of catalytic active site by coke deposition [34, 35].

Lignin-specific depolymerization is a critical step to get renewable bio-products. Ma and coworkers worked on selective depolymerization lignin and used zirconium-supported (Ni/ZrP) Ni catalyst and isopropanol as solvent for hydrogen transfer. A promising 87% organosolv lignin depolymerization was optimized in catalyst conditions of 15 wt% Ni/ZrP-2 and a minimum of 5.2% char (reaction conditions—260 °C for 4 h under 2 MPa H_2).

Product analysis indicated that 15 wt% phenolic monomers were obtained and ~40% of the compounds were found to be *p*-ethylphenol, which is an important bulk chemical produced by the petrochemical industries. These results indicate that the efficient mass yield of fine chemicals from lignin polymer is possible [36].

Lignin and the mono-liganols are interconnected by a number of functional interlinks, which are precursors for valuable compounds [6]. Hydrogenolysis of carbon-oxygen bonds with metal catalysts carried out inside a hydrogen atmosphere is an effective means of transforming lignin to depolymerized aromatic platform compounds. Generally, 70% of lignin bonds are formed by Cβ-O links; and thus,

breakage of these bonds represents an ideal way for degradation of lignin into valuable compounds. In this regard, Zhang et al. investigated the impact of various bi-metallic catalysts—$Ni_{85}M_{15}$—and its effectiveness on degradation of lignin compounds. The reaction was performed in organosolv lignin at 130 °C under 10 bar H_2 for 1 h in water. The bi-metallic catalysts were found to have an upper hand than the monocompounds. The optimized bi-metallic catalysts (85% nickel and 15% ruthenium) were made of ultrasmall atomically mixed Ru-Ni nanoparticles on a Ni-loaded surface. The Ni-Ru catalyst showed a notably higher activity in carbon-oxygen bond hydrogenolysis and aided in rapid direct hydrogenolysis of lignin to aromatic products as compared to monometallic Ni-Ru catalysts. Addition of 15% ruthenium enhances the reaction rate of Ni, resulting in ultrasmall bi-metallic catalyst particles supported with enhanced fraction of surface atoms. $Ni_{85}Ru_{15}$ catalyst prevented the occurrence of non-essential hydrogenation of aromatic ring as compared to pure Ru catalyst that results in increased production of essential aromatic compounds. Additionally, the former exhibited increased TOF at lesser temperature and pressure (100 °C and 1 bar) over the latter which could be related to higher H_2 and substrate activation on electron-rich Ni. Thus, the aforementioned factors are responsible for the synergic effects of Ni and Ru [34].

Similarly, Zhang et al. examined cleavage of $C_β$-O ether bonds by dehydroxylation-hydrogenation with a Ni-Mo sulphide catalyst. The authors chose $C_{14}H_{14}O_2$ as the model compound for the purpose of the study and identified that compounds lost hydroxyl groups (Cα-OH) at acidic sites of the catalyst during the course of the reaction (180 °C for 1 h at H_2 1.0 MPa). Subsequently, the $PhCH^{δ+}CH_2OPh$ transforms to $PhCH^·CH_2OPh$ as it gets an electron in the redox cycle. Intermediate $PhCH^·CH_2OPh$ has a lesser Cβ-OPh bond dissociation energy (66.9 kJ mol^{-1}) as compared with that of Cβ-O bond. The Cβ-OPh bond easily breaks and results the production of styrene, ethylbenzene, phenol and other products via the hydrogenation reaction with alcohol as solvent [37].

Sustainable production of aromatic chemicals from nature's renewable aromatic resource, lignin, using catalytic technology is a popular research topic. Qi and coworkers worked on conversion of birchwood lignin to monomeric phenols over Ni catalysts. Activated carbon-embedded nickel catalysts were formulated through a nascent wet impregnation method and analysed by thermal carbon reduction methodology. High chemo-selectivity to aromatic products was achieved in Ni/C system with coomon alcohol as solvents, such as, methanol, ethanol and ethylene-glycol, resulting in monomeric phenols, propyl-guaiacol and propyl syringol compounds from lignin. The catalysts showed 50% conversion of birchwood lignin, with 97% selectivity for monomeric phenols. Initially small-sized lignin fragments are made from birchwood lignin and ensured that it had more number of benzene rings (MW 1100–1600 m/z) via an alcoholysis reaction and to phenols by further hydrogenolysis. Alcohol as a solvent provides active hydrogen species for the reaction. The catalysts could be repeatedly utilized to about four times by holding its activity. The study thus contributes to the in-depth knowledge of lignin depolymerization and presents ways to a number of such related biomass utilization studies [38].

7 Hydrodeoxygenation of Lignin

Catalytic hydrodeoxygenation is a promising technology for producing bio-oil from lignin, with lesser O_2, higher heating value point, low emission and enhanced stability. It is evident that precious metal-based catalysts exhibit brilliant catalytic performance in the HDO of lignin. However, their extensive application is limited due to low abundance and high cost. Among the non-noble metal catalysts, there is a great number of reports regarding the use of Ni-based catalysts in lignin hydrodeoxygenation. Therefore, we have to essentially consolidate the various positive effects of Ni catalysts and its pivotal role in generating experimental models that are cost-effective, stable and strong for lignin hydrodeoxygenation. Wang et al. conducted experiments on hydrodeoxygenation of diphenyl ether, which is a model compound with a stable ether bonds in lignin substrates, over nickel catalysts on acidic or basic supports. The authors described that Ni/Al-SBA-15 is an ideal one for the hydrodeoxygenation of diphenyl ether, as there is 100% substrate conversion with 98% cyclohexane selectivity. The catalyst can degrade organosolv lignin to a mixture of cycloalkanes, which are important starting materials to make transportation fuels. These results reveal the significance of of Al-SBA-15 as an alternative acidic support to zeolites or other acids for the HDO of phenol-based substrates [39]. Jinet and coworkers performed cracking of ether compounds with Ni nanoparticles placed over Ni/xNbAC complex in normal experimental setup (180–260 °C) and compared the results with those using Ni/AC catalysts.

Due to the coexistance of Bronsted and Lewis acid sites on the wet niobium oxide has accelerated breaking of C-O ether linkages, and the catalytic activity of Ni/xNbAC was higher as compared to that of Ni/AC. Additionally, the Ni/xNbAC performed better at higher temperature (cracking C-O bonds) and at lower H_2 pressure (direct bifurcation of 4-O-5 aryl ether bonds) that leads to production of phenol and benzene intermediate, and the final product obtained was cyclohexane [40]. In another interesting phenomenon, reductive depolymerization with Ni catalysts aided with mixed surface properties (acid and base) was investigated to apprehend the effects of supports on catalysis.

Xu et al. examined depolymerization through hydro-processing of 2-phenoxy-1-phenylethan-1-one ($C_{14}H_{12}O_2$) with a number of Ni-based catalysts over a ZnO-Al_2O_3 compound and checked with different zinc/aluminium ratios (2, 3, 5, ∞) at 250 °C. Among the various tested catalysts, Ni/ZnO-Al_2O_3-5 catalyst showed 100% conversion and had more specificity for ethyl-cyclohexane. Further, findings were made which confirmed that Zn/Al displayed a pivotal role in deciding the products. The suggested pathways for 2-phenoxy-1-phenylethanone conversion on Ni/ZnO-Al_2O_3-5 confirmed that lesser temperature rapidly catalysed the hydrogenation of keto group and resulted in β-O4-ketone leading to formation of β-O-4-alcohol and avoided cleavage of β-O-4 ether bond. When experiments were performed at elevated temperature (>200 °C), the first resultant product was acetophenone and phenol, and subsequent hydrogenolysis to form cyclohexanol and ethyl-cyclohexane [41].

Alda-Onggar et al. investigated hydrodeoxygenation of phenolics (Scheme 2), isoeugenol, guaiacol and vanillin, over Ir/ZrO_2 and Ni/ZrO_2 as heterogeneous catalysts formulated by incipient wetness method (Scheme 2). Both the catalysts possessing Lewis acidity and Ni/ZrO_2 catalyst possess Bronsted acidity too. Hydrodeoxygenation of isoeugenol was studied at 150, 200 and 250 °C for 4 h over 10 wt% Ni/ZrO_2 and 3 wt% Ir/ZrO_2 catalysts, respectively.

The efficiency of Ni/ZrO_2 calibre to deoxygenate isoeugenol at 150 °C under 30 bar H_2 pressure was initially low, however increased with increasing temperature. Ir/ZrO_2 also gave a similar conversion (~33% yield of propyl-cyclohexane). The lower activity of these catalysts could be attributed to reduced liquid-phase balance. In case of guaiacol HDO at 250 °C and 30 bar H_2 pressure, the Ni/ZrO_2 yielded cyclohexanol (36%) as the major product and cyclohexane (2%) as the secondary product. The Ni/ZrO_2 catalyst achieved partial HDO of vanillin at 100 °C in H_2O in 30 bar H_2 pressure, which resulted in production of vanillyl alcohol as the end product [33].

Active research oriented towards finding robust and value-added products from lignin essential. Guaiacol is the most promising model compound for lignin depolymerization as it contains the phenolic and methoxy functional groups, which are the major functional groups found in lignin. Guaiacol typically possess Ar-O, C-O and C-H bonds, thereby making hydrogenation more complicated. Long et al. carried out the hydrogenation of guaiacol to cyclohexanol in a specific manner over Ni/MgO catalyst (Scheme 3). Cyclohexanol production is a significant process with immense applications, since it is an important feedstock for the polymer industry and an excellent source compound for manufacture of bio-based fuel. The catalyst showed a higher conversion rate of 98% with 100% cyclohexanol and an outstanding rate of recyclability. The basicity of MgO has considerable impacts on Ni result in high conversion and selectivity. Mechanistic study of the reaction further revealed that demethoxylation of guaiacol determines the rate of the catalysis [42].

Anisole, a methoxy-superlative lignin model compound, was examined over a series of Ni catalysts on charged carbon, SBA-15, SiO_2 and-aluminium trioxide supports under ambient conditions (210 °C, 3.0 MPa), with a view to understanding the impact of supports on the removal of OCH_3 from anisole. All the catalysts presented increased reaction for hydrogenation saturation of aromatic rings in lesser temperature (180–210 °C) and average H_2 pressure (0.5–3.0 MPa). Of the different catalyst studied, nickel supported on silica showed higher rate
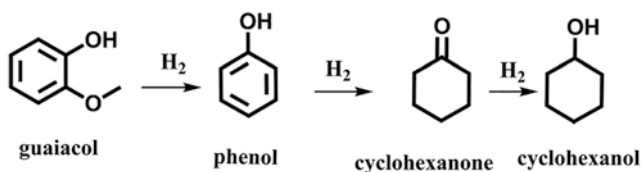
Scheme 3 Proposed reaction pathway for guaiacol hydrogenation (Referred from [42] with due consent from Elsevier)

Scheme 4 Hydrocarbon products from lignin HDO of phenolics (Extracted from [45] upon consent from Elsevier)

o-cresol   methyl cyclohexane
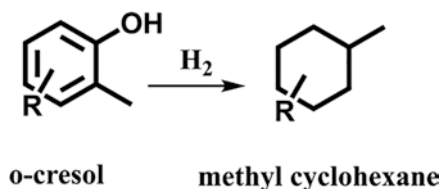
(90%) of deoxygenation in HDO process. The well-dispersed metallic Ni particles on acidic supports resulted in appreciable HDO rate production as compared to Ni/SiO$_2$ catalysts. The catalyst also showed direct demethoxylation of anisole to form benzene, even at atmospheric pressure [43]. Sankaranarayanan et al. explored the catalytic activity of supported metallic Ni or Co for the HDO of anisole. When selecting the support compounds, features like acid/basic nature and texture were considered. ZSM-5 (h-ZSM-5) was supported with Si/Al = 47 and Si/Al-47 (pure silica SBA-1. The results showed that anisole hydrodeoxygenation was highly favoured by acidity of the support associated with the metals, which implies the synergic effect between metallic and acidic sites. Maximum HDO of anisole was achieved with Ni/C as compared with the Co catalysts. The Ni/H-ZSM-5 revealed a high degree of hydrodeoxygenation, hydro-de-aromatization and isomerization reactions, which may be due to the well-dispersed Ni particles in the channels of ZSM-5 [44]. In another experiment lignin-based phenols were hydrodeoxygenated to hydrocarbons (Scheme 4) with Ni/SiO$_2$-ZrO$_2$ catalysts (300 °C and 5.0 MPa H$_2$ pressure) that resulted in 100% conversion of phenolic compounds, with greater than 98% selectivity for hydrocarbons. The amphoteric character of the SiO$_2$-ZrO$_2$ support confers anti-coking performance to the Ni/SZ-3 catalyst, thereby ensuring excellent recyclability in the hydrodeoxygenation reaction of model phenolic compounds [45].

8 Ruthenium-Based Catalysts for the Hydrodeoxygenation of Lignin

As mentioned previously, the Earth's most abundant aromatic natural polymer, lignin, consists of a three-dimensional structure of phenolic monomer that is interconnected by different Cβ-O linkages. β-O-4 is the common bonds studied and represents ~50% cross-linkages in lignin. Lignin is the most known feedstock for extraction of several value-added chemicals, phenols, fuel, flavourings and drug intermediates, thus making its depolymerization studies more challenging for researchers. Through C-O-C bond cleavage, lignin gets converted to monomers and dimers by a number of techniques, namely, pyrolysis, hydrolysis, hydrogenolysis, oxidation or hydrocracking. In addition, metals, namely, Pt, Rh and Ru, placed on carbon support play a crucial role in lignin depolymerization [46]. Wu et al. carried out reaction to cleave aromatic ether bonds in lignin compounds using Ru/C catalyst
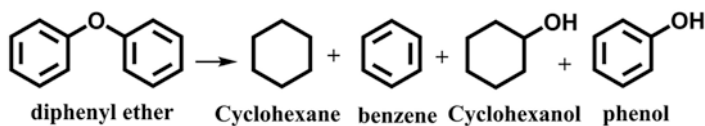
Scheme 5 Image showing hydrogenolysis of diphenyl ether (Obtained from [47] with due consent from the American Chemical Society)

and isopropanol in H_2 atmosphere. Interestingly Ru/C cleaved lignin-based compounds resulting in aliphatic alcohols, alkanes and aromatics in ambient experimental parameters (Scheme 5). Further mechanistic findings affirmed that the catalyst adopts the hydrogenolytic mode to cleave the ether bonds wherein intermediate compounds such as cyclohexyl phenyl ether are also formed [47].

A study on the hydro-pyrolysis activity of phenethyl phenyl ether (PPE) over Ru/C and Ru/Al$_2$O$_3$ was explored. PPE was selected because it is an important model compound that contains significant β-O-4 linkages, the most essential ether bonds. The findings suggested that the above mentioned catalyst was highly specific for lysis of CO bond over HDO of the aromatics. Also, carbon-supported Ru/C facilitated C$_{aryl}$-O hydrogenolysis as compared to alumina. The reason for the increased rate of reaction and enhanced selectivity is due to size of the Ru cluster (4 nm) that is comparatively less than that of γ-alumina (50 nm). In a typical reaction, C$_β$-O ether and C$_{aryl}$-O bond are hydrogenolysed leading to saturation of PPE rings followed by cracking of ether bond which results in one of the two reactions. Either the saturated dimers are broken down to monomer, or they are totally saturated [48].

A number of heterogeneous catalysts have been explored to establish their specific role in degradation of lignin and in accelerating the reaction rate or product yield. The positive effect of the acid-base sites and the metal counterparts encourages the rate of the lignin depolymerization and results in higher yield of phenols. In a study conducted by Limarta, the combined impact of the metal and solid-base catalysts in Kraft lignin conversion to monophenol-based bio-oil was studied. Based on the earlier reports that strongly supports the positive role of Ru/C in lignin hydrogenolysis, it was chosen as a metal catalyst with basic MgO support in combination with carbon, Al$_2$O$_3$ and ZrO$_2$ supports. Additionally, a multi-functional-catalyst Ru/C-MgO/ZrO$_2$ combination was also investigated, and properties such as molecular weight, distribution of the monomers, O/C and H/C rations and oil properties were explored to study the synergistic effect.

The studies unraveled that lignin was effectively degraded by Ru/C-MgO/ZrO$_2$, and the reaction was catalysed by the synergic effect of base catalysed solvolysis and Ru catalysed hydrogenolysis and resulting in the formation of high quality bio-oil with high calorific value enriched with essential phenolic monomers. In comparison with Al$_2$O$_3$ and carbon supports, the ZrO$_2$ support promoted enhanced basicity and reactivity of MgO [49].

Ru catalysts showed a potential application in the hydrotreatment of platform molecules to target chemicals by the effective removal of oxygen moieties and

hydrogenation of unsaturated bonds. Lignin-based phenolics are essential feed crops for yield of hydrocarbons (alkenes) usually achieved through HDO which yields commercial grade fuel. Conversion of phenols from lignin sources has been studied over ruthenium supported on carbon nanotube catalyst in bi-phasic system. In a typical reaction, hydrodeoxygenationof phenolic monomers and dimers was carried out over Ru/CNT in an *n*-dodecane/H_2O biphasic system which resulted 99% conversion of eugenol to propyl-cyclohexane (94%) and propyl-cyclopentane (4%). Thus it can be concluded that biphasic systems have an upper hand over the single-phase setups in terms of conversion rate and selectivity (56% fuel production). Studies affirmed that hydrogenation is the first step of eugenol conversion resulted in the formation of 4-propyl-cyclohexanol, followed by dehydration and hydrogenation to form propyl-cyclohexane [50].

In another study, hydrotreatment of eugenol has been carried out with Ru/C--Fe_2O_3. In a tpical experiment, Ru nanoparticles were annealed to the metal supports at increasing temperatures (0, 300, 500, 600 and 750 °C), and the HDO performance was evaluated in a batch slurry reactor at ambient conditions (275 °C and 5 MPa H_2). The experimental results suggested that the non-annealed catalyst was inactive in HDO of eugenol and with the increase in annealing temperature, the material showed higher hydrogenation and deoxygenation activity, reaching a maximum at 600 °C. Catalyst annealed at 600 °C exhibited superior catalytic performance in deoxygenation of saturated intermediates compared to market grade Ru/C. Thus well-dispersed Ru nanoparticles are accredited for enhanced reaction rate, and the Fe components are believed to play a neutral role [51].

9 Rhodium-Based Catalysts for the Hydrodeoxygenation of Lignin

The recent focus of the researchers for lignin breakdown is rhodium (Rh) catalysts, and comparative studies have been done with the platinum- and palladium-based catalysts [52]. For example, carbon-supported Rh catalysts achieved the successful hydrodeoxygenation of 4-Propylphenol dissolved in H_2O medium at 280 °C under 4 MPa H_2 (initial pressure at RT). The conversion rate for the reaction was 100%, and an 83% yield of propyl-cyclohexane was produced [53]. Deng et al. outperformed experiments on hydrogenation and HDO of lignin-based compounds and relevant model compounds using metal-based catalysts. The HDO of guaiacol with Pt, Pd or Rh yielded catechol as the primary product; however the co-presence of both these compounds resulted in coke production. This has led to a reduced surface area for Pt, Pd and Rh catalysts in the course of the reaction. In comparison with the oxidic support, activated carbon is preferable due to the neutral surface and minimal interaction with the metal [54]. Hydrodeoxygenation of guaiacol was also investigated using mono- and bi-metallic Rh/C. A notable impact of temperature on HDO was also experimented in temperature between 300 and 400 °C, where yield of

cyclohexane was found to be increased with increasing temperature. The monometallic Rh catalyst yielded maximum cyclohexane accompanied with an enhanced HDO reaction on par the other catalysts tested. Generally, guaiacol is hydrogenated in binary catalytic reaction steps, namely, hydrogenation that produces benzene rings from guaiacol and demethoxylation and dihydroxylation [55].

Recently, hydrodeoxygenation of guaiacol was investigated over a zirconia-based Rh catalyst. Guaiacol was hydrotreated in a batch reactor under 3–7 H_2 pressure at 150–350 °C. The optimum condition for the HDO process of guaiacol was found to be 300 °C, 7 MPa and 5 wt% guaiacol. Under these conditions, complete deoxygenation of guaiacol takes place with around 88 mol.% cyclohexane in 3 h, and the support only yielded a maximum of approximately 11% conversion. Without the use of a catalyst, under thermal conditions, guaiacol mainly converted to coke, with the formation of trace amounts of cyclohexanone and cyclohexanol. When rhodium/zirconium dioxide catalyst was used at 150 and 250 °C, the main products were trans and cis 1-methyl-1,2-cyclohexanediol respectively (Scheme 6). As the reaction temperature increased, guaiacol was completely deoxygenated and yielded cyclohexane and alkanes as the major products [56].

Catalytic upgrade of pyrolysis oil using 5% Rh on a carbon-supported catalyst showed good HDO reactivity under 300–1000 psi H_2 pressure at 200–280 °C. The reaction was performed in a bar batch reactor (300 mL vol) using polyethylene glycol as the solvent. Catalytic upgrade of switchgrass-derived oil was conducted with ruthenium/carbon and rhodium/carbon, revealing that the former had upper-hand aliphatic and aromatic hydrocarbons and other upgraded products [57]. Yan et al. formulated a panel of bi-metallic catalysts for lignin valorization. Bi-metallic Ni-Rh catalysed the lysis of lignin C-O bonds and was found to be extremely functional and specific than the mono catalyst, thus having an upper hand in degrading lignin
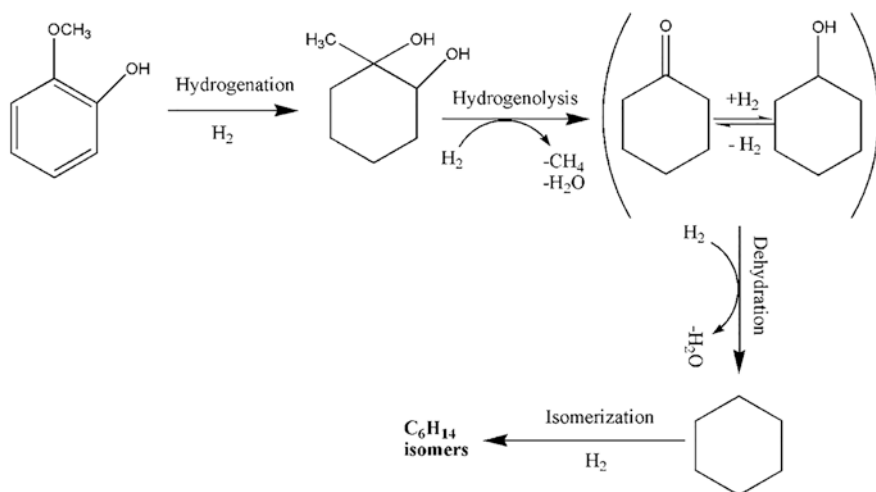
Scheme 6 Proposed pathway for guaiacol hydrodeoxygenation on rhodium/zirconium dioxide catalyst (Extracted with from ref. with due permission [56])

products. The combination of the two metals enhanced the catalytic performance. The depolymerization was carried out using H_2O under a H_2 pressure of 10 bar at 130 °C [34].

10 Significance of Palladium in the Catalytic Conversion of Lignin

Palladium on carbon (Pd/C) catalysts is widely used for hydrogenation reactions in several industries due to their excellent activity and selectivity in ambient reaction setup. Wang et al. [58] explored hydrogenation of alkali-lignin using 5% Pd/C catalysts at 393 K under H_2 pressure of 1.5–4 MPa and evaluated the functional groups and structural variation. It was evident that the use of Pd catalysts facilitates the reduction of carbonyl and carboxyl functionalities present in the alkali-lignin and increased the concentration of phenolics (37%) and aliphatic hydroxyl (89%) groups [58]. Similarly, Hartwig et al. reported less fragmentation of β-O in lignin using commercially available Pd/C catalysts. The authors postulated that the compound, 2-phenoxy-1-phenylethanol, was converted to phenol and acetophenone, with greater than 90% yield within 2 h, suggesting that the reaction first proceeded by dehydrogenation, with subsequent cleavage of β-O linkages. The Pd/C catalysts were also studied using several organosolv lignins, where the double bond present in the molecules was reduced first via the in situ H_2 production by alcohol catalysis succeeded by cracking of the alkyl C-O bond [59]. Cracking of 2-phenoxy-1-phenylethanol over M/C catalysts (where M = Pd, Rh, Ir, Re and Ni) with formic acid acted as a source of H_2 was experimented. An experiment was conducted with ammonia as the base, which promoted the catalytic activity. Among the various catalysts studied, palladium on carbon showed a better activity, with the formation of phenol and acetophenone at 80 °C [60]. The reaction was further studied using various bases, such as ammonia, ethylamine, diethylamine and *p*-allylamine and several hydrogen sources, such as H_2, HCOOH, propanol and $NaBH_4$. The use of $NaBH_4$ favoured complete conversion [61].

Attempts have been made to depolymerize lignin along with palladium and Nafion®SAC-3 catalyst, with formic acid as the H_2 source and H_2O as a green solvent [62]. The pyrolysis of lignin (10 g) at 300 °C was carried out in the presence of Pd/C (0.02 g) Nafion®SAC-3 (0.1–0.2 g) as the catalyst yielded guaiacol (4a), pyrocatechol (5c) and resorcinol, which were further separated and quantified as prime products of catalytic reaction (Scheme 7). Subsequently, other lignin model compounds, such as 2-isopropyl-5-methylphenol (1), 2-ethylphenol (2), 2-methoxy-4-propylphenol (3), 2-hydroxy-3-methoxybenzaldehyde (4) and 3-hydroxy-4-methoxybenzaldehyde (5), were used, yielding hydro-deoxygenated, demethylated and demethoxylated products (Scheme 7) [62].

Experiments were performed with 2-Phenoxy-1-phenylethanol $(C_{14}H_{14}O_2)$-using Pd nanoparticles [63]. Triggered palladium was used in the
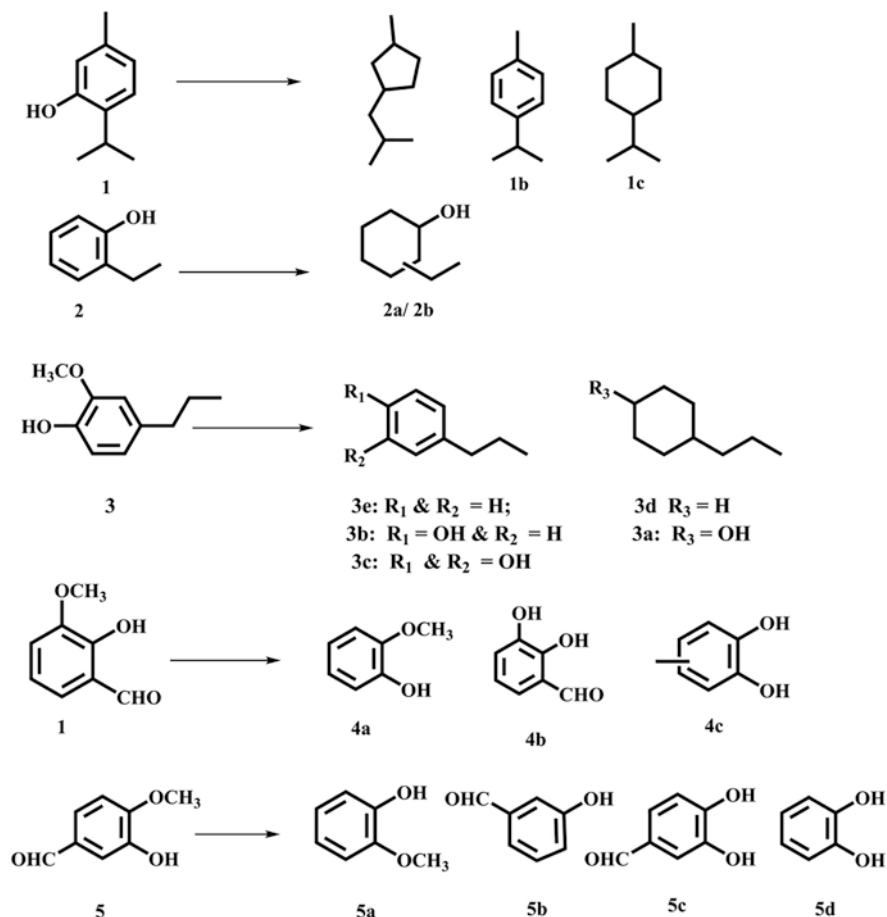
Scheme 7 Pyrolysis of lignin model compounds using the Pd-Nafion®SAC-3 catalyst (Reproduced with permission from [62])

experiment which played a crucial part in converting α-hydroxyl to α-ketone which eventually produced major products from the reaction [7]. The catalyst also showed high specificity in converting organosolv to vanillin, guaiacol and 4-hydroxybenzaldehyde under ambient conditions (185 °C). In situ generated Pd-zeolite-Y was explored for the depolymerization of lignin [64] at a relatively low temperature (180–200 °C). The studies established that there exist a synergic effect between Pd and acidic zeolite-Y which effectively catalysed the reaction [8]. Scheme 8 shows the mechanistic pathway for the products 2-methoxyphenol, 4-ethylphenol, 4-ethyl-2-methoxy-phenol, 2-methoxy-4-propyl phenol, 2-methoxy-4(1-propenyl)-(E)-phenol and 2,6,-dimethoxy-4-(2-propenyl)-phenol [64]. The Pd-zeolite-Y catalyst initially dehydrated the of the Cα hydroxyl group of the lignin and resulted in a double 'C' bond formation prior to the breakage of β-O-4 bond. The
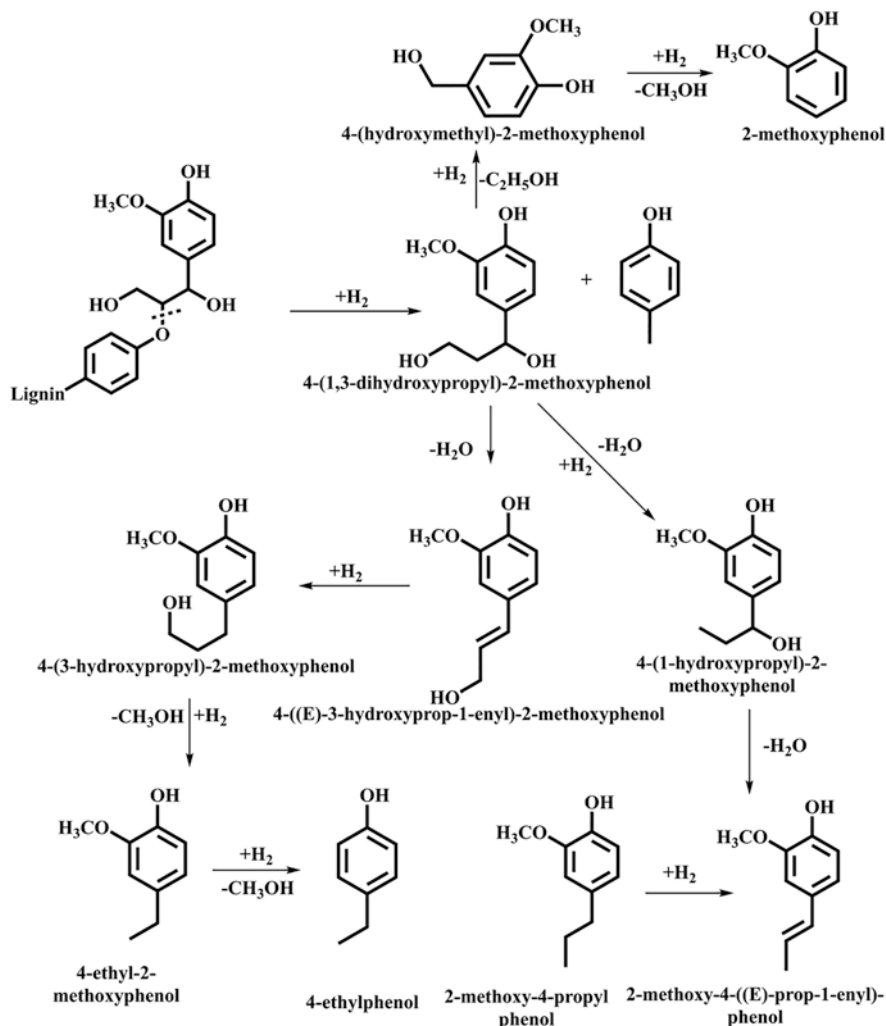
Scheme 8 Lignin depolymerization pathway over Pd-zeolite-Y catalyst (Reproduced with permission from [8])

presence of Pd on zeolite-Y facilitated the hydrogenolysis route [64]. Pd, Rh, Ru and Pt supported on carbon catalysts were also utilized for depolymerization of white birchwood sawdust via the reductive cleavage of lignin-related ethers in water/dioxane mixture, under 40 bar H_2 at 200 °C in the presence of phosphoric acid (H_3PO_4), and the final products were guaiacylpropane, guaiacylpropanol, syringyl-propane and syringylpropanol [65]. Pt is an established compound for lignin depolymerization, while Rh shows a narrowed selectivity. The order in which Pd-based catalyst catalyses HDO reaction in phenolic compounds is through hydrogenation/dehydration along with H_3PO_4 [65]. In particular, zeolite-based Bronsted acid

catalysts promoted hydrodeoxygenation in combination with Pd on carbon, which cleaved C_β-O bonds [65]. Other combinations of catalyst such as Pd over alumina, bi-metallic Pd-Ni nanoparticles on zirconia were employed to catalyse lignin and lignin-based compounds (2-phenoxy-1-phenylethanol). The catalyst with a Pd-to-Ni ratio of 1:8 facilitated cyclohexanol formation using molecular hydrogen as a hydrogen source [66]. Thus, the overall understanding from the study is that Pd catalysts are very effective in breaking lignin and model compounds in combination with acid catalyst (zeolite, alumina and Nafion) to a number of industrially viable products.

11   Iridium-Based Catalysts for Lignin Valorization

Haibach reported a novel phenomenon in which the C-O bonds cleaved by pincer iridium complexes with complete atom economy. The dehydro-aryloxylation by iridium-based catalysts resulted in moderate to excellent conversion of a large number of alkyl aryl ethers [67]. Bruijnincx et al. explored on selective lignin degradation by iridium-based catalysts and utilized cyclopentadienyl iridium-bipyridonate complex for the purpose of the study. The reaction was performed under ambient conditions that resulted in non-phenolic mono-aromatics from selective dehydrogenation of β-O-4 bonds. The depolymerization occurred via breakage of C_α-C_β bonds and is sensitive alcohol oxidation. The major products were bifunctional monoaromatic compounds. The resinol units were inert under the reaction conditions, and the phenyl-coumarins gave ring-opened oxidized products using iridium-based catalysts [68].

12   Role of Platinum in the Conversion of Lignin to Value-Added Chemicals

Lignin is an aromatic polymer, and its conversion to monomeric chemicals, such as vanillin, alkyl guaiacol, syringol and benzoquinone derivatives, is generally studied using Group VIII-based multifunctional catalysts. This part of the chapter throws light on the role of Pt in producing viable products from lignin.

Weckhuysen et al. developed an approach in which organosolv, kraft and sugarcane bagasse lignin were converted to monoaromatic compounds with a two step process. In the first step, a liquid layer reformation was done to produce monoaromatics in low O_2 phase with 1 wt% Pt/γ-Al_2O_3 catalyst at 225 °C in alkaline ethyl alcohol water, followed by HDO over cobalt-molybdenum/aluminium dioxide and Mo_2C/CNF catalyst. This method yielded greater than 57% of mono-oxygenated phenolic derivatives as major products [69]. In another study HDO of 1-(2,4-dihydroxyphenyl)-2-(4-methoxyphenoxy)-ethanone was studied using Pt

catalyst supported with carbon in water-ethanol environment at 275 °C. The end products were methoxyphenol, 6-hydroxy-3-coumaranone and 2,4 dihydroxyacetophenone produced by the breaking of β-O-4 linkage and cyclization of 2,4 dihydroxyacetophenone to 6-hydroxy-3-coumaranone. The platinum catalysts were also used for hydrogenolysis of guaiacylglycerol-β-guaiacyl ether (GGGE) that yielded 2-methoxyphenol and 4-propyl-2-methoxyphenol as primary products [70].

Studies were carried out to understand hydrogenolysis of six lignin molecules extracted from black liquor, birch, maple, pine and corn stalk over Pt/TiO$_2$, Re/TiO$_2$, PtRe/TiO$_2$, Pd/C and HZSM-5 catalysts. Pt-Re with isopropyl alcohol as the hydrogen donor was found to be the best catalyst among the various catalysts studied. The acid-extracted birch lignin (ABL), containing 36 Cβ-O bonds per 100 phenylpropene units, yielded 15 types of monophenols: 4-ethylphenol; 4-propylphenol; guaiacol; 4-ethylguaiacol; 4-propylguaiacol; 4-propenylguaiacol; 4-hydoxy-3-methoxyphenylacetone; 3-(4-hydroxy-3-methoxyphenyl) propionic acid; 4-methylsyringol; 4-ethylsyringol; 4-propylsyringol; 4-propenylsyringol; 4-hydroxy-3,5-dimethoxyacetophenone; 4-hydroxy-3,5-dimethoxyphenylacetone; and 3-(4-hydroxy-3,5-dimethoxyphenyl)propionic acid. Among the various catalysts, Pt-Re/TiO$_2$ produced twice the amount of products as the commercial ZSM-5 and Pd/C catalysts, with a monophenol yield of approximately 19%. The better activity of Pt-Re/TiO$_2$ can be explained based on the high oxophilicity of ReO$_x$, which polarized the carbonyl and hydroxyl groups on the linkages in lignin and facilitated C-O bond cleavage via the highly reducible Pt [71]. Organosolv switchgrass has been subjected to hydrogenolysis with Pt/C catalyst using ethanol solvent [72]. Similarly, when the reaction was performed with formic acid over a Pt/C catalyst, *p*-propyl-guaiacol as the resultant product was obtained not only as less molecular mass product but also with better H/C and O/C ratios, and the total yield was 21 wt%.

Very recently, Hensen et al. performed a single-step reaction for converting plant lignin (wood sawdust) to monomeric phenol derivatives by 1 wt% Pt on γ-Al$_2$O$_3$ under a 30 bar nitrogen atmosphere (inert) using methanol and water as the solvents [73]. The Pt catalyst facilitated partial reforming of the solvent and yielded the required hydrogen, stabilizing the intermediate by hydrogenation. A very high phenol production (46%) was attained at 230 °C in 3 h using 0.5 g catalyst with a methanol to water molar ratio of 1:2 (40 mL for 2 g wood dust). The use of methanol as a co-solvent for Pt catalyst at a high process temperature enabled delignification of lignin from wood dust by solvolysis. The dissolved lignin components were depolymerized to phenolic monomers by β-O-4 bond cleavage [73]. Similarly, Pt-deposited hyper-cross-linked polystyrene (Pt/MN270) and Pd-deposited hyper-cross-linked polystyrene (Pd/MN270) were used as catalysts for the hydrogenolysis of lignin isolated from softwood sawdust at 300 °C under 2 MPa hydrogen in the presence of isopropanol as a solvent [74]. The catalyst with 5% Pt-containing polymer showed the highest conversion, with a hydrocarbon selectivity of 92%.

Model Co-Pt bi-metallic catalysts, formulated by vapour-deposition of Co atoms on Pt(111), were experimented for deoxygenation of the lignin-derived model compound, anisole, and it was observed that cobalt atoms open up several sites for O$_2$ to attach which further facilitated bifurcation of carbon-oxygen bonds with Pt,

yielding benzene and phenyl groups [75]. The real-time structural modification of lignin compound aided by Pt/C supported over alumina was critically observed with four lignin model compounds, and the results suggested that β-O-4 plays a critical role and determined the fate of the end products (monomers). Exceedingly condensed polymers yielded non-alkylated phenolic monomers, and the less condensed or non-condensed lignin produced propyl phenolic derivatives as primary products in large concentrations [76]. Overall, the oxophilic character of Pt facilitated lignin depolymerization and the formation of a greater number of monomeric species.

13   Conclusion

In summary, this chapter discussed the importance of catalysts containing various Group VIII metals, namely, Fe, Co, Ni, Ru, Rh, Pd and Ir, in conversion of biomass to valuable chemicals. In particular, this chapter explained the role of individual metal ions on the hydro-process, briefly elaborating on the hydrodeoxygenation of lignin molecules. In general, catalysts containing Group VIII metals show excellent catalytic performance in hydrogenolysis of lignin and its compounds, namely, eugenol, coniferyl alcohol and guaiacol. The use of a support, such as resin, zeolite, titania, zirconia or carbon, facilitates the preparation of the best dispersed Group VIII metal catalysts and enhances the lignin hydrogenation and hydrodeoxygenation process. The uses of iron-based catalysts facilitate deoxygenation, whereas nickel- and ruthenium-based catalysts favoured hydrogenation and hydrodeoxygenation. The use of Pd-based catalysts, particularly on acidic support, facilitates β-O-4 cleavage. Overall, this chapter summarizes the broad spectrum of knowledge and insight regarding the value of individual metal ion addition in lignin-derived model compound conversion. The chapter provides notable information's towards methodology development for production of industrially viable products from lignin.

References

1. Chen X, Guan W, Tsang CW, Hu H, Liang C (2019) Lignin valorizations with Ni catalysts for renewable chemicals and fuels productions. Catalysts 9:488
2. Schutyser W, Renders T, Van den Bosch S, Koelewijn SF, Beckham GT, Sels BF (2018) Chemicals from lignin: an interplay of lignocellulose fractionation, depolymerisation, and upgrading. Chem Soc Rev 47:852–908
3. Hernández WY, Lauwaert J, Van Der Voort P, Verberckmoes A (2017) Recent advances on the utilization of layered double hydroxides (LDHs) and related heterogeneous catalysts in a lignocellulosic-feedstock biorefinery scheme. Green Chem 19:5269–5302

4. Sudarsanam P, Peeters E, Makshina EV, Parvulescu VI, Sels BF (2019) Advances in porous and nanoscale catalysts for viable biomass conversion. Chem Soc Rev 48:2366–2421

5. Li C, Zhao X, Wang A, Huber GW, Zhang T (2015) Catalytic transformation of lignin for the production of chemicals and fuels. Chem Rev 115:11559–11624

6. Zakzeski J, Bruijnincx PC, Jongerius AL, Weckhuysen BM (2010) The catalytic valorization of lignin for the production of renewable chemicals. Chem Rev 110:3552–3599

7. Cheng C, Shen D, Gu S, Luo KH (2018) State-of-the-art catalytic hydrogenolysis of lignin for the production of aromatic chemicals. Cat Sci Technol 8:6275–6296

8. Verma AM, Kishore N (2017) Gas phase conversion of eugenol into various hydrocarbons and platform chemicals. RSC Adv 7:2527–2543

9. Yang L, SeshanK LY (2017) A review on thermal chemical reactions of lignin model compounds. Catal Today 298:276–297

10. Nimmanwudipong T, Runnebaum RC, Ebeler SE, Block DE, Gates BC (2012) Upgrading of lignin-derived compounds: reactions of eugenol catalyzed by HY zeolite and by Pt/γ-Al$_2$O$_3$. Catal Lett 142:151–160

11. Demirbas A (2011) Competitive liquid biofuels from biomass. Appl Energy 88:17–28

12. Bond GC (1968) Periodic variations in the catalytic properties of metals. Platin Met Rev 12:100–105

13. Rezaei PS, Shafaghat H, Daud W (2016) Aromatic hydrocarbon production by catalytic pyrolysis of palm kernel shell waste using a bifunctional Fe/HBeta catalyst: effect of lignin-derived phenolics on zeolite deactivation. Green Chem 18:684–1693

14. Mullen CA, Boateng AA (2015) Production of aromatic hydrocarbons via catalytic pyrolysis of biomass over Fe-modified HZSM-5 zeolites. ACS Sustain Chem Eng 3:1623–1631

15. Jia S, Cox BJ, Guo X, Zhang ZC, Ekerdt JG (2011) Hydrolytic cleavage of β-O-4 ether bonds of lignin model compounds in an ionic liquid with metal chlorides. Ind Eng Chem Res 50:849–855

16. Zeng J, Yoo CG, Wang F, Pan X, Vermerris W, Tong Z (2015) Biomimetic fenton-catalyzed lignin depolymerization to high-value aromatics and dicarboxylic acids. ChemSusChem 8:861–871

17. Mottweiler J, Rinesch T, Besson C, Buendia J, Bolm C (2015) Iron-catalysed oxidative cleavage of lignin and β-O-4 lignin model compounds with peroxides in DMSO. Green Chem 17:5001–5008

18. Yoshikawa T, Shinohara S, Yagi T, Ryumon N, Nakasaka Y, Tago T, Masuda T (2014) Production of phenols from lignin-derived slurry liquid using iron oxide catalyst. Appl Catal B 146:289–297

19. Collard FX, Blin J, Bensakhria A, Valette J (2012) Influence of impregnated metal on the pyrolysis conversion of biomass constituents. J Anal Appl Pyrol 95:213–226

20. Bu Q, Lei H, Zacher AH, Wang L, Ren S, Liang J, Ruan R (2012) A review of catalytic hydrodeoxygenation of lignin-derived phenols from biomass pyrolysis. Bioresour Technol 124:470–477

21. Hong Y, Hensley A, McEwen JS, Wang Y (2016) Perspective on catalytic hydrodeoxygenation of biomass pyrolysis oils: essential roles of Fe-based catalysts. Catal Lett 146:1621–1633

22. Olcese R, Bettahar MM, Malaman B, Ghanbaja J, Tibavizco L, Petitjean D, Dufour A (2013) Gas-phase hydrodeoxygenation of guaiacol over iron-based catalysts. Effect of gases composition, iron load and supports (silica and activated carbon). Appl Catal B Environ 129:528–538

23. Olcese RN, François J, Bettahar MM, Petitjean D, Dufour A (2013) Hydrodeoxygenation of guaiacol, a surrogate of lignin pyrolysis vapors, over iron based catalysts: kinetics and modeling of the lignin to aromatics integrated process. Energ Fuel 27:975–984

24. Guan G, Kaewpanha M, Hao X, Zhu AM, Kasai Y, Kakuta S, Abudula A (2013) Steam reforming of tar derived from lignin over pompom-like potassium-promoted iron-based catalysts formed on calcined scallop shell. Bioresour Technol 139:280–284

25. Liu X, Jia W, Xu G, Zhang Y, Fu Y (2017) Selective hydrodeoxygenation of lignin-derived phenols to cyclohexanols over Co-based catalysts. ACS Sustain Chem Eng 5:8594–8601

26. Xie W, Liang J, Morgan HM Jr, Zhang X, Wang K, Mao H, Bu Q (2018) Ex-situ catalytic micro-wave pyrolysis of lignin over Co/ZSM-5 to upgrade bio-oil. J Anal Appl Pyrol 132:163–170
27. Wu C, Wang Z, Huang J, Williams PT (2013) Pyrolysis/gasification of cellulose, hemicellulose and lignin for hydrogen production in the presence of various nickel-based catalysts. Fuel 106:697–706
28. Akubo K, Nahil MA, Williams PT (2019) Pyrolysis-catalytic steam reforming of agricultural biomass wastes and biomass components for production of hydrogen/syngas. J Energy Inst 92:1987–1996
29. Schmitt CC, Raffelt K, Zimina A, Krause B, Otto T, Rapp M, Dahmen N (2018) Hydrotreatment of fast pyrolysis bio-oil fractions over nickel-based catalyst. Top Catal 61:1769–1782
30. Ben H, Ragauskas AJ (2011) Pyrolysis of kraft lignin with additives. Energy Fuels 25:4662–4668
31. Ma T, Liu Y, Yu H (2017) Catalytic characteristics of pyrolysis volatile matter from biomass/biomass components on a novel Ni-based catalyst supported by iron slag. J Renew Sustain Energy 9:063101
32. Yin W, Venderbosch RH, He S, Bykova MV, Khromova SA, Yakovlev VA, Heeres HJ (2017) Mono-, bi-, and tri-metallic Ni-based catalysts for the catalytic hydrotreatment of pyrolysis liquids. Biomass Convers Bior 7:361–376
33. Alda-Onggar M, Mäki-Arvela P, Aho A, Simakova IL, Murzin DY (2019) Hydrodeoxygenation of phenolic model compounds over zirconia supported Ir and Ni-catalysts. React Kinet Mech Cat 126:737–759
34. Zhang J, Teo J, Chen X, Asakura H, Tanaka T, Teramura K, Yan N (2014) A series of NiM (M = Ru, Rh, and Pd) bimetallic catalysts for effective lignin hydrogenolysis in water. ACS Catal 4:1574–1583
35. Yadagiri J, Koppadi KS, Enumula SS, Vakati V, Kamaraju SRR, Burri DR, Somaiah PV (2018) Ni/KIT-6 catalysts for hydrogenolysis of lignin-derived diphenyl ether. J Chem Sci 130:106
36. Ma H, Li H, Zhao W, Li L, Liu S, Long J, Li X (2019) Selective depolymerization of lignin catalyzed by nickel supported on zirconium phosphate. Green Chem 21:658–668
37. Zhang C, Lu J, Zhang X, MacArthur K, Heggen M, Li H, Wang F (2016) Cleavage of the lignin β-O-4 ether bond via a dehydroxylation–hydrogenation strategy over a NiMosulfide catalyst. Green Chem 18:6545–6555
38. Song Q, Wang F, Cai J, Wang Y, Zhang J, Yu W, Xu J (2013) Lignin depolymerization (LDP) in alcohol over nickel-based catalysts via a fragmentation–hydrogenolysis process. Energy Environ Sci 6:994–1007
39. Wang X, Rinaldi R (2016) Bifunctional Ni catalysts for the one-pot conversion of Organosolv lignin into cycloalkanes. Catal Today 269:48–55
40. Jin S, Xiao Z, Chen X, Wang L, Guo J, Zhang M, Liang C (2015) Cleavage of lignin-derived 4-O-5 aryl ethers over nickel nanoparticles supported on niobic acid-activated carbon composites. Ind Eng Chem Res 54:2302–2310
41. Xu C, Tang SF, Sun X, Sun Y, Li G, Qi J, Li X (2017) Investigation on the cleavage of β-O-4 linkage in dimeric lignin model compound over nickel catalysts supported on ZnO-Al2O3 composite oxides with varying Zn/Al ratios. Catal Today 298:89–98
42. Long J, Shu S, Wu Q, Yuan Z, Wang T, Xu Y, Ma L (2015) Selective cyclohexanol production from the renewable lignin derived phenolic chemicals catalyzed by Ni/MgO. Energy Convers Manag 105:570–577
43. Jin S, Xiao Z, Li C, Chen X, Wang L, Xing J, Liang C (2014) Catalytic hydrodeoxygenation of anisole as lignin model compound over supported nickel catalysts. Catal Today 234:125–132
44. Sankaranarayanan TM, Berenguer A, Ochoa-Hernández C, Moreno I, Jana P, Coronado JM, Pizarro P (2015) Hydrodeoxygenation of anisole as bio-oil model compound over supported Ni and Co catalysts: effect of metal and support properties. Catal. Today 243:163–172
45. Zhang X, Zhang Q, Wang T, Ma L, Yu Y, Chen L (2013) Hydrodeoxygenation of lignin-derived phenolic compounds to hydrocarbons over Ni/SiO2–ZrO2 catalysts. Bioresources 134:73–80

46. Verziu M, Tirsoaga A, Cojocaru B, Bucur C, Tudora B, Richel A, Mikkola JP (2018) Hydrogenolysis of lignin over Ru-based catalysts: the role of the ruthenium in a lignin fragmentation process. Mol Catal 450:65–76

47. Wu H, Song J, Xie C, Wu C, Chen C, Han B (2018) Efficient and mild transfer hydrogenolytic cleavage of aromatic ether bonds in lignin-derived compounds over Ru/C. ACS Sustain Chem Eng 6:2872–2877

48. Gomez-Monedero B, Faria J, BimbelaF RMP (2017) Catalytic hydroprocessing of lignin β-O-4 ether bond model compound phenethyl phenyl ether over ruthenium catalysts. Biomass Convers Bior 7:385–398

49. Limarta SO, Ha JM, Park YK, Lee H, Suh DJ, Jae J (2018) Efficient depolymerization of lignin in supercritical ethanol by a combination of metal and base catalysts. J Ind Eng Chem 57:45–54

50. Chen MY, Huang YB, Pang H, Liu XX, Fu Y (2015) Hydrodeoxygenation of lignin-derived phenols into alkanes over carbon nanotube supported Ru catalysts in biphasic systems. Green Chem 17:1710–1717

51. Bjelić A, Grilc M, Gyergyek S, Kocjan A, Makovec D, Ikozar B (2018) Catalytic hydrogenation, hydrodeoxygenation, and hydrocracking processes of a lignin monomer model compound eugenol over magnetic Ru/C–Fe2O3 and mechanistic reaction microkinetics. Catalysts 8:425

52. Mu W, Ben H, Ragauskas A, Deng Y (2013) Lignin pyrolysis components and upgrading technology review. Bioenergy Res 6:1183–1204

53. Ohta H, Kobayashi H, Hara K, Fukuoka A (2011) Hydrodeoxygenation of phenols as lignin models under acid-free conditions with carbon-supported platinum catalysts. Chem Commun 47:12209–12211

54. Mu W, Ben H, Du X, Zhang X, Hu F, Liu W, Deng Y (2014) Noble metal catalyzed aqueous phase hydrogenation and hydrodeoxygenation of lignin-derived pyrolysis oil and related model compounds. Bioresour Technol 173:6–10

55. Lin YC, Li CL, Wan HP, Lee HT, Liu CF (2011) Catalytic hydrodeoxygenation of guaiacol on Rh-based and sulfided CoMo and NiMo catalysts. Energy Fuel 25:890–896

56. He Y, Bie Y, Lehtonen J, Liu R, Cai J (2019) Hydrodeoxygenation of guaiacol as a model compound of lignin-derived pyrolysis bio-oil over zirconia-supported Rh catalyst: process optimization and reaction kinetics. Fuel 239:1015–1027

57. Nan W, Krishna CR, Kim TJ, Wang LJ, Mahajan D (2014) Catalytic upgrading of switchgrass-derived pyrolysis oil using supported ruthenium and rhodium catalysts. Energ Fuel 28:4588–4595

58. Jie-wang Y, Gui-zhen F, Chun-de J (2012) Hydrogenation of alkali lignin catalyzed by Pd/C. Apcbee Procedia 3:53–59

59. Gao F, Webb JD, Sorek H, WemmerDE HJF (2016) Fragmentation of lignin samples with commercial Pd/C under ambient pressure of hydrogen. ACS Catal 6:7385–7392

60. Galkin MV, Sawadjoon S, Rohde V, DawangeM SJS (2014) Mild heterogeneous palladium-catalyzed cleavage of β-O-4′-ether linkages of lignin model compounds and native lignin in air. ChemCatChem 6:179–184

61. Galkin MV, Dahlstrand C, Samec JS (2015) Mild and robust redox-neutral Pd/C-catalyzed Lignol β-O-4′ bond cleavage through a low-energy-barrier pathway. ChemSusChem 8:2187–2192

62. Liguori L, Barth T (2011) Palladium-Nafion SAC-13 catalysed depolymerisation of lignin to phenols in formic acid and water. J Anal Appl Pyrol 92:477–484

63. Deng W, Zhang H, Wu X, Li R, Zhang Q, Wang Y (2015) Oxidative conversion of lignin and lignin model compounds catalyzed by CeO2-supported Pd nanoparticles. Green Chem 17:5009–5018

64. Qin Y, Wang H, Ruan H, Feng M, Yang B (2018) High catalytic efficiency of lignin depolymerization over low Pd-zeolite Y loading at mild temperature. Front Energy Res 6:2

65. Gillet S, Aguedo M, Petitjean L, Morais ARC, da Costa Lopes AM, Łukasik RM, Anastas PT (2017) Lignin transformations for high value applications: towards targeted modifications using green chemistry. Green Chem 19:4200–4233
66. Zhang JW, Cai Y, Lu GP, Cai C (2016) Facile and selective hydrogenolysis of β-O-4 link-ages in lignin catalyzed by Pd–Ni bimetallic nanoparticles supported on ZrO$_2$. Green Chem 18:6229–6235
67. Haibach MC, Lease N, Goldman AS (2014) Catalytic cleavage of ether C-O bonds by pincer iridium complexes. Angew Chem 53:10160–10163
68. Lancefield CS, Teunissen LW, WeckhuysenBM BPC (2018) Iridium-catalysed primary alcohol oxidation and hydrogen shuttling for the depolymerisation of lignin. Green Chem 20:3214–3221
69. Jongerius AL, BruijnincxPC WBM (2013) Liquid-phase reforming and hydrodeoxygenation as a two-step route to aromatics from lignin. Green Chem 15:3049–3056
70. Besse X, Schuurman Y, Guilhaume N (2017) Reactivity of lignin model compounds through hydrogen transfer catalysis in ethanol/water mixtures. Appl Catal B 209:265–272
71. Hu J, Zhang S, Xiao R, Jiang X, Wang Y, Sun Y, Lu P (2019) Catalytic transfer hydrogenolysis of lignin into monophenols over platinum-rhenium supported on titanium dioxide using iso-propanol as in situ hydrogen source. Bioresour Technol 279:228–233
72. Xu W, Miller SJ, Agrawal PK, Jones CW (2012) Depolymerization and hydrodeoxygenation of switchgrass lignin with formic acid. ChemSusChem 5:667–675
73. Ouyang X, Huang X, Zhu J, Boot MD, Hensen EJ (2019) Catalytic conversion of lignin in woody biomass into phenolic monomers in methanol/water mixtures without external hydro-gen. ACS Sustain Chem Eng 7:13764–13773
74. Shimanskaya E, Sulman M, Tiamina I, Sidorov A, MolchanovV SE (2019) Catalytic hydroge-nolysis of softwood sawdust. Chem Eng Trans 74:229–234
75. Shi D, Vohs JM (2019) J Phys Energy 1:015003
76. Bouxin FP, McVeigh A, Tran F, Westwood NJ, Jarvis MC, Jackson SD (2015) Catalytic depo-lymerisation of isolated lignins to fine chemicals using a Pt/alumina catalyst: part 1—impact of the lignin structure. Green Chem 17:1235–1242

Biochar as a Catalytic Material

Prachi Singh

Abstract Biochar has recently emerged as a class of biomass-derived functional materials with the potential applications in environmental sustainability. The high activity, porosity, flexibility and cost-effectiveness of biochar, makes it a promising alternative to other conventional catalysts. In this chapter, we present a comprehensive review of the catalytic properties and catalytic applications of the biochar. We begin by discussing the biomass conversion and the generation of the biochar catalyst. We then examine the properties, functionalities and discuss the underlying mechanisms of the biochar as a catalyst. This is followed by the discussion of possible applications in biomass hydrolysis, isomerization and dehydration, for energy production, i.e., biofuel production, syngas production and tar decomposition. Further, we discuss its role as an environmental catalyst in the abatement of the contaminants. At the end, we compare the biochar catalysis with the conventional heterogeneous catalysis.

Keywords Biomass · Biochar · Agro residue · Environmental catalysts · Biofuel · Carbonization

1 Introduction

The limited reserve and the environmental concern associated with the fossil fuels have attracted the attention of the humankind to turn to renewable alternatives (solar, wind, and biomass energy) for cleaner and safer energy and chemicals. Among all the types of renewable energies, biomass has been harnessed as a raw material to meet the demands on energy and fuels. Given its inherent rich and intrinsic carbon property, biomass is regarded as one of the most potential renewable resources to solve issues pertaining to energy security and environmental pollution.

P. Singh (✉)

Department of Environmental Sciences, Shaheed Rajguru College of Applied Sciences for Women, University of Delhi, New Delhi, Delhi, India

School of Environmental Sciences, Jawaharlal Nehru University, New Delhi, Delhi, India
e-mail: prachi.singh@rajguru.du.ac.in

Biomass conversion into chars is an ancient practice [1, 2]. These chars were an important additive to improve the soil fertility [3]. Pyrolysis is a technique by which biomass is converted in the absence of oxygen into a carbonaceous solid mass known as biochar [4, 5]. Biochar properties depend on (1) feedstock type (wood-grass, dry-wet, energy crop), (2) types of pyrolysis (fast pyrolysis, slow pyrolysis), and (3) pyrolysis conditions (temperature, residence time, heating rate, pressure) [5–9]. Fast pyrolysis or flash pyrolysis produces bio-oil as a primary product and biochar as a secondary product [5, 10]. Moreover, slow pyrolysis concentrates on "biochar" as a primary product [5, 10].

During pyrolysis, biomass undergoes several chemical transformations including carbonization, dehydrogenation, decomposition, polymerization, graphitization, evaporation, etc. This results in producing a carbonized material with altered chemical and physical properties that has more stable molecular structures, high cation exchange capacity, greater electrical conductivity, high porosity, and greater surface area [9–12]. Due to the invulnerability of biochar towards physio-chemical processes, it shows versatile applications in soil management [13], energy production, climate change mitigation, and pollution control technologies [14, 15].

The efficiency of the biochar has been further improved upon modifications like amination, magnetization, and carboxylation [16]. In recent years, biochar and their composites have found emerging applications in the energy and chemical industry, due to their cost-effectiveness and sustainability [17]. They have shown their applications as an eco-friendly material for latent heat storage [18], as a composite in supporting enzyme mobilization [19], as a sustainable material for supercapacitor-based energy storage [20], and in replacing metal-based photo-activators [21].

Biochar as a catalytic material or catalytic support has played an important role in creating pathways for biofuel and bioethanol production in the energy sector and in value-added chemicals and products for chemical industries [22]. Inherent physio-chemical properties of biochar like unique chemical structure, high surface area, inherent functional groups, and greater stability soar up its utility to act as a potential catalyst or as a tailored catalyst support [22–24]. Moreover, easy activation and functionalization like sulfonation and ionic grafting, gas activation, and metal impregnations of biochar enable tailoring of finest biochar-heterogeneous catalysts [22, 25]. These surface charges and radicals provide active sites for the interactions between biochar-based systems and reactants. Evaluating biochar obtained from the agro wastes used as a supporting matrix for the catalysts further enhances its worthiness with its economic viability [17].

This chapter focuses on the comprehensive overview and the systematic summary of designing of biochar and their catalytic performances. The chapter provides an in-depth understanding on the interrelations between the catalytic activity and the properties required for the synthesis of biochar catalysts. With the knowledge of catalytic properties, the chapter discusses the designing and applications of biochar catalysts based on the type of product and the path of production.

2 Synthesis of Biochar Catalysts

The biochar preparation methods for catalytic activity/degradation and other conventional applications like adsorption are not very different [26]. The process of biochar synthesis starts with the drying of feedstock or biomass. The biomass is pyrolyzed at high temperatures in the absence of oxygen. The heating causes various chemical transformations. The volatile components are formed that are released as permanent gases, condensed to produce complex organic compounds. Subsequent heating causes cracking and polymerization that changes the entire matrix of biomass [6]. These complex chemical reactions result in yielding three products: gases (permanent gases), liquid phase (tar and water), and solid residue (biochar) [10]. The reaction pathways for the production of these products parallel and partly compete with each other. The product of interest is largely influenced by the type of pyrolysis and the pyrolytic conditions. By converting the pathway, every feedstock can be converted into biochar. To maximize the yield of the desired product, certain pyrolytic conditions are followed [10]. In fast (flash) pyrolysis, biomass is rapidly heated to very high temperatures for a concise time interval. The heating rate is very high and the residence time is short. As a result, biomass cannot undergo cracking or polymerization to yield gases or solid residues, respectively. Moreover, volatiles and vapors produced by biomass flash heating get quickly condensed to obtain liquid phases. The goal of slow pyrolysis is to produce a solid residue with high carbon content. This biomass needs lower heating rates and longer residual time for the volatiles and water molecules to undergo polymerization and dehydration. This increases the fixed carbon content to yield solid residue known as biochar [7, 10, 27].

Hydrothermal carbonization is another thermochemical process for the synthesis of biochar. Here no pre-drying of feedstock is required. The biomass is heated in water at a lower temperature (180–260 °C) for 5 min to 6 h. The water here is in a subcritical state and acts as a non-polar solvent. As a result, organic compounds solubilize in water. Moreover, it also destroys polychlorinated dibenzofurans and polychlorinated biphenyls. This results in producing biochar with a high carbon yield (40–70 wt%). However, the biochar produced here is in a slurry phase and needs further dewatering steps [6, 10]. Figure 1 shows the scheme for the synthesis of biochar/biochar-based catalysts.

2.1 Fair Catalyst Without Treatment/Modification

The biochar exhibits inherent properties like active constituents, abundant functional groups, and high porosity and surface area that ables it to act as a good catalyst without any modification or treatment [22]. The alkali and alkaline earth metals present in the biochar provides active sites for the reactions. For instance, during tar reformation, biochar offered active sites for tar adsorption
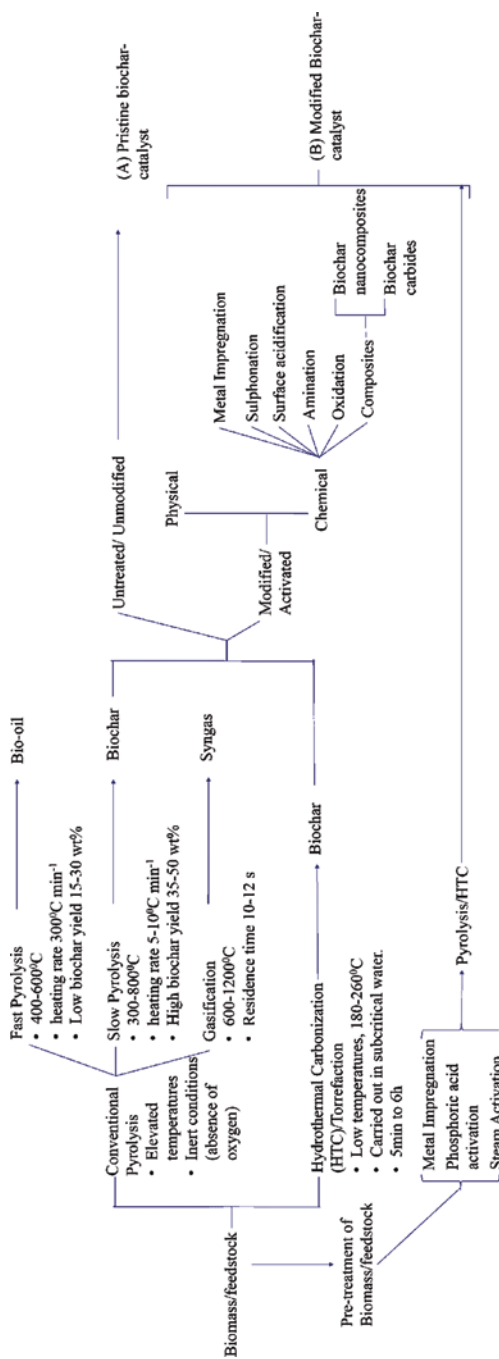
Fig. 1 Scheme showing synthesis of biochar and biochar-based catalysts

[28, 29]. Moreover, the porous surface of biochar allowed adsorption of several complex aromatic compounds released during tar reformation [30]. Yang et al. [31] prepared biochars at different temperatures and utilized them to degrade p-nitrophenol. The free radicals developed over biochar surfaces assisted in the catalytic degradation [31]. Similarly, Huang et al. [32] synthesized biochar at different temperatures using sludge. The sludge biochar was successfully used as a catalyst to decolorize rhodamine B, as the free radicals over its surface, enhanced electron shuttling capacity that assisted in decolorization. Shen et al. [33] synthesized biochar using corn stover and used it for anaerobic digestion. The alkali/alkaline earth metals on the surface of biochar increased the pH of the digester, which converted CO_2 into bicarbonates. Moreover, it increased the methanogenesis activity that resulted in greater methane production. In some cases, biochar showed a decline in catalytic activity with time due to the saturation of active sites or pores' blocking [28]. Thus, the use of unmodified/pristine biochar for complex processes, like transesterification, thermal cracking, and tar decomposition, needed further investigations.

2.2   Biochar catalysts after treatment/modification

The morphology of biochar without activation exhibits lower catalytic activity [34]. Many researchers are directed to modify the biochar to improve its properties like surface functionality, porosity, surface area, pore size, etc. The biochar can be further modified before, during, or after the pyrolysis process [35]. Several surface modification methods like chemical treatment (acid/alkali), steam activation, gasification (CO_2 or N_2), metal impregnation, etc. resulted in increased functionalization, redox properties, pore volume, and active sites over biochar surface [35, 36]. This also enhanced the property of the biochar to act as a solid catalyst support. Dehkhoda et al. [37] treated wood-based biochar with KOH followed by carbonization and sulfonation to increase its surface area and porosity. For tar decomposition, enhanced porous size of the acid-activated biochars promoted easy gasification of the coking agents and other tar by-products [38]. Similarly, acid activation of biochars by methods like sulfonation and fuming sulfuric acid created acid-active sites which promoted the catalytic activity for esterification/transesterification during bio-oil production [37].

2.2.1   Metal Impregnation

Presence of metal and minerals can enhance the sorption efficiency of the biochars [36, 39]. Several metal-impregnated biochars have been used for the adsorption of various heavy metals and contaminants [36]. Min et al. [40] used $FeCl_3$-impregnated biochar for the removal of nitrogen and phosphorus. Singh et al. [41] prepared magnetized rice husk (RHIOB) and wheat husk biochar (WHIOB) using $FeCl_3$ and

utilized it for the removal of arsenite and arsenates. FTIR and XPS studies revealed the deposition of metals in the form of magnetite (Fe_3O_4) nanoparticles. The studies revealed electrostatic attraction between positively charged ($FeOH^+$) biochar surface (pH < pHzpc) and negatively charged arsenic oxyanions which resulted in the adsorption of arsenic [41]. Bi or tri-metal impregnated biochars for example, Fe-/Mn-/La-impregnated biochar composites, have been used for the removal of arsenic [42].

2.2.2 Physical Activation

It involves the activation/modification of biochar or biomass using physical agents such as steam, carbon dioxide, nitrogen, etc. Steam activation subjects the biochar with partial gasification using steam (>700° C) [19]. This results in the crystallization of carbon due to the decomposition of the biochar carbon matrix [43]. In the process, water decomposes to oxygen and hydrogen, where the former binds to the surface carbon to form CO and the latter binds to the carbon to form CH_x matrix. Further oxidation leads to the formation of CO_2 and H_2 [43]. The devolatilization formed the pores in the carbon matrix that incresaed the internal surface area of the biochar. Rajapaksha et al. [16] reported enhanced sulfamethazine removal (55%) using steam-activated biochar as compared to non-activated biochar.

Activation using carbon dioxide and nitrogen also affects the catalytic property of the biochar. Buentello-Montoya et al. [30] selected carbon dioxide over steam as an activating agent. The former led to the formation of micropores and –O groups that led to high reactivity towards tar reformation. Steam-reformed biochars led to the formation of meso- and macropores in the biochar [43]. Such biochars were preferred for the processes where the coking blocks de-blocking could be easily done by gasification.

2.2.3 Chemical Activation

Chemical modification involves the treatment of biochar or biomass with acidic solutions or hydroxides. This alters the crucial physio-chemical properties of the biochar by introducing surface functional groups [36]. Treatment with acidic agents like sulfuric acid or fuming sulfuric acid resulted in the addition of oxygen-rich functional groups (−COOH, −OH), increased O/C ratio, and increased hydrophilicity by the mineral elements [19, 36]. Moreover, it also increased the surface area. Such acid-activated biochars also increase the catalytic activity of processes like esterification/transesterification [44] (mechanism is provided in the section "Esterification/Transesterification Process for Biodiesel Production"). Alkaline modification also provided a significant increase in the total pore volume, pore distribution, and non-polarity of the biochar. Moreover, they produced negative surface charges that adsorbed negatively charged species [35]. Dehkhoda et al. [45] reported the mechanism of KOH on the porosity of the biochar. In the first step, KOH gets

Fig. 2 Mechanism of KOH activation of biochar
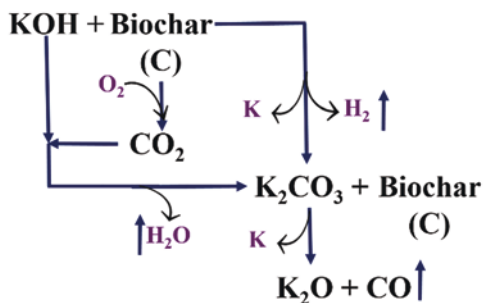
converted to K_2CO_3 and K_2O that caused the etching of the biochar. In the second step, gaseous products CO and H_2 that were generated during secondary reactions lead to macropores formation. In the third step, formation of H_2O and CO_2 during carbonization increased the porosity. Lastly, metallic K increased biochar lattice space by intercalating into the biochar matrix. Figure 2 shows the systematic fate of KOH treatment with biochar. Han et al. [46] synthesized KOH-activated peanut shell biochar for the adsorption of methylene blue from aqueous solution.

H_3PO_4 is another chemical activator that has effectively led to increased surface area and pore volume of the biochar. H_3PO_4 cleaves aryl ether bonds that aid in the hydrolysis of hemicellulose and cellulose [24]. Moreover, H_3PO_4 activation also helps in building cross-link polymer chains by forming ester linkages with –OH groups [47]. It increased the aromaticity of biochar catalyst with the breaking of P-O-P bonds due to cyclization and condensation reaction [47].

3 Properties and Underlying Mechanism of Biochar Catalysts

3.1 Properties of Biochar as Catalysts

For supporting the catalyst, the material must be highly stable [48]. Biochar acts as a solid support to the catalysts in terms of high surface area and porosity, acid density, stable chemical structures, oxygen-rich surface functional groups, reusability, and chemical inertness [49]. These physio-chemical properties enable higher resistivity of biochar catalysts towards the changes in pH of media and higher adaptability towards the changes in polarity and hydrophobicity, that enables its stability towards high temperatures, metal dispersion and higher speciation [17, 24]. These key features are conducive for the good performance of biochar catalysts [49, 50]. Out of these key features, porosity and surface area, functionality, biochar matrix, and inorganic minerals are essential components for enabling biochar to act as a catalyst or a catalyst support [24].

3.1.1 Porosity and Surface Area

Performance of the catalyst relies on the availability of the active sites and easy diffusion of the reactants and products formed [24]. First, porous nature and greater surface area of the biochar provides greater catalytic activity terms of easy accessibility [51]. Moreover, italso improves the interactions between catalytic sites and reactants and favors the adsorption of substrates. Second, it enhances the easy dispersion of active substances and metals commonly used to catalyze reactions for example during hydrogenation of the organic functional groups or in tar steam reformation [30, 51]. Third, selectivity of pore size plays a significant role in regulating the size-selective catalytic activity [30, 52]. Fourth, high porosity provides catalytic microenvironments such as methanogenic activity, chirality, hydrogen bond formation, etc. that assists in reactivity of the molecules [52]. For instance, Shen et al. [33] reported enhanced methanogenic activity and higher carbon dioxide loss due to greater surface area in biochar which resulted in the increased methane production [29].

In the studies conducted by Buentello-Montoya et al. [30], biochar with macro- and mesopores showed higher catalytic performance towards the tar conversion as compared to the biochar with micropores. They also indicated that porosity and surface area were the key factors that created differences in the catalytic activity of biochars towards tar reformation. In contrast, surface functional groups had negligible impact here [30]. As compared to the micropores, macro- and mesopores provided better gasification of the pores that were intitially blocked by the volatile condensates [17]. In another study, Xiong et al. [17] reported higher transesterification activity for sulfonated biochar catalysts as compared to the activated carbon. This was due to larger pore radius and pore value. Greater access to the substrate-active sites facilitated the transesterification process for the production of biodiesel [17].

3.1.2 Surface Functional Groups, Biochar Matrix, and Inorganic Minerals

Biochar possesses abundant surface functional groups. During pyrolysis these functional groups undergo various physico-chemical processes like decomposition, aromatization, decarboxylation, dehydration, polymerization, and intermolecular condensations [6]. The Decomposition and dehydration of the lignocellulosic component of biomass results in generating various oxygen-containing functional groups ($-COO$, $-OH$, $-CO$, $-NO_2$), some N- and S-based functional groups, free radicals, and heteroatoms depending on the pyrolysis conditions and the type of feedstock [6, 15]. These functional groups present over the biochar surface help in the functionalization of biochar and enhance its catalytic activity [17, 24]. First, the functional groups facilitated the loading of metals/metal precursors with catalytic activity. Pierri et al. [49] facilitated anchoring of Mn^{II}-based catalysts over carboxylate functional groups of biochar for epoxidation of olefins. Lyu et al. [26]

investigated the role of Fe(II) and Cu(II) metal-based biochar catalysts for facilitating the production of persistent free radicals. Second, the functional groups facilitated certain catalytic reactions through acting as solid acid catalysts, transesterification process, and redox reactions. Cao et al. [23] prepared solid acid catalysts by the sulfonation of biochar for polysaccharide hydrolysis and biodiesel production. Third, functional groups facilitate the adsorption of compounds formed during the catalytic process. Lamichhane et al. [53] used biochar-based catalyst to adsorb polyaromatic hydrocarbons while producing liquid oil from plastic wastes.

Biochar is amorphous in nature and develops crystalline structures under varied pyrolysis conditions. Keiluweit et al. [54] suggested four types of biochar matrix depending upon pyrolysis condition. The graphene or conjugated aromatic sheets in turbostratic biochars develop chemical heterogeneity [15]. This creates a difference in the electronegativity of the heteroatoms (N, P, S) relative to the carbon atoms of the aromatic or graphene structures [15, 24]. Moreover, defects are formed between graphene sheets and amorphous carbon [55]. The chemical heterogeneity and defects played an important role in catalytic activity [56]. The composition affected the type of carbon units (e.g., sp^3 or sp^2) which in turn affected the bounding in the carbon matrix. Pierre et al. [49] reported higher catalytic activity for the catalysts with sp^3 carbon as comapred to sp^2 carbon in the biochar matrix.

Presence of Inorganic species like Na, K, Mg, Ca, Cl, N, P, and S in the biomass altered the functionality of the biochars [6]. Waqas et al. [57] showed that the oxides of Al and Si minerals in the biochar facilitated the degradation of plastic polymers by breaking complex bonds through binding and cracking. Detailed mechanisms of the processes are explained in Sect. 3.3.

3.2   Factors Affecting Properties of the Biochar Catalysts

3.2.1   Type of Biomass Feedstock

Biomass is made up of cellulose, hemicellulose, lignin, and various mineral components. Due to the differences in the structural and behavioral properties of these components towards pyrolysis conditions, the biomass selection affects the properties of the biochar [54]. Hence, it becomes inevitable to understand the fate of each component that affects the functionality of biochar and hence assists in the synthesis of biochar-based catalysts.

Depending on the moisture content, source, and lignin content, biomass can be dry or wet, energy or waste biomass, and wood or grassbased feedstock [6, 10]. Biomasses with higher lignin content have higher char yield and lower volatile matter and possess greater stability as compared to the biomass with higher cellulosic content [54]. Hence, composition of biochar depends largely on the composition of the biomass. Figure 3 illustrates the fate and mechanism of pyrolysis of cellulose, hemicellulose, and lignin present in biomass. Composition of biochar determines the catalytic activity. For instance, biochar with high carbon and high ash content is
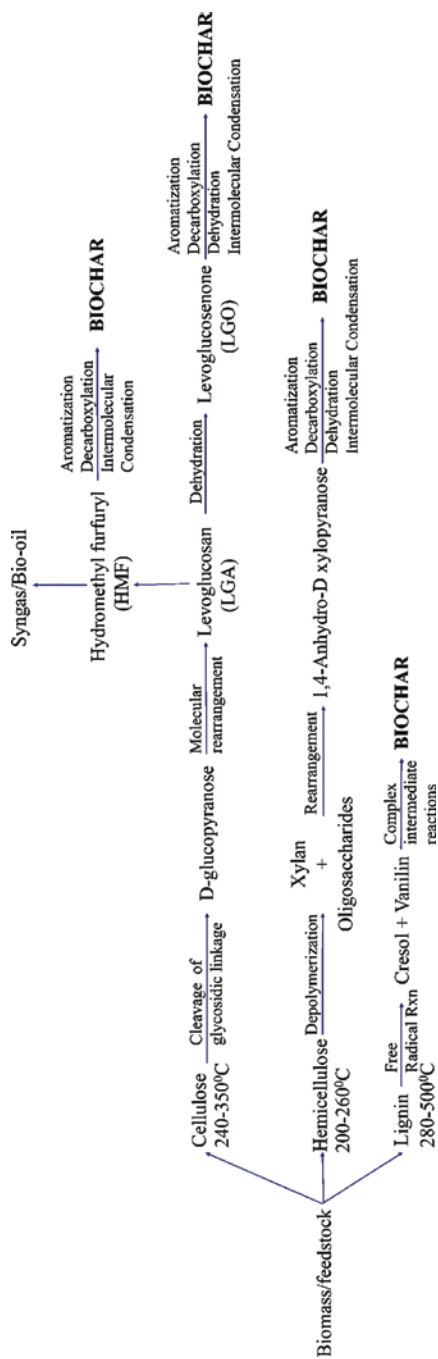
Fig. 3 Scheme showing conversion of different components of biomass during pyrolysis of biochar

less suitable for tar decomposition as it causes deactivation of the process by blocking the pores due to coking [30].

3.2.2 Pyrolysis/Gasification Conditions

The catalytic performance of the biochar depends largely upon the pyrolysis conditions like reaction rate, residence time, type of gas, and temperature. Different types of pyrolysis types have been discussed in detail in Sect. 2. High pyrolysis temperature, faster heating rate, and long residence time affects the surface area, biochar matrix, carbon percentage, and heating value of the biochar. Heating rate ensures secondary pyrolysis conditions that results in cracking. Thus, there is increase in char yield as compared to the lower heating rate [6]. Moreover, at higher heating rates (>10 °C/min) due to rapid volatilization, the porosity increases. A Slower heating rate formsbiochar with a more stable matrix. In slow pyrolysis, greater residence time allows repolymerization of char that increases the char yield [43].

Depending upon the pyrolysis conditions, studies from XRD and spectroscopic analysis, Keiluweit et al. [54] suggested following four distinct categories of biochars: *transition chars*, with the intact crystalline character of the minerals in chars; *amorphous chars*, with aromatic polycondensates and heat-altered molecules; *composite chars*, the amorphous form containing embedded graphene stacks; and *turbostratic chars*, i.e. biochars with graphitic crystallites. The Pyrolysis process causes the formation of unpaired electrons/radicals that induces complex reactions at the biochar's surface [1]. Formation of the defects also takes place between graphene sheets and amorphous carbon and in between various other carbon structures and biochar minerals [55].

3.2.3 Pyrolysis Temperature

Biochars obtained by biomass pyrolysis at very high temperatures have significantly low H/C and O/C ratios [58]. Table 1 shows the properties of biochars as a function of the temperature. Catalysts with such biochar support produce fuels with lower H/C and O/C values that are highly favorable [54]. Such fuels produce less smoke, less water vapors, and more energy [57]. Moreover, such biochar catalysts were unfavorable for the transesterification process due to the reduction in heteroatoms and the acid density [59]. Uchimiya et al. [9] studied in detail the impact of pyrolysis temperature on the properties of biochar. High-temperature biochars with low O/C ratio are expected to be π donors, while those obtained at lower temperatures with high O/C ratio are π acceptors. Thermogravimetric (TGM) studies of chars at low temperatures showed release of CO_2 and H_2O as compared to high-temperature chars that released CO, CH_4, and H_2 [9, 58] (Table 1).

Table 1 The properties of biochars as a function of temperature

Low-temperature biochars (<400 °C)	Low- to medium-temperature biochars (400–500 °C)	High-temperature biochars (>500 °C)
Higher oxygen contains functional groups carboxylic acids, ketones, aldehydes, hydroxyl, quinones, lactone, cyclic peroxides, furanone, etc.	A Higher concentration of organic compounds and acid and basic functional groups. Dominated by low molecular weight acids and neutrals	A Higher concentration of dense organic molecules. Benzene, toluene, ethyl benzene, xylene, and possibly polycyclic aromatic hydrocarbons
Higher water- and organic-soluble compounds	–	Higher absorptivity of heavy metals by some biochars
Lower cation exchange capacity (CEC) and lower water-holding capacity	Higher CEC and higher water-holding capacity	Lower CEC. Decrease in abundance of oxygenated functional groups
Higher surface negative charges	–	–
Low pH (usually <7.5)	–	High pH (usually >8.5)
–	–	Higher surface area and pore volume
Higher O/C ratios	Moderate O/C and H/C ratio depending upon the feedstock	Low H/C ratios. High stability

3.3 Mechanism of Catalytic Functioning of Biochar

Before proceeding on the mechanism of the catalytic functioning of biochar, it is important to understand the phenomena of heterogeneous catalysis. Heterogeneous catalysis follows the mass transfer phenomena. The process is divided into seven steps. (1) diffusion of the reactant from bulk phase to the external surface of the catalyst; (2) diffusion of the reactant from the external surface to the internal surface of the catalyst via catalyst pores; (3) adsorption of reactants on the catalyst surface; (4) reactions on the active sites of the catalyst surface; (5) generation of the product and its diffusion from catalyst surface to the internal surface of the catalyst; (6) diffusion of the products from the internal surface to the external surface of the catalyst via catalytic pores; and (7) diffusion of the products from the external surface of the catalyst to the bulk phase [34, 51]. Adsorption of the reactants (step 3) and desorption of the products (step 5) are the two most necessary and sufficient steps in governing the activity of catalyst [51]. Thus, a catalyst that provides sites to facilitate easy adsorption-desorption is chemically suited for its role. Adsorption can be chemi- or physio-sorption depending upon the type of interaction.

The decomposition of the organic components of biomass during pyrolysis creates several active sites that facilitate the sorption-desorption of the reactants and product molecules over biochar [60]. This explains the potential role of biochar in catalysis. The surface of the biochar contains oxygen-rich functional groups like –OH, –COOH, and –C=O. FTIR and XRD studies also reveals that when the biochars are impregnated with the metals they are likely to develop the deposits of oxides of their corresponding metals. For example, Fe-treated biochar that were

reported by Singh et al. [41] developed into iron nanoparticles in the form of Fe_3O_4. In the basic solutions (pH > pHzpc), oxygen-rich functional sites gets deprotonated and become negatively charged. On the contrary, when the solution is acidic with lots of H^+ ions, the oxygen-rich functional groups get protonated to generate a positively charged surface. The charge development over the surface of biochar creates, (1) electrostatic attraction between the adsorbing ions and the charged functional groups; (2) the charged functional group facilitates redox reactions by acting as electron acceptor/donor depending upon the conditions. For example, at pH < pHzpc, Fe_3O_4 sites were protonated to $FeOH^+$ active sites that facilitated the adsorption of negatively charged arsenites through electrostatic attraction [41]. In another instance, sulfonated functional groups on the biochar promoted transesterification by serving as proton donors [44]. Hydrogen bonding also explains the mechanism of sorption of various anionic species like phosphate, organic oxyanions, and perchlorates [60]. Surface complexation is another mechanism that explains the function of biochar. For example, Halder et al. [61] explained the adsorption of fluoride over MgFe-impregnated biochar by K_2MgF_4 and $KFeF_3$ surface complex formation. π-π interaction explains the adsorption of contaminants with aromatic structures. High-temperature pyrolysis biochar has an aromatic graphene-like structure that acts as π-electron donors. For example, Yang et al. [62] explained the removal of Congo red dye using biochar through electron donor-acceptor interaction. Figure 4 illustrates possible mechanisms of biochar-facilitated adsorption.
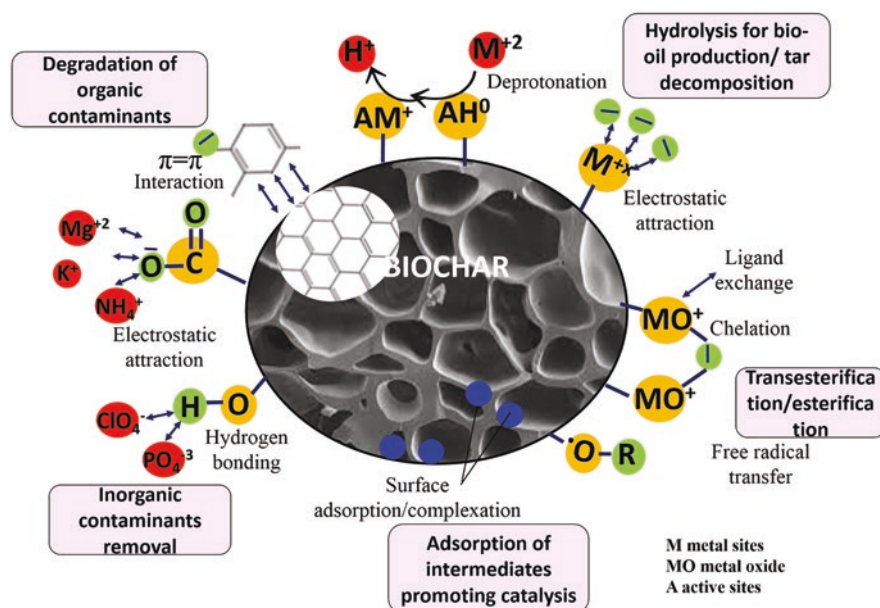
Fig. 4 Illustration of the possible mechanisms over biochar for its catalytic role

4 Applications of the Biochar-Based Catalysts

Biomass is regarded as best renewable resource that has huge potential for producing high-valued platform compounds, like furfural, HMF, furans, phenols, acetic acid, formaldehyde, L-glucosenone, etc., during energy fuel production like bio-oil, biodiesel, and syngas. It has surpassed its role by covering the industrial sector, biorefineries, energy sector, and environmental sector. Lignocellulosic masses are made up of carbohydrates (cellulose and hemicellulose) and aromatic (lignin) polymers that interact via intra- and intermolecular hydrogen bonds. It involves the breakdown and transformation of these compounds through hydrolysis, isomerization, dehydration, and rehydration [17]. Biochar catalysts have played an important role in catalyzing these reactions. In the following section, applications of biochar/biochar supported catalysts have been discussed. Moreover, the mechanism and the catalytic activity of the biochar catalysts will be discussed in detail.

4.1 Biochar Catalysts for the Energy Production

Bioenergy, that is the energy obtained from biomass, is one of the potential alternatives to drive the dependency of the world away from the non-renewable resources. It aims at resolving the problems associated with the environmental pollution and the limited reserves of fossil fuels [63]. Bioenergy is more adaptable, environment-friendly, cost-effective and energy-efficient [63, 64]. However, traditional biomass combustion practices were abandoned due to low energy efficiency and greater air pollution. Thus, researchers worked intensively on the use of biochar as catalysts in biorefineries and energy production.

Biomass conversion technologies includes three main processes: the biochemical process, the thermochemical process, and the physio-chemical process [63]. There are several pathways by which biomass can be converted into bioenergy, (1) by the esterification/transesterification of the biomass to yield biodiesel, (2) by the hydrolysis and fermentation of the biomass to produce bioethanol, (3) by the gasification of the biomass to produce syngas, and (4) by anaerobic digestion of the biomass to obtain biogas [24]. Further, bio-oil can be upgraded by hydrodeoxygenation and hydrodenitrogenation [24].

Biochars have been extensively studied for their higher potentialties as catalysts or catalyst supports in the biomass conversion to biofuels in biorefineries [24, 34, 57]. High surface area, porosity, and the surface functional groups assisted its catalytic activity for the same. Modification techniques like chemical treatment, physical treatment, and composite formation further increased the surface area and functionalization in biochar that was necessary for bioenergy generation. Its catalytic activity also contributes in tar cracking [29]. Moreover, during biomass conversion, biochar is produced as a common by-product that makes the process more integrated and sustainable in terms of reduction in cost and dependency over the

metal-based catalysts [24]. In the following sections, the role of biochar catalysts has been highlighted in bioenergy productions through different pathways.

4.1.1 Biofuel Production

Catalysts play an important role in initiating the reaction and solubilizing the alcohols for biofuel production [65]. Biochars are widely investigated for their catalytic activity in biodiesel/bioethanol production via esterification/transesterification, hydrolysis, and catalytic upgrading [24]. As compared to the conventional homogeneous acid-base catalysts, they are more renewable, environment-friendly, and sustainable [64]. Moreover, physio-chemical properties of the biochar can be tailored using various modification techniques. In the following subsections, the role of biochar catalysts has been highlighted in the production of biodiesel and bioethanol.

Esterification/Transesterification Process for the Biodiesel Production

Biodiesel is a mono-alkyl fatty acid ester that is obtained from the thermochemical reaction between triglycerides, free fatty acids (FFAs), alcohol, and other contaminants. These reactants are obtained from vegetable oils, animal fats, and greases as primary raw materials. Catalysts enhance the solubility of alcohol and increase the rate of reaction by lowering down the activation energy [65]. The strong mineral base catalysts enhance the transesterification processes, while mineral acid catalysts are used in the esterification processes [65]. The Esterification process becomes significant when the biomass contains higher FFAs. However, high FFAs containing biomass hinders the transesterification process [37].

Lee et al. [64] synthesized maize residue biochar to study the catalytic effect of transesterification process over mixture of waste cooking oil and methanol. As compared to the conventional silica catalysts where the maximum yield of fatty acid methyl ester (FAME) was obtained at 400 °C, higher amount of yield (~90%) was obtained using maize residue biochar at 300 °C. The higher porosity of the biochars increased the number of collisions between triglycerides (liquid phase) and methanol (gaseous phase) in their pores.

The Aacid catalysts are well known for offering lower production costs and easy operational methodology as they have the potential to catalyze the esterification and transesterification process simultaneously [14, 24, 37]. Sulfonation of the biochar using concentrated sulfuric acid and fuming sulfuric acid thus enhances the catalytic activity for esterification and transesterification process. These solid biochar acid catalysts offered high oxygen content in the form of phenolic and carboxylic acidic group which in turn increased the acidity of the biochar and facilitated the adsorption of the reactant molecules on the surface [44].

The catalytic effect of the solid biochar acid catalysts on the biodiesel production using hardwood biochar was studied by Dehkhoda et al. [37] by using two different sulfonation processes : (a) Cat A- wet impregnation in the liquid

concentrated H_2SO_4 (98%) and (b) Cat B- chemical treatment using KOH followed by the treatment with fuming H_2SO_4 (20% free SO_3) at 150 °C. The Conversion of FFAs increased on increasing the amount of Cat A (obtained using method a) in the reaction mixture due to the increase in the active sites that facilitated the esterification. The protons released from the acid-active sites over biochar attacked the carboxyl group on FFAs accounting for greater biodiesel production. Moreover, it was found that the esterification process was not affected when the FFA content was increased and it reported higher conversion into biodiesel (92%). However, Cat A showed less efficiency and catalytic activity towards transesterification. This was due to low acid density and lower surface area and porosity. Sulfonation by method A resulted in the functionalization of biochars with –OH, –COOH, and few –SO_3H groups. These functional groups were weaker enough to catalyze transesterification. On the contrary, Cat B (obtained using method b) had acid-active sites rich in –SO_3H, they had higher surface area, and high porosity. This gave biochar Cat B the strength to catalyze the transesterification of the canola oil. Cat B reported 100 times higher acid density as compared to Cat A. Moreover, high surface area and porosity of both the biochars facilitated good intra-particle diffusion of the reactants [37].

In another study, Dehkhoda et al. [44] chemically treated wood-based biochar using KOH followed by carbonization at 750 °C. The activated biochar was sulfonated using fuming sulfuric acid to obtain the solid acid catalyst. There was significant increase in the catalytic activity for the transesterification process. The yield of biodiesel increased from 28% to 48%.

Yu et al. [59] and Waqas et al. [57] conducted the studies to find the effect of temperature and matrix on the catalytic activity of biochar catalysts on transesterification process to produce bio-oils. Biochars produced at higher temperatures reported low H/C and O/C ratios. Due to the evaporation of heteroatoms from the aromatic rings, there was decline in the acid density that lowered the transesterification process. Moreover, carbon sheets produced at high temperatures were rigid and reported poor sulfonation. Biochar produced at 675 °C reported greater yield as compared to the biochar produced at 875 °C. Thus, by controlling the temperatures, biochar catalysts produced at lower temperatures were used to increase the yield of biodiesel from canola oil [59].

Hydrolysis of Biomass and Fermentation of Sugars for Bioethanol Production

Hydrolysis of lignocellulosic biomass into sugars and its subsequent conversion into useful compounds are highly desirable. Bioethanol is most commonly used as an extender of petrol in "flexible-fuel vehicles" (FFVs) [63]. Sugar-rich biomasses like sugarcane, maize, sugar beet, and wheat undergo fermentation with microbial assistance to produce bioethanol.

Significant research efforts are undertaken to enable the fermentation of the lignocellulosic feedstocks by pre-treatment and/or identification of appropriate catalysts [63]. However, during the production of bioethanol, the fermentation process

is often inhibited, that resulted in decreasing the productivity. Biochar catalysts can assist biological fermenters like yeast in bringing the stability to the fermentation process and in enhancing the production of bioethanol. First, they improve the cell activity and growth, facilitate interspecies electron transfer, induce buffering capacity, and allow nutrient adsorption over its surface [66]. Second, high surface charge density, high internal porosity, and presence of polar and non-polar surfaces promote immobilization of microbes that assist in fermentation [66, 67]. For instance, Kyriakou et al. [67] reported increase in ethanol production from citrus peel hydrolysates (composed of glucose, sucrose, fructose, galactose, etc.) by immobilizing S. cerevisiae and *K. marxianus* promoters in fermentation. Biocatalysts were prepared through immobilization of S. cerevisiae and *K. marxianus* over biochars obtained from the seagrass residues (SGR) and vineyard pruning (VP). SEM studies showed densely and homogeneously adhered yeast over biochar surface by (1) physical adsorption, (2) electrostatic attraction, (3) natural entrapment into pores, or (4) covalent bindings between the membrane and the support. The bioethanol production increased from 51 to 72 g/L in the presence of biochar support. The studies showed that addition of biochar led to the increase in the biological activity and in the formation of the biofilm as a significant electron acceptor and donor. This substantially increased the enzymatic activity for alcohol fermentation and ethanol yield from 0.62 mol ethanol/mol xylose to 1.35 mol ethanol/mol xylose [67].

4.1.2 Biogas Production Using Biochar/Biochar Supported Catalysts

Gasification of Biomass for the Syngas Production

Syngas or synthesis gas is produced by gasification, reformation, and/or partial oxidation of the biomass. It is mainly composed of carbon oxides (CO and CO_2) and hydrogen (H_2). Syngas has numerous applications such as in the manufacture of wide range of chemicals through Fischer-Tropsch synthesis and Haber's process, in methanation, in downstream processes, and as fuels [68, 69]. However, presence of other components in syngas other than CO/CO_2 and H_2 decreases its efficiency, propensity and the energy density [68]. For instance, presence of N_2 in the syngas lead to the formation of NO_x [70]. Higher CH_4 in the syngas deteriorated its quality due to coking by the formation of C-C bond. It resulted in formation the blockage of the active sites and in the poisoning of the catalysts [71]. Moreover, for better syngas production, increased steam utilization through integrated gasification system increased the overall cost of the process.

Researchers investigated the use of biochar/biochar-supported catalysts in biomass gasification for enhancing the production efficiency and the quality of syngas. They found significant improvement in the performance of the process as well as in the quality of the syngas [68]. Biochar provided higher surface area, porosity, and modified electronic states that determined the selectivity of the product in enhancing the syngas production [72]. Ni-impregnated biochar catalysts, synthesized via wet impregnation methods, have been widely used to enhance the conversion of

natural gas into syngas. Lee et al. [73] synthesized biochar-supported Ni catalyst (MBC-Ni) and studied the effect of the gasification of microalgal biomass on the syngas production. The Studies were conducted to compare the activity and performance of MBC-Ni with the non-catalytic and pristine biochar's (MBC) catalytic activity in the syngas production. It was found that the syngas production was enhanced in the order non-catalytic < MBC < MBC-Ni. In addition, concentrations of H_2, CH_4, and CO were also enhanced using MBC and MBC-Ni. Thus, both biochar supported and Ni metal in the biochar synergistically enhanced the syngas production. Pyrolysis condition(s) also affected the catalytic activity of biochar catalysts in the syngas production. Biochar catalysts that were obtained in CO_2 atmosphere resulted in higher syngas production with elevated H_2-to-CO ratios as compared to those obtained in inert N_2 atmosphere. This was attributed to the effectiveness of CO_2 as an oxidant in CO production, thereby shifting the reaction towards higher H_2 synthesis [73].

Zhu et al. [72] synthesized biochar-supported Ru catalyst for studying the mechanism and enhancing the syngas production. The catalytic performances of prepared catalysts with (Ru/ABC) and without activation (Ru/BC) over different temperatures were studied for the syngas production. Due to activation, high surface area of Ru/ABC higher CO conversion was obtained as compared to Ru/BC that had comparatively lesser surface area. The enhanced surface area of the biochar catalysts promoted, first, better dispersal of Ru crystallites. Second, it favored greater particle size formation of Ru crystallites. Third, it gave the appropriate electronic state to the catalysts that favored the selectivity of CO and H_2 formation in the syngas production.

Yip et al. [74] studied the catalytic effect of alkali/alkaline earth metals in wood biochar on biomass gasification for enhanced syngas production. Alkali/alkaline earth metals catalyzed biomass gasification with little CH_4 and CO/CO_2:H_2 production. This enhanced the quality of syngas with less methane and high percentage of hydrogen. Wan-cho et al. [75] had similar observations using biochar obtained from the paper mill sludge. Higher mineral content of the biochar enhanced thermal cracking of biomass to produce higher CO and H_2 in the presence of CO_2. Hydrogenation of syngas further promotes its upgrading, cleaning, and production of several useful compounds. The details are discussed in Sect. 4.2.

Reformation and Decomposition of Tar(s)

During the thermochemical gasification of biomass for the production of syngas, a complex mixture of condensable and non-condensable hydrocarbons is also produced. Tar is a mixture of these compounds containing single- to five-membered aromatic rings and polycyclic and oxygen-containing hydrocarbons [29, 30, 76]. This includes toluene, naphthalene, styrene, phenols, and other polycyclic aromatic hydrocarbons (PAHs) [34]. Based on the experimental studies, tars can be primary (acetol, acetic acid, guaiacols), secondary (phenols, cresols, toluene), or tertiary (naphthalene) tars [38]. However, tars can cause the mechanical breakdown of the

entire system by condensing down the pipes, heat exchangers, and equipment that may result in blocking downstream processes [34]. Moreover, it also deactivates the catalytic activity [29, 30, 38, 76]. For the commercial production of syngas in power generation and synthetic fuel production, it becomes important to reduce the levels of tars. Due to fast reaction rate, stability, and reliability, catalytic reforming is considered as a promising technique for large-scale tar reformation or decomposition. Several studies report use of noble metal catalysts like Pt, Pd, and Rh for the tar decomposition. Moreover, tar cracking is conducted using base metals such as Ni, dolomite, and olivines. However, deactivation of the catalytic activity due to coking and recovery of catalysts remains a challenge for their application.

Biochar/biochar-based catalysts have shown high conversion rates and high removal efficiency for tar. Moreover, biochar is naturally produced inside the gasifier. High surface area of biochar enhances the reforming activity of the biochar catalysts for tar, whereas the reforming mechanism of the tars is followed by the active sites inside the pores [29, 30]. The mechanism of tar reformation over biochar occurs as deposition, dehydrogenation, and soot gasification [29]. As the tar encounters the fresh batch of char, they get adsorbed over the active sites and undergo polymerization reaction to produce soot and hydrogen. This is followed by the deposition of soot over the char surfaces in the form of solid deposits. As the active sites over chars are blocked and coke deposition stops, it hinders the interaction of active sites with tar, thereby promoting homogenous reformation of tars. The homogenous reforming decomposes hydrocarbons to produce more stable compounds like benzene rather than tar [30]. The alkali/alkaline earth metals on the chars also affect soot gasification through tar-char interactions that influences its catalytic activity [77]. In addition, by steam or CO_2 gasification, catalytic activity of the biochar catalysts can be reformed to CO and H_2. The role of pore size in retaining the catalytic activity is discussed in Sect. 3.1.1.

Shen et al. [38] synthesized rice husk biochar-based Ni-Fe catalyst (RH Ni-Fe) for the reformation of tar. RH Ni-Fe catalyst played a significant role by producing seven-time less tars during syngas production. First, they reduced the intermediate metal oxides and CO_2 to their metallic states. Second, the biochar Ni-Fe catalyst provided active support for the adsorption of tar and, hence, prevented deactivation of catalytic activity and accelerated its reformation. Third, the water molecules retained in the pores of biochar allowed dissolution of certain aromatic hydrocarbons. Besides this, the catalyst also checked the reduction of Ni-Fe from $Ni^{+2}/Fe^{+2/+3}$ to their metallic Ni^0/Fe^0 states that was necessary for the catalytic activity. The biochar-based Ni-Fe catalyst reported ~92.0% efficiency for the tar removal as compared to Ni-Fe catalyst. Moreover, syngas yield increased by 2.11 L/g in comparison to Ni-Fe catalyst.

Liu et al. [76] deduced the mechanism and highlighted the importance of O-functionality over steam-reformed biochar catalysts in tar destruction. The catalytic activity and tar destruction were significantly higher for greater O-containing active sites. O-containing functional groups on biochar served as intermediates that accelerated tar destruction. Furthermore, coking decomposed the tar molecules once they were bonded over the active sites through O-containing functional groups.
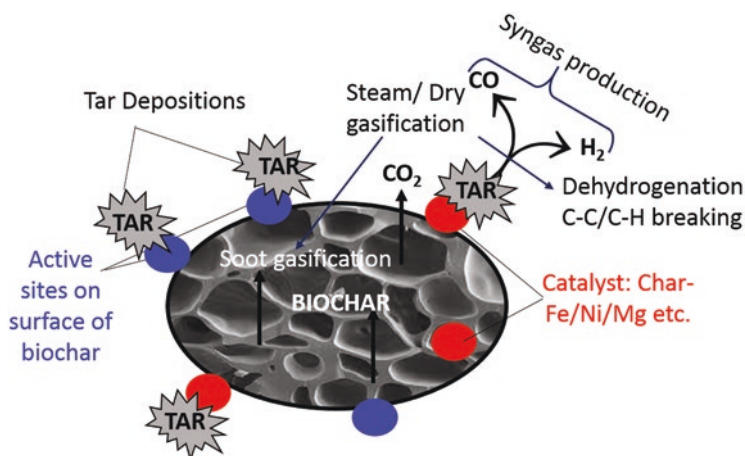
Fig. 5 Application of biochar showing pathways and mechanisms for syngas production and tar degradation

Tar molecules interacted with O-functional groups via H radical that resulted in their breakdown and the consumption of O groups. Figure 5 shows the role of biochar catalysts in tar decomposition/reformation and syngas production.

Anaerobic Digestion of Biomass for Biogas Production

Anaerobic digestion/decomposition (AD) is a two-way sustainable method for stabilization and conversion of wastes into renewable energy sources [78]. First, it manages and disposes municipal/sludge wastes. Second, it produces biogas that reduces the dependency of the energy sector on fossil fuels [79]. By managing the conditions of the digester, biogas's composition and quality can be upscaled for commercial purposes [79]. Catalysts have played a significant role in AD either by reducing activation energy of the reactions, by acting as adsorbents to the inhibitors, or by triggering electron transfer in syntropic microorganisms [80]. For instance, Yang et al. [81] added GAC-MnO_2 nanocomposite-based catalysts in anaerobic digester to enrich biogas with high percentage methane. Das and Mondal [82] used tungsten for maximizing biogas yield.

Adding biochars into AD systems has played a significant role in catalyzing the process in terms of stability and upscaling of the biofuels [80, 83]. Porous structure, high surface area, and alkaline surface functional groups increased methanogenesis, remove CO_2, and enhance CH_4 production [29]. First, during the AD process, a complex series of redox reactions takes place between microbial consortiums. This happens by the H2/formate electron transfer system. Biochar predominates this system by direct interspecies electron transfer (DIET) between syntropic microbes that enhances methanogenesis activity [29, 80], thus causing enrichment of biogas with a high methane percentage. Second, it promotes hydrolysis, acido−/acetogenesis by

the immobilization of microbes, and increment of cell concentrate [80]. Duan et al. [84] reported 1.4 times higher hydrolysis rate with biochars as compared to AD digesters without biochars. Third, biochars act as buffers for the acidic stress generated in sludge due to acidic products released by acid-oxidizing microbes. Biochars produced at elevated temperatures cause leaching of alkali and alkaline earth metals from their surfaces and result in increasing the pH of the sludge. This also contributes in CO_2 conversion to carbonates that assists hydrogentropic methanogens to produce more methane via reduction. Thus, biochar improves sludge digestion by elevating pH, alleviating NH_3 and H_2S in biogas, reducing CO_2, and increasing electrical conductivity of the digester [85]. For instance, Shen et al. [85] reported as high as 96.7% methane production as compared to the one without biochar (67.9% methane content). The CO_2 content of the AD digester also went low by 86.3% against the digester without biochar. Moreover, the reaction rate of the digester went up by 27.6% in the presence of the biochar. FTIR and XRD studies revealed high alkali/alkaline metal functional groups over the surface of corn stover biochars. Fourth, biochar acts as a favorable adsorbent for the by-products and intermediates. For instance, Shen et al. [86] observed that corn stover biochar significantly reduced total ammonia nitrogen (TAN) by 6.2–13.2% as compared to the AD digesters without biochar. Figure 6 shows the role of the biochar catalyst in the AD process. Thus, catalytic ability of biochar in AD attributes by providing archaeal growth for methanization, by enhancing DIET for the microbial activity, by selective colonization of the microbes, by alleviating inhibitors, and by maintaining the buffer capacity [87].
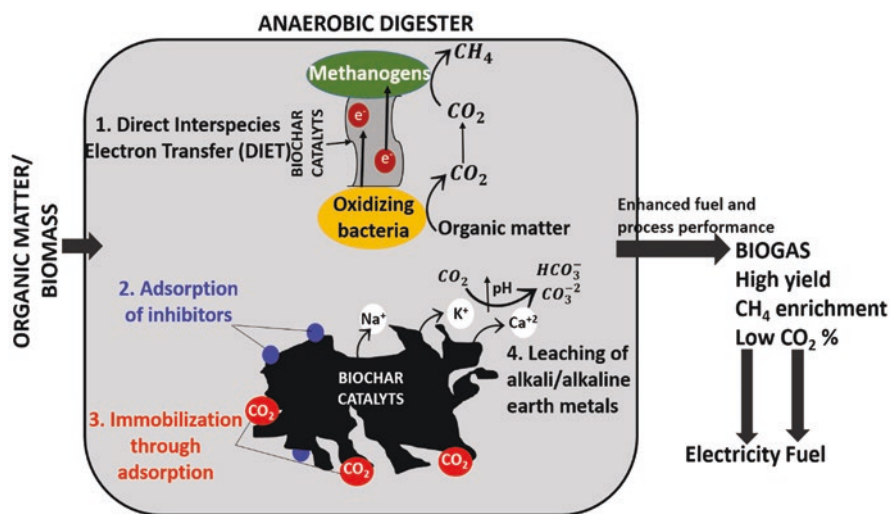
Fig. 6 Pathways and mechanisms showing anaerobic decomposition of biomass for bio-oil production

4.2   Biochar Catalysts for the Chemical Production by Biomass Conversion

Biochar offers a promising role as a catalytic material in the synthesis of value-added platform chemicals by biomass conversion [88].

4.2.1   Hydrogenation

Hydrogenation is a chemical process that involves addition of hydrogen on unsaturated bonds of fatty compounds to their saturated analogs [89]. This results in an increase in stability of the compounds which otherwise are susceptible to photo-oxidation or auto-oxidation [90].

Fischer-Tropsch process is a gas to liquid polymerization technique that converts syngas to various hydrocarbon fuels and chemical products via hydrogenation [17, 69]. Biochar-based Fe, Ru, Ni, and Co catalysts have supported Fischer-Tropsch synthesis by converting 95% CO to useful hydrocarbon compounds [69]. Comb-like structural arrangements, high surface area, and high porosity of biochars intensified mass transfer between syngas and liquid products [69]. Yan et al. [91] synthesized biochar-supported Fe catalysts and tested it for Fischer-Tropsch synthesis of hydrocarbons from syngas. It showed ~68% selectivity towards liquid hydrocarbons, converting ~95% of CO at 310 °C.

Methanol is widely used in the production of formaldehyde, methyl acrylate, and terephthalate [69]. Biochar-based Zn and Cu oxides have been widely used in producing methanol. Catalytic conversion of syngas by partial hydrogenation of CO and CO_2 using H_2 leads to methanol production.

Cyclohexanol and cyclohexane are used as chemical intermediates, stabilizers, and homogenizers in the manufacture of value-added chemical compounds like esters, plasticizers, etc. Kumar et al. synthesized seaweed biochar impregnated with Ni and Co (NiCo/SDSW-ABC) for cyclohexanol and cyclohexane production. The biochar catalysts with and without activation were compared for their catalytic activity on hydrogenation of phenols to produce cyclohexanol and cyclohexane [92]. High phenol conversion was reported in the presence of NiCo/SDSW-ABC. The greater surface area of the biochar facilitated greater dispersion of Ni and Co metals, which served as active sites for phenol dehydrogenation. NiCo/SDSW-ABC showed >99.9% of phenols conversion and selectivity for cyclohexanol production >99.9% as compared to NiCo catalysts. Subsequent increase in the dose of the catalyst resulted in the cracking of cyclohexanol to cyclohexane. No hydrogenation of phenols was observed in the absence of catalyst.

In another study, Adarsh et al. [43] produced phenols using biochar supported catalysts. They synthesized biochar catalysts (NiCo/SDSW-ABC) to evaluate the hydrogenation activity on other lignin model compounds like anisole, m-cresol, pyrocatechol, guaiacol, and 2,6-dimethoxyphenols for phenol production. Depending on the structure and the groups of the compounds, bulky groups offered

more steric hindrance towards hydrogenation. The results showed hydrogenation activity and the phenol yield in the order: anisole → m-cresol → pyrocatechol → guaiacol → 2,6-dimethoxyphenol.

Tetrahydrofuran (THF), 1,4-butanediol, and succinaldehyde are another group of value-added chemical compounds that are obtained by hydrogenation, hydrogen lysis, and hydrolysis reaction of furan. Furans are obtained from furfural that is isolated from lignocellulosic mass via hydrolysis (refer to Sect. 4.2.2). For instance, Lee et al. [93] synthesized rice straw biochar catalyst support using Ru-ReO$_x$ in N$_2$ (Ru-ReO$_x$/RSB-N$_2$) and CO$_2$ atmospheres (Ru-ReO$_x$/RSB-CO$_2$). The catalysts were tested for their catalytic activity for furan conversion to THF via hydrogenation and 1,4-butanediol via hydrogenolysis. Biochar supported catalysts enhance the catalytic activity. First, the inherent alkali groups present in biochars altered the bonding structure of terminal oxygen (Re=O) to the bridging oxygen (Re-O-biochar supported), which led to the stabilization of species and favored stronger interactions. Second, greater surface area is attributed to greater dispersal of Re-RuO$_x$ species. Third, biochar provided bi-functional surface sites, both metal and acid sites. THF is produced by hydrogenation of C=C bonds in furan at metal (Ru) sites, since Re does not adsorb H$_2$ [88]. While hydrogenolysis of C-O bonds at acidic functional sites results in 1-butanol and 1,4-butanediol production, dehydrogenation of 1,4-butanediol subsequently resulted in butyrolactone production. Lee et al. showed that when the process was mediated in the presence of water, furan rings opened to form succinaldehyde [93]. The results from experiments reported by Lee et al. reaction rate of 310 h^{-1} and ~80% furan hydrogenation to THF by (Ru-ReO$_x$/RSB-CO$_2$). Moreover, 46% higher activity for furan and twice higher for 1,4-butanediol were reported for Ru-ReO$_x$/RSB-N$_2$ as compared to Ru-ReO$_x$/RSB-CO$_2$ due to differences in surface properties.

4.2.2 Hydrolysis, Isomerization, and Dehydration

Hydrolysis enables conversion of complex polysaccharides into more accessible and active compounds [94]. The hydrolysis of biomass for the production of mono- and oligosaccharides is an important process for the synthesis of value-added chemicals and fuels, such as hydroxymethylfurfural (HMF), furfural, and ethanol [6, 94]. Biochar-based materials followed by sulfonation offer high surface area, porosity, and acid functionalization for the hydrolysis of polysaccharides into HMF and furfural compounds. First, hydrophobic carbon surfaces bond carbohydrates through CH-π interactions. Second, acidic functional groups provide active sites for hydrolysis by adsorbing cellulose or glucan chains via hydrogen bonds. This causes conformational changes, which induces the attack on glycosidic linkages. Third, fused rings of the biochars allow greater π binding that causes hydrothermal stability [94]. Equation 1 shows hydrolysis of lignocellulose in the production of MHF.

$$\text{Lignocellulose} \xrightarrow{\text{Hydrolysis}} \text{Glucose} \xrightarrow{\text{Isomerization}} \text{Fructose} \xrightarrow{\text{Dehydration}} \text{HMF} \xrightarrow{\text{Polymerization}} \text{Humins}$$

$$(1)$$
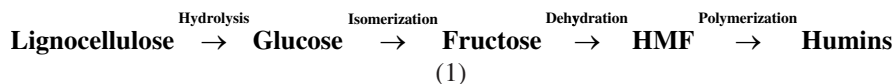
Cao et al. [25] studied the catalytic activity of chemically activated biochar using H_3PO_4 (PAB) in the conversion of carbohydrate-rich food waste into glucose and HMF. PABs were obtained by wet impregnation of pinewood sawdust in H_3PO_4 (60% w/w; 60 °C) for 24 h followed by its pyrolysis. The results indicated high HMF and glucose yields as compared to the processes without PABs. HMF yield of 24.5 Cmol% from bread waste was reported as compared to 3.3 Cmol% in the absence of PABs. The enhanced catalytic conversion is attributed to the high surface area and $P^+\text{-}O^-$ functionalities of PABs. This resulted in an increase in hydrolysis of polymeric starch into glucose. Glucose underwent subsequent dehydration to yield HMF. PABs also controlled glucose isomerization to fructose.

Similar experiments were conducted by Cao et al. [95] using biochar obtained from forest wood waste. Sulfonation was carried out by soaking biochar in 98% H_2SO_4, at 150 °C for 12 h. Sulfonated biochars were tested for their catalytic activity in converting bread waste to glucose and HMF. Highest yield of 46.4 Cmol% glucose was reported. HMF formation was subsequently catalyzed by $-SO_3H$ and other acidic sites of biochars by (a) direct dehydration of glucose and (b) indirect dehydration of fructose obtained from isomerization of glucose.

Liu et al. [96] prepared Sn-Co support-based biochar catalyst ($SnO_2\text{-}Co_3O_4$/C) by pyrolyzing lignocellulosic residues obtained from corncob degradation, followed by its metal impregnation using co-precipitation method (Sn(IV) and Co(II) hydroxides). The catalyst was tested for the hydrolysis of hemicellulose in corncob to yield furfural via isomerization of xylose to xylulose and dehydration of xylulose. Equation 2 shows the stepwise production of furfural. Maximum yield of 30% was achieved for furfural at 180 °C for ~3 h as compared to 15.2% without catalyst. Biochar catalyst support enhanced the catalytic activity as follows: First, unsaturated cationic sites in biochar lead to the formation of Lewis sites that left Sn^{4+} and Co^{2+} exposed to attract hydroxyl groups from water molecules and lignocellulose. This facilitated the xylose isomerization to xylulose that further led to the increase in the yield of furfural. Second, increased surface area and high porosity of biochar led to enhanced dispersion of Sn and Co species that helped in the aggregation of xylose and xylulose molecules for their further dehydration to yield furfural.

$$\text{Hemicellulose} \atop \text{(Corncob)} \xrightarrow{\text{Saccharification}} \text{Monosaccharide} \xrightarrow{\text{Hydrolysis}} \text{Xylose} \xrightarrow{\text{Isomerization}} \text{Xylulose}$$
$$\xrightarrow{\text{Dehydration}} \text{Furfural} \xrightarrow{\text{Polymerization}} \text{Humins}$$

$$(2)$$
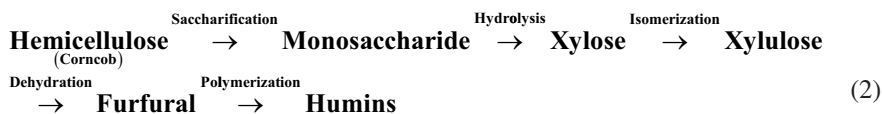
Ormsby et al. 2017 [97] conducted experiments on the hydrolysis of cellobiose and xylan using sulfonated pine chip biochar. Hydrolysis of cellobiose into selective glucose formation was reported higher using sulfonated biochar catalyst (85%) as

compared to the commercial activated carbons. Similarly, xylan hydrolysis was explored in hemicellulose using the biochar catalysts. Ninety percentage xylan conversion was reported at 120 °C using biochar catalysts as compared to 50% conversion by commercial activated carbons.

Phenols are important platform compounds that are used for the production of bisphenol A, caprolactam, pharmaceutical products, phenolic resins, etc. [98]. In order to increase the yield of phenols, Chen et al. [98] prepared biochar from bamboo wastes and doped it with nitrogen (N) at 600 °C for 30 min. The experiments were conducted to test the catalytic activity using biochar catalysts and N-doped biochar catalysts. N-doped biochar increased the affinity of the biochar for water molecules and enhanced pH. This promoted the dehydration reactions that inhibited the formation of acid products. Moreover, it increased the stability of bio-oil by avoiding its acid corrosion. With the addition of biochar catalysts, the phenols' yield increased significantly to 59%. It was further increased to 77% with the addition of N-doped biochar catalyst. Biochar promoted the decarboxylation and dehydration and removed alkyl chains, leading to more phenol production and less O species and acetic acid releasing them in the form of CO_2. Second, the increase in NH_3 concentration using N-doped biochar catalyst increased the phenol production taking maximum yield up to 82%. Third, active O- and N-containing groups in the catalyst promoted β-O-4 linkage to form more phenol intermediates. Fourth, biochar catalysts increased H-donors from the decomposition of hemicellulose and cellulose to form more phenols. Fifth, doped biochar catalysts promoted the decomposition of lignin and inhibited the cracking of hemicellulose and cellulose, thereby increasing the phenolic content in bio-oil. Sixth, it promoted –O-CH_3 cracking in complex phenols to yield simpler phenols.

Pierri et al. [49] synthesized epoxide catalyst using biochar Mn^{II} catalysts. These biochar-based epoxide catalysts were kinetically faster than silica-based catalysts. This was due to the hydrophobicity of the carbon structures that favored olefin-active metal complexation to generate epoxides. Moreover, it also repelled the water generated during catalysis reactions.

4.3 Biochar Catalysts for the Abatement of Pollutants

Water pollution has caused substantial release of pollutants in water. Hazardous chemicals, like antibiotics, dyes, and pesticides, have been detected in water. Use of biochar as an adsorbent for the abatement of pollutants is economically viable and readily accessible. The carbon matrix, medium to high surface area, and high porosity of the biochar enable it to adsorb/absorb organic pollutants from surroundings [99]. In the following section, the role and mechanism of biochar catalysts have been discussed via two most commonly used pathways, oxidation (ozonation, photocatalysis) and reduction.

4.3.1   Advanced Oxidation Processes and Degradation of Organic Contaminants

Advanced oxidation processes (AOPs) have proven a highly efficient noble process that accelerates the degradation of a wide range of organic and inorganic contaminants via oxidation. It aims at producing transitory free radicals (hydroxyl, keto, peroxides, metal oxide free radicals, etc.) that acts upon the target pollutant species and degrades it to CO_2, H_2O, and mineral acids. Photocatalysis, ozonation, and UV photolysis are some of the commonly used AOPs [100]. Ozone-driven AOPs are effective in the degradations of antibiotics, pharmaceuticals, and amino compounds [101]. The excellent properties of biochar, i.e., high adsorption capacity, environmental friendliness, low cost, and defect structure generation of reactive/oxidizing species, make biochar an emerging catalyst for the degradation of the pollutants [102]. Addition of activators to the biochar system like persulfates (PS), peroxymonosulfate (PMS), and peroxodisulfate (PDS) produces ·OH species, $SO_4^{·-}$ radicals, singlet oxygen ($1O_2$) species, surface-bound radicals (SBRs), and reactive oxygen species (ROSs). At $pH < pH_{pzc}$, the positively charged surface of biochars favors the bonding with these activator species. This creates Fenton-like reactions. First, biochar surface provides persistent free radicals (PFRs) for activating PS/PMS/PDS. Second, high-temperature pyrolysis for biochar synthesis creates biochar defects that leads to biochar activation potency towards activators. These defect edges of the biochars are susceptible to oxidation that facilitates the donation of electrons for activator species. As a result, $SO_4^{·-}$ species, ·OH species, singlet O species, SBRs, and ROS species attack the contaminants and degrade the molecules. Figure 7 shows various AOP pathways and mechanisms of degradation of contaminants over biochar catalysts.

Ouyang et al. [102] synthesized pine needle biochar and investigated the potency of 1,4-dioxane degradation. The reaction was catalyzed in the presence of peroxymonosulfate (PMS) over biochar support. The degradation efficiency for 1,4-dioxane increased from 40.6% to 100% as the dose of biochar and PMS increased. Singlet oxygen species generated within the biochar/PMS system contributed to the degradation of 1,4-dioxane. Moreover, $SO_4^{·-}$ and ·OH species were also produced by PMS activation. These species attacked 1,4-dioxane molecules and enhanced its degradation.

In a similar study, Zhang et al. [103] proposed catalytic impact of biochar/peroxydisulfate (PDS) system, for the effective removal of sulfamethoxazole (SMX) and N_4-acetyl-sulfamethoxazole (NSMX) in urine. The biochar/PDS system produced ·OH and $SO_4^{·-}$ radicals as major species, along with singlet oxygen species, surface-bound radicals (SBRs), and some reactive oxygen species (ROSs) that transformed SMX in urine to the products that were easily degraded by microbial activity.

Diao et al. [104] prepared novel sludge biochar catalysts with dispersed Fe^0 and Al^0 particles in its pores. The prepared biochar was combined with persulfates (PS). ·OH free radical generation was enhanced by the oxidation of reaction between dissolved oxygen and Fe^0/Al^0 which led to the increase in the degradation efficiency of bisphenol A (BPA). Fe^{2+} on the biochar's surface further decomposed PS to release $SO_4^{·-}$. The efficiency of BPA degradation went up to 97.8% from 22.1% in the presence of Fe/Al biochar/PS catalyst system.
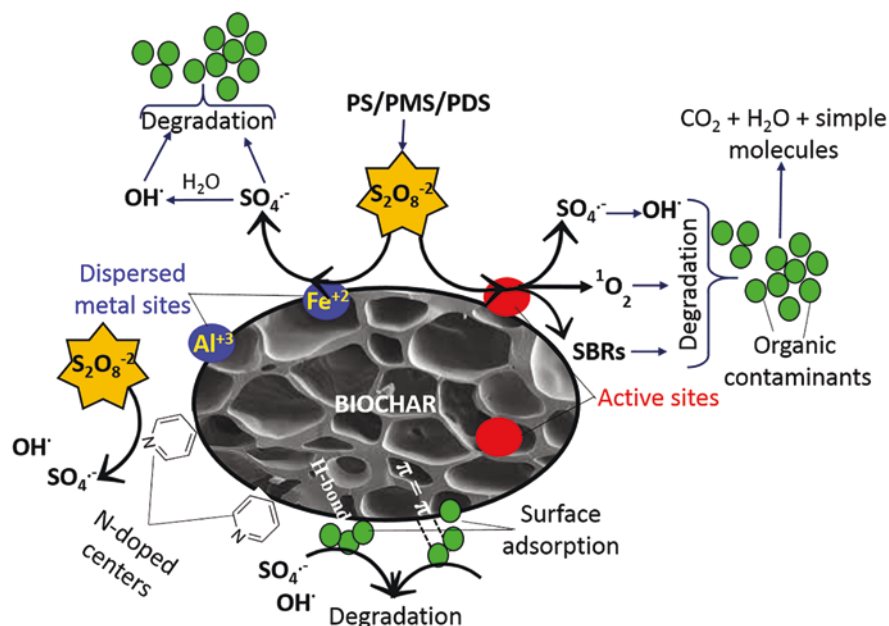
Fig. 7 Pathways and mechanisms showing degradation of organic pollutants by advanced oxidation processes (AOPs)

Based on similar principles, Chen et al. [105] reported degradation of proteins and extracellular polymer substances in sludge using biochar-based peroxodisulfate/zero-valent iron (Fe-ADSBC); Li et al. [106] studied the degradation of trichloroethylene in groundwater using biochar (maize cob) supported on nano-zero-valent iron with PMS activator. Li et al. [107] synthesized wheat straw Fe, N-co-doped biochar (Fe-N-BC) using urea and iron salts and activated it with persulfate (peroxydisulfate, PS) for organic contaminant degradation. Xu et al. [108] synthesized saw dust-based biochar and doped with N followed by activating it with PMS (N-C-d-4-800/PMS system). The pyridine N and graphitic rich defects, larger surface area, and porous structure of biochar/PMS system activated PMS to obtain superior catalytic degradation of bisphenol A (BPA), phenol, acetaminophen (AAP), and sulfamethoxazole (SMX). Similarly, Ding et al. [109] also tested the catalytic activity of N-doped biochar/PMS systems derived from rice straw over the degradation of metolachlor (MET). Oxidation of surface ketonic group and PMS resulted in the formation of ·OH and SO_4^- species that enhance degradation. Moreover, sp^2 carbon of biochar with free-flowing π-electrons, in conjunction with doped N atoms, increased the adsorption capacity of MET over biochar/PMS system.

Duan et al. used biochar derived from sludge as an effective oxidation process activator for the nonradical degradation and disinfection of micropollutants [110]. Ahmed et al. [111] used biochars derived from soybean stover (S-BC700) and peanut shells (P-BC700) for the adsorption of trichloroethylene (TCE), a chlorinated

hydrocarbon that poses threat to the groundwater. The high adsorption capacity of biochars towards TCE was attributed to low H/C and O/C ratio for biochars at 700 °C. Decrease in O-functionality resulted in increased hydrophobicity of the biochars. This prevented the hindrance over non-polar C-sites for the adsorption of hydrophobic TCE. Moreover, lower H/C ratio indicates greater aromaticity and tough carbon matrix that favored the removal of organic contaminants.

4.3.2 Photocatalytic Degradation of Organic Contaminants

Biochar serves as potential photocatalysts in degrading organic pollutants [17]. This is ascribed to the following: First, well-developed porous structures and oxygen-rich containing functional groups facilitate the adsorption of contaminants and hence provide greater opportunity for contact with the catalysts. Second, dispersal of well-organized active sites that facilitates dispersal of activator particles (TiO_2, H_2O_2, etc.) over biochar supports generates electrons from valence band to the conduction band on photoexcitation. Third, biochars facilitate fast charge shuttling by preventing the recombination of the vacant valance bands and diverting the stream of electrons by acting as acceptors towards them. Fourth, electrons also react with oxygen functionalities to generate superoxide and hydroxyl radicals to oxidize contaminants into CO_2 and H_2O. Fifth, stable interconnected framework of biochar catalyst provides stability to the complete process [22, 26, 112, 113]. Lu et al. [113] effectively photodegraded methyl orange (MO) over biochar support with the dispersed TiO_2 particles under UV radiations. The decolorization efficiency of MO in the presence of biochar catalyst increased from 3.43% to 76.69%. Photocatalytic holes, hydroxyl radicals, and superoxide anions were the primary species that oxidized methyl orange into CO_2 [112].

4.3.3 Catalytic Reduction of Inorganic Contaminants

Biochar/biochar supported catalysts can facilitate the removal of inorganic contaminants by reducing them to their less toxic state. For instance, more toxic Cr(VI) has been reduced to Cr(III) that is less toxic and of low risk to the environment. Xu et al. [114] utilized biochar prepared from peanut shells to reduce Cr(VI) to Cr(III). The oxygen-containing functional groups –C=O and –COOH of biochar acted as electron donor moieties. Moreover, biochar acted as an electron shuttle for lactates that increased the reduction rate. It was concluded that both biochar and lactates worked synergistically in enhancing the reduction of Cr(VI) to Cr(III) by up to 25 times. The O-centered, semiquinone-type radicals acted as electron shuttle and reduced Cr(VI) to CrOOH.

Shows the method of pyrolysis, surface characteristics, and catalytic applications of biochar-based catalysts.

5   Concluding Remarks

The chapter highlighted the impact of biochar physio-chemical properties (surface area, porosity, functional groups, mineral content, stable matrix, active sites, -SO$_3$H density, metal dispersion, etc.) over biochar-based catalysts for the production of value-added products. The chapter discussed mechanistic studies of char synthesis/ activation/loading of metal and its catalytic property. Moreover, it discussed the mechanism of various processes like hydrolysis, isomerization, reduction, oxidation, transesterification/esterification, fermentation, anaerobic decomposition, and tar cracking. Depending upon the relative significance of the catalysis process, a relationship between catalytic activity and physio-chemical properties of biochar along with their tuning with the synthesis/activation process was established. Thus, biochar emerges as a sustainable, versatile, and low-cost catalyst/catalyst support for chemical synthesis, biofuel production, and pollution control. It can be used in multiple ways and can be maneuvered through innovative modification techniques. Thus, after proper designing of biochar/biochar-based catalysts, they have potential to replace expensive, non-renewable, and environment-unfriendly catalysts.

References

1. Joseph SD, Camps-Arbestain M, Lin Y, Munroe P, Chia CH, Hook J et al (2010) An investigation into the reactions of biochar in soil. Soil Res 48(7):501–515
2. Lehmann J, Rillig MC, Thies J, Masiello CA, Hockaday WC, Crowley D (2011) Biochar effects on soil biota – a review. Soil Biol Biochem 43(9):1812–1836. https://doi.org/10.1016/j.soilbio.2011.04.022
3. Graber E, Elad Y (2013) Biochar impact on plant resistance to disease. In: Rineau F, Ladygina N (eds) Biochar and soil biodata. Taylor & Francis, London, pp 41–68
4. Deem ML, Crow S (2017) Biochar
5. Tan Z, Lin CSK, Ji X, Rainey TJ (2017) Returning biochar to fields. Appl Soil Ecol 116:1–11. https://doi.org/10.1016/j.apsoil.2017.03.017
6. Lee J, Sarmah AK, Kwon EE (2019) Production and formation of biochar. In: Ok YS, Tsang DCW, Bolan N, Novak JM (eds) Biochar from biomass and waste. Elsevier, Amsterdam, pp 3–18
7. Masek O, Buss W, Roy-poirier A, Lowe W, Peters C, Brownsort P et al (2018) Consistency of biochar properties over time and production scales: a characterisation of standard materials. J Anal Appl Pyrol. https://doi.org/10.1016/j.jaap.2018.02.020
8. Mohan D, Sharma R, Singh VK, Steele P, Pittman CU (2012) Fluoride removal from water using bio-char, a green waste, low-cost adsorbent: equilibrium uptake and sorption dynamics modeling. Ind Eng Chem Res 51(2):900–914. https://doi.org/10.1021/ie202189v
9. Uchimiya M, Wartelle LH, Klasson KT, Fortier CA, Lima IM (2011) Influence of pyrolysis temperature on biochar property and function as a heavy metal sorbent in soil. J Agric Food Chem 59(6):2501–2510. https://doi.org/10.1021/jf104206c
10. Weber K, Quicker P (2018) Properties of biochar. Fuel 217:240–261. https://doi.org/10.1016/j.fuel.2017.12.054
11. de Almeida LS, Oreste EQ, Maciel JV, Heinemann MG, Dias D (2020) Electrochemical devices obtained from biochar: advances in renewable and environmentally-friendly tech-

nologies applied to analytical chemistry. Trends Environ Anal Chem 26:e00089. https://doi.org/10.1016/j.teac.2020.e00089

12. Zimmerman A, Gao B (2013) The stability of biochar in the environment. In: Rineau F, Ladygina N (eds) Biochar and soil biodata. Taylor & Francis, London, pp 1–40

13. Majumder S, Neogi S, Dutta T, Powel MA, Banik P (2019) The impact of biochar on soil carbon sequestration: meta-analytical approach to evaluating environmental and economic advantages. J Environ Manag 250:109466. https://doi.org/10.1016/j.jenvman.2019.109466

14. Lee HW, Lee H, Kim Y-M, Park R-s, Park Y-K (2019) Recent application of biochar on the catalytic biorefinery and environmental processes. Chin Chem Lett 30(12):2147–2150. https://doi.org/10.1016/j.cclet.2019.05.002

15. Lehmann J, Joseph S (2009) Biochar for environmental management: an introduction. Biochar for environmental management. Science and technology. Earthscan Publishers Ltd, London

16. Rajapaksha AU, Chen SS, Tsang DCW, Zhang M, Vithanage M, Mandal S et al (2016) Engineered/designer biochar for contaminant removal/immobilization from soil and water: potential and implication of biochar modification. Chemosphere 148:276–291. https://doi.org/10.1016/j.chemosphere.2016.01.043

17. Xiong X, Yu IKM, Cao L, Tsang DCW, Zhang S, Ok YS (2017) A review of biochar-based catalysts for chemical synthesis, biofuel production, and pollution control. Bioresour Technol 246:254–270. https://doi.org/10.1016/j.biortech.2017.06.163

18. Jeon J, Park JH, Wi S, Yang S, Ok YS, Kim S (2019) Latent heat storage biocomposites of phase change material-biochar as feasible eco-friendly building materials. Environ Res 172:637–648. https://doi.org/10.1016/j.envres.2019.01.058

19. Pandey D, Daverey A, Arunachalam K (2020) Biochar: production, properties and emerging role as a support for enzyme immobilization. J Clean Prod 255:120267. https://doi.org/10.1016/j.jclepro.2020.120267

20. Thomas P, Lai CW, Bin Johan MR (2019) Recent developments in biomass-derived carbon as a potential sustainable material for super-capacitor-based energy storage and environmental applications. J Anal Appl Pyrolysis 140:54–85. https://doi.org/10.1016/j.jaap.2019.03.021

21. Norouzi O, Kheradmand A, Jiang Y, Di Maria F, Masek O (2019) Superior activity of metal oxide biochar composite in hydrogen evolution under artificial solar irradiation: a promising alternative to conventional metal-based photocatalysts. Int J Hydrog Energy 44(54):28698–28708. https://doi.org/10.1016/j.ijhydene.2019.09.119

22. Do Minh T, Song J, Deb A, Cha L, Srivastava V, Sillanpää M (2020) Biochar based catalysts for the abatement of emerging pollutants: a review. Chem Eng J 394:124856. https://doi.org/10.1016/j.cej.2020.124856

23. Cao X, Sun S, Sun R (2017) Application of biochar-based catalysts in biomass upgrading: a review. RSC Adv 7(77):48793–48805. https://doi.org/10.1039/C7RA09307A

24. Cheng F, Li X (2018) Preparation and application of biochar-based catalysts for biofuel production. Catalysts 8(9):346

25. Cao L, Yu IKM, Tsang DCW, Zhang S, Ok YS, Kwon EE et al (2018) Phosphoric acid-activated wood biochar for catalytic conversion of starch-rich food waste into glucose and 5-hydroxymethylfurfural. Bioresour Technol 267:242–248. https://doi.org/10.1016/j.biortech.2018.07.048

26. Lyu H, Zhang Q, Shen B (2020) Application of biochar and its composites in catalysis. Chemosphere 240:124842. https://doi.org/10.1016/j.chemosphere.2019.124842

27. Mohan D, Pittman CU, Bricka M, Smith F, Yancey B, Mohammad J et al (2007) Sorption of arsenic, cadmium, and lead by chars produced from fast pyrolysis of wood and bark during bio-oil production. J Colloid Interface Sci 310(1):57–73. https://doi.org/10.1016/j.jcis.2007.01.020

28. Fuentes-Cano D, von Berg L, Diéguez-Alonso A, Scharler R, Gómez-Barea A, Anca-Couce A (2020) Tar conversion of biomass syngas in a downstream char bed. Fuel Process Technol 199:106271. https://doi.org/10.1016/j.fuproc.2019.106271

29. Shen Y (2015a) Chars as carbonaceous adsorbents/catalysts for tar elimination during biomass pyrolysis or gasification. Renew Sust Energ Rev 43:281–295. https://doi.org/10.1016/j.rser.2014.11.061

30. Buentello-Montoya D, Zhang X, Li J, Ranade V, Marques S, Geron M (2020) Performance of biochar as a catalyst for tar steam reforming: effect of the porous structure. Appl Energy 259:114176. https://doi.org/10.1016/j.apenergy.2019.114176

31. Yang J, Pan B, Li H, Liao S, Zhang D, Wu M, Xing B (2016) Degradation of p-nitrophenol on biochars: role of persistent free radicals. Environ Sci Technol 50(2):694–700

32. Huang Z, Wang T, Shen M, Huang Z, Chong Y, Cui L (2019) Coagulation treatment of swine wastewater by the method of in-situ forming layered double hydroxides and sludge recycling for preparation of biochar composite catalyst. Chem Eng J 369:784–792

33. Shen Y, Linville JL, Urgun-Demirtas M, Schoene RP, Snyder SW (2015) Producing pipeline-quality biomethane via anaerobic digestion of sludge amended with corn stover biochar with in-situ CO2 removal. Appl Energy 158:300–309. https://doi.org/10.1016/j.apenergy.2015.08.016

34. Lee J, Kim K-H, Kwon EE (2017) Biochar as a catalyst. Renew Sust Energ Rev 77:70–79. https://doi.org/10.1016/j.rser.2017.04.002

35. Ahmed MB, Zhou JL, Ngo HH, Guo W, Chen M (2016) Progress in the preparation and application of modified biochar for improved contaminant removal from water and wastewater. Bioresour Technol 214:836–851

36. Trakal L, Vítková M, Hudcová B, Beesley L, Komárek M (2019) Biochar and its composites for metal(loid) removal from aqueous solutions. In: Ok YS, Tsang DCW, Bolan N, Novak JM (eds) Biochar from biomass and waste. Elsevier, Amsterdam, pp 113–141

37. Dehkhoda AM, West AH, Ellis N (2010) Biochar based solid acid catalyst for biodiesel production. Appl Catal A Gen 382(2):197–204. https://doi.org/10.1016/j.apcata.2010.04.051

38. Shen Y, Zhao P, Shao Q, Ma D, Takahashi F, Yoshikawa K (2014) In-situ catalytic conversion of tar using rice husk char-supported nickel-iron catalysts for biomass pyrolysis/gasification. Appl Catal B Environ 152-153:140–151. https://doi.org/10.1016/j.apcatb.2014.01.032

39. Mohan D, Singh P, Sarswat A, Steele PH, Pittman CU (2015) Lead sorptive removal using magnetic and nonmagnetic fast pyrolysis energy cane biochars. J Colloid Interface Sci 448:238–250. https://doi.org/10.1016/j.jcis.2014.12.030

40. Min L, Zhongsheng Z, Zhe L, Haitao W (2020) Removal of nitrogen and phosphorus pollutants from water by FeCl3-impregnated biochar. Ecol Eng 149:105792. https://doi.org/10.1016/j.ecoleng.2020.105792

41. Singh P, Sarswat A, Pittman CU, Mlsna T, Mohan D (2020) Sustainable low-concentration arsenite [As(III)] removal in single and multicomponent systems using hybrid iron oxide–biochar nanocomposite adsorbents—a mechanistic study. ACS Omega 5(6):2575–2593. https://doi.org/10.1021/acsomega.9b02842

42. Lin L, Song Z, Khan ZH, Liu X, Qiu W (2019) Enhanced As(III) removal from aqueous solution by Fe-Mn-La-impregnated biochar composites. Sci Total Environ 686:1185–1193. https://doi.org/10.1016/j.scitotenv.2019.05.480

43. Kumar A, Saini K, Bhaskar T (2020) Advances in design strategies for preparation of biochar based catalytic system for production of high value chemicals. Bioresour Technol 299:122564. https://doi.org/10.1016/j.biortech.2019.122564

44. Dehkhoda AM, Ellis N (2013) Biochar-based catalyst for simultaneous reactions of esterification and transesterification. Catal Today 207:86–92. https://doi.org/10.1016/j.cattod.2012.05.034

45. Dehkhoda AM, Gyenge E, Ellis N (2016) A novel method to tailor the porous structure of KOH-activated biochar and its application in capacitive deionization and energy storage. Biomass Bioenergy 87:107–121. https://doi.org/10.1016/j.biombioe.2016.02.023

46. Han X, Chu L, Liu S, Chen T, Ding C, Yan J et al (2015) Removal of methylene blue from aqueous solution using porous biochar obtained by KOH activation of peanut shell biochar. Bioresources 10(2):2836–2849

47. Jagtoyen M, Derbyshire F (1998) Activated carbons from yellow poplar and white oak by H3PO4 activation. Carbon 36(7–8):1085–1097

48. Aasberg-Petersen K, Christensen TS, Dybkjaer I, Sehested J, Østberg M, Coertzen RM et al (2004) Synthesis gas production for FT synthesis. In: Steynberg A, Dry M (eds) Studies in surface science and catalysis, vol 152. Elsevier, Amsterdam, pp 258–405

49. Pierri L, Gemenetzi A, Mavrogiorgou A, Borges Regitano J, Deligiannakis Y, Louloudi M (2020) Biochar as supporting material for heterogeneous Mn(II) catalysts: efficient olefins epoxidation with H2O2. Mol Catalysis 489:110946. https://doi.org/10.1016/j.mcat.2020.110946

50. Tsang DCW, Yu IKM, Xiong X (2019) Novel application of biochar in stormwater harvesting. In: Ok YS, Tsang DCW, Bolan N, Novak JM (eds) Biochar from biomass and waste. Elsevier, Amsterdam, pp 319–347

51. Bartholomew CH, Farrauto RJ (2011) Fundamentals of industrial catalytic processes. John Wiley & Sons, Hoboken, NJ

52. Li D, Xu H-Q, Jiao L, Jiang H-L (2019) Metal-organic frameworks for catalysis: state of the art, challenges, and opportunities. Energy Chem 1(1):100005. https://doi.org/10.1016/j.enchem.2019.100005

53. Lamichhane S, Bal Krishna KC, Sarukkalige R (2016) Polycyclic aromatic hydrocarbons (PAHs) removal by sorption: a review. Chemosphere 148:336–353. https://doi.org/10.1016/j.chemosphere.2016.01.036

54. Keiluweit M, Nico PS, Johnson MG, Kleber M (2010) Dynamic molecular structure of plant biomass-derived black carbon (biochar). Environ Sci Technol 44(4):1247–1253. https://doi.org/10.1021/es9031419

55. Bourke J, Manley-Harris M, Fushimi C, Dowaki K, Nunoura T, Antal MJ (2007) Do all carbonized charcoals have the same chemical structure? 2. A model of the chemical structure of carbonized charcoal. Ind Eng Chem Res 46(18):5954–5967. https://doi.org/10.1021/ie070415u

56. Wen X, Guan J (2019) Recent progress on MOF-derived electrocatalysts for hydrogen evolution reaction. Appl Mater Today 16:146–168. https://doi.org/10.1016/j.apmt.2019.05.013

57. Waqas M, Aburiazaiza AS, Miandad R, Rehan M, Barakat MA, Nizami AS (2018) Development of biochar as fuel and catalyst in energy recovery technologies. J Clean Prod 188:477–488. https://doi.org/10.1016/j.jclepro.2018.04.017

58. Novak JM, Johnson MG (2019) Elemental and spectroscopic characterization of low-temperature (350°C) lignocellulosic- and manure-based designer biochars and their use as soil amendments. In: Ok YS, Tsang DCW, Bolan N, Novak JM (eds) Biochar from biomass and waste. Elsevier, Amsterdam, pp 37–58

59. Yu JT, Dehkhoda AM, Ellis N (2011) Development of biochar-based catalyst for transesterification of canola oil. Energy Fuel 25(1):337–344. https://doi.org/10.1021/ef100977d

60. Li X, Zhao C, Zhang M (2019) Biochar for anionic contaminants removal from water. In: Ok YS, Tsang DCW, Bolan N, Novak JM (eds) Biochar from biomass and waste. Elsevier, Amsterdam, pp 160–143

61. Halder G, Khan AA, Dhawane S (2016) Fluoride sorption onto a steam-activated biochar derived from *Cocos nucifera* shell. Clean Soil Air Water 44(2):124–133

62. Yang G, Wu L, Xian Q, Shen F, Wu J, Zhang Y (2016) Removal of congo red and methylene blue from aqueous solutions by vermicompost-derived biochars. PLoS One 11(5):e0154562

63. Adams P, Bridgwater T, Lea-Langton A, Ross A, Watson I (2018) Biomass conversion technologies. In: Thornley P, Adams P (eds) Greenhouse gas balances of bioenergy systems. Academic, Cambridge, MA, pp 107–139

64. Lee J, Jung J-M, Oh J-I, Ok YS, Lee S-R, Kwon EE (2017) Evaluating the effectiveness of various biochars as porous media for biodiesel synthesis via pseudo-catalytic transesterification. Bioresour Technol 231:59–64. https://doi.org/10.1016/j.biortech.2017.01.067

65. Pruszko R (2020) Biodiesel production. In: Dahiya A (ed) Bioenergy, 2nd edn. Academic, Cambridge, MA, pp 491–514

66. Chakraborty R, Chatterjee S, Mukhopadhyay P, Barman S (2016) Progresses in waste biomass derived catalyst for production of biodiesel and bioethanol: a review. Procedia Environ Sci 35:546–554. https://doi.org/10.1016/j.proenv.2016.07.039

67. Kyriakou M, Chatziiona VK, Costa CN, Kallis M, Koutsokeras L, Constantinides G, Koutinas M (2019) Biowaste-based biochar: a new strategy for fermentative bioethanol overproduction via whole-cell immobilization. Appl Energy 242:480–491. https://doi.org/10.1016/j.apenergy.2019.03.024

68. Kraisornkachit P, Vivanpatarakij S, Amornraksa S, Simasatitkul L, Assabumrungrat S (2016) Performance evaluation of different combined systems of biochar gasifier, reformer and CO2 capture unit for synthesis gas production. Int J Hydrog Energy 41(31):13408–13418

69. Palma V, Ruocco C, Martino M, Meloni E, Ricca A (2017) Catalysts for conversion of synthesis gas. In: Dalena F, Basile A, Rossi C (eds) Bioenergy systems for the future. Woodhead Publishing, Cambridge, pp 217–277

70. Schuster G, Löffler G, Weigl K, Hofbauer H (2001) Biomass steam gasification – an extensive parametric modeling study. Bioresour Technol 77(1):71–79. https://doi.org/10.1016/S0960-8524(00)00115-2

71. Boerner LK (2020) Light-activated catalyst makes syngas greener. C&EN Global Enterprise 98(3):11–11. https://doi.org/10.1021/cen-09803-scicon9

72. Zhu L, Yin S, Yin Q, Wang H, Wang S (2015) Biochar: a new promising catalyst support using methanation as a probe reaction. Energy Sci Eng 3(2):126–134

73. Lee T, Nam I-H, Jung S, Park Y-K, Kwon EE (2020) Synthesis of nickel/biochar composite from pyrolysis of microcystis aeruginosa and its practical use for syngas production. Bioresour Technol 300:122712. https://doi.org/10.1016/j.biortech.2019.122712

74. Yip K, Tian F, Hayashi J-i, Wu H (2010) Effect of alkali and alkaline earth metallic species on biochar reactivity and syngas compositions during steam gasification. Energy Fuel 24(1):173–181. https://doi.org/10.1021/ef900534n

75. Cho D-W, Kwon G, Yoon K, Tsang YF, Ok YS, Kwon EE, Song H (2017) Simultaneous production of syngas and magnetic biochar via pyrolysis of paper mill sludge using CO2 as reaction medium. Energy Convers Manag 145:1–9. https://doi.org/10.1016/j.enconman.2017.04.095

76. Liu Y, Paskevicius M, Wang H, Parkinson G, Veder J-P, Hu X, Li C-Z (2019) Role of O-containing functional groups in biochar during the catalytic steam reforming of tar using the biochar as a catalyst. Fuel 253:441–448. https://doi.org/10.1016/j.fuel.2019.05.037

77. Schwan J, Ulrich S, Batori V, Ehrhardt H, Silva S (1996) Raman spectroscopy on amorphous carbon films. J Appl Phys 80(1):440–447

78. Manchala KR, Sun Y, Zhang D, Wang Z-W (2017) Anaerobic digestion modelling. Adv Bioenergy 2:69–141

79. Gould MC (2015) Bioenergy and anaerobic digestion. Paper presented at the Bioenergy

80. Pan J, Ma J, Zhai L, Luo T, Mei Z, Liu H (2019) Achievements of biochar application for enhanced anaerobic digestion: a review. Bioresour Technol 292:122058. https://doi.org/10.1016/j.biortech.2019.122058

81. Yang B, Xu H, Liu Y, Li F, Song X, Wang Z, Sand W (2020) Role of GAC-MnO2 catalyst for triggering the extracellular electron transfer and boosting CH4 production in syntrophic methanogenesis. Chem Eng J 383:123211. https://doi.org/10.1016/j.cej.2019.123211

82. Das A, Mondal C (2013) Catalytic effect of tungsten on anaerobic digestion process for biogas production from fruit and vegetable wastes. Int J Sci Eng Technol 2(4):216–221

83. Zheng R, Liu Z, Wang Y, Xie Z (2020) Industrial catalysis: strategies to enhance selectivity. Chin J Catal 41(7):1032–1038. https://doi.org/10.1016/S1872-2067(20)63578-1

84. Duan X, Chen Y, Yan Y, Feng L, Chen Y, Zhou Q (2019) New method for algae comprehensive utilization: algae-derived biochar enhances algae anaerobic fermentation for short-chain fatty acids production. Bioresour Technol 289:121637

85. Shen Y e a (2015b) Producing pipeline-quality biomethane via anaerobic digestion of sludge amended with corn stover biochar with in-situ CO2 removal. Appl Energy 158:300–309. https://doi.org/10.1016/j.apenergy.2015.08.016

86. Shen Y, Forrester S, Koval J, Urgun-Demirtas M (2017) Yearlong semi-continuous operation of thermophilic two-stage anaerobic digesters amended with biochar for enhanced biomethane production. J Clean Prod 167:863–874. https://doi.org/10.1016/j.jclepro.2017.05.135

87. Mumme J, Srocke F, Heeg K, Werner M (2014) Use of biochars in anaerobic digestion. Bioresour Technol 164:189–197. https://doi.org/10.1016/j.biortech.2014.05.008

88. Lee Y, Kim YT, Kwon EE, Lee J (2020) Biochar as a catalytic material for the production of 1,4-butanediol and tetrahydrofuran from furan. Environ Res 184:109325. https://doi.org/10.1016/j.envres.2020.109325

89. Tang D (2019) Hardstock triglycerides. In: Melton L, Shahidi F, Varelis P (eds) Encyclopedia of food chemistry. Academic Press, Oxford, pp 128–131

90. Dijkstra AJ, van Duijn G (2016) Vegetable oils: oil production and processing. In: Caballero B, Finglas PM, Toldrá F (eds) Encyclopedia of food and health. Academic Press, Oxford, pp 373–380

91. Yan Q, Wan C, Liu J, Gao J, Yu F, Zhang J, Cai Z (2013) Iron nanoparticles in situ encapsulated in biochar-based carbon as an effective catalyst for the conversion of biomass-derived syngas to liquid hydrocarbons. Green Chem 15(6):1631–1640

92. Kumar A, Kumar J, Bhaskar T (2020) High surface area biochar from Sargassum tenerrimum as potential catalyst support for selective phenol hydrogenation. Environ Res 186:109533. https://doi.org/10.1016/j.envres.2020.109533

93. Lee Y, Lee SW, Tsang YF, Kim YT, Lee J (2020) Engineered rice-straw biochar catalysts for the production of value-added chemicals from furan. Chem Eng J 387:124194. https://doi.org/10.1016/j.cej.2020.124194

94. Chen SS, Maneerung T, Tsang DCW, Ok YS, Wang C-H (2017) Valorization of biomass to hydroxymethylfurfural, levulinic acid, and fatty acid methyl ester by heterogeneous catalysts. Chem Eng J 328:246–273. https://doi.org/10.1016/j.cej.2017.07.020

95. Cao L, Iris K, Chen SS, Tsang DC, Wang L, Xiong X et al (2018) Production of 5-hydroxymethylfurfural from starch-rich food waste catalyzed by sulfonated biochar. Bioresour Technol 252:76–82

96. Liu Q-y, Yang F, Liu Z-h, Li G (2015) Preparation of SnO2–Co3O4/C biochar catalyst as a Lewis acid for corncob hydrolysis into furfural in water medium. J Ind Eng Chem 26:46–54

97. Ormsby R, Kastner JR, Miller J (2012) Hemicellulose hydrolysis using solid acid catalysts generated from biochar. Catal Today 190(1):89–97. https://doi.org/10.1016/j.cattod.2012.02.050

98. Chen W, Fang Y, Li K, Chen Z, Xia M, Gong M et al (2020) Bamboo wastes catalytic pyrolysis with N-doped biochar catalyst for phenols products. Appl Energy 260:114242. https://doi.org/10.1016/j.apenergy.2019.114242

99. Cao X, Harris W (2010) Properties of dairy-manure-derived biochar pertinent to its potential use in remediation. Bioresour Technol 101(14):5222–5228. https://doi.org/10.1016/j.biortech.2010.02.052

100. Michael I, Frontistis Z, Fatta-Kassinos D (2013) Removal of pharmaceuticals from environmentally relevant matrices by advanced oxidation processes (AOPs). In: Petrovic M, Barcelo D, Pérez S (eds) Comprehensive analytical chemistry, vol 62. Amsterdam, Elsevier, pp 345–407

101. Blaney L (2014) Ozone treatment of antibiotics in water. In: Ahuja S (ed) Water reclamation and sustainability. Elsevier, Boston, pp 265–316

102. Ouyang D, Chen Y, Yan J, Qian L, Han L, Chen M (2019) Activation mechanism of peroxymonosulfate by biochar for catalytic degradation of 1,4-dioxane: important role of biochar defect structures. Chem Eng J 370:614–624. https://doi.org/10.1016/j.cej.2019.03.235

103. Zhang R, Li Y, Wang Z, Tong Y, Sun P (2020) Biochar-activated peroxydisulfate as an effective process to eliminate pharmaceutical and metabolite in hydrolyzed urine. Water Res 177:115809. https://doi.org/10.1016/j.watres.2020.115809

104. Diao Z-H, Dong F-X, Yan L, Chen Z-L, Qian W, Kong L-J et al (2020) Synergistic oxidation of bisphenol A in a heterogeneous ultrasound-enhanced sludge biochar catalyst/persulfate process: reactivity and mechanism. J Hazard Mater 384:121385. https://doi.org/10.1016/j.jhazmat.2019.121385

105. Chen Y-d, Bai S, Li R, Su G, Duan X, Wang S et al (2019) Magnetic biochar catalysts from anaerobic digested sludge: production, application and environment impact. Environ Int 126:302–308. https://doi.org/10.1016/j.envint.2019.02.032

106. Li Z, Sun Y, Yang Y, Han Y, Wang T, Chen J, Tsang DCW (2020) Biochar-supported nanoscale zero-valent iron as an efficient catalyst for organic degradation in groundwater. J Hazard Mater 383:121240. https://doi.org/10.1016/j.jhazmat.2019.121240

107. Li X, Jia Y, Zhou M, Su X, Sun J (2020) High-efficiency degradation of organic pollutants with Fe, N co-doped biochar catalysts via persulfate activation. J Hazard Mater 397:122764. https://doi.org/10.1016/j.jhazmat.2020.122764

108. Xu L, Wu C, Liu P, Bai X, Du X, Jin P et al (2020) Peroxymonosulfate activation by nitrogen-doped biochar from sawdust for the efficient degradation of organic pollutants. Chem Eng J 387:124065. https://doi.org/10.1016/j.cej.2020.124065

109. Ding D, Yang S, Qian X, Chen L, Cai T (2020) Nitrogen-doping positively whilst sulfur-doping negatively affect the catalytic activity of biochar for the degradation of organic contaminant. Appl Catal B Environ 263:118348. https://doi.org/10.1016/j.apcatb.2019.118348

110. Duan X, Zhang C, Wang S, Ren N-q, Ho S-H (2020) Graphitic biochar catalysts from anaerobic digestion sludge for nonradical degradation of micropollutants and disinfection. Chem Eng J 384:123244

111. Ahmad M, Lee SS, Dou X, Mohan D, Sung J-K, Yang JE, Ok YS (2012) Effects of pyrolysis temperature on soybean stover-and peanut shell-derived biochar properties and TCE adsorption in water. Bioresour Technol 118:536–544

112. Chen X-L, Li F, Chen H, Wang H, Li G (2020) Fe2O3/TiO2 functionalized biochar as a heterogeneous catalyst for dyes degradation in water under Fenton processes. J Environ Chem Eng 8(4):103905. https://doi.org/10.1016/j.jece.2020.103905

113. Lu L, Shan R, Shi Y, Wang S, Yuan H (2019) A novel TiO2/biochar composite catalysts for photocatalytic degradation of methyl orange. Chemosphere 222:391–398. https://doi.org/10.1016/j.chemosphere.2019.01.132

114. Xu X, Huang H, Zhang Y, Xu Z, Cao X (2019) Biochar as both electron donor and electron shuttle for the reduction transformation of Cr (VI) during its sorption. Environ Pollut 244:423–430

Biomass Conversion and Green Chemistry

Avinash Ammanagi, Praveen Satapute, Shakeel Ahmed Adhoni, Shivakantkumar S. Adhikari, Sanjay Kumar Gupta, and Sikandar I. Mulla

Abstract Chemicals and biofuels can be obtained from biological systems (biomass). Currently, biomass expenditures should be decreased by planning alternate methods and catalytic arrangements, because those used for hydrocarbons have not been efficiently adapted for the molecular structures of biological compounds. To avoid competitiveness with food sources, lignocellulosic feedstocks must to be used differently for expected yields, mostly in the biological production of fuel. A valuation of the life-cycle of feedstocks should be completed to determine environmental impacts and can be used as a exploratory tool for the development of products. Reasonable and modern advance needs nearing destruction, practical incomes of life. For the development of sustainable, low-cost, natural, basic materials, novel approaches in research, manufacturing, and the economy are crucial. This chapter focuses on cost-efficient tools and processes to convert biomass into valuable biological fuels and bioproducts, with particular emphasis on biorefinery concepts to create the diverse feedstocks that are used to manufacture high-value products. This chapter also explores the biological characteristics of developments, because the use of renewables as raw materials does not exempt them from green chemistry principles.

Keywords Biomass · Biofuels · Biorefinery · Green chemistry

Avinash Ammanagi and Praveen Satapute contributed equally to this work.

A. Ammanagi · P. Satapute · S. A. Adhoni · S. S. Adhikari
Department of Biotechnology and Microbiology, Karnatak University,
Dharwad, Karnataka, India

S. K. Gupta
Environmental Engineering, Department of Civil Engineering, Indian Institute of Technology
Delhi, New Delhi, Delhi, India

S. I. Mulla (✉)
Department of Biochemistry, School of Applied Sciences, REVA University,
Bangalore, Karnataka, India
e-mail: sikandar.mulla@reva.edu.in

1 Introduction

Much research has focused on the expansion of coal, petroleum, and gas-based plants to supplement fossil fuel feedstocks. The feedstocks are used in industries to harvest numerous materials such as biofuel, soap, pesticides, waxes, and coke. [1, 2]. Currently, assets of fossil fuels are not considered to be financially feasible or eco-friendly [3]. Petroleum derivatives are major contributors to the collective carbon dioxide (CO_2) level in the environment, which is recognized to contribute to climate change [4]. The adverse effects of greenhouse gas (GHG) discharge in the atmosphere, combined with deteriorating fuel reserves, have persisted. Henceforth, the search for acceptable, biologically harmless, and cost-effective sources of energy for industrial users and consumers has been become crucial in recent years [5]. Consequently, there is great interest in the creation and utilization of biofuels from terrestrial plants and other waste materials.

Biological fuels produced from ecofriendly materials can help to decrease petrochemical and CO_2 emissions. Biofuels created from terrestrial plants and organic materials can reduce the world's oil dependencies and carbon dioxide creation. These biological fuels may reduce carbon dioxide release because the terrestrial plants absorb CO_2 as they grow [6]. Hence, researchers are investigating new industrial stocks and green practices to harvest these complexes from ecological biomass assets [7].

Some biological fuels can address CO_2 emissions and support progress in urban energy safety. However, there are concerns with sourcing raw materials, effects on biodiversity and land practices, and problems with agricultural yields. Biodiesel can be combined with petroleum-based ingredients, combusted in internal combustion engines, and circulated through existing or new technology, such as flexible fuel vehicles. First-generation biofuels are currently manufactured at 50×10^9 L annually. Additionally, biogas has resulted in the anaerobic management of compost as well as additional mass resources. However, the amount of biological gas used for transport has been decreasing [4], although first-generation biofuels appear to be trusted by experts. The main weakness of first-generation biofuels lies in the food-versus-fuel debate: one of the reasons for increasing food rates is due to the increased creation of these fuels [8]. Moreover, biodiesel is not a cost-effective technology to reduce GHG emissions. Therefore, other ecological and conventional technologies are needed to decrease GHG emissions [9].

Consequently, lignocellulosic feedstocks are being investigated as novel second-generation biofuels [10]. These biofuels are created from the biomass of plants, mostly from lignocellulosic sources. This makes up the majority of the low-cost nonfood resources obtainable from plants. Nonetheless, at present, the creation of such fuels is not profitable. There are numerous practical problems that need to be overcome before their potential can be understood [9]. Plant biomass is one of the richest and most exploited organic raw materials on the earth. For basic needs, the raw material can be merely burned in order to generate heat and electricity. Plant raw materials are excessively used in production of liquid biofuels these days.

However, biofuel creation from intermediate products can supplement the increasing demand for liquid fuels. This has attracted attention in expanding the use of biomass crops as feedstock for biofuel creation [11]. It is estimated that second-generation biological fuels could meaningfully decrease CO_2 emissions, do not compete with nutrition crops, and may improve machine performance. Once commercialized, the rate of second-generation biological fuels will likely be similar to regular gasoline and would be the most cost-effective path to renewable, lower-carbon energy for vehicles [4, 61]. The methods for the expanded use of biomass are reasonable, with all parts of the plant (such as leaves, bark, fruits, and seeds) being used as valuable products.

In 1990, the term "biorefinery" was originally recognized by the National Renewable Energy Laboratory to indicate the use of biomass to create fuels and further bioproducts. This term denotes a group of facilities that creates resources or fuel goods [12]. The system of a biorefinery comprises biomass creation, biomass alteration/processing, and end use. Global biomass creation is approximately 100×10^9 tons of organic dry biomass per year. Some is recycled as food and manufacturing raw resources, whereas food usage is only 1.25% of the complete terrestrial biomass. Leftover biomass can be discarded into the ecosystem and recycled as raw material for chemical manufacturing.

2 Biomass as Multiple Feedstocks for Biorefineries

Biomass from agro-timberland, amphibian plants, and yields is an important multi-purpose ecological feedstock for chemical manufacturing[13, 14]. Through photosynthesis, plants transform CO_2 and water into various metabolites, which together are critical biochemicals. The primary metabolites are sugar and lignin. The subordinate metabolites are high-value biochemicals, such as waxes, elastics, steroids, terpenoids, fatty substances, and terpenes, which occur in low amounts in the plants [15]. The subordinate byproducts can be utilized for the formation of high-value synthetic substances, using combined preparation strategies. Advances in biomass manufacturing require massive endeavors to improve biomass creation, modification, and resulting bio-based items [6]. However, such achievements are dependent upon current knowledge on modifying fossil fuels to organic waste resources. Thus, numerous researchers are investigating these topics, including the re-evacuation of hemicellulose and other significant synthetics, ethanol division, and dried up. Potential separation methods for biorefineries include refinement with ionic fluids and hyperbranched polymers, adsorption with sub-atomic sifters, and bio-based adsorbents. Clark et al. [16] used green innovation to modify low-value, undesirable biomass into synthetics such as waxes and ethanol. Chew et al. [17] investigated different synergist methods for the production of biofuels in a trademark oil in Malaysia. Inedible oilseeds such as *Jatropha curcas*, raised erucic mustard, *Pongamia glabra* (*Pongamia pinnata*), unpracticed canola seeds, and microalgae can be used for biofuels containing diesel, whereas marine biomass can be used for bioethanol and biodiesel [61].

2.1 Biorefinery Concept/System

The biorefinery structure relies upon biomass as the planning input (feedstocks) for the production of various bio-based items [18, 19]. The major aim of a biorefinery system is to create biofuel and engineered materials from biomass. Previous studies focused on three types of biorefineries: sustained feedstocks, quantity based adaptabilities and element. The first type deals with limits and use of dry grain as feedstock to make ethanol, dried distillers' grain, feed yields, and carbon dioxide. The second type of biorefinery uses a comparative feedstock and has more technical adaptabilities than the first type. It can make starch, high-fructose syrup, ethanol, carbon dioxide, dried distillers' grain, and corn oil. The third kind of biorefinery is commonly top tier and uses a mix of biomass feedstocks and to manufacture different products using a blend of materials. It may be built using both the high-value/low-volume and low-value/high-volume concepts. Biorefineries comprise three classes—whole crop, lignocellulose feedstock, and green bioprocessing plants—that are in the examination and improvement stages [12]. According to the National Renewable Energy Laboratory, a biorefinery uses biomass change cycles and equipment to produce power and synthetic compounds from biomass. Complex engineering science and innovation are required to create and change biomass [20]. A biorefinery refines and changes organic crude materials into a wide variety of significant items [21, 61].

3 First-Generation Biofuels

Increasing oil costs over recent decades have allowed liquid biofuels to become cost-effective options for transportation. The three main types of biofuels used commercially are biodiesel (bio-esters), ethanol, and biogas. Biodiesel is a substitute for diesel and is made through the transesterification of plant oils and fats, with minimal engine alterations. Bioethanol, which is a complete substitute for gasoline in flexi-fuel vehicles, is created through the maturation of sugar or starch. Bioethanol can similarly fill in as feedstock for ethyl tertiary radical ether (ETBE) when blended with gas. Biogas (biomethane) is a fuel that can be reused in gas vehicles with minor adaptations. It is generally conveyed through anaerobic osmosis of liquid compost and another absorbable feedstock. At present, biodiesel, bioethanol, and biogas are made from resources that are also used for food. However, the demand for edible oils is increasing, so it is difficult to use green food crops for biofuel creation [22]. Some harvests are used for biodiesel creation, which can be taken up as industrial yields on wasteful land. Such multipurpose uses for oilseed yields will occur when their biomass can be utilized for the production of various bio-based products [61].

3.1 Conversion Processes for First-Generation Biofuels

3.1.1 Transesterification

The fatty acid methyl esters (FAME) in biodiesel are attracting attention as a diesel fuel substitute or extender. Biodiesel is created using a number of common sources, such as vegetable oils and animal fats, by artificially reacting oil or fat with alcohol inside a homogeneous and heterogeneous catalyst. The product of the reaction is a mix of methyl esters that comprise biodiesel, as well as glycerol (which is a high-value co-product) [23, 24, 61].

Homogeneous Catalysis

Transesterification is a reversible reaction in which the forces could be a liquid destructive or a liquid base. The strategy is known as transesterification [61].

Heterogeneous Catalysis

A goal is to attain a fundamental transesterification method for prime free fatty acid (FFA) oil and reduce the modification of emollient to a methyl group organic compound through a chemical reaction. The use of solid catalysts is recommended for high free fatty acid-containing oil [23]. The solid acid catalyzes biological fuel production by co-occurring transesterification and esterification of quality oil containing high FFA, as performed by Kulkarni et al. [23]. The retort mechanism of co-occurring transesterification and esterification is through a Lewis acid. The esterification takes place between free fatty acids (RCOOH) and wood alcohol (CH_3OH), whereas transesterification takes place between lipids and wood alcohol adsorbate on acidic site (L+) of the catalyst surface. The interaction of the carbonyl O of free fatty acid or monoglyceride with acidic constituents forms carbocation.

Transesterification will be protracted to triglycerides and diglycerides. Transesterification may be a stepwise reaction. Within the reaction sequence, the lipid is converted stepwise to di glyceride and monoglyceride and finally alcohol. The tetrahedral intermediate reaction eliminates diglycerides, monoglycerides, and alcohol once triglycerides and monoglycerides are available to contact with the acidic sites, respectively, to allow one mole of organic compound ($RCOOCH_3$) in every step. In this case, esterification and transesterification manufacture methyl group esters, an equivalent final product. The catalyst is regenerated in the cooccurring esterification and transesterification reactions [23].

3.2   Whole-Crop Biorefinery

A whole-crop biorefinery uses the full crop to obtain useful products. Raw materials such as oilseed are used as feedstock within the operations of a full-crop biorefinery. Rosid dicot genus seeds contain 35–40% oil and 1–1.5 tons of oil are created per angular distance [28, 61]. The method of changing biomass into energy is characterized by the alteration of biomass into totally different elements that are then conserved singly. The oil initially acts as the starting point for fuel manufacturing or undergoes chemical modification to produce oleochemical products, whereas the de-oiled cake is used after purification because of the basic raw components for the synthesis of valuable chemicals or for chemical action.

3.2.1   Oleochemicals

Oleochemicals are converted to fabricated materials from the ordinary oils and fats of plants and animals. Essentially, oleochemicals are unsaturated fats and alcohol obtained from cutting off the fatty oil structures of oils and fats. In any case, these subordinates are jointly treated by altering the carboxylic destructive array of unsaturated fats by engineered or natural strategies, and various mixtures obtained from any reactions of these auxiliaries. Oleochemicals are mainly fundamental oleochemicals such as unsaturated fats, oily methyl pack esters, oily alcohols, oily amines, and alcohol. Until the 1980s, approximately 95% of trademark oils and oils were used in food products, with a small percentage used in non-food applications such as chemical manufacturing and drying oils. In the 1980s, oleochemicals found wide use in food and non-food applications, including as "engineered blends"'from fossil oils or petrochemicals. Currently, oleochemicals are used in the creation of food products and quality fats, chemicals, cleaning agents, oils, surface coatings, polymers, and biofuels. On a basic level, oleochemicals should supersede petrochemicals considering their applications [29]. Oleochemicals are obtained from manageable resources, whereas petrochemicals are procured from nonessential or nonrenewable fossil oil. Secondly, products derived from oleo processed mixtures are extremely short and thus do not pose a danger to the environment. Thirdly, the additional imperative for source derived from fossil oil sources is to cause higher spikes in harmful substances such as NO_x, SO_2, CO, and hydrocarbons.

3.2.2   De-oiled Cake

Biomass used for the manufacturing of biodiesel would create millions of tons of extra protein (de-oiled cake). At present, the use of protein for non-food applications is logically limited to the use of auxiliary unsaturated fats. The palatable protein can be utilized for te production of fundamental amino acids for animal feeds and human usage. Some of the nonedible oilseed cakes, such as jatropha, neem, and

karanja, can be used to make biopesticides and amino acids for non-food applications. Sanders et al. [30, 61] described the utilization of protein-based unrefined materials for the production of 1,2-ethanediamine and 1,4-butanediamine from amino acids. The formation of amino acids from de-oiled cake would increase the production of biofuel crops. 1,2-Ethanediamine and 1,4-butanediamine can be coordinated from amino acids, such as serine and arginine independently. Decarboxylation of serine creates ethanolamine, which is converted into diamine by the development of a soluble base. Arginine can be hydrolyzed to ornithine and urea. Ornithine will produce 1,4-butanediamine after carboxylation. Protein-based surfactants are the most significant smooth surfactants. Because the structure and properties of the amino acids in the surfactants resemble the tissue of the skin's amino acids, they show strong favoritism and fragility on skin. Acyl subordinates from glutamic acid and serine are incredibly suitable for use with customary surfactants. The formation of protein-based surfactants incorporates the hydrolysis of protein with sulphuric acid followed by acylation with RCOCl (R55C12–C18) to produce acyl amino acid sodium salts, which are transformed into acyl esters of amino acids by esterification with oily alcohol [30, 61].

4   Second-Generation Biofuels

Second-generation biofuels are created utilizing biomass in a carbon-neutral or even carbon-negative process with regard to their impact on carbon dioxide emissions. With respect to biofuel creation, the term "plant biomass" implies an extraordinary amount of lignocellulosic material as this makes up most of the nonfood material from plants [11, 31]. In present situation, due to their fair quantity collection of exceptional barriers which need to be resolved before their inactive limit is usually enfolded up. Plant biomass is one of the most available but underutilized natural resources in the world. Plant biomass has the potential for use as liquid biofuel. Plant biomass generally consists of plant cell dividers, which are 75% polysaccharides [32]. These polysaccharides comprise a significant pool of sugars; for example, in traditional food crops such as wheat (*Triticum aestivum*), sugar is contained inside the stems as well as inside the starch of the grains. To date, the ability of many yield stores, like straws and squeezing, to use sugar feedstocks in biofuel creation has not been investigated. In any case, there is great potential to use designated biomass crops as feedstock for biofuel creation [22].

Lignocellulosic materials in feedstocks for biofuels may be obtained either through a reaction and maturation (e.g., bioethanol) or through complex mixtures. Typical resources include short-term crops (e.g., poplar, willow, eucalyptus), grasses (miscanthus, switchgrass, reed canary grass) and stores from the wood trade and agriculture. Advanced biofuels are carbon-based compounds that are directly designed by innovative methods. Bioethanol (advanced) is a full substitute for gas in flexi-fuel vehicles. Through a reaction, sugars are eliminated from the lignocellulosic feedstock, after which the sugars are converted into ethyl alcohol.

Fischer–Tropsch diesel and biomass-to-liquids may be full substitutes for diesel; here, lignocellulosic biomass is volatilized to syngas that is converted into liquid hydrocarbons, mostly diesel and kerosene. Bio-synthetic natural gas may be used in gas vehicles with slight developments; in this case, lignocellulosic biomass is volatilized to syngas that is continuously converted into gas. Bio-dimethyl ether (DME) may be used in diesel vehicles with slight adaptations; for this fuel, lignocellulosic biomass is volatilized to syngas that is continuously converted into DME [33, 61].

4.1 Conversion Processes for Second-Generation Biofuels

There are two main methods for manufacturing liquid biofuels from biomass. The first involves a thermochemical process and different organic chemistry processes. The thermochemical process defines the conversion of biomass into a variety of products by thermal decay and chemical reformation, and basically involves heating biomass in the presence of various concentrations of oxygen. A clear advantage of the thermochemical process is that it will basically convert all organic elements of the biomass, whereas the organic chemistry process focuses mostly on the polysaccharides [11]. The next section focuses on the conversion processes for lignocellulosic biomass and technologies to produce additional chemicals of value.

4.1.1 Physical Conversion

Mechanical Extraction

Vegetable oils can be extracted from oil seeds using a screw press (expeller). The screw press is typically used in two ways: pre-crushing and full crushing. In pre-crushing, only a bit of the oil is recovered; thus, the de-oiled cake (with 18–20% oil) is also treated by dissolvable extraction. Solidified pre-crushing and dissolvable extraction are commonly used for oilseeds with high oil content (30–40%). Full crushing needs 95,000 kPa to press out as much oil as possible—ideally up to 3–5% fat for animal materials. Full crushing may be controlled in during prepress and the last press [7, 61].

Briquetting of Biomass

Agricultural and waste biomass are often difficult to use as biological fuels because of their large and varied structures. This challenge is often overcome by concentrating the residual into stable, consistent shapes. Throughout concentration, biomass is contained in compact chamber presses. There are two major methods of concentration: pressing and drenching. Sometimes, these two processes are combined. In pressing, there is an increase in applied pressure within the original segment of

compression; however, the speed of increase in density decreases as the density of pressed material approaches the density of water. There's no such closed explanation of density and drenched degree that can be cutting, destructive and beating. A rough chopping of some materials could also be as effective as ultrafine grinding. For example, tree branches experience intensive volume reduction once broken, but fine grinding supplies very little, if any, extra reduction in volume [6, 7, 61].

Distillation

Compression is the most important methodology for extracting volatile oil and depends upon isolating volatile compounds. Plant are crushed to encourage them to release their oils. The plants are steam distilled; therefore, the significant oils are released with the steam. The vapors are captured and allowed to condense back to liquid form. Molecular distillation is used to manufacture fragrances that cannot be distilled by standard methods [7].

4.1.2 Thermo-Chemical Conversion

Biomass is converted to energy by two main processes: thermochemical or biological. The thermochemical conversion method includes direct combustion, chemical action, liquefaction, and transformation. Once biomass is heated under chemical-deficient conditions, it generates synthesis gas, or syngas, that consists primarily of a chemical element and carbon monoxide. This syngas is directly burned or further processed for different evaporated or liquid products. During this process, the thermal or chemical conversion of biomass is almost like that of coal [26, 61].

4.1.3 Hydrotreating of Vegetable Oils/Green Diesel

Vegetable oils are renewable feedstocks that can be easily used to manufacture biofuels from biomass resources. Plant oils such as oilseed, soybean, canola, and vegetable can be processed via transesterification into FAME or biodiesel. The future potential of biofuels depends on the development of new procedures to make high-quality transportation fuels from naturally derived feedstocks. These new biofuels must be acceptable for current fuel and transportation technologies to be financially viable. Researchers are investigating the transformation of vegetable oils into high-quality diesel fuel or diesel mix stock that may totally replace gasoline. The paraffin-rich diesel ("green diesel") is created from a sustainable feedstock containing fatty oils and unsaturated fats by creation movement backlog, hydrodeoxygenation, substance change, and hydroisomerization. This natural diesel is pleasant smelling, without sulfur. Inside the device, the fuel properties are modified to satisfy the sensitivities of air in either the pure or emulsified fuel [39]. Green diesel has a higher cetane (One of the most important product qualities for diesel) cost and incredible

contamination properties. It also has extraordinary storage stability and is able to mix well with oil-based diesel fuels. Unlike to carboxylic acid alkyl esters, natural diesel does not depend on food source and system arrangement; thus, the totally deoxygenated biofuel is promptly blended with fuel [61].

4.1.4 Bio-oil

Biological oils are made by a quick transformation method. In this process, organic compounds such as polyose, hemicellulose, and lignin are heated to moderate temperatures (400–600 °C) in the absence of chemicals to supply a liquid product of char (13–25%), gas (e.g., CO, H_2), lightweight hydrocarbons (13–25%), and bio-oil (60–70%). The outcome and chemical components of biological oil depend upon feedstocks and methods used, including the particle size of biomass (2–5 mm), continuance (0.1–2 s), and reactor type. The bio-oil could be used in furnaces and stationary engines. Biological oils have a complex chemical component containing chemicals from lignocelluloses biomass such as open-chain alcohols/aldehydes, furanoids, and pyrenoids. The physiochemical properties of bio-oil are presented in Table 1. These constituents are mixed with water (25–45%) in the transformation method to make an emulsion with organic constituents. Hence, many "green chemicals" are extracted from bio-oil by solvent extraction. Supercritical fluid extraction, such as greenhouse gases, selectively extracts specific chemicals from bio-oil. These chemical compounds are used for plant products, food flavors, wood preservatives, slow-release chemicals, and prescription drugs, among others [40–45, 61].

4.1.5 FT Oil and Motor Fuel from Biomass

Franz Fisher and Hans Tropsch starting investigating the transformation of syngas (CO + H_2) into many common blends in 1923. The syngas made by the manufacturing process for biomass may be converted into a sizable number of normal blends.

Physiological properties	Content
Water content (wt%)	12–30
Carbon (wt%)	40.70–69.50
Hydrogen (wt%)	5.70–9.40
Oxygen (wt%)	19.45–50.30
Nitrogen (wt%)	0–9.80
Sulfur (wt%)	0–0.77
Ash (wt%)	<0.25
pH	2.30–4.50
Viscosity (pa-s)	11.10–62.20 at 25°C
Density (g/mL)	0.95–1.20

Table 1 Physiological properties of biological oil

The procedure for changing the CO and H_2 mix into watery invigorates or hydrocarbons over advanced metal stimuli creates Fisher-Tropsch oil (FT oil); fuel made by the Fischer-Tropsch synthesis (FTS) methodology is that it yields very high nuclear mass waxes, which need to be hydrocracked to give green diesel. The biggest drawback of the FTS methodology is that it yields very high nuclear mass waxes, which need to be hydrocracked to give green diesel. Some of the recent publications exhibit that the use of FT advancement for biomass change to artificial hydrocarbon could moreover be promising and carbon alternative different from conventional fuels. The biomass gasification produces syngas that contains the debased products of biomass, such as sugar (cellulose, hemicellulose) and lignin [33].

The method for biomass gasification of syngas is depicted in Fig. 1. Here, n is the typical length of the normal compound chain and m is the number of particles per carbon. All the reactions are exothermic. The result may be a mix of various hydrocarbons, in which paraffin and olefins are principal segments. In FTS, 1 mol of CO reacts with 2 mol of H_2 in the proximity of a stimulus to make a hydrocarbon chain. The $-CH_2-$ is the construction mass for the longer hydrocarbons. The products of FTS are mostly open-chain hydrocarbons. In addition, extended hydrocarbons and first alcohol is framed in a long time. The item dispersal obtained from FTS handle light regular compound gas (CH_4), olefin (C_2H_4) and alkane (C_2H_5), LPG (C3–C4), fuel (C3), paraffin (C4), gas (C5–C12), diesel fuel (C13–C22), and wax (C23–C33). Some unrefined biomass contains trace contaminants such as NH_3, H_2S, HCl, buildup, and acid neutralizer. The scattering of products depends on the driving force and reaction limits such as temperature, weight, and length [45, 61].
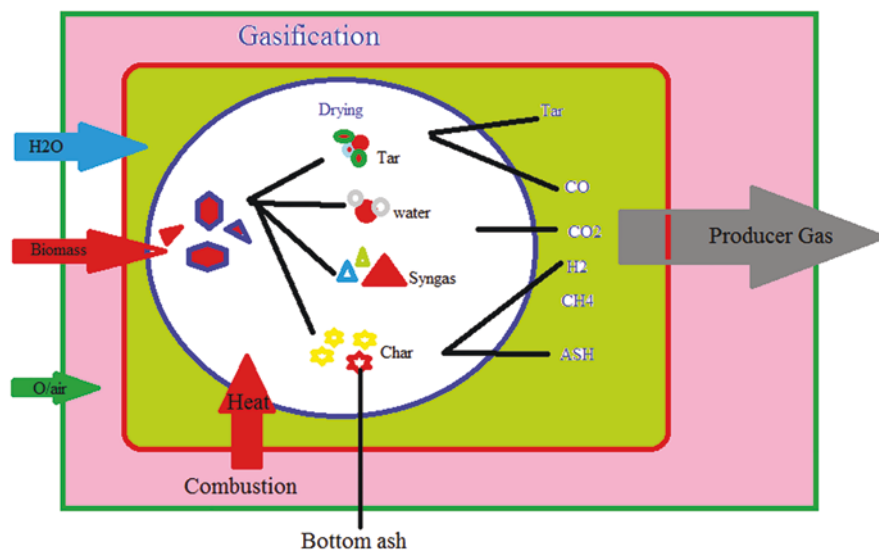
Fig. 1 Process of biogas gasification for syngas

4.1.6   Bioethanol Production from Lignin-Containing Biomass

Biological strategies are maintained by microorganisms and the enzymatic methodology for producing sugars from biomass such as lignocellulosic, starch, and cellulosic. The sugars may later recuperate into alcohol and various solvents that are required for fuel and engineered products. Solid waste has been used to make gas through anaerobic preparations in digesters or swamps. The collective matter of plant materials from corn, sugarcane by biochemical means that has been recently commercially recognized. It is crucial to hydrolyze lignocellulose for biotic change [25–27]. Excellent element manufactured action of lignocellulosic biomass required some assessment and natural system work to increase the yield of alcohol. The modification from biomass feedstock's to liquid fuels such as ethanol requires the level of central unit activities identified with pretreatment, enzyme production, hydrolysis, fermentation, and ethanol recovery. Biomass to ethanol conversion has decreased cost requirements, improved saccharide and hemicellulose conversion to sugar, combined supermolecule and hexose development, less pretreatment requirements, alteration of lignin to worth added yields, and well-organized separation process for alcohol [25, 26].

Agrarian stores, forest development, and industrial food crops produce a great amount of sugar-containing lignocellulosic waste [46, 61]. This lignin-containing biomass has three fundamental parts: saccharide, hemicellulose, and lignin. Cellulose is a crystal-like hexose substance and hemicellulose is undefined polymers of super molecule, arabinose, and mixture compound great polyaromatic mixtures. The change from lignocellulosic biomass to alcohol is progressively extreme for starch-based feedstocks. The conversion from lignocellulosic biomass to alcohol needs a three-step technique: pretreatment of biomass, acid or enzymatic hydrolysis and fermentation/refining. The pretreatment structures separate sugars and engineered blends from the translucent saccharide [47, 61]. The process of steam explosion is an important pre-processing for conversion of lignocellulosic biomass. Biomass samples are sited in a density vessel (i.e. digester) in this procedure and evaporated for a short period (20 s to 20 min) at a temperature of 473–543 K and high pressure of 14–16 bar using saturated steam. By opening the steam, the pressure in the digester is formerly fast dropped and the material is exposed to normal atmospheric pressure to cause an explosion that fragments lignocellulosic biomass. Different machines are used for the steam impact. The eruption of steam reasons the wood hemicellulose and lignin to be decomposed and changed into portions of low molecular weight that can simply be removed. Most of the water soluble portion of hemicellulose can then be removed through enzymatic hydrolysis procedure by water removal down to glucose. At the same, a constituent of lignin's low molecular weight portion is also removed. Xylose can be fermented into ethanol and it is likely to further procedure lignin for the treating of the other fuels. After pretreatment, the crystalline cellulose leftovers solid and ultimately breaks down to glucose by enzymatic hydrolysis. Glucose is additional fermented into alcohol and xylose is changed into the hemicellulose portion. The change of xylose to ethanol is a challenging method, so pretreatment is significant to decrease cellulose crystallinity to

minimalize the average polymerization of cellulose and hemicellulose-lignin sheath nearby the cellulose and to increase the enzyme's available surface area to attack. To create an oxygenated one, ethanol can be mixed with gasoline. Low hydrocarbon fuels and greenhouse gas emissions, there is a rise in such aldehydes, which could cause health problems. Automobiles will run on 5% ethanol/gasoline mixtures without alterations to engine equipment or configuration up to 25%. The fuel properties of mixed gasoline and pure alcohol, big problem with engine processes fuel quality, volatility, octane number with alcohol mixed fuels are fuel quality, hot service, cold start and fuel consumption.

4.1.7   Biochemical Adaptations

Chemical Reaction

The necessary components of a chemical reaction are surface-to-volume ratio, acid concentration, time, and temperature. The surface-to-volume ratio is particularly important; therein, it also standardizes the amount of aldohexose. Therefore, smaller particle sizes result in more hydrolysis in amount and rate of reaction. A greater liquid-to-solid volume ratio results in a quicker reaction [48, 61].

Extraction of Solvent

Solvent removal includes numerous unit operations: removal of the oil from the oil seeds using hexane as solvent; solvent vaporization; oil-hexane mixture distillation (called miscella); and de-oiled meal toasting. Other solvents can be used in special cases; halogenated (mostly dichloromethane) solvents, acetone ethanol or isopropanol. It is also likely to do supercritical extraction using carbon dioxide [7]. Removal refer to a phase in which the unwanted material was removed selectively from the raw materials by allowing the preferred material to be dissolved, finally extracted in the solvent [35, 36]. To remove a specific substance usually biomass removal and separation are also essential. The high molecular weight macromolecules like polysaccharide, cellulose, the main metabolite is called hemicellulose and lignin are found in biomass like wood, wheat straw, aromatic grasses, etc [37, 38]. The other small, next low biochemical molecules such as terpenoids, by volume and high value, secondary waxes, resins, sterols, and alkaloids are known as extractive biomass or metabolities. In the method of biorefinery, intially chemicals are extracted from biomass using solvents.

Dewarte et al. [49] and Clark et al. [16] investigated straw-based biorefineries and high-value products such as waxes, polycosanol, and steroids using fundamental CO_2. Fluid extraction can be used for sweet-smelling woods (cedarwood, sandalwood, pinewood) to isolate extractives. The removed lignocellulosic biomass can be used for engineered reactions and development for the production of biofuels. Dissolvables such as ethanol, $(CH_3)2CO$, methanol, and water isolate the desired extractive from biomass [7, 61].

Supercritical Water Conversion of Biomass

A critical fluid is a substance with temperature and pressure conditions that are higher than its vapor-liquid crossroads (e.g., 644 K and 22 MPa for water; 304 K and 7.4 MPa for greenhouse gas). In some circumstances, a water-like substance is neither fluid nor gas because it does not boil by decreasing the pressure at continuous temperature and does not condense by cooling at constant pressure [50]. The supercritical fluid process of biomass to biochemicals is an alternative route to an acid or catalyst reaction of polysaccharide to sugars. With acid hydrolysis, acid recovery can be a pricey and polluting issue. Catalyst scarification requires pretreatment of lignocellulosic biomass. Critical water will rapidly alter cellulose to sugar and converts biomass into a mix of oils, organic acids, alcohol, and alkane series. Close to the vital state (523–573 K), the acid (H+) and base (OH−) elements of water are separate and dissolve within the biomass. The dissolved critical water breaks the bonds of polysaccharide and hemicellulose apace to supply small sugar molecules, glucose, and carbohydrates [51, 52]. Such characteristics make supercritical water very promising reaction medium without the use of any conversion catalyst biomass for added value items [53, 61].

5 Types of Biorefinery

5.1 Green Biorefinery

A green biorefinery is a system of multiple products that manages its cuts, goods, and fractions of refineries in compliance with the physiology of the corresponding material of the plant as defined by Kamm and Kamm [21] and Fernando et al. [12]. A natural biorefinery uses trademark wet feedstocks obtained from untreated items such as grass, fresh plants, or natural harvests. The plant treats the fresh biomass using wet-fractionation to obtain a fiber-rich press cake and an enhancement-rich solution. Cellulose, sugar, valuable dyes and pigments, crude medicines and other organics are included in the press cake, while protein, free amino acids, organic acids, colorants, enzymes, hormones, other organic substances and minerals are included in the green juice. The cake can also be used for fresh feed pellets, as an unrefined material for engineered products, as levulinic acid, and for changes to syngas and synthetic fills [61].

5.2 Forest and Lignocellulosic-Based Biorefinery

Lignocellulosic materials contain two types of polysaccharides, cellulose and hemicellulose, and lignin. Lignocellulosic biomass (LCB) has three main components: (1) hemicellulose, a pentose sugar; (2) a polysaccharide that is an aldohexose compound; and (3) a polymer that consists phenolic compounds [54]. LCB principally

uses strong plant materials obtained from mistakes or common waste. The material is isolated into its three parts (hemicellulose, cellulose, and lignin) by assimilation or a driving force reaction. Hemicellulose and polysaccharide are made by a solvent and sulfite (acidic, bisulfite, etc.). The sugar polymers (cellulose and hemicellulose) are restored through the reaction. Any hemicellulose contains extended chains of sugars, with five-carbon sugars (typically D-xylose and arabinose), six-carbon sugars, and uronic acid. The reaction of the polysaccharide to aldohexose is completed either by desire technique or combination quantity that produces stable products such as ethyl alcohol, carboxylic acid, propanone [$(CH_3)_2CO$], and butanol. The hemicellulose and polysaccharide components have various usages. Some undesirable materials extend the LCB, such as the utilization of polymers as fuel. The polymer stage contains critical proportions of mono-fragrant hydrocarbons that may change the basic process. The final products include a wide range of substances, engineered solution, materials, and power sources. As such, five stages are proposed: sugar stage, thermochemical or syngas stage, biogas stage, carbon chains, and plant stock [61].

5.3 Aquatic or Algae-Based Biorefinery

Green development uses microorganisms that convert sunlight, water, and carbon dioxide to lipids or triacylglycerol. The lipids may include polar lipids, wax esters, sterols, hydrocarbons, and phenyl subordinates such as tocopherols, carotenoids, terpenes, quinones, and phenylated pyrrole auxiliaries (e.g., chlorophylls). Algae have high improvement rates and resistance to fluctuating biological conditions, with an ability to live and reproduce in high-saline water [6]. This characteristics has allowed algae to be used in slop treatment. In addition, they need high carbonic acid gas thorough and fixation, so they can be utilized to reduce CO_2 release from power plants and different endeavors with high carbon dioxide surges [55]. Algae or cyanobacteria can be used in bioreactors to reduce carbonic acid emissions from power plants and as green development biomass for oil extraction and biodiesel creation. Green development uses unsaturated fats for the esterification of glycerol, mainly lipids with 5–20% of their dry cell weight (DCW). Unsaturated fats may have medium-chain (C10–C14), long-chain (C16–C18) or very-long-chain (C20) carboxylic acid auxiliaries.

Hydrocarbons and other lipids are found in algae at an aggregate of 5%. *Bortyococcus braunii* has large amounts (up to 80% DCW) of very-long-chain (C23–C20) hydrocarbons, much like those found in oil and investigated as feedstocks for biofuel and biomaterials. The oil substance of some alga species exceeds 80% DWC [56]. Traditional oil crops such as soybean, rapeseed, and palm are commonly used in biodiesel. For example, palm oil yields approximately 6000 l of oil for each genuine quantity; however, microalgae yield approximately 58,700 l/ha of oil [57].

Algae are attractive feedstocks (biofuels and biomaterials) for a biorefinery, for the following reasons:

1. Alga consolidate and store large amounts of lipids/oil (20–50% DCW).
2. They have high advancement rates (1–3 doublings/day).
3. They thrive in high-saline water.
4. Algae live in unusual locations (e.g., deserts, dry and semi-dry land) that do not have all the characteristics of being suitable for standard cultivation.
5. Develop growth supplements like atomic number 7 and phosphorus from the sort of wastewater hotspots (for instance Agrarian getaway, mechanical and metropolitan wastewater).
6. They can isolate carbonic acid from gases emitted from power plants and other sources.
7. They have valuable co-products (e.g., biopolymers, proteins, polysaccharides, hues, animal feed, excrement, and H_2).
8. Algae can be grown in a culture vessel (photo bioreactor) for biomass creation [61].

5.4   Integrated Biorefinery

The previously described biorefinery types are reliant on one change expansion to able mixed manufactured blends. Certain process expansions can be combined to allow more flexibility, such as thermochemical, sugar, and non-stage or current progresses an area unit assisted. Accessory in treatment facilitated biorefinery produces changed stock, that grip power made from thermochemical and bioproducts from the mixture of sugar and particular current change growth stages. A new concept in the biorefinery field is a change of bio-oil, an item from the biomass trans-change that can be coordinated by methods for common endeavors to include other synthetic materials [53]. The advantage of this approach is having one significant system for the allotment and purifying of an item made sector unit starting at set up. This idea is attractive because most oil treatment plants can manage variable feedstocks with the reservation that no two clusters of non-sustainable power source region unit an equal. Bio-oil properties vary with the feedstock; for example, woody biomass has a combination of water, phenolics, two hundredth aldehydes and ketones, alcohols, and 100% spontaneous mixtures [58]. A method called hydrodeoxygenation can convert the bio-oil into a solution with similar properties as the oil subordinate. The deoxygenated bio-oils can be refined in existing oil treatment plants with only minor changes using a hydrodesulfurization technique [59, 61].

6 Environmental Issues: Impact of Biomass Process

Biomass processes should limit waste creation and essentialness usage and to lightly in the stock in uncommon returns. Currently, some techniques do not achieve these objectives. For example, the production of biodiesel by the transesterification of vegetable oils with liquid base catalysts is not an ideal method because of the resulting pollution and waste. This system was introduced for different biofuels in western countries to decrease their oil dependency. Moreover, biofuels are attractive because of their potential to reduce the level of greenhouses gas emissions. However, the ECU Commission (see JRC/EUCAR/CONCAWE report [60]) reported that GHG emission reductions depend on the raw materials, the manufacturing process, and, as such, the resulting byproducts. The initial decline attributed to the introduction of first-generation biofuels was discussed in a report by Crutzen et al. A United Nations office showed that food crops developed with nitrogen-containing fertilizers discharged N_2O at levels 300 times that of carbon dioxide, thus negating the advantages of carbon dioxide reduction [34].

Thus, biofuels are not CO_2-neutral, and observing on the emerging apply here could moreover be no benefit in any respect for lessening initial surge transmissions. The impact of monoculture applies to reasonable variety and land use in making countries was conjointly assessed. It has been suggested that any new biomass manufacturing process for biofuels or bioproducts should undergo a life-cycle assessment (LCA). Quantitative LCA is confounded on account of the whole stock required and possible excellence in effect assessment. LCA should be applied as a decision-making tool prior to implementation and can be valuable even at the exploration stage [62].

7 Conclusions

The chapter discussed first-generation and second-generation biofuel, the construction of biorefineries, the different types of biorefineries, and associated technical challenges. However, increasing concerns about the production of biofuels in terms of their impact on food costs and also the situation has connection to associate degree increasingly unsafe within recent years. The unfortunate result is that biofuel is beginning to generate resistance, notably in poor countries with environmental agendas. The replacement of fossil fuels will occur despite these concerns, but the negative effects of manufacturing biofuels from food should be avoided.

Lignocellulosic-derived fuels have the shortest production time (i.e., second-generation biofuels). However, the immediate use of first-generation biofuels involves provisional changes to use the biofuels. A commitment to biofuels can help the transition to second-generation biofuels be more economically beneficial. However, the technology to use these replacement fuels is still being developed. Biorefineries for lignocellulosic-derived fuels will be able to access a far wider

variety of feedstocks, as well as forest biomass. Therefore, an integrated manufacturing method is desirable. The reactor and catalyst should enhance the effectiveness of the various processes used for bioproducts and biofuel production in a typical biorefinery system.

A main objective of a biorefinery is to provide multiple produce misuse combinations of technologies. Furthermore, chemistry knowledge is required for the manufacturing of bio-based products and biorefinery systems and to implement a combination for the biotechnological and chemical conversion of drugs. These competencies are mainly found in large government or industrial centers. Researchers must be aware of the economic, environmental, social, and moral aspects of this field. Clearly, research and development should be centered on renewable materials that do not compete with food and land use—notably in a way that biofuel production considers. A variety of processes should be developed to address the value, usefulness, and purity of the feedstocks.

References

1. Bender M (2000) Potential conservation of biomass in the production of synthetic organics. Resour Conserv Recycling 30:49–58
2. Demirbas MF (2006) Current technologies for biomass conversion into chemicals and fuels. Energy Sour A 28:1181–1188
3. Kamm B, Gruber PR, Kamm M (2006) Biorefinery industrial processes and products. Status and future direction, vols. 1 and 2. Wiley-Verlay Gmbtt and Co KGaA, Weinheim
4. www.shell.com
5. Mabee WE, Gregg DJ, Saddler JN (2005) Assessing the emerging biorefinery sector in Canada. Appl Biochem Biotechnol 121–124:765–778
6. Osamu K, Carl HW (1989) Biomass handbook. Gordon & Breach Science Publisher, London
7. Stevens CV, Verhe R (2004) Renewable bioresources scope and modification for nonfood application. John Wiley and Sons Ltd., London
8. Laursen W (2006) Students take a green initiative. Chem Eng 774:32–34
9. Eisberg N (2006) Harvesting energy. Chem Ind 17:24–25
10. Simpson-Holley M, Higson A, Evans G (2007) Bring on the biorefinery. Chem Eng 795:46–49
11. Gomez LD, Clare GS, McQueen-Mason J (2008) Sustainable liquid biofuels from biomass: the writing's on the walls. New Phytol 178:473–485
12. Fernando S, Adhikari S, Chandrapal C, Murali N (2006) Biorefineries: current status challenges and future direction. Energy Fuel 4:1727–1737
13. Deswarte FEI, Clark JH, Hardy JJE, Rose PM (2008) The fractionation of valuable wax products from wheat straw using CO_2. Green Chem 8:39–42
14. Haung HJ, Ramaswamy S, Tschirner UW, Ramarao BV (2008) A review of separation technologies in current and future biorefineries. Sep Purif Technol 62:1–21
15. Clark JH (2007) Green chemistry for the second generation biorefinery-sustainable chemical manufacturing based on biomass. J Chem Technol Biotechnol 82:603–609
16. Clark JH, Buldarni V, Deswarte FIE (2006) Green chemistry and the biorefinery: a partnership for a sustainable future. Green Chem 8:853–860
17. Chew TL, Bhatia S (2008) Catalytic processes towards the production of biofuels in a palm oil and oil palm biomass-based biorefinery. Bioresour Technol 99:7911–7922
18. Rowlands WN, Masters A, Maschmeyer T (2008) The biorefinery-challenges, opportunities, and an Australian perspective. Bull Sci Technol Soc 28(2):149–158

19. Koutinas AA, Wang RH, Webb C (2007) The biochemurgist—bioconversion of agricultural raw materials for chemical production. Biofuel Bioproduct Biorefin 1:24–38
20. www.NREL.com
21. Kamm B, Kamm M (2004) Principles of biorefineries. Appl Microbiol Biotechnol 64:137–145
22. www.task39.org
23. Kulkarni M, Gopinath R, Meher LC, Dalai AK (2006) Solid acid catalyzed biodiesel production by simultaneous esterification and transesterification. Green Chem 8:1056–1062
24. Meher LC, Vidyasagar D, Naik SN (2006) Technical aspects of biodiesel production by transesterification—a review. Renew Sustain Energy Rev 10:248–268
25. Shelley M (2006) Alcoholic fuels. CRC Taylor and Francis Group, Boca Raton, FL
26. Lee S, Speight JG, Loyalka SK (2007) Hand book of alternative fuel technologies. Boca Raton, FL, CRC Taylor and Francis Group
27. Shapouri H, Duffield JA, Graboski MS (1995) Estimating the net energy balance of corn ethanol. Agricultural economic report number 721. U S Department of Agriculture, Washington, DC
28. Pradhan RC, Naik SN, Bhatnagar N, Vijay VK (2009) Moisture-dependent physical properties of jatropha fruit. Ind Crop Prod 29:341–347
29. Soon TK (2000) An overview of the Asian oleochemical market. The Second World Oleochemicals Conference, Amsterdam
30. Sanders J, Scott E, Weusthuis R, Mooiboek H (2007) Bio-refinery as the bio-inspired process to bulk chemicals. Macromol Biosci 7:105–117
31. Zabaniotou A, Ioannidou O, Skoulou V (2008) Rapeseed residues utilization for energy and 2nd generation biofuels. Fuel 87:1492–1502
32. Pauly M, Keegstra K (2008) Cell-wall carbohydrates and their modification as a resource for biofuels. Plant J 54:559–568
33. Balat M (2006) Sustainable transportation fuels from biomass materials. Energ Educ Sci Technol 17:83–103
34. Steen EV, Claeys M (2008) Fischer–Tropsch catalysts for the biomass-to-liquid (BTL) process. Chem Eng Technol 31(5):655–660
35. Demirbas A (2004) Current technologies for the thermo-conversion of biomass into fuels and chemicals. Energy Sources 26:715–730
36. Appell HR, Fu YC, Friedman S, Yavorsky PM, Wender I (1971) Technical report of investigation 7560. US Bureau of Mines, Pittsburgh, PA
37. Shafizadeh F (1982) Introduction to pyrolysis of biomass. J Anal Appl Pyrolysis 3:283–305
38. Mohan D, Pitman CU, Steele PH (2006) Pyrolysis of wood/biomass for bio-oil: a critical review. Energy Fuel 20:848–889
39. Kalnes T, Marker T, Shonnard DR (2007) Green diesel: a second generation biofuel. Int J Chem React Eng 5:748
40. Elliott DC (2007) Historical developments in hydroprocessing bio-oils. Energy Fuel 21:1792–1815
41. Ates F, Isikday MA (2008) Evaluation of the role of the pyrolysis temperature in straw biomass samples and characterization of the oils by GC/MS. Energy Fuel 22:1936–1943
42. Scott D, Piskorz J, Radlein D (1993) Yield of chemicals from biomass based fast pyrolysis oils. In: Klass DL (ed) Energy from biomass and wastes XVI. Institute of Gas Technology, Des Plaines, IL
43. Ozbay N, Putun AE, Putun E (2006) Bio-oil production from rapid pyrolysis of cottonseed cake: product yields and compositions. Int J Energ Res 30:501–510
44. Naik SN, Goud VV, Rout PK, Dalai AK (2010) Supercritical CO_2 fractionation of bio-oil produced from wheat-hemlock biomass. Bioresour Technol 101(19):7605–7613
45. Rout PK, Naik M, Naik SN, Goud VV, Das LM, Dalai AK Supercritical CO_2 fractionation of bio-oil produced from wheat-sawdust biomass. Energy Fuel. https://doi.org/10.1021/ef900663a

46. Huber GW, Corma A (2007) Synergies between bio- and oil refineries for the production of fuels from biomass. Angew Chem Int Ed 46:7184–7201
47. Naik SN, Goud VV, Rout PK, Jacobson K, Dalai AK (2010) Characeisation of Canadian biomass for alternate renewable biofuel. Renew Energy 35(8):1624–1631
48. Jensen J, Morinelly J, Aglan A, Mix A, Shonard DR (2008) Kinetic characterization of biomass dilute sulfuric acid hydrolysis: mixtures of hardwoods, softwood, and switchgrass. AICHE J 54:1637–1645
49. Dewarte FEI, Clark JH, Wilson AJ, Hardy JJE, Marriott R, Chahal SP, Jackson C, Heslop G (2007) Toward an integrated straw-based biorefinery. Biofuel Bioprod Bior 1:245–254
50. Saka S, Ehara K, Sakaguchi S, Yoshida K (2006) Useful products from lignocellulosics by supercritical water technologies. In: The second joint international conference on sustainable energy and environment, pp 485–489
51. Sasaki M, Kabyemela B, Malaluan R, Hirose S, Takeda N, Adschiri T, Arai K (1998) Cellulose hydrolysis in subcritical and supercritical water. J Supercrit Fluid 13:261–268
52. www.biorefinery.euroview.eu
53. Serani AL, Aymonier C, Cansell F (2008) Current and foreseeable applications of supercritical water for energy and the environment. Chem Sustain Chem 1:486–503
54. Tyson KS, Bozell J, Wallace R, Petersen E, Moens L (2005) Biomass oil analysis: research needs and recommendations. NREL technical report. http://www.eere.energy.gov/biomass/pdfs/34796.pdf
55. Brown LM, Zeiler KG (1993) Aquatic biomass and carbon dioxide trapping. Energ Convers Manage 34:1005–1013
56. Hu Q, Sommerfeld M, Jarvis E, Ghirardi M, Posewitz M, Seibert M, Darzins A (2008) Microalgal triacylglycerols as feedstocks for biofuel production: perspectives and advances. Plant J 54:621–639
57. Chisti Y (2008) Biodiesel from microalgae beats bioethanol. Trends Biotechnol 26(3):126–131
58. Bridgewater A, Czernik C, Diebold J, Mekr D, Radlein P (1999) Fast pyrolysis of biomass: a handbook. CPL Scientific Publishing Services, Ltd, Newbury
59. Bridgewater AV, Cottam ML (1992) Opportunities for biomass pyrolysis liquids production and upgrading. Energy Fuel 6:113–120
60. http://ies.jrc.ec.europa.eu/wtw.html
61. Naik SN, Goud VV, Rout PK, Dalai AK (2010) Production of first and second generation biofuels: a comprehensive review. Renew Sustain Energy Rev 14:578–597
62. Gallezot P (2008) Catalytic conversion of biomass: challenges and issues. ChemSusChem 1:734–737

Nanostructured Photocatalysts for Degradation of Environmental Pollutants

Shafali, Surinder Singh, and Sushil Kumar Kansal

Abstract Water is the most essential life form on earth and a prerequisite for human survival. Due to manifold anthropogenic and industrial activities, voluminous discharge of diverse organic and inorganic pollutants has blown up into the water bodies. Organic pollutants, in particular, have a major contribution to the degradation of water quality on a vast scale. There is an exigent need for the abatement of these organic contaminants from water and wastewater. There are many conventional techniques of wastewater treatment including sedimentation, filtration, adsorption, reverse osmosis, ion exchange, coagulation and flocculation, and Fenton process. Photocatalysis is a highly efficient technique for the degradation of organic contaminants from water and wastewater. Several semiconducting materials have been used as photocatalysts, including ZnO, WO_3, TiO_2, Fe_2O_3, and ZnS, for the photocatalytic decomposition of multifarious organic pollutants. These semiconducting materials are highly beneficial for their application in the photocatalytic treatment of wastewater due to their favorable properties. They have favorable electronic structure, excellent charge transfer properties, a long lifetime in the excited state, high stability, low cost, and strong capability to absorb light. However, due to the wide gap, their application is limited to ultraviolet region with only 5% of the total spectrum of available solar light. So, modified metal oxide-based photocatalysts have been employed for the effective utilization of a wide visible spectrum of light. To modify and enhance the efficacy of these catalysts, various methodologies such as nano-structuring, metal doping, and genesis of nanocomposites have been engineered. These modified nanostructured photocatalysts provide an effective treatment potential to degrade organic water pollutants. This chapter outlines the potential and efficacy of metal oxide and modified metal oxide-based photocatalysts for the treatment of contaminants from water and wastewater.

Keywords Metal oxide · Organic pollutants · Photocatalysis · Modified metal oxide-based photocatalysts

Shafali · S. Singh (✉) · S. K. Kansal
Dr. S. S. Bhatnagar University Institute of Chemical Engineering and Technology, Panjab University, Chandigarh, India

1 Introduction

Water happens to be the most vital and essential natural commodity for the survival of different forms of life on earth. However, providing access to clean and safe drinking water for everyone has become a daunting task globally [1, 2]. According to an annual report by WHO published in 2018, around two billion people were forced to consume water that is contaminated with fecal material, while 4.5 billion had access to poor sanitation systems [3]. It is estimated by the United Nations that around 1.7 million or nearly 3.1% of worldwide deaths every year are due to the consumption of contaminated water [4]. Globally, more than one-fifth of children die from water-related diseases such as diarrhea under 5 years of age, and about 4500 children get demised every day due to diarrhea [5]. The scarcity of safe drinking water is attributed to the competing and selfish needs of the rapidly growing population which have been overrun by water supplies. It is expected that this issue will become even more serious as the population increases by around two billion by the year 2050 [6]. Besides the increasing population, the rapid release of harmful chemicals by industrialization and anthropogenic activities into the water also have an equal contribution to the scarcity of water. On average, about two million tons of waste including agricultural, sewage, and industrial waste is released into water bodies daily [7, 8]. This dumping of waste leads to the introduction of inorganic, organic, radioactive, and biological pollutants into the water bodies and causes a massive deterioration in the quality of water. Among all these pollutants, organic pollutants, in particular, pose a serious threat to society because they have been widely used in textile, agricultural, and pharmaceutical and other chemical industries. Various types of organic pollutants, such as polychlorinated biphenyls (PCBs), dyes, phenolic compounds, pharmaceutical drugs, cosmetics, polycyclic aromatic hydrocarbons (PAHs), pesticides, and herbicides, have detrimental effects on human health such as cancer, disturbance in the endocrine system, obesity, and reproductive system disorders [9–12]. The effects of these pollutants are not just limited to human health, but entire ecosystems have been disrupted by these pollutants. Marine life, in particular, has been the worst affected with around 50% of the fish species and one-third of the amphibian population reportedly extinct [13]. The removal of organic contaminants from water/wastewater is necessary because of their consistent and tremendously increasing occurrence in water in the present time. They are ubiquitous due to their semi-volatility, meager hydrophilicity, toxicity, bioaccumulation, and non-biodegradability under ambient conditions [12, 14]. Due to the detrimental effects of organic pollutants on all living organisms and the environment, it becomes necessary to remove them from water/wastewater so that the treated water can be efficiently reused for the world's sustainable and economic growth. The problem of shortage of water can be overcome by developing suitable methods and materials which are economic, reliable, and efficient and that can meet the high environmental standards. The conventional water purification techniques like flocculation, activated sludge, biological trickling filters, chlorination, ozonation, filtration, precipitation, sedimentation, coagulation, adsorption, oxidation, distillation,

reverse osmosis, etc. had been employed to remove organic pollutants from water/wastewater, but these methods have some limitations also. These techniques are not sufficient individually to remove a wide spectrum of organic pollutants since most of them are not capable to remove microbes that cause diseases like cholera, typhoid, etc. Also, some of these techniques can only transform the phase of the pollutants and/or lead to the generation of secondary pollution that needs further treatment [15, 16]. Recently, semiconductor photocatalysis has emerged as the most effective technique for the degradation of organic impurities from water/wastewater. This technique is simple, is economical, and can completely mineralize the organic contaminants to non-toxic compounds such as CO_2 and H_2O without the formation of secondary pollutants. The most important and unique features of photocatalysis are usage of solar irradiation, the most abundant source of light, and its conversion into chemical energy for its use for the treatment of water contaminants [17–19]. Several semiconducting materials had been utilized for photocatalytic decomposition of organic impurities. Among them, metal oxides such as TiO_2, ZnS, and ZnO are the most widely used traditional heterogeneous photocatalysts for organic wastewater treatment. They have excellent properties such as good stability, an efficient capability to absorb light, complimentary electronic structure, charge transfer properties, and lifetime in the excited state. However, these catalysts suffer from one major limitation that they have a wide bandgap, so they can utilize the ultraviolet region of electromagnetic spectrum only [20–27]. Since metal oxides have some inherent limitations, physical or chemical modifications in their structure are required to enhance their photocatalytic activity. These modifications or changes in metal oxide catalysts include imparting nanostructure to these materials, doping, and formation of composites with other materials [28–30]. Nanostructure engineering involves reducing the size of the catalyst to a nanoscale, which ultimately changes the material properties tremendously. One major advantage of both the nanostructured materials is excellent recyclability and the ability to regenerate for several cycles [31, 32]. Similarly, the formation of composites and doping methods have also been reported to enhance some properties such as to broaden the light absorption spectrum, reduced recombination of charge carriers, reduced bandgap energy, and high specific surface area [33–36]. Although photocatalysis has emerged as an economical and environmentally friendly sustainable technology, it is yet to fulfill the requirements of the industry. The development of a perfect photocatalyst possessing outstanding photocatalytic efficiency, large surface area, the ability to completely utilize sunlight, and superior recyclability remains, by far, the biggest challenge on the path to its commercialization.

The current chapter aims to describe the overview about the most basic principles of photocatalysis and the role and application of traditional photocatalysts such as metal oxide catalysts in the removal of harmful organic contaminants from water. This chapter also includes discussion on methods to enhance photocatalytic efficiencies such as nanostructure engineering, the addition of external materials or doping, and the formation of composites, and finally, the chapter concludes with potential prospects in the area of photocatalysis.

2 Scope of Photocatalysis for the Degradation of Organic Pollutants

The removal of toxic, burgeoning, and recalcitrant organic pollutants from water has now become an imperative task. Organic pollutants are the pollutants that have the potential to persist for a prolonged time, are produced extensively by industries, have high stability at ambient temperatures and in sunlight, and have a strong resistance to degradation. They have great adverse implications on the human and animal's health, aquatic species, other living beings, and the environment. They can cause cancer, reproductive system disorder, and disturbance in the immune system, affect the growth of children, and cause mutagenic and carcinogenic effects on human health [12, 14, 37]. As a result, the immediate development of an ideal and most reliable treatment method has become an essential need for society at present. To date, many physico-chemical and biological techniques have been explored for the decomposition of organic pollutants from water/wastewater as shown in Fig. 1.

The most commonly used methods are coagulation-flocculation, activated sludge process, membrane process, ozonation, biological treatment, filtration, reverse osmosis, ion exchange, Fenton process, adsorption, and photocatalysis [15, 16]. However, the coagulation-flocculation process is only effective in removing turbidity and color and is unable to remove organic/inorganic pollutants, dissolved impurities, and heavy metals [38]. The activated sludge process has its own sets of limitations such as the formation of loose flocs, high operating costs, sludge expansion, and poor effluent quality [39]. The ozonation process is often used for water disinfection, but it leads to the formation of carcinogenic bromates as byproducts in the treated water and is also an expensive process [40]. Biological treatment is not

Fig. 1 Methods to remove pollutants from water/wastewater
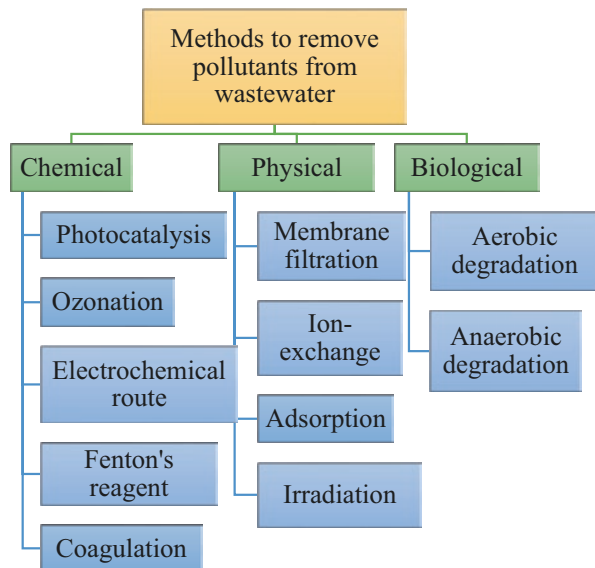
effective in eliminating high concentration pollutants, requires a high level of oxygen and qualified operators, and is unable to remove certain organic pollutants that are resistant to biological degradation [41]. The filtration process can efficiently remove pathogens and turbidity adequately, but has poor response towards the removal of organic materials and also causes the formation of excess amount of disinfection byproducts when chemical disinfectants are added [42]. Membrane processes such as reverse osmosis suffer from the limitation of clogging of pores by the pollutants which makes them inefficient in removing contaminates after a short time. They also produce fouling odor caused by the scaling of colloidal, particulate, organic, and biological pollutants [40]. In the ion-exchange method, the majority of the resins get polluted in the presence of organic materials [43]. The Fenton process produces iron sludge that causes secondary pollution, is an expensive process, requires a narrow working pH range, and includes risks of handling, storage, and transportation of reagents [44]. The adsorption technique is the most widely employed and efficient method for wastewater treatment, but this process has also some major drawbacks like high cost, small capacity, and unsuitable for large-scale applications [45]. Moreover, all these abovementioned methods are not easy to use, i.e., need additional equipments/resins, and are not economic and environmentally friendly as they are only capable of transferring the phase of pollutants from one phase to another. These methods may also produce secondary pollutants that need further treatment and therefore increase the cost of the treatment process [15, 16]. Therefore, we need a method that can meet the essential requirements such as environmentally benign, have a low cost, capable to completely mineralize the parent as well as intermediate pollutants, flexible, highly efficient, and possessing high recycling capacity. Until now, semiconductor-based photocatalysis played an important part in the advanced oxidation processes (AOPs). It is the most reliable and promising approach that can meet all the abovementioned requirements for the decontamination of organic pollutants from water/wastewater [15–19]. The number of publications on environmental remediation using photocatalysis technique has increased productively over the last 16 years. The number of publications was found to have increased ten times in 2002 as compared to 2001, and more than 6000 publications were published during 2017 [46]. Also, the number of publications on photocatalysis displayed a significant increase from 2000 to 2019 as shown in Fig. 2 [47].

2.1 Photocatalysis

It is defined as the chemical reaction involving a catalyst which accelerates the reaction rate, utilizing the solar spectrum. The phenomenon of photocatalysis was initially discovered by the scientists Fujishima and Honda in 1972 during their experiment on splitting of water on TiO_2 electrode [48]. Since then, extensive study and research have been carried out by the scientists for understanding the basic mechanism and parameters affecting photocatalysis so that this technique may be
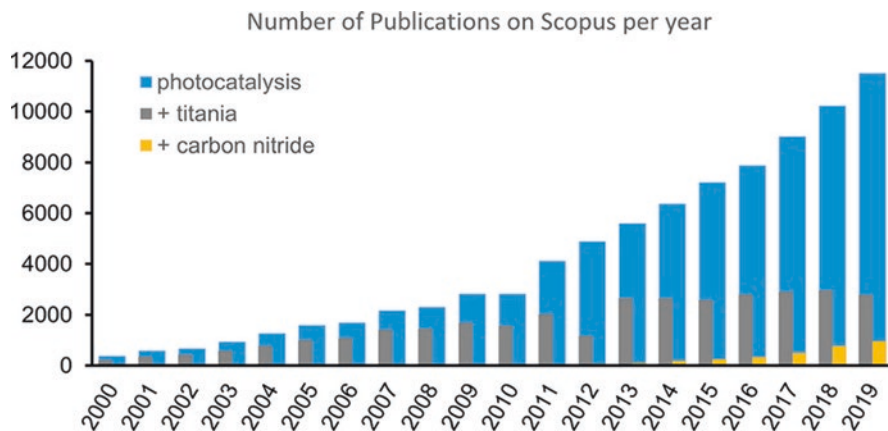
Fig. 2 Histogram of the number of publications on photocatalysis (blue bars) and on photocatalysis with TiO_2 and C_3N_4 (gray and yellow bars, respectively) from 2000 to 2019 (Data source: Scopus March 12, 2020) (Reproduced from Melchionna et al. 2020 [47])

applied to water/wastewater treatment applications. Photocatalysis technique can be categorized into two categories: (1) homogeneous and (2) heterogeneous photocatalysis. During the process of homogeneous photocatalysis, all reagents and photocatalysts are present in the same phase. Commonly utilized catalysts in this process are transition metal complexes, e.g., iron, chromium, and copper. However, during heterogeneous photocatalysis, all reagents and photocatalysts tend to present in different phases. The process includes semiconducting materials like TiO_2, ZnO, SnO_2, etc. However, due to the outstanding properties of the semiconducting materials used in the latter process, it has gained huge attention compared to the former. These materials have exceptional properties such as suitable electronic structure, excellent stability, high absorption coefficients, high ability to generate charge carriers when the light of suitable energy falls on them, biocompatibility, high charge transfer properties, and excited lifetimes of metal oxides. Also, heterogeneous photocatalysis proves to be highly efficient in degrading distinct organic impurities to biodegradable intermediates and also mineralizing them completely to non-toxic carbon dioxide and water molecules by undergoing a suitable photocatalytic mechanism [49–51].

2.1.1 Mechanism of Heterogeneous Photocatalysis

Heterogeneous photocatalytic mechanism incorporates the following basic steps:

1. The electrons from the valence band (VB) of the semiconductor material get transferred to the conduction band (CB) when the light of suitable energy (i.e., equal to or more than the bandgap energy) is incident on the surface of semiconductor.

2. Holes that are generated in valence band (VB) after the transfer of electrons participate in the oxidation of donor molecules and generate hydroxyl (OH·) radicals after reaction with water.
3. The electrons in the conduction band (CB) can react with species of the dissolved oxygen to form superoxide ions. Redox reactions are induced by these electrons followed by successive reduction and oxidation reactions that occur between any species that might have been adsorbed on semiconductor surface. The mechanism of semiconductor photocatalysis is shown by the following schematic, i.e., in Fig. 3.

The formation of radicals is initiated by a series of steps as shown below:

- $TiO_2 + h\nu \rightarrow e^-$(conduction band) $+ h^+$(valence band.).

- $O_2 + e^- \rightarrow \cdot O_2^-$.

- $\cdot O_2^- + H_2O \rightarrow HO_2^-$.
- $H_2O/OH^- + h^+ \rightarrow HO\cdot$.

- $\cdot O_2^- / \cdot O_2H / OH\cdot + $organic pollutants $\rightarrow CO_2 + H_2O$.

The generated $OH\cdot$ and $\cdot O_2^-$ ions play a major role to degrade organic pollutants. Firstly, the pollutants are transferred from the bulk liquid phase (BLP) to the surface of catalyst. Secondly, the surface of the photon-activated photocatalyst is used for adsorbing the impurities on its surface, followed by generation of $OH\cdot$ and $\cdot O_2^-$ radicals which will further degrade the impurities to non-toxic mineralized products, e.g., CO_2 and H_2O. Finally, the intermediates or the final products formed during the
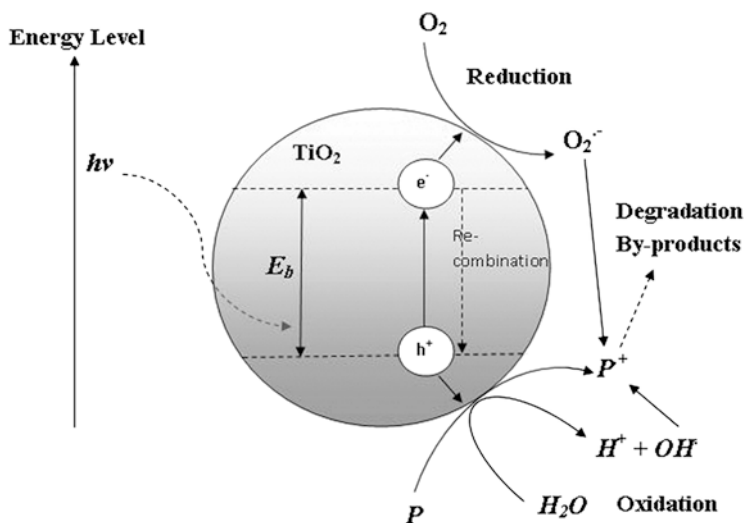
Fig. 3 Photo-induced formation mechanism of electron-hole pair in a semiconductor TiO_2 particle with the presence of water pollutant (P) (Reproduced from Chong et al. 2010 [54])

reaction are desorbed from the catalyst surface and transferred to the bulk liquid phase (BLP) [52–54].

Various catalysts had been discussed in literature by researchers for the degradation of organic contaminants, but only a few of them, which are highly efficient due to their characteristic properties, e.g., metal oxides and their composites, will be discussed in the present chapter to fully understand the potential, applications, and merits of these photocatalytic materials in water/wastewater treatment.

3   Metal Oxide-Based Photocatalysts for the Treatment of Organic Pollutants

To date, a wide variety of photocatalysts have been reported for the treatment of organic species from water/wastewater. Photocatalysts are core of the photocatalysis technique; therefore, the design of an ideal photocatalyst is an essential task. An excellent photocatalyst is one that possesses a remarkable ability to harness visible or UV light coupled with high photocatalytic efficiency and stability towards photocorrosion. In addition to these properties, it also needs to possess biological and chemical inertness, has a low cost, and should be environmentally benign [55, 56]. During the last years, major research has been centered on semiconducting materials like metal oxides to treat wastewater possessing harmful organic impurities. Metal oxide photocatalysts like TiO_2, ZrO_2, ZnO, SnO_2, WO_3, Fe_2O_3, CeO_2, etc. have shown tremendous potential in photocatalysis due to their exceptional characteristics like diverse morphology, composition, structure, and size. Thanks to the electronic structure of these catalysts, due to which they can serve as sensors for light-induced redox processes, absorption of the light by semiconducting materials causes the charge transfer process due to the formation of holes that can oxidize the organic species [51, 57]. TiO_2 and ZnO are, by far, two of the most extensively studied metal oxide semiconducting materials [58–63]. Additionally, Fe_2O_3, SnO_2, and WO_3 are also the commonly used catalysts used for the treatment of organic impurities.

3.1   Discovery of TiO₂ as a Photocatalyst

TiO_2 is a metal oxide that occurs naturally and can be easily obtained from a mineral called ilmenite which is a titanium iron oxide mineral [64]. It can exist in three polymorphic forms: (a) anatase, (b) rutile, and (c) brookite [65]. Rutile happens to be the most commonly utilized and stable type of TiO_2 utilized at high temperatures; however, anatase form is only stable at low temperatures. Brookite form is in-between phase formed during anatase-to-rutile phase transformation. This form is metastable, is uncommon, and rarely exists [64, 65]. The ability of TiO_2 to exist and

to get converted in various physical forms such as powdered TiO_2, dispersed colloidal particles in water, thin films, nanoparticles, nanorods, etc. underlines their possible applications in TiO_2 photocatalytic technology [64].

The groundbreaking work of Fujishima and Honda initially unfolded titania (TiO_2)-based photocatalysis, sometimes quoted as "Honda-Fujishima effect." After that, numerous efforts to explore the photocatalytic properties of TiO_2 have been made. An early attempt on photocatalysis using an aqueous suspension of TiO_2 was initiated by scientists Frank and Bard during the year 1977 for the photo-oxidation of CN^- and SO_3^{2-} ions under sunlight [66]. A report displaying the ability of titania (TiO_2) to reduce CO_2 under visible light further drew the attraction of the researchers towards titania photocatalysts [67]. Since the 1980s, the photocatalytic decomposition of various harmful aqueous and air pollutants using powdered TiO_2 has become the subject of extensive research [68].

3.1.1 Photocatalytic Properties of TiO_2

TiO_2 basically is an n-type semiconductor material with an energy bandgap value ranging from 3.0 to 3.2 eV, the bandgap being low as compared to ZnO and tin oxide (SnO_2) which happens to be 3.35 eV and 3.6 eV, respectively (at about 400 nm wavelength). Thus, light having wavelength less than 400 nm will be required to initiate a photo-reaction using TiO_2 [69–71]. TiO_2, however, possesses remarkably high thermal and chemical stability coupled with its strong UV light absorption capacity that allows it to perform effectively in the degradation of organic pollutants. A strong oxidizing ability, high stability in any pH, hydrophilicity, environmental friendliness, ease of preparation, and high pigmentary properties are some of the other properties that make TiO_2 a great photocatalytic material [67–72]. The ability to yield results over a range of pH values is in stark comparison to ZnO, another widely used photocatalytic material, which can easily undergo corrosion in the acidic medium [72]. An important feature of TiO_2 is that the holes in the VB bear more oxidation potential as compared to electrons of CB. Also, the oxidation potential of VB holes is higher than the normal hydrogen electrode potential (NHE). Furthermore, the conduction band energy (CBE) possessed by TiO_2 catalyst remains higher than the reduction potential of oxygen, O_2 (a predominant electron acceptor), which induces electrons to move towards the conduction band to O_2 which results in the absolute mineralization of organic pollutants to H_2O and CO_2 [73]. Most of the photocatalytic chemical reactions involve water, air, pollutant, and photocatalyst. In terms of photocatalytic activity, anatase type of TiO_2 happens to be more efficient than rutile type because the former has an indirect bandgap as compared to the latter, which has a direct bandgap. As a result, anatase has a longer life, which drives the energetic separation of e^-/h^+ (electron-hole) pairs and inhibits the recombination [74, 75]. Also, position of CB of the anatase phase is such that it can drive more efficient conjugate reactions of electrons [76]. Other approaches, including the combination of rutile-type and anatase-type phases, have been employed to enhance the photocatalytic effect of TiO_2 as the e^-/h^+ recombination rate gets

declines in composite [77, 78]. As the edge of anatase CB is reported to exceed the rutile phase by a bandgap of 0.2 eV which makes the transfer of electrons smooth [79], this results in the jump of anatase electron to rutile phase, hence reducing e^-/h^+ recombination rates and evolution of holes on anatase site [80, 81]. Degussa type P25 TiO_2, containing 75% of anatase, and of 25% rutile part, is one such combination of the two phases of TiO_2 that is well known and has been commonly used commercial catalyst [77]. The photocatalytic efficiency of the TiO_2 greatly relates to charge carriers and surface densities of charge carriers. The e^-/h^+ pairs take a few femtoseconds (fs) to generate. Then within some picoseconds (ps) or nanoseconds (ns), charge carriers that have been induced by light can be trapped [82]. The electron and hole can be recombined in a few tens of nanoseconds [83].

Various TiO_2 photocatalysts got reported for studies related to decomposition of toxic organic pollutants present in aqueous medium. For example, TiO_2 Degussa P-25 was utilized in photodegradation of cationic dye malachite green (MG) under UV light. The as-prepared photocatalyst displayed 99.9% degradation of MG which was observed to decrease with decreasing pH. At low pH, the structure of MG dye got cleaved and so the dye adsorbed with difficulty at surface of the TiO_2, hence producing slow degradation efficiency. Under high pH, several intermediates were formed, and the dye got adsorbed at TiO_2 surface easily, the degradation rate being higher at high pH. Also, rate of degradation of MG dye was found to decrease with increasing catalyst concentration. This is because, at high concentrations of 0.5 g L^{-1}, less active sites got induced by aggregation of TiO_2 particles [84]. The influence of the pH value during photocatalytic treatment of MG using TiO_2 is displayed in Fig. 4.

The photocatalytic degradation of two dyes, i.e., acridine orange and ethidium bromide, under UV irradiation was also performed by using TiO_2 suspensions. It has been found that acridine orange was decomposed completely in 75 min, while ethidium bromide has undergone complete decomposition in 195 min. Further, the comparison of TiO_2 types like Degussa P25, Hombikat UV100, and PC500 was also

Fig. 4 pH effect on the MG photodegradation rate with concentrations of TiO_2 to be 0.5 g L^{-1} and MG to be 0.05 g L^{-1} (Reproduced from Chen et al. 2007 [84])
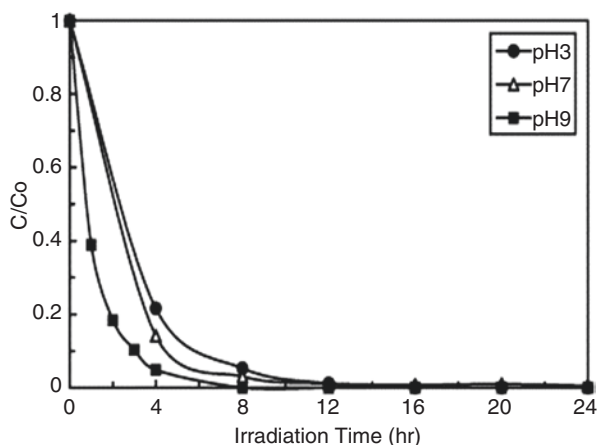
investigated. Degussa P25 was found to display maximum photocatalytic efficiency among the three types. Also, the photocatalytic capability enhanced with enhanced catalyst concentration, but after a particular concentration called optimum concentration, the reverse trend was observed, i.e., efficiency photocatalytic declined. This is because, beyond optimum concentration, the TiO_2 particles would start aggregating resulting in less active sites at surface of TiO_2 [85]. Yang et al. utilized Degussa P25 TiO_2 as a photocatalyst to degrade paracetamol utilizing UV light. Various important factors such as the effect of UV light, initial drug concentration, catalyst dose, pH, oxygen concentration in solution, and intensity of light were explored to determine the optimal set of conditions. Degradation of paracetamol utilizing UV A (365 nm) light was found to be negligible, while significant degradation was observed under UV C (254 nm) irradiation. The degradation rate enhanced with an increase in the intensity of light and oxygen concentration. Amount of drug degraded initially enhanced with an enhancement in catalyst dose but decreased when the loading was further increased. There was a slow rise in the drug degradation rate as the pH was raised from 3.5 to 9.5, and a further enhancement in solution pH beyond 9.5 led to a significant fall in degradation rate. Under the optimized conditions, more than 95% of the drug was degraded within 80 min [86]. Ohko et al. studied the photocatalytic treatment of bisphenol A employing commercially available anatase TiO_2 using UV irradiation. It was found that the adsorption isotherm of bisphenol A followed a Langmuir model and only 4% of the initial pollutant in the solution was adsorbed at surface of photocatalyst till 12 h. Nearly all of the bisphenol A present initially was degraded by the photocatalyst in a time period of 15 h, the degradation process being following the first-order-type kinetics. Another thing observed was the formation of intermediates during the early stages of photocatalytic degradation, and these intermediates were found to have been completely converted to CO_2 in 20 h under UV light irradiation [87].

3.2 ZnO and Its Advantages

ZnO has emerged as an equally good alternative to TiO_2 catalyst for treating organic impurities owing to its marvelous properties such as similar bandgap energy as that of TiO_2. Additionally, it is identical to TiO_2 in the dynamics of charge carriers upon excitation, as well as formation of the reactive oxygen atoms when suspended in the aqueous medium. The reasons behind its utilization as a photocatalyst include high photosensitivity, high redox potential, high thermal and mechanical stability, anisotropic growth, and ease of crystallization. Also, its low production costs, availability in nature in abundance, synthesis versatility with hierarchical morphology, and large bandgap make it hugely popular in photocatalysis [88].

The electron mobility of ZnO is in the range of 200–300 cm^2 V^{-1} s^{-1}, and the lifetime of generated e^-(electron) is greater than 10 s. This makes ZnO having reduced electrical resistance, thus promoting the transfer of electrons with high speed [89, 90]. Also, the valence band possessed by ZnO is located below the valence

band of TiO_2, so hydroxyl radicals generated by ZnO will have enhanced oxidation potential (+3.06 V) when compared to TiO_2 (+2.7 V). While electrons generated from CB of ZnO are found to be more negative than TiO_2 (+2.7 V), the edges of CB of both the catalysts are believed to be located at the same position at the neutral condition of pH (−0.5 V vs. NHE) [91, 92]. Additionally, ZnO has high absorption efficiency over a broad spectrum of solar light than TiO_2. Fenoll et al. in their study investigated the photocatalytic effectiveness of ZnO and TiO_2 in degrading the fungicides in leaching water employing solar light [93]. Comparative study of both ZnO and TiO_2 for the treatment of cyprodinil and fludioxonil fungicides is shown in Fig. 5.

They found that the ZnO was more efficient than TiO_2 because of its non-stoichiometry. The photocatalytic activity was also examined for both ZnO catalyst and P25 TiO_2 catalyst for the treatment of acid brown 14. ZnO showed higher degradation when compared with TiO_2 due to the absorption of more quanta of light [94]. Also, the performance of ZnO catalyst was matched with TiO_2 for photocatalytic degradation of terephthalic acid (TPA) from wastewater using UV light. The degradation rate of TPA using ZnO was much faster than utilizing P25 TiO_2 under optimized conditions [95]. Furthermore, the degradation efficiencies of ZnO catalyst and P25 TiO_2 catalyst were calculated to ascertain decomposition of estrone in aqueous medium using artificial ultraviolet (UVA) and solar irradiation. Under UVA irradiation, ZnO exhibited a three times more degradation rate as compared to P25 TiO_2, whereas under solar irradiation ZnO showed 2.7 times more degradation efficiency when compared to results obtained utilizing UVA irradiation [96]. ZnO was also found to be more capable than TiO_2 in degrading congo red azo dye [97]. Also, it was reported that ZnO displayed better photocatalytic activity for degrading the methylene blue (MB) dye than TiO_2 [98].

3.2.1 Significance of ZnO in the Efficient Removal of Organic Pollutants

The prominent feature of ZnO is that its photocatalytic reactions can be best performed at conditions of neutral pH. Furthermore, its emission properties render it to perform effectively in removing the pollutants from the environment [89, 99, 100], thus allowing the transfer of charge carriers generated by light to the surface in high concentration, which further contributes to the efficient removal of pollutants. Also, ZnO can absorb a significant fraction of quanta of light from a UV spectrum rendering it to perform better in wastewater treatment applications [101]. Moreover, ZnO scatters the light seldomly because of its smaller refractive index (RI = 2.0) as compared to TiO_2 catalyst (RI = 2.5–2.7), which results in boosting the transparency of ZnO [89]. The unique bending of the ZnO surface band in an upward direction in the air indicates that E (electric field strength) which is directed from the inner surface to the outer surface promotes the movement of electrons from the surface to the bulk. The holes move from the bulk to the surface, thus facilitating the adequate separation of e⁻ and holes [99]. Furthermore, immense binding energy of excitons (60 meV) and the defects like oxygen and zinc interstitials, vacancies, and hydroxyl and superoxide ions also enhance the photocatalytic capability of ZnO [101]. ZnO exhibits high photocatalytic capability than TiO_2 for treating organic impurities [93,
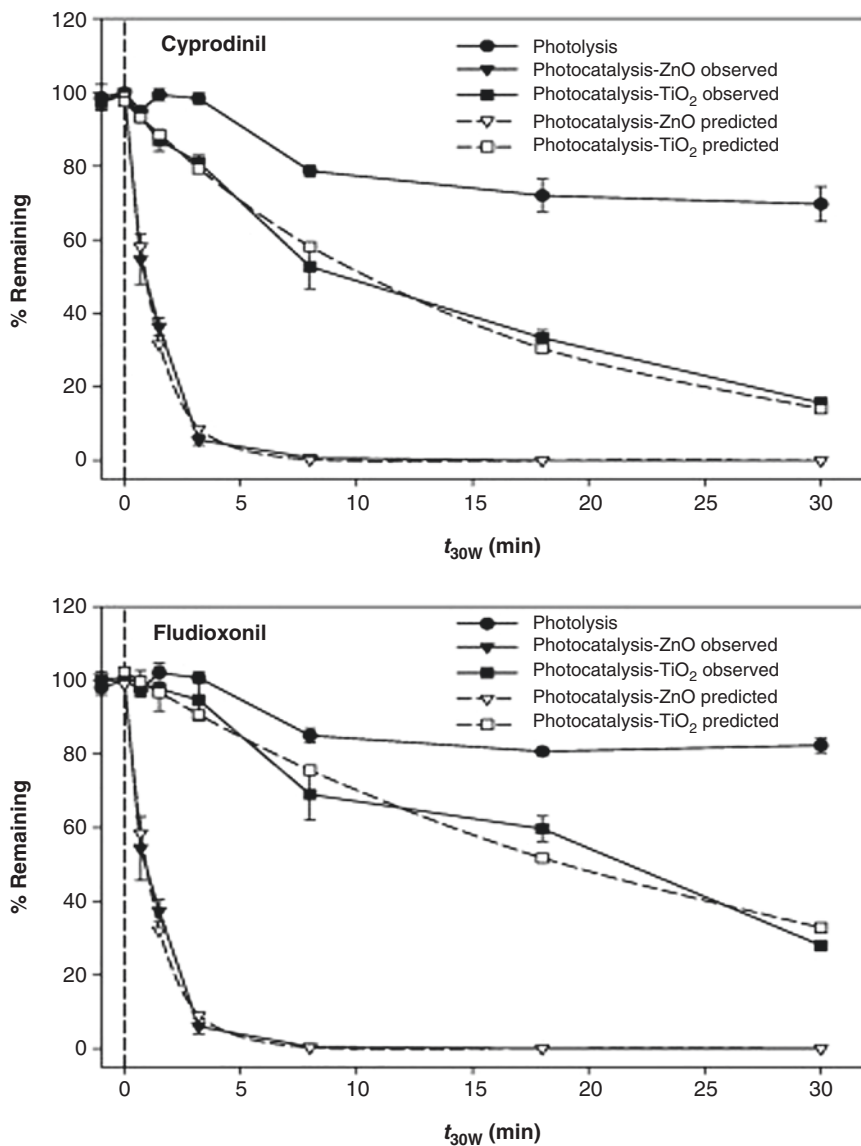
Fig. 5 Disappearance kinetics of cyprodinil and fludioxonil by photolysis (filled circle) and photocatalysis with ZnO (filled inverted triangle) and TiO_2 (filled square) during the photoperiod (as t_{30W}). Error bars denote standard deviation. Predicted kinetics according to a first-order model for photocatalysis experiments are shown, ZnO (triangle) and TiO_2 (square) (Reproduced from Fenoll et al. 2011 [93])

94, 102–106]. Degradation of insecticide diazinon from water under UV irradiation by using ZnO nanocrystals was also reported [107]. ZnO nanocrystals were synthesized by precipitation and calcination method, and maximum degradation rate was achieved with ZnO crystals of mean size of 14 nm. Around 80% of diazinon degraded within 80 min, and the degradation rate was excellent and more than the commercial ZnO catalyst. The enhanced photocatalytic efficiency of the prepared ZnO nanocrystals was due to the reduced size of nanocrystals from 33 to 14 nm [107]. El-Kemary et al. prepared nanostructured ZnO photocatalyst using chemical precipitation method for the treatment of ciprofloxacin (CF) using UV irradiation. The amount of drug degraded enhanced with enhancement in the solution pH in the range 4–10, with maximum degradation of 48% when the pH was 10. Higher degradation efficiencies under basic conditions were ascribed to the formation of hydroxyl ions which possess high oxidation capability. The degradation of drug followed the pseudo-first-order-type reaction kinetics [108]. The absorption spectra and the pseudo-first-order-type kinetics of CF are shown in Fig. 6.

The degradation of phenol was reported using commercially available ZnO under ultraviolet (UV), ultrasound (US), and a combination of UV and US irradiation. Sonophotocatalytic treatment of phenol was much more effective as compared to either photocatalytic or sonocatalytic degradation of the pollutant. Acidic pH and lower reaction volumes were observed to favor sonophotocatalytic degradation of phenol, with 85% of it getting degraded within 120 min. Phenol degradation process exhibited variable kinetics that depend on the pollutant concentration, and presence of anions such as chloride and sulfate could lead to a significant reduction in the amount of drug degraded [109]. ZnO photocatalysts bearing variable molar ratios of oxalic acid to zinc acetate precursors were prepared using sol-gel technique. The synthesized ZnO photocatalysts were explored for the treatment of dyes, e.g., congo red, direct black 38, and methyl orange, employing UV light from aqueous medium. ZnO sampled synthesized with precursor materials in the ratio 4:1 and further calcined at 400 °C exhibited high activity. Acidic conditions were determined to be the most favorable for the treatment of dyes; rates of removal of dyes were found to increase as the photocatalyst dose was increased and declined with enhancement of dye concentration. The photocatalyst was able to degrade 99.70% methyl orange, 97.53% congo red, and 89.59% of direct black 38 dyes in 30 min under UV light irradiation [110].

3.3   Other Metal Oxide Photocatalysts

3.3.1 Fe_2O_3

Recyclability is a very crucial aspect of the performance of photocatalyst. Recently, magnetic separation technology has emerged as the best alternative for the effective separation and recyclability of photocatalyst. Development of efficient catalysts having photocatalytic and magnetic properties has been the focus of researchers. In this context, Fe_2O_3 is being considered the most promising photocatalyst because of
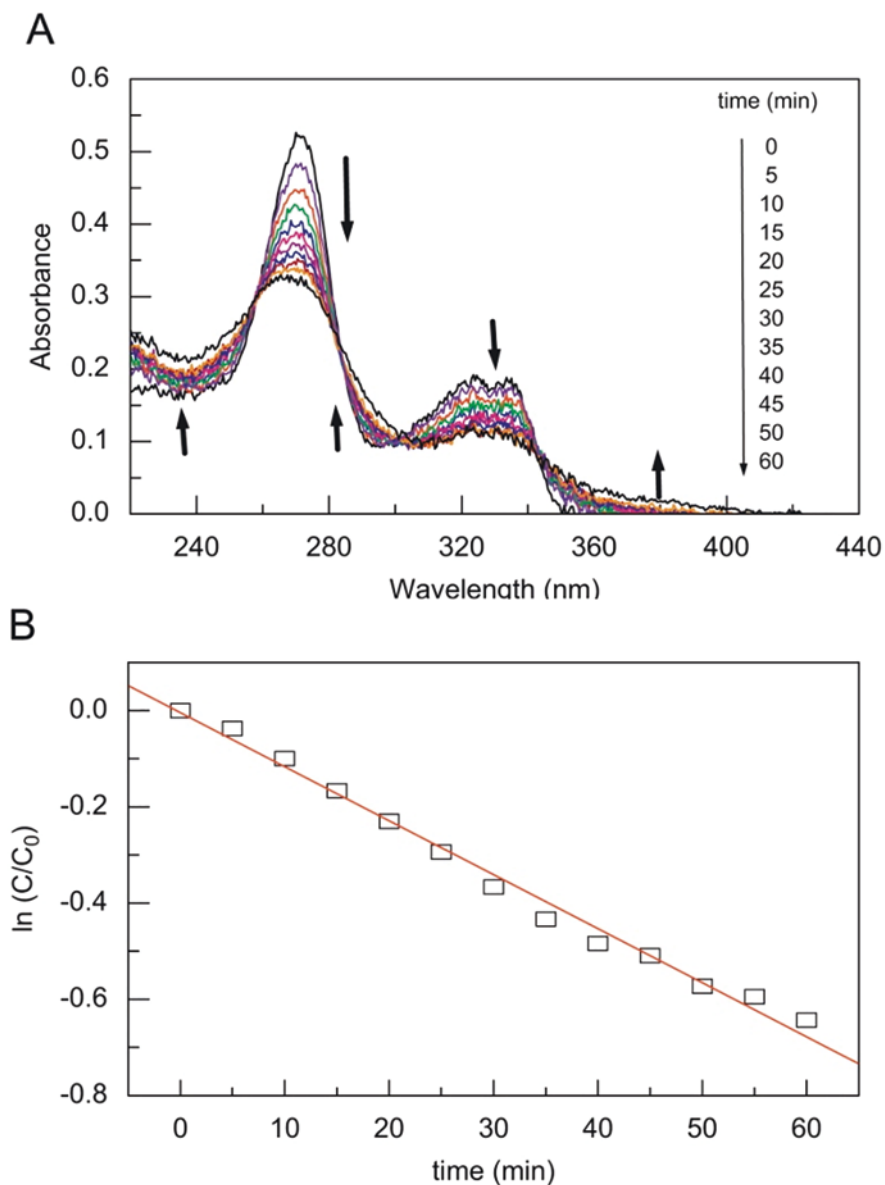
Fig. 6 (**a**) Change of absorption spectra of CF solution of pH 7 during photocatalytic degradation by ZnO nanoparticles and (**b**) pseudo-first-order plot for the kinetic photodegradation of CF in the presence of ZnO nanoparticles (Reproduced from El-Kemary et al. 2010 [108])

its favorable valence state and chemical composition, high resistance to corrosion, low toxicity, narrow bandgap energy (2.3 eV), excellent recyclability, natural availability in abundance, and high chemical stability. Additionally, it can harvest nearly 40% of the abundant solar light and has a saturated magnetization value of 1 emu g^{-1} which helps in the separation of photocatalyst via external magnetic field [111–114]. After absorption of light, generated e$^-$ charge carrier species in Fe_2O_3 initiate chemical reactions through the activation of chemical compounds [115]. Fe_2O_3 catalyst plays a significant role in the separation of photocatalyst from solution and its degradation [116, 117]. Porous Fe_2O_3 nanorods were prepared by chemical solution technique and calcination. The as-synthesized catalyst was used for the photodegradation of methyl orange (MO), p-nitrophenol (pNP), rhodamine B (RhB), eosin B, and methylene blue (MB) utilizing solar light. The photocatalytic efficiency was found to be more efficient than the commercial Fe_2O_3 nanopowder degrading 87.2% of RhB in 180 min and 86.4% of eosin in 210 min. Other dyes were also degraded by Fe_2O_3 nanorods following an order of degradation as RhB > eosin B > MB > pNP > MO. The enhanced photocatalytic capability of prepared photocatalyst was by virtue of its porous nanostructure and larger specific surface area [115]. The photocatalytic degradation plot for RhB utilizing both the catalysts is shown in Fig. 7.

Use of UV laser was reported to be highly effective than conventional UV lamps, as in the study done by Gondal et al. In their work, α-Fe_2O_3 powder was employed for the photocatalytic degradation of phenol under UV laser irradiation. The results were estimated to be more efficient than those measured under conventional UV lamps. Photocatalytic degradation efficiency of phenol was recorded to be 90% in 1 h [118]. Shao et al. prepared ultrathin nanosheets of α-Fe_2O_3 using a dissolution-recrystallization method mediated by silica hydrogel. The prepared nanosheets were then explored using visible light photocatalytic degradation of bisphenol S. It was observed from the results of the study that the as-synthesized α-Fe_2O_3 nanosheets were able to remove 91% of bisphenol S present within 120 min under visible light illumination; by comparison, α-Fe_2O_3 nanoparticles and commercial TiO_2 were only able to degrade 16% and 62% within the same time period. Furthermore, rate constant for degradation of bisphenol S over α-Fe_2O_3 nanosheets was found to be 16.4 and 2.6 times greater than the rate constants obtained for degradation using α-Fe_2O_3 nanoparticles and commercial TiO_2, respectively. Similarly, the quantum efficiency of α-Fe_2O_3 nanosheets was found to be 4.5 and 1.9 times the quantum efficiencies of α-Fe_2O_3 nanoparticles and commercial TiO_2, respectively. The excellent performance of α-Fe_2O_3 nanosheets was attributed to the careful designing of the nanoarchitecture [119].

3.3.2 SnO_2

The structure of SnO_2 is the key to its effectiveness as a photocatalyst. Crystallographic structure of SnO_2 resembles rutile-type phase structure of titania TiO_2 [120]. The structural features of SnO_2 like the octahedral network are an essential prerequisite
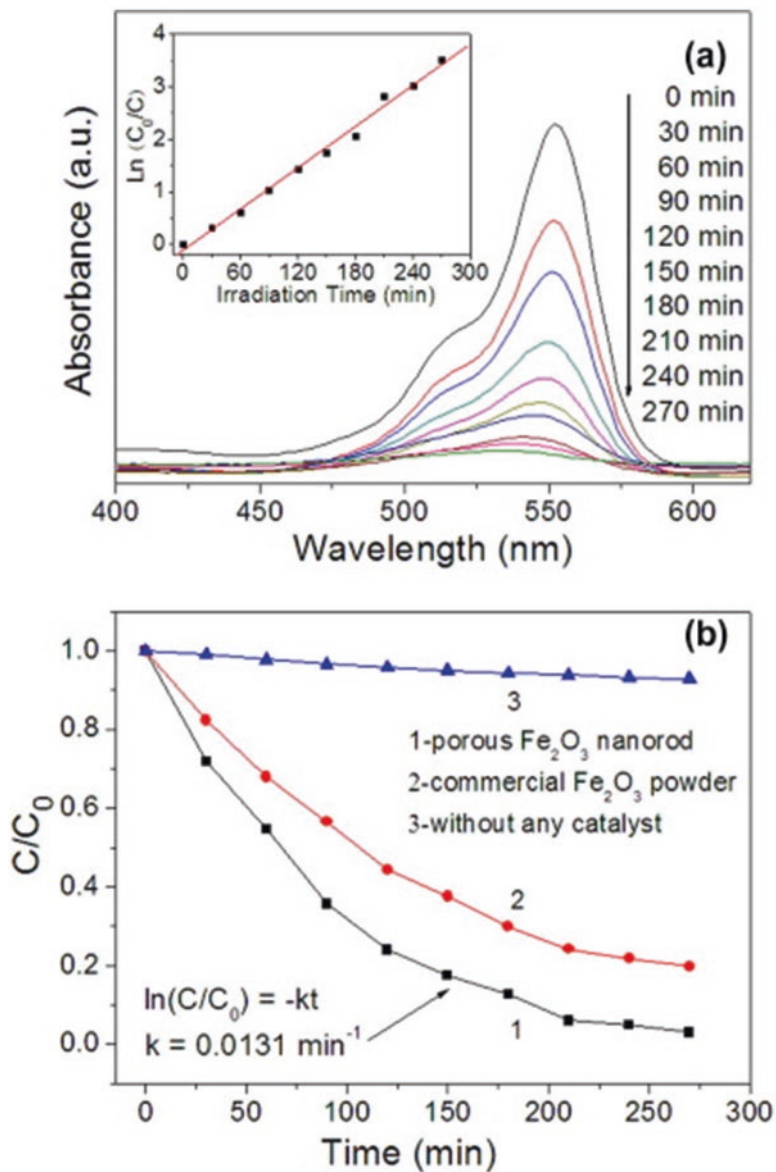
Fig. 7 (**a**) Changes in the absorbance spectra of the RhB in aqueous solution (10 mg/L, 50 mL) in the presence of porous Fe_2O_3 nanorods under the simulated solar light. (**b**) Photodegradation plots of RhB under the simulated solar light for different times in the presence/absence of the catalysts (Reproduced from Liu et al. 2015 [115])

for the high efficiency of photocatalyst as it helps in enabling increased mobility of electron-hole pairs, leading to the increase in probability of electron-hole pairs to reach the reactive sites on the photocatalyst surface [121, 122]. Some other essential properties of SnO_2 are high thermostability and photosensitivity, low cost and toxicity, low electrical resistance, high optical transparency, large bandgap, and high electrical conductivity owing to inherent structural defects [123, 124]. The presence of defects can lead to a significant decline in bandgap, thus enhancing the properties of SnO_2. In this context, more anions of oxygen cause oxidation of Sn from +2 to +4 state, to provide neutrality of SnO_2 [125, 126]. Due to the abovementioned properties, SnO_2 had been employed to treat toxic organic impurities from aqueous medium. Paramarta et al. described the synthesis of SnO_2 nanoparticles prepared using sol-gel technique for the removal of congo red (CR) and methylene blue under ultra-sonication and UV light. The photocatalytic activity was found to be greatly influenced by ultra-sonication irradiation. The sonocatalytic activity was estimated to possess a higher degradation rate, i.e., 48.5% for the dye congo red and 77.1% for the dye MB, as compared to a photocatalytic activity which displayed 32.6% and 64.1% for the dyes CR and MB [127]. Two-dimensional nanoflakes of SnO_2 were prepared employing hydrothermal technique for the sonophotocatalytic treatment of tetracycline hydrochloride utilizing visible light. The prepared nanoflakes of the photocatalyst displayed excellent photocatalytic activity towards tetracycline hydrochloride employing visible light. Furthermore, sonophotocatalytic process was much more efficient in degrading the drug as compared to photocatalysis or sonocatalysis; the sonophotocatalytic route was able to degrade nearly 89% of the drug present initially in 135 min utilizing visible light illumination. The degradation process exhibited pseudo-first-order-type kinetics; furthermore, the results of the scavenger study demonstrated that photo-induced holes along with superoxide radicals exhibited a major role in the sonophotocatalytic degradation of target drug [128]. Viet et al. used SnO_2 nanoparticles synthesized via hydrothermal route degradation of MB dye employing UV light irradiation. The synthesized nanoparticles of the photocatalyst were able to degrade nearly 89% of the initially present pollutant in 30 min utilizing UV light; degradation efficiency, thereafter, grew slowly and reached 90% after 120 min utilizing UV light. In comparison, commercial SnO_2 powder was able to degrade just 20.5% of the methylene blue initially present after 30 min of UV light illumination. When the same study was conducted under direct sunlight, synthesized SnO_2 nanoparticles were able to degrade 79.26% of the pollutant solution in 90 min, while the commercial SnO_2 nanoparticles degraded 36.23% of the pollutant solution in the same time period [129].

3.3.3 WO₃

WO_3 is an oxygen-deficient semiconductor that possesses bandgap energy varying from 2.4 to 2.8 eV. Its bandgap energy differs significantly with the defects or the stoichiometric ratio. It is photosensitive, is inexpensive, exhibits durable stability in various electrolytes, is non-toxic, and displays a higher light absorption coefficient

over a wide area of the solar spectrum (UV-visible). Additionally, it is resistant to photo decay, has a strong capability to convert the photoelectrons, is chemically inert, possesses high mechanical strength, and has long lifetimes of charge carriers [130]. Moreover, WO_3 can reduce charge carriers' recombination rate, exhibits a favorable rate of oxidation, and displays excellent efficiency to absorb light. It is capable of utilizing about 30% of abundantly present solar light. Furthermore, the valence and conduction band positions of WO_3 are favorable to degrade the organic pollutants, and, also, it is efficient to degrade acidic organic compounds because it can persist in the acidic climate for a prolonged time [64]. Three-dimensional WO_3 octahedra were prepared using simple hydrothermal technique for the photocatalytic degradation of MB dye employing visible light. The synthesized sample displayed higher degradation efficiencies as its dose in the pollutant solution was increased, with a photocatalyst dose of 100 mg degrading 95% of the initially present methylene blue in just 60 min. The degradation of MB dye followed pseudo-first-order-type reaction kinetics. Furthermore, it was observed that the WO_3 octahedra displayed a photocatalytic activity that was about 5.33 times more than bulk WO_3; higher photocatalytic activity of synthesized WO_3 octahedra was attributed to good crystallinity, high surface area, sufficient bandgap value, and more catalytically active sites [131]. Huang et al. employed simple hydrothermal route to synthesize nanoplates and hierarchical flower-like assemblies of WO_3 for the treatment of rhodamine B (RhB) dye utilizing the visible light illumination. The nanoplates and flower-like assemblies displayed degradation rates that were 7.6 and 3.3 greater than those of commercial WO_3 particles. The best photocatalytic activity was demonstrated by the nanoplates which were able to degrade almost all of the rhodamine-B after 150 min of visible light illumination [132]. The rate of degradation of rhodamine B using different morphologies of WO_3 photocatalyst is displayed in Fig. 8.
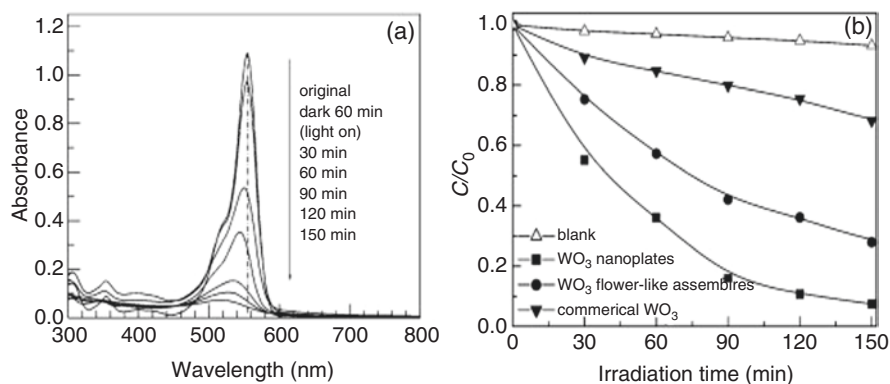
Fig. 8 (**a**) UV-Vis spectral changes of RhB aqueous solution in the presence of WO_3 nanoplates under visible light irradiation; (**b**) degradation rate of RhB over different photocatalysts (Reproduced from Huang et al. 2013 [132])

A hydrothermal route was employed to synthesize WO_3 photocatalyst for treating amoxicillin employing simulated sunlight. The study was conducted by making use of Box-Behnken design with initial concentration (of drug), catalyst dose, and solution pH as the independent variables and involving 30 experimental runs. It was observed from the study that while the amount of drug degraded enhanced as the catalyst dose was enhanced, it decreased as the solution pH and initial concentration of the drug both increased. The photocatalyst WO_3 was able to complete degrade amoxicillin in 180 min of simulated solar light illumination; however, the dissolved organic carbon (DOC) removal rate is only 36% in the same time period, which indicates the incomplete mineralization of the intermediates which were formed in the degradation process. The degradation process was found to follow pseudo-first-order kinetics; experimental data was best described using second-order polynomial regression models [133].

3.4 Strategies to Improve the Photocatalytic Efficiency of Metal Oxide-Based Catalysts

Over the years, metal oxide catalysts have been considered to be potential photo-induced catalytic materials due to their excellent properties. They have generally provided good results for the treatment of organic impurities found in wastewater. Still, their industrial applications have so far been limited due to factors such as e^-/h^+ pair recombination, lower quantum yield, and lower photocatalytic performances. Also, they are unable to utilize the full spectrum of sunlight due to their wide band-gap energies that allow them to use only the highly energetic UV region, which makes up only about 5% of the solar light spectrum. Recently, a series of strategies have been employed to make efficient use of these photocatalysts like nanostructure engineering, doping, and formation of composites [28–36].

3.4.1 Nanostructure Engineering

Nanostructure engineering involves the synthesis of nanostructured materials, which will change or manipulate the properties and functionalities of the photocatalytic materials at the nanoscale. The conversion of macro- and microstructures to nanoscale by nanostructure engineering has broadened the applications of photocatalysts. Recently, nanostructured metal oxides possessing enhanced photocatalytic properties have drawn the attention of researchers. Nanostructured metal oxides (NMOs) have been reported to possess optical, mechanical, electronic, and magnetic properties that do not exist in the bulk forms. Additionally, NMOs have also been reported to possess large surface area-to-volume ratios and small sizes than bulk materials, which result in increased photocatalytic activities [134, 135]. For instance, nanosized TiO_2 is reported to have a higher rate of photo-conversion

of organic compounds to mineralized products [136, 137]. Also, TiO_2 nanotubes displayed high photocatalytic efficiency as compared to available commercial TiO_2 (P-25 TiO_2) [138]. Furthermore, crystalline TiO_2 nanoparticles synthesized in our lab displayed superior photocatalytic performance for the degradation of Eriochrome Black T (EBT). The as-synthesized TiO_2 nanoparticles displayed higher degradation rate than commercially available PC-50, PC-500, and ZnO [139]. Nanostructured ZnO nanomaterials also exhibit better photocatalytic performance than pure ZnO, e.g., nanostar ZnO showed enhanced mass transfer of hydroxyl radicals during the photochemical reaction of methyl orange degradation [140]. The SEM images of nanostar ZnO photocatalyst at different reaction times are displayed in Fig. 9.

Also, ZnO nanoparticles synthesized by facile hydrothermal process displayed enhanced photocatalytic performance to degrade Alizarin Red S dye than commercial PC-500 photocatalyst [141]. Furthermore, porous Fe_2O_3 nanorods were synthesized and displayed more efficient photocatalytic efficiency, superior reusability, and stability than commercial Fe_2O_3 powder [116]. In another study, Fe_2O_3 nanowires were used for RhB degradation which also displayed better photocatalytic performance [142]. SnO_2 nanocrystals also resulted in the 100% degradation of RhB [143]. The enhancement in the photocatalytic efficiency of the abovementioned studies was due to the increased surface area, decreased distance of electron-hole transmission, and decreased electron-hole recombination rate.

3.4.2 Doping

Doping is considered to be the most promising, effective, facile, and practical approach to enhance photocatalytic properties because it can reduce the bandgap values of metal oxides, lead to enhanced charge separation, and result in shift in the absorption band to visible region. Also, this method leads to a change in the coordination environment of the host metal ion in the lattice. It introduces localized energy levels in bandgap states, which will modify the electronic band structure. The dopant can be introduced into the semiconducting materials either individually or
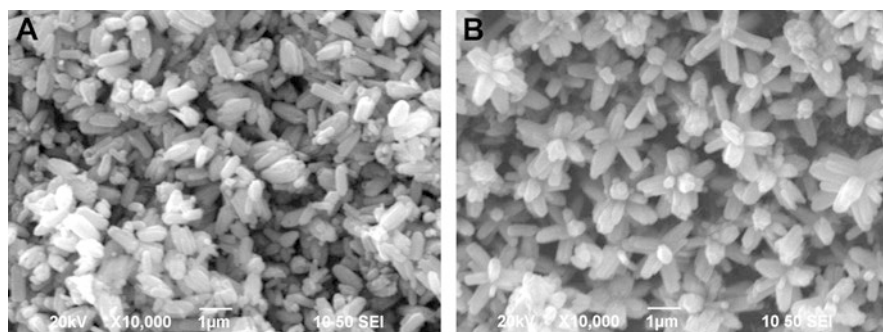
Fig. 9 SEM images of the ZnO products taken at different reaction times: 0.5 h (**a**) and 16 h (**b**) (Reproduced from Fang et al. 2013 [140])

simultaneously. Over the years, various metals, metalloids, and nonmetals have been used as dopants to increase the performance of metal oxide photocatalysts with excellent results [144–150]. For instance, doping of 13.36% Se on TiO_2 displayed outstanding photocatalytic capability employing visible light due to the narrowing of bandgap [151]. Also, N-doped Ti_4O_7 exhibited marvelous photocatalytic activity degrading 100% dye due to a reduction in bandgap energy from 2.9 to 2.7 eV of Ti_4O_7 [152]. Bimetallic-doped TiO_2 displayed more efficient results than single-doped TiO_2, e.g., the absorption band of Er-W-co-doped TiO_2 shifted to the near-IR range (800–1000 nm) [153]. The effect of doping various species on degradation efficiency of TiO_2 is displayed in Fig. 10.

ZnO has also been found to be affected significantly by the doping species, e.g., Pd^{2+}-doped ZnO displayed more efficient results towards the treatment of methyl orange (MO) dye. The incorporation of Pd^{2+} ions gave rise to electronic energy level in bandgap states, which helps in the trapping of charge species carriers. And the charge was efficiently separated with an increase in Pd^{2+} content from 2% to 3%, followed by a sudden decrease at high concentration [154]. ZnO plates doped with Ag ions have been used for the degradation of ofloxacin drug under solar irradiation. The as-prepared photocatalyst displayed enhanced degradation rate with 98% removal of ofloxacin in 150 min. The enhanced degradation rate was due to the trapping of electrons by silver ions which inhibited recombination of e^-/h^+ pairs [155]. Also, nitrogen-doped ZnO showed visible light photoactivity towards the degradation of bisphenol A due to the formation of isolated nitrogen 2p states above the valence band, which intensifies the visible light absorption [156]. Similarly, Pt-doped Fe_2O_3 showed a significant increase in the performance because Pt plays the role of conduction band electron sinker owing to its lower Fermi level, which
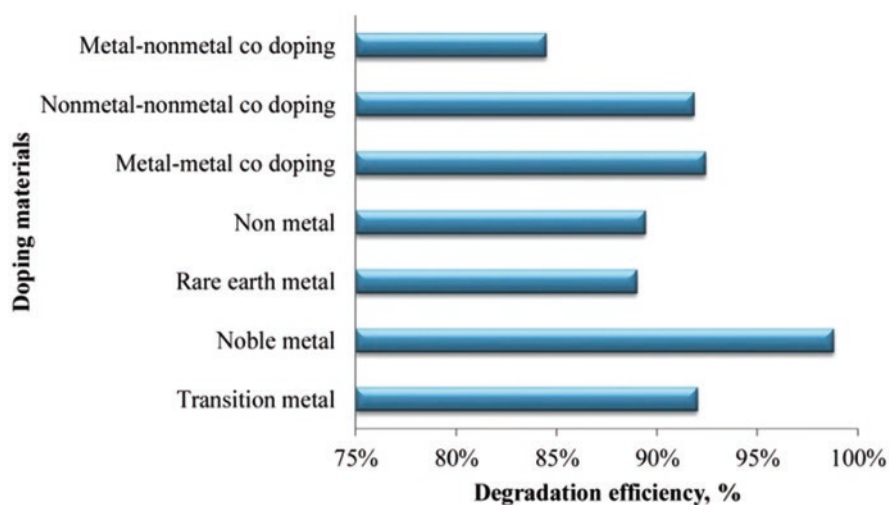
Fig. 10 Diagram for average photocatalytic degradation of different doping materials by using TiO_2 photocatalyst in the presence of UV irradiation (Reproduced from Al-Mamun et al. 2019 [73])

Table 1 Doped metal oxides that have been used for the degradation of organic pollutants from water

Pollutant	Photocatalyst	Synthesis method	Light source	Degradation efficiency (%)	Reference
Eosin yellow	Pd-/N-doped TiO$_2$	Nebulized-pray pyrolysis	UV irradiation	99.3	[158]
Congo red	Cu-/Zn-doped TiO$_2$	Sol-gel	Visible irradiation	98	[159]
Methylene blue	C-/F-doped TiO$_2$	Hydrothermal	300 W Xe lamp	75	[160]
P-nitrophenol	(a) Li-doped ZnO (b) Na-doped ZnO (c) K-doped ZnO	Sol-gel	Visible irradiation	Li-ZnO = 97 Na-ZnO = 72 K-ZnO = 84	[161]
Methyl orange	Au-doped ZnO	Hydrothermal	300 W Xe lamp	100	[162]
Methylene blue	ZnO-doped SnO$_2$ nanoparticles	Hydrothermal	UV irradiation	75	[163]
Formaldehyde	N-doped ZnO	Calcination	1000 W Xe lamp	97	[164]
Methylene blue	CdO-doped ZnO	Electrospinning	Sunlight irradiation	100	[165]
Phenol	Ce-doped ZnO	Chemical precipitation	Visible irradiation	80.7	[166]

improves the separation of electron-hole pairs [150]. Similarly, a considerable improvement was observed in Sb-doped SnO$_2$ due to the improved electrical conductivity of SnO$_2$ and modification in its band structure. This is because Sb traps the e$^-$/h$^+$ pairs and causes effective charge separation in the catalyst [157]. Some other examples of doped metal oxides are displayed in Table 1.

3.4.3 Formation of Composites

Formation of different composites/heterojunctions has drawn the utmost attention in recent years because of their facile synthesis, stability, and outstanding performance in the visible/solar light region. A heterojunction comprises two or more semiconducting materials, with one of them having a wide bandgap and the other having a narrow bandgap. While wide bandgap semiconductors such as TiO$_2$ are unable to absorb visible light, the narrow bandgap semiconductors, despite their ability to utilize the broad spectrum of light, suffer from the limitation of recombination of charge carriers. The formation of heterojunction results in the shifting of the absorption region beyond the UV region and also improves the separation of e$^-$/h$^+$ pairs [72, 167]. Therefore, the formation of heterojunction is necessary to explore
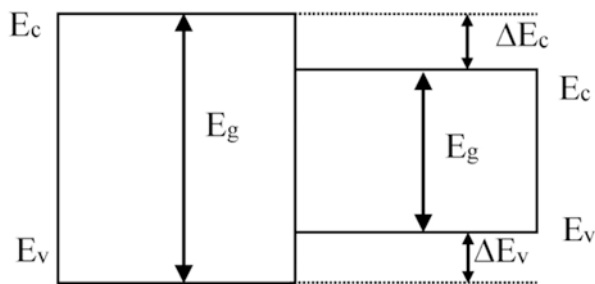
Fig. 11 Type I heterojunction with redox potential energy of CB (Ec) and VB (Ev) (Reproduced from Ani et al. 2018 [72])
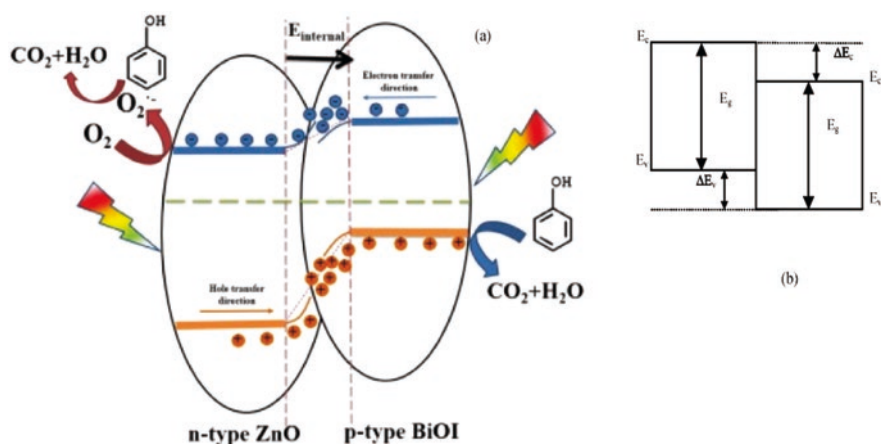
Fig. 12 (**a**) Photocatalytic mechanism scheme for separation and transfer of carriers under simulated solar light irradiated based on BiOI/ZnO photocatalyst. The red and blue lines represent the different reaction courses. (For interpretation of the references to color in this figure legend, the reader is referred to the web version of this article.) (Reproduced from Jiang et al. 2017 [172]). (**b**) Type II heterojunction with redox potential energy of CB (Ec) and VB (Ev) (Reproduced from Ani et al. 2018 [72])

the photocatalytic properties of these materials [72, 168–170]. Three types of heterojunctions that can be formed are type I, type II, and type III [72, 171] as shown in Figs. 9, 10, and 11. Type I heterojunction is displayed in Fig. 11.

A type II heterojunction involves the movement of electrons from CB which is more positive to a CB which is less negative, while the holes move from VB which is more positive to a less positive VB. The formation of type II heterojunction is shown in Fig. 12.

However, in type III heterojunction, electrons from the less negative CB move and recombine with the less positive VB holes, leaving behind holes and electrons with strong oxidation and reduction potential [72, 169]. This movement of charge carriers in the opposite direction helps in improving the effective e$^-$/h$^+$ pair
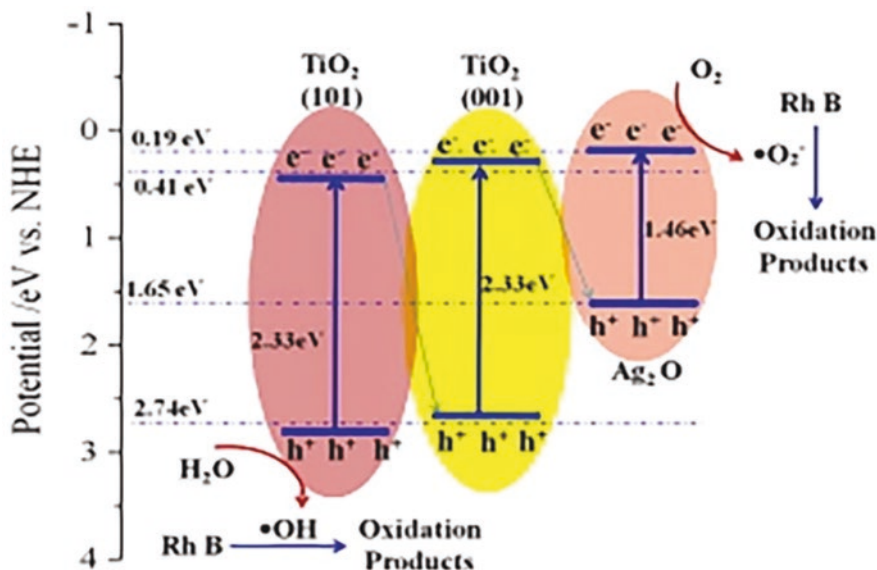
Fig. 13 Photocatalytic mechanism of Ag_2O-0.13-TiO_2 (Reproduced from Li et al. 2017 [173])

separation and hence enhances the photocatalytic performance of photocatalyst. This effective charge separation and improved photocatalytic performance along with better durability as a result of strong redox ability and wide photon response make materials with type III heterojunction the best [72, 153]. The type III heterojunction is displayed in Fig. 13.

Various composites of metal oxide-based photocatalysts have been reported for the degradation of organic pollutants. For example, a multicomponent photocatalyst was synthesized for the very first time by incorporating graphene into TiO_2 nanowires (G-Pd@TiO_2-CNW). A facile hydrothermal method and electrochemical spinning were used for the synthesis of this catalyst which possessed a porous and rough surface. The as-obtained composite was used for the degradation of 4-nitrophenol from different water samples under visible irradiation. The synergistic effect of graphene and palladium helps in enhancing the photocatalytic performance resulting in 100% degradation of 4-nitrophenol from pond water in just 30 min, while 97.2% and 80.5% degradation efficiencies were observed to reduce 4-nitrophenol from tap water and river water, respectively [174]. The mechanism of degradation of 4-nitrophenol by G-Pd@TiO_2-CNW is shown in Fig. 14.

Novel Fe_2O_3-TiO_2 nanocomposites were also prepared by using the photodeposition method and utilized for the degradation of an herbicide called 2,4-dichlorophenoxyacetic acid under both UV and visible irradiation. The as-prepared photocatalyst displayed enhanced photocatalytic performance than pristine P25 TiO_2 with maximum results for 10% Fe-TiO_2-H_2O sample. The rate constant for a composite was determined to be 2.36 min^{-1} which is 78% more than that measured with pristine P25 TiO_2. The enhanced performance was due to the
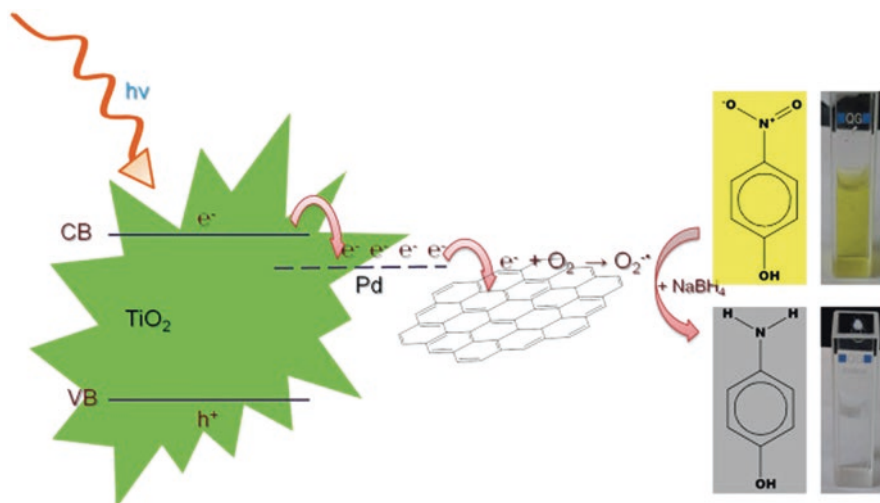
Fig. 14 Photocatalytic reduction of 4-nitrophenol by G-Pd@TiO$_2$-CNW (Reproduced from Lee et al. 2015 [174])

improved separation of e$^-$/h$^+$ pairs [175]. Also, MoS$_2$/TiO$_2$ photocatalyst was fabricated by hydrothermal treatment for the decomposition of paracetamol (PCM) in the presence of sunlight. The as-prepared photocatalyst was capable to decompose 40% of PCM in 25 min as compared to TiO$_2$ which showed decomposition of only 8% PCM. The enhanced photocatalytic performance was due to the effective charge separation inTiO$_2$/MoS$_2$ composite and the increased number of active sites to absorb visible light [176]. Furthermore, Liu et al. reported the synthesis of novel TiO$_{2-x}$/Ag$_3$PO$_4$composite with oxygen vacancies on which the visible light absorption depends. The photocatalytic activity of the as-synthesized photocatalyst was found to greatly depend upon the calcination temperature and the optimum temperature at which maximum degradation efficiency obtained was 400 °C. The degradation rate of TiO$_{2-x}$/Ag$_3$PO$_4$ was measured to be 95% for bisphenol A over 16 min of visible light irradiation which is more than pristine Ag$_3$PO$_4$ and TiO$_2$ [177]. Jiang et al. reported the synthesis of BiOI/ZnO photocatalyst by employing a simple and easy two-step hydrothermal method. The obtained photocatalyst was used for the photodegradation of phenol in the presence of solar light with degradation efficiency of 99.9% in 2 h. The composite showed enhanced photocatalytic activity than pure ZnO which degraded only 40% of phenol in 2 h [172]. Multifunctional photocatalyst film was also synthesized by integrating ZnO nanosheets, BiVO$_4$ particles, and conductive magnetic cilia through hydrothermal treatment. When visible light falls on the surface of the as-synthesized photocatalyst, it displayed the enhanced degradation rate towards the removal of RhB dye. The enhanced degradation rate is attributed to the improved charge separation and increased absorption and mass transfer. The degradation efficiency was calculated to be 100% in 120 min [178]. Three-dimensional SnO$_2$/α-Fe$_2$O$_3$ heterostructure was synthesized by

employing a facile hydrothermal approach. The obtained catalyst has displayed efficient removal efficiency towards the removal of methylene blue when visible light falls on the surface of the catalyst. The calculated degradation efficiency for methylene blue was found to be 98.4% in 240 min. The efficient removal of methylene blue contributed to the improved separation of photogenerated e^-/h^+ pairs [179]. Novel $WO_3/CdWO_4$ photocatalyst synthesized by hydrothermal and chemisorption method has been reported for the degradation of MB, MO, and RhB dyes under visible light. Maximum photocatalytic degradation was obtained for MB exhibiting 97% degradation in 50 min which was about 2.3 times more than that of pure WO_3 and seven times more than pure $CdWO_4$. The enhancement in the degradation efficiency was due to the increased surface area [180]. In another study, the synthesis of WO_3/TiO_2 photocatalyst synthesized by a sol-gel method and that displayed better photocatalytic efficiency than pure TiO_2 towards the degradation of pesticide called malathion was reported. Approximately 99% of malathion degraded in 120 min by using 2 wt% of WO_3 in the as-prepared catalyst. The improvement in the photocatalytic efficiency of TiO_2 after the introduction of WO_3 was due to the enhanced surface area and the formation of smaller clusters [181]. The nitrogen adsorption-desorption isotherm for the degradation of organophosphorus pesticide malathion is shown in Fig. 15.

Some other examples of composites of metal oxide photocatalysts for the removal of organic pollutants from water are displayed in Table 2.

4 Future Prospects

Photocatalysis has emerged as the most efficient and extensively used technique for wastewater treatment. This technique has shown remarkable progress with a long history for many years, and the progress is still ongoing. But its rate of progress still
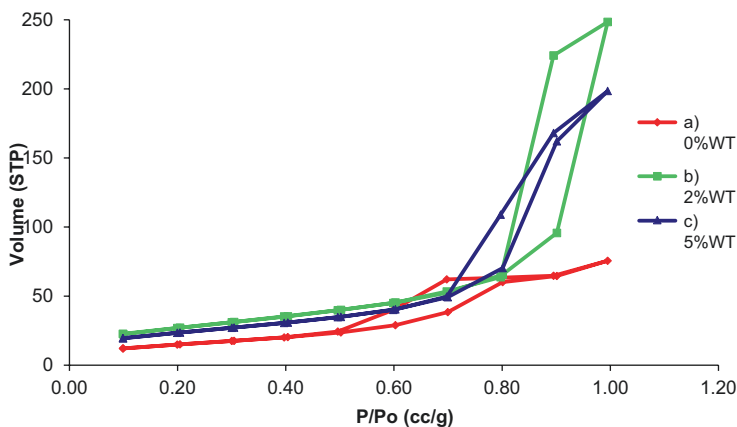
Fig. 15 Nitrogen adsorption-desorption isotherms: (**a**) 0%WT, (**b**) 2%WT, and (**c**) 5%WT (Reproduced from Ramos-Delgado et al. 2013 [181])

Table 2 List of reported metal oxide-based photocatalysts for the removal of organic pollutants from water

Pollutant	Photocatalyst	Synthesis method	Light source	Degradation efficiency (%)	Reference
2,4-Dichlorophenol	ZnO/CuO	Microwave-assisted combustion	300 W tungsten-halogen lamp	82	[182]
Rhodamine 6G	CuO/ZnO/SiNWs	Chemical precipitation	Sunlight irradiation	100	[183]
Ofloxacin	CdS/TiO$_2$	Hydrothermal	Visible light irradiation	86	[184]
Bisphenol A	Bi$_2$O$_3$/SnO$_2$	Hydrothermal	Sunlight irradiation	93.42	[185]
Rhodamine B, methylene blue, and methyl orange	g-C$_3$N$_4$/SiO$_2$/SnO$_2$	Sol-gel	Visible light irradiation	Methylene blue = 99.73 Methyl orange = 95.58 Rhodamine B = 95.10	[186]
Acid orange 7	WO$_3$/g-C$_3$N$_4$	Wet impregnation	Visible light irradiation	100	[187]
Methylene blue	WO$_3$-CuS heterojunction	Hydrothermal	300 W Xe lamp	96	[188]
Tetracycline	WO$_3$/Ag$_3$PO$_4$	Hydrothermal	Visible light irradiation	96	[189]
Toluene and methylene blue	CNT/TiO$_2$	Electrospinning and calcination	Visible irradiation	52 for toluene and 58 for methylene blue	[190]
Rhodamine B, nitrobenzene	SWCNT/TiO$_2$	Solvothermal	UV irradiation	100 both	[191]
Amoxicillin	Activated carbon-supported TiO$_2$ nanoparticle(s)	Ultrasonic impregnation	UV irradiation	90	[192]
Diphenhydramine	Reduced graphene oxide-TiO$_2$	Liquid-phase deposition	UV-Vis and visible light irradiation	>95	[193]
2,4-Dichlorophenoxy acetic acid	TiO$_2$-WO$_3$	Sol-gel	Sunlight	94.6	[194]
Tetracycline	N-TiO$_2$/CaFe$_2$O$_4$/diatomite	Sol-gel	150 W xenon lamp	91.7	[195]
Tetracycline	TiO$_2$/Fe$_2$O$_3$/CNT	Hydrothermal	300 W xenon lamp	89.41	[196]
Tetrabromodiphenyl ethers	TiO$_2$-Cu$_2$O film	Electrochemical deposition	300 W xenon lamp	90	[197]

Pollutant	Photocatalyst	Synthesis method	Light source	Degradation efficiency (%)	Reference
Ofloxacin	Bi_2O_3-TiO_2	Hydrothermal	70.3 K lux	92	[198]
17β-Estradiol	CdS nanorod/TiO_2 nano-belt composite	Hydrothermal	Visible irradiation	92	[199]
Ciprofloxacin	Au-CdS/TiO_2 nanowire	Molten flux	Solar light	99	[200]
Levofloxacin	Bi_2WO_6/C-dots/TiO_2	Chemical wet technique	Sunlight irradiation	99	[201]
Ciprofloxacin	Ag/Fe_2O_3/ZnO heterostructure	Precipitation method	Sunlight irradiation	76.4	[202]
2,4-Dichlorophenol	MoO_3/ZnO	Hydrothermal precipitation	55 W fluorescent lamp	99.2	[203]
Methyl orange and 4-nitrophenol	In_2O_3/ZnO	Hydrothermal	Solar light irradiation	100 for both	[204]
Methylene blue	MoS_2-ZnO heterostructure	Hydrothermal	Solar light irradiation	97	[205]
4-Chlorophenol	C/ZnO/CdS	Micro-emulsion and hydrothermal	65 W fluorescent lamp	98	[206]
Amaranth dye	Ag_2O-decorated ZnO nanorod heterostructures	Precipitation	Visible irradiation	94	[207]
Tetracycline	AgI/WO_3	Precipitation	Visible irradiation	75	[208]
Methylene blue	WO_3/g-C_3N_4	In situ liquid-phase process	Visible irradiation	97	[209]
Tetracycline	CdS/SnO_2	Hydrothermal	Visible irradiation	85	[210]
Direct blue 15	ZnO-SnO_2 nanosheets	Hydrothermal	Visible light irradiation	87	[211]
Ciprofloxacin	MoS_2-SnO_2 heterojunction anchored on expanded graphite (EG)	Hydrothermal	100 W xenon lamp	78.5	[212]

lacks to compete with the rate of deterioration of water quality. To overcome this problem, the development of widely used, economic, green, and efficient technique is necessary. Photocatalysis, although the most favorable technique for this purpose, is still unable to meet the multifarious demands of an ideal technique, as most of the studies of this technique are limited to the laboratory scale and the implementation of this technique in industries has not been achieved yet. From an industrial application point of view, the development of reactor design and an ideal photocatalytic material is a paramount task. Cost is one of the major aspects of a photocatalyst from a broad application point of view followed by environment friendliness and efficiency. These three parameters form the basis of an ideal photocatalyst. Conventional photocatalysts such as TiO_2 and ZnO have many advantages such as low cost, environment friendliness, chemical and physical stability, etc. However, they are inefficient to explore the wide spectrum of solar light. Due to their wide bandgap, they are only photoactive in the UV region which is only 5% of the solar spectrum. Thus, expensive artificial UV light is necessary for the efficient work of these catalysts, thereby increasing the cost of a photocatalyst. Therefore, visible light active materials or low bandgap materials are economic as they can be used under visible light which is nearly 48% of the solar spectrum. Recyclability is also the major aspect associated with the cost of the catalyst by ensuring their reuse. In this context, several supporting materials were reported to be used to immobilize the catalyst such as concrete, quartz, inert surface, etc. But this will lead to a decrease in the efficiency of the catalyst, hence reducing the efficiency of the operation. Thus, for the practical reuse of the material, a good support possessing specific features such as chemical stability, photochemically inert, good adsorption capability, nontoxicity, low cost, and availability in abundance is required. Another important aspect of an ideal catalyst is its toxicity. Most of the photocatalyst can convert the pollutants to mineralized products, but some of them produce intermediates that are toxic to the environment. Thus, the identification of these toxic intermediates is an imperative task, but only a few studies have focused on their identification. Therefore, extensive research is necessary to develop a prominent number of eco-toxicological tests or kits. The efficiency of the catalyst is also an important part of an ideal catalyst. Till now, various composite materials have been developed to enhance the efficiency of the catalyst, but they were still not capable to achieve up to the mark results. Nowadays, the focus of most of the researchers relies on combining photocatalysis with other wastewater treatment methods such as biological treatment, activated sludge process, ozonation, etc. which gives more efficient results. The photocatalytic efficiency not only depends upon the properties of a catalyst but also depends upon other parameters such as atmospheric conditions, properties of effluent, and the properties of a reactor. Therefore, these parameters should be optimized during the degradation of pollutants to achieve excellent efficiency. In conclusion, it is suggested that future studies should be focused on designing photocatalytic materials having good recyclability, efficiency, low cost, and environmental friendliness. Additionally, to extend the application of photocatalysis on a large scale, i.e., in industries, the focus should also be towards designing a reactor that is reliable, cost-effective, and environmentally friendly.

References

1. Mara DD (2003) Water, sanitation and hygiene for the health of developing nations. Public Health 117(6):452–456
2. Moore M, Gould P, Keary BS (2003) Global urbanization and impact on health. Int J Hyg Environ Health 206(4–5):269–278
3. World Health Organization (2018) Water sanitation hygiene. WHO global water, sanitation and hygiene annual report. https://www.who.int/water_sanitation_health/publications/global-water-sanitation-and-hygiene-annual-report-2018/en/
4. World Health Organization (2015) Progress on sanitation and drinking water. Update and MDG assessment. WHO, Geneva. https://www.unicef.org/publications/index_82419.html
5. UNICEF (2006) UNICEF, human development report. Children and water, sanitation and hygiene: the evidence. UNICEF, New York, NY. http://hdr.undp.org/en/content/children-and-water-sanitation-and-hygiene-evidence
6. United Nations, Department of Economics and Social Affairs, Population Division (2019) World Population Prospects 2019: highlights. ST/ESA/SER. A/423
7. Geissen V, Mol H, Klumpp E, Umlauf G, Nadal M, Ploega M, Zee SEATM, Ritsema CJ (2015) Emerging pollutants in the environment: a challenge for water resource management. Int Soil Water Conserv Res 3(1):57–65
8. UNESCO WWAP (2003) Water for people, water for life: 3rd world water forum in Kyoto, Japan. http://www.unesco.org/new/en/naturalsciences/environment/water/wwap/wwdr/wwdr1-2003/
9. Saxena R, Saxena M, Lochab A (2020) Recent progress in nanomaterials for adsorptive removal of organic contaminants from wastewater. Chem Select 5(1):335–353
10. Szabo E, Vajda K, Vereb G, Dombi A, Mogyorosi K, Abraham I, Majer M (2011) Removal of organic pollutants in model water and thermal wastewater using clay minerals. J Environ Sci Health A Tox Hazard Subst Environ Eng 46(12):1346–1356
11. Karpinska J, Kotowska U (2019) Removal of organic pollution in the water environment. Water 11(10):2017
12. Bhomick PC, Supong A, Sinha D (2017) Organic pollutants in water and its remediation using biowaste activated carbon as greener adsorbent. Int J Hydro 1(3):91–92
13. Vie JC, Taylor CH, Stuart SN (eds) (2009) Wildlife in a changing world – an analysis of the 2008 IUCN red list of threatened species. IUCN, Gland, Switzerland, p 180
14. Gutierreza AM, Dziublaa TD, Hilt JZ (2017) Recent advances on iron oxide magnetic nanoparticles as sorbents of organic pollutants in water and wastewater treatment. Rev Environ Health 32(1–2):111–117
15. Donde OO (2017) Wastewater management techniques: a review of advancement on the appropriate wastewater treatment principles for sustainability. Environ Manag Sustain Dev 6(1):10137
16. Rajasulochana P, Preethy V (2016) Comparison on efficiency of various techniques in treatment of waste and sewage water – a comprehensive review. Resour Eff Technol 2(4):175–184
17. Koe WS, Lee JW, Chong WC (2020) An overview of photocatalytic degradation: photocatalysts, mechanisms, and development of photocatalytic membrane. Environ Sci Pollut Res 27:2522–2565

18. Wankhade AV, Gaikwad GS, Dhonde MG, Khaty NT, Thakare SR (2013) Removal of organic pollutant from water by heterogenous photocatalysis: a review. Res J Chem Environ 17(1):84

19. Li Y, Chen F, He R, Wang Y, Tang N (2019) Semiconductor photocatalysis for water purification. Nanoscale Mater Water Purif 2019:689–705

20. Herrmann JM, Disdier J, Pichat P, Malato S, Blanco J (1998) TiO_2-based solar photocatalytic detoxification of water containing organic pollutants. Case studies of 2,4-dichlorophenoxyaceticacid (2,4-D) and of benzofuran. Appl Catal B Environ 17(1–2):15–23

21. Dong H, Zeng G, Tang L, Fan C, Zhang C, He X, He Y (2015) An overview on limitations of TiO_2-based particles for photocatalytic degradation of organic pollutants and the corresponding countermeasures. Water Res 79:128–146

22. Chakraborty S, Farida JJ, Simon R, Kasthuri S (2020) Averrhoa carambola fruit extract assisted green synthesis of ZnO nanoparticles for the photodegradation of congo red dye. Surf Interfaces 19:100488

23. Heidari Z, Alizadeh R, Ebadi A, Oturan N, Oturan MA (2020) Efficient photocatalytic degradation of furosemide by a novel sonoprecipited ZnO over ion exchanged clinoptilolite nanorods. Sep Purif Technol 242:116800

24. Sharma S, Basu S (2020) Highly reusable visible light active hierarchical porous WO_3/SiO_2 monolith in centimeter length scale for enhanced photocatalytic degradation of toxic pollutants. Sep Purif Technol 231:115916

25. Hitam CNC, Jalil AA (2020) A review on exploration of Fe_2O_3 photocatalyst towards degradation of dyes and organic contaminants. J Environ Manag 258:110050

26. Hojamberdiev M, Czech B, Goktaş AC, Yubuta K, Kadirova ZC (2020) SnO_2@ZnS photocatalyst with enhanced photocatalytic activity for the degradation of selected pharmaceuticals and personal care products in model wastewater. J Alloys Compd 827:154339

27. Mohanta D, Ahmaruzzaman M (2020) Biogenic synthesis of SnO_2 quantum dots encapsulated carbon nanoflakes: an efficient integrated photocatalytic adsorbent for the removal of bisphenol A from aqueous solution. J Alloys Compd 828:154093

28. Djurisic AB, Leung YH, Ng AMC (2014) Strategies for improving the efficiency of semiconductor metal oxide photocatalysis. Mater Horiz 1:400–410

29. Lu F, Astruc D (2020) Nanocatalysts and other nanomaterials for water remediation from organic pollutants. Coord Chem Rev 408:213180

30. Basavarajappa PS, Patil SB, Ganganagappa N, Reddy KR (2020) Recent progress in metal-doped TiO_2, non-metal doped/codoped TiO_2 and TiO_2 nanostructured hybrids for enhanced photocatalysis. Int J Hydrog Energy 45(13):7764–7778

31. Rani A, Reddy R, Sharma U, Mukherjee P, Mishra P, Kuila A, Sim LC, Saravanan P (2018) A review on the progress of nanostructure materials for energy harnessing and environmental remediation. J Nanostruct Chem 8:255–291

32. Ren Z, Guo Y, Liu CH, Gao PX (2013) Hierarchically nanostructured materials for sustainable environmental applications. Front Chem 1:18

33. Khairy M, Zakaria W (2014) Effect of metal-doping of $TiO2$ nanoparticles on their photocatalytic activities toward removal of organic dyes. Egypt J Pet 23(4):419–426

34. Tan YN, Wong CL, Mohamed AR (2011) An overview on the photocatalytic activity of nano-doped-TiO_2 in the degradation of organic pollutants. ISRN Mater Sci 2011:261219

35. Zhao C, Zhou Y, Ridder DJD, Zhai J, Wei Y (2014) Advantages of TiO_2/5A composite catalyst for photocatalytic degradation of antibiotic oxytetracycline in aqueous solution: comparison between TiO_2 and TiO_2/5A composite system. Chem Eng J 248:280–289

36. Guo Y, Wang P, Qian J, Hou J, Ao Y, Wang C (2018) Construction of a composite photocatalyst with significantly enhanced photocatalytic performance through combination of homojunction with hetero-junction. Cat Sci Technol 8:486–498

37. Xiao J, Xie Y, Cao H (2015) Organic pollutants removal in wastewater by heterogeneous photocatalytic ozonation. Chemosphere 121:1–17

38. Iwuozor KO (2019) Prospects and challenges of using coagulation-flocculation method in the treatment of effluents. Adv J Chem A 2(2):105–127

39. Fang F, Qiao LL, Ni BJ, Cao JS, Yu HQ (2017) Quantitative evaluation on the characteristics of activated sludge granules and flocs using a fuzzy entropy-based approach. Sci Rep 7:42910

40. Al-Abri M, Al-Ghafri B, Bora T, Dobretsov S, Dutta J, Castelletto S, Rosa L, Boretti A (2019) Chlorination disadvantages and alternative routes for biofouling control in reverse osmosis desalination. NPJ Clean Water 2:2

41. Yalcinkaya F, Boyraz E, Maryska J, Kucerova K (2020) A review on membrane technology and chemical surface modification for the oily wastewater treatment. Materials (Basel) 13(2):493

42. Boddu VM, Paul T, Page MA, Byl C, Ward L, Ruan J (2016) Gray water recycle: effect of pretreatment technologies on low pressure reverse osmosis treatment. J Environ Chem Eng 4(4):4435–4443

43. Esmaeili H, Foroutan R (2015) Investigation into ion exchange and adsorption methods for removing heavy metals from aqueous solutions. Int J Biol Pharm Allied Sci 4:620–629

44. Zhang M, Dong H, Zhao L, Wang DX, Meng D (2019) A review on Fenton process for organic wastewater treatment based on optimization perspective. Sci Total Environ 670:110–121

45. Khulbe KC, Matsuura T (2018) Removal of heavy metals and pollutants by membrane adsorption techniques. Appl Water Sci 8:19

46. Li X, Xie J, Jiang C, Yu J, Zhang P (2018) Review on design and evaluation of environmental photocatalysts. Front Environ Sci Eng 12(5):14

47. Melchionna M, Fornasiero P (2020) Updates on the roadmap for photocatalysis. ACS Catal 10:5493–5501

48. Fujishima A, Honda K (1972) Electrochemical photolysis of water at a semiconductor electrode. Nature 238:37–38

49. Saravanan R, Gracia F, Stephen A (2017) Basic principles, mechanism, and challenges of photocatalysis. In: Khan M, Pradhan D, Sohn Y (eds) Nanocomposites for visible light-induced photocatalysis. Springer series on polymer and composite materials. Springer, Cham

50. Zhang F, Wang X, Liu H, Liu C, Wan Y, Long Y, Cai Z (2019) Recent advances and applications of semiconductor photocatalytic technology. Appl Sci 9:2489

51. Khan MM, Adil SF, Mayouf AA (2015) Metal oxides as photocatalysts. J Saudi Chem Soc 19(5):462–464

52. Ahmed SN, Haider W (2018) Heterogeneous photocatalysis and its potential applications in water and wastewater treatment: a review. Nanotechnology 29:342001

53. Zhu D, Zhou Q (2019) Action and mechanism of semiconductor photocatalysis on degradation of organic pollutants in water treatment: a review. Environ Nanotechnol Monit Manag 12:100255

54. Chong M, Jin B, Chow CWK, Saint C (2010) Recent developments in photocatalytic water treatment technology: a review. Water Res 44(10):2997–3027

55. Ibhadon AO, Fitzpatrick P (2013) Heterogeneous photocatalysis: recent advances and applications. Catalysts 3(1):189–218

56. Al-Rasheed R, Arabia S (2005) Water treatment by heterogeneous photocatalysis an overview. Chemistry 2005:15

57. Shaheen K, Suo H, Arshad T, Shah Z, Khan SA, Khan SB, Khan MN, Liu M, Ma L, Cui J, Ji YT, Wang Y (2020) Metal oxides nanomaterials for the photocatalytic mineralization of toxic water wastes under solar light illumination. J Water Process Eng 34:101138

58. Hoffmann MR, Martin ST, Choi W, Bahnemann DW (1995) Environmental applications of semiconductor photocatalysis. Chem Rev 95(1):69–96

59. Nakata K, Fujishima A (2012) TiO_2 photocatalysis: design and applications. J Photochem Photobiol C Photochem Rev 13(3):169–189

60. Shayegan Z, Lee CS, Haghighat F (2018) TiO_2 photocatalyst for removal of volatile organic compounds in gas phase – a review. Chem Eng J 334:2408–2439

61. Khalilova HK, Hasanova SA, Aliyev FG (2018) Photocatalytic removal of organic pollutants from industrial wastewater using TiO$_2$ catalyst. J Environ Prot 9(6):691–698

62. Ong CB, Ng LY, Mohammad AW (2018) A review of ZnO nanoparticles as solar photocatalysts: synthesis, mechanisms and applications. Renew Sust Energ Rev 81(1):536–551

63. Qiu R, Zhang D, Mo Y, Song L, Brewer E, Huang X, Xiong Y (2008) Photocatalytic activity of polymer-modified ZnO under visible light irradiation. J Hazard Mater 156(1–3):80–85

64. Karthikeyan C, Arunachalam P, Ramachandran K, Mayouf AMA, Karuppuchamy S (2020) Recent advances in semiconductor metal oxides with enhanced methods for solar photocatalytic applications. J Alloys Compd 828:154281

65. Pinho L, Mosquera MJ (2013) Photocatalytic activity of TiO$_2$–SiO$_2$ nanocomposites applied to buildings: influence of particle size and loading. Appl Catal B Environ 134-135:205–221

66. Frank SN, Bard AJ (1977) Heterogeneous photocatalytic oxidation of cyanide and sulfite in aqueous solutions at semiconductor powders. J Phys Chem 81(15):1484–1488

67. Inoue T, Fujishima A, Konishi S, Honda K (1979) Photoelectrocatalytic reduction of carbon dioxide in aqueous suspensions of semiconductor powders. Nature 277:637–638

68. Horikoshi S, Serpone N (2020) Can the photocatalyst TiO$_2$ be incorporated into a wastewater treatment method? Background and prospects. Catal Today 340:334–346

69. Shvadchina YO, Vakulenko VF, Levitskaya EE, Goncharuk VV (2012) Photocatalytic destruction of anionic SAS with oxygen and hydrogen peroxide in the TiO$_2$ suspension. J Water Chem Technol 34:218–226

70. Teh CM, Mohamed AR (2011) Roles of titanium dioxide and ion-doped titanium dioxide on photocatalytic degradation of organic pollutants (phenolic compounds and dyes) in aqueous solutions: a review. J Alloys Compd 509(5):1648–1660

71. Hernandez-Alonso MD, Fresno F, Suarez S, Coronado JM (2009) Development of alternative photocatalysts to TiO$_2$: challenges and opportunities. Energy Environ Sci 2:1231–1257

72. Ani IJ, Akpan UG, Olutoye MA, Hameed BH (2018) Photocatalytic degradation of pollutants in petroleum refinery wastewater by TiO$_2$- and ZnO-based photocatalysts: recent development. J Clean Prod 205:930–954

73. Al-Mamun MR, Kader S, Islam MS, Khan MZH (2019) Photocatalytic activity improvement and application of UV-TiO$_2$ photocatalysis in textile wastewater treatment: a review. J Environ Chem Eng 7(5):103248

74. Zhang J, Zhou P, Liu J, Yu J (2014) New understanding of the difference of photocatalytic activity among anatase, rutile and brookite TiO$_2$. Phys Chem Chem Phys 16:20382–20386

75. Fisher K, Gawel A, Rosen D, Krause M, Latif AA, Griebel J, Prager A, Schulze A (2017) Low-temperature of anatase/rutile/brookite TiO$_2$ nanoparticles on a polymer membrane for photocatalysis. Catalysts 7(7):209

76. Guimaraes RR, Parussulo ALA, Araki K (2016) Impact of nanoparticles preparation method on the synergic effect in anatase/rutile mixtures. Electrochim Acta 222:378–1386

77. Hussain M, Ceccarelli R, Marchisio DL, Fino D, Russo N, Geobaldo F (2010) Synthesis, characterization, and photocatalytic application of novel TiO$_2$ nanoparticles. Chem Eng J 157(1):45–51

78. Chen H, Nanayakkara CE, Grassian VH (2012) Titanium dioxide photocatalysis in atmospheric chemistry. Chem Rev 112(11):5919–5948

79. Pfeifer V, Erhart P, Li S, Rachut K, Morasch J, Brotz J, Reckers P, Mayer T, Ruhle S, Zaban A, Sero IM, Bisquert J, Jaegermann W, Klein A (2013) Energy band alignment between anatase and rutile TiO$_2$. J Phys Chem Lett 4(23):4182–4187

80. Hussain M, Russo N, Saracco G (2011) Photocatalytic abatement of VOCs by novel optimized TiO$_2$ nanoparticles. Chem Eng J 166(1):138–149

81. Wang C, Wu T (2015) TiO$_2$ nanoparticles with efficient photocatalytic activity towards gaseous benzene degradation. Ceram Int 41(2):2836–2839

82. Colombo DP Jr, Bowman RM (1996) Chemical physics of nanostructured semiconductors. J Phys Chem 100:18445

83. Gaya UI, Abdullah AH (2008) Heterogeneous photocatalytic degradation of organic contaminants over titanium dioxide: a review of fundamentals, progress and problems. J Photochem Photobiol C Photochem Rev 9(1):1–12

84. Chen C, Lu C, Chung Y, Jan J (2007) UV light induced photodegradation of malachite green on TiO_2 nanoparticles. J Hazard Mater 141(3):520–528

85. Faisal M, Tariq MA, Muneer M (2007) Photocatalysed degradation of two selected dyes in UV-irradiated aqueous suspensions of titania. J Dyes Pigments 72:233–239

86. Yang L, Yu LE, Ray MB (2008) Degradation of paracetamol in aqueous solutions by TiO2 photocatalysis. Water Res 42:3480–3488

87. Ohko Y, Ando I, Niwa C, Tatsuma T, Yamamura T, Nakashima T, Kubota Y, Fujishima A (2001) Degradation of bisphenol A in water by TiO_2 photocatalyst. Environ Sci Technol 35:2365–2368

88. Kumar SG, Rao KSRK (2015) Zinc oxide based photocatalysis: tailoring surface-bulk structure and related interfacial charge carrier dynamics for better environmental applications. RSC Adv 5:3306–3351

89. Look DC, Reynolds DC, Sizelove JR, Jones RL, Litton CW, Cantwell G, Harsch WC (1998) Electrical properties of bulk ZnO. Solid State Commun 105(6):399–401

90. Chandiran AK, Jalebi MA, Nazeeruddin MK, Gratzel M (2014) Analysis of electron transfer properties of ZnO and TiO_2 photoanodes for dye-sensitized solar cells. ACS Nano 8(3):2261–2268

91. Kamat PV, Bedja I, Hotchandani S (1994) Photoinduced charge transfer between carbon and semiconductor clusters. One-electron reduction of C60 in colloidal TiO_2 semiconductor suspensions. J Phys Chem 98(37):9137–9142

92. Daneshvar N, Salari D, Khatatee AR (2004) Photocatalytic degradation of azo dye acid red 14 in water on ZnO as an alternative catalyst to TiO_2. J Photochem Photobiol A Chem 162(2–3):317–322

93. Fenoll J, Ruiz E, Hellín P, Flores P, Navarro S (2011) Heterogeneous photocatalytic oxidation of cyprodinil and fludioxonil in leaching water under solar irradiation. Chemosphere 85(8):262–1268

94. Sakthivel S, Neppolian B, Shankar MV, Arabindoo B, Palanichamy M, Murugesan V (2003) Solar photocatalytic degradation of azo dye: comparison of photocatalytic efficiency of ZnO and TiO_2. Sol Energy Mater Sol Cells 77(1):65–82

95. Shafaei A, Nikazar M, Arami M (2010) Photocatalytic degradation of terephthalic acid using titania and zinc oxide photocatalysts: comparative study. Desalination 252(1–3):8–16

96. Han J, Liu Y, Singhal N, Wang L, Gao W (2012) Comparative photocatalytic degradation of estrone in water by ZnO and TiO_2 under artificial UVA and solar irradiation. Chem Eng J 213:150–162

97. Movahedi M, Mahjoub AR, Janitabar-Darzi S (2009) Photodegradation of Congo red in aqueous solution on ZnO as an alternative catalyst to TiO_2. JICS 6:570–577

98. Mohabansi NP, Patil VB, Yenkie N (2011) A comparative study on photo degradation of methylene blue dye effluent by advanced oxidation process by using TiO_2/ZnO photo catalyst. Rasayan J Chem 4(4):814–819

99. Kamat PV, Huehn R, Nicolaescu R (2002) A "sense and shoot" approach for photocatalytic degradation of organic contaminants in water. J Phys Chem B 106(4):788–794

100. Quintana M, Edvinsson T, Hagfeldt A, Boschloo G (2007) Comparison of dye-sensitized ZnO and TiO_2 solar cells: studies of charge transport and carrier lifetime. J Phys Chem C 111(2):1035–1041

101. Muruganandham M, Zhang Y, Suri R, Lee GJ, Chen PK, Hsieh SH, Sillanpyaa M, Wu JJ (2015) Environmental applications of ZnO materials. J Nanosci Nanotechnol 15(9):6900–6913

102. Tian C, Zhang Q, Wu A, Jiang M, Liang Z, Jiang B, Fu H (2012) Cost-effective large-scale synthesis of ZnO photocatalyst with excellent performance for dye photodegradation. Chem Commun 48:2858–2860

103. Poulios I, Kositzi M, Kouras A (1998) Photocatalytic decomposition of triclopyr over aqueous semiconductor suspensions. J Photochem Photobiol A Chem 115(2):175–183
104. Hariharan C (2006) Photocatalytic degradation of organic contaminants in water by ZnO nanoparticles: revisited. Appl Catal A Gen 304:55–61
105. Colon G, Hidalgo MC, Navio JA, Melian EP, Diaz OG, Rodriguez JMD (2008) Highly photoactive ZnO by amine capping-assisted hydrothermal treatment. Appl Catal B Environ 83:30–38
106. Liao Y, Xie C, Liu Y, Huang Q (2013) Metal oxide-based photocatalysis: fundamentals and prospects for application. J Alloys Compd 550:190–197
107. Daneshvar N, Aber S, Dorraji MSS, Khataee AR, Rasoulifard MH (2007) Photocatalytic degradation of the insecticide diazinon in the presence of prepared nanocrystalline ZnO powders under irradiation of UV-C light. Sep Purif Technol 58(1):91–98
108. El-Kemary M, El-Shamy H, El-Mehasseb I (2010) Photocatalytic degradation of ciprofloxacin drug in water using ZnO nanoparticles. J Lumin 130:2327–2331
109. Anju SG, Yesodharan S, Yesodharan EP (2012) Zinc oxide mediated sonophotocatalytic degradation of phenol in water. Chem Eng J 189–190:84–93
110. Chen X, Wu Z, Liu D, Gao Z (2017) Preparation of ZnO photocatalyst for the efficient and rapid photocatalytic degradation of azo dyes. Nanoscale Res Lett 12:143–152
111. Zhang Z, Hossain MF, Takahashi T (2010) Self-assembled hematite (α-Fe2O3) nanotube arrays for photoelectrocatalytic degradation of azo dye under simulated solar light irradiation. Appl Catal B 95(3–4):423–429
112. Cong Y, Chen M, Xu T, Zhang Y, Wang Q (2014) Tantalum and aluminum co-doped iron oxide as a robust photocatalyst for water oxidation. Appl Catal B 147:733–740
113. Pradhan GK, Sahu N, Parida KM (2013) Fabrication of S, N co-doped α-Fe$_2$O$_3$ nanostructures: effect of doping, OH radical formation, surface area, [110] plane and particle size on the photocatalytic active. RSC Adv 3:7912–7920
114. Wu W, Jiang C, Roy VAL (2015) Recent progress in magnetic iron oxide–semiconductor composite nanomaterials as promising photocatalysts. Nanoscale 7:38–58
115. Liu X, Chen K, Shim JJ, Huang J (2015) Facile synthesis of porous Fe$_2$O$_3$ nanorods and their photocatalytic properties. J Saudi Chem Soc 19:479–484
116. Lu AH, Salabas EL, Schuth F (2007) Magnetic nanoparticles: synthesis, protection, functionalization, and application. Angew Chem Int Ed 46:1222–1244
117. Laurent S, Forge D, Port M, Roch A, Robic C, Elst LV, Muller RN (2008) Magnetic iron oxide nanoparticles: synthesis, stabilization, vectorization, physicochemical characterizations, and biological applications. Chem Rev 108:2064–2110
118. Gondal MA, Sayeed MN, Yamani ZH, Al-Arfaj AR (2009) Efficient removal of phenol from water using Fe$_2$O$_3$ semiconductor catalyst under UV laser irradiation. J Environ Sci Health A Tox Hazard Subst Environ Eng 44(5):515–521
119. Shao P, Ren Z, Tian J, Gao S, Luo X, Shi W, Yan B, Li J, Cui F (2017) Silica hydrogel-mediated dissolution-recrystallization strategy for synthesis of ultrathin α-Fe$_2$O$_3$nanosheets with highly exposed (1 1 0) facets: a superior photocatalyst for degradation of bisphenol S. Chem Eng J 323:64–73
120. Dou M, Persson C (2013) Comparative study of rutile and anatase SnO$_2$ and TiO$_2$: band-edge structures, dielectric functions, and polaron effects. J Appl Phys 113(2013):083703
121. Abe R, Higashi M, Sayama K, Abe Y, Sugihara H (2006) Photocatalytic activity of R$_3$MO$_7$ and R$_2$Ti$_2$O$_7$ (R = Y, Gd, La; M = Nb, Ta) for water splitting into H$_2$ and O$_2$. J Phys Chem B 110:2219–2226
122. Madelung O, Rossler U, Schulz M (1998) Tin dioxide (SnO$_2$) crystal structure, lattice parameters, thermal expansion non-tetrahedrally bonded elements and binary compounds I. Springer, Berlin, pp 1–2
123. Mistry BV, Avasthi DK, Joshi US (2016) Tuning of optical and electrical properties of wide band gap Fe:SnO$_2$/Li:NiO p–n junctions using 80 MeV oxygen ion beam. Appl Phys A Mater Sci Process 122:1024

124. Zhang G, Xie C, Zhang S, Zhang S, Xiong Y (2014) Defect chemistry of the metal cation defects in the p-and n-doped SnO_2 nanocrystalline films. J Phys Chem C 118:18097–18109

125. Sanal KC, Jayaraj MK (2013) Growth and characterization of tin oxide thin films and fabrication of transparent p-SnO/n-ZnO p–n hetero junction. Mater Sci Eng B 178:816–821

126. Zulfiqar Y, Yang J, Wang W, Ye Z, Ye JL (2016) Structural and optical properties of (Zn, Co) co-doped SnO_2 nano particles. J Mater Sci Mater Electron 27:12119–12127

127. Paramarta V, Taufik A, Munisa L, Saleh R (2017) Sono- and photocatalytic activities of SnO_2 nanoparticles for degradation of cationic and anionic dyes. AIP Conf Proc 1788:030125

128. Yashas SR, Shivaraju HP, Thinley T, Pushparaj KS, Maleki A, Shahmoradi B (2020) Facile synthesis of SnO_2 2D nanoflakes for ultrasound-assisted photodegradation of tetracycline hydrochloride. Int J Environ Sci Technol 17:2593–2604

129. Viet PV, Thi CM, Hieu LV (2016) The high photocatalytic activity of SnO_2 nanoparticles synthesized by hydrothermal method. Photochem Photobiol 87(2):267–274

130. Tahir MB, Ali S, Rizwan M (2019) A review on remediation of harmful dyes through visible light-driven WO_3 photocatalytic nanomaterials. Int J Environ Sci Technol 16:4975–4988

131. Aslam I, Cao C, Khan WS, Tanveer M, Abid M, Idrees F, Riasat R, Tahir M, Butta FK, Alia Z (2014) Synthesis of three-dimensional WO_3 octahedra: characterization, optical and efficient photocatalytic properties. RSC Adv 4:37914–37920

132. Huang J, Xiao L, Yang X (2013) WO_3 nanoplates, Hierarchical flower-like assemblies and their photocatalytic properties. Mater Res Bull 48:2782–2785

133. Nguyen TT, Nam S-N, Son J, Oh J (2019) Tungsten trioxide (WO_3)-assisted photocatalytic degradation of amoxicillin by simulated solar irradiation. Sci Rep 9:9349

134. Jeevanandam J, Barhoum A, Chan YS, Dufresne A, Danquah MK (2018) Review on nanoparticles and nanostructured materials: history, sources, toxicity and regulations. Beilstein J Nanotechnol 9:1050–1074

135. Yu X, Hu Y, Zhou L, Cao F, Yang Y, Liang T, He J (2011) Research progress of nanostructured materials for heterogeneous catalysis. Curr Nanosci 7(4):11

136. Xu Z, Meng X (2009) Size effects of nanocrystalline TiO_2 on As(V) and As(III) adsorption and As(III) photooxidation. J Hazard Mater 168:747

137. Falk GS, Borlaf M, Lopez-Munoz MJ, Farinas JC, Neto JBR, Moreno R (2018) Microwave-assisted synthesis of TiO_2 nanoparticles: photocatalytic activity of powders and thin film. J Nanopart Res 20:23

138. Liu Z, Zhang X, Nishimoto S, Murakami T, Fujishima A (2008) Efficient photocatalytic degradation of gaseous acetaldehyde by highly ordered TiO_2 nanotube arrays. Environ Sci Technol 42:8547

139. Kansal SK, Sood S, Umar A, Mehta SK (2013) Photocatalytic degradation of Eriochrome Black T dye using well-crystalline anatase TiO2 nanoparticles. J Alloys Compd 51:392–397

140. Fang K, Wang Z, Zhang M, Wang A, Meng Z, Feng J (2013) Gelatin-assisted hydrothermal synthesis of single crystalline zinc oxide nanostars and their photocatalytic properties. J Colloid Interface Sci 402:68–74

141. Kansal SK, Lamba R, Mehta SK, Umar A (2013) Photocatalytic degradation of Alizarin Red S using simply synthesized ZnO nanoparticles. Mater Lett 106:385–389

142. Deng J, Liu J, Dai H, Wang W (2018) Preparation of α-Fe_2O_3 nanowires through electrospinning and their Ag_3PO_4 heterojunction composites with enhanced visible light photocatalytic activity. Ferroelectrics 528:58–65

143. Wu S, Cao H, Yin S, Liu X, Zhang X (2009) Amino acid-assisted hydrothermal synthesis and photocatalysis of SnO_2 nanocrystals. J Phys Chem C 113:17893–17898

144. Asahi R, Morikawa T, Irie H, Ohwaki T (2014) Nitrogen-doped titanium dioxide as visible-light-sensitive photocatalyst: designs, developments, and prospects. Chem Rev 114(19):9824–9852

145. Huang J, Guo X, Wang B, Li L, Zhao M, Dong L, Liu X, Huang Y (2015) Synthesis and photocatalytic activity of Mo-doped TiO_2 nanoparticles. J Spectrosc 2015:681850

146. Qiu L, Luo X (2018) ZIF-8 derived Ag-doped ZnO photocatalyst with enhanced photocatalytic activity. RSC Adv 8:4890–4894
147. Bousslama W, Elhouichet H, Ferid M (2017) Enhanced photocatalytic activity of Fe doped ZnO nanocrystals under sunlight irradiation. Optik 134:88–98
148. Arshad M, Ehtisham-ul-Haque S, Bilal M, Ahmad N, Ahmad A, Abbas M, Nisar J, Khan MI, Nazir A, Ghaffar A, Iqbal M (2020) Synthesis and characterization of Zn doped WO_3 nanoparticles: photocatalytic, antifungal and antibacterial activities evaluation. Mater Res Express 7:015407
149. Wang Y, Chan K, Li X, So S (2006) Electrochemical degradation of 4-chlorophenol at nickel–antimony doped tin oxide electrode. Chemosphere 65:1087–1093
150. Chen L, Li F, Ni B, Xu J, Fu Z, Lu Y (2012) Enhanced visible photocatalytic activity of hybrid Pt/α-Fe_2O_3 nanorods. RSC Adv 2:10057–10063
151. Xie W, Li R, Xu Q (2018) Enhanced photocatalytic activity of Se-doped TiO_2 under visible light irradiation. Sci Rep 8:1–10
152. Maragatha J, Rani C, Rajendran S, Karuppuchamy S (2017) Microwave synthesis of nitrogen doped Ti_4O_7 for photocatalytic applications. Phys E 93:78–82
153. Kubacka A, Munoz-Batista MJ, Ferrer M, Fernandez-Garcia M (2018) Er-W codoping of TiO_2-anatase: structural and electronic characterization and disinfection capability under UV-vis, and near-IR excitation. Appl Catal B Environ 228:113–129
154. Zhong JB, Li JZ, He XY, Zeng J, Lu Y, Hu W, Lin K (2012) Improved photocatalytic performance of Pd-doped ZnO. Curr Appl Phys 12:998–1001
155. Kaur A, Gupta G, Ibhadon AO, Salunke DB, Sinha ASK, Kansal SK (2018) A Facile synthesis of silver modified ZnO nanoplates for efficient removal of ofloxacin drug in aqueous phase under solar irradiation. J Environ Chem Eng 6(3):3621–3630
156. Qiu Y, Yang M, Fan H, Xu Y, Shao Y, Yang X, Yang S (2013) Synthesis and characterization of nitrogen doped ZnO tetrapods and application in photocatalytic degradation of organic pollutants under visible light. Mater Lett 99:105–107
157. Fadavieslam MR (2016) Effect of Sb doping on the structural, electrical, and optical properties of SnO_2 thin films prepared through spray pyrolysis. J Mater Sci Mater Electron 27:4943–4950
158. Kuvarega AT, Krause RWM, Mamba BB (2012) Multiwalled carbon nanotubes decorated with nitrogen, palladium co-doped TiO_2 (MWCNT/N, Pd co-doped TiO_2) for visible light photocatalytic degradation of eosin yellow in water. J Nanopart Res 2012:776–779
159. Chelli VR, Golder AK (2017) Bimetal doping on TiO_2 for photocatalytic water treatment: a green route. Eur Water 58:53–60
160. Yan H, Kochuveedu ST, Quan LN, Lee SS, Kim DH (2013) Enhanced photocatalytic activity of C, F-codoped TiO_2 loaded with AgCl. J Alloys Comp 560:20–26
161. Benhebal H, Chaib M, Malengreaux C, Leonard A, Lambert SD, Leonard A, Crine M, Heinrichs B (2014) Visible-light photo-activity of alkali metal doped ZnO. J Taiwan Inst Chem Eng 45(1):249–253
162. Lu J, Wang H, Peng D, Chen T, Dong S, Chang Y (2016) Synthesis and properties of Au/ZnO nanorods as a plasmonic photocatalyst. Phys E Low Dimens Syst Nanostruct 78:41
163. Lamba R, Umar A, Mehta SK, Kansal SK (2015) ZnO doped SnO_2 nanoparticles heterojunction photo-catalyst for environmental remediation. J Alloys Compd 653:327–333
164. Wu C (2014) Facile one-step synthesis of N-doped ZnO micropolyhedrons for efficient photocatalytic degradation of formaldehyde under visible-light irradiation. Appl Surf Sci 319:237
165. Yousef A, Barakat NAM, Amna T, Unnithan AR, Al-Deyab SS, Yong Kim H (2012) Influence of CdO-doping on the photoluminescence properties of ZnO nanofibers: effective visible light photocatalyst for waste water treatment. J Lumin 132(7):1668–1677
166. Sin J, Lam S, Lee K, Mohamed AR (2015) Preparation of cerium-doped ZnO hierarchical micro/nanospheres with enhanced photocatalytic performance for phenol degradation under visible light. J Mol Catal A Chem 409:1–10

167. Wang H, Cai Y, Zhou J, Fang J, Yang Y (2017) Crystallization-mediated amorphous $CuxO$ (x = 1, 2)/crystalline CuI p–p type heterojunctions with visible light enhanced and ultraviolet light restrained photocatalytic dye degradation performance. Appl Surf Sci 402:31–40

168. Lan H, Li L, An X, Liu F, Chen C, Liu H (2017) Microstructure of carbon nitride affecting synergetic photocatalytic activity : hydrogen bonds vs. structural defects. Appl Catal B Environ 204:49–57

169. Wang J, Xia Y, Zhao H, Wang G, Xiang L, Xu J, Komarneni S (2017) Oxygen defects-mediated Z-scheme charge separation in g-C_3N_4/ZnO photocatalysts for enhanced visible-light degradation of 4-chlorophenol and hydrogen evolution. Appl Catal B Environ 206:406–416

170. Yao J, Chen H, Jiang F, Jiao Z, Jin M (2017) Titanium dioxide and cadmium sulfide co-sensitized graphitic carbon nitride nanosheets composite photocatalysts with superior performance in phenol degradation under visible-light irradiation. J Colloid Interface Sci 490:154–162

171. Heng H, Gan Q, Meng P, Liu X (2017) The visible-light-driven type III heterojunction $H_3PW_{12}O_{40}$/TiO_2-In_2S_3: a photocatalysis composite with enhanced photocatalytic activity. J Alloy Comp 696:51–59

172. Jiang J, Wang H, Chen X, Li S, Xie T, Wang D, Lin Y (2017) Enhanced photocatalytic degradation of phenol and photogenerated charges transfer property over BiOI-loaded ZnO composites. J Colloid Interface Sci 494:130–138

173. Li M, Liu H, Liu T, Qin Y (2017) Design of a novel dual Z-scheme photocatalytic system composited of Ag_2O modified Ti^{3+} self doped TiO_2 nanocrystals with individual exposed (001) and (101) facets. Mater Charact 124:136–144

174. Lee H, Sai-Anand G, Komathi S, Gopalan AI, Kang SW, Lee KP (2015) Efficient visible-light-driven photocatalytic degradation of nitrophenol by using graphene-encapsulated TiO_2 nanowires. J Hazard Mater 283:400–409

175. Moniz SJA, Shevlin SA, An X, Guo ZX, Tang J (2014) Fe_2O_3-TiO_2 nanocomposites for enhanced charge separation and photocatalytic activity. Chem Eur J 20:15571–15579

176. Kumar N, Bhadwal AS, Mizaikoff B, Singh S, Kranz C (2019) Electrochemical detection and photocatalytic performance of MoS_2/TiO_2 nanocomposite against pharmaceutical contaminant: paracetamol. Sens Bio-Sens Res 24:100288

177. Liu J, Xie F, Li R, Li T, Jia Z, Wang Y, Wang Y, Zhang X, Fan C (2019) TiO_2-x/Ag_3PO_4 photocatalyst: oxygen vacancy dependent visible light photocatalytic performance and BPA degradative pathway. Mater Sci Semicond Process 97:1–10

178. Construction (2017) Construction of ZnO nanosheet arrays within $BiVO_4$ particles on a conductive magnetically driven cilia film with enhanced visible photocatalytic activity. J Alloys Compd 690:953

179. Zhang S, Li J, Niu H, Xu W, Xu J, Hu W, Wang X (2013) Visible-light photocatalytic degradation of methylene blue using SnO_2/α-Fe_2O_3 hierarchical nanoheterostructures. ChemPlusChem 78(2):192–199

180. Aslam I, Cao C, Tanveer M, Farooq MH, Khan WS, Tahir M, Idrees F, Khalid S (2015) A novel Z-scheme WO_3/$CdWO_4$ photocatalyst with enhanced visible-light photocatalytic activity for the degradation of organic pollutants. RSC Adv 5:6019–6026

181. Ramos-Delgado NA, Gracia-Pinilla MA, Maya-Trevino L, Hinojosa-Reyes L, Guzman-Mar JL, Hernandez-Ramirez A (2013) Solar photocatalytic activity of TiO_2 modified with WO_3 on the degradation of an organophosphorus pesticide. J Hazard Mater 263(1):36–44

182. Sherly ED, Vijaya JJ, Kennedy LJ (2015) Visible-light-induced photocatalytic performances of ZnO–CuO nanocomposites for degradation of 2,4-dichlorophenol. Chin J Catal 36:1263

183. Feng Q, Li SY, Ma WH, He X, Zou YX (2017) Hydrothermal synthesis of flower-like CuO/ZnO/SiNWs photocatalyst for degradation of r6g under visible light irradiation. Key Eng Mater 727:847

184. Kaur A, Umar A, Anderson WA, Kansal SK (2018) Facile synthesis of CdS/TiO_2 nanocomposite and their catalytic activity for ofloxacin degradation under visible illumination. J Photochem Photobiol A 360:34–43

185. Chu L, Zhang J, Wu Z, Wang C, Sun Y, Dong S, Sun J (2020) Solar-driven photocatalytic removal of organic pollutants over direct Z-scheme coral-branch shape Bi_2O_3/SnO_2 composites. Mater Charact 159:110036

186. Peng L, Zheng R, Feng D, Yu H, Dong X (2020) Synthesis of eco-friendly porous $g-C_3N_4/SiO_2/SnO_2$ composite with excellent visible-light responsive photocatalysis. Arab J Chem 13(2):4275–4285

187. Priya A, Senthil RA, Selvi A, Arunachalam P, Kumar CKS, Madhavan J, Boddula R, Pothu R, Al-Mayouf AM (2020) A study of photocatalytic and photoelectrochemical activity of as-synthesized $WO_3/g-C_3N_4$ composite photocatalysts for AO_7 degradation. Mater Sci Energy Technol 3:43–50

188. Liu Y, Li M, Zhang Q, Qin P, Wang X, He G, Li L (2020) One-step synthesis of a WO_3-CuS nanosheet heterojunction with enhanced photocatalytic performance for methylene blue degradation and Cr(VI) reduction. Chem Technol Biotechnol 95(3):665–674

189. Pudukudy M, Shan S, Miao Y, Gu B, Jia Q (2020) WO_3 nanocrystals decorated Ag_3PO_4 tetrapods as an efficient visible-light responsive Z-scheme photocatalyst for the enhanced degradation of tetracycline in aqueous medium. Colloids Surf A Physicochem Eng Asp 589:124457

190. Wongaree M, Chiarakorn S, Chuangchote S, Sagawa T (2016) Photocatalytic performance of electrospun CNT/TiO_2 nanofibers in a simulated air purifier under visible light irradiation. Environ Sci Pollut Res 23:21395–21406

191. Zhou W, Pan K, Qu Y, Sun F, Tian C, Ren Z, Fu H (2010) Photodegradation of organic contamination in wastewaters by bonding TiO_2/single-walled carbon nanotube composites with enhanced photocatalytic activity. Chemosphere 81(5):555–561

192. Basha S, Barr C, Keane D, Nolan K, Morrissey A, Oelgemoller M, Tobin JM (2011) On the adsorption/photodegradation of amoxicillin in aqueous solutions by an integrated photocatalytic adsorbent (IPCA): experimental studies and kinetics analysis. Photochem Photobiol Sci 10:1014–1022

193. Pastrana-Martinez LM, Morales-Torres S, Likodimos V, Figueiredo JL, Faria JL, Falaras P, Silva AMT (2012) Advanced nanostructured photocatalysts based on reduced graphene oxide-TiO_2 composites for degradation of diphenhydramine pharmaceutical and methyl orange dye. Appl Catal B Environ 2012:123–124

194. Macias-Tamez R, Villanueva-Rodriguez M, Ramos-Delgado NA, Maya-Trevino L, Hernandez-Ramirez A (2017) Comparative study of the photocatalytic degradation of the herbicide 2,4-D Using WO_3/TiO_2 and Fe_2O_3/TiO_2 as catalysts. Water Air Soil Pollut 228:379

195. Chen Y, Wu Q, Wang J, Song Y (2019) The fabrication of magnetic recyclable nitrogen-doped titanium dioxide/calcium ferrite/diatomite heterojunction nanocomposite for improved visible-light-driven degradation of tetracycline. J Chem Technol Biotechnol 94:2702–2712

196. Lu C, Guan W, Zhang G, Ye L, Zhou Y, Zhang X (2013) TiO_2 /Fe_2O_3/CNTs magnetic photocatalyst: a fast and convenient synthesis and visible-light-driven photocatalytic degradation of tetracycline. Micro Nano Lett 8:749–752

197. Hu Z, Wang X, Dong H, Li S, Li X, Li L (2017) Efficient photocatalytic degradation of tetrabromodiphenyl ethers and simultaneous hydrogen production by TiO_2-Cu_2O composite films in N_2 atmosphere: influencing factors, kinetics and mechanism. J Hazard Mater 340:1–15

198. Sood S, Mehta SK, Sinha ASK, Kansal SK (2016) Bi_2O_3/TiO_2 heterostructures: synthesis, characterization and their application in solar light mediated photocatalyzed degradation of an antibiotic, ofloxacin. Chem Eng J 290:45–52

199. Luo L, Long J, Zhao S, Dai J, Ma L, Wang H, Xia L, Shu L, Jiang F (2019) Effective visible-light-driven photocatalytic degradation of 17α-ethynylestradiol by crosslinked CdS nanorod/TiO_2 (B) nano-belt composite. Process Saf Environ Prot 130:77–851

200. Kandi D, Behera A, Martha S, Naik B, Parida KM (2019) Quantum confinement chemistry of CdS QDs plus hot electron of Au over TiO_2 nanowire protruding to be encouraging photo-

catalyst towards nitrophenol conversion and ciprofloxacin degradation. J Environ Chem Eng 7:102821

201. Sharma S, Ibhadon AO, Francesconi MG, Mehta SK, Elumalai S, Kansal SK, Umar A, Baskoutas S (2020) Bi_2WO_6/C-Dots/TiO_2: a novel z-scheme photocatalyst for the degradation of fluoroquinolone levofloxacin from aqueous medium. Nano 10(5):910

202. Kaur A, Anderson WA, Tanvir S, Kansal SK (2019) Solar light active silver/iron oxide/zinc oxide heterostructure for photodegradation of ciprofloxacin, transformation products and antibacterial activity. J Colloid Interface Sci 557:236–253

203. Lam S, Sin J, Abdullah AZ, Mohamed AR (2013) Investigation on visible-light photocatalytic degradation of 2,4-dichlorophenoxyacetic acid in the presence of MoO_3/ZnO nanorod composites. J Mol Catal A Chem 370:123

204. Liu H, Zhai H, Hu C, Yang J, Liu Z (2017) Hydrothermal synthesis of In_2O_3 nanoparticles hybrid twins hexagonal disk ZnO heterostructures for enhanced photocatalytic activities and stability. Nanoscale Res Lett 12:466

205. Ritika M, Kaur A, Umar SK, Mehta S, Singh SK, Kansal HF, Alothman OY (2018) Rapid solar-light driven superior photocatalytic degradation of methylene blue using MoS_2-ZnO heterostructure nanorods photocatalyst. Materials (Basel) 11(11):2254

206. Lavand AB, Malghe YS (2015) Visible light photocatalytic degradation of 4-chlorophenol using C/ZnO/CdS nanocomposites. J Saudi Chem Soc 19(5):471–478

207. Lamba R, Umar A, Mehta SK, Kansal SK (2017) Enhanced visible light driven photocatalytic application of Ag2O decorated ZnO nanorods heterostructures. Sep Purif Technol 183:341–349

208. Wang T, Quan W, Jiang D, Chen L, Li D, Meng S, Chen M (2016) Synthesis of redox-mediator-free direct Z-scheme AgI/WO_3 nanocomposite photocatalysts for the degradation of tetracycline with enhanced photocatalytic activity. Chem Eng J 300:280–290

209. Liu X, Jin A, Jia Y, Xia T, Deng C, Zhu M, Chen C, Chen X (2017) Synergy of adsorption and visible-light photocatalytic degradation of methylene blue by a bifunctional Z-scheme heterojunction of WO_3/g-C_3N_4. Appl Surf Sci 405:359–371

210. Zhang L, Niu CG, Liang C, Wen X, Huang D, Guo H, Zhao X, Zeng G (2018) One-step in situ synthesis of CdS/SnO_2 heterostructure with excellent photocatalytic performance for Cr(VI) reduction and tetracycline degradation. Chem Eng J 352:863–875

211. Lamba R, Umar A, Mehta SK, Kansal SK (2015) Well-crystalline porous ZnO–SnO_2 nanosheets: an effective visible-light driven photocatalyst and highly sensitive smart sensor material. Talanta 131:490–498

212. Umukoro EH, Kumar N, Ngila JC, Arotiba OA (2018) Expanded graphite supported p-n MoS_2-SnO_2 heterojunction nanocomposite electrode for enhanced photo-electrocatalytic degradation of a pharmaceutical pollutant. J Electroanal Chem 827:193–203

Biohydrometallurgy: A Sustainable Approach for Urban Mining of Metals and Metal Refining

Prashant Ram Jadhao, Snigdha Mishra, Ashish Pandey, K. K. Pant, and K. D. P. Nigam

Abstract Electronic waste (e-waste) is termed as "urban mines" due to high metal content. Metals are major components of e-waste and have a share of 61 wt% of e-waste. E-waste contains various valuable metals such as gold, silver, platinum, palladium, copper, nickel, etc. Therefore, metal recovery is important to conserve the resources. Apart from this, the unregulated accumulation and improper recycling of e-waste have harmful effects on human health and environment. Therefore, environmentally friendly e-waste recycling is the need of the hour to mitigate the harmful effects. Currently, pyrometallurgy and hydrometallurgy are the conventional processes employed for recovery of metals from e-waste. However, these technologies are non-selective and energy-intensive, employ hazardous chemicals, and produce toxic gases. Biohydrometallurgy is a promising alternative and is an eco-friendly approach to recycle e-waste as it employs microorganisms for metal recovery. Biohydrometallurgy employs different approaches such as autotrophic bacteria bioleaching, heterotrophic bacteria bioleaching, and heterotrophic fungi bioleaching for leaching of metals and has been discussed in this chapter. In addition, the refining of metals from metal leached solution has also been discussed in this chapter. The development of continuous process for metal recovery is important, and we have discussed a coiled flow inverter (CFI) reactor as a promising option for the same.

Keywords E-waste · Urban mining · Biohydrometallurgy · Bioleaching · Coiled flow inverter · Waste management

P. R. Jadhao · S. Mishra · A. Pandey · K. K. Pant (✉) · K. D. P. Nigam
Department of Chemical Engineering, Indian Institute of Technology Delhi, New Delhi, India
e-mail: kkpant@chemical.iitd.ac.in

1   Introduction

Electronic waste (e-waste) is rapidly growing, and 53.6 million tons (Mt) of e-waste was generated in 2019 [1]. It is expected that the e-waste generation will be around 74.7 Mt by 2030 [1, 2]. In 2019, Asia produced 24.9 Mt of e-waste and followed by America, Europe, Africa, and Oceania which have generated 13.1, 12, 2.9, and 0.7 Mt of e-waste, respectively [1]. The e-waste generation is increasing with an annual growth of 2 Mt from 2014 and is shown in Fig. 1 along with projected values till 2030 [1]. However, the recycling rate is not keeping pace with the e-waste generation. Europe is leading in the e-waste recycling with a recycling rate of 42.5%, while Asia is at the second position with an 11.7% recycling rate and followed by America, Oceania, and Africa which have a recycling rate of 9.4%, 8.8%, and 0.9%, respectively [1]. Only 17.4% of e-waste was properly recycled, while the fate of around 82.6% of e-waste generated in 2019 is not known [1].

   The amount of e-waste which is not documented in 2019 contains 71 kilotons of brominated flame retardants (BFR), 98 Mt of CO_2 in the form of hydrochlorofluorocarbons (HCFCs) and chlorofluorocarbons (CFCs), and 50 t of mercury [1]. Apart from this, e-waste contains various toxic substances such as Sb, As, Ba, Cd, Pb, polychlorinated biphenyls, etc. [3]. Unregulated accumulation of e-waste leads to the leaching of these substances into the soil and water and then containment the food chain. Table 1 shows the different harmful substances existing in e-waste and their hazardous effects. In addition, informal recycling, i.e., open burning of e-waste, leads to the formation of harmful chemicals such as dioxins and furans.

   Although e-waste contains various toxic substances, it can also act as a secondary source of valuable metals owing to its high metal content. E-waste mainly
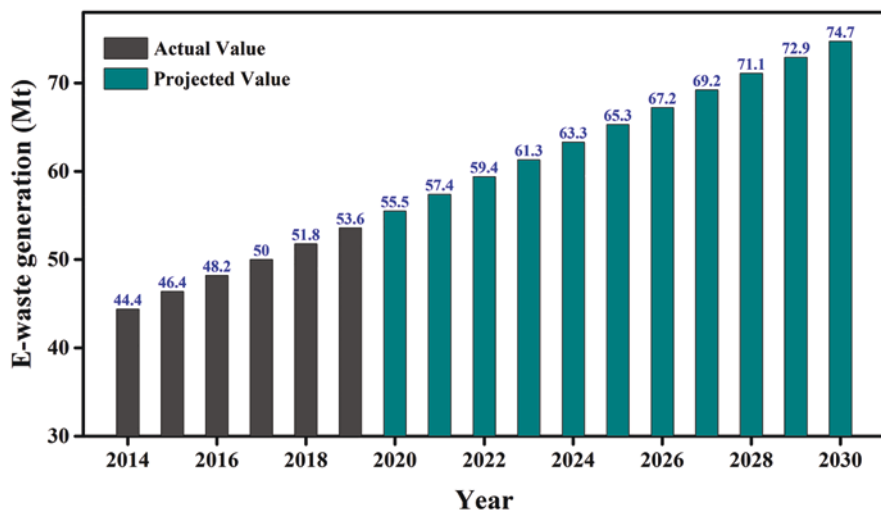
Fig. 1 E-waste generation data from 2014 to 2030

Table 1 Harmful substances in e-waste and their hazardous effects [3, 4]

Toxic substance	Hazardous effect on human health
Antimony	Can cause stomach ulcer
Arsenic	Leads to skin disease and lung cancer
Barium	Brain swelling, damage to the heart and liver
Beryllium	Lung cancer, skin disease
Brominated flame retardants	Leads to hormonal disorder
Cadmium	Damage to the kidney
Chlorofluorocarbons (CFCs)	Can cause skin cancer
Lead	Can damage the brain and kidneys
Nickel	Can cause bronchitis and lung cancer
Polychlorinated biphenyls	Liver damage in human
Polyvinyl chloride (PVC)	Can cause respiratory problems

consists of metals, plastics, rubber, ceramics, and glass [5]. Out of these, metals are the main components and have a share of 61% by wt. of e-waste [6]. E-waste contains different heavy metals, like Cu, Ni, Hg, Cd, and Pb, and precious metals like Au, Ag, Pt, and Pd [7]. Electrical and electronic equipment industry consumes over 50% of the ruthenium, antimony, and indium and more than 30% of silver, copper, and tin produced annually [8]. Hence, recovery of metals from e-waste is necessary to mitigate the scarcity of metals. The printed circuit board (PCB) of a personal computer contains 20% Cu and 250 g/ton of Au, whereas the concentrations of Cu and Au in ores are 0.5–1% and 1–10 g/ton, respectively [9, 10]. The metal recovery from e-waste will provide advantages such as the conservation of primary metal resources, energy-saving, and prevention of environmental pollution caused due to leaching of metals.

It is clear from the above discussion that it is very important to not dump the e-waste or treat it inappropriately. E-waste recycling is important from the aspect of recovery of metals and mitigating the environmental and human health hazards. Therefore, various technologies like pyrometallurgy [11–13], hydrometallurgy [14–16], and biohydrometallurgy [17–19] have been employed for the recovery of metals from e-waste. Out of these, pyrometallurgy and hydrometallurgy are conventional processes employed for the recovery of metals from e-waste. However, both these technologies have disadvantages associated with them. The use of pyrometallurgical approach leads to the generation of dioxins and furans due to the presence of halogenated flame retardants in e-waste [20]. In addition, pyrometallurgy uses very high temperature, i.e., above 1000 °C, for metal recovery and makes this process energy-intensive [21]. In the case of hydrometallurgy, there is no or less formation of toxic gases, but the hydrometallurgical process uses toxic solvents such as acid, cyanide, halide, thiosulfate, and thiourea for the recovery of metals [22, 23]. The use of these chemicals limits the industrial application of hydrometallurgy. Compared to pyrometallurgy and hydrometallurgy, biohydrometallurgy uses microorganisms for the recovery of metals which makes this process an eco-friendly approach. Biohydrometallurgy is proven efficient for the recovery of metal from primary ores

and can play an important role in the efficient recovery of metal from e-waste [24, 25]. Biohydrometallurgy provides advantages such as selectivity toward valuable metals, cost-effectiveness, and lower environmental hazards [26, 27]. Bioleaching of e-waste is a new field compared to hydrometallurgy and pyroometallurgy, and it can be seen from Fig. 2. The numbers of publication in the field of e-waste are
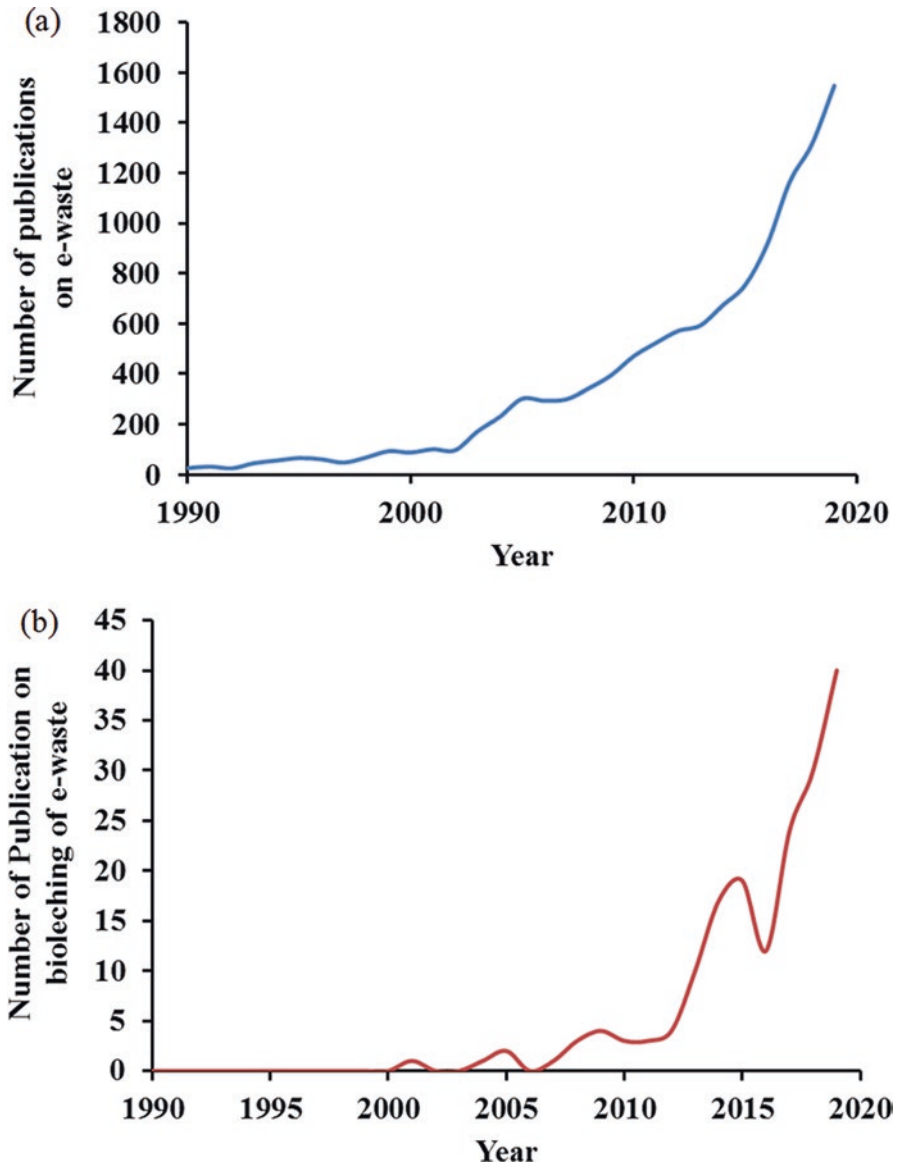
Fig. 2 Number of publication (**a**) on e-waste and (**b**) bioleaching of e-waste

constantly increasing. The biohydrometallurgy is a new technique in the field of e-waste which can be seen from Fig. 2b.

This chapter focuses on the recent development in the recovery of valuable metals from e-waste using biohydrometallurgy. In this chapter, various biohydrometallurgical approaches, i.e., autotrophic bacteria bioleaching, heterotrophic bacteria bioleaching, and heterotrophic fungi bioleaching, have been discussed. In addition, this chapter also focuses on the different approaches such as biosorption and bioelectrochemical process for the recovery of metals from the metal leach solution.

2   Different Bioleaching Approaches for Metal Recovery

Bioleaching of metals has been investigated using various microorganisms, and these microorganisms have the natural capability to leach the metals into aqueous solution. Usually, autotrophic bacteria, heterotrophic bacteria, and heterotrophic fungi are the most frequently used microorganisms for the recovery of metals from different sources as shown in Fig. 3. The bioleaching using each of these is discussed in the following subsections.
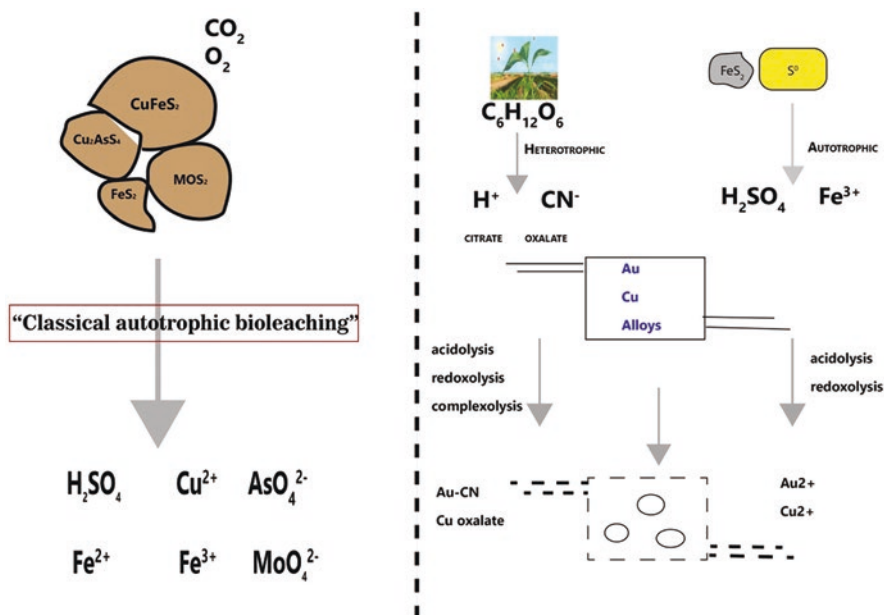
Fig. 3 Bioleaching of primary ores and secondary raw materials

2.1 Autotrophic Bacteria Bioleaching

The autotrophic bioleaching is mainly carried out using chemolithotrophic and aci-dophilic bacteria. These organisms use carbon dioxide from the atmosphere as a carbon source and ferrous ion (Fe^{2+}), elemental sulfur (S^o), and/or reduced sulfur compounds as an energy source [28, 29]. Most chemolithotrophic bacteria have a high tolerance for heavy metal toxicity and therefore are the most widely used microorganisms to recover metals from polymetallic sources such as e-waste [30]. The microorganisms used in autotrophic bioleaching are sulfur-oxidizing bacteria, iron- and sulfur-oxidizing bacteria, and iron-oxidizing bacteria [19]. The above men-tioned microorganisms lead to the sulfur and iron oxidation which causes metal sulfide solubilization and decreases the pH of the environment which ultimately causes the solubilization of other metal compounds. These microorganisms flourish on the iron- and sulfur-containing sources (e.g., pyrite, pentlandite, and chalcopy-rite) at 45–75 °C [31]. However, in the case of e-waste, autotrophic bacteria cannot grow directly on the oxidation/dissolution of the e-waste matrix. Therefore, it is important to mixed e-waste with sulfur- or iron-containing sources such as pyrite, pentlandite, and chalcopyrite to provide energy for the growth of autotrophic bacte-ria [32]. As a result, the microbial oxidation of sulfur- and iron-containing sources will produce acidic environment and ferric ion, and this will help in the leaching of metals from e-waste. It is important to notice that the autotrophic bioleaching of sulfidic ores only leaches the metallic fraction of e-waste, while the non-metallic fraction remains as it is. The recovery of rare earth metals from other sources will also need to mix with the sulfur- and iron-containing sources for the growth of auto-trophic bacteria. The research work carried for metal recovery from e-waste using autotrophic bacteria is mainly focused on transition metal and also rare earth ele-ment (REE) recovery.

Hong et al. investigated the bioleaching of copper using *Acidithiobacillus thio-oxidans* bacteria and studied abiotic leaching and direct and indirect bioleaching [33]. The acidophilic bacteria were cultivated and during which the sulfuric acid was produced. This acid was used for indirect bioleaching. However, in the case of direct bioleaching, the sterilized e-waste was directly added during the growth phase of bacteria. The direct leaching was performed at 30 °C, and 10 g/dm^3 e-waste were added to the microbe culture when pH was reached to 1. At the same process condition, there is not much difference between the Cu leaching in both direct and indirect bioleaching. Therefore, it can be concluded that the toxicity of e-waste at the concentration of 10 g/dm^3 doesn't have a significant effect on microorganism metabolism. The indirect leaching was also carried out at 90 °C, and the results were compared with abiotic leaching. It was observed that for 8 h of leaching time, the copper leaching is lower in the case of indirect leaching (60%) compared to abiotic leaching (98%). It was found that after 6 h of leaching, there is the formation of CuS on the surface which results in the passivation of Cu surface and decreases the leaching of Cu in biogenic acid. The formation of CuS can be attributed to the presence of incompletely oxidized sulfide and sulfates.

In a different study, Chen et al. studied the application of *Acidithiobacillus ferrooxidans* for copper leaching from WPCB [34]. Sulfuric acid and ferric ion play an important role during the bioleaching process. During the bioleaching, ferrous ions are oxidized to ferric ions as shown in Eq. (1), while Cu oxidizes to Cu^{2+} by Fe^{3+}, and Fe^{3+} reduces to Fe^{2+} as shown in Eq. (2). This Fe cycle increases the rate of reaction significantly. The column bioleaching was employed for the copper recovery, and the temperature of the column reactor was maintained at 30 °C during the complete process. For a typical experiment, 250 g of washed sample was added to the column, and then 495 L of prepared 4.5 K medium along with 0.05 L of *A. ferrooxidans* culture was added into the column reactor. The pH of the solution in the column was maintained at 2.25 (±0.05) using 5 M of H_2SO_4. The maximum leaching of copper was measured to be 94.8% in 28 days. It was found that pH is an important factor and greatly influences the copper leaching. The kinetics of the bioleaching process does not change as the size and morphology of precipitates remain the same as the pH was maintained at 2.25. The addition of sulfuric acid and maintaining an acidic pH of solution aid in preventing the formation of jarosite precipitate, and this helps in the Fe^{2+}–Fe^{3+} cycle to go on to create a favorable environment for copper bioleaching.

$$4Fe^{2+} + 4H^+ + O_2 \xrightarrow{\text{A.ferrooxidans}} 4Fe^{3+} 2H_2O \tag{1}$$

$$Cu + 2Fe^{3+} \rightarrow Cu^{2+} + 2Fe^{2+} \tag{2}$$
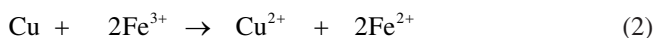
Isildar et al. studied the bioleaching of copper using *Acidithiobacillus ferrivorans*, *Acidithiobacillus thiooxidans*, and a mixture of both [35]. The leaching efficiencies of 94%, 89%, and 98% were reported using a pure culture of *A. ferrivorans*, *A. thiooxidans*, and a mixture of both, respectively, at a pulp density of 1%. It is reported that the pulp density below 2.5% is efficient for the bioleaching of copper. The hazardous components of PCB such as metals, phenols, and BFRs are harmful to the bacterial activity, and therefore, to prevent the toxic effect of these components on bacteria, a pre-growth method was applied. A pre-growth method was also helpful in producing favorable bioleaching conditions. The microorganisms were incubated in the bioleaching medium, and the culture was prepared in the absence of waste PCB. The waste PCBs were added after attaining the optimal bioleaching conditions. The measurement of pH and ORP helps in monitoring the bacterial activity, and these parameters also show the presence of both acidolysis and redoxolysis mechanisms. The increase in pulp density from 0% to 5% increases the pH due to the basic nature of waste material. When the pulp density is 2.5% or higher, then pH value does not drop below 2.5 where acidophiles thrive. The pulp density of 1% and lower is best suited for the growth of microorganisms. Acidophiles play an important role to catalyze the oxidation of Fe^{2+} to Fe^{3+} as shown in Eq. (1) and elemental sulfur (S_0) to sulfuric acid as shown in Eq. (3):

$$S_0 + 1.5O_2 + H_2O \rightarrow 2H^+ + SO_4^{2-} \tag{3}$$
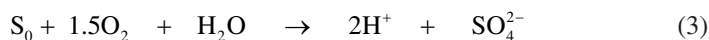
The recovery of Cu takes places under low pH and high ORP conditions as shown in Eqs. (2) and (4):

$$Cu_0 + H_2SO_4 + \ 0.5\,O_2 \quad \rightarrow \quad Cu^{2+} + \ SO_4^{2-} \ + \ H_2O \tag{4}$$

The copper leaching is higher in the case of a co-culture of iron- and sulfur-oxidizing acidophiles. Therefore, it is reported that the involvement of redoxolysis and acidolysis is beneficial for metal recovery. Table 2 shows the summary of research works carried out for metal recovery using autotrophic bioleaching.

2.2   Heterotrophic Bioleaching

The scientific community has recently started to explore the various biotechnological approaches to recover REE from secondary metal sources [42–44]. Heterotrophic bioleaching is an encouraging technique for the recovery of metals from the sources which do not contain metal sulfides [44]. Microorganisms such as bacteria, fungi, and archaea are commonly employed during heterotrophic bioleaching [19, 45]. Heterotrophic bioleaching is microbial leaching where organisms get energy from organic carbon sources for growth during the leaching process [46]. The metabolic by-products of organic carbon such as acetic acid, citric acid, oxalic acid, and gluconic acid are responsible for the leaching of metals when the pH is between 4 and 6 [47]. Apart from this, the protein catabolism produces non-acidic complexion agents which can be employed during alkaline leaching [19]. The metal recovery using heterotrophic bioleaching mainly occurs via cyanide- and organic acid-producing organisms. The cyanogenic bioleaching is employed to recover precious and platinum group metals. However, chelation is used for the recovery of critical metals such as cobalt, gallium, germanium, lithium, antimony, and tungsten. The heterotrophic microorganism can be used for metal leaching in higher pH conditions and, therefore, can be employed to treat alkaline wastes compared to acidophiles [45].

2.2.1   Heterotrophic Bacterial Bioleaching

Pseudomonas aeruginosa, *Pseudomonas fluorescens*, and *Pseudomonas putida* are the *Pseudomonas* strains used for metal leaching. These microorganisms are omnipresent, and in soil, they solubilize metals due to various metabolic products.

Jujun et al. found a new strain of *Pseudomonas* which has the ability to produce CN^- and can recover precious metals [48]. The ability to produce CN^- of different strains such as *Pseudomonas aeruginosa*, *Pseudomonas chlororaphis*, *Pseudomonas putida*, *Pseudomonas mosselii*, *Pseudomonas fluorescens*, and *Pseudomonas* sp. was investigated. The experiments were performed to find out the concentration of produced CN^- by the above mentioned strains. These strains were cultured for 24 h

Table 2 Summary of research work on metal recovery using autotrophic bioleaching

E-waste	Microorganism	Bioleaching conditions	Metal recovery, %	Reference
Mobile PCB	*Acidithiobacillus ferrooxidans*	pH = 1, pulp density = 8.5 g/L, Fe^{3+} concentration = 4.18 g/L, particle size = 100 mesh, time = 55 days, temp. = 30 °C, stirring speed = 170 rpm	Cu=100 Ni=100	[36]
Electronic waste	*Acidithiobacillus thiooxidans*	25 g/L of sulfur in culture medium, temp. = 90 °C, pH < 1, particle size = 40–104 μm, time = 14 days, pulp density—10 g/dm³	Cu = 90	[33]
Computer PCB	*Acidithiobacillus ferrooxidans*	pH = 3, Fe^{3+} conc. = 8.4 g/L, pulp density = 20 g/L, particle size = 95 μm, temp. = 30 °C, time = 80 days, stirring speed = 170 rpm	Cu = 100 Ni = 100	[37]
Mobile PCB	*Acidithiobacillus ferrooxidans*	pH = 2, time = 14–17 days, particle size = 93 μm, pulp density = 20 g/L	Cu = 80	[38]
Computer PCB	*Acidithiobacillus ferrooxidans*	pH = 3, time = 17–20 days, particle size = 93 μm, pulp density = 20 g/L	Cu = 90	[38]
PCBs	*Acidithiobacillus ferrooxidans + Acidithiobacillus thiooxidans*	Stirring speed = 200 rpm, temp. = 32 °C, pH = 1.5, pulp density = 18 g/L, particle size = 100–200 μm, time = 10 days	Cu = 94 Ni = 89 Zn = 90 Pb = 86	[39]
Spent batteries	*Acidithiobacillus ferrooxidans*	Stirring speed = 160 rpm, pH = 1, temp. = 30 °C, particle size = 62 μm, Fe^{3+} conc. = 9.7 g/L, pulp density = 10 g/L, time = 20 days	Ni = 85.6 Cd = 66.1 Co = 90.6	[40]
PCB	*Acidithiobacillus ferrooxidans*	Stirring speed = 165 rpm, pH = 2.25, temp. = 30 °C, particle size = 178–250 μm, Fe^{3+} conc. = 9 g/L, pulp density = 12 g/L, time = 3 days	Cu = 92	[41]

at 25 °C, and then the CN$^-$ concentration was tested. It was reported that the *Pseudomonas chlororaphis* has produced the highest concentration of CN$^-$ (7.11 mg/L). Afterward, *Pseudomonas chlororaphis* was selected to investigate the metal recovery, and the effect of various process variables like culture condition, pH, temperature, additive, and stirring speed on the ability to produce CN$^-$ was studied. The optimized conditions for producing maximum CN$^-$ were pH 7 and adding glycine (4.4 g/L) + methionine (2 g/L) into NB culture medium which is cultured for 72 h at 25 °C with a stirring speed of 60 rpm. At the optimized conditions, the recovery of gold, silver, and copper was 8.2%, 12.1%, and 52.3%, respectively, from the metallic particles obtained from crushed waste PCBs.

Chi et al. studied the copper and gold recovery using *Chromobacterium violaceum* (*C. violaceum*) from waste mobile phone printed circuit boards [49]. The bioleaching was performed in the presence of YP medium (yeast extraction, polypeptone, and glycine), and the effect of pH and hydrogen peroxide on copper and gold recovery was investigated. It is reported that gold leaching increase from 7.78% to 10.9% when pH was increased from 8 to 11 in 8 days. Similarly, the copper leaching was also increased from 4.9% to 11.4% with an increase in pH from 8 to 10. Marsden and House reported that the Cu(CN)$^{2-}$ is formed when pH is less than 9, while at higher pH, more amounts of Cu(CN)$^{3-}$ and Cu(CN)$_4^{3-}$ will form [50]. Metal leaching is improved at higher pH due to the high stability of metal cyanide complexes and increases the stability of HCN at pH > 10 [51]. Similarly, Au(CN)$^{2-}$ forms at higher pH, and high dissolved oxygen favors gold leaching [52]. The hydrogen peroxide was employed to increase the dissolved oxygen to facilitate more metal leaching. The hydrogen peroxide concentration above 0.004% negatively hampers the bacteria, and therefore, 0.004% hydrogen peroxide was considered as the optimum for metal leaching. The increase in hydrogen peroxide concentration leads to an increase in the metal leaching from 7.23% to 24.6% with an increase in pH from 8.5 to 10 in 8 days. The recovery of gold is increased slightly from 8.1% to 11.32% when pH was increased from 8.5 to 11 in the presence of hydrogen peroxide. The higher copper recovery compared to gold can be attributed to the galvanic interaction and gold being nobler than copper. Therefore, it is important to leach copper prior to gold leaching to improve the gold bioleaching.

Cu is a major component of the e-waste, and as mentioned above, it is important to recover Cu before Au and Ag for their efficient recovery. Therefore, Isiladar et al. developed a two-stage bioleaching process for Cu and Au recovery. In the first step, 98% Cu was leached using a mixture of *Acidithiobacillus ferrivorans* and *Acidithiobacillus thiooxidans* [35]. In the next step, Au was recovered using *Pseudomonas putida* at 25 °C, and a 44% recovery of Au was reported. The low recovery of gold can be attributed to the lower amount of cyanide generation (21.4 mg/L) from *Pseudomonas* cultures, and this did not allow complete gold recovery. Marra et al. have also investigated metal bioleaching in two steps [53]. In the first step, rare earth metals such as cerium, europium, neodymium, lanthanum, and yttrium were recovered using *Acidithiobacillus thiooxidans* from e-waste dust. During the first step, recovery of cerium, europium, and neodymium was 99%,

while that of lanthanum and yttrium is around 80%. In the second step, gold was recovered using the *Pseudomonas putida* and reported the 48% recovery of Au within 3 h.

Several researchers have tried to increase the production of biogenic cyanide using different approaches such as sequential nutrient addition, medium modification, and genetic modification. Natarajan et al. tried to improve the production of biogenic cyanide than *Chromobacterium violaceum*; two metabolically engineered stains, pBAD hcn (induced by L-arabinose) and pTAC hcn (induced by IPTG), were prepared [54]. It is reported that the pBAD (induced with 0.002% L-arabinose) and pTAC (induced with 1 mM IPTG) have produced 34.5 and 31 mg/L of cyanide, respectively, whereas *Chromobacterium violaceum* has produced 20 mg/L cyanide. The increase in the cyanide concentration results in higher gold leaching. The pBAD and pTAC showed 30% and 27% gold leaching at 0.5% w/v pulp density compared to 11% gold leaching using wild-type bacteria. Similarly, Natarajan and Ting studied the effect of mutation of *Chromobacterium violaceum* bacteria to grow under alkaline environment on the production of biogenic cyanide for gold bioleaching [55]. The mutation of bacteria was performed by exposing the wild *C. violaceum* to 100 mM of the mutagen, i.e., N-nitroso-N-ethyl urea (ENU), at pH 9, 9.5, and 10. The gold recovery reported using the *C. violaceum* mutated at pH 9, 9.5, and 10 was 18%, 22.5%, and 19%, respectively. Under alkaline conditions, there are a growth of bacteria and production of cyanide which increases the availability of cyanide ion, thereby increasing the gold leaching. The lower gold leaching using the *C. violaceum* mutated at pH 10 as it has significantly lower growth compared to others. The wild strain of *C. violaceum* grown at pH 9 and 9.5 showed 14% and 16% gold leaching, respectively, whereas wild strain grown at pH 10 showed no gold leaching. Therefore, from these studies, it is clear that genetic modification or medium modification can lead to higher metal leaching. Table 3 shows the summary of research work on metal recovery using heterotrophic bacterial leaching.

2.2.2 Heterotrophic Fungi Bioleaching

Heterotrophic fungi bioleaching involves the metal leaching using the organically excreted acid (acidolysis and complexolysis) and changing the oxidation potential of the medium (redoxolysis) or a combination of acidolysis, complexolysis, and redoxolysis [31, 59]. The fungal redoxolysis leaching occurs at comparatively higher pH, i.e., near pH 7 or above [31]. *Aspergillus niger* and *Penicillium simplicissimum* are the most used microorganisms in the fungal leaching of metal from various waste sources [59]. Brandl et al. investigated the bioleaching of metals form electronic waste using *Aspergillus niger* and *Penicillium simplicissimum* [60]. During the growth, various organic acids such as citrate, gluconate, and oxalate were formed which are responsible for the metal leaching. It is reported that *P. simplicissimum* has been more efficient for the leaching of metals compared to *A. niger* under identical conditions. Both the fungal species were able to recover 65% of Cu and Sn, whereas the recovery of Al, Ni, Pb, and Zn was more than 95%. Authors

Table 3 Summary of research work on metal recovery using heterotrophic bioleaching

E-waste	Microorganism	Bioleaching conditions	Metal recovery, %	Reference
PCB	*Chromobacterium violaceum*	Stirring speed = 150 rpm, pH = 6.8, temp. = 30 °C, particle size = 200 mesh, time = 7 days	Au = 70.6	[56]
Electrical scrap	*Chromobacterium violaceum*	Stirring speed = 150 rpm, pH = 10, temp. = 30 °C, pulp density = 15 g/L, particle size = 1 × 1 mm^2, H$_2$O$_2$ = 0.004% v/v, time = 8 days	Au = 24.6	[49]
Computer PCB	*P. aeruginosa + C. violaceum*	Stirring speed = 150 rpm, pH = 7.2, temp. = 30 °C, pulp density = 1% (w/v), particle size =37–149 μm, time = 7 days	Cu = 83.46 Au = 73.17 Zn = 49.11 Fe = 13.98 Ag = 8.42	[57]
Computer PCB	*P. aeruginosa*	Stirring speed = 150 rpm, pH = 7.2, temp. = 30 °C, pulp density = 1% (w/v), particle size =37–149 μm, time = 7 days	Au = 52 Cu = 52 Zn = 39	[57]
Electronic scrap	*C. violaceum*	Stirring speed = 150 rpm, pH = 9.5, temp. = 30 °C, pulp density = 0.5% (w/v), particle size <100 μm, time = 8 days	Au = 22.5	[55]
Electrical scrap	*P. plecoglossicida*	Stirring speed = 150 rpm, pH = 7.2, temp. = 30 °C, particle size <71 μm, time = 4 days	Au = 68.5	[58]

have suggested a two-step approach for the bioleaching of metals as e-scrap has negative impact on growth of microorganisms. It is recommended that in the first step, growth of the microorganisms will take place without e-scrap and in the next step, the metabolites produced will be employed for metal leaching. It is previously recommended for the treatment of fly ash for metal leaching using bacteria and fungi leaching and has the following advantages [61, 62]:

1. Microorganisms can be recycled.
2. Optimization of acid formation due to absence of waste material.
3. The high concentration of waste material can be used during the leaching step.

Desouky et al. studied the leaching of rare earth metals from the waste material using *A. ficuum* [63]. The metabolite containing organic acids was produced using *A. ficuum* at pH 3. The waste material (0.75 g) was then added to the metabolite, and then the mixture was stirred using rotary shaker at 175 rpm for 24 h. The leaching of uranium, thorium, lanthanum, cerium, and yttrium was reported as 30%, 29%, 20%, 33%, and 2.5%, respectively. It is also reported that thorium was precipitated from the leached solution as thorium oxalate using oxalic acid at pH 0.9 and uranium was precipitated as ammonium diuranate using ammonia solution at pH 5–6.

In addition to this, rare earth metals were precipitated as rare earth oxalate using oxalic acid at pH 8–8.3.

Hassanien et al. compared the bioleaching efficiencies of one- and two-step bioleaching processes for rare earth metal leaching from Egyptian monazite and thorium-uranium concentrate using *A. ficuum* [64]. In one-step bioleaching, *A. ficuum* was grown in the media in the presence of the 1 g of monazite or thorium-uranium concentrate. However, in the indirect bioleaching process, the *A. ficuum* was grown in the media in the absence of monazite or thorium-uranium concentrate. The 1 g of monazite and thorium-uranium concentrate was added after the separation of microbial biomass. In the case of direct bioleaching, the leaching of rare earth elements using *A. ficuum* was reported as 60.6% and 50.3% within 10 days from monazite and thorium-uranium concentrate, respectively, whereas, in the case of indirect bioleaching, the leaching of rare earth metals was 55.0% and 47.7% from monazite and thorium-uranium concentrate, respectively. The pH was decreased from 3.9 to 3 due to the formation of amino acid and other metabolites during the growth of *A. ficuum*. These metabolites help in the leaching of metals using hydrogen ions or forming the metal complexes, whereas there is an increase in the pH during indirect bioleaching due to the consumption of proton to convert oxides present in a sample to soluble metal salts. The organic acid formed plays an important role and acts as leaching agents during the fungi bioleaching process. The organic acids such as citric, tartaric, oxalic, and gluconic acids were produced during the growth of *A. ficuum*. The complex formation reaction between rare earth element cations (Re_2O_3) and citric acid may take place as below:

$$C_6H_8O_7 \quad \rightarrow \quad \left(C_6H_5O_7\right)^{3-} \quad + \quad 3H^+\left(pKa = 6.93\right) \tag{5}$$

$$\left(C_6H_5O_7\right)^{3-} \quad + \quad Re_2O_3 \quad \rightarrow \quad Re\left(C_6H_5O_7\right)$$
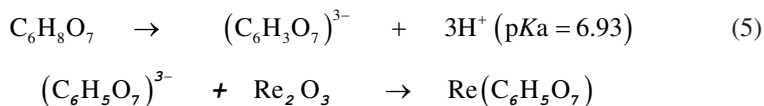
The possible reactions between the oxalic acid and rare earth elements are as follows:

$$C_2H_2O_4 \quad \rightarrow \quad \left(C_2HO_4\right)^{1-} \quad + \quad H^+\left(pK_a = 1.2\right) \tag{6}$$

$$3\left(C_2HO_4\right)^{1-} \quad + \quad Re_2O_3 \quad \rightarrow \quad Re\left(C_2HO_4\right)_3$$

$$C_2H_2O_4 \quad \rightarrow \quad \left(C_2O_4\right)^{2-} \quad + \quad 2H^+\left(pK_a = 4.2\right) \tag{7}$$

$$3\left(C_2O_4\right)^{2} \quad + \quad 2\,Re_2O_3 \quad \rightarrow \quad Re_2\left(C_2O_4\right)_3$$
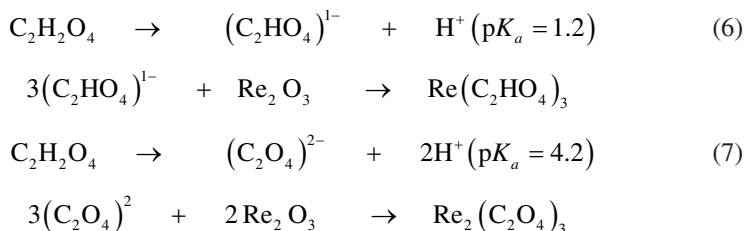
Similarly, the gluconic acid reacts with the rare earth elements as follows:

$$C_6H_{12}O_7 \quad \rightarrow \quad \left(C_6H_{11}O_7\right)^{1-} \quad + \quad H^+\left(pK_a = 3.66\right) \tag{8}$$

$$3\left(C_6H_{11}O_7\right)^{1-} \quad + \quad Re_2O_3 \quad \rightarrow \quad Re\left(C_6H_{11}O_7\right)_3$$
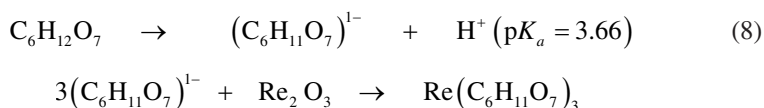
3   Metal Refining

In recent years, significant research for environmental protection is focused on the removal of metals from industrial wastewater, soil, and ground wastewater. The bio-based technologies are being employed for this purpose. Biosorption and bioprecipitation are some of the bio-based technologies employed for metal recovery which are low-cost, eco-friendly biological strategies with a low waste generation [65]. An integrated approach combining conventional metallurgical systems with bioelectrochemical and biosorption processes will be a great leap toward the development of green technology.

3.1   *Biosorption*

Biosorption is a combination of adsorption and absorption which depends on the binding capacity of potential biological sorbents like algae, bacteria [66, 67], yeasts [68], and fungi with metal [69, 70]. Various living or dormant biological materials like fungus, bacteria, agriculture residue, and biomass residual of fermentation process have been studied for the biosorption process [71–73]. Generally, the biosorption process is an interaction of metal ions present in aqueous solution with the biological material surface, thereby reducing metal ion concentration in aqueous solution as shown in Fig. 4. There are several mechanisms of biosorption which include ion exchange, reduction, precipitation, etc., and due to the complex process and nature of biomaterials, there is a possibility of a combination of mechanism [66].

The cell structure of biosorbent plays a vital role in the sorption process. Bacteria are one of the widely used biosorbent and are classified based on the composition of the cell wall, which highly affects the efficiency of metal absorption [66, 70]. Teichoic acid is present in the cell membrane of gram-positive bacteria, and
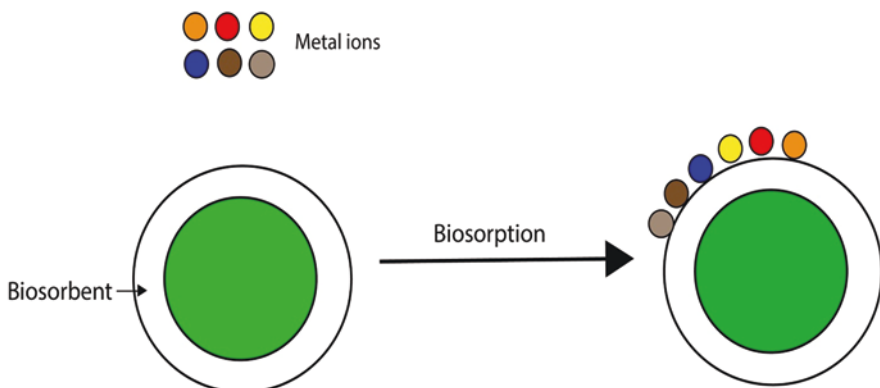
Fig. 4   Biosorption process

phosphodiester bonds between the teichoic acid impart negative charge which enhances the sorption of metal ions. Similarly, phospholipid and lipopolysaccharide layers are present in the outer layer of gram-negative bacteria which imparts negative charge and expedites metal biosorption [74]. Potential bacterial biosorbents are *Bacillus* [75, 76] and *Streptomyces* [77, 78] in gram-positive genus and *Pseudomonas* [76, 79] in gram-negative genus.

In addition to bacteria, fungal biosorbents have a huge potential in metal biosorption as it is easier to grow and can be modified genetically or chemically. Chitin, lipids, polyphosphates, and proteins are some species of fungi with metal binding groups such as amines, phosphates, carboxyl, hydroxyl, etc. *Aspergillus* [80], *Rhizopus* [81], and *Penicillium* [82, 83] are important fungal biosorbents. Cheap production and least sensitivity toward alteration in nutrients and process parameters (pH, temperature, aeration) make fungi fit for industrial use [84]. Yeast biomass is also used for specific metal biosorption. *Saccharomyces cerevisiae* is one of the widely used yeast biomass with high biosorption capacity [85]. Extensive use of microorganisms in food/pharmaceutical industries generates immense amounts of waste which can be reutilized in the metal sorption process [86, 87]. Functional groups of sorbent material play a major role in biosorption mechanism, and alteration of the functional group via physical or chemical means affects the sorption capacity [88]. Functional groups (mainly COOH, NH_2, OH, and SH) present on biosorbent surface form complexes with metal ions in solution via chemical binding, microprecipitation, ion exchange, etc. [89]. Tuning of functional groups of biomaterials can be done by surface modification techniques like ultrasonication, heat treatment, or changing crosslinking by acid/alkali treatment [90]. The pre-treatment technique modifies surface groups by removing, masking, or exposing binding sites. It was observed that biosorption capacity is immensely affected by pretreatment technique and time [90].

Various researchers have studied the effect of process parameters such as pH, contact time, the concentration of feed, and amount of biosorbent on the biosorption [64, 65]. Kalak et al. studied the effect of process parameters like pH, biosorbent dosage, and initial concentration of metal ions which directly affect the efficiency of biosorption of Fe (III) onto *elderberry* [91]. The initial concentration of metal ions in aqueous solution affects the saturation of biosorbent surface, whereas considerable pH change leads to deprotonation of the acid group present on biomass, surging probability of adsorption of positive metal ions onto elderberry. Vendruscolo et al. discussed different microbial systems to recover Cr (VI) from industrial effluent and concluded that versatile biosorbents in their viable or non-viable forms can be used in the batch, fed-batch, or continuous reactors [92]. Further, it is also reported that microorganism's isolation, novel selection, and genetic alterations are the key parameters for the technological advancement of biosorption in metal absorption. The summary of research work on the recovery of metals using biosorbent from aqueous solution is shown in Table 4.

Nicomal et al. recovered indium, a major component in the optical electronic industry, using microalgae biomass [94]. Microalgal biomass has shown high

Table 4 Recovery of major metals via biosorption from an aqueous solution

Metal ions	Biosorbent	Biosorption capacity (mg/g)	Reference
Ag (I)	*Klebsiella sp. 3S1*	114.1 mg/g	[86]
	Bacillus cereus biomass	91.75 mg/g	[93]
Fe (III)	*Elderberry (Sambucus nigra)*	33.25 mg/g	[91]
	Chlorella vulgaris	129.83 mg/g	[71]
In (III)	*Microalgae biomass*	0.144 mmol/g	[94]
Cd (II)	*Phanerochaete chrysosporium*	47.85 mg/g	[65]
	Cronobacter muytjensii	72.45 mg/g	[95]
Cu (II)	*Eichhornia crassipes (Aguapé)*	10 mg/g	[96]
	Aspergillus nomius	987.21 mg/g to 100 min	[87]
	Macroalgae Macrocystis pyrifera	1.251 mmol/g	[97]
	Zeolite 13X-Algal-Alginate Beads (ZABs)	85.88 mg/g	[98]
	Cronobacter muytjensii	76.51 mg/g	[95]
Pb (II)	*Eichhornia crassipes (Aguapé)*	10 mg/g	[96]
	Aspergillus nomius	298.81 mg/g to 60 min	[87]
	Phanerochaete chrysosporium	29.09 mg/g	[65]
Ni (II)	*Aspergillus nomius*	684.2 mg/g to 80 min	[87]
Mn (II)	*Chlorella vulgaris*	115.90 mg/g	[71]
Zn (II)	*Chlorella vulgaris*	105.29 mg/g	[71]

binding capacities for several metals as various functional groups, like carboxyl, amino, phosphate, etc., present in microalgal biomass act as binding sites for metals.

Immobilization of microbial biomass is an innovative way to improve biosorbent capacity along with enhancement in strength and durability. Various polymeric or biopolymeric materials are used for the immobilization process. Ahmed et al. investigated the biosorption of different metals on free and immobilized algae biomass. Free and immobilized biomass are equally effective for the metal aqueous solution in the batch system; however, biosorption via immobilized algae biomass shows better biosorption capacity and biosorbent reusability [71]. Chatterjee et al. recovered nickel from spent batteries using *Aspergillus nominus* (*A. nominus*), a fungal strain [87]. Further, they have studied the effect of the production of enzymes and alcohol on the tolerance level of *A. nominus*. A phenomenon of a sudden rise in biosorption of heavy metal with an increase in pH was termed as absorption edge, and in this case, the pH was 5. Desorption capacity of fungal strain *A. nominus* was observed, and it is reported that fungal biosorbent could be reused multiple times. Sheel et al. used ammonium thiosulfate (AT) and *Lactobacillus acidophilus* for selective sorption of gold from the printed circuit board [99]. The combination of leaching and sorption method leads to a recovery of 85% gold. Several major challenges like metal binding capacity, renewability, stability, and cost efficiency should be addressed in the biosorption process [90].

To conclude, biosorption is a versatile process with certain advantages such as (a) selective absorption of metals at low concentration, (b) mild operating conditions like pH and temperature, (c) energy-efficient, and (d) regeneration of

biosorbent [94]. One of the major challenges in biosorption is to find high biosorption capacity biosorbent for metal absorption. Even though it has several advantages, its limited commercial success and lack of understanding of its kinetics, mechanism, and thermodynamics limit its use. In the case of electronic waste, there are certain challenges, like multi-metal-rich feedstream, dissolution of metal ions into the aqueous solution, and chemical modifications for better selectivity, which need to be addressed. Till now, the recovery of metals from e-waste using biosorption is still at early stages; however, versatile biosorption process holds great potential in the near future [66, 99].

3.2 Bioelectrochemical Process (BES)

BES is a fusion of conventional electrochemical systems and microbial systems. It reduces organic matter and produces electrical energy from chemical energy via the metabolism of microorganisms [100]. BES is also referred to as microbial fuel cell (MFC) or microbial electrolytic cell and is a promising option because of its sustainable approach of harnessing energy and in the production of bioproducts and waste remedy. The microbial fuel cell has several advantages over conventional metallurgy techniques in terms of cost, energy, and environment hazard [101]. Low anode corrosion and recovery of material as well as harnessing electrical energy are the advantages of BES systems over conventional systems [101]. The general structure of BES reactors includes anode, cathode, and separator as shown in Fig. 5 [102]. An anode chamber is filled with oxidized biodegradable material. BES is a promising modern technology for metal recovery from electronic waste due to major improvements in electrode material and designs in the last decade [103]. In recent years, BES applications to remove metals from aqueous solutions are intensively studied with a hope that BES could be applied to metallurgical systems to recover base metals, precious metals, and rare earth metals.

The general methodology of the BES system is the biological conversion at the anode which releases electrons to the cathode and, therefore, reduces metals to its precipitate by considering metals as terminal electron acceptor (TEA). TEA is a compound that accepts electron during oxidation of organic source and plays a crucial role in BES if it is used for waste minimization. Several metal ions can substitute oxygen in a series of oxidation and reduction reactions and can act as an effective TEA [104].

Nachariah et al. discussed about several BES systems to remove metal ions such as Ag(I), Au(III), Co(II), etc. [105]. BES along with microbial electrolysis cell for individual metals recovery were discussed in detail. Biocathode usage was also discussed where cathodes use metal-reducing bacteria to enhance metal reduction on the cathode, with an additional separation method to recover metals.

Huang et al. recovered cobalt from lithium cobalt powder using a microbial electrolysis cell [106]. Overall cobalt recovery was 0.15 ± 0.01 g Co/g Co. This study could be linked to recover cobalt from spent lithium batteries with minimum energy
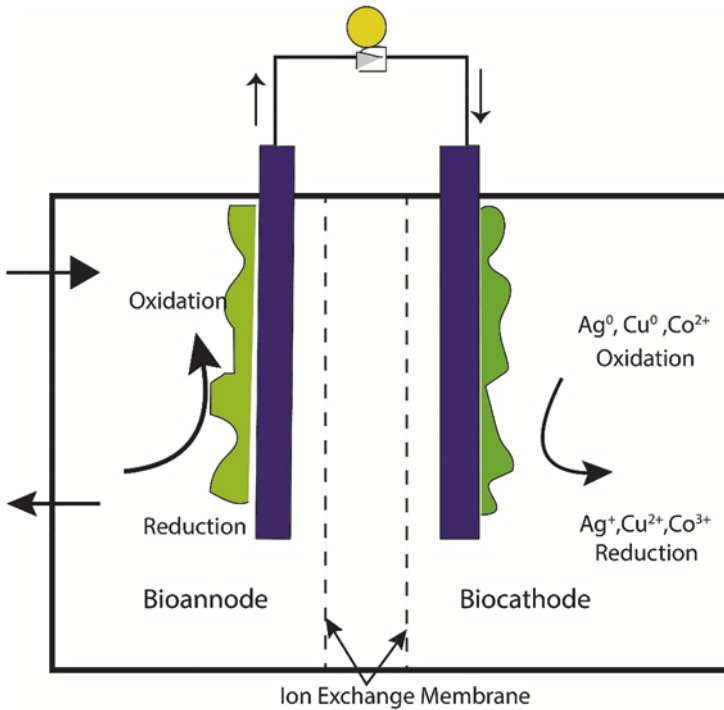
Fig. 5 General structure of BES

consumption. Heijne et al. recovered copper using a MFC with the bipolar membrane [107]. Aerobic and anaerobic condition effect on copper and electricity generation was evaluated, and it was observed that there is improvement in power density of the MFC in aerobic conditions.

Hu et al. have recovered platinum group metals like palladium and rhodium on cathode from wastewater using microbial fuel cell [108]. The electromotive force was utilized to recover Pd, Pt, and Rh on the cathode with a removal efficiency of 99.2%, 99.5%, and 98.7%, respectively. The purity of metals was verified by SEM and EDS analysis. The bioelectrochemical system is a versatile process for the recovery of metals from waste or industrial effluent waste stream. A combination of cathodic reduction with organic component oxidation can be an effective tool to leach out several metals and remove metals. Configuration of BES in terms of cathode-anode along with applied potential, voltage, and initial metal concentration will vastly affect metal removal efficiency. The mechanism part of BES is still not explored well, and much research is needed to verify the mechanism. An integrated approach of combining hydrometallurgy with BES, along with its use in the leaching and extraction of metals from aqueous solution, still needs to be explored.

4 Future Perspective

4.1 Development of Continuous Process for Metal Extraction

The development of a continuous process is important from the aspect of the economic efficiency of the process. The continuous process will also help in mitigating the variation in the quality of the product compared to the batch process and provides more control over the quality of the product. Some recent studies showed that a novel coiled flow inverter (CFI) can be an attractive option for the development of a continuous process for metal extraction [109–112]. CFI was designed by Saxena and Nigam in 1984 [113]. CFI works on the principle of flow inversion, and it is the combination of coiling and 90° bends.

Due to superior efficiency, CFI has been used in various applications such as heat exchanger, gas-liquid-solid reactions, two-phase flow, food processing, mass transfer, pharmaceutical and biotechnology, micro-reactor for metal extraction, etc. as shown in Fig. 6 [114–120]. Different types of CFI designs such as standard CFI,
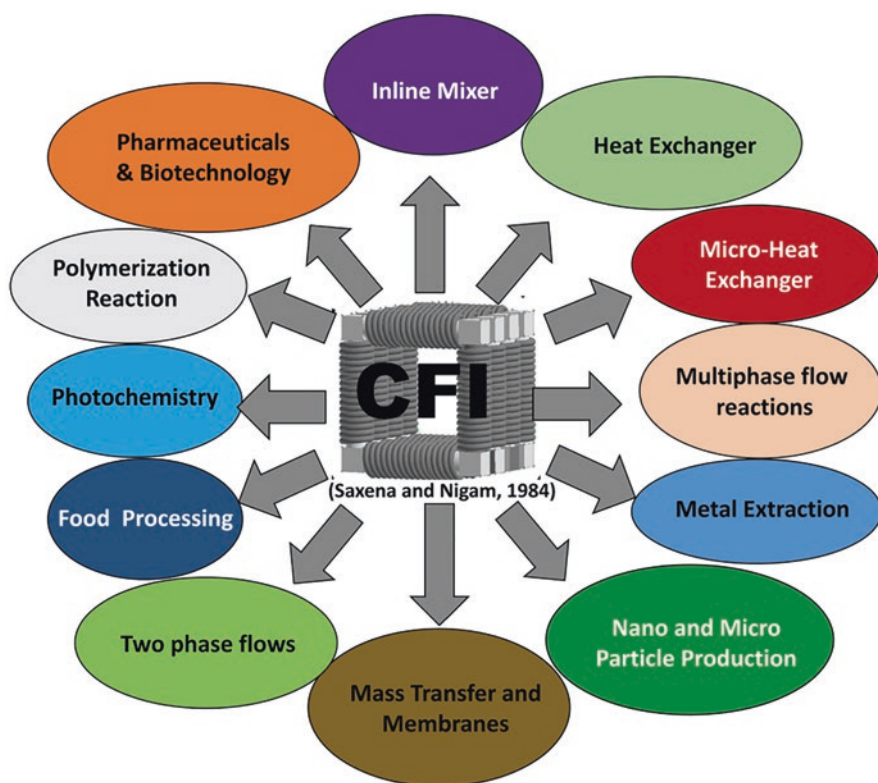
Fig. 6 Application of CFI in different fields (Reproduced with permission from [114])

symmetrical compact CFI, and asymmetrical compact CFI have been employed for process intensification as shown in Fig. 7 [114]. Very few studies have been carried out in the field of metal extraction using CFI. Zhang et al. employed CFI for the extraction of Co from Ni sulfate solution using Cyanex 272 [121]. The experimental setup employed in the study for the continuous extraction of metals is shown in Fig. 8. The two syringe pumps were employed to pump aqueous and organic solutions. A T-type joint was used to join the aqueous and organic phases. A CFI reactor of square shape with four 90° bends was employed in the study to facilitate more efficient mixing. Zhang et al. reported that CFI leads to the higher extraction of Co and separation factor between Co and Ni compared to batch operation. In addition, the optimized residence time in a continuous process using CFI was 60 s and it is very less compared to a batch process residence time of 450 s. The use of CFI provides advantages such as lower reagent consumption, higher productivity and
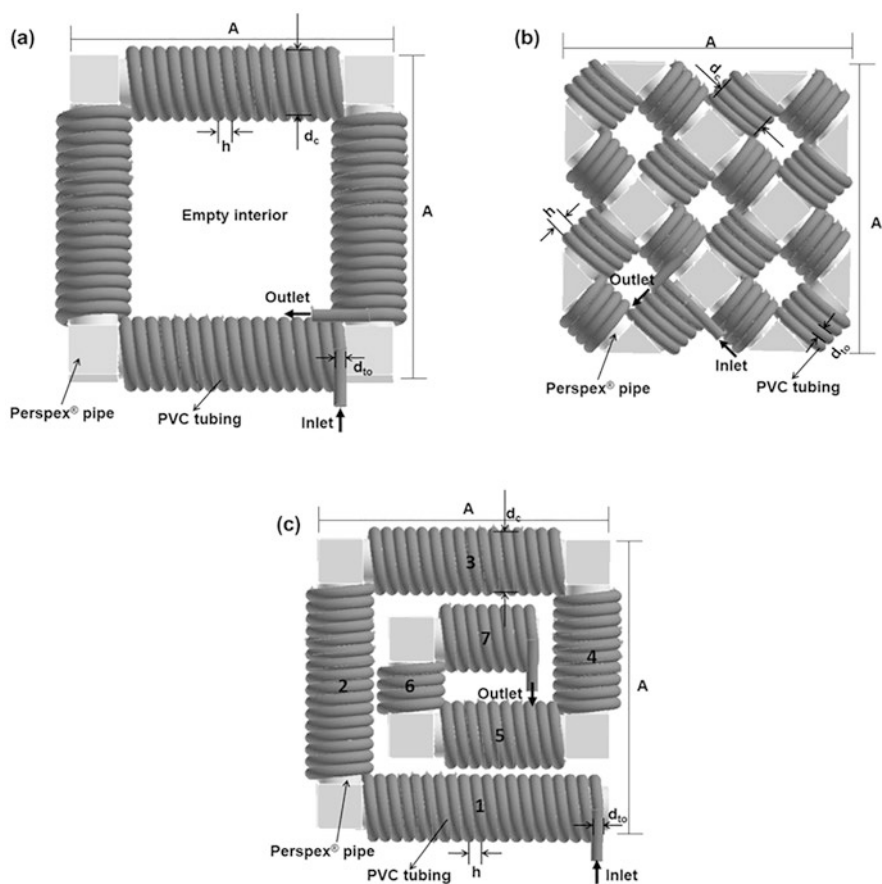
Fig. 7 Schematic diagrams for CFI designs: (**a**) standard CFI, (**b**) symmetrical compact CFI, and (**c**) asymmetrical compact CFI (Reproduced with permission from [114])
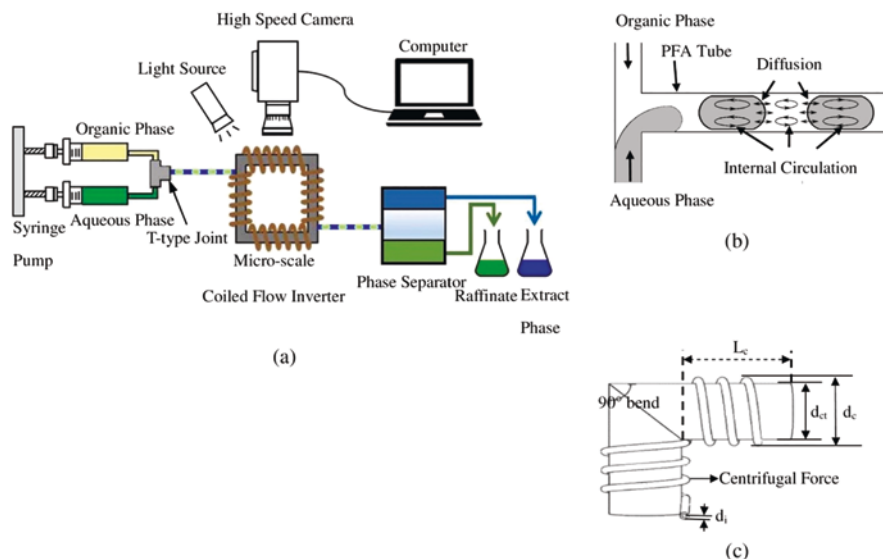
Fig. 8 (**a**) Schematic diagram for the setup of micro-flow extraction and separation system, (**b**) T-type joint, and (**c**) CFI structure (Reproduced with permission from [121])

recycle rate, and smaller plant footprint. The use of CFI leads to intensified liquid-liquid mass transfer and can provide a viable solution for the extraction and separation of metal ions at the industrial scale. A similar study was carried out by Gursel et al. and employed CFI to develop a continuous metal extraction process and efficiently recovered 99% Cu [122].

The use of CFI for metal extraction offers a significant advantage for the development of a continuous process. However, the scale-up and industrial application of this process are still a concern, and there is a need to explore this technique in more detail for application in the field of metal extraction.

4.2 Synthesis of the Catalyst Using Recovered Metals from E-Waste

The real bottom profitability of any process depends on its ability to ensure the usability of the products obtained from it. In this regard, the treatment of e-waste for obtaining precious metals offers several advantages in terms of reusability of the metals for useful purposes, more specifically, the use of extracted metals such as Cu, Ag, Au, Pt, Zn, Ni, etc. in both homo- and heterogeneous catalysis. This can be easily defined in terms of the gap in meeting the demand for the extensive use of such metals in preparing efficient catalysts for a range of commercially relevant processes such as biomass valorization, CO_2 conversion, and water splitting for H_2

generation, among many others. Though the precious metals as mentioned above are used prevalently in preparing catalysts, still, there are several issues like low natural abundance, difficulty in availability, and high cost which are responsible for fluctuations in their continuous supply, hence raising concerns over the use of such strategically important metals in the preparation of valuable catalysts. Moreover, the incessant demand for precious metals creates economic concerns, and it also has substantial repercussions for the environment.

The underlying principles of "sustainable development" which stresses on meeting the present demands without compromising future needs can be truly replicated by the use of metals extracted from electronic waste. The sustainable use of extracted metals from e-waste can play a major role in subsidizing the heavy demand and scarcity of metals important for catalysis. As such, the overdependence of current industrial processes over precious metals can also be minimized through the sustainability of the overall electronic waste treatment process. Ultimately, such electronic waste derived from homo−/heterogeneous catalysts will go a long way in improving the energy efficiency of many current and neoteric chemical practices.

5   Summary

The global e-waste generation is increasing year by year, and it will reach to 74.7 Mt by 2030. E-waste is a rich source of metals and, therefore, can play an important role in mitigating the scarcity of metals. However, unregulated accumulation and improper recycling techniques lead to the loss of critical metals and also pose a threat to the environment and human health. Therefore, it is important to find a sustainable solution for the sound management of the e-waste and recovery of metals. Biohydrometallurgy is a promising option for the recovery of metals from e-waste in an environmentally friendly way. Biotechnology has been employed for the recovery of metals from ores, but e-waste is a different challenge due to the large number of metals and its complex structure. Biohydrometallurgy mainly uses autotrophic bacteria bioleaching, heterotrophic bacteria bioleaching, and heterotrophic fungi bioleaching. Out of these, autotrophic bacteria bioleaching is a conventional bioleaching process that uses sulfur-oxidizing bacteria, iron- and sulfur-oxidizing bacteria, and iron-oxidizing bacteria. These organisms use carbon dioxide from the atmosphere as a carbon source and ferrous ion (Fe^{2+}), elemental sulfur (S^o), and/or reduced sulfur compounds as an energy source. However, e-waste includes metals in their metallic form, and therefore, there is a need to supply the microorganism with an additional energy source. Heterotrophic bioleaching uses microorganisms such as bacteria (e.g., *Pseudomonas aeruginosa*, *Pseudomonas fluorescens*, and *Pseudomonas putida*) and fungi (e.g., *Aspergillus niger* and *Penicillium simplicissimum*). Heterotrophic bioleaching is microbial leaching where organisms get energy from organic carbon sources for growth during the leaching process. The metabolic by-products of organic carbon such as acetic acid, citric acid, oxalic acid, and gluconic acid are responsible for the leaching of metals. Biosorption and bioelectrochemical processes are bio-based

technologies used for the recovery of metals from aqueous solutions. Also, there is a need to explore technique to develop continuous process for metal recovery, and CFI can provide a viable solution for this. However, there is a need to extensively explore the application of CFI for metal recovery.

There is a need to carry out further investigation in the biohydrometallurgical approach for metal recovery from e-waste as some of the main leaching mechanisms are not clear. In addition, it is also important to carry out the pilot-scale studies to find out the feasibility of the biohydrometallurgical process for full-scale industrial applications.

References

1. Forti V, Blade CP, Kuehr R, Bel G (2020) The global e-waste monitor 2020: quantities, flows and the circular economy potential, no. July. United Nations University (UNU)/United Nations Institute for Training and Research (UNITAR) – Co-hosted SCYCLE Programme, International Telecommunication Union (ITU) & International Solid Waste Association (ISWA), Geneva
2. Jadhao PR, Ahmad E, Pant KK, Nigam KDP (2020) Environmentally friendly approach for the recovery of metallic fraction from waste printed circuit boards using pyrolysis and ultra-sonication. Waste Manag 118:150–160
3. Kiddee P, Naidu R, Wong MH (2013) Electronic waste management approaches : an overview. Waste Manag 33:1237–1250
4. Babu BR, Parande AK, Basha CA (2007) Electrical and electronic waste : a global environmental problem. Waste Manag Res 25:307–318
5. Ongondo FO, Williams ID, Cherrett TJ (2011) How are WEEE doing ? A global review of the management of electrical and electronic wastes. Waste Manag 31:714–730
6. Widmer R, Krapf H, Khetriwal D, Schnellmann M, Boni H (2005) Global perspectives on e-waste. Environ Impact Assess Rev 25:436–458
7. Das A, Vidyadhar A, Mehrotra SP (2009) A novel flowsheet for the recovery of metal values from waste printed circuit boards. Resour Conserv Recycl 53:464–469
8. Buekens A, Yang J (2014) Recycling of WEEE plastics: a review. J Mater Cycles Waste Manag 16:415–434
9. Tuncuk A, Stazi V, Akcil A, Yazici EY, Deveci H (2012) Aqueous metal recovery techniques from e-scrap : hydrometallurgy in recycling. Miner Eng 25:28–37
10. Kusch S, Hills CD (2017) The link between E-waste and GDP – new insights from data from the Pan-European region. Resources 6:1–10
11. Hsu E, Barmak K, West AC, Park A-H (2019) Advancements in the treatment and processing of electronic waste with sustainability : a review of metal extraction and recovery technologies. Green Chem 21:919–936
12. Khaliq A, Rhamdhani M, Brooks G, Masood S (2014) Metal extraction processes for electronic waste and existing industrial routes: a review and australian perspective. Resources 3:152–179
13. Hagelüken C (2007) Metals recovery from e-scrap in a global environment. In: 6th Session of OEWG Basel convention
14. Jadhao P, Chauhan G, Pant KK, Nigam KDP (2016) Greener approach for the extraction of copper metal from electronic waste. Waste Manag 57:102–112
15. Panda R, Jadhao PR, Pant KK, Naik SN, Bhaskar T (2020) Eco-friendly recovery of metals from waste mobile printed circuit boards using low temperature roasting. J Hazard Mater 395:122642

16. Chauhan G, Jadhao PR, Pant KK, Nigam KDP (2018) Novel technologies and conventional processes for recovery of metals from waste electrical and electronic equipment : challenges & opportunities – a review. J Environ Chem Eng 6:1288–1304

17. Baniasadi M, Vakilchap F, Bahaloo-horeh N, Mousavi SM, Farnaud S (2019) Advances in bioleaching as a sustainable method for metal recovery from e-waste : a review. J Ind Eng Chem 76:75–90

18. Kumar A, Li J (2017) An overview of the potential of eco-friendly hybrid strategy for metal recycling from WEEE. Resour Conserv Recycl 126:228–239

19. Habibi A, Kourdestani SS, Hadadi M (2020) Biohydrometallurgy as an environmentally friendly approach in metals recovery from electrical waste : a review. Waste Manag Res 38:232–244

20. Cui J, Zhang L (2008) Metallurgical recovery of metals from electronic waste: a review. J Hazard Mater 158:228–256

21. Shuey SA, Taylor P (2005) Review of pyrometallurgical treatment of electronic scrap. In: SME annual meeting, pp 1–4

22. Zhang Y, Liu S, Xie H, Zeng X, Li J (2012) Current status on leaching precious metals from waste printed circuit boards. Proc Environ Sci 16:560–568

23. Akcil A, Erust C, Gahan CS, Ozgun M, Sahin M, Tuncuk A (2015) Precious metal recovery from waste printed circuit boards using cyanide and non-cyanide lixiviants – a review. Waste Manag 45:258–271

24. Morin D et al (2006) BioMinE - integrated project for the development of biotechnology for metal-bearing materials in Europe. Hydrometallurgy 83:69–76

25. Jain R et al (2016) Preferential adsorption of Cu in a multi-metal mixture onto biogenic elemental selenium nanoparticles. Chem Eng J 284:917–925

26. Muñoz AJ, Espínola F, Ruiz E (2017) Biosorption of Ag(I) from aqueous solutions by Klebsiella sp. 3S1. J Hazard Mater 329:166–177

27. Ilyas S, Lee J (2014) Biometallurgical recovery of metals from waste electrical and electronic equipment: a review. ChemBioEng Rev 1:148–169

28. Ilyas S, Anwar MA, Niazi SB, Afzal Ghauri M (2007) Bioleaching of metals from electronic scrap by moderately thermophilic acidophilic bacteria. Hydrometallurgy 88:180–188

29. Beolchini F, Fonti V, Dell'Anno A, Rocchetti L, Vegliò F (2012) Assessment of biotechnological strategies for the valorization of metal bearing wastes. Waste Manag 32:949–956

30. Orell A, Navarro CA, Arancibia R, Mobarec JC, Jerez CA (2010) Life in blue: copper resistance mechanisms of bacteria and archaea used in industrial biomining of minerals. Biotechnol Adv 28:839–848

31. Işıldar A et al (2019) Biotechnological strategies for the recovery of valuable and critical raw materials from waste electrical and electronic equipment (WEEE) – a review. J Hazard Mater 362:467–481

32. Bas AD, Deveci H, Yazici EY (2013) Bioleaching of copper from low grade scrap TV circuit boards using mesophilic bacteria. Hydrometallurgy 138:65–70

33. Hong Y, Valix M (2014) Bioleaching of electronic waste using acidophilic sulfur oxidising bacteria. J Clean Prod 65:465–472

34. Chen S, Yang Y, Liu C, Dong F, Liu B (2015) Chemosphere column bioleaching copper and its kinetics of waste printed circuit boards (WPCBs) by acidithiobacillus ferrooxidans. Chemosphere 141:162–168

35. Isildar A, Van De Vossenberg J, Rene ER, Van Hullebusch ED, Lens PNL (2016) Two-step bioleaching of copper and gold from discarded printed circuit boards (PCB). Waste Manag 57:149–157

36. Arshadi M, Mousavi SM (2015) Multi-objective optimization of heavy metals bioleaching from discarded mobile phone PCBs: simultaneous Cu and Ni recovery using *Acidithiobacillus ferrooxidans*. Sep Purif Technol 147:210–219

37. Arshadi M, Mousavi SM (2014) Simultaneous recovery of Ni and Cu from computer-printed circuit boards using bioleaching: statistical evaluation and optimization. Bioresour Technol 174:233–242

38. Arshadi M, Mousavi SM (2015) Statistical evaluation of bioleaching of mobile phone and computer waste PCBs: a comparative study. Adv Mater Res 1104:87–92

39. Liang G, Li P, Liu W, Wang B (2016) Enhanced bioleaching efficiency of copper from waste printed circuit boards (PCBs) by dissolved oxygen-shifted strategy in Acidithiobacillus ferrooxidans. J Mater Cycles Waste Manag 18:742–751

40. Bajestani MI, Mousavi SM, Shojaosadati SA (2014) Bioleaching of heavy metals from spent household batteries using Acidithiobacillus ferrooxidans: statistical evaluation and optimization. Sep Purif Technol 132:309–316

41. Yang T, Xu Z, Wen J, Yang L (2009) Factors influencing bioleaching copper from waste printed circuit boards by Acidithiobacillus ferrooxidans. Hydrometallurgy 97:29–32

42. Muravyov MI, Bulaev AG, Melamud VS, Kondrat'eva TF (2015) Leaching of rare earth elements from coal ashes using acidophilic chemolithotrophic microbial communities. Microbiology 84:194–201

43. Machado MD, Soares EV, Soares HMVM (2010) Removal of heavy metals using a Brewer's yeast strain of *Saccharomyces cerevisiae* : chemical speciation as a tool in the prediction and improving of treatment efficiency of real electroplating effluents. J Hazard Mater 180:347–353

44. Das N, Das D (2013) Recovery of rare earth metals through biosorption : an overview. J Rare Earths 31:933–943

45. Burgstaller W, Schinner F (1993) Leaching of metals with fungi. J Biotechnol 27:91–116

46. Shabani MA, Irannajad M, Azadmehr AR, Meshkini M (2013) Bioleaching of copper oxide ore by Pseudomonas Aeruginosa. Int J Miner Metall Mater 20:1130–1133

47. Rezza I, Salinas E, Sanz de Tosetti M, Donati E (2001) Mechanisms involved in bioleaching of an aluminosilicate by heterotrophic microorganisms. Process Biochem 36:495–500

48. Jujun R, Xingjiong Z, Yiming Q, Jian H (2014) A new strain for recovering precious metals from waste printed circuit boards. Waste Manag 34:901–907

49. Chi TD, Lee JC, Pandey BD, Yoo K, Jeong J (2011) Bioleaching of gold and copper from waste mobile phone PCBs by using a cyanogenic bacterium. Miner Eng 24:1219–1222

50. Marsden JO, House CI (2006) The chemistry of gold extraction, second. Society of Mining, Metallurgy, and Exploration, Inc., Englewood, CO

51. Rees KL, Van Deventer JSJ (1999) The role of metal-cyanide species in leaching gold from a copper concentrate. Miner Eng 12:877–892

52. Kita Y, Nishikawa H, Ike M, Takemoto T (2009) Enhancement of Au dissolution by microorganisms using an accelerating cathode reaction. Metall Mater Trans B Process Metall Mater Process Sci 40B:39–44

53. Marra A, Cesaro A, Rene ER, Belgiorno V, Lens PNL (2018) Bioleaching of metals from WEEE shredding dust. J Environ Manag 210:180–190

54. Natarajan G, Tay SB, Yew WS, Ting YP (2015) Engineered strains enhance gold biorecovery from electronic scrap. Miner Eng 75:32–37

55. Natarajan G, Ting YP (2014) Pretreatment of e-waste and mutation of alkali-tolerant cyanogenic bacteria promote gold biorecovery. Bioresour Technol 152:80–85

56. Li J, Liang C, Ma C (2015) Bioleaching of gold from waste printed circuit boards by Chromobacterium violaceum. J Mater Cycles Waste Manag 17:529–539

57. Pradhan JK, Kumar S (2012) Metals bioleaching from electronic waste by *Chromobacterium violaceum* and *Pseudomonads* sp. Waste Manag Res 30:1151–1159

58. Faramarzi MA, Brandl H (2006) Formation of water-soluble metal cyanide complexes from solid minerals by *Pseudomonas plecoglossicida*. FEMS Microbiol Lett 259:47–52

59. Lee J, Pandey BD (2012) Bio-processing of solid wastes and secondary resources for metal extraction – a review. Waste Manag 32:3–18

60. Brandl H, Bosshard R, Wegmann M (2001) Computer-munching microbes : metal leaching from electronic scrap by bacteria and fungi. Hydrometallurgy 59:319–326

61. Brombacher C, Bachofen R, Brandl H (1998) Development of a laboratory-scale leaching plant for metal extraction from fly ash by *Thiobacillus* strains. Appl Environ Microbiol 64:1237–1241

62. Bosshar PP, Bachofen R, Brandl H (1996) Metal leaching of fly ash from municipal waste incineration by *Aspergillus niger*. Environ Sci Technol 30:3066–3070

63. Desouky OA, El-Mougith AA, Hassanien WA, Awadalla GS, Hussien SS (2016) Extraction of some strategic elements from thorium – uranium concentrate using bioproducts of *Aspergillus ficuum* and Pseudomonas Aeruginosa. Arab J Chem 9:S795–S805

64. Hassanien WAG, Desouky OAN, Hussien SSE (2014) Bioleaching of some rare earth elements from Egyptian Monazite using *Aspergillus ficuum* and *Pseudomonas Aeruginosa*. Walailak J Sci Tech 11:809–823

65. Lu N, Hu T, Zhai Y, Qin H, Aliyeva J, Zhang H (2020) Fungal cell with artificial metal container for heavy metals biosorption: equilibrium, kinetics study and mechanisms analysis. Environ Res 182:109061

66. Arshadi M, Mousavi SM, Rasoulnia P (2016) Enhancement of simultaneous gold and copper recovery from discarded mobile phone PCBs using *Bacillus megaterium*: RSM based optimization of effective factors and evaluation of their interactions. Waste Manag 57:158–167

67. Huang H et al (2016) A novel *Pseudomonas Gessardii* strain LZ-E simultaneously degrades naphthalene and reduces hexavalent chromium. Bioresour Technol 207:370–378

68. Mahmoud A, Cezac P, Hoadley AFA, Contamine F, D'Hugues P (2017) A review of sulfide minerals microbially assisted leaching in stirred tank reactors. Int Biodeterior Biodegradation 119:118–146

69. Xia M et al (2018) Bioleaching of low-grade waste printed circuit boards by mixed fungal culture and its community structure analysis. Resour Conserv Recycl 136:267–275

70. Veglio F, Beolchini F (1997) Removal of metals by biosorption : a review. Hydrometallurgy 44:301–316

71. Ahmad A, Bhat AH, Buang A (2018) Biosorption of transition metals by freely suspended and Ca-alginate immobilised with chlorella vulgaris : kinetic and equilibrium modeling. J Clean Prod 171:1361–1375

72. Ilyas S, Lee J, Chi R (2013) Bioleaching of metals from electronic scrap and its potential for commercial exploitation. Hydrometallurgy 131–132:138–143

73. Salvadori MR, Ando RA, Nascimento CAO, Correa B (2017) Dead biomass of Amazon yeast : a new insight into bioremediation and recovery of silver by intracellular synthesis of nanoparticles. J Environ Sci Heal A 52:1–9

74. Paknikar KM, Pethkar AV, Puranik PR (2003) Bioremediation of metalliferous wastes and products using inactivated microbial biomass. Indian J Biotechnol 2:426–443

75. Baran MF (2019) Biosorption of Pb 2 + from aqueous solutions by Bacillus licheniformis Isolated from Tigris River with a comparative study. Int J Latest Eng Manag Res 4:108–121

76. Joo JH, Hassan SHA, Oh SE (2010) Comparative study of biosorption of Zn2+ by *Pseudomonas aeruginosa* and *Bacillus cereus*. Int Biodeterior Biodegrad 64:734–741

77. Sahmoune MN (2018) Performance of Streptomyces Rimosus biomass in biosorption of heavy metals from aqueous solutions. Microchem J 141:87–95

78. Selatnia A, Bakhti MZ, Madani A, Kertous L, Mansouri Y (2004) Biosorption of Cd2+ from aqueous solution by a NaOH-treated bacterial dead Streptomyces rimosus biomass. Hydrometallurgy 75:11–24

79. Ahmady-Asbchin S, Safari M, Tabaraki R (2015) Biosorption of Zn (II) by Pseudomonas aeruginosa isolated from a site contaminated with petroleum. Desalin Water Treat 54:3372–3379

80. Mulligan CN, Yong RN, Gibbs BF (2001) An evaluation of technologies for the heavy metal remediation of dredged sediments. J Hazard Mater 85:145–163

81. Park D, Yun YS, Park JM (2010) The past, present, and future trends of biosorption. Biotechnol Bioprocess Eng 15:86–102

82. Dursun AY, Uslu G, Tepe O, Cuci Y, Ekiz HI (2003) A comparative investigation on the bioaccumulation of heavy metal ions by growing *Rhizopus arrhizus* and *Aspergillus niger*. Biochem Eng J 15:87–92

83. Say R, Yilmaz N, Denizli A (2003) Removal of heavy metal ions using the fungus *Penicillium canescens*. Adsorpt Sci Technol 21:643–650

84. Leitão AL (2009) Potential of Penicillium species in the bioremediation field. Int J Environ Res Public Health 6:1393–1417

85. Ponce de León CA, Bayón MM, Paquin C, Caruso JA (2002) Selenium incorporation into Saccharomyces cerevisiae cells: a study of different incorporation methods. J Appl Microbiol 92:602–610

86. Munoz AJ, Espínola F, Ruiz E (2017) Biosorption of Ag (I) from aqueous solutions by Klebsiella sp . 3S1. J Hazard Mater 329:166–177

87. Chatterjee A, Das R, Abraham J (2020) Bioleaching of heavy metals from spent batteries using *Aspergillus nomius* JAMK1. Int J Environ Sci Technol 17:49–66

88. Abdallah MAM, Mahmoud ME, Osman MM, Ahmed SB (2017) New Biosorbent in removing some metals from industrial wastewater in El Mex Bay, Egypt. Appl Water Sci 7:1931–1942

89. Escudero LB, Quintas PY, Wuilloud RG, Dotto GL (2019) Recent advances on elemental biosorption. Environ Chem Lett 17:409–427

90. Vieira RHSF, Volesky B (2000) Biosorption: a solution to pollution? Int Microbiol 3:17–24

91. Kalak T, Dudczak-Halabuda J, Tachibana Y, Cierpiszewski R (2020) Effective use of elderberry (Sambucus nigra) pomace in biosorption processes of Fe (III) Ions. Chemosphere 246:125744

92. Vendruscolo F, Ferreira GLR, Filho NRA (2017) Biosorption of hexavalent chromium by microorganisms. Int Biodeterior Biodegradation 119:87–95

93. Li L, Hu Q, Zeng J, Qi H, Zhuang G (2011) Resistance and biosorption mechanism of silver ions by *Bacillus cereus* biomass. J Environ Sci 23:108–111

94. Nicomel NR et al (2020) Microalgae : a sustainable adsorbent with high potential for upconcentration of indium (III) from liquid process and waste streams. Green Chem 22:1985–1995

95. Saranya K, Sundaramanickam A, Shekhar S, Meena M, Sathishkumar RS, Balasubramanian T (2018) Biosorption of multi-heavy metals by coral associated phosphate solubilising Bacteria Cronobacter Muytjensii KSCAS2. J Environ Manag 222:396–401

96. De Freitas F, Battirola LD, Arruda R, de Andrade RT (2019) Assessment of the Cu (II) and Pb (II) removal efficiency of aqueous solutions by the dry biomass Aguapé : kinetics of adsorption. Env Monit Assess 191:751

97. Cid H, Ortiz C, Pizarro J, Moreno-pirajàn JC (2020) Effect of copper (ii) biosorption over light metal cation desorption in the surface of Macrocystis Pyrifera Biomass. J Environ Chem Eng 8:103729

98. Moghaddam SAE, Harun R, Mokhtar MN, Zakaria R (2020) Kinetic and equilibrium modeling for the biosorption of metal ion by zeolite 13X-algal-alginate beads (ZABs). J Water Process Eng 33:101057

99. Sheel A, Pant D (2018) Recovery of Gold from Electronic Waste using Chemical Assisted Microbial Biosorption (hybrid) Technique. Bioresour Technol 247:1189–1192

100. Ai C et al (2020) Recovery of metals from acid mine drainage by bioelectrochemical system Inoculated with a Novel Exoelectrogen, Pseudomonas sp. E8. Microorganisms 8:1–16

101. Chaturvedi V, Verma P (2016) Microbial fuel cell: a green approach for the utilization of waste for the generation of bioelectricity. Bioresour Bioprocess 3:1–14

102. Tugtas AE, Calli B (2018) Removal and recovery of metals by using bio-electrochemical system. In: Das D (ed) Microbial fuel cell. New Delhi, Capital Publishing Company, pp 307–333

103. Huang T, Liu L, Zhang S (2019) Microbial fuel cells coupled with the bioleaching technique that enhances the recovery of cu from the secondary mine tailings in the bio-electrochemical system. Environ Prog Sustain Energy 38:1–9

104. Velvizhi G, Goud RK, Mohan SV (2014) Anoxic bio-electrochemical system for treatment of complex chemical wastewater with simultaneous bioelectricity generation. Bioresour Technol 151:214–220

105. Nancharaiah YV, Mohan SV, Lens PNL (2015) Metals removal and recovery in bioelectrochemical systems: a review. Bioresour Technol 195:102–114

106. Huang L, Yao B, Wu D, Quan X (2014) Complete cobalt recovery from lithium cobalt oxide in self-driven microbial fuel cell - microbial electrolysis cell systems. J Power Sources 259:54–64

107. Ter Heijne A, Liu F, Van Der Weijden R, Weijma J, Buisman CJN, Hamelers HVM (2010) Copper recovery combined with electricity production in a microbial fuel cell. Environ Sci Technol 44:4376–4381

108. Hu N, Cui Y, Choi C (2019) Recovery of platinum-group metals using a microbial fuel cell. Trends Diabetes Metab 2:1–9

109. Vural Gürsel I, Kockmann N, Hessel V (2017) Fluidic separation in microstructured devices – concepts and their integration into process flow networks. Chem Eng Sci 169:3–17

110. Kurt SK, Vural Gürsel I, Hessel V, Nigam KDP, Kockmann N (2016) Liquid-liquid extraction system with microstructured coiled flow inverter and other capillary setups for single-stage extraction applications. Chem Eng J 284:764–777

111. Kurt SK, Akhtar M, Nigam KDP, Kockmann N (2016) Modular concept of a smart scale helically coiled tubular reactor for continuous operation of multiphase reaction systems. In: Proceedings of the ASME 2016 14th international conference on nanochannels, microchannels, and minichannels, pp 1–12

112. Vural Gürsel I et al (2016) Utilization of milli-scale coiled flow inverter in combination with phase separator for continuous flow liquid-liquid extraction processes. Chem Eng J 283:855–868

113. Chauhan G, Kaur P, Pant KK, Nigam KDP (2020) Sustainable metal extraction from waste streams. WILEY-VCH Verlag GmbH, Berlin

114. Soni S, Sharma L, Meena P, Roy S, Nigam KDP (2019) Compact coiled flow inverter for process intensification. Chem Eng Sci 193:312–324

115. Mandal MM, Aggarwal P, Nigam KDP (2011) Liquid-liquid mixing in coiled flow inverter. Ind Eng Chem Res 50:13230–13235

116. Singh J, Nigam KDP (2016) Pilot plant study for effective heat transfer area of coiled flow inverter. Chem Eng Process Process Intensif 102:219–228

117. Singh J, Choudhary N, Nigam KDP (2014) The thermal and transport characteristics of nano-fluids in a novel three-dimensional device. Can J Chem Eng 92:2185–2201

118. Kateja N, Agarwal H, Saraswat A, Bhat M, Rathore AS (2016) Continuous precipitation of process related impurities from clarified cell culture supernatant using a novel coiled flow inversion reactor (CFIR). Biotechnol J 11:1320–1331

119. Parida D et al (2014) Coil flow inversion as a route to control polymerization in microreactors. Macromolecules 47:3282–3287

120. Vashisth S, Nigam KDP (2008) Experimental investigation of void fraction and flow patterns in coiled flow inverter. Chem Eng Process Process Intensif 47:1281–1291

121. Zhang L, Hessel V, Peng J, Wang Q, Zhang L (2017) Co and Ni extraction and separation in segmented micro-flow using a coiled flow inverter. Chem Eng J 307:1–8

122. Gürsel IV, Aldiansyah F, Wang Q, Noël T, Hessel V (2015) Continuous metal scavenging and coupling to one-pot copper-catalyzed azide-alkyne cycloaddition click reaction in flow. Chem Eng J 270:468–475

Index